

AEC-tr

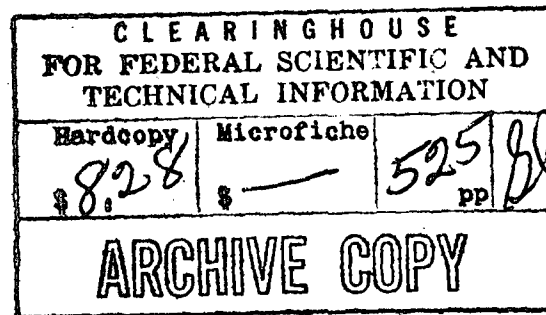
6630

Clifford Anderson

I.E. Idel'chik

**HANDBOOK OF HYDRAULIC
RESISTANCE**

Coefficients of Local Resistance and of Friction



Translated from Russian

Published for the U.S. Atomic Energy Commission
and the National Science Foundation, Washington, D.C.
by the Israel Program for Scientific Translations

I.E. IDEL'CHIK

HANDBOOK OF HYDRAULIC RESISTANCE

Coefficients of Local Resistance and of Friction

(Spravochnik po gidravlicheskim sопротивлениям.
Koeffitsienty mestnykh sопротивлений i sопротивleniya treniya)

Gosudarstvennoe Energeticheskoe Izdatel'stvo
Moskva-Leningrad
1960

Translated from Russian

Israel Program for Scientific Translations
Jerusalem 1966

Published Pursuant to an Agreement with
THE U.S. ATOMIC ENERGY COMMISSION
and
THE NATIONAL SCIENCE FOUNDATION, WASHINGTON, D.C.

Copyright © 1966
Israel Program for Scientific Translations Ltd.
IPST Cat. No. 1505

Translated by A. Barouch, M.Sc.
Edited by D. Grunaer, P.E. and IPST Staff

Printed in Jerusalem by S. Monson

Price: \$8.28

Available from the
U.S. DEPARTMENT OF COMMERCE
Clearinghouse for Federal Scientific and Technical Information
Springfield, Va. 22151

Table of Contents

FOREWORD	vii
Section One. GENERAL INFORMATION AND RECOMMENDATIONS FOR USING THE HANDBOOK		1
1-1.	List of general symbols used throughout the book	1
1-2.	General directions	2
1-3.	Properties of fluids	3
a.	Specific gravity	3
b.	Viscosity	4
1-4.	Equilibrium of fluids	12
1-5.	Motion of fluids	14
a.	Discharge, and mean stream velocity	14
b.	Equation of continuity of a stream	15
c.	Bernoulli equation. Head loss	16
1-6.	The flow of fluids through an orifice	21
a.	Flow of an incompressible fluid	21
b.	Discharge of a compressible gas	25
1-7.	Fluid-flow states	26
1-8.	Fluid resistance	29
1-9.	Work of a compressor in systems	32
1-10.	Examples of the calculations of the fluid resistance of systems	35
Section Two. STREAM FLOW THROUGH STRAIGHT PIPES AND CHANNELS (FRICTION COEFFICIENTS AND ROUGHNESS)		53
2-1.	List of symbols	53
2-2.	Explanations and practical recommendations	53
2-3.	Roughness of pipes and channels	62
2-4.	List of the diagrams of friction coefficients of section II	65
2-5.	Diagrams of friction coefficients	66
Section Three. STREAM INTAKE IN PIPES AND CHANNELS (RESISTANCE COEFFICIENTS OF INLET SECTIONS)		80
3-1.	List of symbols	80
3-2.	Explanations and recommendations	81
3-3.	List of the diagrams of resistance coefficients of section III	91
3-4.	Diagrams of resistance coefficients	92
Section Four. SUDDEN VARIATION OF VELOCITY IN STREAM PASSAGE THROUGH AN ORIFICE (RESISTANCE COEFFICIENTS OF STRETCHES WITH SUDDEN EXPANSION, ORIFICE PLATES, APERTURES, ETC.)		112
4-1.	List of symbols	112
4-2.	Explanations and practical recommendations	112
4-3.	List of diagrams of resistance coefficients of section IV	127
4-4.	Diagrams of resistance coefficients	128
Section Five. SMOOTH VELOCITY VARIATION (RESISTANCE COEFFICIENTS OF DIFFUSERS)		151
5-1.	List of symbols	151
5-2.	Explanations and recommendations	151

5-3. List of the diagrams of resistance coefficients of section V	165
5-4. Diagrams of resistance coefficients	166
Section Six. VARIATION OF THE STREAM DIRECTION (RESISTANCE COEFFICIENT OF CURVES STRETCHES-BRANCHES, ELBOWS, ETC.)	189
6-1. List of symbols	189
6-2. Explanations and recommendations	190
6-3. List of the diagrams of resistance coefficients of section VI	204
6-4. Diagrams of resistance coefficients	206
Section Seven. STREAM JUNCTIONS AND DIVISIONS (RESISTANCE COEFFICIENTS OF WYES, TEES, AND CROSSES)	247
7-1. List of symbols	247
7-2. Explanations and recommendations	247
7-3. List of diagrams for resistance coefficients of section VII	258
7-4. Diagrams of resistance coefficients	260
Section Eight. FLOW PAST OBSTRUCTIONS UNIFORMLY DISTRIBUTED OVER CONDUIT CROSS SECTIONS (RESISTANCE COEFFICIENTS OF GRIDS, SCREENS, PIPE BUNDLES, PACKINGS, ETC.)	305
8-1. List of symbols	305
8-2. Explanations and recommendations	306
8-3. List of the diagrams of resistance coefficients of section VIII	319
8-4. Diagrams of resistance coefficients	321
Section Nine. STREAM FLOW THROUGH PIPE FITTINGS AND LABYRINTH SEALS (RESISTANCE COEFFICIENTS OF THROTTLES, VALVES, LABYRINTHS, ETC.)	350
9-1. List of symbols	350
9-2. Explanations and recommendations	350
9-3. List of the diagrams of resistance coefficients of section IX	358
9-4. Diagrams of resistance coefficients	359
Section Ten. FLOW PAST OBSTRUCTIONS IN A CONDUIT (RESISTANCE COEFFICIENTS OF STRETCHES WITH PROJECTIONS, TRUSSES, GIRDERS, AND OTHER OBSTRUCTIONS)	379
10-1. List of symbols	379
10-2. Explanations and recommendations	379
10-3. List of the diagrams of resistance coefficients of section X	387
10-4. Diagrams of resistance coefficients	388
Section Eleven. STREAM DISCHARGE FROM PIPES AND CHANNELS (RESISTANCE COEFFICIENTS OF EXIT STRETCHES)	400
11-1. List of symbols	400
11-2. Explanations and recommendations	400
11-3. List of the diagrams of resistance coefficients of section XI	414
11-4. Diagrams of resistance coefficients	416
Section Twelve. STREAM FLOW THROUGH VARIOUS APPARATUS (RESISTANCE COEFFICIENTS OF APPARATUS AND OTHER DEVICES)	442
12-1. List of symbols	442
12-2. Explanations and recommendations	442
12-3. List of the diagrams of resistance coefficients (or resistance magnitudes) of section XII	456
12-4. Diagrams of resistance coefficients	458
BIBLIOGRAPHY	492
INDEX	509

This handbook contains data on the friction coefficients of straight pipes and channels and the coefficients of fluid resistance of fittings, throttles, obstructions, elements of hydraulic or gas-air lines, and several devices used in industrial systems for gas purification, heat exchange, and ventilation.

The handbook is divided into twelve sections. The first section contains general information on hydraulics and mechanics of fluids. The other sections are each devoted to a definite group of fittings or other elements of pipes and obstructions with similar conditions of fluid motion, and contain data on their fluid resistances. Each of these sections is divided into descriptive material and separate diagrams for practical calculations, each of which corresponds to a certain element of the pipe or obstruction. In most instances these diagrams contain formulas for calculating the resistance coefficient of the element as a function of its main characteristics, a graphical representation of this functional relationship, and tables of the values of the resistance coefficients.

This handbook is intended for a wide range of specialists: scientists, designing and operating engineers of all branches of hydroengineering, and students of universities and technical institutes.

FOREWORD

There is almost no branch of engineering which is not somehow concerned with the necessity of moving fluids through pipes, conduits, or machinery. The degree of complexity of a hydraulic or gas-air line can be quite varied. In some cases these are large-scale systems of pipes, gas mains, water conduits, steam pipes, air ducts, etc., while in other cases these are pipelines of relatively small length, but having a large number of fittings and branches, various obstructions such as throttles and adjusting devices, grids, protruding parts, etc.

The network through which a fluid moves usually represents a single unit such as boilers, furnaces, heat exchangers, motors, scrubbers, chemical instruments, and wind tunnels.

The correct calculation of the fluid resistance of these systems is necessary in all cases, and a special handbook on the friction coefficients and the coefficients of local resistances should be available for this.

Until recently only restricted data were available on the subject, and these were scattered among various textbooks on hydraulics and aerodynamics and in scientific papers. In many cases these data are contradictory or dated, and deal with only a limited number of local resistances. Furthermore, the coefficients of local resistances generally were given only for special geometric and physical characteristics.

In order to fill this gap, in 1954 the author published a book "Gidravlicheskie sопротивления" (Fluid Resistances), Gosenergoizdat, 1954, on the general problems of fluid resistances, based on the processing, collating, and classification of materials obtained from our studies and those of others. We present here in the same spirit this special handbook on the local fluid and friction resistances.

The writing of this handbook presented considerable difficulties, mainly due to the range of local resistances, their geometric boundaries, and the states of flow in them, which are much narrower than required by practice. Furthermore, much of the data obtained is insufficiently accurate and reliable; this is particularly true of the coefficients of local resistances.

Therefore, it would have been better to delay the publication of this handbook until all coefficients of local resistances could have been checked and refined experimentally by some standard method, based on the contemporary level of metrology. Unfortunately, it seems unlikely that such a series of experiments would be completed in the near future.

A different approach was also possible: to include in the handbook only such data as can be considered reliable. The amount of such data is, however, very small, and this approach would result in a book which does not fulfill our object — to present the necessary material for the hydraulic calculation of gas-air and hydraulic lines.

Taking into account the great need of even tentative data for assessing the resistance of conduits made of stretches of quite varied configurations, we decided to include

in this handbook not only data checked satisfactorily by laboratory studies, but also data obtained by crude experiments, and those obtained theoretically or by approximate calculations, etc.

We feel that such an approach is justified, since the accuracy with which conduits and components are manufactured and installed under industrial conditions can differ considerably from installation to installation and also from the laboratory conditions under which most coefficients of fluid resistances were obtained.

We have found it necessary to add to the basic material in the handbook some general principles of hydraulics and mechanics of fluids, with descriptions of the contents of each section, as well as additional explanations and recommendations for calculating and selecting hydraulic components.

The coefficient of local resistance is usually a function of many parameters and is therefore represented by an expression with many terms. In order to obtain the numerical value of such a coefficient it is therefore necessary to use several curves or tables.

The different formulas for calculating the resistance coefficients frequently contain similar terms. The curves representing these terms are not repeated each time, but are given once and for all in one of the diagrams; the number of this diagram is then indicated in the other diagrams.

This arrangement naturally complicates the use of the handbook; it is, however, dictated by the necessity of reducing the volume of the book as much as possible.

These shortcomings are probably not the only ones. Nevertheless it is our hope that this handbook will be of use to specialists in the calculation of the fluid resistances of various conduits.

The author will be grateful for any suggestions for correcting the mistakes that are found.

The author acknowledges the help of A. D. Al'tshul, A. S. Ginevskii, I. S. Mochan, L. A. Rikhter, Candidates of Engineering Sciences, and of Engineer L. E. Medovar in reading the MS, and giving many valuable suggestions.

The Author

Section One

GENERAL INFORMATION AND RECOMMENDATIONS FOR USING THE HANDBOOK

1-1. LIST OF GENERAL SYMBOLS USED THROUGHOUT THE BOOK

- F = cross-section area, m^2 ;
 D = cross-section diameter, m;
 D_h , d_h = hydraulic diameters ($4 \times$ hydraulic radius), m;
 Π = cross-section perimeter, m;
 f = cross-section coefficient;
 l = length of the stretch, m;
 h = height, m;
 R , r = radii of cross sections or curvature, respectively, m;
 Δ = mean height of roughness peaks, m;
 $\bar{\Delta} = \frac{\Delta}{D_h}$ = relative roughness;
 n = area ratio or number of elements;
 α = angle of divergence or convergence of the conduit, or angle of attack of the stream;
 w = stream velocity, m/sec ;
 p = pressure (absolute), kg/m^2 ;
 H = gage pressure, kg/m^2 ;
 ΔH = pressure loss or resistance, kg/m^2 ;
 ΔE = energy loss, $\text{kg} \cdot \text{m/sec}$;
 Q = volume flow rate, m^3/sec ;
 G = mass flow rate, kg/sec ;
 γ = specific gravity of the flowing medium, kg/m^3 ;
 $\rho = \frac{\gamma}{g}$ = density of the flowing medium, $\text{kg} \cdot \text{sec}^2/\text{m}^2$;
 g = gravitational acceleration, m/sec^2 ;
 η = dynamic viscosity;
 ν = kinematic viscosity;
 T = absolute temperature of the medium, $^\circ\text{K}$;
 t = temperature of the medium, $^\circ\text{C}$;
 c_p , c_v = mean specific heats at $p = \text{const}$ and $v = \text{const}$, respectively, $\text{kcal/kg} \cdot \text{degree}$;
 $\kappa = \frac{c_p}{c_v}$ = specific-heat ratio;
 ζ = coefficient of fluid resistance;
 λ = friction coefficient of unit relative length (length in section-diameter units) of the stretch calculated;
 C_d = coefficient of drag;
 φ = velocity coefficient;
 ϵ = coefficient of jet contraction;
 μ = discharge coefficient;
 Re = Reynolds number.

1-2. GENERAL DIRECTIONS

1. The basic reference data given here are the friction coefficients ζ_{fr} in straight pipes and channels and the coefficients of local fluid resistance ζ_1 of pipe fittings, throttles, obstructions, and industrial instruments.

2. When using this handbook it is assumed that all magnitudes in the well-known formula for calculating the resistance (cf. (1-66)):

$$\Delta H_{sum} = \zeta_{sum} \frac{\gamma w_0^2}{2g} = \zeta_{sum} \frac{\gamma}{2g} \left(\frac{Q}{F_0} \right)^2 [kg/m^2], \quad (1-1)$$

except the total coefficient of fluid resistance $\zeta_{sum} = \zeta_{fr} + \zeta_1$, and all geometric parameters of the system element being considered, are given. The only unknowns are ζ_{sum} , or simply ζ^* , and its components ζ_{fr} and ζ_1 .

3. The coefficient of local resistance can be considered equal to the total coefficient ζ in all diagrams for elements of conduits of relatively short length, since the values of ζ_{fr} in such elements can be neglected compared with the values of ζ_1 .

4. Diagrams referring to elements of relatively long pipes and channels give the values of both the coefficients of local resistance ζ_1 and the friction coefficients ζ_{fr} .

The values of resistance coefficients appearing in diagrams giving tentative data are to be considered as total coefficients ζ ; accordingly, the frictional losses in these fittings are not to be added separately when summing all losses in the lines.

5. The values of ζ_1 given in this handbook include the local pressure losses in the immediate proximity of a variation in the system configuration and also the pressure losses associated with the subsequent equalization of velocities over the straight exit section. Since, however, local losses are arbitrarily determined as the difference between the total and frictional losses in the exit section, the frictional losses have to be taken into account.

6. In the case of a stream discharged from a fitting or some other element into a large volume (such as the atmosphere), the given coefficients of local resistance take into account the losses of dynamic pressure $\frac{\gamma w_{ex}^2}{2g}$ at the exit (w_{ex} = velocity at outlet section).

7. All values of local resistance coefficients given in the handbook, with certain exceptions, are given for conditions of uniform velocity distribution in the inlet section of the element considered; as a rule, such conditions prevail behind a smooth inlet.

8. The influence on the local resistance of an element, due to fittings, obstructions, or lengthy straight stretches located downstream, is not allowed for by the values given for ζ in the handbook, except as noted. In certain cases this influence causes an increase in the value of ζ_1 of the element considered, and in other cases a decrease. As yet there is no general method of allowing for this.

9. The dependence of the coefficients of local resistance on the Reynolds number Re , is only given in those cases where the influence of the latter is known or can be estimated.

In practice, Re has an influence on the local resistance in the range $Re < 10^5 - 2 \times 10^5$. At $Re > 10^5 - 2 \times 10^5$ it can almost always be assumed that the coefficients of local resistance are independent of Re . At smaller values of Re it is necessary to allow for its influence on the basis of the data given in the handbook.

* In what follows, the subscript "sum" in the symbols for the total resistance coefficient ζ and the total resistance ΔH will be omitted.

If there is no indication of the values of Re for which the values given for ζ_1 were obtained, it can be assumed, in the case of turbulent flow ($Re > 10^3$), that the resistance coefficient is practically independent of the value of Re . In the case of laminar flow ($Re < 10^3$), the data given in the handbook can be used only for a rough estimate of the resistance.

10. All values of the resistance coefficients given in this handbook, except as noted, were obtained for Mach numbers $M = \frac{w}{a} \leq 0.3$. In practice, however, the values given for ζ , ζ_1 , and ζ_{fr} are correct even for higher subsonic velocities, roughly up to $M = 0.7-0.8$. In some cases the relationship between ζ and M is given.

11. Most of the data on the coefficients of local resistance were obtained for smooth channel walls; the influence of roughness on the local resistance has not been extensively studied. Therefore, unless otherwise specified, the walls of the stretches given here should be considered smooth. In practice the influence of the roughness (for Reynolds numbers $Re > 4 \times 10^4$) can be approximated by introducing into the coefficient ζ a factor of the order of 1.1 to 1.2 (higher at large roughness).

12. The shape of the cross section of fittings is indicated in the handbook when it has a bearing on the value of the resistance coefficient or when the values of this coefficient were obtained for specific cross sections. In all cases where the cross section is not indicated, or when no additional data on the resistance of elements of noncircular section are given, the value of the resistance coefficient for a polygonal or rectangular section of side ratio $0.6 \leq \frac{a_0}{b_0} \leq 1.7$ is to be considered equal to the value for a circular section.

13. The curves and tables of resistance coefficients given are based either on calculations or empirical data. In the latter case the values of ζ given by approximate formulas can differ somewhat from the data of the curves and tables. These formulas can be used for tentative calculations only.

14. Since the coefficients of fluid resistance are independent of the medium* flowing through a system, and are determined chiefly by the geometric characteristics of the given element or in some cases by the flow conditions (the Reynolds or Mach numbers), the data given in the handbook are suitable for calculating resistances of purely hydraulic lines as well as gas, air, and other lines and elements.

15. A complete calculation of the fluid resistance of the entire network can be performed by means of the proposed tables (cf. examples of hydraulic calculation, Table 1-10, etc.).

16. This handbook gives the values of the resistance coefficients for various shapes and parameters of pipe and channel elements. The minimum values of ζ can be easily established on the basis of the curves and tables of resistance given in the diagram, and on the basis of the recommendations given in the explanatory part of each section of the handbook.

17. The list of diagrams of resistance coefficients given at the beginning of each section indicates both the source and the method (experimental, theoretical, or tentative) by which these coefficients were obtained, so that it is possible to form some opinion on their reliability.

1-3. PROPERTIES OF FLUIDS

a. Specific gravity

1. The specific gravity γ is defined as the ratio of the weight of a given body to its volume (weight of a unit volume). In technical units it is usually measured in kg/m^3 .

* Where the medium is homogeneous.

2. The values of the specific gravity of water are given in Table 1-1. The specific gravity of some other liquids at different temperatures is given in Table 1-2.

The values of the specific gravity of some gases at standard conditions (0°C, 760 mm mercury, 100% dry) and of their weight relative to air (whose specific gravity is taken as unity) are given in Table 1-3.

TABLE 1-1
Specific gravity of water /1-21/

$t^{\circ}\text{C}$	0	10	20	30	40	50	60	70	80	90	100	120	140	160
$\gamma \text{ kg/m}^3$	999.87	999.73	998.23	995.67	992.24	988.07	983.24	977.81	971.83	965.34	958.38	943.4	926.4	907.5

3. For multicomponent gases (blast-furnace gas, coke gas) the specific gravity of the mixture is determined by the formula:

$$\gamma_m = \frac{\gamma_{x1}v_1 + \gamma_{x2}v_2 + \gamma_{x3}v_3 + \dots + \gamma_{xn}v_n}{100} (\text{kg/m}^3 \text{ dry}),$$

where $\gamma_{x1}, \gamma_{x2}, \dots, \gamma_{xn}$ are the specific gravities of the mixture components at 0°C and 760 mm mercury (cf. Table 1-3), kg/m^3 dry; v_1, v_2, \dots, v_n are the volume percentages of the mixtures components according to data obtained from a gas analysis.

b. Viscosity

1. Viscosity is a property of all fluids and manifests itself as internal friction during motion.

There is a difference between: 1) the absolute or dynamic viscosity η , defined as the ratio between the shearing stress and the velocity gradient:

$$\eta = \frac{\tau}{\frac{dy}{dx}}, \quad (1-2)$$

where τ is the shearing stress; $\frac{dy}{dx}$ is the velocity gradient in the direction of the normal y ;

2) the kinematic viscosity ν , defined as the ratio between the dynamic viscosity of the fluid and its density.

2. The dynamic viscosity is measured in the CGS system in poises (ps); the corresponding units of measurement of the shearing stress and the velocity gradient are dyn/cm^2 and $\text{cm/sec} \times \text{cm}$, respectively:

$$1 \text{ poise} = 1 \frac{\text{dyn} \times \text{sec}}{\text{cm}^2} = 1 \frac{\text{g}}{\text{cm} \times \text{sec}}.$$

The centipoise (cps), which is 10^2 times smaller, or the micropoise (μ ps), which is 10^6 times smaller, are more generally used:

$$\frac{\text{dyn} \times \text{sec}}{\text{cm}^2} = 1 \text{ ps} = 100 \text{ cps} = 10^6 \mu\text{ps}.$$

TABLE 1-2
Specific gravity of various liquids at a pressure of 1 atm /1-7, 1-8/

Type of liquid	°C	γ, kg/m ³
Ammonia	-34	684
Aniline	15	1,004
Acetone	15	790
Gasoline	15	680-740
Benzene	15	900
	60	882
Bromine	15	3,190
Butane (normal)	-0.5	601
Water	(see Table 1-1)	-
Sea water	15	1,020-1,030
Glycerine (anhydrous)	15	1,270
	18	1,260
	20	1,250
Coal tar	15	1,200
Dichloroethane.	15	1,175-1,200
Nitrogen dioxide	3.2	1,484
Sulfur dioxide	-10	1,472
Kerosene	15	790-820
Lignite oil	20	970
Wood oil	15	920
Castor oil	15	970
Coconut oil	15	930
Linseed oil (boiled)	15	940
Light machine oil	10	899
	20	898
	50	895
Medium machine oil	10	899
	20	898
	50	895
Mineral lubricating oil	15	890-960
Olive oil.	15	920
Paraffin oil	18	925
Turpentine oil	15	870
Cotton oil	15	930
Natural mineral oil	15	700-900
Liquefied ozone	-5	537
Carbon bisulfide	15	1,290
Sulfuric acid (87%)	15	1,800
Sulfuric acid (fuming)	15	1,890
Turpentine	18	870
Mercury	20	13,546
Methyl alcohol (methanol)	15	810
Ethyl alcohol (ethanol)	15-18	790
Tetrabromoethane	15	2,964
Chlorine	0	1,469
Methyl chloride	0	954
Ethyl chloride	0	919
Chloroform	15-18	1,480
Hydrogen	0	715
Ethyl ether	15-18	740

TABLE 1-3
Specific gravity of dry gas at 0°C and 1 atm and specific heats at 20°C of 1 kg dry gas /1-8/

Type of gas	Chemical formula	Specific gravity γ_1 , kg/m ³	Weight relative to air	c_p	c_v	$\frac{c_p}{c_v}$
Nitrogen	N ₂	1.2507	0.9672	0.250	0.178	1.40
Ammonia	NH ₃	0.7710	0.5962	0.530	0.400	1.29
Argon	A	1.7820	1.3781	0.127	0.077	1.66
Acetylene	C ₂ H ₂	1.1710	0.9056	0.402	0.323	1.25
Benzene	C ₆ H ₆	3.4840	2.6950	0.299	0.272	1.10
Butane	C ₄ H ₁₀	2.6730	2.0672	0.458	0.414	1.11
Isobutane	C ₄ H ₁₀	2.6680	2.0633	0.390	-	-
Air	-	1.2930	1.0000	0.241	0.172	1.40
Hydrogen	H ₂	0.0899	0.6450	3.410	2.420	1.41
Water vapor	H ₂ O	0.8040	0.6218	-	-	-
Helium	He	0.1785	0.1380	1.260	0.760	1.66
Nitrous oxide	N ₂ O	1.9780	1.5297	0.210	0.164	1.28
Oxygen	O ₂	1.4290	1.1051	0.218	0.156	1.40
Krypton	Kr	3.7080	2.8677	0.060	0.036	1.67
Xenon	Xe	5.8510	4.5252	0.038	0.023	1.70
Methane	CH ₄	0.7170	0.5545	0.531	0.405	1.31
Neon	Ne	0.9002	0.6962	0.248	0.148	1.68
Ozone	O ₃	2.2200	1.7169	-	-	1.29
Nitric oxide	NO	1.3400	1.0363	0.233	0.166	1.38
Carbon oxide	CO	1.2500	0.9667	0.250	0.180	1.40
Propane	C ₃ H ₈	2.0200	1.5622	0.445	0.394	1.13
Propylene	C ₃ H ₆	1.9140	1.4802	0.390	0.343	1.17
Hydrogen sulfide	H ₂ S	1.5390	1.1902	0.253	0.192	1.30
Carbon oxy sulfide	COS	2.7210	2.1044	-	-	-
Sulfur dioxide	SO ₂	2.9270	2.2637	0.151	0.120	1.25
Carbon dioxide	CO ₂	1.9760	1.5282	0.200	0.156	1.30
Chlorine	Cl ₂	3.2170	2.4880	0.115	0.085	1.36
Methyl chloride	CH ₃ Cl	2.3080	1.7772	0.177	0.139	1.28
Ethane	C ₂ H ₆	1.3570	1.0486	0.413	0.345	1.20
Ethylene	C ₂ H ₄	1.2610	0.9752	0.365	0.292	1.25

In industry the unit of measurement of the dynamic viscosity is $\frac{\text{kg}}{\text{m} \times \text{hour}}$ (where kg is the unit of mass), or $\frac{\text{kg} \times \text{sec}}{\text{m}^2}$ (where kg is the unit of force).

The unit of measurement of kinematic viscosity in the CGS system is the stoke (st), $\frac{\text{cm}^2}{\text{sec}}$, or the centistoke (cst), $\frac{\text{mm}^2}{\text{sec}}$, which is 10^2 smaller; its unit of measurement in industry is $\frac{\text{m}^2}{\text{sec}}$.

3. Conversion factors for the different systems are given in Table 1-4 for the dynamic viscosity η , and in Table 1-5 for the kinematic viscosity ν .

4. Examples of conversion of the viscosity units of measurement.

a. Given the value of the dynamic viscosity of a gas in poises: $\eta_{ps} = 180.9 \times 10^{-6} \frac{\text{g}}{\text{cm} \times \text{sec}}$.

It is required to convert it to the industrial system of units ($\eta_{I.S.}$ ($\text{kg} \times \text{sec}/\text{m}^2$)).

TABLE 1-4
Conversion factors for dynamic viscosity (η)

Unit of measurement given	Micropoise (μ ps)	Centipoise (cps)	Poise, $\frac{g}{cm \times sec}$ (ps)	$\frac{kg}{m \times sec}$	$\frac{kg}{m \times hour}$	$\frac{kg \times sec}{m^2}$	$\frac{lb}{ft \times sec}$	$\frac{lb}{ft \times hour}$
μ ps	1	10^{-4}	10^{-6}	10^{-7}	3.6×10^{-4}	1.02×10^{-3}	6.72×10^{-3}	2.42×10^{-4}
cps	10^4	1	10^{-2}	10^{-3}	3.6	1.02×10^{-4}	6.72×10^{-4}	2.42
Poise, $\frac{g}{cm \times sec}$ (ps)	10^6	10^2	1	10^{-1}	3.6×10^2	1.02×10^{-2}	6.72×10^{-2}	2.42×10^2
$\frac{kg}{m \times sec}$	10^7	10^3	10	1	3.6×10^3	1.02×10^{-1}	6.72×10^{-1}	2.42×10^3
$\frac{kg}{m \times hour}$	2.78×10^3	2.78×10^{-1}	2.78×10^{-3}	2.78×10^{-4}	1	2.84×10^{-5}	1.863×10^{-4}	6.72×10^{-1}
$\frac{kg \times sec}{m^2}$	9.81×10^7	9.81×10^3	9.81×10^2	9.81	3.53×10^4	1	6.592	2.374×10^4
$\frac{lb}{ft \times sec}$	1.488×10^7	1.488×10^3	1.488×10	1.488	4.13×10^3	1.52×10^{-1}	1	3.6×10^3
$\frac{lb}{ft \times hour}$	4.13×10^3	4.13×10^{-1}	4.13×10^{-3}	4.13×10^{-4}	1.488	4.21×10^{-5}	2.77×10^{-4}	1

According to Table 1-4, the conversion factor is equal to 1.02×10^{-2} . Then

$$\eta_{I.S.} = 1.02 \cdot 10^{-2} \eta_{ps} = 1.02 \cdot 10^{-2} \times 180.9 \cdot 10^{-6} \approx 1.85 \cdot 10^{-6} \text{ kg} \times \text{sec}/\text{m}^2.$$

b. Given the value of the dynamic viscosity of water in the foot-pound-second system of units: $\eta_{fps} = 6.92 \times 10^{-6} \text{ lb}/\text{ft} \times \text{sec}$. It is required to convert it to the CGS system ($\text{kg} \times \text{sec}/\text{m}^2$).

According to Table 1-4, the conversion factor is equal to 1.52×10^{-1} . Then

$$\eta_{I.S.} = 1.52 \cdot 10^{-1} \cdot 6.92 \cdot 10^{-6} = 1.05 \cdot 10^{-6} \text{ kg} \times \text{sec}/\text{m}^2.$$

c. Given the value of the kinematic viscosity of air in centistokes $\nu_{cst} = 15.0$. It is required to convert it to industrial units ($\sim I.S.$, m^2/sec).

According to Table 1-5, the conversion factor is equal to 10^{-6} . Then

$$\nu_{I.S.} = 10^{-6} \nu_{cst} = 15.0 \cdot 10^{-6} \text{ m}^2/\text{sec}.$$

d. Given the value of the kinematic viscosity of water in the foot-pound-hour system of units (ft^2/hour):

$$\nu_{fh} = 5.78 \cdot 10^{-1}.$$

It is required to convert it to CGS units (stokes).

According to Table 1-5, the conversion factor is equal to 2.60×10^{-1} . Then

$$\nu_{st} = 2.60 \cdot 10^{-1} \cdot \nu_{fh} = 2.60 \cdot 10^{-1} \cdot 5.78 \cdot 10^{-1} = 1.50 \cdot 10^{-1} \text{ cm}.$$

5. When the kinematic viscosity is determined as the ratio: dynamic viscosity/specific gravity, care should be taken to use consistent units of measurement in numerator and denominator. In order to obtain the value of the kinematic viscosity ν in stokes (st), the dynamic viscosity η must be in ps and the specific gravity in g/cm^3 (the result is cm^2/sec , i.e., st); in order to obtain ν in m^2/sec , η is taken in $\text{kg} \times \text{sec}/\text{m}^2$ and is divided by the density

$\rho = \frac{\gamma}{g}$ in $\frac{\text{kg} \times \text{sec}^2}{\text{m}^4}$; in order to obtain ν in m^2/hour , γ is taken in $\text{kg}/\text{m} \times \text{hour}$ and is divided by the specific gravity γ in $\frac{\text{kg}}{\text{m}^3}$.

6. The dynamic and kinematic viscosities depend on the characteristics of the medium. The dynamic viscosity of fluids is a function of the temperature only and, for perfect gases, is independent of the pressure. The viscosity of vapors and gases increases with the increase of the temperature, while that of liquids decreases. The kinematic viscosity of liquids and gases is a function of both temperature and pressure.

TABLE 1-5
Conversion factors for kinematic viscosity (ν)

Unit of measurement given	Centistoke, mm^2/sec (cst)	Stoke, cm^2/sec (st)	$\frac{\text{m}^2}{\text{sec}}$	$\frac{\text{m}^2}{\text{hour}}$	$\frac{\text{ft}^2}{\text{sec}}$	$\frac{\text{ft}^2}{\text{hour}}$
Centistoke, mm^2/sec (cst)	1	10^{-2}	10^{-6}	3.60×10^{-3}	1.07×10^{-5}	3.85×10^{-2}
Stoke, cm^2/sec (st)	10^2	1	10^{-4}	3.60×10^{-1}	1.07×10^{-3}	3.85
$\frac{\text{m}^2}{\text{sec}}$	10^6	10^4	1	3.60×10^3	1.07×10	3.85×10^4
$\frac{\text{m}^2}{\text{hour}}$	2.78×10^2	2.78	2.78×10^{-4}	1	2.98×10^{-3}	1.07×10
$\frac{\text{ft}^2}{\text{sec}}$	9.35×10^4	9.35×10^2	9.35×10^{-2}	36×10^2	1	3.60×10^3
$\frac{\text{ft}^2}{\text{hour}}$	2.60×10	2.60×10^{-1}	2.60×10^{-5}	9.35×10^{-2}	2.78×10^{-4}	1

7. The relationship between the viscosity of gases and the temperature can be expressed approximately by Sutherland's formula:

$$\eta = \eta_0 \frac{273 + C}{T + C} \left(\frac{T}{273} \right)^{3/2}, \quad (1-3)$$

where η_0 is the dynamic viscosity of the gas at 0°C ; T is the absolute temperature, $^\circ\text{K}$; C is a constant depending on the gas.

The values of the dynamic viscosity η in micropoises for various gases as a function of the temperature, and the values of the constant C and the maximum temperature at which the value of this constant has been corroborated experimentally, are given in Table 1-6.

The values of the kinematic viscosity ν in cst for the same gases as a function of the temperature at a pressure of 1 atm are given in Table 1-7.

The values of ν for air in m^2/sec are also given in Figure 1-1.

8. The kinematic viscosity of a gas mixture can be determined by Mann's approximate formula:

$$\nu_m = \frac{100}{\frac{v_1}{v_1} + \frac{v_2}{v_2} + \dots + \frac{v_n}{v_n}}, \quad (1-4)$$

where v_1, v_2, \dots, v_n are the dynamic viscosities of the components; v_1, v_2, \dots, v_n are the percentage weights of the mixture components.

TABLE 1-6
Dynamic viscosity of gases η , μ ps, at a pressure of 1 atm as a function of the temperature, and the values of the constant C in the Sutherland formula
/1-7, 1-8, 1-19-21/

Gas	Formula	Temperature, °C														Temperature range, °C
		-20	0	20	40	60	80	100	150	200	300	400	600	800	C	
Nitrogen	N ₂	157.5	166.0	174.8	183.5	192.5	200.0	208.2	229.0	246.0	281.0	311.0	366.0	413.0	104	25-280
Ammonia	NH ₃	86.0	93.0	100.5	107.8	114.5	121.5	128.0	146.0	—	—	—	—	—	503	20-300
Argon	A	—	212.0	222.0	—	—	—	271.0	—	321.0	367.0	410.0	487.0	554.0	142	20-827
Acetylene	C ₂ H ₂	90.2	96.0	102.1	108.2	114.5	120.2	126.0	—	—	—	—	—	—	215	—
Benzene	C ₆ H ₆	62.0	68.0	73.5	79.0	84.0	89.5	95.0	108.0	121.0	147.0	—	—	—	448	130-313
Butane	C ₄ H ₁₀	—	69.0	74.0	—	—	—	95.0	—	—	—	—	—	—	358	—
Hydrogen	H ₂	80.4	84.0	88.0	91.8	95.9	99.6	103.0	113.0	121.0	139.0	154.0	183.0	210.0	71.0	20-100
Water vapor	H ₂ O	82.0	89.3	96.7	104.0	111.3	118.7	126.0	—	160.4	200.0	239.0	314.5	386.5	961	20-406
Air	—	162.0	171.2	180.9	190.4	199.8	208.9	219.0	—	260.2	297.2	330.1	390.6	443.0	111	16-825
Helium	He	175.0	186.0	195.5	204.0	213.5	220.5	229.0	—	270.0	307.0	342.0	407.0	465.0	0	21-100
Sulfur dioxide	SO ₂	—	116.0	126.0	—	—	—	163.0	—	207.0	246.0	—	—	—	306	300-825
Nitrous oxide	N ₂ O	—	137.0	146.0	—	—	—	183.0	—	225.0	265.0	—	—	—	260	25-280
Oxygen	O ₂	181.5	192.0	202.5	213.0	223.5	234.0	244.0	—	290.0	331.0	369.0	435.0	493.0	125	20-280
Krypton	Kr	—	233.0	246.0	—	—	—	306.0	—	—	—	—	—	—	188	—
Xenon	Xe	—	211.0	226.0	—	—	—	287.0	—	—	—	—	—	—	252	—
Methane	CH ₄	95.5	102.0	108.0	115.0	121.4	127.0	133.0	147.0	161.0	186.0	—	—	—	164	20-250
Nitric oxide	NO	—	179.0	188.0	—	—	—	227.0	—	268.0	—	—	—	—	128	20-250
Carbon monoxide	CO	159.5	168.0	176.8	185.5	191.5	202.4	210.2	229.0	247.0	279.0	—	—	—	100	До 130
Pentane (p)	C ₅ H ₁₂	—	62.0	—	—	—	—	—	100.0	103.0	—	—	—	—	383	—
Propane	C ₃ H ₈	70.0	75.0	80.0	85.4	90.5	95.8	100.1	113.0	125.0	144.0	—	—	—	278	20-250
Propylene	C ₃ H ₆	—	78.0	83.5	—	—	—	107.0	141.0	—	—	—	—	—	487	—
Hydrogen sulfide	H ₂ S	—	116.0	124.0	—	—	—	159.0	—	—	—	—	—	—	331	—
Carbon dioxide	CO ₂	128.0	138.0	147.0	157.0	167.0	175.5	184.5	—	226.0	264.0	299.0	362.0	413.5	254	—
Chlorine	Cl	114.5	123.0	132.0	141.0	150.0	159.0	168.0	189.0	210.0	250.0	—	—	—	350	100-250
Methyl chloride	CH ₃ Cl	—	98.0	106.0	—	—	—	136.0	—	175.0	—	—	—	—	454	—
Ethyl chloride	C ₂ H ₅ Cl	—	94.0	105.0	—	—	—	—	143.0	—	—	—	—	—	411	—
Hydrogen cyanide	HCN	—	—	74.0	—	—	—	—	—	—	—	—	—	—	901	—
Ethane	C ₂ H ₆	—	86.0	92.0	—	—	—	115.0	128.0	142.0	—	—	—	—	252	20-250
Ethylene	C ₂ H ₄	88.5	94.5	101.0	107.0	112.0	118.5	124.0	140.0	154.0	—	—	—	—	225	20-250

TABLE 1-7

Kinematic viscosity ν , cst, at a pressure of 1 atm as a function of temperature /1-7, 1-8, 1-19-1-21/

Gas	Formula	Temperature, °C												
		-20	0	20	40	60	80	100	150	200	300	400	600	800
Nitrogen	N ₂	11.67	13.30	15.00	16.85	18.80	20.65	22.30	28.30	34.10	47.20	61.40	93.50	130.00
Ammonia	NH ₃	6.81	12.00	14.00	16.00	18.10	20.35	22.70	29.30	36.00	—	—	—	—
Argon	A	—	11.90	13.30	—	—	—	20.70	—	31.20	43.30	56.50	87.50	123.00
Acetylene	C ₂ H ₂	4.73	8.20	9.35	10.60	11.94	13.25	14.70	—	—	—	—	—	—
Benzene	C ₆ H ₆	1.66	11.95	2.26	2.60	2.94	3.33	3.73	4.80	6.02	8.85	—	—	—
Butane	C ₄ H ₁₀	—	25.80	29.70	—	—	—	48.50	—	—	—	—	—	—
Hydrogen	H ₂	84.00	93.50	105.00	117.30	130.00	143.00	156.60	195.00	233.00	324.00	423.00	651.00	918.00
Water vapor	H ₂ O	9.50	11.12	12.90	14.84	16.90	18.66	21.50	—	—	—	—	—	—
Air	—	11.66	13.20	15.00	16.98	18.85	20.89	23.00	30	34.90	48.20	63.20	96.50	134.00
Helium	He	9.12	10.40	11.74	13.12	14.55	15.97	17.50	—	26.20	36.10	47.30	72.80	102.50
Sulfur dioxide	SO ₂	—	4.00	4.60	—	—	—	7.60	—	12.20	17.60	—	—	—
Nitrous oxide	N ₂ O	—	6.82	7.93	—	—	—	12.70	—	19.70	28.20	—	—	—
Oxygen	O ₂	11.04	13.40	15.36	17.13	19.05	21.16	23.40	—	35.20	48.70	63.80	97.50	135.70
Krypton	Kr	—	6.26	7.13	—	—	—	13.70	—	—	—	—	—	—
Xenon	Xe	—	3.59	4.15	—	—	—	6.70	—	—	—	—	—	—
Methane	CH ₄	12.57	14.20	16.50	18.44	20.07	22.90	25.40	31.8	39.00	54.50	—	—	—
Nitric oxide	NO	—	13.30	15.10	—	—	—	23.20	—	30.50	—	—	—	—
Carbon monoxide	CO	11.86	13.50	15.16	17.00	18.96	21.00	22.70	28.4	34.30	46.85	—	—	—
Propane	C ₃ H ₈	3.04	3.70	4.26	4.90	5.52	6.18	6.76	8.70	10.84	15.10	—	—	—
Propylene	C ₃ H ₆	—	4.08	4.70	—	—	—	7.70	11.4	—	—	—	—	—
Hydrogen sulfide	H ₂ S	—	7.62	8.70	—	—	—	14.10	—	19.80	28.00	37.30	65.20	82.00
Carbon dioxide	CO ₂	5.62	7.00	8.02	9.05	10.30	12.10	12.80	—	—	—	—	—	—
Chlorine	Cl ₂	3.09	3.80	4.36	5.02	5.66	6.36	7.15	9.10	11.50	16.25	—	—	—
Methyl chloride	CH ₃ Cl	—	4.28	4.90	—	—	—	8.05	—	13.10	—	—	—	—
Ethane	C ₂ H ₆	—	6.35	7.28	—	—	—	11.60	14.70	18.10	—	—	—	—
Ethylene	C ₂ H ₄	6.80	7.50	8.66	9.73	10.85	12.15	13.40	17.30	21.20	—	—	—	—

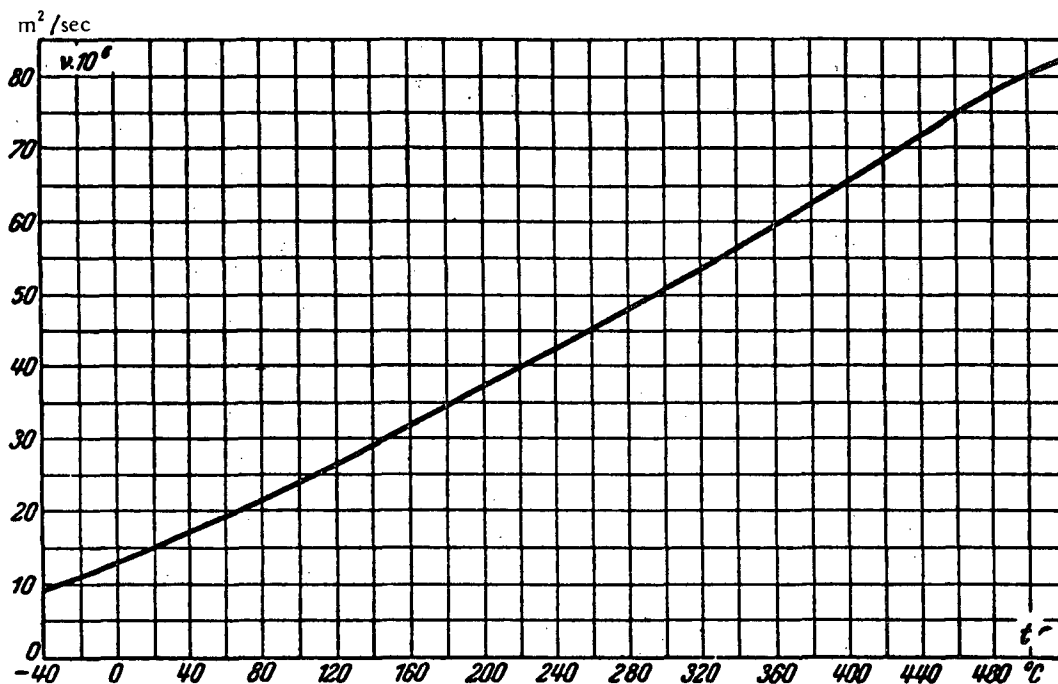


FIGURE 1-1. Kinematic viscosity of air as a function of its temperature at $p = 1.0$ atm.

The dynamic viscosity of the mixture can be determined by the approximate formula

$$\eta = \frac{100}{\frac{G_1}{\eta_1} + \frac{G_2}{\eta_2} + \dots + \frac{G_n}{\eta_n}}, \quad (1-5)$$

where $\eta_1, \eta_2, \dots, \eta_n$ are the dynamic viscosities of the components; G_1, G_2, \dots, G_n are the percentage weights of the mixture components.

9. The dependence of the dynamic $\left(\frac{\text{kg} \times \text{sec}}{\text{m}^2}\right)$ and kinematic (m^2/sec) viscosities of water on the temperature and pressure is given in Table 1-8. The dependence of $v \left(\frac{\text{m}^2}{\text{sec}}\right)$ of water on the temperature at 1 atm is given in Figure 1-2.

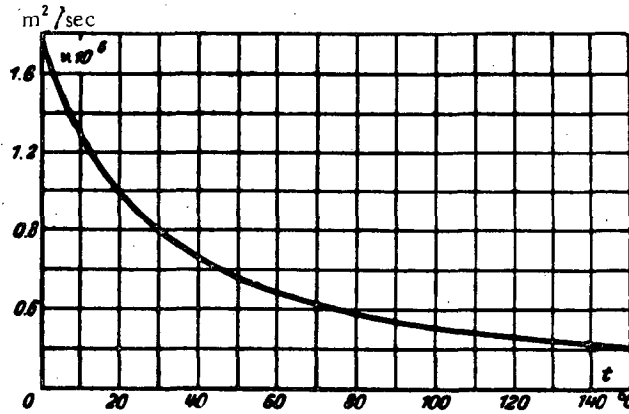


FIGURE 1-2. Kinematic viscosity of water as a function of its temperature.

TABLE 1-8
Dynamic and kinematic viscosities of water as functions of temperature
and pressure /1-21/

<i>t</i> , °C	0	10	20	30	40	50	60	70	80	90	100	110	120	130
<i>p</i> , kg/cm ²	1.0	1.0	1.0	1.0	1.0	1.0	1.0	1.0	1.0	1.0	1.03	1.46	2.02	2.75
$\eta \times 10^6$, $\frac{\text{kg} \times \text{sec}}{\text{m}^2}$	182.3	133.1	102.4	81.7	66.6	56.0	47.9	41.4	36.2	32.1	28.8	26.4	24.2	22.5
$\nu \times 10^6$, $\frac{\text{m}^2}{\text{sec}}$	1.792	1.306	1.006	0.805	0.659	0.556	0.478	0.415	0.365	0.326	0.295	0.272	0.252	0.233
<i>t</i> , °C	140	150	160	170	180	190	200	210	220	230	240	250	260	270
<i>p</i> , kg/cm ²	3.68	4.85	6.30	8.08	10.23	12.80	15.86	19.46	23.46	28.53	34.14	40.56	47.87	56.14
$\eta \times 10^6$, $\frac{\text{kg} \times \text{sec}}{\text{m}^2}$	20.5	19.0	17.7	16.6	15.6	14.7	13.9	13.3	12.7	12.2	11.7	11.2	10.8	10.4
$\nu \times 10^6$, $\frac{\text{m}^2}{\text{sec}}$	0.217	0.203	0.191	0.181	0.173	0.165	0.158	0.153	0.148	0.145	0.141	0.137	0.135	0.133
<i>t</i> , °C	280	290	300	310	320	330	340	350	360	370				
<i>p</i> , kg/cm ²	65.46	75.92	87.61	100.64	115.12	131.18	149.96	168.63	180.42	214.68				
$\eta \times 10^6$, $\frac{\text{kg} \times \text{sec}}{\text{m}^2}$	10.0	9.60	9.30	9.00	8.70	8.30	7.90	7.40	6.80	5.80				
$\nu \times 10^6$, $\frac{\text{m}^2}{\text{sec}}$	0.131	0.129	0.128	0.128	0.128	0.127	0.127	0.126	0.126	0.126				

1-4. EQUILIBRIUM OF FLUIDS

1. A fluid is in equilibrium if the resultant of all the forces acting on any part of it is equal to zero.

2. The equation of equilibrium of a fluid in one and the same volume* at constant specific gravity can be written in the form:

$$z_1 + \frac{p_1}{\gamma} = z_2 + \frac{p_2}{\gamma}, \quad (1-6)$$

where z_1 and z_2 are the coordinates of two fluid particles in the given volume relative to the reference plane (Figure 1-3); p_1 and p_2 are the absolute static pressures at the levels of these particles, kg/m^2 ; γ is the specific gravity of the fluid, kg/m^3 .

* The expression "one and the same volume" is to be understood as meaning a volume such that any two points of it can be connected by a line contained inside the volume. The volumes of liquids filling communicating vessels are one and the same volume in this sense.

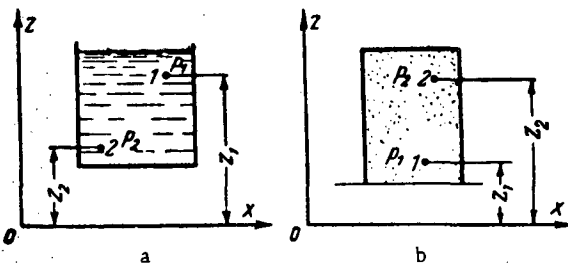


FIGURE 1-3. Determination of the pressure at an arbitrary point of a fluid volume from the pressure at a given point: a) $\gamma_f > \gamma_a$; b) $\gamma_f < \gamma_a$. [γ_a = specific gravity of air.]

3. The pressure at an arbitrary point of the fluid volume can be determined if the pressure at some other point of the same volume is given and the difference in depth $h = z_s - z_i$ of one point relative to the other one is known (Figure 1-3):

$$\left. \begin{aligned} p_s &= p_i - \gamma(z_s - z_i) = p_i - \gamma h; \\ p_i &= p_s + \gamma(z_s - z_i) = p_s + \gamma h. \end{aligned} \right\} \quad (1-7)$$

It follows that the pressure on the wall of a vessel filled with a stationary burning gas ($\gamma < \gamma_a$) at a level $h = z_g - z_a$ above the surface of separation of the gas and the surrounding air (Figure 1-4) is lower on both sides of the wall (p_g = the gas pressure, and p_h = the air pressure at level h) than the pressure p_a at the surface of separation:

$$p_g = p_a - \gamma_g h \quad (1-8)$$

and

$$p_h = p_a - \gamma_a h, \quad (1-9)$$

where γ_g = specific gravity of the gas (average value over the height h), $\frac{\text{kg}}{\text{m}^3}$; γ_a = specific gravity of surrounding air (averaged over height h), $\frac{\text{kg}}{\text{m}^3}$.

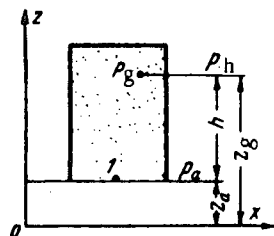


FIGURE 1-4. Determination of the excess pressure of a burning gas in a vessel at an arbitrary height, over the atmospheric pressure at the same level.

4. The excess pressure H_g of a stationary burning gas in a vessel at level $h = z_g - z_a$, over the atmospheric pressure of air at the same height h will be, on the strength of (1-8) and (1-9):

$$H_g = p_g - p_a = h(\gamma_a - \gamma_g). \quad (1-10)$$

1-5. MOTION OF FLUIDS

a. Discharge, and mean flow velocity

1. The amount of fluid flowing across a given cross section of a pipe per unit of time is called the fluid discharge. It is measured in industrial units either as weight, rate of flow (G kg/sec), or as volume rate of flow (Q m³/sec).

2. At any flow-velocity distribution over the section, the volume discharge is represented in a general form by the formula:

$$Q = \int dQ = \int w dF. \quad (1-11)$$

where w is velocity at the given point of the conduit section, m/sec; F is the area of the conduit cross section, m².

The weight discharge is connected with the volume discharge by the formula:

$$G = \gamma Q. \quad (1-12)$$

3. The distribution of the velocities over the conduit section is practically never uniform. The analysis of problems is simplified by the introduction of the mean flow velocity:

$$w_m = \frac{\int w dF}{F} = \frac{Q}{F}, \quad (1-13)$$

whence

$$Q = w_m F. \quad (1-14)$$

4. The volume discharge (and also the flow velocity) of a gas is a function of its temperature, pressure, and humidity*.

Designate the volume discharge at normal conditions (0°C, 760 mm mercury, dry gas) by Q_n (m³/sec); and the corresponding mean velocity by w_n (m/sec); the corresponding magnitudes at operating conditions will be:

$$Q_{op} = Q_n \frac{T}{273} \cdot \frac{p_n}{p_{op}} \left(1 + \frac{m}{0.804}\right) [\text{m}^3/\text{sec}], \quad (1-15)$$

* We consider the case of a perfect gas, satisfying the equation

$$pv = RT,$$

and for which the internal energy is a function of the temperature only; here v = specific volume, R = gas constant.

and

$$w_{op} = w_n \frac{T}{273} \cdot \frac{p_n}{p_{op}} \left(1 + \frac{m}{0.804}\right) [\text{m/sec}], \quad (1-16)$$

where T is the absolute temperature of the gas, °K; m is the content of water vapor in the gas, kg/m³ dry gas (at normal conditions $m = 0.804$); p_{op} is the absolute pressure of the gas considered in the given section F , kg/m²; p_n is the absolute pressure of the gas at normal conditions ($p_n = 10,330 \text{ kg/m}^2$).

The volume discharge and the flow velocity at operating conditions for a dry gas at atmospheric pressure ($p = p_n$) will be:

$$Q_{op} = Q_n \frac{T}{273} \left[\frac{\text{m}^3}{\text{sec}} \right] \quad (1-17)$$

and

$$w_{op} = w_n \frac{T}{273} \left[\frac{\text{m}}{\text{sec}} \right]. \quad (1-18)$$

5. The specific gravity of a gas at operating conditions is equal to

$$\gamma_{op} = (\gamma_n + m) \frac{273}{T} \cdot \frac{1}{1 + \frac{m}{0.804}} \cdot \frac{p_{op}}{p_n} \left[\frac{\text{kg}}{\text{m}^3} \right], \quad (1-19)$$

where γ_n is the specific gravity of the dry gas at normal conditions, kg/m³.

In the case of a dry gas at atmospheric pressure:

$$\gamma_{op} = \gamma_n \frac{273}{T} = \frac{\gamma_n}{1 + \frac{t}{273}} \left[\frac{\text{kg}}{\text{m}^3} \right]. \quad (1-20)$$

b. Equation of continuity of a stream

1. The equation of continuity is a result of the application of the law of mass conservation to a moving medium (fluid).

The equation of continuity can be represented in the following general form, at any distribution of the velocities, for two conduit sections I-I and II-II (Figure 1-5):

$$\int_{F_1} \gamma_1 w dF = \int_{F_2} \gamma_2 w dF. \quad (1-21)$$

In the case of an incompressible homogeneous medium the specific gravity over the section is always constant, and therefore:

$$\gamma_1 \int w dF = \gamma_2 \int w dF, \quad (1-21')$$

where F_1 and F_2 are the areas of sections I-I and II-II, respectively, m²; w is the flow velocity at the given point, m/sec; γ_1 and γ_2 are the specific gravities of the moving medium at sections I-I and II, respectively, kg/m³.

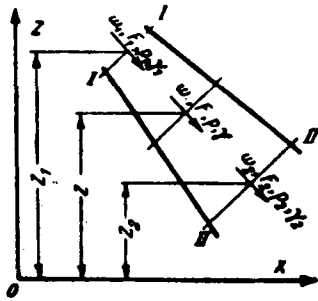


FIGURE 1-5. Application of the equation of continuity, the energy equation and the Bernoulli equation to two conduit sections.

2. On the strength of expressions (1-12) to (1-14), the equation of continuity (equation of discharge) for a uniform compressible flow and for an arbitrary incompressible flow can be written in the form:

$$\left. \begin{aligned} \gamma_1 w_1 F_1 &= \gamma_2 w_2 F_2 = \gamma w F, \\ \gamma_1 Q_1 &= \gamma_2 Q_2 = \gamma Q. \end{aligned} \right\} \quad (1-22)$$

where w_1 and w_2 are the mean velocities over sections I-I and II-II, respectively, m/sec.

If the specific gravity of the moving medium does not vary along the conduit, i.e., $\gamma_1 = \gamma_2 = \gamma$, the equation of continuity (discharge) reduces to

$$w_1 F_1 = w_2 F_2 = w F \quad (1-23)$$

or

$$Q_1 = Q_2 = Q = \frac{G}{\gamma}.$$

c. Bernoulli equation. Head loss

1. The law of energy conservation, when applied to a medium moving through a conduit, states that the energy of the flow per unit time across section I-I (Figure 1-5) is equal to the energy of the flow per unit time across section II-II plus the heat and mechanical energy dissipated along the stretch between these sections.

2. In the general case of flow of an inelastic liquid or a gas with nonuniform velocity and pressure distributions over the section, the corresponding energy equation will be:

$$\int_{F_1} (p + \frac{\gamma w^2}{2g} + z\gamma + \frac{U}{A} \gamma) w dF = \int_{F_2} (p + \frac{\gamma w^2}{2g} + z\gamma + \frac{U}{A} \gamma) w dF + \Delta E_{tot}, \quad (1-24)$$

where z is the geometric height of the centroid of the corresponding section, m; p is the absolute hydrostatic pressure at the point of the corresponding section, kg/m^2 ; A is the mechanical equivalent of heat $= \frac{1}{427} \frac{\text{kcal}}{\text{kg} \times \text{m}}$; $\int z\gamma w dF$ is the gravitational potential

energy of the flow per unit time across the corresponding section, $\text{kg} \times \text{m/sec}$;

$\int p w dF$ is the potential pressure energy of the flow per unit time across the corresponding section, $\text{kg} \times \text{m/sec}$; $\int_F \frac{\gamma w^2}{2g} w dF$ is the kinetic energy of the flow per unit time across the corresponding section, $\text{kg} \times \text{m/sec}$; $U = c_v T$ is the specific internal energy of the gas, kcal/kg ; $\int_F \frac{U}{A} \gamma w dF$ is the internal thermal energy of the flow per unit time across the corresponding section, $\text{kg} \times \text{m/sec}$; ΔE is the energy (thermal and mechanical) lost in the stretch between section I-I and II-II, $\text{kg} \times \text{m/sec}$; c_v is the mean specific heat of the gas at constant volume, $\text{kcal/kg} \times \text{deg}$.

3. The static pressure p is, in most cases, constant over the section even with a considerably nonuniform velocity distribution. The variation of specific gravity over the section, due to a variation of velocities, can be neglected in practice. Equation (1-24) can therefore be replaced by the equation:

$$(\gamma_1 z_1 + p_1) w_1 F_1 + \int_{F_1} \frac{\gamma_1 w_1^2}{2g} dF + \frac{U_1}{A} \gamma_1 w_1 F_1 = (\gamma_2 z_2 + p_2) w_2 F_2 + \int_{F_2} \frac{\gamma_2 w_2^2}{2g} dF + \frac{U_2}{A} \gamma_2 w_2 F_2 + \Delta E$$

Substituting

$$\left. \begin{aligned} N_1 &= \frac{1}{F_1} \int_{F_1} \left(\frac{w}{w_1} \right)^3 dF \\ N_2 &= \frac{1}{F_2} \int_{F_2} \left(\frac{w}{w_2} \right)^3 dF \end{aligned} \right\} \quad (1-25)$$

the last equation can now be written

$$(\gamma_1 z_1 + p_1) w_1 F_1 + N_1 \frac{\gamma_1 w_1^2}{2g} w_1 F_1 + \frac{U_1}{A} \gamma_1 w_1 F_1 = (\gamma_2 z_2 + p_2) w_2 F_2 + N_2 \frac{\gamma_2 w_2^2}{2g} w_2 F_2 + \frac{U_2}{A} \gamma_2 w_2 F_2 + \Delta E_{\text{tot}},$$

or

$$\left(\gamma_1 z_1 + p_1 + N_1 \frac{\gamma_1 w_1^2}{2g} + \frac{U_1}{A} \right) Q = \left(\gamma_2 z_2 + p_2 + N_2 \frac{\gamma_2 w_2^2}{2g} + \frac{U_2}{A} \right) Q + \Delta E \quad (1-26)$$

where N_1 and N_2 are the kinetic-energy coefficients for sections I-I and II-II, respectively; they characterize the degrees of nonuniformity of both kinetic-energy distribution and velocity distribution.

4. If the flow energy per second is divided by the weight or volume discharge, we obtain the generalized Bernoulli equation corresponding to a real fluid and allowing for specific losses in the stretch considered:

$$\begin{aligned} z_1 + \frac{p_1}{\gamma_1} + N_1 \frac{w_1^2}{2g} + \frac{U_1}{A} &= z_2 + \frac{p_2}{\gamma_2} + \\ &+ N_2 \frac{w_2^2}{2g} + \frac{U_2}{A} + \frac{\Delta E}{G} \end{aligned} \quad (1-27)$$

or

$$\gamma_1 z_1 + p_1 + N_1 \frac{\gamma_1 w_1^2}{2g} + \frac{\gamma_1 U_1}{A} = \gamma_2 z_2 + p_2 + N_2 \frac{\gamma_2 w_2^2}{2g} + \frac{\gamma_2 U_2}{A} + \frac{\Delta E}{Q}. \quad (1-28)$$

5. In the case of an incompressible liquid, or a gas at low flow velocities (up to $w = 150$ to 200 m/sec), and low pressure drop (up to 1000 kg/m²), $U_1 = U_2$ and $\gamma_1 = \gamma_2 = \gamma$; the Bernoulli equation then reduces to:

$$z_1 + \frac{p_1}{\gamma} + N_1 \frac{w_1^2}{2g} = z_2 + \frac{p_2}{\gamma} + N_2 \frac{w_2^2}{2g} + H \quad (1-29)$$

or

$$\gamma z_1 + p_1 + N_1 \frac{\gamma w_1^2}{2g} = \gamma z_2 + p_2 + N_2 \frac{\gamma w_2^2}{2g} + \Delta H. \quad (1-30)$$

6. All terms in (1-29) have the dimension of length, and they are accordingly all called "heads":

z_1 and z_2 = potential head, m;

$\frac{p_1}{\gamma}$, $\frac{p_2}{\gamma}$ = pressure head, m

$N_1 \frac{w_1^2}{2g}$, $N_2 \frac{w_2^2}{2g}$ = velocity head, m;

H = total head loss, m.

7. All the terms in (1-30) have the dimension of pressure (kg/m² or mm water column) and are called:

γz_1 , γz_2 = specific energy of position, kg/m²;

p_1 , p_2 = specific pressure energy or static pressure, kg/m²;

$N_1 \frac{\gamma w_1^2}{2g}$, $N_2 \frac{\gamma w_2^2}{2g}$ = specific kinetic energy or dynamic pressure, kg/m²;

$\Delta H = \frac{\Delta E}{Q}$ = lost pressure, spent on overcoming the total resistance of the stretch between sections I-I and II-II, kg/m².

8. In the particular case of a uniform velocity field $N_1 = N_2$ [=1] Bernoulli's equation reduces to:

$$z_1 + \frac{p_1}{\gamma} + \frac{w_1^2}{2g} = z_2 + \frac{p_2}{\gamma} + \frac{w_2^2}{2g} + H \quad (1-31)$$

or

$$\gamma z_1 + p_1 + \frac{\gamma w_1^2}{2g} = \gamma z_2 + p_2 + \frac{\gamma w_2^2}{2g} + \Delta H. \quad (1-32)$$

9. The addition and subtraction of p_{z_1} to the left-hand side of (1-30), and of p_{z_2} to its right-hand side, gives:

$$\gamma z_1 + p_1 + p_{z_1} - p_{z_1} + N_1 \frac{\gamma w_1^2}{2g} = \gamma z_2 + p_2 + p_{z_2} - p_{z_2} + N_2 \frac{\gamma w_2^2}{2g} + \Delta H, \quad (1-33)$$

where p_{s_1} is the atmospheric pressure at height z_1 , kg/m^2 ; p_{s_2} is the atmospheric pressure at height z_2 , kg/m^2 .

On the basis of (1-9)

$$\left. \begin{aligned} p_{s_1} &= p_a - \gamma_a z_1 \\ p_{s_2} &= p_a - \gamma_a z_2 \end{aligned} \right\} \quad (1-34)$$

where p_a is the atmospheric pressure in the reference plane (Figure 1-6), kg/m^2 ; γ_a is the mean specific gravity of atmospheric air over height z ; in the given case the specific gravity is considered as equal at the two heights z_1 and z_2 , kg/m^3 .

Equation (1-33) can therefore be replaced by:

$$(\gamma - \gamma_a) z_1 + (p_1 - p_{s_1}) + N_1 \frac{\gamma w_1^2}{2g} = (\gamma - \gamma_a) z_2 + (p_2 - p_{s_2}) + N_2 \frac{\gamma w_2^2}{2g} + \Delta H \quad (1-35)$$

10. The resistance of the stretch between sections I-I and II-II is equal, on the basis of (1-35), to:

$$\Delta H = (p_1 - p_{s_1}) - (p_2 - p_{s_2}) + N_1 \frac{\gamma w_1^2}{2g} - N_2 \frac{\gamma w_2^2}{2g} + (\gamma_a - \gamma)(z_2 - z_1) \quad (1-36)$$

or

$$\Delta H = (H_{1st} - H_{2st}) + (H_{1d} - H_{2d}) + H_L = H_{1tot} - H_{2tot} + H_L, \quad (1-37)$$

where $H_d = N \frac{\gamma w^2}{2g}$ is the dynamic pressure at the given stream section (always a positive magnitude), kg/m^2 ; $H_{st} = p - p_s$ is the excess hydrostatic pressure, i.e., the difference between the absolute pressure p in the stream section at height z and the atmospheric pressure p_s at the same height, kg/m^2 ; this pressure can be either positive or negative; $H_{tot} = H_d + H_{st}$ is the total pressure in the given stream section, kg/m^2 ; H_L is the excess potential head, kg/m^2 :

$$H_L = (z_2 - z_1)(\gamma_a - \gamma) \quad (1-38)$$

11. The excess potential head is caused by the tendency of the fluid to go up or down, depending on the medium in which it is located. This head can be positive or negative depending on whether it promotes or hinders the flow.

If at $\gamma > \gamma_a$ the flow is directed upward (Figure 1-6a) and at $\gamma < \gamma_a$ downward (Figure 1-6b), the excess head $H_L = (z_2 - z_1)(\gamma_a - \gamma)$ is negative and hinders the flow. If the flow is directed downward at $\gamma > \gamma_a$ (Figure 1-6c) and upward at $\gamma < \gamma_a$ (Figure 1-6d), the excess head $H_L = (z_2 - z_1)(\gamma_a - \gamma)$ is positive and contributes to the flow.

12. When the specific gravities of a flowing medium γ and the surrounding atmosphere are equal, or when the conduit is horizontal, the geometric head equals zero, and equation (1-37) simplifies to

$$\Delta H_{tot} = H_{1tot} - H_{2tot} [\text{kg/m}^2]. \quad (1-39)$$

13. In those cases when both the static pressure and the velocity are nonuniform over the section and this nonuniformity cannot be neglected, the resistance of the stretch must

be determined as the difference between total specific energies plus or minus the excess head (if the latter is not equal to zero):

$$\Delta H = \frac{1}{Q} \int_{F_1} (H_{st} + H_d) w dF - \frac{1}{Q} \int_{F_2} (H_{st} + H_d) w dF \pm H_L, \quad (1-40)$$

where $\frac{1}{Q} \int_F (H_{st} + H_d) w dF$ is the total specific energy of the flow through the given section F , kg/m^2 ; $H_{st} + H_d$ is the total pressure at the point of the section, kg/m^2 .

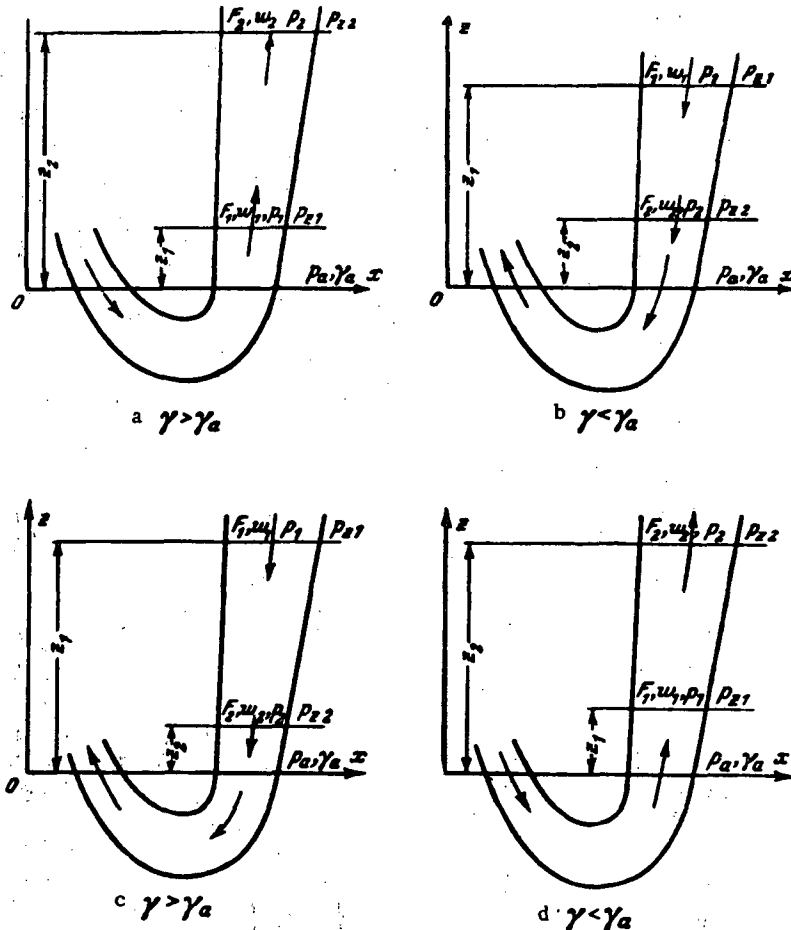


FIGURE 1-6. Determination of sign of the head.

1-6. THE FLOW OF FLUIDS THROUGH AN ORIFICE

a. Flow of an incompressible fluid

1. The discharge velocity of fluid from a vessel or reservoir, through an orifice in the bottom or wall (Figure 1-7), is determined by the formula*:

$$w_c = \frac{\sqrt{\frac{2g}{\gamma} \left[\gamma(z+l) + p_i - p_c + N_1 \frac{\gamma w_i^2}{2g} \right]}}{\sqrt{N_c + \zeta}}, \quad (1-41)$$

or

$$w_c = \varphi \sqrt{2gH_{t.\text{dis}}}, \quad (1-42)$$

where w_c and w_i are the velocities of flow in the vena contracta of the jet and in the vessel, respectively, in m/sec;

$$\varphi = \frac{1}{\sqrt{N_c + \zeta}} \text{ is the velocity coefficient; } \quad (1-43)$$

$$H_{t.\text{dis}} = \frac{1}{\gamma} \left[\gamma(z+l) + p_i - p_c + N_1 \frac{\gamma w_i^2}{2g} \right] \quad (1-44)$$

is the total discharge pressure, kg/m²; p_c and p_i are the static pressures (absolute) in the vena contracta and the vessel, respectively, kg/m²; z is the height of the liquid level above the centroid of the exit section of the orifice, m; l is the vertical distance from the exit orifice to the reference plane (Figure 1-7) or nozzle depth, m; N_c and N_1 are the kinetic-energy coefficients in the vena contracta and the vessel, respectively; ζ is the resistance coefficient of the orifice, referred to the velocity in the vena contracta of the jet; it is determined from the same data as for any stretch of pipe.

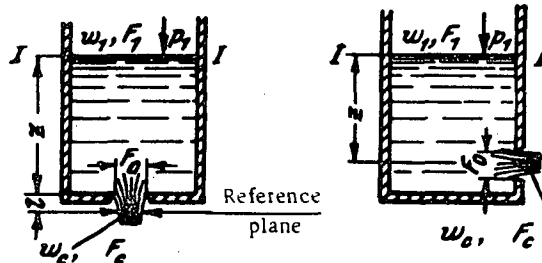


FIGURE 1-7. Discharge from a vessel through an orifice in the bottom or wall.

* The magnitudes z and l are neglected in the case of a gas.

2. In the general case, the jet issuing from an orifice contracts somewhat just below the orifice, so that

$$F_c = \epsilon F_o. \quad (1-45)$$

where F_c and F_o are the areas of the contracted section (the vena contracta) and the orifice, respectively (Figure 1-8), m^2 ; $\epsilon = \frac{F_c}{F_o}$ is the coefficient of jet contraction, which depends mainly on the shape of the inlet edge of the orifice, on the ratio $\frac{F_o}{F_1}$ (F_1 = area of the vessel cross section), and on the Reynolds number.

Using (1-45) and the continuity equation, formula (1-41) can be reduced to

$$w_c = \varphi \frac{\sqrt{\frac{2g}{\gamma} [\gamma(z+l) + p_1 - p_c]}}{\sqrt{1 - N_1 \left(\frac{F_o}{F_1} \cdot \varphi\right)^2}} = \varphi \frac{\sqrt{2gH_{\text{dis}}}}{\sqrt{1 - N_1 \left(\frac{F_o}{F_1} \cdot \varphi\right)^2}} \quad (1-46)$$

where $H_{\text{dis}} = \frac{1}{\gamma} [\gamma(z+l) + p_1 - p_c]$ is the discharge pressure, kg/m^2 .

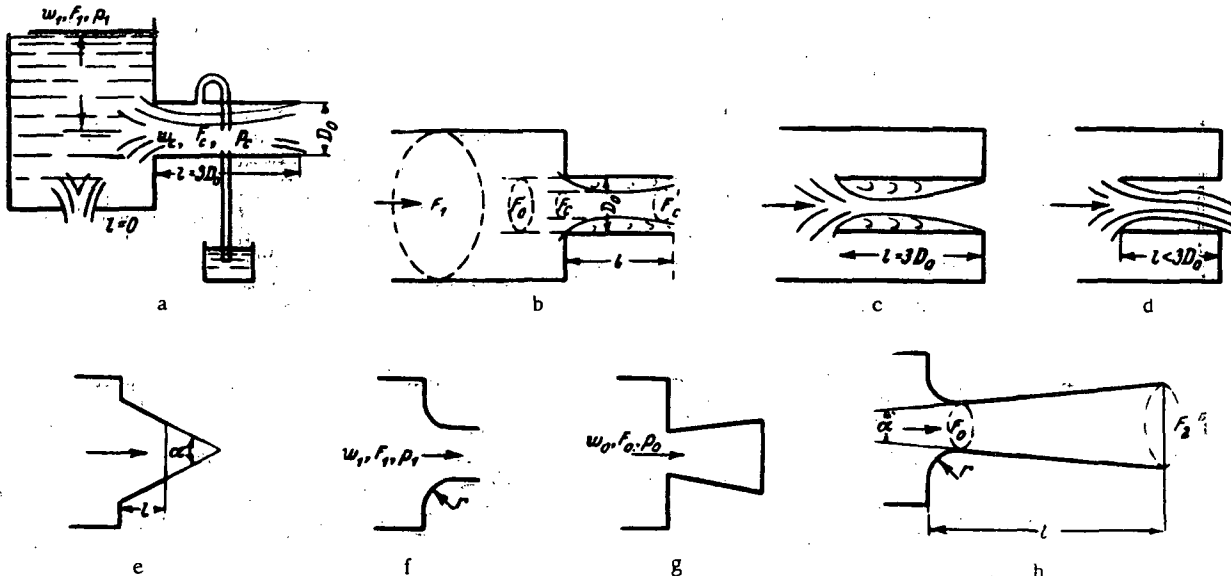


FIGURE 1-8. Discharge from a vessel through various nozzles.

3. If the cross-sectional area of the orifice can be neglected compared with the area of the vessel cross section, (1-46) simplifies to

$$\begin{aligned} w_c &= \varphi \sqrt{\frac{2g}{\gamma} [\gamma(z+l) + p_1 - p_c]} = \\ &= \varphi \sqrt{2gH_{\text{dis}}} \end{aligned} \quad (1-47)$$

4. The volume discharge of a fluid through an orifice is given by the formula:

$$Q = w_c \cdot F_0 \cdot \frac{\sqrt{2gH_{dis.}}}{\sqrt{1 - N_1 \left(\epsilon \varphi \frac{F_0}{F_1} \right)^2}} = \mu F_0 \cdot \frac{\sqrt{2gH_{dis.}}}{\sqrt{1 - N_1 \left(\mu \frac{F_0}{F_1} \right)^2}}, \quad (1-48)$$

where $\mu = \epsilon \varphi$ is the discharge coefficient of the orifice.

At $F_0 \ll F_1$:

$$Q = \mu F_0 \sqrt{2gH_{dis.}}. \quad (1-49)$$

5. The discharge coefficient μ of the orifice is a function of the shape of its inlet edge and of the area ratio $\frac{F_0}{F_1}$, and also of the Reynolds number (due to the dependence of ϵ, φ, ζ on these parameters).

6. The dependence of the coefficients ϵ, φ, μ on the Reynolds number $Re_r = \frac{w_r D_0}{v}$ (where $w_r = \sqrt{\frac{2g}{l} [\gamma z + p_1 - p_c]}$ is the theoretical velocity of discharge through an orifice in a thin wall in the vena contracta, D_0 is the orifice diameter, v is the kinematic viscosity coefficient of the liquid or gas) can be determined at $\frac{F_0}{F_1} = 0$ on the basis of the curves of Figure 1-8, proposed by Al'tshul /1-2/.

7. At $Re > 10^4$ the values of μ for the case considered can be determined approximately by the following formulas:

1) circular orifice

$$\mu_o \approx 0.59 + \frac{5.5}{\sqrt{Re_r}}$$

(Al'tshul formula /1-2/);

2) rectangular orifice

$$\mu_r \approx 0.59 + \frac{8.9}{\sqrt{Re_r}}$$

(Frenkel formula /1-24/);

3) square orifice

$$\mu_s = 0.58 + \frac{8.9}{\sqrt{Re_r}}$$

(Frenkel formula /1-24/).

8. The values of μ at $Re > 10^4$ for different types of nozzles (Figure 1-8) can be determined approximately as a function of the area ratio $\frac{F_0}{F_1}$ by the formulas given in Table 1-9*.

9. The velocity and quantity of a liquid discharged from a submerged orifice (Figure 1-10) are determined by the same formulas (1-41) to (1-49) as for a nonsubmerged orifice; the different symbols are understood in this case as follows:

* Author's data.

$z = z_A$ = immersion depth of the centroid of the exit section relative to the free liquid level in the reservoir A , m;

$p_i = p_A$ = pressure at the free surface in the reservoir A , kg/m²;

$p_c = p_B + \gamma z_B$ = pressure in the vena contracta of the jet, where p_B is the pressure at the free surface of reservoir B , kg/m²; z_B is the immersion depth of the center of gravity of the orifice relative to the free level in reservoir B , m.

TABLE 1-9

Shape of the nozzle	Values of μ	
	different $\frac{F_0}{F_1}$	$\frac{F_0}{F_1} \rightarrow 0$
Orifice in a thin wall (bottom) (Figure 1-8a, $l=0$)	$\frac{1}{1+0.707\sqrt{1-\frac{F_0}{F_1}}} + \frac{5}{\sqrt{Re}}$	$0.59 + \frac{5}{\sqrt{Re}}$
External cylindrical nozzle (Figure 1-8,a and b, $l \approx 3D_0$)	$\sqrt{\frac{1}{1.5 - 0.5\frac{F_0}{F_1}}}$	0.82
Internal cylindrical nozzle (Figure 1-8, c, $l \approx 3D_0$)	$\sqrt{\frac{1}{2 - \frac{F_0}{F_1}}}$	0.71
Conical converging nozzle (Figure 1-8, e, $\alpha \approx 13^\circ$)	$\sqrt{\frac{1}{1.12 - 0.2\frac{F_0}{F_1}}}$	0.94
Rounded approach nozzle (Figure 1-8,f)	$\sqrt{\frac{1}{1.07 - 0.07\frac{F_0}{F_1}}}$	0.97
Diverging nozzle (Venturi tube) with rounded entrance (Figure 1-8h, $\alpha = 6 \div 8^\circ$, $\frac{F_2}{F_0} \geq 7$)	—	2.4

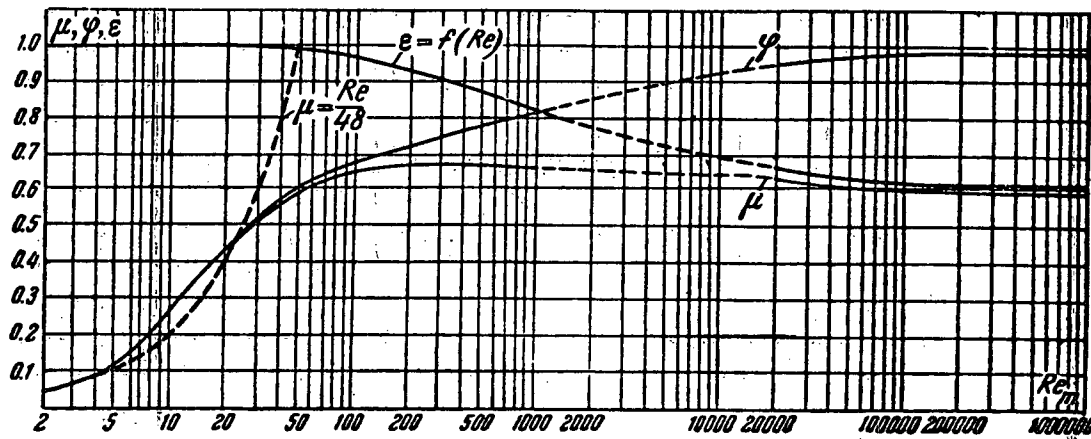


FIGURE 1-9. Curves of the velocity coefficient φ , the contraction coefficient ϵ , and the discharge coefficient μ , for a sharp-edged orifice, as a function of Re .

Introduce the designation $H_1 = \gamma(z_A - z_B) = \gamma z_0$; then, at $l \approx 0$ and $\frac{F_0}{F_1} = 0$:

$$w_c = \varphi \sqrt{\frac{2g}{\gamma} (H_1 + p_A - p_B)} \quad (1-50)$$

and

$$Q = \mu F_0 \sqrt{\frac{2g}{\gamma} (H_1 + p_A - p_B)}. \quad (1-51)$$

10. If p_A and p_B are equal to the atmospheric pressure, then for a relatively small opening:

$$w_c = \varphi \sqrt{2g \frac{H_1}{l}} \quad (1-52)$$

and

$$Q = \mu F_0 \sqrt{2g \frac{H_1}{l}}. \quad (1-53)$$

The same values are used for φ and μ as above.

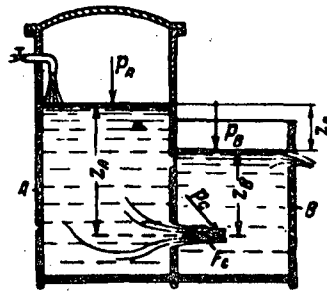


FIGURE 1-10. Discharge from a submerged orifice.

b. Discharge of a compressible gas

1. When a gas is discharged at high pressure to the atmosphere, a sharp variation occurs in its volume. In this case it is necessary to take its compressibility into account. Neglecting the nozzle losses (Figure 1-8f) for a perfect gas and the influence of the gas weight, the velocity of the adiabatic discharge can be determined by the Saint-Venant and Wantzel formula:

$$w_0 = \sqrt{2g \frac{\kappa}{\kappa-1} \frac{p_1}{T_1} \left[1 - \left(\frac{p_0}{p_1} \right)^{\frac{\kappa-1}{\kappa}} \right]} \text{ [m/sec]} \quad (1-54)$$

or

$$w_0 = \sqrt{2g \frac{\kappa}{\kappa-1} RT_1 \left[1 - \left(\frac{p_0}{p_1} \right)^{\frac{\kappa-1}{\kappa}} \right]} \text{ [m/sec]}, \quad (1-55)$$

where w_0 is the velocity of the gas jet in the nozzle throat, m/sec; p_i and p_0 are the inlet and back pressures, respectively, kg/m²; T_1 is the absolute temperature of the gas before the nozzle throat, °K; γ_1 is the specific gravity of the gas at pressure p_i and temperature T_1 , kg/m³; R is the gas constant; $\kappa = \frac{c_p}{c_v}$ is the specific-heats ratio (cf. Table 1-3); c_p , c_v are the mean specific heats of the gas at constant pressure and constant volume, respectively, $\frac{\text{kcal}}{\text{kg} \times \text{deg}}$.

2. When p_0 decreases, the discharge velocity w_0 increases until p_0 becomes equal to the critical pressure:

$$p_{cr} = \left(\frac{2}{\kappa+1} \right)^{\frac{1}{\kappa-1}} p_i \quad (1-56)$$

When $p_0 = p_{cr}$, the velocity in the nozzle throat F_0 is equal to the speed of sound in the given medium.

The subsequent decrease of p_0 has no influence on the velocity at the throat, which remains equal to the speed of sound, but leads to the expansion of the jet at the exit. Thus, when the pressure is reduced below its critical value, the mass discharge of gas remains constant and equal to

$$G = \gamma_0 F_0 w_0 = F_0 \left(\frac{2}{\kappa+1} \right)^{\frac{1}{\kappa-1}} \sqrt{\frac{2\kappa}{\kappa+1} g \gamma_1 p_i} \quad (1-57)$$

Formula (1-54) or (1-55) can therefore be used for calculating the velocity and discharge at $p_0 \geq p_{cr}$ only. Formula (1-57) is to be used at $p_0 < p_{cr}$.

1-7. FLUID-FLOW STATES

1. The state of flow of a fluid can be laminar or turbulent. In the first case the flow is stable, the fluid layers move without mixing with each other and flow smoothly past the obstacles in their way. The second state of flow is characterized by a random motion of finite masses of fluid mixing strongly with each other.

2. The state of flow of a fluid is a function of the ratio between the inertial forces and the viscosity forces in the stream. This ratio is characterized by the dimensionless Reynolds number:

$$Re = \frac{\gamma w_0 D_0}{\eta} = \frac{w_0 D_0}{v} \quad (1-58)$$

where w_0 is the determining flow velocity (i. e., the mean velocity over the pipe section), m/sec; D_0 is the determining linear dimension of the flow (the pipe diameter), m.

3. For each installation there exists a certain range of "critical" values of Reynolds number at which the passage from laminar to turbulent flow takes place. The lower limit of the critical Reynolds number for a circular pipe is about 2300. The upper limit of Re depends strongly on the inlet conditions, the state of the wall surface, and other factors.

4. When a viscous fluid flows between solid boundaries, the layer contiguous to the solid surface adheres to it, leading to a transverse velocity gradient: the velocity increases in the region near the solid surface from zero to the velocity w of the undisturbed stream (Figure 1-11). The region in which this variation of the velocity takes place is called the boundary layer.

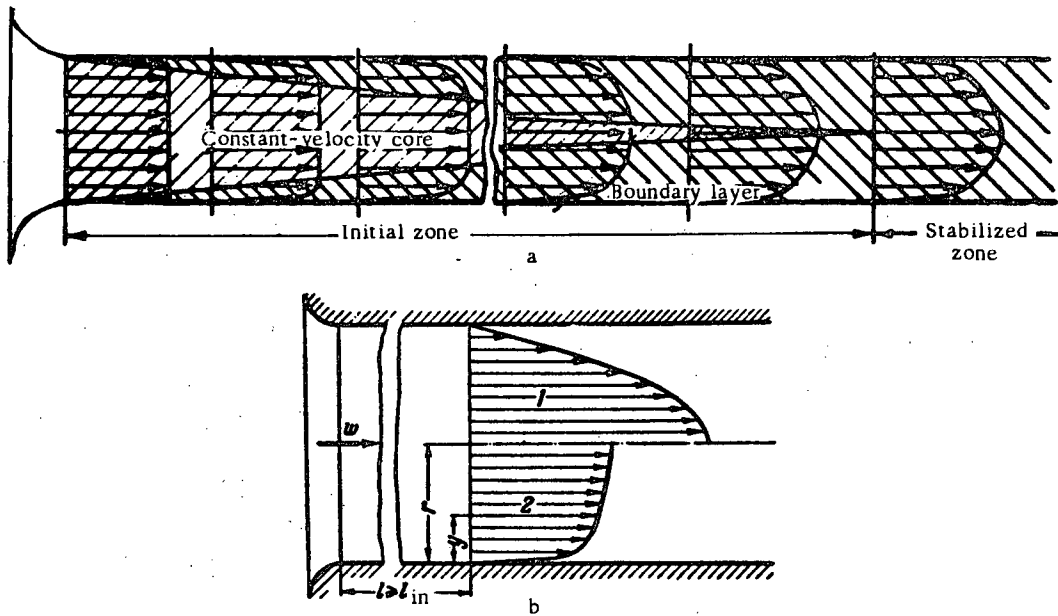


FIGURE 1-11. Velocity distributions over the pipe cross section:

a—stream deformation in the initial zone; b—velocity profile in the stabilized zone;
1—laminar flow; 2—turbulent flow.

5. A distinction is made in the case of flow in straight conduits, between the initial zone of flow and the zone of stabilized flow (Figure 1-11a).

The initial zone is the stretch along which the uniform velocity profile observed at the inlet is gradually transformed into the normal profile corresponding to stabilized flow.

6. The stabilized velocity profile is parabolic for laminar flow (Figure 1-11b, 1) and roughly logarithmic or exponential for turbulent flow (Figure 1-11b, 2).

7. The length of the initial stretch, i. e., the distance from the inlet section to the section in which the velocity differs from the velocity of the stabilized stream by only 1%, of a circular or rectangular pipe with a side ratio of between 0.7 and 1.5, can be determined in the case of laminar flow by Shiller's formula /1-25/:

$$\frac{L_{in}}{D_h} = 0.029 \text{ Re}, \quad (1-59)$$

where L_{in} is the length of the initial stretch, m; D_h is the hydraulic diameter of the pipe, m; $\text{Re} = \frac{w_0 D_h}{\nu}$ is the Reynolds number.

8. In the case of turbulent flow the length of the initial stretch of an annular pipe with smooth walls can be determined by the Solodkin-Ginevskii formula /1-18/:

$$\frac{L_{in}}{D_h} = b' \lg \text{Re} + (a' - 4.3b'), \quad (1-60)$$

where $a' = f_1 \left(\frac{D_{in}}{D_{out}} \right)$ and $b' = f_2 \left(\frac{D_{in}}{D_{out}} \right)$ are determined from the corresponding curves of Figure 1-12; D_{in} and D_{out} are diameters of the inner and outer pipes, respectively.

The annular pipe is transformed in the limiting case $\frac{D_{in}}{D_{out}} = 0$ ($D_{in} = 0$) into a circular pipe, for which formula (1-60) reduces to:

$$\frac{L_{in}}{D_h} = 7.88 \lg \text{Re} - 4.35. \quad (1-61)$$

In the limiting case $\frac{D_{in}}{D_{out}} = 1.0$ the annular pipe is transformed into a plane one, for which formula (1-60) reduces to:

$$\frac{L_{in}}{D_h} = 3.28 \lg \text{Re} - 4.95. \quad (1-62)$$

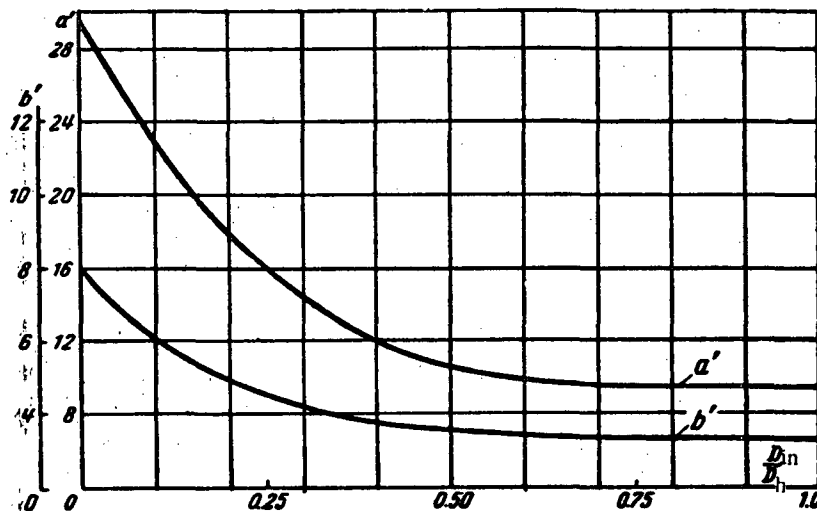


FIGURE 1-12. Curves of the coefficients a' and b' as a function of the ratio of diameters of an annular pipe.

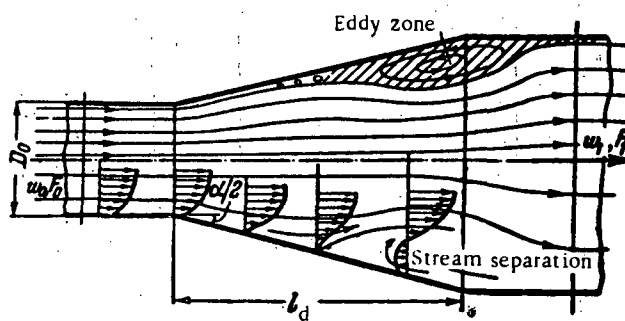


FIGURE 1-13. Flow separation and formation of eddies in a diffuser.

9. The thickness of the boundary layer at a given distance from the initial section of a straight conduit can increase or decrease, depending upon whether the medium moves in a decelerating motion or an accelerating motion.

A too sudden expansion can lead to the phenomenon of flow separation from the wall, accompanied by the formation of eddies (Figure 1-13).

1-8. FLUID RESISTANCE

1. The fluid losses in the course of the motion of a fluid are due to the irreversible transformation of mechanical energy into heat. This energy transformation is due to the molecular and turbulent viscosity of the moving medium.

2. There exist two different types of fluid losses:

- 1) the frictional losses ΔH_{fr} ;
- 2) the local losses ΔH_l .

3. The frictional losses are due to the viscosity (molecular and turbulent) of the fluids, which manifests itself during their motion and is a result of the exchange of momentum between molecules at laminar flow and between individual particles of adjacent fluid layers moving at different velocities, at turbulent flow. These losses take place along the entire length of the pipe.

4. The local losses appear at a disturbance of the normal flow of the stream, such as its separation from the wall and the formation of eddies at places of alteration of the pipe configuration or at obstacles in the pipe. The losses of dynamic pressure occurring with the discharge of the stream from a pipe into a large volume must also be classed as local losses.

5. The phenomenon of flow separation and eddy formation is linked with the difference between the flow velocities in the cross section, and with a positive pressure gradient along the stream, which appears when the motion is slowed down in an expanding channel, in accordance with Bernoulli's equation. The difference between the velocities in the cross section at a negative pressure gradient does not lead to flow separation. The flow in smoothly converging stretches is even more stable than in stretches of constant section.

6. All kinds of local pressure losses, except the dynamic-pressure losses at the exit of a pipe, occur along a more or less extended stretch of the pipe and cannot be separated from the frictional losses. For ease of calculation they are, however, arbitrarily assumed to be concentrated in one section; it is also assumed that they do not include friction losses. The summing is conducted according to the principle of superposition of losses, according to which the total loss is equal to the arithmetic sum of the friction and local losses:

$$\Delta H_{sum} = \Delta H_{fr} + \Delta H_l \text{ [kg/m}^2\text{].} \quad (1-63)$$

In practice, it is necessary to take ΔH_{fr} into account only for relatively long fittings or when its value is commensurable with ΔH_l .

7. Hydraulic calculations use the dimensionless coefficient of fluid resistance, which has the same value in dynamically similar streams, i. e., streams having geometrically similar stretches, equal values of Re , and equal values of other similitude criteria, independent of the nature of the fluid. This is especially true of the flow velocity and the dimensions of the stretches being calculated.

8. The fluid-resistance coefficient represents the ratio of the pressure loss ΔH to the dynamic pressure in the section F considered:

$$\zeta = \frac{\Delta H}{\frac{\gamma w^2}{2g}}. \quad (1-64)$$

The numerical value of ζ is thus a function of the dynamic pressure, and therefore of the cross section. The passage from the value of the resistance coefficient in section (F_1) to its value in section F_0 is realized by means of the formula:

$$\zeta_0 = \zeta_1 \frac{\gamma_1}{\gamma_0} \left(\frac{w_1}{w_0} \right)^2 = \zeta_1 \frac{\gamma_0}{\gamma_1} \left(\frac{F_0}{F_1} \right)^2 \quad (1-65)$$

or at $\gamma_0 = \gamma_1$:

$$\zeta_0 = \zeta_1 \left(\frac{F_0}{F_1} \right)^2. \quad (1-65')$$

9. The total fluid resistance of any element of the pipe is determined by the formula:

$$\Delta H_{\text{sum}} = \zeta_{\text{sum}} \frac{\gamma w^2}{2g}$$

or

$$\Delta H_{\text{sum}} = \zeta_{\text{sum}} \frac{\gamma_{\text{op}} w_{\text{op}}^2}{2g} = \zeta_{\text{sum}} \frac{\gamma_{\text{op}}}{2g} \left(\frac{Q_{\text{op}}}{r} \right)^2 [\text{kg/m}^2]. \quad (1-66)$$

In accordance with the principle of superposition of losses:

$$\zeta_{\text{sum}} = \zeta_{\text{fr}} + \zeta_1. \quad (1-67)$$

where $\zeta_{\text{fr}} = \frac{\Delta H_{\text{fr}}}{\frac{\gamma_{\text{op}} w_{\text{op}}^2}{2g}}$ is the friction coefficient in the given element of the pipe; $\zeta_1 = \frac{\Delta H_1}{\frac{\gamma_{\text{op}} w_{\text{op}}^2}{2g}}$ is the coefficient of local resistance of the given element of the pipe; w_{op} is the mean flow velocity at section F at operating conditions, m/sec (cf. (1-16) or (1-18)); Q_{op} is the volume rate of flow of the fluid, m^3/sec (cf. (1-15), (1-17)); γ_{op} is the specific gravity of the fluid, kg/m^3 (cf. (1-19), (1-20)); F is the cross-sectional area of the element considered, m^2 .

10. The friction coefficient of the entire element is expressed through the friction coefficient per unit relative length by:

$$\zeta_{\text{fr}} = \lambda \frac{l}{D_h}, \quad (1-68)$$

where λ is the friction coefficient of unit relative length of the pipe element considered; l is the length of the element considered, m; $D_h = \frac{4F}{\Pi}$ is the hydraulic diameter (four times the hydraulic radius) of the element section adopted, m; Π is the perimeter of the section, m.

11. The friction coefficient λ , and hence ζ_{fr} at constant $\frac{l}{D_h}$, is a function of two factors: the Reynolds number Re and the roughness of the channel walls $\bar{A} = \frac{A}{D_h}$.

12. The coefficient of local resistance ζ_l is mainly a function of the geometric parameters of the system element considered, and also of several general factors of motion, including:

a) the velocity profile at the inlet of the element. This in turn is a function of the state of flow, the inlet shape, the shape and distance of the various fittings or obstacles located ahead of the element, the length of the preceding straight stretch, etc.;

b) the Reynolds number $Re = \frac{\omega D_h}{v}$;

c) the Mach number $M = \frac{\omega}{a}$, where a is the speed of sound.

13. The principle of superposition of losses is used not only with respect to a separate element of the conduit, but also in the hydraulic calculation of the entire system. This means that the losses found for separate elements of the system are summed arithmetically which gives the total resistance of the entire system ΔH_{sys} .

14. The principle of superposition of losses can be applied by two methods:

1) by summing the absolute values of the hydraulic resistance of the separate elements of the system:

$$\Delta H_{sys} = \sum_{i=1}^n \Delta H_i, \quad (1-69)$$

where i is the number of the system element; n is the total number of system elements; ΔH_i is the total resistance of the i -th element of the system, determined by a formula similar to (1-66):

$$\Delta H_i = \zeta_i \frac{\gamma_i w_i^2}{2g} = \zeta_i \frac{\gamma_i}{2g} \left(\frac{Q_i}{F_i} \right)^2; \quad (1-70)$$

b) by summing the resistance coefficients of the separate elements expressed in terms of the same velocity w_0 and then expressing the total resistance of the system in terms of this summed resistance coefficient:

$$\zeta_{0sys} = \sum_{i=1}^n \zeta_{0i}, \quad (1-71)$$

where

$$\zeta_{0i} = \zeta_i \frac{\gamma_0}{\gamma_i} \left(\frac{F_0}{F_i} \right)^2; \quad (1-72)$$

ζ_{0i} is the total resistance coefficient of the given i -th element of the system expressed in terms of the velocity w_0 in the section F_0 ; ζ_i is the total resistance coefficient of the given i -th element of the system, expressed in terms of the velocity w_i in section F_i . Hence,

$$\Delta H_{sys} = \zeta_{0sys} \frac{\gamma_0 w_0^2}{2g} = \sum_{i=1}^n \zeta_{0i} \frac{\gamma_0 w_0^2}{2g} = \sum_{i=1}^n \zeta_i \frac{\gamma_0}{\gamma_i} \left(\frac{F_0}{F_i} \right)^2 \frac{\gamma_0 w_0^2}{2g} = \sum_{i=1}^n \zeta_i \frac{\gamma_0}{\gamma_i} \left(\frac{F_0}{F_i} \right)^2 \frac{\gamma_0}{2g} \left(\frac{Q_0}{F_0} \right)^2 \quad (1-73)$$

or

$$\Delta_{sys} = \sum_{i=1}^n \zeta_i \left(\frac{\gamma_{iop}}{F_i} \right)^2 \frac{\gamma_{iop}}{2g} \left(\frac{Q_{iop}}{F_i} \right)^2,$$

and at $\gamma_i = \gamma_0$:

$$\Delta H_{sys} = \sum_{i=1}^n \zeta_i \left(\frac{F_0}{F_i} \right)^2 \frac{\gamma_{0op}}{2g} \left(\frac{Q_{0op}}{F_0} \right)^2. \quad (1-73')$$

The first method is more convenient when a considerable variation of temperature and pressure takes place in the line (roughly at $t > 100^\circ\text{C}$ and $H > 500-1000 \text{ kg/m}^2$). In this case the line is split in separate successive stretches, for each of which the mean values of γ_i and w_i are used.

The second method is more convenient in the absence of a substantial variation of the temperature and pressure along the line.

1-9. WORK OF A COMPRESSOR IN A SYSTEM

1. In order to start motion of a fluid in a system it is necessary to give it a suitable head H ; this head is created by a compressor or pump (fan, supercharger, etc.).

2. The head created by a compressor is used in the most general sense: a) to overcome the difference between the pressures of the intake and discharge volumes; b) to overcome the excess physical head, i. e., to raise a heavier-than-air fluid by height z from the initial section of the system to its final section; c) to create a dynamic head at the exit of the flow from the pipe (Figure 1-14), i. e.,

$$H = (H_{in} - H_{dis}) \pm H_L + (\Delta H_{dis} + \Delta H_{in}) + \frac{\gamma w_{ex}^2}{2g} \left[\frac{\text{kg}}{\text{m}^2} \right]^*, \quad (1-74)$$

where H is the total head developed by the compressor, kg/m^2 ; H_{in} is the excess pressure in the intake volume, kg/m^2 ; H_{dis} is the excess pressure in the discharge volume, kg/m^2 ; H_L is the excess potential head (lift); ΔH_{in} is the pressure losses along the intake stretch of the pipe, kg/m^2 ; ΔH_{dis} is the pressure losses in the discharge stretch, kg/m^2 ; w_{ex} is the outlet velocity, m/sec .

3. In the case where the pressures of the intake and the discharge volumes are equal ($H_{in} = H_{dis}$), this formula reduces to:

$$H = \Delta H_{in} + \Delta H_{dis} + \frac{\gamma w_{ex}^2}{2g} \pm H_L = \Delta H_{sys} \pm H_L, \quad (1-75)$$

where ΔH_{sys} is calculated for the entire system as a sum of the losses in the intake and discharge stretches of the system, including the losses of dynamic pressure at the exit of the system, by formula (1-69) or (1-73); H_L is calculated by formula (1-38).

4. Since, at $H_L = 0$, the sum of all the losses in the system is equal to the difference

* For pumps H is given in meters of the displaced liquid column.

between the total pressures before and after the compressor, then:

$$H = \left(H_{st,dis} + \frac{\gamma w_{dis}^2}{2g} \right) - \left(H_{st,in} + \frac{\gamma w_{in}^2}{2g} \right) = H_{tot,dis} - H_{tot,in}. \quad (1-76)$$

where $H_{tot,in}$ and $H_{tot,dis}$ are the excess total pressure before and after the compressor, kg/m^2 ; $H_{st,in}$ and $H_{st,dis}$ are the excess static pressure before and after the compressor, kg/m^2 ; w_{in} and w_{dis} are the mean stream velocity before and after the compressor, m/sec.

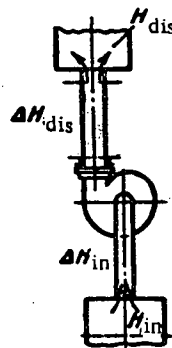


FIGURE 1-14. Work of a compressor in a system.

5. The value of H is positive at normal operating conditions of the compressor, i.e.,

$$H_{tot,dis} > H_{tot,in}.$$

At the same time, either the static or the dynamic pressure can be smaller after the compressor than before it.

6. Where the intake and discharge orifices have the same cross section:

$$\frac{\gamma w_{dis}^2}{2g} = \frac{\gamma w_{in}^2}{2g},$$

and therefore the total head of the compressor will be :

$$H = H_{st,dis} - H_{st,in}, \quad (1-77)$$

i.e., the total head of the compressor is equal to the difference between the static pressures immediately before and after the compressor.

7. The power on the compressor shaft is determined by the formula:

$$\left. \begin{aligned} N &= \frac{Q_{op}H}{3600 \cdot 102 \eta_{ov}} [\text{kW}], \\ N &= \frac{Q_{op}H}{3600 \cdot 75 \eta_{ov}} [\text{h.p.}] \end{aligned} \right\} \quad (1-78)$$

or

where Q_{op} is the volume rate of flow of the medium being displaced at operating conditions (compressor), m^3/hr^* ; H is the compressor head at operating conditions, kg/m^2* ; η_{ov} is the overall efficiency of the compressor.

8. The compressor output is usually specified. The head of the compressor is calculated by (1-74) to (1-77) for the specified conditions of the lines, i.e., for a given difference between the pressures in the intake and discharge volumes ($H_{dis} - H_{in}$), excess potential head $\pm H_L$, and shape and dimensions of all the elements of the system. These latter determine the magnitude of the resistance coefficients ζ_{fr} and ζ_l , the flow velocity in each element, and, therefore, the magnitude of ΔH_{sys} .

9. In order to determine whether the compressor satisfies the specified values of Q_{op} and H it is necessary first to convert these magnitudes to the conditions for which the compressor characteristic is given. If the rate of flow of the medium being displaced is given in m^3/hr , it may be converted to operating conditions by formulas (1-15) or (1-17).

The head of the compressor is calculated by the formula:

$$H = H_{ch} \frac{\gamma_{ch}}{\gamma_n} \cdot \frac{273 + t_{op}}{273 + t_{ch}} \cdot \frac{p_{ch}}{p_{op}}, \quad (1-79)$$

where H_{ch} is the design value of the compressor head, kg/m^2 ; γ_{ch} is the specific gravity of the medium for which the characteristic was obtained under standard conditions (0°C , $B = 760 \text{ mm column of mercury, kg/m}^3$); γ_n is the specific gravity of the medium for which the compressor is used, at standard conditions, kg/m^3 ; t_{op} is the operating temperature of the displaced medium in the compressor, $^\circ\text{C}$; t_{ch} is the temperature at which the compressor characteristic was obtained, $^\circ\text{C}$; p_{op} is the absolute operating pressure of the displaced medium in the compressor, kg/m^2 ; p_{ch} is the absolute pressure of the medium, at which the compressor characteristic was determined; in the case of fans $p_{ch} = 10.330 \text{ kg}/\text{m}^2$.

10. In the case of high head, the value used for the specific gravity of the medium being displaced is related to the mean pressure on the rotor. In that case p_{op} in (1-79) is replaced by the mean absolute pressure on the rotor:

$$p_m = p_{op} + (\Delta H_{com} - 0.5\Delta H_{sys}) [\text{kg}/\text{m}^2],$$

where ΔH_{com} is the pressure loss in the compressor, kg/m^2 ; ΔH_{sys} is the total pressure loss in the whole line, kg/m^2 .

11. The rated power consumption of the compressor is determined by the formula:

$$N_{ch} = \frac{Q_{op} H_{ch}}{3600 \cdot 102 \eta_{ov}} = \frac{Q_{op} H}{3600 \cdot 102 \eta_{ov}} \cdot \frac{\gamma_n}{\gamma_{ch}} \times \frac{273 + t_{ch}}{273 + t_{op}} \cdot \frac{p_{op}}{p_{ch}} = \\ N \times \frac{\gamma_n}{\gamma_{ch}} \cdot \frac{273 + t_{ch}}{273 + t_{op}} \times \frac{p_{op}}{p_{ch}} [\text{kw}], \quad (1-80)$$

where N_{ch} is the power output of the compressor according to the manufacturer's rating, kw .

* In the case of pumps Q_{op} is the weight rate of flow of the fluid being displaced, $\frac{\text{kg}}{\text{hr}}$, and H is the head in meters of the displaced liquid column.

1-10. EXAMPLES OF THE CALCULATIONS OF THE FLUID RESISTANCE OF SYSTEMS

Example 1-1. Forced ventilation system

A ventilation-system network is shown schematically in Figure 1-15.

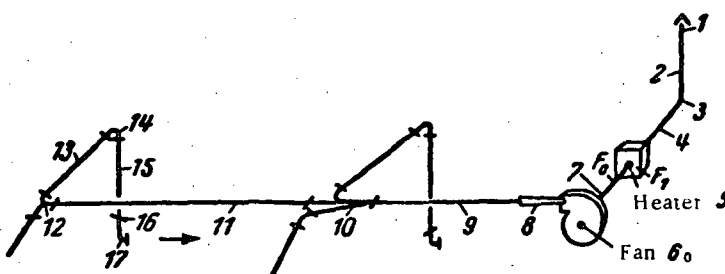


FIGURE 1-15. Schematic layout of a ventilation-system network.

Given:

- 1) the output of the blower $Q = 3200 \text{ m}^3/\text{hour}$;
 - 2) discharge through each of the four lateral branches $Q_1 = 800 \text{ m}^3/\text{hour}$;
 - 3) temperature of the external (atmospheric) air $t = -20^\circ\text{C}$;
 - 4) air temperature at the heater outlet $t = +20^\circ\text{C}$;
 - 5) material from which the ducts are made — sheet steel, oil-coated roughness $\Delta \approx 0.15 \text{ mm}$ (cf. Table 2-1, group A).
- Since the gas temperature varies in the ducts (due to the heater), the first method of summing the losses will be used: summing the absolute losses in the separate elements of the ducts.

The calculation of the resistance is given in Table 1-10. The following values are obtained according to this table for selecting the fan:

$$Q_{op} = 0.955 \text{ m}^3/\text{sec} \text{ and } H = \Delta H_{sys} = 23 \text{ kg}/\text{m}^2.$$

The power on the fan rotor at a fan efficiency $\eta_{ov} = 0.6$ is equal to:

$$N = \frac{Q_w H}{102 \eta_{ov}} = \frac{0.955 \cdot 23}{102 \cdot 0.6} \approx 0.36 \text{ kw.}$$

Example 1-2. Installation for the scrubbing of sintering gases

The installation layout is shown in Figure 1-16.

Given:

- 1) total flow rate of the gas under standard conditions ($t = 0^\circ\text{C}$ and $B = 760 \text{ mm mercury}$) $Q = 10^6 \text{ m}^3/\text{hour} = 278 \text{ m}^3/\text{sec}$;
 - 2) specific gravity of the gas under standard conditions $\gamma = 1.3 \text{ kg/m}^3$;
 - 3) kinematic viscosity of the gas under standard conditions $\nu = 1.3 \times 10^{-5} \text{ m}^2/\text{sec}$;
 - 4) internal coating of the gas mains: sheet steel; its roughness: same as seamless corroded steel pipes, equal to $\Delta \approx 1.0 \text{ mm}$ (cf. Table 2-1, A);
 - 5) the gas cleaning is done in a wet scrubbing tower; the rate of spraying $A \approx 50 \text{ m}^3/\text{hour} \times \text{m}^2$ (Figure 1-17).
- In the example the gas temperature varies through the conduits due to cooling; the first method of summing the losses will therefore be used, i. e., summation of the absolute losses in the separate elements of the main.

The calculation of the resistance is given in Table 1-11.

The draft created by the exhaust pipe is equal to:

$$H_L = H_p (\gamma_a - \gamma_g)$$

where $H_p = 62\text{ m}$ = height of the pipe; γ_a = specific gravity of atmospheric air, kg/m^3 ; γ_g = specific gravity of the gas at the inlet to the exhaust pipe, kg/m^3 .

The specific gravity of atmospheric air at temperature $t_a = 0^\circ\text{C}$ is:

$$\gamma_a = 1.29 \text{ kg/m}^3.$$

The specific gravity of the gas at temperature $t_g = 40^\circ\text{C}$ is:

$$\gamma_g = 1.13 \text{ kg/m}^3.$$

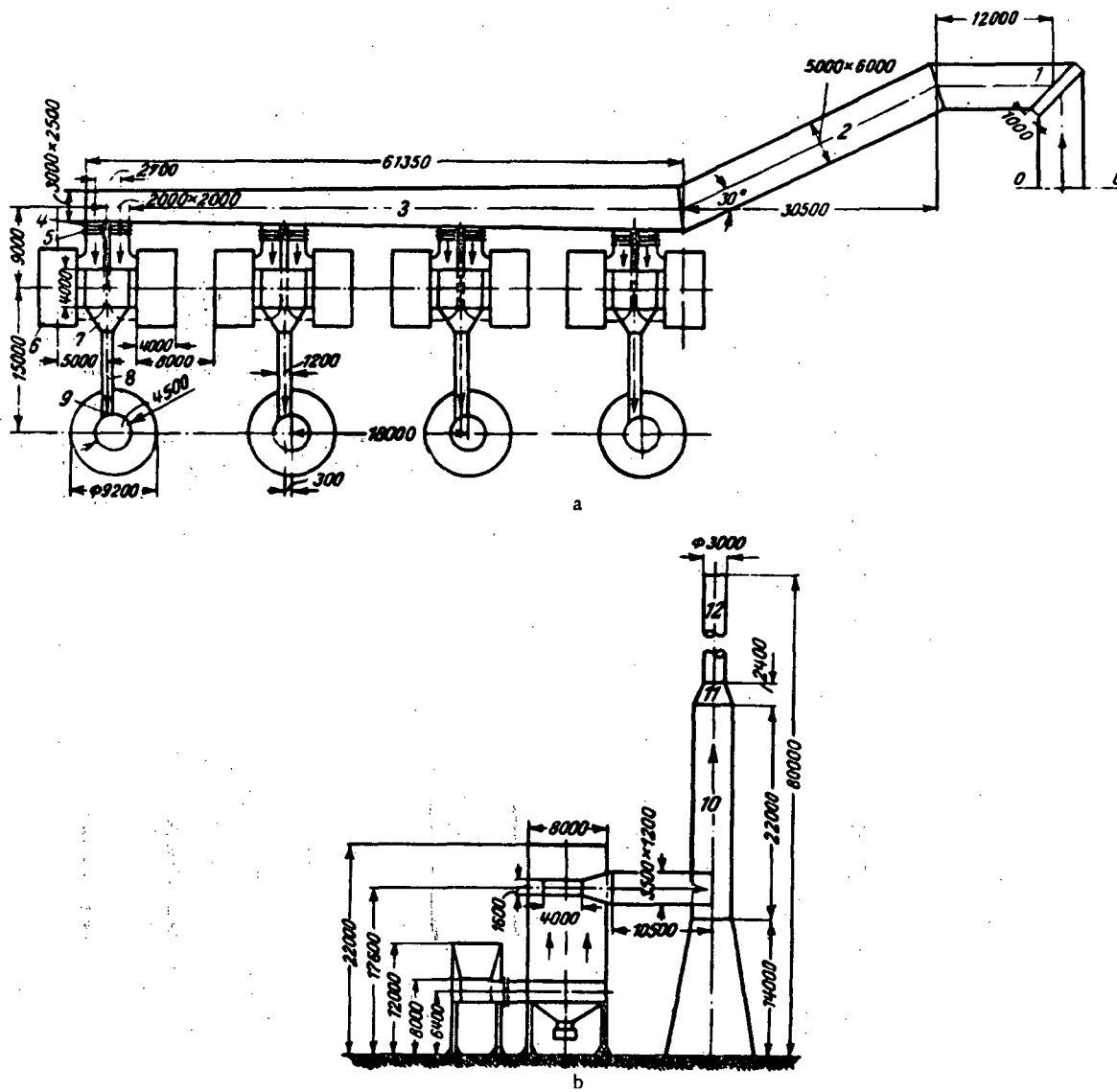


FIGURE 1-16. Plan of an installation for scrubbing sintering gases:

a – plan view; b – side view.

Therefore

$$H_L = 62(1.29 - 1.13) \approx 10 \text{ kg/m}^2.$$

This is a positive head, which contributes to the stream motion, and therefore has to be subtracted from the total losses (cf. Table 1-11).

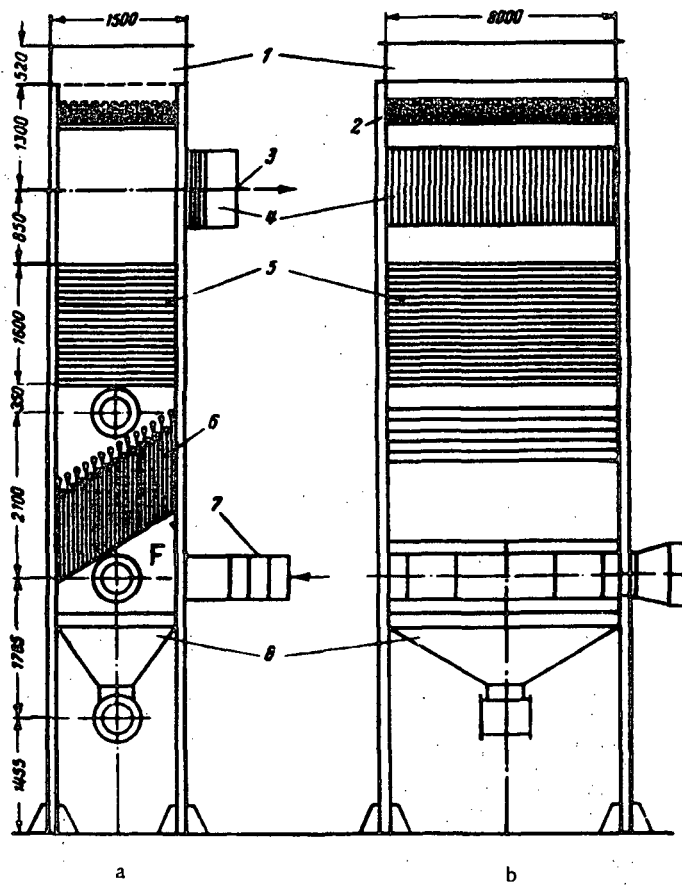


FIGURE 1-17. Wet scrubbing tower (cf. the plan Figure 1-16 and Table 1-11)

1—sprinkler tank; 2—distributing nozzles; 3—gas outlet; 4—louvers;
5—main nozzles; 6—spray nozzles; 7—diffuser for gas inlet;
8—scrubber bunker;
a — front view; b — side view.

Calculation of the

No. of the system element	Type of the main element	Diagram and dimensions of the system elements	Geometric parameters of the system elements	Q_{pd} , m^3/sec	t_1 , $^\circ\text{C}$	w , kg/m^3	w , m^2/sec
1	Supply vent		$\frac{h}{D_o} = 0.6$	0.825	-20	1.40	$1.17 \cdot 10^{-5}$
2	Straight stretch (vertical)		$\frac{l}{D_o} = 8.0$ $\bar{\Delta} = \frac{\Delta}{D_o} = 0.0003$	0.825	-20	1.40	$1.17 \cdot 10^{-5}$
3	Bend		$\theta = 90^\circ$ $\frac{r}{D_o} = 0.2$ $\bar{\Delta} = 0.0003$	0.825	-20	1.40	$1.17 \cdot 10^{-5}$
4	Straight stretch (horizontal)		$\frac{l}{D_o} = 2.0$ $\bar{\Delta} = 0.0003$	0.825	-20	1.40	$1.17 \cdot 10^{-5}$
5	Air heater with 3 rows of smooth pipes		$T_m w_0 = 4.0 \text{ kg}/\text{m}^2 \cdot \text{sec}$	-	-	-	-

TABLE 1-10.

resistance of the conduits

w_i , m/sec	$\frac{\rho_i^2}{2g}$, kg/m ²	$Re = \frac{w_i D h}{v}$	$\epsilon_{i,l}$	λ_i	$\epsilon_{fr,i} = \lambda_i \frac{l_i}{D_{hl}}$	$\epsilon_i = \epsilon_{i,l} + \epsilon_{fr,i}$	$\Delta H_i = \epsilon_i \frac{\rho_i^2}{2g}$, kg/m ²	Basis for the determination of ϵ_i (reference to diagram)
4.27	1.30	$1.80 \cdot 10^5$	0.30	-	-	0.30	0.390	3-16
4.27	1.30	$1.80 \cdot 10^5$	-	0.018	0.144	0.144	0.187	2-3
4.27	1.30	$1.80 \cdot 10^5$	0.44	0.018	0.024	0.464	0.605	6-9
4.27	1.30	$1.80 \cdot 10^5$	-	0.018	0.036	0.036	0.047	2-3
-	-	-	-	-	-	-	1.100	12-30

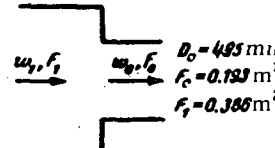
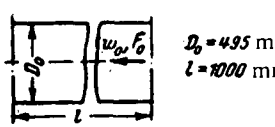
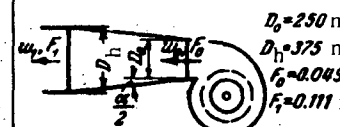
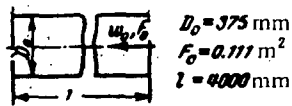
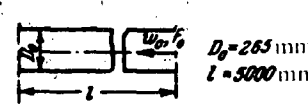
No. of the system element	Type of the main element	Diagram and dimensions of the system elements	Geometric parameters of the system elements	Q_{pri} , m^3/sec	t_i , $^{\circ}\text{C}$	\bar{w} , kg/m^3	γ , $\text{N}/\text{m}^2/\text{sec}$	
6	Sudden sharp contraction		$D_o = 495 \text{ mm}$ $f_c = 0.189 \text{ m}^2$ $f_s = 0.388 \text{ m}^2$	$\frac{F_o}{F_t} = 0.5$	0.955	+20	1.20	$1.5 \cdot 10^{-5}$
7	Horizontal straight stretch		$D_o = 495 \text{ mm}$ $l = 1000 \text{ mm}$	$\frac{l}{D_o} = 2.0;$ $\Delta = 0.0003$	0.955	+20	1.20	$1.5 \cdot 10^{-5}$
8	Pyramidal diffuser behind the fan working in the mains		$D_o = 250 \text{ mm}$ $D_h = 375 \text{ mm}$ $f_s = 0.049 \text{ m}^2$ $f_c = 0.111 \text{ m}^2$	$n = \frac{F_t}{F_o} = 2.25;$ $\alpha = 10^\circ$	0.955	+20	1.20	$1.5 \cdot 10^{-5}$
9	Horizontal straight stretch		$D_o = 375 \text{ mm}$ $f_c = 0.111 \text{ m}^2$ $l = 4000 \text{ mm}$	$\frac{l}{D_o} = 10.7;$ $\Delta = 0.0004$	0.955	+20	1.20	$1.5 \cdot 10^{-5}$
10	Flow divider		$D_c = 375 \text{ mm}$ $D_n = 265 \text{ mm}$ $f_c = 0.111 \text{ m}^2$ $f_n = 0.056 \text{ m}^2$	$\frac{F_s}{F_c} = 0.5;$ $\frac{Q_s}{Q_c} = 0.5; \frac{w_s}{w_c} = 1.0;$ $\alpha = 15^\circ$	0.478	+20	1.20	$1.5 \cdot 10^{-5}$
11	Horizontal straight stretch		$D_o = 265 \text{ mm}$ $l = 5000 \text{ mm}$	$\frac{l}{D_o} = 18.8;$ $\Delta = 0.00056$	0.478	+20	1.20	$1.5 \cdot 10^{-5}$

TABLE 1-10 (cont'd)

v_t , m/sec	$\frac{v_t^2}{2g}$, kg/m ²	$Re = \frac{v_tD}{\nu}$	ϵ_{lf}	λ_t	$\epsilon_{fr} = \lambda_t \frac{l_t}{D_D}$	$\epsilon_t = \epsilon_{lf} + \epsilon_{fr}$	$\Delta H_t = \epsilon_t \frac{v_t^2}{2g}$, kg/m ²	Basis for the determination of ϵ_t (reference to diagram)
4.95	1.50	$1.64 \cdot 10^5$	0.25	—	—	0.25	0.374	3-9
4.95	1.50	$1.64 \cdot 10^5$	—	0.0185	0.037	0.037	0.056	2-3
19.5	23.3	$3.25 \cdot 10^5$	0.19	—	—	0.19	4.40	5-16
8.6	4.54	$2.15 \cdot 10^5$	—	0.018	0.193	0.193	0.875	2-4
8.6	4.54	$1.5 \cdot 10^5$	0	—	—	—	0	7-23 (as a supply tee)
8.6	4.54	$1.5 \cdot 10^5$	—	0.019	0.36	0.36	1.630	2-3

No. of the system element	Type of the main element	Diagram and dimensions of the system elements	Geometric parameters of the system elements	q_{dp} , m ³ /sec	t_1 , °C	η_t , kg/m ³	ψ , m ² /sec
12	Symmetrical smooth tee	<p> $D_o = 195 \text{ mm}$ $D_c = 285 \text{ mm}$ $F_o = 0.03 \text{ m}^2$ $F_c = 0.058 \text{ m}^2$ </p>	$\frac{Q_o}{Q_c} = 0.5;$ $\frac{F_o}{F_c} = 0.50;$ $\frac{R}{D_c} = 1.5$	0.239	+20	1.20	$1.5 \cdot 10^{-5}$
13	Horizontal straight stretch	<p> $D_o = 195 \text{ mm}$ $l = 4000 \text{ mm}$ </p>	$\frac{l}{D_o} = 20.5;$ $\Delta = 0.00077$ $\delta = 90^\circ$	0.239	+20	1.20	$1.5 \cdot 10^{-5}$
14	90° curve	<p> $D_o = 195 \text{ mm}$ $F_o = 0.03 \text{ m}^2$ $R = 400 \text{ mm}$ </p>	$\frac{R_o}{D_o} = 2.0;$ $\Delta = 0.00077$	0.239	+20	1.20	$1.5 \cdot 10^{-5}$
15	Horizontal straight stretch	<p> $D_o = 195 \text{ mm}$ $l = 4000 \text{ mm}$ </p>	$\frac{l}{D_o} = 20.5;$ $\Delta = 0.00077$	0.239	+20	1.20	$1.5 \cdot 10^{-5}$
16	Throttle valve	<p> $D_o = 195 \text{ mm}$ </p>	$\delta = 5^\circ$	0.239	+20	1.20	$1.5 \cdot 10^{-5}$
17	Intake nozzle at exit from the bend	<p> $D_o = 195 \text{ mm}$ $l = 4000 \text{ mm}$ $r = 40 \text{ mm}$ </p>	$\frac{l}{D_o} = 2.0$ $\frac{r}{D_o} = 0.20$ $\Delta = 0.00077$	0.239	+20	1.20	$1.5 \cdot 10^{-5}$

TABLE 1-10 (cont'd)

v_i , m/sec	$\frac{v_i^2}{2g}$, kg/m ²	$Re = \frac{v_i D_{hi}}{\nu}$	ϵ_{li}	λ_f	$\epsilon_{frf} = \lambda_f \frac{H}{D_{hi}}$	$\epsilon_l = \epsilon_{li} + \epsilon_{frf}$	$\Delta H_f = \epsilon_l \frac{v_i^2}{2g}$, kg/m ²	Basis for the determination of ϵ_l (reference to diagram)
8.0	3.9	$1.04 \cdot 10^5$	0.25	0.019	0.05	0.30	1.170	7-30
8.0	3.9	$1.04 \cdot 10^5$	—	0.02	0.41	0.41	1.600	2-3
8.0	3.9	$1.04 \cdot 10^5$	0.15	0.02	0.065	0.215	0.840	6-2
8.0	3.9	$1.04 \cdot 10^5$	—	0.02	0.41	0.41	1.600	2-4
8.0	3.9	$1.04 \cdot 10^5$	0.25	—	—	0.28	0.980	9-4
8.0	3.9	$1.04 \cdot 10^5$	1.70	0.02	0.06	1.76	6.870	11-20
$\Delta H_{sys} = 22.764 \approx 23.0$ kg/m ²								

Resistance of pipelines and fittings of the unit for

No. of pipe-line element	Type of element	Plan and basic dimensions of the element	Geometric parameters of the element	Q_{pl} , m ² /sec
1	Square elbow	<p>$F_0 = 30 \text{ m}^2$ $F_1 = 30 \text{ m}^2$ $b_0 = 5000 \times 6000 \text{ mm}$ $t_0 = 2500 \text{ m}$ $D_h = \frac{4F_0}{H_0} = \frac{4 \cdot 30}{22} = 5450 = 5.45 \text{ m}$</p>	$\frac{F_1}{F_0} = 1.0; \frac{t_0}{b_0} = \frac{2500}{5000} = 0.5;$ $\bar{A} = \frac{A}{b_0} = \frac{1}{5000} = 0.0002$	430
2	Compound bend	<p>$l_y = 28500 \text{ mm}, b_0 = 5000 \times 6000 \text{ mm}, D_h = 5.5 \text{ m}$</p>	$\frac{l_0}{b_0} = 5.6;$ $\bar{A} = 0.0002;$ $a = 30^\circ$	430
3	Duct of the distributing header	<p>$l_0 = 60000 \text{ mm}; b_0 = 3000 \times 2500 \text{ mm}; D_h = 2.78 \text{ m};$ $l_1 = 60000 \text{ mm}; b_0 = 3000 \times 2000 \text{ mm}; D_h = 2.78 \text{ m};$ $l_2 = 60000 \text{ mm}; b_0 = 3000 \times 2000 \text{ mm}; D_h = 2.78 \text{ m}$</p>	$\frac{w_{1a}}{w_0} = \frac{w_{2a}}{w_0} = \frac{w_{3a}}{w_0} = \frac{w_{4a}}{w_0} = 1.0;$ $\frac{l_0}{D_{hm}} = \frac{60000}{411} = 14.5;$ $\bar{A} = \frac{A}{D_{hm}} = \frac{1.0}{411} = 0.0025$	430
4	Lateral branch of the distributing header	<p>$F_0 = 2.4 \text{ m}^2$ $F_c = 7.5 \text{ m}^2$ $w_n = w_c$</p>	$a = 90^\circ;$ $\frac{F_0}{F_c} = \frac{2.4}{7.5} \approx 1.0;$ $\frac{Q_6}{Q_c} = \frac{Q_6}{Q_{n6}} = 1.0; \frac{w_6}{w_c} = 1.0$	$\frac{430}{4} \frac{273+120}{273+150} = 107 \cdot 0.93 \approx 100$
5	Throttle valve (at 10% closing, $\theta = 5^\circ$)	<p>$F = 32 \text{ m}^2$</p>	$\frac{F}{F_0} = 0.9 (6 = 5^\circ)$	$\frac{100}{2} = 50$
6	Wet scrubber	(cf. Figure 1-17); $F = 32 \text{ m}^2$	at the inlet: $t = 120^\circ \text{C}$; at the exit: $t = 50^\circ \text{C}$; wetting intensity $A = 50 \text{ m}^3/\text{m}^2 \cdot \text{hr}$	$\frac{50}{50} \frac{273+85}{273+120} = 50 \cdot 0.91 = 45.5$
7	Exit stretch of the scrubber—symmetric tee	<p>$F_s = 4000 \times 1800 = 5.4 \text{ m}^2$ $F_c = 3500 \times 1200 = 4.2 \text{ m}^2$</p>	$\frac{F_c}{2F_s} = \frac{4.2}{2 \cdot 5.4} = 0.33;$ $\frac{Q_s}{Q_c} = 0.5$	$\frac{45.5}{45.5} \frac{273+50}{273+85} = 45.5 \cdot 0.9 = 41$

TABLE 1-11

the scrubbing of sintering gases (Figure 1-16)

t_i °C	τ_i kg/m ²	v_i m ² /sec	w_i m/sec	$\frac{\gamma_i w_i^2}{2g}$ kg/m ²	$= \frac{Re = w_i D_{H,i}}{v_i}$	$c_{1,i}$	λ_i	$c_{fr,i} = \lambda_i \frac{t_i}{D_{H,i}}$	$c_i = c_{1,i} + c_{fr,i}$	$\Delta H_{f,i} = c_i \frac{w_i^2}{2g}$ kg/m ²	Basis for the determination of c_i (reference to diagram)
150	0.84	$3 \cdot 10^{-5}$	14.3	8.8	$2.6 \cdot 10^6$	0.60	—	—	0.60	5.30	6-11
150	0.84	$3 \cdot 10^{-5}$	14.3	8.8	$2.6 \cdot 10^6$	0.20	0.014	0.079	0.28	2.46	6-18
150	0.84	$3 \cdot 10^{-5}$	14.3	8.8	$\sim 2.0 \cdot 10^6$	0	0.013	0.19	0.19	1.70	7-23
120	0.90	$2.7 \cdot 10^{-5}$	$w_0 = w_c = 13.3$	8.12	—	1.45	—	—	1.45	11.80	7-21
120	0.90	$2.7 \cdot 10^{-5}$	12.5	7.2	—	0.28	—	—	0.28	2.00	9-4
$\frac{120+50}{2} = 85$	1.0	—	1.42	0.103	—	960	—	—	960	99.00	12-7
50	1.0	—	9.8	5.40	—	≈ 2.0	—	—	2.0	10.80	Tentatively, as in diagram 3-9 (converging inlet) and symmetric 90° tee (diagram 7-29)

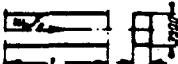
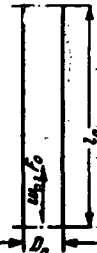
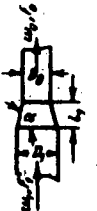
No. of pipeline element	Type of element	Plan and basic dimensions of the element	Geometric parameters of the element	q_{pl} , m^2/sec
8	Horizontal straight stretch	 <p> $l_0 = 10500 \text{ mm}$ $F_0 = 3500 \times 1200 = 4.2 \text{ m}^2$ $D_0 = \frac{0.42}{2(3.14)} = 1.0 \text{ m}^2$ </p>	$\frac{l_0}{D_0} = \frac{10500}{1600} = 6.6;$ $\bar{\Delta} = \frac{1.0}{1600} = 0.0006$	$2 \cdot 40 = 80$
9	Inlet to the stack	 <p> w_0, f_0 $F_0 = 4.2 \text{ m}^2$ $F_1 = 15.8 \text{ m}^2$ </p>	$\frac{F_0}{F_1} = \frac{4.2}{15.8} = 0.27$	$2 \cdot 40 = 80$
10	First straight stretch of the stack	 <p> $D_0 = 4500 \text{ mm}$ $F_0 = 15.8 \text{ m}^2$ $l_0 = 22000 \text{ mm}$ </p>	$\frac{l_0}{D_0} = \frac{22000}{4500} = 4.9;$ $\bar{\Delta} = \frac{1.0}{4500} = 0.00022$	$80 \cdot \frac{273+40}{273+50} = 77.5$
11	Transition passage	 <p> $D_0 = 4500 \text{ mm}$ $D_1 = 3000 \text{ mm}$ $F_0 = 15.8 \text{ m}^2$ $F_1 = 7.05 \text{ m}^2$ $l_0 = 22000 \text{ mm}$ $\alpha = 30^\circ$ </p>	$\frac{F_0}{F_1} = \frac{7.05}{15.8} = 0.45;$ $\frac{l_1}{D_0} = \frac{2400}{3000} = 0.8;$ $\bar{\Delta} = \frac{1.0}{3000} = 0.00033$	$80 \cdot \frac{273+40}{273+50} = 77.5$
12	Second straight stretch of the stack	 <p> $D_0 = 3000 \text{ mm}$ $F_0 = 7.05 \text{ m}^2$ $l_0 = 41500 \text{ mm}$ </p>	$\frac{l_0}{D_0} = \frac{41500}{3000} = 14;$ $\bar{\Delta} = \frac{1.0}{3000} = 0.00033$	$80 \cdot \frac{273+40}{273+50} = 77.5$
13	Exit from the stack			$80 \cdot \frac{273+40}{273+50} = 77.5$
14	Draft in the entire stack			—

TABLE 1-11 (cont'd)

t_L °C	γ_l kg/m ²	v_L m ² /sec	w_L m/sec	$\frac{\gamma_l w_L^2}{2g}$ kg/m ²	$Re = \frac{w_L D_{hl}}{v_l}$	c_{Ll}	λ_l	$c_{fr} = \frac{c_{Ll}}{\lambda_l} + c_{fr}$	$\Delta H_f = \frac{\gamma_l w_L^2}{2g}$ kg/m ²	Basis for the determina- tion of c_L (refer- ence to diagram)	
50	1.10	$1.8 \cdot 10^{-5}$	19.0	20.2	$1.9 \cdot 10^6$	—	0.018	0.12	0.12	2.42	2-3
50	1.10	$1.8 \cdot 10^{-5}$	19.0	20.2	$1.9 \cdot 10^6$	0.53	—	—	0.53	10.70	4-1 (sudden expansion)
40	1.13	$1.7 \cdot 10^{-5}$	4.9	1.38	$1.3 \cdot 10^6$	—	0.015	0.074	0.074	0.10	2-3
40	1.13	$1.7 \cdot 10^{-5}$	11.0	7.00	$\sim 2 \cdot 10^6$	0.054	0.014	0.01	0.064	0.45	3-7
40	1.13	$1.7 \cdot 10^{-5}$	11.0	7.00	$2.15 \cdot 10^6$	—	0.014	0.20	0.2	1.40	2-3
40	1.13	$1.7 \cdot 10^{-5}$	11.0	7.00	$2.15 \cdot 10^6$	1.0	—	—	1.0	7.00	11-1
—	1.13	—	—	—	—	—	—	—	—	—	Formula (1-38): $H_L = z(\gamma_s - \gamma_g)$, where $\gamma_s = 1.29$ at $t = 0^\circ C$ $\Delta H_{sys} = 155.13 \approx 155 \text{ kg/m}^2$

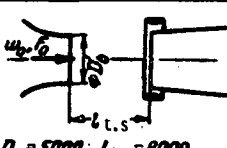
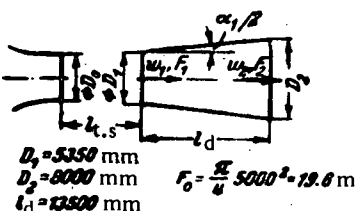
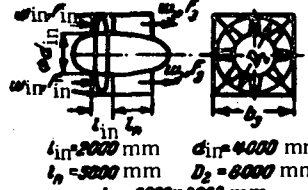
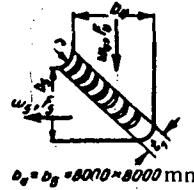
No. of turn- nel ele- ment	Type of element	Plan and dimensions of element	Geometric parameters of the element
1	Circular open throat	 $D_0 = 5000 \text{ mm}$, $l_{t,s} = 8000 \text{ mm}$	$\frac{l_{t,s}}{D_0} = \frac{8000}{5000} = 1.6$
2	First diffuser	 $D_1 = 5350 \text{ mm}$, $D_2 = 8000 \text{ mm}$, $l_{t,s} = 8000 \text{ mm}$, $F_0 = \frac{\pi}{4} 5000^2 = 19.6 \text{ m}^2$, $l_d = 32500 \text{ mm}$	$a = 7^\circ$; $n = \frac{F_1}{F_0} = \left(\frac{8000}{5000}\right)^2 = 2$; $\frac{w_{max}}{w_0} > 1.12$; $k_1 \approx 1.8$; $\bar{A} = \frac{A}{D_1} \approx 0.0004$
3	Adapter (from an angular section to a square)	 $d_{in} = 4000 \text{ mm}$, $D_1 = 8000 \text{ mm}$, $D_2 = 8000 \text{ mm}$, $b_2 = 8000 - 4000 = 4000 \text{ mm}$	$\bar{d}_{in} = \frac{d_{in}}{D_2} = 0.5$ $n = \frac{F_3}{F_{in}} = \frac{F_3}{(1 - \bar{d}_{in}^2) F_{in}} = \frac{8000^2}{(1 - 0.25)^2 \cdot 8000^2} = 1.7$ $a_s \approx 15^\circ$; $\bar{A} \approx 0.0004$ $\frac{w_{max}}{w_0} > 1.12$; $k_1 \approx 1.8$
4	Elbow No. 1 with reduced number of guide vanes	 $D_2 = 8000 - 8000 = 8000 \text{ mm}$, $r = 2000 \text{ mm}$, $t = 1000 \text{ mm}$	$\frac{b_1}{b_2} = 1.0$; $\frac{r}{b_2} = 0.2$; $\bar{A} = 0.0003$
5	Cylindrical stretch	 $D_2 = 8000 - 6000 = 2000 \text{ mm}$, $D_1 = 6000 \text{ mm}$	$\frac{l_1}{b_1} = \frac{6000}{8000} = 0.75$; $\bar{A} = 0.0003$
6	Elbow No. 2; guide vanes as for elbow No. 1	 $D_2 = 8000 - 8000 = 8000 \text{ mm}$, $r = 1000 \text{ mm}$, $t = 2200 \text{ mm}$	$\frac{b_3}{b_4} = 1.0$; $\frac{r}{D_2} = 0.2$

TABLE 1-12

tunnel (Figure 1-18)

Area ratio $\frac{F_0}{F_t}$	$\left(\frac{P_0}{F_t}\right)^2$	w_t , m/sec	$Re = \frac{w_t D_{ht}}{\nu}$	ζ_{lt}	λ_t	$\zeta_{frt} = \frac{\zeta_t}{D_{ht}}$	$\zeta_t = \zeta_{lt} + \zeta_{frt}$	$\zeta_t \times \left(\frac{P_0}{F_t}\right)^2$	Basis for the determination of ζ_t (reference to diagram)
1.0	1.0	60	$2.0 \cdot 10^7$	0.13	—	—	0.13	0.130	4-27
$\left(\frac{5000}{5350}\right)^2 = 0.875$	0.77	52.5	$1.9 \cdot 10^7$	0.05	0.01	0.016	0.066	0.051	5-2
$\frac{F_0}{F_{in}} = \frac{5000^2}{0.75 \cdot 8000^2} = 0.52$	0.27	31	$1.8 \cdot 10^7$	0.19	0.011	0.01	0.20	0.054	5-1
$\frac{\frac{x}{4} \cdot 5000^2}{8000^2} = 0.306$	0.096	18	10^7	0.18	0.011	0.015	0.195	0.019	6-32; ζ is increased by 1.2 in order to allow for the influence of the diffuser placed before it
0.306	0.096	18	10^7	—	0.011	0.008	0.008	0.001	2-3
0.306	0.096	18	10^7	0.15	0.011	0.015	0.165	0.016	6-32

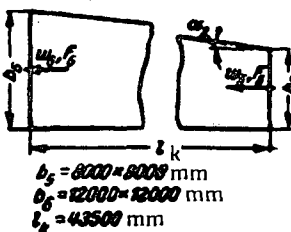
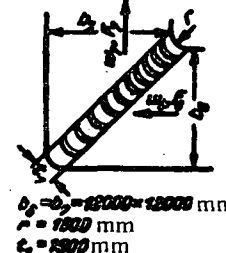
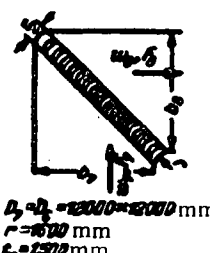
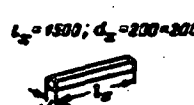
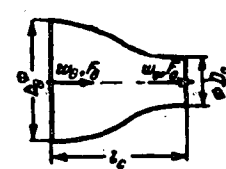
No. of turn- nel ele- ment	Type of element	Plan and dimensions of element	Geometric parameters of the element
7	Second diffuser	 <p> $b_6 = 8000 \times 8000 \text{ mm}$ $b_7 = 12000 \times 12000 \text{ mm}$ $l_k = 13500 \text{ mm}$ </p>	$\alpha_1 = 5.5^\circ; n = \frac{F_6}{F_5} = \left(\frac{12000}{8000} \right)^2 = 2.25$ $\frac{w_{\max}}{w_0} \approx 1.1; k_1 \approx 1.8$
8	Elbow No. 3; same conditions as elbow No. 1	 <p> $b_6 = b_7 = 12000 \times 12000 \text{ mm}$ $r = 15200 \text{ mm}$ $l_k = 13500 \text{ mm}$ </p>	$\frac{b_7}{b_6} = 1.0; \frac{r}{D_6} = 0.13$
9	Elbow No. 4; same conditions as elbow No. 3, but the number of guide vanes is normal	 <p> $b_6 = b_7 = 12000 \times 12000 \text{ mm}$ $r = 15200 \text{ mm}$ $l_k = 13500 \text{ mm}$ </p>	$\frac{b_7}{b_6} = 1.0;$ $\frac{r}{D_6} = 0.13$
10	Honeycomb (coated sheet iron)	 <p> $l_x = 1500; d_x = 200 \times 200$ </p>	$\frac{l_x}{d_x} = 7.5; \bar{l} = \frac{F_x}{F_i} = 0.9;$ $\bar{\Delta} = \frac{0.2}{200} = 0.001$
11	Nozzle	 <p> $b_6 = 5000 \text{ mm}$ $b_7 = 12000 \times 12000 \text{ mm}$ $l_c = 13500 \text{ mm}$ </p>	$\alpha_2 \approx 35^\circ;$ $n = \frac{12000^2}{\frac{\pi}{4} \cdot 5000^2} = 7.35$

TABLE 1-12 (cont'd)

Area ratio $\frac{F_0}{F_l}$	$\left(\frac{F_0}{F_l}\right)^2$	w_l , m/sec	$Re = \frac{w_l D_{hl}}{\nu}$	ϵ_{ll}	λ_l	$\zeta_{frl} = \frac{l_l}{D_{hl}}$	$\zeta_l = \epsilon_{ll} + \zeta_{frl}$	$\zeta_l \times \left(\frac{F_0}{F_l}\right)^2$	Basis for the determination of ζ_l (reference to diagram)
0.306	0.096	18	10^7	0.046	0.011	0.011	0.057	0.006	5-1
$\frac{\pi}{4} \cdot \frac{5000^2}{12000^2} = 0.137$	0.0181	8.2	$6.5 \cdot 10^6$	0.20	0.011	0.015	0.215	0.004	6-32
0.137	0.0181	8.2	$6.5 \cdot 10^6$	0.21	0.011	0.015	0.225	0.004	6-32
$\frac{0.137}{0.9} = 0.152$	0.0232	9.1	$\frac{w_l d_x}{\nu} = -1.2 \cdot 10^8$	0.11	0.060	0.45	0.56	0.013	$\zeta = \zeta_{in} + \zeta_{ex} + \zeta_{fr}$ $\zeta_{in} \approx 1 - \bar{f}$ (diagram 3-1); $\zeta_{ex} = (1 - \bar{f})^2$ (diagram 4-1); $\zeta_{fr} = \lambda \frac{l_x}{d_x}$ 3-7
7.35	54	60	$2 \cdot 10^7$	—	0.008	0.003	0.003	0.003	$\sum_{l=1}^{11} \zeta_{ol} = 0.301 \approx 0.30$

Example 1-3. Low-velocity closed-circuit wind tunnel with an open throat

A plan of the wind tunnel is shown in Figure 1-18.

Given:

- 1) diameter of the exit section of the nozzle outlet:

$$D_0 = 5.00 \text{ m};$$

- 2) length of the test section $l_{t.s.} = 8.00 \text{ m}$;

- 3) flow velocity in the test section (nozzle outlet) $w_0 = 60 \text{ m/sec}$;

- 4) air temperature $t \approx 20^\circ \text{C}$;

- 5) kinematic viscosity $\Delta = 1.5 \times 10^{-5} \text{ m}^2/\text{sec}$;

- 6) tunnel: concrete; state of the internal surface: average; roughness of surface $A = 2.5 \text{ mm}$ (cf. Table 2-1, B).

At low stream velocities the variation of the pressure and temperature along the tunnel can be neglected in hydraulic calculation. Therefore, it is convenient here to use the second method of summing the losses: summation of the reduced resistance coefficients of the separate elements (cf. § 1-8).

The calculation of tunnel resistance is given in Table 1-12. According to this table the total resistance is:

$$\Delta H_{sys} = \sum_i^{11} \zeta_i \frac{T w_0^2}{2g} = 0.30 \frac{1.22}{19.6} 60^2 \approx 67 \text{ [kg/m}^2\text{]}.$$

The rate of flow of air through the nozzle is:

$$Q = w_0 F_0 = 60 \cdot 19.6 = 1175 \text{ m}^3/\text{sec}.$$

The power on the fan rotor at a fan efficiency $\eta_{ov} \approx 0.7$ is equal to:

$$N = \frac{Q \Delta H_{sys}}{102 \eta_{ov}} = \frac{1175 \cdot 67}{102 \cdot 0.7} = 1100 \text{ kw.}$$

The concept of "quality" of the tunnel is used in aerodynamic calculations. The tunnel quality λ_{tun} is defined as the inverse of the losses in it. In the given case:

$$\lambda_{tun} = \frac{1}{\sum \zeta_i} = \frac{1}{0.30} \approx 3.3.$$

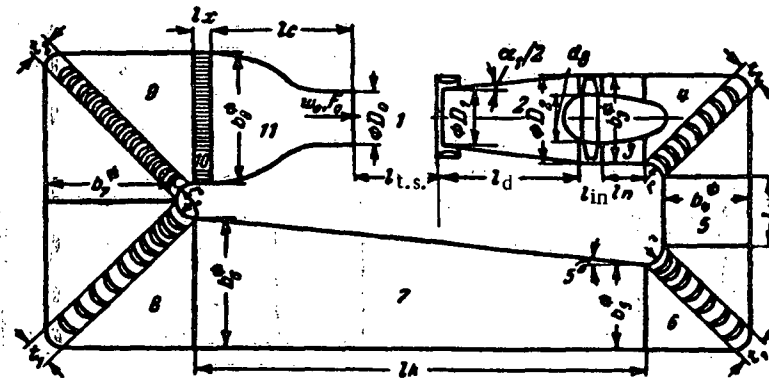


FIGURE 1-18. Plan of a closed-circuit open-throat wind tunnel (dimensions in meters):

$$D_0 = 5.00; D_1 = 5.35; D_2 = 8.00;$$

$$l_s = 1.50; l_{t.s.} = 8.00; l_d = 13.50;$$

$$d_{in} = 4.00; b_1 = 8.00; b_2 = 8.00; b_3 = 8.00; l_{in} = 2.00; l_n = 5.00; l_t = 6.00; l_k = 43.50;$$

$$b_4 = 12.00; b_5 = 12.00; b_6 = 12.00; l_1 = 2.20; l_x = 1.50; l_e = 13.50; r = 1.60; \alpha_1 = 7^\circ; \alpha_2 = 5^\circ.$$

Section Two

STREAM FLOW THROUGH STRAIGHT PIPES AND CHANNELS *(Friction coefficients and roughness)*

2-1. LIST OF SYMBOLS

- F_o = area of conduit cross section, m^2 ;
 S_o = friction surface, m^2 ;
 H_o = perimeter of the conduit cross section, m;
 D_o = diameter of the conduit cross section, m;
 D_h = hydraulic diameter of the conduit cross section = $4 \times$ hydraulic radius;
 D_{in}, D_{out} = inner and outer diameters of an annular pipe, m;
 a_o, b_o = sides of the rectangular cross section of a conduit, m;
 l = length, m;
 Δ = mean height of the roughness peaks of the conduit walls, m;
 $\bar{\Delta}$ = relative roughness of the walls;
 w_o = mean flow velocity over the conduit cross section, m/sec ;
 ΔH = pressure losses, kg/m^2 ;
 ΔH_{fr} = frictional pressure losses, kg/m^2 ;
 λ = friction coefficient of referred length (l/Dia) of conduit;
 ζ = friction coefficient of conduit length considered;
 Re = Reynolds number.

2-2. EXPLANATIONS AND PRACTICAL RECOMMENDATIONS

1. The friction losses through a straight conduit of constant cross section are calculated by the Darcy-Weisbach formula:

$$\Delta H_{fr} = \frac{\lambda}{4} \frac{S_o \tau w_0^2}{F_o \frac{2g}{m^2}} \quad (2-1)$$

or

$$\Delta H_{fr} = \lambda \frac{l}{D_h} \cdot \frac{\tau w_0^2}{2g} = \zeta \frac{\tau w_0^2}{2g} \left[\frac{\text{kg}}{\text{m}^2} \right] \quad (2-2)$$

where

$$\left. \begin{aligned} D_h &= D_o; \\ \text{for a circular section, } & \\ D_h &= 2 \frac{a_o b_o}{a_o + b_o}; \end{aligned} \right\} \quad (2-3)$$

* The engineering unit of measurement of H_{fr} for water is meters: $\Delta H_{fr} = \zeta \frac{w_0^2}{2g}$ [m].

for a rectangular section, and

$$D_h = D_{\text{out}} - D_{\text{in}} \quad \left. \right\}$$

(2-3) cont'd

for an annular section.

2. The resistance to fluid motion at laminar flow is due to the viscosity forces which occur during the motion of one layer of a fluid relative to an adjacent one. Viscosity forces are proportional to the stream velocity. Due to the predominance of these forces at laminar flow, even the flow past protuberances of a rough surface is smooth. As a result, a small amount of roughness has no effect on the magnitude of the resistance, and the friction coefficient at laminar flow is a function of the Reynolds number only ($\text{Re} = \frac{\omega_0 D_h}{\nu}$).

3. An increase in the value of Re is accompanied by an increase in the inertia forces which are proportional to the square of the velocity. At a certain value of Re the flow becomes turbulent. This flow condition is characterized by the appearance of cross-current velocities and by the resulting mixing of the fluid in the whole stream. In turbulent flow the resistance to motion, caused by an exchange of momentum between fluid masses moving in a random motion, is much greater than in laminar flow*.

In the case of a rough wall surface, the flow past the protuberances is accompanied by jet separation, and the friction coefficient becomes a function not only of Re, but also of the relative roughness $\bar{A} = \frac{A}{D_h}$.

4. Conduits can be either smooth or rough, and the roughness can be either uniform or nonuniform. The two types of roughness differ in the shape of the protuberances, dimensions, spacing, etc. Most industrial pipes are nonuniformly rough.

5. The mean height A of the roughness protuberances is called the absolute geometric roughness. The ratio of the mean height of the protuberances to the pipe diameter, i.e., $\bar{A} = \frac{A}{D_h}$, is called the relative roughness. Since the geometric characteristics of the

roughness cannot uniquely define the pipe resistance, we introduce the concept of hydraulic or equivalent roughness, which is determined by measuring the resistance.

6. The equivalent roughness is a function of:

a) the material and method of manufacture of a pipe. Thus, cast-iron pipes manufactured by centrifugal casting are smoother than those cast by conventional methods; seamless steel pipes are less rough than welded ones, etc. Pipes manufactured by the same method have, as a rule, the same equivalent roughness, independent of their diameter;

b) the properties of the medium flowing through a pipe. The influence of the fluid on the inner surface of a pipe can result in corrosion of the walls, the formation of protuberances, and the deposition of scale;

c) the length of time the pipe has been in use.

* At the same time, since the friction coefficient λ is always determined as the ratio of the loss of pressure to the dynamic pressure $\left(\lambda = \frac{\Delta H_{\text{fr}}}{\frac{l}{D_h} \frac{\rho w_0^2}{2g}} \right)$, the magnitude of λ will be larger at laminar flow than turbulent flow, when ΔH_{fr} is directly proportional to the velocity.

b) the zone in which the curves obtained for pipes with different roughness coincide with the Blasius curve /2-57/ for smooth pipes:

$$\lambda = \frac{0.3164}{Re^{0.25}}. \quad (2-5)$$

The accuracy of this expression decreases with an increase of the relative roughness;

c) the zone in which the resistance curves diverge from each other and from the straight line (2-5) for pipes of different roughness. The values of friction coefficients in certain ranges of Re^* increase with an increase in relative roughness.

The third regime of flow is called square-law flow, flow at completely rough walls, or turbulent flow, and is characterized by friction coefficients independent of Re and constant for a given roughness.

8. The same three regimes of flow are also observed in the friction-coefficient curves $\lambda = f(Re, \Delta)$ for nonuniform roughness (industrial pipes); however, the trough in the transition region of the curves corresponding to uniform roughness, is lacking, since here the friction-coefficient curves drop gradually and smoothly, reaching the lowest position at turbulent flow.

9. It follows from Nikuradze's resistance formulas /2-66/ for rough pipes, and Filonenko-Al'tshul's resistance formula /2-8, 2-48/ for smooth pipes, that pipes with uniform roughness can be considered as hydraulically smooth if

$$\bar{\Delta} < \bar{\Delta}_{lim},$$

where

$$\bar{\Delta}_{lim} = \left(\frac{\Delta}{D_h} \right)_{lim} = \frac{18 \lg Re - 16.4}{Re}. \quad (2-6)$$

From this it follows, by using Blasius's formula, that for $Re < 10^5$

$$\bar{\Delta}_{lim} \approx 17.85 Re^{-0.875}. \quad (2-6')$$

For the case of nonuniform roughness the following formula will give results which are accurate within 3 to 4 % (Al'tshul' /2-14/ and Lyatkher /2-31/):

$$\Delta_{lim} \approx \frac{23}{Re}. \quad (2-7)$$

It follows that the limiting Reynolds numbers at which the influence of roughness begins to be felt are:

for uniform roughness ($Re \approx 10^5$)

$$Re'_{lim} = \frac{26.9}{\Delta^{1.143}}. \quad (2-8)$$

* The increase of λ ceases in these ranges of Re .

for nonuniform roughness

$$Re'_{lim} \approx \frac{23}{\Delta}. \quad (2-9)$$

10. The limiting value of Reynolds number at which the square law of resistance starts to apply is determined at uniform roughness by the formula:

$$Re''_{lim} = \frac{217.6 - 382.2 \lg \Delta}{\Delta}, \quad (2-10)$$

which follows from Nikuradze's formulas /2-66/ for the transition and square-law regions.

For the case of nonuniform roughness the following formula will give results which are accurate within 3 to 4% (Al'tshul' /2-14/ and Lyatkher /2-31/):

$$Re''_{lim} \approx \frac{560}{\Delta}. \quad (2-11)$$

11. At laminar flow ($Re \approx 2000$), the friction coefficient λ is independent of the wall roughness and for a circular pipe is determined by formula (2-4) or by curve (a) of diagram 2-1.

For rectangular pipes with sides ratio $0 < \frac{a_0}{b_0} < 1.0$, the friction coefficient is given by the formula:

$$\lambda_r = k_r \lambda. \quad (2-12)$$

where λ_r = friction coefficient for conduits of rectangular section; λ = friction coefficient for conduits of circular section; k_r = coefficient allowing for the influence of the value of the sides ratio $\frac{a_0}{b_0}$ /2-42/.

For annular pipes made from two concentric cylinders (pipe within a pipe) of diameters D_{in} and D_{out} , respectively, the friction coefficient is determined by:

$$\lambda_{an} = k_a \lambda, \quad (2-13)$$

where λ_{an} = friction coefficient of an annular pipe; λ = friction coefficient of a circular pipe; k_a = coefficient allowing for the influence of the diameter ratio

$$\frac{D_{in}}{D_{out}}. \quad (2-42)$$

12. The friction coefficient λ for circular conduits with hydraulically smooth walls in the critical region ($2000 \leq Re \leq 4000$) can be determined from the curve $\lambda = f(Re)$ of diagram 2-2.

13. The friction coefficient λ for circular conduits with hydraulically smooth walls at $Re > 4000$ (turbulent flow) can be determined from the curve $\lambda = f(Re)$ of diagram 2-2, or from Filolenko-Al'tshul's formula /2-8 and 2-48/*:

* This formula is almost the same as the formulas obtained by Konakov /2-29/, Murin /2-32/, and Yakimov /2-56/.

$$\lambda = \frac{1}{(1.8 \lg Re - 1.64)^2} . \quad (2-14)$$

14. The friction coefficient λ of circular pipes with uniform roughness in the transition region, i.e., within the limits

$$\frac{26.9}{\Delta^{1.143}} < Re < \frac{217.6 - 382.4 \lg \Delta}{\Delta} ,$$

is determined from the curve $\lambda = f(Re, \Delta)$ of diagram 2-3 or from Nikuradze's formula /2-66/:

$$\lambda = \frac{1}{[a_1 + b_1 \lg(Re \sqrt{\lambda}) + c_1 \lg \Delta]^2} . \quad (2-15)$$

where at $3.6 < \Delta Re \sqrt{\lambda} < 10$ $a_1 = -0.8$; $b_1 = +2.0$; $c_1 = 0$ (smooth walls);

$$10 < \Delta Re \sqrt{\lambda} < 20 \quad a_1 = +0.068; \quad b_1 = +1.13; \\ c_1 = -0.87;$$

$$20 < \Delta Re \sqrt{\lambda} < 40 \quad a_1 = +1.538; \quad b_1 = 0; \\ c_1 = -2.0;$$

$$40 < \Delta Re \sqrt{\lambda} < 191.2 \quad a_1 = +2.471; \\ b_1 = -0.588; \quad c_1 = -2.588;$$

$$\Delta Re \sqrt{\lambda} \geq 191.2 \quad a_1 = +1.138; \quad b_1 = 0; \\ c_1 = -2.0 \text{ (square law).}$$

15. With the exception of special pipes (for which the values of λ are given separately), the friction coefficient λ of all commercial pipes can be determined in the transition region from the curves of diagram 2-4 plotted on the basis of the Colebrook-White formula /2-58/* :

$$\lambda = \frac{1}{\left[-2 \lg \frac{2.51}{Re \sqrt{\lambda}} + \frac{\Delta}{3.7} \right]^2} . \quad (2-16)$$

or, in the range $0.00008 < \Delta < 0.0125$, by the simplified formula of Al'tshul' /2-11/** :

$$\lambda = 0.1 \left(1.46 \Delta + \frac{100}{Re} \right)^{0.25} \quad (2-17)$$

-
- * The Colebrook-White curves are 2 to 4% higher than the similar curves obtained by Murin /2-32/, and therefore give a certain factor of safety in the calculations. Similar formulas were obtained by Adamov /2-5/, Al'tshul' /2-15/, Filonenko /2-49/, and Frenkel' /2-52/.
 - ** A formula similar to (2-17) was also obtained by Adamov /2-6/, /2-7/. The error introduced by the assumption that the coefficients are actually constant /2-52/ can be neglected in practical calculations.

A simple convenient formula for the determination of λ in the transition region (within the limits $0.0001 \leq \Delta \leq 0.01$) was proposed by Lobaev /2-30/:

$$\lambda = \frac{1.42}{\left(\lg \frac{Re}{\Delta}\right)^2}. \quad (2-18)$$

16. With the exception of special pipes (for which the value of λ is given separately), the friction coefficient λ of all circular pipes can be determined in the square-law region (that is roughly at $Re > \frac{560}{\Delta}$) for any type of roughness (uniform or nonuniform) from the curve of diagram 2-5 plotted on the basis of the Prandtl-Nikuradze formula /2-40/ and /2-66/*:

$$\lambda = \frac{1}{2 \lg \left(\frac{3.7}{\Delta} \right)^2}. \quad (2-19)$$

17. At turbulent flow the friction coefficient of rectangular pipes with small sides ratio ($0.5 \leq \frac{a_0}{b_0} \leq 2.0$) can be determined in the same way as for circular pipes. The friction coefficient of annular pipes can be determined by the formula:

$$\lambda_{an} = k_s \lambda, \quad (2-20)$$

where k_s is determined from the data of Ginevskii and Solodkin /2-21/ given in curve (c) of diagram 2-1 as a function of the diameter ratio $\frac{D_{in}}{D_{out}}$ and Re .

At $\frac{D_{in}}{D_{out}} = 1.0$ the annular pipe becomes a plane pipe, and therefore the friction coefficient of a plane pipe is determined by the same formula (2-20), with k_s determined for $\frac{D_{in}}{D_{out}} = 1.0$.

18. When the friction coefficients are determined as under points 14 to 17, the values of the pipe roughness Δ to be used are those given in Table 2-1. These values of Δ apply to formula (2-19).

19. The resistance of steel pipes with welded joints, which lead to the formation of metal burrs, is higher than the resistance of seamless pipes /2-52/. The additional resistance of welded pipes when the joints are located at a distance $\frac{b_j}{D_0} \geq 30$ from each other can be roughly considered equal to the resistance of a restrictor ξ_d **.

In the range $\frac{b_j}{D_0} \leq 30$ the influence of the joints decreases with the decrease of the relative distance between them, so that

$$\xi_j = k_s \xi_d. \quad (2-21)$$

* The error introduced by the assumption that the coefficients are actually constant /2-52/ can be neglected in practical calculations

** New experiments for more accurate determination of the influence of joints on pipe resistance are being conducted.

where k_4 is the correction factor determined as a function of $\frac{l_j}{D_0}$ from curve (a) of diagram 2-6; ζ_d is determined as a function of $\frac{d}{D_0}$ from curve (b) of diagram 2-6.

The total resistance of a pipe section with joints is equal to

$$\zeta = z \left(\lambda \frac{l_j}{D_0} + \zeta_j \right). \quad (2-22)$$

where z is the number of joints in the pipe section to be calculated; ζ_j is the resistance coefficient of the joint.

20. In practice the resistance of steel pipes with coupled joints can be considered equal to the resistance of welded pipes /2-52/.

When pipes made from cast iron are being calculated, the additional resistance caused by the presence of bell-and-spigot joints can be neglected.

21. Shevelev's formula /2-52/, can be used to calculate the increase in the coefficient of friction of steel and cast-iron water pipes through their service life:

1) in the transition region, defined by the condition $Re = \frac{\omega_0 D_0}{v} < 9.2 \cdot 10^5 D_0$,

$$\lambda = \left(\frac{1.5 \cdot 10^{-6}}{D_0} + \frac{1}{Re} \right)^{0.3}; \quad (2-23)$$

2) in the square-law region, defined by the condition $Re \geq 9.2 \cdot 10^5 D_0$.

$$\lambda = \frac{0.021}{D_0^{0.3}}, \quad (2-24)$$

where D_0 is in meters.

22. The friction coefficient λ of reinforced rubber sleeves, whose characteristics are given in diagram 2-8, is independent of the Reynolds number for $Re > 4000$, due to the considerable roughness of these sleeves. The value of λ increases with the increase of the sleeve diameter, since this increase is accompanied by an increase in the height of the internal seams (Tol'tsman and Shevelev /2-46/).

When the pressure losses are determined by (2-2), the diameter to be used is not the nominal sleeve diameter d_{nom} but the diameter d_{cal} calculated according to curve (b) of diagram 2-8 as a function of the mean internal pressure.

23. The friction coefficient λ of smooth rubber sleeves, whose characteristics are given in diagram 2-9, can be determined by the Tol'tsman-Shevelev formula /2-46/:

$$\lambda = \frac{A}{Re^{0.265}}, \quad (2-25)$$

where, for $5000 \leq Re = \frac{\omega_0 d_{nom}}{v} \leq 120,000$, A varies from 0.38 to 0.52 depending on the quality of the rubber sleeve. When the pressure losses are being determined by (2-2), the value of the calculated diameter is to be determined on the basis of the mean internal pressure from curve (b) of diagram 2-9.

24. The friction coefficient λ of smooth reinforced rubber sleeves is determined from the curves of λ as a function of $Re = \frac{w_0 d_{\text{nom}}}{\nu}$, given in diagram 2-10 for different values of the mean internal pressure and d_{nom} .

When the pressure loss is being determined by (2-2), the diameter to be used is not the nominal sleeve diameter but the calculated diameter, and the sleeve length is to be multiplied by a correction coefficient k , given in curves (b) and (c) of diagram 2-10 as a function of the mean internal pressure.

25. The total resistance of large-diameter pipes (300 to 500 mm) of rubberized material used for mine ventilation, usually with connections made by means of wire rings closed at the ends by pipe sockets (Figure 2-2), is equal to the sum of the frictional resistance and the resistance of the connections:

$$\zeta = \frac{\Delta H}{\frac{\gamma w_0^2}{2g}} = z \left(\lambda \frac{l_j}{D_0} + \zeta_c \right). \quad (2-26)$$

where z is the number of connections; λ = friction coefficient of unit relative length of the pipe, determined as a function of the Reynolds number $Re = \frac{w_0 D_0}{\nu}$ for different degrees of tension, small with large wrinkles and fractures, medium with small wrinkles, and large without wrinkles (cf. diagram 2-11); l_j = distance between joints; m; D_0 = pipe diameter, m; ζ_c = resistance coefficient of one connection, determined as a function of the Reynolds number (cf. diagram 2-11).

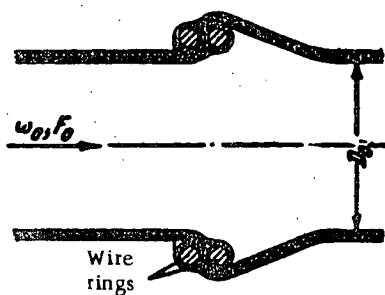


FIGURE 2-2. Circular pipe from tar-paulin-type rubberized material with a ring connection.

26. The friction coefficients λ of plywood pipes (made from birch plywood with the grain running lengthwise) are determined on the basis of the data of Adamov and Idel'chik /2-3/, given in diagram 2-12.

27. All the values of λ recommended above apply to Mach numbers $M = \frac{w_0}{a}$ not larger than 0.75 to 0.80.

28. When determining the relative roughness of the walls of a section, the data given in Table 2-1 can be used.

2-3. ROUGHNESS OF PIPES AND CHANNELS

TABLE 2-1

Group	Type of pipe and materials	State of pipe surface and conditions of use	Δ , mm	Reference
A. Metal pipes				
I	Seamless pipes made from brass, copper lead or aluminum	Commercially smooth	0.0015–0.0100	/2-61, 2-65/
		The same	0.015–0.06	
II	Seamless steel pipes (commercial)	1. New, unused	0.02–0.10*	/2-22, 2-53, 2-63, 2-68/
		2. Cleaned after many years of use	Up to 0.04	/2-65/
		3. Bituminized	Up to 0.04	/2-65/
		4. Superheated-steam pipes of heating systems and water pipes of heating systems with deaeration and chemical treatment of running water	0.10	/2-33/
		5. After one year of use in gas pipelines	0.12	/2-22/
		6. After several years of use as tubings in gas wells under various conditions	0.04–0.20	/2-7/
		7. After several years of use as casings in gas wells under various conditions	0.06–0.022	/2-7/
		8. Saturated-steam pipes and water pipes of heating systems with insignificant water leakages (up to 0.5%) and deaeration of water added for making up leakage losses	0.20	/2-33/
		9. Heating-system water pipes independent of their feed source	0.20	/2-18/
		10. Oil pipelines for medium conditions of operation	0.20	/2-33/
		11. Slightly corroded	≈ 0.4	/2-68/
		12. Small depositions of scale	≈ 0.4	/2-68/
		13. Steam pipes in intermittent operation, and condensate pipes in an open condensate system	0.5	/2-33/
		14. Compressed-air ducts from piston compressors and turbocompressors	0.8	/2-33/
		15. After several years of use under various other conditions, i.e., corroded or with small scale deposits	0.15–1.0	/2-7, 2-47, 2-65/
		16. Condensate pipes working intermittently, and water-heating pipes in the absence of deaeration and chemical treatment of the water, with large leakage (up to 1.5–3%)	1.0	/2-33/
		17. Water pipelines in operation	1.2–1.5	/2-53/
		18. Large depositions of scale	≈ 3.0	/2-65/
		19. Pipe surface in poor state. Nonuniform overlapping of pipe joints	>5.0	/2-60/
III	Welded steel pipes	1. New or old pipes in satisfactory state; welded or riveted pipe joints	0.04–0.10	/2-61 and 2-68/
		2. New, bituminized pipes	≈ 0.15	/2-64/
		3. Used pipes, corroded bitumen partially dissolved	≈ 0.10	/2-68/
		4. Used pipes, uniform corrosion	≈ 0.15	/2-68/
		5. Without noticeable unevenness at the joints; lacquered on the inside (layer thickness about 10 mm); satisfactory state of surface	0.3–0.4	/2-62/
		6. Gas main after many years' use	≈ 0.5	/2-68/
		7. With simple or double transverse riveted joints; inside lacquered (layer thickness 10 mm) or without lacquer but not corroded	0.6–0.7	/2-61/

TABLE 2-1 (cont'd)

Group	Type of pipe and materials	State of pipe surface and conditions of use	Δ , mm	Reference
III	Welded steel pipes	8. Lacquer-coated on the inside, but not rust-free; soiled in the process of carrying water, but not corroded 9. Layer deposits; gas mains after 20 years' use 10. With double transverse riveted joints, not corroded; soiled by passage of water 11. Small deposits 12. With double transverse riveted joint, heavily corroded 13. Considerable deposits 14. 25 years' use in municipal gas mains, uneven depositions of resin and naphthalene 15. Pipe surface in poor state; uneven overlap of joints	0.95-1.0 1.1 1.2-1.5 1.5 2.0 2.0-4.0 2.4 $\Delta 5.0$	/2-61/ /2-68/ /2-68, 2-53/ /2-68/ /2-61/ /2-68/ /2-68/ /2-61/
IV	Riveted steel pipes	1. Riveted along and across with one line of rivets; lacquered on the inside (layer thickness 10 mm); satisfactory state of the surface 2. With double longitudinal riveted joints and simple transverse riveted joints lacquered on the inside (layer thickness 10 mm), or without lacquer but not corroded 3. With simple transverse and double longitudinal riveted joints; coated on the inside with tar or lacquer (layer thickness 10 to 20 mm) 4. With four to six longitudinal rows of rivets; long period of use 5. With four transverse and six longitudinal rows of rivets; joints overlapped on the inside 6. Pipe surface in very poor state; uneven overlap of the joints	0.3-0.4 0.6-0.7 1.2-1.3 2.0 4.0 $\Delta 5.0$	/2-61/ /2-61/ /2-61/ /2-61/ /2-61/ /2-61/
V	Roofing steel sheets	1. Not oiled 2. Oiled	0.02-0.04 0.10-0.15	/2-43/ /2-43/
VI	Galvanized steel pipes	1. Bright galvanization, new pipes 2. Ordinary galvanization	0.07-0.10 0.1-0.15	/2-68/ /2-68/
VII	Galvanized sheet steel	1. New pipes 2. Used (in water pipelines)	0.15 0.18	/2-63/ /2-58/
VIII	Cast-iron pipes	1. New ones 2. New, bituminized 3. Asphalt-coated 4. Used water pipes 5. Used and corroded pipes 6. With deposits 7. Considerable deposits 8. Cleaned after many years of use 9. Strongly corroded	0.25-1.0 0.10-0.15 0.12-0.30 1.4 1.0-1.5 1.0-1.5 2.0-4.0 0.3-1.5 Up to 3.0	/2-58/ /2-68/ /2-63/ /2-53/ /2-68/ /2-63 and 2-68/ /2-65 and 2-68/ /2-68/

B. Conduits made from concrete, cement or other materials

I	Concrete pipes	1. Good surface, plaster finish 2. Average conditions 3. Coarse (rough) surface	0.3-0.8 2.5 3-9	/2-68/ /2-68/ /2-68/
II	Reinforced-concrete pipes		2.5	/2-47/

TABLE 2-1 (cont'd)

Group	Type of pipe and materials	State of pipe surface and conditions of use	Δ , mm	Reference
III	Asbestos-cement pipes	1. New 2. Average	0.05-0.10 ≈ 0.60	/2-47/ /2-47/
IV	Cement pipes	1. Smoothed surfaces 2. Nonsmoothed surfaces 3. Mortar in the joints not smoothed	0.3-0.8 1.0-2.0 1.9-6.4	/2-65/ /2-47 and 2-65/ /2-61/
V	Channel with a cement-mortar plaster	1. Good plaster from pure cement with smoothed connections; all unevennesses removed 2. With steel-troweling	0.05-0.22 0.5	/2-61/ /2-47/
VI	Plaster over a metallic grid		10-15	/2-18/
VII	Ceramic salt-glazed channels		1.4	/2-47/
VIII	Slag-concrete tiles		1.5	/2-18/
IX	Slag and alabaster-filling tiles	Carefully finished plates	1.0-1.5	/2-18 and 2-58/

C. Wood, plywood, and glass pipes

I	Wooden pipes	1. Very thoroughly dressed boards 2. Dressed boards 3. Well-fitted undressed boards 4. Undressed boards 5. Wood-stave pipes	0.15 0.30 0.70 1.0 0.6	Tentatively /2-68/ /2-47/
II	Plywood pipes	1. From good-quality birch plywood with transverse grain 2. From good-quality birch plywood with longitudinal grain	0.12 0.03-0.05	/2-3/ /2-3/
III	Glass pipes	Plain glass	0.0015-0.010	/2-63/

2-4. LIST OF THE DIAGRAMS OF FRICTION COEFFICIENTS OF SECTION II

Name of diagram	Source	Number	Note
Conduit. Friction coefficient at laminar flow — $Re < 2000$	Hagen-Poiseuille formula /2-59 and 2-67/	2-1	—
Conduit with smooth walls. Friction coefficient at $Re > 2000$	Al'tshul' /2-8/, Blasius /2-57/, Karman /2-27/, Konakov /2-29/, Murin /2-32/, Nikuradze /2-34/, Prandtl /2-40/, Filonenko /2-48/, Yakimov /2-56/	2-2	Maximum difference of λ according to the various formulas is 3-4%
Conduit with uniform wall roughness. Friction coefficient at $Re > 2000$	Nikuradze /2-66/	2-3	Extrapolation of experimental data
Conduit with nonuniform wall roughness (commercial pipes). Friction coefficient at $Re > 2000$	Adamov /2-5/, Al'tshul' /2-11/, Colebrock /2-58/, Lobaev /2-30/, Murin /2-32/, Filonenko /2-48/, Frenkel' /2-51/	2-4	Maximum difference of λ according to the various formulas is 3-4%
Conduit with rough walls. Friction coefficient. Flow conditions according to square law of resistance ($Re_{lim} > \frac{560}{\Delta}$)	Prandtl /2-40/, Nikuradze /2-66/	2-5	According to a calculating formula
Welded pipe with joints. Friction coefficient	Shevelev /2-52/	2-6	Experimental data. To be used until refined by new experiments
Steel and cast-iron water pipes with allowance for the increase in resistance with use. Friction coefficient	The same	2-7	Experimental data
Steel-reinforced rubber hose. Friction coefficient	Tol'tsman and Shevelev /2-46/	2-8	" "
Smooth rubber hose. Friction coefficient	" "	2-9	" "
Smooth steel-reinforced rubber hose. Friction coefficient	" "	2-10	" "
Pipe from tarpaulin-type rubberized material. Friction coefficient	Adamov	2-11	" "
Plywood pipe (birch with longitudinal grain). Friction coefficient at turbulent flow	Adamov and Idel'chik /2-3/	2-12	" "

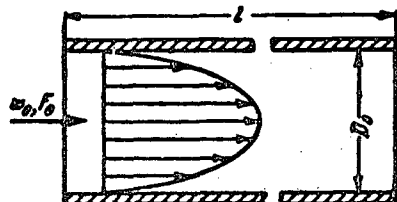
2-5. DIAGRAMS OF FRICTION COEFFICIENTS

Conduit. Friction coefficient at laminar flow. $Re < 2000$

Section II

Diagram 2-1

$$D_h = \frac{4F_0}{\Pi_0}; \quad \Pi_0 = \text{perimeter}$$

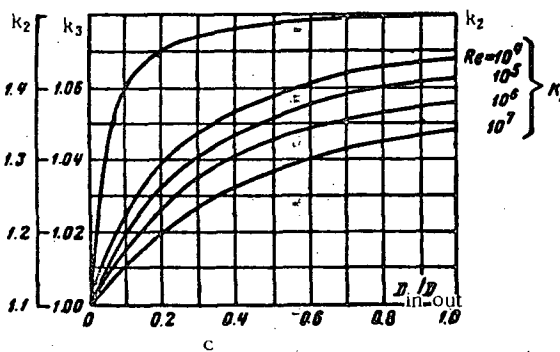
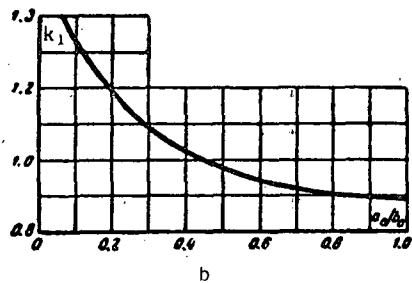
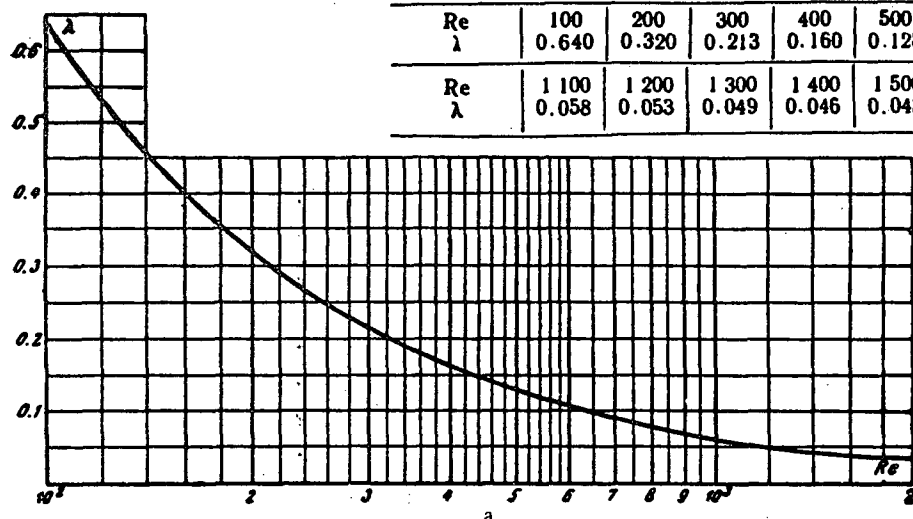


1. Circular section: $\lambda = \frac{\Delta H}{\frac{\gamma w_0^2}{2g} l / D_h} = \frac{64}{Re}$ is determined by curve a.

2. Rectangular section of side ratio $a_0/b_0 = 0-1.0$:

$$\lambda_r = k_1 \lambda_c$$

where k_1 is determined from curve b.



$\frac{a_0}{b_0}$	0	0.1	0.2	0.4	0.6	0.8	1.0
k_1	1.50	1.34	1.20	1.02	0.94	0.90	0.89

$\frac{D_o}{D_h}$	0	0.1	0.2	0.3	0.4	0.5	0.6	0.7	0.8	1.0
-------------------	---	-----	-----	-----	-----	-----	-----	-----	-----	-----

$Re > 2 \cdot 10^2$

k_2	1.0	1.40	1.45	1.47	1.48	—	1.49	—	—	1.50
-------	-----	------	------	------	------	---	------	---	---	------

$Re = 10^4$

k_2	1.0	1.03	1.04	1.05	1.05	1.06	1.06	1.07	1.07	1.07
-------	-----	------	------	------	------	------	------	------	------	------

$Re = 10^5$

k_2	1.0	1.02	1.03	1.04	1.05	1.06	1.06	1.06	1.06	1.06
-------	-----	------	------	------	------	------	------	------	------	------

$Re = 10^6$

k_2	1.0	1.02	1.03	1.04	1.05	1.05	1.05	1.05	1.05	1.06
-------	-----	------	------	------	------	------	------	------	------	------

$Re = 10^7$

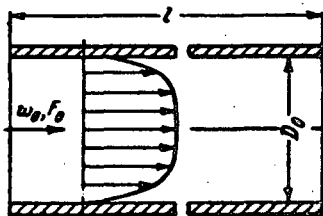
k_2	1.0	1.01	1.02	1.03	1.03	1.04	1.04	1.04	1.05	1.05
-------	-----	------	------	------	------	------	------	------	------	------

Conduit with smooth walls. Friction coefficient at $Re > 2000$

Section II

Diagram 2-2

$$D_h = \frac{4F_0}{P_0}; \quad P_0 = \text{perimeter}$$


 1. Circular and rectangular sections ($\frac{a_0}{b_0} \approx 0.5 + 2.0$):

 1) $2000 < Re < 4000$
 λ is determined from curve a;

 2) $4000 < Re < 100,000$

$$\lambda = \frac{\Delta H}{\gamma w_0^2 \cdot l} = \frac{0.3164}{\sqrt{Re}} \text{ is determined from curve a;}$$

 3) any $Re > 4000$

$$\lambda = \frac{\Delta H}{\gamma w_0^2 \cdot l} = \frac{1}{(1.8 \lg Re - 1.64)^2} \text{ is determined from curves a and b.}$$

 2. Annular section: $\lambda_{an} = k_a \lambda$,

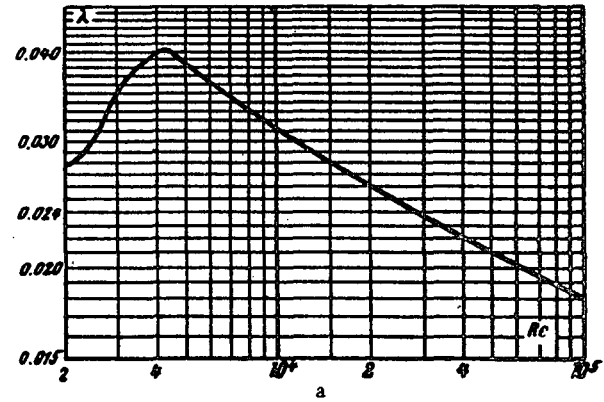
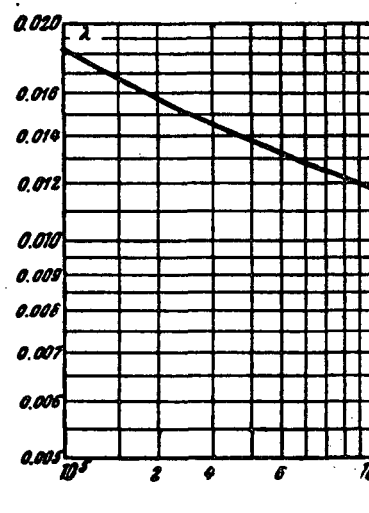
 where k_a is determined from curve c of diagram 2-1;

$$Re = \frac{w_0 D_h}{v}; v \text{ is taken according to § 1-3,b.}$$

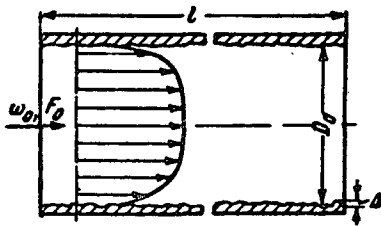
Re	$2 \cdot 10^3$	$2.5 \cdot 10^3$	$3 \cdot 10^3$	$4 \cdot 10^3$	$5 \cdot 10^3$	$6 \cdot 10^3$	$8 \cdot 10^3$	10^4	$1.5 \cdot 10^4$	$2 \cdot 10^4$	$3 \cdot 10^4$	$4 \cdot 10^4$	$5 \cdot 10^4$	$6 \cdot 10^4$	$8 \cdot 10^4$
λ	0.052	0.046	0.045	0.041	0.038	0.036	0.033	0.032	0.028	0.026	0.024	0.022	0.021	0.020	0.019

Re	10^5	$1.5 \cdot 10^5$	$2 \cdot 10^5$	$3 \cdot 10^5$	$4 \cdot 10^5$	$5 \cdot 10^5$	$6 \cdot 10^5$	$8 \cdot 10^5$	10^6	$1.5 \cdot 10^6$	$2 \cdot 10^6$	$3 \cdot 10^6$	$4 \cdot 10^6$	$5 \cdot 10^6$	$8 \cdot 10^6$
λ	0.018	0.017	0.016	0.015	0.014	0.013	0.013	0.012	0.012	0.011	0.011	0.010	0.010	0.009	0.009

Re	10^7	$1.5 \cdot 10^7$	$2 \cdot 10^7$	$3 \cdot 10^7$	$6 \cdot 10^7$	$8 \cdot 10^7$	10^8
λ	0.008	0.008	0.008	0.007	0.007	0.006	0.006



$$D_h = \frac{4F_0}{\Pi_0}; \Pi_0 = \text{perimeter}$$



1. Circular and rectangular sections ($\frac{a_0}{b_0} \approx 0.5 + 2.0$):

$$\lambda = \frac{\Delta H}{\frac{\gamma w_0^2}{2g} \frac{l}{D_h}} = \frac{1}{[a_1 + b_1 \lg(\text{Re} \sqrt{\lambda}) + c_1 \lg \Delta]^2}$$

is determined from curve a and Table 2-2 (p. 69); the values of a_1 , b_1 and c_1 are given below:

$\bar{\Delta} \text{ Re} \sqrt{\lambda}$	a_1	b_1	c_1
3.6-10	-0.800	2.000	0
10-20	0.068	1.130	-0.870
20-40	1.538	0.000	-2.000
40-191.2	2.471	-0.588	-2.588
>191.2	1.138	0	-2.000

2. Annular section:

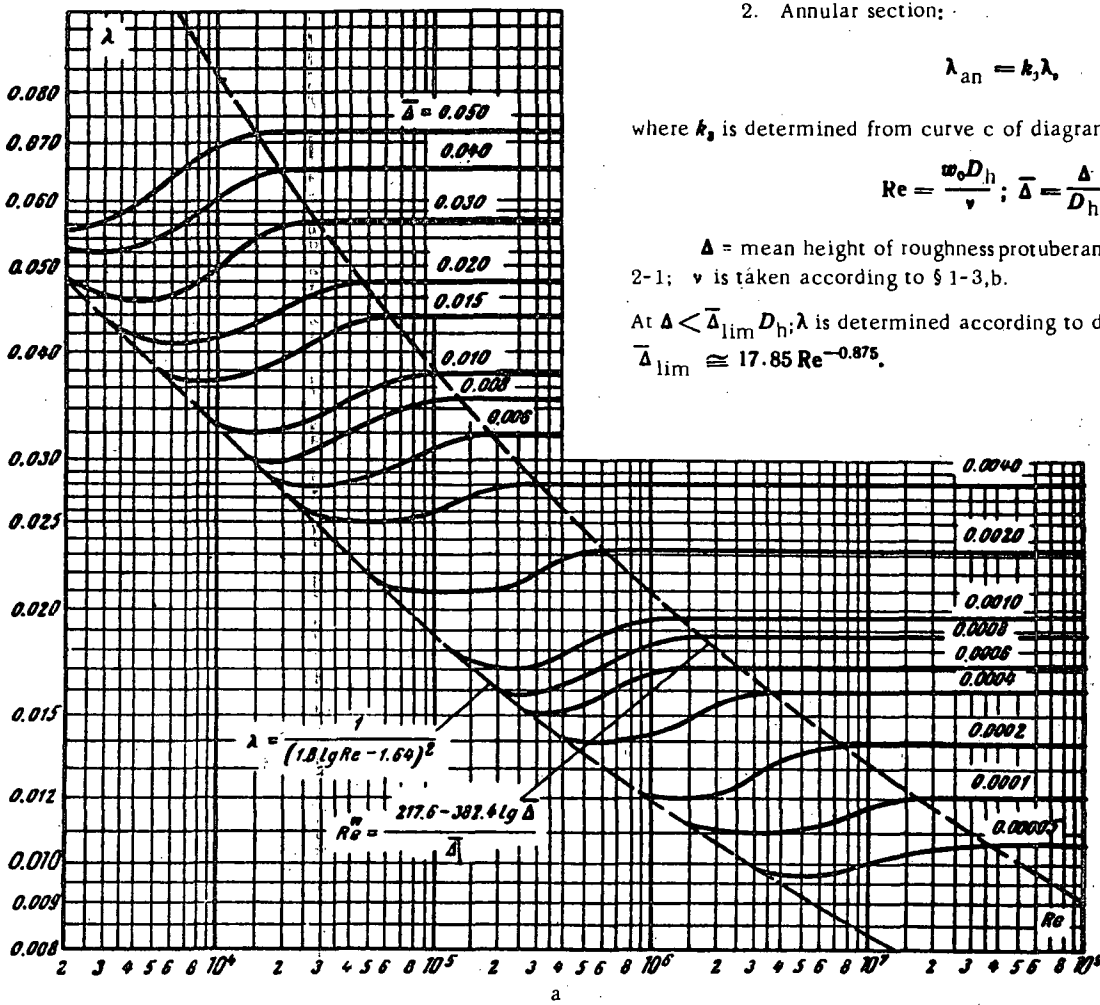
$$\lambda_{an} = k_s \lambda_s$$

where k_s is determined from curve c of diagram 2-1;

$$\text{Re} = \frac{w_0 D_h}{v}; \bar{\Delta} = \frac{\Delta}{D_h};$$

Δ = mean height of roughness protuberances according to Table 2-1; v is taken according to § 1-3,b.

At $\Delta < \bar{\Delta}_{lim} D_h$, λ is determined according to diagram 2-2, where $\bar{\Delta}_{lim} \cong 17.85 \text{ Re}^{-0.875}$.



Conduit with uniform wall roughness. Friction coefficient
at $Re > 2000$ (continuation of diagram 2-3)

Section II
Table 2-2

Values of λ

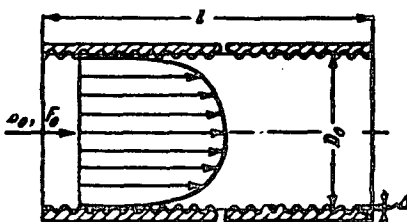
Re	$2 \cdot 10^3$	$4 \cdot 10^3$	$6 \cdot 10^3$	10^4	$2 \cdot 10^4$	$4 \cdot 10^4$	$6 \cdot 10^4$	10^5	$2 \cdot 10^5$
$\bar{A} = \frac{A}{D_h}$									
0.05	0.056	0.060	0.063	0.069	0.072	0.072	0.072	0.072	0.072
0.04	0.053	0.053	0.055	0.060	0.065	0.065	0.065	0.065	0.065
0.03	0.048	0.046	0.046	0.050	0.056	0.057	0.057	0.057	0.057
0.02	0.048	0.042	0.041	0.042	0.044	0.048	0.049	0.049	0.049
0.015	0.048	0.042	0.038	0.037	0.039	0.042	0.044	0.044	0.044
0.010	0.048	0.042	0.038	0.033	0.032	0.035	0.036	0.038	0.038
0.008	0.048	0.042	0.038	0.033	0.030	0.032	0.033	0.035	0.035
0.006	0.048	0.042	0.038	0.033	0.028	0.028	0.029	0.030	0.032
0.004	0.048	0.042	0.038	0.033	0.027	0.025	0.025	0.026	0.028
0.002	0.048	0.042	0.038	0.033	0.027	0.023	0.021	0.021	0.021
0.001	0.048	0.042	0.038	0.033	0.027	0.023	0.021	0.018	0.017
0.0008	0.048	0.042	0.038	0.033	0.027	0.023	0.021	0.018	0.016
0.0006	0.048	0.042	0.038	0.033	0.027	0.023	0.021	0.018	0.016
0.0004	0.048	0.042	0.038	0.033	0.027	0.023	0.021	0.018	0.016
0.0002	0.048	0.042	0.038	0.033	0.027	0.023	0.021	0.018	0.016
0.0001	0.048	0.042	0.038	0.033	0.027	0.023	0.021	0.018	0.016
0.00005	0.048	0.042	0.038	0.033	0.027	0.023	0.021	0.018	0.016

Values of λ

Re	$4 \cdot 10^3$	$6 \cdot 10^3$	10^4	$2 \cdot 10^4$	$4 \cdot 10^4$	$6 \cdot 10^4$	10^5	$2 \cdot 10^5$	$> 10^5$
$\bar{A} = \frac{A}{D_h}$									
0.05	0.072	0.072	0.072	0.072	0.072	0.072	0.072	0.072	0.072
0.04	0.065	0.065	0.065	0.065	0.065	0.065	0.065	0.065	0.065
0.03	0.057	0.057	0.057	0.057	0.057	0.057	0.057	0.057	0.057
0.02	0.049	0.049	0.049	0.049	0.049	0.049	0.049	0.049	0.049
0.015	0.044	0.044	0.044	0.044	0.044	0.044	0.044	0.044	0.044
0.010	0.038	0.038	0.038	0.038	0.038	0.038	0.038	0.038	0.038
0.008	0.035	0.035	0.035	0.035	0.035	0.035	0.035	0.035	0.035
0.006	0.032	0.032	0.032	0.032	0.032	0.032	0.032	0.032	0.032
0.004	0.028	0.028	0.028	0.028	0.028	0.028	0.028	0.028	0.028
0.002	0.022	0.023	0.023	0.023	0.023	0.023	0.023	0.023	0.023
0.001	0.018	0.018	0.020	0.020	0.020	0.020	0.020	0.020	0.020
0.0008	0.016	0.017	0.018	0.019	0.019	0.019	0.019	0.019	0.019
0.0006	0.015	0.016	0.017	0.017	0.017	0.017	0.017	0.017	0.017
0.0004	0.014	0.014	0.014	0.015	0.016	0.016	0.016	0.016	0.016
0.0002	0.014	0.013	0.012	0.012	0.013	0.014	0.014	0.014	0.014
0.0001	0.014	0.013	0.012	0.011	0.011	0.011	0.011	0.012	0.012
0.00005	0.014	0.013	0.012	0.011	0.010	0.010	0.010	0.010	0.011

Conduit with nonuniform wall roughness (commercial pipes).
Friction coefficient at $Re > 2000$

Section II
Diagram 2-4



$$D_h = \frac{4F_0}{U_0}; \quad U_0 = \text{perimeter}$$

1. Circular and rectangular sections:

$$\lambda = \frac{\Delta H}{\frac{rw_0^2}{2g} l/D_h} = \frac{1}{\left[-2 \lg \frac{2.51}{Re \sqrt{\lambda}} + \frac{\bar{\Delta}}{3.7} \right]^2}$$

$$\text{or within the limits } \bar{\Delta} = 0.00008 + 0.0125$$

$$\lambda = 0.1 \left(1.46 \bar{\Delta} + \frac{100}{Re} \right)^{0.25}$$

is determined from curve a or Table 2-3 (p. 71).

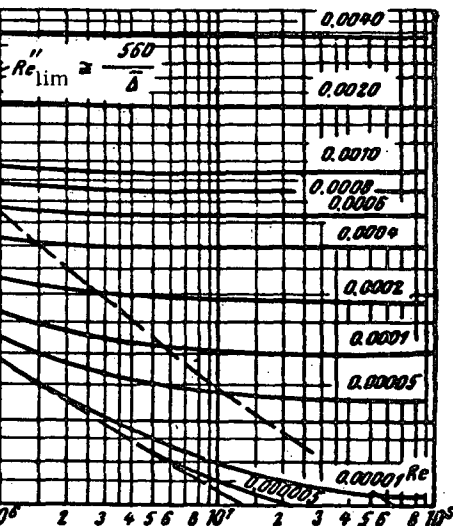
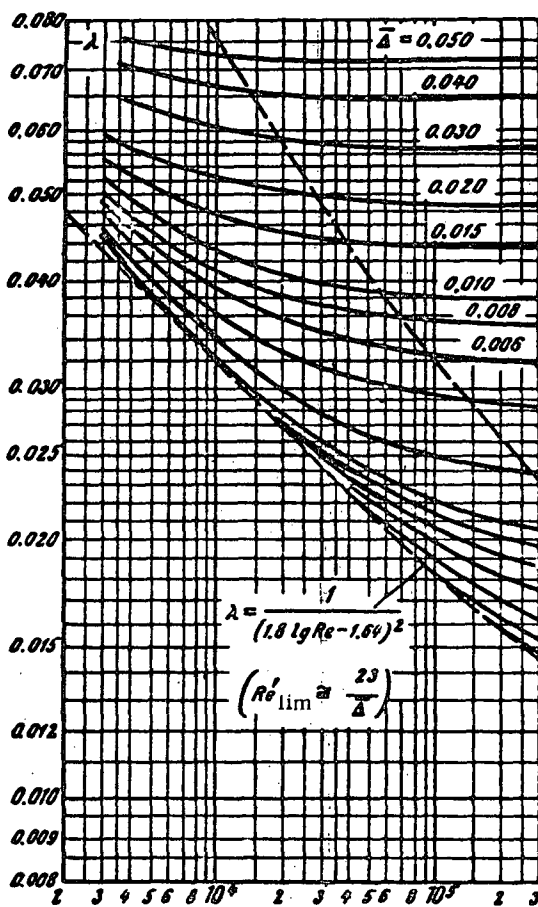
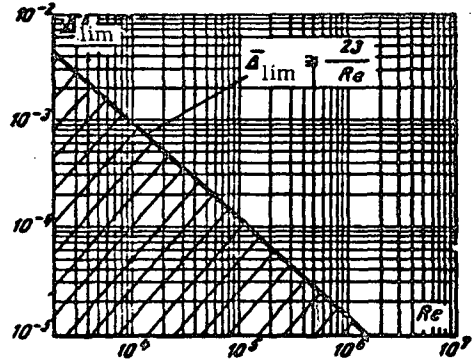
2. Annular section:

$$\lambda_{an} = k \lambda_0$$

where k is determined from curve c of diagram 2-1;

$Re = \frac{w_0 D_h}{v}; \bar{\Delta} = \frac{\Delta}{D_h}; \Delta = \text{mean height of roughness}$
protuberances taken according to Table 2-1; v is taken according to § 1-3, b.

At $\Delta < \bar{\Delta}_{lim}$ $D_h; \lambda$ is determined from diagram 2-2;
 $\bar{\Delta}_{lim}$ is determined from curve b of diagram 2-4.



Conduit with nonuniform wall roughness (commercial pipes).
Friction coefficient at $Re > 2000$

Section II
Table 2-3

Values of λ

Re $\bar{A} = \frac{A}{D_h}$	$3 \cdot 10^3$	$4 \cdot 10^3$	$6 \cdot 10^3$	10^4	$2 \cdot 10^4$	$4 \cdot 10^4$	$6 \cdot 10^4$	10^5	$2 \cdot 10^5$
0.05	0.077	0.076	0.074	0.073	0.072	0.072	0.072	0.072	0.072
0.04	0.072	0.071	0.068	0.067	0.065	0.065	0.065	0.065	0.065
0.03	0.065	0.064	0.062	0.061	0.059	0.057	0.057	0.057	0.057
0.02	0.059	0.057	0.054	0.052	0.051	0.050	0.049	0.049	0.049
0.015	0.055	0.053	0.050	0.048	0.046	0.045	0.044	0.044	0.044
0.010	0.052	0.049	0.046	0.043	0.041	0.040	0.039	0.038	0.038
0.008	0.050	0.047	0.044	0.041	0.038	0.037	0.036	0.035	0.035
0.006	0.049	0.046	0.042	0.039	0.036	0.034	0.033	0.033	0.032
0.004	0.048	0.044	0.040	0.036	0.033	0.031	0.030	0.030	0.028
0.002	0.045	0.042	0.038	0.034	0.030	0.027	0.026	0.026	0.024
0.001	0.044	0.042	0.037	0.032	0.028	0.025	0.024	0.023	0.021
0.0008	0.043	0.040	0.036	0.032	0.027	0.024	0.023	0.022	0.020
0.0006	0.040	0.040	0.036	0.032	0.027	0.023	0.022	0.021	0.018
0.0004	0.036	0.040	0.036	0.032	0.027	0.023	0.022	0.020	0.018
0.0002	0.036	0.040	0.036	0.032	0.027	0.022	0.021	0.019	0.017
0.0001	0.036	0.040	0.036	0.032	0.027	0.022	0.021	0.019	0.017
0.00005	0.036	0.040	0.036	0.032	0.027	0.022	0.021	0.019	0.016
0.00001	0.036	0.040	0.036	0.032	0.027	0.022	0.021	0.019	0.016
0.000005	0.036	0.040	0.036	0.032	0.027	0.022	0.021	0.019	0.016

Values of λ

Re $\bar{A} = \frac{A}{D_h}$	$4 \cdot 10^5$	$6 \cdot 10^5$	10^6	$2 \cdot 10^6$	$4 \cdot 10^6$	$6 \cdot 10^6$	10^7	$2 \cdot 10^7$	$> 10^8$
0.05	0.072	0.072	0.072	0.072	0.072	0.072	0.072	0.072	0.072
0.04	0.065	0.065	0.065	0.065	0.065	0.065	0.065	0.065	0.065
0.03	0.057	0.057	0.057	0.057	0.057	0.057	0.057	0.057	0.057
0.02	0.049	0.049	0.049	0.049	0.049	0.049	0.049	0.049	0.049
0.015	0.044	0.044	0.044	0.044	0.044	0.044	0.044	0.044	0.044
0.010	0.038	0.038	0.038	0.038	0.038	0.038	0.038	0.038	0.038
0.008	0.035	0.035	0.035	0.035	0.035	0.035	0.035	0.035	0.035
0.006	0.032	0.032	0.032	0.032	0.032	0.032	0.032	0.032	0.032
0.004	0.028	0.028	0.028	0.028	0.028	0.028	0.028	0.028	0.028
0.002	0.024	0.023	0.023	0.023	0.023	0.023	0.023	0.023	0.023
0.001	0.021	0.020	0.020	0.020	0.020	0.020	0.020	0.020	0.020
0.0008	0.020	0.019	0.019	0.019	0.019	0.019	0.019	0.019	0.019
0.0006	0.018	0.018	0.017	0.017	0.017	0.017	0.017	0.017	0.017
0.0004	0.017	0.017	0.016	0.016	0.016	0.016	0.016	0.016	0.016
0.0002	0.016	0.015	0.015	0.014	0.014	0.014	0.014	0.014	0.014
0.0001	0.015	0.014	0.013	0.013	0.012	0.012	0.012	0.012	0.012
0.00005	0.014	0.013	0.013	0.012	0.011	0.011	0.011	0.011	0.011
0.00001	0.014	0.013	0.012	0.011	0.010	0.009	0.009	0.009	0.009
0.000005	0.014	0.013	0.012	0.011	0.009	0.009	0.009	0.008	0.008

Conduit with rough walls. Friction coefficient.
Flow conditions according to square law of resistance

$$(Re_{\text{lim}} > \frac{560}{\Delta})$$

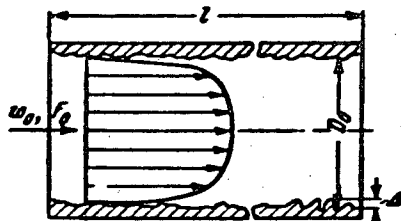
Section II

Diagram 2-5

$$D_h = \frac{4F_0}{U_0}; \quad U_0 = \text{perimeter}$$

1. Circular and rectangular sections:

$$\left(\frac{a_0}{b_0} \approx 0.5 \div 2.0 \right)$$



$$\lambda = \frac{\Delta H}{\frac{\tau w_0^2}{2g} l/D_h} = \frac{1}{\left(2 \lg \frac{3.7}{\Delta} \right)^2}$$

is determined from the curve $\lambda = f(\bar{\Delta})$.

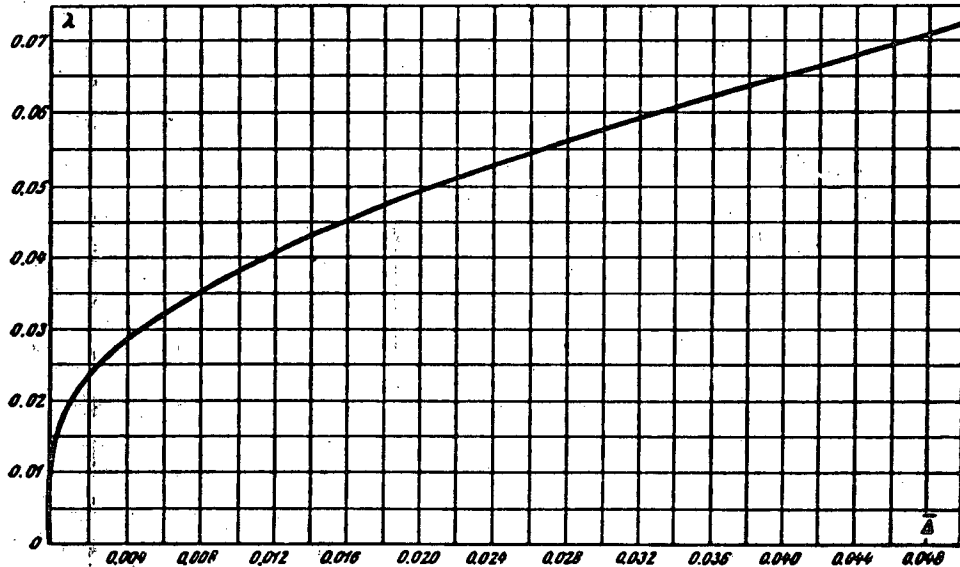
2. Annular section

$$\lambda_{\text{an}} = k_3 \lambda$$

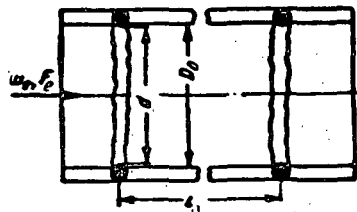
where k_3 is determined from curve c of diagram 2-1;

$$\bar{\Delta} = \frac{\Delta}{D_h}; \quad \Delta = \text{mean height of the roughness protuberances according to Table 2-1}; \quad v \text{ is taken according to § 1-3,b.}$$

$\bar{\Delta} = \frac{\Delta}{D_h}$	0.00005	0.0001	0.0002	0.0003	0.0004	0.0005	0.0006	0.0007	0.0008	0.0009	0.001	0.002	0.003
λ	0.010	0.012	0.013	0.014	0.015	0.016	0.017	0.018	0.018	0.019	0.020	0.023	0.026
$\bar{\Delta} = \frac{\Delta}{D_h}$	0.004	0.005	0.006	0.008	0.010	0.015	0.020	0.025	0.030	0.035	0.040	0.045	0.050
λ	0.028	0.031	0.032	0.035	0.038	0.044	0.049	0.053	0.057	0.061	0.065	0.068	0.072



Welded pipes with joints. Friction coefficient

 Section II
 Diagram 2-6


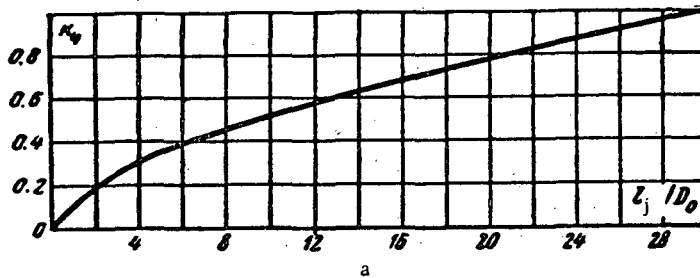
$$\xi = \frac{\Delta H}{\frac{\gamma w_0^2}{2g}} = z \left(\lambda \frac{l_j}{D_0} + \xi_j \right),$$

where z = number of joints in the pipeline; λ = friction coefficient, determined from diagrams 2-2 to 2-5 as a function of $Re = \frac{w_0 D_0}{\nu}$ and $A = A/D_0$; ξ_j = resistance coefficient of one joint:

1) at $\frac{l_j}{D_0} < 30$

$$\xi_j = \frac{\Delta H}{\frac{\gamma w_0^2}{2g}} = k_a \xi_d,$$

$\frac{l_j}{D_0}$	4	8	12	16	20	24	30
k_a	0.30	0.45	0.58	0.68	0.78	0.87	1.00

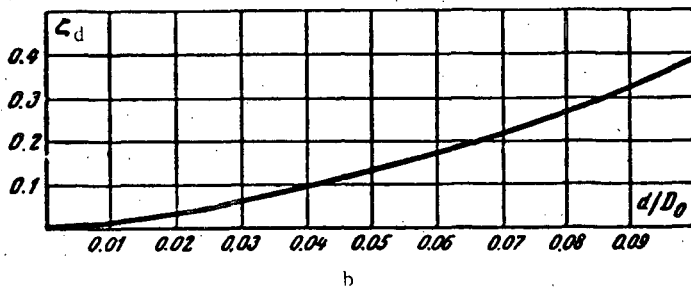


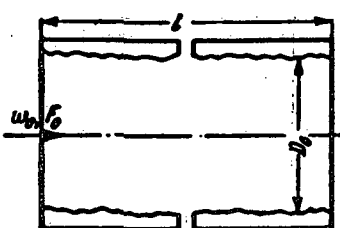
where k_a is determined from curve a as a function of $\frac{l_j}{D_0}$; ξ_d is determined from curve b as a function of $\frac{d}{D_0}$;

2) at $\frac{l_j}{D_0} > 30$

$$\xi_j = \frac{\Delta H}{\frac{\gamma w_0^2}{2g}} = \xi_d,$$

$\frac{d}{D_0}$	0.01	0.02	0.03	0.04	0.05	0.06	0.07	0.08	0.09	0.10
ξ_d	0.015	0.035	0.06	0.09	0.13	0.17	0.27	0.26	0.32	0.38





$$1. \text{Re} = \frac{\omega D_0}{v} < 9.2 \cdot 10^5 D_0;$$

$\lambda = \left(\frac{1.5 \cdot 10^{-6}}{D_0} + \frac{1}{\text{Re}} \right)^{0.3}$ is determined from the curves $\lambda = f(\text{Re}, D_0)$

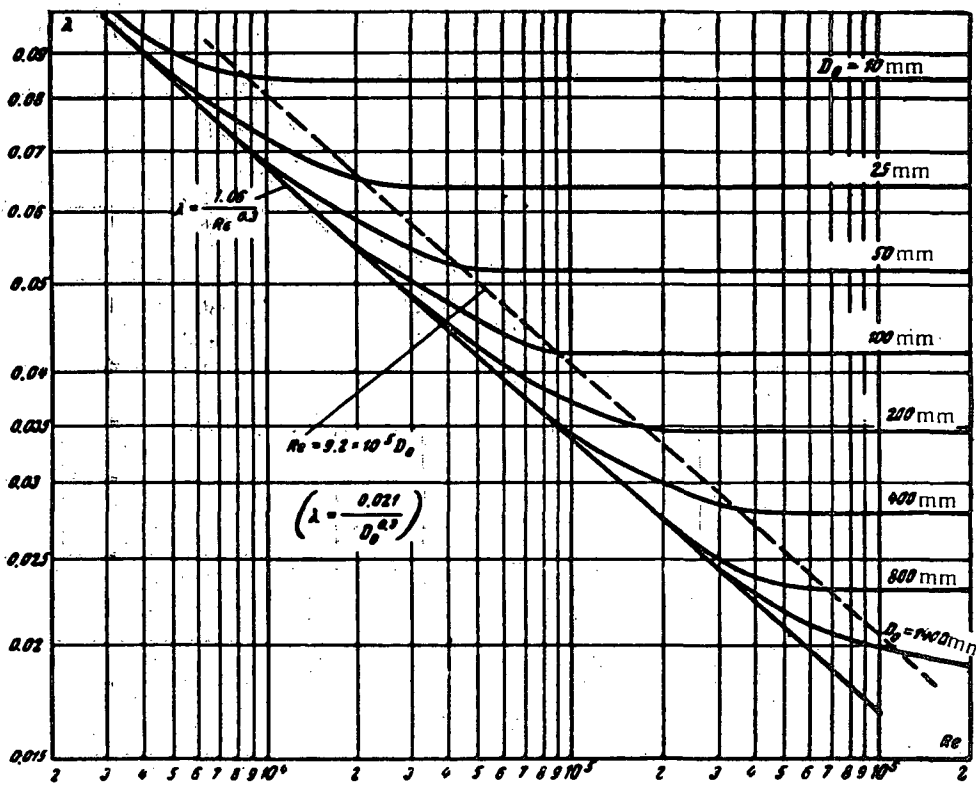
$$2. \text{Re} \geq 9.2 \cdot 10^5 D_0;$$

$\lambda = \frac{0.021}{D_0^{0.3}}$ is determined from the curves $\lambda = f(\text{Re}, D_0)$

(D_0 is in meters; v is taken from § 1-3, b)

Values of λ

D_0 , mm	Re														
	$3 \cdot 10^3$	$4 \cdot 10^3$	$6 \cdot 10^3$	$8 \cdot 10^3$	10^4	$2 \cdot 10^4$	$4 \cdot 10^4$	$6 \cdot 10^4$	$8 \cdot 10^4$	10^5	$2 \cdot 10^5$	$4 \cdot 10^5$	$6 \cdot 10^5$	$8 \cdot 10^5$	10^6
10	1.101	0.094	0.088	0.086	0.084	0.084	0.084	0.084	0.084	0.084	0.084	0.084	0.084	0.084	0.084
25	—	—	0.081	0.076	0.072	0.065	0.064	0.064	0.064	0.064	0.064	0.064	0.064	0.064	0.064
50	—	—	—	0.072	0.068	0.059	0.053	0.052	0.052	0.052	0.052	0.052	0.052	0.052	0.052
100	—	—	—	—	—	0.055	0.048	0.045	0.042	0.042	0.042	0.042	0.042	0.042	0.042
200	—	—	—	—	—	—	0.045	0.041	0.038	0.037	0.034	0.034	0.034	0.034	0.034
400	—	—	—	—	—	—	—	0.039	0.036	0.035	0.030	0.028	0.028	0.028	0.028
800	—	—	—	—	—	—	—	—	—	0.033	0.028	0.023	0.023	0.023	0.023
1400	—	—	—	—	—	—	—	—	—	—	0.027	0.023	0.021	0.021	0.020

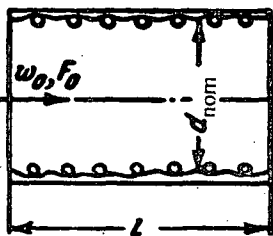


Steel-reinforced rubber hose. Friction coefficient

$$Re = \frac{u_0 d_{\text{cal}}}{v} > 4 \cdot 10^3$$

Section II

Diagram 2-8



$$\xi = \frac{\Delta H}{\gamma u_0^2} = \lambda \frac{l}{d_{\text{cal}}} \cdot$$

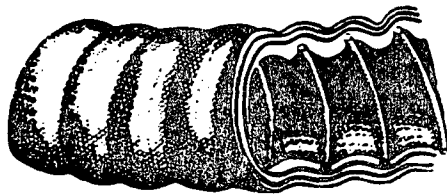
where λ is determined from curve a as a function of the nominal diameter d_{nom} :

d_{cal} = calculated diameter, determined as a function of the internal pressure p_{atm} from curve b for different values of d_{nom} :

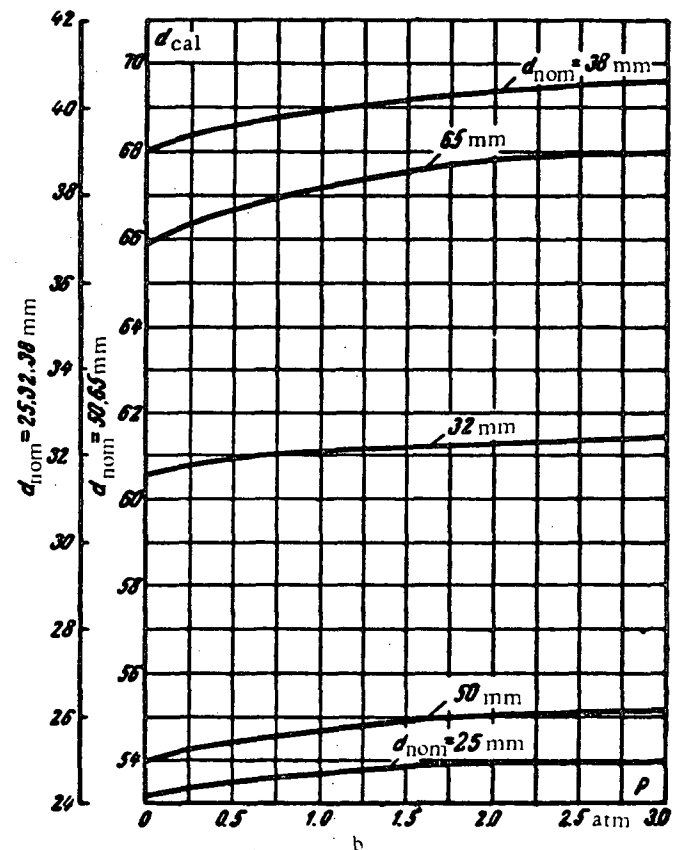
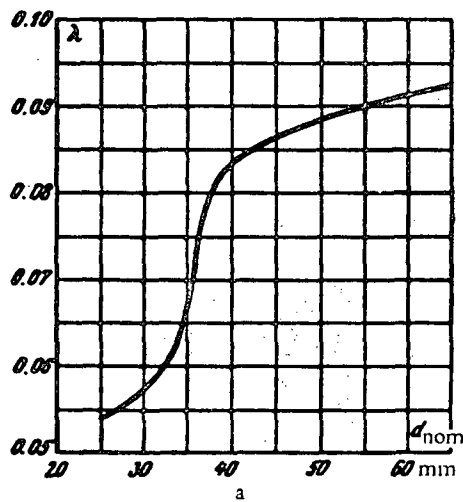
ν is taken according to § 1-3.b.

Hose dimensions

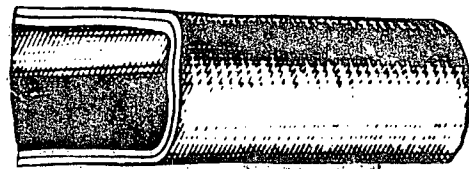
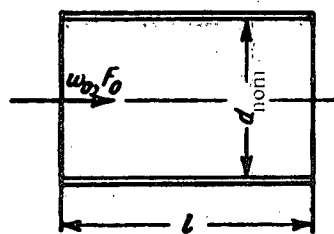
Nominal internal diameter d_{nom} , mm	25	32	38	50	65
Spiral-wire diameter, mm	2.8	2.8	2.8	3.0	3.4
Pitch, mm	15.6	15.6	17.6	20.0	20.8
Fabric insert 1.1 mm thick, nos.	1	1	1	1	1
Rubber layer, mm	1.5	1.5	2.0	2.0	2.0
Cotton thread, spiral-thread diameter, mm	1.8	1.8	1.8	1.8	1.8
Rubber layer, mm	1.5	1.5	1.5	1.5	1.5
Cloth insert 1.1 mm thick, nos.	2	2	2	2	3



d_{nom} , mm	25	32	38	50	65
λ	1.051- 0.057	0.053- 0.066	0.072- 0.090	0.083- 0.094	0.085- 0.100



Smooth rubber hose. Friction coefficient

 Section II
 Diagram 2-9


$$\zeta = \frac{\Delta H}{\gamma w_0^2} = \lambda = \frac{l}{d_{cal}} \cdot \frac{2g}{w_0^2}$$

where $\lambda = \frac{A}{Re^{0.265}}$ is determined from the curve $\lambda = f(Re)$
on graph a;
 $A = 0.38$ to 0.52 within the limits

$$Re = \frac{w_0 d_{cal}}{v} = 5000 \div 120000$$

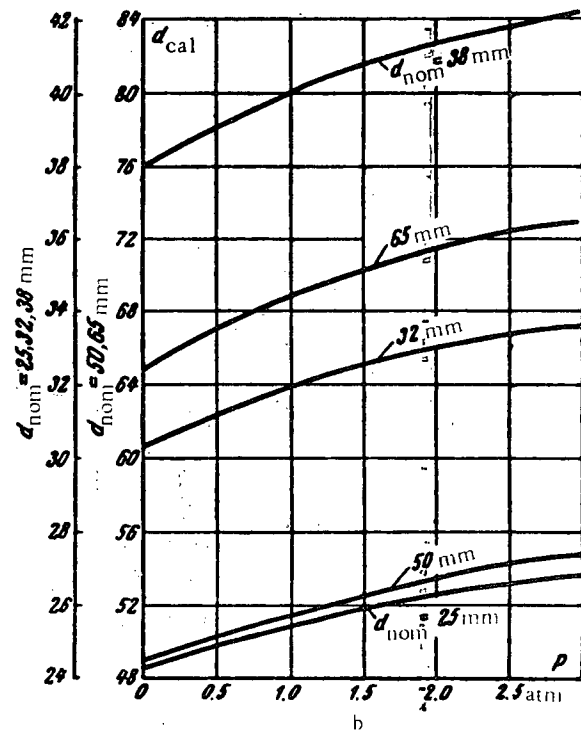
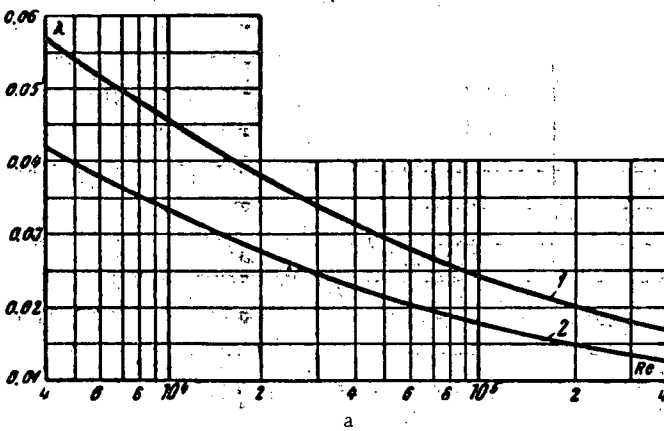
and depending upon the sleeve quality;

d_{cal} = calculated diameter, determined as a function of the internal pressure p_{atm} from curve b;
 v is taken according to § 1-3, b.

Hose dimensions

Nominal internal diameter d_{nom} , mm	25	32	38	50	65
Rubber layer (internal), mm	2	2	2	2.2	2.2
Fabric insert, thickness 1.1 mm, nos.	2	2	2	3	3
Rubber layer (external), mm	0.9	0.9	0.9	1.2	1.2

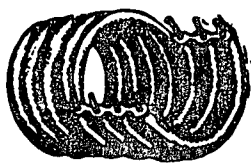
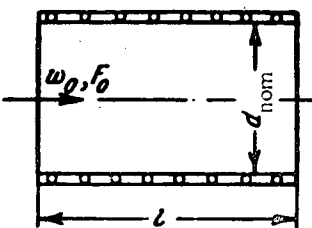
Re	$4 \cdot 10^3$	$6 \cdot 10^3$	10^4	$2 \cdot 10^4$	$4 \cdot 10^4$	$6 \cdot 10^4$	10^5	$2 \cdot 10^5$
1. $A = 0.52$								
λ	0.057	0.052	0.046	0.038	0.031	0.028	0.025	0.020
2. $A = 0.38$								
λ	0.042	0.038	0.033	0.028	0.023	0.020	0.018	0.015



Steel-reinforced rubber hose. Friction coefficient

Section II

Diagram 2-10



$$\zeta = \frac{\Delta H}{\gamma w_0^2} = \lambda \frac{l_{tr}}{d_{calc}} \cdot \frac{2g}{2g}$$

where λ is determined from the curves $\lambda=f(Re, d_{nom}, p_{atm})$ of graph a;

d_{calc} = calculated diameter, determined as a function of the mean internal pressure p_{atm} from graph b;

$$l_{tr} = kl,$$

where k is determined as a function of the mean internal pressure p_{atm} from graph c;

$$Re = \frac{w_0 d_{nom}}{v}, v \text{ is taken according to § 1-3,b.}$$

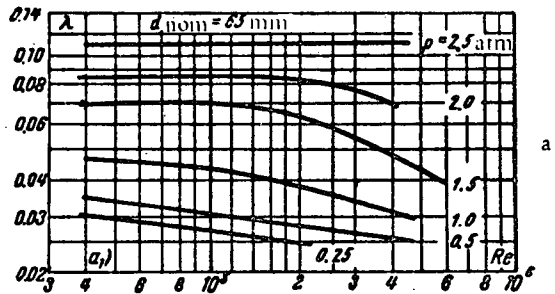


Table for Graph a₁: Friction coefficient λ vs. Reynolds number Re for $d_{nom} = 65 \text{ mm}$ at $p = 2.5 \text{ atm}$.

p_{atm}	$4 \cdot 10^4$	$6 \cdot 10^4$	$8 \cdot 10^4$	10^5	$1.4 \cdot 10^5$	$2 \cdot 10^5$	$2.5 \cdot 10^5$	$4 \cdot 10^5$
0.25	0.03	0.03	0.03	0.03	0.03	0.03	—	—
0.5	0.04	0.03	0.03	0.03	0.03	0.03	0.03	0.03
1.0	0.05	0.05	0.05	0.04	0.04	0.04	0.04	0.03
1.5	0.07	0.07	0.07	0.07	0.07	0.06	0.06	0.06
2.0	0.09	0.09	0.09	0.09	0.09	0.08	0.08	0.07
2.5	0.11	0.11	0.11	0.11	0.11	0.11	0.11	—

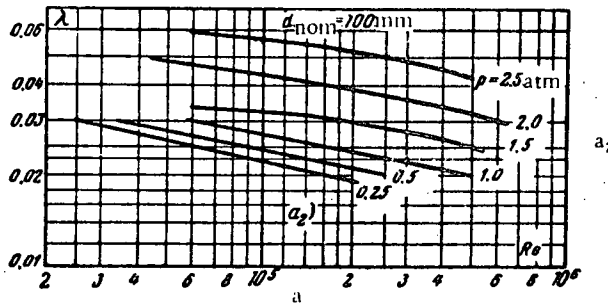
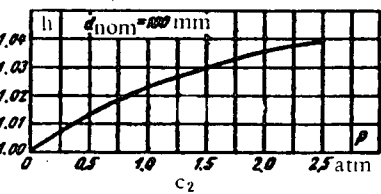
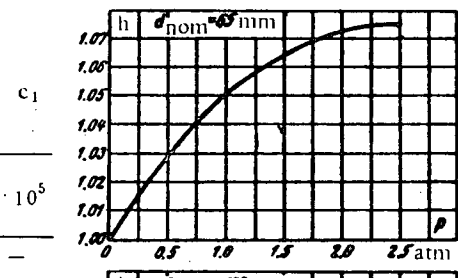
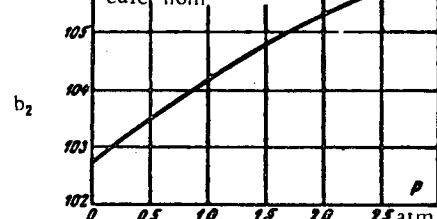
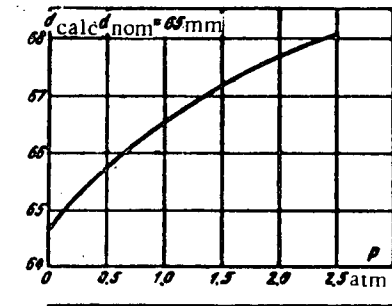
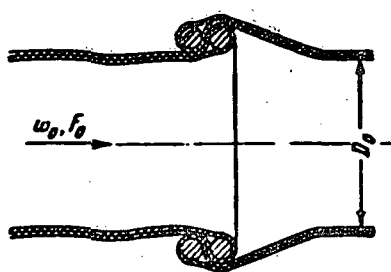


Table for Graph a₂: Friction coefficient λ vs. Reynolds number Re for $d_{nom} = 100 \text{ mm}$ at $p = 2.5 \text{ atm}$.

p_{atm}	$2.5 \cdot 10^4$	$4 \cdot 10^4$	$6 \cdot 10^4$	$8 \cdot 10^4$	10^5	$1.4 \cdot 10^5$	$2 \cdot 10^5$	$2.5 \cdot 10^5$	$4 \cdot 10^5$	$6 \cdot 10^5$
0.25	0.03	0.03	0.03	0.02	0.02	0.02	—	—	—	—
0.5	—	0.03	0.03	0.03	0.02	0.02	—	—	—	—
1.0	—	—	0.03	0.03	0.03	0.03	0.02	0.02	0.02	—
1.5	—	—	0.03	0.03	0.03	0.03	0.03	0.03	0.03	0.02
2.0	—	—	0.05	0.05	0.04	0.04	0.04	0.04	0.04	0.03
2.5	—	—	—	0.06	0.06	0.06	0.05	0.05	0.05	—





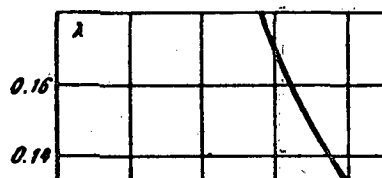
$$\xi = \frac{\Delta H}{\frac{w_0^2}{2g} \cdot \frac{l_j}{D_0}} = z \left(\lambda \frac{l_j}{D_0} + \xi_c \right).$$

where z = number of pipe joints; l_j = distance between joints;

$$\lambda = \frac{\Delta H}{\frac{w_0^2}{2g} \cdot \frac{l_j}{D_0}} \text{ is determined from curve a for different degrees of pipe tension;}$$

$$\xi_c = \frac{\Delta H}{\frac{w_0^2}{2g} \cdot \frac{l_j}{D_0}} \text{ is determined from curve b;}$$

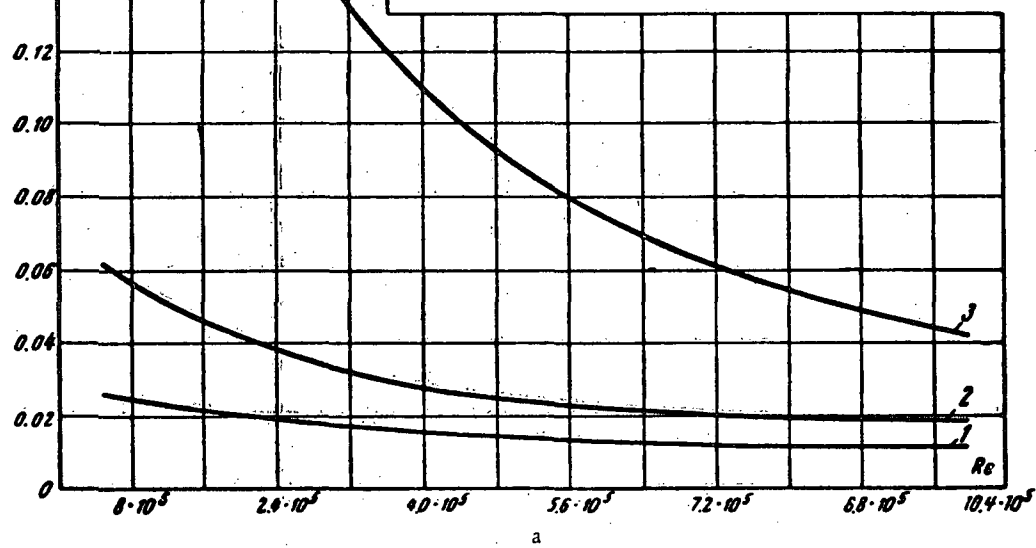
$$Re = \frac{w_0 D_0}{\nu}; \nu \text{ is taken according to § 1-3.b.}$$



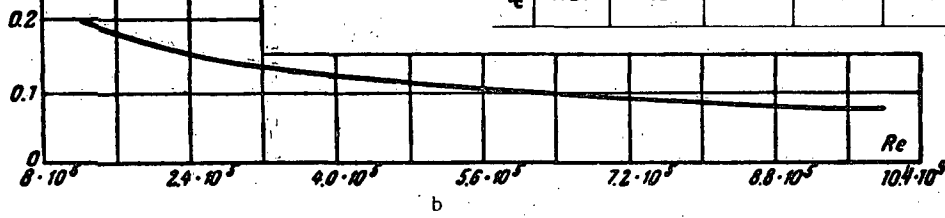
Re No.	10^5	$2 \cdot 10^5$	$3 \cdot 10^5$	$4 \cdot 10^5$	$5 \cdot 10^5$	$6 \cdot 10^5$	$7 \cdot 10^5$	$8 \cdot 10^5$	$9 \cdot 10^5$
1	0.024	0.020	0.018	0.016	0.014	0.013	0.012	0.011	0.011
2	0.064	0.042	0.034	0.028	0.025	0.023	0.021	0.020	0.019
3	0.273	0.195	0.139	0.110	0.091	0.074	0.063	0.054	0.048

Pipe tension

1. large
2. medium
3. small



Re	10^5	$2 \cdot 10^5$	$3 \cdot 10^5$	$4 \cdot 10^5$	$5 \cdot 10^5$	$6 \cdot 10^5$	$7 \cdot 10^5$	$8 \cdot 10^5$	10^6
ξ_c	0.20	0.17	0.14	0.12	0.11	0.10	0.09	0.08	0.08

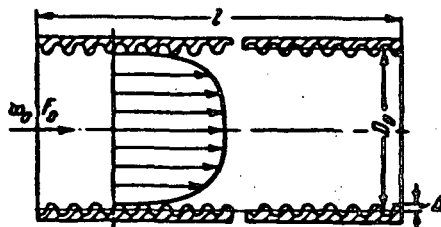


Plywood pipe (birch with longitudinal grain). Friction coefficient at turbulent flow

Section II

Diagram 2-12

$$D_h = \frac{4F_0}{\Pi_0}; \Pi_0 = \text{perimeter}$$



$$1. \text{ Circular cross section: } A = \frac{\Delta H}{\frac{\gamma w_0^2}{2g} \frac{l}{D_h}}$$

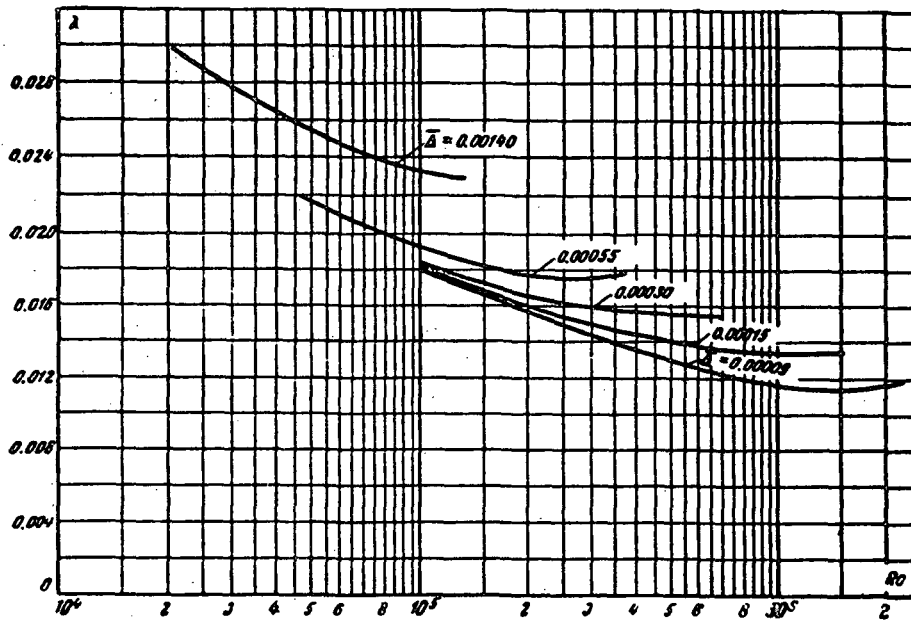
is determined from the curves $\lambda = f(Re)$ for different $\bar{\Delta}$:

$$\bar{\Delta} = \frac{\Delta}{D_h}; \Delta = \text{mean height of the roughness protuberances taken}$$

$$\text{from Table 2-1; } Re = \frac{w_0 D_h}{v}$$

v is taken according to § 1-3,b.

$\bar{\Delta}$	Re													
	$2 \cdot 10^4$	$3 \cdot 10^4$	$4 \cdot 10^4$	$6 \cdot 10^4$	$8 \cdot 10^4$	10^5	$1.5 \cdot 10^5$	$2 \cdot 10^5$	$3 \cdot 10^5$	$4 \cdot 10^5$	$6 \cdot 10^5$	$8 \cdot 10^5$	10^6	$2 \cdot 10^6$
0.00140	0.030	0.028	0.027	0.025	0.024	0.023	—	—	—	—	—	—	—	—
0.00055	—	—	—	0.021	0.021	0.019	0.018	0.017	0.018	0.018	—	—	—	—
0.00030	—	—	—	—	—	0.018	0.017	0.017	0.016	0.016	0.016	—	—	—
0.00015	—	—	—	—	—	0.018	0.017	0.016	0.015	0.014	0.014	0.014	0.013	—
0.00009	—	—	—	—	—	0.018	0.017	0.016	0.014	0.014	0.013	0.012	0.012	0.011



Section Three

STREAM INTAKE IN PIPES AND CHANNELS (Resistance coefficients of inlet sections)

3-1. LIST OF SYMBOLS

- F_0 = area of the narrowest cross section of the inlet stretch, m²;
 F_1 = area of the widest cross section of the inlet stretch, m²;
 F_{or} = cross-section area (total area of the orifices) of the perforated plate, screen or orifice, m²;
 F_p = frontal area of the perforated plate, screen, or orifice, m²;
 F_c = area of the contracted jet section at entrance into a channel orifice, m²;
 f_o = area of one orifice of the plate, screen, m²;
 \bar{f} = $\frac{F_{or}}{F_p}$ = cross-section coefficient of the plate or screen;
 n = $\frac{F_1}{F_0}$ = area-contraction ratio of the conduit section;
 s = $\frac{F_c}{F_0}$ = coefficient of jet contraction;
 P_0 = perimeter of the cross section of the conduit or the orifice of the plate, m;
 D_0, D_1 = diameters of the narrowest and widest sections of the stretch, m;
 D_{or}, D_c = diameters of the perforated plate orifice and contracted jet section at channel inlet, m;
 D_h = hydraulic diameter, four times the hydraulic radius of conduit section, m;
 d_h = hydraulic diameter of the perforated plate orifice, m;
 b' = width of the slit of a standard louver, distance between the louver slats in the direction perpendicular to their axis, m;
 b = distance from the inlet edge to wall in which conduit is fixed, m;
 h = distance of the screen from the inlet orifice of the conduit, m;
 l = length of the contracting inlet stretch, depth of orifices in the perforated plate, m;
 r = radius of curvature, m;
 ζ = resistance coefficient of the inlet stretch.
 δ_1 = thickness of the inlet-pipe wall (edge), m;
 α = central convergence angle of the inlet stretch or of the edge of the perforated plate orifice;
 w_0, w_1 = mean velocity of the stream in the narrowest and widest sections of the stretch, m/sec;
 w_{or}, w_c = mean velocity in the perforated plate (screen) orifice and the contracted jet section, m/sec;
 ΔH = pressure loss (resistance) in the stretch, kg/m²;

3-2. EXPLANATIONS AND RECOMMENDATIONS

1. The entry of a stream into a straight pipe or channel of constant cross section (Figure 3-1) depends on two characteristics: the relative thickness $\frac{\delta_1}{D_h}$ of the pipe-inlet wall, and the relative distance $\frac{b}{D_h}$ from the pipe edge to the wall where it is mounted.

The coefficient of resistance ζ of the straight inlet stretch is maximum at a completely sharp edge ($\frac{\delta_1}{D_h} = 0$) and infinite distance of the pipe edge from the wall ($\frac{b}{D_h} = \infty$). In this case $\zeta = 1.0$. Its minimum value is equal to 0.5, and is obtained at a thick inlet edge, or at a pipe orifice flush with the wall ($\frac{b}{D_h} = 0$).

The effect of the wall on the coefficient of resistance of the inlet almost ceases at $\frac{b}{D_h} \geq 0.5$. This case corresponds to a stream entrance into a conduit whose edge is at a great distance from the wall.

2. When entering a straight conduit the stream flows past the inlet edge; if, however, this is insufficiently rounded, the stream separates near the entrance (Figure 3-1). This stream separation, and the resulting formation of eddies, are the main cause of pressure losses at the inlet. The stream separation from the pipe walls leads to a decrease of the jet cross section. The coefficient of jet contraction $\epsilon = \frac{F_c}{F}$ for a sharp-edged straight inlet orifice is equal to 0.5 in the case of turbulent flow.

3. The thickening, cutting, or rounding of the inlet wall, and the nearness of the conduit edge to the wall in which the pipe is mounted, all lead to a smoother motion of the stream about the inlet edge and to a smaller zone of stream separation with a smaller inlet resistance.

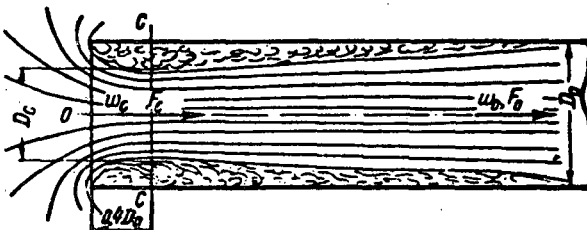


FIGURE 3-1. Flow at the inlet to a straight pipe from an unlimited space.

4. The greatest decrease of resistance is obtained for a stream entrance through a smooth bellmouth whose section forms an arc of a curve (circle, lemniscate, etc.) (Figure 3-2,a). Thus, in the case of a circular intake with relative radius of curvature

$\frac{r}{D_h} = 0.2$, the resistance coefficient ζ drops to 0.04 or 0.05 as against $\zeta = 1.0$ at $\frac{r}{D_h} = \frac{\delta_1}{D_h} = 0$ (sharp edge).

5. A relatively low resistance is also created by a stream entrance through inlets shaped as truncated cones (Figure 3-2,b,c) or as contracting stretches with transitions from rectangular to circular or from circular to rectangular (Figure 3-2,d). The resistance coefficient of such transition pieces is a function of both the convergence angle

α and the relative length $\frac{l}{D_h}$. For each length of a conical transition section there is an optimum value of α at which the resistance coefficient ζ is minimum. The optimum value of α for a relatively wide range of $\frac{l}{D_h}$, $0.1 \leq \frac{l}{D_h} \leq 1.0$, lies within the limits 40 to 60°. At such angles, e.g., $\frac{l}{D_h} = 0.2$, the resistance coefficient is only 0.2.

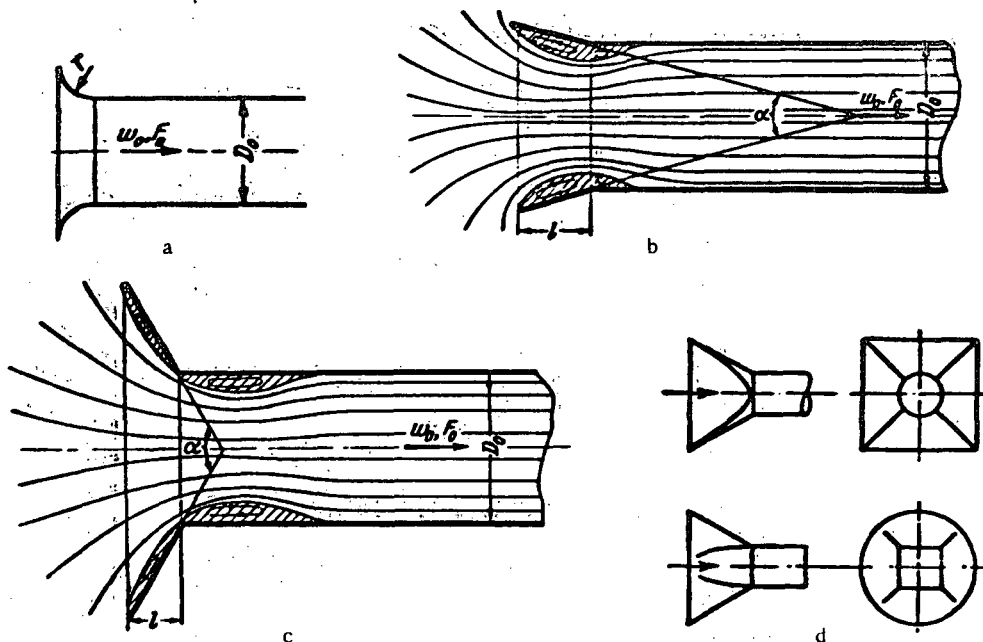


FIGURE 3-2. Plan of smooth inlet stretches:

a—bellmouth whose section forms arc of a circle; b and c—bellmouths shaped like truncated cones; d—transition pieces.

6. When an inlet stretch is mounted in the end wall under an angle δ (Figure 3-3), the inlet resistance increases. The resistance coefficient is determined in this case by the Weisbach formula /3-15/:

$$\zeta = \frac{\Delta H}{\frac{1}{2} \rho u_0^2} = 0.5 + 0.3 \cos \delta + 0.2 \cos^2 \delta. \quad (3-1)$$

7. The mounting of a screen (Figure 3-4) at a relative distance $\frac{h}{D_h} < 0.8 - 1.0$ before the inlet stretch increases the resistance of the inlet; the nearer the screen to the inlet opening of the conduit, i.e., the smaller is $\frac{h}{D_h}$ the greater is this increase.

The resistance coefficient of inlet stretches of different thickness, with rounded or cut-off inlet edges, without a screen can be determined by the author's approximate formula /3-3/:

$$\zeta = \frac{\Delta H}{\frac{\rho w_0^2}{2g}} \approx \zeta' + \frac{\sigma_1}{n^2}, \quad (3-2)$$

where ζ' is the coefficient allowing for the influence of the inlet edge shape and is determined as ζ' from diagrams 3-1, 3-3, and 3-5; σ_1 is the coefficient allowing for the influence of the screen and determined from the curve $\sigma_1 = f\left(\frac{h}{D_h}\right)$ of diagram 3-8.

The resistance coefficient of smooth intakes mounted flush with the wall is determined in the presence of a screen, determined from the curve $\zeta = f\left(\frac{h}{D_h}, \frac{r}{D_h}\right)$ of diagram 3-4.

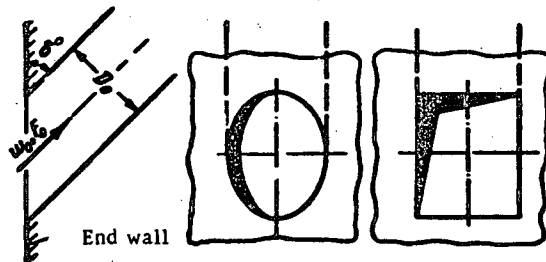


FIGURE 3-3. Entrance at an angle to the wall.

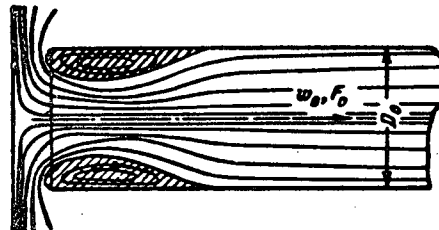


FIGURE 3-4. Inlet stretch with screen before the entrance.

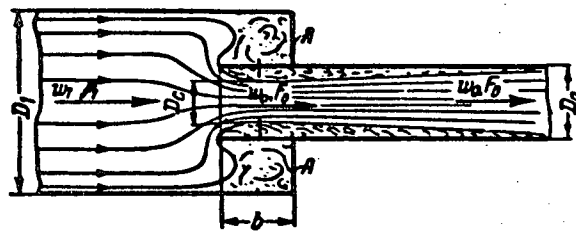


FIGURE 3-5. Flow pattern at sudden contraction.

8. The phenomenon observed in inlet stretches in which the stream suddenly contracts, i.e., passes suddenly from a large section F_1 to a smaller section F_2 (Figure 3-5), is similar to the one observed at the entrance to a straight inlet from a very large volume. The only difference here is that at large values of Reynolds number ($Re = \frac{w_0 D_h}{v} > 10^4$), the

resistance coefficient is a function of the area ratio $\frac{F_0}{F_1}$. This coefficient is calculated by the following formula established by the author /3-1/:

$$\zeta = \frac{\Delta H}{\frac{1}{2} w_0^2} = \zeta' \left(1 - \frac{F_0}{F_1} \right), \quad (3-3)$$

where ζ' is a coefficient depending on the shape of the inlet edge of the narrow channel and is determined as ζ from diagrams 3-1, 3-5, and 3-6.

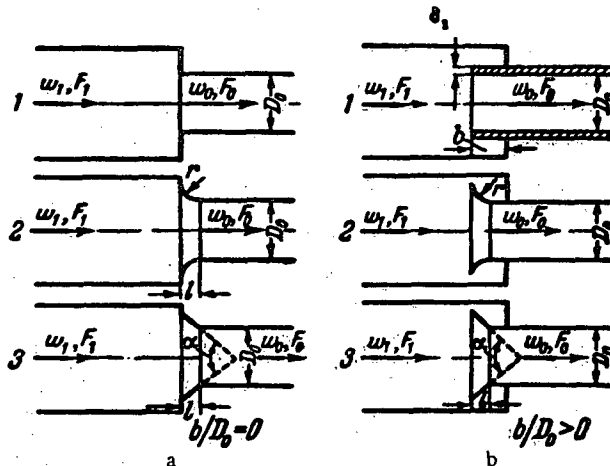


FIGURE 3-6. Sudden contraction:

a — inlet edge of a pipe of smaller section mounted flush with the end wall of a pipe of larger section; b — inlet edge of the pipe of smaller section moved forward.

In the case of the inlet edge of a narrow channel mounted flush with the end wall of a wider channel (Figure 3-6,a), the resistance coefficient can vary within the limits $0 \leq \zeta \leq 0.5$; when this edge is moved forward (Borda mouthpiece, Figure 3-6,b), it can vary within the limits $0 \leq \zeta \leq 1.0$.

9. The resistance coefficient of an inlet with a sudden contraction at Reynolds numbers within the limits $10 < Re < 10^4$ is a function not only of the area ratio $\frac{F_0}{F_1}$ but also of the Reynolds number, and at $Re < 10$ of this number only.

The values of ζ in the case of a sudden contraction, with the narrow inlet section mounted flush with the wall, can be determined at $10 < Re < 10^4$ from Karev's data /3-5/, (diagram 3-10) and at $Re < 10$ from the usual formula of resistance at laminar flow:

$$\zeta = \frac{\Delta H}{\frac{1}{2} w_0^2} = \frac{A}{Re}, \quad (3-4)$$

where, according to Karev's experiments /3-5/, $A \approx 27$.

10. The resistance of a contracting stretch can be decreased considerably if the transition from the wide section to the narrow one is accomplished smoothly by means of a rectilinear or curvilinear adapter (Figure 3-7). The contraction losses decrease with the increase of the transition smoothness. In the case of a perfectly smooth contraction of the section, where the convergence angle is very small or the length of the contracting stretch sufficiently large, and where this stretch has a very smooth curvilinear generatrix, the stream does not separate from the wall, and the pressure losses reduce to friction losses.

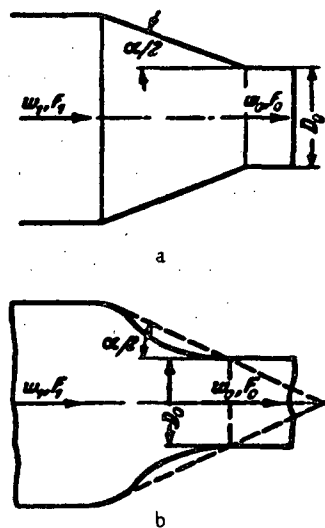


FIGURE 3-7. Adapters

a — rectilinear; b — curvilinear.

11. The resistance coefficient of a rectilinear transition section (Figure 3-7,a) can be approximately determined by the formula:

$$\zeta = \frac{\Delta H}{\frac{\gamma w_0^2}{2g}} \approx \zeta' \left(1 - \frac{F_0}{F_1} \right) + \zeta_{fr}, \quad (3-5)$$

where the first term on the right is determined as in formula (3-3); the second term is determined as friction coefficient of a transition piece with the same geometric parameters as for a convergent nozzle (diagrams 5-2 to 5-4).

The resistance coefficient of a smooth curvilinear adapter (Figure 3-7,b) is determined either as the friction coefficient of a bell-mouth orifice given in diagram 5-7, or as the friction coefficient of a rectilinear adapter with the same length and contraction ratio, from the data of diagrams 5-2 to 5-4:

$$\zeta = \frac{\Delta H}{\frac{\gamma w_0^2}{2g}} = \zeta_{fr}. \quad (3-6)$$

12. The resistance coefficient of inlet sections is also a function of their location and method of mounting in the wall [of the vessel or container into which they discharge]. A low resistance coefficient can be achieved by installing an annular rib or ledge before the inlet stretch enclosing the opening (Figure 3-8). If the rib or ledge has a sharp edge, the phenomenon of stream separation will occur at the entrance to the widened section which is formed by these devices. The eddies formed in the region of separation contribute to the smooth flow of the stream into the main inlet stretch of the pipe without separation. As a result, the resistance of the inlet is considerably reduced.

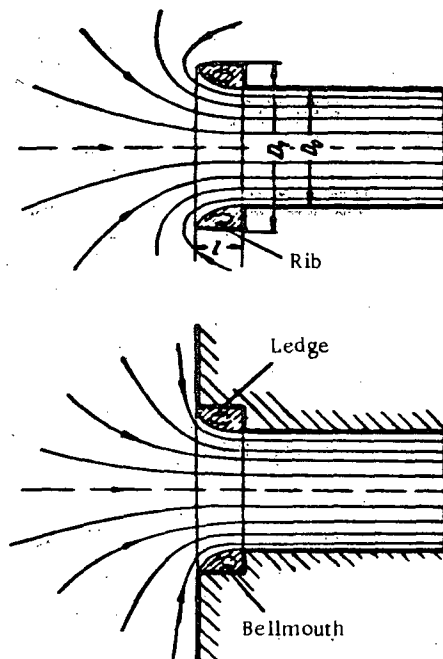


FIGURE 3-8. Entrance through an annular bellmouth.

The optimum dimensions of the widened stretch in which a bell-mouth ledge is placed, must closely correspond to the dimensions of the eddy region: a) at a point upstream from the most contracted section of the stream jet at the inlet into a straight pipe with sharp edges; b) to a pipe mounted flush with the wall. In fact, Khanzhonkov's experiments established /3-11/ that the minimum resistance coefficient $\zeta \approx 0.10$ is obtained in the case of a rib at $\frac{l}{D_0} \approx 0.25$ and $\frac{D_1}{D_0} \approx 1.3$, and in the case of a ledge at $\frac{l}{D_0} \approx 0.2$ and $\frac{D_1}{D_0} \approx 1.2$.

The values of ζ with various other methods of mounting the inlet stretches in the end wall or between walls are given in diagrams 3-11 and 3-12.

13. The pressure losses in the case of a lateral entrance of a stream through the first orifice in a constant-section collecting pipe are much larger than in the case of a straight entrance. The resistance of a one-way entrance is much smaller than that of a two-way entrance through two orifices located on two opposite sides (cf. diagram 3-13).

In this last diagram the resistance coefficients of a side entrance in a circular pipe through a lateral slit of constant height, $h = 0.875 D_0$, are given.

The resistance coefficients of side entrances corresponding to rectangular pipes and to slits of different relative heights can differ somewhat from the values given in diagram 3-13*.

14. Entrance through side orifices is frequently used in rectangular-section ventilating shafts. In order to prevent the penetration of sediments, louvers are mounted in the orifices. The resistance coefficient of such shafts is a function not only of the relative area of the orifices, but of their relative location as well. The resistance coefficients of intake shafts with differently disposed lateral orifices are given in diagrams 3-14 and 3-15. The values of ζ are given for both orifices with and without fixed louvers.

15. The resistance of intake shafts with straight entrance and canopies (cf. diagram 3-16) is similar to the resistance of ordinary inlet stretches with screens. In the case of normal ventilating shafts of circular section, in which the relative thickness of the inlet edges lies within the limits $0.002 \leq \delta \leq 0.01$, the influence of this parameter can be neglected and the value of the resistance coefficient ζ of all shafts can be determined from diagrams corresponding to sharp-edged shafts.

The ratio $\frac{h}{D_h}$ between the canopy hood and the inlet edge of the shaft can be taken as equal to 0.4. An increase of this distance would require building too large a canopy hood in view of the possibility of rain or snow entering the shaft.

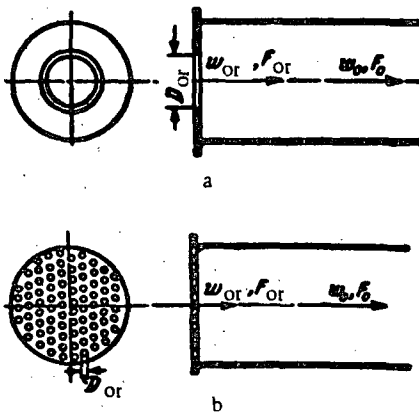


FIGURE 3-9. Stream entrance in a straight stretch:

a — through an orifice; b — through a perforated plate; F_{or} = cross section.

The recommended shaft design is the one with conical inlet stretch. This shaft is characterized by a minimum resistance coefficient $\zeta = 0.48 / 3-9/$.

16. The resistance coefficient of an inlet stretch through an orifice or perforated plate with sudden expansion ($F_1 = \infty$) (Figure 3-9) at $Re = \frac{w_{or} d_h}{\nu} > 10^4$ is calculated in the general case by the author's approximate formulas (3-2) and (3-3):

$$\zeta = \frac{\Delta H}{\frac{\rho w_0^2}{2g}} = \left[\zeta' + (1 - \bar{l})^2 + \epsilon (1 - \bar{l}) + 2 \frac{l}{d_h} \right] \frac{1}{\bar{l}^2}, \quad (3-7)$$

* More detailed studies of such entrances are currently being conducted.

where ζ' is determined as the coefficient ζ for inlet stretches in the presence of walls, from diagrams 3-1 to 3-3, and 3-6; τ is a coefficient allowing for the influence of the perforated-plate wall thickness, the inlet-edge shape, and the conditions of stream flow through the orifice; λ is determined from diagrams 2-2 to 2-5 as a function of Re and $\bar{A} = \frac{A}{d_h}$; $\bar{f} = \frac{f_{or}}{F_0}$ is the cross-section coefficient of the perforated plate.

17. The general case of entrance through orifice or perforated plate is reduced to a number of particular cases:

a) sharp orifice edges ($\frac{l}{d_h} \approx 0$), at which $\zeta' = 0.5$ and $\tau = 1.41$, and expression (3-7) is reduced to the following formula of the author /3-1 to 3-3/:

$$\zeta = \frac{\Delta H}{\frac{\gamma w_0^2}{2g}} = (1.707 - \bar{f})^2 \frac{1}{\bar{f}^2} = \left(\frac{1.707}{\bar{f}} - 1 \right)^2; \quad (3-8)$$

b) thick orifice edges, at which $\zeta' = 0.5$ and τ is determined from the curve $\tau = f(\frac{l}{d_h})$ of diagram 3-18*;

c) orifice edges beveled or rounded, at which it is assumed that $\lambda \frac{l}{d_h} = 0$
 $\tau \approx 2\sqrt{\zeta}$; as a result it is obtained that

$$\zeta = \frac{\Delta H}{\frac{\gamma w_0^2}{2g}} = (1 - \sqrt{\zeta} - \bar{f})^2 \frac{1}{\bar{f}^2}, \quad (3-9)$$

where the coefficient ζ' is determined in the case of edges beveled along the flow direction as ζ for a conical collector with end wall, from curve (a) of diagram 3-19, as a function of the contraction angle α and the length ratio $\frac{l}{d_h}$, and in the case of rounded edges, as ζ' of a circular collector with end wall from curve (b) of the same diagram, as a function of $\frac{l}{d_h}$.

18. At $Re < 10^5$ and sharp orifice edges, the resistance coefficient of an inlet through an orifice or perforated plate is calculated by the following formula, proposed by the author /3-4/:

$$\zeta = \frac{\Delta H}{\frac{\gamma w_0^2}{2g}} = \left[\left(\frac{1}{\varphi^2} - 1 \right) + \frac{0.342}{(\epsilon_0^{Re})^2} (1.707 - \bar{f})^2 \right] \frac{1}{\bar{f}^2} = [\zeta_\varphi + \epsilon_0^{Re} (1.707 - \bar{f})^2] \frac{1}{\bar{f}^2}, \quad (3-10)$$

where φ = velocity coefficient of the stream discharge from a sharp-edged orifice, and depends on Re and \bar{f} ; ϵ_0^{Re} = coefficient of filling of the section of a sharp-edged orifice at $\frac{f_{or}}{F_0} = 0$, and depends on Re ; $\zeta_\varphi = \left(\frac{1}{\varphi^2} - 1 \right)$ is determined from the curve $\zeta_\varphi = f_1(Re, \bar{f})$ on graph (a) of diagram 4-10; $\epsilon_0^{Re} = \frac{0.342}{(\epsilon_0^{Re})^2}$ is determined from the curve $\epsilon_0^{Re} = f_2(Re)$ on the same graph (a).

* The calculation as under b and c can be performed for $Re = 10^4$ and more.

At $Re < 10^5$ and thick orifice edges the resistance coefficient of an inlet with perforated plate or orifice is calculated from the formula:

$$\xi = \frac{\Delta H}{\frac{1}{2} \rho_0 v_0^2} = \left\{ \xi_v + \xi_p \left[0.5 + (1 - \bar{f})^2 + \epsilon(1 - \bar{f}) + 2 \frac{l}{d_h} \right] \right\} \frac{1}{F_p}. \quad (3-11)$$

19. When a perforated plate is installed at the stream entrance, the total resistance coefficient can be approximately determined as sum of the resistance coefficients of the plate and the inlet:

$$\xi = \frac{\Delta H}{\frac{1}{2} \rho_0 v_0^2} \approx \xi_v + \frac{\xi_p}{n^2}, \quad (3-12)$$

where ξ_v = resistance coefficient of the inlet, without a plate, determined as ξ for a given shape of the inlet edge from the corresponding curves of diagrams 3-1 to 3-6; ξ_p = resistance coefficient of the plate, determined as ξ from the corresponding curves of diagram 8-6; $n = \frac{F_l}{F_p}$ = ratio of area of the cross section where the plate is mounted, to the narrowest cross section of the inlet stretch.

20. The resistance coefficient of a fixed louver is a function both of its cross-section coefficient $\bar{f} = \frac{F_{or}}{F_p}$ and of the relative depth of the channels $\frac{l}{b_l}$. To each cross-section coefficient there is an optimum value of the relative depth $\left(\frac{l}{b_l}\right)_{opt}$ at which the resistance coefficient is minimum. The selection of the louver with the optimum value of $\frac{l}{b_l}$ is recommended. This can be determined by using the formula:

$$\left(\frac{l}{b_l}\right)_{opt} \approx 11(1 - \bar{f}). \quad (3-13)$$

21. In the case of standard grids with fixed louvers, the inlet edges of the slats are cut along the vertical (Figure 3-10,a). From the point of view of the resistance it is more expedient, however, to use louvers with inlet edges cut along the horizontal (Figure 3-10,b). A 40% decrease in the resistance is achieved as a result /3-13/.

22. The following formulas are proposed for calculating the resistance coefficient of grids with fixed louvers installed at the entrance to a channel** :

$$1) \frac{l}{b_l} \geq \left(\frac{l}{b_l}\right)_{opt}$$

$$\xi = \frac{\Delta H}{\frac{1}{2} \rho_0 v_0^2} = k \left[0.85 + \left(1 - \bar{f} \frac{F_p}{F_o} \right)^2 + \xi_{fr} \right] \frac{1}{F_g} \left(\frac{F_o}{F_p} \right)^2; \quad (3-14)$$

* This formula was obtained on the basis of Bevier's data /3-13/.

** The agreement between these formulas and the experimental data of Bevier /3-13/ and Cobb /3-14/ is satisfactory

3-3. LIST OF THE DIAGRAMS OF RESISTANCE COEFFICIENTS OF SECTION III

Type of diagram	Source	No. of diagram	Note
Straight entrance into a conduit of constant cross section, $Re > 10^4$	Idel'chik /3-1/	3-1	Some of the curves were obtained approximately by extrapolating experimental data
Straight entrance into a conduit mounted flush in the wall at an arbitrary angle δ° , $Re > 10^4$	Weissbach /3-15/	3-2	Experimental data
Smooth converging bellmouth made by an arc of a circle, without screen, $Re > 10^4$	Idel'chik /3-1/	3-3	The same
Smooth converging bellmouth made by an arc of a circle, with flat end wall and with screen, $Re > 10^4$	Nosova /3-6/	3-4	" "
Conical converging bellmouth with end wall, $Re > 10^4$	Idel'chik /3-1/	3-5	Some of the curves were obtained approximately by extrapolating experimental data
Conical converging bellmouth without end wall, $Re > 10^4$	The same	3-6	The same
Inlet with smooth contraction $Re > 10^4$	—	3-7	Tentative
Various inlets with screen, $Re > 10^4$	Idel'chik /3-1/	3-8	Experimental data
Various inlets with sudden contraction (or sudden contraction only), $Re > 10^4$	The same	3-9	Calculating formula
Inlet with sudden contraction (or sudden contraction only); inlet section in the end wall, $Re < 10^4$	Karev /3-5/	3-10	Experimental data; some of the curves were obtained approximately by extrapolation
Straight inlets with various mountings in the end wall, $Re > 10^4$	Idel'chik /3-1/	3-11	Experimental data
Straight inlets with various mountings between walls, $Re > 10^4$	The same	3-12	The same
Side entrance into a circular straight pipe through the first orifice $Re > 10^4$	—	3-13	Author's experimental data
Straight intake shafts of rectangular section; side orifices with fixed louvers and without them	Nosova and Tarasov	3-14	Experimental data
Rectangular-section intake shafts with a bend; side orifices with fixed louvers or without them	The same	3-15	The same
Straight in-draft shafts of circular section, $Re > 10^4$	Khanzhonkov /3-9/	3-16	" "
Entrance to a straight conduit through a perforated plate with sharp-edged orifices	Idel'chik /3-1/	3-17	Calculating formula
Entrance to a straight conduit through a perforated plate with thick-edged orifices ($\frac{l}{d_h} = 0.015$)	Idel'chik /3-2/	3-18	The same
Entrance to a straight conduit through a perforated plate with orifice edges beveled or rounded $Re > 10^3$	The same	3-19	" "
Various entrances to a conduit with a screen at the inlet	—	3-20	Approximate
Entrance to a straight channel through a fixed louver $f = 0.1$ to 0.9	—	3-21	According to the author's approximate formula, allowing for the experiments of Bevier /3-13/ and Cobb /3-14/
Entrance to a straight channel through stamped or cast shaped perforated plates	—	3-22	Approximate, based on the author's formula for entrance through a flat grid

3-4. DIAGRAMS OF RESISTANCE COEFFICIENTS

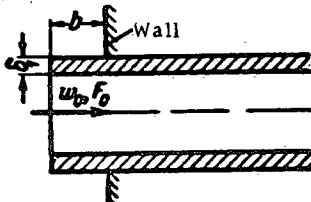
Straight entrance into a conduit of constant cross section

$$Re = \frac{w_0 D_h}{\nu} > 10^4$$

Section III

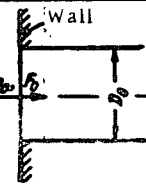
Diagram 3-1

1) Entrance at a distance $\left(\frac{b}{D_h} < 0.5\right)$ from the wall in which the conduit is mounted;



2) Entrance flush with the wall $\left(\frac{b}{D_h} = 0\right)$

$$D_h = \frac{4f_0}{H_0};$$



H_0 — perimeter

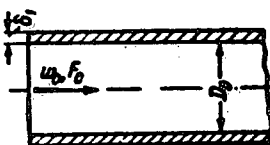
3) Entrance at a large distance $\left(\frac{b}{D_h} > 0.5\right)$ from the wall in which the conduit is mounted

$$\zeta = \frac{\Delta H}{\frac{1}{2} w_0^2} \text{ is determined from the curve } \zeta = f\left(\frac{b}{D_h}\right)$$

at $\frac{b}{D_h} \geq 0.5$; w is taken from § 1-3, b.

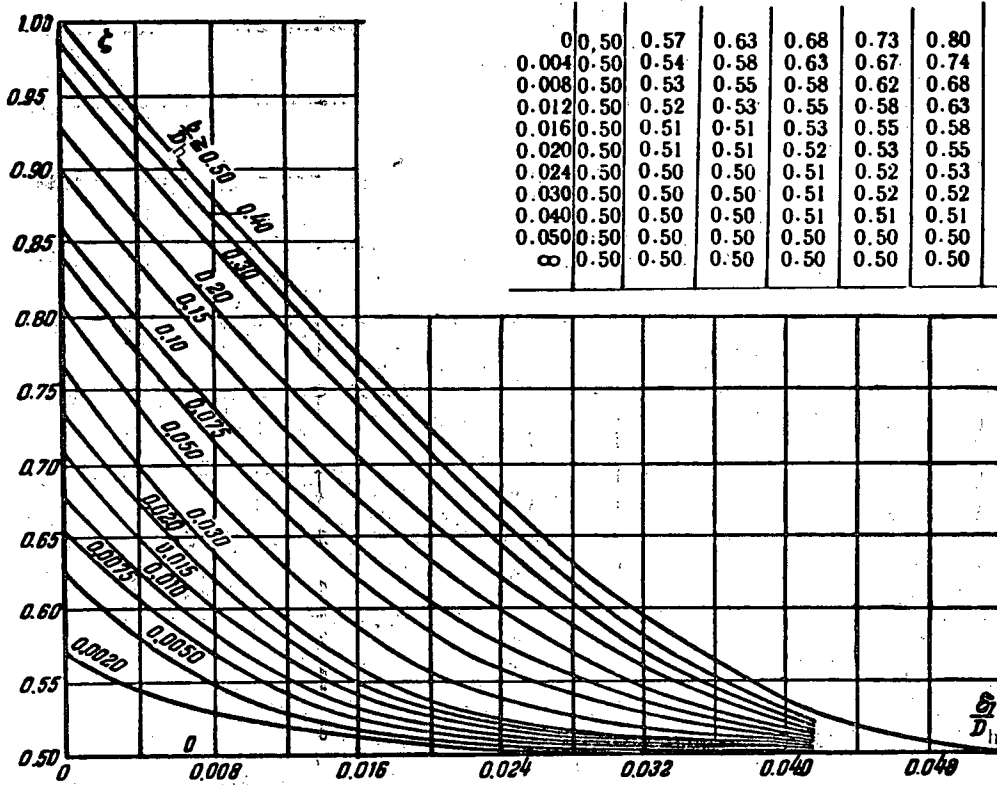
$$1) \text{ and } 2) \zeta = \frac{\Delta H}{\frac{1}{2} w_0^2}$$

$$\zeta = f\left(\frac{b}{D_h}\right) \text{ at given } \frac{b}{D_h};$$



Values of ζ

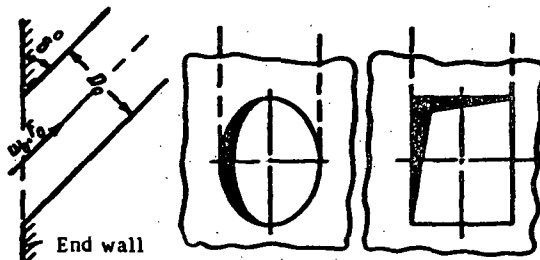
$\frac{b}{D_h}$	$\frac{b}{D_h}$										
	0	0.002	0.005	0.010	0.020	0.050	0.100	0.200	0.300	0.500	∞
0	0.50	0.57	0.63	0.68	0.73	0.80	0.86	0.92	0.97	1.00	1.00
0.004	0.50	0.54	0.58	0.63	0.67	0.74	0.80	0.86	0.90	0.94	0.94
0.008	0.50	0.53	0.55	0.58	0.62	0.68	0.74	0.81	0.85	0.88	0.88
0.012	0.50	0.52	0.53	0.55	0.58	0.63	0.68	0.75	0.79	0.83	0.83
0.016	0.50	0.51	0.51	0.53	0.55	0.58	0.64	0.70	0.74	0.77	0.77
0.020	0.50	0.51	0.51	0.52	0.53	0.55	0.60	0.66	0.69	0.72	0.72
0.024	0.50	0.50	0.50	0.51	0.52	0.53	0.58	0.62	0.65	0.68	0.68
0.030	0.50	0.50	0.50	0.51	0.52	0.52	0.54	0.57	0.59	0.61	0.61
0.040	0.50	0.50	0.50	0.51	0.51	0.51	0.51	0.52	0.52	0.54	0.54
0.050	0.50	0.50	0.50	0.50	0.50	0.50	0.50	0.50	0.50	0.50	0.50
∞	0.50	0.50	0.50	0.50	0.50	0.50	0.50	0.50	0.50	0.50	0.50



Straight entrance into a conduit mounted flush with the wall at an arbitrary angle θ° , $Re = \frac{w_0 D_h}{\nu} > 10^4$

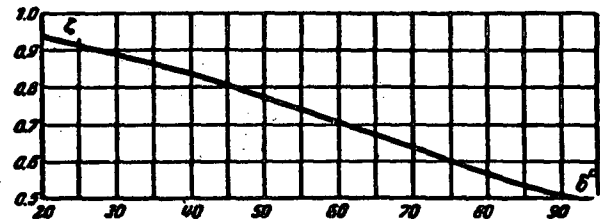
Section III
Diagram 3-2

$$D_h = \frac{4F_0}{H_0}; H_0 = \text{perimeter}$$



θ°	20	30	45	60	70	80	90
ζ	0.96	0.91	0.81	0.70	0.63	0.56	0.50

$$\zeta = \frac{\Delta H}{\frac{V^2}{2g}} = 0.5 + 0.3 \cos \theta + 0.2 \cos^2 \theta \text{ is determined from the curve } \zeta = f(\theta); \nu \text{ is taken from § 1-3, b.}$$

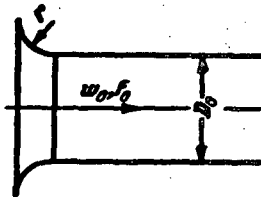


Smooth converging bellmouth made by an arc of a circle, without screen, $Re = \frac{w_0 D_h}{\nu} > 10^4$

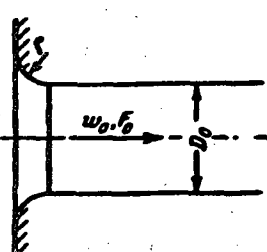
Section III
Diagram 3-3

$$D_h = \frac{4F_0}{H_0}; H_0 = \text{perimeter}$$

1) Without end wall



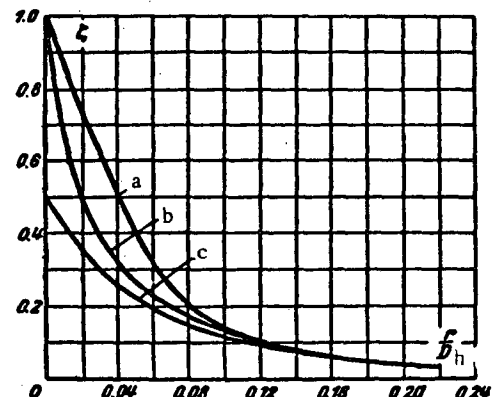
2) With end wall



$$\zeta = \frac{\Delta H}{\frac{V^2}{2g}}$$

is determined from curves a, b, c as a function of r/D_h ; ν is taken from § 1-3, b.

r/D_h	0	0.01	0.02	0.03	0.04	0.05	0.06	0.08	0.12	0.16	> 0.20
a) Without end wall (not sharpened)											
ζ	1.0	0.87	0.74	0.61	0.51	0.40	0.32	0.20	0.10	0.06	0.03
b) Without end wall (sharpened)											
ζ	1.0	0.65	0.49	0.39	0.32	0.27	0.22	0.18	0.10	0.06	0.03
c) With end wall (not sharpened)											
ζ	0.50	0.43	0.36	0.31	0.26	0.22	0.20	0.15	0.09	0.06	0.03

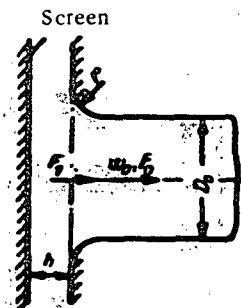


Smooth converging bellmouth made by an arc of a circle, with flat end wall and with screen, $Re = \frac{w_0 D_h}{\nu} > 10^4$

Section III
Diagram 3-4

$$D_h = \frac{4F_0}{U_0}; \quad U_0 = \text{perimeter}$$

$$\xi = \frac{\Delta H}{\frac{\tau w_0^2}{2g}}$$

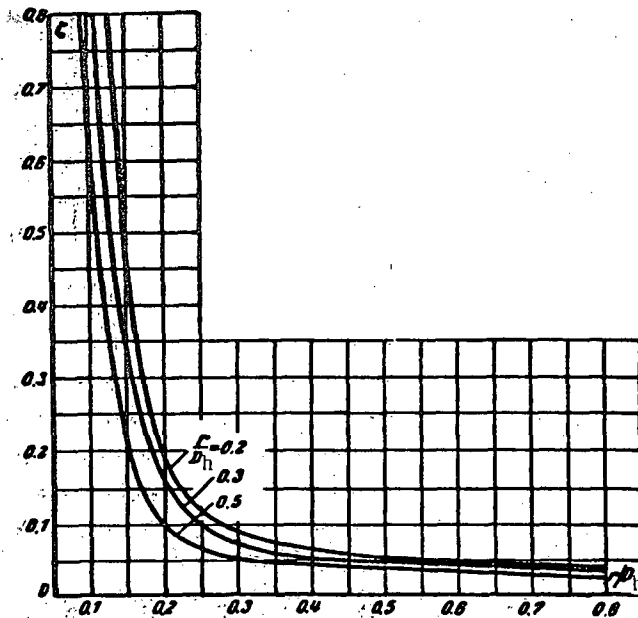


$$n = \frac{F_1}{F_0}$$

is determined from the curves

$$\xi = f\left(\frac{h}{D_h}, \frac{r}{D_h}\right);$$

is taken from § 1-3,b.



$\frac{h}{D_h}$	0.10	0.125	0.15	0.20	0.25	0.30	0.40	0.50	0.60	0.80
-----------------	------	-------	------	------	------	------	------	------	------	------

$$r/D_h = 0.2$$

ξ	-	0.80	0.45	0.19	0.12	0.09	0.07	0.06	0.05	0.05
-------	---	------	------	------	------	------	------	------	------	------

$$r/D_h = 0.3$$

ξ	-	0.50	0.34	0.17	0.10	0.07	0.06	0.05	0.04	0.04
-------	---	------	------	------	------	------	------	------	------	------

$$r/D_h = 0.5$$

ξ	0.65	0.36	0.25	0.10	0.07	0.05	0.04	0.04	0.03	0.03
-------	------	------	------	------	------	------	------	------	------	------

Conical converging bellmouth without end wall,

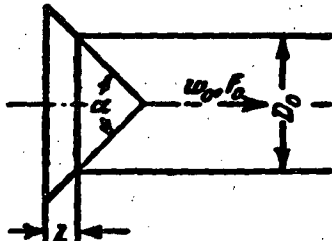
Section III

$$Re = \frac{w_0 D_h}{v} > 10^4$$

Diagram 3-5

$$D_h = \frac{4F_0}{\Pi_0}; \quad \Pi_0 = \text{perimeter}$$

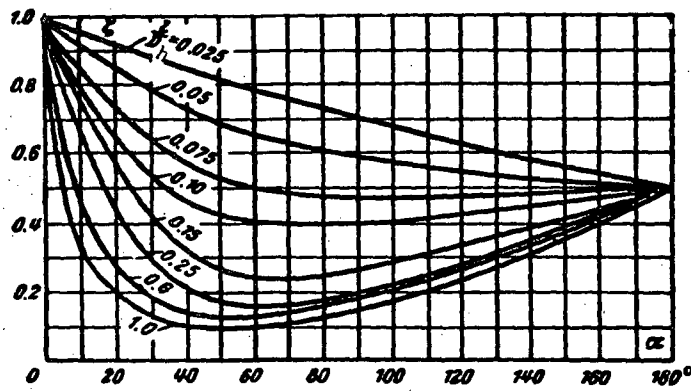
$$\xi = \frac{\Delta H}{\frac{\rho v^2}{2g}}$$



is determined approximately from the curves $\xi = f(\alpha^\circ)$
for different $\frac{l}{D_h}$:
 v is taken from §1-3,b.

 Values of ξ (approximately)

l/D_h	α°								
	0	10	20	30	40	60	100	140	180
0.025	1.0	0.96	0.93	0.90	0.86	0.80	0.69	0.59	0.50
0.050	1.0	0.93	0.86	0.80	0.75	0.67	0.58	0.53	0.50
0.075	1.0	0.87	0.75	0.65	0.58	0.50	0.48	0.49	0.50
0.10	1.0	0.80	0.67	0.55	0.48	0.41	0.41	0.44	0.50
0.15	1.0	0.76	0.58	0.43	0.33	0.25	0.27	0.38	0.50
0.25	1.0	0.68	0.45	0.30	0.22	0.17	0.22	0.34	0.50
0.60	1.0	0.46	0.27	0.18	0.14	0.13	0.21	0.33	0.50
1.0	1.0	0.32	0.20	0.14	0.11	0.10	0.18	0.30	0.50



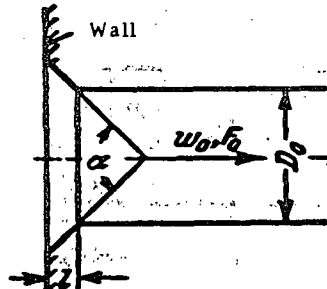
Conical converging bellmouth with end wall,

$$Re = \frac{w_0 D_h}{\nu} > 10^4$$

Section III

Diagram 3-6

$$D_h = \frac{4F_0}{H_0}; \quad H_0 \text{ — perimeter}$$



$$\zeta = \frac{\Delta H}{\frac{w_0^2}{2g}}$$

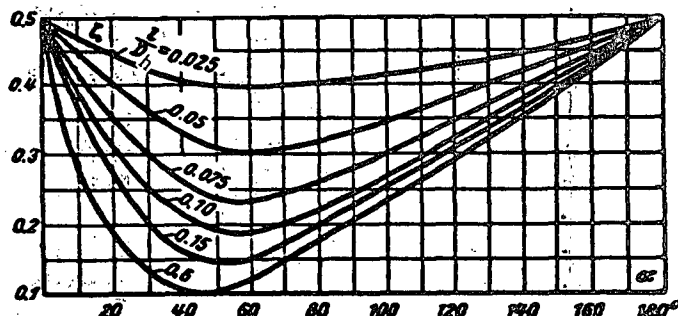
is determined approximately from the curves

$$\zeta = f(\alpha) \text{ for different } l/D_h;$$

it is taken from §1-3,b.

Values of ζ (approximately)

l/D_h	0	10	20	30	40	60	100	140	180
0.025	0.50	0.47	0.45	0.43	0.41	0.40	0.42	0.45	0.50
0.050	0.50	0.45	0.41	0.36	0.33	0.30	0.35	0.42	0.50
0.075	0.50	0.42	0.35	0.30	0.26	0.23	0.30	0.40	0.50
0.10	0.50	0.39	0.32	0.25	0.22	0.18	0.27	0.38	0.50
0.15	0.50	0.37	0.27	0.20	0.16	0.15	0.25	0.37	0.50
0.60	0.50	0.27	0.18	0.13	0.11	0.12	0.23	0.36	0.50



Inlet with smooth contraction

$$Re = \frac{w_0 D_0}{\nu} > 10^4$$

Section III

Diagram 3-7

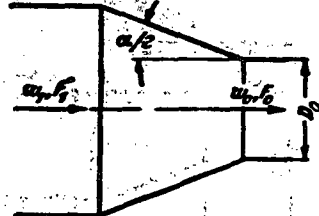
Inlet conditions

Scheme

Resistance coefficient

$$\zeta = \frac{\Delta H}{\frac{w_0^2}{2g}}$$

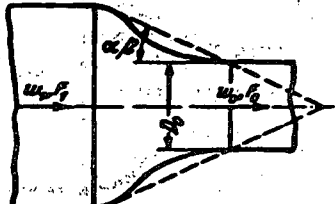
Rectilinear converging bellmouth



$$\zeta = \zeta' \left(1 - \frac{F_0}{F_1} \right) + \zeta_{fr},$$

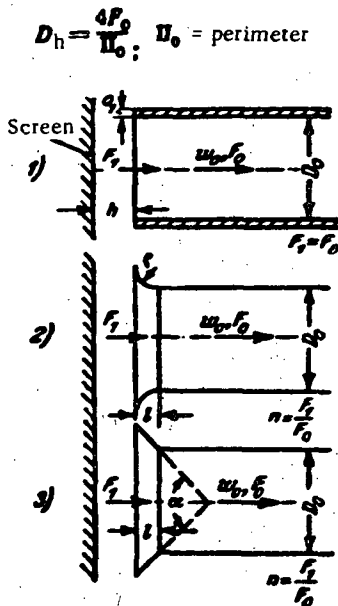
where ζ' is determined as ζ from diagram 3-6; ζ_{fr} is determined from diagrams 5-2 – 5-5

Curvilinear converging bellmouth

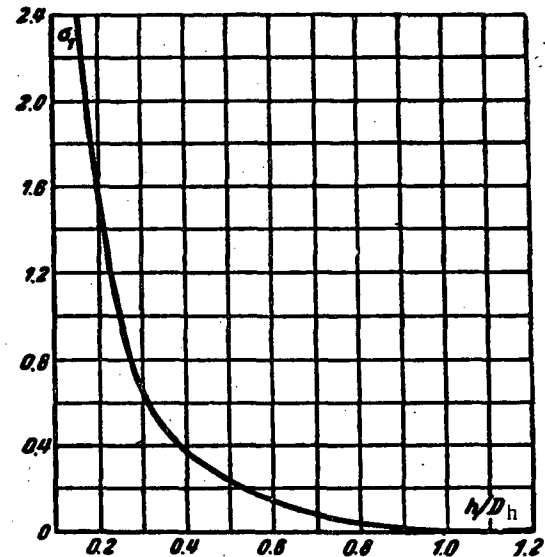


$$\zeta = \zeta_{fr},$$

where ζ_{fr} is determined from diagrams 5-2 – 5-5



h/D_h	0.20	0.30	0.40	0.50	0.60	0.70	0.80	1.0	∞
σ_1	1.60	0.65	0.37	0.25	0.15	0.07	0.04	0	0



$$\zeta = \frac{\Delta H}{\frac{1}{2} \rho v_0^2} \approx \zeta + \frac{\sigma_1}{n^2} \text{ (approximate), where}$$

1) ζ is determined from the curve $\zeta = f\left(\frac{\delta_1}{D_h}\right)$ at $\frac{b}{D_h} \geq 0.50$ on diagram 3-1;

2) ζ is determined from the curves $\zeta = f\left(\frac{r}{D_h}\right)$ on diagram 3-3 (curves a and b);

3) ζ is determined from the curve $\zeta = f\left(a^\circ, \frac{l}{D_h}\right)$ on diagram 3-5;

σ_1 is determined from the curve $\sigma_1 = f(h/D_h)$;

ν is taken from § 1-3, b.

Various inlets with sudden contraction (or sudden
contraction only) $\text{Re} = \frac{w_0 D_h}{\nu} > 10^4$

Section III

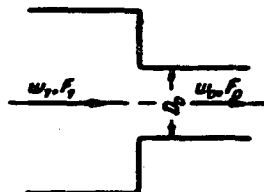
Diagram 3-9

Inlet conditions	Diagram	Resistance coefficient $\zeta = \frac{\Delta H}{\frac{\rho w_0^2}{2g}}$
		A. Inlet section in the end wall ($\frac{b}{D_h} = 0$): $D_h = \frac{4F_0}{P_0}$; P_0 = perimeter
Inlet edge blunt		$\zeta = 0.5 \left(1 - \frac{F_0}{F_1}\right)$
Inlet edge rounded		$\zeta = \zeta' \left(1 - \frac{F_0}{F_1}\right)$, where ζ' is determined from the curves $\zeta' = f\left(\frac{b}{D_h}\right)$ on diagram 3-3 (curve c)
Inlet edge beveled		$\zeta = \zeta' \left(1 - \frac{F_0}{F_1}\right)$, where ζ' is determined from the curve $\zeta' = f\left(\alpha^\circ, \frac{l}{D_h}\right)$ on diagram 3-6
		B. Inlet edge moved forward relative to the end wall ($\frac{b}{D_h} > 0$)
Inlet edge sharp or thick		$\zeta = \zeta' \left(1 - \frac{F_0}{F_1}\right)$, where ζ' is determined from the curves $\zeta' = f\left(\frac{b_1}{D_h}, \frac{b}{D_h}\right)$ on diagram 3-1
Inlet edge rounded		$\zeta = \zeta' \left(1 - \frac{F_0}{F_1}\right)$, where ζ' is determined from the curves $\zeta' = f\left(\frac{r}{D_h}\right)$ on diagram 3-3 (curves a and c)
Inlet edge beveled		$\zeta = \zeta' \left(1 - \frac{F_0}{F_1}\right)$, where ζ' is determined from the curve $\zeta' = f\left(\alpha^\circ, \frac{l}{D_h}\right)$ on diagram 3-5; α is taken from § 1-3,b.

Inlet with sudden contraction (or sudden contraction only);
 inlet section in the end wall, $\text{Re} = \frac{w_0 D_h}{v} < 10^4$

Section III
 Diagram 3-10

$$D_T = \frac{4F_0}{P_0}; P_0 - \text{perimeter}$$



$$1) \text{ At } 10 < \text{Re} = \frac{w_0 D_h}{v} < 10^4;$$

$$\zeta = \frac{\Delta H}{\frac{\gamma w_0^2}{2g}}$$

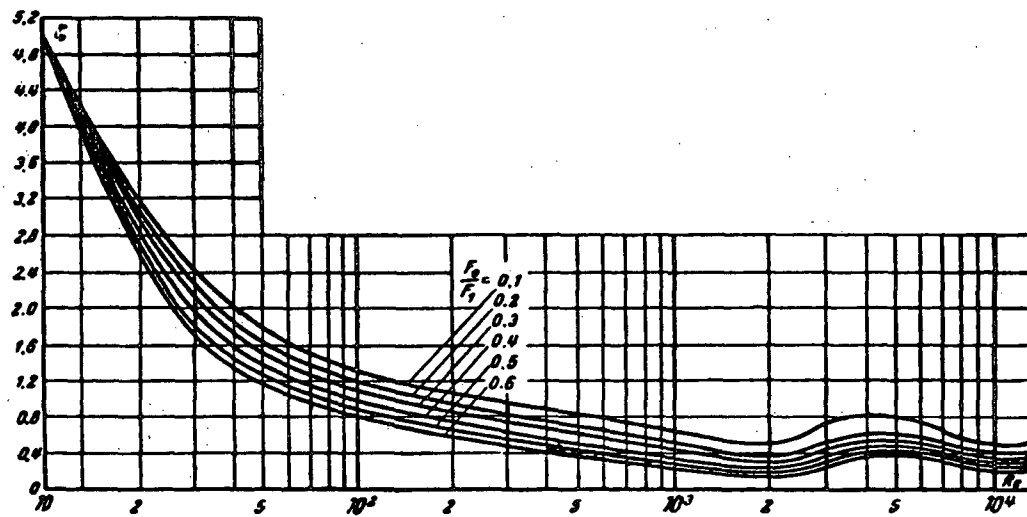
is determined from the curves $\zeta = f(\text{Re})$ corresponding to different $\frac{F_0}{F_1}$.

$$2) \text{ At } 1 < \text{Re} < 8$$

$$\zeta = \frac{\Delta H}{\frac{\gamma w_0^2}{2g}} = \frac{27}{\text{Re}};$$

v is taken from § 1-3, b.

$\frac{F_0}{F_1}$	10	20	30	40	50	10^2	$2 \cdot 10^2$	$5 \cdot 10^2$	10^3	$2 \cdot 10^3$	$4 \cdot 10^3$	$5 \cdot 10^3$	10^4	10^4
Re														
0.1	5.00	3.20	2.40	2.00	1.80	1.30	1.04	0.82	0.64	0.50	0.80	0.75	0.50	0.45
0.2	5.00	3.10	2.30	1.84	1.62	1.20	0.95	0.70	0.50	0.40	0.60	0.60	0.40	0.40
0.3	5.00	2.95	2.15	1.70	1.50	1.10	0.85	0.60	0.44	0.30	0.55	0.55	0.35	0.35
0.4	5.00	2.80	2.00	1.60	1.40	1.00	0.78	0.50	0.35	0.25	0.45	0.50	0.30	0.30
0.5	5.00	2.70	1.80	1.46	1.30	0.90	0.65	0.42	0.30	0.20	0.40	0.42	0.25	0.25
0.6	5.00	2.60	1.70	1.35	1.20	0.80	0.56	0.35	0.24	0.15	0.35	0.35	0.20	0.20



Straight inlets with various mountings in the end wall.

Section III

$$Re = \frac{w_0 a_0}{v} > 10^4$$

Diagram 3-11

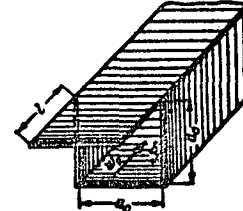
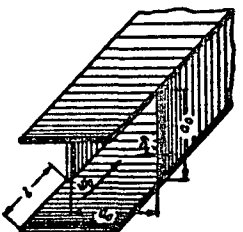
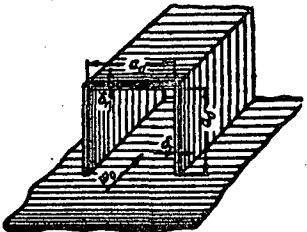
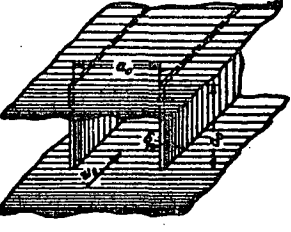
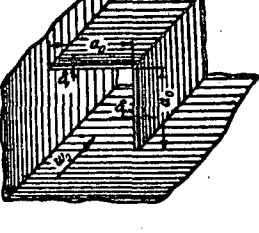
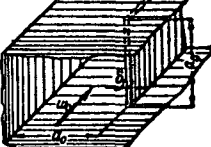
Inlet conditions	Diagram	Resistance coefficient $C = \frac{\Delta H}{\frac{1}{2} w_0^2}$
Entrance with end wall on one side of the conduit		0.58
Entrance with end walls on two opposite sides of the conduit		0.55
Entrance with end walls on two adjacent sides of the conduit		0.55
Entrance with end walls on three sides of the conduit		0.52
Entrance with end walls on four sides of the conduit		0.50
<i>w</i> is taken from § 1-3,b		

Straight inlets with various mountings between walls.

Section III

$$Re = \frac{\rho_0 d_0}{\mu} > 10^4$$

Diagram 3-12

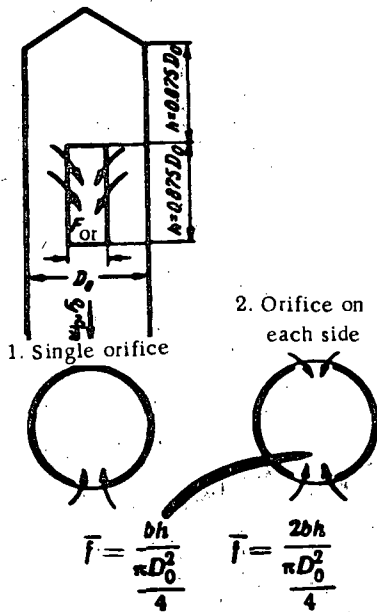
Inlet conditions	Resistance coefficient $\zeta = \frac{\Delta H}{\frac{V_0^2}{2g}}$
Entrance with deflector at one side of the conduit at $\frac{l}{a_0} = 0.5$	 0.60
Entrance with deflector at two sides of the conduit at $\frac{l}{a_0} = 0.5$	 0.63
Entrance to a conduit mounted on a wall	 0.67
Entrance to a conduit mounted between two walls	 0.68
Entrance to a conduit in an angle between two walls	 0.71
Entrance to a conduit clamped between three walls	 0.77
	0.92

Side entrance into a circular straight pipe through the first orifice,

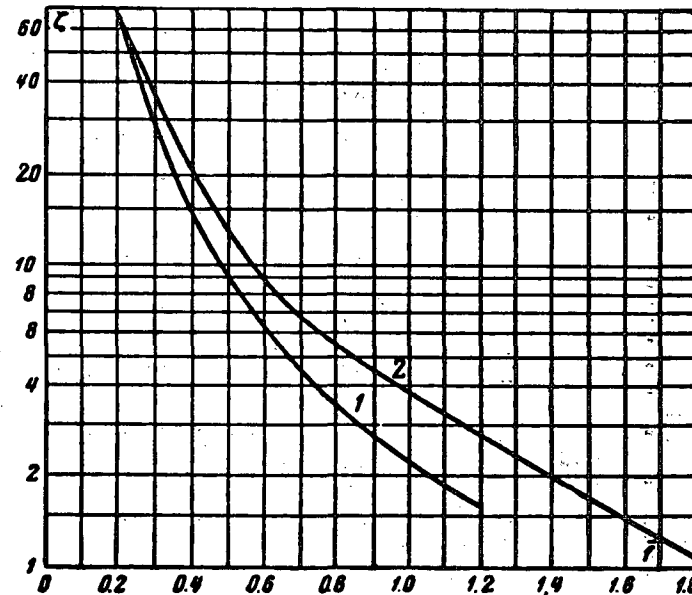
Section III

$$Re = \frac{w_{or} b}{v} > 10$$

Diagram 3-13

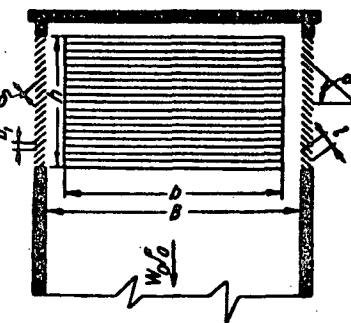


$\zeta = \frac{\Delta H}{\frac{\gamma w_0^2}{2g}}$ is determined from the curves $\zeta = f(\bar{f})$



\bar{f}	0.2	0.3	0.4	0.5	0.6	0.7	0.8	0.9	1.0	1.2	1.4	1.6	1.8
1. One orifice													
ζ	64.5	30.0	14.9	9.00	6.27	4.54	3.54	2.70	2.28	1.60	—	—	—
2. Two orifices													
ζ	65.5	36.5	17.0	12.0	8.75	6.85	5.50	4.54	3.84	2.76	2.01	1.40	1.10

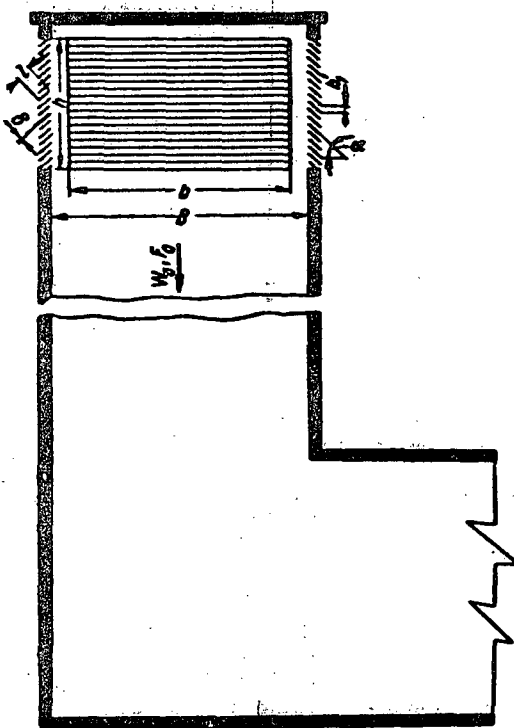
$$\frac{h}{B} = 0.5; I' = \frac{n b h}{F_0} = \frac{F_p}{F_0}$$



Number of orifices	Layout of the orifices		I'	$\frac{b}{h}$	Resistance coefficient $\frac{\Delta H}{T^2 F_0^2 / 2g}$		
	without louvers	with louvers			Without grids	$\alpha=30^\circ$: $b'_1/h = 0.029$, $I'/I = 1.6$, $b/b'_1 = 0.058$	$\alpha=45^\circ$: $b'_1/h = 0.034$, $I'/I = 1.4$, $b/b'_1 = 0.07$
1			0.44	1.5	12.6	17.5	—
2			0.88	1.5	3.60	5.40	—
2			0.88	1.5	4.20	6.30	—
3			1.30	1.5	1.80	3.20	—
4			1.74	1.5	1.20	2.50	3.80
4			1.16	1.0	2.00	3.60	6.00
4			0.58	0.5	8.00	13.7	21.5

Number of orifices n	Layout of the orifices		\bar{P}	$\frac{b}{h}$	Resistance coefficient $c = \frac{\Delta H}{\frac{T^2}{F_0} \frac{2g}{z}}$	
	without louvers	with louvers			Without grids	$\alpha=30^\circ$; $b'_1/h = 0.029$; $b'_1/b = 1.8$; $b'_1/s = 0.058$
1			0.44	1.5	14.0	18.6
1			0.44	1.5	16.0	19.0
1			0.44	1.5	16.7	20.0
2			0.88	1.5	4.50	6.50
2			0.88	1.5	5.20	7.00
2			0.88	1.5	5.30	7.20
2			0.88	1.5	5.30	7.50
3			1.30	1.5	2.60	3.90
3			1.30	1.5	3.00	4.50
3			1.30	1.5	3.40	5.10
4			1.74	1.5	2.70	4.00
4			1.16	1.0	3.10	4.70
4			0.58	0.5	9.00	14.4
						22.0

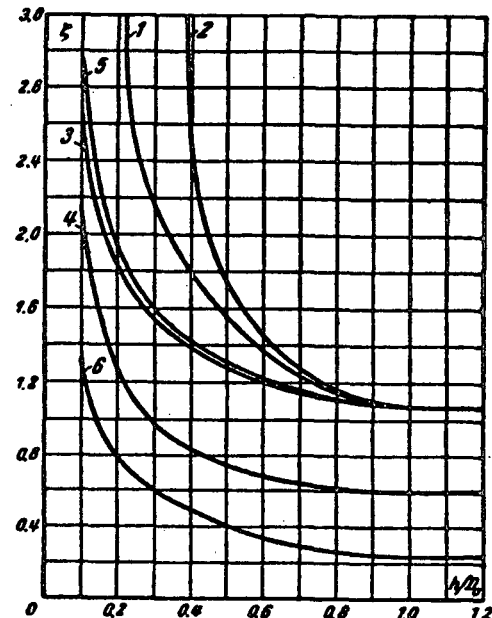
$$\frac{h}{B} = 0.5; \bar{P} = \frac{n b h}{F_0} = \frac{P_p}{F_0}$$



Straight indraft shafts of circular section, $Re = \frac{w_0 D_0}{\nu} > 10^4$

Section III
Diagram 3-16

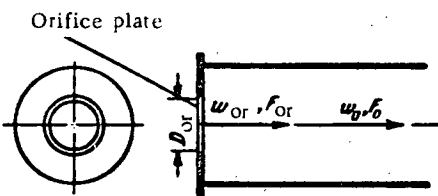
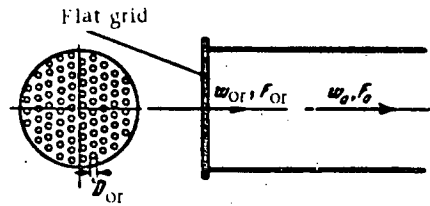
Shaft characteristic	Diagram	Resistance coefficient
No. 1 with flat screen		$\zeta = \frac{\Delta H}{\frac{1}{2} w_0^2}$ is determined from the curves $\zeta = f\left(\frac{h}{D_0}\right)$
No. 2 with section		Values of ζ
No. 3 with hood at sharp inlet edge		Draw- ing No.
No. 4 with hood at thickened inlet edge		$\frac{h}{D_0}$
No. 5 with hood and slots		0.1 0.2 0.3 0.4 0.5 0.6 0.7 0.8 0.9 1.0 ∞
No. 6 with diffuser and hood		1 — 4.40 2.15 1.78 1.58 1.35 1.23 1.13 1.10 1.06 1.06 2 — 48.0 6.40 2.72 1.73 1.47 1.26 1.16 1.07 1.06 1.06 3 2.63 1.83 1.53 1.39 1.31 1.19 1.15 1.08 1.07 1.06 1.06 4 2.13 1.30 0.95 0.84 0.75 0.70 0.65 0.63 0.60 0.60 0.60 5 2.90 1.90 1.59 1.41 1.33 1.25 1.15 1.10 1.07 1.06 1.06 6 1.32 0.77 0.60 0.48 0.41 0.30 0.29 0.28 0.25 0.25 0.25



Entrance to a straight conduit through a
perforated plate with sharp-edged orifices ($\frac{l}{d_h} = 0 + 0.015$)

Section III

Diagram 3-17



$$d_h = \frac{4f_{or}}{\Pi_{or}}; \Pi_{or} = \text{perimeter of the orifices}$$

$$f_{or} = \text{area of one orifice}; \bar{f} = \frac{F_{or}}{F_p} = \frac{F_{or}}{F_0}$$

$$1) Re = \frac{w_{or} d_h}{v} \geq 10^5:$$

$$\zeta = \frac{\Delta H}{T w_0^2} \approx (1.707 - \bar{f})^2 \frac{1}{\bar{f}^2} \text{ is determined from the curve } \zeta = f(\bar{f})$$

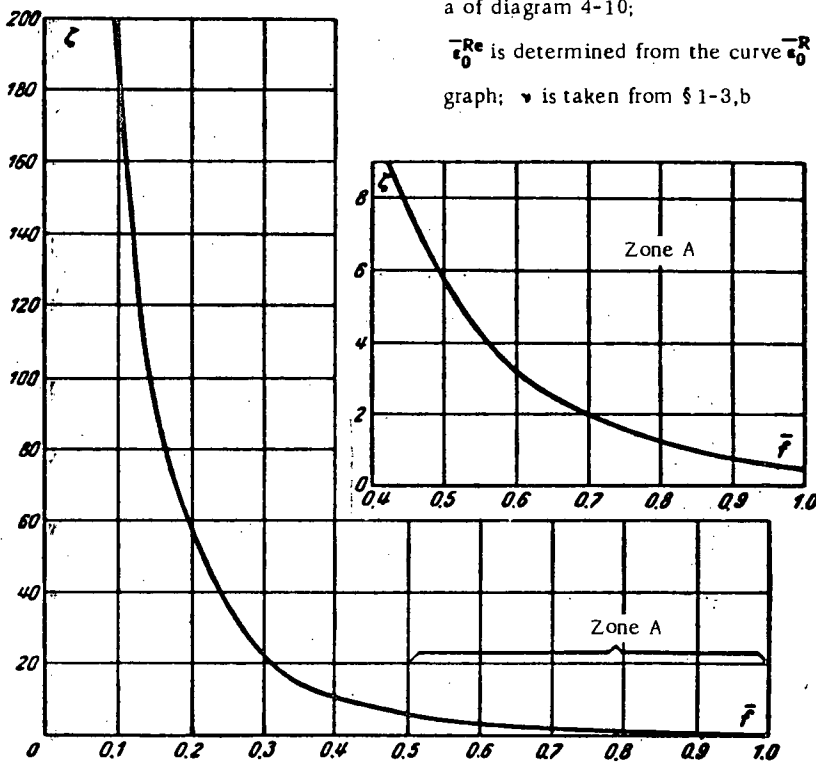
$$2) Re < 10^5 \text{ (approximate)}$$

$$\zeta = \frac{\Delta H}{T w_0^2} \approx [\zeta_p + \zeta_0^{Re} (1.707 - \bar{f})^2] \frac{1}{\bar{f}^2},$$

\bar{f}	0.05	0.10	0.15	0.20	0.25	0.30	0.35	0.40	0.45	0.50	0.55	0.60	0.65	0.70	0.75	0.80	0.90	1.0
ζ	1100	258	98	57	38	24	15	11	7.8	5.8	4.4	3.5	2.6	2.0	1.7	1.3	0.8	0.5

where ζ_p is determined from the curve $\zeta_p = f_1(Re, \bar{f})$ on graph of diagram 4-10;

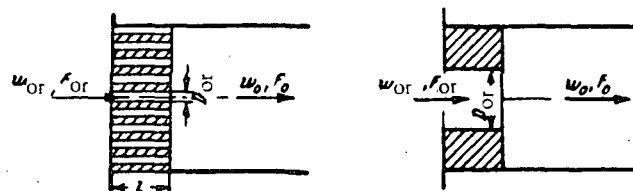
ζ_0^{Re} is determined from the curve $\zeta_0^{Re} = f_2(Re)$ on the same graph; v is taken from § 1-3,b



Entrance to a straight conduit through a perforated plate
with thick-edged orifices ($\frac{l}{d_h} > 0.015$)

Section III

Diagram 3-18



$$d_h = \frac{4f_{or}}{\Pi_{or}}$$

Π_{or} = perimeter

f_{or} = area of one orifice

F_{or} = free grid (washer) section

$$\bar{f} = \frac{F_{or}}{F_0} = \frac{\Sigma f_{or}}{F_0}$$

$$1) Re = \frac{w_{or} d_h}{v} > 10^5$$

$$\zeta = \frac{\Delta H}{\frac{T w_0^2}{2g}} \cong \left[0.5 + (1 - \bar{f})^2 + \tau(1 - \bar{f}) + \lambda \frac{l}{d_h} \right] \frac{1}{\bar{f}^2} = \left(\zeta_0 + \lambda \frac{l}{d_h} \right) \frac{1}{\bar{f}^2}$$

where τ is determined from the curve $\tau = f\left(\frac{l}{d_h}\right)$; λ is determined as a function of Re and $\Delta = \frac{\Delta}{d_h}$ from diagrams 2-2 - 2-5; Δ is taken from Table 2-1; v is taken from § 1-3, b.

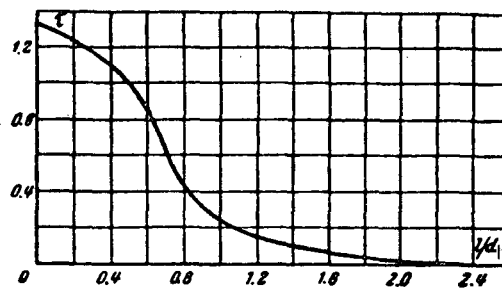
$$2) Re < 10^5 \text{ (approximate)}$$

$$\zeta = (\zeta_0 + \bar{e}_0^{Re} \zeta_0) \frac{1}{\bar{f}^2}$$

where ζ_0 and \bar{e}_0^{Re} are found from diagram 4-10;

$$\zeta_0 = 0.5 + (1 - \bar{f})^2 + \tau(1 - \bar{f})$$

l/d_h	0	0.2	0.4	0.6	0.8	1.0	1.2	1.6	2.0	2.4
τ	1.35	1.22	1.10	0.84	0.42	0.24	0.16	0.07	0.02	0

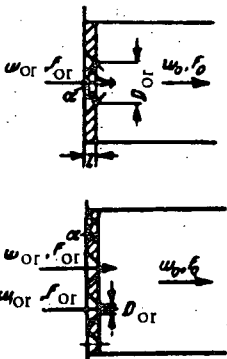
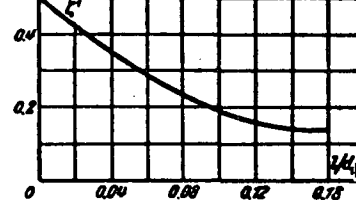
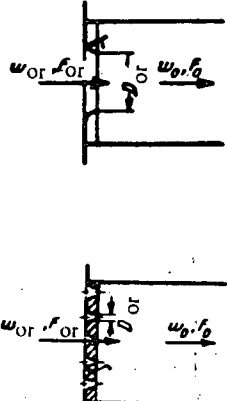
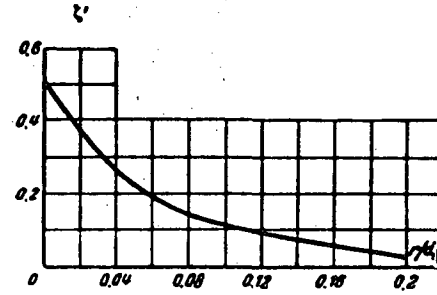


Entrance to a straight conduit through a perforated plate
with orifice edges beveled or rounded

Section III:

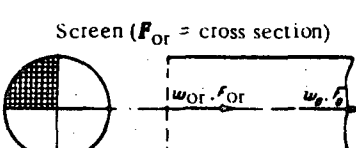
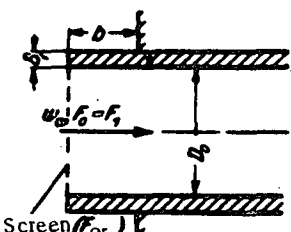
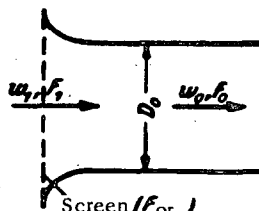
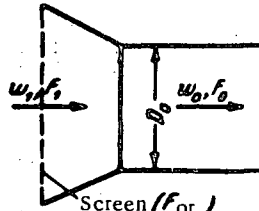
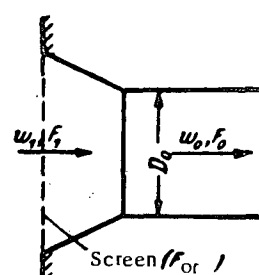
$$Re = \frac{w_{or} d_h}{\nu} > 10^3$$

Diagram 3-19

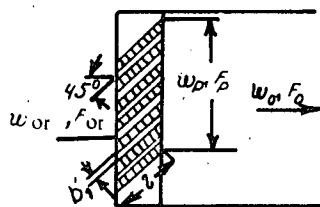
Grid characteristic	Plan	Resistance coefficient $\xi = \frac{\Delta H}{\frac{1}{2} u_0^2}$																								
Orifices with beveled edges		$\xi = (1 + \sqrt{\zeta} - \bar{f})^2 \frac{1}{\bar{f}^2},$ <p>where ζ is determined from the curve $\zeta = f\left(\frac{l}{d_h}\right)$.</p> <table border="1"> <thead> <tr> <th>l/d_h</th><th>0.01</th><th>0.02</th><th>0.03</th><th>0.04</th><th>0.06</th><th>0.08</th><th>0.12</th><th>0.16</th></tr> </thead> <tbody> <tr> <th>ζ</th><td>0.46</td><td>0.42</td><td>0.38</td><td>0.35</td><td>0.29</td><td>0.23</td><td>0.16</td><td>0.13</td></tr> </tbody> </table>  <p>a</p>	l/d_h	0.01	0.02	0.03	0.04	0.06	0.08	0.12	0.16	ζ	0.46	0.42	0.38	0.35	0.29	0.23	0.16	0.13						
l/d_h	0.01	0.02	0.03	0.04	0.06	0.08	0.12	0.16																		
ζ	0.46	0.42	0.38	0.35	0.29	0.23	0.16	0.13																		
Orifices with rounded edges		$\xi = (1 + \sqrt{\zeta} - \bar{f})^2 \frac{1}{\bar{f}^2},$ <p>where ζ is determined from the curve $\zeta = f\left(\frac{r}{d_h}\right)$</p> <table border="1"> <thead> <tr> <th>$\frac{r}{d_h}$</th><th>0</th><th>0.01</th><th>0.02</th><th>0.03</th><th>0.04</th><th>0.05</th><th>0.06</th><th>0.08</th><th>0.12</th><th>0.16</th><th>0.20</th></tr> </thead> <tbody> <tr> <th>ζ</th><td>0.50</td><td>0.44</td><td>0.37</td><td>0.31</td><td>0.26</td><td>0.22</td><td>0.19</td><td>0.15</td><td>0.09</td><td>0.06</td><td>0.02</td></tr> </tbody> </table>  <p>b</p>	$\frac{r}{d_h}$	0	0.01	0.02	0.03	0.04	0.05	0.06	0.08	0.12	0.16	0.20	ζ	0.50	0.44	0.37	0.31	0.26	0.22	0.19	0.15	0.09	0.06	0.02
$\frac{r}{d_h}$	0	0.01	0.02	0.03	0.04	0.05	0.06	0.08	0.12	0.16	0.20															
ζ	0.50	0.44	0.37	0.31	0.26	0.22	0.19	0.15	0.09	0.06	0.02															

Various entrances to a conduit with a screen at the inlet

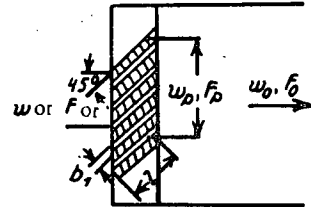
 Section III
 Diagram 3-20

Entrance characteristic	Diagram	Resistance coefficient $\zeta = \frac{\Delta H}{\frac{V^2}{2g}}$
Entrance with sharp inlet edge $(\frac{\delta_1}{D_h} = 0)$		$\zeta \approx 1 + \zeta_s$, where ζ_s is determined as ζ for a screen from diagram 3-6
Entrance with reinforced inlet edge $(\frac{\delta_1}{D_h} > 0)$		$\zeta \approx \zeta' + \zeta_s$, where ζ' is determined from the curves $\zeta = f(\frac{\delta_1}{D_h} \cdot \frac{b}{D_h})$ on diagram 3-1; ζ_s — as above.
Converging bell-mouth orifice forming the arc of a circle		$\zeta \approx \zeta' + \frac{\zeta_s}{n^2}$, where ζ' is determined from the curve $\zeta = f(\frac{r}{D_h})$ on diagram 3-3. ζ_s — as above.
Conic converging bellmouth orifice	a) Without end wall  b) With end wall 	$\zeta \approx \zeta' + \frac{\zeta_s}{n^2}$, where ζ' is determined from the curve $\zeta = f(\alpha^\circ, \frac{l}{D_{hi}})$ on diagrams 3-5 and 3-6 respectively; ζ_s — as above

No. 1 — inlet edges of the fins
 cut vertically



No. 2 — inlet edges of the fins
 cut horizontally



$$\text{No. 1 } \frac{l}{b'_1} \geq \left(\frac{l}{b'_1} \right)_{\text{opt}} \left[\text{ где } \left(\frac{l}{b'_1} \right)_{\text{opt}} \cong 11(1 - \bar{n}) \right]:$$

$$\zeta = \frac{\Delta H}{\frac{\tau w_0^2}{2g}} \cong k \left[0.85 + \left(1 - \bar{F} \frac{F_p}{F_0} \right)^2 + \zeta_{fr} \right] \frac{1}{\bar{F}^2} \left(\frac{F_0}{F_p} \right)^2 = k$$

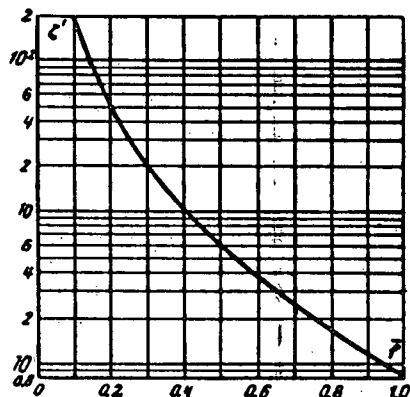
$$\text{No. 2 } \frac{l}{b'_1} < \left(\frac{l}{b'_1} \right)_{\text{opt}} : \quad \zeta = \frac{\Delta H}{\frac{\tau w_0^2}{2g}} \cong k\zeta + \Delta\zeta$$

where $k = 1.0$ for No. 1; $k = 0.6$ for No. 2;

$$\Delta\zeta \cong 0.5 \left[11(1 - \bar{n}) - \frac{l}{b'_1} \right]; \quad \zeta_{fr} = \lambda \frac{l}{b'_1} :$$

λ is determined from diagrams 2-1 to 2-5;

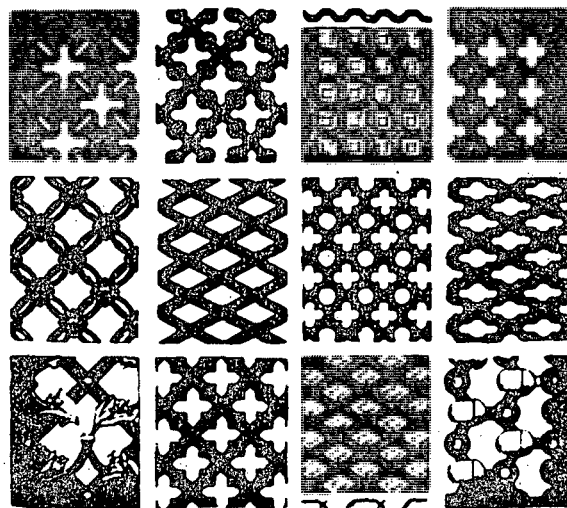
\bar{F}	0.1	0.2	0.3	0.4	0.5	0.6	0.7	0.8	0.9	1.0
ζ	235	52.5	20.5	10.5	6.00	3.60	2.35	1.56	1.18	0.85



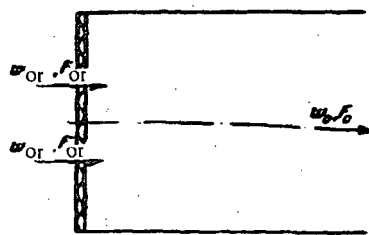
$$\bar{F} = \frac{F_{or}}{F_p} \quad (F_p - \text{grid front area}; \quad F_{or} - \text{grid cross section})$$

$$\text{At } \frac{l}{b'_1} = \left(\frac{l}{b'_1} \right)_{\text{opt}} \cdot \frac{F_{or}}{F_p} = \frac{F_{or}}{F_0} \text{ and } \lambda = 0.064$$

(at $(Re = \frac{w_{or} b'_1}{v} \cong 10^4)$; the values of ζ are determined from the curve $\zeta = \bar{F}(l)$; v is taken from § 1-3, b.)



$$w_{or} = \frac{Q}{F_{or}}; F_{or} = \text{free grid section}$$



$$\zeta = \frac{\Delta H}{\frac{1}{2} w_o^2} \quad \text{is determined approximately from the curve } \zeta = f(\bar{H})$$

on diagram 3-17.

Section Four

SUDDEN VARIATION OF VELOCITY IN STREAM PASSAGE THROUGH AN ORIFICE

(Resistance coefficients of stretches with sudden expansion,
orifice plates, apertures, etc.)

4-1. LIST OF SYMBOLS

- F_0 = area of the narrowest section of the stretch of the orifice, m²;
 F_1 = area of the channel section before the narrow section of the stretch of the orifice, m²;
 F_2 = area of the channel section behind the narrow section of the stretch of orifice, m²;
 F_c = area of the contracted-jet section at the entrance to the orifice, m²;
 $\epsilon = \frac{F_c}{F_0}$ = coefficient of jet contraction;
 $\epsilon_0^{\text{Re}} = \frac{F_c}{F_0}$ = coefficient depending on Re, of jet contraction in the section of a sharp-edged orifice at $\frac{F_0}{F_1} = 0$;
 $n = \frac{F_2}{F_0}$ = area ratio;
 Π_0 = section perimeter, m;
 D_0 = diameter of the narrowest section of the orifice, m;
 D_1, D_2 = diameters of the section before the orifice and the section behind it respectively, m;
 D_h = hydraulic diameter, 4X hydraulic radius, m;
 a_0, b_0 = sides of the rectangular section or semiaxes of the ellipse, m;
 t = length of the stretch, depth of the orifice, m;
 r = radius of curvature of the inlet-orifice edge, m;
 α = central angle of divergence of the diffuser or of convergent bell mouth, or of the opening of the aperture flaps in the wall;
 w_0 = mean stream velocity in the narrowest section of the orifice, m/sec;
 w_1, w_2 = mean stream velocities in the sections before and behind it, m/sec;
 ΔH = pressure loss or resistance of the stretch, kg/m²;
 ζ = resistance coefficient of the stretch;
 M = momentum coefficient, or Mach number;
 N = kinetic-energy coefficient.

4-2. EXPLANATIONS AND RECOMMENDATIONS

1. The sudden enlargement of the cross section of a conduit is the cause of so-called "shock" losses*. The resistance coefficient of a shock, with uniform velocity distribution over the section before the expansion and turbulent flow ($Re = \frac{w_0 D_h}{\nu} > 3500$), is a function of

* [Not to be confused with shock losses in supersonic flow.]

the area ratio $n = \frac{F_2}{F_1}$ only, and is calculated by the Borda-Carnot formula:

$$\zeta = \frac{\Delta H}{\frac{1}{2} w_0^2} = \left(1 - \frac{F_0}{F_2}\right)^2. \quad (4-1)$$

2. When a stream suddenly expands, a jet is formed in the expanded section. This jet is separated from the remaining part of the medium by a surface of separation which disintegrates into powerful eddies (Figure 4-1). The length l_s of the stretch along which the formation of eddies, their gradual reabsorption, and the complete spreading of the stream over the section takes place equals 8 to 10 D_{2h} (D_{2h} = hydraulic diameter of the expanded section). The shock losses at sudden expansion are due to the formation of eddies in stretch l_s .

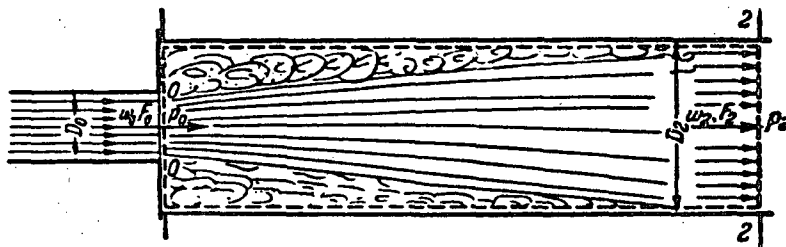


FIGURE 4-1. Flow pattern at sudden expansion.

3. Within the limits of Reynolds number $10 < Re < 3500$, the resistance coefficient of shock is a function not only of the area ratio $\frac{F_0}{F_2}$, but of Re as well, and at $Re < 10$ of Re only.

The values of ζ at $10 < Re < 3500$ can be determined from the data of diagram 4-1, and at $1 < Re < 10$ from the formula

$$\zeta = \frac{\Delta H}{\frac{1}{2} w_0^2} = \frac{A}{Re}, \quad (4-2)$$

where $A = 26$ according to Karev's data /4-15/.

4. Actually, the velocity distribution in the stretch before a sudden expansion is generally nonuniform (Figure 4-2). This has a strong effect on the actual pressure losses, and considerably increases them above the values given by (4-1).

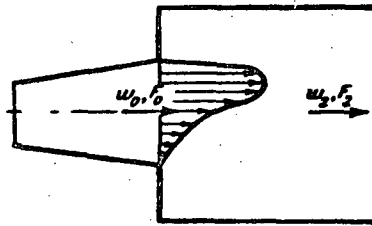


FIGURE 4-2. Nonuniform velocity distribution before a sudden expansion.

In order to calculate the resistance coefficient of a shock in a stream with nonuniform velocity distribution, it is necessary to use a general formula for the shock, which allows

for this nonuniformity if the velocity distribution over the channel section is known* :

$$\zeta = \frac{\Delta H}{\frac{1}{2} w_0^2} = \frac{1}{n^2} + N - \frac{2M}{n}, \quad (4-3)$$

where $M = \frac{1}{F_0} \int_{F_0}^F \left(\frac{w}{w_0}\right)^2 dF$ = coefficient of momentum at the exit from the narrow channel into the wide one; $N = \frac{1}{F_0} \int_{F_0}^F \left(\frac{w}{w_0}\right)^3 dF$ = coefficient of kinetic energy of the stream in the same section.

It can be approximated that

$$N \approx 3M - 2.$$

The accuracy of this formula is the higher, the nearer N and M are to unity.

Using the last expression, the following approximate formula is obtained for the resistance coefficients:

$$\zeta = \frac{\Delta H}{\frac{1}{2} w_0^2} \approx N \left(1 - \frac{2}{3n}\right) + \frac{1}{n^2} - \frac{4}{3n}. \quad (4-3')$$

5. If the velocity distribution over a section is known, the coefficients M and N can be easily determined. If the velocity distribution is unknown, it must be determined empirically. The values of M and N can then be determined by graphic integration from the velocity profiles obtained.

6. The velocity distribution is roughly exponential in the sections of expanding channels of divergence angles $\alpha = 8$ to 10° (Figure 4-3), in lengthy straight stretches of constant cross section with developed turbulent velocity profile (cf. § 1-7, and other stretches).

$$\frac{w}{w_{\max}} = \left(1 - \frac{y}{R_0}\right)^{\frac{1}{m}}. \quad (4-4)$$

where w , w_{\max} = the velocity at the given point and the maximum velocity over the section, m/sec; R_0 = radius of the section, m; y = distance from the pipe axis, m; m = exponent which can vary in the general case between 1 and ∞ .

7. At $m = 1$ the velocity profile resembles a triangle (Figure 4-4). At $m = \infty$ it resembles a rectangle, meaning that the velocity distribution over the section is completely uniform. In practice a velocity profile approximating a rectangle is obtained for m as low as 8 to 10 (Figure 4-4). Such a value of m can be assumed for lengthy

* The general formula for shock with allowance for a nonuniform velocity distribution was derived separately by Frenkel /4-19/ and the author /4-11/.

straight stretches at turbulent flow. The values $m = 2$ to 6 can be assumed for lengthy diffusers ($n > 2$), in accordance with the following table:

$$\begin{aligned} \text{at } \alpha = 2^\circ - m \approx 6; & \quad \text{at } \alpha = 6^\circ - m \approx 3; \\ \text{at } \alpha = 4^\circ - m \approx 4; & \quad \text{at } \alpha = 8^\circ - m \approx 2. \end{aligned}$$

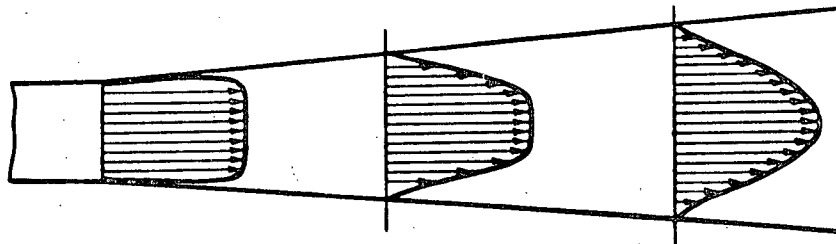


FIGURE 4-3. Smooth diffuser ($\alpha = 8$ to 10°).

8. The values of M and N in (4-3) can be calculated at the exponential velocity profile from the following formulas obtained by the author /4-11/:

a) in the case of conduits of circular and square sections;

$$M = \frac{(2m+1)^2(m+1)}{4m^2(m+2)} \quad (4-5)$$

and

$$N = \frac{(2m+1)^2(m+1)^2}{4m^4(2m+3)(m+3)}; \quad (4-6)$$

b) in the case of a plane pipe or diffuser with sides ratio of the rectangular section $\frac{a_0}{b_0} = 0.3 + 3.0$:

$$M = \frac{(m+1)^2}{m(m+2)} \quad (4-7)$$

and

$$N = \frac{(m+1)^2}{m^2(m+3)}. \quad (4-8)$$

9. The velocity profile in lengthy straight stretches of conduits, with a distance from the inlet larger than $10D_h$ and laminar flow, is parabolic (Figure 4-4):

$$\frac{w}{w_{\max}} = 1 - \left(\frac{y}{R_o}\right)^2. \quad (4-9)$$

The values of M and N obtained here are $M = 1.33$, $N = 2$ in the case of a conduit of circular or square section, and $M = 1.2$, $N = 1.55$ in the case of a plane pipe.

10. The velocity profile is roughly sinusoidal (Figure 4-5) in conduits in the vicinity of grids, elbows behind guide vanes, and in other similar obstructions; in the case of a plane channel it is calculated by the following formula /4-11/:

$$\frac{w}{w_0} = 1 + \frac{\Delta w}{w_0} \sin 2k\pi \frac{2y}{b_0}. \quad (4-10)$$

where b_0 = width of the plane channel, m; Δw = deviation of the velocity at the given point of a narrow channel section from the mean velocity w_0 over that section, m/sec; k = integer; $\pi \approx 3.14 \dots$

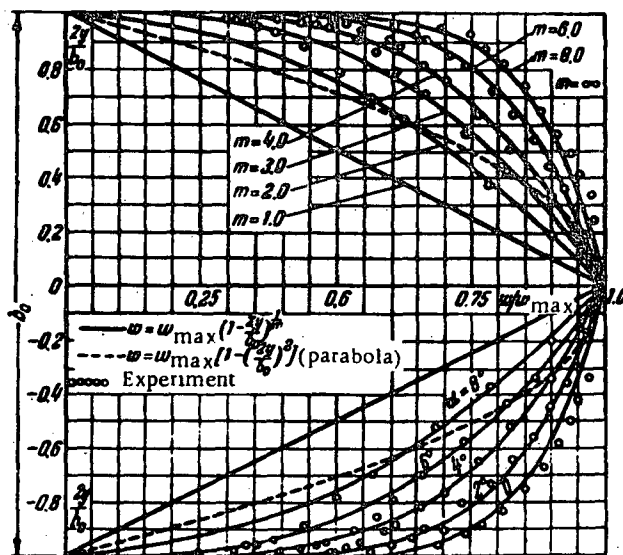


FIGURE 4-4. Velocity distribution in plane diffusers with divergence angles not wider than 8° , and comparison with the exponential law.

Here the coefficients M and N are expressed as follows:

$$M = 1 + \frac{1}{2} \left(\frac{\Delta w}{w_0} \right)^2 \quad (4-11)$$

and

$$N = 1 + \frac{3}{2} \left(\frac{\Delta w}{w_0} \right)^2. \quad (4-12)$$

11. A nonsymmetrical velocity field is established behind diffusers with divergence angles sufficient to cause stream separation ($\alpha > 10^\circ$), behind elbows, branches, etc. (Figure 4-6). In particular, the velocity distribution in plane diffusers with divergence angles $\alpha = 15$ to 20° and in straight elbows ($\delta = 90^\circ$) is found by the following formula /4-11/:

$$\frac{w}{w_0} = 0.585 + 1.64 \sin \left(0.2 + 1.95 \frac{2y}{b_0} \right). \quad (4-13)$$

The values obtained in this case for M and N are: $M = 1.87$ and $N = 3.7$.

12. When a nonuniform velocity field is established in a conduit of constant cross section ($n = 1$), the equalization of stream velocity is accompanied by irreversible pressure

losses, which are calculated by the following formula derived from (4-3):

$$\zeta = \frac{\Delta H}{\frac{1}{2} w_0^2} = 1 + N - 2M \quad (4-14)$$

or

$$\zeta = \frac{\Delta H}{\frac{1}{2} w_0^2} \approx \frac{1}{3} (N - 1), \quad (4-14')$$

where M and N are determined in accordance with the nonuniform pattern obtained. These losses are taken into account only where they have been neglected in determining the local resistance of fittings or obstructions in the straight stretch.

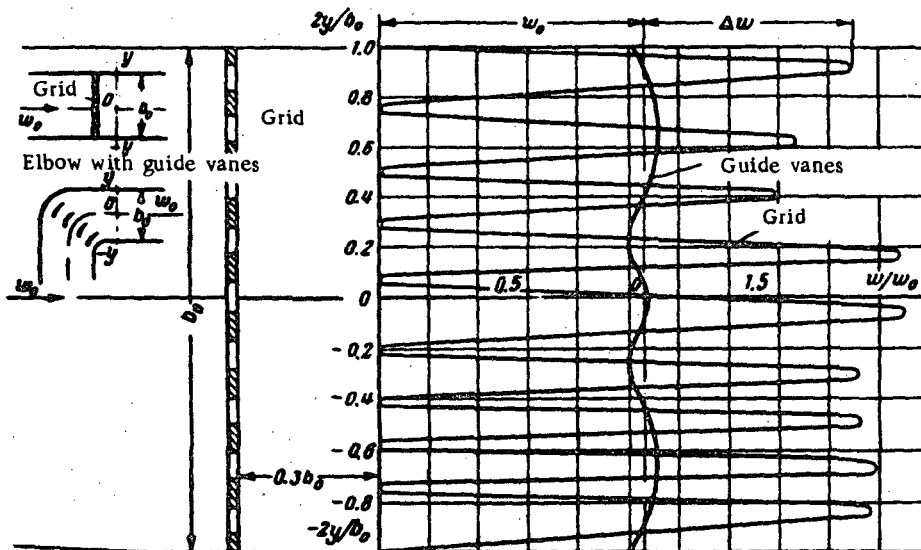


FIGURE 4-5. Sinusoidal velocity profile behind grids and guide vanes.

13. The coefficients M and N for the intake of the mixing chamber of an ejector at the point of entry of the "main" zone of the free jet (Figure 4-7) are calculated by the following formulas, /4-11/:

$$M = \frac{1}{q^2} \cdot \frac{F_2}{F_0} \quad (4-15)$$

and

$$N = \frac{1}{q^2} \left(\frac{F_2}{F_0} \right)^2 e, \quad (4-16)$$

* For the definition of the concept of "main" zone of a free jet, cf. Section XI.

where F_1 = section of free jet in mixing chamber; F_0 = section of jet in inlet nozzle; \bar{q} = dimensionless discharge through the given section, i.e., ratio of the discharge through the pipe to the discharge through the inlet nozzle; \bar{e} = ratio of the energy of the jet at its entry to the mixing chamber, to the initial energy of the jet.

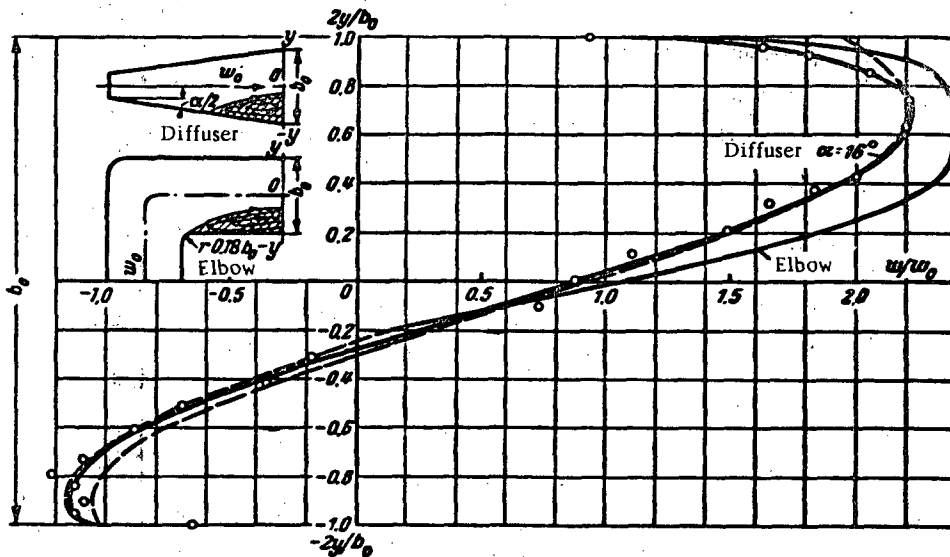


FIGURE 4-6: Nonsymmetric velocity distribution behind an elbow or a diffuser with a divergence angle causing stream division.

The magnitudes $\frac{F_1}{F_0} = \frac{F_1}{F_0} \cdot \bar{q}$, and \bar{e} are functions of the relative length of the free jet $\frac{s_i}{D_h}$ and are determined from the corresponding graphs of diagrams 11-32 and 11-33.

14. The resistance of a stretch with a sudden enlargement can be reduced by installing baffles (cf. diagram 4-1). Correct installation* of these baffles reduces the losses by 35 to 40 %, so that the resistance coefficient of such a stretch can be approximated by the formula

$$\zeta = \frac{\Delta H}{\frac{1}{2} \rho_0 u^2} \approx 0.6 \zeta' \quad (4-17)$$

where ζ' = resistance coefficient of a stretch with sudden enlargement without baffles, determined from the data in diagram 4-1.

15. In the general case, the passage of a stream from one volume into another through a hole in a wall is accompanied by the phenomena illustrated in Figure 4-8. The stream passes from channel 1, located before the partition A with orifice of diameter D_o , into channel 2, located behind this partition. The two channels can have cross sections of arbitrary dimensions, provided they are not smaller than the cross section of the orifice of passage. The passage of the stream through the orifice is accompanied by the bending of the trajectories of the particles, the inertial forces causing them to continue

* The basic data to be used in the installation of such baffles are given in § 5-2 (paragraph 16).

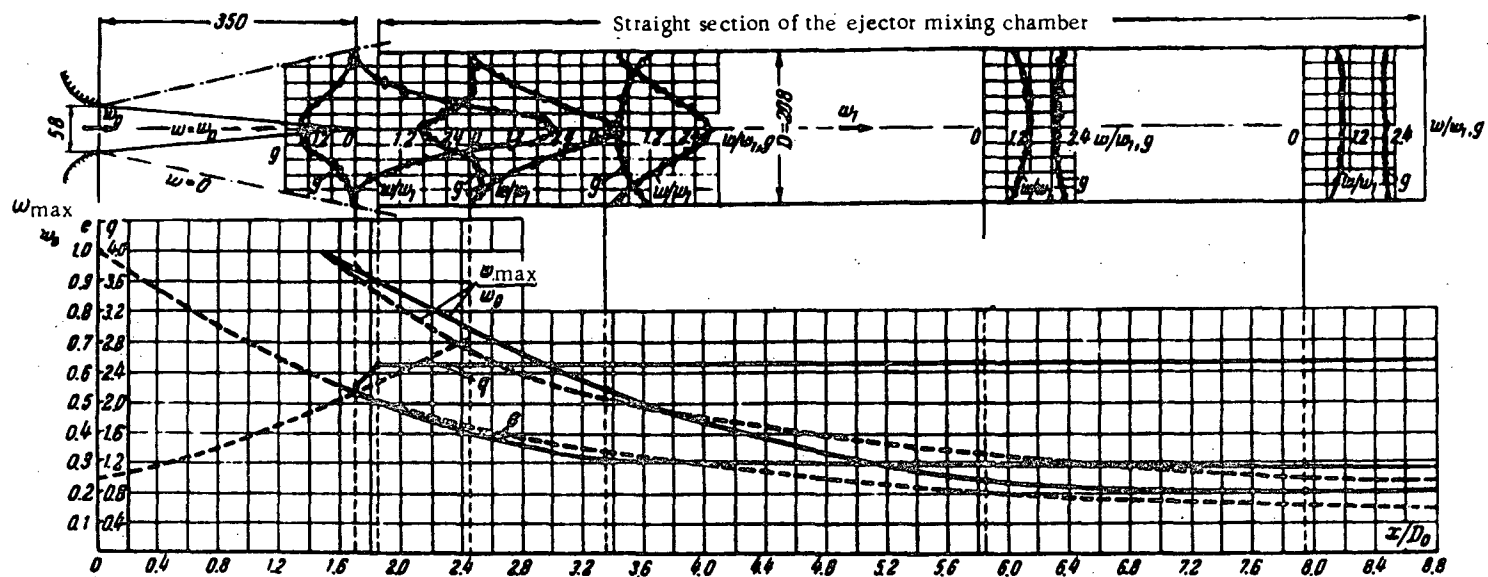


FIGURE 4-7. Velocity distribution in the main zone of the free jet after its entrance into the mixing chamber of the ejector:

--- theoretical curve for the free jet; —— experimental curve for the jet in the channel.

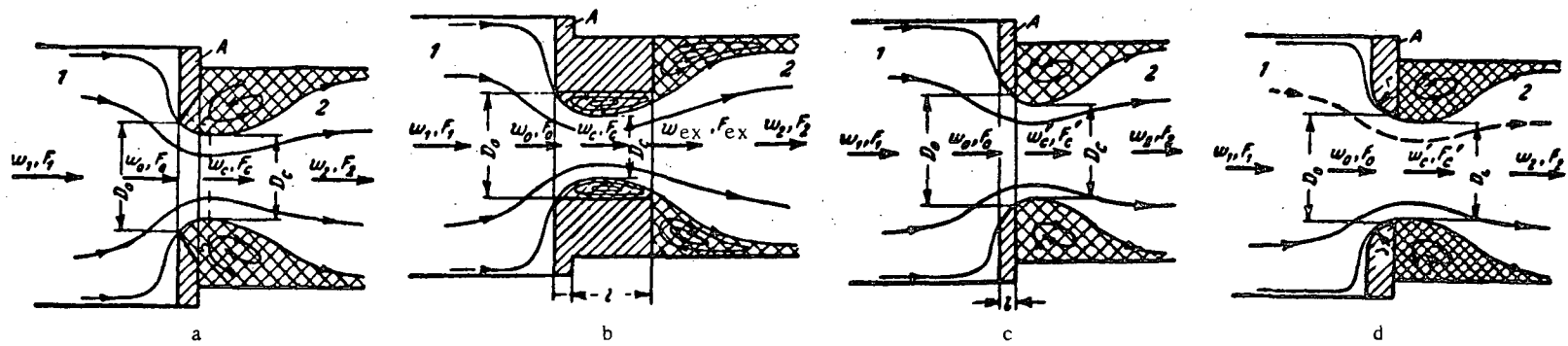


FIGURE 4-8. General case of stream flow from one volume into another through an orifice:

a — sharp-edged orifice ($D_h/l \approx 0$); b — thick-walled orifice ($D_h/l > 0$); c — orifice with edges beveled in the flow direction; d — orifice edges rounded in the flow direction.

their motion toward the orifice axis. This leads to a decrease of the jet section from its initial area F_1 to an area F_c (section $c-c$) smaller than the area F_0 of the orifice section. Starting with section $c-c$, the trajectories of the moving particles are straightened, and the normal phenomenon of sudden jet expansion takes place farther on.

16. The resistance coefficient of the stream passage through a sharp-edged orifice $\frac{l}{D_h} = 0$, Figure 4-8, a) is calculated in the general case described under 15, at $Re = \frac{w_0 D_h}{\nu} > 10^5$ by the formula /4-10/:

$$\zeta = \frac{\Delta H}{\frac{1}{2} w_0^2} = \left(1 + 0.707 \sqrt{1 - \frac{F_0}{F_1} - \frac{F_0}{F_2}} \right)^2. \quad (4-18)$$

At $Re < 10^5$ the resistance coefficient can be calculated by the approximate formula /4-14/:

$$\zeta = \frac{\Delta H}{\frac{1}{2} w_0^2} \approx \left(\frac{1}{\varphi^2} - 1 \right) + \frac{0.342}{(\epsilon_0^{Re})^2} \left(1 + 0.707 \sqrt{1 - \frac{F_0}{F_1} - \frac{F_0}{F_2}} \right)^2 = \zeta_v + \bar{\epsilon}_0^{Re} \left(\zeta_v - \frac{F_0}{F_2} \right)^2. \quad (4-19)$$

where φ = velocity coefficient at discharge from a sharp-edged orifice, depending on the Reynolds number Re and the area ratio $\frac{F_0}{F_1}$; $\epsilon_0^{Re} = \frac{F_c}{F_0}$ = coefficient of filling of the section of a sharp-edged orifice at $\frac{F_0}{F_1} = 0$, depending on Reynolds number; $\zeta_v = \left(\frac{1}{\varphi^2} - 1 \right)$ is determined from the curves $\zeta_v = f_1(Re, \frac{F_0}{F_1})$ on graph a of diagram 4-10; $\bar{\epsilon}_0^{Re} = \frac{0.342}{(\epsilon_0^{Re})^2}$ is determined from the curve $\bar{\epsilon}_0^{Re} = f_2(Re)$ on graph a of the same diagram;

$$\zeta_v = 1 + 0.707 \sqrt{1 - \frac{F_0}{F_1}}.$$

17. The thickening (Figure 4-8, b), beveling (Figure 4-8, c), or rounding (Figure 4-8, d) of the orifice edges lead to the weakening of the jet-contraction effects in the orifice, i.e., to the decrease of the jet velocity in its narrowest section ($F'_c > F_c$, $w'_c < w_c$). Since it is this velocity which basically determines the shock losses at the discharge from the orifice, the total resistance of the passage through the orifice is decreased.

18. The resistance coefficient of the passage of a stream through a wall orifice of arbitrary edge shape and thickness is calculated as described under 15, at large Reynolds numbers (practically at $Re \geq 10^5$), by the author's formulas /4-12/ and /4-13/:

$$\zeta = \frac{\Delta H}{\frac{1}{2} w_0^2} = \zeta' \left(1 - \frac{F_0}{F_1} \right) + \left(1 - \frac{F_0}{F_2} \right)^2 + \epsilon \sqrt{1 - \frac{F_0}{F_1} \left(1 - \frac{F_0}{F_2} \right)} + \zeta_{fr}. \quad (4-20)$$

where ζ' is a coefficient, depending on the shape of the inlet edge of the orifice, and is determined as ζ from diagrams 3-1 to 3-3, and 3-6; ϵ = coefficient allowing for the influence of wall thickness, the inlet edge shape, and conditions of passage of a stream across the orifice; it is determined at thick-walled orifices from the

curve $\tau = f\left(\frac{l}{D_h}\right)$ of diagram 4-11, and approximately, at orifices with rounded or beveled edges, by the formula $\tau \approx 2\sqrt{\ell}$; $\zeta_{fr} = \lambda \frac{l}{D_h}$ = friction coefficient of the entire depth of the orifice; λ = friction coefficient of unit depth of the orifice, determined by diagrams 2-1 to 2-5.

In the case of beveled or rounded orifice edges, ζ_{fr} is assumed to be equal to zero.

The following formula, similar to (4-19), can be used at $Re < 10^5$ for thick-walled orifices:

$$\zeta = \frac{\Delta H}{\frac{\gamma w_0^2}{2g}} \approx \zeta_0 + \zeta_{fr}^{Re} \left[0.5 \left(1 - \frac{F_0}{F_1} \right) + \left(1 - \frac{F_0}{F_2} \right)^2 + \sqrt{1 - \frac{F_0}{F_1}} \left(1 - \frac{F_0}{F_2} \right) \right] + \zeta_{fr}. \quad (4-21)$$

19. In general, flow through an orifice in a wall can assume several distinct forms:

- a) $F_1 = F_0$ — sudden expansion of the section (Figure 4-1), for which the resistance formula (4-20) reduces to (4-1);
- b) $F_2 = F_0$ — sudden contraction of the section (Figure 3-6,a), for which the resistance formula (4-20) reduces to (3-3);
- c) $F_1 \rightarrow \infty$ — entrance with sudden enlargement (entrance through a flat plate orifice or perforated plate, Figure 3-9), for which the resistance formula (4-20) reduces to the following (if ζ is expressed through the velocity w_2 behind the orifice)* :

$$\zeta = \frac{\Delta H}{\frac{\gamma w_2^2}{2g}} = \left[\zeta' + \left(1 - \frac{F_0}{F_2} \right)^2 + \zeta \left(1 - \frac{F_0}{F_2} \right) + \zeta_{fr} \right] \left(\frac{F_2}{F_0} \right)^2. \quad (4-22)$$

- d) $F_2 \rightarrow \infty$ — discharge from the orifice into an unlimited space (stream discharge through an orifice plate or perforated plate at the pipe end, Figure 11-3), for which the resistance formula (4-20) reduces to the following (if ζ is expressed through the velocity w_1 before the orifice)** :

$$\zeta = \frac{\Delta H}{\frac{\gamma w_1^2}{2g}} = \left[1 + \zeta' \left(1 - \frac{F_0}{F_1} \right) + \zeta \sqrt{1 - \frac{F_0}{F_1}} + \zeta_{fr} \right] \left(\frac{F_1}{F_0} \right)^2. \quad (4-23)$$

- e) $F_1 = F_2$ — restrictor, orifice plate, etc. (Figure 4-9), for which the resistance formula (4-20) reduces to the following (if ζ is expressed through the velocity w_1 before the orifice):

$$\zeta = \frac{\Delta H}{\frac{\gamma w_1^2}{2g}} = \left[\left(\zeta' + \zeta \sqrt{1 - \frac{F_0}{F_1}} \right) \left(1 - \frac{F_0}{F_1} \right) + \left(1 - \frac{F_0}{F_1} \right)^2 + \zeta_{fr} \right] \left(\frac{F_1}{F_0} \right)^2. \quad (4-24)$$

* The subscript "o" corresponds here to the subscript "or", and the subscript "2" to the subscript "o" in Section III.

** The subscript "o" corresponds here to the subscript "or", and the subscript "1" to the subscript "o" in Section XI.

f) $F_1 = F_2 \rightarrow \infty$ — aperture in a wall of unlimited area (flow through an orifice from some large volume into another large volume, Figure 4-10), for which the resistance formula (4-20) reduces to the following:

$$\zeta = \frac{\Delta H}{\frac{\gamma w_0^2}{2g}} = \zeta' + \tau + 1 + \zeta_{fr}. \quad (4-25)$$

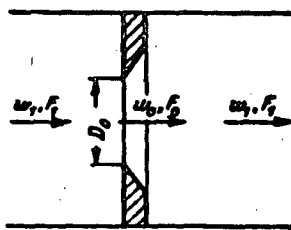


FIGURE 4-9. Restrictor.

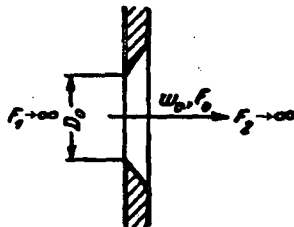


FIGURE 4-12. Open test section of a wind tunnel.

20. The resistance coefficient of a restrictor reduces to the following expressions at different shapes of the orifice edges and $Re \geq 10^5$:

a) Sharp-edged orifice. In this case $\zeta' = 0.5$ and $\tau = 1.41$, so that formula (4-24) reduces to the following formula (/4-10/, /4-12/, and /4-13/):

$$\zeta = \frac{\Delta H}{\frac{\gamma w_1^2}{2g}} = \left(0.707 \sqrt{1 - \frac{F_0}{F_1}} + 1 - \frac{F_0}{F_1} \right)^2 \left(\frac{F_1}{F_0} \right)^2. \quad (4-26)$$

b) Thick-walled orifice. In this case too $\zeta' = 0.5$, so that:

$$\zeta = \frac{\Delta H}{\frac{\gamma w_1^2}{2g}} = \left[\left(0.5 + \tau \sqrt{1 - \frac{F_0}{F_1}} \right) \left(1 - \frac{F_0}{F_1} \right) + \left(1 - \frac{F_0}{F_1} \right)^2 + \zeta_{fr} \right] \left(\frac{F_1}{F_0} \right)^2. \quad (4-27)$$

where τ is determined from the curve $\tau = f\left(\frac{l}{D_h}\right)$ of diagram 4-11.

c) Orifice edges beveled or rounded. Assuming approximately $\tau \approx 2\sqrt{\frac{F_o}{F_i}}$ and $\zeta_{fr} = 0$, the following expression is obtained for the resistance coefficient:

$$\zeta = \frac{\Delta H}{\frac{\gamma w_i^2}{2g}} = \left[1 + \sqrt{\zeta' \left(1 - \frac{F_o}{F_i} \right) - \frac{F_o}{F_i}} \right]^2 \left(\frac{F_i}{F_o} \right)^2.$$

where ζ' is determined in the case of beveled edges from graph a of diagram 4-12 as a function of $\frac{l}{D_h}$, and in the case of rounded edges as ζ' from graph b of diagram 4-12 as a function of $\frac{l}{D_h}$.

21. The resistance coefficient of a restrictor at $Re < 10^5$ and sharp-edged orifices, is calculated by a formula derived from the general formula (4-19):

$$\zeta = \frac{\Delta H}{\frac{\gamma w_i^2}{2g}} \approx \left[\left(\frac{1}{\varphi^2} - 1 \right) + \frac{0.342}{(\zeta_0^{Re})^2} \left(1 + 0.707 \sqrt{1 - \frac{F_o}{F_i}} - \frac{F_o}{F_i} \right)^2 \right] \left(\frac{F_i}{F_o} \right)^2 = \left[\zeta_\varphi + \zeta_0^{Re} \left(\zeta_0 - \frac{F_o}{F_i} \right)^2 \right] \left(\frac{F_i}{F_o} \right)^2. \quad (4-29)$$

where φ , ζ_0^{Re} , ζ_φ , ζ_0 and ζ_o are determined as indicated under 16.

At $Re < 10^5$ and with a thick-edged orifice it follows from (4-21) and (4-27) that:

$$\zeta = \frac{\Delta H}{\frac{\gamma w_i^2}{2g}} \approx \left\{ \zeta_\varphi + \zeta_0^{Re} \left[\left(0.5 + \tau \sqrt{1 - \frac{F_o}{F_i}} \right) \left(1 - \frac{F_o}{F_i} \right) + \left(1 - \frac{F_o}{F_i} \right)^2 \right] + \zeta_{fr} \right\} \left(\frac{F_i}{F_o} \right)^2. \quad (4-30)$$

22. The resistance coefficient of an aperture in a wall, at different shapes of the orifice edges and $Re \geq 10^5$, reduces to the following expressions:

a) Sharp-edged orifice. In this case $\zeta' = 0.5$, $\tau = 1.41$, and $\zeta_{fr} = 0$, so that, on the basis of (4-25):

$$\zeta = \frac{\Delta H}{\frac{\gamma w_0^2}{2g}} \approx 2.9*. \quad (4-31)$$

b). Thick-edged orifice. In this case too $\zeta' = 0.5$, so that (4-25) gives:

$$\zeta = \frac{\Delta H}{\frac{\gamma w_0^2}{2g}} 1.5 + \tau + \zeta_{fr} = \zeta' + \zeta_{fr}, \quad (4-32)$$

where $\zeta' = 1.5 + \tau$ was obtained experimentally by the author and is plotted in graph a of diagram 4-18 as a function of $\zeta' = f\left(\frac{l}{D_h}\right)$.

* According to the author's experiments $\zeta \approx 2.8$.

c) Orifice edges beveled or rounded. Assuming $\zeta_{fr} = 0$ and $r \approx 2\sqrt{\zeta}$, we obtain:

$$\zeta = \frac{\Delta H}{\frac{\gamma w_0^2}{2g}} = (1 + \sqrt{\zeta})^2, \quad (4-33)$$

where ζ is determined from the curves $\zeta = f\left(\frac{l}{D_h}\right)$ (graph b) and $\zeta = f\left(\frac{r}{D_h}\right)$ (graph c) of diagram 4-18, respectively.

23. The resistance coefficient of an aperture in a wall with sharp-edged orifice at $Re < 10^5$, is determined from the following formula, which follows from (4-19):

$$\zeta = \frac{\Delta H}{\frac{\gamma w_0^2}{2g}} = \left(\frac{1}{r^2} - 1\right) + \frac{1}{(\epsilon_0^{Re})^2} = \zeta_{v_0} + \epsilon_0^{Re},$$

where ζ_{v_0} is determined from the curve $\zeta_{v_0} = f_1(Re)$ of diagram 4-17, ϵ_0^{Re} is determined from the curve $\epsilon_0^{Re} = f_2(Re)$ of the same diagram.

At $Re < 10^5$ and thick-walled orifice it follows from (4-21) and (4-32):

$$\zeta = \frac{\Delta H}{\frac{\gamma w_0^2}{2g}} = \left(\frac{1}{r^2} - 1\right) + \left(\frac{0.585}{\epsilon_0^{Re}}\right)^2 \zeta + \zeta_{fr} = \zeta_{v_0} + 0.342 \epsilon_0^{Re} \zeta + \zeta_{fr}, \quad (4-35)$$

where ζ_{v_0} and ϵ_0^{Re} are determined as in the case of an aperture with sharp-edged orifice; ζ is determined as under 22,b.

24. At low cross-section coefficients $\frac{F_0}{F_1}$ of the restrictor, large velocities are obtained in its orifice even at relatively low stream velocities in the pipe. The influence of compression begins to be felt here, leading to an increase in the resistance coefficient of the restrictor.

The resistance coefficient of a restrictor, taking the influence of compression into account, can be determined by the formula

$$\zeta_M = \frac{\Delta H}{\frac{\gamma_1 w_1^2}{2g}} = k_M \zeta, \quad (4-36)$$

where ζ_M = resistance coefficient of the restrictor at large Mach numbers; ζ = resistance coefficient of the restrictor at low Mach numbers, determined as indicated under 14 to 17; k_M = coefficient allowing for the influence of compressibility in the vena contracta of the jet at its passage through an orifice, determined from the graph (diagram 4-19); $M_1 = \frac{w_1}{a}$ = Mach number before the restrictor; $a = \sqrt{\gamma g p_1} =$ velocity of propagation of sound, m/sec; $\gamma = \frac{c_p}{c_v}$ = ratio of specific heats; p_1, γ_1 = static pressure (absolute, kg/m²) and specific gravity (kg/m³), respectively, of the medium before the restrictor.

25. As with entry into a straight channel, a sharp decrease of orifice resistance is achieved by installing an annular rib or ledge at the orifice inlet (Figure 4-11). Thus, according to Khanzhonkov's experiments /3-11/, the installation of an annular rib with $\frac{D_1}{D_0} \approx 1.22$ and $\frac{l}{D_0} \approx 0.25$ reduces the resistance coefficient ζ of an orifice in a wall from 2.7 - 2.8 to 1.15.

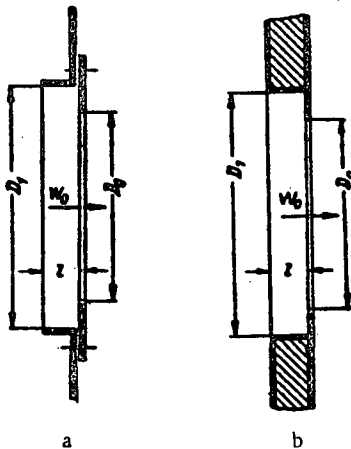


FIGURE 4-11. Entrance to an orifice through an annular rib (a) or ledge(b).

26. When the stream passes through a smooth bellmouth orifice set into a wall (cf. diagram 4-20), the resistance is equal to the sum of the resistances of: entrance into the bell mouth, frictional resistance in the straight stretch, and exit resistance. The resistance coefficient of such a stretch can be determined by the formula

$$\zeta = \frac{\Delta H}{\frac{\gamma v_0^2}{2g}} = \zeta' + \zeta_{fr}, \quad (4-37)$$

where ζ' = coefficient simultaneously allowing for the inlet and exit losses, and determined from the curves $\zeta' = f\left(\frac{l}{D_h}, \frac{r}{D_h}\right)$ of diagram 4-20; $\zeta_{fr} = \lambda \frac{l}{D_h}$ = friction coefficient of the straight stretch of a bellmouth.

27. When the stream passes through apertures in a wall fitted with various flaps, the resistance is higher than in the absence of flaps, since they cause a complex flow pattern. Here the resistance coefficient becomes a function of the angle of opening of the flaps α and their relative length $\frac{l_{fl}}{b_{fl}}$.

28. The open test section of a wind tunnel (Figure 4-12) can likewise be considered as a stretch with sudden enlargement.

Ejection dissipation of energy is the main cause of losses in the open test section of a wind tunnel. Another cause of losses is that part of the free jet is cut off by the diffuser. The kinetic energy of this portion of the jet is lost for the wind tunnel and, therefore, represents a part of the resistance of the throat.

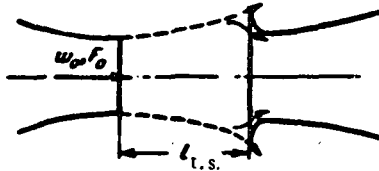


FIGURE 4-12. Open test section of a wind tunnel.

The coefficient of total resistance of the test section is calculated by Abramovich's formula /4-1/:

$$\zeta = \frac{\Delta H}{\frac{\gamma w_0^2}{2g}} = 0.0845 \frac{l_{t.s.}}{D_h} - 0.0053 \left(\frac{l_{t.s.}}{D_h} \right)^2. \quad (4-38)$$

where $D_h = \frac{4F_0}{\Pi_0}$ = hydraulic diameter of the exit section of the tunnel nozzle, m; and in the case of an elliptic cross section of the test section, approximately:

$$D_h \approx \frac{a_0 b_0}{1.5(a_0 + b_0) - \sqrt{a_0 b_0}}; \quad (4-39)$$

$l_{t.s.}$ = length of the test section, m; a_0, b_0 = ellipse semiaxes, m.

4-3. LIST OF DIAGRAMS OF RESISTANCE COEFFICIENTS OF SECTION IV

Diagram	Source	No. of diagram	Note
Sudden expansion of a stream with uniform velocity distribution	—	4-1	Bordat-Carnot formula; at low Re — Karev's experiments /4-15/ Calculation formulas
Sudden expansion after a long straight stretch, diffuser, etc., with exponential velocity distributions. Circular or rectangular cross section. $Re > 3.5 \times 10^3$	Idel'chik /4-11/	4-2	
Sudden expansion after long plane and straight stretches, plane diffusers, etc., with exponential velocity distribution. $Re > 3.5 \times 10^3$	The same	4-3	The same
Sudden enlargement of a plane channel behind orifice plates, baffles in elbows, etc., with sinusoidal velocity distribution $Re > 3.5 \times 10^3$	" "	4-4	" "
Sudden expansion behind plane diffusers with $\alpha > 10^\circ$, elbows, etc., with asymmetric velocity distribution. $Re > 3.5 \times 10^3$	" "	4-5	" "
Sudden expansion after stretches with parabolic velocity distributions. $Re > 3.5 \times 10^3$	" "	4-6	" "
Stream deformation in a straight conduit. $Re > 3.5 \times 10^3$	" "	4-7	" "
Stream deformation in a straight conduit with the entry of a free jet into it (ejector). $Re > 3.5 \times 10^3$	" "	4-8	" "
Sharp-edged ($l/D_h = 0 \div 0.015$) orifice at the passage of the stream from a conduit of one size to another. $Re > 10^5$	Idel'chik /4-12, 4-13/	4-9	" "
The same for $Re < 10^5$	Idel'chik /4-14/	4-10	" " (approximate)
Thick-edged ($l/D_h > 0.015$) orifice at the passage of the stream from a conduit of one size to another	Idel'chik /4-12, 4-13/	4-11	" "
The same, but beveled or rounded orifice edges	The same	4-12	" "
Sharp-edged ($l/D_h = 0 \div 0.015$) orifice in a straight conduit	Idel'chik /4-12, 4-14/	4-13	" "
Thick-edged ($l/D_h > 0.015$) orifice in a straight conduit	The same	4-14	" "
Orifice with edges beveled facing the stream flow ($\alpha = 40 \div 60^\circ$) in a straight pipe. $Re > 0^4$	" "	4-15	" "
Orifice with rounded edges in a straight pipe. $Re > 10^4$	" "	4-16	" "
Sharp-edged orifice ($\frac{l}{D_h} = 0 \div 0.015$) in a large wall	" "	4-17	" "
Orifices with various orifice edges in large walls	" "	4-18	" "
Perforated plate at high Mach numbers	—	4-19	On the basis of calculating data /4-21/ Experimental data
Bellmouth set in a large wall. $Re > 10^4$	Khanzhonkov /4-20/	4-20	
Exhaust flap, single, top-hinged	Bromlei /4-7/	4-21	The same
Intake flap, single, top-hinged	The same	4-22	" "
Single flap, center-hinged	" "	4-23	" "
Double flap, both top-hinged	" "	4-24	" "
Double flap, top- and bottom-hinged	" "	4-25	" "
Stamped louver with adjustable slats in a large wall $\tilde{f} \approx 0.8$; complete opening of the louver	" "	4-26	Tentative
Test section of a wind tunnel	Abramovich /4-1/	4-27	Theoretical formula

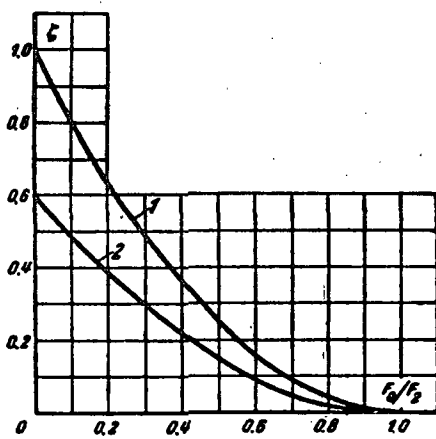
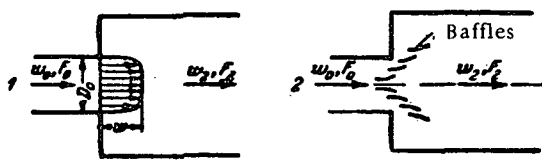
4.4. DIAGRAM OF THE RESISTANCE COEFFICIENTS

Sudden expansion of a stream with uniform velocity distribution

Section IV

Diagram 4-1

$$D_h = \frac{4F_0}{\Pi_0}; \quad \Pi_0 = \text{perimeter}$$



a.

$$1. \quad Re = \frac{\omega_0 D_h}{v} \geq 3.5 \cdot 10^3$$

a) Without baffles

$$\zeta = \frac{\Delta H}{\gamma w_0^2} = \left(1 - \frac{F_0}{F_2}\right)^2 \text{ is determined from the curve}$$

$$\zeta = f\left(\frac{F_0}{F_2}\right) \text{ (curve 1) on graph a.}$$

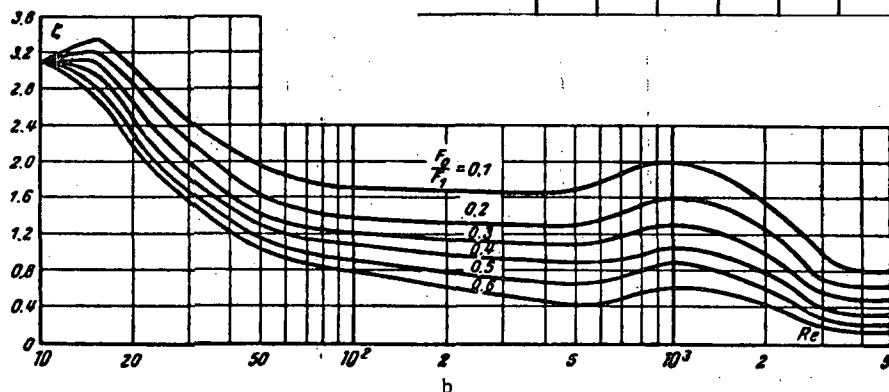
b) With baffles

$$\zeta = \frac{\Delta H}{\gamma w_0^2} \approx 0.6 \left(1 - \frac{F_0}{F_2}\right)^2 \text{ is determined from the curve}$$

$$\zeta = f\left(\frac{F_0}{F_2}\right) \text{ (curve 2) on graph a.}$$

$\frac{F_0}{F_2}$	0	0.1	0.2	0.3	0.4	0.5	0.6	0.7	0.8	1.0
1. Without baffles										
ζ	1.00	0.81	0.64	0.50	0.36	0.25	0.16	0.09	0.04	0
2. With baffles										
ζ	0.60	0.49	0.39	0.30	0.21	0.15	0.10	0.05	0.02	0

$\frac{F_0}{F_2}$	Re												
	10	15	20	30	40	50	10^2	$2 \cdot 10^2$	$5 \cdot 10^2$	10^3	$2 \cdot 10^3$	$3 \cdot 10^3$	
0.1	3.10	3.20	3.00	2.40	2.15	1.95	1.70	1.65	1.70	2.00	1.60	1.00	0.81
0.2	3.10	3.20	2.80	2.20	1.85	1.65	1.40	1.30	1.30	1.60	1.25	0.70	0.64
0.3	3.10	3.10	2.60	2.00	1.60	1.40	1.20	1.10	1.10	1.30	0.95	0.60	0.50
0.4	3.10	3.00	2.40	1.80	1.50	1.30	1.10	1.00	0.85	1.05	0.80	0.40	0.36
0.5	3.10	2.80	2.30	1.65	1.35	1.15	0.90	0.75	0.65	0.90	0.65	0.30	0.25
0.6	3.10	2.70	2.15	1.55	1.25	1.05	0.80	0.60	0.40	0.60	0.50	0.20	0.16



b

$$2. \quad 10 < Re < 3.5 \cdot 10^3:$$

$$\zeta = \frac{\Delta H}{\gamma w_0^2} \text{ is determined from}$$

the curves $\zeta = f(Re, \frac{F_0}{F_2})$ on graph b.

$$3. \quad 1 < Re < 8:$$

$$\zeta = \frac{\Delta H}{\gamma w_0^2} = \frac{26}{Re}$$

is determined from § 1-3, b.

Sudden expansion after a long straight stretch, diffuser, etc.,
with exponential velocity distribution

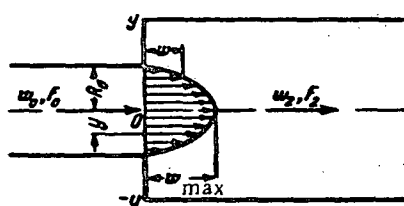
Section IV

Circular or rectangular cross section. $Re = \frac{w_0 D_h}{\nu} > 3.5 \cdot 10^4$

Diagram 4-2

$$D_h = \frac{4F_0}{U_0}; \quad U_0 \text{— perimeter; } n = \frac{F_0}{F_1}$$

$$\frac{w}{w_{\max}} = \left(1 - \frac{y}{R_0}\right)^{\frac{1}{m}}; \quad m \geq 1$$



$$\zeta = \frac{\Delta H}{\gamma w_0^2} = \frac{1}{n^2} + N - \frac{2M}{n} \text{ is determined from graph a;}$$

$$M = \frac{(2m+1)^2(m+1)}{4m^2(m+2)}$$

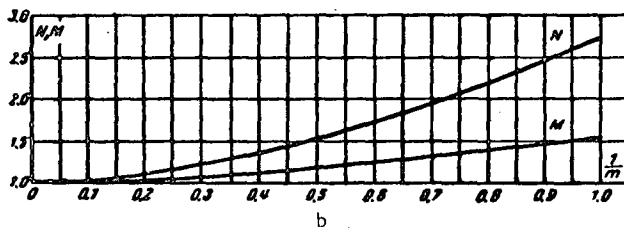
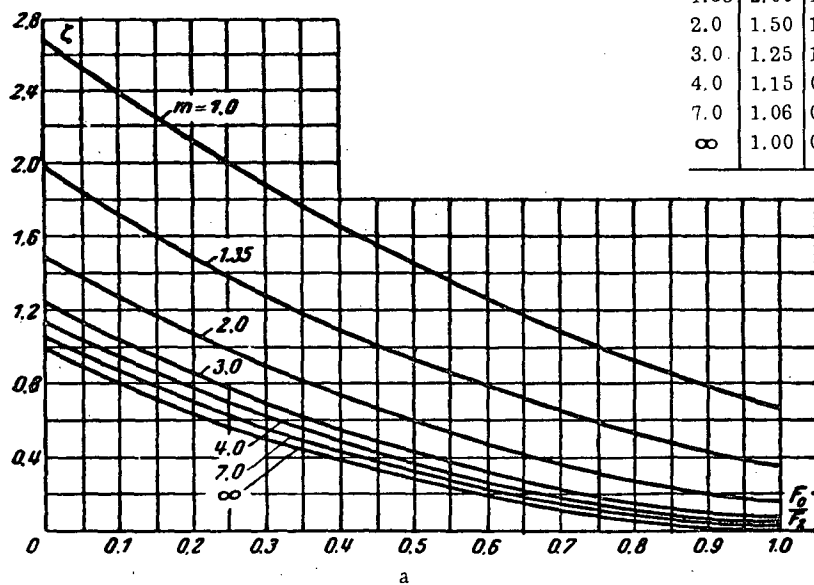
$$N = \frac{(2m+1)^2(m+1)^2}{4m^4(2m+3)(m+3)}$$

ν is taken from § 1-3, b

} are determined from graph b;

Values of ζ

m	F_0/F_1									
	0	0.1	0.2	0.3	0.4	0.5	0.6	0.7	0.8	1.0
1.0	2.70	2.42	2.14	1.90	1.66	1.45	1.26	1.09	0.94	0.70
1.35	2.00	1.74	1.51	1.29	1.00	0.93	0.77	0.65	0.53	0.36
2.0	1.50	1.28	1.08	0.89	0.72	0.59	0.46	0.35	0.27	0.16
3.0	1.25	1.04	0.85	0.68	0.53	0.41	0.30	0.20	0.14	0.07
4.0	1.15	0.95	0.77	0.62	0.47	0.35	0.25	0.17	0.11	0.05
7.0	1.06	0.86	0.69	0.53	0.41	0.29	0.19	0.12	0.06	0.02
∞	1.00	0.82	0.64	0.48	0.36	0.25	0.16	0.09	0.04	0



m	1.0	1.35	2.0	3.0	4.0	7.0	∞
N	2.70	2.00	1.50	1.25	1.15	1.06	1.0
M	1.50	1.32	1.17	1.09	1.05	1.02	1.0

Sudden expansion after long plane and straight stretches,
plane diffusers, etc., with exponential velocity

$$\text{distribution. } \text{Re} = \frac{w_0 D_h}{\nu} > 3.5 \cdot 10^3$$

Section IV

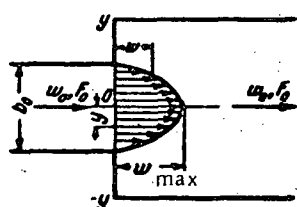
Diagram 4-3

$$D_h = \frac{4F_0}{U_0}; \quad U_0 - \text{perimeter; } n = \frac{F_0}{F_z}$$

$$\zeta = \frac{\Delta H}{\gamma w_0^2} = \frac{1}{n^2} + N - \frac{2M}{n}$$

is determined from graph a;

$$\frac{w}{w_{\max}} = \left(1 - \frac{2y}{b_0}\right)^{\frac{1}{m}}; \quad m \geq 1$$



$$M = \frac{(m+1)^2}{m(m+2)}$$

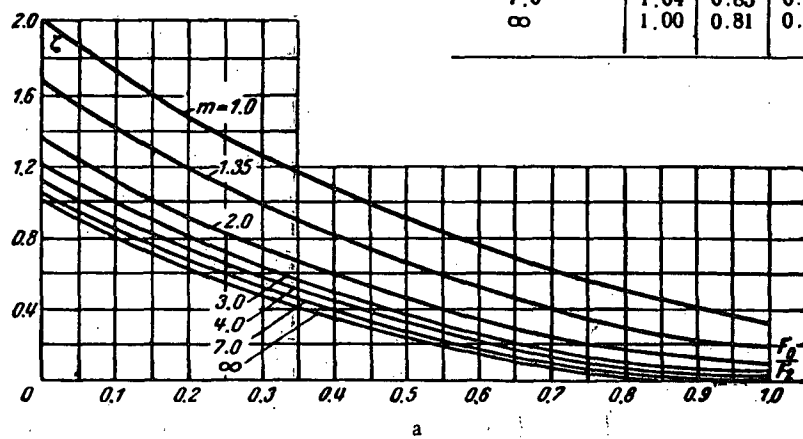
$$N = \frac{(m+1)^2}{m^2(m+3)}$$

are determined from graph b;

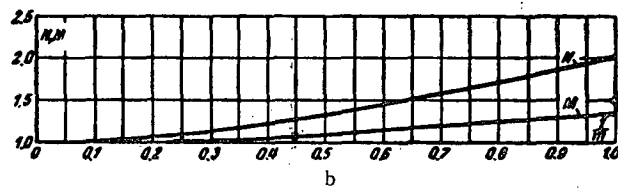
ν is taken from § 1-3, b.

Values of ζ

m	F_0/F_z									
	0	0.1	0.2	0.3	0.4	0.5	0.6	0.7	0.8	1.0
1.0	2.00	1.74	1.51	1.28	1.19	0.92	0.77	0.64	0.51	0.34
1.35	1.65	1.40	1.20	1.00	0.83	0.67	0.53	0.41	0.32	0.20
2.0	1.35	1.14	0.94	0.77	0.62	0.48	0.36	0.26	0.19	0.10
3.0	1.19	0.98	0.80	0.64	0.49	0.37	0.24	0.18	0.12	0.05
4.0	1.12	0.92	0.74	0.60	0.46	0.33	0.23	0.14	0.09	0.04
7.0	1.04	0.85	0.67	0.54	0.41	0.28	0.18	0.08	0.05	0.02
∞	1.00	0.81	0.64	0.49	0.36	0.25	0.15	0.08	0.04	0



a



b

m	1.0	1.35	2.0	3.0	4.0	7.0	∞
N	2.00	1.64	1.35	1.18	1.12	1.04	1.0
M	1.33	1.22	1.13	1.07	1.04	1.02	1.0

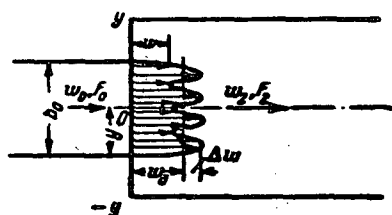
Sudden enlargement of a plane channel behind orifice plates,
baffles in elbows, etc., with sinusoidal velocity
distribution. $Re = \frac{w_0 D_h}{v} > 3.5 \cdot 10^3$

Section IV

Diagram 4-4

$$D_{11} = \frac{4F_0}{U_0}; \quad U_0 - \text{perimeter}; \quad n = \frac{F_2}{F_0}$$

$$\frac{w}{w_0} = 1 + \frac{\Delta w}{w_0} \sin 2k\pi \frac{2y}{b_0}; \quad k - \text{integer}$$



$$\zeta = \frac{\Delta H}{\gamma w_0^2} = \frac{1}{n^2} + N - \frac{2M}{n}$$

is determined from graph a;

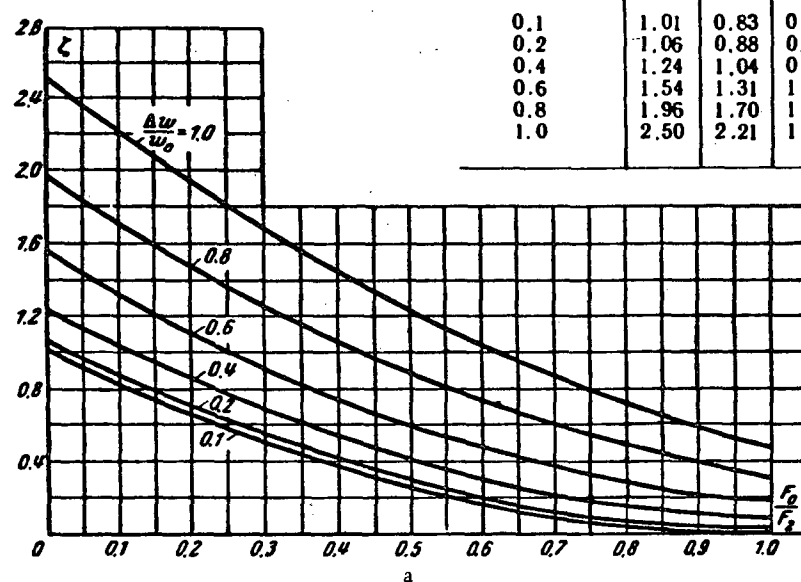
$$M = 1 + \frac{1}{2} \left(\frac{\Delta w}{w_0} \right)^2$$

$$N = 1 + \frac{3}{2} \left(\frac{\Delta w}{w_0} \right)^2$$

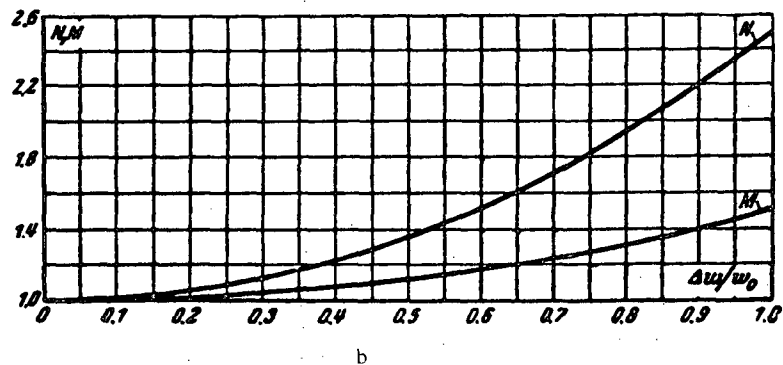
is determined from graph b;
 γ is taken from § 1-3, b.

Values of ζ

$\Delta w/w_0$	F_0/F_2									
	0	0.1	0.2	0.3	0.4	0.5	0.6	0.7	0.8	1.0
0.1	1.01	0.83	0.66	0.50	0.38	0.26	0.17	0.10	0.06	0.01
0.2	1.06	0.88	0.70	0.54	0.40	0.29	0.20	0.13	0.07	0.02
0.4	1.24	1.04	0.84	0.68	0.54	0.41	0.30	0.22	0.16	0.08
0.6	1.54	1.31	1.18	0.92	0.75	0.61	0.48	0.39	0.29	0.18
0.8	1.96	1.70	1.47	1.27	1.07	0.89	0.75	0.60	0.49	0.32
1.0	2.50	2.21	1.95	1.70	1.46	1.25	1.05	0.88	0.74	0.50



a



b

$\frac{\Delta w}{w_0}$	0.1	0.2	0.3	0.4	0.5
N	1.0	1.06	1.13	1.24	1.37
M	1.00	1.02	1.04	1.08	1.12

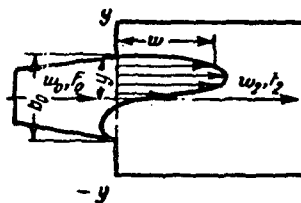
$\frac{\Delta w}{w_0}$	0.6	0.7	0.8	0.9	1.0
N	1.54	1.73	1.96	2.22	2.50
M	1.18	1.24	1.32	1.40	1.50

Sudden expansion behind plane diffusers with $\alpha > 10^\circ$, elbows, etc., with asymmetric velocity distribution.

$$Re = \frac{w_0 D_{h1}}{v} > 3.5 \cdot 10^3$$

Section IV

Diagram 4-5



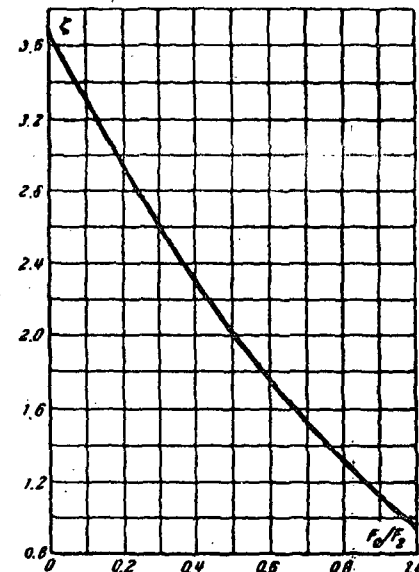
$$D_{h1} = \frac{4F_0}{H_0}; \quad H_0 = \text{perimeter}; \quad n = \frac{F_2}{F_0}$$

$$\frac{w}{w_0} = 0.585 + 1.64 \sin \left(0.2 + 1.95 \frac{2y}{h_0} \right)$$

$$\zeta = \frac{\Delta H}{\frac{\gamma w_0^2}{2g}} = \frac{1}{n^2} + 3.7 - \frac{3.74}{n} \quad \text{is also determined from the curve } \zeta = f \left(\frac{F_0}{F_2} \right);$$

* is taken from § 1-3, b.

F_0/F_2	0	0.1	0.2	0.3	0.4	0.5	0.6	0.7	0.8	1.0
ζ	3.70	3.34	2.99	2.66	2.36	2.09	1.82	1.58	1.35	0.96

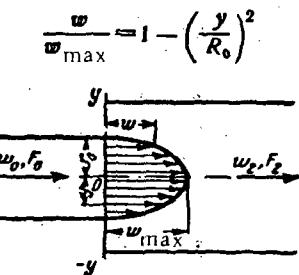


Sudden expansion after stretches with parabolic velocity

$$\text{distribution. } Re = \frac{w_0 D_{h1}}{v} > 3.5 \cdot 10^3$$

Section IV

Diagram 4-6



R_0/R_1	0	0.1	0.2	0.3	0.4	0.5	0.6	0.7	0.8	1.0
-----------	---	-----	-----	-----	-----	-----	-----	-----	-----	-----

a) Circular pipe

ζ	2.00	1.75	1.51	1.30	1.10	0.92	0.78	0.63	0.51	0.34
---------	------	------	------	------	------	------	------	------	------	------

b) Rectangular pipe

ζ	1.55	1.32	1.11	0.92	0.75	0.60	0.47	0.36	0.27	0.15
---------	------	------	------	------	------	------	------	------	------	------

$$D_{h1} = \frac{4F_0}{H_0}; \quad H_0 = \text{perimeter}; \quad n = \frac{F_2}{F_0}$$

a) Circular pipe

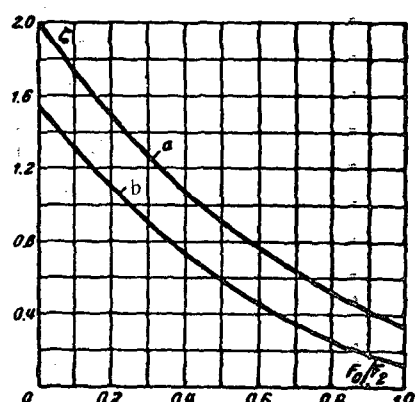
$$\zeta = \frac{\Delta H}{\frac{\gamma w_0^2}{2g}} = \frac{1}{n^2} + 2 - \frac{2.66}{n}$$

b) Rectangular pipe

$$\zeta = \frac{\Delta H}{\frac{\gamma w_0^2}{2g}} = \frac{1}{n^2} + 1.55 - \frac{2.4}{n}$$

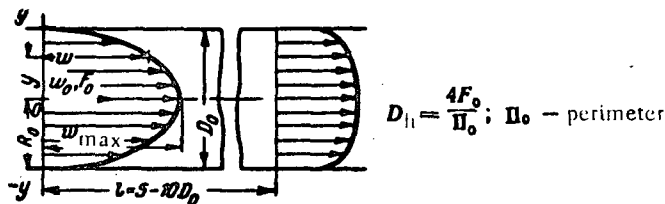
are also determined from the corresponding curves

$$\zeta = f \left(\frac{F_0}{F_2} \right);$$



* is taken from § 1-3, b.

1. Exponential velocity profile

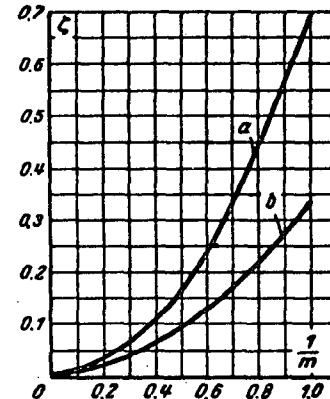


$$\frac{w}{w_{\max}} = \left(1 - \frac{y}{R_0}\right)^{\frac{1}{m}}; m \geq 1$$

$$\zeta = \frac{\Delta H}{\frac{\rho w_0^2}{2g}} = 1 + N - 2M \text{ is determined from the corresponding curve } \zeta = f\left(\frac{1}{m}\right);$$

M and N are determined from graph b of diagrams 4-2 and 4-3

m	1.0	1.35	2.0	4.0	7.0	∞
a) Circular pipe						
ζ	0.7	0.36	0.16	0.05	0.02	0
b) Rectangular pipe						
ζ	0.31	0.19	0.10	0.04	0.02	0



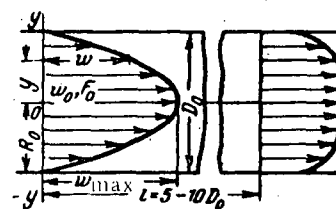
2. Parabolic velocity profile

$$\frac{w}{w_{\max}} = 1 - \left(\frac{y}{R_0}\right)^2$$

a) circular pipe $\zeta = \frac{\Delta H}{\frac{\rho w_0^2}{2g}} = 0.34$

b) rectangular $\zeta = \frac{\Delta H}{\frac{\rho w_0^2}{2g}} = 0.15$

w is taken from § 1-3, b.

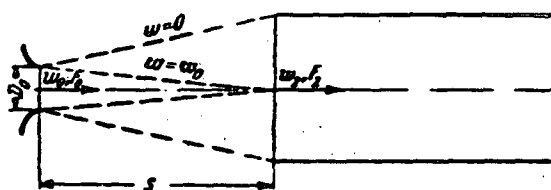


Stream deformation in a straight conduit with the entry of a free jet into it (ejector). $\text{Re} = \frac{w_0 D_h}{\nu} > 3.5 \cdot 10^4$

Section IV

Diagram 4-8

$$D_h = \frac{4F_0}{\Pi_0}; \quad \Pi_0 \text{ — perimeter}$$



$$\zeta = \frac{\Delta H}{\gamma w_0^2} = 1 + N - 2M$$

$$M = \frac{1}{q^2} \left(\frac{F_2}{F_0} \right);$$

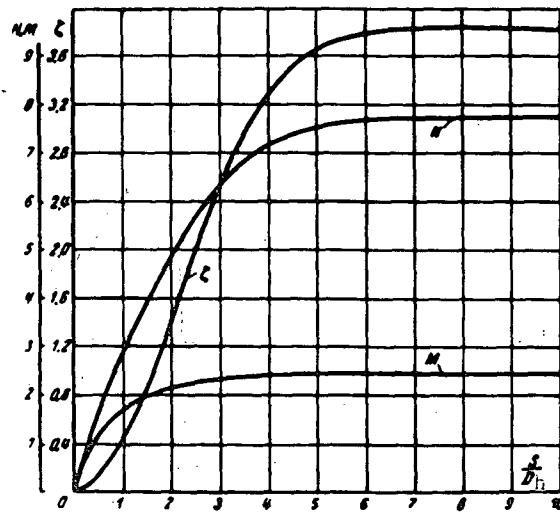
$$N = \frac{1}{q^2} \left(\frac{F_2}{F_0} \right)^2 e$$

The magnitudes ζ , M , and N are determined from the graph of this diagram as a function of the length $\frac{S}{D_h}$ of the free jet;

$$\bar{F} = \frac{F_2}{F_0} = \frac{F_j}{F_0}, \quad \bar{q} \text{ and } \bar{e}$$

are determined as a function of the length $\frac{S}{D_h}$ of the free jet from the corresponding graphs of diagrams 11-32 and 11-33; ν is taken from § 1-3, b.

S/D_h	0.5	1.0	1.5	2.0	2.5	3.0	4.0	5.0	6.0	8.0	10
ζ	0.16	0.46	0.84	1.43	2.02	2.54	3.26	3.65	3.80	3.81	3.81
N	1.65	2.89	3.90	4.85	5.65	6.35	7.20	7.55	7.68	7.70	7.70
M	1.25	1.71	2.00	2.20	2.30	2.40	2.45	2.45	2.45	2.45	2.45

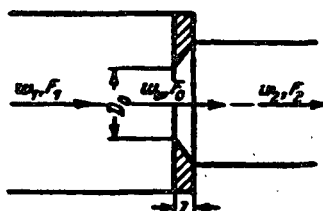


Sharp-edged ($\frac{l}{D_h} = 0 \div 0.015$) orifice at the passage of the stream from a conduit of one size to another. $Re = \frac{\omega_0 D_h}{\nu} > 10^3$

Section IV

Diagram 4-9

$$D_h = \frac{4F_0}{\Pi_0}; \Pi_0 = \text{perimeter}$$



$$\zeta = \frac{\Delta H}{\frac{\rho u_0^2}{2g}} = \left(1 + 0.707 \sqrt{1 - \frac{F_0}{F_1} - \frac{F_0}{F_2}} \right)^2$$

is determined from

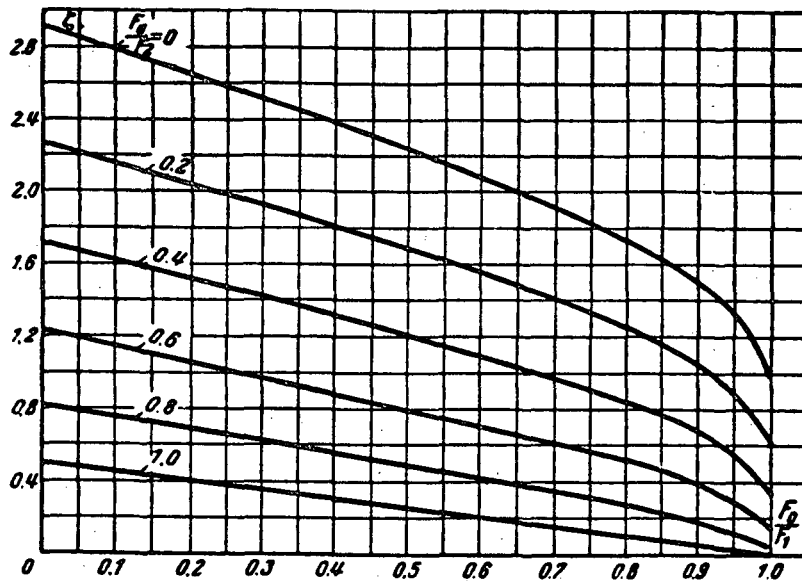
the curves

corresponding to different $\frac{F_0}{F_2}$:

ν is taken from § 1-3, b.

Values of ζ

F_0/F_2	F_0/F_1										
	0	0.1	0.2	0.3	0.4	0.5	0.6	0.7	0.8	0.9	1.0
0	2.90	2.80	2.67	2.53	2.40	2.25	2.09	1.98	1.75	1.50	1.00
0.2	2.27	2.17	2.05	1.94	1.82	1.69	1.55	1.40	1.26	1.05	0.64
0.4	1.70	1.62	1.52	1.42	1.32	1.20	1.10	0.98	0.85	0.68	0.36
0.6	1.23	1.15	1.07	0.98	0.90	0.80	0.72	0.62	0.52	0.39	0.16
0.8	0.82	0.76	0.69	0.63	0.56	0.49	0.42	0.35	0.28	0.18	0.04
1.0	0.50	0.45	0.40	0.35	0.30	0.25	0.20	0.15	0.10	0.05	0



Sharp-edged

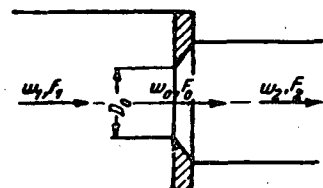
orifice at the passage of the stream

Section IV

from a conduit of one size to another. $Re = \frac{\omega_0 D_h}{v} < 10^4$

Diagram 4-10

$$D_h = \frac{4F_0}{H_0}; H_0 = \text{perimeter}$$



$$\zeta = \frac{\Delta H}{\frac{1}{2} \omega_0^2} = \zeta_p + \bar{\epsilon}_0^{Re} \left(\zeta_0 - \frac{F_0}{F_1} \right)^2 \quad (\text{approximate}),$$

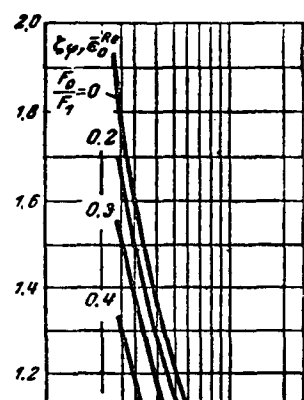
where ζ_p is determined from the curves $\zeta_p = f_1 \left(Re, \frac{F_0}{F_1} \right)$ of graph a;

$\bar{\epsilon}_0^{Re}$ is determined from the curves $\bar{\epsilon}_0^{Re} = f_2 (Re)$ of graph a;

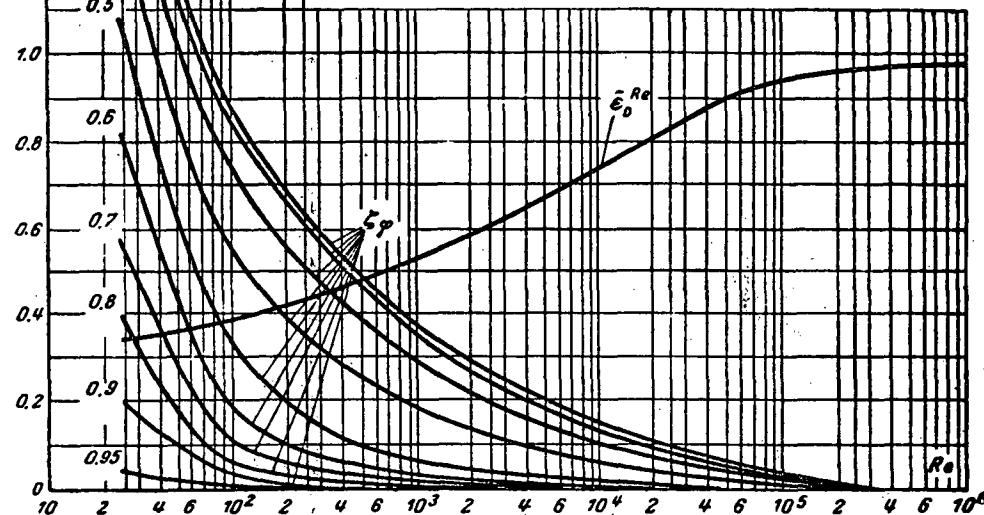
$$\zeta_0 = 1 + 0.707 \sqrt{1 - \frac{F_0}{F_1}} \quad \text{is determined from the curve } \zeta_0 = f_3 \left(\frac{F_0}{F_1} \right)$$

of graph b

v is taken from § 1-3, b.



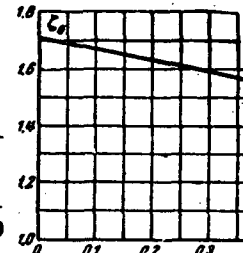
Re	2.5·10	4·10	6·10	10 ¹	2·10 ¹	4·10 ¹	10 ²	2·10 ²	4·10 ²	10 ³	2·10 ³	4·10 ³	10 ⁴	2·10 ⁴	4·10 ⁴	10 ⁵	2·10 ⁵	4·10 ⁵	10 ⁶
$\bar{\epsilon}_0^{Re}$	0.34	0.36	0.37	0.40	0.42	0.46	0.53	0.59	0.64	0.74	0.81	0.94	0.99	0.99	0.99	0.99	0.99	0.99	0.99
Values of ζ_p																			
0	1.94	1.38	1.14	0.89	0.69	0.64	0.39	0.30	0.22	0.15	0.11	0.04	0.01	0					
0.2	1.78	1.36	1.05	0.85	0.67	0.57	0.36	0.26	0.20	0.13	0.09	0.03	0.01	0					
0.3	1.57	1.16	0.88	0.75	0.57	0.43	0.30	0.22	0.17	0.10	0.07	0.02	0.01	0					
0.4	1.35	0.99	0.79	0.57	0.40	0.28	0.19	0.14	0.10	0.06	0.04	0.02	0.01	0					
0.5	1.10	0.75	0.55	0.34	0.19	0.12	0.07	0.05	0.03	0.02	0.01	0.01	0	0	0	0	0	0	0
0.6	0.85	0.56	0.30	0.19	0.10	0.06	0.03	0.02	0.01	0	0	0	0	0	0	0	0	0	0
0.7	0.58	0.37	0.23	0.11	0.06	0.03	0.02	0.01	0	0	0	0	0	0	0	0	0	0	0
0.8	0.40	0.24	0.13	0.06	0.03	0.02	0.01	0	0	0	0	0	0	0	0	0	0	0	0
0.9	0.20	0.13	0.08	0.03	0.01	0	0	0	0	0	0	0	0	0	0	0	0	0	0
0.95	0.03	0.03	0.02	0	0	0	0	0	0	0	0	0	0	0	0	0	0	0	0



a

Values of ζ_p

$\frac{F_0}{F_1}$	0	0.1	0.2	0.3	0.4	0.5	0.6	0.7	0.8	0.9	1.0
ζ_p	1.71	1.67	1.63	1.59	1.55	1.50	1.45	1.39	1.32	1.22	1.00



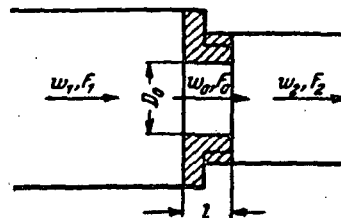
b

Thick-edged ($\frac{l}{D_h} > 0.015$) orifice at the passage of the stream from a conduit of one size to another

Section IV

Diagram 4-11

$$D_h = \frac{4F_0}{\Pi_0}; \quad \Pi_0 \text{ — perimeter}$$



$$1. \quad Re = \frac{w_0 D_h}{\nu} > 10^5:$$

$$\zeta = \frac{\Delta H}{\gamma w_0^2} = 0.5 \left(1 - \frac{F_0}{F_1} \right) + \left(1 - \frac{F_0}{F_2} \right)^2 + \tau \sqrt{1 - \frac{F_0}{F_1}} \times \left(1 - \frac{F_0}{F_2} \right) + \lambda \frac{l}{D_h} = \zeta_0 + \lambda \frac{l}{D_h},$$

where τ is determined from the curve $\tau = f \left(\frac{l}{D_h} \right)$; λ is

determined from diagrams 2-2 to 2-5 as a function of Re and
 $\lambda = \frac{\Delta}{D_h}$; Δ is taken from Table 2-1; ν is taken from § 1-3,b;

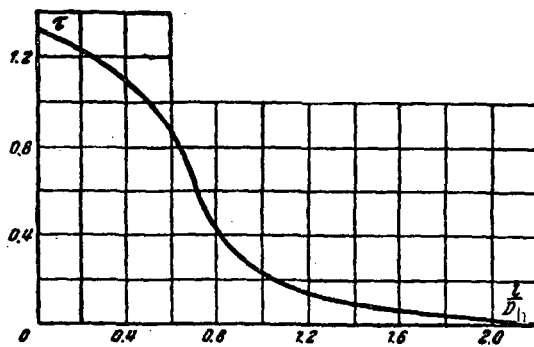
2. $Re < 10^5$ (approximately):

$$\zeta = \zeta_0 + \zeta_0^{Re} \zeta_0,$$

where ζ_0 and ζ_0^{Re} — cf. diagram 4-10;

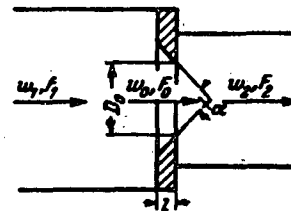
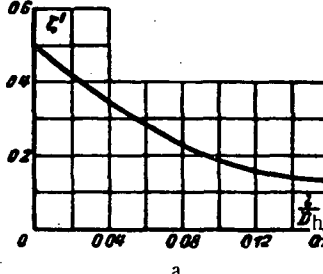
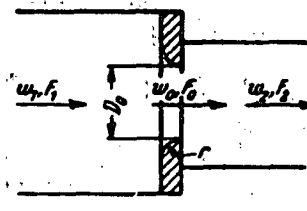
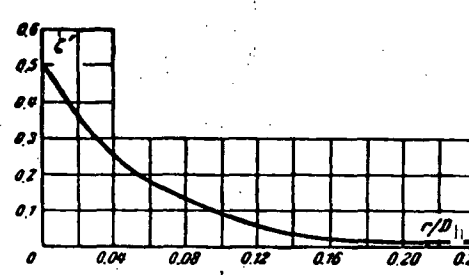
$$\zeta_0 = 0.5 \left(1 - \frac{F_0}{F_1} \right) + \left(1 - \frac{F_0}{F_2} \right)^2 + \tau \sqrt{1 - \frac{F_0}{F_1}} \left(1 - \frac{F_0}{F_2} \right)$$

l/D_h	0	0.2	0.4	0.6	0.8	1.0	1.2	1.6	2.0	2.4
τ	1.35	1.22	1.10	0.84	0.42	0.24	0.16	0.07	0.02	0



Thick-edged ($t/D_h > 0.015$) orifice with edges beveled or rounded at the passage of a stream from a conduit of one size to another

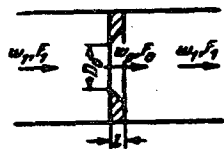
Section IV
Diagram 4-12

	Schematic diagram	Resistance coefficient $\xi = \frac{\Delta H}{\frac{V^2}{2g}}$																							
Orifice with beveled edges		$\xi \approx \zeta \left(1 - \frac{F_0}{F_1}\right) + \left(1 - \frac{F_0}{F_2}\right)^2 + 2 \sqrt{\zeta' \left(1 - \frac{F_0}{F_1}\right) \left(1 - \frac{F_0}{F_2}\right)}$ <p>where ζ' is determined from the curve $\zeta' = f\left(\frac{t}{D_h}\right)$ of graph a</p> <table border="1"> <thead> <tr> <th>t/D_h</th> <th>0.01</th> <th>0.02</th> <th>0.03</th> <th>0.04</th> <th>0.06</th> <th>0.08</th> <th>0.12</th> <th>≥ 0.16</th> </tr> </thead> <tbody> <tr> <td>ζ'</td> <td>0.46</td> <td>0.42</td> <td>0.38</td> <td>0.35</td> <td>0.29</td> <td>0.23</td> <td>0.16</td> <td>0.13</td> </tr> </tbody> </table> 	t/D_h	0.01	0.02	0.03	0.04	0.06	0.08	0.12	≥ 0.16	ζ'	0.46	0.42	0.38	0.35	0.29	0.23	0.16	0.13					
t/D_h	0.01	0.02	0.03	0.04	0.06	0.08	0.12	≥ 0.16																	
ζ'	0.46	0.42	0.38	0.35	0.29	0.23	0.16	0.13																	
Orifice with rounded edges		$\xi = \zeta' \left(1 - \frac{F_0}{F_1}\right) + \left(1 - \frac{F_0}{F_2}\right)^2 + 2 \sqrt{\zeta' \left(1 - \frac{F_0}{F_1}\right) \left(1 - \frac{F_0}{F_2}\right)}$ <p>where ζ' is determined from the curve $\zeta' = f\left(\frac{r}{D_h}\right)$ of graph b</p> <table border="1"> <thead> <tr> <th>r/D_h</th> <th>0</th> <th>0.01</th> <th>0.02</th> <th>0.03</th> <th>0.04</th> <th>0.05</th> <th>0.06</th> <th>0.08</th> <th>0.12</th> <th>≥ 0.16</th> </tr> </thead> <tbody> <tr> <td>ζ'</td> <td>0.50</td> <td>0.44</td> <td>0.37</td> <td>0.31</td> <td>0.26</td> <td>0.22</td> <td>0.19</td> <td>0.15</td> <td>0.09</td> <td>0.06</td> <td>0.03</td> </tr> </tbody> </table> 	r/D_h	0	0.01	0.02	0.03	0.04	0.05	0.06	0.08	0.12	≥ 0.16	ζ'	0.50	0.44	0.37	0.31	0.26	0.22	0.19	0.15	0.09	0.06	0.03
r/D_h	0	0.01	0.02	0.03	0.04	0.05	0.06	0.08	0.12	≥ 0.16															
ζ'	0.50	0.44	0.37	0.31	0.26	0.22	0.19	0.15	0.09	0.06	0.03														

Sharp-edged $\left(\frac{l}{D_h} = 0 \div 0.015\right)$ orifice in a straight conduit

Section IV
Diagram 4-13

$$D_h = \frac{4F_0}{H_0}; H_0 - \text{perimeter}$$

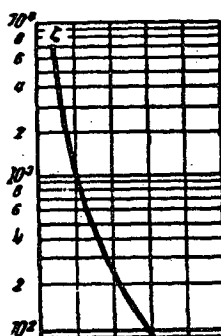


$$1. Re = \frac{w_0 D_h}{v} > 10^5:$$

$$\zeta = \frac{\Delta H}{\gamma w_1^2} \approx \left(1 + 0.707 \sqrt{1 - \frac{F_0}{F_1}} - \frac{F_0}{F_1} \right)^2 \left(\frac{F_1}{F_0} \right)^2$$

is determined from the curve $\zeta = f\left(\frac{F_0}{F_1}\right)$.

$$2. Re < 10^5 \text{ (approximately):}$$



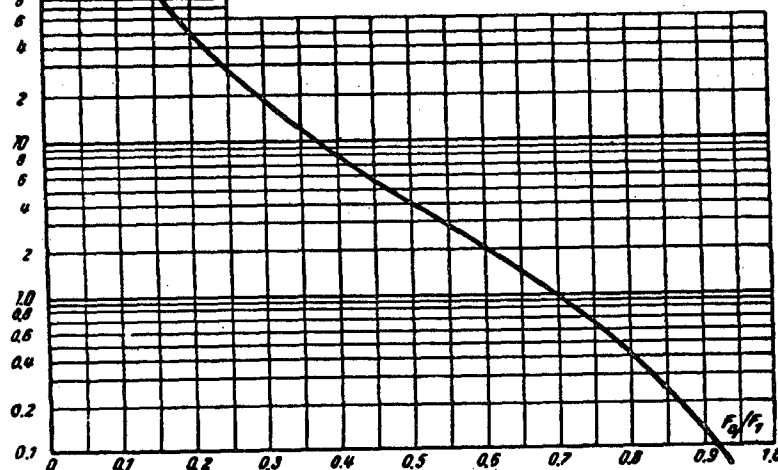
where ζ_p is determined from the curves $\zeta_p = f_1(Re, \frac{F_0}{F_1})$ on graph a of diagram 4-10;

ζ_0^{Re} is determined from the curve $\zeta_0^{Re} = f_2(Re)$ on the same graph a of diagram 4-10;

$\zeta_0 = 1 + 0.707 \sqrt{1 - \frac{F_0}{F_1}}$ is determined from the curve on graph b of the same diagram 4-10

(p. 136);

v is taken from § 1-3, b.



$\frac{F_0}{F_1}$	0.02	0.03	0.04	0.05	0.06	0.08	0.10	0.12	0.14	0.16	0.18	0.20	0.22	0.24	0.26	0.28	0.30	0.32
ζ	7 000	3 100	1 670	1 050	730	400	245	165	117	86.0	65.5	51.5	40.6	32.0	26.8	22.3	18.2	15.6

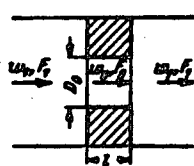
$\frac{F_0}{F_1}$	0.34	0.36	0.38	0.40	0.43	0.47	0.50	0.52	0.55	0.60	0.65	0.70	0.75	0.80	0.85	0.90	0.95	1.00
ζ	13.1	11.6	9.55	8.25	6.62	4.95	4.00	3.48	2.85	2.00	1.41	0.97	0.65	0.42	0.25	0.13	0.05	0

Thick-edged ($\frac{l}{D_h} > 0.015$) orifice in a straight conduit

Section III
Diagram 4-14

$$D_{hi} = \frac{4F_0}{\Pi_e}; \Pi_e - \text{perimeter}$$

$$1. Re = \frac{\omega_0 D_{hi}}{v} > 10^4$$

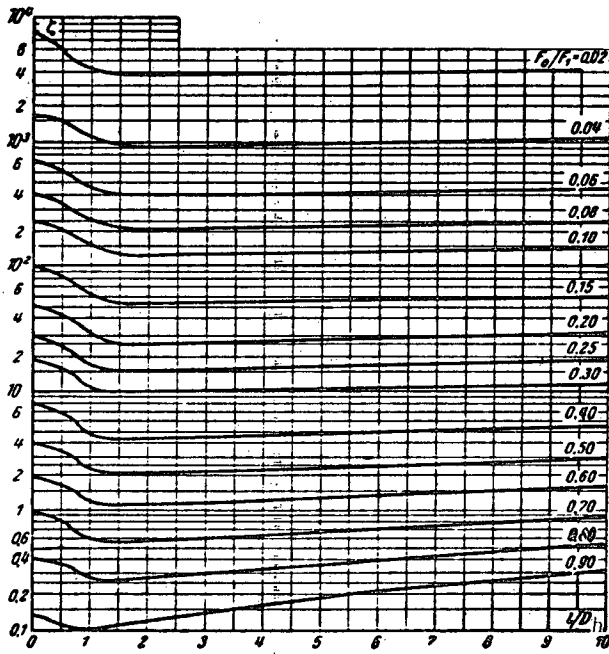


$$\zeta = \frac{\Delta H}{\gamma w_1^2} \approx \left[\left(0.5 + \tau \sqrt{1 - \frac{F_0}{F_1}} \right) \left(1 - \frac{F_0}{F_1} \right) + \left(1 - \frac{F_0}{F_1} \right)^2 + \lambda \frac{l}{D_{hi}} \right] \left(\frac{F_1}{F_0} \right)^2 = \left(\zeta_0 + \lambda \frac{l}{D_{hi}} \right) \left(\frac{F_1}{F_0} \right)^2$$

where $\tau = f\left(\frac{l}{D_{hi}}\right)$ is determined from the table or more accurately from the graph of diagram 4-11;

Values of ζ

$\frac{l}{D_{hi}}$	ζ	F_0/F_1															
		0.02	0.04	0.06	0.08	0.10	0.15	0.20	0.25	0.30	0.40	0.50	0.60	0.70	0.80	0.90	1.0
0	1.35	7000	1670	730	400	245	96.0	51.5	30.0	18.2	8.25	4.00	2.00	0.97	0.42	0.13	0
0.2	1.22	6600	1600	687	374	230	94.0	48.0	28.0	17.4	7.70	3.75	1.87	0.91	0.40	0.13	0.01
0.4	1.10	6310	1530	660	356	221	89.0	46.0	26.5	16.6	7.40	3.60	1.80	0.88	0.39	0.13	0.01
0.6	0.84	5700	1380	590	322	199	81.0	42.0	24.0	15.0	6.60	3.20	1.60	0.80	0.36	0.12	0.01
0.8	0.42	4680	1130	486	264	164	66.0	34.0	19.6	12.2	5.50	2.70	1.34	0.66	0.31	0.11	0.02
1.0	0.24	4260	1030	443	240	149	60.0	31.0	17.8	11.1	5.00	2.40	1.20	0.61	0.29	0.11	0.02
1.4	0.10	3930	950	408	221	137	55.6	28.4	16.4	10.3	4.60	2.25	1.15	0.58	0.28	0.11	0.03
2.0	0.02	3770	910	391	212	134	53.0	27.4	15.8	9.30	4.40	2.20	1.13	0.58	0.28	0.12	0.04
3.0	0	3765	913	392	214	132	53.5	27.5	15.9	10.0	4.50	2.24	1.17	0.61	0.31	0.15	0.06
4.0	0	3775	930	400	215	132	53.8	27.7	16.2	10.0	4.60	2.25	1.20	0.64	0.35	0.16	0.08
5.0	0	3850	936	400	220	133	55.5	28.5	16.5	10.5	4.75	2.40	1.28	0.69	0.37	0.20	0.10
6.0	0	3870	940	400	222	133	55.8	28.5	16.6	10.5	4.80	2.42	1.32	0.70	0.40	0.21	0.12
7.0	0	4000	950	405	230	135	55.9	29.0	17.0	10.9	5.00	2.50	1.38	0.74	0.43	0.23	0.14
8.0	0	4000	965	410	236	137	56.0	30.0	17.2	11.2	5.10	2.58	1.45	0.78	0.45	0.25	0.16
9.0	0	4080	985	420	240	140	57.0	30.0	17.4	11.4	5.30	2.62	1.50	0.80	0.50	0.28	0.18
10	0	4110	1000	430	245	146	59.7	31.0	18.2	11.5	5.40	2.80	1.57	0.89	0.53	0.32	0.20



λ is determined from diagrams 2-2 to 2-5 as a function of

$$Re \text{ and } \bar{\Delta} = \frac{\Delta}{D_h}$$

At $\lambda = 0.02$ the values of ζ are completely determined from the curves $\zeta = f\left(\frac{l}{D_h}\right)$ corresponding to different F_0/F_1 or from the table.

2. $Re < 10^5$ (approximately):

$$\zeta = \frac{\Delta H}{\gamma w_1^2} \approx \left(\zeta_0 + \zeta_0^{Re} \zeta_0 + \lambda \frac{l}{D_h} \right) \left(\frac{F_1}{F_0} \right)^2$$

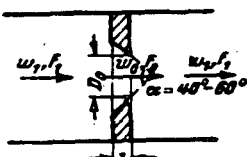
where ζ_0 and ζ_0^{Re} cf. diagram 4-10; ζ_0 is determined as under 1; y is taken from § 1-3, b; Δ is taken from Table 2-1.

Orifice with edges beveled facing the stream flow
 $(\alpha = 40-60^\circ)$ in a straight pipe. $Re = \frac{w_0 D_h}{\nu} > 10^4$

Section IV

Diagram 4-15

$$D_h = \frac{4F_0}{\Pi_0}; \Pi_0 \text{ — perimeter}$$



$$\zeta = \frac{\Delta H}{\frac{\gamma w_1^2}{2g}} \approx \left[1 + \sqrt{\zeta' \left(1 - \frac{F_0}{F_1} \right) - \frac{F_0}{F_1}} \right]^2 \left(\frac{F_1}{F_0} \right)^2,$$

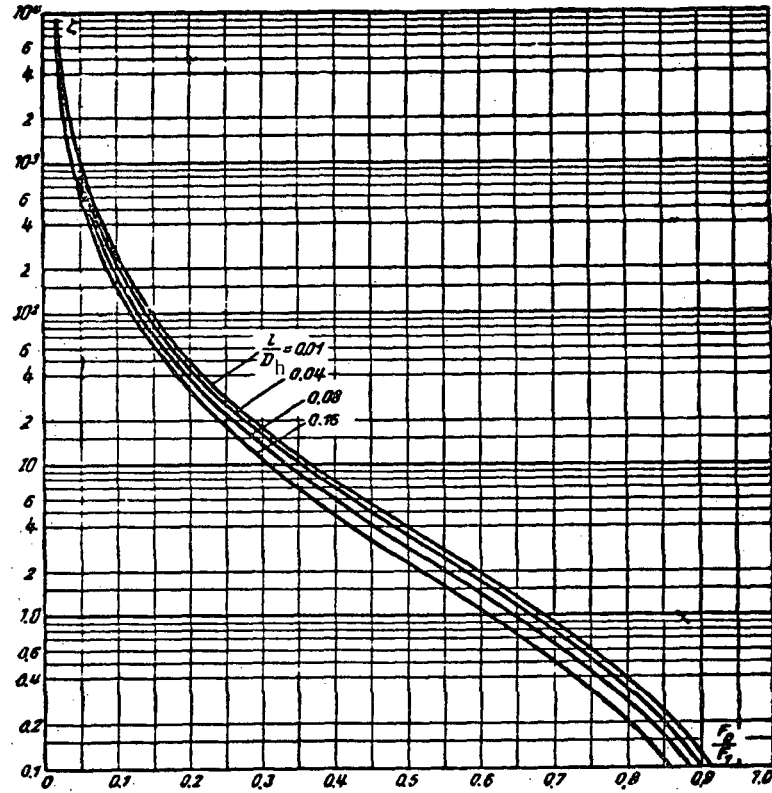
where $\zeta' = f \left(\frac{l}{D_h} \right)$ is taken from the table or more accurately from graph a of diagram 4-12.

The values of ζ are completely determined from the curves $\zeta = f \left(\frac{F_0}{F_1} \cdot \frac{l}{D_h} \right)$ or from the table;

ν is taken from § 1-3, b.

Values of ζ

$\frac{l}{D_h}$	ν	$\frac{F_0}{F_1}$															
		0.02	0.04	0.06	0.08	0.10	0.15	0.20	0.25	0.30	0.40	0.50	0.60	0.70	0.80	0.90	1.0
0.01	0.46	6.800	1.650	710	386	238	96.8	49.5	28.6	17.9	7.90	3.84	1.92	0.92	0.40	0.12	0
0.02	0.42	6.540	1.590	683	371	230	93.2	47.7	27.5	17.2	7.60	3.68	1.83	0.88	0.38	0.12	0
0.03	0.38	6.310	1.530	657	357	220	89.4	45.7	26.4	16.5	7.25	3.50	1.72	0.83	0.35	0.11	0
0.04	0.36	6.130	1.480	636	345	214	86.5	44.2	25.6	15.8	7.00	3.36	1.67	0.80	0.34	0.10	0
0.06	0.29	5.750	1.385	600	323	200	80.0	41.2	23.4	14.6	6.85	3.08	1.53	0.73	0.30	0.09	0
0.08	0.23	5.300	1.275	549	298	184	74.3	37.8	21.8	13.5	5.92	2.80	1.37	0.64	0.27	0.08	0
0.12	0.16	4.730	1.140	490	265	164	66.0	33.5	19.2	11.9	5.18	2.44	1.18	0.55	0.22	0.06	0
0.16	0.13	4.460	1.080	462	251	154	62.0	31.6	18.1	11.2	4.80	2.28	1.10	0.50	0.20	0.05	0



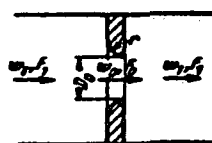
Orifice with rounded edges in a straight pipe.

Section IV

$$Re = \frac{w_0 D_h}{\nu} > 10^4$$

Diagram 4-16

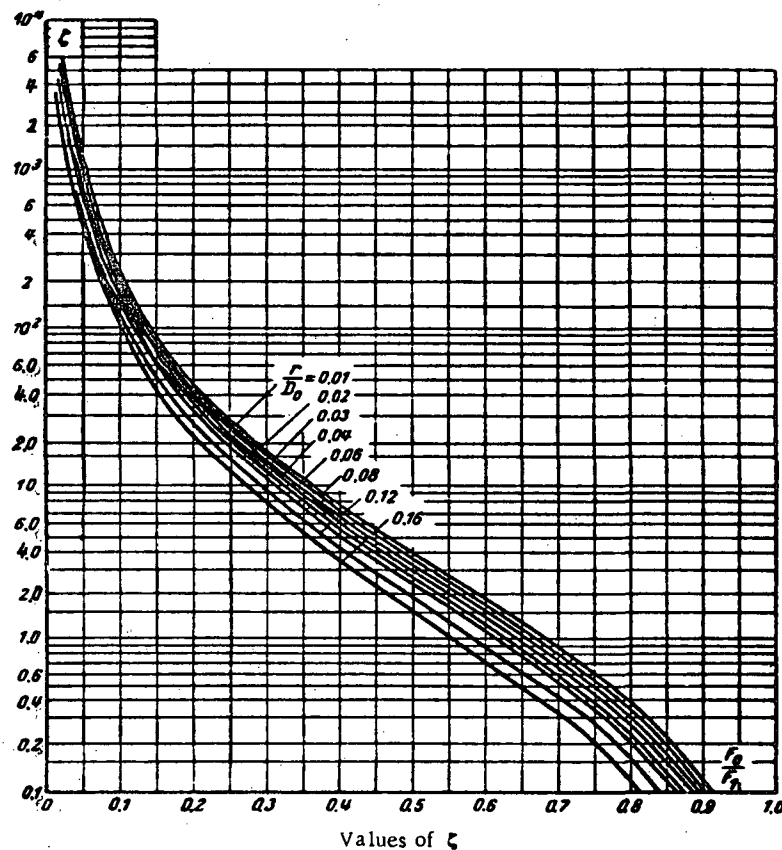
$$D_h = \frac{4F_0}{H_0}; H_0 - \text{perimeter}$$



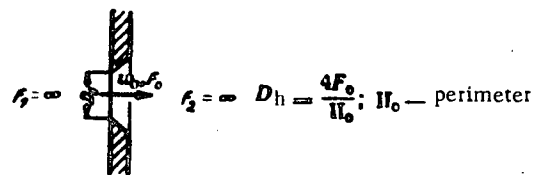
$$\frac{\Delta H}{\frac{\rho w_1^2}{2g}} \approx \left[1 + \sqrt{\zeta \left(1 - \frac{F_0}{F_1} \right) - \frac{F_0}{F_1}} \right]^2 \left(\frac{F_1}{F_0} \right)^2$$

where $\zeta = f_1 \left(\frac{r}{D_h} \right)$ is taken from the table or more accurately from graph b of diagram 4-12.

The values of ζ are determined from the curves $\zeta = f \left(\frac{F_0}{F_1}, \frac{r}{D_h} \right)$ or from the table; ν is taken from § 1-3, b.



$\frac{r}{D_h}$	ζ'	$\frac{F_0}{F_1}$																			
		0.02	0.04	0.06	0.08	0.10	0.15	0.20	0.25	0.30	0.35	0.40	0.45	0.50	0.55	0.60	0.65	0.70	0.75	0.81	0.90
0.01	0.44	6620	1600	690	375	232	94.0	48.0	27.7	17.3	11.0	7.70	5.60	3.70	2.65	1.84	1.25	0.90	0.60	0.38	0.12
0.02	0.37	6200	1500	642	348	216	87.6	45.5	25.8	16.1	10.7	7.10	5.00	3.48	2.33	1.69	1.18	0.82	0.56	0.34	0.10
0.03	0.31	5850	1400	600	327	201	82.0	42.0	24.2	14.9	9.9	6.56	4.50	3.20	2.22	1.55	1.10	0.75	0.50	0.31	0.09
0.04	0.26	5510	1330	570	310	192	77.5	39.0	22.7	14.1	9.00	6.19	4.20	3.00	2.00	1.45	0.95	0.70	0.45	0.29	0.08
0.06	0.19	5000	1200	518	278	173	69.9	36.5	20.3	12.58	8.00	5.50	4.00	2.60	1.72	1.27	0.85	0.60	0.40	0.24	0.07
0.08	0.15	4450	1100	437	255	158	63.6	32.2	18.5	11.47	5.05	3.00	3.40	2.30	1.52	1.13	0.78	0.53	0.34	0.21	0.06
0.12	0.09	3860	925	398	216	133	53.5	27.0	15.0	9.30	6.50	4.16	3.00	1.90	1.24	0.89	0.60	0.40	0.27	0.16	0.04
0.16	0.06	3320	797	340	184	113	45.4	23.0	12.9	7.90	5.30	3.40	2.20	1.60	1.00	0.70	0.50	0.32	0.20	0.12	0.03



$$1. Re = \frac{w_0 D_h}{v} > 10^5$$

$$\zeta = 2.85$$

2. $Re < 10^5$: (approximately);

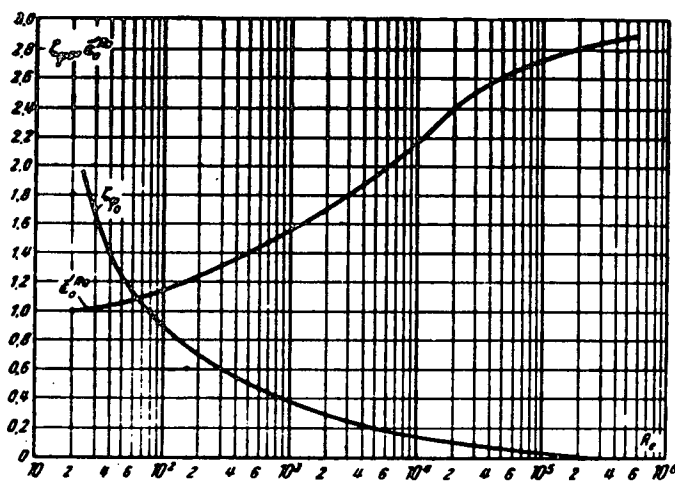
$$\zeta = \zeta_{p_0} + \bar{\zeta}_0^{Re}$$

where ζ_{p_0} is determined from the curve $\zeta_{p_0} = f_1(Re)$

$\bar{\zeta}_0^{Re} = \frac{1}{(\zeta_0^{Re})^2}$ is determined from the curve $\bar{\zeta}_0^{Re} = f_2(Re)$

v is taken from § 1-3, b.

	$2 \cdot 10^4$	$4 \cdot 10^4$	$6 \cdot 10^4$	10^5	$2 \cdot 10^5$	$4 \cdot 10^5$	10^6	$2 \cdot 10^6$	$4 \cdot 10^6$	10^7	$2 \cdot 10^7$	10^8	$2 \cdot 10^8$	10^9
ζ_{p_0}	1.94	1.38	1.14	0.89	0.69	0.54	0.39	0.30	0.22	0.15	0.11	0.04	0.01	0
$\bar{\zeta}_0^{Re}$	1.00	1.05	1.09	1.15	1.23	1.37	1.56	1.71	1.88	2.17	2.38	2.56	2.72	2.85

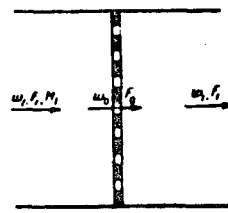


Orifices with various edges in large walls

Section IV

Diagram 4-18

Orifice characteristic	Schematic design	Resistance coefficient $\xi = \frac{\Delta H}{\frac{1}{2} u_0^2}$																										
Thick-walled orifice (deep orifice) $(\frac{l}{D_h} > 0.015)$		<p>1. $Re = \frac{w_0 D_h}{v} \geq 10^5$: $\xi = \zeta + \lambda \frac{l}{D_h}$, where ζ' is determined from the curve $\zeta' = f(\frac{l}{D_h})$ on graph a); λ is determined from diagrams 2-2 to 2-5 as a function of Re and $\bar{\Delta} = \frac{\Delta}{D_h}$; Δ is taken from Table 2-1; v is taken from § 1-3,b.</p> <p>2. $Re < 10^5$ (approximately) $\xi = \xi_{\infty} + 0.342 \epsilon_0^{Re} \zeta' + \lambda \frac{l}{D_h}$, where ξ_{∞} and ϵ_0^{Re} are determined as in diagram 4-17; ζ' is determined as for $Re \geq 10^5$.</p>																										
		<table border="1"> <thead> <tr> <th>l/D_h</th><th>0</th><th>0.2</th><th>0.4</th><th>0.6</th><th>0.8</th><th>1.0</th><th>1.2</th><th>1.4</th><th>1.6</th><th>1.8</th><th>2.0</th><th>4.0</th> </tr> </thead> <tbody> <tr> <th>ζ'</th><td>2.85</td><td>2.72</td><td>2.60</td><td>2.34</td><td>1.95</td><td>1.76</td><td>1.67</td><td>1.62</td><td>1.60</td><td>1.58</td><td>1.55</td><td>1.55</td> </tr> </tbody> </table>	l/D_h	0	0.2	0.4	0.6	0.8	1.0	1.2	1.4	1.6	1.8	2.0	4.0	ζ'	2.85	2.72	2.60	2.34	1.95	1.76	1.67	1.62	1.60	1.58	1.55	1.55
l/D_h	0	0.2	0.4	0.6	0.8	1.0	1.2	1.4	1.6	1.8	2.0	4.0																
ζ'	2.85	2.72	2.60	2.34	1.95	1.76	1.67	1.62	1.60	1.58	1.55	1.55																
Orifice with beveled edges		ζ' is determined from the curve $\zeta' = f(\frac{l}{D_h})$ on graph b.																										
		<table border="1"> <thead> <tr> <th>l/D_h</th><th>0</th><th>0.01</th><th>0.02</th><th>0.03</th><th>0.04</th><th>0.05</th><th>0.06</th><th>0.08</th><th>0.10</th><th>0.12</th><th>0.16</th><th>0.20</th> </tr> </thead> <tbody> <tr> <th>ζ'</th><td>2.85</td><td>2.80</td><td>2.70</td><td>2.60</td><td>2.50</td><td>2.41</td><td>2.33</td><td>2.18</td><td>2.08</td><td>1.98</td><td>1.84</td><td>1.80</td> </tr> </tbody> </table>	l/D_h	0	0.01	0.02	0.03	0.04	0.05	0.06	0.08	0.10	0.12	0.16	0.20	ζ'	2.85	2.80	2.70	2.60	2.50	2.41	2.33	2.18	2.08	1.98	1.84	1.80
l/D_h	0	0.01	0.02	0.03	0.04	0.05	0.06	0.08	0.10	0.12	0.16	0.20																
ζ'	2.85	2.80	2.70	2.60	2.50	2.41	2.33	2.18	2.08	1.98	1.84	1.80																
Orifice with rounded edges		ζ is determined from the curve $\zeta = f(\frac{r}{D_h})$ of graph c.																										
		<table border="1"> <thead> <tr> <th>r/D_h</th><th>0.01</th><th>0.02</th><th>0.03</th><th>0.04</th><th>0.06</th><th>0.08</th><th>0.12</th><th>0.16</th><th>0.20</th> </tr> </thead> <tbody> <tr> <th>ζ</th><td>2.72</td><td>2.56</td><td>2.40</td><td>2.27</td><td>2.06</td><td>1.88</td><td>1.60</td><td>1.38</td><td>1.37</td> </tr> </tbody> </table>	r/D_h	0.01	0.02	0.03	0.04	0.06	0.08	0.12	0.16	0.20	ζ	2.72	2.56	2.40	2.27	2.06	1.88	1.60	1.38	1.37						
r/D_h	0.01	0.02	0.03	0.04	0.06	0.08	0.12	0.16	0.20																			
ζ	2.72	2.56	2.40	2.27	2.06	1.88	1.60	1.38	1.37																			



1. Sharp-edged orifices:

$$\zeta_M = k_M \zeta$$

where ζ is determined from the data of diagrams 4-9 to 4-11, 4-13, and 4-14; k_M is

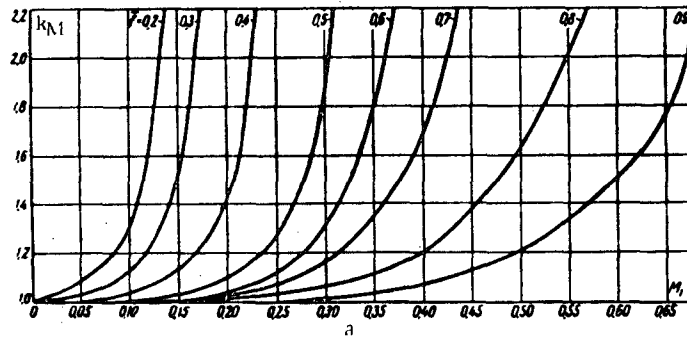
determined from the curves $k_M = f(M_1)$; $M_1 = \frac{w_1}{a}$; $a = \sqrt{xg \frac{p_1}{\gamma_1}}$ = velocity of sound;

$x = \frac{c_p}{c_v}$ = specific-heat ratio, determined from Table 1-3.

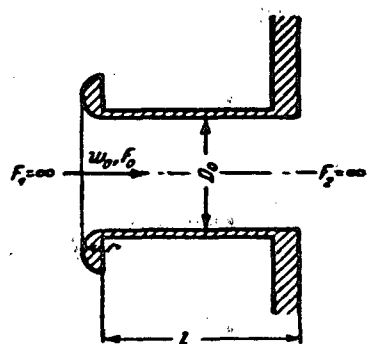
2. Orifice edges beveled or rounded, cf. diagram 8-8.

Values of k_M

\bar{f}	M_1														
	0	0.05	0.10	0.15	0.20	0.25	0.30	0.35	0.40	0.45	0.50	0.55	0.60	0.65	
0.2	1.00	1.09	1.30	—	—	—	—	—	—	—	—	—	—	—	—
0.3	1.00	1.03	1.13	1.51	—	—	—	—	—	—	—	—	—	—	—
0.4	1.00	0.00	1.03	1.41	1.41	—	—	—	—	—	—	—	—	—	—
0.5	1.00	1.00	1.00	1.03	1.10	1.27	1.85	—	—	—	—	—	—	—	—
0.6	1.00	0.00	1.00	1.00	1.12	1.30	1.30	1.77	—	—	—	—	—	—	—
0.7	1.00	1.00	1.00	1.00	1.03	1.08	1.18	1.35	1.68	—	—	—	—	—	—
0.8	1.00	1.00	1.00	1.00	1.01	1.03	1.07	1.12	1.20	1.37	1.63	2.01	—	—	—
0.9	1.00	1.00	1.00	1.00	1.00	1.00	1.02	1.04	1.07	1.13	1.21	1.33	1.50	1.75	—



$$D_h = \frac{4F_o}{\Pi_o}; \Pi_o \text{ — perimeter}$$

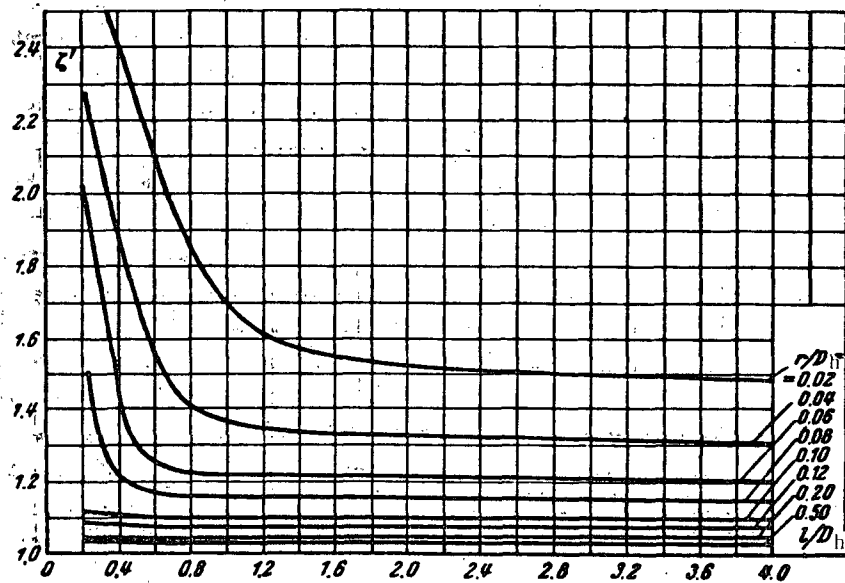


$$\zeta = \frac{\Delta H}{\frac{1}{2} w_0^2} = \zeta + \zeta_{fr},$$

where $\zeta_{fr} = \lambda \frac{l}{D_h}$; λ is determined from the curves $\zeta = f\left(\frac{l}{D_h}\right)$ corresponding to different r/D_h ; λ is determined from diagrams 2-2 to 2-5 as a function of $Re = \frac{w_0 D_h}{v}$ and $\Delta = \frac{\Delta}{D_h}$; v is taken from § 1-3,b; Δ is taken from Table 2-1.

 Values of ζ

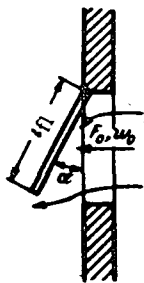
r/D_h	l/D_h											
	0.25	0.50	0.75	1.00	1.25	1.50	1.75	2.0	2.5	3.0	3.5	4.0
0.02	2.64	2.25	1.89	1.68	1.60	1.56	1.54	1.58	1.51	1.50	1.49	1.48
0.04	2.20	1.70	1.42	1.37	1.34	1.33	1.33	1.32	1.32	1.32	1.31	1.30
0.06	1.90	1.30	1.23	1.22	1.22	1.21	1.21	1.21	1.21	1.21	1.20	1.20
0.08	1.44	1.19	1.16	1.15	1.15	1.15	1.15	1.15	1.15	1.15	1.15	1.15
0.10	1.12	1.10	1.10	1.10	1.10	1.10	1.10	1.10	1.10	1.10	1.10	1.10
0.12	1.08	1.08	1.08	1.07	1.07	1.07	1.07	1.07	1.07	1.08	1.08	1.08
0.20	1.04	1.04	1.04	1.04	1.04	1.04	1.04	1.04	1.04	1.05	1.05	1.05
0.50	1.03	1.03	1.03	1.03	1.03	1.03	1.03	1.03	1.03	1.03	1.03	1.03



Exhaust flap, single, top-hinged

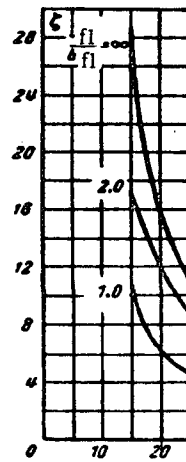
 Section IV
 Diagram 4-21

$$l_{fl} = \text{flap length}; \quad w_0 = \frac{Q}{F_0};$$



$$\zeta = \frac{\Delta H}{\gamma w_0^2 / 2g}$$

is determined from the curves $\zeta = f(\alpha^\circ)$ corresponding to different values of $\frac{l_{fl}}{b_{fl}}$.

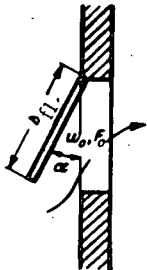


a_0	15	20	25	30	45	60	90
1) $\frac{l_{fl}}{b_{fl}} = 1.0$							
ζ	11	6.3	4.5	4.0	3.0	2.5	2.0
2) $\frac{l_{fl}}{b_{fl}} = 2.0$							
ζ	17	12	8.5	6.9	4.0	3.1	2.5
3) $\frac{l_{fl}}{b_{fl}} = \infty$							
ζ	30	16	11	8.6	4.7	3.3	2.5

Intake flap, single, top-hinged

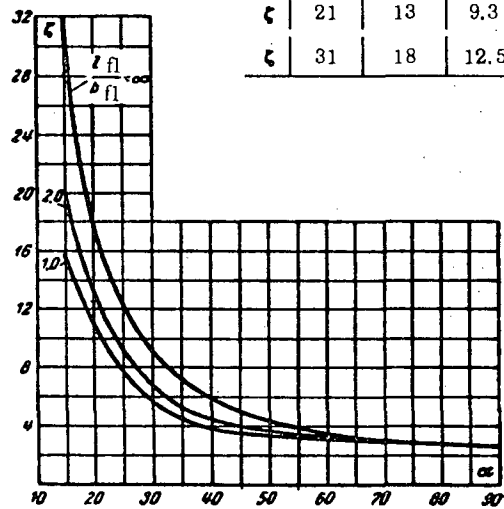
 Section IV
 Diagram 4-22

$$l_{fl} = \text{flap length}; \quad w_0 = \frac{Q}{F_0};$$



$$\zeta = \frac{\Delta H}{\gamma w_0^2 / 2g}$$

is determined from the curves $\zeta = f(\alpha^\circ)$ corresponding to different values of $\frac{l_{fl}}{b_{fl}}$.



a_0	15	20	25	30	45	60	90
ζ	16	11	8.0	5.7	3.7	3.1	2.6
ζ	21	13	9.3	6.9	4.0	3.2	2.6
ζ	31	18	12.5	9.2	5.2	3.5	2.6

$$1) \frac{l_{fl}}{b_{fl}} = 1.0$$

$$2) \frac{l_{fl}}{b_{fl}} = 2.0$$

$$3) \frac{l_{fl}}{b_{fl}} = \infty$$

Single flap, center-hinged

Section IV

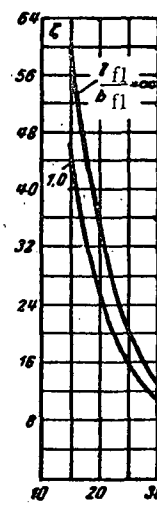
Diagram 4-23

$$l_{fl} = \text{flap length}, w_0 = \frac{Q}{F_0};$$



$$\zeta = \frac{\Delta H}{\frac{T w_0^2}{2g}}$$

is determined from the curves $\zeta = f(\alpha^\circ)$ corresponding to different values of $\frac{l_{fl}}{b_{fl}}$.



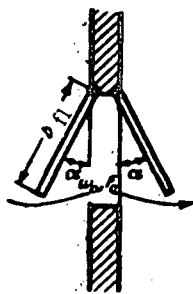
α°	15	20	25	30	45	60	90
1) $\frac{l_{fl}}{b_{fl}} = 1.0$	46	26	16	11	5.0	3.0	2.0
2) $\frac{l_{fl}}{b_{fl}} = \infty$	59	35	21	14	5.0	3.0	2.4

Double flaps, both top-hinged

Section IV

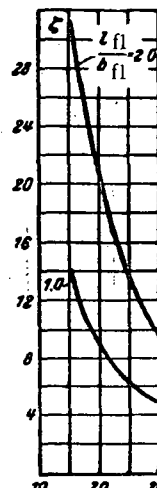
Diagram 4-24

$$l_{fl} = \text{flap length}, w_0 = \frac{Q}{F_0};$$



$$\zeta = \frac{\Delta H}{\frac{T w_0^2}{2g}}$$

is determined from the curves $\zeta = f(\alpha^\circ)$ corresponding to different values of $\frac{l_{fl}}{b_{fl}}$.

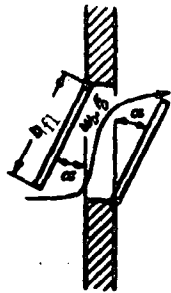


α°	15	20	25	30	45	60	90
1) $\frac{l_{fl}}{b_{fl}} = 1.0$	14	9.0	6.0	4.9	3.8	3.0	2.4
2) $\frac{l_{fl}}{b_{fl}} = 2.0$	31	21	14	9.8	5.2	3.5	2.4

Double flaps, top- and bottom-hinged

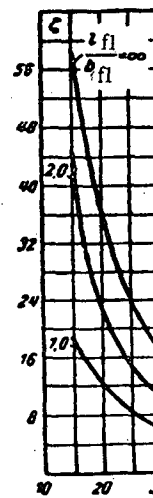
Section IV
Diagram 4-25

$$f_1 = \text{flap length}; w_0 = \frac{Q}{F_0}$$



$$\zeta = \frac{\Delta H}{\frac{T w_0^2}{2g}}$$

is determined from the curves $\zeta = f(\alpha^\circ)$ corresponding to different values of $\frac{l_{fl}}{b_{fl}}$.



α°	15	20	25	30	45	60	90
1) $\frac{l_{fl}}{b_{fl}} = 1.0$							
ζ	19	13	8.5	6.3	3.8	3.0	2.4
2) $\frac{l_{fl}}{b_{fl}} = 2.0$							
ζ	44	24	15	11	6.0	4.0	2.8
3) $\frac{l_{fl}}{b_{fl}} = \infty$							
ζ	59	36	24	17	8.6	5.7	2.8

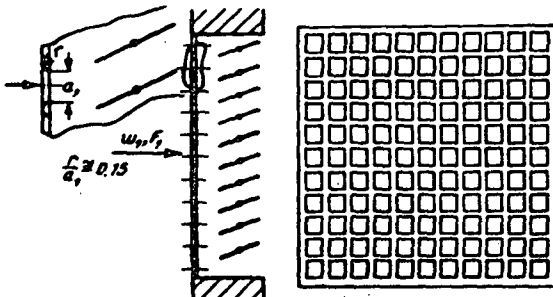
Stamped louver with adjustable slats in a large wall;
 $f \approx 0.8$; complete opening of the louver

Section IV
Diagram 4-26

$$\bar{f} = \frac{F_0}{F_1}$$

F_0 = louver cross section

$$\zeta = \frac{\Delta H}{\frac{T w_1^2}{2g}} \approx 1.6$$



w_1 = mean velocity over the total section of the louver in the wall.

$$D_h = \frac{4F_0}{U_0}; \quad U_0 = \text{perimeter}$$

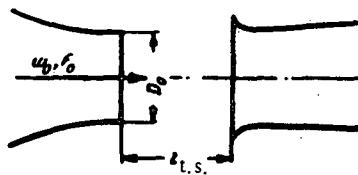
For a rectangle

$$D_h = \frac{a_0 b_0}{a_0 + b_0};$$

for an ellipse

$$D_h = \frac{4a_0 b_0}{1.5(a_0 + b_0) - \sqrt{a_0 b_0}}.$$

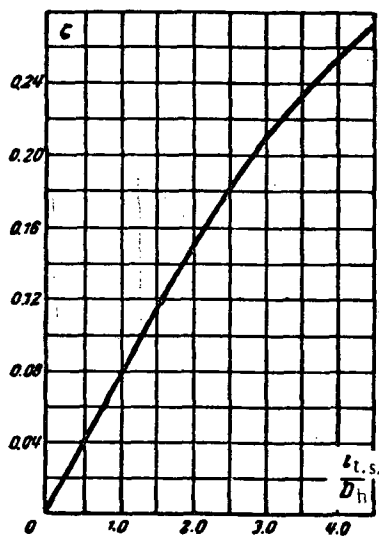
where a_0 and b_0 = sides of the rectangle or semiaxes of the ellipse;



$$\zeta = \frac{\Delta H}{\frac{\rho u_0^2}{2g}} = 0.0845 \frac{l_{t.s.}}{D_h} - 0.0053 \left(\frac{l_{t.s.}}{D_h} \right)^2$$

is determined from the curve $\zeta = f\left(\frac{l_{t.s.}}{D_h}\right)$

$\frac{l_{t.s.}}{D_h}$	0	0.5	1.0	1.5	2.0	2.5	3.0	3.5	4.0	4.5	5.0
ζ	0	0.04	0.08	0.12	0.15	0.18	0.21	0.23	0.25	0.27	0.29



Section Five

SMOOTH VELOCITY VARIATION (Resistance coefficients of diffusers)

5-1. LIST OF SYMBOLS

- F_0 = area of the narrow section of the diffuser, m²;
 F_1 = area of the wide section of the diffuser (in the case of a multistage diffuser — of the wide section of its smooth part), m²;
 F_2 = area of the widest section of a multistage diffuser, m²;
 $n_1 = \frac{F_1}{F_0}$ = area ratio of the diffuser (in the case of a multistage diffuser — area ratio of its smooth part);
 $n_2 = \frac{F_2}{F_1}$ = area ratio of sudden enlargement of a multistage diffuser;
 $n = \frac{F_2}{F_0}$ = total area ratio of a multistage diffuser;
 Π_0 = perimeter of the narrow section of the diffuser, m;
 D_0 = diameter of the narrow section of the diffuser, m;
 D_h = hydraulic diameter of the narrow section of the diffuser, m;
 a_0, b_0 = sides of the rectangular narrow section of the diffuser, m;
 a_1, b_1 = sides of the rectangular wide section of the diffuser, m;
 l_d = diffuser length, m;
 α = central divergence angle of a diffuser of arbitrary shape;
 w_0, w_1 = mean stream velocity in the narrow and wide sections of the diffuser, respectively, m/sec;
 w_0 = mean stream velocity before the perforated plate, m/sec;
 w_{\max} = maximum stream velocity through the cross section, m/sec;
 ΔH = pressure loss or resistance, kg/m²;
 ζ = total resistance coefficient of the diffuser;
 ζ_{exp} = coefficient of local resistance due to diffuser enlargement;
 ζ_{fr} = friction coefficient of diffuser;
 φ_d = total coefficient of shock allowing for the total losses in the diffuser;
 φ_{exp} = coefficient of shock allowing for the local losses due to diffuser enlargement only.

5-2. EXPLANATIONS AND RECOMMENDATIONS

1. A diffuser is a gradually widening passage to make the transition from a narrow conduit to a wide one and the transformation of the kinetic energy of the stream into pressure energy, with minimum pressure losses. In such a divergent pipe the intensity of turbulence is greater than in a straight pipe, and the local friction resistances are also greater. The increase in the pipe section is accompanied by a drop in the mean stream velocity. Therefore, the total resistance coefficient of the diffuser, expressed in terms of the velocity in the initial section, is less for divergence angles below a certain

value, than for the equivalent length of a constant-section pipe, whose area is equal to the initial section of the diffuser.

An increase of the divergence angle beyond this limit leads to a considerable increase in the resistance coefficient, so that it finally becomes much larger than for the equivalent length of straight pipe.

2. The increase of the resistance coefficient of a diffuser with the increase of its divergence angle, is mainly a result of the separation of the boundary layer from the diffuser walls, and of intensification of the stream turbulence with the resulting formation of turbulence in the entire stream.

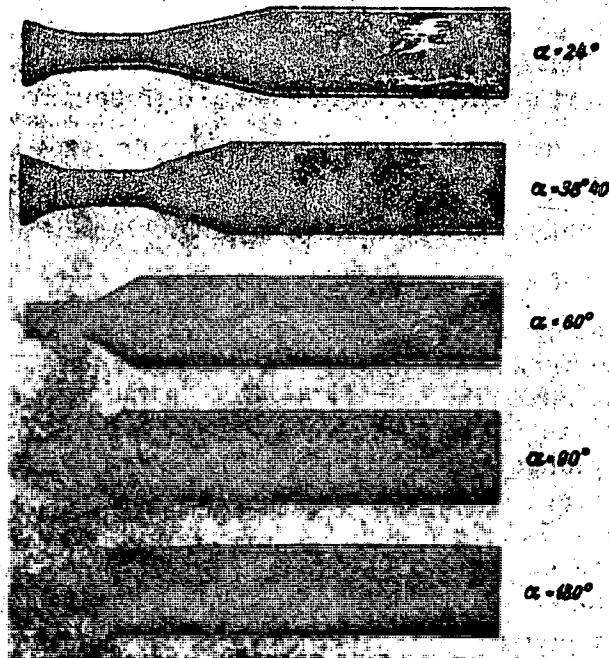


FIGURE 5-1. Flow patterns in diffusers with different

$$n = \frac{F_1}{F_0} = 3.3$$

a - $\alpha = 24^\circ$; b - $\alpha = 38^\circ 40'$; c - $\alpha = 60^\circ$; d - $\alpha = 90^\circ$;
e - $\alpha = 180^\circ$

The separation of the boundary layer from the walls (Figure 5-1) is due to a positive pressure gradient existing in the diffuser as a result of the velocity drop which accompanies the increase in cross section (Bernoulli equation).

The beginning of stream separation in a plane diffuser* can be approximately determined from the following relation, proposed by Levin /5-20/:

$$\frac{F_{sep}}{F_0} = \frac{1}{1 - \frac{1.95}{c^{4/5} \sqrt{Re}}} \quad (5-1)$$

* A plane diffuser is a length of conduit with expansion in one plane only.

where F_{sep} is the area of the section in which the stream separation starts.

3. The velocities over the cross section in narrow-angle diffusers with nonseparating boundary layers are distributed symmetrically about the longitudinal axis (Figure 4-4).

The separation in wide-angle diffusers (up to $\alpha = 50-60^\circ$) generally starts from only one of the walls, i.e., from the wall where the velocity is lowest. With the beginning of stream separation from one of the walls, the pressure increase through the diffuser is interrupted or reduced, and as a result there will be no stream separation from the opposite wall. Consequently, the distribution of velocities over the diffuser section will be asymmetric (Figures 5-1 and 5-2).

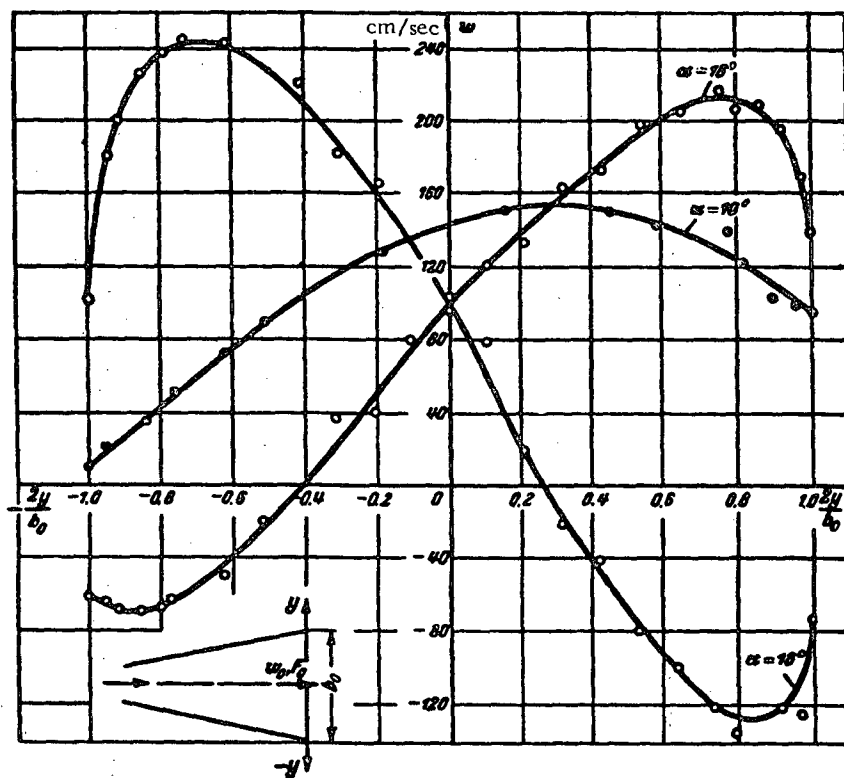


FIGURE 5-2. Velocity profiles in plane diffusers with different divergence angles.

In a perfectly symmetrical wide-angle diffuser the separation occurs alternately at one or the other side of the diffuser (Figure 5-2), leading to strong fluctuations of the whole stream.

4. The resistance coefficient of a diffuser is a function of several parameters:

- 1) the divergence angle α ;
- 2) the area ratio $n_1 = \frac{F_1}{F_0}$;
- 3) the cross-section shape;
- 4) the shape of the generatrix;
- 5) the inlet conditions;
- 6) the regime of flow (value of $Re = \frac{w_0 D_1}{\nu}$);
- and 7) the Mach number $M = \frac{w_0}{a}$.

$$\zeta = \frac{\Delta H}{\frac{\gamma w_0^2}{2g}} = f(Re, M, \alpha, n_1, k_1, k_2, k_3), \quad (5-2)$$

where k_1 is the coefficient characterizing the state of the boundary layer (the velocity distribution) at the diffuser inlet; k_2 is the coefficient characterizing the shape of the diffuser cross section; k_3 is the coefficient characterizing the shape of the diffuser generatrix; a is the velocity of propagation of sound in the stream, m/sec.

5. In practice an arbitrary method of loss separation is used. This is due to the scarcity of available data on the dependence of diffuser resistance on these parameters, and particularly on the Reynolds number. With this method, the total resistance of the diffuser ΔH_{dif} is considered as the sum of the local resistance, due to the stream "expansion" ΔH_{exp} , and the frictional resistance ΔH_{fr} . The total resistance coefficient ζ_{dif} is correspondingly considered as the sum of the local resistance coefficient due to the expansion ζ_{exp} and the friction coefficient ζ_{fr} *.

$$\zeta_{\text{dif}} = \frac{\Delta H}{\frac{1}{2} w_0^2} = \zeta_{\text{exp}} + \zeta_{\text{fr}}. \quad (5-3)$$

Here, the influence of the Reynolds number is accounted for by the friction coefficient ζ_{fr} , while ζ_{exp} is considered practically independent of Re^* .

6. It is convenient to express the expansion losses by the coefficient of shock (cf. /5-16/), defined as the ratio of expansion losses in a smooth diffuser to the theoretical losses at shock, in the case of sudden expansion of the cross section ($\alpha = 180^\circ$):

$$\varphi_{\text{exp}} = \frac{\Delta H}{\frac{1}{2} g (w_0 - w_1)^2}. \quad (5-4)$$

In the case of uniform velocity distribution at the inlet ($k_1 = 1.0$) the coefficient of shock of diffusers with divergence angles $\alpha = 0 - 40^\circ$ can be calculated by the following approximate formula, /5-16/:

$$\varphi_{\text{exp}} = k_2 \operatorname{tg} \frac{\alpha}{2} \sqrt{\operatorname{tg} \frac{\alpha}{2}}. \quad (5-5)$$

where α is the general divergence angle. In the case of a pyramidal diffuser with unequal divergence angles in the two planes, α is the larger angle.

The following value of k_2 is used for conical and plane diffusers:

$$k_2 \approx 3.2;$$

the following value is tentatively used in lieu of more accurate experimental data for pyramidal diffusers with expansion in two planes:

$$k_2 \approx 4.0.$$

- * The subscript "dif" will be dropped in what follows.
- * The recent studies of Solodkin and Ginevskii /5-8, 5-9, and 5-26 to 5-29/, Bam-Zelikovich /5-2, 5-3/, and Ovchinnikov /5-24/, in regard to the boundary layer in pipes with positive pressure gradient, enable the establishment of a relationship between the total resistance coefficient of a narrow-angle diffuser and the boundary layer before the diffuser entrance.

Currently there is no theoretical analysis of the corresponding situation for wide-angle diffusers, which is by far the most interesting case.

The value of φ_{exp} for the entire range of α from 0 to 180° is determined from the curves $\varphi_{\text{exp}} = f(\alpha)$ in diagrams 5-2 to 5-4.

The coefficient of local resistance of expansion is expressed through the coefficient of shock as follows:

$$\zeta_{\text{exp}} = \frac{\Delta H}{\frac{\gamma w_0^2}{2g}} = \varphi_{\text{exp}} \left(1 - \frac{1}{n_1}\right)^2 = k_s \operatorname{tg} \frac{\alpha}{2} \sqrt{\operatorname{tg} \frac{\alpha}{2} \left(1 - \frac{1}{n_1}\right)^2}. \quad (5-6)$$

7. The friction coefficient of a diffuser of circular or rectangular section, with equal divergence angles in the two planes, is calculated by the formula** :

$$\zeta_{\text{fr}} = \frac{\Delta H}{\frac{\gamma w_0^2}{2g}} = \frac{\lambda}{8 \sin \frac{\alpha}{2}} \left(1 - \frac{1}{n_1^2}\right), \quad (5-7)$$

where λ is the friction coefficient of unit length of the diffuser, determined from the corresponding graphs of diagrams 2-2 to 2-5 as a function of the Reynolds number

$\text{Re} = \frac{w_0 D_h}{v}$ and the relative roughness $\bar{\Delta} = \frac{\Delta}{D_h}$.

The friction coefficient of a pyramidal diffuser with unequal divergence angles ($\alpha^\circ \neq \beta^\circ$) in the two planes is calculated by the following formula, cf. /5-16/:

$$\zeta_{\text{fr}} = \frac{\Delta H}{\frac{\gamma w_0^2}{2g}} = \frac{\lambda}{16} \frac{1}{\sin \frac{\alpha}{2}} \left(1 - \frac{1}{n_1^2}\right) + \frac{\lambda}{16} \frac{1}{\sin \frac{\beta}{2}} \left(1 - \frac{1}{n_1^2}\right) = \Delta \zeta_{\text{fr}} + \Delta' \zeta_{\text{fr}}. \quad (5-8)$$

The friction coefficient of a plane diffuser with inlet-section sides a_0 and b_0 , where b_0 is constant along the diffuser, is calculated by:

$$\zeta_{\text{fr}} = \frac{\Delta H}{\frac{\gamma w_0^2}{2g}} = \frac{\lambda}{4} \left[\frac{a_0}{b_0} \cdot \frac{1}{\operatorname{tg} \frac{\alpha}{2}} \left(1 - \frac{1}{n_1} + \frac{1}{2 \sin \frac{\alpha}{2}} \left(1 - \frac{1}{n_1^2}\right)\right) \right].$$

The following simplified formula can be used in practice:

$$\zeta_{\text{fr}} = \frac{\lambda}{4} \frac{1}{\sin \frac{\alpha}{2}} \left[\frac{a_0}{b_0} \left(1 - \frac{1}{n_1}\right) + 0.5 \left(1 - \frac{1}{n_1^2}\right) \right]. \quad (5-9)$$

8. The resistance coefficients of diffusers where the rectangular section changes to circular or vice versa, can be determined from the data for pyramidal diffusers with equivalent divergence angles. The equivalent angle α_e is determined on the basis of the following formulas:

* Obviously, at $n_1 = \frac{F_1}{F_0} = \infty$ $\varphi_{\text{exp}} = \zeta_{\text{exp}}$.

** For the derivation cf. Eiffel /5-39/ and also /5-16/.

The magnitude of λ actually varies along the diffuser, but in practice it is assumed to be constant.

1) transition from circle to rectangle

$$\operatorname{tg} \frac{\alpha_e}{2} = \frac{2 \sqrt{\frac{a_1 b_1}{\pi}} - D_0}{2 l_d}; \quad (5-10)$$

2) transition from rectangle to circle

$$\operatorname{tg} \frac{\alpha_e}{2} = \frac{D_1 - 2 \sqrt{\frac{a_0 b_0}{\pi}}}{2 l_d}. \quad (5-11)$$

9. In the case of a nonuniform velocity distribution at the inlet section, i.e., at $k_1 > 1.0$, as when the diffuser is placed behind a long straight stretch or any other fitting, behind a throttle, etc., the coefficient of local resistance due to expansion in the diffuser is determined by the formula

$$\zeta_{\text{exp}} = k_1 \zeta_{\text{exp}} \quad (5-12)$$

where ζ_{exp} is determined as ζ_{exp} of a diffuser with uniform velocity distribution at the inlet (cf. point 6);

k_1 is determined as a function of the velocity profile at the inlet of the diffuser and of its divergence angle.

10. At the inlet, the dependence of the diffuser resistance coefficient on the state of the boundary layer (the velocity distribution) is complex. In narrow-angle diffusers a nonuniform symmetric velocity profile with a maximum at the center and minimum at the walls leads to a decrease of the total resistance, since the frictional stress at the walls is decreased. At the same time this velocity profile increases the possibility of stream separation, and displaces the point of separation toward the initial section of the diffuser, so that with the subsequent increase of the divergence angle the resistance will increase compared with resistance at a uniform velocity distribution.

In a nonuniform velocity profile, with lower velocities at the center and higher ones at the walls, the opposite will be observed; the total resistance of the diffuser being higher at small divergence angles and lower at larger ones.

11. The dependence of the coefficient k_1 on the divergence angle for a symmetric velocity profile at the inlet has been plotted in diagram 5-1 for different values of the ratio of the maximum to the mean velocities $\frac{w_{\max}}{w_0}$ over the section. The dependence of the ratio $\frac{w_{\max}}{w_0}$ on the relative length $\frac{l}{D_h}$ of the initial straight stretch has likewise been plotted in the same diagram for different values of Re (Solodkin and Ginevskii /5-26/).

In the case of a nonsymmetric velocity profile, which exists behind various fittings, throttles, etc., limited use can be made of the values of k_1 given in diagrams 5-6 and 5-18. The data of diagram 5-6 were obtained on the basis of the processing of results of Winter's investigations /5-65/ of a conic diffuser placed behind branches with different geometric parameters. The data of diagram 5-18 were obtained on the basis of the processing of the results of Johnson's investigations /5-47/ of annular diffusers at whose inlet different velocity distributions were created by means of special screens.

12. Up to $\alpha = 40$ to 50° , the coefficient of shock φ_{exp} is smaller than unity. This shows that losses in a diffuser are smaller than shock losses in the case of sudden expansion ($\alpha = 180^\circ$). At divergence angles $50 \leq \alpha \leq 90^\circ$ the value of φ_{exp} becomes

somewhat larger than unity, i.e., losses in a diffuser increase slightly compared with losses at shock. Starting with $\alpha = 90^\circ$, and up to $\alpha = 180^\circ$, the value of φ_{exp} again drops and approaches unity, indicating that the losses in the diffuser approach the losses at sudden expansion. If, therefore, a uniform velocity distribution at the diffuser exit is not required, it will be inexpedient to use diffusers with divergence angle $\alpha > 40$ to 50° .

If a very short transition stretch is required by design considerations, this can be achieved by means of sudden expansion ($\alpha = 180^\circ$).

If it is required to obtain a uniform velocity profile behind the transition stretch and if this purpose is to be achieved by means of baffles, dividing walls, or grids, then any diffuser, even with a large divergence angle ($\alpha > 50^\circ$), is to be preferred to sudden expansion ($\alpha = 180^\circ$).

13. Since the smooth increase of a pipe section with narrow divergence angles leads to a decrease in the pressure losses compared with those in a pipe of constant section, and at wide divergence angles to the increase of these losses, there must obviously exist an optimum divergence angle at which minimum losses are obtained. This angle can be calculated for the case of a straight diffuser of circular section by:

$$\alpha_{\text{opt}} = 0.43 \left(\frac{\lambda}{k_1} \cdot \frac{n_1 + 1}{n_1 - 1} \right)^{4/5}. \quad (5-13)$$

Thus, at $\lambda = 0.015$, $n_1 = 2.25$, and $k_1 = 1.0$ one obtains $\alpha_{\text{opt}} \approx 6^\circ$. For a diffuser of rectangular section, α_{opt} lies approximately within the same limits. For a plane diffuser this angle lies within the limits $\alpha_{\text{opt}} = 10$ to 12° .

14. The flow conditions of a stream in short wide-angled diffusers can be considerably improved by preventing stream separation or reducing the formation of eddies.

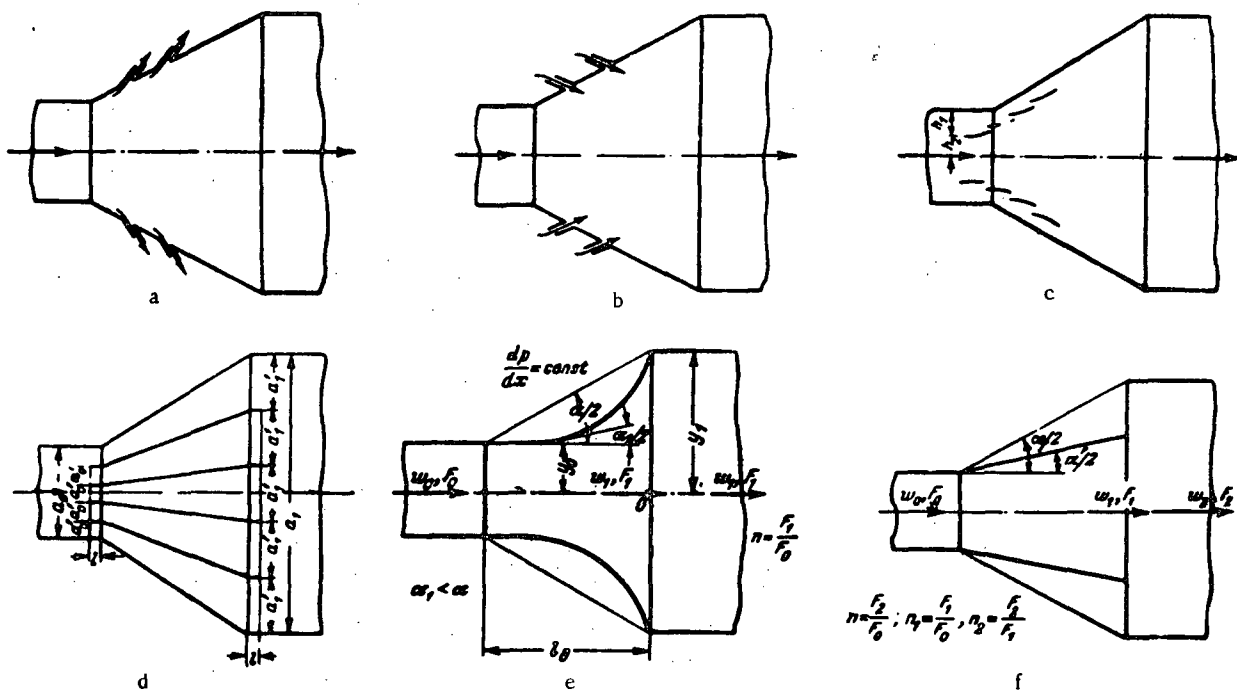


FIGURE 5-3. Different methods for improving the work of short diffusers:

a — suction of the boundary layer; b — blowing away of the boundary layer; c — guide vanes or baffles; d — dividing walls; e — curved diffuser; f — multistage (stepped) diffuser.

The main measures contributing to an improvement of flow in diffusers are (Figure 5-3):

- 1) the suction of the boundary layer;
- 2) the blowing away of the boundary layer;
- 3) the installation of baffles or guide vanes;
- 4) the installation of dividing walls;
- 5) the use of curved walls;
- 6) the use of stepped walls.

15. When the boundary layer is sucked (Figure 5-3,a), the part of the stream separated from the wall again adheres to the surface, and as a result the zone of separation is displaced downstream, the flow becomes smoother, and the resistance decreases. A 30 to 50 % reduction of losses can be achieved as a result.

The blowing away of the boundary layer (Figure 5-3,b) leads to an increase of stream velocity near the walls. As a result, the separation zone is also displaced downstream.

16. Guide vanes or baffles (Figure 5-3,c) deflect a part of the high-velocity stream core toward the boundary zone of separation. The latter is reduced or even completely eliminated as a result. The effect of guide vanes is greatest at wide divergence. At $\alpha = 50$ to 180° the resistance coefficient is reduced by a factor of almost two.

Several general rules can be given for positioning the baffles in the diffuser /5-56/:

a) The vanes should be placed before and behind the entrance angle to the diffuser (Figure 5-3,c), and their number should be increased with the increase of the divergence angle.

b) The channels between the vanes and the walls must contract as a rule; however, at wide divergence angles, satisfactory results can be obtained even with expanding channels. It is necessary to permit the stream to expand in the peripheral channels just as in the main channel.

c) The relative distance $\frac{h_1}{h_2}$ must be equal to 0.95 for $\alpha = 90^\circ$, and to 1.4 for $\alpha = 180^\circ$ (Figure 5-3,c).

d) The vanes must have a small curvature and can be made of sheet metal.

e) The chord of the vanes can represent 20 to 25% of the diameter or the height of the diffuser section.

f) The best angle of inclination of the vanes can be selected by arranging them first one behind the other and rotating each of them through an angle until the diffuser resistance becomes minimum.

17. The dividing walls divide a wide-angle diffuser into several narrow-angle diffusers (Figure 5-3,d). As a result, the resistance is decreased and a more uniform velocity distribution over the section is achieved /5-19/.

The dividing walls are more efficient with the increase of the total divergence angle of the diffuser. At relatively narrow divergence angles the dividing walls can even increase the diffuser resistance, since they increase the total friction surface.

The following procedure is used when selecting and installing dividing walls in wide-angle diffusers:

a) The number z of dividing walls is selected from Table 5-1 as a function of the divergence angle.

TABLE 5-1

α°	30	45	60	90	120
z	2	4	4	6	8

b) The dividing walls are positioned so that the distances a'_0 between them at the diffuser inlet are exactly equal, and the distances a'_1 between them at the exit are approximately equal.

c) The dividing walls extend in both directions beyond the diffuser, with protruding parts parallel to the diffuser axis. The length of the protruding parts must not be smaller than $0.1a_0$ and $0.1a_1$, respectively.

18. The variation of the pressure gradient along the diffuser is smoother in a diffuser with curved walls (Figure 5-3,e), in which the rate of increase of the cross-section area is lower in the initial section than in the end section. As a result, the main cause of stream separation is weakened, and the main source of losses is attenuated. A diffuser in which the pressure gradient remains constant along the channel ($\frac{dp}{dx} = \text{const}$) at potential flow will be the best choice.

The losses in such diffusers may be as much as 40% lower than corresponding straight diffusers at divergence angles $25^\circ \leq \alpha \leq 90^\circ$, the reduction increasing with an increase of the divergence angle within these limits /5-16/. At lower divergence angles, e.g., $\alpha < 15$ to 20° , the losses in curved diffusers are higher than in straight ones. The use of curved diffusers is therefore expedient at wide divergence angles only.

The equation of the generatrix of a curved diffuser with a section which fulfills the condition $\frac{dp}{dx} = \text{const}$ (Figure 5-3,e) is:

$$y = \frac{y_1}{\sqrt[4]{1 + \left[\left(\frac{y_1}{y_0} \right)^4 - 1 \right] \frac{x}{l_d}}}. \quad (5-14)$$

The equation of the generatrix for a plane diffuser is:

$$y = \frac{y_1}{\sqrt{1 + \left[\left(\frac{y_1}{y_0} \right)^2 - 1 \right] \frac{x}{l_d}}}. \quad (5-15)$$

The resistance coefficient of a curvilinear diffuser at $\frac{dp}{dx} = \text{const}$ within the limits $0.1 \leq \frac{F_0}{F_1} < 0.9$ can be calculated by the following approximate formula /5-16/:

$$\zeta = \frac{\Delta H}{\frac{\rho w_0^2}{2g}} = \varphi_0 \left(1.43 - \frac{1.3}{n_1} \right) \left(1 - \frac{1}{n} \right)^2 * \quad (5-16)$$

where φ_0 is a coefficient depending on the relative length $\frac{l_d}{D_h}$ of the curved diffuser and determined from the data of diagram 5-7.

19. In a multistage diffuser (Figure 5-3,f), in which a sudden expansion takes place after a smooth variation of cross-section area, the main shock losses occur at relatively low velocities. As a result, the losses in the diffuser are reduced by a factor of two to

* The frictional losses in very wide-angled diffusers are quite small. It is not necessary, therefore, to separate these losses from the total losses with curved diffusers which correspond to wide-angle straight diffusers.

three. The coefficient of total resistance of a multistage diffuser of circular or rectangular section can be approximately calculated by the following formula /5-16/:

$$\zeta = \frac{\Delta H}{\frac{\gamma w_0^2}{2g}} = (1 + \alpha) \left[\frac{\lambda}{8 \sin \frac{\alpha}{2}} \cdot \frac{\left(1 + 2 \frac{l_d}{D_h} \operatorname{tg} \frac{\alpha}{2} \right)^2 + 1}{\left(1 + 2 \frac{l_d}{D_h} \operatorname{tg} \frac{\alpha}{2} \right)^2 - 1} + k_s \operatorname{tg} \frac{\alpha}{2} \sqrt[4]{\operatorname{tg} \frac{\alpha}{2}} \right] \times \\ \times \left[1 - \frac{1}{\left(1 + 2 \frac{l_d}{D_h} \operatorname{tg} \frac{\alpha}{2} \right)^2} \right]^2 + \left[\frac{1}{\left(1 + 2 \frac{l_d}{D_h} \operatorname{tg} \frac{\alpha}{2} \right)^2} - \frac{1}{n} \right]^2, \quad (5-17)$$

where $k_s = 3.2$ for a diffuser of circular section; $k_s = 4$ to 6 for a diffuser of rectangular section*; $n = \frac{F_2}{F_0}$ is total area ratio of the multistage diffuser, i.e., ratio of the area of the widest part of the diffuser to the area of its narrowest part (Figure 5-3,f).

The coefficient of total resistance of a plane multistage diffuser can be approximately calculated as follows /5-16/:

$$\zeta = \frac{\Delta H}{\frac{\gamma w_0^2}{2g}} = (1 + \alpha) \left\{ \frac{\lambda}{8 \frac{l_d}{a_0} \operatorname{tg} \frac{\alpha}{2}} \left[\frac{a_0}{b_0} \cdot \frac{1}{\operatorname{tg} \frac{\alpha}{2}} \times \left(1 + 2 \frac{l_d}{a_0} \operatorname{tg} \frac{\alpha}{2} \right) + \frac{1}{\sin \frac{\alpha}{2}} \left(1 + \frac{l_d}{a_0} \operatorname{tg} \frac{\alpha}{2} \right) \right] + \right. \\ \left. + 3.2 \operatorname{tg} \frac{\alpha}{2} \sqrt[4]{\operatorname{tg} \frac{\alpha}{2}} \right\} \left(1 - \frac{1}{1 + 2 \frac{l_d}{a_0} \operatorname{tg} \frac{\alpha}{2}} \right)^2 + \left[\frac{1}{\left(1 + 2 \frac{l_d}{a_0} \operatorname{tg} \frac{\alpha}{2} \right)} - \frac{1}{n} \right]^2 \quad (5-18)$$

with b_0 constant along the diffuser.

20. To each area ratio n and each relative length $\frac{l_d}{D_h}$ (or $\frac{l_d}{a_0}$) of the multistage diffuser, there corresponds an optimum divergence angle α_{opt} at which the total coefficient of resistance is minimum (cf. diagrams 5-8 to 5-10). The use of multistage diffusers with optimum expansion angles is recommended.

The resistance coefficient of such diffusers is determined by the formula /5-16/:

$$\zeta = \frac{\Delta H}{\frac{\gamma w_0^2}{2g}} = (1 + \alpha) \zeta_{min} \quad (5-19)$$

where ζ_{min} = minimum resistance coefficient, depending on the relative length of the smooth part of the diffuser $\frac{l_d}{D_h}$ or $\frac{l_d}{a_0}$, and the total area ratio n of the multistage diffuser;

* The curves of diagram 5-10 were calculated for $k_s = 6.0$, which gives a certain safety factor in the calculation.

this relationship has been plotted in diagrams 5-8 to 5-10; σ is a corrective factor, determined from the same diagrams as a function of $\frac{F_1}{F_2}$.

21. The limiting divergence angle α_{lim} of the smooth part of the multistage diffuser, i.e., the angle at which, for the given overall area ratio n and relative length $\frac{l_d}{D_h}$ or $\frac{l_d}{a_0}$ of the smooth part, a straight diffuser is obtained, is given by

$$\left. \begin{aligned} \operatorname{tg} \frac{\alpha_{lim}}{2} &= \frac{\sqrt{n-1}}{2 \frac{l_d}{D_h}} \\ \text{or} \\ \operatorname{tg} \frac{\alpha_{lim}}{2} &= \frac{n-1}{2 \frac{l_d}{a_0}} \end{aligned} \right\} \quad (5-20)$$

In practice, it is expedient to select the relative length $\frac{l_d}{D_h}$ of the multistage diffuser not on the basis of the minimum value ζ_{min} , but on a value approximately 10% higher, which makes possible a considerable reduction in diffuser length without noticeably increasing the losses in it. The lines of optimum values of $\frac{l_d}{D_h}$ are represented in graphs a of diagrams 5-8 to 5-10 by dotted lines.

22. If the diffuser is installed behind a fan, it becomes necessary to allow for the flow pattern at the fan exit, which is quite different from that at an inlet to an isolated diffuser placed behind a straight stretch of constant section.

As a rule, the velocity profile behind a centrifugal fan is nonsymmetric, due to a certain stream deflection in the direction of fan rotation. The velocity profile is a function of the type of fan and its type of work, characterized by the output coefficient $\frac{Q}{Q_{opt}}$, where Q_{opt} = output at maximum efficiency of the fan.

23. The stream deflection in the direction of fan rotation makes it possible to use unusually wide divergence angles behind centrifugal fans and diffusers. If these are plane diffusers of divergence angle $\alpha > 25^\circ$, it is best to make them asymmetric, so that the outer wall is either a continuation of the housing or deviates from it by a small angle (up to 10°) toward the side of the housing, while the inner wall deviates toward the side of the impeller.

The deflection of the diffuser axis toward the side of the fan housing is impractical, since the resistance of such diffusers at $\alpha > 15^\circ$ is 2 to 2.5 times higher than that of symmetric diffusers in which the axis is deflected toward the side of the impeller (cf. Lokshin and Gazirbekova /5-22/).

24. The resistance coefficient of plane diffusers with divergence angles $\alpha < 15^\circ$ and pyramidal diffusers with divergence angles $\alpha < 10^\circ$, installed behind centrifugal fans of any type, can be calculated from the data given above for isolated diffusers, taking for their inlet section the ratio of velocities

$$\frac{w_{max}}{w_0} \approx 1.1.$$

The values of ζ obtained for isolated diffusers cannot be used at wider divergence angles than those given above; here the values of ζ must be determined from the data of diagrams 5-12 to 5-17. These are applicable for $Q = Q_{\text{opt}}$ and $Q \leq Q_{\text{opt}}$.

25. When the space available for the diffuser behind the centrifugal fan is restricted, use can be made of a multistage diffuser, which is much shorter than a straight diffuser at equal resistance. The optimum divergence angle of the diffuser, at which a minimum coefficient is obtained, can be calculated from the corresponding curves of diagram 5-17.

26. The resistance coefficient of an annular diffuser formed by installing a conical diffuser behind an axial fan or compressor with converging back fairing (cf. diagram 15-18) can be determined by the formula

$$\zeta = \frac{\Delta H}{\frac{\gamma w_0^2}{2g}} = k_i \varphi_d \left(1 - \frac{F_0}{F_i}\right)^2. \quad (5-21)$$

where φ_d = total coefficient of shock, determined from graph a of diagram 5-18 as a function of the divergence angle α^* ; k_i is a correction coefficient, characterizing the velocity distribution in the narrow section of the diffuser and determined from graph b of the same diagram as a function of the divergence angle α ; these curves correspond to different velocity profiles in the narrow section of the diffuser, represented in graph c of the same diagram**; F_0 and F_i are cross-section areas (less the cross-section area of the fairing) in the narrow and wide parts of the diffuser, respectively.

27. The resistance coefficient of an annular diffuser formed by installing a conic diffuser behind an axial fan with diverging back fairing can be approximated by the formula

$$\zeta = \frac{\Delta H}{\frac{\gamma w_0^2}{2g}} = k_i \zeta'. \quad (5-22)$$

where ζ' = resistance coefficient of the same diffuser at uniform velocity distribution at the inlet, determined from table 5-3 in diagram 5-18; k_i = correction coefficient determined under 11.

28. Axial turbines use radial-annular diffusers in which the increase of area is mainly due to the radial dimensions of the diffuser (Figure 5-4,a). The area-expansion ratio of radial-annular diffusers can be determined from the relation

$$n = 2 \frac{b}{h} \frac{\bar{D}}{1 + \bar{d}}, \quad (5-23)$$

where $\bar{D} = \frac{D_d}{D_0}$ and $\bar{d} = \frac{d}{D_0}$ are the relative diameters of the diffuser and of the hub, respectively; $\frac{b}{h}$ is the relative width of the exit section of the diffuser.

The resistance coefficient of a radial-annular diffuser mounted behind an operating turbo-compressor is 15% to 20% greater than the corresponding value for the same diffuser when the compressor is not operating. The magnitude of the resistance

* The total coefficient of shock allows for the total losses in diffusers /5-16/.

** It is assumed that the approximate velocity distribution to be expected behind the fan or compressor is known.

coefficient is also a function of the type of work of the compressor, that is of the discharge coefficient $\bar{c}_{d0} = \frac{Q}{\frac{\pi}{4}(D_0^2 - d^2)u}$ where u = peripheral impeller velocity at the maximum radius (cf. Dovzhik and Ginevskii /5-12/).

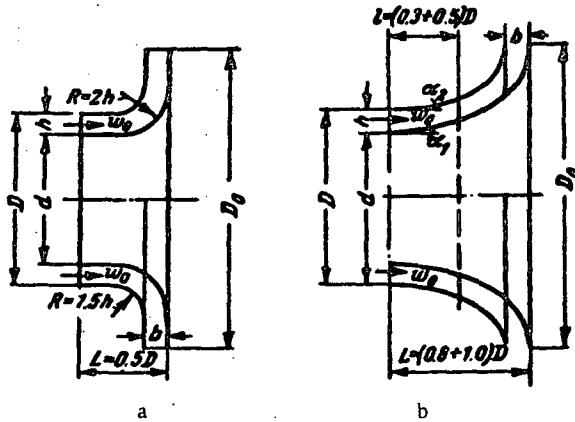


FIGURE 5-4

a — radial annular diffuser; b — axial-radial-annular.

The values of the resistance coefficients of radial-annular diffusers of an operating (at $\bar{c}_{d0} = 0.5$) and nonoperating compressor are given in diagram 5-19.

29. The axial-radial-annular diffuser is somewhat better from the aerodynamic point of view. Here, a radial bend follows a short annular diffuser (Figure 5-4, b).

In this diffuser the radial turn is achieved at lower stream velocities, and the pressure losses are, accordingly, somewhat lower. At the same time the axial dimensions are much larger than those of a radial-annular diffuser.

When installed behind an operating turbo-compressor, at $\bar{c}_{d0} = 0.5$, the values of the resistance coefficients are given in diagram 5-19.

30. The existence of a uniformly distributed resistance behind the diffuser promotes orderly streamline flow in the diffuser itself and in the channel behind it. This somewhat reduces the losses in the diffuser itself. The total losses in the diffuser, however, remain roughly the same.

Specifically for curved diffusers, and for straight diffusers of divergence angles from 40 to 60°, these losses remain equal to the sum of the losses taken separately for the diffuser and the grid, screen, etc. (cf. /5-17/):

$$\zeta = \frac{\Delta H}{\frac{\rho u_0^2}{2g}} = \zeta_d + \frac{\zeta_g}{\frac{\rho u_1^2}{2g}}. \quad (5-24)$$

where $\zeta_d = \frac{\Delta H}{\frac{\rho u_0^2}{2g}}$ = resistance coefficient of the diffuser, determined as ζ from the data

of the corresponding diagrams of this section; $\zeta_g = \frac{\Delta H}{\frac{1}{2} w_0^2}$ = resistance coefficient in front of
the grids, screens, nozzles, etc., expressed through the stream velocity, determined as
 ζ from the data of the corresponding diagrams of section VIII; $n_i = \frac{F_i}{F_0}$ = area ratio of
the diffuser.

5-3. LIST OF THE DIAGRAMS OF RESISTANCE COEFFICIENTS OF SECTION V

Diagram description	Source	No. of diagram	Note
Diffusers of arbitrary shape located at the discharge of long stretches with nonuniform but symmetric velocity profile	Abramovich /5-1/, Solodkin and Ginevskii /5-26/, Peters /5-57/	5-1	The nonuniformity is compensated for approximately
Conical diffuser in a line	Gibson /5-6, 5-43, 5-44/, Idel'chik /5-16, 5-18/, Peters /5-57/	5-2	Experimental data; at large divergence angles the curves are an extrapolation
Pyramidal diffuser in a line	The same	5-3	Very tentative; to be used until refined by new data
Plane diffuser in a line	The same	5-4	Experimental data; the curves are extrapolated for large divergence angles
Transition diffuser (transition from circle to rectangle or from rectangle to circle) in a line	—	5-5	Tentative
Diffusers of arbitrary shape at $\alpha = 8-12^\circ$, located at discharges of branches or other fittings with similar velocity profiles	Winter /5-65/	5-6	Experimental data
Curved diffusers ($dp/dx = \text{const}$) in a line	Idel'chik /5-16/	5-7	Based on experimental data
Stepped conical diffuser of optimum divergence angle α_{opt}	The same	5-8	Approximate calculations
Stepped pyramidal diffuser of optimum divergence angle α_{opt}	The same	5-9	" "
Stepped plane diffuser of optimum divergence angle α_{opt} at $0.5 < \frac{a_0}{b_0} < 2.0$	The same	5-10	" "
Short diffusers with guiding devices or with resistance at the exit	Idel'chik /5-19/	5-11	First one according to the author's experimental data, the other tentative
Plane symmetric diffuser behind a centrifugal fan in a duct (forced draft)	Lokshin and Gazirbekova /5-22/	5-12	Experimental data
Plane asymmetric diffuser at $a_1 = 0$ behind a centrifugal fan in a duct (forced draft)	The same	5-13	The same
Plane asymmetric diffuser at $a_1 = 10^\circ$ behind a centrifugal fan in a duct (forced draft)	" "	5-14	" "
Plane asymmetric diffuser at $a_1 = -10^\circ$ behind a centrifugal fan in a duct (forced draft)	" "	5-15	" "
Pyramidal diffuser behind a centrifugal fan in a duct (forced draft)	" "	5-16	" "
Multistage diffuser of optimum divergence angle α_{opt} behind a centrifugal fan in a duct (forced draft)	" "	5-17	" "
Annular diffusers with deflecting baffles in a duct	Bushel' /5-4/, Johnston /5-47/	5-18	" "
Radial-annular and axial-radial-annular diffusers in a line	Dovzhik and Ginevskii /5-12/	5-19	" "

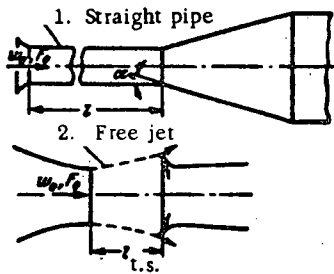
5-4. DIAGRAMS OF RESISTANCE COEFFICIENTS

Diffusers of arbitrary shape located at the discharge of long stretches with nonuniform but symmetric velocity profile

Section V
Diagram 5-1

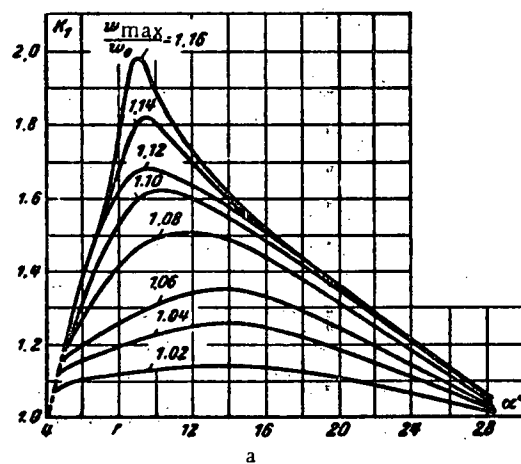
$$D_h = \frac{4P_0}{\Pi_0}; \Pi_0 \text{ — perimeter}$$

Initial zone



$$\zeta = \frac{\Delta H}{\gamma w_0^2} = k_1 \zeta_{exp} + \zeta_{fr.}$$

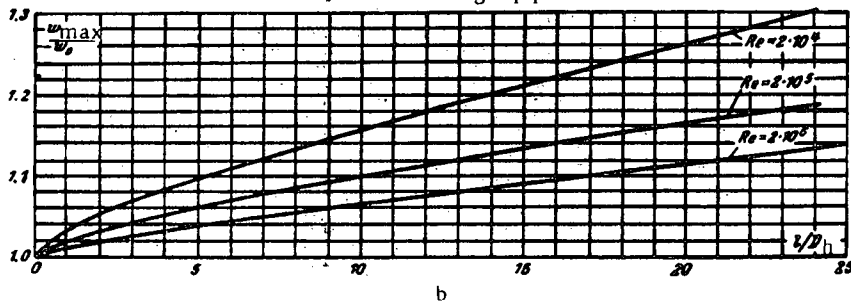
where ζ_{exp} and $\zeta_{fr.}$ are taken from the diagrams of Section V; k_1 is determined as a function of α° from the curves of graph a corresponding to different $\frac{w_{max}}{w_0}$; $\frac{w_{max}}{w_0}$ is determined as a function of I/D_h from the curves of graphs b and c corresponding to different values of $Re = \frac{w_0 D_h}{v}$; v is taken from § 1-3, b.



a

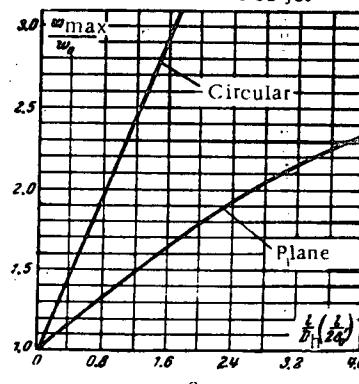
$\frac{w_{max}}{w_0}$	Values of k_1							
	α°	5	8	10	14	20	24	30
1.00	1.00	1.00	1.00	1.00	1.00	1.00	1.00	1.00
1.02	1.10	1.12	1.14	1.15	1.00	1.07	1.02	
1.04	1.14	1.20	1.23	1.26	1.19	1.10	1.03	
1.06	1.17	1.27	1.31	1.36	1.24	1.14	1.04	
1.08	1.19	1.42	1.49	1.49	1.31	1.18	1.05	
1.10	1.19	1.54	1.62	1.54	1.34	1.20	1.06	
1.12	1.22	1.62	1.68	1.57	1.36	1.21	1.06	
1.14	1.22	1.68	1.81	1.60	1.36	1.21	1.06	
1.16	1.22	1.78	1.89	1.61	1.36	1.21	1.06	

1. Initial zone — straight pipe.



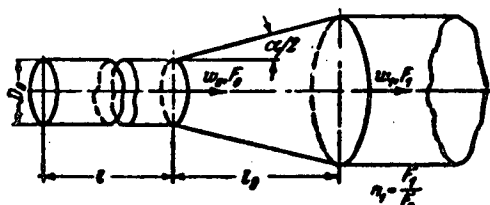
b

2. Initial zone — free jet



c

Conical diffuser in a line

 Section V
 Diagram 5-2


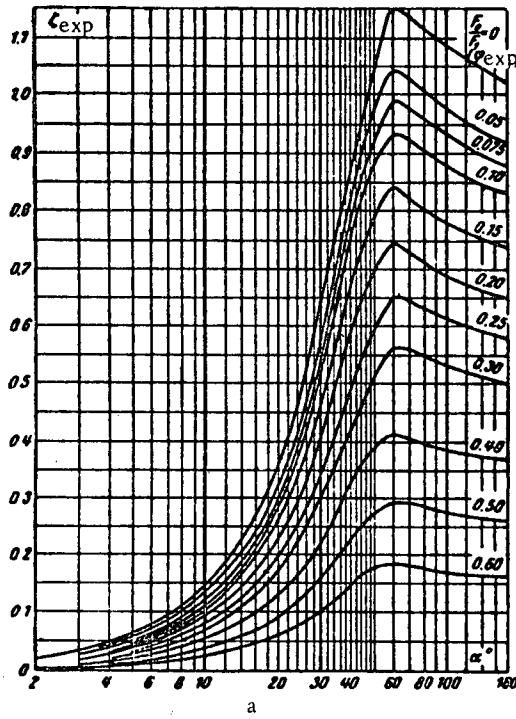
1. Uniform velocity distribution at the diffuser inlet:

$$\zeta = \frac{\Delta H}{\frac{1}{2} w_0^2} = \xi_{\text{exp}} + \xi_{\text{fr}}$$

$$\text{where } \xi_{\text{exp}} = \varphi_{\text{exp}} \left(1 - \frac{F_2}{F_1}\right)^2;$$

 Values of ξ_{exp}

$\frac{F_2}{F_1}$	n_1	α°													
		3	6	8	10	12	14	16	20	24	30	40	60	90	
0	∞	0.03	0.08	0.11	0.15	0.19	0.23	0.27	0.36	0.47	0.65	0.92	1.15	1.10	1.02
0.05	20	0.03	0.07	0.10	0.14	0.16	0.20	0.24	0.32	0.42	0.58	0.83	1.04	0.99	0.92
0.075	13.3	0.03	0.07	0.09	0.13	0.16	0.19	0.23	0.30	0.40	0.55	0.79	0.99	0.95	0.88
0.10	10	0.03	0.07	0.09	0.12	0.15	0.18	0.22	0.29	0.38	0.52	0.75	0.93	0.89	0.83
0.15	6.7	0.02	0.06	0.08	0.11	0.14	0.17	0.20	0.26	0.34	0.46	0.67	0.84	0.79	0.74
0.20	5.0	0.02	0.05	0.07	0.10	0.12	0.15	0.17	0.23	0.30	0.41	0.59	0.74	0.70	0.65
0.25	4.0	0.02	0.05	0.06	0.08	0.10	0.13	0.15	0.20	0.26	0.35	0.47	0.65	0.62	0.58
0.30	3.3	0.02	0.04	0.05	0.07	0.09	0.11	0.13	0.18	0.23	0.31	0.40	0.57	0.54	0.50
0.40	2.5	0.01	0.03	0.04	0.06	0.07	0.08	0.10	0.13	0.17	0.23	0.33	0.41	0.39	0.37
0.50	2.0	0.01	0.02	0.03	0.04	0.05	0.06	0.07	0.09	0.12	0.16	0.23	0.29	0.28	0.26
0.60	1.7	0.01	0.01	0.02	0.03	0.03	0.04	0.05	0.06	0.08	0.10	0.15	0.18	0.17	0.16



φ_{exp} is determined from the curve $\zeta_{\text{exp}} = f(\alpha^\circ)$ at $\frac{F_0}{F_1} = \sigma$ on graph a.

Within the limits $0 < \alpha < 40^\circ$:

$$\varphi_{\text{exp}} = 3.2 \operatorname{tg} \frac{\alpha}{2} \sqrt{\operatorname{tg} \frac{\alpha}{2}}.$$

The values of ζ_{exp} are determined from the curves $\zeta_{\text{exp}} = f\left(\alpha^\circ, \frac{F_0}{F_1}\right)$ of graph a;

$$\zeta_{\text{fr}} = \frac{\lambda}{8 \sin \frac{\alpha}{2}} \left[1 - \left(\frac{F_0}{F_1} \right)^2 \right];$$

at $\lambda = 0.02$ ζ_{fr} is determined from the curves $\zeta_{\text{fr}} = f\left(\alpha^\circ, \frac{F_0}{F_1}\right)$ of graph b;

λ is determined from the curves $\lambda = f\left(\operatorname{Re} = \frac{w_0 D_0}{v}, \bar{A} = \frac{A}{D_0}\right)$ on diagrams 2-2 to 2-5;

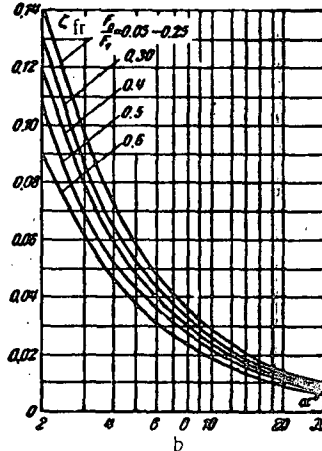
v is taken from § 1-3, b; A is taken from Table 2-1.

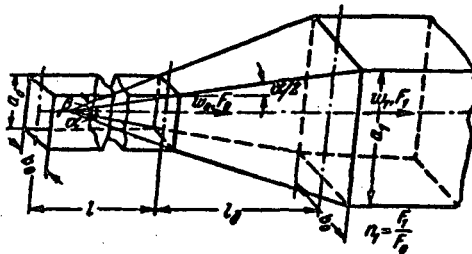
2. Nonuniform velocity distribution at the diffuser inlet:

$$\zeta = \frac{\Delta H}{\frac{\gamma w_0^2}{2g}} = k_1 \zeta_{\text{exp}} + \zeta_{\text{fr}},$$

where k_1 is determined from the data of diagrams 5-1, 5-6, and 5-18.

$\frac{F_0}{F_1}$	α°									
	20	2	3	6	8	10	12	14	16	20
0.05	20	0.14	0.10	0.05	0.04	0.03	0.03	0.02	0.02	0.01
0.075	13.3	0.14	0.10	0.05	0.04	0.03	0.02	0.02	0.02	0.01
0.10	10	0.14	0.10	0.05	0.04	0.03	0.02	0.02	0.02	0.01
0.15	6.7	0.14	0.10	0.05	0.04	0.03	0.02	0.02	0.02	0.01
0.20	5.0	0.14	0.10	0.05	0.03	0.03	0.02	0.02	0.02	0.01
0.25	4.0	0.14	0.10	0.05	0.03	0.03	0.02	0.02	0.02	0.01
0.30	3.3	0.13	0.09	0.04	0.03	0.03	0.02	0.02	0.02	0.01
0.40	2.5	0.12	0.08	0.04	0.03	0.02	0.02	0.02	0.02	0.01
0.50	2.0	0.11	0.07	0.04	0.03	0.02	0.02	0.02	0.02	0.01
0.60	1.7	0.09	0.06	0.03	0.02	0.02	0.02	0.02	0.02	0.01





$$D_h = \frac{4F_0}{\Pi_0}; \quad \Pi_0 = \text{perimeter}$$

1. Uniform velocity distribution at the diffuser inlet:

$$\zeta = \frac{\Delta H}{\frac{\gamma w_0^2}{2g}} = \zeta_{\text{exp}} + \zeta_{\text{fr.}}$$

$$\text{where } \zeta_{\text{exp}} = \varphi_{\text{exp}} \left(1 - \frac{F_0}{F_1} \right)^2;$$

φ_{exp} is only approximately determined from the curve $\zeta_{\text{exp}} = f(\alpha^\circ)$ corresponding to $\frac{F_0}{F_1} = 0$ on graph a.

Within the limits $0 < \alpha < 25^\circ$:

$$\varphi_{\text{exp}} \approx 4.0 \tan \frac{\alpha}{2} \sqrt{\tan \frac{\alpha}{2}}.$$

The values of ζ_{exp} are determined from the curves $\zeta_{\text{exp}} = f\left(\alpha^\circ, \frac{F_0}{F_1}\right)$ on graph a;

$$\zeta_{\text{fr}} \approx \frac{\lambda}{16 \sin \frac{\alpha}{2}} \left[1 - \left(\frac{F_0}{F_1} \right)^2 \right] + \frac{\lambda}{16 \sin \frac{\alpha}{2}} \left[1 - \left(\frac{F_0}{F_1} \right)^4 \right] = \Delta \zeta_{\text{fr}} + \Delta \zeta'_{\text{fr}}.$$

$$\text{At } \alpha = \beta: \quad \zeta_{\text{fr}} = \frac{\lambda}{8 \sin \frac{\alpha}{2}} \left[1 - \left(\frac{F_0}{F_1} \right)^2 \right] = 2 \Delta \zeta_{\text{fr}}.$$

At $\lambda \approx 0.02$, $\Delta \zeta_{\text{fr}}$ is determined from the curves $\Delta \zeta_{\text{fr}} = f(\alpha^\circ)$ on graph b;

$\Delta \zeta'_{\text{fr}}$ is determined from the curve $\Delta \zeta'_{\text{fr}} = f(\beta^\circ)$ on graph b;

λ is determined from the curves $\lambda = f\left(\text{Re} = \frac{w_0 D_h}{v}; \frac{\Delta}{D_h}\right)$ on diagrams 2-2 to 2-5;

v is taken from § 1-3, b; Δ is taken from Table 2-1.

2. Nonuniform velocity distribution at the diffuser inlet:

$$\zeta = \frac{\Delta H}{\frac{\gamma w_0^2}{2g}} = k \zeta_{\text{exp}} + \zeta_{\text{fr.}}$$

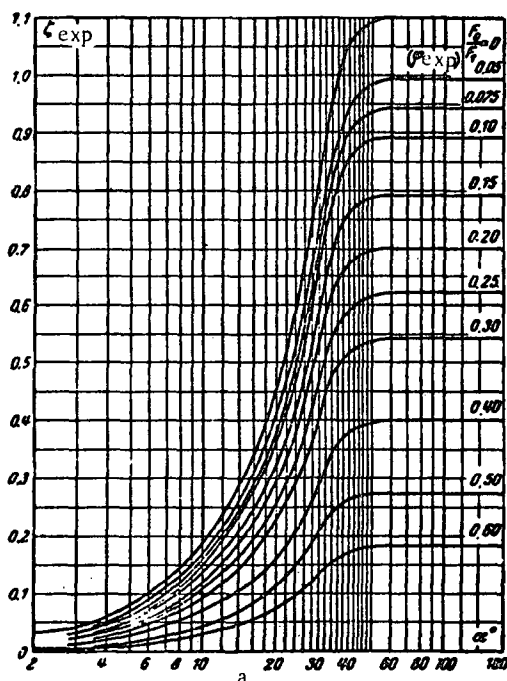
where k is determined from the data of diagrams 5-1, 5-6, and 5-18.

Pyramidal diffuser in a line (cont'd)

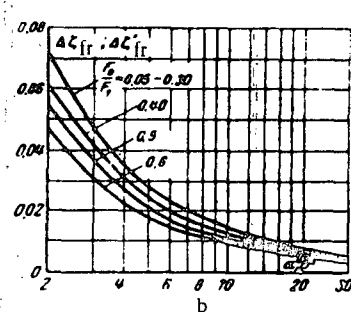
 Section V
 Diagram 5-3

 Values of ξ_{exp}

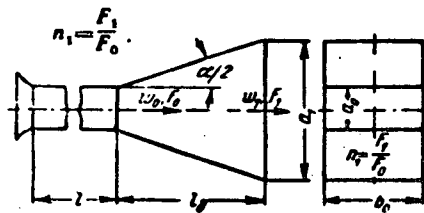
$\frac{F_0}{F_1}$	n_i	a_{av}																
		2	4	6	8	10	12	14	16	18	20	24	28	32	40	60	80	160
0	∞	0.03	0.06	0.10	0.14	0.19	0.23	0.29	0.34	0.40	0.45	0.59	0.73	0.89	1.05	1.10	1.10	1.10
0.05	20	0.03	0.05	0.09	0.13	0.17	0.21	0.26	0.31	0.36	0.40	0.53	0.66	0.80	0.94	0.99	0.99	0.99
0.075	13.3	0.03	0.05	0.08	0.12	0.16	0.20	0.25	0.29	0.34	0.38	0.50	0.62	0.76	0.90	0.91	0.94	0.94
0.10	10	0.02	0.05	0.08	0.11	0.15	0.19	0.24	0.28	0.32	0.36	0.48	0.59	0.72	0.85	0.89	0.89	0.89
0.15	6.7	0.02	0.04	0.07	0.10	0.14	0.17	0.21	0.24	0.29	0.32	0.42	0.52	0.64	0.76	0.79	0.79	0.79
0.20	5.0	0.02	0.04	0.06	0.09	0.12	0.15	0.18	0.22	0.26	0.29	0.38	0.47	0.57	0.67	0.70	0.70	0.70
0.25	4.0	0.02	0.03	0.06	0.08	0.11	0.13	0.16	0.19	0.22	0.25	0.33	0.41	0.50	0.59	0.62	0.62	0.62
0.30	3.3	0.01	0.03	0.05	0.07	0.09	0.11	0.14	0.17	0.20	0.22	0.29	0.36	0.44	0.51	0.54	0.54	0.54
0.40	2.5	0.01	0.02	0.04	0.05	0.07	0.08	0.10	0.12	0.14	0.16	0.21	0.26	0.32	0.33	0.40	0.40	0.40
0.50	2.0	0.01	0.01	0.02	0.03	0.05	0.06	0.07	0.08	0.10	0.11	0.15	0.18	0.22	0.26	0.27	0.27	0.27
0.60	1.7	0.01	0.01	0.02	0.02	0.03	0.04	0.05	0.05	0.06	0.07	0.09	0.12	0.14	0.17	0.18	0.18	0.18


 Values of $\Delta\xi_{fr}$ or $\Delta\xi'_{fr}$

$\frac{F_0}{F_1}$	n_i	α^*, β^*									
		2	4	6	8	10	12	14	16	20	
0.05	20	0.07	0.04	0.02	0.02	0.02	0.02	0.02	0.01	0.01	
0.10	10	0.07	0.03	0.02	0.02	0.02	0.02	0.02	0.01	0.01	
0.15	6.7	0.07	0.03	0.02	0.02	0.02	0.02	0.02	0.02	0.01	
0.20	5.0	0.07	0.03	0.02	0.02	0.02	0.02	0.02	0.01	0.01	
0.25	4.0	0.07	0.03	0.02	0.02	0.02	0.02	0.02	0.01	0.01	
0.30	3.3	0.07	0.03	0.02	0.02	0.02	0.02	0.02	0.01	0.01	
0.40	2.5	0.06	0.03	0.02	0.02	0.02	0.01	0.01	0.01	0.01	
0.50	2.0	0.06	0.03	0.02	0.02	0.01	0.01	0.01	0.01	0.01	
0.60	1.7	0.05	0.02	0.02	0.01	0.01	0.01	0.01	0.01	0.01	



$$D_h = \frac{4F_0}{\Pi_0}; \quad \Pi_0 - \text{perimeter};$$



1. Uniform velocity distribution at the diffuser inlet:

$$\zeta = \frac{\Delta H}{\gamma w_0^2} = \zeta_{\text{exp}} + \zeta_{\text{fr}},$$

$$\text{where } \zeta_{\text{exp}} = \varphi_{\text{exp}} \left(1 - \frac{F_0}{F_1}\right)^2;$$

φ_{exp} is determined approximately from the curve $\zeta_{\text{exp}} = f(\alpha^\circ)$ at $\frac{F_0}{F_1} = 0$ on graph a;

Values of ζ_{exp}

$\frac{F_0}{F_1}$	a°														
		3	6	8	10	12	14	16	20	21	30	40	60	90	180
0	∞	0.03	0.08	0.11	0.15	0.19	0.23	0.27	0.36	0.47	0.65	0.92	1.15	1.10	1.02
0.05	20	0.03	0.07	0.10	0.14	0.16	0.20	0.24	0.32	0.42	0.58	0.83	1.04	0.99	0.92
0.075	13.3	0.03	0.07	0.09	0.13	0.16	0.19	0.23	0.30	0.40	0.55	0.79	0.99	0.95	0.88
0.10	10	0.02	0.07	0.09	0.12	0.15	0.18	0.22	0.29	0.38	0.52	0.75	0.93	0.89	0.83
0.15	6.7	0.02	0.06	0.08	0.11	0.14	0.17	0.20	0.26	0.34	0.46	0.67	0.84	0.79	0.74
0.20	5.0	0.02	0.05	0.07	0.10	0.12	0.15	0.17	0.23	0.30	0.41	0.59	0.74	0.70	0.65
0.25	4.0	0.02	0.04	0.06	0.08	0.10	0.13	0.15	0.20	0.26	0.35	0.47	0.65	0.62	0.58
0.30	3.3	0.02	0.04	0.05	0.07	0.09	0.11	0.13	0.18	0.23	0.31	0.40	0.57	0.54	0.50
0.40	2.5	0.01	0.03	0.04	0.05	0.07	0.08	0.10	0.13	0.17	0.23	0.33	0.41	0.39	0.37
0.50	2.0	0.01	0.02	0.03	0.04	0.05	0.06	0.07	0.09	0.12	0.16	0.23	0.29	0.28	0.26
0.60	1.7	0.01	0.01	0.02	0.03	0.03	0.04	0.05	0.06	0.08	0.10	0.15	0.18	0.17	0.16

In the range $0 < \alpha < 40^\circ$:

$$\varphi_{\text{exp}} \approx 3.2 \operatorname{tg} \frac{\alpha}{2} \sqrt{\operatorname{tg} \frac{\alpha}{2}}.$$

The values of ζ_{exp} are determined from the curves $\zeta_{\text{exp}} = f(a^\circ, \frac{F_0}{F_1})$ on graph a;

$$\zeta_{\text{fr}} \approx \frac{\lambda}{4 \sin \frac{\alpha}{2}} \left\{ \frac{a_0}{b_0} \left(1 - \frac{F_0}{F_1} \right) + 0.5 \left[1 - \left(\frac{F_0}{F_1} \right)^2 \right] \right\}$$

At $\lambda = 0.02$: $\Delta \zeta_{\text{fr}}$ is determined from the curves $\zeta_{\text{fr}} = f(a^\circ, \frac{a_0}{b_0}, \frac{F_0}{F_1})$ on graphs b, c, d, e, and f;

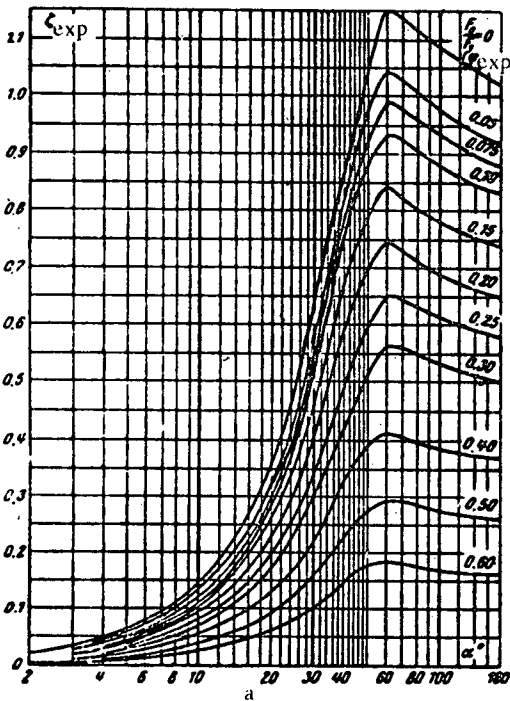
λ is determined from the curves $\lambda = f(R_e = \frac{w_0 D_h}{v}; \Delta = \frac{\Delta}{D_h})$ on diagrams 2-2 to 2-5;

v is taken from § 1-3, b; Δ is taken from Table 2-1.

2. Nonuniform velocity distribution at the diffuser inlet:

$$\zeta = \frac{\Delta H}{\gamma w_0^2} = k_1 \cdot \zeta_{\text{exp}} + \zeta_{\text{fr}},$$

where k_1 is determined from the data of diagrams 5-1, 5-6, and 5-18.

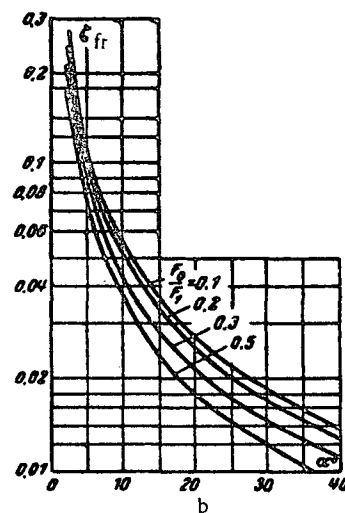


Plane diffuser in a line (cont'd)

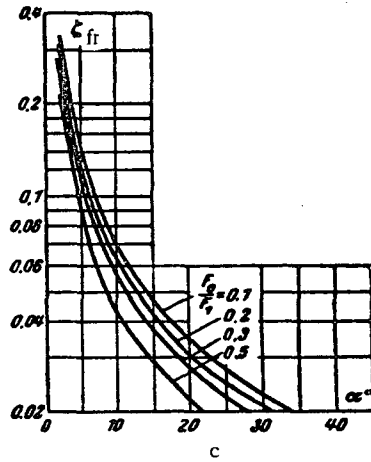
 Section V
 Diagram 5-4

 Values of ζ_{fr} at $a_0/b_0 = 0.5$

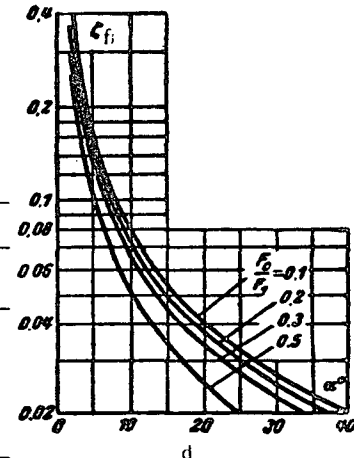
F_d/F_1	n_1	α°							
		2°	4°	6°	8°	10°	20°	30°	40°
0.10	10.	0.27	0.14	0.09	0.07	0.05	0.03	0.02	0.01
0.20	5.0	0.25	0.13	0.08	0.06	0.05	0.03	0.02	0.01
0.30	3.3	0.22	0.11	0.08	0.06	0.05	0.02	0.02	0.01
0.50	2.0	0.18	0.09	0.06	0.04	0.04	0.02	0.01	0.01


 Values of ζ_{fr} at $a_0/b_0 = 0.75$

F_d/F_1	n_1	α°							
		2°	4°	6°	8°	10°	20°	30°	40°
0.10	10.	0.34	0.17	0.11	0.08	0.07	0.03	0.02	0.02
0.20	5.0	0.31	0.15	0.10	0.08	0.06	0.03	0.02	0.02
0.30	3.3	0.28	0.14	0.09	0.07	0.06	0.03	0.02	0.01
0.50	2.0	0.21	0.11	0.07	0.05	0.04	0.02	0.01	0.01

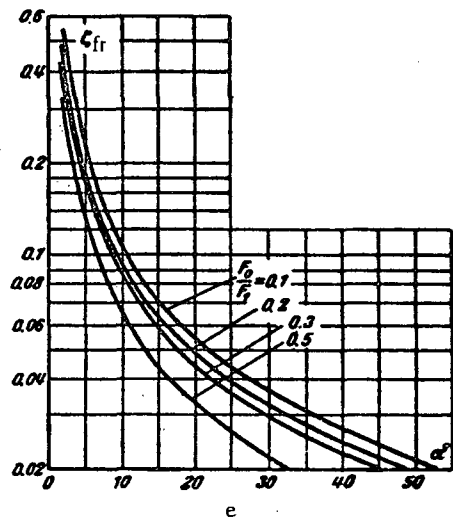

 Values of ζ_{fr} at $a_0/b_0 = 1.0$

F_d/F_1	n_1	α°								
		2°	4°	6°	8°	10°	20°	30°	40°	50°
0.10	10	0.40	0.20	0.13	0.10	0.08	0.04	0.03	0.02	0.02
0.20	5.0	0.37	0.18	0.13	0.09	0.07	0.04	0.03	0.02	0.02
0.30	3.3	0.33	0.17	0.11	0.08	0.07	0.03	0.02	0.02	0.02
0.50	2.0	0.25	0.13	0.08	0.06	0.05	0.03	0.02	0.01	0.01

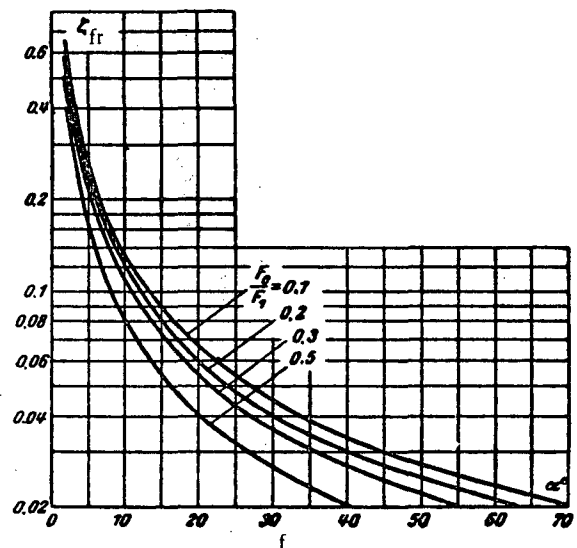


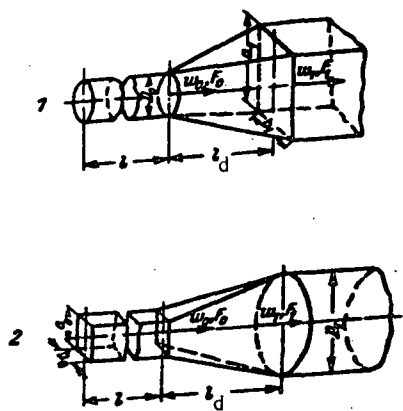
Values of ξ_{fr} at $a_0/b_0 = 1.5$

F_0/F_1	R_1	α°							
		2°	4°	6°	8°	10°	20°	30°	40°
0.10	10	0.53	0.26	0.18	0.13	0.11	0.25	0.04	0.03
0.10	5.0	0.48	0.24	0.16	0.12	0.10	0.05	0.03	0.02
0.30	3.3	0.43	0.21	0.14	0.10	0.09	0.04	0.03	0.02
0.50	2.0	0.32	0.16	0.10	0.08	0.06	0.03	0.02	0.02

Values of ξ_{fr} at $a_0/b_0 = 2.0$

F_0/F_1	R_1	α°									
		2°	4°	6°	8°	10°	20°	30°	40°	50°	60°
0.10	10	0.65	0.33	0.22	0.16	0.13	0.06	0.04	0.03	0.03	0.02
0.20	5.0	0.60	0.30	0.28	0.15	0.12	0.06	0.04	0.03	0.03	0.02
0.30	3.3	0.53	0.26	0.18	0.13	0.11	0.05	0.04	0.03	0.02	0.02
0.50	2.0	0.39	0.19	0.13	0.10	0.08	0.04	0.03	0.02	0.02	0.01





$$\zeta = \frac{\Delta H}{\gamma w_0^2} \cdot \frac{2g}{2}$$

is determined from the data in diagram 5-3 for a pyramidal diffuser with equivalent divergence angle, determined from the relations:

1) transition from circle to rectangle

$$\operatorname{tg} \frac{\alpha}{2} = \frac{2 \sqrt{\frac{a_0 b_1}{\pi}} - D_0}{2 l_d};$$

2) transition from rectangle to circle

$$\operatorname{tg} \frac{\alpha}{2} = \frac{D_1 - 2 \sqrt{\frac{a_0 b_0}{\pi}}}{2 l_d}.$$

$$D_h = \frac{4F_0}{\Pi_0}; \Pi_0 - \text{perimeter}$$

$$\zeta = \frac{\Delta H}{\gamma w_0^2} = k_i \zeta_i$$

where ζ is determined, depending on the diffuser shape, as ζ from the corresponding one of diagrams 5-2 to 5-5;

k_i is taken from Table 5-2 as a function of the branch characteristics or the velocity profile; the velocity profiles themselves are represented on the graph

$$\left[\text{the curves } \frac{w}{w_0} = f\left(\frac{y}{r_0}\right) \right]$$

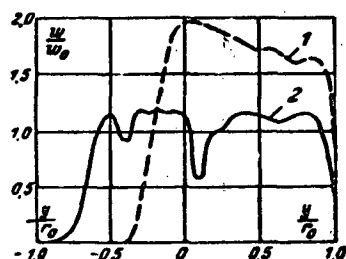
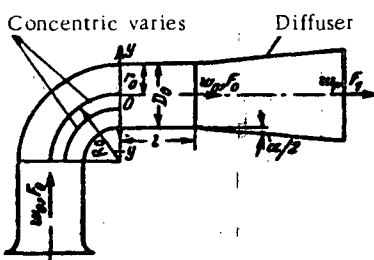


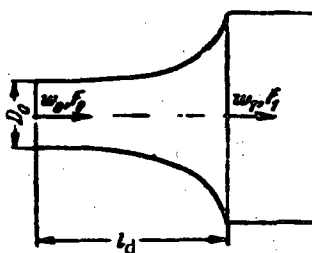
TABLE 5-2
Branch parameters

Velocity profile	$\frac{R_0}{D_h}$	$\frac{l}{D_h}$	Number of concentric vanes	k_i
1	0.8 - 1.0	0	0	6.8
2	0.8 - 1.0	0	2	2.1
-	0.8 - 1.0	0	3	1.9
-	2.0	0	0	2.6
-	2.0	1.0	0	1.0
-	≥ 3	0	0	1.0

Curved diffusers ($\frac{dp}{dx} = \text{const}$) in a line

 Section V
 Diagram 5-7

No. 1. Circular or pyramidal diffuser



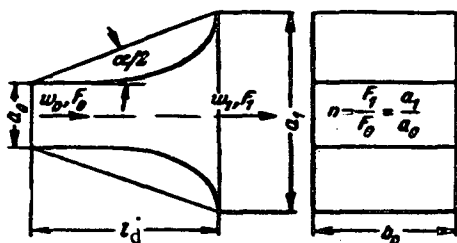
$$\zeta = \frac{\Delta H}{\gamma w_0^2} \approx \varphi_0 \sigma_0 d \quad (\text{formula applicable in the range } 0.1 \leq \frac{F_0}{F_1} \leq 0.9), \text{ where}$$

$\sigma_0 = 1.43 - \frac{1.3F_0}{F_1}$ is determined from the curve $\sigma_0 = f\left(\frac{F_0}{F_1}\right)$ of graph a;

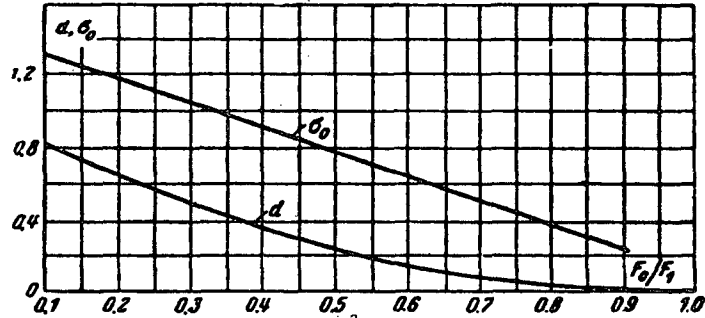
$d = \left(1 - \frac{F_0}{F_1}\right)^2$ is determined from the curve $d = f_2\left(\frac{F_0}{F_1}\right)$ of graph a;

$\varphi_0 = f\left(\frac{l}{D_h}\right)$ and $\varphi_0 = f\left(\frac{l}{a_0}\right)$ is determined from the corresponding curves of graph b.

No. 2. Plane diffuser



F_0/F_1	0.1	0.2	0.3	0.4	0.5	0.6	0.7	0.8	0.9
σ_0	1.30	1.17	1.04	0.91	0.78	0.65	0.52	0.39	0.26
d	0.81	0.64	0.49	0.36	0.25	0.16	0.09	0.04	0.01



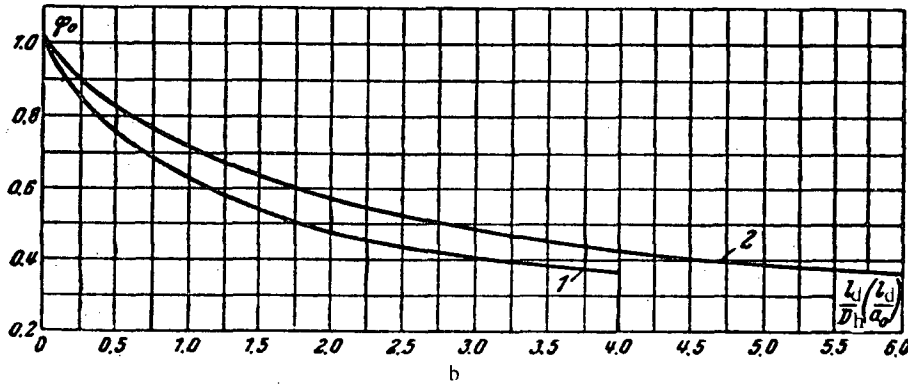
$\frac{l_d}{D_h} \left(\frac{F_0}{\sigma_0} \right)$	0	2.5	1.0	1.5	2.0	2.5	3.0	3.5	4.0	4.5	5.0	6.0
---	---	-----	-----	-----	-----	-----	-----	-----	-----	-----	-----	-----

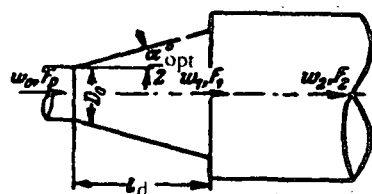
No. 1. Circular or pyramidal diffuser

φ_0	1.02	0.75	0.62	0.53	0.47	0.43	0.40	0.38	0.37	-	-	-
-------------	------	------	------	------	------	------	------	------	------	---	---	---

No. 2. Plane diffuser

φ_0	0.12	0.83	0.72	0.64	0.57	0.52	0.48	0.45	0.43	0.41	0.39	0.37
-------------	------	------	------	------	------	------	------	------	------	------	------	------





$$\zeta = \frac{\Delta H}{\gamma w_0^2} \approx (1 + \alpha) \xi_{\min}$$

The formula may be used for selecting the optimum angle $\alpha^{\circ}_{\text{opt}}$ from graph b;

ξ_{\min} is determined from graph a as a function of $\frac{l_d}{D_0}$ and a ;

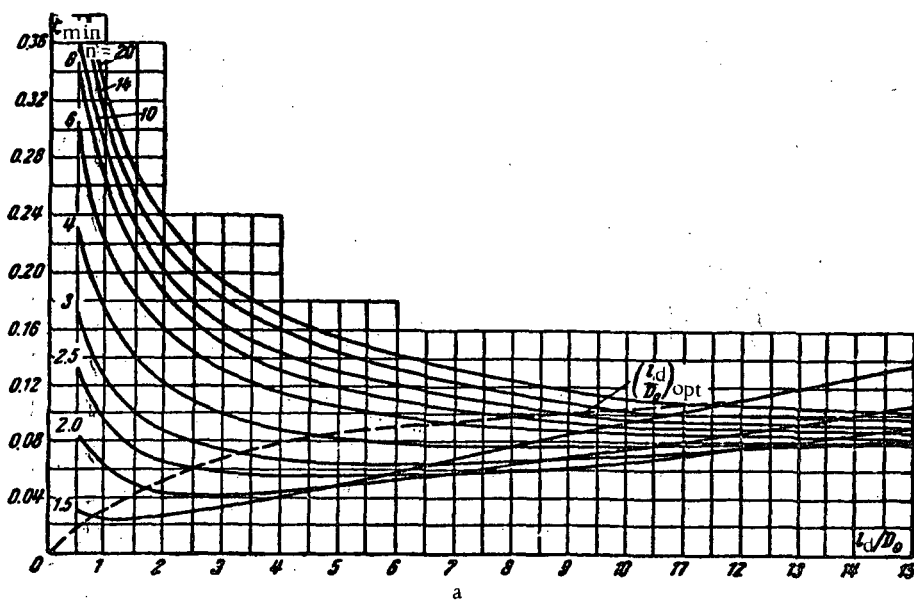
α is determined approximately from graph c as a function of $\frac{F_0}{F_1}$.

$$n_1 = \frac{F_1}{F_0} = \left(1 + 2 \frac{l_d}{D_0} \lg \frac{a}{2} \right)^2$$

$$n_2 = \frac{F_2}{F_1}; \quad n = \frac{F_2}{F_0}$$

Values of ξ_{\min}

a	$\frac{l_d}{D_0}$											
	0.5	1.0	2.0	3.0	4.0	5.0	6.0	8.0	10	12	14	
1.5	0.03	0.02	0.03	0.03	0.04	0.05	0.06	0.08	0.10	0.11	0.13	
2.0	0.08	0.06	0.04	0.04	0.04	0.05	0.05	0.06	0.08	0.09	0.10	
2.5	0.13	0.09	0.06	0.06	0.06	0.06	0.06	0.06	0.07	0.08	0.09	
3.0	0.17	0.12	0.09	0.07	0.07	0.06	0.06	0.07	0.07	0.08	0.08	
4.0	0.23	0.17	0.12	0.10	0.09	0.08	0.08	0.08	0.08	0.08	0.08	
6.0	0.30	0.22	0.16	0.13	0.12	0.10	0.10	0.09	0.09	0.09	0.08	
8.0	0.34	0.26	0.18	0.15	0.13	0.12	0.11	0.10	0.09	0.09	0.09	
10	0.36	0.28	0.20	0.16	0.14	0.13	0.12	0.11	0.10	0.09	0.09	
14	0.39	0.30	0.22	0.18	0.16	0.14	0.13	0.12	0.10	0.10	0.10	
20	0.41	0.32	0.24	0.20	0.17	0.15	0.14	0.12	0.11	0.11	0.10	

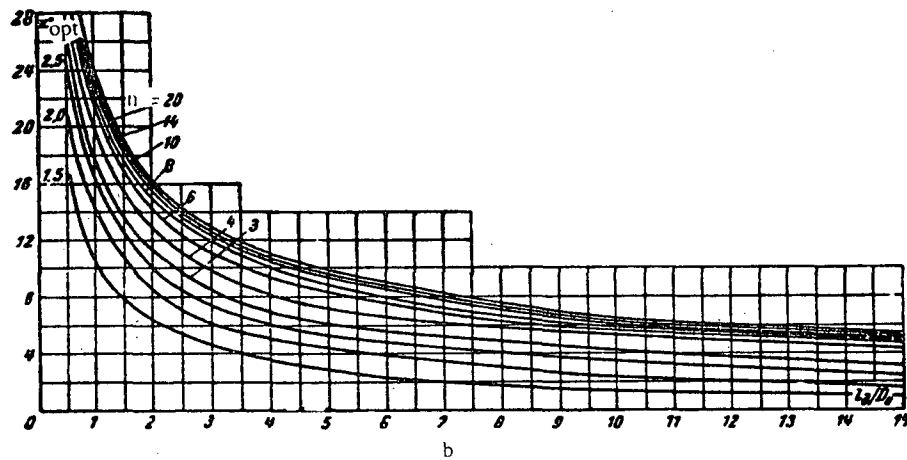


Stepped conical diffuser of optimum divergence angle
 α_{opt} (cont'd)

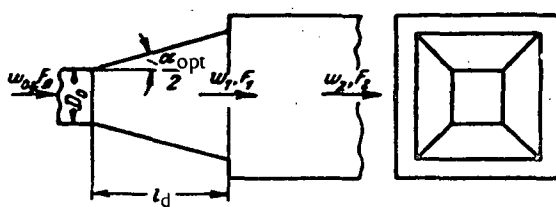
Section V
 Diagram 5-8

Values of α_{opt}

n	t_d/D_c											
	0.5	1.0	2.0	3.0	4.0	5.0	6.0	8.0	10	12	14	
1.5	17	10	6.5	4.5	3.5	2.8	2.2	1.7	1.2	1.0	0.8	
2.0	21	14	8.5	6.2	5.0	4.3	3.8	3.0	2.3	2.0	1.6	
2.5	25	16	10	7.4	6.0	5.4	4.8	4.0	3.5	3.0	2.5	
3.0	27	17	11	8.5	7.0	6.1	5.6	4.8	4.2	3.8	3.2	
4.0	29	20	13	9.8	8.0	7.2	6.6	5.8	5.2	4.8	4.4	
6.0	31	21	14	11	9.4	8.2	7.4	6.2	5.6	5.2	4.7	
8.0	32	22	15	12	10	8.8	8.0	6.6	5.8	5.4	5.0	
10	33	23	15	12	11	9.4	8.4	7.0	6.2	5.5	5.2	
14	33	24	16	13	11	9.6	8.7	7.3	6.3	5.6	5.4	
20	34	24	16	13	11	9.8	9.0	7.5	6.5	6.0	5.6	



$$D_h = \frac{4F_0}{\Pi_0}; \Pi_0 \text{ — perimeter}$$



$$\zeta = \frac{\Delta H}{\gamma w_0^2} \cong (1 + \sigma) \zeta_{\min}$$

The formula may be used for selecting the optimum angle α_{opt} from graph b;

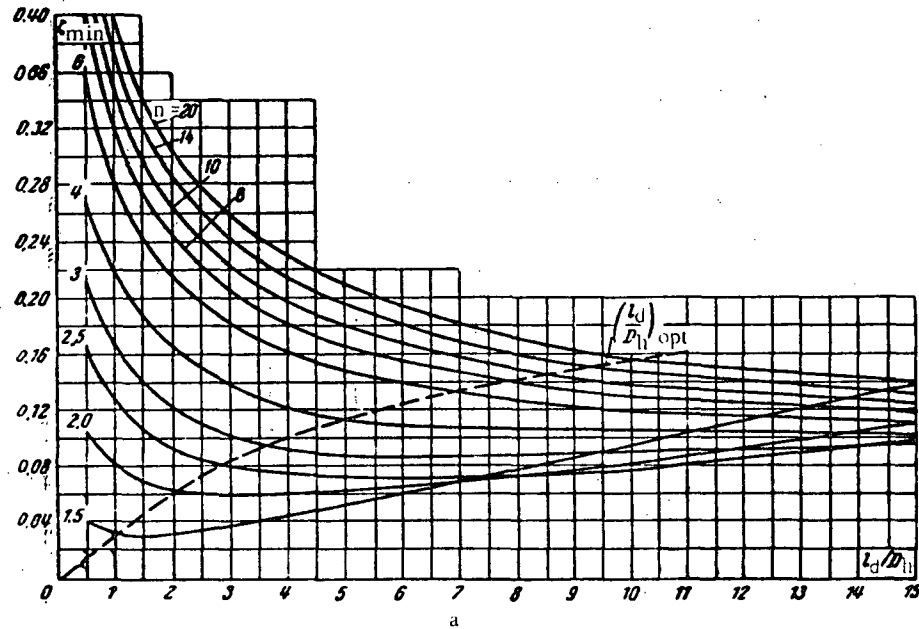
ζ_{\min} is determined from graph a as a function of l_d/D_h and n . σ is determined approximately from graph c as a function of F_0/F_1 .

$$n_1 = \frac{F_1}{F_0} = \left(1 + 2 \frac{l_d}{D_h} \operatorname{tg} \frac{\alpha}{2} \right)^2;$$

$$n_2 = \frac{F_2}{F_1}; n = \frac{F_2}{F_0}$$

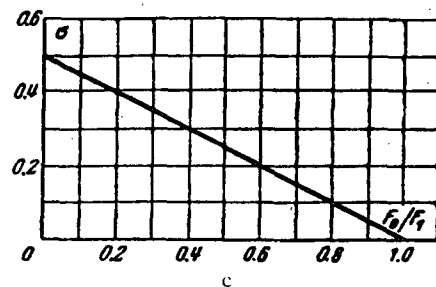
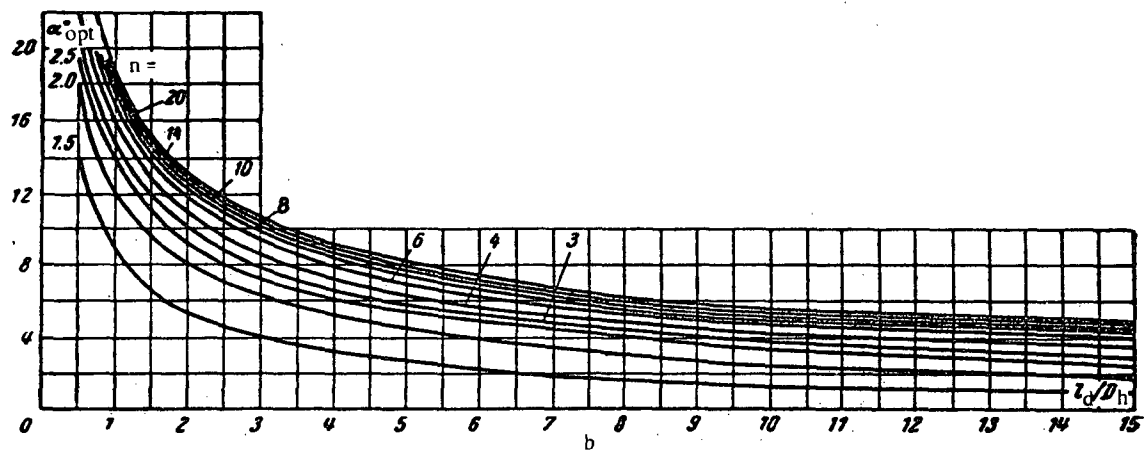
Values of ζ_{\min}

n	l_d/D_h											
	0.5	1.0	2.0	3.0	4.0	5.0	6.0	8.0	10	12	14	
1.5	0.04	0.03	0.03	0.04	0.05	0.05	0.06	0.08	0.10	0.11	0.13	
2.0	0.11	0.08	0.06	0.06	0.06	0.06	0.07	0.07	0.08	0.09	0.10	
2.5	0.16	0.13	0.09	0.08	0.08	0.07	0.08	0.07	0.08	0.08	0.09	
3.0	0.21	0.17	0.12	0.10	0.09	0.09	0.09	0.09	0.09	0.09	0.09	
4.0	0.27	0.22	0.17	0.14	0.12	0.11	0.11	0.11	0.11	0.10	0.10	
6.0	0.36	0.28	0.21	0.18	0.16	0.15	0.14	0.13	0.12	0.12	0.11	
8.0	0.41	0.32	0.24	0.21	0.18	0.17	0.16	0.14	0.13	0.12	0.12	
10	0.44	0.35	0.26	0.22	0.20	0.18	0.17	0.15	0.14	0.13	0.13	
14	0.47	0.37	0.28	0.24	0.21	0.20	0.18	0.16	0.15	0.14	0.14	
20	0.49	0.40	0.30	0.26	0.23	0.21	0.19	0.17	0.16	0.15	0.14	



Values of $\alpha^{\circ}\text{opt}$

n	I_d/D_h											
	0.5	1.0	2.0	3.0	4.0	5.0	6.0	8.0	10	12	14	
1.5	14	9.0	5.3	4.0	3.3	2.7	2.2	1.7	1.2	1.0	1.0	
2.0	18	12	8.0	6.3	5.2	4.5	3.8	3.0	2.3	2.0	1.8	
2.5	20	14	9.0	7.2	6.1	5.4	4.8	4.0	3.2	2.9	2.4	
3.0	21	15	10	7.8	6.5	5.8	5.2	4.4	3.6	3.3	2.9	
4.0	22	16	11	8.5	7.1	6.2	5.5	4.8	4.0	3.6	3.5	
6.0	24	17	12	9.4	8.0	6.9	6.2	5.2	4.5	4.3	4.0	
8.0	25	17	12	9.7	8.3	7.3	6.5	5.5	4.8	4.6	4.2	
10	25	18	12	10	8.7	7.6	6.9	5.8	5.0	4.8	4.5	
14	26	18	13	10	9.0	7.8	7.1	6.1	5.2	5.0	4.7	
20	26	19	13	11	9.2	8.1	7.3	6.4	5.5	5.2	4.9	

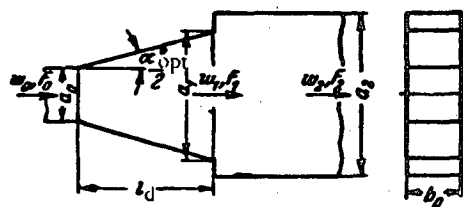


Stepped plane diffuser of optimum divergence angle $\alpha_{\text{opt}}^{\circ}$

 at $0.5 \leq \frac{a_0}{b_0} \leq 2.0$

Section V

Diagram 5-10



$$n_1 = \frac{a_1}{a_0} = 1 + 2 \frac{l_d}{a_0} \tan \frac{\alpha}{2};$$

$$n_2 = \frac{a_2}{a_1}; \quad n = \frac{F_2}{F_1} = \frac{a_2}{a_0}.$$

$$\xi = \frac{\Delta H}{\gamma w_0^2} \approx (1 + \epsilon) \xi_{\min}.$$

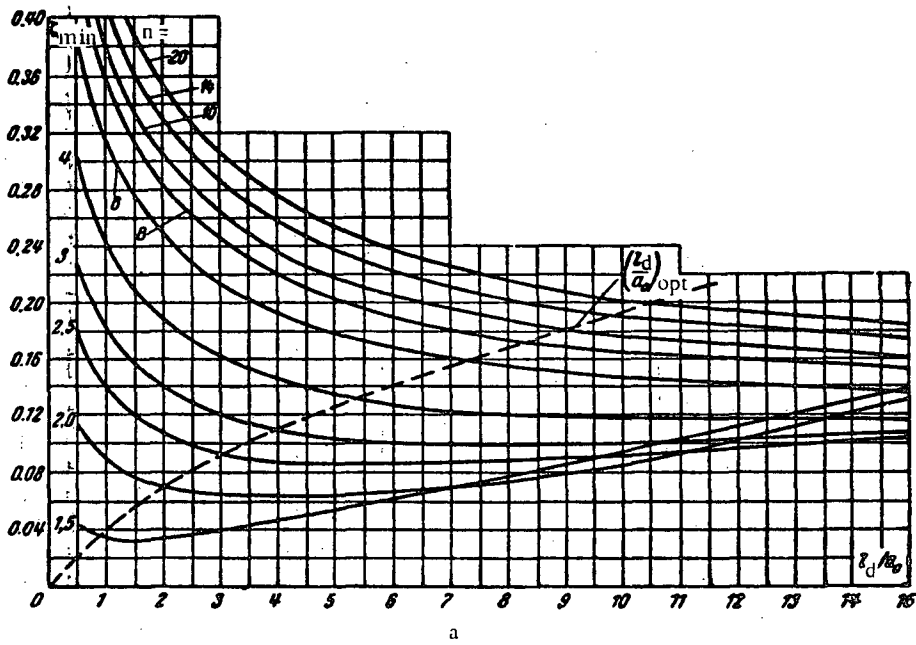
The formula may be used for selecting the optimum angle α_{opt} from graph b;

ξ_{\min} is determined from graph a as a function of l_d/a_0 and n ;

ϵ is determined approximately from graph c as a function of F_0/F_1 .

 Values of ξ_{\min}

n	l_d/a_0										
	0.5	1.0	2.0	3.0	4.0	5.0	6.0	8.0	10	12	14
1.5	0.04	0.04	0.04	0.04	0.05	0.06	0.06	0.08	0.10	0.11	0.13
2.0	0.12	0.09	0.07	0.07	0.06	0.07	0.07	0.07	0.08	0.10	0.12
2.5	0.18	0.14	0.11	0.10	0.09	0.09	0.09	0.09	0.09	0.10	0.10
3.0	0.23	0.18	0.14	0.12	0.11	0.11	0.10	0.10	0.10	0.10	0.11
4.0	0.30	0.24	0.19	0.16	0.15	0.14	0.13	0.12	0.12	0.12	0.12
6.0	0.38	0.31	0.25	0.21	0.19	0.18	0.17	0.16	0.15	0.14	0.14
8.0	0.43	0.36	0.28	0.25	0.22	0.20	0.19	0.17	0.16	0.16	0.15
10	0.46	0.38	0.30	0.26	0.24	0.22	0.21	0.19	0.18	0.17	0.16
14	0.50	0.41	0.33	0.29	0.26	0.24	0.22	0.20	0.19	0.18	0.18
20	0.53	0.44	0.35	0.31	0.28	0.25	0.24	0.22	0.20	0.19	0.19



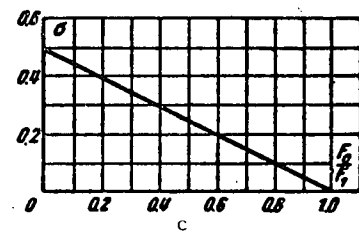
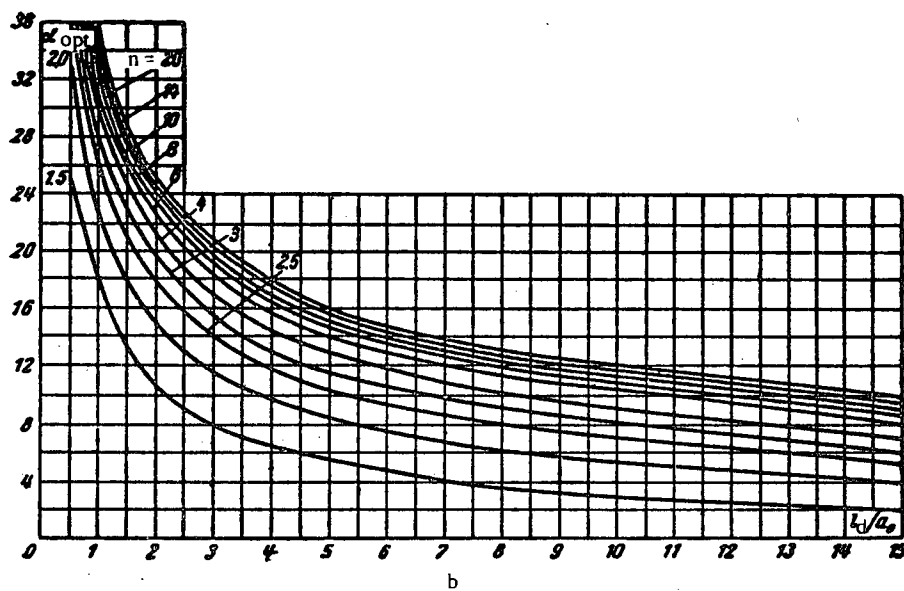
a

Stepped plane diffuser of optimum divergence angle $\alpha_{\text{opt}}^{\circ}$
 at $0.5 \leq \frac{a_0}{b_0} \leq 2.0$ (cont'd)

Section V

Diagram 5-10

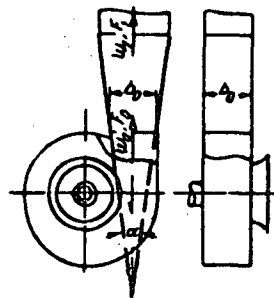
n	Values of $\alpha_{\text{opt}}^{\circ}$											
	0.5	1.0	2.0	3.0	4.0	5.0	6.0	8.0	10	12	14	
1.5	25	18	11	8.0	6.4	5.4	4.7	3.5	2.8	2.4	2.0	
2.0	33	23	15	12	9.7	8.4	7.5	6.0	5.2	4.7	4.3	
2.5	37	26	18	14	12	10	9.4	8.0	7.0	6.3	5.6	
3.0	39	27	20	16	13	12	11	9.1	8.0	7.2	6.4	
4.0	42	30	21	17	15	13	12	10	9.0	8.2	7.4	
6.0	45	31	23	18	16	14	13	11	10	9.4	8.5	
8.0	47	32	23	19	17	15	14	12	11	10	9.1	
10	48	33	24	20	17	15	14	12	11	10	9.5	
14	49	34	25	20	17	16	14	13	12	11	9.9	
20	50	35	25	21	18	16	15	13	12	11	10	



Guiding device	Schematic diagram	Resistance coefficient $\zeta = \frac{\Delta H}{\frac{w_0^2}{2g}}$
With dividing walls Number of dividing walls z	$\frac{a'_e}{a_0} = \frac{a'_1}{a_0} = \frac{1}{z+1}$ <p>$\alpha > 30^\circ$</p>	$\zeta \approx 0.65 \zeta_d,$ <p>where ζ_d is determined as ζ from diagrams 5-2 to 5-5</p>
With baffles	<p>$\alpha > 30^\circ$</p>	$\zeta \approx 0.65 \zeta_d,$ <p>where ζ_d is determined as ζ from diagrams 5-2 to 5-5</p>
With resistance at the exit (screen, perforated plate)		<p>a) $\alpha = 0$ to 60°</p> $\zeta = \zeta_0 + \frac{\zeta_g}{n_1^2};$ <p>b) $\alpha > 60^\circ$</p> $\zeta = (1.2 \text{ to } 1.3) \left(\zeta_0 + \frac{\zeta_g}{n_1^2} \right),$ <p>where ζ_0 is determined as ζ from diagrams 5-2 to 5-5; ζ_g is determined as ζ of a screen or grid from diagram 8-1 to 8-7;</p> $n_1 = \frac{F_1}{F_0}.$

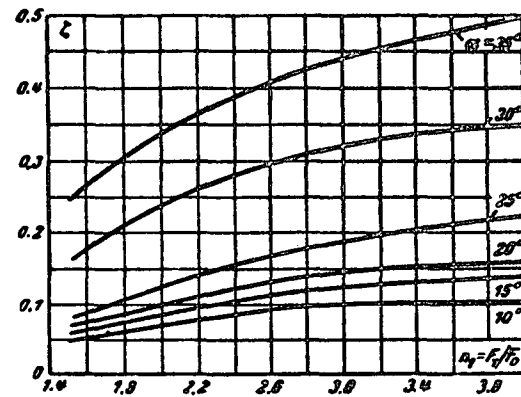
Plane symmetric diffuser behind a centrifugal fan
in a duct (forced draft)

Section V
Diagram 5-12



Values of ζ

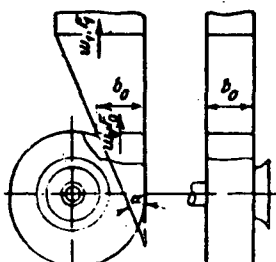
α°	$\frac{F_1}{F_0}$					
	1.5	2.0	2.5	3.0	3.5	4.0
10	0.05	0.07	0.09	0.10	0.11	0.11
15	0.06	0.09	0.11	0.13	0.13	0.14
20	0.07	0.10	0.13	0.15	0.16	0.16
25	0.08	0.13	0.16	0.19	0.21	0.23
30	0.16	0.24	0.29	0.32	0.34	0.35
35	0.24	0.34	0.39	0.44	0.48	0.50



$\zeta = \frac{\Delta H}{\frac{\gamma w_0^2}{2g}}$ is determined from the curves $\zeta = f\left(\frac{F_1}{F_0}\right)$ corresponding to different α° .

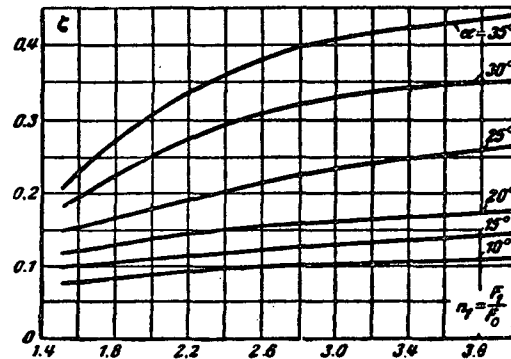
Plane asymmetric diffuser at $\alpha_1 = 0$ behind a centrifugal fan
in a duct (forced draft)

Section V
Diagram 5-13



Values of ζ

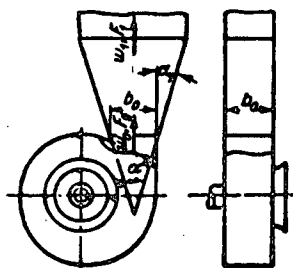
α°	F_1/F_0					
	1.5	2.0	2.5	3.0	3.5	4.0
10	0.08	0.09	0.10	0.10	0.11	0.11
15	0.10	0.11	0.12	0.13	0.14	0.15
20	0.12	0.14	0.15	0.16	0.17	0.18
25	0.15	0.18	0.21	0.23	0.25	0.26
30	0.18	0.25	0.30	0.33	0.35	0.35
35	0.21	0.31	0.38	0.41	0.43	0.44



$\zeta = \frac{\Delta H}{\frac{\gamma w_0^2}{2g}}$ is determined from the curves $\zeta = f\left(\frac{F_1}{F_0}\right)$ corresponding to different α° .

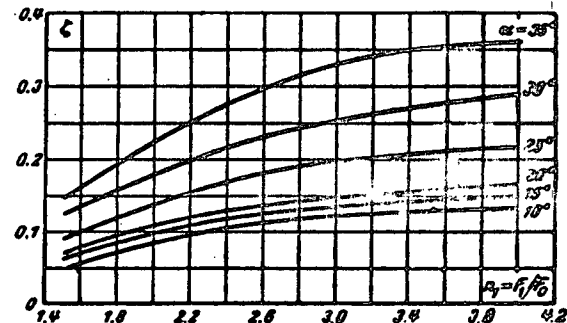
Plane asymmetric diffuser at $\alpha_1 = 10^\circ$ behind a centrifugal fan in a duct (forced draft)

Section V
Diagram 5-14



Values of ζ

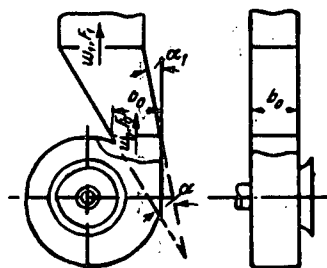
α°	F_1/F_0					
	1.5	2.0	2.5	3.0	3.5	4.0
10	0.11	0.13	0.14	0.14	0.14	0.14
15	0.13	0.15	0.16	0.17	0.18	0.18
20	0.19	0.22	0.24	0.26	0.28	0.30
25	0.29	0.32	0.35	0.37	0.39	0.40
30	0.36	0.42	0.46	0.49	0.51	0.51
35	0.44	0.54	0.61	0.64	0.66	0.66



$\zeta = \frac{\Delta H}{\frac{\rho u_0^2}{2g}}$ is determined from the curves $\zeta = f\left(\frac{F_1}{F_0}\right)$ corresponding to different α° .

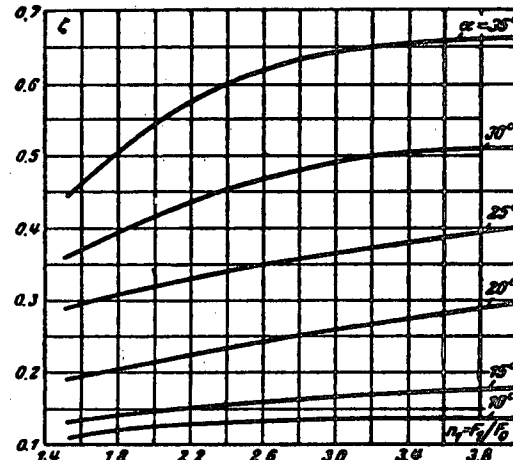
Plane asymmetric diffuser at $\alpha_1 = -10^\circ$ behind a centrifugal fan in a duct (forced draft)

Section V
Diagram 5-15

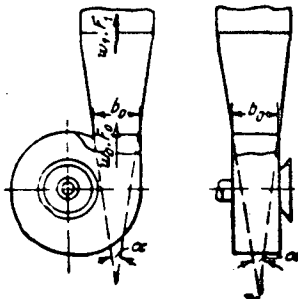


Values of ζ

α°	F_1/F_0					
	1.5	2.0	2.5	3.0	3.5	4.0
10	0.05	0.08	0.11	0.13	0.13	0.14
15	0.06	0.10	0.12	0.14	0.15	0.15
20	0.07	0.11	0.14	0.15	0.16	0.16
25	0.09	0.14	0.18	0.20	0.21	0.22
30	0.13	0.18	0.23	0.26	0.28	0.29
35	0.15	0.23	0.28	0.33	0.35	0.36

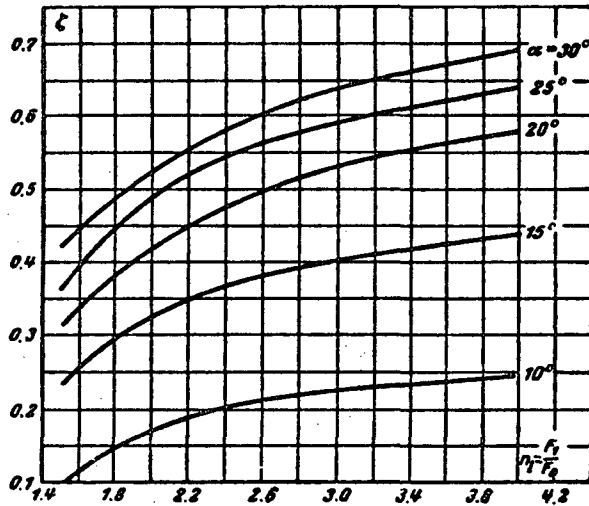


$\zeta = \frac{\Delta H}{\frac{\rho u_0^2}{2g}}$ is determined from the curves $\zeta = f\left(\frac{F_1}{F_0}\right)$ corresponding to different α° .



$\zeta = \frac{\Delta H}{\frac{\gamma w_0^2}{2g}}$ is determined from the curves $\zeta = f\left(\frac{F_1}{F_0}\right)$
corresponding to different α°

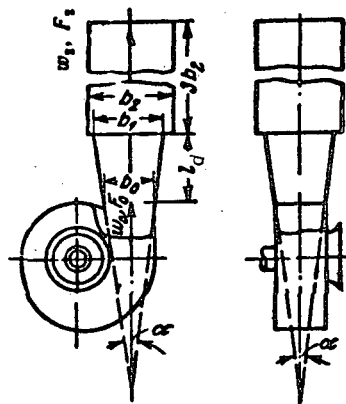
α	Value of ζ					
	F_1/F_0					
	1.5	2.0	2.5	3.0	3.5	4.0
10°	0.10	0.18	0.21	0.23	0.24	0.25
15°	0.23	0.33	0.38	0.40	0.42	0.44
20°	0.31	0.43	0.48	0.53	0.56	0.58
25°	0.36	0.49	0.55	0.58	0.62	0.64
30°	0.42	0.53	0.59	0.64	0.67	0.69



Multistage diffuser of optimum divergence angle $\alpha_{\text{opt}}^{\circ}$
behind a centrifugal fan in a duct (forced draft)

Section V

Diagram 5-17

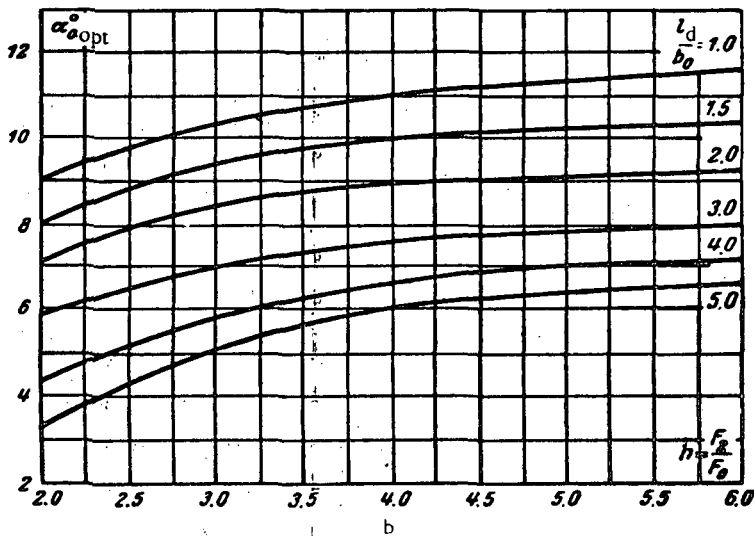
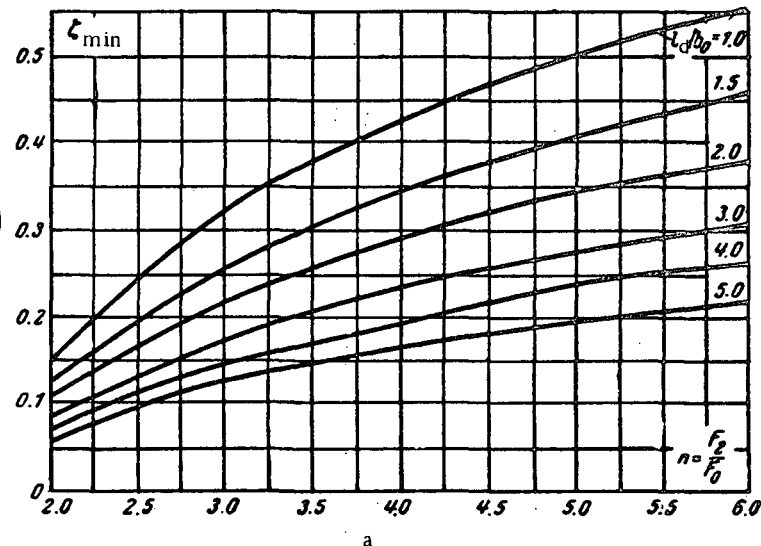


I_d/b_0	Values of ζ_{min}							
	F_2/F_0							
2.0	2.5	3.0	3.5	4.0	4.5	5.0	6.0	
1.0	0.16	0.25	0.33	0.38	0.43	0.47	0.50	0.56
1.5	0.13	0.20	0.26	0.31	0.34	0.38	0.41	0.46
2.0	0.12	0.17	0.22	0.26	0.29	0.33	0.35	0.38
3.0	0.09	0.13	0.18	0.21	0.24	0.26	0.28	0.31
4.0	0.08	0.12	0.15	0.18	0.20	0.22	0.24	0.26
5.0	0.06	0.10	0.13	0.15	0.17	0.18	0.20	0.22

$\zeta = \frac{\Delta H}{\frac{\rho w_0^2}{2g}}$ is determined from the curves $\zeta_{\text{min}} = f\left(\frac{F_2}{F_0}\right)$

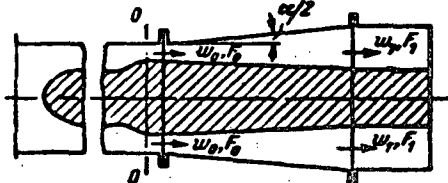
corresponding to different values of $\frac{I_d}{b_0}$ on graph a;

$\alpha_{\text{opt}}^{\circ}$ is determined from the curves $\alpha_{\text{opt}}^{\circ} = f\left(\frac{F_2}{F_0}\right)$
corresponding to different $\frac{I_d}{b_0}$ on graph b.



I_d/b_0	Values of $\alpha_{\text{opt}}^{\circ}$							
	F_2/F_0							
2.0	2.5	3.0	3.5	4.0	4.5	5.0	6.0	
1.0	9	10	10	11	11	11	11	12
1.5	8	9	9	10	10	10	10	10
2.0	7	8	8	9	9	9	9	9
3.0	6	7	7	7	7	8	8	8
4.0	4	5	6	6	7	7	7	8
5.0	3	4	5	6	6	6	6	7

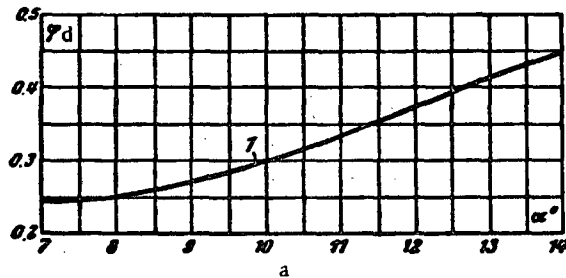
1. Diffuser with converging fairing:



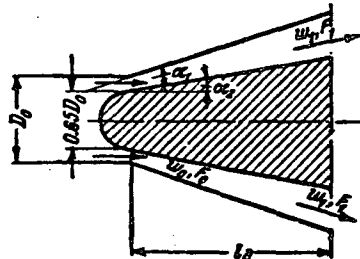
$$\zeta = \frac{\Delta H}{\gamma w_0^2} = k_1 \varphi_d \left(1 - \frac{F_0}{F_1}\right)^2,$$

where φ_d is determined from graph a as a function of the divergence angle α :

k_1 is determined from graph b as a function of the divergence angle α for the different velocity profiles shown in graph c.



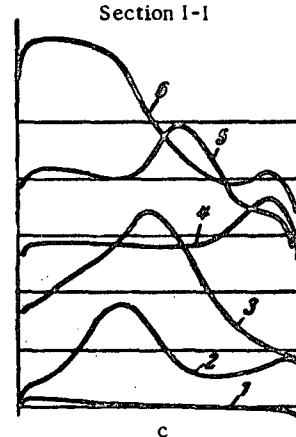
2. Diffuser with diverging fairing:



$$\zeta = \frac{\Delta H}{\gamma w_0^2} = k_1 \kappa,$$

where κ is taken from Table 5-3;

k_1 is taken from the data in diagrams 5-1, 5-6, and 5-18, 1.



a°	φ_d	Values of k_1						
		1	2	3	4	5	6	
7	0.25	7	1.0	1.40	2.00	1.16	0.90	2.74
8	0.25	8	1.0	1.60	2.10	1.21	1.15	2.98
10	0.30	10	1.0	1.60	2.10	1.20	1.36	3.02
12	0.37	12	1.0	1.45	2.00	1.10	1.42	2.70
14	0.44	14	1.0	1.40	1.86	1.08	1.50	2.48

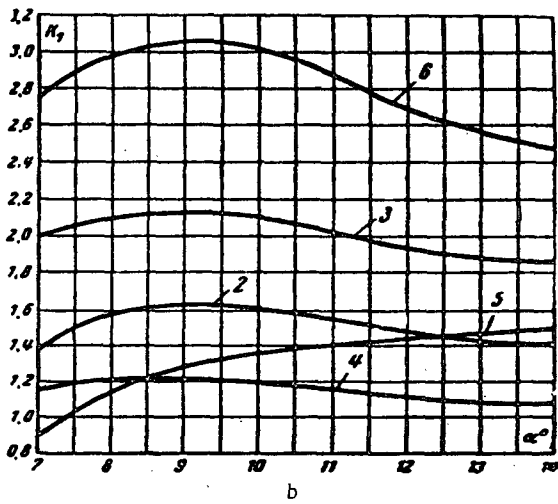
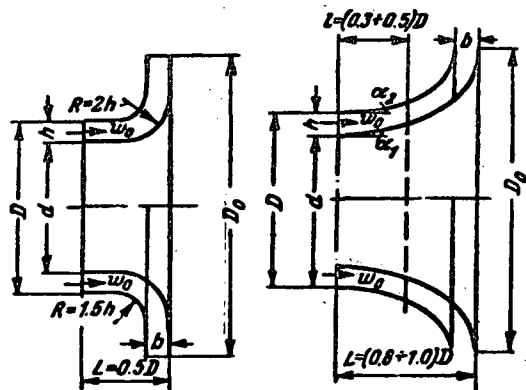


TABLE 5-3

$\frac{l_d}{D_0}$	0.75	1.0	1.5	1.75	2.0
a_1°	12.5	17	8.7	6.7	6.0
a_2°	0	9	6	3	3
ζ	0.17	0.27	0.11	0.09	0.08

1. Radial-annular
2. Axial-radial-annular

$$\bar{D} = 2.06; \alpha_2 = 8^\circ; \bar{c}_{a0} = 0.5$$

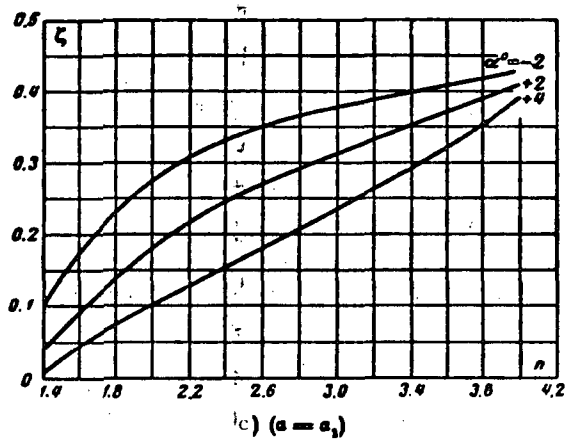


$$n = 2 \frac{b}{h} \bar{D} \frac{1}{1+\bar{d}}; \bar{D} = \frac{D_d}{D_o}; \bar{d} = \frac{d}{D_o};$$

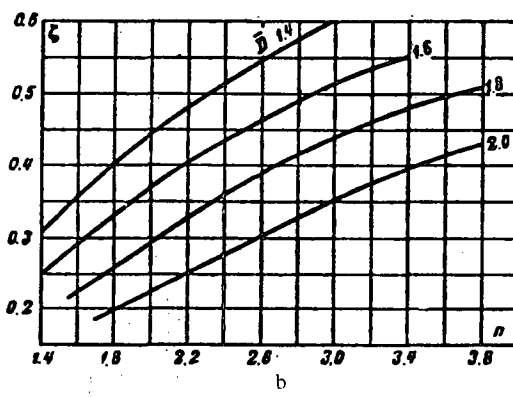
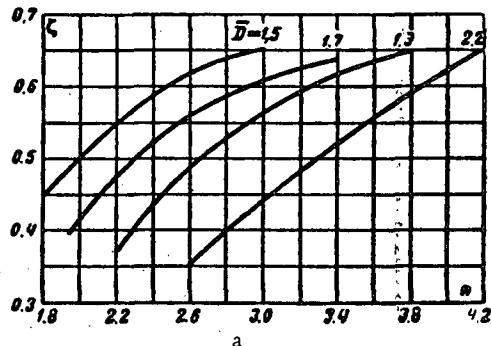
$$\bar{c}_{a0} = w_0 = \frac{Q}{\frac{\pi}{4} (D_o^2 - d^2)} \quad \bar{c}_{a0} = \frac{c_{a0}}{u};$$

Q = discharge, m^3/sec , u = peripheral velocity at the maximum radius, m/sec .

$\zeta = \frac{\Delta H}{\frac{1}{2} u^2}$ is determined from the curves $\zeta = f(n, \bar{D})$ (graphs a and b), and $\zeta = f(n, \alpha_2)$ (graph c).



\bar{D}	1. Values of ζ							
	1.4	1.8	2.2	2.6	3.0	3.4	3.8	4.2
a) Diffuser behind operating compressor at $\bar{c}_{a0} = 0.5$								
1.5	—	0.45	0.55	0.62	0.65	—	—	
1.7	—	0.34	0.48	0.56	0.61	0.62	—	
1.9	—	—	0.37	0.49	0.56	0.62	0.65	
2.2	—	—	—	0.35	0.45	0.52	0.60	0.65
b) Diffuser without operating compressor								
1.4	0.31	0.41	0.48	0.55	0.60	—	—	
1.6	0.25	0.33	0.40	0.46	0.52	0.55	—	
1.8	0.19	0.26	0.33	0.39	0.44	0.48	0.51	
2.0	—	0.20	0.25	0.30	0.35	0.40	0.43	



α_2	2. Values of ζ						
	1.8	2.2	2.6	3.0	3.4	3.6	4.0
-2	0.28	0.31	0.35	0.38	0.40	0.41	0.43
+2	0.14	0.22	0.27	0.31	0.35	0.37	0.41
+4°	0.08	0.13	0.18	0.24	0.29	0.32	0.39

Section Six

VARIATION OF THE STREAM DIRECTION (Resistance coefficient of curved stretches - branches, elbows, etc.)

6-1. LIST OF SYMBOLS

- F_0, F_1 = areas of the inlet and exit cross sections, respectively, of a curved conduit, m^2 ;
 D_0, D_1 = diameters of the inlet and exit cross sections, respectively, of the curved conduit, m;
 D_h = hydraulic diameter of the inlet section of the curved conduit;
 a_0 = height of the section of the curved conduit, m;
 b_0 = width of section at inlet } (measured in plane of bending of
 b_1 = width of section at outlet } curved conduit);
 b_{ch} = width of section in intermediate channel;
 l = length along the axis of a curved conduit, m;
 l_0 = length of the intermediate straight stretch of the curved pipe (the stretch between two branches or elbows), m;
 l' = distance between the axes of coupled elbows, m;
 R_0 = mean radius of curvature of the bend or elbow, m;
 r = radius of curvature of the elbow wall, m;
 r_0, r_1 = radii of curvature of the inner and outer bend walls, respectively, m;
 t_1 = chord of the guide vanes, m;
 Δ = mean height of roughness peaks of the walls, m;
 $\bar{\Delta}$ = relative roughness of the walls;
 δ = angle of bend of the curved channel;
 α = angle between the direction of the impinging stream and the chord (angle of attack) of the guide vanes;
 θ = angle at which guide vanes are mounted in the elbow;
 φ_1 = angle subtended by the arc of curvature of the guide vanes;
 w_0, w_1 = mean stream velocity at the inlet and exit sections of the curved channel, respectively, m/sec ;
 ΔH = pressure loss or resistance, kg/m^2 ;
 ζ = total resistance coefficient of the curved conduit;
 ζ_1 = local resistance coefficient of the curved conduit;
 ζ_{ff} = friction coefficient of the entire length of the curved conduit;
 λ = friction coefficient of unit relative length of the curved conduit.

6-2. EXPLANATIONS AND RECOMMENDATIONS

1. The variation of the stream direction in curved conduits (elbows, branches, bends and by-passes)* leads to the appearance of centrifugal forces directed from the center of curvature toward the outer wall of the pipe. As a result, the passage of a stream from the straight to the curved portion of the pipe is accompanied by an increase of the pressure at the outer wall and its decrease at the inner wall, and by a corresponding decrease of the stream velocity at the outer wall and its increase at the inner wall (Figure 6-1). At the bend, therefore, a diffuser effect occurs near the outer wall, and a bellmouth effect near the inner wall. The passage of a stream from the curved part of a pipe to the straight part following it is accompanied by the opposite effect, i. e., diffuser effect near the inner wall and the opposite effect near the outer wall.

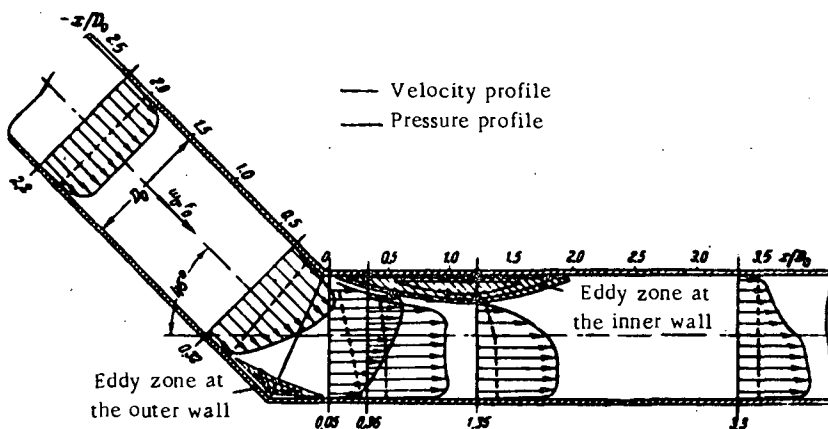


FIGURE 6-1. Variation of the profiles of velocities and pressures in an elbow and the straight stretch following it.

2. The diffuser phenomena lead to a separation of the stream from both walls (Figure 6-2). The separation from the inner wall is intensified by the inertial forces acting in the curved zone, which tend to move the stream particles toward the outer wall. The eddy zone which is formed as a result of the separation from the inner wall propagates far ahead and across, considerably reducing the main stream section.

3. The appearance of a centrifugal force and the existence of a boundary layer at the walls explain the appearance of a transverse flow in a curved pipe. It also explains

* An elbow is a curved stretch with equal radii of curvature of the inner and outer walls; a bend is a stretch whose inner and outer walls represent arcs of concentric circles:

$$r_{in} \geq 0 \text{ and } r_{out} = r_{in} + b_0$$

where r_{in} is the radius of curvature of the inner wall; and r_{out} is the radius of curvature of the outer wall.

Since the two walls of a bend have the same center of curvature, the bend can be characterized by the radius of curvature R_0 of its axis, which always satisfies the inequality

$$R_0/b_0 \geq 0.5$$

the formation of the so-called vortex pair which, superimposed on the main stream parallel to the channel axis, gives the streamlines a helical shape (Figure 6-3).

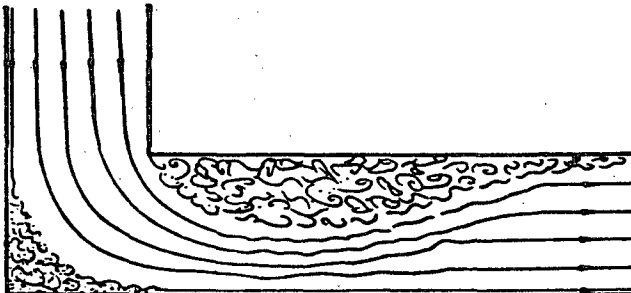


FIGURE 6-2. Stream pattern in a 90° elbow.

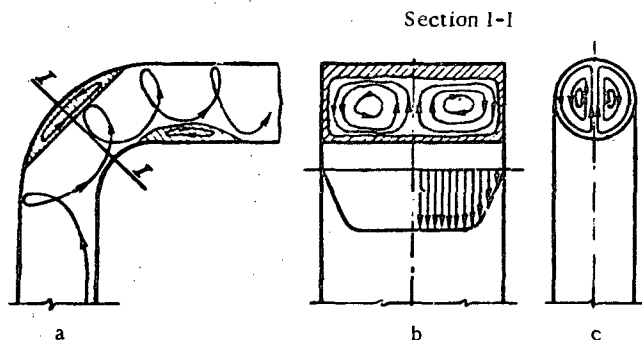


FIGURE 6-3. Vortex pair in an elbow:

a — longitudinal section; b — cross section of rectangular conduit;
c — cross section of a circular pipe.

4. The pressure losses in curved pipes are mainly due to the formation of eddies at the inner wall. This eddy formation also determines the pattern of velocity distribution beyond the bend.

The magnitude of the resistance coefficient in curved pipes varies as a function of the factors determining the turbulent intensity, the Reynolds number $Re = \frac{w_0 D_h}{\nu}$, the relative roughness of the walls $\bar{\Delta} = \frac{\Delta}{D_h}$, the inlet conditions, etc. It is also a function of the pipe shape, the angle of bend δ° , the relative radius of curvature $\frac{R_o}{D_h}$, the side ratio of the cross section $\frac{a_o}{b_o}$, the ratio of the inlet to exit areas $\frac{F_i}{F_o}$, etc.

5. The total resistance coefficient of bends and elbows is determined as the sum of the coefficient of local resistance of the bend ζ_1 and the friction coefficient ζ_{fr} :

$$\zeta = \frac{\Delta H}{\frac{\gamma w_0^2}{2g}} = \zeta_1 + \zeta_{fr}, \quad (6-1)$$

where ζ_1 is determined from the data given in this section; $\zeta_{fr} = \lambda \frac{l}{D_h}$ is calculated as ζ for straight stretches, with λ determined from diagrams 2-1 to 2-5 as a function of Re and the relative roughness $\bar{\Delta} = \frac{\Delta}{D_h}$; l = length of the bend or elbow, measured along the axis, so that:

$$\frac{l}{D_h} = \pi \frac{\delta^\circ}{180^\circ} \frac{R_o}{D_h} = 0.0175 \frac{R_o}{D_h} \delta^\circ. \quad (6-2)$$

Thus,

$$\zeta_{fr} = 0.0175 \lambda \frac{R_o}{D_h} \delta^\circ. \quad (6-3)$$

6. With other conditions constant, the resistance of a curved pipe is highest when its inner wall makes a sharp corner at the bend; the stream separation from this wall is then most intense. At an angle of bend $\delta = 90^\circ$ (Figure 6-2), the zone of stream separation at the inner wall beyond the bend reaches 0.5 of the pipe width /6-23/. It follows that the intensity of eddy formation and the resistance of a curved conduit increase with an increase in the angle of bend. The rounding of the corners (especially the inner wall) considerably attenuates the separation and reduces the resistance as a result.

7. If only the inner corner of the elbow is rounded (radius of curvature $r_1 = 0$, radius of curvature $r_0 > 0$, Figure 6-4), the resistance of a 90° elbow will be minimum at $\frac{r_0}{b_0} = 1.2$ to 1.5. With the subsequent increase of $\frac{r_0}{b_0}$ the resistance starts to increase considerably (Figure 6-4). Such an increase of resistance is explained in that, when the inner corner is rounded, a substantial area increase and a corresponding velocity drop are obtained at the bend. This leads to the intensification of the separation of the stream at the place of passage from the inlet stretch to the elbow.

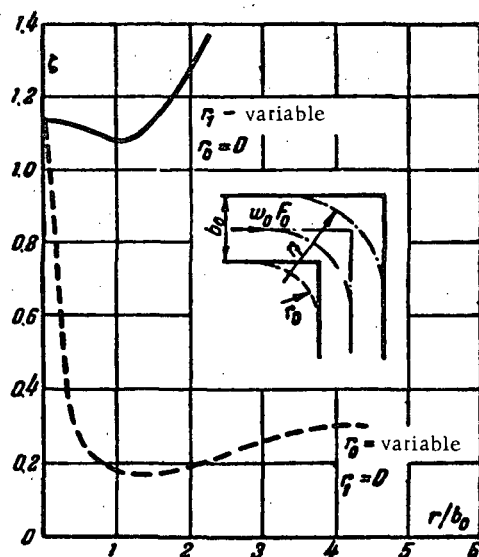


FIGURE 6-4. Plan of the rounding of an elbow, and resistance coefficient of the elbow as a function of the radius of curvature $\frac{r_0}{b_0}$.

8. The rounding of the outer wall while the inner corner is kept sharp ($r_0 = 0$) does not lead to a noticeable drop in the elbow resistance. A considerable increase of the radius of curvature of the outer wall will lead to an increase in the elbow resistance (Figure 6-4). In fact, the rounding of the outer wall only (sharp inner corner) reduces the stream area at the place of the bend and so increases the diffuser losses accompanying the passage of the stream from the elbow to the exit stretch of the pipe.

Minimum resistance is achieved in an elbow where $\frac{r_1}{b_0} = \frac{r_0}{b_0} + 0.6$ (elbow of optimum shape); a resistance close to the minimum is achieved in a bend or in a "normal" elbow

in which $\frac{r_1}{b_0} = \frac{r_0}{b_0} + 1.0$. Since a bend is easier to make, it can replace the optimum elbow in most cases.

9. A considerable reduction in elbow resistances can also be achieved simply by cutting off (along the chord) the sharp corners, particularly the inner one (cf. diagrams 6-10 and 6-11).

10. The variation of the ratio of areas $\frac{F_1}{F_0}$ of the elbow inlet and exit sections leads to a variation of the resistance. The increase of this ratio intensifies the diffuser effect beyond the turn, which leads to a greater stream separation, the formation of eddies and a simultaneous decrease (at constant discharge) of the stream velocity in the exit section. Expressed as a decrease of pressure losses, the effect of this drop in the velocity is greater (up to a certain value of $\frac{F_1}{F_0}$) than the effect of increase of the eddy zone, which leads to an increase of the losses. As a result, when the elbow section widens up to a limit, the total losses decrease.

11. The resistance of right-angled elbows ($\delta = 90^\circ$) with sharp corners is a minimum for $1.2 \leq \frac{F_1}{F_0} \leq 2.0$. The optimum value of $\frac{F_1}{F_0}$ in elbows and bends with smooth turns is closer to unity, and in some cases is even smaller than unity. If no data are available on the resistance of diverging elbows and bends, the decreases of pressure losses in the above range of $\frac{F_1}{F_0}$ can be neglected, and the resistance coefficient can be considered equal to its value for $\frac{F_1}{F_0} = 1.0$. The increase of resistance cannot be neglected at values of $\frac{F_1}{F_0}$ lower than unity or considerably higher than the optimum values.

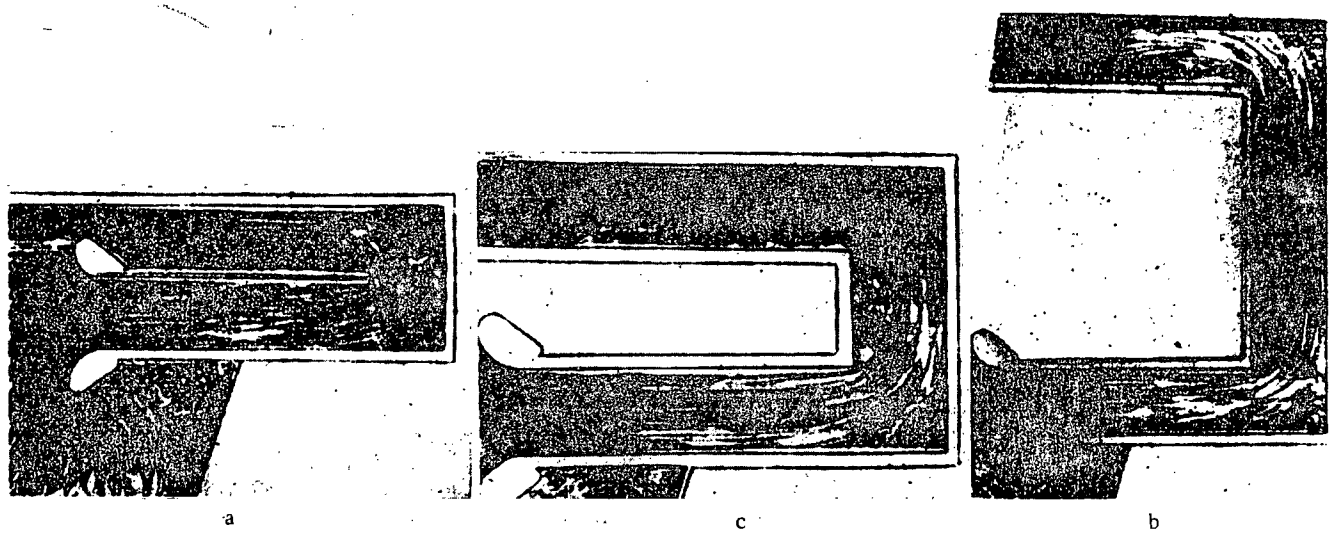


FIGURE 6-5. Flow patterns in Π-shaped conduits.

12. The resistance of curved conduits decreases with the increase of the side ratio of the elbow cross section $\frac{a_0}{b_0}$ and increases with the decrease of $\frac{a_0}{b_0}$ in the range below unity.

13. The resistance of combined elbows depends a great deal on the relative distance $\frac{l_0}{b_0}$ between the two elbows. In the case of a Π -shaped elbow, made from a couple of 90° elbows with sharp corners and small relative distance ($\frac{l_0}{b_0} \approx 0$), the stream separation from the inner wall takes place only after the complete turn by an angle $\delta = 180^\circ$ (Figure 6-5,a). The stream separation is most intense at such a large angle of turn, and the resistance coefficient is highest as a result.

When the relative distance is considerably increased ($\frac{l_0}{b_0} = 4$ to 5 and more), the stream will spread almost completely over the section in the straight stretch following the first 90° turn, and the conditions of the stream turning at the following 90° will be roughly the same as for the first turn (Figure 6-5,b). As a result, the total resistance coefficient of such a Π -shaped elbow will be close to twice the resistance coefficient of a right-angled elbow ($\delta = 90^\circ$).

At some intermediate value of $\frac{l_0}{b_0}$ near 1.0, the zone of separation behind the first 90° turn will not develop completely. Thus, at the inner wall before the second 90° turn, smooth rounding of the main stream will occur (Figure 6-5, c). Under these conditions the second turn of the stream takes place almost without separation, and therefore with low pressure losses. The total resistance coefficient of such a Π -shaped elbow is therefore minimum.

The rounding of the corners of Π -shaped elbows decreases the difference between the values of ζ corresponding to different values of $\frac{l_0}{b_0}$, but does not alter the pattern of the resistance curves or of the flow.

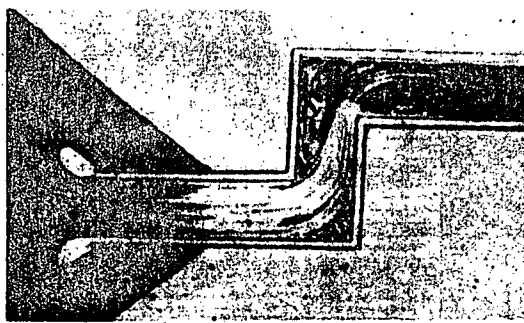


FIGURE 6-6. Flow pattern in a Z-shaped elbow.

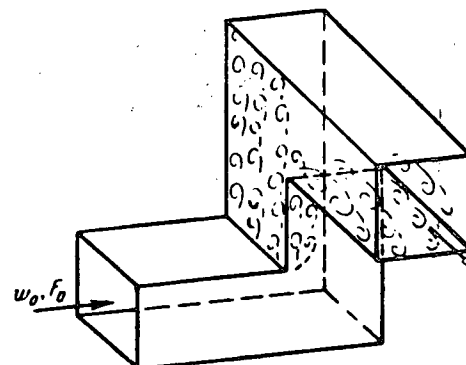


FIGURE 6-7. Flow pattern in a combined elbow with a 90° turn in two mutually perpendicular planes.

14. In the case of a Z formed by right-angled elbows (Figure 6-6), the increase of the relative distance $\frac{l_0}{b_0}$ between the axes of the two single elbows leads at the beginning to a sharp increase of the total resistance coefficient. As this ratio continues to increase, the resistance passes through a maximum and then gradually drops until it reaches a magnitude roughly equal to twice the resistance coefficient of a single right-angled elbow ($\delta = 90^\circ$).

The resistance coefficient of a Z-shaped conduit is a maximum when the second of the two single elbows forming it is placed near the widest section of the eddy zone formed after the first 90° turn (Figure 6-6). A maximum reduction of the stream cross section is then obtained at the second turn.

15. The total resistance coefficient of combined elbows in two mutually perpendicular planes (Figure 6-7), increases with the increase of the relative distance $\frac{r_0}{b_0}$ between the axes of the two constituent right-angled elbows. This increase from an initial value equal to the resistance coefficient of a single right-angled elbow, reaches a maximum at a small value of $\frac{r_0}{b_0}$. It then decreases with the further increase of this ratio, and tends to a value approximately equal to twice the resistance coefficient of a right-angled elbow ($\delta = 90^\circ$).

16. The coefficient of local resistance of smooth bends is calculated by the following formula, proposed by Abramovich /6-1/*:

$$\zeta_1 = \frac{\Delta H}{\frac{\gamma w_0^2}{2g}} = A_1 B_1 C_1, \quad (6-4)$$

where A_1 is a coefficient allowing for the influence of the bend angle δ° ; B_1 is a coefficient allowing for the influence of the relative radius of curvature of the bend $\frac{R_0}{D_h}$; C_1 is a coefficient allowing for the influence of the side ratio of the bend cross section $\frac{a_t}{b_0}$.

The value of A_1 is found from the following table, established by Nekrasov /6-11/:

at $\delta = 90^\circ$	$A_1 = 1.0$	}
at $\delta < 70^\circ$	$A_1 = 0.9 \sin \delta$	
at $\delta > 100^\circ$	$A_1 = 0.7 + 0.35 \frac{\delta}{90^\circ}$	

(6-5)

or from graph a of diagrams 6-1 or 6-2.

The value of B_1 can be calculated by the following approximate formulas:

at $\frac{R_0}{D_h} < 1.0$	$B_1 = \frac{0.21}{\left(\frac{R_0}{D_h}\right)^{2.5}}$	}
at $\frac{R_0}{D_h} > 1.0$	$B_1 = \frac{0.21}{\sqrt{\frac{R_0}{D_h}}}$	

(6-6)

or from graph b of diagrams 6-1 or 6-2.

The value of C_1 is determined from graph c of diagrams 6-1 or 6-2.

17. The coefficient of local resistance of elbows with sharp corners can be calculated in the entire range $0 \leq \delta \leq 180^\circ$ by the formula

$$\zeta_1 = \frac{\Delta H}{\frac{\gamma w_0^2}{2g}} = C_1 A' \quad (6-7)$$

* The formula given in /6-1/ contains a numerical factor 0.73, which is included here in the magnitude B_1 .

where ζ' is determined by Weisbach's formula /6-43/:

$$\zeta' = 0.95 \sin^2 \frac{\delta}{2} + 2.05 \sin^4 \frac{\delta}{2}; \quad (6-8)$$

A is the correction coefficient, obtained from Richter's /6-13, 6-37/ and Schubart's /6-39/ data, and determined from the curve $A=f(\delta)$ of diagram 6-7.

18. The coefficient of local resistance of bends and elbows can be considered as constant and independent of Re only for $Re = \frac{w_0 D_h}{\nu} > 2 \cdot 10^5$ to $2.5 \cdot 10^5$. Below this value, Re starts to influence the value of the local resistance coefficient, and this influence is the stronger, the lower the value of Re . This is particularly true of bends, and also of elbows with smooth inner curvature. The analytic relationship between the local resistance coefficient and Re is complex (cf. /6-8/) and so far has not been accurately determined.

19. The value of ζ_1 for elbows and bends of very small relative radii of inner curvature, within the range $0 < \frac{r}{D_h} < 0.05$ ($0.5 < \frac{R_0}{D_h} < 0.55$), can be considered practically constant and independent of the Reynolds number at $Re \geq 4 \cdot 10^4$. The following formula can be tentatively used for determining the resistance coefficient in the range $3 \cdot 10^3 < Re < 4 \cdot 10^4$:

$$\zeta_1 = \frac{\Delta H}{\frac{\gamma w_0^2}{2g}} = k_{Re} \zeta_{Re \geq 4 \cdot 10^4} \quad (6-9)$$

where

$$k_{Re} = \frac{\lambda_{Re}}{\lambda_{Re=4 \cdot 10^4}} \approx 45 \lambda_{Re}; \quad (6-10)$$

ζ_1 is the coefficient of local resistance of the bend or elbow considered at a given $Re < 4 \cdot 10^4$; $\zeta_{Re \geq 4 \cdot 10^4}$ is the coefficient of local resistance of the bend or elbow considered, determined as ζ_1 for $Re > 4 \cdot 10^4$ from the data of diagrams 6-1 and 6-6; k_{Re} is the coefficient allowing for the influence of the Reynolds number; $\lambda_{Re=4 \cdot 10^4}$ is the friction coefficient of unit relative length of a smooth pipe, equal to 0.022 (at $Re = 4 \cdot 10^4$); λ_{Re} is the friction coefficient of unit relative length of a smooth pipe, determined as λ at $Re < 4 \cdot 10^4$ from the data of diagrams 2-2 to 2-5.

20. The value of ζ_1 of elbows and bends with relative radius of inner curvature $\frac{r}{D_h} > 0.05$ ($\frac{R_0}{D_h} > 0.55$) can be considered as practically constant at all values $Re \geq 2 \cdot 10^5$; its value in the range $3 \cdot 10^3 < Re < 2 \cdot 10^5$ can be tentatively determined by formulas similar to (6-9) and (6-10):

$$\zeta_1 = \frac{\Delta H}{\frac{\gamma w_0^2}{2g}} = k_{Re} \zeta_{Re \geq 2 \cdot 10^5} \quad (6-11)$$

where

$$k_{Re} = \frac{\lambda_{Re}}{\lambda_{Re=2 \cdot 10^5}} \approx 64 \lambda_{Re}; \quad (6-11a)$$

$\zeta_{Re \geq 2 \cdot 10^5}$ is the local resistance coefficient of the bend or elbow considered, determined as ζ_1 at $Re \geq 2 \cdot 10^5$ from the data of diagrams 6-1, 6-2, and 6-9.

21. The total resistance of very smoothly curved pipes and channels ($\frac{R_o}{D_h} \gg 1.5$), such as are used in coils, can be considered as an increased friction coefficient, depending not only on Reynolds number and roughness, but also on the relative radius of curvature $\frac{R_o}{D_h}$:

$$\zeta = \zeta_{fr} = \lambda \frac{l}{D_h} = 0.0175 \lambda \frac{R_o}{D_h} \delta^*,$$

where λ is the friction coefficient of unit length of the curved pipe.

The value of λ for smooth pipes (made of glass, brass, lead, rubber, etc.) can be calculated by the following formulas obtained by Aronov /6-2/ on the basis of his experiments and those of Adler /6-22/ and White /6-44/*:

$$50 < Re \sqrt{\frac{D_h}{2R_o}} < 600$$

$$\lambda = \frac{20}{Re^{0.65}} \left(\frac{D_h}{2R_o} \right)^{0.175}; \quad (6-12)$$

$$600 < Re \sqrt{\frac{D_h}{2R_o}} < 1400$$

$$\lambda = \frac{10.4}{Re^{0.55}} \left(\frac{D_h}{2R_o} \right)^{0.225}; \quad (6-13)$$

$$1400 < Re \sqrt{\frac{D_h}{2R_o}} < 5000$$

$$\lambda = \frac{5}{Re^{0.45}} \left(\frac{D_h}{2R_o} \right)^{0.275}. \quad (6-14)$$

22. The state of the inner surface of bends and elbows immediately before the turn has a stronger influence on the coefficient of local resistance than on the friction coefficient at high values of Reynolds number /6-8/. The exact determination of the influence of this factor is impossible at present as it has not been widely studied.

23. The influence of the general roughness Δ is for very small relative radii $0 < \frac{R_o}{D_h} < 0.05$ or $0.5 < \frac{R_o}{D_h} < 0.55$ considerably weaker than for smoothly curved elbows and bends since the place of stream separation is near the corner of the bend. The influence of the general roughness in such elbows and bends can be tentatively

* These formulas were given by Aronov, and before him by Prandtl and Adler /6-13/ in a somewhat different form, namely:

$$\tau' = \frac{\lambda}{64} = k \left(Re \sqrt{\frac{D_h}{2R_o}} \right)^n.$$

where k is a numerical coefficient.

calculated by the formula

$$\zeta = \frac{\Delta H}{\frac{1}{2} w_0^2} = k_A \zeta_{sm} \quad (6-15)$$

where

$$\left. \begin{array}{l} Re > 4 \cdot 10^4 \text{ and } \bar{\Delta} < 0.001 \\ k_A \approx (1 + 0.5 \cdot 10^3 \bar{\Delta}) \end{array} \right\} \quad (6-16)$$

and

$$\left. \begin{array}{l} Re > 4 \cdot 10^4 \text{ and } \bar{\Delta} > 0.001 \\ k_A \approx 1.5 \end{array} \right\} \quad (6-17)$$

ζ_{sm} is determined as ζ_1 for smooth walls ($\bar{\Delta} \approx 0$).

24. The influence of general roughness in elbows and bends with relative radii of curvature within the limits $0.05 < \frac{r}{D_h} < 1.0$ ($0.55 < \frac{R_o}{D_h} < 1.5$), can be allowed for by the coefficient k_A in expression (6-15), which for $4 \cdot 10^4 < Re < 2 \cdot 10^5$ and $\bar{\Delta} < 0.001$, is given tentatively by Abramovich's formula /6-1/:

$$k_A = \frac{\lambda_A}{\lambda_{sm}} \quad (6-18)$$

at $Re > 2 \cdot 10^5$ and $\bar{\Delta} < 0.001$ tentatively by the following formula, based on the author's data /6-8/:

$$k_A \approx 1 + \bar{\Delta} \cdot 10^3, \quad (6-19)$$

and at $Re > 4 \cdot 10^4$ and $\bar{\Delta} > 0.001$ tentatively by the formula

$$k_A \approx 2, \quad (6-20)$$

where λ_{sm} = friction coefficient of a smooth pipe, determined as λ , at given $Re > 4 \cdot 10^4$, from diagram 2-4; λ_A is friction coefficient of a rough pipe, determined as λ at given $Re > 4 \cdot 10^4$ and $\bar{\Delta} = 0 - 0.001$, from the data of diagrams 2-2 to 2-5.

25. The influence of the general roughness on bends with $\frac{R_o}{D_h} > 1.5$ can be allowed for approximately, on the basis of the author's /6-8/ and Hofman's /6-32/ data, at $Re > 4 \cdot 10^4$ and $\bar{\Delta} < 0.001$ by the formula

$$k_A \approx 1 + \bar{\Delta}^2 \cdot 10^6, \quad (6-21)$$

and at $Re > 4 \cdot 10^4$ and $\bar{\Delta} > 0.001$ by the formula

$$k_A \approx 2.0. \quad (6-22)$$

26. At $Re < 4 \cdot 10^4$, the resistance coefficient of all bends and elbows can be considered practically independent of the general roughness, being a function of the Reynolds number only. It is accordingly calculated according to points 19 to 21 of this section.

27. The resistance coefficient of elbows with rounded corners and converging or diverging discharge sections ($n = \frac{F_1}{F_0} = \frac{b_1}{b_0} \geq 1.0$) can be approximated by the following formula, proposed by Richter /6-16/ on the basis of a large amount of experimental data:

$$\zeta = \frac{\Delta H}{\frac{\rho w_c^2}{2g}} = A_1 C_1 e^{-\frac{k}{n}},$$

where $A_1 = f(\delta^\circ)$ and $C_1 = f\left(\frac{a_0}{b_c}\right)$ are determined as above;

$$k = \ln \frac{1}{\zeta_0};$$

ζ = resistance coefficient of the elbow at $\frac{F_1}{F_0} = 1.0$ and $\delta = 90^\circ$; w_c = mean velocity in the narrow section of the elbow; b_c = width of the narrow section of the elbow; $e = 2.718$.

28. The coefficients of local resistance of welded branches are higher than those of nonwelded branches with all other conditions unchanged; since welding seams on the inner surfaces increase the local roughness. The relative magnitude of this local roughness decreases with the increase in diameter, and the resistance coefficient will accordingly decrease.

The coefficient of local resistance of corrugated bends is higher than for welded or nonwelded bends; the absolute dimensions of the corrugations increasing with the increase of the bend diameter, the resistance coefficient will increase likewise.

Bends from sheet material, either corrugated or made from several interlocked links, also belong to the category of curved stretches of increased resistance coefficient.

29. In the case of cast-iron or steel bends with threaded joints, a projection is formed at the junction between the straight part and the curved one, causing a sharp variation of cross section at this point (Figure 6-8); which creates additional pressure losses. The smaller the dimensions of such bends, the larger is the relative magnitude of the projection. As a result, small standard gas fittings have a resistance coefficient much higher than that of ordinary bends with a flanged joint.

The data given in diagram 6-4 on the resistance coefficients of gas fittings can be extended to all standard OST* bends of dimensions similar to those given.

30. The resistance of elbows can be decreased not only by rounding or cutting off corners, but also by installing guide vanes. These have the advantage that they do not lead to an increase in the channel dimensions. The guide vanes can be airfoils (Figure 6-9,a), simplified, and bent along the surface of a circular cylinder (Figure 6-9,b and c), or thin concentric (Figure 6-9,d) arcs of circles.

Vanes of identical shape and dimensions are usually mounted in the elbows, and, in a majority of cases, they are placed along the line of bend of the conduit (Figure 6-9, a, b, and c).

Concentric vanes should be used in bends (Figure 6-9,d).

31. An aerodynamic cascade in an elbow, formed of guide vanes, deflects the stream toward the inner wall as a result of the aerodynamic force developed in it. When the dimensions, number, and angle of the vanes are correctly selected, this stream deflection will prevent the separation of the jet from the wall and the formation of an eddy zone. The velocity distribution over the section behind the turn is improved as a result (Figure 6-10), and the elbow resistance is decreased.

* [Obshchesoyuznyi Standart (All-Union Standard).]

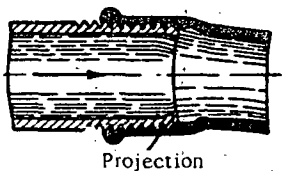


FIGURE 6-8. Threaded cast-iron bends.

Designa-tion	Relative dimensions
t	1.0 t
x_1	0.519 t
x_2	0.489 t
r_1	0.663 t
r_2	0.553 t
y_1	0.463 t
y_2	0.215 t
z_1	0.139 t
z_2	0.338 t
z_3	0.268 t
ρ	0.033 t

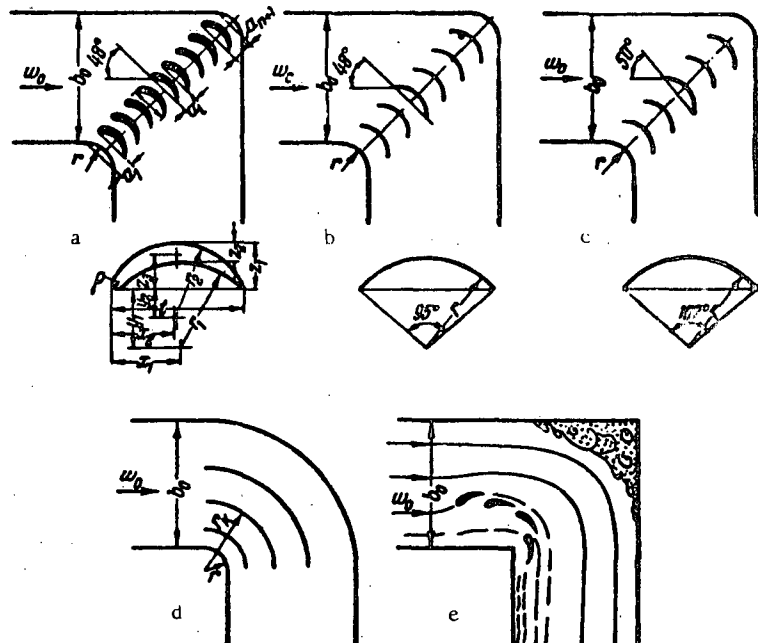


FIGURE 6-9. Guide vanes in elbows and bends:

a — airfoils; b — thin, along a 95° arc; c — thin, along a 107° arc; d — concentric; e — staggered.

32. Since the most effective means for decreasing the resistance and equalizing the velocity distribution is the elimination of the eddy zone at the inner wall of the channel, the vanes located near the inner rounding will produce the largest effect. This makes it possible to remove some of the vanes located near the outer wall without altering the flow characteristics (cf. Baulin and Idel'chik /6-3/).

33. In those cases when it is especially important to obtain a uniform velocity distribution immediately after the turn, the number of vanes is not reduced (the "normal" number of vanes is used) and is determined by the formula /6-6/:

$$n_{\text{norm}} = 2.13 \left(\frac{r}{D_h} \right)^{-1} - 1. \quad (6-23)$$

In most practical cases it is sufficient to use a reduced number of vanes determined by the following formulas obtained by the author /6-6/:

$$n_{\text{opt}} \approx 1.4 \left(\frac{r}{D_h} \right)^{-1} \quad (6-24)$$

or

$$n_{\text{min}} \approx 0.9 \left(\frac{r}{D_h} \right)^{-1}. \quad (6-25)$$

In ordinary elbows, lower resistance and a better distribution of the velocities are obtained with the optimum number of vanes (cf. formula (6-24)).

The chord t_1 of the airfoil vane is taken as the chord of a 90° arc of circle, i.e., as the chord of the inner curvature of the elbow, and therefore

$$t_1 = r\sqrt{2}, \quad (6-26)$$

or

$$t_1 = D_h \left(\frac{r}{D_h} \right) \sqrt{2}. \quad (6-27)$$

Formulas (6-23) to (6-25) are only correct for this relation between the dimensions of the vane chord and the radius of curvature of the elbow. The profiles of the guide vanes are plotted on the basis of the data given in Figure 6-9.

34. If the elbow does not have smooth curvatures but sharp or cut-off corners, the vane-chord length can be taken within the limits $t_1 = 0.15$ to $0.6D_h$. The number of vanes can be determined in this case by the following formulas /6-6/:

$$n_{\text{norm}} = \frac{3D_h}{t_1} - 1; \quad (6-28)$$

$$n_{\text{opt}} \approx 2 \frac{D_h}{t_1}; \quad (6-29)$$

$$n_{\text{min}} \approx 1.5 \frac{D_h}{t_1}. \quad (6-30)$$

35. The number of vanes in elbows with diverging section ($b_1 > b_0$) is determined by the following formulas, respectively:

$$n_{\text{norm}} = 2.13 \frac{s}{t_1} - 1; \quad (6-31)$$

$$n_{\text{opt}} \approx 1.4 \frac{s}{t_1}; \quad (6-32)$$

$$n_{\text{min}} \approx 0.9 \frac{s}{t_1}, \quad (6-33)$$

$$s = \sqrt{b_0^2 + b_1^2}. \quad (6-34)$$

36. When the "normal" number of vanes are used they are uniformly mounted along the line of bending of the elbow, so that the distance between the chords of the vanes is $a = \frac{s}{n+1}$.

When a reduced number is used, it is recommended /6-6/ that a distance a between the chords be taken, varying according to an arithmetic progression, such, that in the case of the optimum number of vanes, $\frac{a_{n+1}}{a_1} = 2$, and in the case of the minimum number, $\frac{a_{n+1}}{a_1} = 3$. Here a_1 is the distance from the chord of the arc of the inner rounding of the elbow to the chord of the first vane (Figure 6-9); a_{n+1} is the distance between the chords of the last vane and the outer rounding.

The distances between vanes are determined by the following formulas /6-7/:

when the optimum number of vanes is used

$$a_i = 0.67 \frac{s}{n+1} \left(1 + \frac{i-1}{n} \right); \quad (6-35)$$

when the minimum number of vanes is used

$$a_i = \frac{s}{n+1} \left(0.5 + \frac{i-1}{n} \right). \quad (6-36)$$

37. The vanes used in practice in a majority of the cases in elbows are the simplified thin vanes, disposed, in the case of a 90° turn, on the average along a circular arc of angle $\varphi_1 = 95^\circ$ independently of the elbow parameters (the relative radius of curvature, the area ratio, etc.). The disposition and the angle of installation of such vanes are selected according to the same criteria as for airfoil vanes. The resistance coefficient of elbows with such vanes is considerably higher than for elbows with airfoil vanes.

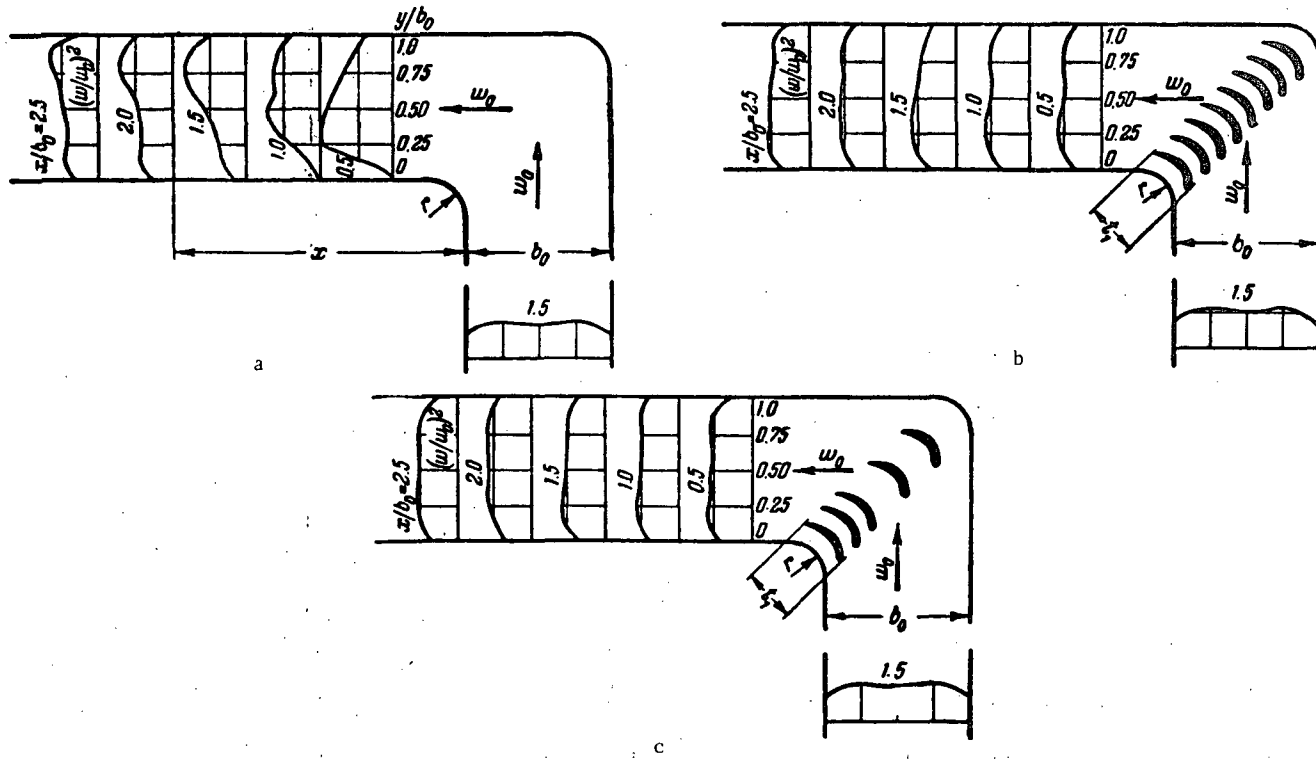


FIGURE 6-10. Distribution of dimensionless velocities in an elbow:

a — without vanes; b — with a normal number of vanes; c — with a reduced number of vanes.

38. A low value of resistance, similar to the resistance of elbows with airfoil vanes, is obtained by selecting thin vanes by the Yudin method /6-20/. The optimum angle of the vane arc and the vane angle are a function of both the relative radius of curvature of the elbow and its area ratio. This relationship is represented in diagrams 6-34 to 6-36.

39. The installation of guide vanes in elbows is expedient as long as the relative radius of curvature is small. In the case of elbows of constant section, the installation of vanes is efficient as long as $\frac{r}{D_h} < 0.4 - 0.5$. In the case of diffuser elbows, the limiting value of $\frac{r}{D_h}$ is increased roughly to 1.0. In the case of elbows with reduced exit section, this value is decreased roughly to 0.2.

40. The action of concentric vanes installed in bends mainly results in splitting the given bend into a number of bends of more elongated cross section, which leads to a decrease of the pressure losses. The normal number z of thin optimally installed concentric vanes in a bend is determined on the basis of the data of Khanzhonkov and Taliev /6-18/ (Table 6-1).

TABLE 6-1

$\frac{r}{b_0}$	0 - 0.1	0.1 - 0.4	0.4 - 1.0	1.0
z	3 - 4	2	1	0

The optimum disposition of the vanes in the bend is determined by the formula

$$r_i = 1.26 r_{i-1} + 0.07 b_0. \quad (6-37)$$

41. The resistance coefficient of a bend with normal number of optimally installed concentric vanes can be determined approximately by the following formula of the above authors /6-18/:

$$\zeta = \frac{\Delta H}{\frac{\rho w_0^2}{2g}} = \left(0.46 \frac{R_0}{b_0} + 0.04 \right) \zeta_{w.v} \quad (6-38)$$

where $\zeta_{w.v}$ is the resistance coefficient of the bend without vanes.

42. When guide vanes are installed in combined elbows, the resistance coefficient is determined as the sum of the resistance coefficients of the single elbows with vanes:

$$\zeta = 2\zeta_v, \quad (6-39)$$

where ζ_v is resistance coefficient of a single elbow with vanes.

6-3. LIST OF THE DIAGRAMS OF RESISTANCE COEFFICIENTS OF SECTION VI

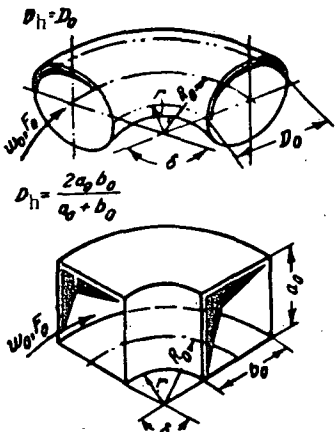
Diagram description	Source	No. of diagram	Note
Sharp bends at $0.5 < \frac{R_o}{D_h} < 1.5$ and $0 < \delta^\circ < 180^\circ$	Abramovich /6-1/, Vasilevskii /6-42/, Idel'chik /6-8/, Nekrasov /6-11/, Nippert /6-36/, Richter /6-13/, Fritzsche /6-28/, Hofmann /6-32/	6-1	Based on experiments. The influence of Reynolds number and the roughness allowed for approximately on the basis of the data from /6-1, 6-8, and 5-13/. To be used until refined by experimental data
Smooth bends at $R_o/D_h > 1.5$ and $0 < \delta^\circ < 180^\circ$ Very smooth bends ($R_o/D_h \gg 1.5$) in conduits cast-iron bends, $8.50 < Re < 2 \cdot 10^4$	The same Aronov /6-2/, Adler /6-22/, Richter /6-13/ Vuskovich /6-41/	6-2 6-3 6-4 6-5	The same Experimental data
Standard threaded cast-iron bends $Re \geq 2 \cdot 10^4$ Combined bends (U-shaped, S-shaped) at different δ° and $\frac{R_o}{D_h} \geq 0.5$	—	—	The same Approximately according to diagrams (6-1 and 6-2); the influence of $\frac{L_o}{D_h}$ allowed for by the data of /6-29/. To be used until refined on the basis of new experiments
Sharp $(\frac{r}{D_h} = 0)$ elbows of rectangular section with converging or diverging exit section Sharp $(r/D_h = 0)$ elbows at $0 < \delta^\circ < 180^\circ$	Data according to /6-12/	6-6	Experimental data
Elbows with rounded corners and converging or diverging exit section $(\frac{F_1}{F_0} \geq 1.0)$	Abramovich /6-1/, Weisbach /6-43/, Idel'chik /6-6/, Nippert /5-36/, Richter /6-13/, Schubart /6-39/ and Richter /6-16/	6-7	Cf. (diagram 6-1)
Elbows with rounded corners at $0.05 \leq r/D_h \leq 0.5$ and $0 < \delta^\circ < 180^\circ$	Cf. diagram 6-1	6-9	Cf. diagram 6-1
90° elbows of rectangular section with rounded inner corner and sharp outer corner	Nippert /6-36/, Richter /6-15/	6-10	Experimental data
90° elbows of rectangular section with cut-off corners	Richter /6-15/	6-11	The same
Elbows made from separate elements at different δ°	Kirchbach /6-34/, Schubart /6-39/	6-12	" "
90° elbow made from five elements	The same	6-13	" "
90° elbow made from four elements	" "	6-14	" "
90° elbow made from three elements	" "	6-15	" "
90° elbow made from three elements at $R_o/D_o = 2.4$, welded (with welding seams), at $Re \geq 10^4$	Kamershtein and Karev /6-9/	6-16	" "
Corrugated bend; $\frac{R_o}{D_o} \approx 2.5$; $Re > 2 \cdot 10^4$	The same	6-17	" "
Z-shaped elbow made from two 30° elbows	Kirchbach /6-34/, Schubart /6-39/	6-18	" "
Z-shaped elbow, $Re \geq 10^4$	Data according to /6-12/	6-19	" "
Combined elbow made from two 90° elbows lying in different planes, $Re > 10^4$	The same	6-20	" "

Diagram description	Source	Diagram number	Note
Π-shaped elbow (180°) with equal inlet and exit sections ($\frac{F_1}{F_0} = \frac{b_1}{b_0} = 1.0$). $Re > 4 \cdot 10^4$	Data according to /6-12/	6-21	Experimental data
Π-shaped elbow (180°) with airfoil guide vanes. section ($\frac{F_1}{F_0} = \frac{b_1}{b_0} = 0.5$)	The same	6-22	The same
Π-shaped elbow (180°) with widened exit section ($\frac{F_1}{F_0} = \frac{b_1}{b_0} = 1.4$)	" "	6-23	" "
Π-shaped elbow (180°) with widened exit section ($\frac{F_1}{F_0} = \frac{b_1}{b_0} = 2.0$)	" "	6-24	" "
U-shaped elbow (180°) with contracted exit section ($\frac{F_1}{F_0} = \frac{b_1}{b_0} = 0.5$)	" "	6-25	" "
U-shaped elbow (180°) with equal inlet and exit sections ($\frac{F_1}{F_0} = \frac{b_1}{b_0} = 1.0$)	" "	6-26	" "
U-shaped elbow (180°) with widened exit section ($\frac{F_1}{F_0} = \frac{b_1}{b_0} = 1.4$)	" "	6-27	" "
U-shaped elbow (180°) with widened exit section ($\frac{F_1}{F_0} = \frac{b_1}{b_0} = 2.0$). $Re \geq 10^4$	" "	6-28	" "
Parts made from galvanized sheet for $R_0/D_0 = 1.0$; $D_0 = 100$ mm. $Re \geq 1.5 \cdot 10^4$	Conn, Colborne and Brown /6-24/	6-29	" "
Corrugated elbows made from galvanized sheet for $R_0/D_0 = 0.7$; $D_0 = 100$ mm. $Re \geq 1.5 \cdot 10^4$	The same	6-30	" "
90° bend with concentric guide vanes. $Re \geq 10^4$	Khanzhonkov and Taliev /6-18/	6-31	" "
90° elbow of rectangular section at different r/b_0 with airfoil guide vanes. $Re \geq 10^4$	Baulin and Idel'chik /6-3/	6-32	" "
90° elbow of rectangular section at different r/b_0 with thin guide vanes ($\varphi_1 = 90^\circ$). $Re \geq 10^4$	The same	6-33	" "
90° elbow of rectangular section with thin guide vanes ($\varphi_1 = 95^\circ$) under different conditions. $Re \geq 10^4$	" "	6-34	" "
90° smooth elbow ($r/b_0 = 0.2$) of rectangular section at $\frac{F_1}{F_0} = 0.5$ with thin guide vanes ($\varphi_1 = 103^\circ$). $Re \geq 10^4$	Yudin /6-20/	6-35	" "
90° smooth elbow ($r/b_0 = 0.2$) of rectangular section at $\frac{F_1}{F_0} = 1.0$ with thin guide vanes ($\varphi_1 = 107^\circ$). $Re \geq 10^4$	The same	6-36	" "
90° elbow of rectangular section at $F_1/F_0 = 2.0$ with thin guide vanes. $Re \geq 10^4$	" "	6-37	" "
90° elbow of circular section with airfoil guide vanes $Re \geq 10^4$	Idel'chik /6-6/	6-38	" "

6-4. DIAGRAMS OF RESISTANCE COEFFICIENTS

Sharp bends at $0.5 < \frac{R_o}{D_h} < 1.5$ and $0 < \delta^\circ \leq 180^\circ$

Section VI
Diagram 6-1



1. Smooth walls ($\Delta = 0$) and $Re = \frac{w_0 D_h}{\nu} \geq 2 \cdot 10^5$

$$\zeta = -\frac{\Delta H}{\frac{1}{2} w_0^2} = \zeta_1 + \zeta_{fr.}$$

where $\zeta_1 = A_1 B_1 C_1$; $\zeta_{fr.} = 0.0175 \lambda \frac{R_o}{D_h} \delta^\circ$; at $\lambda \approx 0.02$ $\zeta_{fr.} = 0.00035 \frac{R_o}{D_h} \delta^\circ$

A_1 is determined as a function of δ° from graph a or approximately by the formulas of Table 6-2.

B_1 is determined as a function of $\frac{R_o}{D_h}$ from graph b or approximately by the formulas of Table 6-3.

C_1 is determined approximately from graph c as a function of $\frac{a_0}{b_0}$ (in the case of circular or square section $C_1 = 1.0$)

ν	0	20	30	45	60	75	90	110	130	150	180
A_1	0	0.31	0.45	0.60	0.78	0.90	1.00	1.13	1.20	1.28	1.40

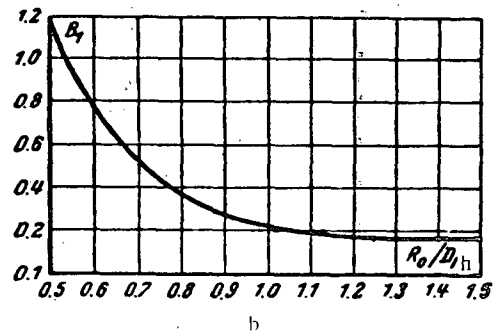
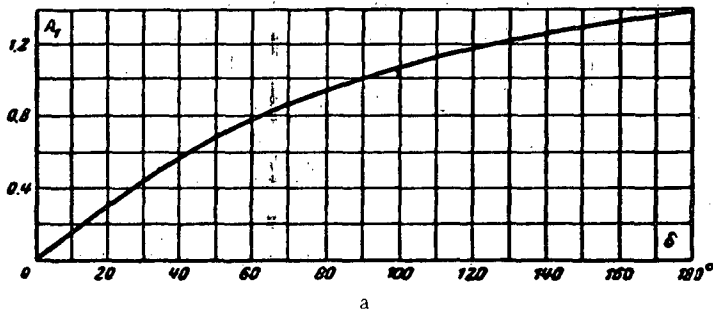
$\frac{R_o}{D_h}$	0.50	0.60	0.70	0.80	0.90	1.00	1.25	1.50
B_1	1.18	0.77	0.51	0.37	0.28	0.21	0.19	0.17

TABLE 6-2

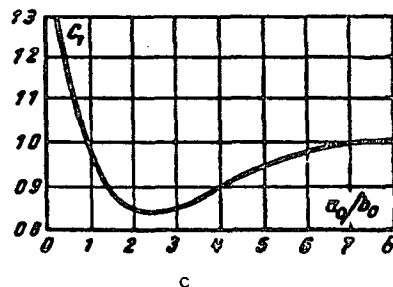
δ°	$\leq 70^\circ$	90°	$\geq 100^\circ$
A_1	$0.9 \sin \delta^\circ$	1.0	$0.7 + 0.35 \frac{\delta^\circ}{90^\circ}$

TABLE 6-3

$\frac{R_o}{D_h}$	0.5-1.0	1.0
B_1	$\frac{0.21}{(\frac{R_o}{D_h})^{2.5}}$	$\frac{0.21}{\sqrt{R_o/D_h}}$



$\frac{a_0}{b_0}$	0.25	0.50	0.75	1.0	1.5	2.0	3.0	4.0	5.0	6.0	7.0	8.0
C_1	1.30	1.17	1.09	1.00	0.90	0.85	0.85	0.90	0.95	0.98	1.00	1.00


 2. Rough walls ($\Delta > 0$) and $Re \leq 2 \cdot 10^5$:

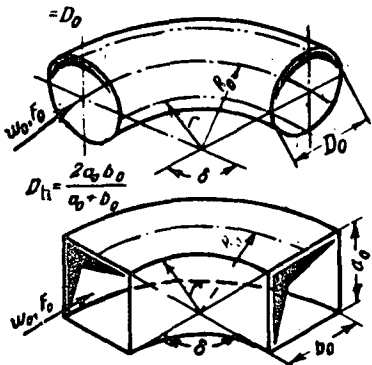
$$\zeta = \frac{\Delta H}{\frac{\rho g}{2} u_0^2} = k_\Delta k_{Re} \xi_1 + \xi_{fr},$$

where k_Δ and k_{Re} are determined (tentatively) from Table 6-4 as a functions of Re and $\bar{\Delta} = \frac{\Delta}{D_h}$

TABLE 6-4

$\bar{\Delta}$	R_o/D_h									
	0.5-0.55				0.55-1.5					
	Re									
	$3 \cdot 10^3 - 4 \cdot 10^4$		$> 4 \cdot 10^4$		$3 \cdot 10^3 - 4 \cdot 10^4$		$3 \cdot 10^4 - 2 \cdot 10^5$		$> 2 \cdot 10^5$	
	k_{Re}	k_Δ	k_{Re}	k_Δ	k_{Re}	k_Δ	k_{Re}	k_Δ	k_{Re}	k_Δ
0	$45 k_{Re}$	1.0	1.0	1.0	$64 k_{Re}$	1.0	$64 k_{Re}$	1.0	1.0	1.0
$0-0.001$	$45 k_{Re}$	1.0	1.0	$1 + 0.5 \cdot 10^{-3} \bar{\Delta}$	$64 k_{Re}$	1.0	$64 k_{Re}$	λ_Δ/k_{sm}	1.0	$1 + \bar{\Delta} \cdot 10^3$
> 0.01	$45 k_{Re}$	1.0	1.0	≈ 1.5	$64 k_{Re}$	1.0	$64 k_{Re}$	≈ 2.0	1.0	≈ 2.0

λ_{Re} and λ_{sm} are determined as λ for commercially smooth pipes ($\Delta = 0$) at given Re from diagram 2-2
 λ and λ_Δ are determined as λ for rough pipes ($\Delta > 0$) at given Re and $\bar{\Delta} = \frac{\Delta}{D_h}$ from diagrams 2-3 to 2-5;
 λ is taken from § 1-3, b; Δ is taken from Table 2-1.

1. Smooth bends ($\Delta = 0$) and $Re = \frac{w_0 D_h}{\nu} \geq 2 \cdot 10^4$:where $\zeta_1 = A_1 B_1 C_1$:

$$\zeta = \frac{\Delta H}{\gamma w_0^2} = \zeta_1 + \zeta_{fr},$$

$$\zeta_{fr} = 0.01751 \frac{R_o}{D_h} \delta^\circ;$$

$$\lambda \approx 0.02 - \zeta_{fr} = 0.00035 \frac{R_o}{D_h} \delta^\circ;$$

 A_1 is determined as a function of δ° from graph a or by the formulas of Table 6-5

TABLE 6-5

δ°	$\leq 70^\circ$	90°	$\geq 100^\circ$
A_1	$0.9 \sin \delta^\circ$	1.0	$0.7 + 0.35 \frac{\delta^\circ}{90^\circ}$

 B_1 is determined as a function of $\frac{R_o}{D_h}$ from graph b, or by the formula

$$B_1 = \frac{0.21}{\sqrt{R_o/D_h}};$$

 C_1 is determined from graph c as a function of $\frac{a_o}{b_o}$ (for circular or square cross section $C_1 = 1.0$)2. Rough walls ($\Delta > 0$) and $Re \geq 2 \cdot 10^4$:

$$\zeta = \frac{\Delta H}{\gamma w_0^2} = k_A k_{Re} \zeta_1 + \zeta_{fr},$$

where k_A , k_{Re} are determined (tentatively) from Table 6-6 as a function of Re and $\bar{\Delta} = \frac{\Delta}{D_h}$

TABLE 6-6

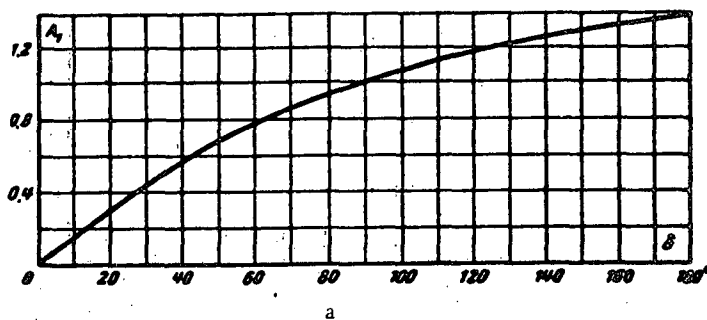
$\bar{\Delta}$	Re					
	$3 \cdot 10^3 - 4 \cdot 10^4$		$4 \cdot 10^4 - 2 \cdot 10^5$		$> 2 \cdot 10^5$	
k_{Re}	k_A	k_{Re}	k_A	k_{Re}	k_A	k_A
0	$64 k_{Re}$	1.0	$64 k_{Re}$	1.0	1.0	1.0
$0 - 0.001$	$64 k_{Re}$	1.0	$64 k_{Re}$	$1 + \bar{\Delta} \cdot 10^{-6}$	1.0	$1 + \bar{\Delta} \cdot 10^{-6}$
> 0.001	$64 k_{Re}$	1.0	$64 k_{Re}$	≈ 2.0	1.0	≈ 2.0

 λ is determined as a function of the given Re and $\bar{\Delta}$ from diagrams 2-2 to 2-5; k_{Re} is determined as λ for commercially smooth pipes ($\Delta = 0$) at given Re from diagram 2-2; ν is taken from § 1-3, b; Δ is taken from Table 2-1.

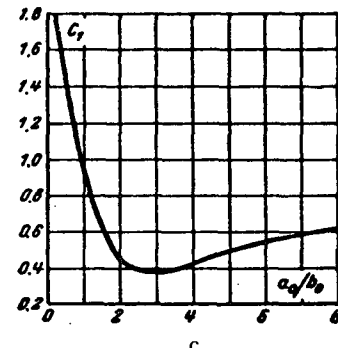
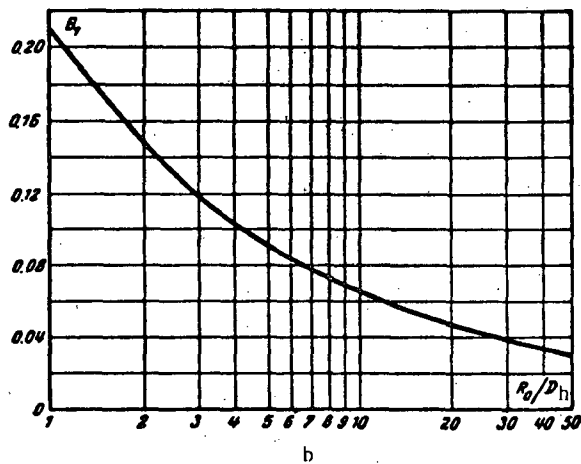
Smooth bends at $\frac{R_b}{D_h} > 1.5$ and $0 < \delta^\circ \leq 180^\circ$ (cont'd)

Section VI
Diagram 6-2

θ°	0	20	30	45	60	75	90	110	130	150	180
A_1	0	0.31	0.45	0.60	0.78	0.90	1.00	1.13	1.20	1.28	1.40



$\frac{R_b}{D_h}$	1.0	2.0	4.0	6.0	8.0	10	15	20	25	30	35	40	45	50
B_1	0.21	0.15	0.11	0.09	0.07	0.07	0.06	0.05	0.05	0.04	0.04	0.03	0.03	0.03



$\frac{a_0}{b_0}$	0.25	0.50	0.75	1.0	1.5	2.0	3.0	4.0	5.0	6.0	7.0	8.0
C_1	1.80	1.45	1.20	1.00	0.68	0.45	0.40	0.43	0.48	0.55	0.58	0.60

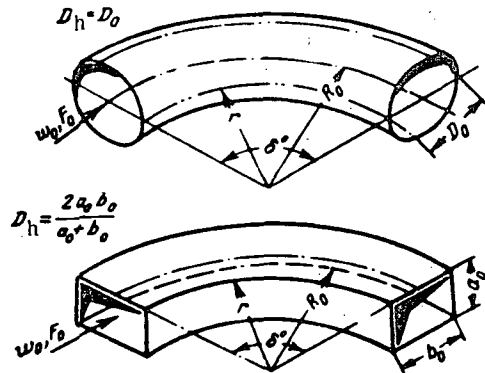
Very smooth bends ($\frac{R_o}{D_h} \gg 1.5$) in conduits (coils) of arbitrary angle of bend δ° . $50 < Re = \frac{w_0 D_h}{\nu} < 2 \cdot 10^4$

Section VI

Diagram 6-3

$$D_h = \frac{4F_0}{\Pi_0}; \quad \Pi_0 \text{ — perimeter}$$

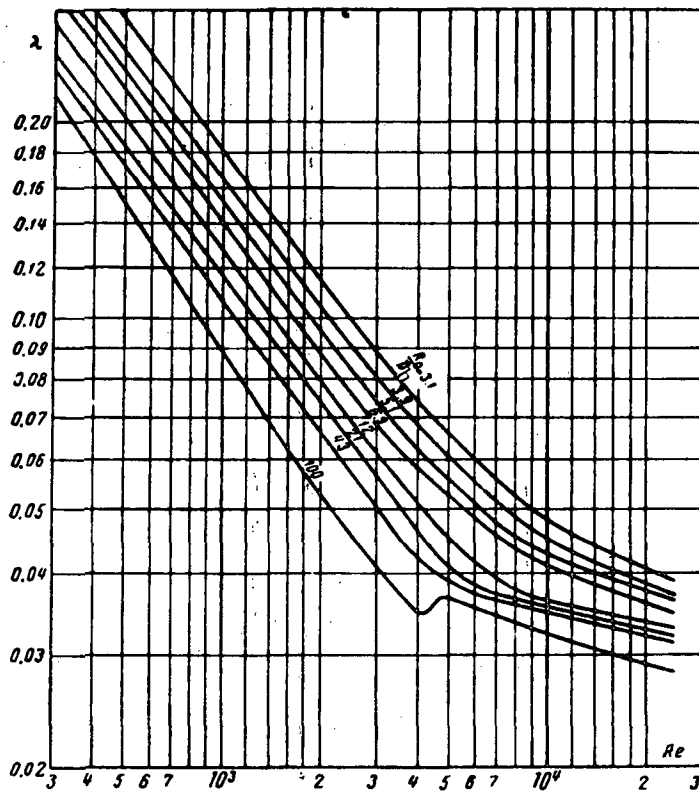
$$\zeta = \frac{\Delta H}{\frac{1}{2} w_0^2} = 0.0175 \lambda \frac{R_o}{D_h} \delta^\circ$$



where λ is determined from the curve $\lambda = f\left(Re, \frac{R_o}{D_h}\right)$
or from the following table:

- a) $50 < Re < 600 \quad \sqrt{\frac{D_h}{2R_o}} < 600 \quad \lambda = \frac{20}{Re^{0.65}} \left(\frac{D_h}{2R_o}\right)^{0.175};$
- b) $600 < Re < 1400 \quad \sqrt{\frac{D_h}{2R_o}} < 1400 \quad \lambda = \frac{10.4}{Re^{0.65}} \left(\frac{D_h}{2R_o}\right)^{0.225};$
- c) $1400 < Re < 5000 \quad \sqrt{\frac{D_h}{2R_o}} < 5000 \quad \lambda = \frac{5}{Re^{0.45}} \left(\frac{D_h}{2R_o}\right)^{0.275};$

ν is taken from § 1-3, b.



Re | 4 · 10² | 6 · 10² | 8 · 10² | 10³ | 2 · 10³ | 4 · 10³ | 6 · 10³ | 10⁴

$$\frac{R_o}{D_h} = 3.1$$

λ | 0.34 | 0.26 | 0.21 | 0.18 | 0.12 | 0.08 | 0.06 | 0.05

$$\frac{R_o}{D_h} = 3.9$$

λ | 0.30 | 0.23 | 0.19 | 0.17 | 0.10 | 0.07 | 0.06 | 0.05

$$\frac{R_o}{D_h} = 5.1$$

λ | 0.28 | 0.21 | 0.18 | 0.15 | 0.10 | 0.06 | 0.05 | 0.04

$$\frac{R_o}{D_h} = 6.9$$

λ | 0.26 | 0.20 | 0.17 | 0.14 | 0.09 | 0.06 | 0.05 | 0.04

$$\frac{R_o}{D_h} = 12$$

λ | 0.24 | 0.18 | 0.15 | 0.13 | 0.08 | 0.05 | 0.04 | 0.04

$$\frac{R_o}{D_h} = 21$$

λ | 0.22 | 0.16 | 0.14 | 0.12 | 0.07 | 0.05 | 0.04 | 0.03

$$\frac{R_o}{D_h} = 43$$

λ | 0.20 | 0.15 | 0.13 | 0.11 | 0.07 | 0.04 | 0.04 | 0.03

$$\frac{R_o}{D_h} = 100$$

λ | 0.18 | 0.13 | 0.11 | 0.09 | 0.05 | 0.04 | 0.04 | 0.03

Characteristics of bends	Schematic diagram	Resistance coefficient $\zeta = \frac{\Delta H}{\frac{w_0^2}{2g}}$				
		D_0	$\frac{1}{2}"$	1"	$1\frac{1}{2}"$	2"
$\delta = 30^\circ$		L mm	30	44	56	66
		$\bar{\Delta} = \frac{\Delta}{D_0}$	0.020	0.010	0.0075	0.005
		ζ	0.81	0.52	0.32	0.19
$\delta = 45^\circ$		L mm	36	52	68	81
		$\bar{\Delta} = \frac{\Delta}{D_0}$	0.020	0.010	0.0075	0.005
		ζ	0.73	0.38	0.27	0.23
$\delta = 90^\circ$ (knee bend)		L mm	30	40	55	65
		$\bar{\Delta} = \frac{\Delta}{D_0}$	0.020	0.010	0.0075	0.005
		ζ	2.19	1.98	1.60	1.07
$\delta = 90^\circ$ $\frac{R_o}{D_0} = 1.36 \text{ to } 1.67$		L mm	45	63	85	98
		$\bar{\Delta} = \frac{\Delta}{D_0}$	0.02	0.01	0.0075	0.005
		ζ	1.20	0.80	0.81	0.58

Standard threaded cast-iron bends $R_e = \frac{w_0 D_0}{v} \geq 2 \cdot 10^3$ (cont'd)

Section VI
Diagram 6-4

Bend characteristic	Schematic diagram	Resistance coefficient $\zeta = \frac{\Delta H}{\frac{T w_0^2}{2g}}$				
		D_0	$\frac{1}{2}"$	1"	$1\frac{1}{2}"$	2"
$\delta = 90^\circ$ $\frac{R_0}{D_0} \text{ to } 2.13$		$L \text{ mm}$ $\bar{A} = \frac{A}{D_0}$ ζ	55 0.020 0.82	85 0.010 0.53	116 0.0075 0.53	140 0.005 0.35
$\delta = 180^\circ$		$L \text{ mm}$ $\bar{A} = \frac{A}{D_0}$ ζ	38 0.020 1.23	102 0.010 0.70	102 0.0075 0.65	127 0.005 0.58

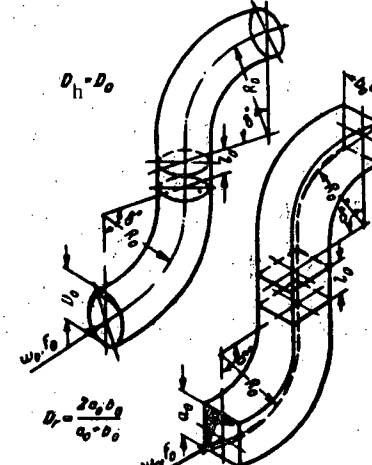
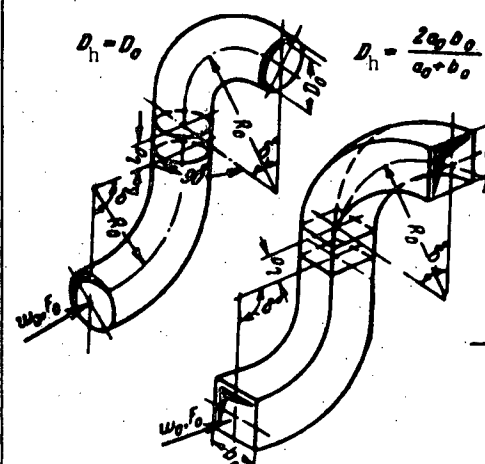
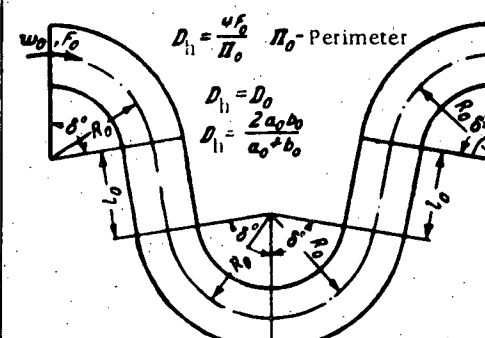
Combined bends at different δ and $\frac{R_0}{D_h} \geq 0.5$

Section VI
Diagram 6-5

No.	Bend characteristic	Schematic diagram	Resistance coefficient $\zeta = \frac{\Delta H}{\frac{T w_0^2}{2g}}$
1	U-shaped		$\zeta = A \zeta'$, where ζ' is determined as ζ for a single bend from diagrams 6-1 and 6-2; ζ_{fr} is determined by the formula $\zeta_{fr} = \left(\frac{l_0}{D_h} + 0.035 \frac{R_0}{D_h} \delta^\circ \right) \lambda;$ at $\lambda \approx 0.02$: $\zeta_{fr} = 0.02 \frac{l_0}{D_h} + 0.0007 \frac{R_0}{D_h} \delta^\circ$; any λ is determined from diagrams 2-2 to 2-5. A is taken from Table 6-7 (tentatively).

TABLE 6-7

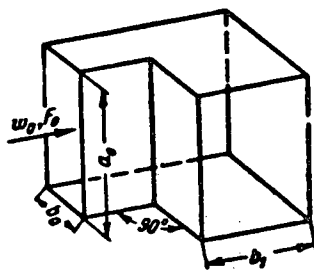
l_0/D_h	0	≥ 1.0
A	1.4	2.0

No	Bend characteristic	Schematic diagram	Resistance coefficient $\zeta = \frac{\Delta H}{\frac{1}{2} \rho v_0^2}$						
2	S-shaped (gooseneck)	 <p>$D_h = D_o$</p> <p>$D_i = \frac{2a_o b_o}{a_o + b_o}$</p>	<p>The same as in No. 1, but the values of A are taken from Table 6-8 (tentatively)</p> <table border="1" data-bbox="1067 759 1537 865"> <tr> <th>I_o/D_h</th> <th>0</th> <th>≥ 1.0</th> </tr> <tr> <td>A</td> <td>3.0</td> <td>2.0</td> </tr> </table>	I_o/D_h	0	≥ 1.0	A	3.0	2.0
I_o/D_h	0	≥ 1.0							
A	3.0	2.0							
3	S-shaped in two planes	 <p>$D_h = D_o$</p> <p>$D_i = \frac{2a_o b_o}{a_o + b_o}$</p>	<p>The same as in No. 1, but the values of A are taken from Table 6-9 (tentatively)</p> <table border="1" data-bbox="1067 1223 1537 1350"> <tr> <th>I_o/D_h</th> <th>0</th> <th>≥ 1.0</th> </tr> <tr> <td>A</td> <td>2.5</td> <td>2.0</td> </tr> </table>	I_o/D_h	0	≥ 1.0	A	2.5	2.0
I_o/D_h	0	≥ 1.0							
A	2.5	2.0							
4	By-pass	 <p>$D_h = D_o$</p> <p>$D_i = \frac{2a_o b_o}{a_o + b_o}$</p> <p>$P_o$ - Perimeter</p>	<p>The same as in No. 1, but the values of A are taken from Table 6-10 (tentatively)</p> <table border="1" data-bbox="1067 1434 1537 1582"> <tr> <th>I_o/D_h</th> <th>0</th> <th>≥ 1.0</th> </tr> <tr> <td>A</td> <td>6.0</td> <td>4.0</td> </tr> </table> <p>ζ_{fr} is determined by formula</p> $\zeta_{fr} = 2 \left(\frac{l_o}{D_h} + 0.035 \frac{R_o}{D_h} \delta^\circ \right) \lambda;$ <p>λ - cf. No. 1.</p>	I_o/D_h	0	≥ 1.0	A	6.0	4.0
I_o/D_h	0	≥ 1.0							
A	6.0	4.0							

Sharp ($\frac{r}{D_h} = 0$) elbows of rectangular section
with converging or diverging exit section

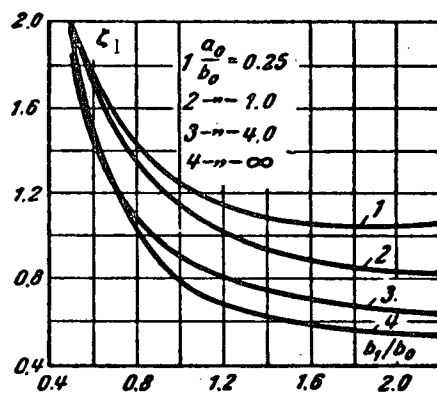
Section VI

Diagram 6-6



$$D_h = \frac{2a_0 b_0}{a_0 + b_0}$$

$\frac{b_1}{b_0}$	0.6	0.8	1.0	1.2	1.4	1.6	2.0
1) $a_0/b_0 = 0.25$							
ζ_1	1.76	1.43	1.24	1.14	1.09	1.06	1.06
2) $a_0/b_0 = 1.0$							
ζ_1	1.70	1.36	1.15	1.02	0.95	0.90	0.84
3) $a_0/b_0 = 4.0$							
ζ_1	1.46	1.10	0.90	0.81	0.76	0.72	0.66
4) $a_0/b_0 = \infty$							
ζ_1	1.50	1.04	0.79	0.69	0.63	0.60	0.55



1. Smooth walls ($\Delta = 0$) and $Re = \frac{w_0 D_h}{\nu} \geq 2 \cdot 10^5$:

$$\zeta = \frac{\Delta H}{\frac{\gamma w_0^2}{2g}} = \zeta_1$$

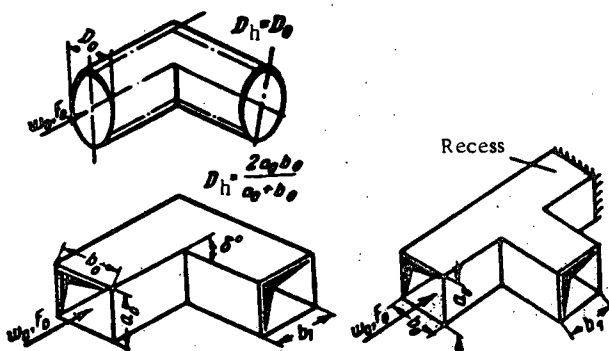
is determined from the curves $\zeta_1 = f\left(\frac{b_1}{b_0}\right)$ corresponding to different values of $\frac{a_0}{b_0}$.

2. Rough walls ($\Delta > 0$) and $Re \leq 2 \times 10^5$:

$$\zeta = \frac{\Delta H}{\frac{\gamma w_0^2}{2g}} = k_\Delta k_{Re} \zeta_1,$$

where k_Δ and k_{Re} are determined from diagram 6-7 as functions of Re and $\Delta = \frac{\Delta}{D_h}$,

ν is taken from § 1-3,b; Δ is taken from Table 2-1.



1. Elbow without recess

 1. Smooth walls ($\Delta = 0$ and $Re = \frac{\omega_0 D_h}{v} \geq 4 \cdot 10^4$):

$$\zeta = \frac{\Delta H}{\gamma w_0^2} = C_1 A \zeta_1 \quad (\zeta_{fr} = 0),$$

where C_1 is determined approximately from graph a as a function of a_0/b_0 (in the case of circular or square section $C_1 = 1.0$);

A is determined from the curve $A = f_1(\delta^\circ)$ of graph b;

$\zeta_1 = 0.95 \sin^2 \frac{\delta}{2} + 2.05 \sin^4 \frac{\delta}{2}$ is determined from the curve

$\zeta_1 = f_2(\delta^\circ)$ of graph b;

$\frac{a_0}{b_0}$	0.25	0.50	0.75	1.0	1.5	2.0	3.0	4.0	5.0	6.0	7.0	8.0
C_1	1.10	1.07	1.04	1.00	0.95	0.90	0.83	0.78	0.75	0.72	0.71	0.70

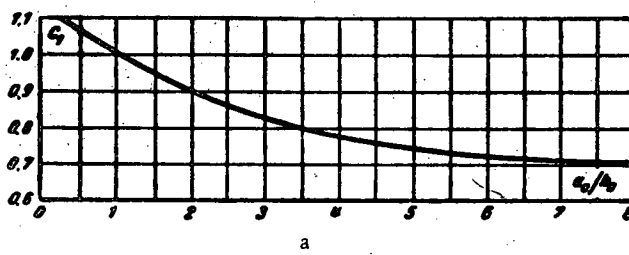


TABLE 6-11

$\bar{\Delta}$	Re			
	$3 \cdot 10^4 - 4 \cdot 10^4$		$\geq 4 \cdot 10^4$	
	k_{Re}	k_A	k_{Re}	k_A
0	$45 k_{Re}$	1.0	1.1	1.0
$0 - 0.001$	$45 k_{Re}$	1.0	1.0	$1 + 0.5 \cdot 10^3 \bar{\Delta}$
> 0.001	$45 k_{Re}$	1.0	1.0	≈ 1.5

2. Rough walls ($\Delta > 0$) and any Re:

$$\zeta = \frac{\Delta H}{\gamma w_0^2} = k_A k_{Re} C_1 A \zeta_i$$

where k_A and k_{Re} are determined (tentatively) from Table 6-11 as a function of Re and $\bar{\Delta} = \frac{\Delta}{D_h}$.

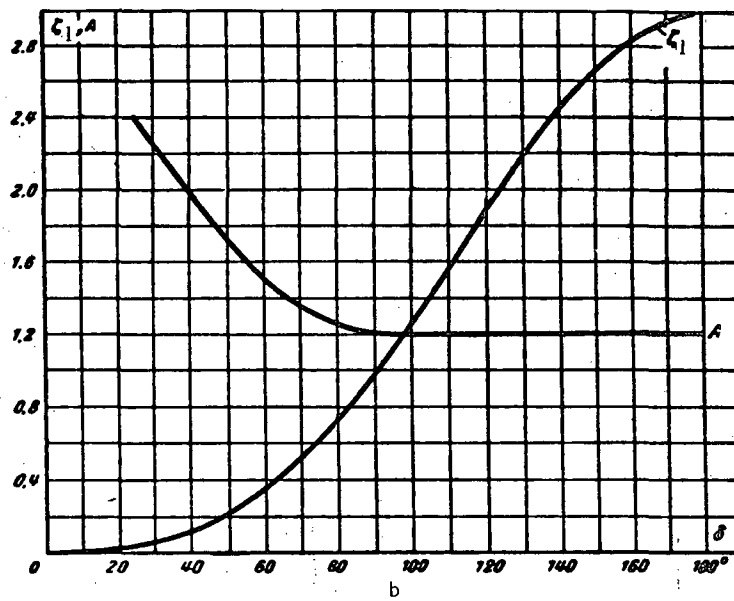
λ is determined from diagrams 2-2 to 2-5 as a function of Re and $\bar{\Delta}$;

k_{Re} is determined from diagram 2-2 as λ for commercially smooth pipes ($\Delta = 0$) at given Re;

$\bar{\Delta}$ is taken from Table 2-1;

w is taken from § 1-3, b.

θ°	0	20	30	45	60	75	90	110	130	150	180
ζ_1	0	0.05	0.07	0.17	0.37	0.63	0.99	1.56	2.16	2.67	3.00
A	—	2.50	2.22	1.87	1.50	1.28	1.20	1.20	1.20	1.20	1.20



II. Elbow with recess

$$\zeta = \frac{\Delta H}{\gamma w_0^2} \approx 1.2 \zeta_{w.r.}$$

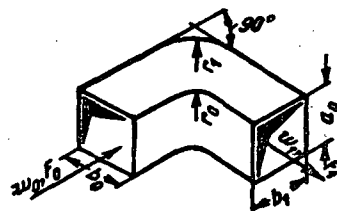
where $\zeta_{w.r.}$ is determined as ζ for an elbow without recess.

Elbows with rounded corners and converging or diverging exit section ($F_1 \geq 1.0$)

Section VI
Diagram 6-8

b_c = width of the narrow section;

$$n = \frac{F_1}{F_0}$$



1. Smooth walls ($\Delta = 0$) and $Re = \frac{w_0 b_c}{v} > 2 \cdot 10^5$:

$$\zeta = \frac{\Delta H}{\frac{\gamma w_c^2}{2g}} = A_1 C_1 e^{-\frac{k}{n}} = A_1 C_1 \zeta'$$

where $\zeta' = e^{-\frac{k}{n}}$ is determined from the curves $\zeta' = f\left(\frac{F_1}{F_0}, \frac{r}{b_c}\right)$ of graph a;

A_1 is determined from the curve $A_1 = f(90^\circ)$ of graph b;

C_1 is determined approximately from the curve $C_1 = f\left(\frac{b_0}{b_c}\right)$ of graph c;

$k = \ln \frac{1}{\zeta'}$; ζ'_0 = resistance coefficient of the elbow at $\frac{F_1}{F_0} = 1.0$ and $\theta = 90^\circ$;

w_c = mean stream velocity in the narrow section.

2. Rough walls ($\Delta > 0$) and $Re = 2 \times 10^5$:

$$\zeta = \frac{\Delta H}{\frac{\gamma w_c^2}{2g}} = k_A k_{Re} A_1 C_1 \zeta'$$

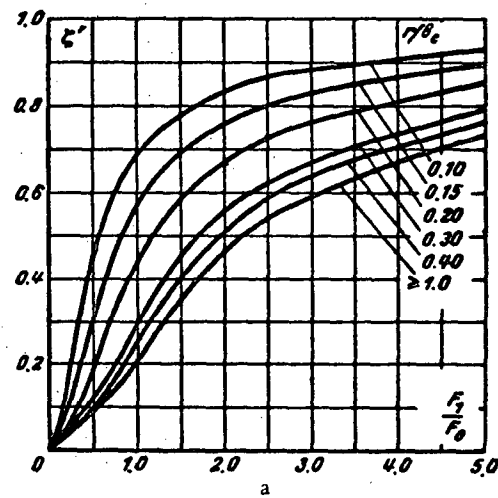
where k_A and k_{Re} are determined as functions of Re and $\bar{A} = \frac{A}{b_c}$ from Table 6-12 of diagram 6-9;

v is taken from § 1-3, b;

Δ is taken from Table 2-1.

Values of ζ'

$\frac{r}{b_c}$	$\frac{F_1}{F_0}$							
	0.2	0.5	1.0	1.5	2.0	3.0	4.0	5.0
0.1	0.20	0.45	0.69	0.78	0.83	0.88	0.91	0.93
0.15	0.13	0.32	0.57	0.68	0.76	0.83	0.87	0.89
0.20	0.08	0.20	0.45	0.58	0.67	0.76	0.81	0.85
0.30	0.06	0.13	0.30	0.45	0.56	0.67	0.74	0.79
0.40	0.04	0.10	0.25	0.40	0.51	0.64	0.70	0.76
1.0	0.04	0.09	0.21	0.35	0.47	0.59	0.67	0.73

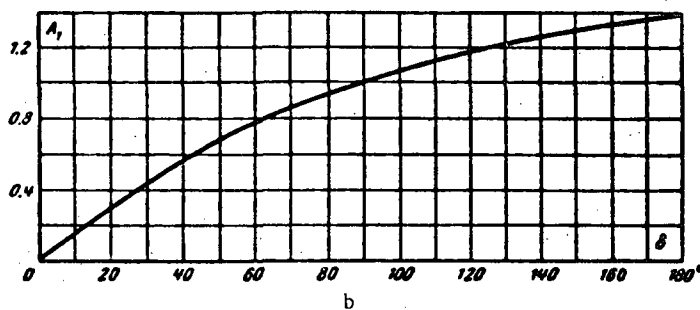


Elbows with rounded corners and converging or diverging
exit section ($\frac{F_1}{F_0} \leq 1.0$) (cont'd)

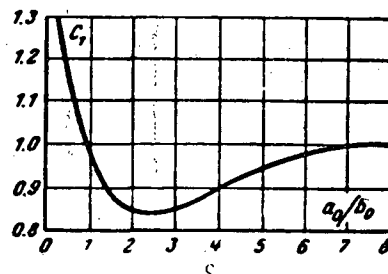
Section VI

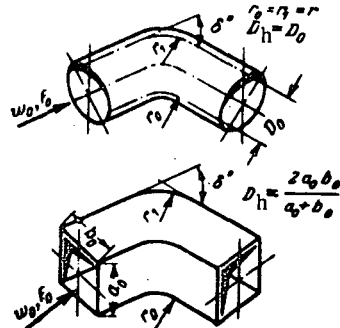
Diagram 6-8

θ	0	20	30	45	60	75	90	110	130	150	160
A_1	0	0.31	0.45	0.60	0.78	0.90	1.00	1.13	1.20	1.28	1.40



$\frac{a_0}{b_0}$	0.25	0.50	0.75	1.0	1.5	2.0	3.0	4.0	5.0	6.0	7.0	8.0
C_1	1.30	1.17	1.09	1.00	0.90	0.85	0.85	0.90	0.95	0.98	1.00	1.00





1. Smooth walls ($\Delta = 0$) and $Re > \frac{w_0 D_h}{\nu} > 2 \cdot 10^5$:

$$\zeta = \frac{\Delta H}{\frac{\gamma w_0^2}{2g}} = \zeta_1 + \zeta_{fr},$$

where $\zeta_1 = A_1 B_1 C_1$

$$\zeta_{fr} = \left(1 + 0.0175 \frac{r}{D_h} \delta^\circ \right) \lambda;$$

at $\lambda = 0.02$: $\zeta_{fr} \approx 0.02 + 0.00035 \frac{r}{D_h} \delta^\circ$;

A_1 is determined from graph a as a function of δ° ;

B_1 is determined approximately from graph b as a function of $\frac{r}{D_h}$;

C_1 is determined approximately from graph c as a function of $\frac{a_o}{b_o}$;

2. Rough walls ($\Delta > 0$) and $Re \geq 2 \cdot 10^5$:

$$\zeta = \frac{\Delta H}{\frac{\gamma w_0^2}{2g}} = k_A k_{Re} \zeta_1 + \zeta_{fr},$$

where k_A and k_{Re} are tentatively determined from Table 6-12 as functions of Re and $\bar{\Delta} = \frac{\Delta}{D_h}$;

λ_{Re} and λ_{sm} are determined from diagram 2-2 as λ (for commercially smooth pipes $\Delta = 0$) at given Re ;

λ and λ_A are determined from diagrams 2-3 to 2-5 as λ for rough pipes ($\Delta > 0$) at given $\bar{\Delta} = \Delta/D_h$;

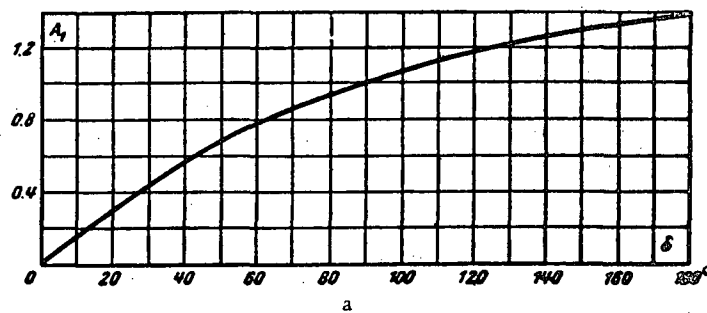
ν is taken from § 1-3, b;

$\bar{\Delta}$ is determined by Table 2-1.

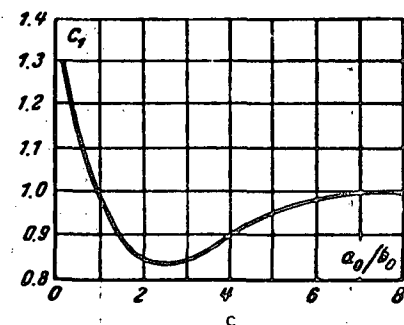
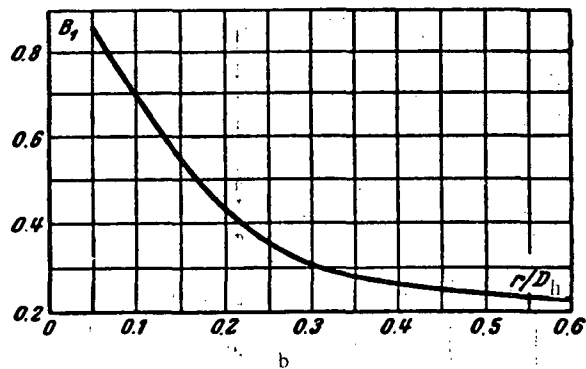
TABLE 6-12

$\bar{\Delta}$	Re					
	$3 \cdot 10^5 - 4 \cdot 10^6$		$4 \cdot 10^6 - 2 \cdot 10^7$		$> 2 \cdot 10^7$	
	k_{Re}	k_A	k_{Re}	k_A	k_{Re}	k_A
0	$64k_{Re}$	1.0	$64k_{Re}$	1.0	1.0	1.0
$0 - 0.001$	$64k_{Re}$	1.0	$64k_{Re}$	λ / λ_{sm}	1.0	$1 + \bar{\Delta} \cdot 10^3$
> 0.001	$64k_{Re}$	1.0	$64k_{Re}$	≈ 2.0	1.0	≈ 2.0

θ°	0	20	30	45	60	75	90	110	130	150	160
A_1	0	0.31	0.45	0.60	0.78	0.90	1.00	1.13	1.20	1.28	1.40



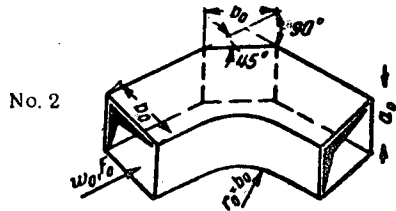
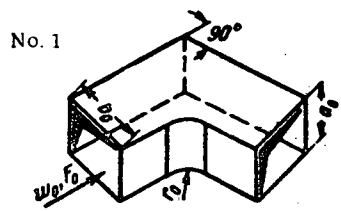
r/D_h	0.05	0.10	0.20	0.30	0.40	0.50	0.60
B_1	0.87	0.70	0.44	0.31	0.26	0.24	0.22



a_0/b_0	0.25	0.50	0.75	1.0	1.5	2.0	3.0	4.0	5.0	6.0	7.0	8.0
C_1	1.30	1.77	1.09	1.00	0.90	0.85	0.85	0.90	0.95	0.98	1.00	1.00

90° elbows of rectangular section with rounded inner corner
and sharp outer corner

Section VI
Diagram 6-10



$$D_h = \frac{4F_0}{H_0}; H_0 - \text{perimeter}$$

1. Smooth walls ($\Delta = 0$) and $Re = \frac{w_0 D_h}{\nu} \geq 2 \cdot 10^5$:

$$\zeta = \frac{\Delta H}{\frac{\gamma w_0^2}{2g}} = C_1 \zeta_1 + \zeta_{fr}.$$

where for No. 1, ζ_1 is determined from graph a as a function of $\frac{r_0}{D_h}$;

for No. 2, $\zeta_1 = 0.20C_1$;

$$\zeta_{fr} = \left(1 + 1.57 \frac{r_0}{D_h}\right) \lambda;$$

$$\text{at } \lambda \approx 0.02 \quad \zeta_{fr} = 0.02 + 0.031 \frac{r_0}{D_h};$$

C_1 is determined approximately from graph b as a function of $\frac{a_0}{b_0}$.

2. Rough walls ($\Delta > 0$) and any Re:

$$\zeta = \frac{\Delta H}{\frac{\gamma w_0^2}{2g}} = k_A k_{Re} C_1 \zeta_1.$$

where k_A and k_{Re} are determined from Table 6-12 of diagram 6-9;

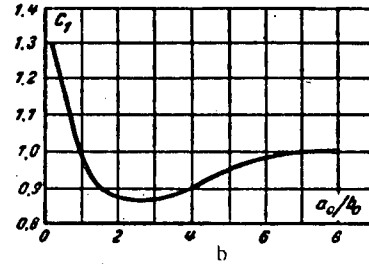
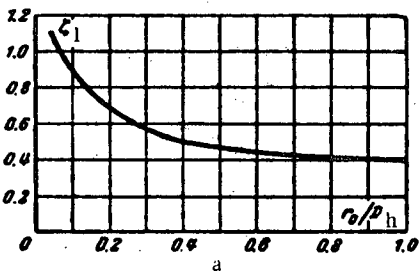
λ is determined from diagrams 2-2 to 2-5 as a function of Re and $\bar{\Delta} = \frac{\Delta}{D_h}$;

ν is taken from § 1-3, b;

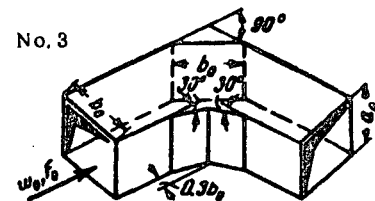
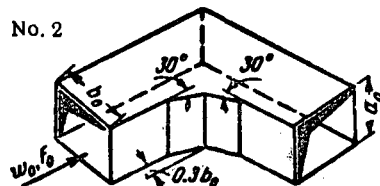
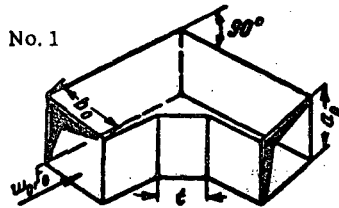
Δ is taken from Table 2-1

r_0/D_h	0.05	0.1	0.2	0.3	0.5	0.7	1.0
ζ	1.10	0.88	0.70	0.56	0.48	0.43	0.40

a_0/b_0	0.25	0.50	0.75	1.00	1.50	2.0	3.0	4.0	5.0	6.0	7.0	8.0
C_1	1.30	1.17	1.09	1.00	0.90	0.85	0.85	0.90	0.95	0.98	1.00	1.00



$$D_h = \frac{4F_0}{\Pi}; \quad \Pi_0 \text{ — perimeter}$$



1. Smooth walls ($\Delta = 0$) and $Re = \frac{\nu_0 D_h}{\mu} \geq 2 \cdot 10^5$:

$$\zeta = \frac{\Delta H}{\gamma w_0^2} = C_s \zeta_1,$$

where for No. 1, ζ_1 is determined from the curve

$$\zeta_1 = f\left(\frac{\ell_1}{D_h}\right);$$

for No. 2: $\zeta_1 = 0.47C_s$;

for No. 3: $\zeta_1 = 0.28C_s$.

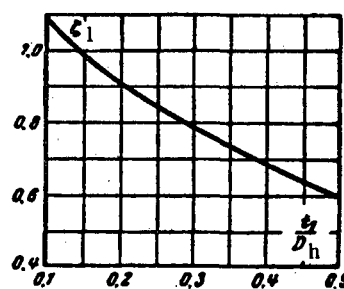
C_s is determined approximately from graph b of diagram 6-10.

2. Rough walls ($\Delta > 0$) and $Re \geq 2 \times 10^5$:

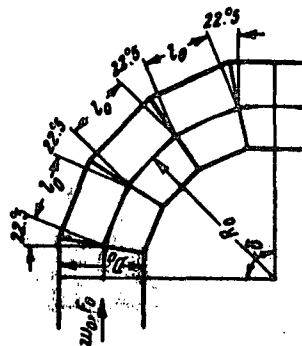
$$\zeta = \frac{\Delta H}{\gamma w_0^2} = k_A k_{Re} C_s \zeta_1.$$

where k_A and k_{Re} are determined from Table 6-12 of diagram 6-9;
 ν is taken from § 1-3, b.

$\frac{\ell_1}{D_h}$	0.1	0.2	0.3	0.4	0.5
ζ_1	1.10	0.90	0.80	0.69	0.60



No.	Elbow characteristic	Schematic diagram	Resistance coefficient $\zeta = \frac{\Delta H}{\frac{V^2 g}{2g}}$
1	$\delta = 45^\circ$; three elements		<p>1. Smooth walls ($\Delta = 0$) and $Re = \frac{w_0 D_0}{v} \geq 2 \cdot 10^5$:</p> $\zeta = \zeta_1 + \zeta_{fr}$ <p>2. Rough walls ($\Delta > 0$) and $Re \geq 2 \cdot 10^5$:</p> $\zeta = k_A k_{Re} \zeta_1 + \zeta_{fr},$ <p>where $\zeta_1 = 0.11$; $\zeta_{fr} = \lambda \frac{l_0}{D_0}$; at $\lambda \approx 0.02$ $\zeta_{fr} = 0.02 \frac{l_0}{D_0}$; λ, k_A, k_{Re}, Δ, and ζ_1 cf. diagram 6-1.</p>
2	$\delta = 60^\circ$; three elements		The same as in No. 1, but $\zeta_1 = 0.15$.
3	$\delta = 60^\circ$; four elements		The same as in No. 1, but $\zeta_{fr} = 2\lambda \frac{l_0}{D_0}$ at $\lambda \approx 0.02$ $\zeta_{fr} = 0.04 \frac{l_0}{D_0}$
4	$\delta = 90^\circ$; three elements		The same as in No. 1, but $\zeta_1 = 0.40$



$\frac{l_o}{D_o}$	0	0.2	0.4	0.6	0.8	1.0	2.0	3.0	4.0	5.0	6.0
R_o/D_o	0	0.49	0.98	1.47	1.90	2.50	5.00	7.50	10.0	12.5	15.0
ζ_1	1.10	0.75	0.45	0.34	0.35	0.12	0.10	0.12	0.14	0.14	0.14

1. Smooth walls ($\Delta = 0$) and $Re = \frac{\omega_0 D_h}{v} > 2 \cdot 10^5$:

$$\zeta = \frac{\Delta H}{\frac{\gamma w_0^2}{2g}} = k_A k_{Re} \zeta_1 + \zeta_{fr},$$

where ζ_1 is determined from the curve $\zeta_1 = f\left(\frac{l_o}{D_o}\right)$ or $f\left(\frac{R_o}{D_o}\right)$

$$\zeta_{fr} = 3\lambda \frac{l_o}{D_o}; \text{ at } \lambda \approx 0.02, \zeta_{fr} = 0.06 \frac{l_o}{D_o}.$$

2. Rough walls ($\Delta > 0$) and $Re \geq 2 \times 10^5$:

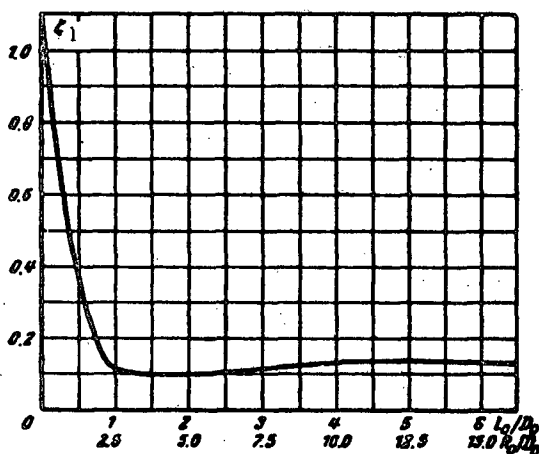
$$\zeta = \frac{\Delta H}{\frac{\gamma w_0^2}{2g}} = \zeta_1 + \zeta_{fr},$$

where k_A and k_{Re} are determined from Table 6-4 of diagram 6-1;

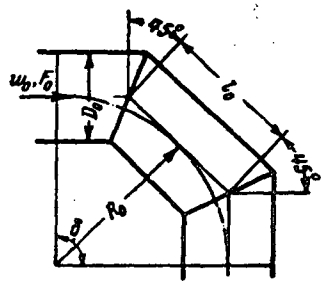
λ is determined by diagrams 2-2 to 2-5;

v is taken from § 1-3, b;

Δ is taken from Table 2-1.



90° elbow from three elements

Section VI
Diagram 6-15

$\frac{l_0}{D_0}$	0	0.2	0.4	0.6	0.8	1.0	2.0	3.0	4.0	5.0	6.0
R_0/D_0	0	0.24	0.48	0.70	0.97	1.20	2.35	3.60	4.60	6.00	7.25
ζ_1	1.10	0.95	0.72	0.60	0.42	0.38	0.32	0.38	0.41	0.41	0.41

1. Smooth walls ($\Delta = 0$) and $Re = \frac{w_0 D_0}{v} \geq 2 \cdot 10^5$:

$$\zeta = \frac{\Delta H}{\frac{\gamma w_0^2}{2g}} = \zeta_1 + \zeta_{fr},$$

where ζ_1 is determined from the curve $\zeta_1 = f\left(\frac{l_0}{D_0}\right)$ or $f\left(\frac{R_0}{D_0}\right)$:

$$\zeta_{fr} = \lambda \frac{l_0}{D_0}; \quad \text{at } \lambda \approx 0.02, \zeta_{fr} = 0.02 \frac{l_0}{D_0}.$$

2. Rough walls ($\Delta > 0$) and $Re \geq 2 \times 10^5$:

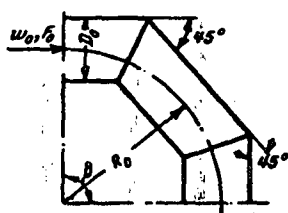
$$\zeta = \frac{\Delta H}{\frac{\gamma w_0^2}{2g}} = k_A k_{Re} \zeta_1 + \zeta_{fr},$$

where k_A and k_{Re} are taken by Table 6-4 of diagram 6-1;
 λ is determined by diagrams 2-2 to 2-5;
 v is taken from § 1-3, b;
 Δ is taken from Table 2-1.

90° elbow made from three elements at $\frac{R_0}{D_0} = 2.4$ welded (with welding seams), at $Re = \frac{w_0 D_0}{v} \geq 10^5$

Section VI

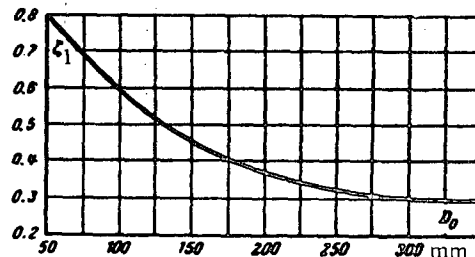
Diagram 6-16

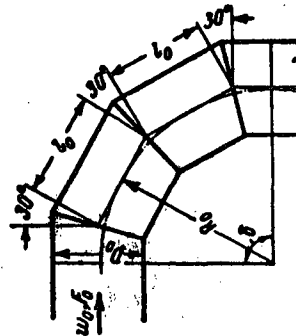


$$\zeta = \frac{\Delta H}{\frac{\gamma w_0^2}{2g}}$$

is determined from the curve $\zeta = f(D_0 \text{ mm})$;
 v is taken from § 1-3, b.

$D_0 \text{ mm}$	50	100	150	200	250	300	350
ζ	0.80	0.60	0.45	0.38	0.32	0.30	0.30





$\frac{l_o}{D_o}$	0	0.2	0.4	0.6	0.8	1.0	2.0	3.0	4.0	5.0	6.0
R_o/D_o	0	0.37	0.75	1.12	1.50	1.97	3.74	5.60	7.46	9.30	11.3
ζ_1	1.10	0.92	0.70	0.58	0.40	0.30	0.16	0.19	0.20	0.20	0.20

1. Smooth walls ($\Delta = 0$) and $Re = \frac{w_o D_h}{v} > 2 \cdot 10^5$:

$$\zeta = \frac{\Delta H}{\frac{\gamma w_o^2}{2g}} = \zeta_1 + \zeta_{fr},$$

where ζ_1 is determined from the curve $\zeta_1 = f\left(\frac{l_o}{D_o}\right)$ or $f\left(\frac{R_o}{D_o}\right)$;

$$\zeta_{fr} = 2\lambda \frac{l_o}{D_o}; \quad \text{at } \lambda \approx 0.02, \zeta_{fr} = 0.04 \frac{l_o}{D_o}.$$

2. Rough walls ($\Delta > 0$) and $Re \geq 2 \times 10^5$:

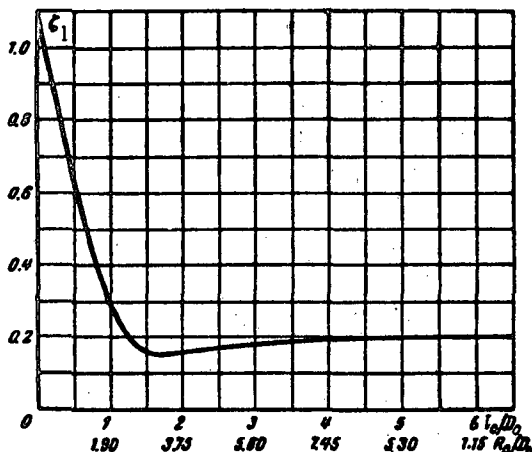
$$\zeta = \frac{\Delta H}{\frac{\gamma w_o^2}{2g}} = k_A k_{Re} \zeta_1 + \zeta_{fr},$$

where k_A and k_{Re} are taken from Table 6-4 of diagram 6-1;

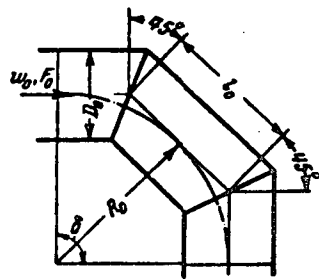
λ is determined by diagrams 2-2 to 2-5;

v is taken from § 1-3, b;

Δ is taken from Table 2-1.



90° elbow from three elements

Section VI
Diagram 6-15

$\frac{l_0}{D_0}$	0	0.2	0.4	0.6	0.8	1.0	2.0	3.0	4.0	5.0	6.0
R_0/D_0	0	0.24	0.48	0.70	0.97	1.20	2.35	3.60	4.60	6.00	7.25
ζ_1	1.10	0.95	0.72	0.60	0.42	0.38	0.32	0.38	0.41	0.41	0.41

1. Smooth walls ($\Delta = 0$) and $Re = \frac{w_0 D_0}{\nu} \geq 2 \cdot 10^5$:

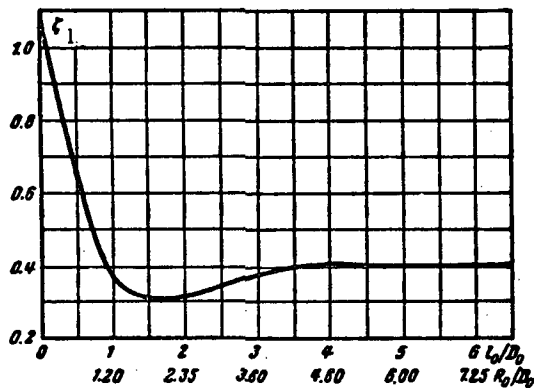
$$\zeta = \frac{\Delta H}{\frac{\gamma w_0^2}{2g}} = \zeta_1 + \zeta_{fr},$$

where ζ_1 is determined from the curve $\zeta_1 = f\left(\frac{l_0}{D_0}\right)$ or $f\left(\frac{R_0}{D_0}\right)$:

$$\zeta_{fr} = \lambda \frac{l_0}{D_0}; \quad \text{at } \lambda \approx 0.02, \zeta_{fr} = 0.02 \frac{l_0}{D_0}.$$

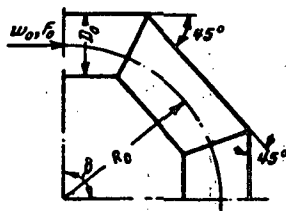
2. Rough walls ($\Delta > 0$) and $Re \geq 2 \times 10^5$:

$$\zeta = \frac{\Delta H}{\frac{\gamma w_0^2}{2g}} = k_A k_{Re} \zeta_1 + \zeta_{fr},$$

where k_A and k_{Re} are taken by Table 6-4 of diagram 6-1; λ is determined by diagrams 2-2 to 2-5; ν is taken from § 1-3, b; Δ is taken from Table 2-1.90° elbow made from three elements at $\frac{R_0}{D_0} = 2.4$ welded (with welding seams), at $Re = \frac{w_0 D_0}{\nu} \geq 10^5$

Section VI

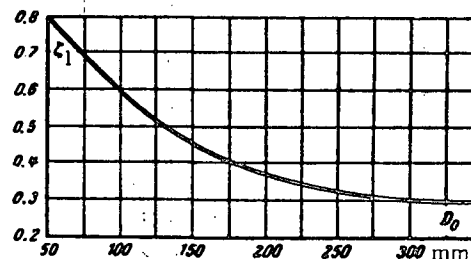
Diagram 6-16



$$\zeta = \frac{\Delta H}{\frac{\gamma w_0^2}{2g}}$$

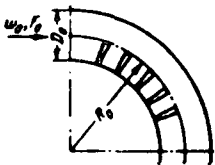
is determined from the curve $\zeta = f(D_0 \text{ mm})$;
 ν is taken from § 1-3, b.

$D_0 \text{ mm}$	50	100	150	200	250	300	350
ζ	0.80	0.60	0.45	0.38	0.32	0.30	0.30



Corrugated bend; $\frac{R_o}{D_0} \approx 2.5$; $Re = \frac{\omega_0 D_0}{\nu} > 2 \cdot 10^5$

Section VI
Diagram 6-17



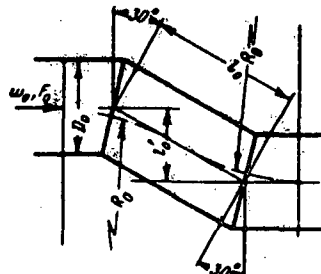
D_0 , mm	50	100	150	200	250	300	350
ζ	0.25	0.3	0.33	0.37	0.42	0.45	0.50

ν is taken from § 1-3,b.

$$\zeta = \frac{\Delta H}{\gamma \omega_0^2} \text{ is taken from the table.}$$

Z-shaped elbow made from two 30° elbows

Section VI
Diagram 6-18



1. Smooth walls ($\Delta = 0$) and $Re = \frac{\omega_0 D_h}{\nu} > 2 \cdot 10^5$:

$$\zeta = \frac{\Delta H}{\gamma \omega_0^2} = \zeta_1 + \zeta_{fr},$$

where ζ_1 is determined from the curve $\zeta_1 = f\left(\frac{l_0}{D_0}\right)$ or $f\left(\frac{R_0}{D_0}\right)$;

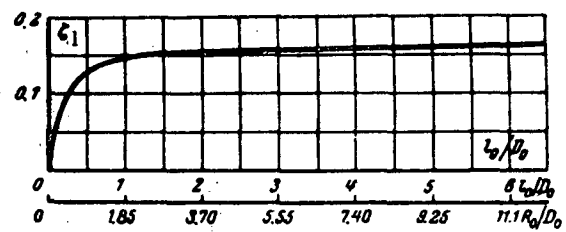
$$\zeta_{fr} = \lambda \frac{l_0}{D_0}; \text{ at } \lambda = 0.02 \quad \zeta_{fr} = 0.02 \frac{l_0}{D_0}.$$

2. Rough walls ($\Delta > 0$) and $Re \geq 2 \times 10^5$:

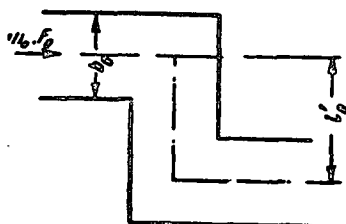
$$\zeta = \frac{\Delta H}{\gamma \omega_0^2} = k_A k_{Re} \zeta_1 + \zeta_{fr}.$$

where k_A and k_{Re} are taken from Table 6-4 of diagram 6-1;
 λ is determined by diagrams 2-2 to 2-5;
 ν is taken from § 1-3,b;
 Δ is taken from Table 2-1.

$\frac{l_0}{D_0}$	0	1.0	2.0	3.0	4.0	5.0	6.0
R_o/D_0	0	1.90	3.74	5.60	7.46	9.30	11.3
ζ_1	0	0.15	0.15	0.16	0.16	0.16	0.16



$$D_h = \frac{4F_0}{\Pi_0}; \quad \Pi_0 - \text{perimeter}$$



$\frac{l'_0}{b_0}$	0	0.4	0.6	0.8	1.0	1.2	1.4	1.6	1.8	2.0
ζ_1	0	0.62	0.90	1.61	2.63	3.61	4.01	4.18	4.22	4.18
$\frac{l'}{b_0}$	2.4	2.8	3.2	4.0	5.0	6.0	7.0	9.0	10.0	∞
ζ_1	3.65	3.30	3.20	3.08	2.92	2.80	2.70	2.60	2.45	2.30

1. Smooth walls ($\Delta = 0$) at any Re :

$$\xi = \frac{\Delta H}{\frac{\gamma w_0^2}{2g}} = C_1 \zeta_1 + \xi_{fr}$$

where ζ_1 is determined from the curve $\zeta_1 = f\left(\frac{l'_0}{b_0}\right)$;

C_1 is determined approximately from graph b of diagram 6-21;

$$\xi_{fr} = \lambda l'_0 / b_0 \quad \text{at } \lambda \approx 0.02, \quad \xi_{fr} = 0.02 \frac{l'_0}{b_0}.$$

2. Rough walls ($\Delta > 0$) (tentatively):

$$\xi = \frac{\Delta H}{\frac{\gamma w_0^2}{2g}} = k_A C_1 \zeta_1 + \xi_{fr}$$

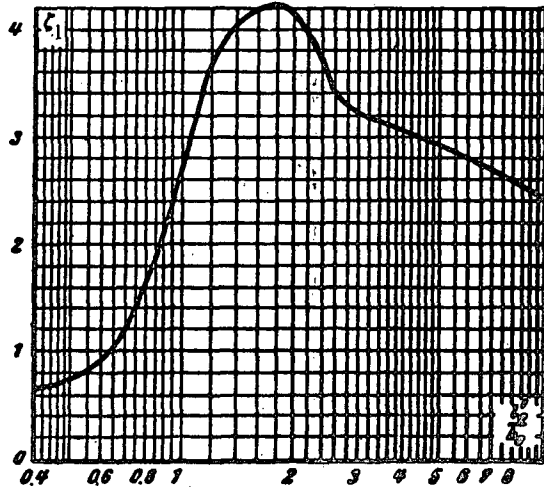
where k_A is calculated by the following expressions:

- a) $k_A = 1.0$ at $Re < 4 \cdot 10^4$;
- b) $k_A = 1 + 0.5 \cdot 10^{-3} \bar{\Delta}$ at $Re > 4 \cdot 10^4$ and $0 < \bar{\Delta} < 0.001$;
- c) $k_A \approx 1.5$ at $Re > 4 \cdot 10^4$ and $\bar{\Delta} > 0.001$;

$\bar{\Delta}$ is determined from diagrams 2-2 to 2-5;

w is taken from § 1-3, b;

Δ is taken from Table 2-1; $\bar{\Delta} = \frac{\Delta}{D_h}$.

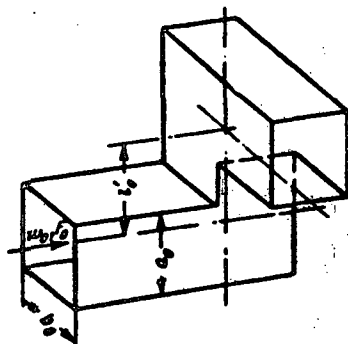


Combined elbow made from two 90° elbows lying in different planes. $Re = \frac{\omega_0 D_h}{v} > 10^4$

Section VI

Diagram 6-20

$$D_h = \frac{4F_0}{P_0}; P_0 - \text{perimeter}$$



$\frac{l'0}{b_0}$	0	0.4	0.6	0.8	1.0	1.2	1.4	1.6	1.8	2.0
ζ_1	1.15	2.40	2.90	3.31	3.44	3.40	3.36	3.28	3.20	3.11
$\frac{l'0}{b_0}$	2.4	2.8	3.2	4.0	5.0	6.0	7.0	9.0	10.00	∞
ζ_1	3.16	3.18	3.15	3.00	2.89	2.78	2.70	2.50	2.41	2.30

1. Smooth walls ($\Delta = 0$) at any Re :

$$\zeta = \frac{\Delta H}{\frac{\gamma \omega_0^2}{2g}} = C_1 \zeta_1 + \zeta_{fr},$$

where ζ_1 is determined from the curve $\zeta_1 = f\left(\frac{l'0}{b_0}\right)$;

C_1 is determined tentatively from graph b of diagram 6-21;

$$\zeta_{fr} = \lambda \frac{l'0}{b_0}; \quad \text{at } \lambda \approx 0.02, \quad \zeta_{fr} = 0.02 \frac{l'0}{D_h}.$$

2. Rough walls ($\Delta > 0$) (tentatively):

$$\zeta = \frac{\Delta H}{\frac{\gamma \omega_0^2}{2g}} = k_A C_1 \zeta_1 + \zeta_{fr},$$

where k_A is calculated by the following expressions:

a) $k_A = 1.0$ at $Re < 4 \cdot 10^4$;

b) $k_A = 1 + 0.5 \cdot 10^3 \bar{\Delta}$ at $Re > 4 \cdot 10^4$ and $0 < \bar{\Delta} < 0.001$;

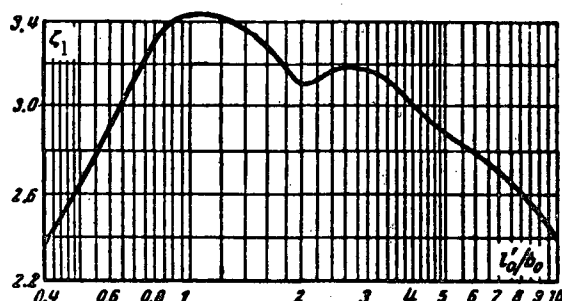
c) $k_A \approx 1.5$ at $Re > 4 \cdot 10^4$ and $\bar{\Delta} >$

λ is determined from diagrams 2-2 to 2-5;

v is taken from § 1-3, b;

Δ is taken from Table 2-1;

$$\bar{\Delta} = \frac{\Delta}{D_h}.$$



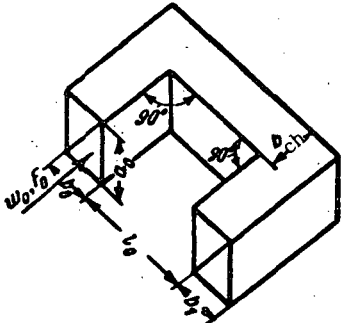
Π-shaped elbow (180°) with equal inlet and exit sections

$$\left(\frac{F_1}{F_0} = \frac{b_1}{b_0} = 1.0 \right), \quad Re = \frac{w_0 D_h}{v} > 4 \cdot 10^4$$

Section VI

Diagram 6-21

$$D_h = \frac{4F_0}{\Pi_0}; \quad \Pi_0 - \text{perimeter}$$



1. Smooth walls ($\Delta = 0$) at any Re :

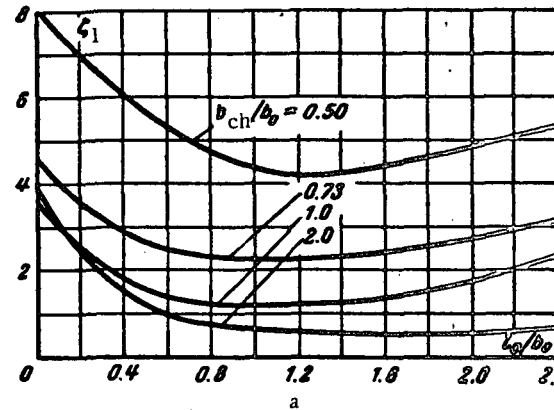
$$\zeta = \frac{\Delta H}{\frac{1}{2} w_0^2} = C_1 \zeta_1 + \zeta_{fr}$$

where ζ_1 is determined from the curves $\zeta_1 = f\left(\frac{l_0}{b_0}, \frac{b_{ch}}{b_0}\right)$ of graph a;

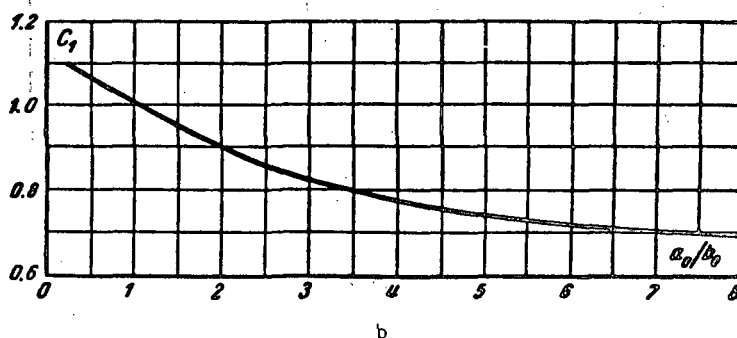
$$\zeta_{fr} = \lambda \left(1 + \frac{l_0}{b_0}\right); \quad \text{at } \lambda \approx 0.02, \quad \zeta_{fr} = 0.02 + 0.02 \frac{l_0}{b_0};$$

C_1 is determined tentatively from the curve $C_1 = f\left(\frac{a_0}{b_0}\right)$ of graph b.

a/b_0	0	0.2	0.4	0.6	0.8	1.0	1.2	1.4	1.6	1.8	2.0	2.4
1. $b_{ch}/b_0 = 0.5$												
ζ_1	7.9	6.9	6.1	5.4	4.7	4.3	4.2	4.3	4.4	4.6	4.8	5.3
2. $b_{ch}/b_0 = 0.73$												
ζ_1	4.5	3.6	2.9	2.5	2.4	2.3	2.3	2.3	2.4	2.6	2.7	3.2
3. $b_{ch}/b_0 = 1.0$												
ζ_1	3.6	2.5	1.8	1.4	1.3	1.2	1.2	1.3	1.4	1.5	1.6	2.3
4. $b_{ch}/b_0 = 2.0$												
ζ_1	3.9	2.4	1.5	1.0	0.8	0.7	0.7	0.6	0.6	0.6	0.6	0.7



$\frac{a_0}{b_0}$	0.25	0.50	0.75	1.0	1.5	2.0	3.0	4.0	5.0	6.0	7.0	8.0
C_1	1.10	1.07	1.04	1.00	0.95	0.90	0.83	0.78	0.75	0.72	0.71	0.70



2. Rough walls ($\Delta > 0$) (tentatively):

$$\zeta = \frac{\Delta H}{\frac{1}{2} w_0^2} = k_d C_1 \zeta_1,$$

where: a) $k_d = 1.0$ at $Re < 4 \cdot 10^4$;
b) $k_d = 1 + 0.5 \cdot 10^3 \bar{\Delta}$ at $Re > 4 \cdot 10^4$ and
 $0 < \bar{\Delta} < 0.001$;
c) $k_d \approx 1.5$ at $Re > 4 \cdot 10^4$ and $\bar{\Delta} > 0.001$

$\bar{\Delta}$ is determined from diagrams 2-2 to 2-5 as a function of Re and $\bar{\Delta}$:

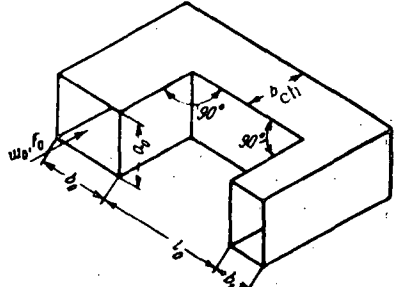
v is taken from § 1-3, b;

Δ is taken from Table 2-1; $\bar{\Delta} = \frac{\Delta}{D_h}$

$$D_{\text{h}} = \frac{4F_0}{\Pi_0}; \quad \Pi_0 = \text{perimeter}$$

1. Smooth walls ($\Delta = 0$) at any $Re = \frac{w_0 D_h}{v}$ and $\frac{l_0}{b_0} < 1.0$:

$$\zeta = \frac{\Delta H}{\gamma w_0^2 / 2g} = C_1 \zeta_1 + \zeta_{\text{fr}},$$



where ζ_1 is determined from the curves $\zeta_1 = f\left(\frac{a_0}{b_0}\right)$ of graph a; C_1 is determined tentatively from graph c) of diagram 6-21; $\zeta_{\text{fr}} = \lambda\left(1 + \frac{l_0}{b_0}\right)$; at $\lambda = 0.02$

$$\zeta_{\text{fr}} = 0.02 + 0.02 \frac{l_0}{b_0}$$

2. Smooth walls ($\Delta = 0$), $Re < 2 \cdot 10^5$ and $\frac{l_0}{b_0} \geq 1.0$:

$$\zeta = k_{\text{Re}} C_1 \zeta_1 + \zeta_{\text{fr}},$$

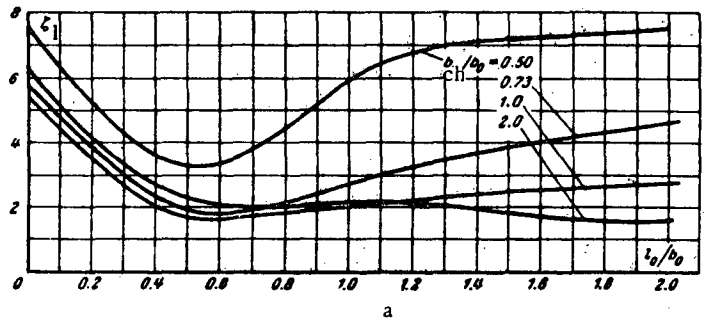
where k_{Re} is determined from the curve $k_{\text{Re}} = f(\text{Re})$ of graph b.

3. Rough walls ($\Delta > 0$) (tentatively):

$$\zeta = \frac{\Delta H}{\gamma w_0^2 / 2g} = k_{\Delta} k_{\text{Re}} C_1 \zeta_1 + \zeta_{\text{fr}},$$

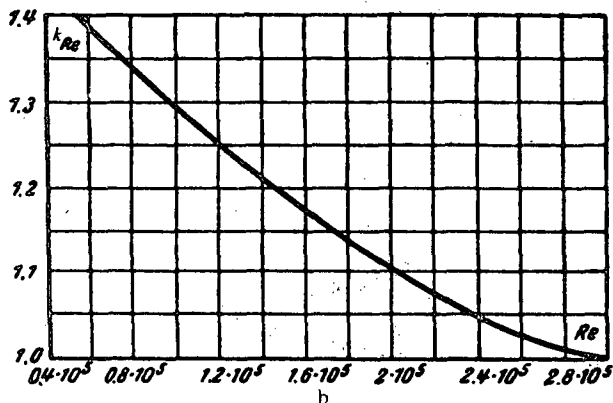
where k_{Δ} and k_{Re} are calculated by the following expressions:

- a) $k_{\text{Re}} = 1.0$ for all Re and $l_0/b_0 < 1.0$;
- b) k_{Re} is taken from graph b for $Re < 2 \cdot 10^5$ and $l_0/b_0 > 1.0$;
- c) $k_{\Delta} = 1.0$ for $Re < 4 \cdot 10^4$;
- d) $k_{\Delta} = 1 + 0.5 \cdot 10^3 \Delta$ for $Re > 4 \cdot 10^4$ and $0 < \Delta < 0.001$;
- e) $k_{\Delta} \approx 1.5$ for $Re > 4 \cdot 10^4$ and $\Delta > 0.001$;
- λ is determined from diagrams 2-2 to 2-5;
- v is taken from § 1-3, b;
- Δ is taken from Table 2-1; $\Delta = \frac{\Delta}{D_h}$.



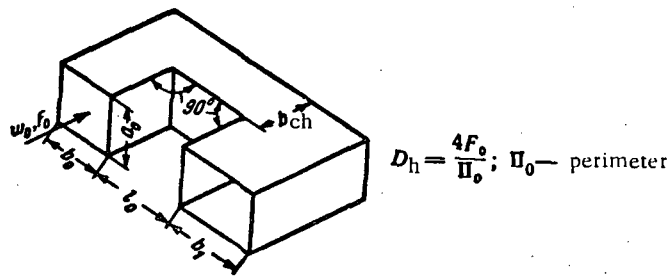
a

Re	$0.4 \cdot 10^5$	$0.8 \cdot 10^5$	$1.2 \cdot 10^5$	$1.6 \cdot 10^5$	$2.0 \cdot 10^5$	$2.4 \cdot 10^5$	$2.8 \cdot 10^5$
k_{Re}	1.45	1.34	1.26	1.17	1.10	1.05	1.0



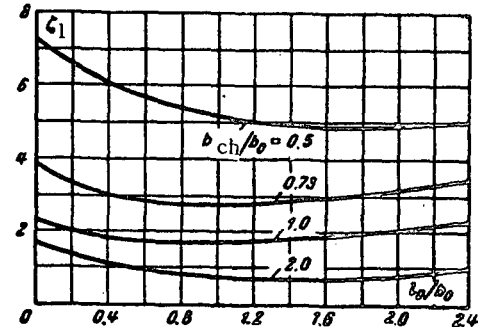
b

l_0/b_0	0	0.2	0.4	0.6	0.8	1.0	1.2	1.4	1.6	1.8	2.0
1) $b_{\text{ch}}/b_0 = 0.5$	7.5	5.2	3.6	3.4	4.5	6.0	6.7	7.1	7.3	7.5	7.6
2) $b_{\text{ch}}/b_0 = 0.73$	5.8	3.8	2.4	1.9	2.2	2.7	3.3	3.7	4.0	4.3	4.7
3) $b_{\text{ch}}/b_0 = 1.0$	5.5	3.5	2.1	1.7	1.9	2.1	2.3	2.4	2.6	2.7	2.7
4) $b_{\text{ch}}/b_0 = 2.0$	6.3	4.2	2.7	2.1	2.1	2.2	2.2	2.0	2.0	1.8	1.6



$$D_h = \frac{4F_0}{\Pi_0}; \Pi_0 - \text{perimeter}$$

l_0/b_0	0.0	0.2	0.4	0.6	0.8	1.0	1.2	1.4	1.6	1.8	2.0
ζ_1	7.3	6.6	6.1	5.7	5.4	5.2	5.1	5.0	4.9	4.9	5.0
	2) $b_{ch}/b_0 = 0.73$										
ζ_1	3.9	3.3	3.0	2.9	2.8	2.8	2.8	2.9	2.9	3.0	3.2
	3) $b_{ch}/b_0 = 1.0$										
ζ_1	2.3	2.1	1.9	1.8	1.7	1.7	1.8	1.8	1.9	2.0	2.1
	4) $b_{ch}/b_0 = 2.0$										
ζ_1	1.7	1.4	1.2	1.0	0.9	0.8	0.8	0.7	0.7	0.8	0.8



1. Smooth walls ($\Delta = 0$) at any $Re = \frac{w_0 D_h}{v}$:

$$\zeta = \frac{\Delta H}{\frac{\gamma w_0^2}{2g}} = C_1 \zeta_1 + \zeta_{fr},$$

where ζ_1 is determined from the curves $\zeta_1 = f\left(\frac{l_0}{b_0}\right)$ corresponding to different values of $\frac{b_{ch}}{b_0}$;

C_1 is determined tentatively from graph b of diagram 6-21;

$$\zeta_{fr} = \lambda \left(1 + \frac{l_0}{b_0} \right);$$

at $\lambda \approx 0.02$:

$$\zeta_{fr} = 0.02 + 0.02 \frac{l_0}{b_0}.$$

2. Rough walls ($\Delta > 0$) (tentatively):

$$\zeta = \frac{\Delta H}{\frac{\gamma w_0^2}{2g}} = k_A C_1 \zeta_1 + \zeta_{fr},$$

where k_A is calculated by the following expressions:

- a) $k_A = 1.0$ at $Re < 4 \cdot 10^4$;
- b) $k_A = 1 + 0.5 \cdot 10^3 \bar{\Delta}$ at $Re > 4 \cdot 10^4$ and $0 < \bar{\Delta} < 0.001$;
- c) $k_A \approx 1.5$ at $Re > 4 \cdot 10^4$ and $\bar{\Delta} > 0.001$;

λ is determined from diagrams 2-2 to 2-5;

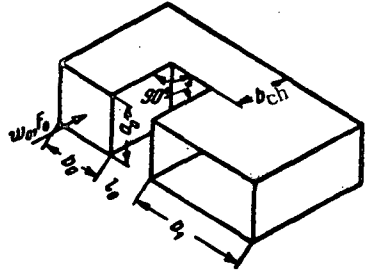
v is taken from § 1-3, b;

Δ is taken from Table 2-1; $\bar{\Delta} = \frac{\Delta}{D_h}$.

Π -shaped elbow (180°) with widened exit section ($\frac{F_1}{F_0} = \frac{b_1}{b_0} = 2.0$)

Section VI
Diagram 6-24

$$D_h = \frac{4F_0}{\Pi_0}; \quad \Pi_0 - \text{perimeter}$$



$\frac{l_0}{b_0}$	0.0	0.2	0.4	0.6	0.8	1.0	1.2	1.4	1.6	1.8	2.0
1) $b_{ch}/b_0 = 0.5$											
ζ_1	8.4	7.8	7.3	6.8	6.3	5.9	5.6	5.3	5.2	5.0	4.9
	2) $b_{ch}/b_0 = 0.73$										
ζ_1	4.1	3.9	3.8	3.6	3.5	3.4	3.2	3.1	3.0	3.0	2.9
	3) $b_{ch}/b_0 = 1.0$										
ζ_1	2.5	2.5	2.4	2.3	2.2	2.1	2.0	2.0	1.9	1.9	1.9
	4) $b_{ch}/b_0 = 2.0$										
ζ_1	1.2	1.1	1.0	1.0	0.9	0.9	0.8	0.8	0.8	0.9	0.9

1. Smooth walls ($\Delta = 0$) at any $Re = \frac{\omega_0 D_h}{v}$:

$$\zeta = \frac{\Delta H}{\frac{\gamma w_0^2}{2g}} = C_1 \zeta_1 + \zeta_{fr},$$

where ζ_1 is determined tentatively from the curves $\zeta_1 = f(l_0/b_0)$ corresponding to different $\frac{b_{ch}}{b_0}$;

C_1 is determined from graph b of diagram 6-21;

$$\zeta_{fr} = \lambda \left(1 + \frac{l_0}{b_0} \right);$$

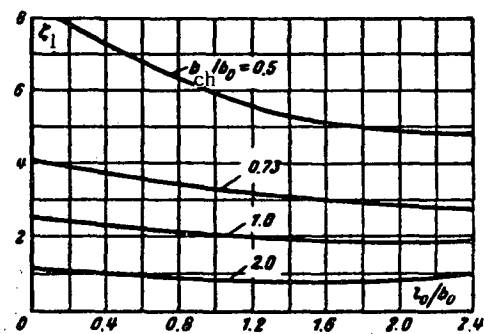
$$\text{at } \lambda \approx 0.02: \quad \zeta_{fr} = 0.02 + 0.02 \frac{l_0}{b_0}.$$

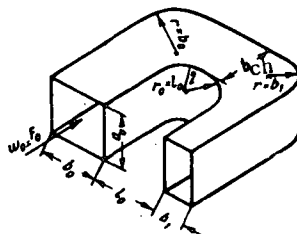
2. Rough walls ($\Delta > 0$) (tentatively):

$$\zeta = \frac{\Delta H}{\frac{\gamma w_0^2}{2g}} = k_A C_1 \zeta_1 + \zeta_{fr},$$

where k_A is calculated by the following expressions:

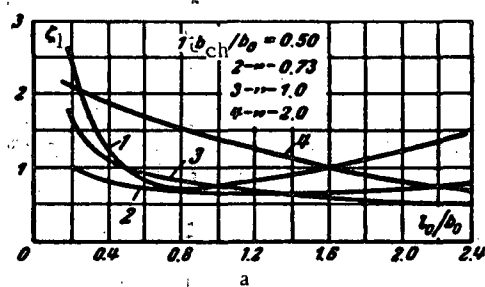
- a) $k_A = 1.0$ at $Re < 4 \cdot 10^4$;
 - b) $k_A = 1 + 0.5 \cdot 10^3 \bar{\Delta}$ at $Re > 4 \cdot 10^4$ and $0 < \bar{\Delta} < 0.001$;
 - c) $k_A \approx 1.5$ at $Re > 4 \cdot 10^4$ and $\bar{\Delta} > 0.001$;
- λ is determined from diagrams 2-2 to 2-5;
 v is taken from § 1-3, b;
 Δ is taken from Table 2-1; $\bar{\Delta} = \frac{\Delta}{D_h}$.



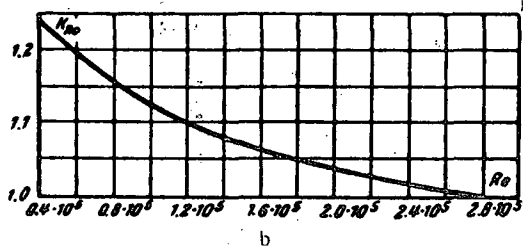


$$D_h = \frac{4F_0}{\Pi_0}; \quad \Pi_0 = \text{perimeter}$$

l_0/b_0	0.2	0.4	0.6	0.8	1.0	1.2	1.4	1.6	1.8	2.0
1) $\frac{b_{ch}}{b_0} = 0.5$										
ζ_1	2.6	1.3	0.8	0.7	0.7	0.8	0.9	1.0	1.1	1.2
2) $\frac{b_{ch}}{b_0} = 0.73$										
ζ_1	1.1	0.8	0.7	0.7	0.6	0.6	0.6	0.7	0.7	0.7
3) $\frac{b_{ch}}{b_0} = 1.0$										
ζ_1	1.8	1.1	0.9	0.8	0.8	0.7	0.6	0.6	0.6	0.5
4) $\frac{b_{ch}}{b_0} = 2.0$										
ζ_1	2.1	1.9	1.7	1.5	1.4	1.3	1.1	1.0	1.9	1.8



Re	$0.4 \cdot 10^5$	$0.8 \cdot 10^5$	$1.2 \cdot 10^5$	$1.6 \cdot 10^5$	$2.0 \cdot 10^5$	$2.4 \cdot 10^5$	$2.8 \cdot 10^5$
k_{Re}	1.24	1.16	1.11	1.07	1.04	1.02	1.0



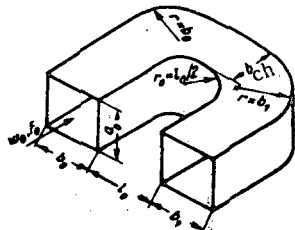
U-shaped elbow (180°) with equal inlet and exit sections

$$\left(\frac{F_1}{F_0} - \frac{b_1}{b_0} = 1.0 \right)$$

Section VI

Diagram 6-26

$$D_h = \frac{4P_0}{\Pi_0}; \quad \Pi_0 = \text{perimeter}$$



l_0/b_0	0.2	0.4	0.6	0.8	1.0	1.2	1.4	1.6	1.8	2.0
-----------	-----	-----	-----	-----	-----	-----	-----	-----	-----	-----

 1) $b_{ch}/b_0 = 0.5$

ζ_1	4.5	2.6	1.9	1.7	1.5	1.3	1.2	1.1	1.0	0.9
-----------	-----	-----	-----	-----	-----	-----	-----	-----	-----	-----

 2) $b_{ch}/b_0 = 0.75$

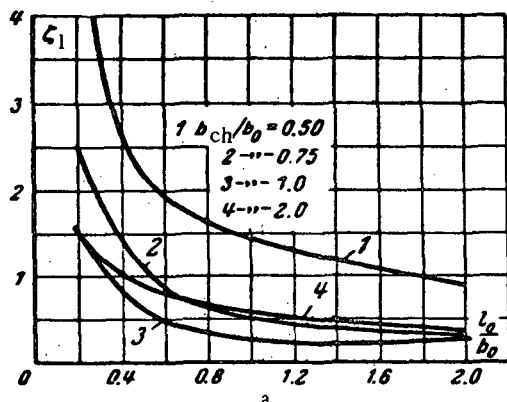
ζ_1	2.5	1.5	0.9	0.7	0.5	0.5	0.4	0.4	0.4	0.3
-----------	-----	-----	-----	-----	-----	-----	-----	-----	-----	-----

 3) $b_{ch}/b_0 = 1.0$

ζ_1	1.6	0.9	0.5	0.3	0.3	0.3	0.2	0.2	0.2	0.3
-----------	-----	-----	-----	-----	-----	-----	-----	-----	-----	-----

 4) $b_{ch}/b_0 = 2.0$

ζ_1	1.6	1.0	0.8	0.7	0.6	0.5	0.5	0.4	0.4	0.4
-----------	-----	-----	-----	-----	-----	-----	-----	-----	-----	-----



Re	$0.4 \cdot 10^5$	$0.8 \cdot 10^5$	$1.2 \cdot 10^5$	$1.6 \cdot 10^5$	$2.0 \cdot 10^5$	$2.4 \cdot 10^5$	$2.8 \cdot 10^5$
------	------------------	------------------	------------------	------------------	------------------	------------------	------------------

 1) $b_1/b_0 = 1.0; l_0/b_0 \leq 0.3$

k_{Re}	1.24	1.16	1.11	1.07	1.04	1.02	1.0
----------	------	------	------	------	------	------	-----

 2) $b_1/b_0 = 1.0; l_0/b_0 > 0.3$

k_{Re}	1.35	1.25	1.18	1.12	1.07	1.04	1.0
----------	------	------	------	------	------	------	-----

 1. Smooth walls ($\Delta = 0$) at $Re = \frac{w_0 D_h}{v} \geq 2 \cdot 10^5$;

$$\zeta = \frac{\Delta H}{\gamma w_0^2} = C_1 \zeta_1 + \zeta_{fr},$$

where ζ_1 is determined from the curves $\zeta_1 = f\left(\frac{l_0}{b_0}\right)$ of graph a;
 C_1 is determined tentatively from graph b of diagram 6-21;

$$\zeta_{fr} = \lambda \left(1 + \frac{l_0}{b_0} \right);$$

at $\lambda \approx 0.02, \zeta_{fr} = 0.02 + 0.02 \frac{l_0}{b_0}$.

 2. Smooth ($\Delta = 0$) and rough ($\Delta > 0$) walls at any Re :

$$\zeta = \frac{\Delta H}{\gamma w_0^2} = k_A k_{Re} C_1 \zeta_1 + \zeta_{fr},$$

where k_A and k_{Re} are calculated by the following expressions (tentatively):

 a) $k_{Re} = 1.0$ at $Re \geq 2 \cdot 10^5$;

 b) k_{Re} is taken from curve 1 of graph b for $Re < 2 \cdot 10^5$

 and $\frac{l_0}{b_0} \leq 0.3$;

 c) k_{Re} is taken from curve 2 of graph b for $Re < 2 \cdot 10^5$

 and $\frac{l_0}{b_0} > 0.3$;

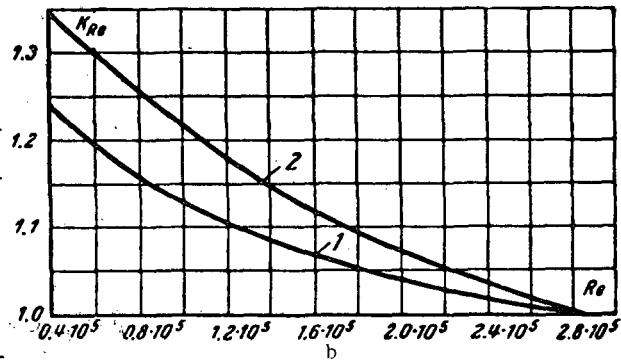
 d) $k_A = 1.0$ for $Re \leq 4 \cdot 10^4$;

 e) $k_A = 1 + 1.5 \cdot 10^3 \bar{\Delta}$ for $Re > 4 \cdot 10^4$ and $0 < \bar{\Delta} < 0.001$;

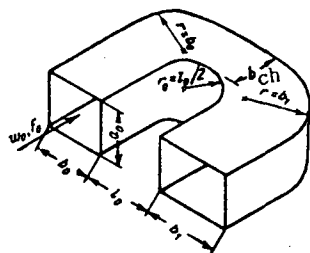
 f) $k_A \approx 1.5$ for $Re > 4 \cdot 10^4$ and $\bar{\Delta} > 0.001$;

λ is determined from diagrams 2-2 to 2-5;

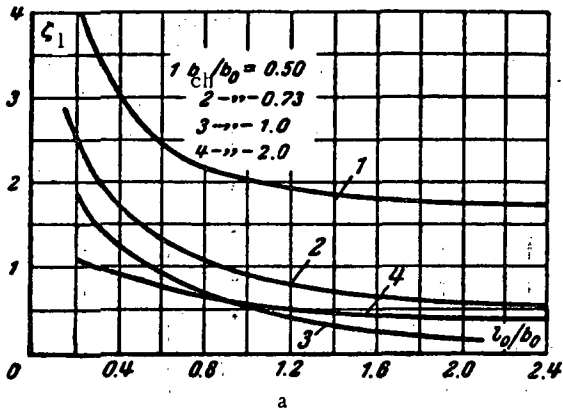
ν is taken from § 1-3, b;

 Δ is taken from Table 2-1; $\bar{\Delta} = \frac{\Delta}{D_h}$.


$$D_h = \frac{4P_0}{B_0}; B_0 - \text{perimeter}$$



l_0/b_0	0.2	0.4	0.6	0.8	1.0	1.2	1.4	1.6	1.8	2.0
1) $b_{ch}/b_0 = 0.5$										
ζ_1	4.2	3.1	2.5	2.2	2.0	1.9	1.9	1.8	1.8	1.8
2) $b_{ch}/b_0 = 0.75$										
ζ_1	2.8	1.8	1.4	1.1	0.9	0.8	0.8	0.7	0.7	0.7
3) $b_{ch}/b_0 = 1.0$										
ζ_1	1.9	1.3	0.9	0.7	0.5	0.4	0.3	0.3	0.2	0.2
4) $b_{ch}/b_0 = 2.0$										
ζ_1	1.2	0.9	0.8	0.7	0.6	0.5	0.4	0.4	0.4	0.4



Re	$0.4 \cdot 10^5$	$0.8 \cdot 10^5$	$1.2 \cdot 10^5$	$1.6 \cdot 10^5$	$2.0 \cdot 10^5$	$2.4 \cdot 10^5$	$2.8 \cdot 10^5$
k_{Re}	1.24	1.16	1.11	1.07	1.04	1.02	1.0

1. Smooth walls ($\Delta = 0$) at any Re and $\frac{l_0}{b_0} < 0.5$:

$$\zeta = \frac{\Delta H}{\frac{1}{2} g} = C_s \zeta_1 + \zeta_{fr},$$

where ζ_1 is determined from the curves $\zeta_1 = f\left(\frac{l_0}{b_0}\right)$ of graph a;

C_s is determined from graph b of diagram 6-21;

$$\zeta_{fr} = \lambda \left(1 + \frac{l_0}{b_0}\right);$$

$$\text{at } \lambda \approx 0.02: \quad \zeta_{fr} = 0.02 + 0.02 \frac{l_0}{b_0}.$$

2. Smooth walls ($\Delta = 0$) at $Re < 2 \cdot 10^5$ and $\frac{l_0}{b_0} \geq 0.5$:

$$\zeta = \frac{\Delta H}{\frac{1}{2} g} = k_{Re} C_s \zeta_1 + \zeta_{fr},$$

where k_{Re} is determined tentatively from the curve $k_{Re} = f(Re)$ of graph b.

3. Rough walls ($\Delta > 0$) (tentatively):

$$\zeta = \frac{\Delta H}{\frac{1}{2} g} = k_A k_{Re} C_s \zeta_1 + \zeta_{fr},$$

where k_A and k_{Re} are calculated by the following expressions:

a) $k_{Re} = 1.0$ at any Re and $\frac{l_0}{b_0} < 0.5$

b) k_{Re} is determined from graph b for $Re < 2 \cdot 10^5$ and $\frac{l_0}{b_0} > 0.5$;

c) $k_A = 1.0$ for $Re < 4 \cdot 10^4$;

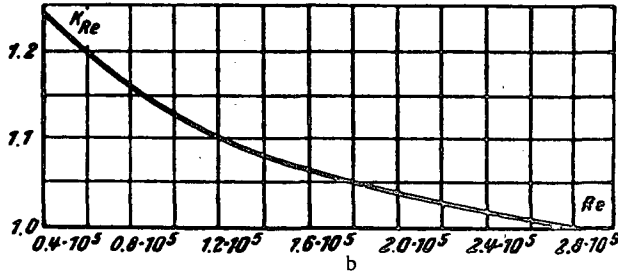
d) $k_A = 1 + 0.5 \cdot 10^3 \Delta$ for $Re > 4 \cdot 10^4$ and $0 < \Delta < 0.001$;

e) $k_A \approx 1.5$ for $Re > 4 \cdot 10^4$ and $\Delta > 0.001$;

λ is determined from diagrams 2-2 to 2-5;

ν is taken from § 1-3, b;

Δ is taken from Table 2-1; $\Delta = \frac{\Delta}{D_h}$.



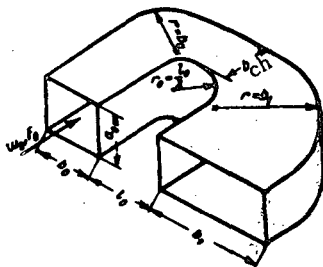
U-shaped elbow (180°) with widened exit section

$$\left(\frac{F_1}{F_c} = \frac{b_1}{b_c} = 20 \right), \text{Re} = \frac{w_0 D_h}{v} \geq 10^4$$

Section VI

Diagram 6-28

$$D_h = \frac{4F_0}{\Pi_0}; \quad \Pi_0 = \text{perimeter}$$


 1. Smooth walls ($\Delta = 0$) at any Re:

$$\zeta = \frac{\Delta H}{\frac{1}{2} w_0^2} = C_1 \zeta_1 + \zeta_{fr},$$

 where ζ_1 is determined from the curves

$$\zeta_1 = f\left(\frac{l_c}{b_c}\right)$$

 corresponding to different b_{ch}/b_o ;

 C_1 is determined tentatively by graph b of diagram 6-21;

$$\zeta_{fr} = \lambda \left(1 + \frac{l_o}{b_o} \right);$$

$$\text{at } \lambda \approx 0.02, \quad \zeta_{fr} = 0.02 + 0.02 \frac{l_o}{b_o}.$$

 2. Rough walls ($\Delta > 0$) (tentatively):

$$\zeta = \frac{\Delta H}{\frac{1}{2} w_0^2} = k_A C_1 \zeta_1 + \zeta_{fr},$$

 where k_A is calculated by the following expressions:

$$\text{a)} k_A = 1.0 \text{ at } \text{Re} < 4 \cdot 10^4;$$

$$\text{b)} k_A = 1 + 0.5 \cdot 10^3 \bar{\Delta} \text{ at } \text{Re} > 4 \cdot 10^4 \text{ and } 0 < \bar{\Delta} < 0.001;$$

$$\text{c)} k_A \approx 1.5 \text{ at } \text{Re} > 4 \cdot 10^4 \text{ and } \bar{\Delta} > 0.001;$$

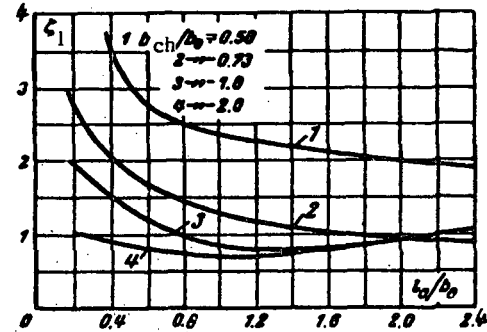
 λ is determined from diagrams 2-2 to 2-5;

 v is taken from § 1-3, b;

 Δ is taken from Table 2-1;

$$\bar{\Delta} = \frac{\Delta}{D_h}.$$

l_o/b_o	0.2	0.4	0.6	0.8	1.0	1.2	1.4	1.6	1.8	2.0
1) $b_{ch}/b_o = 0.5$										
ζ_1	6.0	3.5	2.8	2.5	2.4	2.3	2.2	2.1	2.1	2.0
2) $b_{ch}/b_o = 0.73$										
ζ_1	2.9	2.1	1.7	1.5	1.3	1.2	1.1	1.0	1.0	0.9
3) $b_{ch}/b_o = 1.0$										
ζ_1	2.0	1.6	1.2	1.0	0.9	0.8	0.8	0.8	0.9	0.9
4) $b_{ch}/b_o = 20$										
ζ_1	1.0	0.9	0.8	0.7	0.7	0.7	0.7	0.8	0.9	0.9

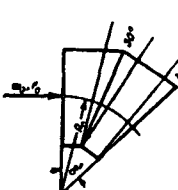
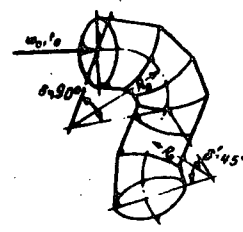
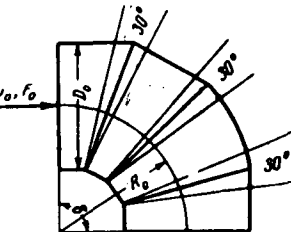
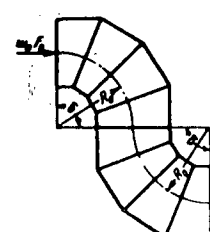
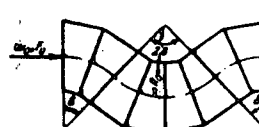


Parts made from galvanized sheet for $\frac{R_o}{D_o} = 1.0$; $D_o = 100$ mm

Section VI

$$Re = \frac{\omega_o D_o}{\nu} \geq 1.5 \cdot 10^4$$

Diagram 6-29

Type	Schematic diagram	Resistance coefficient $\zeta = \frac{\Delta H}{\frac{1}{2} \rho v^2}$	Type	Schematic diagram	Resistance coefficient $\zeta = \frac{\Delta H}{\frac{1}{2} \rho v^2}$
Elbow $\delta' = 45^\circ$		0.60	Offset $\delta + \delta' = 90^\circ + 45^\circ$		1.50
Elbow $\delta = 90^\circ$		0.92	Offset $2\delta = 2 \times 90^\circ$		1.60
Gooseneck $2\delta = 2 \times 90^\circ$		2.16	By-pass $4\delta' = 4 \times 45^\circ$		2.65

ν is taken from § 1-3, b.

Corrugated elbows made from galvanized sheet for

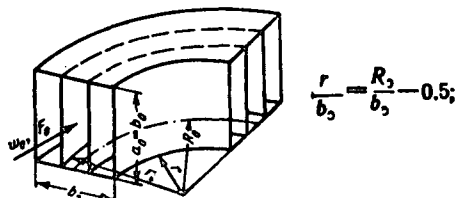
Section VI

$$\frac{R_e}{D_0} = 0.7; D_0 = 100 \text{ mm. } Re = \frac{\rho v D_0}{\mu} > 1.5 \cdot 10^4$$

Diagram 6-30

Type	Schematic diagram	Resistance coefficient $\xi = \frac{\Delta H}{T^2 D^2 / 2g}$	Type	Schematic diagram	Resistance coefficient $\xi = \frac{\Delta H}{T^2 D^2 / 2g}$
Elbow $\delta' = 45^\circ$		0.53	Offset $\delta + \delta' = 90^\circ + 45^\circ$		1.93
Elbow $2\delta' = 2 \times 45^\circ$		0.82			
Elbow $\delta = 90^\circ$		1.33	Offset $\delta = 2 \times 90^\circ$		2.56
Gooseneck $2\delta' = 2 \times 45^\circ$		1.00	By-pass $4\delta' = 4 \times 45^\circ$		2.38
Gooseneck $2\delta = 2 \times 90^\circ$		3.30			

is taken from § 1-3, b.



$$\frac{r_v}{b_0} = \frac{R_2}{b_0} - 0.5;$$

$$\zeta = \frac{\Delta H}{\frac{1}{2} w_0^2} = \zeta_1 + \zeta_{fr},$$

where ζ_1 is determined from the curve $\zeta_1 = f\left(\frac{R_2}{b_0}\right)$ or approximately by the formula

$$\zeta_1 = \left(0.46 \frac{R_0}{b_0} - 0.04\right) \zeta_{w.v.}$$

$$\zeta_{fr} = 1.57 \frac{R_0}{b_0} \lambda$$

$$\text{at } \lambda \approx 0.02; \quad \zeta_{fr} = 0.031 \frac{R_0}{b_0};$$

$\zeta_{w.v.}$ is determined as ζ for a bend without vanes from the data of diagram 6-1;

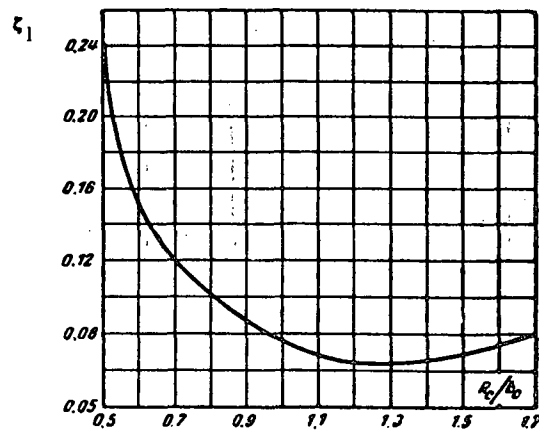
λ is determined from diagrams 2-2 to 2-5;

v is taken from § 1-3,b;

The distance between the vanes is determined by the formula

$$r_i = 1.26 r_{i-1} + 0.07 b_0.$$

$\frac{R_2}{b_0}$	0.5	0.6	0.7	0.8	0.9	1.0	1.1	1.3	1.5
ζ_1	0.24	0.15	0.12	0.10	0.09	0.08	0.07	0.06	0.07

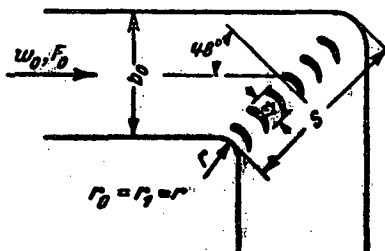


90° elbow of rectangular section at different $\frac{r}{b_0}$ with airfoil guide vanes*. $Re = \frac{w_0 b_0}{v} \geq 10^4$

Section VI

Diagram 6-32

$$r_0 = r_1 = r, \quad t = r\sqrt{2}$$



r/b_0	0	0.1	0.2	0.3	0.4	0.5	0.6
ζ_1	1) n_{norm} 0.33 0.23 0.17 0.16 0.17 0.22 0.31						
ζ_1	2) n_{opt} 0.33 0.23 0.15 0.11 0.13 0.19 0.30						
ζ_1	3) n_{min} 0.45 0.33 0.27 0.22 0.17 0.15 0.17						

1. Normal number of vanes

$$n_{\text{norm}} = 2.13 \left(\frac{r}{b_0}\right)^{-1} - 1 = 2.13 \frac{S}{t_1} - 1.$$

2. Reduced (optimum) number of vanes

$$n_{\text{opt}} \approx 1.4 \left(\frac{r}{b_0}\right)^{-1} = 1.4 \frac{S}{t_1}.$$

3. Minimum number of vanes

$$n_{\text{min}} \approx 0.9 \left(\frac{r}{b_0}\right)^{-1} = 0.9 \frac{S}{t_1};$$

$$\zeta = \frac{\Delta H}{\frac{7w_0^2}{2g}} = \zeta_1 + \zeta_{\text{fr}},$$

where ζ_1 is determined from the curve $\zeta_1 = f\left(\frac{r}{b_0}\right)$;

$$\zeta_{\text{fr}} = (1 + 1.57r/b_0)\lambda;$$

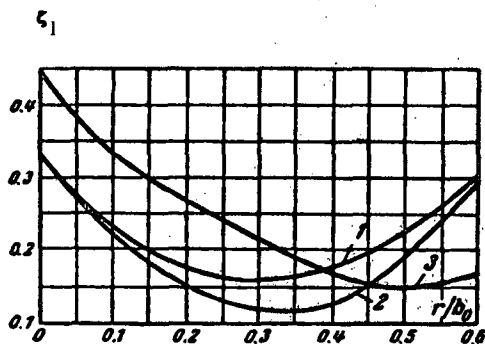
$$\text{at } \lambda \approx 0.02, \quad \zeta_{\text{fr}} = 0.02 + 0.031 \frac{r}{b_0};$$

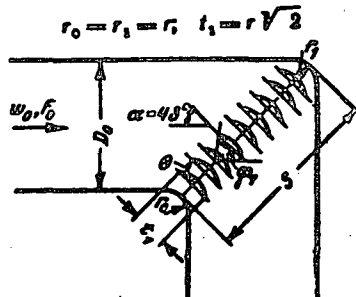
λ is determined from diagrams 2-2 to 2-5;

v is taken from § 1-3, b;

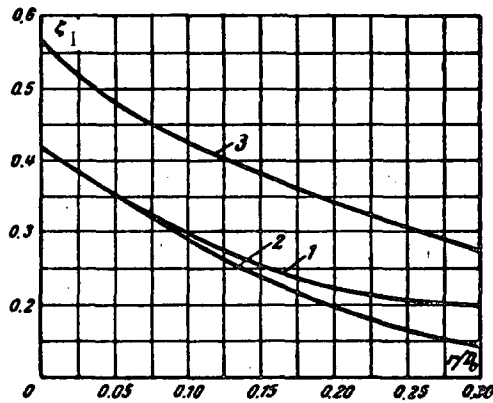
Δ is taken from Table 2-1.

* For location and design of the vanes cf. points 33 and 36 of § 6-2.





r/b_0	0	0.05	0.10	0.15	0.20	0.25	0.30
1) n_{norm}							
ζ_1	0.42 0.35 0.30 0.26 0.23 0.21 0.20						
2) n_{opt}							
ζ_1	0.42 0.35 0.30 0.24 0.20 0.17 0.14						
3) n_{min}							
ζ_1	0.57 0.48 0.43 0.39 0.35 0.31 0.28						



1. Normal number of vanes

$$n_{\text{norm}} = 2.13 \left(\frac{r}{b_0} \right)^{-1} - 1 = 2.13 \frac{S}{t_1} - 1.$$

2. Reduced (optimum) number of vanes

$$n_{\text{m.ad}} \approx 1.4 \left(\frac{r}{b_0} \right)^{-1} = 1.4 \frac{S}{t_1}.$$

3. Minimum number of vanes

$$n_{\text{min}} \approx 0.9 \left(\frac{r}{b_0} \right)^{-1} = 0.9 \frac{S}{t_1}.$$

$$\zeta = \frac{\Delta H}{\frac{\gamma w_0^2}{2g}} = \zeta_1 + \zeta_{\text{fr}},$$

where ζ_1 is determined by the curves $\zeta_1 = f \left(\frac{r}{b_0} \right)$ tentatively:

$$\zeta_{\text{fr}} = \left(1 + 1.57 \frac{r}{b_0} \right) \lambda;$$

$$\text{at } \lambda \approx 0.02, \quad \zeta_{\text{fr}} = 0.02 + 0.031 \frac{r}{b_0};$$

λ is determined from diagrams 2-2 to 2-5;
 λ is taken from § 1-3, b.

* For location of the vanes cf. point 36 of § 6-2.

90° elbow of rectangular section with thin guide vanes*

(θ₁ = 95°) under different conditions. Re = $\frac{w_0 b_0}{v} \geq 10^4$

Section VI

Diagram 6-34

No.	Elbow characteristic	Schematic diagram	Resistance coefficient $t = \frac{\Delta H}{\frac{T w_0^2}{2g}}$
1	Sharp inner corner ($t_1 = 0$); $\alpha = 45^\circ$; normal number of vanes: $n = 2.13 \frac{S}{t_1} - 1$		$\zeta = 0.45 + \lambda$ at $\lambda \approx 0.02$: $\zeta = 0.47$ λ is determined by diagrams 2-2 to 2-5
2	The same as in No. 1, but $\alpha = 50^\circ$		$\zeta = 0.40 + \lambda$ at $\lambda \approx 0.02$: $\zeta = 0.42$
3	The same as in No. 1 but reduced (optimum) number of vanes: $n \approx 1.4S/t_1$		$\zeta = 0.36 + \lambda$ at $\lambda \approx 0.02$: $\zeta = 0.38$
4	The same as in No. 1, but the inner corner is cut off ($t_1 = 0.25b_0$)		$\zeta = 0.32 + 1.28\lambda$ at $\lambda \approx 0.02$: $\zeta = 0.35$
5	Elbow with widening $(\frac{F_1}{F_0} = 1.35)$ $\frac{r}{b_0} = 0.18$; $\alpha \approx 53^\circ$. normal number of vanes: $n = 2.13 \frac{S}{t_1} - 1$		$\zeta = 0.40 + 1.28\lambda$ at $\lambda \approx 0.02$: $\zeta = 0.43$
6	The same as in No. 5, but reduced (minimum) number of vanes: $n \approx 0.9 \frac{S}{t_1}$		$\zeta = 0.60 + 1.28\lambda$ at $\lambda \approx 0.02$: $\zeta = 0.63$

* is taken from § 1-3, b.

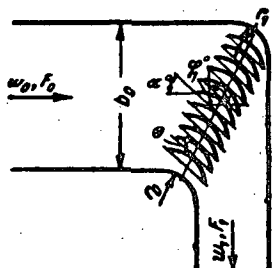
* For location of the vanes cf. point 36 of § 6-2.

90° smooth elbow ($\frac{r}{b_0} = 0.2$) of rectangular section at $\frac{F_1}{F_0} = 0.5$
with thin guide vanes ($\varphi_1 = 103^\circ$). $Re = \frac{w_0 b_0}{v} \geq 10^4$

Section VI

Diagram 6-35

$$r_0 = r_1 = r$$



Number of vanes (optimum)

$$n_{\text{opt}} = 11$$

$$\zeta = \frac{\Delta H}{\gamma w_0^2} = \zeta_1 + \zeta_{fr}; \\ \frac{2g}{\Delta H}$$

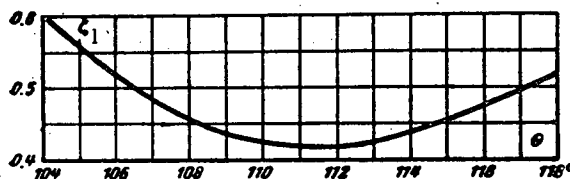
ζ_1 is determined from the curve $\zeta_1 = f(0^\circ)$

$$\zeta_{fr} = \lambda \left(1 + 1.57 \frac{r}{b_0} \right);$$

$$\text{at } \lambda \approx 0.02 \quad \zeta_{fr} = 0.02 + 0.031 \frac{r}{b_0};$$

λ is determined from diagrams 2-2 to 2-5.
 v is taken from § 1-3, b.

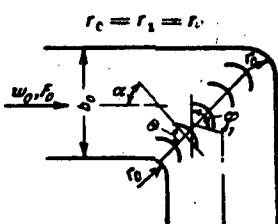
θ°	106	108	110	112	114	116	118
ζ_1	0.52	0.46	0.43	0.42	0.44	0.48	0.52



90° smooth elbow ($\frac{r}{b_0} = 0.2$) of rectangular section at $\frac{F_1}{F_0} = 1.0$
with thin guide vanes ($\varphi_1 = 107^\circ$). $Re = \frac{w_0 b_0}{v} \geq 10^4$

Section VI

Diagram 6-36



θ°	82	84	86	88	90	92	94	96	98
ζ_1	0.50	0.30	0.22	0.17	0.14	0.12	0.11	0.12	0.14

Number of vanes (optimum)

$$n_{\text{opt}} = 5;$$

$$\zeta = \frac{\Delta H}{\gamma w_0^2} = \zeta_1 + \zeta_{fr}; \\ \frac{2g}{\Delta H}$$

where ζ_1 is determined from the curve $\zeta_1 = f(0^\circ)$

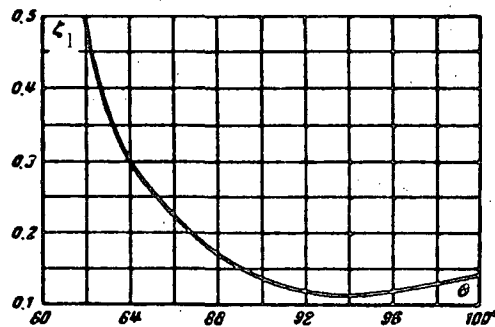
$$\zeta_{fr} = \lambda \left(1 + 1.57 \frac{r}{b_0} \right);$$

at $\lambda \approx 0.02$:

$$\zeta_{fr} = 0.02 + 0.031 \frac{r}{b_0};$$

λ is determined from diagrams 2-2 to 2-5.

v is taken from § 1-3, b.

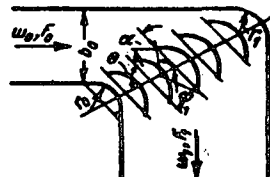


90° elbow of rectangular section at $\frac{F_1}{F_0} = 2.0$ with
thin guide vanes. $Re = \frac{\omega_0 b_0}{v} \geq 10^4$

Section VI

Diagram 6-37

$$r_c = r_s = r$$



Number of vanes (optimum)

$$n_{\text{opt}} = 2 \text{ to } 5;$$

$$\zeta = \frac{\Delta H}{\frac{1}{2} \rho v_0^2} = \zeta_1 + \zeta_{\text{fr}}$$

where ζ_1 is determined from the curves $\zeta_1 = f(\theta^\circ)$

$$\zeta_{\text{fr}} = \left(1 + 1.57 \frac{r}{b_0} \right) \lambda;$$

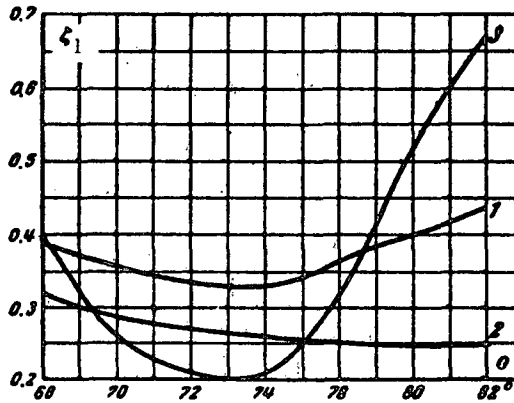
at $\lambda \approx 0.02$,

$$\zeta_{\text{fr}} = 0.02 + 0.031 \frac{r}{b_0};$$

λ is determined from diagrams 2-2 to 2-5;

v is taken from § 1-3, b.

θ°	68	70	72	74	76	78	80	82
ζ	1) $r/b_0 = 0.2; \varphi_1 = 154^\circ; n = 5$ 0.39 0.36 0.34 0.33 0.34 0.37 0.40 0.44							
ζ	2) $r/b_0 = 0.5; \varphi_1 = 138^\circ; n = 2$ 0.32 0.29 0.27 0.26 0.26 0.25 0.25 0.25							
ζ	3) $r/b_0 = 1.0; \varphi_1 = 90^\circ; n = 5$ 0.40 0.26 0.21 0.21 0.25 0.32 0.52 0.67							

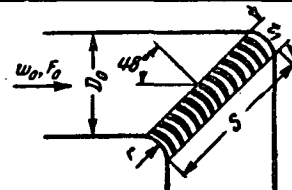
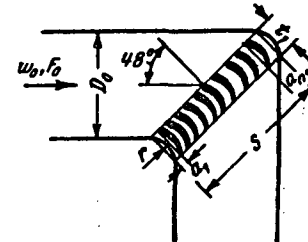
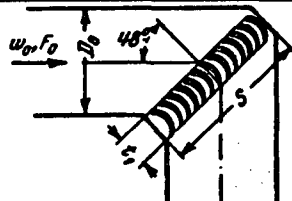
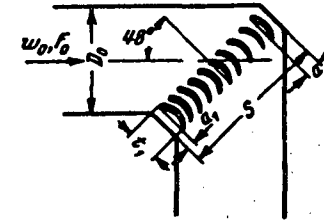
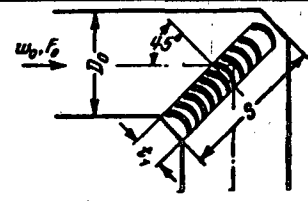


90° elbow of circular section with airfoil guide vanes*.

Section VI

$$Re = \frac{w_0 D_0}{v} \geq 10^4$$

Diagram 6-38

No.	Elbow characteristic	Schematic diagram	Resistance coefficient $\zeta = \frac{\Delta H}{\frac{1}{2} \rho v_0^2}$
1	Smooth turn ($\frac{r}{D_0} = 0.18$) normal number of vanes $n = \frac{3D_0}{t_1} - 1$		$\zeta = 0.23 + 1.28\lambda$ at $\lambda \approx 0.02$, $\zeta = 0.26$ λ is determined from diagrams 2-2 to 2-5
2	Smooth turn ($\frac{r}{D_0} = 0.18$); reduced number of vanes $n = \frac{2D_0}{t_1}$ vanes set according to an arithmetic progression with $\frac{a_{n+1}}{a_1} = 2$		$\zeta = 0.15 + 1.28\lambda$ at $\lambda \approx 0.02$, $\zeta = 0.18$
3	Cut-off corners ($\frac{t_1}{D_0} = 0.25$); normal number of vanes $n = \frac{3D_0}{t_1} - 1$		$\zeta = 0.30 + 1.28\lambda$ at $\lambda \approx 0.02$, $\zeta = 0.33$
4	Cut-off corners ($\frac{t_1}{D_0} = 0.25$); reduced number of vanes $n = \frac{2D_0}{t_1}$ vanes set according to an arithmetic progression with $\frac{a_{n+1}}{a_1} = 2$		$\zeta = 0.23 + 1.28\lambda$ at $\lambda \approx 0.02$, $\zeta = 0.26$
5.	Cut-off corners ($\frac{t_1}{D_0} = 0.25$); reduced number of vanes (the first and third vanes from the outer wall left out)	 <p>* is taken from § 1-3, b.</p>	$\zeta = 0.21 + 1.28\lambda$ at $\lambda \approx 0.02$, $\zeta = 0.24$

* For the location and design of the vanes cf. points 33 and 36 of § 6-2.

Section Seven
STREAM JUNCTIONS AND DIVISIONS
(Resistance coefficients of wyes, tees, and crosses)

7-1. LIST OF SYMBOLS

- F_b, F_s = areas of the cross section of the branch, and the main passage, respectively, m^2 .
- F_c = area of the common channel, m^2 ;
- D_b, D_s = diameters (or sides) of the cross sections of the branch and the main passage, respectively, m;
- D_c = diameter (or side) of the common channel, m;
- D_h = hydraulic diameter of the cross section, m;
- α = branching angle, or divergence angle of the diffuser;
- w_b, w_s = mean velocities in the branch, and the main passage, respectively, m/sec ;
- w_c = mean velocity in the common channel, m/sec ;
- Q_b, Q_s = discharges through the branch, and the main passage, respectively, m^3/sec ;
- Q_c = discharge through the common channel, m^3/sec ;
- ΔH = pressure loss (resistance), kg/m^2 ;
- $\Delta H_b, \Delta H_s$ = pressure losses (resistance) in the branch and the main passage, respectively, kg/m^2 ;
- ζ = resistance coefficient;
- ζ_b, ζ_s = resistance coefficients of the branch, and of the main passage, expressed in terms of the respective velocity;
- $\zeta_{c,b}, \zeta_{c,s}$ = resistance coefficients of the branch and the main passage expressed in terms of the velocity in the common channel.

7-2. EXPLANATIONS AND RECOMMENDATIONS

1. Two basic types of wyes are treated in the handbook:
 - a) wyes in which the sum of the cross-section areas of the branch and the main passage are equal to the cross sections of the common channel: $F_b + F_s = F_c$ (Figure 7-1, a and b);
 - b) wyes in which this sum is larger than the area of the common section: $F_b + F_s > F_c$, with $F_s = F_c$ (Figure 7-1, c)*.
2. Physically, each wye is characterized by a branching angle α and ratios of the cross sections of its three outlets: $\frac{F_s}{F_c}, \frac{F_b}{F_c}$, and $\frac{F_b}{F_s}$. The ratios of discharges $\frac{Q_s}{Q_c}$ and $\frac{Q_b}{Q_c}$ and the corresponding ratios of velocities $\frac{w_s}{w_c}$ and $\frac{w_b}{w_c}$, may vary in every case. All wyes can function with the flow directed either toward or away from the main passage.

* Standard wyes are not treated here due to lack of sufficient data.

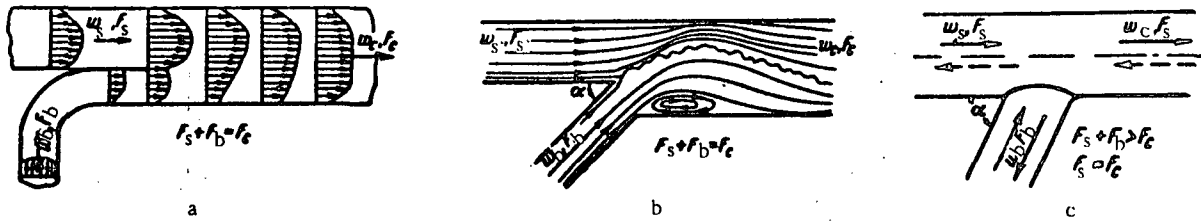


FIGURE 7-1. Plan of the junction of two streams:

a —junction of parallel streams; $f_s + f_b = f_c$; b—junction of streams at an angle; $f_s + f_b = f_c$; c—junction of streams at an angle; $f_s + f_b > f_c$; $f_s = f_c$.

The resistance coefficients of converging wyes are functions of all these parameters. The resistance coefficients of diverging wyes of standard shape are functions of the branching angle α and the velocity ratios $\frac{w_s}{w_c}$ and $\frac{w_b}{w_c}$ only.

The resistance coefficient of wyes of rectangular section is almost independent of the side ratio of their cross section.

3. The junction of two parallel streams moving at different velocities (Figure 7-1, a) is characterized by turbulent mixing of the streams, accompanied by pressure losses. In the course of this mixing an exchange of momentum takes place between the particles moving at different velocities, finally resulting in the equalization of the velocity distributions in the common stream. The jet with higher velocity loses a part of its kinetic energy by transmitting it to the slower moving jet.

The loss in total pressure before and after mixing is always large and positive for the higher-velocity jet, and increases with an increase in the amount of energy transmitted to the lower-velocity jet. Consequently, the resistance coefficient, which is defined as the ratio of the difference of total pressures to the mean dynamic pressures in the given section, will likewise be always positive. As to the lower-velocity jet, the energy stored in it increases as a result of mixing. The loss in total pressure and the resistance coefficient can, therefore, also have negative values for the lower-velocity jet.

4. Generally, junctions are more complex than shown in Figure 7-1, a; the branch makes usually a certain angle α with the common channel (Figure 7-1, b and c). In this case losses due to curving of the stream are added to the losses at mixing. These losses are mainly due to stream separation from the inner wall, which leads to contraction of the jet at the point of turn and its subsequent expansion (Figure 7-1, b). The contraction and expansion of the jet take place after the junction of the two streams, and therefore influence the losses in the branch and main passage.

5. If the branches are conical instead of cylindrical, losses due to the stream expansion in the diffuser part are added to these losses.

In general, the losses in a converging wyes mainly consist of:

- losses due to turbulent mixing of two streams with different velocities;
- losses due to the curving of the stream at its passage from the branch into the common channel;
- losses due to the stream expansion in the diffuser part.

6. The flow pattern in a diverging wye varies with the ratio of velocities $\frac{w_b}{w_s}$ or of discharges $\frac{Q_b}{Q_s}$ /7-15/.

If $Q_b < Q_s$, a wide eddy zone is formed after the stream entrance into the branch. This phenomenon is partially due to the diffuser effect, i.e., to the existence of a considerable positive pressure gradient at the point of stream branching, where the total section area increases sharply compared with the area of the common channel. This high pressure gradient also produces a partial separation of the stream from the opposite straight wall (Figure 7-2, a). The two zones of stream separation from the wall create local jet contractions in both branch and main passage, followed by an expansion of the stream.

At $Q_b \geq Q_s$ the stream separates even more markedly from the outer wall of the main channel. The phenomenon of stream separation from the branch wall also takes place passage. (Figure 7-2, b).

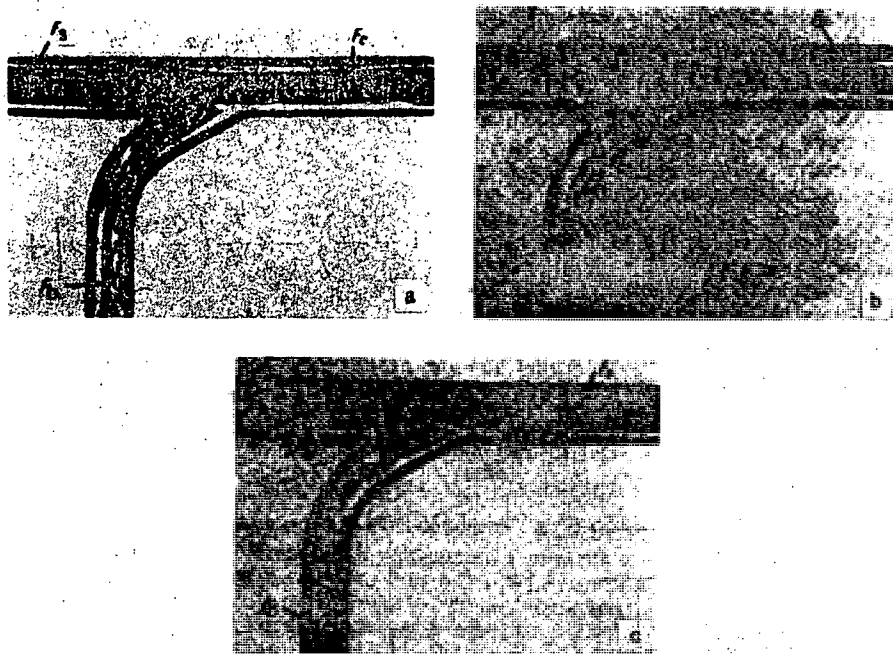


FIGURE 7-2. Flow patterns in diverging wyes:

a - $Q_b < Q_s$; b - $Q_b \geq Q_s$; c - $Q_b = 0$.

At $Q_b = 0$ an eddy zone forms at the branch inlet (Figure 7-2, c), which causes a local contraction and subsequent expansion of the jet entering the straight passage.

7. The losses in a diverging wye usually consist of:

- shock loss accompanying a sudden expansion at the point of flow branching;
- losses due to stream curving along the branch and the accompanying shock in the straight passage.

The resistance coefficient of the straight passage can have a negative value at certain values of the discharges ratio $\frac{Q_b}{Q_c}$, which means an energy increase can occur in this passage. This is caused by the branch receiving a larger share of the slowly moving boundary layer than of the high-velocity core at a stream division. Hence, the energy of unit volume of the medium moving in the main channel will be higher than of unit volume moving in the branch. The energy increase in the main passage is accompanied

by an increase of losses in the branch, so that the whole flow will be accompanied by irreversible pressure losses.

8. The resistance coefficients of converging wyes of normal shape can be calculated by the formulas obtained by Levin /7-5, 7-6/, and later in a somewhat different form by Taliev /7-17/. Correction coefficients have been introduced in these formulas which bring the theoretical results into agreement with the experimental results of Levin /7-6/, Kinne /7-22/, Petermann /7-26/, and Vogel /7-28/.

a. Branch

$$\zeta_{c,b} = \frac{\Delta H_b}{\frac{\gamma w_c^2}{2g}} = A \left[1 + \left(\frac{w_b}{w_c} \right)^2 - 2 \frac{F_s}{F_c} \left(\frac{w_s}{w_c} \right)^2 - 2 \frac{F_b}{F_c} \left(\frac{w_b}{w_c} \right)^2 \cos \alpha \right] + K_b. \quad (7-1)$$

or

$$\zeta_{c,s} = \frac{\Delta H_b}{\frac{\gamma w_c^2}{2g}} = A \left[1 + \left(\frac{Q_b}{Q_c} \cdot \frac{F_c}{F_b} \right)^2 - 2 \frac{F_c}{F_s} \left(1 - \frac{Q_b}{Q_c} \right)^2 - 2 \frac{F_c}{F_b} \left(\frac{Q_b}{Q_c} \right)^2 \cos \alpha \right] + K_b. \quad (7-2)$$

The value of A for wyes of the type $F_s + F_b > F_c$; $F_s = F_c$ is taken from Table 7-1, and the value of K_b is assumed to be zero; the value of A for wyes of the type $F_s + F_b = F_c$ is taken as unity, and the value of K_b from Table 7-2.

TABLE 7-1

a) $\alpha=0-60^\circ$					
$\frac{F_b}{F_c}$	0—0.2	0.3—0.4	0.6	0.8	1.0
A	1.0				
b) $\alpha=90^\circ$					
A	1.0	0.75	0.70	0.65	0.60

TABLE 7-2

α°	0.10		0.20		0.33		0.5	
	K_b	K_s	K_b	K_s	K_b	K_s	K_b	K_s
15°	0	0	0	0	0	0.14	0	0.40
30°	0	0	0	0	0	0.17	0	0.35
45°	0	0.05	0	0.14	0	0.14	0	0.30
60°	0	0	0	0	0	0.10	0.10	0.25
90°	0	0	0.10	0	0.20	0	0.25	0

b. Constant-section main passage

$$\zeta_{c,s} = \frac{\Delta H_s}{\frac{\gamma w_c^2}{2g}} = 1 + \left(\frac{w_s}{w_c} \right)^2 - 2 \frac{F_s}{F_c} \left(\frac{w_s}{w_c} \right)^2 - 2 \frac{F_b}{F_c} \left(\frac{w_b}{w_c} \right)^2 \cos \alpha + K_s, \quad (7-3)$$

or

$$\zeta_{c,s} = \frac{\Delta H_s}{\frac{\gamma w_c^2}{2g}} = 1 + \left(\frac{F_b}{F_s} \right)^2 \left(1 - \frac{Q_b}{Q_c} \right)^2 - 2 \frac{F_c}{F_s} \left(1 - \frac{Q_b}{Q_c} \right)^2 - 2 \frac{F_c}{F_b} \left(\frac{Q_b}{Q_c} \right)^2 \cos \alpha + K_s. \quad (7-4)$$

The value of K_s for wyes of the type $F_s + F_b > F_c$; $F_s = F_c$ is taken as zero; the value of K_s for wyes of the type $F_s + F_b = F_c$ is taken from Table 7-2.

c. Conical main passage

Here the resistance coefficient ζ_d of the diffuser part is added to the values $\zeta_{c,s}$ obtained by (7-3) or (7-4).

$$\zeta_d = \frac{\Delta H}{\frac{\gamma w_c^2}{2g}} = \varphi_{exp} \left(1 - \frac{1}{n_1}\right)^2 \times \left(1 - \frac{Q_b}{Q_c}\right)^2 \left(\frac{F_c}{F_s}\right)^2 + \zeta_{fr}. \quad (7-5)$$

where $n_1 = \frac{F'_s}{F_s} = \frac{F_1}{F_0}$ = area ratio of the diffuser portion of the passage; φ_{exp} = coefficient of shock, determined from the data of diagrams 5-2 to 5-4; ζ_{fr} = friction coefficient of conical part, determined from the data of the same diagrams.

9. The resistance coefficient of diverging wyes of normal shape can be calculated by the following formulas of Levin /7-7/ and Taliev /7-17/, which contain correction coefficients obtained from the comparison with the experimental data of Levin /7-7/, Kinne /7-22/, Petermann /7-26/, and Vogel /7-28/.

a. Branch

$$\zeta_{c,b} = \frac{\Delta H}{\frac{\gamma w_c^2}{2g}} = A' \left[1 + \left(\frac{w_b}{w_c} \right)^2 - 2 \frac{w_b}{w_c} \cos \alpha \right] - K_b \left(\frac{w_b}{w_c} \right)^2. \quad (7-6)$$

or

$$\zeta_{c,b} = \frac{\Delta H_b}{\frac{\gamma w_c^2}{2g}} = A' \left[1 + \left(\frac{Q_b}{Q_c} \cdot \frac{F_c}{F_b} \right)^2 - 2 \frac{Q_b}{Q_c} \cdot \frac{F_c}{F_b} \cos \alpha \right] - K'_s \left(\frac{Q_b}{Q_c} \cdot \frac{F_c}{F_b} \right)^2. \quad (7-7)$$

where according to Levin's data $K_b = \frac{1-2\mu}{\mu^2} \sin^2 \alpha$; μ is the jet contraction coefficient according to Levin.

The value of K_b for wyes of the type $F_s + F_b > F_c$, $F_s = F_c$ is assumed to be zero, and the value of A' as 1.0 for $\frac{w_b}{w_c} < 0.8$, and as roughly 0.9 for $\frac{w_b}{w_c} > 0.8$.

For wyes of the type $F_s + F_b = F_c$, $A' = 1.0$ and the value of K'_s is taken from Table 7-3.

TABLE 7-3

α°	15°	30°	45°	60°	90°
K'_b	0.04	0.16	0.36	0.64	1.0

b. Constant-section main passage

For wyes of the type $F_s + F_b > F_c$; $F_s = F_c$ (within the limits $\frac{w_s}{w_c} \leq 1.0$)

$$\zeta_{c,s} = \frac{\Delta H_s}{\frac{1}{2} w_c^2} \approx 0.4 \left(1 - \frac{w_s}{w_c}\right)^2; \quad (7-8)$$

for wyes of the type $F_s + F_b = F_c$, $\zeta_{c,s}$ is determined over the complete range of $\frac{w_s}{w_c}$ from the curves $\zeta_{c,s} = f\left(\frac{w_s}{w_c}\right)$ of diagram 7-23.

c. Conical main passage

In this case the resistance coefficient ζ_d calculated by (7-5) is added to the values $\zeta_{c,s}$ obtained by formula (7-8) or by diagram 7-23.

The recommended formulas and the corresponding values of the resistance coefficients given in section VII, can be used for all values of Reynolds number $Re = \frac{w_c D_h}{v} \geq 10^4$.

10. Since the resistance coefficient of diverging wyes of normal shape is independent of the area ratios $\frac{F_s}{F_c}$ and $\frac{F_b}{F_c}$, generalized curves can be plotted for this coefficient as

a function of $\frac{w_s}{w_c}$ or $\frac{w_b}{w_c}$, which is impossible in respect to $\frac{Q_s}{Q_c}$ or $\frac{Q_b}{Q_c}$. This is why the resistance coefficients are in some cases given in this section as $\zeta_{c,b} = f\left(\frac{w_b}{w_c}\right)$ and $\zeta_{c,s} = f\left(\frac{w_s}{w_c}\right)$ although most curves are given as $\zeta_{c,s} = f\left(\frac{Q_s}{Q_c}\right)$ and $\zeta_{c,b} = f\left(\frac{Q_b}{Q_c}\right)$.

11. The resistance coefficients of wyes are often expressed through the mean velocity in the corresponding branch. These resistance coefficients are connected with the resistance coefficients expressed through the velocity in the common channel by the following expressions:

$$\zeta_b = \frac{\Delta H_b}{\frac{1}{2} w_b^2} = \frac{\zeta_{c,b}}{\left(\frac{w_b}{w_c}\right)^2} = \frac{\zeta_{c,b}}{\left(\frac{Q_b}{Q_c} \cdot \frac{F_c}{F_b}\right)^2} \quad (7-9)$$

and

$$\zeta_s = \frac{\Delta H_s}{\frac{rw_c^2}{2g}} = \left(\frac{w_s}{w_c} \right)^2 = \frac{\zeta_{c,s}}{\left(1 - \frac{Q_b}{Q_c} \right)^2 \left(\frac{F_c}{F_s} \right)^2}. \quad (7-10)$$

12. The resistance of wyes of normal shape can be considerably reduced by rounding the junction between the branch and the main passage. With converging wyes, only the outside corner has to be rounded (r_1 , Figure 7-3). On the other hand, with diverging wyes both corners have to be rounded (r_1 , Figure 7-3); which makes the flow more stable and reduced the possibility of stream separation near the inner corner (r_2).

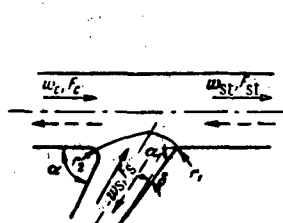


FIGURE 7-3. Improved Y.

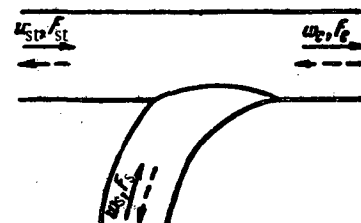


FIGURE 7-4. Y with smooth bend.

A very efficient method for reducing resistance of both converging and diverging wyes is the use of a diffuser in the branch. Here the losses are reduced by reducing the flow velocity in the diverging section, and reducing the true branch angle of the turn ($\alpha_s < \alpha$, Figure 7-3). Together, the rounding of corners and widening of the branch, will give a still larger reduction of the branch resistance.

A minimum resistance is achieved in wyes where the branch is smoothly bent (Figure 7-4); such branches, with small branch angles should be used wherever possible.

13. In gas-heating and water lines the pipes are screwed into wyes [or tees] of larger diameter, so that the inner surface of the pipe does not coincide with the inner surface of the fitting and forms an annular protuberance (Figure 7-5), which increases the resistance of the fitting.

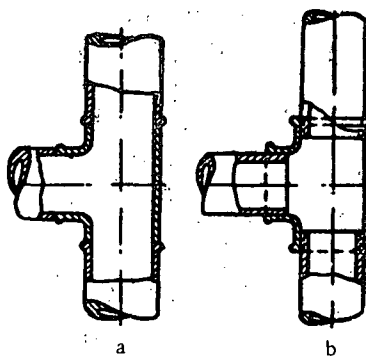


FIGURE 7-5. Annular protuberance in a standard tee.

a — welded tee; b — tee with screwed pipes.

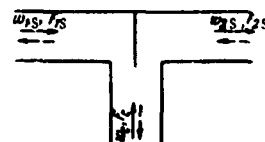


FIGURE 7-6. Equilateral tee with partition.

The values of the resistance coefficients of a number of threaded, malleable-iron tees are given in diagrams 7-16 and 7-25.

14. In the case of tees, which are used for joining two opposite currents (converging tees) (Figure 7-6), the resistance coefficients of the two branches are practically equal.

When a partition is installed at the junction of a tee, the two flows are independent of each other before converging into a common channel. This junction is followed by the usual turbulent mixing of two streams moving at different velocities. Here, the losses in the tee are made up of:

- the loss at mixing, and
- the loss at the 90° turn.

The resistance coefficient of the branch through which the lower-velocity stream moves can have a negative value, just as with a converging wye (due to the additional energy from the higher-velocity stream).

Without a partition the flow pattern is less clearly defined. The pressure drop before and after the stream junction mainly reflects the losses common to both branches.

These losses are positive at any ratio $\frac{w_b}{w_c} \left(\frac{Q_b}{Q_c} \right)$ and are approximately equal to the losses in an expanding elbow.

The resistance coefficient of each branch of the tee before the junction can be calculated by the following formula, proposed by Levin /7-10/:

$$\zeta_{c.b} = \frac{\Delta H_b}{\frac{\gamma w_c^2}{2g}} = 1 + \left(\frac{F_c}{F_b} \right)^2 + 3 \left(\frac{F_c}{F_b} \right)^2 \left[\left(\frac{Q_b}{Q_c} \right)^2 - \frac{Q_b}{Q_c} \right]. \quad (7-11)$$

15. If the tee is used for stream division, the conditions of flow in it are approximately the same as in an ordinary turn. The losses in a diverging tee can therefore be

approximately determined from the data for elbows with different ratios $\frac{b_1}{b_0}$. The resistance coefficient of a diverging tee can also be determined by the following formula, proposed by Levin /7-10/:

$$\zeta_{c.b} = \frac{\Delta H_b}{\frac{\gamma w_c^2}{2g}} = 1 + k \left(\frac{w_b}{w_c} \right)^2. \quad (7-12)$$

where $k \approx 1.5$ for standard, threaded, malleable-iron tees; $k \approx 0.3$ for welded tees.

16. The resistance of a tee can be decreased considerably by making it with smooth bends.

17. At branching angles $\alpha < 90^\circ$ the tee acquires the shape of a Y (cf. diagram 7-36). The resistance coefficient of such true Y-joints with $F_c = 2F_b$ at junctions can be calculated by the following formula, proposed by Lewin /7-10/:

$$\zeta_{c.b} = \frac{\Delta H_b}{\frac{\gamma w_c^2}{2g}} = 4 \frac{Q_b}{Q_c} (0.9 + \cos^2 \alpha) + \left(\frac{Q_b}{Q_c} \right)^4 \left[1 + \left(\frac{Q_c}{Q_b} - 1 \right)^4 \right] (1 - \cos^2 \alpha) - 4 \left(\frac{Q_b}{Q_c} \right)^2 \cos^2 \alpha - 4 (0.2 + 0.5 \cos^2 \alpha). \quad (7-13)$$

The resistance coefficient of the same Y-joints at stream division can be calculated tentatively from diagram 7-22 as the resistance coefficient of the branch of an ordinary wye of the type $F_s + F_b = F_c$.

18. The flow pattern in crosses is basically similar to the flow pattern in single wyes and tees.

The resistance coefficients of double wyes of area $F_s = F_c$ at stream junction (converging double wyes, cf. diagrams 7-31 to 7-35) can be calculated approximately by the following formulas, proposed by Levin /7-8 and 7-9/:

a. One of the branches (No. 1)

$$\zeta_{ic,b} = \frac{\Delta H_{1b}}{\frac{\gamma w_c^2}{2g}} = 1 + \left(\frac{Q_{1b}}{Q_c} \frac{F_c}{F_{1b}} \right)^2 - 8 \left(\frac{Q_{1b}}{Q_c} \right)^2 \frac{\left[\frac{Q_c}{Q_{1b}} - \left(1 + \frac{Q_{2b}}{Q_{1b}} \right) \right]^2}{4 - \left(1 + \frac{Q_{2b}}{Q_{1b}} \right) \frac{Q_{1b}}{Q_c}} - 2 \left(\frac{Q_{1b}}{Q_c} \right)^2 \frac{F_c}{F_{1b}} \left[1 + \left(\frac{Q_{2b}}{Q_{1b}} \right)^2 \right] \cos \alpha. \quad (7-14)$$

The resistance coefficient of the other branch (No. 2) is obtained by interchanging the subscripts 1 and 2.

b. The main passage

$$\zeta_{c,s} = \frac{\Delta H_s}{\frac{\gamma w_c^2}{2g}} = 1 + \left(\frac{Q_s}{Q_c} \right)^2 - \left(\frac{Q_s}{Q_c} \right)^2 \frac{1 + \frac{Q_s}{Q_c}}{\left(0.75 + 0.25 \frac{Q_s}{Q_c} \right)^2} - 2 \left(\frac{Q_s}{Q_c} \right)^2 \frac{F_c}{F_{1s}} \frac{1 + \left(\frac{Q_{2b}}{Q_{1b}} \right)^2}{\left(1 + \frac{Q_{2b}}{Q_{1b}} \right)^2} \left(\frac{Q_c}{Q_s} - 1 \right)^2 \cos \alpha. \quad (7-15)$$

19. The following formulas are recommended for calculating the resistance coefficient of welded converging crosses in cylindrical manifolds for steam, water, etc. (Levin /7-8, 7-9/):

a. One of the branches (No. 1)

$$\zeta_{ic,b} = \frac{\Delta H_{1b}}{\frac{\gamma w_c^2}{2g}} = 1.15 + \left(\frac{Q_{1b}}{Q_c} \frac{F_c}{F_{1b}} \right)^2 - 8 \left(\frac{Q_{1b}}{Q_c} \right)^2 \frac{\left[\frac{Q_c}{Q_{1b}} - \left(1 + \frac{Q_{2b}}{Q_{1b}} \right) \right]^2}{4 - \left(1 + \frac{Q_{2b}}{Q_{1b}} \right) \frac{Q_{1b}}{Q_c}}. \quad (7-16)$$

b. The main passage

$$\zeta_{c,s} = \frac{\Delta H_s}{\frac{\gamma w_c^2}{2g}} = 1.2 + \left(\frac{Q_s}{Q_c} \right)^2 - \left(\frac{Q_s}{Q_c} \right)^2 \frac{1 + \frac{Q_s}{Q_c}}{\left(0.75 + 0.25 \frac{Q_s}{Q_c} \right)^2}. \quad (7-17)$$

For standard crosses made of malleable cast iron and with $\frac{Q_s}{Q_c} > 0.7$, the following magnitude is added to the values obtained for $\zeta_{c,s}$.

$$\Delta\zeta_{c,s} = 2.5 \left(\frac{Q_s}{Q_c} - 0.7 \right). \quad (7-18)$$

20. The resistance coefficients of double wyes at stream division are determined tentatively as for single diverging wyes, from diagrams 7-21 to 7-23.

21. The coefficient of local resistance $\zeta_{c,s} = \frac{\Delta H}{\frac{1}{2}w_c^2}$ of the part of a header between two side openings (Figure 7-7) is a function of the velocities ratio $\frac{w_b}{w_c}$ and the ratio of the pressures $H_{st} = \frac{H_{st}}{\frac{1}{2}w_s^2}$ and $H_{tot} = \frac{H_{tot}}{\frac{1}{2}w_s^2}$ (where H_{st} = static pressure in section 1-1; H_{tot} = total pressure in the same section). This coefficient is also a function of the sides ratio $\frac{a}{b}$ of the pipe section.

The values of $\zeta_{c,s}$ for these passages, determined on the basis of Konokotin's experimental data /7-4/, are given in diagram 7-38*.

22. When several branches start from the same header (Figure 7-8) and the distances between them are larger than the header width, the resistance coefficient of each branch can be calculated as for a single wye.

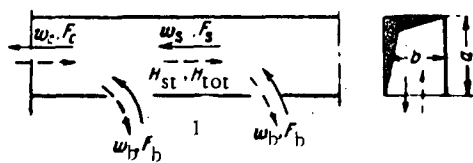


FIGURE 7-7. Side openings in a header.

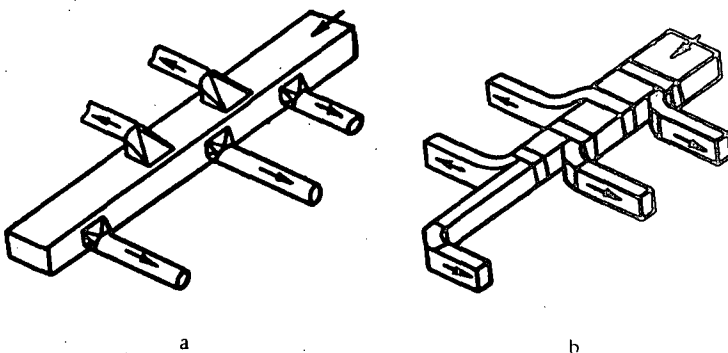


FIGURE 7-8. Header.

a—constant-section header; b—converging-section header.

23. The uniform distribution of the flow to the separate branches of a header is ensured, either by making its cross section constant (Figure 7-8, a) and of area $F_{he} \geq 3\Sigma F_s$ (where ΣF_s is total area of all branches), or by contracting it in such a way that the stream velocity remains constant along the header (cf. Taliev /7-18/). A constant velocity header can be achieved as shown in Figure 7-8, b. Here the resistance of the branches turns out to be considerably higher than in a header of constant section /7-23/.

* For the method of determination of the pressures in such pipes cf. Maksimov /7-11/.

24. It is advisable to design the transitions between the exit openings of the header and the branches perpendicular to it by means of the diagrams given in Figure 7-9. These transitions are of a simple design and have minimum resistance coefficients /7-23/. They can be adopted as standard.

25. The resistance coefficient of the i -th branch $\zeta_{ib} = \frac{\Delta H_b}{\frac{1}{2} \rho (v_{i-1})^2}$ of a header with transitions made according to Figure 7-9 is a function of the ratio of velocities $\frac{v_{ib}}{v_{i-1}}$ only; it is practically independent of Reynolds number for $Re \geq 10^4$, of the sides ratio of the header (for $0.5 \leq \frac{h}{b} \leq 1.0$), and of the areas ratio $\frac{F_b}{F_c}$.

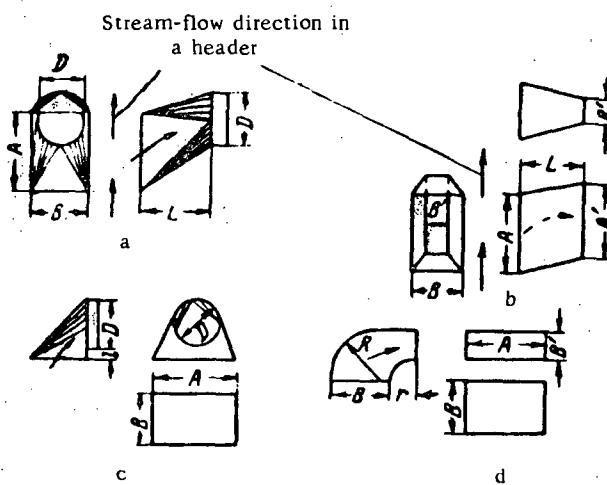


FIGURE 7-9. Transitions of the branches of a header:
a and b—side branches; c and d—upper or lower branch.

The resistance coefficient of a branch at the side is lower than that of a branch at top or bottom, since in the latter case the stream makes two consecutive 90° turns in two mutually perpendicular directions (Figure 7-8).

7-3. LIST OF DIAGRAMS FOR THE RESISTANCE COEFFICIENTS OF SECTION VII

Diagram description	Source	Diagram number	Note
Converging wye of type $F_s + F_b > F_c$; $F_s = F_c$ $\alpha = 30^\circ$. Branch	Levin /7-5, 7-6/ Taliev /7-17/	7-1	Calculating formulas
Main passage of the same	The same	7-2	The same
Converging wye of type $F_s + F_b > F_c$; $F_s = F_c$ $\alpha = 45^\circ$. Branch	" "	7-3	Calculating formulas, refined by Kinne's experiments /7-22/
Main passage of the same	" "	7-4	The same
Converging wye of type $F_s + F_b > F_c$; $F_s = F_c$ $\alpha = 60^\circ$. Branch	" "	7-5	Calculating formulas, refined by Petermann's experiments /7-26/
Main passage of the same	" "	7-6	The same
Converging tee of type $F_s + F_b > F_c$; $F_s = F_c$ $\alpha = 90^\circ$	" "	7-7	Calculating formulas, refined by Vogel's experiments /7-28/
Converging wye of type $F_s + F_b = F_c$ $\alpha = 15^\circ$	" "	7-8	Calculating formulas, refined by Levin's experiments /7-6/
Converging wye of type $F_s + F_b = F_c$ $\alpha = 30^\circ$	" "	7-9	The same
Converging wye of type $F_s + F_b = F_c$ $\alpha = 45^\circ$	" "	7-10	" "
Converging wye of type $F_s + F_b = F_c$ $\alpha = 60^\circ$	" "	7-11	" "
Converging tee of type $F_s + F_b = F_c$ $\alpha = 90^\circ$	" "	7-12	" "
Improved-shape converging wye of type $F_s + F_b > F_c$; $F_s = F_c$ $\alpha = 45^\circ$	Petermann /7-26/	7-13	Experimental data
Improved-shape converging wye of type $F_s + F_b > F_c$; $F_s = F_c$ $\alpha = 60^\circ$	Kinne /7-22/	7-14	The same
Improved-shape converging tee of type $F_s + F_b > F_c$; $F_s = F_c$ $\alpha = 90^\circ$	Vogel /7-28/	7-15	" "
Standard converging threaded malleable-iron tee of type $F_s + F_b > F_c$; $F_s = F_c$ $\alpha = 90^\circ$	Zusmanovich /7-2/	7-16	" "
Circular-section converging wye with smooth side bend ($R_o/D_b = 2.0$) of type $F_s + F_b = F_c$ $\alpha = 12$ to 15° . Branch	Aver'yanov /7-1/	7-17	" "
Main passage of the same		7-18	" "
Rectangular-section converging wye of type $F_b + F_s \geq F_c$ smooth ($r/b_b = 1.0$) $\alpha = 90^\circ$. Branch	Taliev and Tatarchuk /7-16/	7-19	" "
Main passage of the same		7-20	" "
Diverging wye of type $F_s + F_b > F_c$; $F_s = F_c$ Branch. $\alpha = 0$	Levin /7-7/	7-21	Calculating formula; correction co- efficient based on Kinne's /7-22/, Petermann's /7-26/, and Vogel's /7-28/ experiments
Diverging wye of type $F_s + F_b = F_c$ Branch. $\alpha = 0$	The same	7-22	Calculating formula; correction co- efficient based on Levin's experi- ments /7-7/

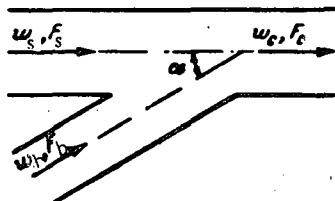
Diagram description	Source	Diagram number	Note
Diverging wye of type $F_s + F_b > F_c$ and $F_s + F_b = F_c$ Main passage. $\alpha = 0-90^\circ$	Levin /7-7/	7-23	Calculating formula; correction coefficient based on Levin's experiments /7-7/
Improved-shape diverging wye of type $F_s + F_b > F_c$; $F_s = F_c$	Kinne /7-22/, Petermann /7-26/, and Vogel /7-28/	7-24	Experimental data
Standard threaded malleable-iron diverging tee of type $F_s + F_b > F_c$; $F_s = F_c$ $\alpha = 90^\circ$	Zusmanovich /7-2/	7-25	The same
Rectangular smooth ($r/b_s = 1.0$) diverging wye of type $F_s + F_b > F_c$ $\alpha = 90^\circ$. Branch	Taliev and Tatarchuk /7-16/	7-26	" "
Main passage of same	The same	7-27	" "
Asymmetrical converging wye of type $F_s + F_{st} \geq F_c$ with smooth bends ($R_b/D_c = 2.0$) $\alpha = 90^\circ$	Franke /7-20/	7-28	" "
Symmetrical tee $\alpha = 90^\circ$	Levin /7-10/ Idel'chik	7-29	Calculating formulas Experimental data
Symmetrical wye (dovetail) $\alpha = 90^\circ$	Franke /7-20/ Taliev and Tatarchuk /7-16/	7-30	The same
Double wye of type $F_{1b} = F_{2b}$; $F_s = F_c$ $\alpha = 15^\circ$	Levin /7-8, 7-9/	7-31	Calculating formulas and experiments
Double wye of type $F_{1b} = F_{2b}$; $F_s = F_c$ $\alpha = 30^\circ$	The same	7-32	The same
Double wye of type $F_{1b} = F_{2b}$; $F_s = F_c$ $\alpha = 45^\circ$	" "	7-33	" "
Double wye of type $F_{1b} = F_{2b}$; $F_s = F_c$ $\alpha = 60^\circ$	" "	7-34	" "
Cross of type $F_{1s} = F_{2b}$; $F_h = F_c$ $\alpha = 90^\circ$	" "	7-35	" "
Wye of type $F_c = 2 F_s$	Levin /7-10/	7-36	" "
Header with transition stretches	Konzo, Gilman, Holl, and Martin /7-23/	7-37	Experimental data
Passage through a side opening of a header pipe of constant cross section	Konokotin /7-4/	7-38	The same
Passage through a side opening of a header pipe of constant cross section	The same	7-39	" "

7-4. DIAGRAMS OF RESISTANCE COEFFICIENTS

 Converging wye of type $F_s + F_b > F_c$; $F_s = F_c$. $\alpha = 30^\circ$. Branch

Section VII

Diagram 7-1



$$\zeta_{c,b} = \frac{\Delta H_b}{\gamma w_c^2} = 1 + \left(\frac{Q_b}{Q_c} \frac{F_c}{F_b} \right)^2 - 2 \left(1 - \frac{Q_b}{Q_c} \right)^2 - 1.74 \frac{F_c}{F_b} \left(\frac{Q_b}{Q_c} \right)^2$$

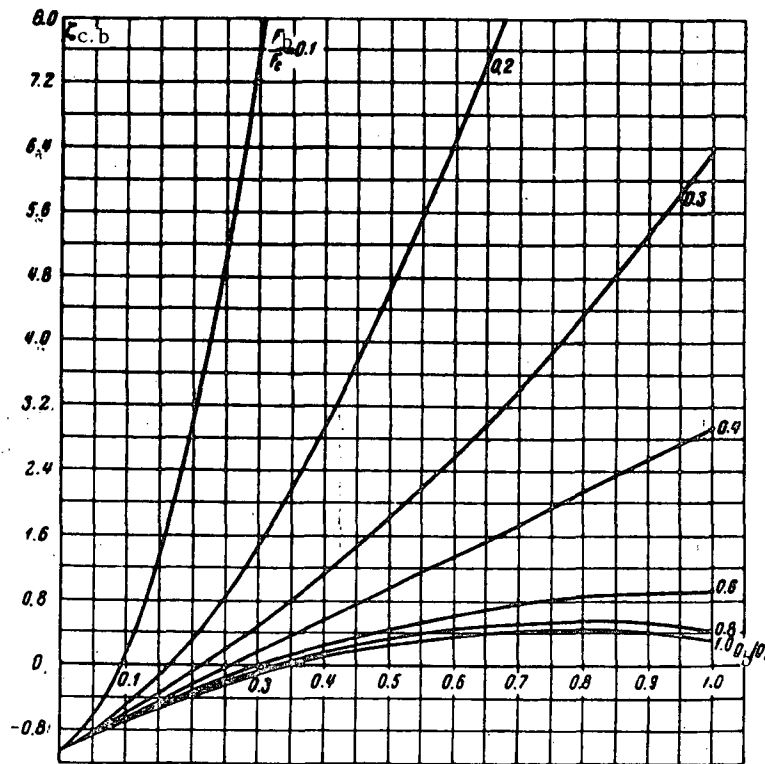
 Values of $\zeta_{c,b}$

$\frac{Q_b}{Q_c}$	$\frac{F_b}{F_c}$						
	0.1	0.2	0.3	0.4	0.6	0.8	1.0
0	-1.00	-1.00	-1.00	-1.00	-1.00	-1.00	-1.00
0.1	+0.21	-0.46	-0.57	-0.60	-0.62	-0.63	-0.63
0.2	3.10	+0.37	-0.06	-0.20	-0.28	-0.30	-0.35
0.3	7.60	1.50	+0.50	+0.20	+0.05	-0.08	-0.10
0.4	13.5	2.95	1.15	0.59	0.26	+0.18	+0.16
0.5	21.2	4.58	1.78	0.97	0.44	0.35	0.27
0.6	30.4	6.42	2.60	1.37	0.64	0.46	0.31
0.7	41.3	8.50	3.40	1.77	0.76	0.50	0.40
0.8	53.8	11.5	4.22	2.14	0.85	0.53	0.45
0.9	58.0	14.2	5.30	2.58	0.89	0.52	0.40
1.0	83.7	17.3	6.33	2.92	0.89	0.39	0.27

 is determined from the curves $\zeta_{c,b} = f\left(\frac{Q_b}{Q_c}\right)$

 corresponding to different $\frac{F_b}{F_c}$;

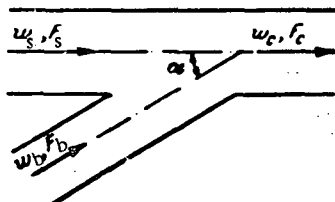
$$\zeta_s = \frac{\Delta H_b}{\gamma w_b^2} = \frac{\zeta_{c,b}}{\left(\frac{Q_b}{Q_c} \frac{F_c}{F_b}\right)^2}$$



(Converging wye of type $F_s + F_b > F_c$; $F_s = F_c$. $\alpha = 30^\circ$. Main passage

Section VII

Diagram 7-2



Values of $\zeta_{c,s}$

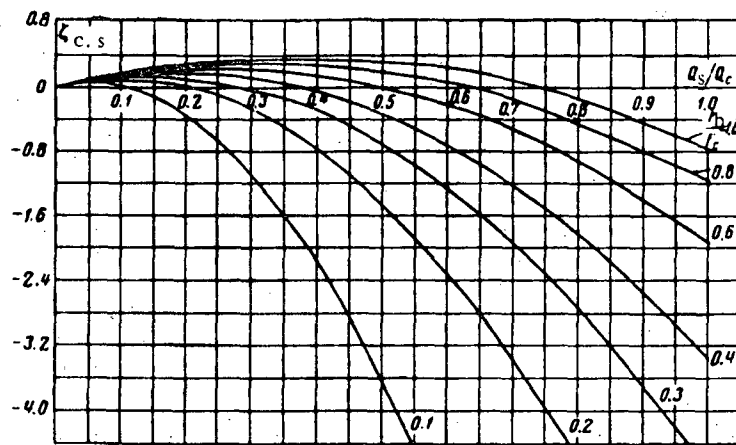
$\frac{Q_b}{Q_c}$	$\frac{F_b}{F_c}$							
	0.1	0.2	0.3	0.4	0.6	0.8	1.0	
0	0.0	0	0	0	0	0	0	0
0.1	+0.02	0.11	0.13	0.15	0.16	0.17	0.17	
0.2	-0.33	+0.01	+0.13	0.19	0.24	0.27	0.29	
0.3	-1.10	-0.25	-0.01	+0.10	0.22	0.30	0.35	
0.4	-2.15	-0.75	-0.30	-0.05	0.17	0.26	0.36	
0.5	-3.60	-1.43	-0.70	-0.35	0.00	0.21	0.32	
0.6	-5.40	-2.35	-1.25	-0.70	-0.20	+0.06	0.25	
0.7	-7.60	-3.40	-1.95	-1.20	-0.50	-0.15	+0.10	
0.8	-10.1	-4.61	-2.74	-1.82	-0.90	-0.43	-0.15	
0.9	-13.0	-6.02	-3.70	-2.55	-1.40	-0.80	-0.45	
1.0	-16.3	-7.70	-4.75	-3.35	-1.90	-1.17	-0.75	

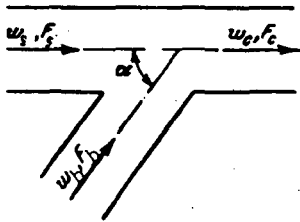
$$\zeta_{c,s} = \frac{\Delta H_s}{\frac{1}{2} w_c^2} = 1 - \left(1 - \frac{Q_b}{Q_c}\right)^2 - 1.74 \frac{F_c}{F_b} \left(\frac{Q_b}{Q_c}\right)^2$$

is determined from the curves $\zeta_{c,s} = f\left(\frac{Q_b}{Q_c}\right)$

corresponding to different $\frac{F_b}{F_c}$:

$$\zeta_s = \frac{\Delta H_s}{\frac{1}{2} w_s^2} = \frac{\zeta_{c,s}}{\left(1 - \frac{Q_b}{Q_c}\right)^2}.$$





$$\zeta_{c,b} = \frac{\Delta H_b}{\frac{\gamma w_c^2}{2g}} = 1 + \left(\frac{Q_b}{Q_c} \frac{F_c}{F_b} \right)^2 - 2 \left(1 - \frac{Q_b}{Q_c} \right)^2 -$$

$$- 1.41 \frac{F_c}{F_b} \left(\frac{Q_b}{Q_c} \right)^2$$

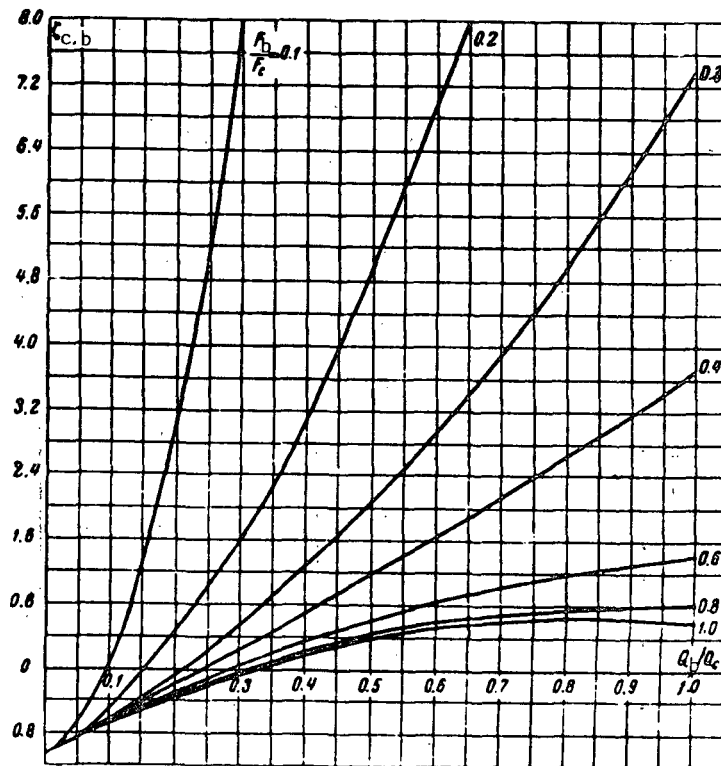
is determined from the curves $\zeta_{c,b} = f\left(\frac{Q_b}{Q_c}\right)$

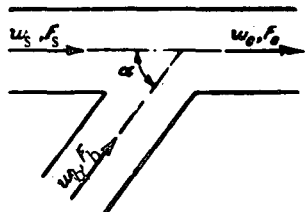
corresponding to different $\frac{F_b}{F_c}$:

$$\zeta_b = \frac{\Delta H_b}{\frac{\gamma w_b^2}{2g}} = \frac{\zeta_{c,s}}{\left(\frac{Q_b}{Q_c} \frac{F_c}{F_b} \right)^2}$$

Values of $\zeta_{c,b}$

$\frac{Q_b}{Q_c}$	$\frac{F_b}{F_c}$						
	0.1	0.2	0.3	0.4	0.6	0.8	1.0
0	-1.00	-1.00	-1.00	-1.00	-1.00	-1.00	-1.00
0.1	+0.24	-0.45	-0.56	-0.59	-0.61	-0.62	-0.62
0.2	3.15	+0.54	-0.02	-0.17	-0.26	-0.28	-0.29
0.3	8.00	1.64	+0.60	+0.30	+0.08	0.00	-0.03
0.4	14.0	3.15	1.30	0.72	0.35	+0.25	+0.21
0.5	21.9	5.00	2.10	1.18	0.60	0.45	0.40
0.6	31.6	6.90	2.97	1.65	0.85	0.60	0.53
0.7	42.9	9.20	3.90	2.15	1.02	0.70	0.60
0.8	55.9	12.4	4.90	2.66	1.20	0.79	0.66
0.9	70.6	15.4	6.20	3.20	1.30	0.80	0.64
1.0	86.9	18.9	7.40	3.71	1.42	0.80	0.59



Values of $\zeta_{c,s}$

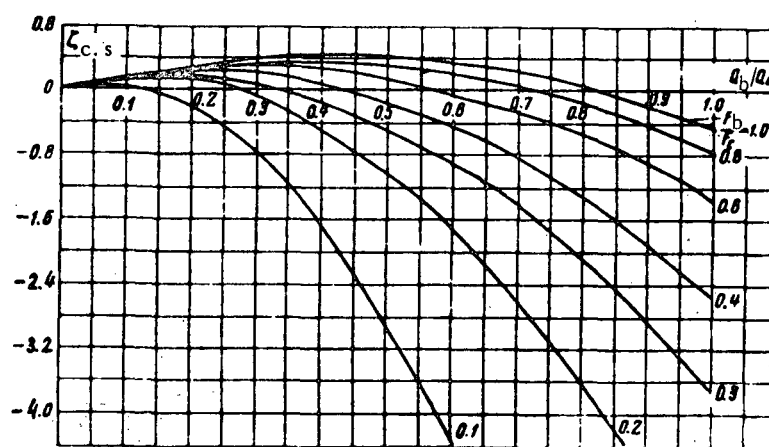
$\frac{Q_b}{Q_c}$	$\frac{F_b}{F_c}$						
	0.1	0.2	0.3	0.4	0.6	0.0	1.0
0	0	0	0	0	0	0	0
0.1	+0.05	0.12	0.14	0.16	0.17	0.17	0.17
0.2	-0.20	+0.17	0.22	0.27	0.27	0.29	0.31
0.3	-0.76	-0.13	+0.08	0.20	0.28	0.32	0.40
0.4	-1.65	-0.50	-0.12	+0.08	0.26	0.36	0.41
0.5	-2.77	-1.00	-0.49	-0.13	+0.16	0.30	0.40
0.6	-4.30	-1.70	-0.87	-0.45	-0.04	0.20	0.33
0.7	-6.05	-2.60	-1.40	-0.85	-0.25	+0.08	0.25
0.8	-8.10	-3.56	-2.10	-1.30	-0.55	-0.17	+0.06
0.9	-10.0	-4.75	-2.80	-1.90	-0.88	-0.40	-0.18
1.0	-13.2	-6.10	-3.70	-2.55	-1.35	-0.77	-0.42

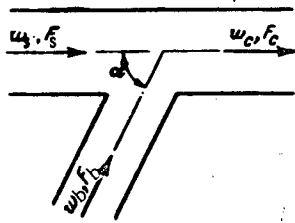
$$\zeta_{c,s} = \frac{\Delta H_s}{\frac{1}{2} w_c^2} = 1 - \left(1 - \frac{Q_b}{Q_c}\right)^2 - 1.41 \frac{F_c}{F_b} \left(\frac{Q_b}{Q_c}\right)^2$$

is determined from the curves $\zeta_{c,s} = f\left(\frac{Q_b}{Q_c}\right)$

corresponding to different $\frac{F_b}{F_c}$;

$$\zeta_s = \frac{\Delta H_s}{\frac{1}{2} w_s^2} = \frac{\zeta_{c,s}}{\left(1 - \frac{Q_b}{Q_c}\right)^2}.$$



Values of $\zeta_{c,b}$

$\frac{Q_b}{Q_c}$	$\frac{F_b}{F_c}$						
	0.1	0.2	0.3	0.4	0.6	0.8	1.0
0	-1.00	-1.00	-1.00	-1.00	-1.00	-1.00	-1.00
0.1	+0.26	-0.42	-0.54	-0.58	-0.61	-0.62	-0.62
0.2	3.35	+0.55	+0.03	-0.13	-0.23	-0.26	-0.26
0.3	8.20	1.85	0.75	+0.40	+0.10	0.00	-0.1
0.4	14.7	3.50	1.55	0.92	0.45	+0.35	+0.28
0.5	23.0	5.50	2.40	1.44	0.78	0.58	0.50
0.6	33.1	7.90	3.50	2.05	1.08	0.80	0.68
0.7	44.9	10.0	4.60	2.70	1.40	0.98	0.84
0.8	58.5	13.7	5.80	3.32	1.64	1.12	0.92
0.9	97.9	17.2	7.65	4.05	1.92	1.20	0.99
1.0	91.0	21.0	9.70	4.70	2.11	1.35	1.00

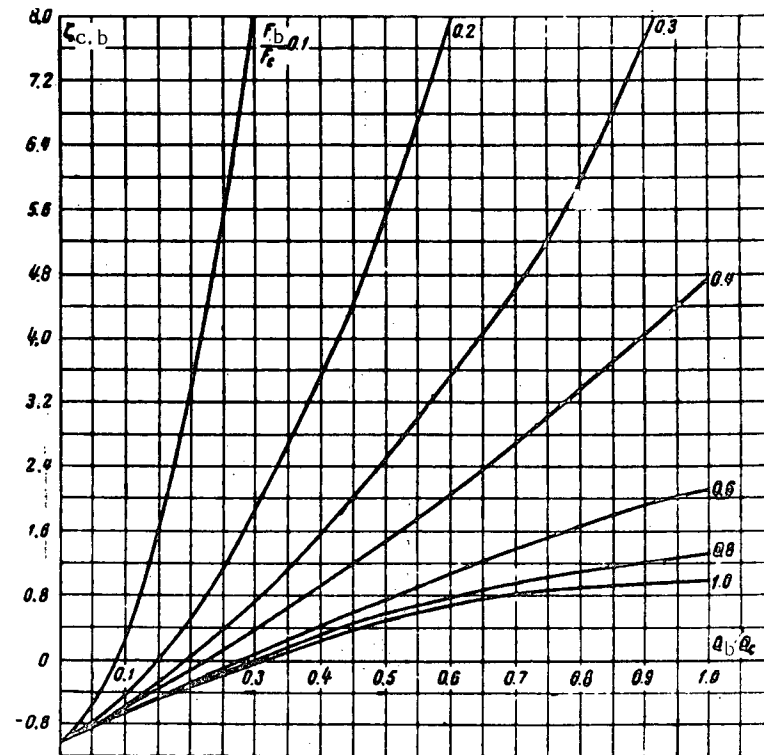
$$\zeta_{c,b} = \frac{\Delta H_b}{\gamma w_c^2} = 1 + \left(\frac{Q_b F_c}{Q_c F_b} \right)^2 -$$

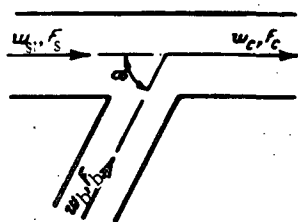
$$- 2 \left(1 - \frac{Q_b}{Q_c} \right)^2 - \frac{F_c}{F_b} \left(\frac{Q_b}{Q_c} \right)^2$$

is determined from the curves $\zeta_{c,b} = f \left(\frac{Q_b}{Q_c} \right)$

corresponding to different $\frac{F_b}{F_c}$:

$$\zeta_b = \frac{\Delta H_b}{\gamma w_b^2} = \frac{\zeta_{c,b}}{\left(\frac{Q_b F_c}{Q_c F_b} \right)^2}$$



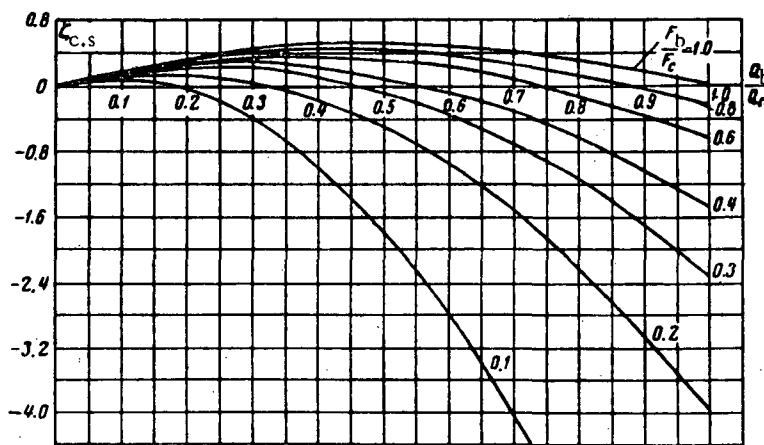
Values of $\zeta_{c,s}$

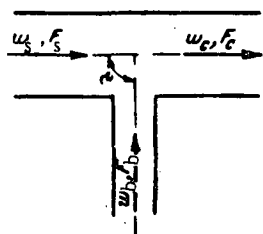
$\frac{Q_b}{Q_c}$	$\frac{F_b}{F_c}$						
	0.1	0.2	0.3	0.4	0.6	0.8	1.0
0	0	0	0	0	0	0	0
0.1	+0.09	0.14	0.16	0.17	0.17	0.18	0.18
0.2	0.00	0.16	0.23	0.26	0.29	0.31	0.32
0.3	-0.40	+0.06	0.22	0.30	0.32	0.41	0.42
0.4	-1.00	-0.16	+0.11	0.24	0.37	0.44	0.48
0.5	-1.75	-0.50	-0.08	+0.13	0.33	0.44	0.50
0.6	-2.80	-0.95	-0.35	-0.10	0.25	0.40	0.48
0.7	-4.00	-1.55	-0.70	-0.30	+0.08	0.28	0.42
0.8	-5.44	-2.24	-1.17	-0.64	-0.11	+0.16	0.32
0.9	-7.20	-3.08	-1.70	-1.02	0.38	-0.08	0.18
1.0	-9.00	-4.00	-2.30	-1.50	-0.68	-0.28	0.00

$$\zeta_{c,s} = \frac{\Delta H_s}{\frac{\gamma w_c^2}{2g}} = 1 - \left(1 - \frac{Q_b}{Q_c}\right) - \frac{F_c}{F_b} \left(\frac{Q_b}{Q_c}\right)^2$$

is determined from the curves $\zeta_{c,s} = f\left(\frac{Q_b}{Q_c}\right)$ corresponding to different $\frac{F_b}{F_c}$:

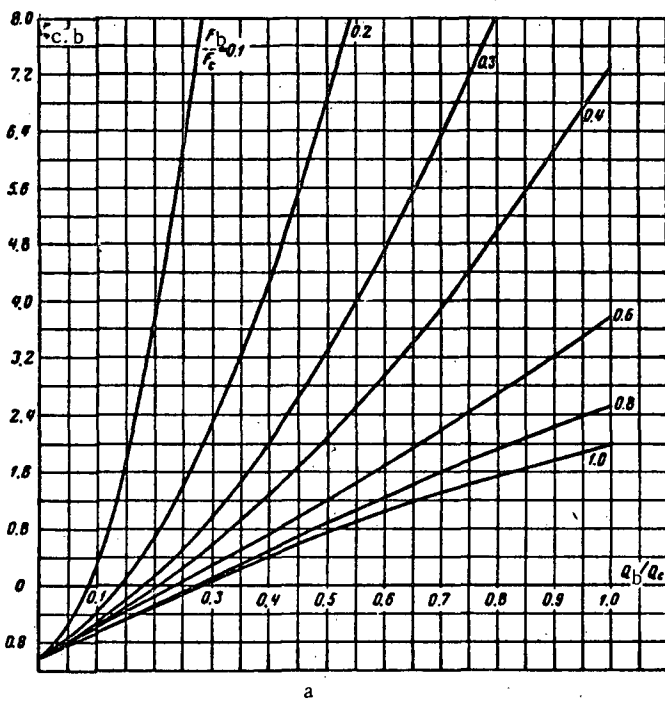
$$\zeta_s = \frac{\Delta H_s}{\frac{\gamma w_s^2}{2g}} = \frac{\zeta_{c,s}}{\left(1 - \frac{Q_b}{Q_c}\right)^2}$$





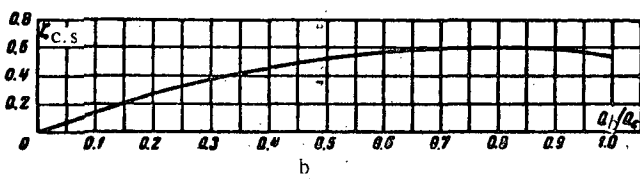
$$\zeta_b = \frac{\Delta H_b}{\gamma w_b^2} = \frac{\zeta'_{c,b}}{\left(\frac{Q_b F_c}{Q_c F_b}\right)^2}$$

$\frac{Q_b}{Q_c}$	Values of $\zeta'_{c,b}$							
	$\frac{F_b}{F_c}$	0.1	0.2	0.3	0.4	0.6	0.8	1.0
0	-1.00	-1.00	-1.00	-1.00	-1.00	-1.00	-1.00	-1.00
0.1	+0.40	-0.37	-0.51	-0.54	-0.59	-0.60	-0.61	
0.2	3.80	+0.72	+0.17	-0.03	-0.17	-0.22	-0.30	
0.3	9.20	2.27	1.00	+0.58	+0.27	+0.15	-0.11	
0.4	16.3	4.30	2.06	1.30	0.75	0.55	0.44	
0.5	25.5	6.75	3.23	2.06	1.20	0.89	0.77	
0.6	36.7	9.70	4.70	2.98	1.68	1.25	1.04	
0.7	42.9	13.0	6.30	3.90	2.20	1.60	1.30	
0.8	64.9	16.9	7.92	4.92	2.70	1.92	1.56	
0.9	82.0	21.2	9.70	6.10	3.20	2.25	1.80	
1.0	101	26.0	11.9	7.25	3.80	2.57	2.00	



a

$\frac{Q_b}{Q_c}$	0	0.1	0.2	0.3	0.4	0.5	0.6	0.7	0.8	0.9	1.0
$\zeta'_{c,s}$	0	0.16	0.27	0.38	0.46	0.53	0.57	0.59	0.60	0.59	0.55



b

1. Branch b

$$\zeta'_{c,b} = \frac{\Delta H_b}{\gamma w_c^2} = A \left[1 + \left(\frac{Q_b F_c}{Q_c F_b} \right)^2 - 2 \left(1 - \frac{Q_b}{Q_c} \right) \right] = A \zeta'_{c,s}$$

where $\zeta'_{c,s}$ is determined from the curves $\zeta'_{c,s} = f \left(\frac{Q_b}{Q_c} \right)$ at different $\frac{F_b}{F_c}$ on graph a;

A is taken from Table 7-4 at different $\frac{F_b}{F_c}$.

TABLE 7-4

$\frac{F_b}{F_c}$	0-0.2	0.3-0.4	0.6	0.8	1.0
A	1.00	0.75	0.70	0.65	0.60

2. Main passage

$$\zeta'_{c,s} = \frac{\Delta H_s}{\gamma w_c^2} \approx 1.55 \frac{Q_b}{Q_c} - \left(\frac{Q_b}{Q_c} \right)^2$$

is determined by the curve

$$\zeta'_{c,s} = f \left(\frac{Q_b}{Q_c} \right)$$

practically true for all values of $\frac{F_b}{F_c}$:

$$\zeta_s = \frac{\Delta H_s}{\gamma w_s^2} = \frac{\zeta'_{c,s}}{\left(1 - \frac{Q_b}{Q_c} \right)^2}$$

Converging wye of type $F_s + F_b = F_c$. $\alpha = 15^\circ$

Section VII

Diagram 7-8

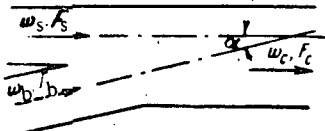


TABLE 7-5

F_b/F_c	K_s
0 - 0.2	0
0.33	0.14
0.50	0.40

1. Branch

$$\zeta_{c,b} = \frac{\Delta H_b}{\gamma w_c^2} = 1 + \left(\frac{Q_b F_c}{Q_c F_b} \right)^2 - 2 \frac{F_c}{F_s} \left(1 - \frac{Q_b}{Q_c} \right)^2 - 1.94 \frac{F_c}{F_b} \left(\frac{Q_b}{Q_c} \right)^2$$

is determined from the curves $\zeta_{c,b} = f\left(\frac{Q_b}{Q_c}\right)$ corresponding to different $\frac{F_b}{F_c}$:

$$\zeta_b = \frac{\Delta H_b}{\gamma w_b^2} = \frac{\zeta_{c,b}}{\left(\frac{Q_b F_c}{Q_c F_b} \right)^2}.$$

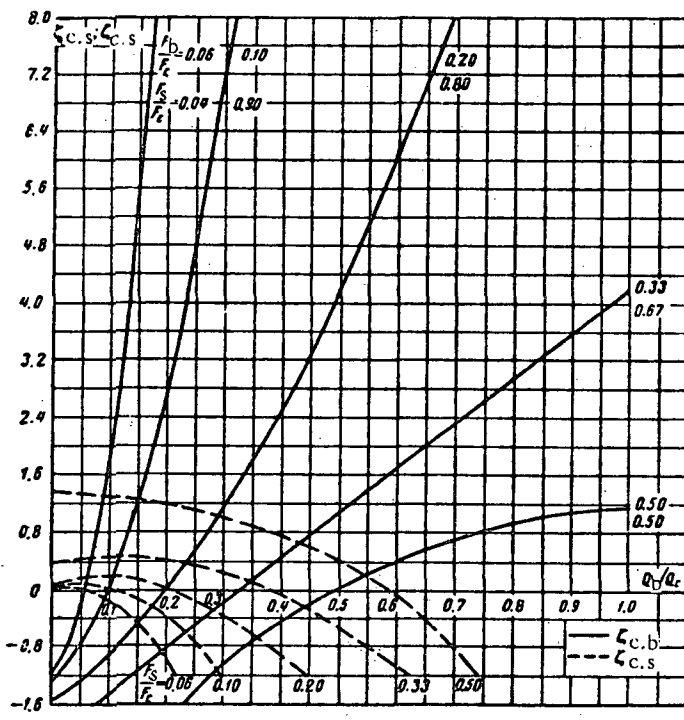
2. Main passage

$$\zeta_{c,s} = \frac{\Delta H_s}{\gamma w_s^2} = 1 + \left(\frac{F_c}{F_s} \right)^2 \left(1 - \frac{Q_b}{Q_c} \right)^2 - 2 \frac{F_c}{F_s} \left(1 - \frac{Q_b}{Q_c} \right)^2 - 1.94 \frac{F_c}{F_b} \left(\frac{Q_b}{Q_c} \right)^2 + K_s$$

is determined from the curves $\zeta_{c,s} = f\left(\frac{Q_b}{Q_c}\right)$ corresponding to different $\frac{F_b}{F_c}$:

K_s is taken from Table 7-5;

$$\zeta_s = \frac{\Delta H_s}{\gamma w_s^2} = \frac{\zeta_{c,s}}{\left(1 - \frac{Q_b}{Q_c} \right)^2 \left(\frac{F_c}{F_s} \right)^2}.$$



F_b/F_c	Q_b/Q_c											
	0	0.03	0.05	0.10	0.2	0.3	0.4	0.5	0.6	0.7	0.8	1.0

 Values of $\zeta_{c,b}$

F_b/F_c	0.06	0.10	0.20	0.33	0.50	0.06	0.10	0.20	0.33	0.50	0.06	0.10
0.06	-1.12	-0.70	-0.20	+1.84	9.92	23.0	41.0	64.3	-	-	-	-
0.10	-1.22	-1.00	-0.72	+0.01	2.80	7.17	13.1	20.6	29.7	-	-	-
0.20	-1.50	-1.40	-1.22	-0.84	+0.02	+1.20	2.55	4.20	6.12	8.20	10.7	-
0.33	-2.00	-1.80	-1.71	-1.40	-0.67	-0.16	+0.42	1.05	1.67	2.30	2.95	4.20
0.50	-3.00	-2.80	-2.60	-2.24	-1.56	-1.00	-0.40	+0.02	0.40	0.66	0.93	1.14

 Values of $\zeta_{c,s}$

F_b/F_c	0.06	0.10	0.20	0.33	0.50	0.06	0.10	0.20	0.33	0.50	0.06	0.10
0.06	0.00	0.06	+0.04	-0.13	-0.95	-2.50	-4.60	-7.50	-	-	-	-
0.10	0.01	0.10	0.12	+0.02	-0.36	-1.20	-2.50	-4.10	-6.12	-	-	-
0.20	0.06	0.15	0.20	0.22	+0.05	-0.28	-0.89	-1.66	-2.63	-3.84	-5.22	-
0.33	0.40	0.42	0.45	0.47	0.42	+0.24	-0.08	-0.52	-1.25	-1.80	-2.60	-4.66
0.50	1.40	1.40	1.39	1.37	1.24	1.01	+0.78	-0.43	-0.10	-0.82	-1.08	-2.46

Converging wye of type $F_b + F_c = F_s$. $\alpha = 30^\circ$

Section VII

Diagram 7-9

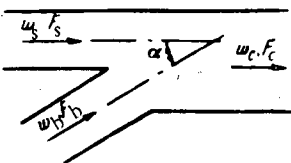


TABLE 7-6

$\frac{F_b}{F_c}$	K_s
0-0.2	0
0.33	0.17
0.50	0.40

1. Branch

$$\xi_{c,b} = \frac{\Delta H_b}{\gamma w_c^2} = 1 + \left(\frac{Q_b}{Q_c} \frac{F_c}{F_b} \right)^2 - 2 \frac{F_c}{F_s} \left(1 - \frac{Q_b}{Q_c} \right)^2 - 1.74 \frac{F_c}{F_b} \left(\frac{Q_b}{Q_c} \right)^2$$

is determined from the curves $\xi_{c,b} = f \left(\frac{Q_b}{Q_c} \right)$ corresponding

to different $\frac{P_b}{F_c}$:

$$\xi_s = \frac{\Delta H_b}{\gamma w_b^2} = \frac{\xi_{c,b}}{\left(\frac{Q_b}{Q_c} \frac{F_c}{F_b} \right)^2}$$

2. Main passage

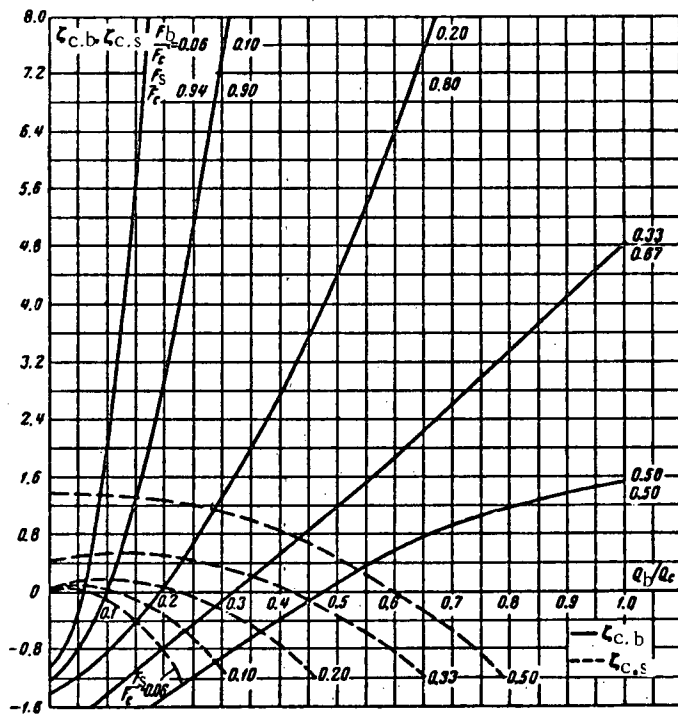
$$\xi_{c,s} = \frac{\Delta H_s}{\gamma w_c^2} = 1 + \left(\frac{F_c}{F_s} \right)^2 \left(1 - \frac{Q_b}{Q_c} \right)^2 - 2 \frac{F_c}{F_s} \left(1 - \frac{Q_b}{Q_c} \right)^2 - 1.74 \frac{F_c}{F_b} \left(\frac{Q_b}{Q_c} \right)^2 + K_s$$

is determined from the curves $\xi_{c,s} = f \left(\frac{Q_b}{Q_c} \right)$ corresponding

to different $\frac{P_b}{F_s}$:

K_s is taken from Table 7-6;

$$\xi_s = \frac{\Delta H_s}{\gamma w_s^2} = \frac{\xi_{c,s}}{\left(1 - \frac{Q_b}{Q_c} \right)^2 \left(\frac{F_c}{F_s} \right)^2}$$



$\frac{F_b}{F_c}$	Q_b/Q_c										
	0	0.03	0.05	0.1	0.2	0.3	0.4	0.5	0.6	0.7	0.8
Values of $\xi_{c,b}$											
0.06	-1.13	-0.07	-0.30	+1.82	10.1	23.3	41.5	65.2	-	-	-
0.10	-1.22	-1.00	-0.76	+0.02	2.88	7.34	13.4	21.1	29.4	-	-
0.20	-1.50	-1.35	-1.22	-0.84	+0.05	+1.40	2.70	4.46	6.48	8.70	11.4
0.33	-2.00	-1.80	-1.70	-1.40	-0.72	-0.12	+0.52	1.20	1.89	2.56	3.30
0.50	-3.00	-2.80	-2.60	-2.24	-1.44	-0.91	-0.36	+0.14	0.56	0.84	1.18
Values of $\xi_{c,s}$											
0.06	0	0.06	+0.04	-0.10	-0.81	-2.10	-4.07	-6.60	-	-	-
0.10	0.01	0.10	0.08	+0.04	-0.33	-1.05	-2.14	-3.60	5.40	-	-
0.20	0.06	0.10	0.13	0.16	+0.06	-0.24	-0.73	-1.40	-2.30	-3.34	-3.59
0.33	0.42	0.45	0.48	0.51	0.52	+0.32	+0.07	-0.32	-0.82	-1.47	-2.19
0.50	1.40	1.40	1.40	1.36	1.26	1.09	0.86	+0.53	+0.15	-0.52	-0.82

Converging wye of type $F_s + F_b = F_c$. $\alpha = 45^\circ$

Section VII

Diagram 7-10

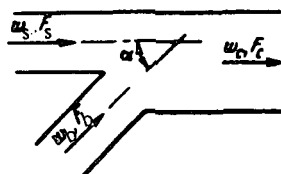


TABLE 7-7

$\frac{F_b}{F_c}$	K_s
0.10	0.05
0.20	0.14
0.33	0.14
0.50	0.30

1. Branch

$$\xi_{c.b} = \frac{\Delta H_b}{\gamma w_e^2} = 1 + \left(\frac{Q_b F_c}{Q_c F_b} \right)^2 - 2 \frac{F_c}{F_s} \left(1 - \frac{Q_b}{Q_c} \right)^2 - 1.41 \frac{F_c}{F_b} \left(\frac{Q_b}{Q_c} \right)^2$$

is determined from the curves $\xi_{c.b} = f \left(\frac{Q_b}{Q_c} \right)$ corresponding

to different $\frac{F_b}{F_c}$:

$$\xi_b = \frac{\Delta H_b}{\gamma w_b^2} = \frac{\xi_{c.b}}{\left(\frac{Q_b F_c}{Q_c F_b} \right)^2}$$

2. Main passage

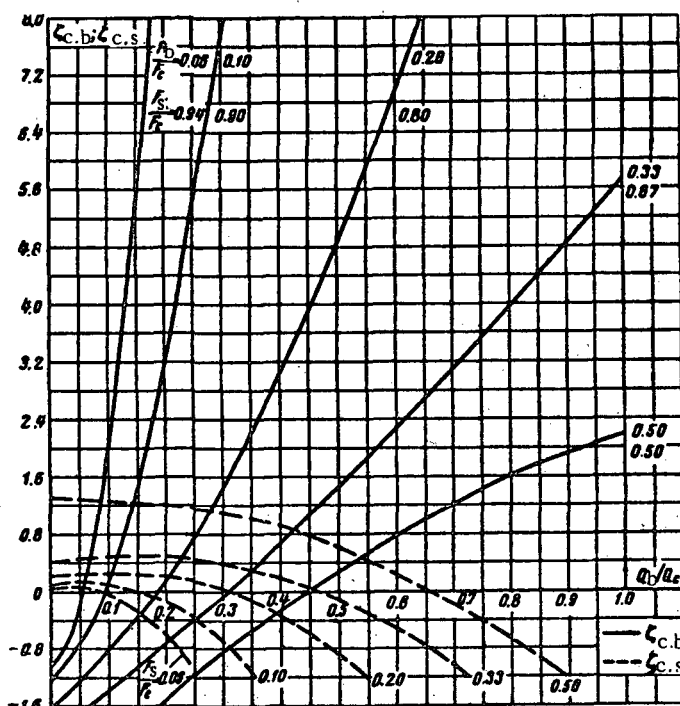
$$\xi_{c.s} = \frac{\Delta H_s}{\gamma w_c^2} = 1 + \left(\frac{F_c}{F_s} \right)^2 \left(1 - \frac{Q_b}{Q_c} \right)^2 - 2 \frac{F_c}{F_s} \left(1 - \frac{Q_b}{Q_c} \right)^2 - 1.41 \frac{F_c}{F_b} \left(\frac{Q_b}{Q_c} \right)^2 + K_s$$

is determined from the curves $\xi_{c.s} = f \left(\frac{Q_b}{Q_c} \right)$ corresponding

to different $\frac{F_b}{F_c}$:

K_s is taken from Table 7-7;

$$\xi_s = \frac{\Delta H_s}{\gamma w_s^2} = \frac{\xi_{c.s}}{\left(1 - \frac{Q_b}{Q_c} \right)^2 \left(\frac{F_c}{F_s} \right)^2}$$



$\frac{F_b}{F_c}$	$\frac{Q_b}{Q_c}$											
	0	0.03	0.05	0.1	0.2	0.3	0.4	0.5	0.6	0.7	0.8	1.0
Values of $\xi_{c.b}$												
0.06	-1.12	-0.70	-0.20	+1.82	10.3	23.8	42.4	64.3	-	-	-	-
0.10	-1.22	-1.00	-0.78	+0.06	3.00	7.64	13.9	22.0	31.9	-	9.50	12.4
0.20	-1.50	-1.40	-1.25	-0.85	+0.12	+1.42	3.00	4.86	7.05	9.50	12.4	-
0.33	-2.00	-1.82	-1.69	-1.38	-0.66	-0.10	+0.70	1.48	2.24	3.10	3.95	5.76
0.50	-3.00	-2.80	-2.60	+2.24	-1.50	-0.85	-0.24	-0.30	0.79	1.26	1.60	2.18
Values of $\xi_{c.s}$												
0.06	0.00	0.05	+0.05	-0.05	-0.59	-1.65	-3.21	-5.13	-	-	-	-
0.10	0.06	0.10	0.12	+0.11	-0.15	-0.71	-1.55	-2.71	-3.73	-	-	-
0.20	0.20	0.25	0.30	0.30	+0.26	+0.04	-0.33	-0.86	-1.52	-2.40	-3.42	-
0.33	0.37	0.42	0.45	0.48	0.50	0.40	+0.20	-0.12	-0.50	-1.01	-1.60	-3.10
0.50	1.30	1.30	1.30	1.27	1.20	1.10	0.90	+0.61	+0.22	-0.20	-0.68	-1.52

Converging wye of type $F_s + F_b = F_c$, $\alpha = 60^\circ$

Section VII

Diagram 7-11

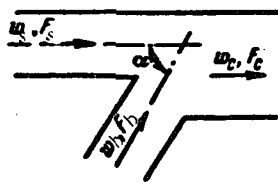
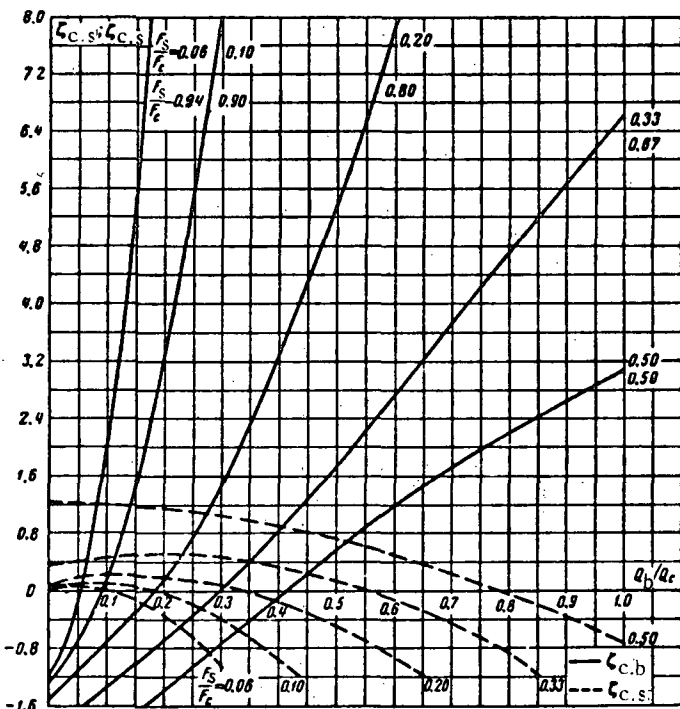


TABLE 7-8

F_b/F_c	K_b	K_s
0 - 0.2	0	0
0.33	0	0.10
0.50	0.10	0.25



1. Branch

$$\xi_{c,b} = \frac{\Delta H_b}{\gamma w_c^2} = 1 + \left(\frac{Q_b}{Q_c} \frac{F_c}{F_b} \right)^2 - 2 \frac{F_c}{F_s} \left(1 - \frac{Q_b}{Q_c} \right)^2 - \frac{F_c}{F_b} \left(\frac{Q_b}{Q_c} \right)^2 + K_b$$

is determined from the curves $\xi_{c,b} = f \left(\frac{Q_b}{Q_c} \right)$ corresponding to different $\frac{F_b}{F_c}$;

K_b is taken from Table 7-8;

$$K_b = \frac{\Delta H_b}{\gamma w_b^2} = \frac{\xi_{c,b}}{\left(\frac{Q_b F_c}{Q_c F_b} \right)^2}$$

2. Main passage

$$\xi_{c,s} = \frac{\Delta H_s}{\gamma w_s^2} = 1 + \left(\frac{F_c}{F_s} \right)^2 \left(1 - \frac{Q_b}{Q_c} \right) - 2 \frac{F_c}{F_s} \left(1 - \frac{Q_b}{Q_c} \right)^2 - \frac{F_c}{F_b} \left(\frac{Q_b}{Q_c} \right)^2 + K_s$$

is determined from the curves $\xi_{c,s} = f \left(\frac{Q_s}{Q_c} \right)$ corresponding to different $\frac{F_b}{F_c}$;

K_s is taken from Table 7-8;

$$\xi_s = \frac{\Delta H_s}{\gamma w_s^2} = \frac{\xi_{c,s}}{\left(1 - \frac{Q_b}{Q_c} \right)^2 \left(\frac{F_c}{F_s} \right)^2}$$

F_b/F_c	Q_b/Q_c											
	0	0.03	0.05	0.1	0.2	0.3	0.4	0.5	0.6	0.7	0.8	1.0
Values of $\xi_{c,b}$												
0.06	-1.12	-0.72	-0.20	+2.00	10.6	24.5	43.5	68.0	-	-	-	-
0.10	-1.22	-1.00	-0.68	+0.10	3.18	8.01	14.6	23.0	33.1	-	-	-
0.20	-1.50	-1.25	-1.19	-0.83	+0.20	+1.52	3.30	5.40	7.80	10.5	13.7	-
0.33	-2.00	-1.81	-1.69	-1.37	-0.67	+0.09	+0.91	1.80	2.73	3.70	4.70	6.60
0.50	-3.00	-2.80	-2.60	-2.13	-1.38	-0.68	-0.02	+0.60	1.18	1.72	2.22	3.10
Values of $\xi_{c,s}$												
0.06	0.00	0.05	0.05	-0.03	-0.32	-1.10	-2.03	-3.42	-	-	-	-
0.10	0.01	0.06	0.09	+0.10	-0.03	-0.38	-0.96	-1.75	-2.75	-	-	-
0.20	0.06	0.10	0.14	0.19	+0.20	+0.09	-0.14	-0.50	-0.95	-1.50	-2.20	-
0.33	0.33	0.39	0.41	0.45	0.49	0.45	+0.34	+0.16	-0.10	-0.47	-0.85	-1.90
0.50	1.25	1.25	1.25	1.23	1.17	1.07	0.90	0.75	+0.48	+0.22	-0.05	-0.78

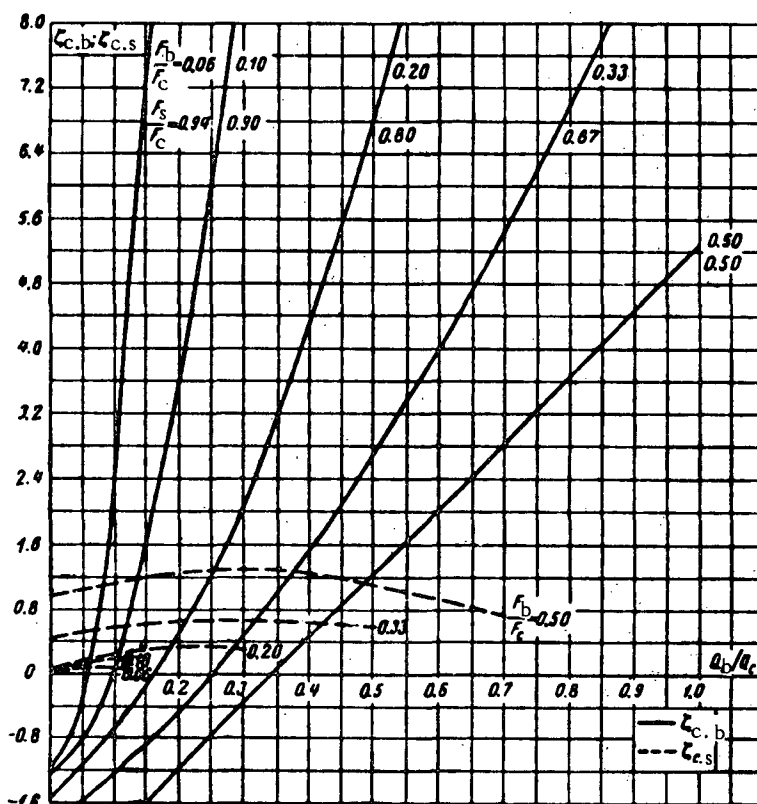
Converging wye of type $F_b + F_s = F_c$

Section VII

Diagram 7-12

TABLE 7-9

$\frac{F_b}{F_c}$	K_b
0.06	0
0.10	0
0.20	0.10
0.33	0.20
0.50	0.25



F_b/F_c	C_b/Q_c											
	0.	0.03	0.05	0.1	0.2	0.3	0.4	0.5	0.6	0.7	0.8	1.0
Values of $\zeta_{c,b}$												
0.06	-1.12	-0.75	-0.20	+2.06	11.2	25.0	46.2	72.5	-	-	-	-
0.10	-1.22	-1.00	-0.75	+0.20	3.58	8.91	16.2	25.5	36.7	-	-	-
0.20	-1.40	-1.25	-1.10	-0.68	+0.50	2.13	4.20	6.70	9.70	13.1	17.0	-
0.33	-1.80	-1.78	-1.50	-1.20	-0.45	+0.56	1.59	2.70	4.05	5.42	6.98	10.4
0.50	-2.75	-2.55	-2.35	-1.96	-1.15	-0.35	+0.42	1.25	2.05	2.80	3.65	5.25
Values of $\zeta_{c,s}$												
0.06	0.02	0.05	0.08	0.08	-	-	-	-	-	-	-	-
0.10	0.04	0.08	0.10	0.20	0.34	0.32	-	-	-	-	-	-
0.20	0.08	0.12	0.18	0.25	-	-	-	-	-	-	-	-
0.33	0.45	0.50	0.52	0.59	0.66	0.64	0.62	0.58	-	-	-	-
0.50	1.00	1.04	1.06	1.16	1.25	1.28	1.22	1.10	0.88	0.70	-	-

1. Branch

$$\zeta_{c,b} = \frac{\Delta H_b}{\gamma w_c^2} = 1 + \left(\frac{Q_b}{Q_c} \frac{F_c}{F_b} \right)^2 - 2 \frac{F_c}{F_b} \left(1 - \frac{Q_b}{Q_c} \right) + K_b$$

is determined from the curves $\zeta_{c,b} = f\left(\frac{Q_b}{Q_c}\right)$

corresponding to different $\frac{F_b}{F_c}$:

K_b is taken from Table 7-9;

$$K_b = \frac{\Delta H_b}{\gamma w_b^2} = \frac{\zeta_{c,b}}{\left(\frac{Q_b}{Q_c} \frac{F_c}{F_b} \right)^2}$$

2. Main passage

$$\zeta_{c,s} = \frac{\Delta H_s}{\gamma w_c^2}$$

is determined from the curves $\zeta_{c,s} = f\left(\frac{Q_b}{Q_c}\right)$

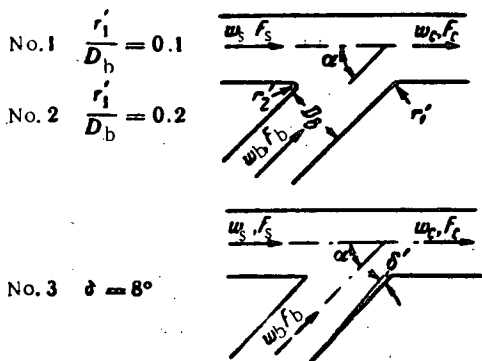
corresponding to different $\frac{F_b}{F_c}$:

$$\zeta_s = \frac{\Delta H_s}{\gamma w_s^2} = \frac{\zeta_{c,s}}{\left(1 - \frac{Q_b}{Q_c} \right) \left(\frac{F_c}{F_s} \right)^2}$$

Section VII

 Improved-shape converging wye of type $F_s + F_b > F_c$; $F_s = F_c$ $\alpha = 45^\circ$

Diagram 7-13


 Values of $\xi_{c,b}$

No.	1 $\left(\frac{r'_1}{D_b} = 0.1\right)$		2 $\left(\frac{r'_1}{D_b} = 0.2\right)$		3 ($\delta' = 8^\circ$)	
	F_b/F_c		1.0		0.122 0.34	
Q_b/Q_c	0.122	0.34	1.0	1.0	0.122	0.34
0.1	0.00	-0.47	-0.62	-0.62	-0.04	-0.58
0.3	4.30	+0.30	-0.17	-0.17	+1.80	0.00
0.6	19.5	2.10	+0.22	+0.22	0.50	0.90
1.0	53.7	5.40	0.38	0.38	22.5	2.10

1. Branch

$$\xi_{c,b} = \frac{\Delta H_b}{\gamma w_c^2} \text{ is determined from the curves } \xi_{c,b} = f\left(\frac{Q_b}{Q_c}\right)$$

 for different $\frac{F_b}{F_c}$ on graph a;

$$\xi_b = \frac{\Delta H_b}{\gamma w_b^2} = \frac{\xi_{c,b}}{\left(\frac{Q_b}{Q_c} \cdot \frac{F_c}{F_b}\right)^2}$$

2. Main passage

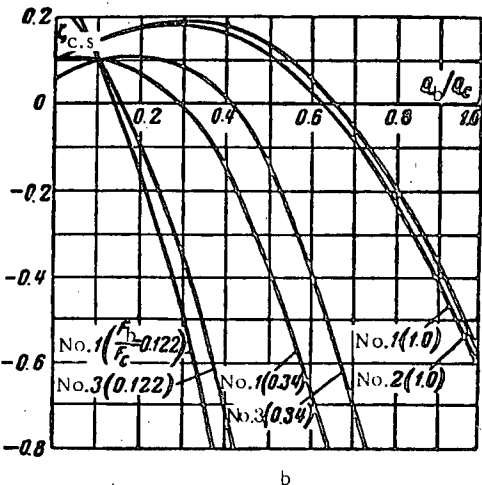
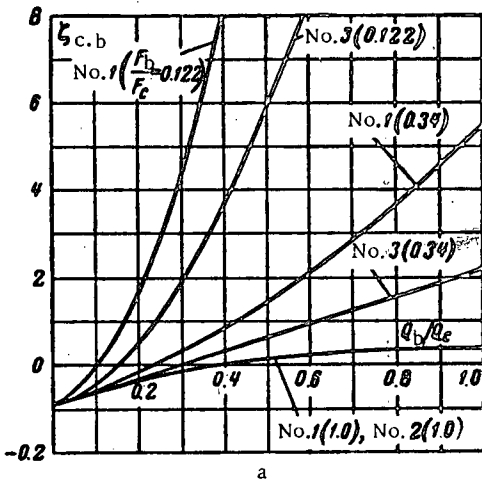
$$\xi_{c,s} = \frac{\Delta H_s}{\gamma w_c^2} \text{ is determined from the curves } \xi_{c,s} = f\left(\frac{Q_b}{Q_c}\right)$$

 for different $\frac{F_b}{F_c}$ on graph b;

$$\xi_s = \frac{\Delta H_s}{\gamma w_s^2} = \frac{\xi_{c,s}}{\left(1 - \frac{Q_b}{Q_c}\right)^2}$$

 Values of $\xi_{c,s}$

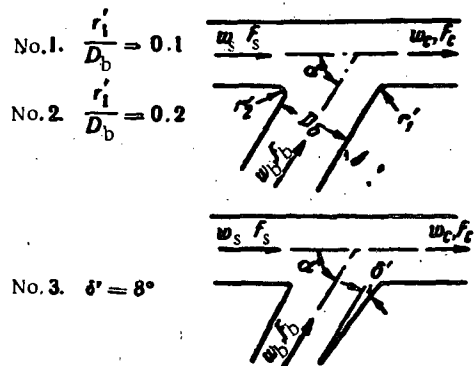
No.	1 $\left(\frac{r'_1}{D_b} = 0.1\right)$		2 $\left(\frac{r'_1}{D_b} = 0.2\right)$		3 ($\delta' = 8^\circ$)	
	F_b/F_c		1.0		0.122 0.34	
Q_b/Q_c	0.122	0.34	1.0	1.0	0.122	0.34
0.1	+0.10	0.10	0.14	0.14	0.10	0.10
0.3	-0.50	0.00	0.19	0.18	0.36	0.09
0.6	-3.20	-0.66	+0.06	0.03	2.20	0.40
1.0	-9.70	-2.90	-0.58	-0.61	-7.10	-1.95



Section VII

 Improved-shape converging wye of type $F_s + F_b > F_c$; $F_s = F_c$. $\alpha \approx 60^\circ$

Diagram 7-14


 Values of $\zeta_{c,b}$

No.	$1 \left(\frac{r'_1}{D_b} = 0.1 \right)$			$2 \left(\frac{r'_1}{D_b} = 0.2 \right)$		$3 (\delta' = 8^\circ)$	
	F_b/F_c						
Q_b/Q_c	0.122	0.34	1.0	1.0	0.122	0.34	
0.1	0.00	-0.43	-0.60	-0.60	-0.50	-0.56	
0.3	5.50	+0.42	-0.14	-0.16	+1.40	0.00	
0.6	21.9	2.30	+0.30	+0.26	7.50	0.87	
1.0	60.0	6.18	0.53	0.50	21.1	2.00	

1. Branch

$$\zeta_{c,b} = \frac{\Delta H_b}{\frac{1}{2} \rho g} \text{ is determined from the curves } \zeta_{c,b} = f\left(\frac{Q_b}{Q_c}\right)$$

 for different $\frac{F_b}{F_c}$ on graph a;

$$\zeta_b = \frac{\Delta H_b}{\frac{1}{2} \rho g} = \frac{\zeta_{c,b}}{\left(\frac{Q_b}{Q_c} \frac{F_c}{F_b}\right)^2}$$

2. Main passage

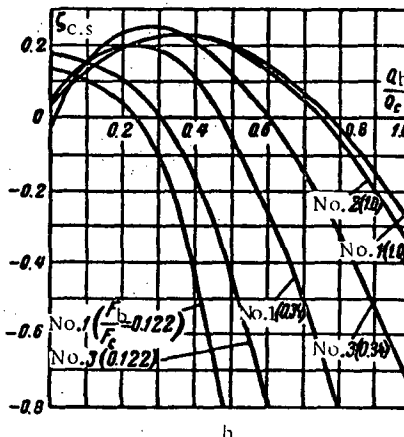
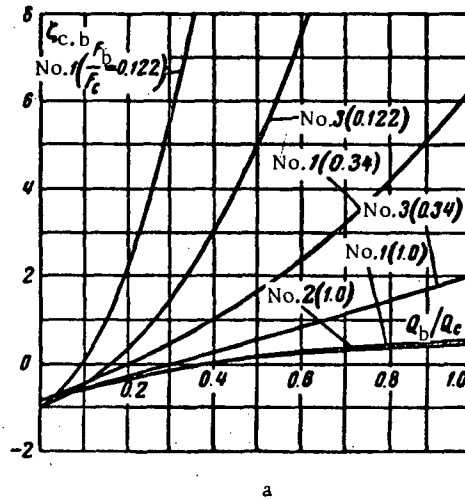
$$\zeta_{c,s} = \frac{\Delta H_s}{\frac{1}{2} \rho g} \text{ is determined from the curves } \zeta_{c,s} = f\left(\frac{Q_b}{Q_c}\right)$$

 for different $\frac{F_b}{F_c}$ on graph b;

$$\zeta_s = \frac{\Delta H_s}{\frac{1}{2} \rho g} = \frac{\zeta_{c,s}}{\left(1 - \frac{Q_b}{Q_c}\right)^2}$$

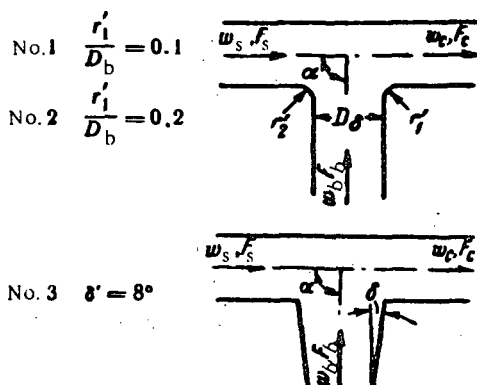
 Values of $\zeta_{c,s}$

No.	$1 \left(\frac{r'_1}{D_b} = 0.1 \right)$			$2 \left(\frac{r'_1}{D_b} = 0.2 \right)$		$3 (\delta' = 8^\circ)$	
	F_b/F_c						
Q_b/Q_c	0.122	0.34	1.0	1.0	0.122	0.34	
0.1	+0.10	0.15	0.13	0.13	0.15	0.15	
0.3	-0.10	+0.19	0.23	0.23	0.00	0.25	
0.6	-1.45	-0.25	+0.14	+0.13	-0.78	0.00	
1.0	-6.14	-1.65	-0.30	-0.35	-3.10	-0.75	



Section VII

Diagram 7-15

 Improved-shape converging tee of type $F_s + F_b > F_c$; $F_s = F_c$. $\alpha = 90^\circ$


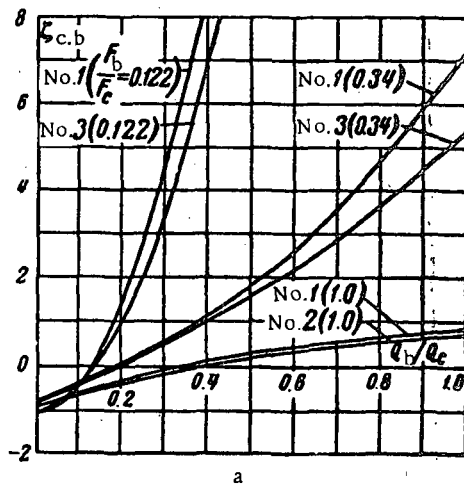
No.	Values of $\xi_{c,b}$					
	1 ($\frac{r'_1}{D_b} = 0.1$)	2 ($\frac{r'_1}{D_b} = 0.2$)	3 ($\delta' = 8^\circ$)	F_b/F_c	0.122	0.34
0.1	-0.50	-0.36	-0.60	-0.64	-0.50	-0.43
0.3	+4.60	+0.54	-0.10	-0.15	+3.24	+0.49
0.6	23.6	2.62	+0.43	+0.31	19.2	2.20
1.0	-	7.11	0.87	0.71	62.0	5.38

1. Branch

$$\xi_{c,b} = \frac{\Delta H_b}{\gamma w_c^2} \text{ is determined from the curves } \xi_{c,b} = f\left(\frac{Q_b}{Q_c}\right)$$

 for different $\frac{F_b}{F_c}$ on graph a;

$$\xi_b = \frac{\Delta H_b}{\gamma w_b^2} = \frac{\xi_{c,b}}{\left(\frac{Q_b}{Q_c} \frac{F_c}{F_b}\right)^2}$$

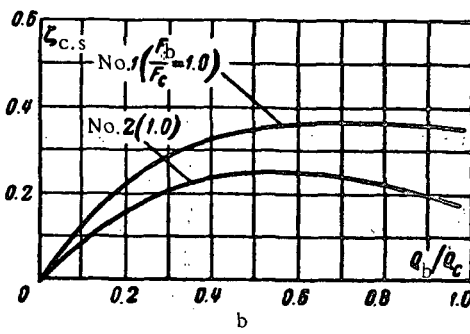


2. Main passage

$$\xi_{c,s} = \frac{\Delta H_s}{\gamma w_c^2} \text{ is determined from the curves } \xi_{c,s} = f\left(\frac{Q_b}{Q_c}\right)$$

 for different $\frac{F_b}{F_c}$ on graph b;

No.	Values of $\xi_{c,s}$	
	1 ($\frac{r'_1}{D_b} = 0.1$)	2 ($\frac{r'_1}{D_b} = 0.2$)
Q_b/Q_c	F_s/F_c	F_s/F_c
1.0	1.0	1.0
0.1	0.12	0.08
0.3	0.29	0.21
0.6	0.36	0.25
1.0	0.35	0.17

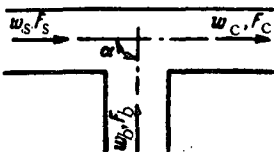


$$\xi_s = \frac{\Delta H_s}{\gamma w_s^2} = \frac{\xi_{c,s}}{\left(1 - \frac{Q_b}{Q_c}\right)^2}$$

Section VII

Standard converging threaded malleable-iron tee of type
 $F_s + F_b > F_c$; $F_s = F_c$. $\alpha = 90^\circ$

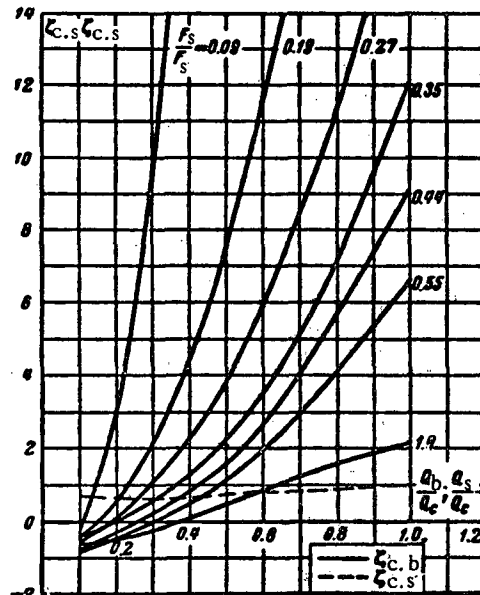
Diagram 7-16



1. Branch

$$\zeta_{c.b} = \frac{\Delta H_b}{\gamma w_c^2 / 2g}$$

is determined from the curves $\zeta_{c.b} = f\left(\frac{Q_b}{Q_c}\right)$ for different $\frac{F_b}{F_s}$:



$$\zeta_{c.b} = \frac{\Delta H_b}{\gamma w_b^2 / 2g} = \frac{\zeta_{c.b}}{\left(\frac{Q_b}{Q_c} \cdot \frac{F_c}{F_b}\right)^2}$$

2. Main passage

$$\zeta_{c.s} = \frac{\Delta H_s}{\gamma w_c^2 / 2g}$$

is determined from the curve $\zeta_{c.s} = f\left(\frac{Q_s}{Q_c}\right)$:

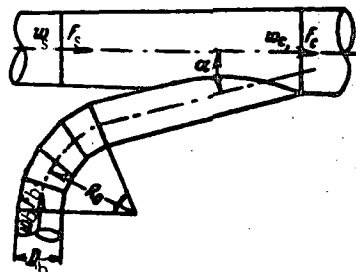
$$\zeta_s = \frac{\Delta H_s}{\gamma w_s^2 / 2g} = \frac{\zeta_{c.s}}{\left(1 - \frac{Q_b}{Q_c}\right)^2}$$

F_b/F_c	Q_b/Q_c									
	0.1	0.2	0.3	0.4	0.5	0.6	0.7	0.8	0.9	1.0
Values of ζ_b										
0.09	-0.50	+2.97	9.90	19.7	32.4	48.8	66.5	86.9	110	136
0.19	-0.53	+0.53	2.14	4.23	7.30	11.4	15.6	20.3	25.8	31.8
0.27	-0.69	0.00	1.11	2.18	3.76	5.90	8.38	11.3	14.6	18.4
0.35	-0.65	-0.09	+0.59	1.31	2.24	3.52	5.20	7.28	9.23	12.2
0.44	-0.80	-0.27	+0.26	0.84	1.59	2.66	4.00	5.73	7.40	9.12
0.55	-0.83	-0.48	0.00	0.53	1.15	1.89	2.92	4.00	5.36	6.60
1.0	-0.65	-0.40	-0.24	+0.10	0.50	0.83	1.13	1.47	1.86	2.30
Values of $\zeta_{c.s}$										
At all F_b/F_c	0.70	0.64	0.60	0.65	0.75	0.85	0.92	0.96	0.99	1.00

Circular-section converging wye with smooth side bend
 $\left(\frac{R_o}{D_b} = 2\right)$ of type $F_s + F_b = F_c$. $\alpha = 12$ to 15° . Branch

Section VII

Diagram 7-17

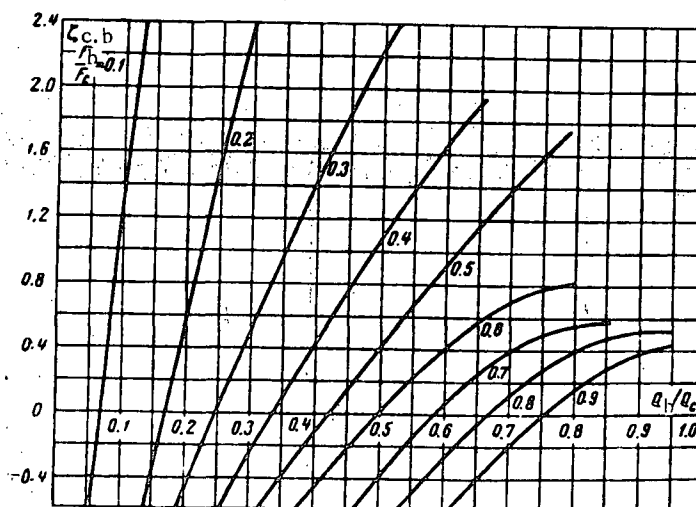


$$\zeta_{c,b} = \frac{\Delta H_b}{\frac{\tau w_c^2}{2g}}$$

is determined from the curves $\zeta_{c,b} = f\left(\frac{Q_b}{Q_c}\right)$ for different $\frac{F_b}{F_c}$

$$\zeta_b = \frac{\Delta H_b}{\frac{\tau w_b^2}{2g}} = \frac{\zeta_b}{\left(\frac{Q_b F_c}{Q_c F_b}\right)^2}$$

F_b/F_c	Q_b/Q_c										
	0.1	0.15	0.2	0.3	0.4	0.5	0.6	0.7	0.8	0.9	1.0
	Values of $\zeta_{c,b}$										
0.1	1.20	+2.90	—	—	—	—	—	—	—	—	—
0.2	—	-0.36	+0.60	2.40	—	—	—	—	—	—	—
0.3	—	—	-0.48	+0.50	1.40	2.22	—	—	—	—	—
0.4	—	—	—	-0.24	+0.44	1.09	1.68	—	—	—	—
0.5	—	—	—	—	-0.10	+0.40	0.92	1.40	—	—	—
0.6	—	—	—	—	-0.44	+0.02	0.40	0.70	—	—	—
0.7	—	—	—	—	—	-0.37	+0.06	0.40	0.56	—	—
0.8	—	—	—	—	—	—	-0.28	+0.12	0.40	0.52	—
0.9	—	—	—	—	—	—	-0.60	-0.20	+0.16	0.39	—

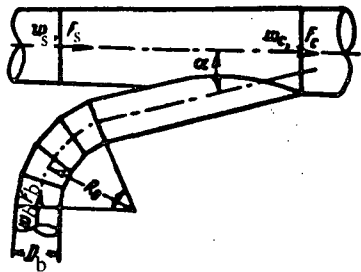


Section VII

 Circular-section converging wye with smooth side bend ($\frac{R_o}{D_s} = 2$)

 $F_s + F_b = F_c$, $\alpha = 12$ to 15° . Straight passage

Diagram 7-18



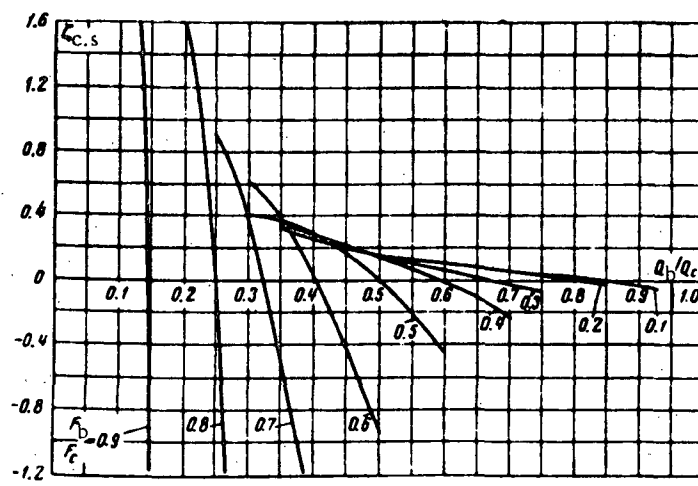
$$\zeta_{c,s} = \frac{\Delta H_s}{\gamma w_s^2}$$

 is determined from the curves $\zeta_{c,s} = f\left(\frac{Q_b}{Q_c}\right)$ for different

$$\frac{F_b}{F_c}$$

$$\zeta_s = \frac{\Delta H_s}{\gamma w_s^2} = \frac{\zeta_{c,s}}{\left(1 - \frac{Q_b}{Q_c}\right)^2 \left(\frac{F_c}{F_s}\right)^2}$$

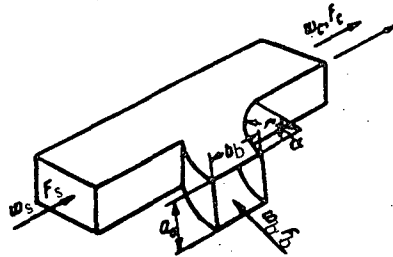
F_b/F_c	Q_b/Q_c										
	0.14	0.15	0.2	0.25	0.3	0.4	0.5	0.6	0.7	0.8	0.9
Values of $\zeta_{c,s}$											
0.1	—	—	—	—	—	—	0.16	0.10	0.06	+0.02	-0.04
0.2	—	—	—	—	—	—	0.16	0.10	0.06	0.00	—
0.3	—	—	—	—	—	0.26	0.16	+0.06	-0.02	—	—
0.4	—	—	—	—	—	0.30	0.16	0.00	-0.24	—	—
0.5	—	—	—	—	0.40	0.30	0.00	-0.44	—	—	—
0.6	—	—	—	—	0.60	+0.03	-0.94	—	—	—	—
0.7	—	—	—	0.90	+0.37	-1.48	—	—	—	—	—
0.8	—	—	1.60	0.00	—	—	—	—	—	—	—
0.9	+0.60	-1.20	—	—	—	—	—	—	—	—	—



Section VII

Rectangular-section converging wye of type $F_s + F_b \geq F_c$, smooth
 $(r/b_b = 1.0)$. $\alpha = 90^\circ$. Branch

Diagram 7-19



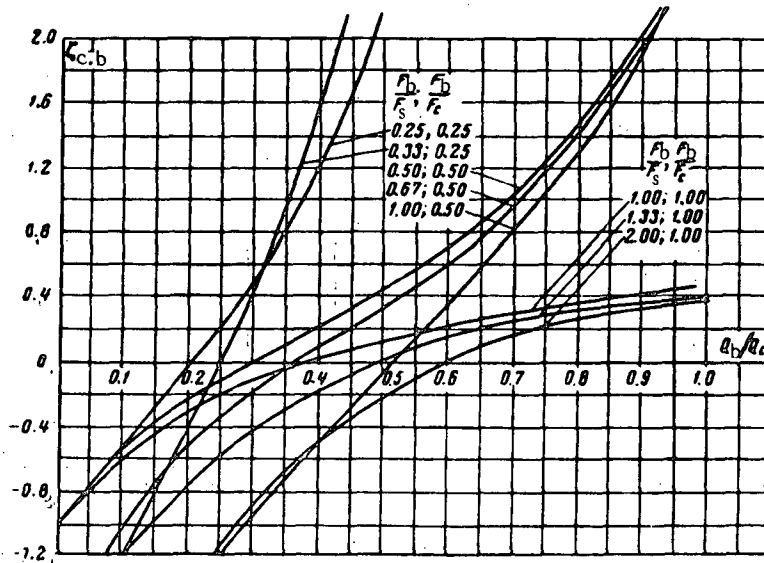
$$\xi_{c,b} = \frac{\Delta H_b}{\gamma w_c^2} \frac{2g}{2g}$$

is determined from the curves $\xi_{c,b} = f\left(\frac{Q_b}{Q_c}\right)$ for different
 $\frac{F_b}{F_s}$ and $\frac{F_b}{F_c}$;

$$\xi_b = \frac{\Delta H_s}{\gamma w_b^2} = \frac{\xi_{c,b}}{\left(\frac{O_b F_c}{Q_c F_b}\right)^2}$$

 Values of $\xi_{c,b}$

F_b/F_s	F_s/F_c	F_b/F_c	Q_b/Q_c										
			0	0.1	0.2	0.3	0.4	0.5	0.6	0.7	0.8	0.9	1.0
0.25	1.00	0.25	-1.00	-0.50	0.00	0.50	1.20	2.20	3.70	5.80	8.40	11.4	14.0
0.33	0.75	0.25	-2.00	-1.20	-0.40	+0.40	1.60	3.00	4.80	6.80	8.90	11.0	13.0
0.50	1.00	0.50	-1.00	-0.50	-0.20	0.00	0.25	0.45	0.70	1.00	1.50	2.00	2.70
0.67	0.75	0.50	-1.70	-1.00	-0.60	-0.20	+0.10	0.30	0.60	1.00	1.45	2.00	2.60
1.00	0.50	0.50	-3.00	-2.15	-1.45	-0.95	-0.50	0.00	0.40	0.80	1.30	1.90	2.80
1.00	1.00	1.00	-1.00	-0.60	-0.30	-0.10	+0.04	0.13	0.21	0.29	0.36	0.42	0.50
1.33	0.75	1.00	-1.80	-1.20	-0.80	-0.40	-0.20	0.00	0.16	0.24	0.32	0.38	0.40
2.00	0.50	1.00	-3.00	-2.10	-1.40	-0.90	-0.50	-0.20	0.00	0.20	0.25	0.30	0.40

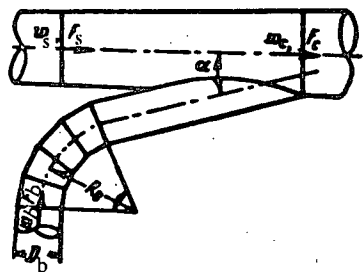


Section VII

 Circular-section converging wye with smooth side bend ($\frac{R_o}{D_s} = 2$)

 $F_s + F_b = F_c$. $\alpha = 12$ to 15° . Straight passage

Diagram 7-18



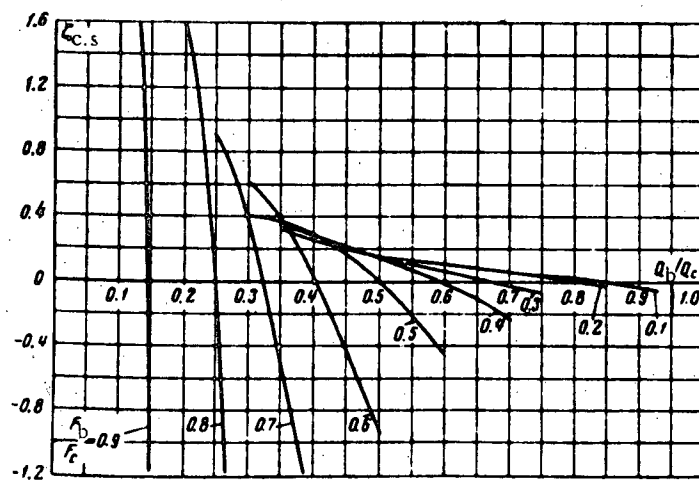
$$\xi_{c,s} = \frac{\Delta H_s}{\gamma v_s^2} \cdot \frac{2g}{2g}$$

 is determined from the curves $\xi_{c,s} = f\left(\frac{Q_b}{Q_c}\right)$ for different

$$\frac{F_b}{F_c}$$

$$\xi_s = \frac{\Delta H_s}{\gamma v_s^2} = \frac{\xi_{c,s}}{\left(1 - \frac{Q_b}{Q_c}\right)^2 \left(\frac{F_c}{F_s}\right)^2}$$

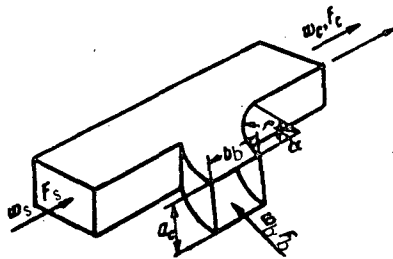
F_b/F_c	Q_b/Q_c											
	0.14	0.15	0.2	0.25	0.3	0.4	0.5	0.6	0.7	0.8	0.9	
Values of $\xi_{c,s}$												
0.1	—	—	—	—	—	—	0.16	0.10	0.06	+0.02	—0.04	
0.2	—	—	—	—	—	—	0.16	0.10	0.06	0.00	—	
0.3	—	—	—	—	—	0.26	0.16	+0.06	-0.02	—	—	
0.4	—	—	—	—	—	0.30	0.16	0.00	-0.24	—	—	
0.5	—	—	—	—	0.40	0.30	0.00	-0.44	—	—	—	
0.6	—	—	—	—	0.60	+0.03	-0.94	—	—	—	—	
0.7	—	—	—	0.90	+0.37	-1.48	—	—	—	—	—	
0.8	—	—	1.60	0.00	—	—	—	—	—	—	—	
0.9	+0.60	-1.20	—	—	—	—	—	—	—	—	—	



Section VII

Rectangular-section converging wye of type $F_s + F_b \geq F_c$, smooth
 $(r/b_b = 1.0)$. $\alpha = 90^\circ$. Branch

Diagram 7-19



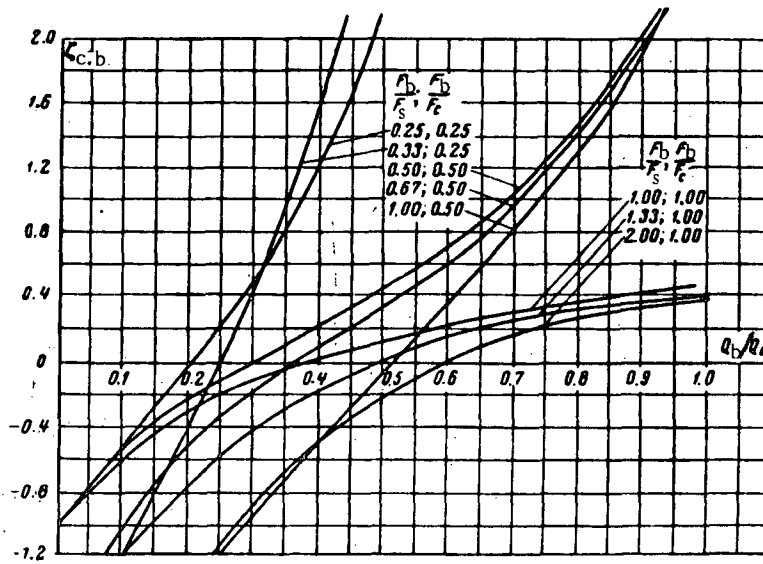
$$\zeta_{c,b} = \frac{\Delta H_b}{\gamma w_c^2}$$

is determined from the curves $\zeta_{c,b} = f\left(\frac{Q_b}{Q_c}\right)$ for different $\frac{F_b}{F_s}$ and $\frac{F_b}{F_c}$:

$$\zeta_b = \frac{\Delta H_s}{\gamma w_b^2} = \frac{\zeta_{c,b}}{\left(\frac{Q_b}{Q_c} \frac{F_c}{F_b}\right)^2}$$

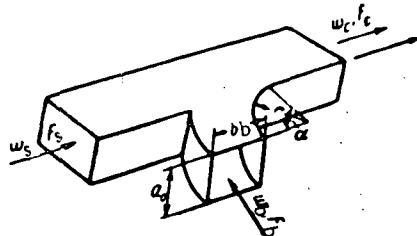
 Values of $\zeta_{c,b}$

F_b/F_s	F_s/F_c	F_b/F_c	Q_b/Q_c										
			0	0.1	0.2	0.3	0.4	0.5	0.6	0.7	0.8	0.9	1.0
0.25	1.00	0.25	-1.00	-0.50	0.00	0.50	1.20	2.20	3.70	5.80	8.40	11.4	14.0
0.33	0.75	0.25	-2.00	-1.20	-0.40	+0.40	1.60	3.00	4.80	6.80	8.90	11.0	13.0
0.50	1.00	0.50	-1.00	-0.50	-0.20	0.00	0.25	0.45	0.70	1.00	1.50	2.00	2.70
0.67	0.75	0.50	-1.70	-1.00	-0.60	-0.20	+0.10	0.30	0.60	1.00	1.45	2.00	2.60
1.00	0.50	0.50	-3.00	-2.15	-1.45	-0.95	-0.50	0.00	0.40	0.80	1.30	1.90	2.80
1.00	1.00	1.00	-1.00	-0.60	-0.30	-0.10	+0.04	0.13	0.21	0.29	0.36	0.42	0.50
1.33	0.75	1.00	-1.80	-1.20	-0.80	-0.40	-0.20	0.00	0.16	0.24	0.32	0.38	0.40
2.00	0.50	1.00	-3.00	-2.10	-1.40	-0.90	-0.50	-0.20	0.00	0.20	0.25	0.30	0.40



Rectangular-section converging wye of type $F_s + F_b \geq F_c$, smooth
 $(r/b_b = 1.0)$. $\alpha = 90^\circ$. Main passage

Section VII
Diagram 7-20



$$\zeta_{c,s} = \frac{\Delta H_s}{\frac{1}{2} w_s^2}$$

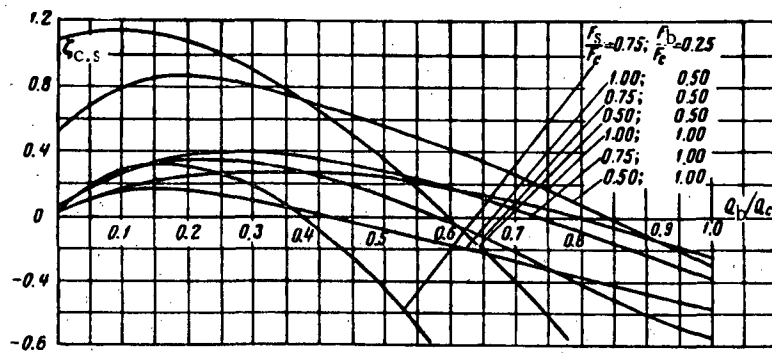
is determined from the curves $\zeta_{c,s} = f\left(\frac{Q_b}{Q_c}\right)$ for different

$$\frac{F_b}{F_c} \text{ and } \frac{F_s}{F_c};$$

$$\zeta_s = \frac{\Delta H_s}{\frac{1}{2} w_s^2} = \frac{\zeta_{c,s}}{\left(1 - \frac{Q_b}{Q_c}\right)^2 \left(\frac{F_c}{F_s}\right)^2}.$$

Values of $\zeta_{c,s}$

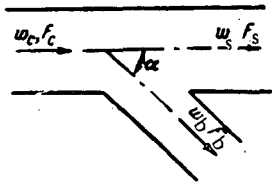
$\frac{F_b}{F_s}$	$\frac{F_s}{F_c}$	$\frac{F_b}{F_c}$	$\frac{Q_b}{Q_c}$											
			0	0.1	0.2	0.3	0.4	0.5	0.6	0.7	0.8	0.9	1.0	
0.33	0.75	0.25	0.00	0.30	0.30	+0.20	-0.10	-0.45	-0.92	-1.45	-2.00	-2.60	-3.30	
0.50	1.00	0.50	0.00	0.17	0.16	0.10	0.00	-0.08	-0.18	-0.27	-0.37	-0.46	-0.55	
0.67	0.75	0.50	0.00	0.27	0.35	0.32	0.25	+0.12	-0.03	-0.23	-0.42	-0.58	-0.70	
1.00	0.50	0.50	1.10	1.15	1.10	0.90	0.65	0.35	0.00	-0.40	-0.80	-1.30	-1.80	
1.00	1.00	1.00	0.00	0.18	0.24	0.27	0.26	0.23	0.18	0.10	0.00	-0.12	-0.25	
1.33	0.75	1.00	0.05	0.75	0.36	0.38	0.35	0.27	0.18	+0.05	-0.08	-0.22	-0.36	
2.00	0.50	1.00	0.50	0.80	0.87	0.80	0.68	0.55	0.40	0.25	+0.08	-0.10	-0.30	



Diverging wye of type $F_s + F_b > F_c$; $F_s = F_c$. $\alpha = 0-90^\circ$. Branch

Section VII

Diagram 7-21



No. 1. $0 < \alpha < 60^\circ$ and $\alpha = 90^\circ$ at $\frac{h_b}{h_c} \leq 2/3$

$$\zeta_{c,b} = \frac{\Delta H_b}{\gamma w_c^2} = A' \left[1 + \left(\frac{w_b}{w_c} \right)^2 - 2 \frac{w_b}{w_c} \cos \alpha \right] = A' \zeta'_{c,b}$$

h_b — height of the branch;
 h_c — height of the common channel

$$\zeta_b = \frac{\Delta H_b}{\gamma w_b^2} = \frac{\zeta_{c,b}}{\left(\frac{w_b}{w_c} \right)^2};$$

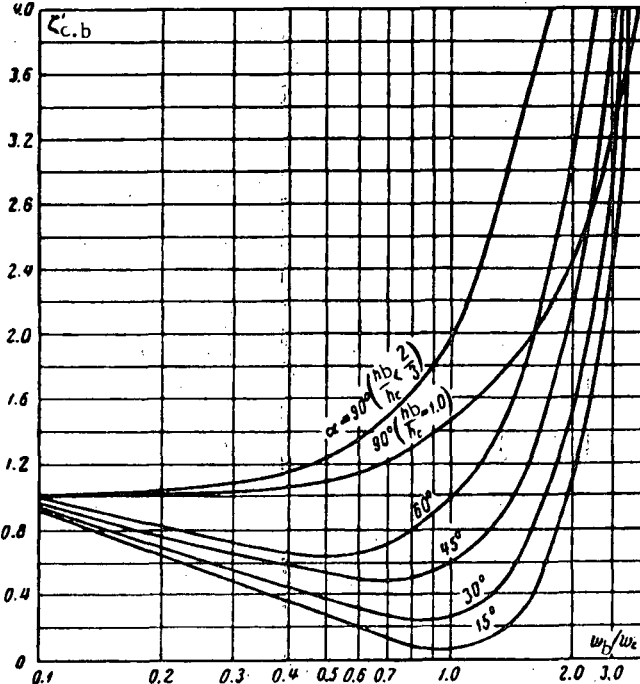
$$\frac{w_b}{w_c} = \frac{Q_b}{Q_c} \frac{F_c}{F_b}.$$

No. 2. $\alpha = 90^\circ$ and $\frac{h_b}{h_c} = 1.0$ (up to $\frac{w_b}{w_c} \geq 2.0$)

$$\zeta_{c,b} = \frac{\Delta H_b}{\gamma w_c^2} = A' \left[0.34 + \left(\frac{w_b}{w_c} \right)^2 \right] = A' \zeta'_{c,b}.$$

where $\zeta'_{c,b}$ is determined from the curves $\zeta'_{c,b} = f\left(\frac{w_b}{w_c}\right)$ for different α° ;

$$A' = 1.0 \text{ for } \frac{w_b}{w_c} \leq 0.8;$$



$$A' \approx 0.9 \text{ for } \frac{w_b}{w_c} > 0.8;$$

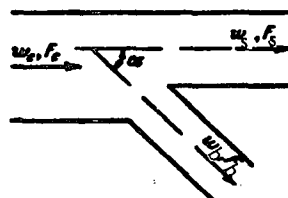
Values of $\zeta'_{c,s}$

w_b/w_c	α°					α°	
	15	30	45	60	$h_b/h_c \leq 2/3$	$h_b/h_c = 1.0$	
0	1.0	1.0	1.0	1.0	1.0	1.0	1.0
0.1	0.92	0.94	0.97	1.0	1.01	1.0	1.0
0.2	0.65	0.70	0.75	0.84	1.04	1.01	1.01
0.4	0.38	0.46	0.60	0.76	1.16	1.05	1.05
0.6	0.20	0.31	0.50	0.65	1.35	1.15	1.15
0.8	0.09	0.25	0.51	0.80	1.64	1.32	1.32
1.0	0.07	0.27	0.58	1.00	2.00	1.45	1.45
1.2	0.12	0.36	0.74	1.23	2.44	1.60	1.60
1.4	0.24	0.70	0.98	1.54	2.96	1.77	1.77
1.6	0.46	0.80	1.30	1.98	3.54	1.95	1.95
2.0	1.10	1.52	2.16	3.00	4.60	2.45	2.45
2.6	2.75	3.23	4.10	5.15	7.76	—	—
3.0	7.20	7.40	7.80	8.10	9.00	—	—
4.0	14.1	14.2	14.8	15.0	16.0	—	—
5.0	23.2	23.5	23.8	24.0	25.0	—	—
6.0	34.2	34.5	35.0	35.0	36.0	—	—
8.0	62.0	62.7	63.0	63.0	64.0	—	—
10	98.0	98.3	98.6	99.0	100	—	—

Diverging wye of type $F_s + F_b = F_c$. $\alpha = 0-90^\circ$. Branch

Section VII

Diagram 7-22



$$\zeta_{c.b} = \frac{\Delta H_b}{\gamma w_c^2} = 1 + \left(\frac{w_b}{w_c} \right)^2 - 2 \frac{w_b}{w_c} \cos \alpha - K'_b \left(\frac{w_b}{w_c} \right)^2,$$

where K'_b is taken from Table 7-10.

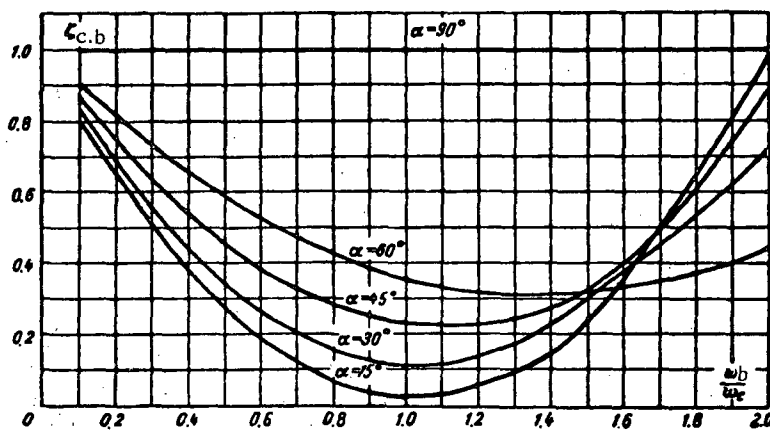
TABLE 7-10

α°	15	30	45	60	90
K'_b	0.04	0.16	0.36	0.64	1.00

$\zeta_{c.b}$ is determined from the curves $\zeta_{c.b} = f \left(\frac{w_b}{w_c} \right)$
for different α° .

Values of $\zeta_{c.b}$

α°	w_b/w_c												
	0.1	0.2	0.3	0.4	0.5	0.6	0.8	1.0	1.2	1.4	1.6	1.8	2.0
15	0.81	0.65	0.51	0.38	0.28	0.19	0.06	0.03	0.06	0.13	0.35	0.63	0.98
30	0.84	0.69	0.56	0.44	0.34	0.26	0.16	0.11	0.13	0.23	0.37	0.60	0.89
45	0.87	0.74	0.63	0.54	0.45	0.38	0.28	0.23	0.22	0.28	0.38	0.53	0.73
60	0.90	0.82	0.79	0.66	0.59	0.53	0.43	0.36	0.32	0.31	0.33	0.37	0.44
90	1.00	1.00	1.00	1.00	1.00	1.00	1.00	1.00	1.00	1.00	1.00	1.00	1.00



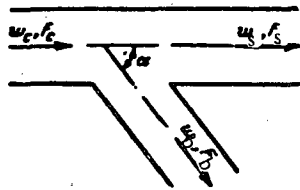
Diverging wye of type $F_s + F_b > F_c$ and $F_s + F_b = F_c$. $\alpha = 0-90^\circ$.

Main passage

Section VII

Diagram 7-23

No.1. $F_s + F_b > F_c$

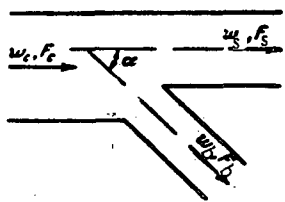


No. 1 $\frac{w_s}{w_c} \leq 1.0$:

$$\epsilon_{c,s} = \frac{\Delta H_s}{\gamma w_c^2} \approx 0.4 \left(1 - \frac{w_s}{w_c} \right)^2.$$

No. 2. $\frac{w_s}{w_c} \leq 1.0$:

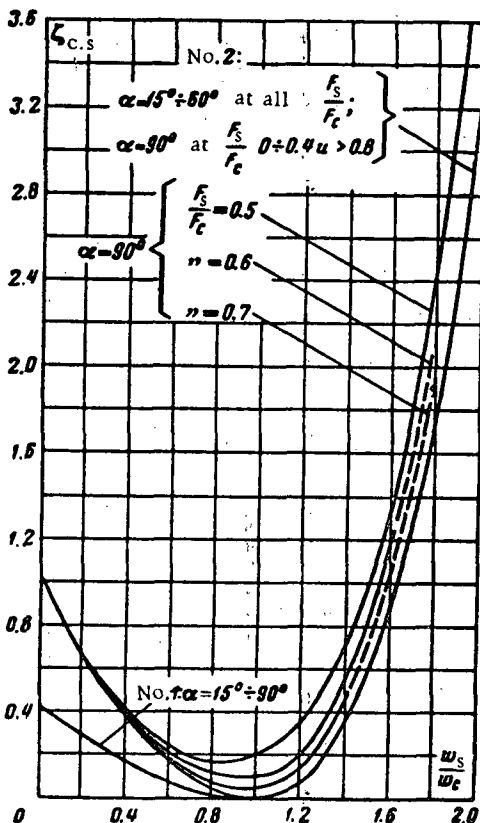
No.2. $F_s + F_b = F_c$



$\epsilon_{c,s} = \frac{\Delta H_s}{\gamma w_c^2}$ is determined from the curves $\epsilon_{c,s} = f\left(\frac{w_s}{w_c}\right)$

$$\epsilon_s = \frac{\Delta H_s}{\gamma w_s^2} = \frac{\epsilon_{c,s}}{\left(\frac{w_s}{w_c}\right)^2};$$

$$\frac{w_s}{w_c} = \frac{Q_s F_c}{Q_e F_s}.$$

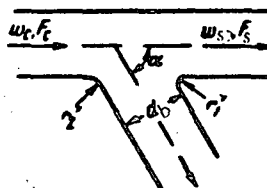


Values of $\epsilon_{c,s}$

α	No.1		No.2					
	15 - 90°	15 - 60°	90°					
w _s w _c	F _s / F _c							
	0 - 1.0	0 - 1.0	0 - 0.4	0.5	0.6	0.7	> 0.8	
0	0.40	1.00	1.00	1.00	1.00	1.00	1.00	
0.1	0.32	0.81	0.81	0.81	0.81	0.81	0.81	
0.2	0.26	0.64	0.64	0.64	0.64	0.64	0.64	
0.3	0.20	0.50	0.50	0.52	0.52	0.50	0.50	
0.4	0.15	0.36	0.36	0.40	0.38	0.37	0.36	
0.5	0.10	0.25	0.25	0.30	0.28	0.26	0.25	
0.6	0.06	0.16	0.16	0.23	0.20	0.18	0.16	
0.8	0.02	0.04	0.04	0.16	0.12	0.07	0.04	
1.0	0.00	0.00	0.00	0.20	0.10	0.05	0.00	
1.2	—	0.07	0.07	0.36	0.21	0.14	0.07	
1.4	—	0.39	0.39	0.78	0.59	0.49	—	
1.6	—	0.90	0.90	1.36	1.15	—	—	
1.8	—	1.78	1.78	2.43	—	—	—	
2.0	—	3.20	3.20	4.00	—	—	—	

1. Branch

No. 1. $\frac{r'_2}{D_b} = 0.1$

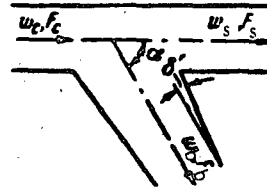


$$\zeta_{c,b} = \frac{\Delta H_b}{\gamma w_c^2}$$

No. 2. $\frac{r'_2}{D_b} = 0.2$

is determined from the curves $\zeta_{c,b} = f\left(\frac{Q_b}{Q_c}\right)$:

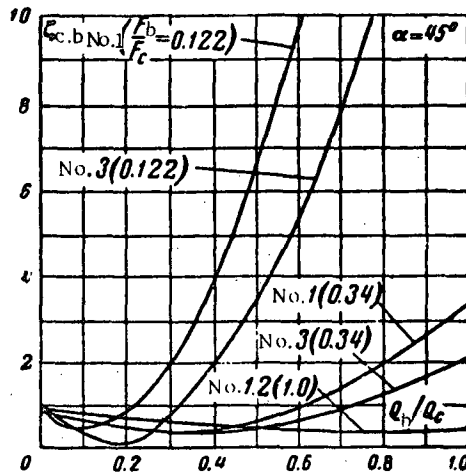
No. 3. $\delta' = 8^\circ$



$$\zeta_b = \frac{\Delta H_b}{\gamma w_b^2} = \frac{\zeta_{c,b}}{\left(\frac{Q_b}{Q_c} \cdot \frac{F_c}{F_b}\right)^2}$$

1. $\alpha = 45^\circ$ Values of $\zeta_{c,b}$

No.	$1 \left(\frac{r'_2}{D_b} = 0.1 \right)$		$2 \left(\frac{r'_2}{D_b} = 0.2 \right)$		$3 (\delta' = 8^\circ)$		
	F_b/F_c						
Q_b/Q_c	0.122	0.34	1.0	1.0	0.122	0.34	
	0.1	0.40	0.62	0.77	0.77	0.40	0.62
0.3	1.90	0.35	0.56	0.56	0.90	0.35	
0.6	9.60	0.90	0.32	0.32	5.40	0.60	
1.0	30.6	3.35	0.32	0.32	17.4	2.00	



1. Branch

 2. $\alpha = 60^\circ$

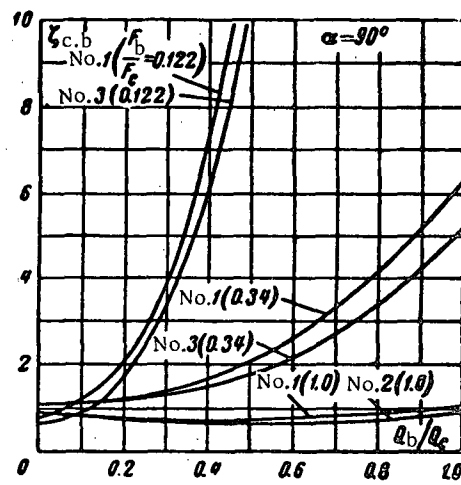
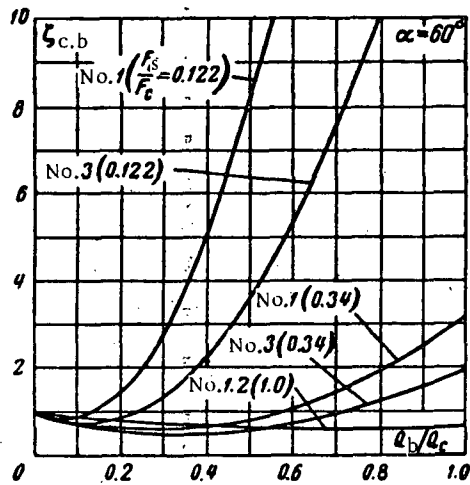
 3. $\alpha = 90^\circ$

 Values of $\zeta_{c,b}$

No.	$1 \left(\frac{r'_2}{D_b} = 0.1 \right)$		$2 \left(\frac{r'_2}{D_b} = 0.2 \right)$		3 ($\theta = 8^\circ$)	
	F_b/F_c					
Q_b/Q_c	0.122	0.34	1.0	1.0	0.122	0.34
0.1	0.90	0.77	0.84	0.84	0.70	0.67
0.3	2.70	0.60	0.67	0.67	1.30	0.44
0.6	12.0	1.10	0.53	0.53	5.40	0.68
1.0	36.7	3.16	0.62	0.62	16.6	1.85

 Values of $\zeta_{c,b}$

No.	$1 \left(\frac{r'_2}{D_b} = 0.1 \right)$		$2 \left(\frac{r'_2}{D_b} = 0.2 \right)$		3 ($\theta' = 8^\circ$)	
	F_b/F_c					
Q_b/Q_c	0.122	0.34	1.0	1.0	0.122	0.34
0.1	1.20	1.15	0.85	0.85	0.80	1.10
0.3	4.00	1.42	0.77	0.74	3.40	1.30
0.6	17.8	2.65	0.78	0.69	17.3	2.17
1.0	—	6.30	1.00	0.91	—	5.20



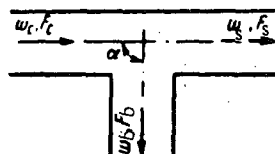
2. Main passage

$$\zeta_{c,s} = \frac{\Delta H_s}{\frac{\rho g}{2} \frac{T^2}{C_p}} \quad \text{is taken from diagram 7-23 (No. 1)}$$

Standard threaded malleable-iron diverging tee of type
 $F_s + F_b > F_c$; $F_s = F_c$. $\alpha = 90^\circ$

Section VII

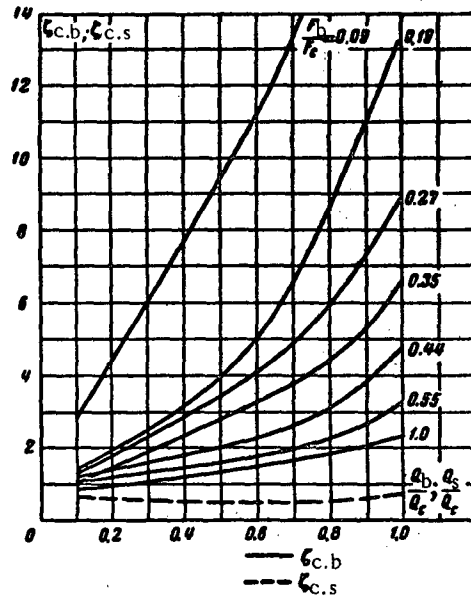
Diagram 7-25



1. Branch

$$\xi_{c,b} = \frac{\Delta H_b}{\gamma w_c^2} \cdot \frac{2g}{F_b}$$

is determined from the curves $\xi_{c,b} = f\left(\frac{Q_b}{Q_c}\right)$ for different $\frac{F_b}{F_c}$:



$$\xi_b = \frac{\Delta H_b}{\gamma w_b^2} = \frac{\xi_{c,b}}{\left(\frac{Q_b F_c}{Q_c F_b}\right)^2} \cdot \frac{2g}{F_b}$$

2. Main passage

$$\xi_{c,s} = \frac{\Delta H_s}{\gamma w_c^2} \cdot \frac{2g}{F_c}$$

is determined from the curve $\xi_{c,s} = f\left(\frac{Q_s}{Q_c}\right)$ for all $\frac{F_b}{F_c}$:

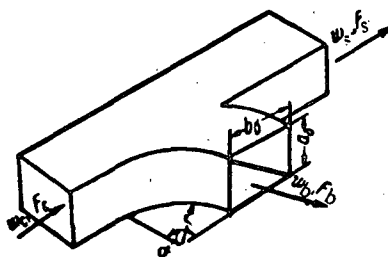
$$\xi_s = \frac{\Delta H_s}{\gamma w_s^2} = \frac{\xi_{c,s}}{\left(1 - \frac{Q_b}{Q_c}\right)^2 \left(\frac{F_c}{F_s}\right)^2} \cdot \frac{2g}{F_s}$$

F_b/F_c	$Q_b/Q_c (Q_s/Q_c)$									
	0.1	0.2	0.3	0.4	0.5	0.6	0.7	0.8	0.9	1.0
Values of $\xi_{c,b}$										
0.09	2.80	4.50	6.00	7.88	9.40	11.1	13.0	15.8	20.0	24.7
0.19	1.41	2.00	2.50	3.20	3.97	4.95	6.50	8.45	10.8	13.3
0.27	1.37	1.81	2.30	2.83	3.40	4.07	4.80	6.00	7.18	8.90
0.35	1.10	1.54	1.90	2.35	2.73	3.22	3.80	4.32	5.28	6.53
0.44	1.22	1.45	1.67	1.89	2.11	2.38	2.58	3.04	3.84	4.75
0.55	1.09	1.20	1.40	1.59	1.65	1.77	1.94	2.20	2.68	3.30
1.00	0.90	1.00	1.13	1.20	1.40	1.50	1.50	1.80	2.06	2.30
Values of $\xi_{c,s}$										
Any F_b/F_c	0.70	0.64	0.60	0.57	0.55	0.51	0.49	0.55	0.62	0.70

Rectangular-section smooth ($r/b_s = 1.0$) diverging wye of type $F_s + F_b > F_e$.
 $\alpha = 90^\circ$. Branch

Section VII

Diagram 7-26



$$\zeta_{c,b} = \frac{\Delta H_b}{\gamma w_e^2} \cdot \frac{2g}{2g}$$

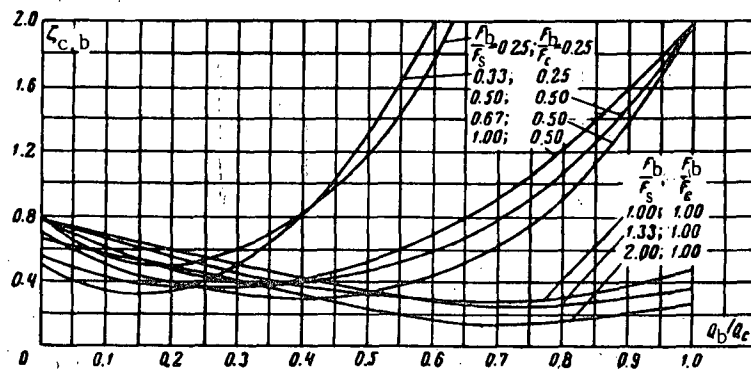
is determined from the curves $\zeta_{c,b} = f\left(\frac{Q_b}{Q_e}\right)$ for different

$$\frac{F_b}{F_s} \text{ and } \frac{F_b}{F_e};$$

$$\zeta_b = \frac{\Delta H_s}{\gamma w_s^2} = \frac{\zeta_{c,s}}{\left(\frac{Q_s F_e}{Q_e F_s}\right)^2}.$$

Values of $\zeta_{c,b}$

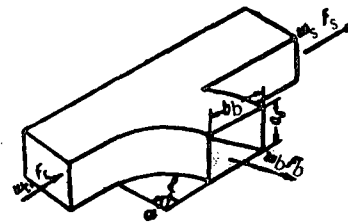
$\frac{F_b}{F_s}$	$\frac{F_s}{F_e}$	$\frac{F_b}{F_c}$	Q_b/Q_e										
			0	0.1	0.2	0.3	0.4	0.5	0.6	0.7	0.8	0.9	1.0
0.25	1.00	0.25	0.80	0.55	0.50	0.60	0.85	1.20	1.80	3.10	4.35	6.00	6.70
0.33	0.75	0.25	0.50	0.35	0.35	0.50	0.80	1.30	2.00	2.80	3.75	5.00	6.50
0.50	1.00	0.50	0.80	0.62	0.48	0.40	0.40	0.48	0.60	0.78	1.08	1.50	2.00
0.67	0.75	0.50	0.70	0.52	0.40	0.32	0.30	0.34	0.44	0.62	0.92	1.38	2.00
1.00	0.50	0.50	0.55	0.44	0.38	0.38	0.41	0.52	0.68	0.92	1.21	1.57	2.00
1.00	1.00	1.00	0.78	0.67	0.55	0.46	0.37	0.32	0.29	0.29	0.30	0.37	0.50
1.33	0.75	1.00	0.78	0.70	0.60	0.51	0.42	0.34	0.28	0.26	0.26	0.29	0.37
2.00	0.50	1.00	0.65	0.60	0.52	0.43	0.33	0.24	0.17	0.15	0.17	0.21	0.25



Rectangular-section smooth ($r/b_b = 1.0$) diverging wye of type $F_b + F_b > F_e$.
 $\alpha = 90^\circ$. Main passage

Section VII

Diagram 7-27



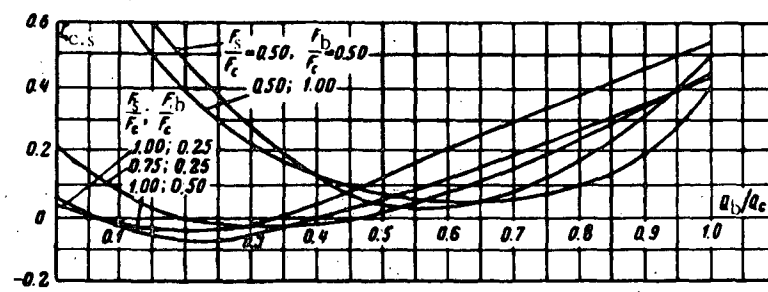
$$\zeta_{c,s} = \frac{\Delta H_s}{\frac{\gamma w_s^2}{2g}}$$

is determined from the curves $\zeta_{c,s} = f\left(\frac{Q_s}{Q_c}\right)$ for different $\frac{F_s}{F_e}$ and $\frac{F_b}{F_e}$;

$$\zeta_s = \frac{\Delta H_s}{\frac{\gamma w_s^2}{2g}} = \frac{\zeta_{c,s}}{\left(1 - \frac{Q_b}{Q_c}\right)^2 \left(\frac{F_e}{F_s}\right)^2}$$

Values of $\zeta_{c,s}$

$\frac{F_b}{F_s}$	$\frac{F_s}{F_c}$	$\frac{F_b}{F_c}$	Q_b/Q_c										
			0	0.1	0.2	0.3	0.4	0.5	0.6	0.7	0.8	0.9	1.0
0.25	1.00	0.25	+0.04	-0.01	-0.03	-0.01	+0.05	0.13	0.21	0.29	0.38	0.46	0.54
0.33	0.75	0.25	0.20	+0.08	0.00	-0.02	-0.01	0.02	0.08	0.16	0.24	0.34	0.45
0.50	1.00	0.50	+0.05	-0.03	-0.06	-0.05	0.00	+0.06	0.12	0.19	0.27	0.35	0.43
0.67	0.75	0.50	0.20	+0.04	-0.02	-0.04	-0.03	-0.01	+0.04	0.12	0.23	0.37	0.50
1.00	0.50	0.50	1.00	+0.72	+0.48	+0.28	+0.13	+0.05	0.04	0.09	0.18	0.30	0.50
1.00	1.00	1.00	+0.05	-0.02	-0.04	-0.04	-0.01	+0.06	0.13	0.22	0.30	0.38	0.45
1.33	0.75	1.00	0.20	+0.10	+0.01	-0.03	-0.03	-0.01	+0.03	0.10	0.20	0.30	0.42
2.00	0.50	1.00	0.95	0.62	0.38	+0.23	+0.13	+0.08	0.05	0.06	0.10	0.20	0.40

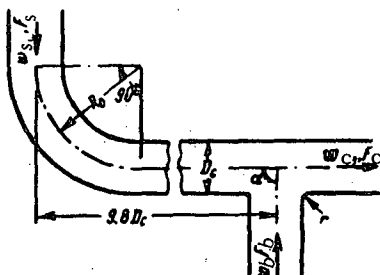


Section VII

Asymmetrical converging wye of type $F_s + F_{st} \geq F_c$; with smooth bends ($\frac{R_o}{D_c} = 2.0$). $\alpha = 90^\circ$

Diagram 7-28

No. 1. Side-branch edge slightly rounded ($\frac{r}{D_c} = 0.1$)



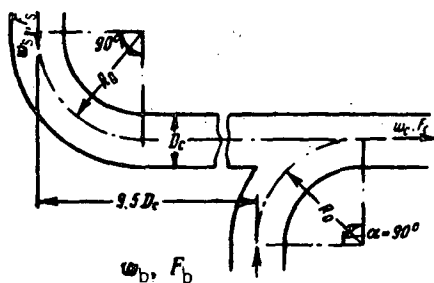
1. Branch

$$\zeta_{c,b} = \frac{\Delta H_b}{\gamma w_c^2} \cdot \frac{2g}{2g}$$

is determined from the curve $\zeta_{c,b} = f\left(\frac{Q_b}{Q_c}\right)$:

$$\zeta_b = \frac{\Delta H_b}{\gamma w_b^2} = \frac{\zeta_{c,b}}{\left(\frac{Q_b}{Q_c}\right)^2}$$

No. 2. Smooth side branch ($\frac{R_o}{D_c} = 2$)



2. Main passage

$$\zeta_{c,s} = \frac{\Delta H_s}{\gamma w_c^2} \cdot \frac{2g}{2g}$$

is determined from the broken curve $\zeta_{c,s} = f\left(\frac{Q_b}{Q_c}\right)$:

$$\zeta_s = \frac{\Delta H_s}{\gamma w_s^2} = \frac{\zeta_{c,s}}{\left(1 - \frac{Q_b}{Q_c}\right)^2}$$

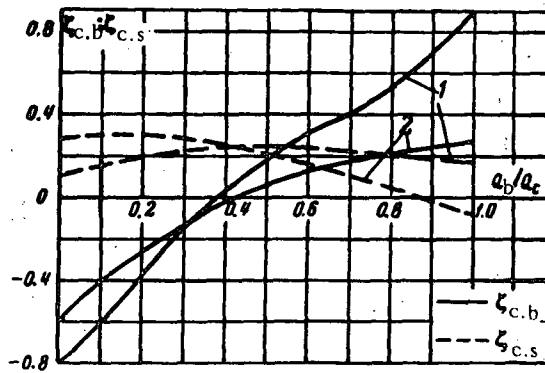
Q_b/Q_c	0	0.1	0.2	0.3	0.4	0.5	0.6	0.7	0.8	0.9	1.0
-----------	---	-----	-----	-----	-----	-----	-----	-----	-----	-----	-----

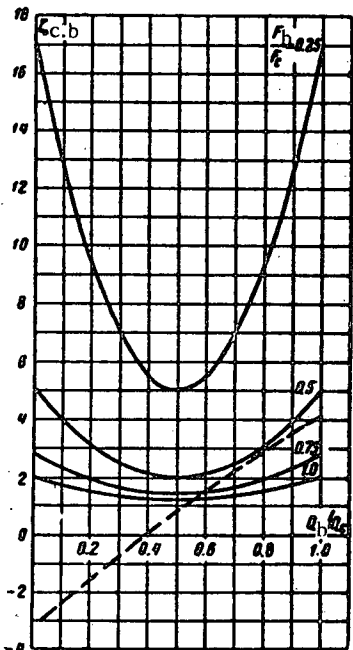
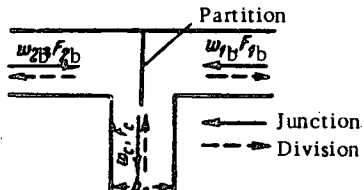
No. 1

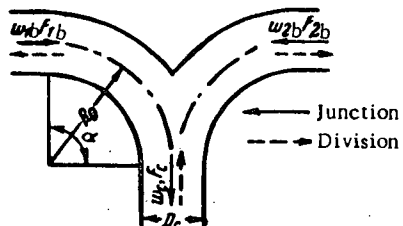
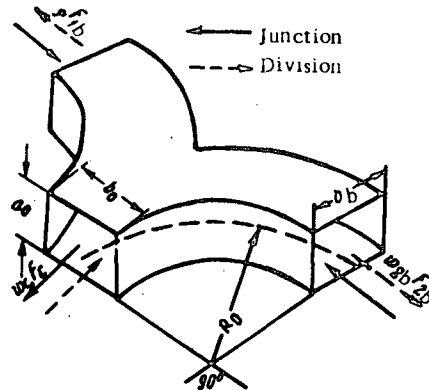
$\zeta_{c,b}$	-0.80	-0.59	-0.35	-0.15	+0.02	0.18	0.31	0.40	0.54	0.70	0.90
$\zeta_{c,s}$	0.11	0.15	0.19	0.22	0.24	0.24	0.23	0.21	0.20	0.19	0.17

No. 2

$\zeta_{c,b}$	-0.60	-0.40	-0.27	-0.14	-0.02	+0.05	0.12	0.15	0.20	0.24	0.27
	0.28	0.30	0.29	0.28	0.25	0.20	0.15	0.10	+0.05	-0.02	-0.08





No. 1. Circular section $\frac{R_o}{D_c} = 2.0$ No. 2. Rectangular section $\frac{R_o}{\delta_c} = 1.5$ 

$\frac{Q_{1b}}{Q_c}$	0	0.10	0.20	0.30	0.40	0.50	0.60	0.70	0.80	0.90	1.0
$\zeta_{lc,b}$	-0.13	-0.10	-0.07	-0.03	0	+0.03	0.30	0.03	0.03	0.05	0.08

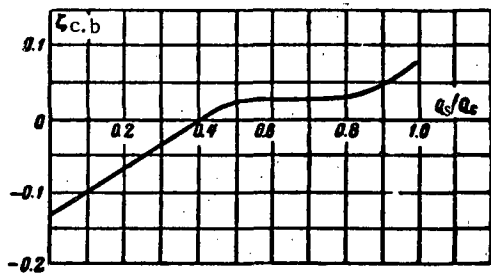


TABLE 7-11

$$\frac{F_{1b}}{F_c} = 0.5; \quad \frac{Q_{1b}}{Q_c} = 0.5$$

$\frac{R_o}{D_c}$	0.50	0.75	1.0	1.5	2.0
ζ_{1b}	1.10	0.60	0.40	0.25	0.20

TABLE 7-12

$$\frac{Q_{1b}}{Q_c} = 0.5$$

$\frac{F_{1b}}{F_c}$	0.50	1.0
Junction $\zeta_{lc,b}$	0.23	0.07
Division $\zeta_{lc,b}$	0.30	0.25

No. 1. Circular section:

$$\zeta_{lc,b} = \frac{\Delta H_{1b}}{\frac{\gamma w_c^2}{2g}} \text{ is determined:}$$

a) at junction — by the curve

$$\zeta_{lc,b} = f\left(\frac{Q_{1b}}{Q_c}\right);$$

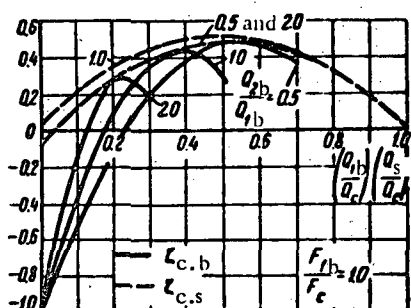
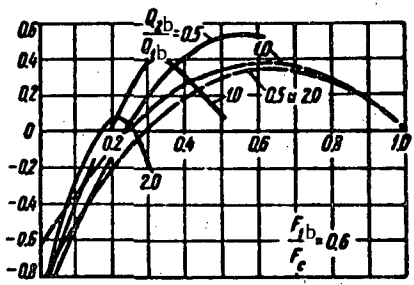
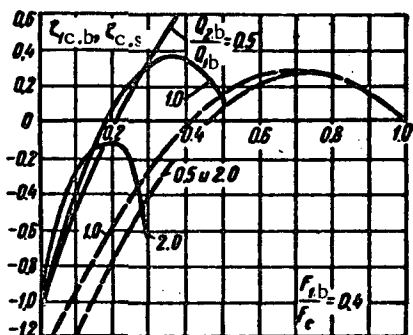
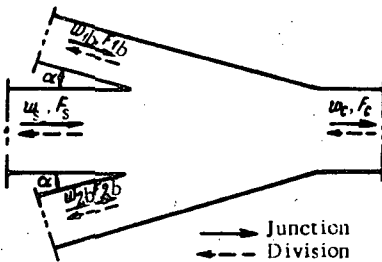
b) at division — by Table 7-11.

$$\zeta_{1b} = \frac{\Delta H_{1b}}{\frac{\gamma w_b^2}{2g}} = \frac{\zeta_{lc,b}}{\left(\frac{Q_{1b}}{Q_c} \cdot \frac{F_c}{F_b}\right)^2};$$

For the second branch, replace subscript "1" by "2".
For a rectangular section, cf. Table 7-12.

No. 2. Rectangular section

$$\zeta_{lc,b} = \frac{\Delta H_{1b}}{\frac{\gamma w_c^2}{2g}} \text{ is determined by Table 7-12.}$$



1. Junction of streams (converging double Y)

a) branch

$$\zeta_{ic,b} = \frac{\Delta H_{1b}}{\gamma w_c^2} = 1 + \left(\frac{Q_{1b}}{Q_c} \cdot \frac{F_c}{F_{1b}} \right)^2 - 8 \left(\frac{Q_{1b}}{Q_c} \right)^2 \times \frac{\left[\frac{Q_c}{Q_{1b}} - \left(1 + \frac{Q_{2b}}{Q_{1b}} \right) \right]^2}{4 - \left(1 + \frac{Q_{2b}}{Q_{1b}} \right) \frac{Q_{1b}}{Q_c}} - 1.93 \left(\frac{Q_{1b}}{Q_c} \right)^2 \frac{F_c}{F_{1b}} \left[1 + \left(\frac{Q_{2b}}{Q_{1b}} \right)^2 \right]$$

is determined from the curves $\zeta_{ic,b} = f\left(\frac{Q_b}{Q_c} \cdot \frac{Q_{2b}}{Q_{1b}}\right)$ for different $\frac{F_{1b}}{F_c}$.

For the second branch, interchange subscripts 1 and 2;

b) main passage

$$\zeta_{c,s} = \frac{\Delta H_s}{\gamma w_c^2} = 1 + \left(\frac{Q_s}{Q_c} \right)^2 - \left(\frac{Q_s}{Q_c} \right)^2 \frac{1 + \frac{Q_s}{Q_c}}{\left(0.75 + 0.25 \frac{Q_s}{Q_c} \right)^2} - 1.93 \left(\frac{Q_s}{Q_c} \right)^2 \frac{F_c}{F_{1s}} \frac{1 + \left(\frac{Q_{2b}}{Q_{1b}} \right)^2}{\left(1 + \frac{Q_{2s}}{Q_{1s}} \right)^2} \left(\frac{Q_c}{Q_s} - 1 \right)^2$$

is determined from the curves $\zeta_{c,s} = f\left(\frac{Q_s}{Q_c} \cdot \frac{Q_{2b}}{Q_{1b}}\right)$ for different $\frac{F_{1b}}{F_c}$.

2. Division of a stream (diverging double wye)

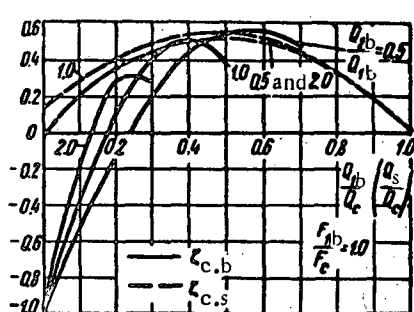
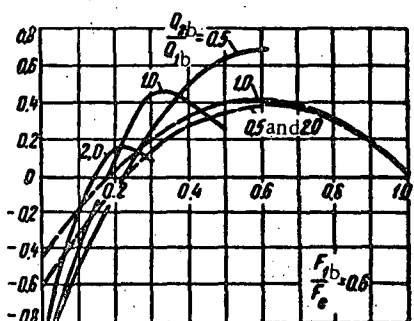
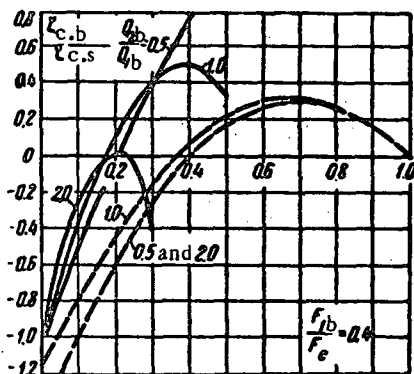
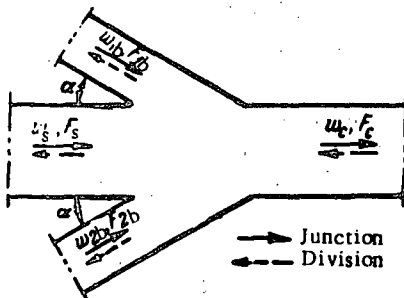
$\zeta_{ic,b}$ and $\zeta_{c,s}$ are determined tentatively by diagrams 7-21 and 7-23 (No. 1) as for diverging wyes.

Double wye of type $F_{1b} = F_{2b} = F_s$; $F_s = F_c$. $\alpha = 15^\circ$ (continued)

Section VII

Diagram 7-31

$\frac{Q_2b}{Q_{1b}}$	$\frac{Q_{1b}}{Q_c} / \frac{Q_s}{Q_c}$										
	0	0.1	0.2	0.3	0.4	0.5	0.6	0.7	0.8	0.9	1.0
$\frac{F_{1b}}{F_c} = 0.2$											
$\zeta_{c,b}$	0.5	-1.0	-0.37	+0.46	1.48	2.69	4.07	5.62	-	-	-
	1.0	-1.0	-0.29	+0.43	+1.23	1.80	2.81	-	-	-	-
	2.0	-1.0	-0.32	-0.31	-1.13	-	-	-	-	-	-
$\zeta_{c,s}$	0.5 and 2.0	-4.37	-2.93	-2.04	-1.44	-1.08	-0.58	-0.22	+0.03	0.16	0.14
	1.0	-3.84	-2.93	-2.13	-1.44	-0.89	-0.45	-0.13	+0.08	0.17	0.14
$\frac{F_{1b}}{F_c} = 0.4$											
$\zeta_{c,b}$	0.5	-1.0	-0.50	-0.05	+0.34	0.65	0.90	1.04	-	-	-
	1.0	-1.0	-0.39	+0.06	+0.31	0.35	0.14	-	-	-	-
	2.0	-1.0	-0.27	-0.10	-0.65	-	-	-	-	-	-
$\zeta_{c,s}$	0.5 and 2.0	-1.70	-1.19	-0.76	-0.40	-0.12	+0.08	0.21	0.27	0.25	0.16
	1.0	-1.42	-0.96	-0.58	-0.26	-0.02	+0.15	0.26	0.29	0.26	0.16
$\frac{F_{1b}}{F_c} = 0.6$											
$\zeta_{c,b}$	0.5	-1.0	-0.51	-0.11	+0.21	0.42	0.55	0.53	-	-	-
	1.0	-1.0	-0.39	+0.05	+0.40	0.31	0.09	-	-	-	-
	2.0	-1.0	-0.22	+0.08	-0.18	-	-	-	-	-	-
$\zeta_{c,s}$	0.5 and 2.0	-0.81	-0.47	-0.19	+0.04	0.20	0.30	0.36	0.35	0.29	0.17
	1.0	-0.61	-0.31	-0.05	+0.13	0.27	0.35	0.39	0.37	0.29	0.17
$\frac{F_{1b}}{F_c} = 1.0$											
$\zeta_{c,b}$	0.5	-1.0	-0.51	-0.12	+0.20	0.39	0.49	0.37	-	-	-
	1.0	-1.0	-0.38	+0.09	0.36	0.44	0.28	-	-	-	-
	2.0	-1.0	-0.18	+0.27	0.19	-	-	-	-	-	-
$\zeta_{c,s}$	0.5 and 2.0	-0.35	-0.11	+0.10	0.26	0.36	0.42	0.43	0.39	0.31	0.18
	1.0	-0.21	+0.02	0.19	0.33	0.41	0.45	0.45	0.41	0.31	0.18



1. Junction of streams (converging double wye)

a) branch

$$\zeta_{1c,b} = \frac{\Delta H_{1b}}{\gamma w_c^2} = 1 + \left(\frac{Q_{1b}}{Q_c} \cdot \frac{F_c}{F_{1b}} \right)^2 - 8 \left(\frac{Q_{1b}}{Q_c} \right)^2 \times$$

$$\times \frac{\left[\frac{Q_c}{Q_{1b}} - \left(1 + \frac{Q_{2b}}{Q_{1b}} \right) \right]^2}{4 - \left(1 + \frac{Q_{2b}}{Q_{1b}} \right) \frac{Q_{1b}}{Q_c}} - 1.73 \left(\frac{Q_{1b}}{Q_c} \right)^2 \frac{F_c}{F_{1b}} \left[1 + \left(\frac{Q_{2b}}{Q_{1b}} \right)^2 \right]$$

is determined from the curves $\zeta_{1c,b} = f\left(\frac{Q_{1b}}{Q_c}, \frac{Q_{2b}}{Q_{1b}}\right)$ for different $\frac{F_{1b}}{F_c}$.

For the second branch, interchange subscripts 1 and 2.

b) main passage

$$\zeta_{c,s} = \frac{\Delta H_s}{\gamma w_c^2} = 1 + \left(\frac{Q_s}{Q_c} \right)^2 - \left(\frac{Q_s}{Q_c} \right)^2 \frac{1 + \frac{Q_s}{Q_c}}{\left(0.75 + 0.25 \frac{Q_s}{Q_c} \right)^2} -$$

$$- 1.73 \left(\frac{Q_s}{Q_c} \right)^2 \frac{F_c}{F_{1b}} \frac{1 + \left(\frac{Q_{2b}}{Q_{1b}} \right)^2}{\left(1 + \frac{Q_{2b}}{Q_{1b}} \right)^2} \left(\frac{Q_c}{Q_s} - 1 \right)^2$$

is determined from the curves $\zeta_{c,s} = f\left(\frac{Q_s}{Q_c}, \frac{Q_{2b}}{Q_{1b}}\right)$ for different $\frac{F_{1b}}{F_c}$.

2. Division of a stream (diverging double wye)

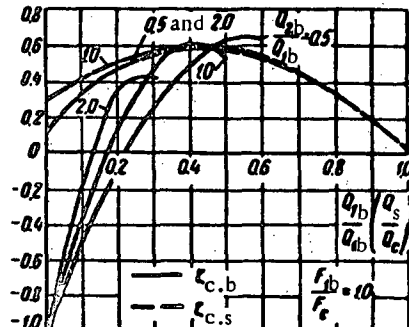
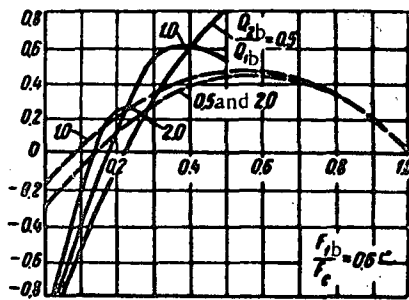
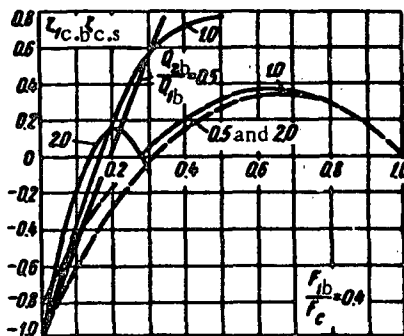
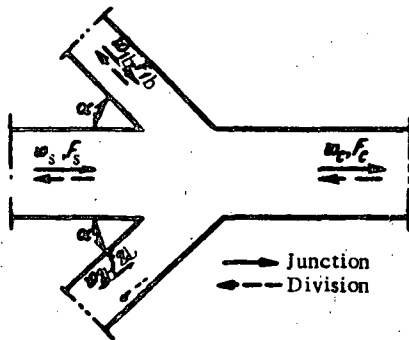
$\zeta_{c,b}$ and $\zeta_{c,s}$ are determined tentatively by diagrams 7-21 and 7-23 (No. 1) as for diverging wyes.

Double wye of type $F_{1b} = F_{2b}$, $F_s = F_c$, $\alpha = 30^\circ$ (continued)

Section VII

Diagram 7-32

$\frac{Q_{2b}}{Q_{1b}}$	$\frac{Q_{1b}/Q_c}{Q_s/Q_c}$										
	0	0.1	0.2	0.3	0.4	0.5	0.6	0.7	0.8	0.9	1.0
$\frac{F_{1b}}{F_c} = 0.2$											
$\zeta_{c,b}$	0.5	-1.0	-0.36	+0.51	1.59	2.89	4.38	6.10	-	-	-
	1.0	-1.0	-0.27	+0.51	1.41	2.12	2.91	-	-	-	-
	2.0	-1.0	-0.27	-0.11	-0.72	-	-	-	-	-	-
$\zeta_{c,s}$	0.5 and 2.0	-3.81	-2.51	-1.81	-1.20	-0.86	-0.44	-0.13	+0.08	0.18	0.14
	1.0	-3.34	-2.53	-1.81	-1.20	-0.71	-0.32	-0.05	+0.12	0.18	0.14
$\frac{F_{1b}}{F_c} = 0.4$											
$\zeta_{c,b}$	0.5	-1.0	-0.49	-0.03	+0.40	0.75	1.06	1.44	-	-	-
	1.0	-1.0	-0.38	+0.10	+0.40	0.51	0.34	-	-	-	-
	2.0	-1.0	-0.25	+0.01	-0.42	-	-	-	-	-	-
$\zeta_{c,s}$	0.5 and 0.2	-1.42	-0.97	-0.58	-0.26	+0.02	0.15	0.26	0.30	0.26	0.17
	1.0	-1.16	-0.76	-0.48	-0.14	+0.07	0.21	0.30	0.31	0.27	0.17
$\frac{F_{1b}}{F_c} = 0.8$											
$\zeta_{c,b}$	0.5	-1.0	-0.51	-0.10	+0.25	0.50	0.65	0.68	-	-	-
	1.0	-1.0	-0.38	+0.08	0.45	0.42	0.25	-	-	-	-
	2.0	-1.0	-0.21	+0.15	0.08	-	-	-	-	-	-
$\zeta_{c,s}$	0.5 and 2.0	-0.62	-0.32	-0.07	+0.13	0.27	0.35	0.39	0.37	0.29	0.17
	1.0	-0.45	-0.18	+0.04	0.21	0.33	0.39	0.41	0.39	0.30	0.18
$\frac{F_{1b}}{F_c} = 1.0$											
$\zeta_{c,b}$	0.5	-1.0	-0.51	-0.11	+0.22	0.43	0.55	0.55	0.48	-	-
	1.0	-1.0	-0.37	+0.10	0.40	0.51	0.38	-	-	-	-
	2.0	-1.0	-0.17	+0.31	0.28	-	-	-	-	-	-
$\zeta_{c,s}$	0.5 and 2.0	-0.03	+0.21	0.34	0.45	0.50	0.52	0.49	0.43	0.32	0.18
	1.0	+0.13	0.29	0.41	0.49	0.54	0.54	0.51	0.44	0.32	0.18



1. Junction of streams (converging double wye)

a) branch

$$\xi_{c,b} = \frac{\Delta H_{1b}}{\gamma w_c^2} = 1 + \left(\frac{Q_{1b}}{Q_c} \frac{F_c}{F_{1b}} \right)^2 - 8 \left(\frac{Q_{1b}}{Q_c} \right)^2 \times \\ \times \frac{\left[\frac{Q_c}{Q_{1b}} - \left(1 + \frac{Q_{2b}}{Q_{1b}} \right) \right]^2}{4 - \left(1 + \frac{Q_{2b}}{Q_{1b}} \right) \frac{Q_{1b}}{Q_c}} - 1.42 \left(\frac{Q_{1b}}{Q_c} \right)^2 \frac{F_c}{F_{1b}} \left[1 + \left(\frac{Q_{2b}}{Q_{1b}} \right)^2 \right]$$

is determined from the curves $\xi_{c,b} = f\left(\frac{Q_{1b}}{Q_c}, \frac{Q_{2b}}{Q_{1b}}\right)$ for different $\frac{F_{1b}}{F_c}$.

For the second branch, interchange subscripts 1 and 2.

b) main passage

$$\xi_{c,s} = \frac{\Delta H_s}{\gamma w_c^2} = 1 + \left(\frac{Q_s}{Q_c} \right)^2 - \left(\frac{Q_s}{Q_c} \right)^2 \frac{1 + \frac{Q_s}{Q_c}}{\left(0.75 + 0.25 \frac{Q_s}{Q_c} \right)^2} - \\ - 1.42 \left(\frac{Q_s}{Q_c} \right)^2 \frac{F_c}{F_{1b}} \frac{1 + \left(\frac{Q_{2b}}{Q_{1b}} \right)^2}{\left(1 + \frac{Q_{2b}}{Q_{1b}} \right)^2} \left(\frac{Q_c}{Q_s} - 1 \right)^2$$

is determined from the curves $\xi_{c,s} = f\left(\frac{Q_s}{Q_c}, \frac{Q_{2b}}{Q_{1b}}\right)$ for different $\frac{F_{1b}}{F_c}$.

2. Division of a stream (diverging double wye)

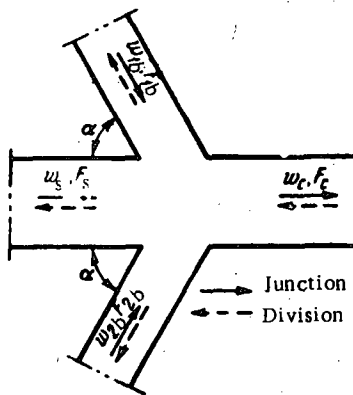
$\xi_{c,b}$ and $\xi_{c,s}$ are determined tentatively by diagrams 7-21 to 7-23 (No. 1) as for diverging wyes.

Double wye of type $F_{1b} = F_{2b}$; $F_s = F_c$. $\alpha = 45^\circ$ (continued)

Section VII

Diagram 7-33

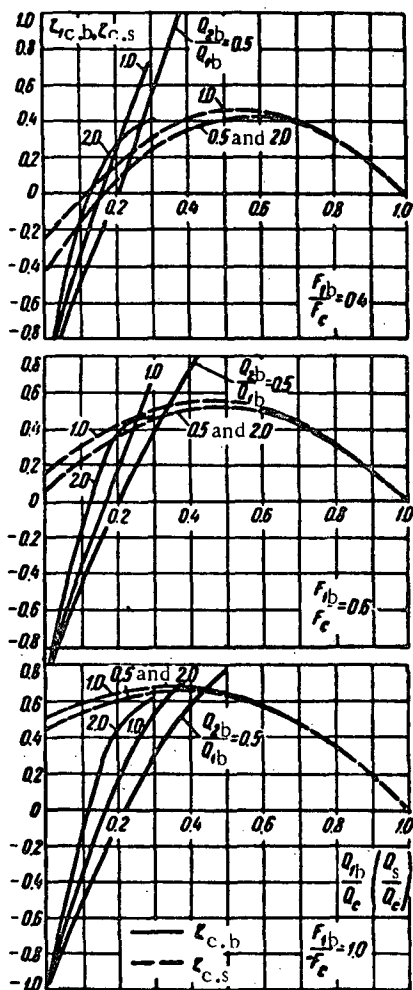
$\frac{Q_{2b}}{Q_{1b}}$	$\frac{F_{1b}}{F_c} (Q_s/Q_c)$										
	0	0.1	0.2	0.3	0.4	0.5	0.6	0.7	0.8	0.9	1.0
$\frac{F_{1b}}{F_c} = 0.8$											
$\zeta_{c,b}$	0.5	-1.0	-0.36	+0.59	1.77	3.20	4.88	6.79	-	-	-
	1.0	-1.0	-0.24	+0.63	1.70	2.64	3.73	-	-	-	-
	2.0	-1.0	-0.19	+0.21	0.04	-	-	-	-	-	-
$\zeta_{c,s}$	0.5 and 2.0	-2.92	-1.87	-1.29	-0.80	-0.56	-0.23	-0.01	+0.16	0.22	0.15
	1.0	-2.54	-1.87	-1.30	-0.80	-0.42	-0.12	+0.08	0.20	0.22	0.15
$\frac{F_{1b}}{F_c} = 0.4$											
$\zeta_{c,b}$	0.5	-1.0	-0.48	-0.02	0.58	0.92	1.31	16.3	-	-	-
	1.0	-1.0	-0.36	+0.17	+0.55	0.72	0.78	-	-	-	-
	2.0	-1.0	-0.18	+0.16	-0.06	-	-	-	-	-	-
$\zeta_{c,s}$	0.5 and 2.0	-0.98	-0.61	-0.30	-0.05	+0.14	0.26	0.33	0.34	0.28	0.17
	1.0	-0.77	-0.44	-0.16	+0.05	0.21	0.31	0.36	0.35	0.29	0.17
$\frac{F_{1b}}{F_c} = 0.6$											
$\zeta_{c,b}$	0.5	-1.0	-0.50	-0.07	+0.31	0.60	0.82	0.92	-	-	-
	1.0	-1.0	-0.37	+0.12	0.55	0.60	0.52	-	-	-	-
	2.0	-1.0	-0.18	+0.26	0.16	-	-	-	-	-	-
$\zeta_{c,s}$	0.5 and 2.0	-0.32	+0.08	+0.11	0.27	0.37	0.43	0.44	0.40	0.31	0.18
	1.0	-0.18	-0.04	0.21	0.34	0.42	0.46	0.46	0.41	0.31	0.18
$\frac{F_{1b}}{F_c} = 1.0$											
$\zeta_{c,b}$	0.5	-1.0	-0.51	-0.09	+0.25	0.50	0.65	0.64	-	-	-
	1.0	-1.0	-0.37	+0.13	0.46	0.61	0.54	-	-	-	-
	2.0	-1.0	-0.15	+0.38	0.42	-	-	-	-	-	-
$\zeta_{c,s}$	0.5 and 2.0	0.11	0.36	0.46	0.53	0.57	0.56	0.52	0.44	0.33	0.18
	1.0	0.29	0.42	0.51	0.57	0.59	0.58	0.54	0.45	0.33	0.18



1. Junction of streams (converging double wye)

a) branch

$$\zeta_{c,b} = \frac{\Delta H_{1b}}{\gamma w_c^2} = 1 + \left(\frac{Q_{1b}}{Q_c} \frac{F_c}{F_{1b}} \right) - 8 \left(\frac{Q_{1b}}{Q_c} \right)^2 \times \\ \times \frac{\left[\frac{Q_c}{Q_{1b}} - \left(1 + \frac{Q_{2b}}{Q_{1b}} \right) \right]^2}{4 - \left(1 + \frac{Q_{2b}}{Q_{1b}} \right) \frac{Q_{1b}}{Q_c}} - \left(\frac{Q_{1b}}{Q_c} \right)^2 \frac{F_c}{F_{1b}} \left[1 + \left(\frac{Q_{2b}}{Q_{1b}} \right)^2 \right]$$



is determined from the curves $\zeta_{c,b} = f\left(\frac{Q_b}{Q_c}, \frac{Q_{2b}}{Q_{1b}}\right)$ for different $\frac{F_{1b}}{F_c}$.

For the second branch, interchange subscripts 1 and 2.

b) main passage

$$\zeta_{c,s} = \frac{\Delta H_s}{\gamma w_c^2} = 1 + \left(\frac{Q_s}{Q_c} \right)^2 - \left(\frac{Q_s}{Q_c} \right)^2 \frac{1 + \frac{Q_s}{Q_c}}{\left(0.75 + 0.25 \frac{Q_s}{Q_c} \right)} - \\ - \left(\frac{Q_s}{Q_c} \right)^2 \frac{F_c}{F_{1b}} \frac{1 + \left(\frac{Q_{2b}}{Q_{1b}} \right)^2}{\left(1 + \frac{Q_{2b}}{Q_{1b}} \right)^2} \left(\frac{Q_c}{Q_s} - 1 \right)^2$$

is determined from the curves $\zeta_{c,s} = f\left(\frac{Q_s}{Q_c}, \frac{Q_{2b}}{Q_{1b}}\right)$ for different $\frac{F_{1b}}{F_c}$.

2. Division of a stream (diverging double wye)

$\zeta_{c,b}$ and $\zeta_{c,s}$ are determined tentatively by diagrams 7-21 and 7-23 (No. 1) as for diverging wyes.

Section VII

Double wye of type $F_{1b} = F_{2b}$, $F_s = F_c$, $\alpha = 60^\circ$ (continued)

Diagram 7-34

$\frac{Q_{2b}}{Q_{1b}}$	$Q_{1b}/Q_c (Q_s/Q_c)$										
	0	0.1	0.2	0.3	0.4	0.5	0.6	0.7	0.8	0.9	1.0

$$\frac{F_{1b}}{F_c} = 0.2$$

$\zeta_{c,b}$	0.5 1.0 2.0	-1.0 -1.0 -1.0	-0.31 -0.20 -0.09	+0.59 +0.80 +0.62	2.00 2.07 0.97	3.62 3.30 -	5.54 4.77 -	7.72 -	-	-	-
$\zeta_{c,s}$	0.5 and 2.0 1.0	-1.77 -1.50	-1.02 -1.03	-0.64 -0.64	-0.30 -0.30	-0.15 -0.05	+0.06 +0.13	0.20 0.24	0.26 0.29	0.26 0.26	0.16 0.16

$$\frac{F_{1b}}{F_c} = 0.4$$

$\zeta_{c,b}$	0.5 1.0 2.0	-1.0 -1.0 -1.0	-0.47 -0.34 -0.15	-0.06 +0.25 +0.27	+0.60 0.73 0.41	1.12 1.10 -	1.63 1.31 -	2.10 -	-	-	-
$\zeta_{c,s}$	0.5 and 2.0 1.0	-0.40 -0.25	-0.14 -0.02	+0.07 +0.16	0.24 0.31	0.35 0.40	0.41 0.44	0.42 0.45	0.39 0.40	0.30 0.31	0.18 0.18

$$\frac{F_{1b}}{F_c} = 0.6$$

$\zeta_{c,b}$	0.5 1.0 2.0	-1.0 -1.0 -1.0	-0.50 -0.36 -0.15	+0.04 +0.18 +0.40	0.38 0.67 0.47	0.74 0.82 -	1.03 0.87 -	1.23 -	-	-	-
$\zeta_{c,s}$	0.5 and 2.0 1.0	0.06 0.16	-0.23 -0.32	0.36 0.43	0.46 0.51	0.51 0.55	0.52 0.55	0.50 0.51	0.43 0.44	0.32 0.33	0.18 0.18

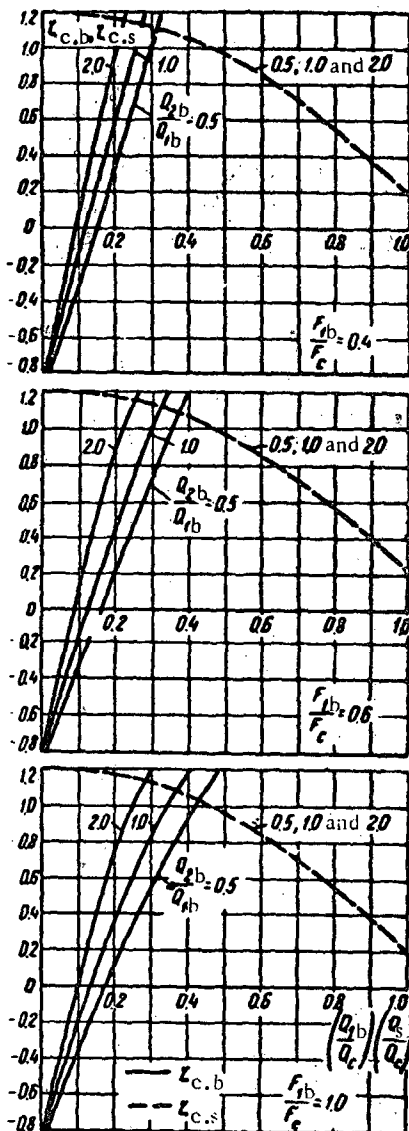
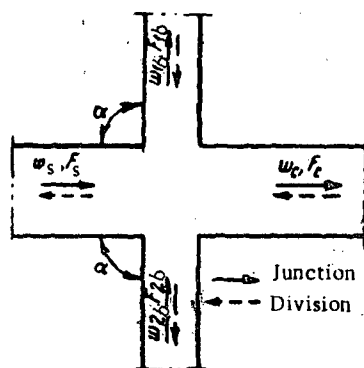
$$\frac{F_{1b}}{F_c} = 1.0$$

$\zeta_{c,b}$	0.5 1.0 2.0	-1.0 -1.0 -1.0	-0.50 -0.36 -0.13	-0.07 +0.16 +0.46	+0.30 0.53 0.61	0.58 0.74 -	0.79 0.75 -	0.88 -	-	-	-
$\zeta_{c,s}$	0.5 and 2.0 1.0	0.44 0.50	0.54 0.59	0.60 0.64	0.65 0.67	0.65 0.67	0.62 0.63	0.56 0.57	0.47 0.47	0.34 0.34	0.18 0.18

C Cross of type $F_{1b} = F_{2b}$; $F_s = F_c$ $\alpha = 90^\circ$

Section VII

Diagram 7-35



1. Junction of streams (converging cross)

a) branch

$$\zeta_{1c,b} = \frac{\Delta H_{1b}}{\gamma w_c^2} = 1 + \left(\frac{Q_{1b}}{Q_c} \frac{F_c}{F_{1b}} \right)^2 - 8 \left(\frac{Q_{1b}}{Q_c} \right)^2 \frac{\left[\frac{Q_c}{Q_{1b}} - \left(1 + \frac{Q_{2b}}{Q_{1b}} \right) \right]^2}{4 - \left(1 + \frac{Q_{2b}}{Q_{1b}} \right) Q_c}$$

is determined from the curves $\zeta_{1c,b} = f \left(\frac{Q_{1b}}{Q_c}, \frac{Q_{2b}}{Q_{1b}} \right)$ for different $\frac{F_{1b}}{F_c}$.

For the second branch, interchange subscripts 1 and 2.

b) main passage

$$\zeta_{c,s} = \frac{\Delta H_s}{\gamma w_c^2} = 1 + \left(\frac{Q_s}{Q_c} \right)^2 - \left(\frac{Q_s}{Q_c} \right)^2 \frac{1 + \frac{Q_s}{Q_c}}{\left(0.75 + 0.25 \frac{Q_s}{Q_c} \right)^2}$$

is determined from the curves $\zeta_{c,s} = f \left(\frac{Q_s}{Q_c}, \frac{Q_{2b}}{Q_{1b}} \right)$ for different $\frac{F_{1b}}{F_c}$.

For standard malleable-iron crosses at $\frac{Q_s}{Q_c} > 0.7$:

$$\zeta'_{c,s} = \frac{\Delta H_s}{\gamma w_c^2} = \zeta_{c,s} + 2.5 \left(\frac{Q_s}{Q_c} - 0.7 \right).$$

2. Division of a stream (diverging cross)

$\zeta_{c,s}$ and $\zeta_{c,b}$ are determined tentatively by diagrams 7-21 and 7-23 (No. 1) as for diverging wyes.

Cross of type $F_{lb} = F_{sh}$; $F_s = F_c$, $\alpha = 90^\circ$ (continued)

Section VII

Diagram 7-35

$\frac{Q_{2b}}{Q_{lb}}$	$\frac{Q_{lb}}{Q_c} \left(\frac{Q_s}{Q_c} \right)$										
	0	0.1	0.2	0.3	0.4	0.5	0.6	0.7	0.8	0.9	1.0

$$\frac{F_{lb}}{F_c} = 0.2$$

$\zeta_{c,b}$	0.5	-0.85	-0.10	+1.09	2.72	4.77	7.25	10.1	-	-	-
	1.0	-0.85	-0.05	+1.35	3.12	5.00	7.40	-	-	-	-
	2.0	-0.85	-0.31	+1.77	3.37	-	-	-	-	-	-

$$\frac{F_{lb}}{F_c} = 0.4$$

$\zeta_{c,b}$	0.5	-0.85	-0.29	+0.34	1.03	1.77	2.56	3.37	-	-	-
	1.0	-0.85	-0.14	+0.60	1.33	2.05	2.71	-	-	-	-
	2.0	-0.85	+0.12	1.02	1.68	-	-	-	-	-	-

$$\frac{F_{lb}}{F_c} = 0.6$$

$\zeta_{c,b}$	0.5	-0.85	-0.82	+0.20	0.72	1.22	1.70	2.13	-	-	-
	1.0	-0.85	-0.18	+0.46	1.02	1.50	1.85	-	-	-	-
	2.0	-0.85	+0.09	0.88	1.37	-	-	-	-	-	-

$$\frac{F_{lb}}{F_c} = 0.8$$

$\zeta_{c,b}$	0.5	-0.85	-0.33	+0.13	0.61	1.02	1.38	1.68	-	-	-
	1.0	-0.85	-0.18	+0.41	0.91	1.30	1.54	-	-	-	-
	2.0	-0.85	+0.08	0.83	1.26	-	-	-	-	-	-

$$\frac{F_{lb}}{F_c} = 1.0$$

$\zeta_{c,b}$	0.5	-0.85	-0.34	+0.13	0.56	0.93	1.25	1.48	-	-	-
	1.0	-0.85	-0.19	+0.39	0.86	1.21	1.40	-	-	-	-
	2.0	-0.85	+0.07	0.81	1.21	-	-	-	-	-	-

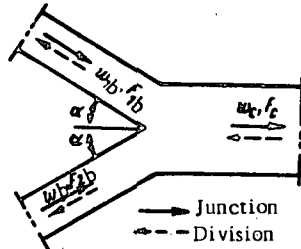
Values of $\zeta_{c,s}$ for any $\frac{F_{lb}}{F_c}$ and any $\frac{Q_{2b}}{Q_{lb}}$

		1.20	1.19	1.17	1.12	1.05	0.96	0.85	0.72	0.56	0.39	0.20
--	--	------	------	------	------	------	------	------	------	------	------	------

Wye of type $F_c = 2F_s$

Section VII

Diagram 7-36



1. Junction of streams (converging wye)

$$a) \alpha = 15^\circ: \zeta_{lc,b} = \frac{\Delta H_{ls}}{\frac{1}{2} \frac{w_e^2}{g}} = 7.3 \frac{Q_{lb}}{Q_c} + 0.07 \left[\left(\frac{Q_{lb}}{Q_c} \right)^4 + \left(1 - \frac{Q_{lb}}{Q_c} \right)^4 \right] - 3.7 \left(\frac{Q_{lb}}{Q_c} \right)^2 - 2.64;$$

$$b) \alpha = 30^\circ: \zeta_{lc,b} = \frac{\Delta H_{lb}}{\frac{1}{2} \frac{w_e^2}{g}} = 6.6 \frac{Q_{lb}}{Q_c} + 0.25 \left[\left(\frac{Q_{lb}}{Q_c} \right)^4 + \left(1 - \frac{Q_{lb}}{Q_c} \right)^4 \right] - 3.0 \left(\frac{Q_{lb}}{Q_c} \right)^2 - 2.30;$$

$$c) \alpha = 45^\circ: \zeta_{lc,b} = \frac{\Delta H_{lb}}{\frac{1}{2} \frac{w_e^2}{g}} = 5.6 \frac{Q_{lb}}{Q_c} + 0.50 \left[\left(\frac{Q_{lb}}{Q_c} \right)^4 + \left(1 - \frac{Q_{lb}}{Q_c} \right)^4 \right] - 2.0 \left(\frac{Q_{lb}}{Q_c} \right)^2 - 1.80.$$

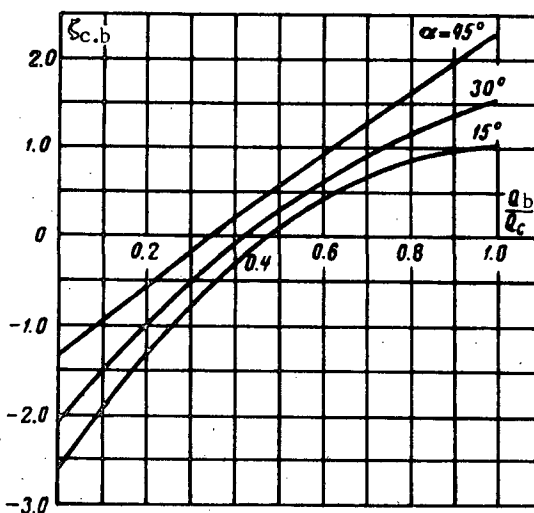
2. Division (diverging wye)

$\zeta_{lc,b} = \frac{\Delta H_{lb}}{\frac{1}{2} \frac{w_e^2}{g}}$ is determined tentatively by diagram 7-23 as for an ordinary wye of type

$$F_c = F_s + F_b$$

 Values of $\zeta_{lc,b}$

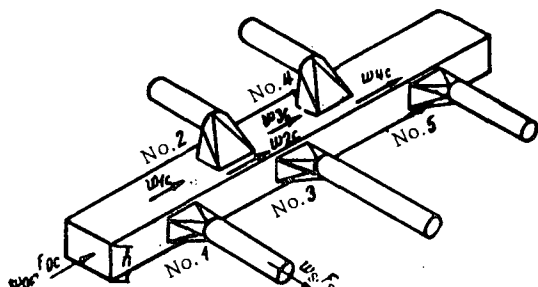
α°	Q_{lb}/Q_c										
	0	0.10	0.20	0.30	0.40	0.50	0.60	0.70	0.80	0.90	1.0
15	-2.56	-1.89	-1.30	-0.77	-0.30	+0.10	0.41	0.67	0.85	0.97	1.04
30	-2.05	-1.51	-1.00	-0.53	-0.10	+0.28	0.69	0.91	1.09	1.37	1.55
45	-1.30	-0.93	-0.55	-0.16	+0.20	0.56	0.92	1.26	1.61	1.95	2.30



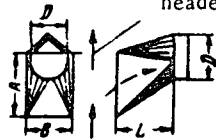
Header with transition stretches

Section VII

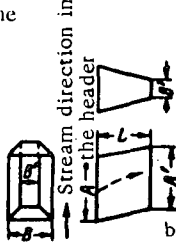
Diagram 7-37



Stream direction in the header



1. Branch at side



$$\zeta_{ib} = \frac{\Delta H_b}{\frac{w_b^2}{2g}} \text{ is determined from the curves } \zeta_{ib} = f \left(\frac{w_b}{w_{(i-1)c}} \right)$$

where $w_{(i-1)s}$ = mean velocity in the header before the i -th branch

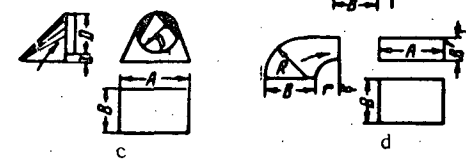
$\frac{w_b}{w_{(i-1)c}}$	0.4	0.6	0.8	1.0	2.0	3.0	4.0	5.0
ζ_{ib}	4.30	1.60	0.88	0.60	0.24	0.20	0.19	0.18
	—	3.00	1.80	1.43	0.92	0.90	1.12	1.67

1. Branch at side

$$\zeta_{ib} \quad 4.30 \quad 1.60 \quad 0.88 \quad 0.60 \quad 0.24 \quad 0.20 \quad 0.19 \quad 0.18$$

2. Branch at top or bottom

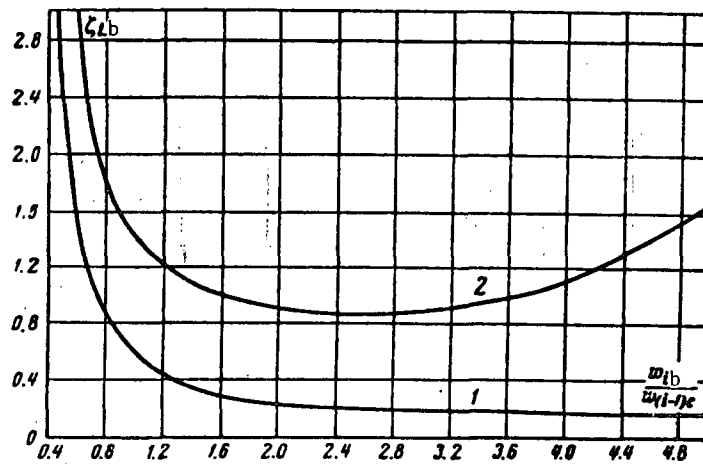
$$\zeta_{ib} \quad — \quad 3.00 \quad 1.80 \quad 1.43 \quad 0.92 \quad 0.90 \quad 1.12 \quad 1.67$$



2. Branch at top or bottom

Dimensions of the different headers (h = height of the header section)

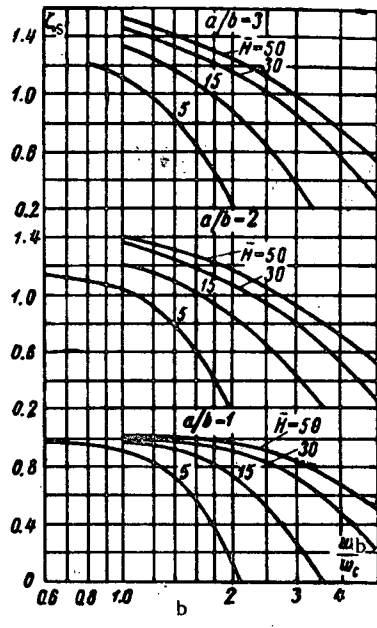
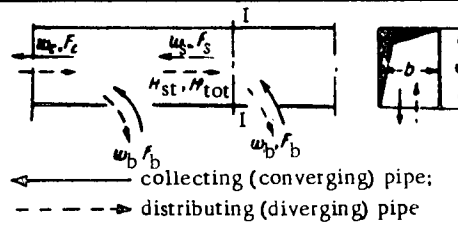
Header	D	A'	B'	A	B	L	R	r
a	$0.6-0.9h$	—	—	$\sim 1.7D$	D	$1-1.3D$	—	—
b	—	$1.15-1.25h$	$0.30-0.45h$	$1-1.5h$	$0.6-0.9h$	$0.6-1.1h$	—	—
c	$0.6-0.9h$	—	—	$\sim 1.7D$	D	—	$0.2D$	—
d	—	$1.15-1.25h$	$0.35-0.45h$	$1.15-1.25h$	$0.6-0.9h$	—	—	$0.6-0.9h$



Passage through a side opening of a header pipe of
constant cross section

Section VII

Diagram 7-38



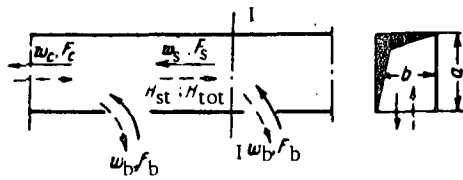
$$\xi_{c,s} = \frac{\Delta H}{\frac{\gamma w_c^2}{2g}} = \text{resistance coefficient of the transition between two openings, is determined from the curves}$$

$$\xi_{c,s} = f \left(\frac{w_b}{w_c} \right) \text{ corresponding to different } \frac{a}{b} \text{ and different } \bar{H}_{st} = \frac{H_{st}}{\frac{\gamma w_s^2}{2g}}, \text{ where}$$

where H_{st} = static pressure in section I-I.

Values of $\xi_{c,s}$

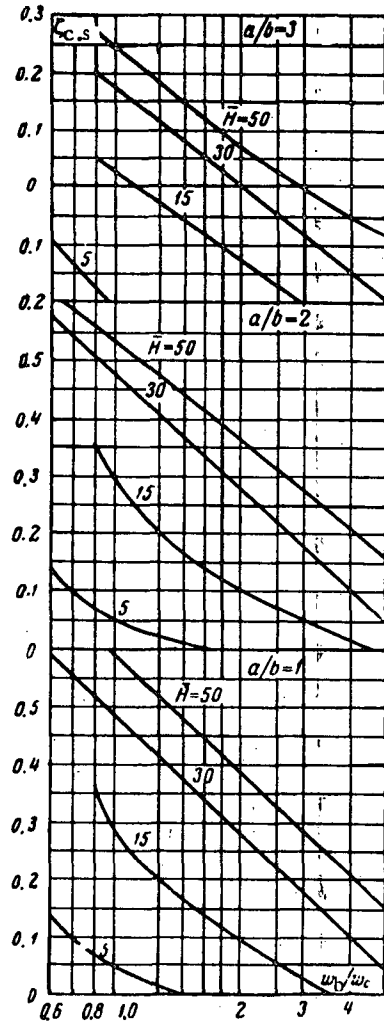
\bar{H}_{st}	$\frac{w_b}{w_c}$											
	0.6	0.8	1.0	1.2	1.4	1.6	1.8	2.0	2.5	3.0	4.0	5.0
$a/b = 1.0$												
5	0.98	0.96	0.91	0.84	0.74	0.56	0.38	0.16	—	—	—	—
15	—	—	0.99	0.96	0.92	0.88	0.82	0.74	0.52	0.28	—	—
30	—	—	1.00	1.02	0.98	0.96	0.94	0.90	0.83	0.74	0.50	0.22
50	—	—	1.02	1.02	1.01	1.00	0.98	0.96	0.92	0.84	0.68	0.51
$a/b = 2.0$												
5	1.15	0.10	1.04	0.93	0.78	0.60	0.40	0.20	—	—	—	—
15	—	—	1.20	1.16	1.02	1.02	0.94	0.86	0.65	0.44	—	—
30	—	—	1.36	1.30	1.24	1.18	1.12	1.07	0.94	0.80	0.52	0.25
50	—	—	1.40	1.36	1.31	1.26	1.16	1.04	0.93	0.71	0.52	—
$a/b = 3.0$												
5	—	1.21	1.10	0.98	0.83	0.64	0.45	0.20	—	—	—	—
15	—	—	1.34	1.25	1.16	1.07	0.98	0.89	0.64	0.39	—	—
30	—	—	1.46	1.40	1.34	1.27	1.22	1.17	1.10	0.86	0.57	0.28
50	—	—	1.52	1.46	1.41	1.36	1.31	1.25	1.12	1.00	0.75	0.55



$$\zeta_{c,s} = \frac{\Delta H}{\frac{\gamma w_c^2}{2g}} = \text{resistance coefficient of the transition}$$

between two openings, is determined from the curves

$$\zeta_{c,s} = f \left(\frac{w_b}{w_c} \right) \text{ corresponding to different } \frac{a}{b} \text{ and different } \bar{H}_{tot} = \frac{H_{tot}}{\frac{\gamma w_s^2}{2g}}, \text{ where } H_{tot} = \text{total pressure in section 1-1.}$$



Values of $\zeta_{c,s}$

\bar{H}_{tot}	0.6	0.8	1.0	1.2	1.4	1.6	1.8	2.0	2.5	3.0	4.0	5.0
-----------------	-----	-----	-----	-----	-----	-----	-----	-----	-----	-----	-----	-----

$a/b = 1.0$

5	0.14	0.07	0.04	0.02	0.00	—	—	—	—	—	—	—
15	—	0.37	0.25	0.20	0.17	0.14	0.12	0.10	0.06	0.03	—	—
30	0.59	0.52	0.46	0.42	0.37	0.34	0.31	0.28	0.22	0.18	0.11	0.05
50	—	—	0.57	0.52	0.48	0.45	0.42	0.39	0.33	0.29	0.21	0.16

$a/b = 2.0$

1	0.14	0.07	0.04	0.02	0.01	0.00	—	—	—	—	—	—
15	—	0.35	0.25	0.20	0.16	0.14	0.12	0.10	0.07	0.05	0.02	—
30	0.58	0.50	0.45	0.40	0.37	0.33	0.30	0.28	0.22	0.18	0.10	0.05
50	—	0.56	0.51	0.47	0.44	0.42	0.39	0.37	0.31	0.28	0.21	0.16

$a/b = 3.0$

5	-0.09	-0.18	—	—	—	—	—	—	—	—	—	—
15	—	+0.05	0.00	-0.03	-0.06	-0.09	-0.11	-0.13	-0.17	—	—	—
30	—	0.20	0.15	0.11	0.08	0.05	0.03	0.00	-0.05	-0.09	-0.15	-0.20
50	—	0.27	0.22	0.19	0.15	0.13	0.10	0.07	0.02	0.00	-0.05	-0.08

Section Eight

FLOW PAST OBSTRUCTIONS UNIFORMLY DISTRIBUTED OVER CONDUIT CROSS SECTIONS

(Resistance coefficients of grids, screens, pipe bundles, packings, etc.)

8-1. LIST OF SYMBOLS

- F_0, F_1 = flow area of the obstruction cross-section and area of the conduit section before the obstruction, respectively, m^2 ;
 F_g = area of the obstruction front, m^2 ;
 f_0 = area of one opening of the grid or screen, m^2 ;
 $\bar{f} = \frac{F_0}{F_g}$ = cross-section coefficient;
 H_0 = perimeter of the section, m;
 D_0 = conduit-section diameter, m;
 D_h = hydraulic diameter of the conduit, m;
 d_0 = diameter of the section of a perforated-plate orifice, m;
 d_h = hydraulic diameter of the orifices of an obstruction or of the pores of a layer of loose or bulk material, etc., m;
 d_{in}, d_{out} = inner and outer diameter of the tubes of a bundle, of rings, etc., m;
 d_{gr} = diameter of a spherical grain, m;
 d_m = bar thickness, m;
 a_0 = width of the gap of a bar grate, radius of the orifices of a disk (plate), m;
 l = depth of the orifices of a grid (wall thickness at the place of the orifice), of the gaps of a bar grate, m;
 l_0 = thickness of a porous layer, total length of a transverse bundle of tubes, of a packing of plates, m;
 S_1, S_2 = vertical and horizontal distances between the axes of adjacent bars of a grate, tubes in a bundle, etc., and also between the orifices of a perforated plate, m;
 S' = diagonal distances between the orifices of a perforated plate, m;
 α_0 = angle of attack of the bar in a bar grate;
 θ = angle of inclination of the bar of a bar grate, of the tubes of a tube bundle toward the stream, and also of the orifices in the case of their checkerboard arrangement in a perforated plate;
 w_0, w_1 = mean velocities of the stream in the gap of the obstruction (grid, grate, screen, bundle of tubes, layer, etc.) and in the conduit in front of the obstruction, respectively, m/sec ;
 $w_{0,in}, w_{0,ex}$ = mean stream velocities in the gap at the inlet of the obstruction and at the exit from it, m/sec ;
 w_{im}, w_{om} = mean stream velocities before the obstruction and in its cross section, dependent on the arithmetic-mean stream temperature along this obstruction, m/sec ;
 ΔH = pressure loss (resistance), kg/m^2 ;
 γ = specific gravity in kg/m^3 of the flowing medium in any section;
 γ_{in} = specific gravity in the inlet section of the obstruction;
 γ_{ex} = specific gravity in the exit section of the obstruction;

γ_m = specific gravity dependent on the arithmetic-mean temperature;
 γ_0 = specific gravity at $t = 0^\circ\text{C}$;
 t = temperature of the flowing medium in any section, $^\circ\text{C}$;
 t_{in} = temperature in the inlet section of the obstruction, $^\circ\text{C}$;
 t_{ex} = temperature in the exit section of the obstruction, $^\circ\text{C}$;
 t_m = arithmetic-mean temperature over the entire depth of the obstruction (bundle, layer, etc.), $^\circ\text{C}$;
 s = jet-contraction coefficient at any area ratio $\frac{F_0}{F_1}$;
 s_0 = jet-contraction coefficient of a sharp-edged orifice at $\frac{F_0}{F_1} = 0$;
 ϵ' = porosity (percentage of pores; free volume) of a porous medium;
 ζ = resistance coefficient of the obstruction;
 $\Delta\zeta$ = additional resistance coefficient, allowing for the pressure loss at the change of stream velocity as a result of a change in its specific gravity with temperature;
 λ = friction coefficient of the conduit (orifice), or thickness of the layer; depends on Reynolds number and relative roughness (for a conduit);
 Re, Re_m = Reynolds number, and average Reynolds number obtained from the arithmetic-mean temperature of the stream along the obstruction;
 M = Mach number.

8-2. EXPLANATIONS AND RECOMMENDATIONS

1. Grids, screens, layers, cloths, checkerboards, etc. made from Raschig rings, bulk material, or arrays of tubes all represent obstructions distributed uniformly over a conduit section

2. A plane grid placed in a straight pipe has the same resistance effect as an orifice plate: the stream contracts during its passage through the grid orifices, and its exit velocity is higher than its inlet velocity. Losses result which are connected both with the entrance to an orifice, and with the sudden expansion at its exit (Figure 8-1).

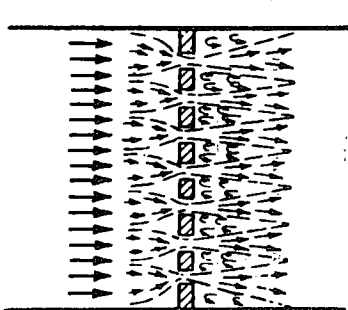


FIGURE 8-1. Pattern of flow through a grid or screen.

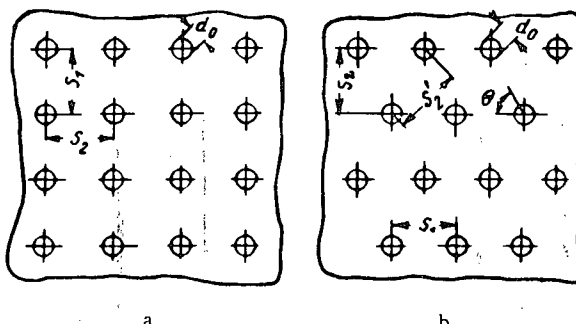


FIGURE 8-2. Designing a perforated grid:
a—orifices in vertical columns; b—orifices staggered.

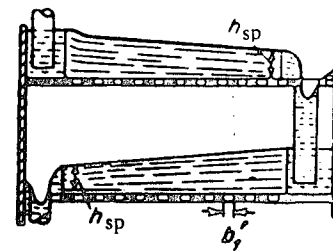


FIGURE 8-3. Screen plates in a rectification column.

The resistance coefficient of a plane, thin-walled grid is a function of its cross-section coefficient $\bar{f} = \frac{F_0}{F_g} = \frac{F_0}{F_1}$ (F_g = grid frontal area), the shape of its orifice edges, and the Reynolds number $Re = \frac{w_0 d_0}{\nu}$. It is calculated by the same formulas as a restrictor, i.e., by formulas (4-24) and (4-26) to (4-30), respectively.

3. The stream velocity in the narrowest section of the jets passing through the grid can turn out to be very high at small values of \bar{f} , even at low inlet velocities, and in some cases approaches the velocity of sound. Under such conditions the resistance coefficient of the grid becomes a function of the Mach number $M_1 = \frac{w_1}{a}$. This is expressed by the formula

$$\zeta_M = \frac{\Delta H}{\frac{T_1 w_1^2}{2g}} = k_M \zeta, \quad (8-1)$$

where k_M is the corrective coefficient for the influence of the Mach number, and is determined on the basis of the data of /8-59/; this coefficient has been plotted in diagram 8-7; ζ is determined as in the case $M_1 = 0$, i.e., by the formulas given in Section IV.

4. The following relationships between the number of orifices z , their transverse (S_1) and longitudinal (S_2) pitches, the orifice diameter d_0 , and the cross-section coefficient of the grid \bar{f} are useful when designing perforated grids:

1) number of orifices

$$z = \frac{1.27 \bar{f} F_g}{d_0^2}; \quad (8-2)$$

- 2) distance between the orifices when these are:
a) arranged in vertical columns (Figure 8-2, a);

$$S_1 = \frac{0.785 d_0^2}{S_2 \bar{f}} \quad (8-3)$$

and

$$S_2 = \frac{0.785 d_0^2}{S_1 \bar{f}}, \quad (8-4)$$

where (8-3) is used when the pitch S_2 is known, and formula (8-4) when the pitch S_1 is known;

in the particular case $S_1 = S_2$:

$$S_1 = \frac{0.89 d_0}{\sqrt{\bar{f}}} \quad (8-5)$$

b) staggered at an angle θ (Figure 8-2, b):

$$S_1 = \frac{1.25d_0 \sqrt{\tan \theta}}{\sqrt{f}} \quad (8-6)$$

and

$$S_2 = \frac{0.625d_0}{\sqrt{f} \tan \theta}. \quad (8-7)$$

In the particular case of equal distances between the orifices in the vertical and diagonal directions ($S_1 = S_2$; $\theta = 30^\circ$), it follows

$$S_1 = \frac{0.95d_0}{\sqrt{f}} \quad (8-8)$$

and

$$S_2 = \frac{0.82d_0}{\sqrt{f}}. \quad (8-9)$$

In the case $S_1 = S_2$, we obtain once more formula (8-5).

5. The resistance coefficients of screens are calculated by the following formula (cf. /8-19/ and /8-20/):

$$\zeta = \frac{\Delta H}{\frac{\gamma w_1^2}{2g}} = k_0 \left(1 - \frac{F_0}{F_1} \right) + \left(\frac{F_1}{F_0} - 1 \right)^2. \quad (8-10)$$

Here $k_0 = 1.3$ (according to Adamov's data) for screens made from circular metal wire not perfectly clean, but with normal surface state (neither rusty nor dusty), $k_0 = 1.0$ for new wire screens, and $k_0 = 2.1$ for silk-thread screens (according to Khanzhonkov's data /8-54/). The resistance coefficient of circular-wire screens is a function of the Reynolds number for $Re = \frac{w_0 d_0}{v} < 400$; the resistance coefficient of silk-thread screens is a function of the Reynolds number for $Re = \frac{w_0 d_0}{v} < 150$. [See diagram 8-6.]

The influence of the Reynolds number can be allowed for by the formula

$$\zeta_{Re} = k_{Re} \zeta, \quad (8-11)$$

where ζ is determined by formula (8-10); k_{Re} is determined from diagram 8-6 as a function of the Reynolds number.

At small values of the cross-section coefficient, the velocity in the screen orifices can approach the velocity of sound. The influence of the Mach number $M_1 = \frac{w_1}{a}$ is allowed

for here by the formula

$$\zeta_M = \frac{\Delta H}{\frac{1_g w_0^2}{2g}} = k'_M \zeta, \quad (8-12)$$

where k'_M is the corrective coefficient allowing for the influence of the Mach number; its value has been plotted in diagram 8-8 on the basis of Cornell's experimental data /8-59/.

6. The installation of two screens close to each other, theoretically should not lead to an increase in resistance, since if the wires of the two screens are accurately superposed the result is equivalent to one screen of doubled wire thickness in the stream direction. Actually, however, the superposition is never quite so accurate, and the result is always a certain decrease of cross-section area as compared to that of a single screen. It follows that the resistance will increase, but rarely by a factor of two. When the two screens are, however, installed at a distance from each other larger than 15 wire diameters, the resistance is doubled. Therefore, in practical calculations the total resistance of screens mounted in series can be considered as equal to the sum of the resistance coefficients of the separate screens:

$$\zeta_z = \sum_i \zeta_i, \quad (8-13)$$

where z is the number of screens.

7. When grids or screens are used as bubbling plates in apparatus where a process of mass exchange takes place (rectification and sorption columns, gas moisteners, etc., Figure 8-3)), their resistance depends upon two factors. One is the type of work of the plate (dry, wetted by the motion of a liquid column with or without bubbling), and the other is the physical properties of the working media and plate dimensions.

8. The resistance coefficient of a dry plate is determined from the data given under points 2 and 5 as for an ordinary grid or screen.

The resistance of a wetted plate with small orifices is higher than the resistance of a dry plate, since a liquid film forms in the orifices whose tearing requires the expenditure of a certain amount of energy by the fluid stream passing through the orifices.

The resistance coefficient of a wetted plate with small orifices can be calculated by the following formula, proposed by Usyukin and Aksel'rod /8-50/:

$$\zeta = \frac{\Delta H}{\frac{1_g w_0^2}{2g}} = \zeta_{dr} \left(\frac{F_0}{F_1} \right)^2 + 2 \cdot 10^{-4} \frac{\sigma/a_0}{\frac{1_g w_0^2}{2g}}, \quad (8-14)$$

where ζ_{dr} = resistance coefficient of a dry plate, determined from diagrams 8-1 to 8-6 as ζ for an ordinary grid; σ = surface-tension coefficient of a liquid at the boundary between the gaseous and liquid phases, kg/m; 1_g = specific gravity of the gas, kg/m²; a_0 = radius of a circular orifice or width of a slit in the plate, m.

Under normal operating conditions the resistance coefficient of a plate with bubbling can be calculated by another formula (proposed by the same authors):

$$\zeta = \frac{\Delta H}{\frac{1_g w_0^2}{2g}} = \zeta_{dr} \left(\frac{F_0}{F_1} \right)^2 + \frac{2 \cdot 10^{-4} \frac{\sigma}{a_0}}{\frac{1_g w_0^2}{2g}} + 0.5 \frac{1_l}{1_w} \frac{h_{sp}}{\frac{1_g w_0^2}{2g}} + 2.3 \frac{1_l}{1_w} \left(\frac{Q_1}{h_{sp}} \right)^{2/3} \frac{1}{\frac{1_g w_0^2}{2g}}. \quad (8-15)$$

where γ_w and γ_1 are the specific gravities of water and the working liquid, kg/m^3 ; h_{sp} , l_{sp} are height and length of the spilling partition of the plate, m.

9. The resistance coefficient of bubbling plates without special spilling devices can be calculated, with sufficient accuracy for technical calculations, by the following formula (proposed by Dil'man, Darovskikh, Aerov, and Aksel'rod /8-10/):

$$\zeta = \frac{\Delta H}{\frac{\gamma_g w_0^2}{2g}} = 2\zeta_{dr} \left(\frac{F_0}{F_1} \right)^2 \frac{1}{(1 - \bar{f})^2} + \frac{\frac{4}{\alpha_0}}{\frac{\gamma_g w_0^2}{2g}}, \quad (8-16)$$

where \bar{f} is the fraction of the cross section of the plate slots through which the liquid flows down; this is calculated by the following formula from the same authors:

$$\bar{f} = \frac{\sqrt[3]{\left(\frac{L_0}{G_0} \right)^2 \gamma_g \frac{0.5}{\zeta_{dr} \left(\frac{F_0}{F_1} \right)^2 \mu_1^2}}}{1 + \sqrt[3]{\left(\frac{L_0}{G_0} \right)^2 \gamma_g \frac{0.5}{\zeta_{dr} \left(\frac{F_0}{F_1} \right)^2 \mu_1^2}}, \quad (8-17)$$

where G_0 , L_0 = mass flow per unit area of gas and liquid, respectively, kg/m^2 ; μ_1 is the discharge coefficient of the fluid through the slot (orifice) of the plate.

10. Just as for ordinary thickened grids, the total losses through bar gratings of different bar cross sections (cf. diagrams 8-9 and 8-10) are comprised of entrance losses, frictional losses, and losses with sudden expansion at the exit from the section between the bars in the grating. The resistance coefficient of gratings at $\frac{l}{a_0} = 5$ and $\frac{a_0}{S_1} \geq 0.5$ can be determined by Kirschmer's formula /8-61/:

$$\zeta = \frac{\Delta H}{\frac{\gamma w_1^2}{2g}} = \beta_1 k_1 \sin \theta, \quad (8-18)$$

where β_1 is the coefficient of bar shape, determined from Table 8-2 of diagram 8-9:

$$k_1 = \left(\frac{S_1}{a_0} - 1 \right)^{4/3}; \quad (8-19)$$

θ is the angle of inclination of the bar toward the stream.

The resistance coefficient of gratings can be determined approximately, at any value of the ratio $\frac{a_0}{S_1}$, and any relative grating thickness $\frac{l}{a_0}$, by the formula

$$\zeta = \frac{\Delta H}{\frac{\gamma w_1^2}{2g}} = \beta_2 \zeta' \sin \theta, \quad (8-20)$$

where β_1 is the coefficient of bar shape, determined from Table 8-2 of diagram 8-9 on the basis of Kirschmer's data /8-61/; C' is the resistance coefficient of an ordinary grid or orifice plate with thick-edged orifices, determined by formula (4-27) or from the graph of diagram 8-4; a_0 , S_1 , t are gap width, distance between the axes of adjacent bars, and bar thickness in the stream direction, m.

11. The resistance coefficient of a bar grating of arbitrary bar cross section, placed immediately behind a stream turn, at an angle of attack α_0 , is determined for $\frac{a_0}{S_1} \geq 0.5$ from the relation (cf. Spandler /8-62/)

$$\zeta = \frac{\Delta H}{\frac{\gamma w_1^2}{2g}} = \sigma_1 \sigma_2, \quad (8-21)$$

where σ_1 is a coefficient depending almost entirely on the angle of attack α_0 , and is determined for given bar shape from graph a (diagram 8-10); σ_2 is a coefficient depending on the angle of attack α_0 and the cross-section coefficient $\frac{a_0}{S_1}$, and is determined from graph b (diagram 8-10).

12. The resistance coefficients of bar gratings used in hydro structures turn out to be higher than the ones determined by these formulas, due to fouling and to design peculiarities of the gratings. Accordingly it is recommended (cf. Dul'nev /8-11/) to introduce a correction coefficient c' into formulas (8-18), (8-20), and (8-21) whose value is to be determined as a function of the nature and amount of flotsam contained in the water, method of cleaning the grating, possibility of deposition of silt before the grating, etc. In the case of mechanical cleaning of the gratings $c' = 1.1-1.3$, and in the case of manual cleaning $c' = 1.5-2.0$.

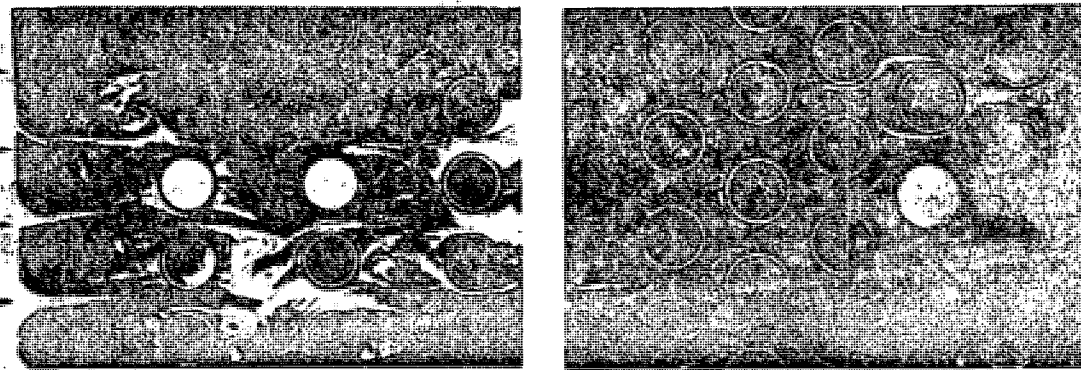
In order to allow for design peculiarities the same author recommends the introduction into the formulas of an additional corrective coefficient c'' :

$$c'' \approx \frac{1}{(1 - \frac{A}{L})}, \quad (8-22)$$

where L = internal height of the grating, m; A = total height of the transverse elements ($A = h z_1 + d z_2$), m; h and z_1 are height and number of intermediate support bars; d and z_2 are diameter and number of bracing elements.

13. The tube bundles of heat exchangers are laid out either in a parallel or in a staggered arrangement. In the first instance the following pattern of flow is observed (cf. Abramovich /8-11/). Jets flow out of the space between the tubes of the first row and enter the space between the rows (Figure 8-4). Here, further masses from the shaded regions are mixed with the main stream core. Upon reaching the second row of tubes the jets divide. The main core passes past the second row of tubes, while the added masses form a closed stream circulation or eddy zone in the shaded regions. The pattern of flow in the spaces between the succeeding rows is similar to the one just described*. Thus, the pressure losses in an array of tubes are similar to losses in a free jet.

* Actually, the flow becomes turbulent after passing the first row of tubes, and the conditions of flow past the succeeding rows are somewhat altered as a result.



a

b

FIGURE 8-4. Arrangement of tubes:

a—vertical columns; b—staggered.

14. The resistance coefficient of a bundle of staggered tubes, including the losses at inlet and exit, can be calculated at $3 \cdot 10^3 < Re_m < 10^5$ by the following formulas, proposed by Mochan and Revzin /8-41/:

$$1) \frac{S_1}{d_{out}} < 2.0 \text{ and } 0.14 < \frac{S_1 - d_{out}}{S'_2 - d_{out}} < 1.7$$

$$\zeta = \frac{\Delta H}{\gamma_m w_{0m}^2} = \left[\left(4.6 - 2.7 \frac{S_1 - d_{out}}{S'_2 - d_{out}} \right) \left(2 - \frac{S_1}{d_{out}} \right) + 3.2 \right] \times Re_m^{-0.27} (z+1); \quad (8-23)$$

$$2) \frac{S_1}{d_{out}} > 2.0 \text{ and } 0.14 < \frac{S_1 - d_{out}}{S'_2 - d_{out}} < 1.7$$

$$\zeta = \frac{\Delta H}{\gamma_m w_{0m}^2} = 3.2 Re_m^{-0.27} (z+1); \quad (8-24)$$

$$3) \frac{S_1}{d_{out}} \geq 1.0 \text{ and } 1.7 < \frac{S_1 - d_{out}}{S'_2 - d_{out}} \leq 5.2$$

$$\zeta = \frac{\Delta H}{\gamma_m w_{0m}^2} = 0.44 \left(\frac{S_1 - d_{out}}{S'_2 - d_{out}} + 1 \right)^n Re_m^{-0.27} (z+1), \quad (8-25)$$

where

$$w_{0m} = w_{0in} \frac{273 + t_m}{273 + t_{in}}; \quad (8-26)$$

$$t_m = \frac{t_{in} + t_{ex}}{2}; \quad (8-27)$$

$$t_m = \frac{t_{in}}{1 + \frac{t_{in}}{273}}; \quad (8-28)$$

$$Re_m = \frac{w_{0m} d_{out}}{v}. \quad (8-29)$$

v is determined by § 1-3, b for the arithmetic-mean temperature t_m .

15. The resistance coefficient of a bundle of vertically arranged tubes, including the losses at inlet and exit, can be calculated at $3 \cdot 10^3 < Re_m < 10^5$ by the following formulas,

proposed by Mochan and Revzin /8-41/:

$$1) \frac{s_1}{d_{out}} < \frac{s_2}{d_{out}}$$

$$\zeta = \frac{\Delta H}{\frac{\gamma_m w_{0m}^2}{2g}} = 1.52 \left(\frac{s_1 - d_{out}}{s_2 - d_{out}} \right)^{-0.2} \left(\frac{s_1}{d_{out}} - 1 \right)^{-0.5} \times Re_m^{-0.2} z; \quad (8-30)$$

$$2) \frac{s_1}{d_{out}} > \frac{s_2}{d_{out}}$$

$$\zeta = \frac{\Delta H}{\frac{\gamma_m w_{0m}^2}{2g}} = 0.32 \left(\frac{s_1 - d_{out}}{s_2 - d_{out}} - 0.9 \right)^{-0.68} \left(\frac{s_1}{d_{out}} - 1 \right)^{-0.5} \times Re_m^{-\frac{0.2}{(s_2 - d_{out})^2}} z. \quad (8-31)$$

If the pitch varies within the limits of the bundle, the resistance is calculated by its mean value.

16. If heat exchange takes place in a tube bundle, it is necessary to add to values of ζ obtained by formulas (8-23) to (8-25), (8-30), and (8-31) a term $\Delta\zeta$, to allow for the pressure loss accompanying change in rate of flow of the stream within the bundle, and which is caused by a change in the specific gravity of the working medium (cf. Mikheev /8-40/):

$$\Delta\zeta = 2 \frac{t_{ex} - t_{in}}{273 + t_m}. \quad (8-32)$$

$\Delta\zeta$ is positive in the case of heating and negative in the case of cooling.

17. When the flow is obliquely directed toward the tube bundle the conditions of flow past the pipes are improved and its resistance is smaller (cf. Kazakevich /8-24/). The

resistance reduction ratio (the coefficient of stream "direction") $\psi = \frac{\zeta_0}{\zeta_{90^\circ}}$ is a function both of the angle of inclination θ and of the other parameters of the bundle. For practical calculations, however, the influence of other parameters can be neglected, and the mean value of ψ can be considered constant for a given inclination angle. These mean values of ψ are:

1. Vertical columns

$$\begin{aligned} \theta = 60^\circ & \psi \approx 0.82; \\ \theta = 45^\circ & \psi \approx 0.54; \\ \theta = 30^\circ & \psi \approx 0.30; \end{aligned}$$

2. Staggered

$$\begin{aligned} \theta = 60^\circ & \psi \approx 0.80; \\ \theta = 45^\circ & \psi \approx 0.57; \\ \theta = 30^\circ & \psi \approx 0.34. \end{aligned}$$

18. Ribbed or finned tubes are frequently used to increase the surface of heating or cooling, and streamlined tubes in order to decrease the resistance of the tube bundle to cross flow. Data for the determination of the resistance coefficients of such tubes in bundles are given in diagrams 8-13 and 8-14.

19. Three main flow states exist in the case of stream passage through porous media: molecular, laminar, and turbulent. The state of flow is molecular when the pore dimensions are equivalent to the free-path length of the molecules (of the order of tenths of a micron). Laminar flow is subject to the Poiseuille-Hagen law, which can be written in the case of a porous medium in the form

$$w_1 = \frac{\epsilon' d_{11}^2 \Delta H}{32 l_{tw}^2 \eta l_0}, \quad (8-33)$$

or in Darcy's form

$$w_i = K \frac{\Delta H}{l_{tw}} = k' \frac{\Delta H}{\eta l_0}, \quad (8-34)$$

where $K = \frac{\epsilon' d_h^2}{32 \eta l_{tw}^2}$ is the seepage coefficient; $k' = \frac{\epsilon' d_h^2}{32 l_{tw}^2}$ is the permeability; this magnitude is constant for a given porous medium and does not depend on the nature of the flowing medium; $\bar{l}_{tw} = \frac{l_{tr}}{l_0}$ = coefficient of twisting of the pores; $d_h = 4 \frac{\epsilon'}{S}$ = hydraulic diameter of the pores, m; ϵ' = porosity (free volume fraction); S = specific surface of the porous medium, m^2/m^3 ; l_0 = layer thickness, m; l_{tr} = true length of the pores, m; η = dynamic viscosity, $kg \times sec/m^2$.

20. A distinctive feature of porous media is the gradual transition from laminar to turbulent flow, starting at low values of Reynolds number and extending over a wide range of values of it. The smooth character of the transition is explained by the twisting of the pores, the contractions and expansions, and also by the roughness of the porous surface, which contribute to formation of eddies and stream disturbances. It is also helped by a gradual propagation of turbulence from large pores toward the smaller ones, which is connected with the distribution of the different sizes of pores in the media.

21. Porous media can be classified into three main groups:

- 1) bonded or cemented media such as: porous ceramics, porous metal;
- 2) loose or bulk media such as: powders, various bulk materials, packings made from regular geometric shapes — spheres, cylinders, rings;
- 3) regular media such as: grid, screen, or chord packings, sieves, tubes, corrugated strips, etc.

22. The porosity and magnitude of the gaps (cross-section coefficient) in a layer made from identical spherical bodies are independent of the grain diameter; they are a function of the mutual disposition of the grains, i. e., of the angle θ (Figure 8-5):

$$\epsilon' = 1 - \frac{\pi}{6(1 - \cos \theta) \sqrt{1 + 2 \cos \theta}} \quad (8-35)$$

and

$$\bar{l} = 1 - \frac{\pi}{4 \sin \theta}.$$

where ϵ' = porosity, m^3/m^3 ;

The extreme values of θ are equal to 60° and 90° . The values of the theoretical porosity ϵ' and of \bar{l} in this range of values of θ are given in Table 8-1.

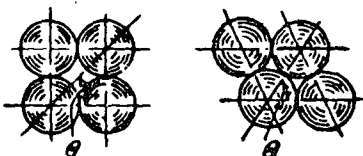


FIGURE 8-5. Arrangement of spherical bodies in a layer.

TABLE 8-1

	60°	60°02'	61°18'	62°38'	64°03'	65°37'	67°21'	69°17'	71°28'	74°03'	77°10'	81°28'	89°00'
ϵ'	0.259	0.26	0.28	0.30	0.32	0.34	0.36	0.38	0.40	0.42	0.44	0.46	0.476
\bar{f}	0.0931	0.0977	0.1045	0.1155	0.1266	0.1337	0.1491	0.1605	0.1719	0.1832	0.1946	0.2057	0.2146

The value of ϵ' for bodies of irregular shape is determined experimentally. The value of \bar{f} can be expressed as a function of the porosity by the following approximate formula, proposed by Bernshtein, Pomerantsev, and Shagalova /8-8/:

$$\bar{f} \approx 0.95 \epsilon'^{1.76}. \quad (8-37)$$

23. The resistance coefficient of both a loose layer of granular bodies, and of cemented porous media of granular material of constant diameter d_{gr} with relative layer thickness $\frac{l_0}{d_{gr}}$, can be calculated by the following formula (proposed by Bernshtein, Pomerantsev, and Shagalova /8-8/):

$$\zeta = \frac{\Delta H}{\gamma w_1^2} = \frac{1.53}{\epsilon'^{4.2}} \left(\frac{30}{Re} + \frac{3}{Re^{0.7}} + 0.3 \right) \frac{l_0}{d_{gr}} = k \lambda' \frac{l_0}{d_{gr}} = \lambda \frac{l_0}{d_{gr}}, \quad (8-38)$$

where λ is the friction coefficient of a layer thickness equal to the grain diameter ($\frac{l_0}{d_{gr}} = 1.0$):

$$k = \frac{1.53}{\epsilon'^{4.2}}; \quad (8-39)$$

$$\lambda' = \frac{30}{Re} + \frac{3}{Re^{0.7}} + 0.3; \quad (8-40)$$

$$Re = \frac{w_1 d_h}{f} = \frac{0.45}{(1 - \epsilon') \sqrt{\epsilon'}} \cdot \frac{w_1 d_{gr}}{v}; \quad (8-41)$$

$$d_h = 0.423 \frac{\epsilon'^{1.25}}{1 - \epsilon'} d_{gr} \quad (8-42)$$

d_h is the hydraulic diameter of the narrowest interval between spheres, m; d_{gr} is the grain (sphere) diameter, m; l_0 = layer thickness, m.

24. The resistance coefficient of a layer made from bodies of any regular shape, except those listed in diagram 8-16, can be calculated by the following formula of Bernshtein, Pomerantsev, and Shagalova /8-8/:

$$\zeta = \frac{\Delta H}{\gamma w_1^2} = \frac{1.53}{\epsilon'^{4.2}} \left(\frac{75}{Re} + \frac{15}{\sqrt{Re}} + 1 \right) = k \lambda', \quad (8-43)$$

where Re and d_h are determined by formulas (8-41) and (8-42).

25. The resistance coefficient of the materials listed in diagram 8-16* and of bonded porous media made from bodies of irregular shape is calculated by the formula

$$\zeta = \frac{\Delta H}{\frac{\gamma w_1^2}{2g}} = \lambda \frac{1}{\epsilon'} \cdot \frac{l_h}{d_h}, \quad (8-44)$$

where according to the data of Ishkin and Kaganer /8-23/ at $Re_h = \frac{w_1 d_h}{\nu} < 3$

$$\lambda = \frac{180}{Re_h}, \quad (8-45)$$

and at $Re_h > 3$,

$$\lambda = \frac{164}{Re_h} + \frac{7.68}{Re_h^{0.11}}. \quad (8-46)$$

The value of d_h here is taken from the data of diagram 8-16.

26. The resistance of "regular" porous media, such as Raschig rings packed in regular rows (cf. diagram 8-20), and of chord packing from wooden laths laid in parallel (cf. diagram 8-21), is mainly determined by the frictional pressure losses in the absence of wetting the liquid.

The resistance coefficient of such packing can be calculated by (8-44), where (according to Zhavoronkov's data /8-12/)

$$\lambda = \frac{3.12}{Re_h^{0.375}}, \quad (8-47)$$

for

$$0.4 \cdot 10^3 < Re_h < 8 \cdot 10^3:$$

and

$$\lambda \approx 0.1 = \text{const.} \quad (8-48)$$

for $Re_h > 8 \cdot 10^3$. Here $Re_h = \frac{w_1 d_h}{\nu} \cdot \frac{1}{\epsilon'}, d_h = \frac{4\epsilon'}{\bar{S}}$ is the hydraulic diameter of the gap between the rings, m; \bar{S} is the specific surface of all rings, m^2/m^3 .

27. The resistance of Raschig rings in a staggered arrangement (cf. diagram 8-20), and of chord packing placed crosswise (cf. diagram 8-21), is determined, in the absence of wetting by the liquid, both by the frictional losses and by the losses accompanying the sudden contraction and expansion of the stream at the places of intersection of the packing.

* The reason for the separate treatment of these media is due to their porosity not always being correctly determined (Zhavoronkov's experiments /8-12/). Also either the size of the bodies is sometimes unknown, or it is impossible to determine it. Formulas (8-45) and (8-46) are meant for use with the values of ϵ' given in the original references.

28. The resistance coefficient of ceramic Raschig rings of diameter ratio $\frac{d_{\text{out}}}{d_{\text{in}}} \approx 1.2$ and relative height $\frac{l_r}{d_{\text{out}}} \approx 1.0$, laid in a staggered pattern can be determined by (8-44), where according to Zhavoronkov /8-12/

$$\lambda = \frac{9.2}{Re_h^{0.375}}. \quad (8-49)$$

for $0.4 \cdot 10^3 < Re_h \leq 6 \cdot 10^3$ λ and

$$\lambda \approx 0.37 = \text{const.} \quad (8-50)$$

for $Re_h > 6 \cdot 10^3$.

Formulas (8-49) and (8-50) can be extended with a certain approximation to rings of other dimensions.

29. The resistance coefficient of chord packings laid crosswise is calculated by (8-44), where according to Zhavoronkov /8-12/

$$\lambda = \frac{k'_1}{Re_h^{0.375}}. \quad (8-51)$$

for $0.4 \cdot 10^3 < Re_h \leq 6 \cdot 10^3$, and

$$\lambda = \lambda' = \text{const.} \quad (8-52)$$

for $Re_h > 6 \cdot 10^3$, where k'_1 and λ' are taken as functions of the grid geometry (cf. diagram 8-21).

30. The resistance to the motion of a gas stream in a wetted packing is considerably larger than in a dry packing. The increase in the resistance is due both to the reduction of the free cross-section area by the liquid stream and to the bubbling of the gas through the liquid retained in the stagnant zones of the packing. The influence of the intensity of wetting on the resistance increases with the decrease of the size of the elements in the packing.

Three states of flow are observed in the case of gas motion by a countercurrent through a wetted packing: a) stable, where the liquid flows down completely; b) unstable, in which there occurs at first a retention of the liquid; and c) a reverse motion of the liquid, leading to flooding and ejection of the liquid from the packing together with the gas. Retention of, and flooding by the liquid occur at a velocity of the gas stream which is the lower the larger the intensity of wetting A of the packing (cf. Zhavoronkov /8-12/).

31. The resistance coefficient of a wetted packing, ordered or disordered, up to the beginning of the retention of the liquid, i.e., at a velocity $w_1 < w_{\text{lim}}$, can be approximately calculated for $A = 50 \text{ m}^3/\text{m}^2 \times \text{hour}$ by the following simplified formula, based on Zhavoronkov's data /8-12/:

$$\zeta = \frac{\Delta H}{\frac{\gamma w_1^2}{2g}} = \zeta_{\text{dr}} (1 + \zeta'_1 A). \quad (8-53)$$

where ζ_{dr} = resistance coefficient of a dry packing, determined as ζ from (8-38) to (8-52); A is the intensity of wetting of the packing by the liquid, $m^3/m^2 \times \text{hour}$; ϵ' is a coefficient allowing for the influence of the type of packing on the resistance increase as a result of the wetting; it is given in diagram 8-21 for different types of packing; w_{lim} is the limiting velocity of the gas stream in the free section of the apparatus (before the packing) at which the retention of the liquid starts; the values of w_{lim} are given in diagrams 8-16, 8-20, and 8-21.

32. The resistance of packings can increase sharply (by a factor of two to three, or more) if the gas passing through them is impure; this should be taken into account in the hydraulic calculation.

33. The resistance coefficient of regenerative packings, serving for heat recovery in heating and other systems, depends on the type of packing. Formulas for calculating the resistance coefficients of such packings are given in diagram 8-22.

34. Where the gas temperature changes as a result of its passage through the packing, the additional term (8-32) should be included in the formula for the resistance coefficient:

$$\zeta = \frac{\Delta H}{\frac{v_m w_{im}}{2g}} = \zeta + \Delta \zeta, \quad (8-54)$$

where ζ is determined by formulas (8-38) to (8-52):

$$w_{im} = w_1 \frac{273 + t_m}{273 + t_{in}}; \quad t_m = \frac{t_{in} + t_{ex}}{2};$$

$$\gamma_m = \frac{t_o}{1 + \frac{t_m}{273}};$$

$$Re_g = \frac{w_{0m} d_h}{v} = \frac{w_{im} d_h}{v} \cdot \frac{1}{\epsilon},$$

where v is taken (cf. § 1-3, b) as a function of the arithmetic-mean temperature t_m .

8-3. LIST OF THE DIAGRAMS OF RESISTANCE COEFFICIENTS OF SECTION VIII

Diagram description	Source	No. of diagrams	Note
Plane grid (perforated sheet) with sharp-edged orifices ($l/d_h = 0 \div 0.015$). $Re > 10^5$	Idel'chik /8-19, 8-20, 8-22/	8-1	Calculating formula and partially experiments
Plane grid (perforated sheet) with sharp-edged orifices ($l/d_h = 0 \div 0.015$). $Re < 10^5$	The same	8-2	The same
Grid with orifice edges beveled facing the flow or made from angle iron. $Re > 10^4$	" "	8-3	Calculating formula
Thickened grid (perforated plate or laths) ($l/d_h > 0.015$)	" "	8-4	" "
Grid with rounded orifice edges. $Re > 10^3$	" "	8-5	" "
Screens	Adamov, Idel'chik /8-19/, Khanzhonkov /8-54/, Cornell /8-59/	8-6	Experimental data and calculating formula
Grids with sharp-edged inlet in the orifice of a wall of arbitrary thickness at high stream velocities (large Mach numbers)	Cornell /8-59/	8-7	The same
Grids with orifice edges beveled or rounded, and screens at high stream velocities (large Mach numbers)	The same	8-8	Screens — experimental data, grids — approximately
Bar grating with an angle of approach $\alpha_0 = 0$. $Re > 10^4$	Dul'nev /8-11/, Idel'chik /8-19/, Kirschmer /8-61/, Spandler /8-62/	8-9	Experimental data, calculating formula, as for an ordinary grid
Bar grating with an angle of approach $\alpha_0 > 0$ and $\frac{\alpha_0}{S_1} > 0.5$. $Re > 10^4$	The same	8-10	The same
Bundle of circular tubes in vertical columns. $3 \times 10^3 < Re_m < 10^5$	Mochan and Revzina /8-41/	8-11	Calculating formulas based on experimental data
Bundle of staggered circular tubes. $3 \times 10^3 < Re_m < 10^5$	The same	8-12	The same
Bundle of ribbed tubes (air heater)	Antuf'ev and Beletskii /8-4/, Timofeev and Karasina /8-48/, Shcherbakov and Zhirnov /8-58/	8-13	" "
Bundles of tubes of different cross-section shapes	Antuf'ev and Beletskii, Sknar', Telegina /8-4/, Tulin /8-49/	8-14	" "
Recuperators (air heaters)	Kuznetsov and Shcherbakov /8-30/, Shcherbakov and Zhirnov /8-58/	8-15	" "
Packing material deposited at random (loose layers from bodies of irregular shape) at given d_h : dry and wetted	Ishkin and Kaganer /8-23/, Zhavoronkov /8-12/	8-16	" "
Packing material deposited at random (loose layers from bodies of irregular shape) at given d_{gr}	The same	8-17	" "

Diagram description	Source	No.of diagram	Note
Packings — loose layer of spherical (granular) bodies or porous cemented layer from granular material (constant diameter)	Bernshtein, Pomerantsev, and Shagalova /8-8/	8-18	Calculating formulas based on experimental data
Packings — bonded porous medium (non-granular)	Ishkin and Kaganer /8-23/	8-19	The same
Packings — ceramic Raschig rings $(\frac{d_{out}}{d_{in}} \approx 1.2)$; dry or wetted	Zhavoronkov /8-12/	8-20	" "
Packings of wooden laths; dry or wetted	The same	8-21	" "
Regenerator checkerwork (of furnaces)	Linchevskii /8-36/	8-22	" "

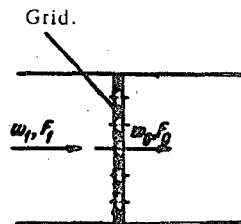
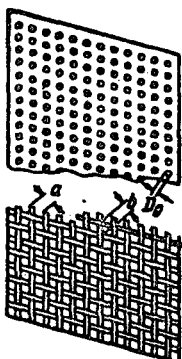
8-4. DIAGRAMS OF RESISTANCE COEFFICIENTS

Plane grid (perforated sheet) with sharp-edged orifices
 $\left(\frac{l}{d_h} = 0 \div 0.015\right)$

$$\left(Re = \frac{w_0 d_h}{v} > 10^3\right)$$

Section VIII

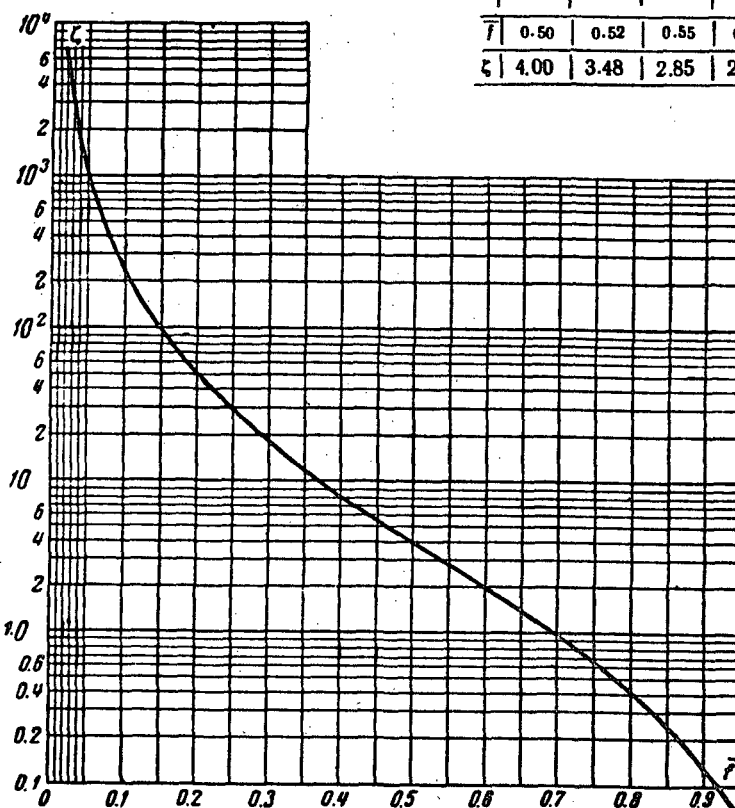
Diagram 8-1



$$\zeta = \frac{\Delta H}{\gamma w_1^2} = (0.707 \sqrt{1 - \bar{f}} + 1 - \bar{f})^2 \frac{1}{f_0}$$

is determined from the curve $\zeta = f(\bar{f})$ or from the table;

\bar{f}	0.02	0.03	0.04	0.05	0.06	0.08	0.10	0.12	0.14	0.15	0.18	0.20
ζ	7 000	3 100	1 670	1 050	730	400	245	165	117	86.0	65.5	51.5
f	0.22	0.24	0.26	0.28	0.30	0.32	0.34	0.36	0.38	0.40	0.43	0.47
ζ	40.6	32.0	26.8	22.3	18.2	15.6	13.1	11.6	9.55	8.25	6.62	4.95
\bar{f}	0.50	0.52	0.55	0.60	0.65	0.70	0.75	0.80	0.85	0.90	0.95	1.0
ζ	4.00	3.48	2.85	2.00	1.41	0.97	0.65	0.42	0.25	0.13	0.05	0.00



$$d_h = \frac{4f_0}{U_e}; \quad \Pi_e \text{ --- perimeter;}$$

$$\bar{f} = \frac{f_0}{f_1};$$

f_0 = orifice area;
 F_0 = total flow area of grid;
 v = is taken from § 1-3, b

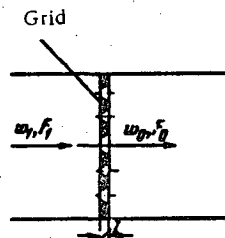
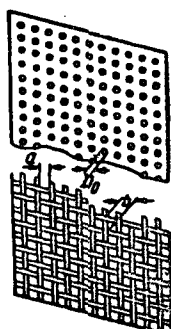
Plane grid (perforated sheet) with sharp-edged orifices

$$\left(\frac{l}{d_h} = 0 \div 0.015 \right)$$

Section VIII

$$(Re = \frac{w_0 d_h}{v} < 10^5)$$

Diagram 8-2



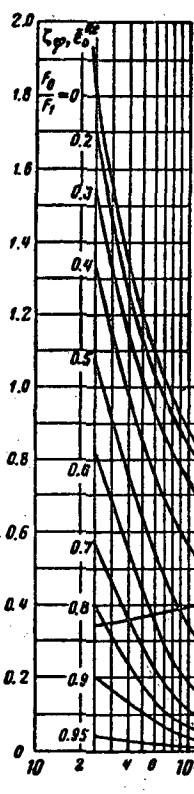
$$\zeta = \frac{\Delta H}{\gamma w_0^2} \approx \left[\zeta_\varphi + \bar{\epsilon}_0^{Re} (\zeta_0 - \bar{f})^2 \right] \frac{1}{f^2} \text{ (approximately)}$$

where ζ_φ is determined from the curves $\zeta_\varphi = f_1(Re)$ for different f on graph a;

$\bar{\epsilon}_0^{Re}$ is determined from $\bar{\epsilon}_0^{Re} = f_2(Re)$ on graph a;

$\zeta_0 = 1 + 0.707 \sqrt{1 - \bar{f}}$ is determined from the curve $\zeta_0 = f(\bar{f})$ on graph b.

Re	2.5-10	4-10	6-10	10 ²	2-10 ²	4-10 ²	10 ³	2-10 ³	4-10 ³	10 ⁴	2-10 ⁴	10 ⁵	2-10 ⁵	>10 ⁵
$\bar{\epsilon}_0^{Re}$	0.34	0.36	0.37	0.40	0.42	0.46	0.53	0.59	0.64	0.74	0.81	0.94	0.98	0.99

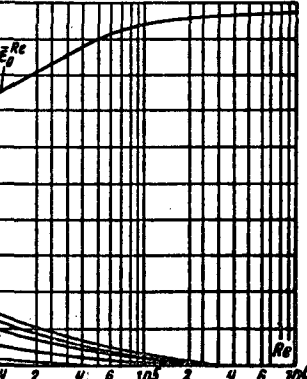


$\frac{F_0}{F_1}$	Values of ζ_φ													
0	1.94	1.38	1.14	0.89	0.69	0.64	0.39	0.30	0.22	0.15	0.11	0.04	0.01	0
0.2	1.78	1.36	1.05	0.85	0.67	0.57	0.36	0.26	0.20	0.13	0.09	0.03	0.01	0
0.3	1.57	1.16	0.88	0.75	0.57	0.43	0.30	0.22	0.17	0.10	0.07	0.02	0.01	0
0.4	1.35	0.99	0.79	0.57	0.40	0.28	0.19	0.14	0.10	0.06	0.04	0.02	0.01	0
0.5	1.10	0.75	0.55	0.34	0.19	0.12	0.07	0.05	0.03	0.02	0.01	0.01	0.01	0
0.6	0.85	0.56	0.30	0.19	0.10	0.06	0.03	0.02	0.01	0	0	0	0	0
0.7	0.58	0.37	0.23	0.11	0.06	0.03	0.02	0.01	0	0	0	0	0	0
0.8	0.40	0.24	0.13	0.06	0.03	0.02	0.01	0	0	0	0	0	0	0
0.9	0.20	0.13	0.08	0.03	0.01	0	0	0	0	0	0	0	0	0
0.95	0.03	0.03	0.02	0	0	0	0	0	0	0	0	0	0	0

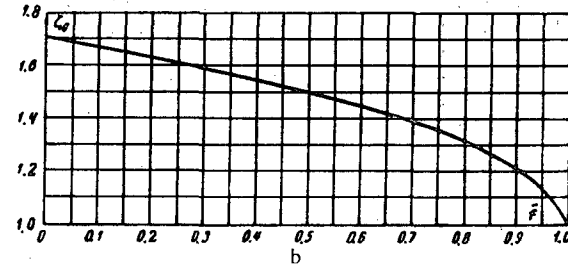
$$d_h = \frac{4f_0}{\Pi_0}; \quad \Pi_0 - \text{perimeters};$$

$$\bar{f} = \frac{F_0}{F_1};$$

v = is taken from § 1-3, b.



\bar{f}	0	0.1	0.2	0.3	0.4	0.5	0.6	0.7	0.8	0.9	1.0
ζ_0	1.71	1.67	1.63	1.59	1.55	1.50	1.45	1.39	1.32	1.22	1.0

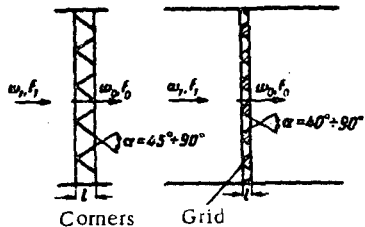


Grid with orifice edges beveled facing the flow or made

$$\text{from angle iron. } \text{Re} = \frac{w_0 d_{\text{h}}}{v} > 10^6$$

Section VIII

Diagram 8-3



$$\zeta = \frac{\Delta H}{\frac{1}{2} w_1^2} = \left[\sqrt{\zeta' (1 - \bar{l})} + (1 - \bar{l}) \right]^2 \frac{1}{\bar{l}^2},$$

where $\zeta' = f \left(\frac{l}{d_h} \right)$ is taken from the

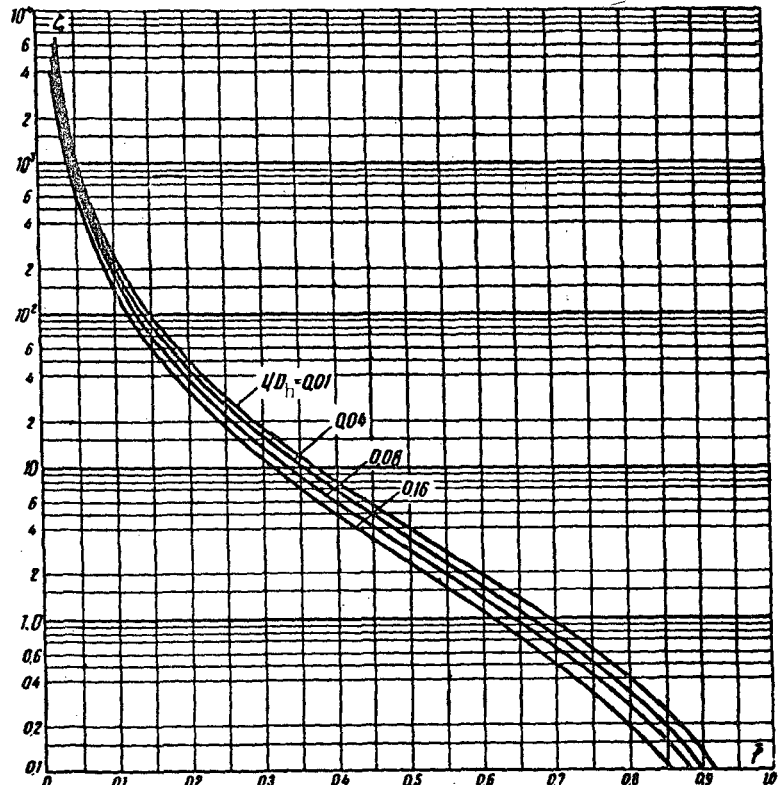
table or more accurately from graph a of diagram 4-12

The values of ζ are determined from the curves

$$\zeta = f \left(\bar{l}, \frac{l}{d_h} \right)$$

or taken from the table;

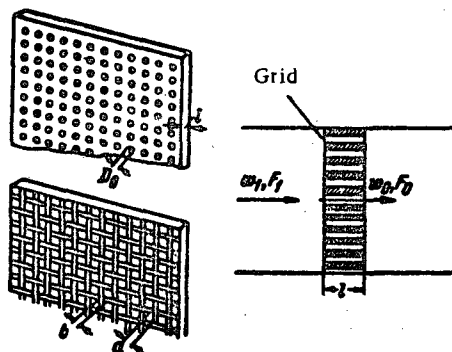
ζ' is taken from § 1-3, b.



Values of ζ

$\frac{l}{d_h}$	ζ'	\bar{l}															
		0.02	0.04	0.06	0.08	0.10	0.15	0.20	0.25	0.30	0.40	0.50	0.60	0.70	0.80	0.90	1.0
0.01	0.46	6 800	1 650	710	386	238	96.8	49.5	28.6	17.9	7.90	3.84	1.92	0.92	0.40	0.12	0
0.02	0.42	6 540	1 590	683	371	230	93.2	47.7	27.5	17.2	7.60	3.68	1.83	0.88	0.38	0.12	0
0.03	0.38	6 310	1 530	657	357	220	89.4	45.7	26.4	16.5	7.25	3.50	1.72	0.83	0.35	0.11	0
0.04	0.35	6 130	1 480	636	345	214	86.5	44.2	25.6	15.8	7.00	3.36	1.67	0.80	0.34	0.10	0
0.06	0.29	5 750	1 385	600	323	200	80.0	41.2	23.4	14.6	6.85	3.08	1.53	0.73	0.30	0.09	0
0.08	0.23	5 300	1 275	549	298	184	74.3	37.8	21.8	13.5	5.92	2.80	1.37	0.64	0.27	0.08	0
0.12	0.16	4 730	1 140	490	265	164	66.0	33.5	19.2	11.9	5.18	2.44	1.18	0.55	0.22	0.06	0
0.16	0.13	4 460	1 080	462	251	154	62.0	31.6	18.1	11.2	4.80	2.28	1.10	0.50	0.20	0.05	0

$$d_h = \frac{4f_0}{D_0}; \quad D_0 \text{ — perimeter; } \bar{l} = \frac{F_0}{F_1};$$



$$d_h = \frac{4f_0}{\Pi_0}; \quad \Pi_0 = \text{perimeter};$$

$$\bar{f} = \frac{f_0}{F_0};$$

$$1. \quad Re = \frac{w_0 d_h}{v} \geq 10^5;$$

$$\zeta = \frac{\Delta H}{\frac{\gamma w_0^2}{2g}} = \left[(0.5 + \tau \sqrt{1 - \bar{f}})(1 - \bar{f}) + (1 - \bar{f})^2 + \lambda \frac{l}{d_h} \right] \frac{1}{\bar{f}^2} = \left(\zeta_0 + \lambda \frac{l}{d_h} \right) \frac{1}{\bar{f}^2}.$$

where $\tau = f \left(\frac{l}{d_h} \right)$ is taken from the table or, more accurately, from the graph of diagram 4-11;

$$\zeta_0 = (0.5 + \tau \sqrt{1 - \bar{f}})(1 - \bar{f}) + (1 - \bar{f})^2;$$

λ is determined from diagrams 2-1 to 2-5 as a function of Re and $\bar{A} = \frac{A}{D_h}$.

At $\bar{A} = 0.02$ the values of ζ are determined from the curves $\zeta = f(\bar{f})$ corresponding to different $\frac{l}{d_h}$ or from the table;

v is taken from § 1-3, b;

\bar{A} is taken from Table 2-1;

2. $Re < 10^5$ (approximately):

$$\zeta_{Re} = \frac{\Delta H}{\frac{\gamma w_0^2}{2g}} = \left(\zeta_0 + \epsilon_0^{Re} \zeta_0 + \lambda \frac{l}{d_h} \right) \frac{1}{\bar{f}^2},$$

where ζ_0 is determined as at $Re > 10^5$; ϵ_0^{Re} and w_0^{Re} — cf. diagram 8-2.

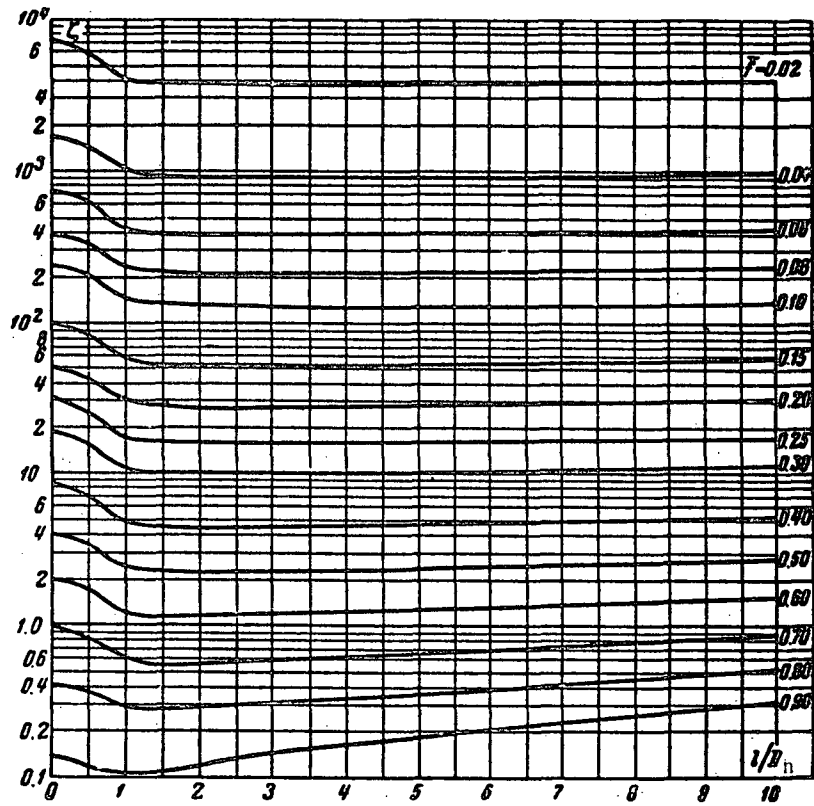
Section VIII

Thickened grid (perforated plate or laths) ($\frac{t}{d_h} > 0.015$) (continued)

Diagram 8-4

Values of ξ

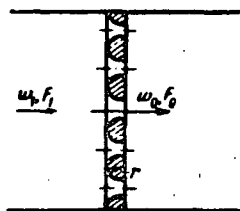
$\frac{t}{d_h}$	1	ξ															
		0.02	0.04	0.06	0.08	0.10	0.15	0.20	0.25	0.30	0.40	0.50	0.60	0.70	0.80	1.0	
0	1.35	7 000	1 670	730	400	245	96.0	51.5	30.0	18.2	8.25	4.00	2.00	0.97	0.42	0.13	0
0.2	1.22	6 600	1 600	687	374	230	94.0	48.0	28.0	17.4	7.70	3.75	1.87	0.91	0.40	0.13	0.01
0.4	1.10	6 310	1 530	660	356	221	89.0	46.0	26.5	16.6	7.40	3.60	1.80	0.88	0.39	0.13	0.01
0.6	0.84	5 700	1 380	590	322	199	81.0	42.0	24.0	15.0	6.60	3.20	1.60	0.80	0.36	0.13	0.01
0.8	0.42	4 680	1 130	486	264	164	66.0	34.0	19.6	12.2	5.50	2.70	1.34	0.66	0.31	0.12	0.02
1.0	0.24	4 260	1 030	443	240	149	60.0	31.0	17.8	11.1	5.00	2.40	1.20	0.61	0.29	0.11	0.02
1.4	0.10	3 930	950	408	221	137	55.6	28.4	16.4	10.3	4.60	2.25	1.15	0.58	0.28	0.11	0.03
2.0	0.02	3 770	910	391	212	134	53.0	27.4	15.8	9.90	4.40	2.20	1.13	0.58	0.28	0.12	0.04
3.0	0	3 765	913	392	214	132	53.5	27.5	15.9	10.0	4.50	2.24	1.17	0.61	0.31	0.15	0.06
4.0	0	3 775	930	400	215	132	53.8	27.7	16.2	10.0	4.60	2.25	1.20	0.64	0.35	0.16	0.08
5.0	0	3 850	936	400	220	133	55.5	28.5	16.5	10.5	4.75	2.40	1.28	0.69	0.37	0.19	0.10
6.0	0	3 870	940	400	222	133	55.8	28.5	16.6	10.5	4.80	2.42	1.32	0.70	0.40	0.21	0.12
7.0	0	4 000	950	405	230	135	55.9	29.0	17.0	10.9	5.00	2.50	1.38	0.74	0.43	0.23	0.14
8.0	0	4 000	965	410	236	137	56.0	30.0	17.2	11.1	5.10	2.58	1.45	0.80	0.45	0.25	0.16
9.0	0	4 080	985	420	240	140	57.0	30.0	17.4	11.4	5.30	2.62	1.50	0.82	0.50	0.28	0.18
10	0	4 110	1 000	430	245	146	59.7	31.0	18.2	11.5	5.40	2.80	1.57	0.89	0.53	0.32	0.20



Grid with rounded orifice edges. $Re = \frac{w_0 d_h}{v} > 3 \cdot 10^4$

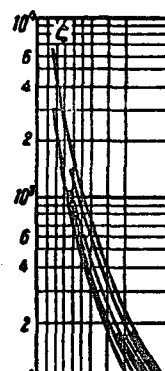
Section VIII

Diagram 8-5



$$d_h = \frac{4f_0}{\Pi_0}; \quad \Pi_0 - \text{perimeter};$$

$$\bar{f} = \frac{F_0}{F_1};$$

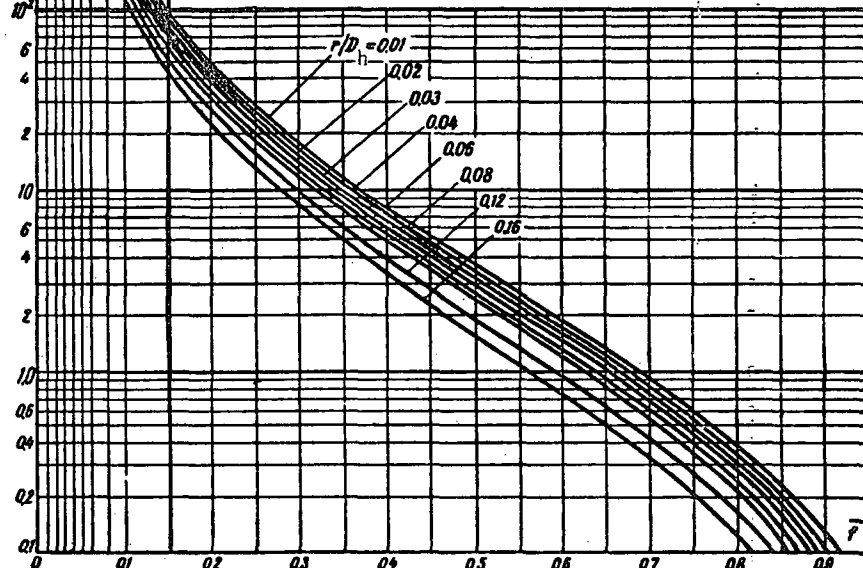


$$\xi = \frac{\Delta H}{\frac{\gamma w_1^2}{2g}} = [\sqrt{\zeta' (1 - \bar{f})} + (1 - \bar{f})]^2 \frac{1}{\bar{f}^2},$$

where ζ' is taken from the table, or more accurately from graph b of diagram 4-12.

The values of ζ are determined from the curves $\zeta = f(\bar{f})$ corresponding to different $\frac{r}{d_h}$ or from the table;

v is taken from § 1-3, b.



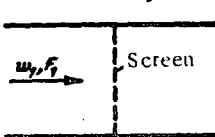
Values of

$\frac{r}{d_h}$	ζ'	\bar{f}																				
		0.02	0.04	0.06	0.08	0.10	0.15	0.20	0.25	0.30	0.35	0.40	0.45	0.50	0.55	0.60	0.65	0.70	0.75	0.80	1.0	
0.01	0.44	6620	1600	690	375	232	94.0	48.0	27.7	17.3	11.0	7.70	5.60	3.70	2.65	1.84	1.25	0.90	0.60	0.38	0.12	0
0.02	0.37	6200	1500	642	348	216	87.6	44.5	25.8	16.1	10.7	7.10	5.00	3.48	2.33	1.69	1.18	0.82	0.56	0.34	0.10	0
0.03	0.31	5850	1400	600	327	201	82.0	42.0	24.2	14.9	9.50	6.56	4.50	3.20	2.22	1.55	1.10	0.75	0.50	0.31	0.09	0
0.04	0.26	5510	1330	570	310	192	77.5	39.0	22.7	14.1	9.00	6.19	4.20	3.00	2.00	1.45	0.95	0.70	0.45	0.29	0.08	0
0.06	0.19	5000	1200	518	278	173	69.9	36.5	20.3	12.5	8.00	5.50	4.00	2.60	1.72	1.27	0.85	0.60	0.40	0.24	0.07	0
0.08	0.15	4550	1100	437	255	158	63.6	32.2	18.5	11.4	7.50	5.00	3.40	2.30	1.52	1.13	0.78	0.53	0.34	0.21	0.06	0
0.12	0.09	3860	928	398	26	133	53.5	27.0	15.6	9.30	6.50	4.16	3.00	1.90	1.24	0.89	0.60	0.40	0.27	0.16	0.04	0
0.16	0.03	3320	797	340	184	113	45.4	23.0	12.9	7.90	5.30	3.40	2.20	1.60	1.00	0.70	0.50	0.32	0.26	0.12	0.03	0

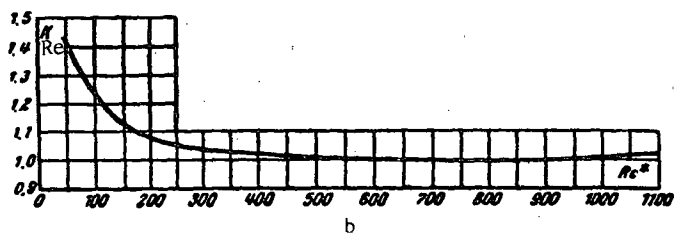
Screens

Section VIII Diagram 8-6

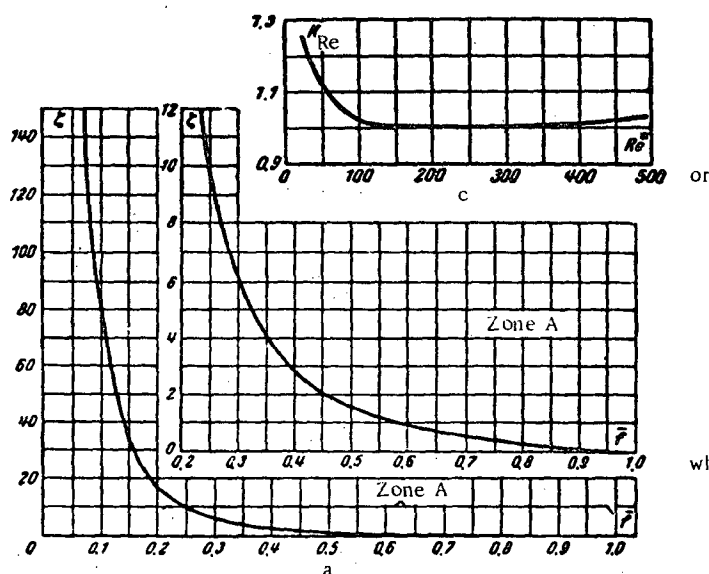
$$\bar{f} = \frac{F_0}{F_1}$$



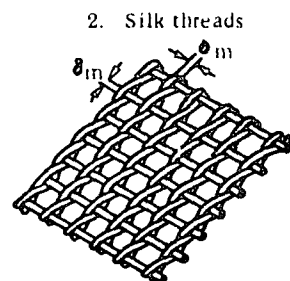
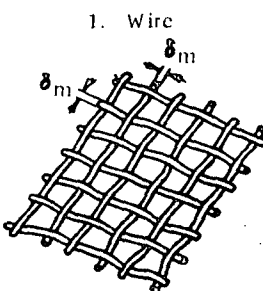
Re*	50	100	150	200	300	400	500	1 000	1 200
k_Re	1.44	1.24	1.13	1.08	1.03	1.01	1.01	1.00	1.02



Re*	40	80	120	300	350	400	500
k_Re	1.16	1.05	1.01	1.00	1.01	1.01	1.03



T	0.05	0.10	0.15	0.20	0.25	0.30	0.35	0.40	0.45	0.50	0.55	0.60	0.65	0.70	0.75	0.80	0.90	1.00
ζ	363	82.0	33.4	17.0	10.0	6.20	4.10	3.00	2.20	1.65	1.26	0.97	0.75	0.58	0.44	0.32	0.14	0.00



1. Circular metal wire.

$$a) Re^* = \frac{w_0 \delta_m}{v} \geq 400:$$

$$\zeta = \frac{\Delta H}{\frac{\tau w_1^2}{2g}} = 1.3(1 - \bar{f}) + \left(\frac{1}{\bar{f}} - 1\right)^2 \text{ is determined from graph a;}$$

graph a;
b) $Re^* < 400$:

$$\zeta_{Re} = \frac{\Delta H}{\frac{\tau w_1^2}{2g}} = k_{Re} \zeta,$$

where k_{Re} is determined from graph b;
 ζ is determined as for $Re > 400$.

In the case of z rows of successively installed screens

$$\zeta_s = \frac{\Delta H}{\frac{\tau w_1^2}{2g}} \approx \sum_1^z \zeta$$

$$\zeta_s \approx \sum_1^z \zeta_{Re}.$$

2. Silk threads

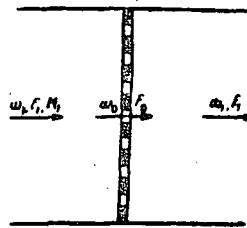
$$\zeta_s = \frac{\Delta H}{\frac{\tau w_1^2}{2g}} = 1.62 \zeta_w,$$

where ζ_w is determined as ζ for circular metal wires;
 k_{Re} is determined from graph c;
 v is taken from § 1-3, b.

Grids with sharp-edged inlet in the orifice of a wall of arbitrary thickness at high stream velocities (large Mach numbers)

Section VIII

Diagram 8-7



$$c_M = \frac{\Delta H}{T_1 w_1^2} = k_M c_s$$

where

ζ is determined as at $M_1 = 0$ from diagrams 8-1, 8-2, and 8-4;

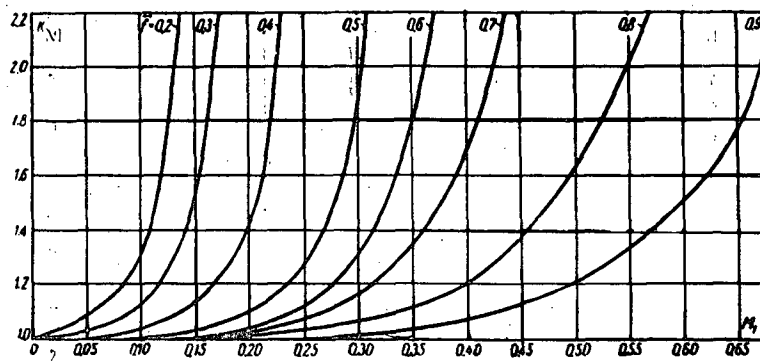
k_M is determined approximately from the curves
 $k_M = f(M_1)$ corresponding to different \bar{f} ;

$M_1 = \frac{w_1}{a}$ = Mach number in front of the grid;

a = sound velocity, m/sec.

Values of k_M

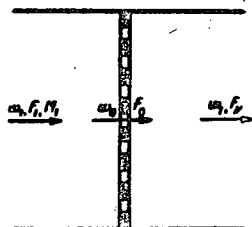
\bar{f}	M_1														
	0	0.05	0.10	0.15	0.20	0.25	0.30	0.35	0.40	0.45	0.50	0.55	0.60	0.65	
0.2	1.00	1.09	1.30	—	—	—	—	—	—	—	—	—	—	—	—
0.3	1.00	1.03	1.13	1.51	—	—	—	—	—	—	—	—	—	—	—
0.4	1.00	1.00	1.03	1.14	1.41	—	—	—	—	—	—	—	—	—	—
0.5	1.00	1.00	1.00	1.03	1.10	1.27	1.85	—	—	—	—	—	—	—	—
0.6	1.00	1.00	1.00	1.00	1.04	1.12	1.30	1.77	—	—	—	—	—	—	—
0.7	1.00	1.00	1.00	1.00	1.03	1.08	1.16	1.35	1.68	—	—	—	—	—	—
0.8	1.00	1.00	1.00	1.00	1.01	1.03	1.07	1.12	1.20	1.37	1.63	2.01	—	—	—
0.9	1.00	1.00	1.00	1.00	1.00	1.00	1.02	1.04	1.07	1.13	1.21	1.33	1.50	1.75	—



Grids with orifice edges beveled or rounded and screens at high stream velocities (large Mach numbers)

Section VIII

Diagram 8-8



$$\zeta_M = \frac{\Delta H}{\frac{1}{2} \rho u_1^2} = k'_M \zeta_0$$

where

ζ is determined as for $M_1 = 0$ from diagrams 8-3 or 8-6;

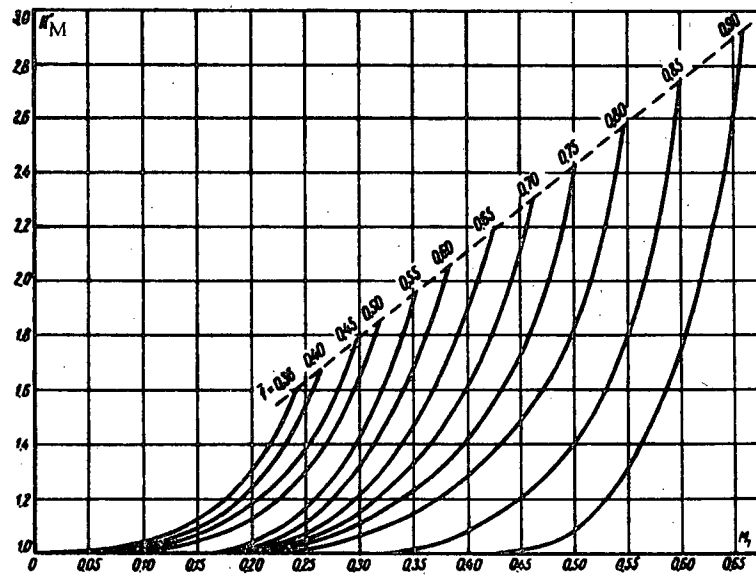
k'_M is determined from the curves $k'_M = f(M_1)$ corresponding to different \bar{f} (tentatively in the case of grids);

$$M_1 = \frac{w_1}{a} = \text{Mach number in front of the screen};$$

$a = \text{sound velocity, m/sec.}$

Values of k'_M

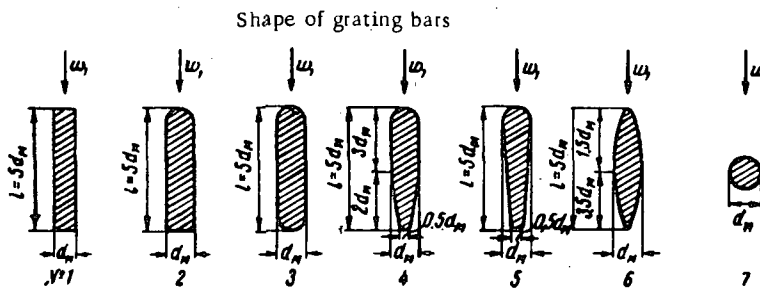
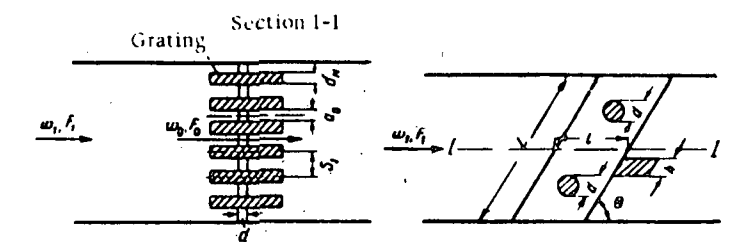
\bar{f}	M_1													
	0	0.05	0.10	0.15	0.20	0.25	0.30	0.35	0.40	0.45	0.50	0.55	0.60	0.65
0.35	1.00	1.01	1.04	1.12	1.30	—	—	—	—	—	—	—	—	—
0.40	1.00	1.00	1.02	1.10	1.25	1.55	—	—	—	—	—	—	—	—
0.45	1.00	1.00	1.01	1.07	1.19	1.40	1.82	—	—	—	—	—	—	—
0.50	1.00	1.00	1.00	1.04	1.13	1.30	1.64	—	—	—	—	—	—	—
0.55	1.00	1.00	1.00	1.00	1.04	1.17	1.42	1.93	—	—	—	—	—	—
0.60	1.00	1.00	1.00	1.00	1.02	1.11	1.32	1.68	—	—	—	—	—	—
0.65	1.00	1.00	1.00	1.00	1.01	1.07	1.22	1.47	1.90	—	—	—	—	—
0.70	1.00	1.00	1.00	1.00	1.00	1.05	1.16	1.33	1.60	2.12	—	—	—	—
0.75	1.00	1.00	1.00	1.00	1.00	1.03	1.12	1.23	1.42	1.73	2.40	—	—	—
0.80	1.00	1.00	1.00	1.00	1.00	1.01	1.06	1.15	1.28	1.49	1.81	—	—	—
0.85	1.00	1.00	1.00	1.00	1.00	1.00	1.00	1.01	1.08	1.20	1.40	1.80	2.71	—
0.90	1.00	1.00	1.00	1.00	1.00	1.00	1.00	1.00	1.00	1.01	1.08	1.32	1.75	2.65



Bar grating with an angle of approach $\alpha_0 = 0$. $Re = \frac{w_0 d_n}{\nu} > 10^4$

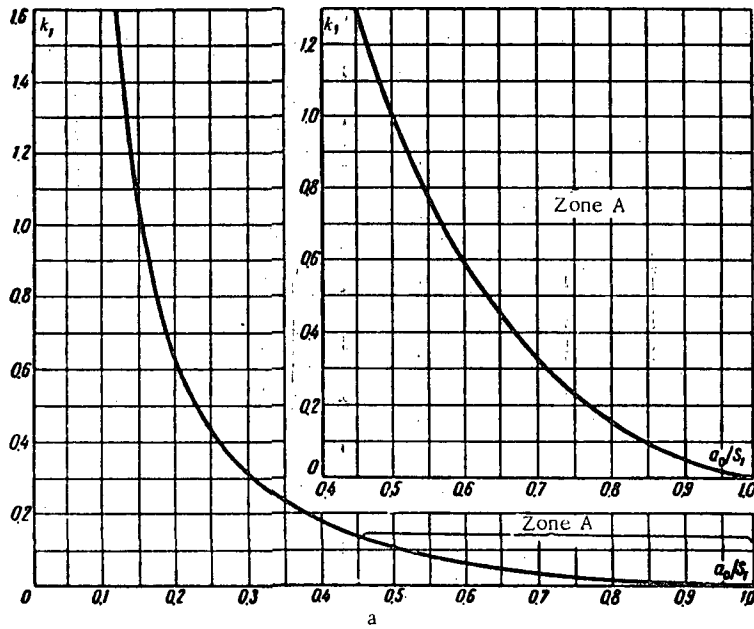
Section VIII

Diagram 8-9



$\frac{a_0}{S_1}$	0	0.1	0.2	0.3	0.4
k_1	∞	18.7	6.35	3.09	1.72

$\frac{a_0}{S_1}$	0.5	0.6	0.7	0.8	0.9	1.0
k_1	1.00	0.58	0.32	0.16	0.05	0



1. Clean grating of screen

$$a) \frac{l}{d_n} = 5 \text{ and } \frac{a_0}{S_1} > 0.5:$$

$$\zeta = \frac{\Delta H}{\gamma w_1^2} = \beta_1 k_1 \sin \theta,$$

where

β_1 is taken from Table 8-2;

$$k_1 = \left(\frac{S_1}{a_0} - 1 \right)^{4/3} \text{ is determined from the curve}$$

$$k_1 = f \left(\frac{a_0}{S_1} \right).$$

$$b) \text{ any } \frac{l}{d_n} \text{ and any } \frac{a_0}{S_1}:$$

$$\zeta = \frac{\Delta H}{\gamma w_1^2} = \beta_1 \zeta' \sin \theta,$$

β_1 is taken from Table 8-2;
 ζ' is determined from diagram
 8-4 as ζ for a thickened grid.

TABLE 8-2

Type of bar	1	2	3	4	5	6	7
β_1	2.34	1.77	1.77	1.00	0.87	0.71	1.73
β_2	1.0	0.76	0.76	0.43	0.37	0.30	0.74

2. Clogged grating

$$\zeta_c = c' \zeta,$$

where $c' = 1.1$ to 1.3 in the case of mechanical cleaning of the grating;

$c' = 1.5$ to 2.0 in the case of manual cleaning of the grating.

3. Grating with additional frame

$$\zeta_{cf} = c'' \zeta_c$$

$$\text{where } c'' = \frac{1}{(1 - \frac{A}{L})^2}$$

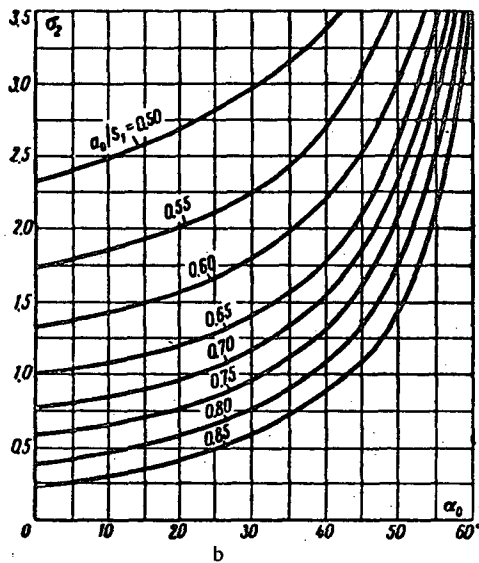
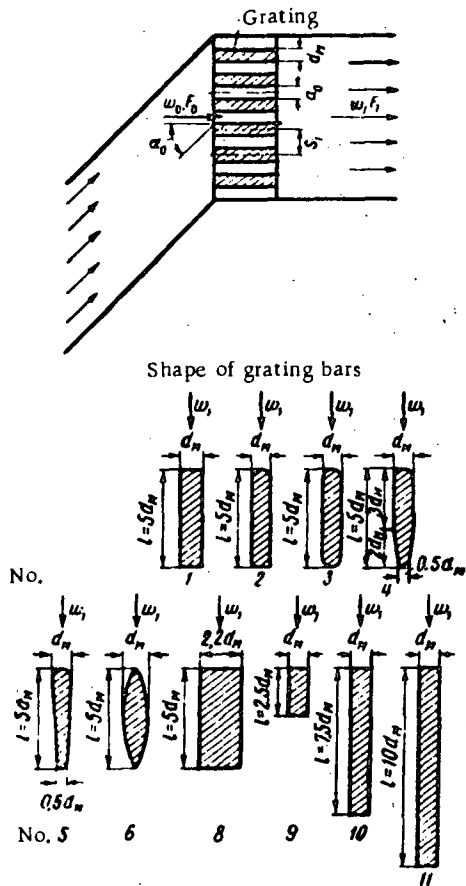
$A = h z_1 + d z_2$ = total height of the transverse elements; z_1 = number of intermediate support bars; z_2 = number of bracing elements; L = internal height of the grating; ν is taken from § 1-3, b.

Bar grating with an angle of approach $\alpha_0 > 0$ and $\frac{a_0}{S_1} \geq 0.5$.

$$Re = \frac{w_0 a_0}{v} > 10^4$$

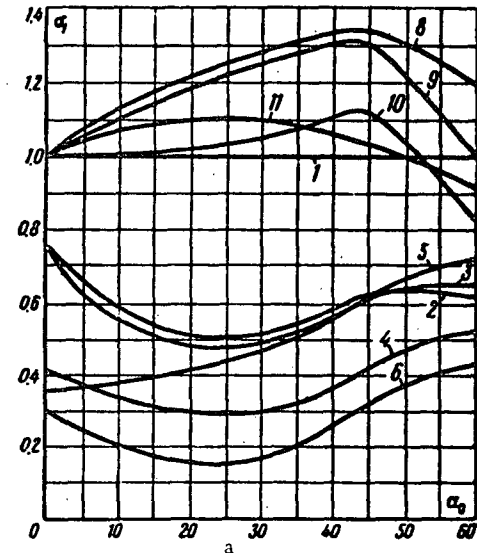
Section VIII

Diagram 8-10



$$\zeta = \frac{\Delta H}{Tw_1^2} = \alpha_1 \alpha_2, \quad \text{where } \alpha_1 \text{ is determined from graph a;} \\ \alpha_2 \text{ is determined from graph b;} \\ v \text{ is taken from § 1-3, b}$$

No.	Values of α_1									
	0	5	10	15	20	25	30	40	50	60
1	1.00	1.00	1.00	1.00	1.00	1.00	1.00	1.00	1.00	1.00
2	0.76	0.65	0.58	0.54	0.52	0.51	0.52	0.58	0.63	0.62
3	0.76	0.60	0.55	0.51	0.49	0.48	0.49	0.57	0.64	0.66
4	0.43	0.37	0.34	0.32	0.30	0.29	0.30	0.36	0.47	0.52
5	0.37	0.37	0.38	0.40	0.42	0.44	0.47	0.56	0.67	0.72
6	0.30	0.24	0.20	0.17	0.16	0.15	0.16	0.25	0.37	0.43
8	1.00	1.08	1.13	1.18	1.22	1.25	1.28	1.33	1.31	1.20
9	1.00	1.06	1.10	1.15	1.18	1.22	1.25	1.30	1.22	1.00
10	1.00	1.00	1.00	1.01	1.02	1.03	1.05	1.10	1.04	0.82
11	1.00	1.04	1.07	1.09	1.10	1.11	1.10	1.07	1.00	0.92



$\frac{a_0}{S_1}$	Values of α_2									
	0	5	10	15	20	25	30	40	50	60
0.50	2.34	2.40	2.48	2.57	2.68	2.80	2.95	3.65	4.00	4.70
0.55	1.75	1.80	1.85	1.90	2.00	2.10	2.25	2.68	3.55	4.50
0.60	1.35	1.38	1.42	1.48	1.55	1.65	1.79	2.19	3.00	4.35
0.65	1.00	1.05	1.08	1.12	1.20	1.30	1.40	1.77	2.56	4.25
0.70	0.78	0.80	0.85	0.89	0.95	1.05	1.17	1.52	2.30	4.10
0.75	0.60	0.62	0.65	0.70	0.75	0.85	0.95	1.30	2.05	3.90
0.80	0.37	0.40	0.45	0.50	0.55	0.64	0.75	1.06	1.75	3.70
0.85	0.24	0.25	0.30	0.36	0.42	0.50	0.60	0.88	1.40	3.50

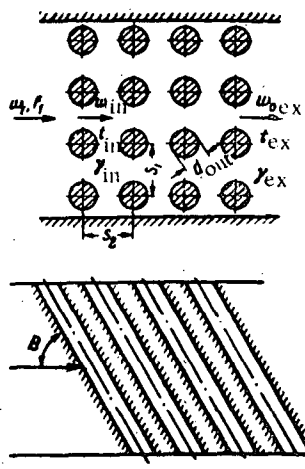
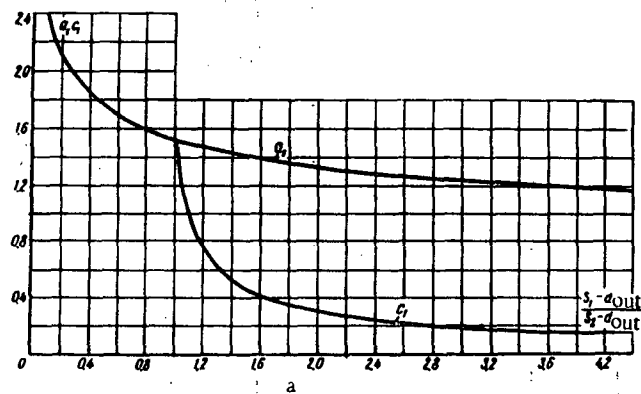


TABLE 8-3

θ°	30	45	60	90
ψ	0.30	0.54	0.82	1.0



$$\zeta = \frac{\Delta H}{\frac{1_m w_0^2 m}{2g}} = \psi A Re^m z + \Delta \zeta_f,$$

$$1) \text{ at } \frac{S_1}{d_{out}} < \frac{S_2}{d_{out}}:$$

$$A = a_1 b_1;$$

$a_1 = 1.52 \left(\frac{S_1 - d_{out}}{S_2 - d_{out}} \right)^{-0.2}$ is determined from the curve

$$a_1 = f \left(\frac{S_1 - d_{out}}{S_2 - d_{out}} \right) \text{ of graph a;}$$

$$b_1 = \left(\frac{S_1}{d_{out}} - 1 \right)^{-0.5} \text{ is determined from the curve}$$

$$b_1 = f \left(\frac{S_1}{d_{out}} \right) \text{ of graph b;}$$

$$m = -0.2;$$

Re^m is determined from the curve $Re^m = f(Re)$ at $\frac{S_1 - d_{out}}{S_2 - d_{out}} = 1.0$ on graph c;

$$2) \text{ at } \frac{S_1}{d_{out}} > \frac{S_2}{d_{out}}$$

$$A = c_1 b_1;$$

$$c_1 = 0.32 \left(\frac{S_1 - d_{out}}{S_2 - d_{out}} - 0.9 \right)^{-0.68} \text{ is determined}$$

from the curve $c_1 = f \left(\frac{S_1 - d_{out}}{S_2 - d_{out}} \right)$ on graph a;

$$m = - \frac{0.2}{\left(\frac{S_1 - d_{out}}{S_2 - d_{out}} \right)^2};$$

Re^m is determined from the curves $Re^m = f(Re)$ for different $\frac{S_1 - d_{out}}{S_2 - d_{out}}$ on graph c;

ψ is taken from Table 8-3 as a function of θ :

$\frac{S_1 - d_{out}}{S_2 - d_{out}}$	0.1	0.2	0.4	0.6	0.8	1.0	1.2	1.6	2.0	2.4	2.8	3.2	3.6	4.0	4.2
a_1	2.40	2.10	1.82	1.70	1.58	1.52	1.46	1.38	1.32	1.28	1.23	1.20	1.18	1.15	1.14
c_1	—	—	—	—	—	1.53	0.72	0.41	0.30	0.24	0.21	0.17	0.15	0.14	0.14

Bundle of ribbed tubes (air heater)

Section VIII

Diagram 8-13

Bundle characteristic

$$\text{Resistance coefficient } \zeta = \frac{\Delta H}{\tau_m w_0^2 \rho_0 g}$$

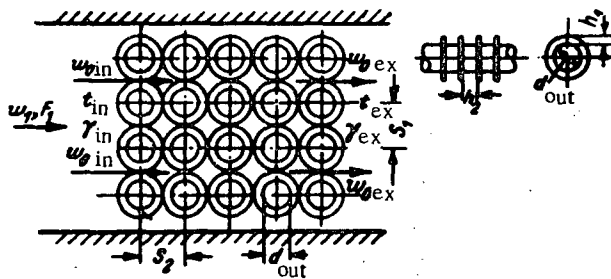
Vertical columns of cast-iron tubes with circular ribs

$$\frac{h_1}{d_{out}} = 0.2 \text{ to } 0.5;$$

$$\frac{h_2}{d_{out}} = 0.2 \text{ to } 0.3;$$

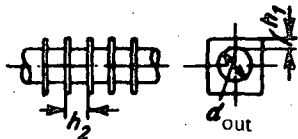
$$\frac{S_1}{d_{out}} = \frac{S_2}{d_{out}} = 2 \text{ to } 4;$$

$$z = 4 \text{ to } 6$$



The same with square ribs and $\frac{h_2}{d_{out}} = 0.33$

$$\zeta = \left(1.80 + 2.75 \frac{h_1}{d_{out}} \right) \frac{1}{S_1} (z - 1) Re^{-0.12} + \Delta \zeta_r$$



$$\Delta \zeta_r = 2 \frac{t_{ex} - t_{in}}{273 + t_m}; t_m = \frac{t_{in} + t_{ex}}{2}; \tau_m = \frac{\gamma_0}{1 + \frac{t_m}{273}}; w_0 m = w_0 \ln \frac{273 + t_m}{273 + t_{in}};$$

z = number of transverse rows of tubes in the bundle;

ν is taken from § 1-3, b as a function of t_m

For fouled bundles $\zeta_f \approx 1.2 - 1.3 \zeta_r$

Bundles of tubes of different cross-section shapes

Section VIII

Diagram 8-14

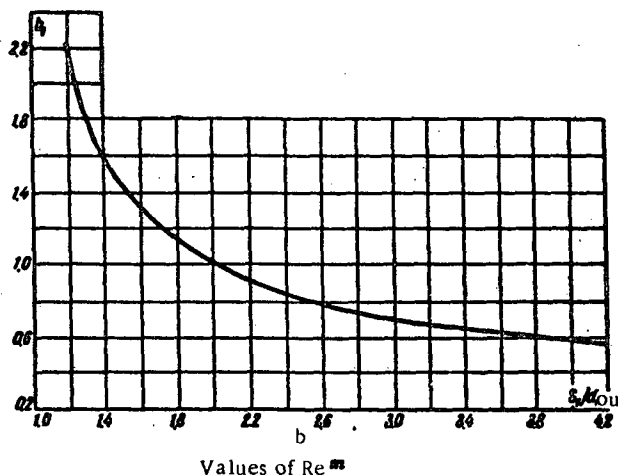
Bundle characteristic	Scheme	Resistance coefficient $\zeta = \frac{\Delta H}{\frac{1}{2} \rho_0 u_m^2}$
Staggered finned tubes		<p>ζ is taken from diagram 8-12. If the fins reduce the gap between the tubes, $w_0 m$ is replaced by</p> $w'_0 m = w_0 m \frac{S_1 - d_{out}}{S_1 - d_{out} - \delta'}$
Oval tubes in vertical columns		$10^4 < Re = \frac{w_0 m d_{out}}{v} < 3 \cdot 10^4;$ $\zeta = 0.059z + 0.31 + \Delta\zeta_y$
Staggered oval tubes		$10^4 < Re = \frac{w_0 m d_{out}}{v} < 3 \cdot 10^4;$ $\zeta = 0.20z + 0.14 + \Delta\zeta_y$
Drop-shaped tubes		$10^4 < Re = \frac{w_0 m d_{out}}{v} < 3 \cdot 10^4;$ $\zeta = 0.12z - 0.016 + \Delta\zeta_y$ <p>v is taken from § 1-3, b.</p>

Bundle of circular tubes in vertical columns, $3 \cdot 10^3 < Re_m = \frac{w_m d_{out}}{\nu} < 10^5$
 (continued)

Section VIII

Diagram 8-11

S_t/d_{out}	1.2	1.4	1.6	1.8	2.2	2.6	3.0	3.4	3.8	4.2
b_1	2.24	1.58	1.30	1.12	0.91	0.78	0.71	0.65	0.60	0.56



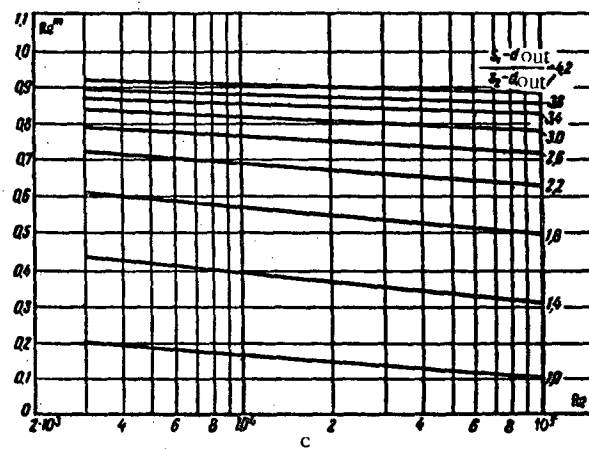
S_t/d_{out}	Re								
	$3 \cdot 10^3$	$4 \cdot 10^3$	$6 \cdot 10^3$	$8 \cdot 10^3$	10^4	$2 \cdot 10^4$	$4 \cdot 10^4$	$6 \cdot 10^4$	$9 \cdot 10^4$
1.0	0.20	0.19	0.18	0.17	0.16	0.14	0.12	0.11	0.10
1.4	0.44	0.43	0.41	0.40	0.39	0.36	0.34	0.32	0.31
1.8	0.61	0.60	0.59	0.57	0.56	0.54	0.52	0.51	0.50
2.2	0.72	0.71	0.70	0.69	0.68	0.66	0.65	0.64	0.63
2.6	0.79	0.78	0.78	0.77	0.76	0.75	0.73	0.72	0.71
3.0	0.84	0.83	0.83	0.82	0.81	0.80	0.80	0.79	0.78
3.4	0.87	0.87	0.86	0.86	0.85	0.84	0.83	0.83	0.82
3.8	0.90	0.89	0.89	0.88	0.88	0.87	0.87	0.86	0.86
4.2	0.92	0.91	0.91	0.90	0.90	0.89	0.89	0.88	0.88

$$\Delta t_f = 2 \frac{t_{ex} - t_{in}}{273 + t_{in}}; \quad t_m = \frac{t_{in} + t_{ex}}{2};$$

$$t_{in} = \frac{T_0}{1 + \frac{T_0}{273}}; \quad w_{0,in} = w_{0,in} \frac{273 + t_{in}}{273 + T_0};$$

z = number of transverse rows of tubes in the bundle;

ν = taken from § 1-3, b as a function of t_m .
 For fouled bundles $\xi_f \approx 1.35$



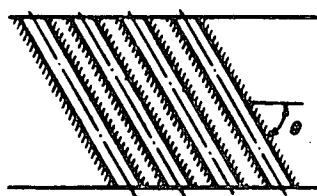
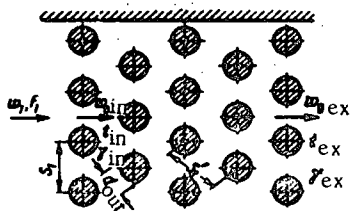
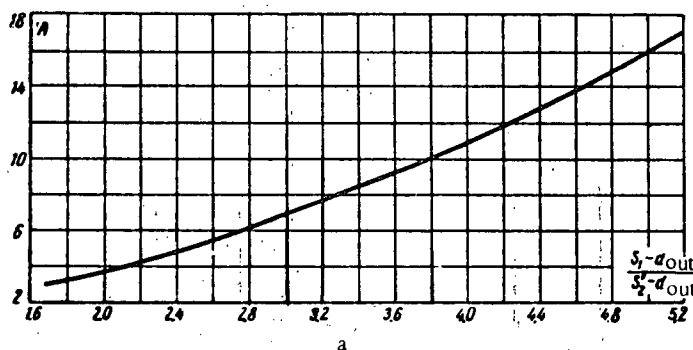


TABLE 8-4

θ°	30	45	60	90
ψ	0.34	0.57	0.80	1.0

Re_m	$3 \cdot 10^3$	$4 \cdot 10^3$	$6 \cdot 10^3$	$8 \cdot 10^3$	10^4	$2 \cdot 10^4$	$4 \cdot 10^4$	$6 \cdot 10^4$	$8 \cdot 10^4$	10^5
$Re_m^{-0.27}$	0.117	0.106	0.095	0.089	0.088	0.069	0.057	0.051	0.047	0.045



$S_1 - d_{out}$	1.7	1.8	2.0	2.4	2.8	3.2	3.6	4.0	4.4	4.8	5.2
A	3.20	3.43	3.96	5.06	6.34	7.70	9.32	11.0	12.8	14.7	16.9

$$\zeta = \frac{\Delta H}{\tau_m w_0^2} = \frac{4A Re_m^{-0.27}(z+1) + \Delta \zeta_f}{2g}$$

1) at $\frac{S_1}{d_{out}} < 2.0$ and $0.14 < \frac{S_1 - d_{out}}{S_2 - d_{out}} < 1.7$:

$$A = \left(4.6 - 2.7 \frac{S_1 - d_{out}}{S_2 - d_{out}} \right) \left(2 - \frac{S_1}{d_{out}} \right) + 3.2;$$

2) at $\frac{S_1}{d_{out}} \geq 2.0$ and $0.14 < \frac{S_1 - d_{out}}{S_2 - d_{out}} < 1.7$:

$$A = 3.2;$$

3) at $\frac{S_1}{d_{out}} \geq 1.0$ and $1.7 < \frac{S_1 - d_{out}}{S_2 - d_{out}} \leq 5.2$:

$A = 0.44 \left(\frac{S_1 - d_{out}}{S_2 - d_{out}} + 1 \right)^2$ is determined from the curve

$$A = f \left(\frac{S_1 - d_{out}}{S_2 - d_{out}} \right)$$
 on graph a;

$Re_m^{-0.27}$ is determined from the curve $Re_m^{-0.27} = f(Re)$

on graph b.

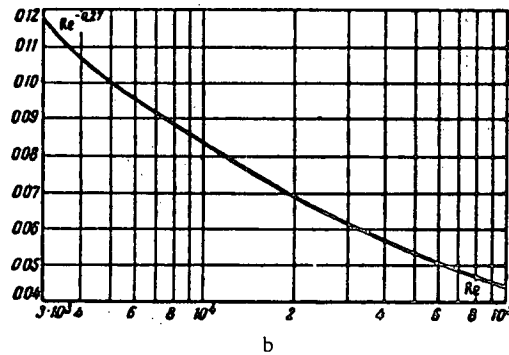
ϕ is taken from Table 8-4 as a function of θ

$$\Delta \zeta_f = 2 \frac{t_{ex} - t_{in}}{273 + t_m}; \quad t_m = \frac{t_{in} + t_{ex}}{2};$$

$$t_m = \frac{T_0}{1 + \frac{t_m}{273}}; \quad w_0 m = w_0 \text{ in } \frac{273 + t_m}{273 + t_{in}};$$

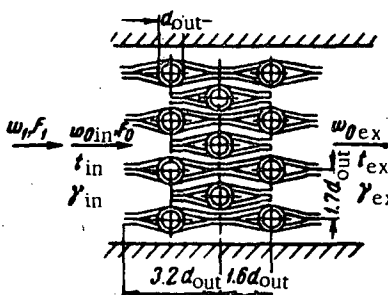
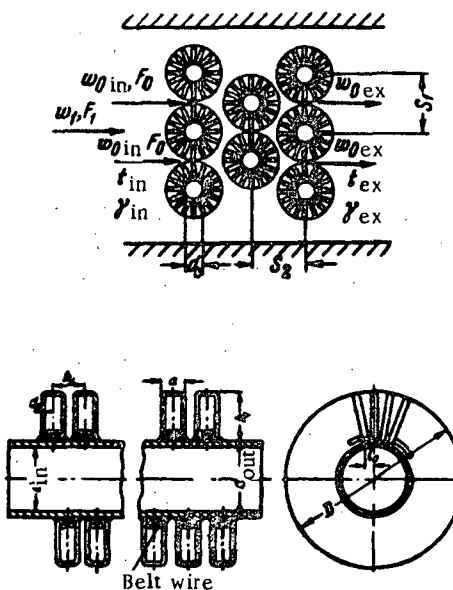
z = number of transverse rows of tubes in the bundle;
 ψ is taken from § 1-3, b as a function of t_m
 For fouled bundles

$$\zeta_f \approx 1.3 \zeta$$



Bundles of tubes of different cross-section shapes (continued)

 Section VIII
 Diagram 8-14

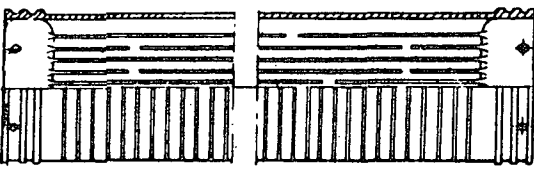
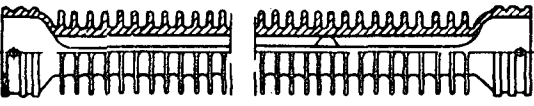
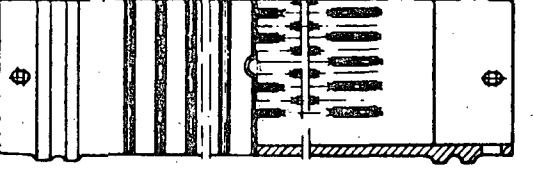
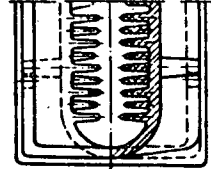
Bundle characteristic	Scheme	Resistance coefficient $\xi = \frac{\Delta H}{T_m^2 \cdot \frac{d}{6} m}$
Staggered "Elesko"-type tubes		$10^4 < Re = \frac{w_0 m d_{out}}{v} < 4 \cdot 10^6;$ $\xi = 0.46z + \Delta\xi_f$
Tubes with wire ribbing $S_1 = 2.1 \text{ to } 3.0; \frac{d_{out}}{d_{out}}$ $\frac{S_2}{d_{out}} = 1.5 \text{ to } 2.5; \frac{l_0}{h_2}$ $\frac{l_0}{h_2} = 0.1 \text{ to } 0.3; \frac{h_1}{h_2} = 0.8 \text{ to } 2.5; \frac{d_{out}}{h_2} = 1.4 \text{ to } 2.2$	 <p> $d_0 = 0.5 \text{ to } 0.7 \text{ mm}; a = 4 \text{ to } 5 \text{ mm}; h_2 = 7 \text{ to } 9 \text{ mm}$ </p>	<p>a) $Re = \frac{w_0 m h_2}{v} = 650 \text{ to } 6000:$</p> $\xi = 3.2zRe^{-0.24} \left(\frac{l_0}{h_2}\right)^{-0.365} \left(\frac{h_1}{h_2}\right)^{0.15} \left(\frac{d_{out}}{h_2}\right)^{0.1}$ <p>b) $Re > 6000:$</p> $\xi = 0.28z \left(\frac{l_0}{h_2}\right)^{-0.365} \left(\frac{h_1}{h_2}\right)^{0.15} \left(\frac{d_{out}}{h_2}\right)^{0.1}$

$$\Delta t_f = 2 \frac{t_{ex} - t_{in}}{273 + t_m}; \quad t_m = \frac{t_{in} + t_{ex}}{2}; \quad T_m = \frac{T_0}{1 + \frac{t_m}{273}}; \quad w_0 m = w_0 \ln \frac{273 + t_m}{273 + t_{in}};$$

z = number of transverse rows in the bundle; v is taken from § 1-3, b as a function of t_m .
 For fouled bundles $\xi_f \cong 1.2 \text{ to } 1.3 \xi$.

Recuperators (air heaters)

 Section VIII
 Diagram 8-15

Characteristic	Resistance coefficient $\zeta = \frac{\Delta H}{T_m w_0^2 g}$
Ribbed cast-iron air heaters (recuperators) ($d_h = 0.0425$ m)   	<ol style="list-style-type: none"> As measured inside the pipes (air flow): $\zeta = 1.06 + 0.040 \frac{l_o}{d_h} + \Delta \zeta_i$ As measured outside the pipes (gas flow): a) $Re = \frac{w_0 m d_h}{\nu} < 10^4$ $\zeta = (1.2 + 1.16z) Re^{-0.12} + \Delta \zeta_g$ b) $Re \geq 10^4$ $\zeta = 0.4 + 0.334z + \Delta \zeta_g$
Ribbed-toothed air heaters (recuperators)   	<ol style="list-style-type: none"> As measured inside the pipes (air flow): a) $Re = \frac{w_0 m d_h}{\nu} < 10^4$ $\zeta = 1.06 + 0.77 \frac{l_o}{d_h} Re^{0.22} + \Delta \zeta_i$ b) $Re \geq 10^4$ $\zeta = 1.06 + 0.10 \frac{l_o}{d_h} + \Delta \zeta_i$ As measured outside the pipes (gas flow): a) $Re < 10^4$ $\zeta = (1.2 + 1.16z) Re^{-0.12} + \Delta \zeta_g$ b) $Re \geq 10^4$ $\zeta = 0.4 + 0.334z + \Delta \zeta_g$

$$\Delta \zeta_i = 2 \frac{t_{ex} - t_{in}}{273 + t_m}; \quad t_m = \frac{t_{in} + t_{ex}}{2}; \quad T_m = \frac{T_0}{1 + \frac{t_m}{273}}; \quad w_0 m = w_0 \ln \frac{273 + t_m}{273 + t_{in}}$$

z = number of transverse rows of the recuperators;

ν is taken from § 1-3, b as a function of t_m

For fouled pipes $\zeta_f = 1.2 \text{ to } 1.3 \zeta_i$.

Packing material deposited at random (loose layers from bodies of irregular shape) at given d_h ; dry and wetted (continued)

Section VIII

Diagram 8-16

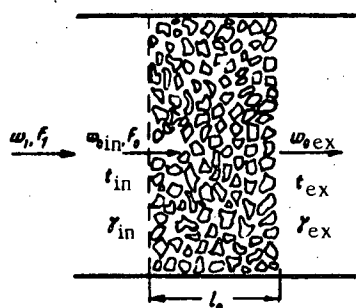


TABLE 8-5

A	$\frac{m^3}{m^2 \cdot hr}$	w_{lim}	$\frac{m}{sec}$
0		∞	
5		0.8	
10		0.7	
25		0.6	
50		0.5	

TABLE 8-6

Type of material	d_h , m	$\frac{s'}{m^3/m^3}$	$\frac{\bar{s}}{m^2/m^3}$
Andesite lumps 43.2 mm	0.0333	0.565	68
Circular gravel 42 mm	0.0193	0.388	80
Catalyst for ammonia synthesis 6.1 mm	0.00194	0.465	960
Catalyst for CO conversion, made in 11.5×6 mm tablets	0.0033	0.380	460
Vanadium sulfuric-acid catalyst, made in 11×6.5 mm tablets	0.00415	0.430	415
Iron rings 35×35×2.5 mm	0.0372	0.830	147
" " 50×50×5 mm	0.036	0.970	104
Ceramic rings 15×15×2 mm	0.0085	0.700	330
" " 25×25×3 mm	0.0145	0.740	204
" " 34×35×4 mm	0.0225	0.780	140
" " 50×50×5 mm	0.0360	0.785	88
Porcelain rings 8×8×1.5 mm	0.0045	0.640	570
Ceramic saddle-shaped elements 12.5 mm	—	0.710-0.760	—
The same 25 mm	—	0.710	—

1. Dry packing

$$\zeta = \frac{\Delta H}{\gamma_m w_{lim}^2} = \lambda \frac{l_0}{d_h} \frac{1}{\epsilon'^2} + \Delta \zeta_f = \zeta_{dr} + \Delta \zeta_f$$

$$a) Re \frac{w_{lim} d_h}{v} \frac{1}{\epsilon'} < 3:$$

$\lambda = \frac{180}{Re_h}$ is determined from the curve $\lambda = f(Re)$;

b) $3 < Re < 1000$:

$$\lambda = \frac{164}{Re_h} + \frac{7.68}{Re_h^{0.11}} \text{ is determined from } \lambda = f(Re).$$

2. Wetted packing (tentatively)

At $A = 50$; $w_1 \leq w_{lim}$; $5 < d_h < 30$ to 35 mm)

$$\zeta = \frac{\Delta H}{\gamma_m w_{lim}^2} \approx \zeta_{dr} (1 + 0.06A) + \Delta \zeta_f$$

A = intensity of wetting by liquid, $m^2 \cdot hr$;

w_{lim} is taken from Table 8-5;

d_h and ϵ' are taken from Table 8-6.

$$\Delta \zeta_f = 2 \frac{t_{ex} - t_{in}}{273 + t_{in}} ;$$

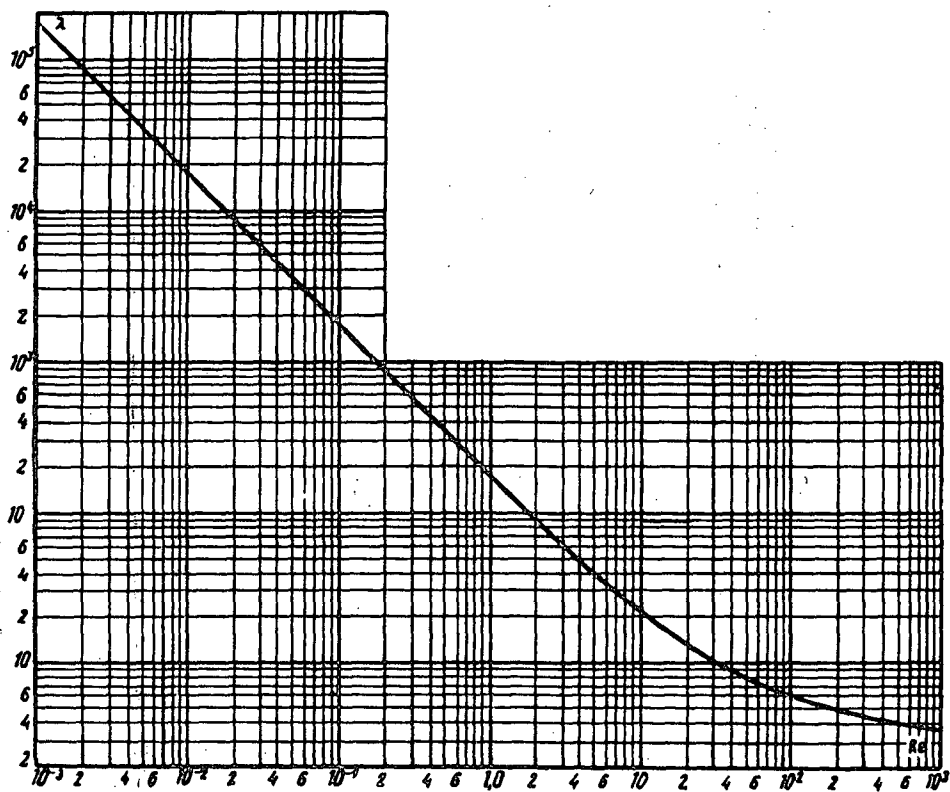
γ_m , t_m , w_{lim} and v cf. diagram 8-15.

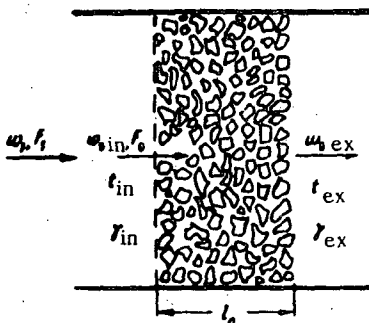
Packing material deposited at random (loose layers from bodies of irregular shape) at given d_{lb} ; dry and wetted (continued)

Section VIII

Diagram 8-16

Re	$1 \cdot 10^{-3}$	$5 \cdot 10^{-3}$	$1 \cdot 10^{-2}$	$5 \cdot 10^{-2}$	$1 \cdot 10^{-1}$	$5 \cdot 10^{-1}$	1	2	3
λ	180,000	36,000	18,000	3,600	1,800	360	180	90	61.5
Re	4	5	6	7	8	9	10	15	20
λ	47.9	39.7	33.7	29.6	26.5	24.3	22.4	16.8	13.7
Re	40	45	50	60	70	80	90	100	150
λ	9.24	8.70	8.30	7.62	7.16	6.80	6.52	6.27	5.62
Re	200	250	300	350					
λ	4.84	4.65	4.49						
Re	400	450	500	600	700	800	900	1,000	
λ	4.37	4.29	4.21	4.07	3.97	3.96	3.81	3.74	





$$\zeta = \frac{\Delta H}{l_m w_{in}^2 m} = \lambda' \frac{l_0}{d_{gr}} + \Delta \zeta_t = \zeta_{dr} + \Delta \zeta_t$$

where $\lambda' = \frac{75}{Re} + \frac{15}{\sqrt{Re}} + 1$ is determined from the curve

$\lambda' = f(Re)$ of graph a;

$k = \frac{1.53}{\epsilon^{4.2}}$ is determined from the curve $k = f(\epsilon')$ of graph b;

$$Re = \frac{0.45}{(1-\epsilon') \sqrt{\epsilon'}} \frac{w_{in} d_{gr}}{v}$$

d_{gr} = mean diameter of body (grain), m;

ϵ' = porosity (free-volume fraction), m^3/m^3 (taken from Table 8-7);

v is taken from § 1-3, b as a function of t_m .

$$\Delta \zeta_t = 2 \frac{t_{ex} - t_{in}}{273 + t_m}; t_m = \frac{t_{in} + t_{ex}}{2}$$

$$t_m = \frac{t_0}{1 + \frac{t_m}{273}}; w_{in} = w_i \frac{273 + t_m}{273 + t_{in}}$$

TABLE 8-7

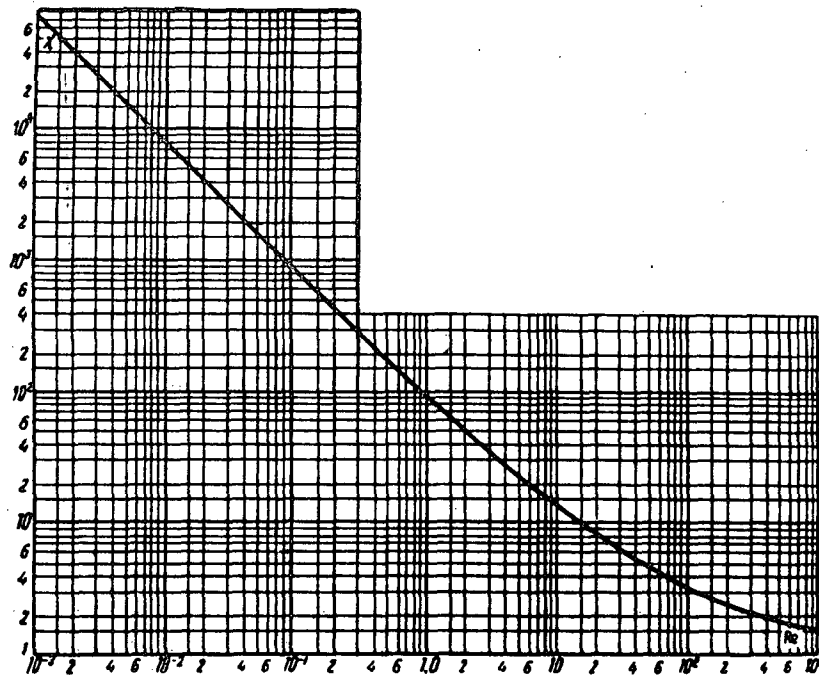
Type of material	d_{gr} mm	ϵ' , m^3/m^3
Anthracite	1-2	0.485
"	3-5	0.466
"	5-7	0.466
"	7-12	0.457
"	12-18	0.465
"	18-25	0.475
Agglomerate	10-20	0.480
"	20-30	0.488
" from rotating furnace	30-50	0.490
Alumina	1-3	0.500
"	3-5	0.500
"	9-10	0.520
Soil	0.517	0.355
"	0.600	0.343
"	0.715	0.352
"	0.800	0.378
"	0.915	0.394
"	1.10	0.401
"	1.22	0.397
"	1.45	0.400
"	1.81	0.395
Coke	10-30	0.435
"	20-50	0.457
"	30-50	0.477
"	68	0.513
Long-flame (gas) coal	5-7	0.466
" "	5-7	0.500
" "	7-12	0.466
" "	12-8	0.466
Silica gel KSM	3-5	0.490
Shale	7-12	0.575
"	18-25	0.575
Hard coal	4-6	0.488
" "	5-7	0.442
" "	7-12	0.447
" "	12-18	0.460

Packing material deposited at random (loose layers from bodies of irregular shape) at given d_{gr} (continued)

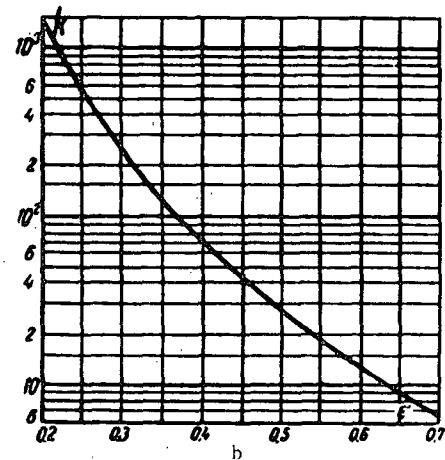
Section VIII

Diagram 8-17

Re	$1 \cdot 10^{-3}$	$5 \cdot 10^{-3}$	$1 \cdot 10^{-2}$	$1 \cdot 10^{-1}$	$1 \cdot 10^{-1}$	$5 \cdot 10^{-1}$	1	2	3	4	5
λ'	75,424	15,212	7,607	1,567	793.5	172.5	91.0	49.2	34.6	26.2	22.7
Re	6	7	8	9	10	2·10	3·10	4·10	5·10	6·10	7·10
λ'	19.6	17.4	15.7	14.3	13.2	8.10	6.22	5.25	4.62	4.20	3.85
Re	$8 \cdot 10$	$9 \cdot 10$	10^2	$2 \cdot 10^2$	$3 \cdot 10^2$	$4 \cdot 10^2$	$5 \cdot 10^2$	$6 \cdot 10^2$	$7 \cdot 10^2$	$9 \cdot 10^2$	10^3
λ'	3.70	3.40	3.25	2.44	2.11	1.94	1.82	1.74	1.68	1.59	1.55



a



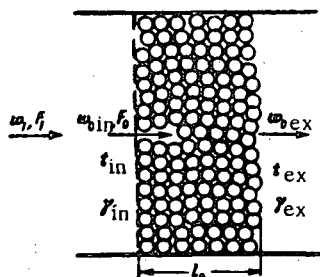
b

ϵ'	0.20	0.25	0.30	0.35	0.40
k	1330	520	238	128	69.8
ϵ'	0.45	0.50	0.55	0.60	0.65
k	44.3	27.8	18.8	13.1	9.45
ϵ'	0.70				6.83

Packing — loose layer of spherical (granular) bodies or porous cemented layer from granular material (constant diameter)

Section VIII

Diagram 8-18



$$\zeta = \frac{\Delta H}{\gamma_m w_{in}^2 l_m} = k \lambda' \frac{l_0}{d_{gr}} + \Delta \zeta_p$$

where $\lambda' = \frac{30}{Re} + \frac{3}{Re^{0.7}} + 0.3$ is determined from the curve

$\lambda' = f(Re)$ of graph a;

$k = \frac{1.53}{\epsilon'^{4.2}}$ is determined from the curve $k = f(\epsilon')$ of graph b;

$$Re = \frac{0.45}{(1 - \epsilon') \sqrt{\epsilon'}} \frac{w_{in} d_{gr}}{v};$$

d_{gr} = diameter of body (grain), m;

ϵ' = porosity (free-volume fraction), m^3/m^3 ;

$$\epsilon' = 1 - \frac{\pi}{6(1 - \cos \theta) \sqrt{1 + 2 \cos \theta}}$$

is determined from Table 8-8.

$$\Delta \zeta_p = 2 \frac{t_{ex} - t_{in}}{273 + t_m};$$

$$t_m = \frac{t_{in} + t_{ex}}{2}; \quad T_m = \frac{T_0}{1 + \frac{t_m}{273}};$$

$$w_{in} = w_{in} \frac{273 + t_m}{273 + t_{in}};$$

v is taken from § 1-3,b as a function of t_m .

TABLE 8-8

ϵ'	60	64	68	72	76	80	84	90
0.260	0.320	0.365	0.405	0.435	0.455	0.470	0.476	

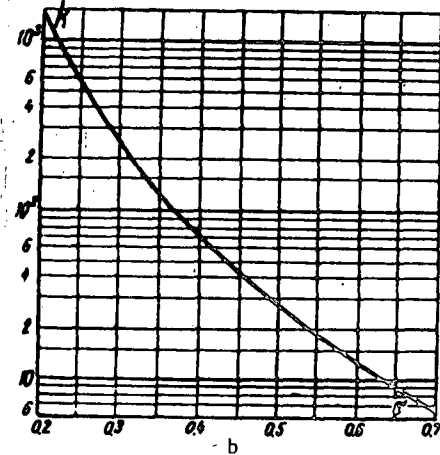
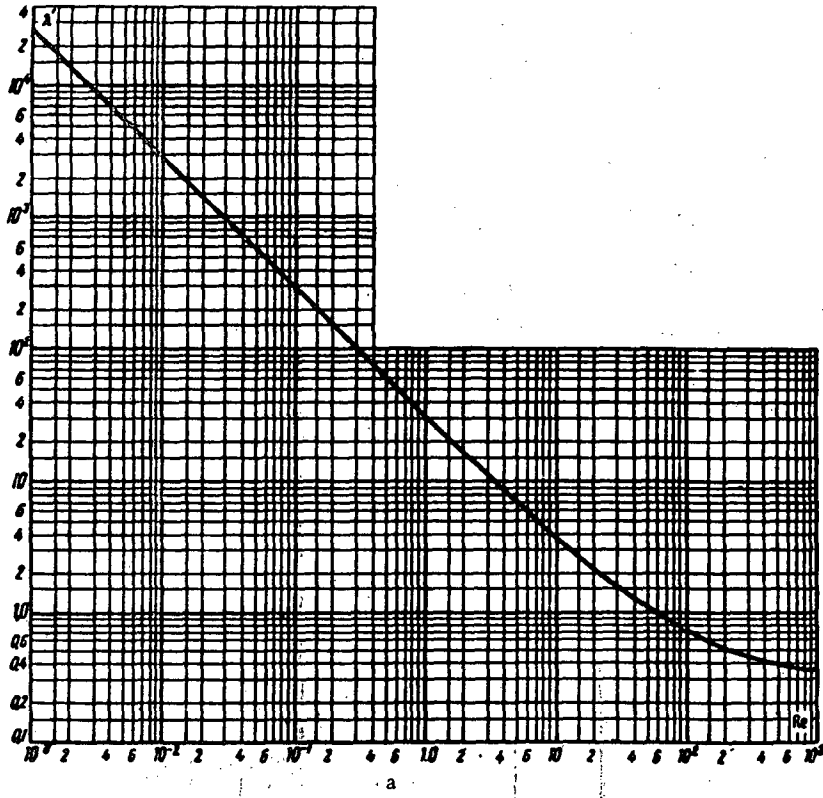
ϵ'	0.20	0.25	0.30	0.35	0.40	0.45	0.50	0.55	0.60	0.65	0.70
k	1,330	520	238	128	69.8	44.3	27.8	18.8	13.1	9.45	6.38

Packing — loose layer of spherical (granular) bodies or porous cemented layer from granular material (constant diameter) (cont'd)

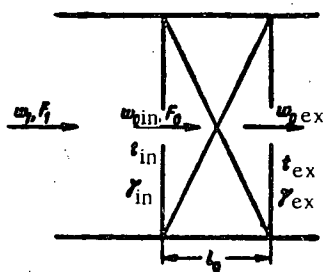
Section VIII

Diagram 8-18

Re	$1 \cdot 10^{-3}$	$5 \cdot 10^{-3}$	$1 \cdot 10^{-2}$	$5 \cdot 10^{-2}$	$1 \cdot 10^{-1}$	$5 \cdot 10^{-1}$	1	2	3	4	5
λ'	30,320	6,125	3,064	634	313	65.2	33.3	17.2	11.7	8.93	7.30
Re	6	7	8	9	10	$2 \cdot 10$	$3 \cdot 10$	$4 \cdot 10$	$5 \cdot 10$	$6 \cdot 10$	$7 \cdot 10$
λ'	6.20	5.05	4.75	4.30	3.90	2.17	1.57	1.28	1.10	0.97	0.88
Re	$8 \cdot 10$	$9 \cdot 10$	10^2	$2 \cdot 10^2$	$3 \cdot 10^2$	$4 \cdot 10^2$	$5 \cdot 10^2$	$6 \cdot 10^2$	$7 \cdot 10^2$	$8 \cdot 10^2$	10^3
λ'	0.81	0.77	0.72	0.52	0.46	0.42	0.40	0.38	0.37	0.36	0.35



Packing — bonded porous medium (nongranular)

 Section VIII
 Diagram 8-19


$$\gamma_m = \frac{\gamma_{t=0}}{1 + \frac{t_m}{273}}$$

$$w_{1m} = w_{in} \frac{273 + t_m}{273 + t_{in}}$$

γ is taken from § 1-3, b as a function of t_m .

$$\zeta = \frac{\Delta H}{\gamma_m w_{1m}^2} = \lambda \frac{l_0}{d_h \epsilon'^2} + \Delta \zeta_t$$

$$a) Re = \frac{w_{1m} d_h}{\nu} \frac{1}{\epsilon'} < 3:$$

$$\lambda = \frac{180}{Re_h}$$

$$\lambda = f(Re)$$

$$b) Re > 3:$$

$$\lambda = \frac{164}{Re_h} + \frac{7.68}{Re_h^{0.11}}$$

is determined from the curve

$\lambda = f(Re)$

d_h and ϵ' are taken from Table 8-9.

$$\Delta \zeta_t = \frac{2(t_{ex} - t_{in})}{273 + t_m}; t_m = \frac{t_{in} + t_{ex}}{2}$$

Re	$1 \cdot 10^{-3}$	$5 \cdot 10^{-3}$	$1 \cdot 10^{-2}$	$5 \cdot 10^{-2}$	$1 \cdot 10^{-1}$	$5 \cdot 10^{-1}$	1	2	3	4	5	6
λ	180,000	36,000	18,000	3,600	1,800	360	180	90	61.5	47.9	39.7	33.7
Re	7	8	9	10	15	20	25	30	35	40	45	50
λ	29.6	26.5	24.3	22.4	16.8	13.7	12.0	10.7	9.90	9.24	8.70	8.30
Re	70	80	90	100	150	200	250	300	350	400	450	500
λ	7.16	6.80	6.52	6.27	5.62	5.12	4.84	4.65	4.49	4.37	4.29	4.21
Re	600	700	800	900	1,000							
λ	4.07	3.97	3.96	3.81	3.74							

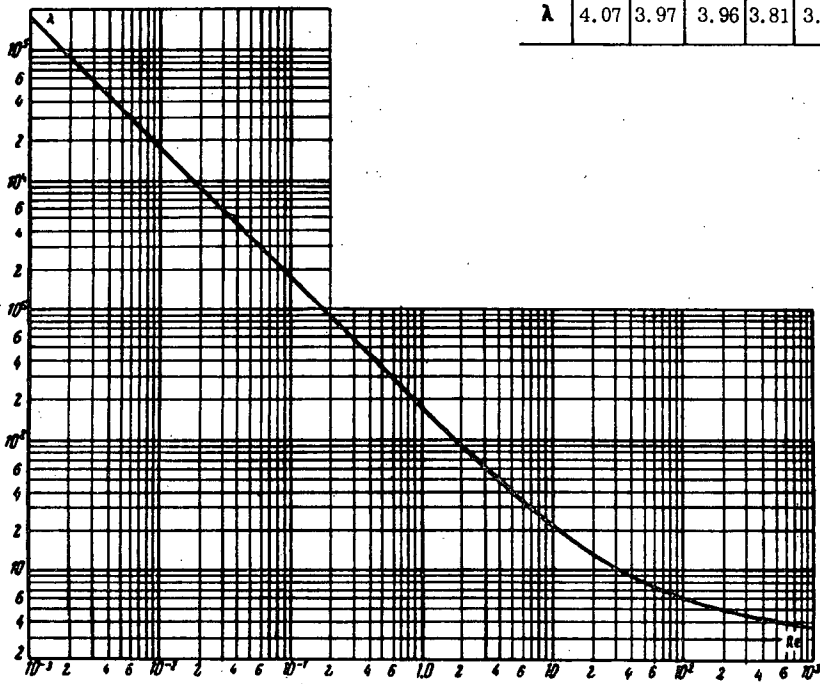


TABLE 8-9

Type of porous medium	d_h	ϵ' , m^3/m^3
Firebrick	0.0000072	0.157
"	0.0000400	0.430
"	0.000130	0.435
Diatomaceous earth	0.0000550	0.485
"	0.0000850	0.443
"	0.0001150	0.461
"	0.0002050	0.426
Quartz	0.0000570	0.361
"	0.0000950	0.502
Glass	0.0000041	0.230
"	0.0000680	0.296
"	0.0000180	0.271
"	0.0000210	0.267
"	0.0000710	0.263
Coal	0.0000061	0.198
"	0.0001270	0.203

No. 1. Rings in vertical columns

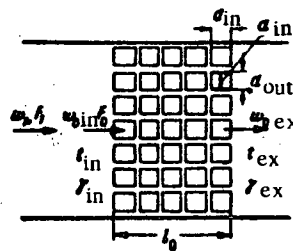


TABLE 8-10

A $\text{m}^3/\text{m}^2 \cdot \text{hr}$	w_{lim} m/sec
0-10	2.0
15-25	1.5
30-50	1.0

No. 2. Rings staggered

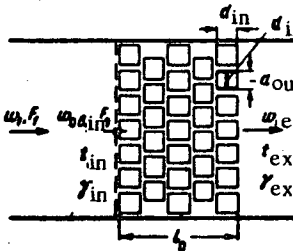
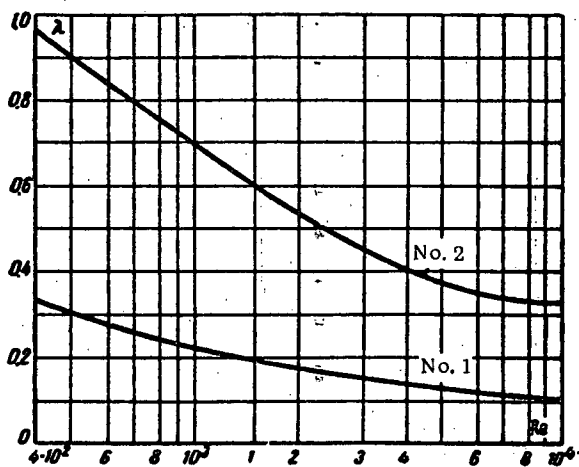


TABLE 8-11

A $\text{m}^3/\text{m}^2 \cdot \text{hr}$	w_{lim} m/sec
0-10	1.5
15-20	1.2
30-50	0.8

TABLE 8-12

d_{out} mm	$d_{\text{h},\text{m}}$	ϵ'	$\frac{1}{\epsilon'}$	$\frac{1}{\epsilon'^2}$	\bar{s} m^2/m^3
50	0.027	0.73	1.36	1.85	108
80	0.036	0.72	1.39	1.93	—
100	0.048	0.72	1.39	1.93	—
150	0.075	0.72	1.39	1.93	—
200	0.100	0.72	1.39	1.93	—



1. Dry packing

$$\zeta = \frac{\Delta H}{\gamma_m w_{\text{lim}}^2} = \lambda \frac{l_0}{d_{\text{h}}} \frac{1}{\epsilon'^2}$$

$$\text{No. 1. a)} 0.4 \cdot 10^3 < Re \frac{w_{\text{lim}} d_{\text{h}}}{\epsilon'} < 8 \cdot 10^3:$$

$\lambda = \frac{3.12}{Re^{0.375}}$ is determined as a function of Re by curve No. 1;
 b) $Re > 8 \cdot 10^3$;

$$\lambda \approx 0.10 = \text{const}$$

$$\text{No. 2. a)} 0.4 \cdot 10^3 < Re < 6 \cdot 10^3:$$

$\lambda = \frac{9.2}{Re^{0.375}}$ is determined as a function of Re by curve No. 2;

$$\text{b) } Re > 6 \cdot 10^3;$$

$$\lambda \approx 0.34 = \text{const}$$

2. Wetted packing (tentatively)

$$(A < 50; w_{\text{1}} \leq w_{\text{lim}})$$

$$\zeta = \frac{\Delta H}{\gamma_m w_{\text{1}}^2} = \lambda \frac{l_0}{d_{\text{h}}} \frac{1}{\epsilon'^2} (1 + 0.04 A) + \Delta \zeta,$$

where A = intensity of wetting by the liquid, $\text{m}^3/\text{m}^2 \cdot \text{hr}$;

w_{lim} is taken from Tables 8-10 and 8-11;

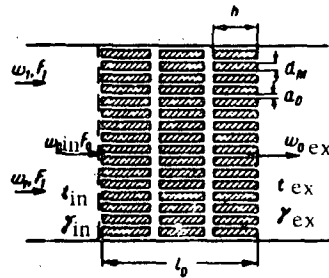
$$\Delta \zeta = 2 \frac{t_{\text{ex}} - t_{\text{in}}}{273 + t_{\text{m}}}; t_{\text{m}} = \frac{t_{\text{in}} + t_{\text{ex}}}{2};$$

$$t_{\text{m}} = \frac{t_{\text{in}}}{1 + \frac{t_{\text{in}}}{273}}; w_{\text{1}} = \frac{273 + t_{\text{m}}}{273 + t_{\text{in}}};$$

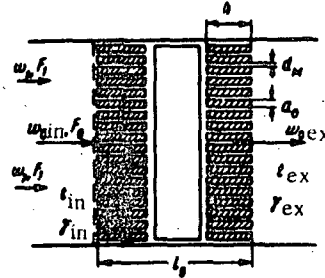
w_{1} is taken as a function of t_{m} from § 1-3 b;
 d_{h} and ϵ' are taken from Table 8-12.

Re	$4 \cdot 10^2$	$6 \cdot 10^2$	$8 \cdot 10^2$	10^3	$1.5 \cdot 10^3$	$2 \cdot 10^3$	$4 \cdot 10^3$	$6 \cdot 10^3$	$8 \cdot 10^3$
No. 1									
λ	0.33	0.28	0.25	0.23	0.20	0.18	0.14	0.12	0.11
No. 2									
λ	0.98	0.84	0.75	0.70	0.60	0.53	0.41	0.36	0.34

No. 1. Chords placed in parallel



No. 2. Chords placed crosswise



1. Dry packing

$$\zeta = \frac{\Delta H}{\frac{v_m^2}{2g}} = \lambda \frac{l_0}{d_h} \frac{1}{\epsilon^2};$$

No. 1. a) $4 \cdot 10^2 < Re = \frac{w_1 m d_h}{v} \frac{1}{\epsilon} < 10^4$;

$\lambda = \frac{3.12}{Re^{0.375}}$ is determined as a function of Re by curve 1;

b) $Re > 10^4$:

$$\lambda \approx 0.10 = \text{const}$$

No. 2. a) $4 \cdot 10^2 < Re = \frac{w_1 m d_h}{v} \frac{1}{\epsilon} \leq 10^4$

$\lambda = \frac{k'_1}{Re^{0.375}}$ is determined as a function of Re by the curves for grids of the corresponding number;

k'_1 is taken from Table 8-13;

b) $Re > 10^4$:

$\lambda = \lambda'$ is taken from Table 8-13.

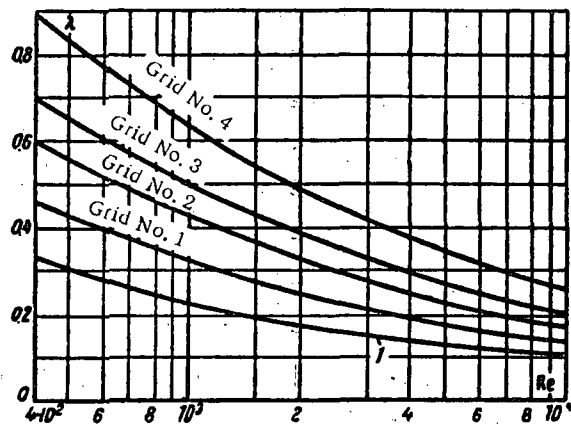
TABLE 8-13

No. of grid	d_{M} , mm	a_0 , mm	h , mm	d_h , mm	d_h , m	ϵ'	$\frac{1}{\epsilon'}$	$\frac{1}{\epsilon'^2}$	\bar{s} , m^2/m^3	k'_1	λ'
1	10	10	100	22	0.022	0.55	1.82	3.31	100	4.4	0.14
2	10	10	50	22	0.022	0.55	1.82	3.31	100	5.7	0.18
3	10	20	100	41	0.041	0.68	1.47	2.16	66	6.7	0.21
4	10	30	100	63	0.063	0.77	1.30	1.69	49	8.5	0.26

Packing of wooden laths; dry or wetted (continued)

 Section VIII
 Diagram 8-21

Re	$4 \cdot 10^2$	$6 \cdot 10^2$	$8 \cdot 10^2$	10^3	$1.5 \cdot 10^3$	$2 \cdot 10^3$	$4 \cdot 10^3$	$6 \cdot 10^3$	$8 \cdot 10^3$	10^4	
$Re = 375$	9.5	10.9	12.3	13.3	15.5	17.3	22.5	26.3	29.8	31.6	No. 1
λ	0.33	0.28	0.25	0.23	0.20	0.18	0.14	0.12	0.11	0.11	
Grid No. 1											
λ	0.46	0.40	0.35	0.33	0.28	0.25	0.20	0.17	0.15	0.14	
Grid No. 2											
λ	0.60	0.52	0.46	0.43	0.37	0.33	0.25	0.22	0.19	0.18	No. 2
Grid No. 3											
λ	0.70	0.61	0.54	0.50	0.43	0.39	0.30	0.25	0.22	0.21	
Grid No. 4											
λ	0.90	0.78	0.69	0.64	0.55	0.49	0.38	0.32	0.28	0.26	



2. Wetted packing (tentatively)
 $(A \leq 50; w_1 \leq w_{1\lim})$

$$\zeta = \frac{\Delta H}{\gamma_m w_{1m}^2} = \lambda \frac{l_0}{d_h} \frac{1}{\epsilon^2} (1 + \epsilon' A) + \Delta \zeta,$$

where A = intensity of wetting by the liquid, $m^3/m^2 \cdot hr.$

$\epsilon' = 0.04$ for No. 1 and 0.06 for No. 2;

$w_{1\lim}$ is taken from Table 8-14;

$$\Delta \zeta_t = 2 \frac{t_{ex} - t_{in}}{273 + t_m}; \quad t_m = \frac{t_{in} + t_{ex}}{2};$$

$$\gamma_m = \frac{\gamma_0}{1 + \frac{t_m}{273}}; \quad w_{1m} = w_1 \frac{273 + t_m}{273 + t_{in}};$$

d_h and ϵ are taken from Table 8-13;

γ is taken from § 1-3, b as a function of t_m .

TABLE 8-14

$A m^3/m^2 \cdot hr.$	10-10	10-25	25-50
No. 1			
$w_{1\lim}, m/sec$	2.0	1.5	1.0
No. 2			
$w_{1\lim}, m/sec$	1.0	0.7	0.5

Regenerator checkerwork (of furnaces)

 Section VIII
 Diagram 8-22

Checkerwork	$d_h = \frac{2a_0 b_0}{a_0 + b_0}$	Resistance coefficient $\zeta = \frac{\Delta H}{\frac{1}{2} \rho v^2 d_h}$
Simple Siemens checkerwork		$\zeta = \frac{0.114}{\sqrt{d_h}} l_0 + \Delta \zeta_t$
Siemens checkerwork		$\zeta = \frac{1.57}{\sqrt{d_h}} l_0 + \Delta \zeta_t$
Checkerwork of "Stal'-proekt" design		<p>a) $Re = \frac{w_0 m d_h}{v} < 700:$</p> $\zeta = \frac{1400}{Re} l_0 + \Delta \zeta_t$ <p>b) $Re > 700:$</p> $\zeta = 2l_0 + \Delta \zeta_t$
Fence-type checkerwork of V. E. Grum-Grzhimailo's system		<p>a) $Re = \frac{w_0 m d_h}{v} < 1000:$</p> $\zeta = \frac{4400}{Re} \sqrt{d_h} l_0 + \Delta \zeta_t$ <p>b) $Re > 1000:$</p> $\zeta = \frac{3}{Re^{0.33} d_h^{0.8}} l_0 + \Delta \zeta_t$ $\Delta \zeta_t = 2 \frac{t_{ex} - t_{in}}{273 + t_m}; \quad t_m = \frac{t_{in} + t_{ex}}{2};$ $t_m = \frac{t_0}{1 + \frac{t_m}{273}}; \quad w_0 m = w_0 \ln \frac{273 + t_m}{273 + t_{in}};$ <p>v is taken from § 1-3, b as a function of t_m.</p>

Section Nine

STREAM FLOW THROUGH PIPE FITTINGS AND LABYRINTH SEALS

(Resistance coefficients of throttles, valves, labyrinth seals, etc.)

9-1. LIST OF SYMBOLS

- F_0 = cross-section area of the inlet, the throttling device, or of the gap of the labyrinth m^2 ;
 P_0 = section perimeter, m;
 F_{ch} = cross-section area of the labyrinth chamber, m^2 ;
 D_0 = diameter of the passage cross-section of the throttling device, m;
 D_h = hydraulic diameter of the passage;
 h = lift of the gate or valve, m;
 h_{ch} = height of the labyrinth chamber, m;
 l = length of the labyrinth gap, m;
 S = length of the free jet (length of the labyrinth chamber), m;
 δ_0 = half-width of the gap for a labyrinth with double grooves, or width of the jet for a labyrinth with one groove, m;
 δ_s = width or half-width of the free jet at the chamber end, m;
 w_0 = mean stream velocity in the passage cross-section of a throttling device, in the gap of a labyrinth, and in a complex fitting, m/sec ;
 p_0 = absolute pressure before the throttling device, kg/m^2 ;
 p_1 = absolute pressure after the throttling device kg/m^2 ;
 ΔH = pressure loss (resistance), kg/m^2 ;
 c = resistance coefficient.

9-2. EXPLANATIONS AND RECOMMENDATIONS

1. The resistance coefficient of throttling and control devices is a function of their design and the shapes of the inside of the body, which determines the stream flow, the uniformity of the section, etc. The quality of finish of the inside of the body also influences the resistance coefficient.

2. The design length of some types of globe and gate valves does not vary in proportion to their flow section, and therefore a complete geometrical similitude is not preserved when the diameter of this section is varied. Further, the relative roughness of the casting increases with the decrease of its size. As a result, the resistance of some globe valves and gate valves varies with the flow cross-section diameter: the resistance coefficient c of globe valves of large dimensions increases with the flow cross-section diameter, while in globe valves of small dimensions it increases with the decrease of the diameter.

3. The resistance of gate valves is similar to the resistance of restrictors, in which a sudden stream contraction is followed by a sudden expansion (Figure 9-1,a). The phenomenon in butterfly valves, taps (faucets), and globe valves is more complex,

(Figure 9-1,b,c, and d), abrupt and complex variations of direction being added to the sudden contractions and expansions. This results in local velocity increases, stream separations, and, consequently, eddy formations which increase the resistance of these elements.

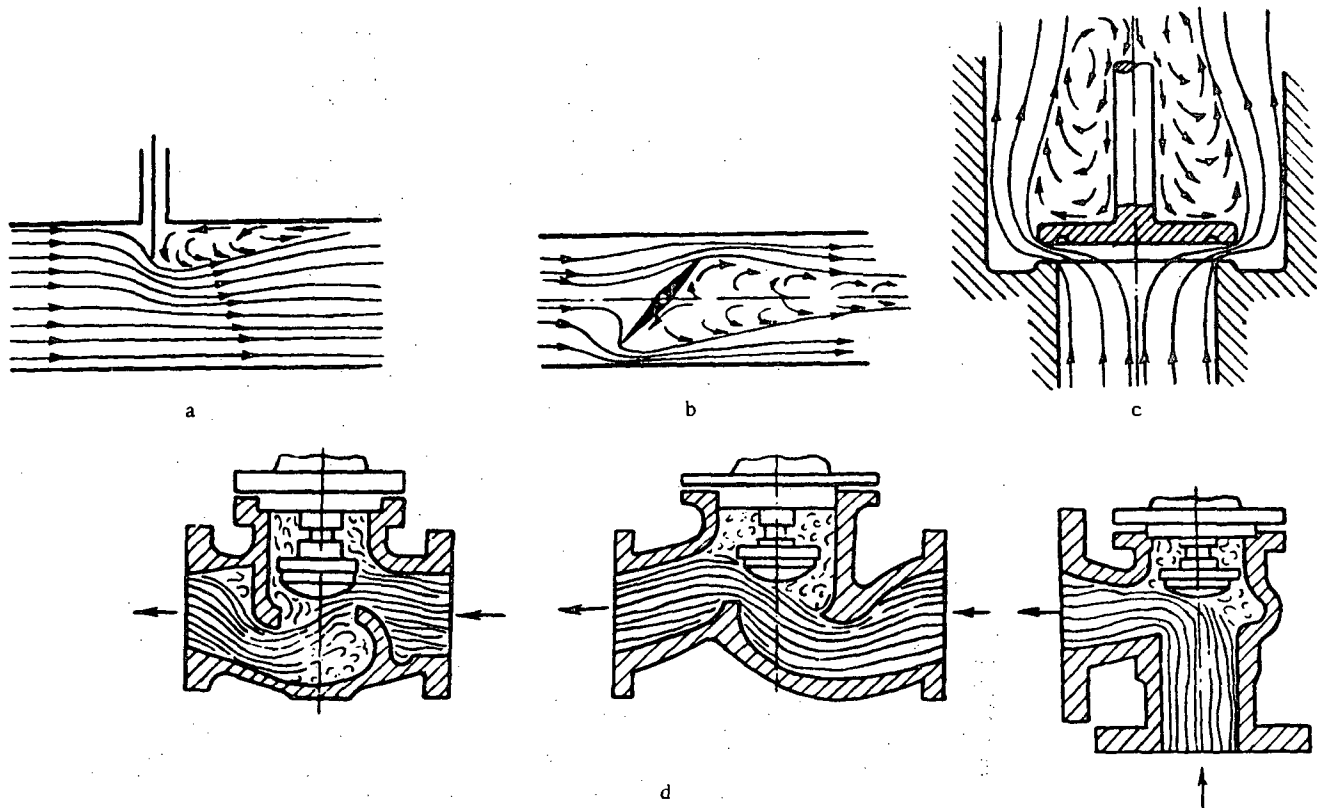


FIGURE 9-1. Flow pattern in throttling and control devices:

a—gate valve; b—butterfly valve; c—disk valve; d—globe valves.

The resistance of each type of throttling device depends largely on the position of the shut-off member.

In order to reduce the size of a gate valve, and the magnitude of forces and torques necessary to control it, the flow section in the valve body is usually contracted. This contraction is usually symmetrical, in the case of one-sided direction of stream motion it can, however, be made asymmetrical (cf. Gurevich /9-6/). The contraction of the passage increases the resistance coefficient of the gate valve.

The best design for minimizing fluid resistance is that of a straightway globe valve. The resistance coefficient of straightway globe valves depends largely on the Reynolds number $Re = \frac{w_0 D_h}{v}$. At small values of Re , ζ decreases rapidly with the increase of Re , passes through a minimum at $Re = 5 \times 10^4$, then increases slowly with the further increase of Re until finally it becomes constant and independent of Re .

6. The resistance coefficient of a straightway globe valve as a function of the valve lift $\frac{h}{D_0}$ can be determined by the following formulas, proposed by Murin /9-12/:

a) at $D_o = 38 \text{ mm}$

$$\zeta = \frac{\Delta H}{\frac{\gamma w_0^2}{2g}} = 1.28 + \frac{0.084}{\left(\frac{h}{D_o}\right)^2}; \quad (9-1)$$

b) at $D_o = 200 \text{ mm}$

$$\zeta = \frac{\Delta H}{\frac{\gamma w_0^2}{2g}} = \frac{0.51}{\left(\frac{h}{D_o}\right)^2}; \quad (9-2)$$

at full opening of the valve within the limits $D_o = 25 \text{ to } 200 \text{ mm}$

$$\zeta = \frac{\Delta H}{\frac{\gamma w_0^2}{2g}} = \frac{5.2}{D_o^{0.5}}. \quad (9-3)$$

7. The resistance coefficient of certain types of valves can be determined by the following formulas (proposed by Bach /9-18/):

a) disk valve without bottom guides within the limits

$$0.1 < \frac{h}{D_o} < 0.25 \text{ and } 0.1 < \frac{b_d}{D_o} < 0.25$$

$$\zeta = \frac{\Delta H}{\frac{\gamma w_0^2}{2g}} = 0.55 + 4 \left(\frac{b_d}{D_o} - 0.1 \right) + \frac{0.155}{\left(\frac{h}{D_o} \right)^2}. \quad (9-4)$$

where b_d = width of the disk flange, m;

b) disk valve with bottom guides within the limits

$$0.125 < \frac{h}{D_o} < 0.25 \text{ and } 0.1 < \frac{b_d}{D_o} < 0.25$$

$$\zeta = \frac{\Delta H}{\frac{\gamma w_0^2}{2g}} = (0.8 \text{ to } 1.0) \left[0.55 + 4 \left(\frac{b_d}{D_o} - 0.1 \right) + \frac{1.73}{\left(\frac{h}{D_o} \right)^2 \left(\pi - \frac{i S_{cl}}{D_o} \right)^2} \right]. \quad (9-5)$$

where S_{cl} = width of the guide shoulder (cf. diagram 9-14); i is the number of guide ribs;

c) conical valve with flat seat within the limits $0.1 < \frac{h}{D_o} < 0.25$ and for $\frac{b_d}{D_o} = 0.1$

$$\zeta = \frac{\Delta H}{\frac{\gamma w_0^2}{2g}} = 2.6 - \frac{0.8}{\frac{h}{D_o}} + \frac{0.14}{\left(\frac{h}{D_o} \right)^2}, \quad (9-6)$$

d) conical valve with conical seat within the limits $0.125 < \frac{h}{D_o} < 0.4$

$$\zeta = \frac{\Delta H}{\frac{\gamma w_0^2}{2g}} = 0.6 + \frac{0.15}{\left(\frac{h}{D_o} \right)^2}, \quad (9-7)$$

e) spherical valve with spherical seal within the limits $0.1 < \frac{h}{D_0} < 0.25$

$$\zeta = \frac{\Delta H}{\frac{\gamma w_0^2}{2g}} = 2.7 - \frac{0.8}{\frac{h}{D_0}} + \frac{0.14}{\left(\frac{h}{D_0}\right)^2}. \quad (9-3)$$

8. Since the motion of a gas through throttling devices is accompanied by large pressure losses, the density of the gas will vary considerably when determining the resistance of the device. This should be taken into account by the formula (cf. Gurevich /9-6/)

$$\Delta H = k_c \zeta \frac{\gamma_{in} w_0^2}{2g} [kg/m^2], \quad (9-9)$$

where w_0 is the mean stream velocity before the throttling device at a pressure p_0 m/sec; γ_{in} is the specific gravity of the gas before the throttling device, kg/m^3 ; k_c is the correction for the gas compressibility, depending on the ratio $\frac{p_1}{p_0}$ between the absolute pressures before and after the throttling device:

$$\frac{p_1}{p_0} = 1 - \frac{\Delta H}{p_0}. \quad (9-10)$$

The following values are obtained for the correction:

a) at $\frac{p_1}{p_0} > 0.9$ or $\Delta H < 0.1 p_0$

$$k_c \approx 1.0;$$

b) at $\left(\frac{p_1}{p_0}\right)_{cr} < \frac{p_1}{p_0} < 0.9$ or $1 - \left(\frac{p_1}{p_0}\right)_{cr} > \frac{\Delta H}{p_0} > 0.1$

$$k_c = \frac{\Delta H}{p_0} \frac{x-1}{x \left[\left(\frac{p_1}{p_0}\right)^{2x} - \left(\frac{p_1}{p_0}\right)^x \right]} \quad (9-11)$$

or, approximately (cf. Aronovich /9-3/):

$$k_c = \frac{1}{\left(1 - 0.46 \frac{\Delta H}{p_1}\right)^{\frac{1}{2}}}. \quad (9-12)$$

where $\left(\frac{p_1}{p_0}\right)_{cr}$ is the critical ratio of the pressures before and after the throttling device at which the stream velocity in the narrow section becomes equal to the local velocity of sound; in the case of air and a diatomic gas $\left(\frac{p_1}{p_0}\right)_{cr} = 0.53$ and $1 - \left(\frac{p_1}{p_0}\right)_{cr} = 0.47$.

The magnitudes ΔH , $\frac{p_1}{p_0}$, and k_c are calculated by the method of successive approximation.

9. The resistance coefficient of a ring-seal gate in a spillway is independent of the tailwater level h_1 (Figure 9-2, a), i. e., it is identical in the cases of discharge

into the atmosphere and discharge under water (cf. Rolle /9-14/). When the ring-seal gate is placed in a stilling chamber which ensures the reliable dissipation of the kinetic energy of the stream in the tailwater (Figure 9-2, b), its resistance coefficient varies somewhat (cf. diagrams 9-17 and 9-18).

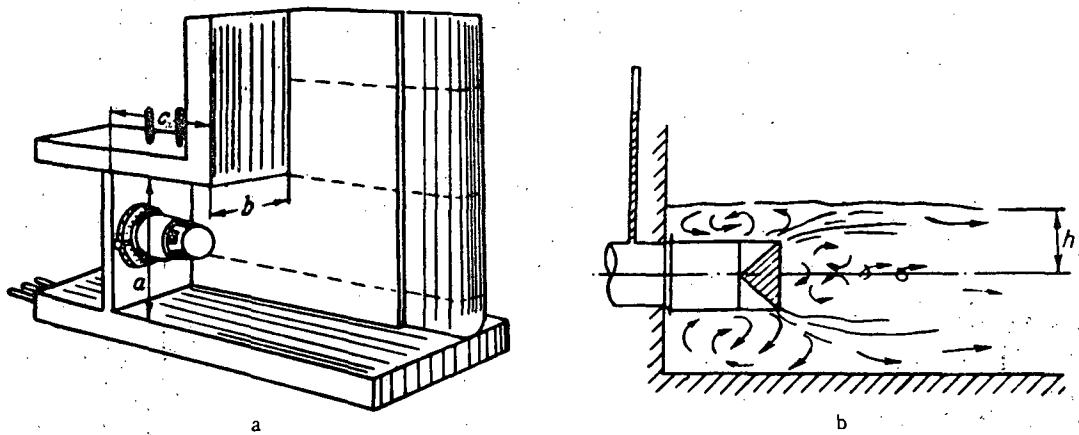


FIGURE 9-2. Ring-seal gate in a spillway:

a — gate design; b — flow pattern.

10. In a labyrinth seal with the intermediate baffles located at one side and on one level, the stream passage is straight. The stream contracts on entering the first gap (Figure 9-3, a) just as in the case of entrance in a straight channel mounted flush in the wall, or in the case of passage through an orifice in a thin wall. It then expands on entering the labyrinth chamber and, due to turbulent mixing, additional fluid is entrained. When the dimensions of the chamber are sufficiently large (relative to the gap size), a core of constant mass separates from the jet at the chamber end and, contracting, enters the second gap. The attached masses of the surrounding medium separate from the stream core at the chamber end and move with a circulatory motion in the chamber until they become once more mixed with the jet. Since the constant core possesses a high kinetic energy before entering the second gap, there is less contraction than at the entrance to the first gap.

11. The resistance of the labyrinth cell (Figure 9-3, a) is due to the frictional losses in the gap and the energy losses in the constant-mass core. The latter are made up of two parts: the difference between the energy stored in the constant-mass core at the beginning and end of the cell, and the loss at the inlet of the next gap.

In the case of relatively small chamber dimensions, fulfilling the inequality

$$\frac{h_{ch}}{\delta_0} < \frac{\delta_s}{\delta_0},$$

the jet issuing from the gap into the chamber will fill the entire section. The resistance in this case is made up of: 1) the frictional losses in the gap; 2) the losses at sudden

expansion; 3) the losses at entering the following gap (according to Abramovich's data /9-1/):

$$\frac{\delta_s}{\delta_0} = 24 \frac{a_{st} s}{\delta_0} + 1, \quad (9-13)$$

where a_{st} is the coefficient of stream turbulence, taken here as 0.1.

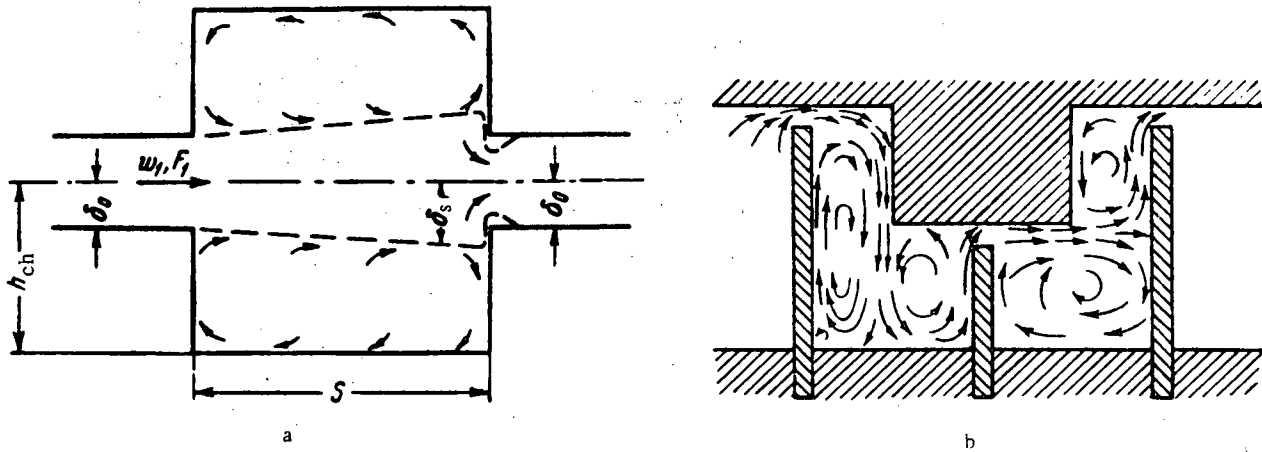


FIGURE 9-3. Flow pattern in labyrinths:

a — cell of simple labyrinth; b — labyrinth with curved stream passage.

12. In the case of labyrinth seals with protuberances, staggered arrangement of baffles, and with large chamber dimensions between the baffles the stream is directed toward the labyrinth protuberance after the compression in the gap (Figure 9-3, b). Here it is deflected through 90° and flows in a straight line up to the lower wall of the chamber. It then circulates in the chamber and flows toward the second gap along the second channel. The flowing stream entrains stationary masses from the surrounding space, causing a motion of these masses and the formation of eddy zones. The existence of protuberances between the labyrinth baffles lengthens the path of the free jet, which contributes to the dissipation of its energy. Labyrinths with curved flow are more effective, since the length of the jet path in them, and correspondingly the resistance, are considerably larger than in labyrinths with straight stream passage.

13. The resistance coefficients of labyrinths with oblong gaps are calculated by the following formulas obtained by the author /9-9/:

a) at $\frac{h_{ch}}{\delta_0} > \frac{\delta_s}{\delta_0}$

$$\zeta = \frac{\Delta H}{\frac{1}{2} w_0^2} = 1 + \zeta' + z(a_1 + \zeta' b_1 + \zeta_{fr}), \quad (9-14)$$

where a_1, b_1 are coefficients depending on the relative length of the labyrinth cell and determined from the corresponding graphs of diagram 9-19; $\zeta_{fr} = \lambda \frac{l}{\delta_0}$ is the friction coefficient

of the gap; λ is the friction coefficient of unit relative length of the gap, determined by the data of diagrams 2-1 to 2-5; ζ' is a coefficient by which allowance is made for the influence of the shape of the inlet edge of the gap; it is determined from the data of diagrams 3-3 and 3-6 as a function of the degree to which the inlet edge is rounded or beveled.

b) at $\frac{h_{ch}}{b_0} < \frac{\delta_s}{b_0}$

$$\zeta = \frac{\Delta H}{\frac{\gamma w_0^2}{2g}} = 1 + \zeta' + z(a_s + \zeta' b_s + \zeta_{fr}). \quad (9-15)$$

where

$$a_s = \left(1 - \frac{F_s}{F_{ch}}\right)^2; \quad (9-16)$$

$$b_s = \left(1 - \frac{F_s}{F_{clif}}\right). \quad (9-17)$$

14. The resistance coefficient of comb-shaped labyrinth seals is calculated by a different set of formulas (/9-9/):

a) at $\frac{h_{ch}}{b_0} > \frac{\delta_s}{b_0}$

$$\zeta = \frac{\Delta H}{\frac{\gamma w_0^2}{2g}} = z c_1 + d_1. \quad (9-18)$$

where c_1, d_1 are coefficients depending on the relative length S/b_0 of the labyrinth chamber and determined from the corresponding graphs of diagram 9-20;

b) at $\frac{h_{ch}}{b_0} < \frac{\delta_s}{b_0}$

$$\zeta = \frac{\Delta H}{\frac{\gamma w_0^2}{2g}} = z c_2 + d_2. \quad (9-19)$$

where

$$c_2 = \left(1 + \frac{0.707}{\sqrt{1 - \frac{F_s}{F_{ch}}}}\right)^2 \left(1 - \frac{F_s}{F_{ch}}\right)^2. \quad (9-20)$$

$$d_2 = \left(1 + 0.707 \sqrt{1 - \frac{F_s}{F_{ch}}}\right)^2. \quad (9-21)$$

15. The flow pattern in complex fittings of conduits in which sharp turns, sudden expansions and contractions, bypasses, etc. follow each other at a very short distance (cf. diagrams 9-23 to 9-25), is similar to curved channels, restrictors, and labyrinth seals with wide gaps.

When calculating the resistance of such complex fittings it is necessary to allow for interaction of the separate elements in each fitting, which considerably increases the total resistance above the sum of the resistances of the separate elements (sometimes by a factor of three and more).

16. If a complex fitting is used as labyrinth seal, its resistance is useful, since it makes operation more efficient (a higher resistance decreases the entry of air through it). Where the complexity of the fitting is necessitated by the limited size of the installations, however, the resistance is harmful and should be reduced. The losses in such fittings can be considerably reduced by enlarging certain cross sections. The installation of guide vanes at sharp-cornered turns is a very efficient method of decreasing the resistance (cf. § 6-2), and, what is more, does not necessitate alterations of the dimensions of the fitting. The resistance is also reduced considerably when the corners are rounded.

The installation of fairings is very useful in the case of obstruction of irregular shape placed in the stream.

**9-3. LIST OF THE DIAGRAMS OF RESISTANCE COEFFICIENTS
OF SECTION IX**

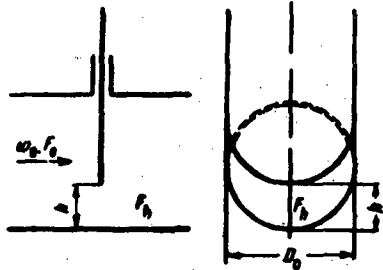
Diagram description	Source	No. of diagram	Note
Gate valve	Idel'chik /9-8/ Weisbach /9-22/	9-1	Calculated by the formula for restrictors; experimental data
Wedge-type gate valve	Idel'chik	9-2	According to the author's experiments
Gate valve with symmetric contraction	Gurevich /9-6/	9-3	Experimental data
Butterfly valve	Weisbach /9-22/	9-4	The same
Stopcock	The same	9-5	" "
Standard globe valve with dividing walls	Bach /9-18/, Erlich /9-17/	9-6	" "
Y-pattern ("Kosva") globe valve	The same	9-7	" "
Direct-flow globe valve	Murin /9-12/	9-8	" "
Various globe valves and gate valves	Bach /9-18/, Erlich /9-17/	9-9	" "
Flap	Aronovich and Slobodkin /9-4/	9-10	" "
Double-seat control valves	Gurevich /9-6/	9-11	Formula given by the author
Check valve, and suction valve with screen	Kuznetsov and Rudomino /9-11/, Frenkel' /9-16/	9-12	Tentatively
Disk valve without bottom guides	Bach /9-18/, Frenkel' /9-16/	9-13	Approximate formulas
Disk valve with bottom guides	The same	9-14	The same
Conical valve on conical seat	" "	9-15	" "
Conical valve on flat seat and ball valve on spherical seat	" "	9-16	" "
Ring-seal gate (free)	Rolle /9-14/	9-17	Experimental data
Ring-seal gate (in a chamber)	The same	9-18	" "
Labyrinth seal with increased gap	Idel'chik /9-9/	9-19	Calculating formulas
Comb-type labyrinth seal	The same	9-20	" "
Various expansion joints	—	9-21	Tentatively
Coils	Aronov /9-2/	9-22	Experimental data
Complex passage from one volume to another through a 90° elbow	Idel'chik	9-23	The same
Complex passage from one volume to another through an oblong 180° elbow	"	9-24	" "
Complex passage from one volume to another through different labyrinth seals	"	9-25	" "

9-4. DIAGRAMS OF THE RESISTANCE COEFFICIENTS

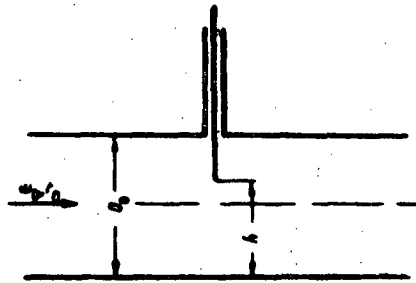
Gate valve

Section IX
Diagram 9-1

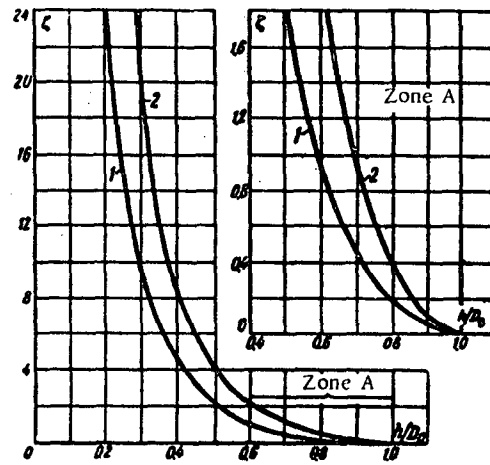
1. Cylindrical pipe



2. Rectangular pipe



$$\xi = \frac{\Delta H}{Tu_0^2} \quad \text{is determined from the curves } \xi = f\left(\frac{h}{D_0}\right)$$



$\frac{h}{D_0}$	0	0.10	0.125	0.2	0.3	0.4	0.5	0.6	0.7	0.8	0.9	1.0
-----------------	---	------	-------	-----	-----	-----	-----	-----	-----	-----	-----	-----

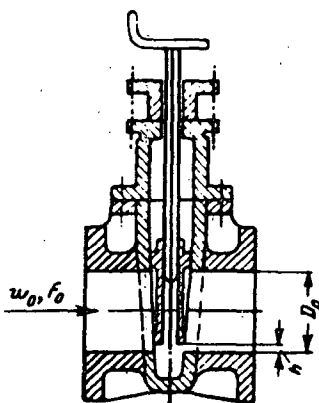
1. Cylindrical pipe

$\frac{F_h}{F_0}$	0	-	0.16	0.25	0.38	0.50	0.61	0.71	0.81	0.90	0.96	1.0
ξ	∞	-	97.8	35.0	10.0	4.60	2.06	0.98	0.44	0.17	0.06	0

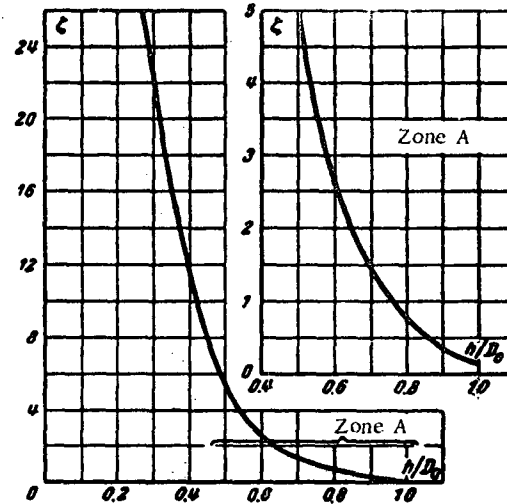
2. Rectangular pipe

ξ	∞	193	-	44.5	17.8	8.12	4.02	2.08	0.95	0.39	0.09	0
-------	----------	-----	---	------	------	------	------	------	------	------	------	---

Wedge-type gate valve

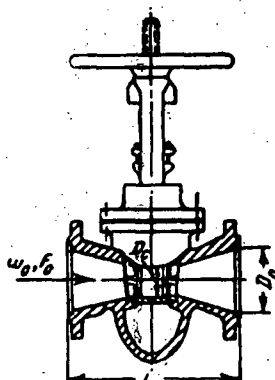
 Section IX
 Diagram 9-2


$\frac{h}{D_0}$	0.25	0.3	0.4	0.5	0.6	0.7	0.8	0.9	1.0
ζ	30.0	22.0	12.0	5.30	2.80	1.50	0.80	0.30	0.15



$$\zeta = \frac{\Delta H}{\frac{1}{2} w_0^2} \text{ is determined from the curve } \zeta = f\left(\frac{h}{D_0}\right)$$

Gate valve with symmetric contraction

 Section IX
 Diagram 9-3


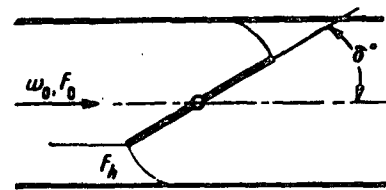
$$\zeta = \frac{\Delta H}{\frac{1}{2} w_0^2} \text{ is taken from the table}$$

D_0 , mm	300	300	200	250
$\frac{D_c}{D_0}$	0.67	0.67	0.75	0.80
$\frac{L}{D_0}$	2.50	1.68	1.33	1.50
ζ	1.45	1.80	0.60	0.39

Butterfly valve

Section IX
Diagram 9-4

$$\zeta = \frac{\Delta H}{\frac{\gamma w_0^2}{2g}} \text{ is determined from the curves } \zeta = f(\delta^\circ)$$



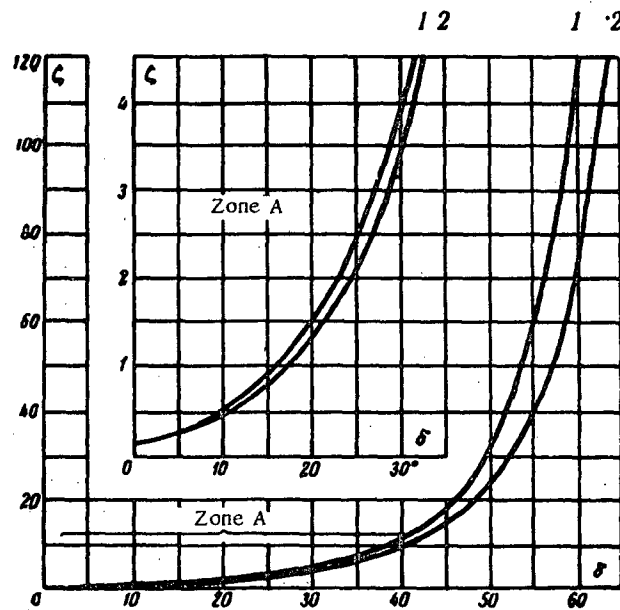
δ°	5	10	15	20	25	30	40	50	60	65	70	90
----	---	----	----	----	----	----	----	----	----	----	----	----

1. Cylindrical pipe

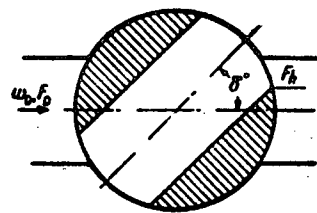
ζ	0.24	0.52	0.90	1.54	2.51	3.91	10.8	32.6	118	256	751	∞
---	------	------	------	------	------	------	------	------	-----	-----	-----	---

2. Rectangular pipe

$\frac{F_h}{F_0}$	0.91	0.83	0.74	0.66	0.58	0.50	0.36	0.23	0.13	0.09	0.06	90
ζ	0.28	0.45	0.77	1.34	2.16	3.54	9.30	24.9	77.4	158	368	∞



$$\xi = \frac{\Delta H}{\gamma w_0^2} \text{ is determined from the curves } \xi = f(\theta)$$

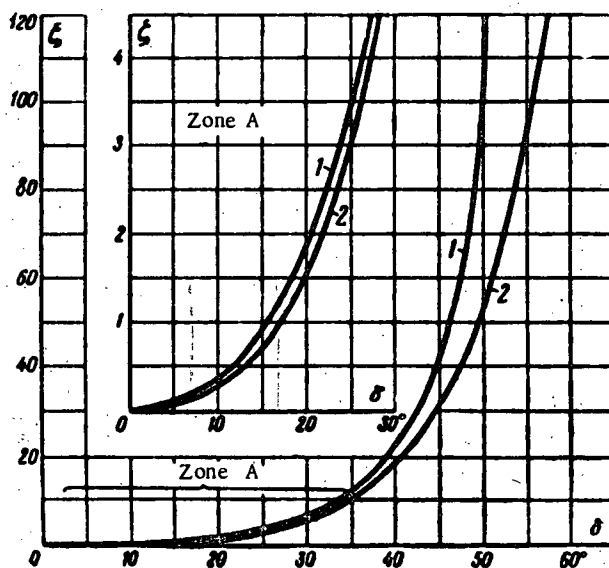


1. Cylindrical pipe

θ°	5	10	15	20	25	30	35	40	45	50	55	67
$\frac{F_h}{F_o}$	0.93	0.85	0.77	0.69	0.60	0.52	0.44	0.35	0.27	0.19	0.11	0
ξ	0.05	0.31	0.88	1.84	3.45	6.15	11.2	20.7	41.0	95.3	275	∞

2. Rectangular pipe

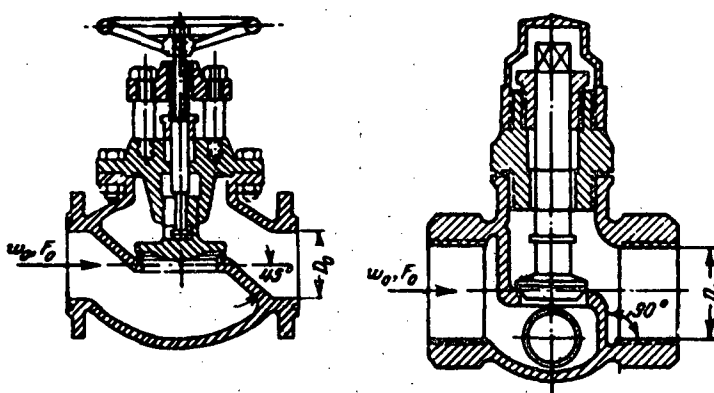
θ°	5	10	15	20	25	30	35	40	45	50	60	82
$\frac{F_h}{F_o}$	0.93	0.85	0.77	0.69	0.61	0.53	0.46	0.38	0.31	0.25	0.14	0
ξ	0.05	0.29	0.75	1.56	3.10	5.47	9.68	17.3	31.2	52.6	205	∞



Standard globe valve with dividing walls

Section IX
Diagram 9-6

1. Dividing walls at an angle of 45° 2. Vertical dividing walls



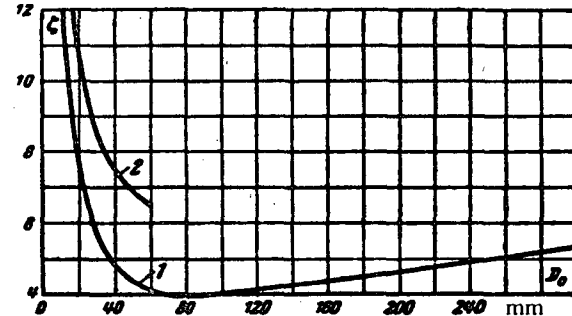
$$\zeta = \frac{\Delta H}{\frac{\gamma w_0^2}{2g}} \text{ is determined from the curves } \zeta = f(D_o)$$

1. Dividing walls at an angle of 45°

D_o , mm	13	20	40	80	100	150	200	250	300	350
ζ	10.8	8.00	4.90	4.00	4.10	4.40	4.70	5.10	5.40	5.50

2. Vertical dividing walls

D_o , mm	13	20	25	30	40	50
ζ	15.9	10.5	9.30	8.60	7.60	6.90

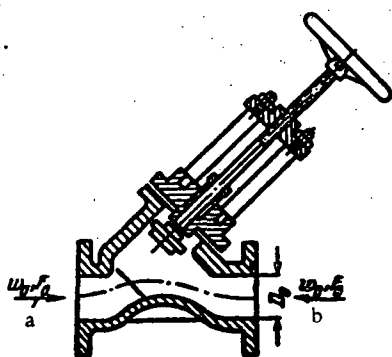


Y-pattern ("Kosva") globe valve

Section IX
Diagram 9-7

$$\zeta = \frac{\Delta H}{\frac{\gamma w_0^2}{2g}} \text{ is determined from the curve } \zeta = f(D_o) \text{ and from}$$

Table 9-1.



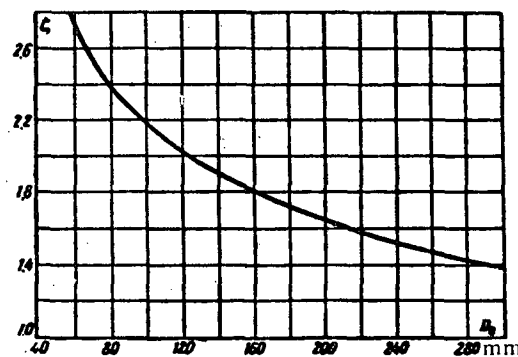
2. With full seat section

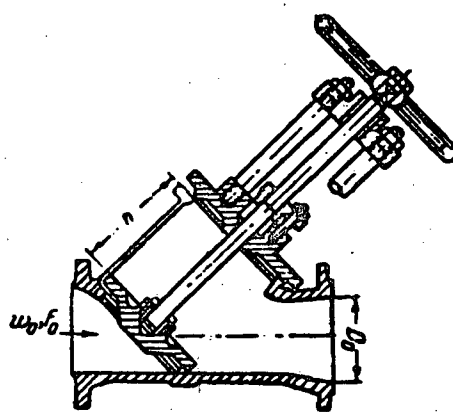
TABLE 9-1

D_o , inches	ζ (flow along arrow a)	ζ (flow along arrow b)
1	1.80	1.70
1 ¼	2.00	1.90
1 ½	1.70	1.60

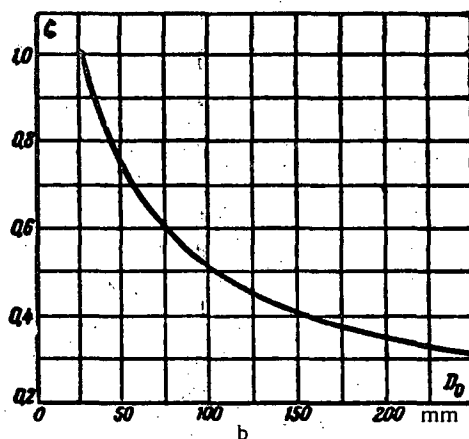
1. With 30% contraction of the seat section
(in direction of arrow a)

D_o , mm	60	80	100	150	200	250	300	350
ζ	2.70	2.40	2.20	1.86	1.65	1.50	1.40	1.30

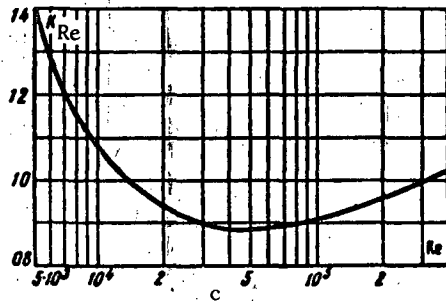




D_0 mm	25	38	50	65	75	100	125	150	200	250
ζ	1.40	0.85	0.73	0.65	0.60	0.50	0.46	0.42	0.36	0.32



Re	$5 \cdot 10^3$	10^4	$2 \cdot 10^4$	$5 \cdot 10^4$	10^5	$2 \cdot 10^5$	$3 \cdot 10^5$
k_{Re}	1.40	1.07	0.94	0.88	0.91	0.96	1.0



$$1. Re = \frac{w_0 D_0}{\nu} > 3 \cdot 10^5$$

A. Incomplete opening

$$a) D_0 = 38 \text{ mm, and } 0.2 < \frac{h}{D_0} < 0.8$$

$$\zeta = \frac{\Delta H}{\frac{\gamma w_0^2}{2g}} = 1.28 + \frac{0.084}{\left(\frac{h}{D_0}\right)^2} \text{ is determined from graph a;}$$

$$b) D_0 = 200 \text{ mm, and } 0.2 < \frac{h}{D_0} < 1.0$$

$$\zeta = \frac{\Delta H}{\frac{\gamma w_0^2}{2g}} = \frac{0.51}{\left(\frac{h}{D_0}\right)^2} \text{ is determined from graph a.}$$

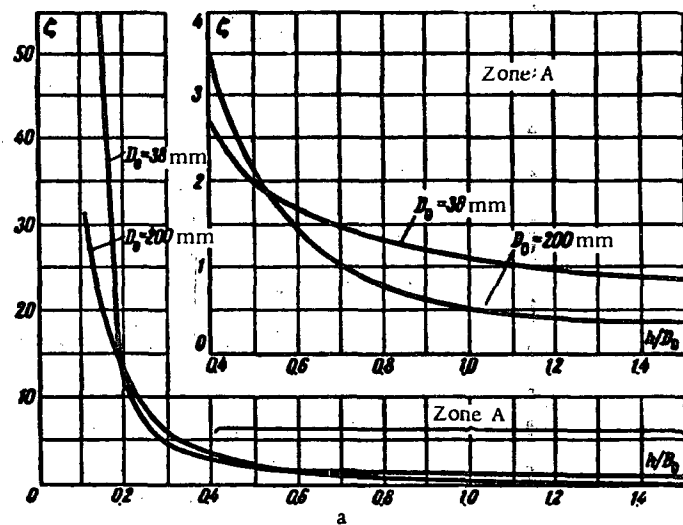
B. Full opening for diameters $D_0 = 25$ to 250 mm

$$\zeta = \frac{\Delta H}{\frac{\gamma w_0^2}{2g}} \approx \frac{5.2}{\sqrt{D_0}} \text{ is determined from graph b.}$$

$$2. Re < 3 \cdot 10^5 \quad \zeta_{Re} = \frac{\Delta H}{\frac{\gamma w_0^2}{2g}} = k_{Re} \zeta,$$

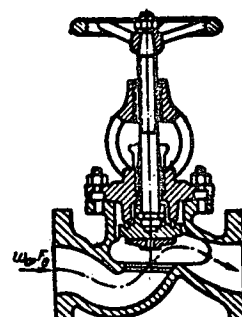
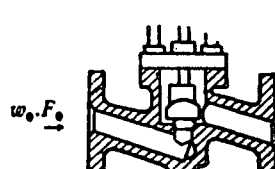
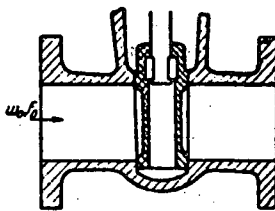
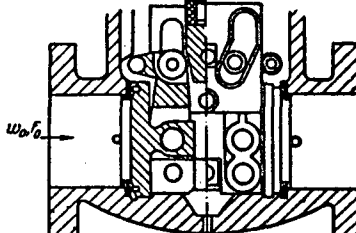
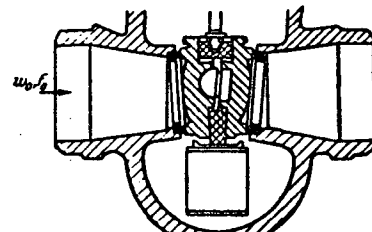
where k_{Re} is determined from graph c; ν is taken from § 1-3, b.

$\frac{h}{D_0}$	0.2	0.3	0.4	0.5	0.6	0.7	0.8	1.0	1.2	1.4
$\zeta_{D_0 = 38 \text{ mm}}$	12.0	4.40	2.60	2.00	1.70	1.50	1.30	1.11	0.95	0.85
$\zeta_{D_0 = 200 \text{ mm}}$	13.0	5.80	3.20	2.00	1.40	1.00	0.80	0.50	0.40	0.36

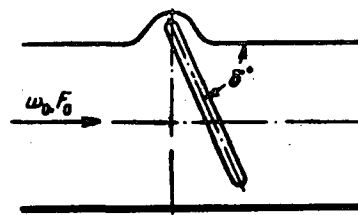


Various globe valves and gate valves

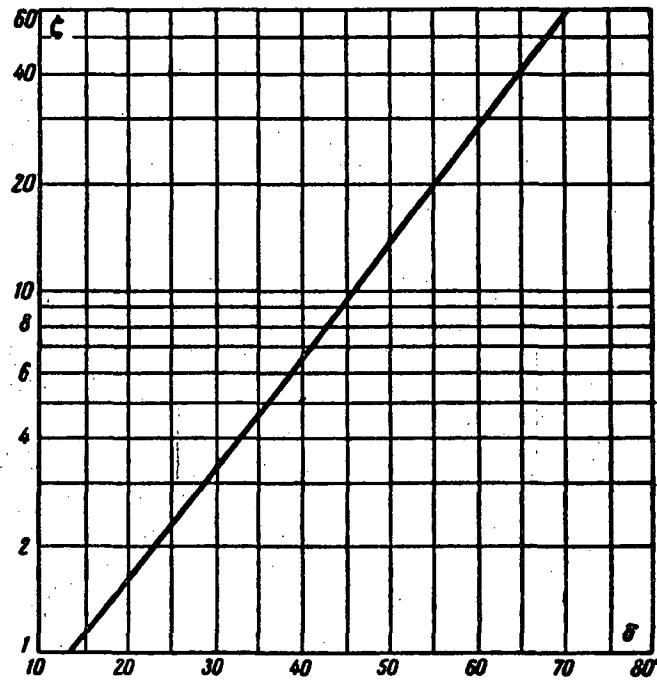
Section IX
Diagram 9-9

Valve type	Sectional view	Resistance coefficient $\zeta = \frac{\Delta H}{\frac{V^2}{2g}}$								
"Rey"-type globe valve		$\zeta = 3.4$								
Forged globe valve		$\zeta = 7.8$								
Wedge-type gate valve		$\zeta = 0.2$								
Steam gate valve with lever gate		$\zeta = 0.75$								
Conduit-type gate valve		<table border="1"> <tr> <td>$\frac{D_g}{D_c}$</td><td>1.2</td><td>1.4</td><td>1.8</td></tr> <tr> <td>ζ</td><td>0.3</td><td>0.7</td><td>2.2</td></tr> </table>	$\frac{D_g}{D_c}$	1.2	1.4	1.8	ζ	0.3	0.7	2.2
$\frac{D_g}{D_c}$	1.2	1.4	1.8							
ζ	0.3	0.7	2.2							

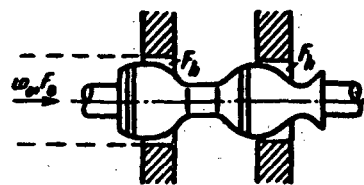
$$\zeta = \frac{\Delta H'}{\frac{T u_0^2}{2g}} \cong 0.35 \cdot 10^{0.0323\theta} \text{ is determined from curve } \zeta = f(\theta)$$



θ°	20	25	30	35	40	45	50	55	60	65	70	75
ζ	1.7	2.3	3.2	4.6	6.6	9.5	14	20	30	42	62	90



Double-seat control valves

 Section IX
 Diagram 9-11


$$\zeta = \frac{\Delta H}{\frac{F_h^2}{2g}} \text{ is determined from the curves } \zeta = f\left(\frac{F_h}{F_0}\right) \text{ for different } D_0 \text{ (mm)}$$

$\frac{F_h}{F_0}$	0.1	0.2	0.3	0.4	0.5	0.6	0.7	0.8	0.9	1.0
-------------------	-----	-----	-----	-----	-----	-----	-----	-----	-----	-----

 $D_0 = 25 \text{ mm}$

ζ	70.0	22.0	11.5	7.40	5.60	4.60	4.00	3.60	3.30	3.20
---------	------	------	------	------	------	------	------	------	------	------

 $D_0 = 50 \text{ mm}$

ζ	70.0	22.5	13.0	9.00	6.75	5.60	4.95	4.50	4.10	4.00
---------	------	------	------	------	------	------	------	------	------	------

 $D_0 = 80 \text{ mm}$

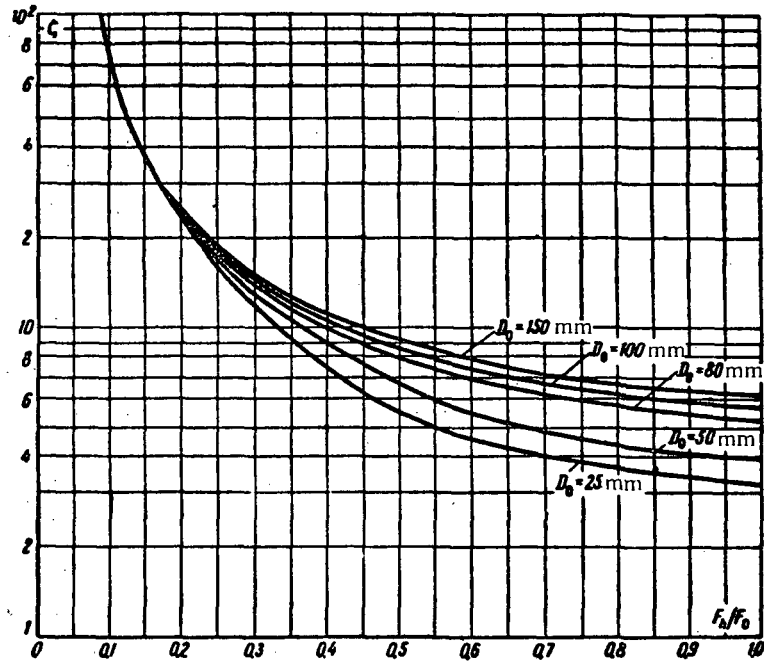
ζ	70.0	23.0	13.5	9.80	8.00	7.00	6.30	5.80	5.40	5.25
---------	------	------	------	------	------	------	------	------	------	------

 $D_0 = 100 \text{ mm}$

ζ	70.0	23.5	14.0	10.5	8.50	7.50	6.80	6.20	6.00	5.80
---------	------	------	------	------	------	------	------	------	------	------

 $D_0 = 150 \text{ mm}$

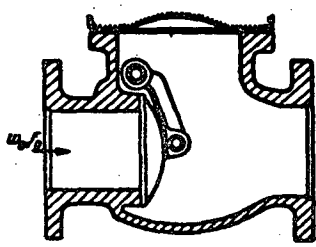
ζ	70.0	24.1	14.5	11.0	9.00	8.00	7.40	6.80	6.50	6.30
---------	------	------	------	------	------	------	------	------	------	------



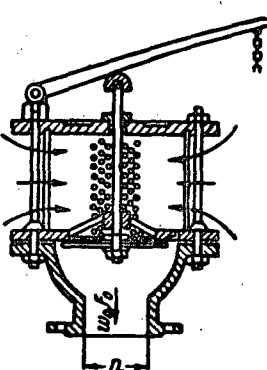
Check valve, and suction valve with screen

 Section IX
 Diagram 9-12

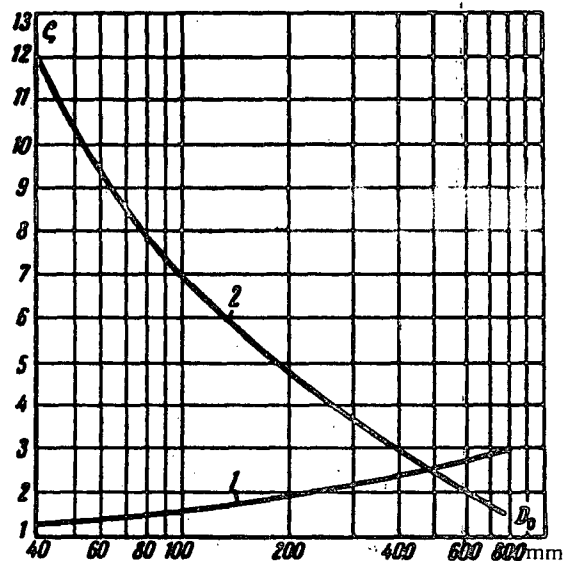
1. Check valve



2. Suction valve with screen

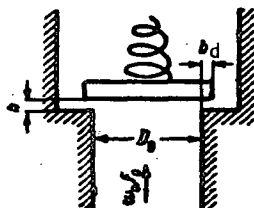


D_0 , mm	40	70	100	200	300	500	750
1. Check valve							
ζ	1.3	1.4	1.5	1.9	2.1	2.5	2.9
2. Suction valve with screen							
ζ	12	8.5	7.0	4.7	3.7	2.5	1.6



$\zeta = \frac{\Delta H}{\frac{\rho w_0^2}{2g}}$ is determined from the curves $\zeta = f(D_0, \text{mm})$

Disk valve without bottom guides

 Section IX,
 Diagram 9-13


$\frac{b_d}{D_0}$	0.10	0.12	0.14	0.16	0.18	0.20	0.22	0.24	0.25
a_0	0.55	0.63	0.71	0.79	0.87	0.95	1.03	1.11	1.15

$$\zeta = \frac{\Delta H}{\frac{\rho w_0^2}{2g}} = a_0 + \beta_0$$

$$\text{where } a_0 = 0.55 + 4 \left(\frac{b_d}{D_0} - 0.1 \right)$$

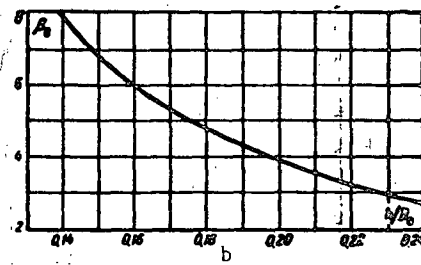
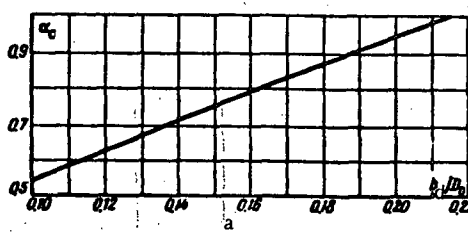
is determined from graph a;

$$\beta_0 = \frac{0.155}{\left(\frac{h}{D_0} \right)^2} \text{ is determined from}$$

graph b.

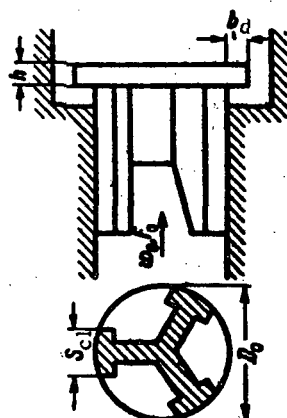
This formula is valid for

$$0.1 < \frac{h}{D_0} < 0.25; 0.1 < \frac{b_d}{D_0} < 0.25$$



$\frac{h}{D}$	0.10	0.12	0.14	0.16	0.18	0.20	0.22	0.24	0.25
β_0	15.5	10.8	7.90	6.05	4.78	3.87	3.20	2.69	2.48

Disk valve with bottom guides

 Section IX
 Diagram 9-14


$$\zeta = \frac{\Delta H}{\gamma w_0^2} = \gamma a_0 + \frac{\beta_1}{(\pi - \frac{i S_{Cl}}{D_o})^2}$$

where $a_0 = 0.55 + 4 \left(\frac{b_d}{D_o} - 0.1 \right)$ is determined from

graph a;

γ_0 is determined from graph b;

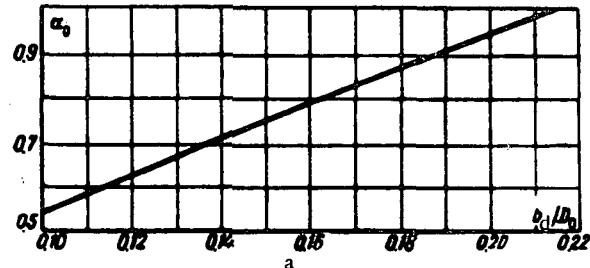
$\beta_1 = \frac{1.73}{\left(\frac{h}{D_o} \right)}$ is determined from graph c;

i = number of guides; F_p = free flow area.

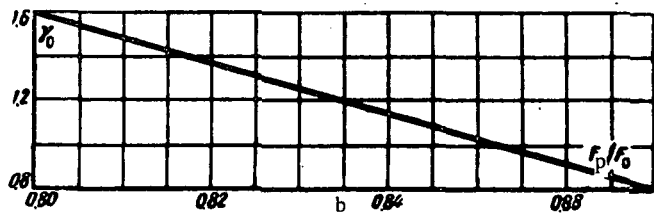
The formula is valid for

$$0.125 < \frac{h}{D_o} < 0.25; 0.10 < \frac{b_d}{D_o} < 0.25.$$

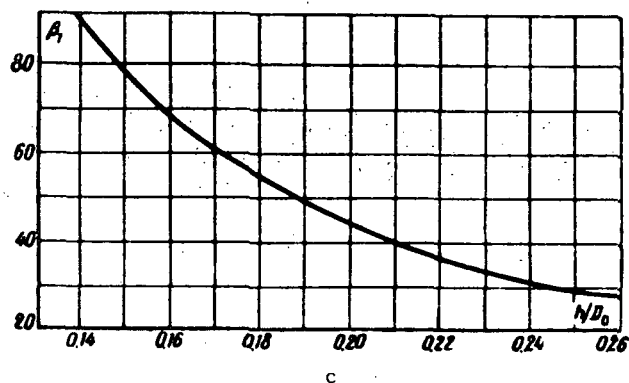
$\frac{b_d}{D_o}$	0.10	0.12	0.14	0.16	0.18	0.20	0.22	0.24	0.25
a_0	0.55	0.63	0.71	0.79	0.87	0.95	1.03	1.11	1.15



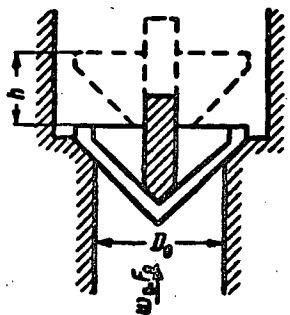
$\frac{F_p}{F_0}$	0.80	0.81	0.82	0.83	0.84	0.85	0.86	0.87
γ_0	1.60	1.48	1.36	1.23	1.14	1.02	0.92	0.80



$\frac{h}{D_o}$	0.125	0.14	0.16	0.18	0.20	0.22	0.24	0.25
β_1	111	88.4	67.5	53.5	43.3	35.8	30.0	27.7



Conical valve on conical seat

 Section IX
 Diagram 9-15


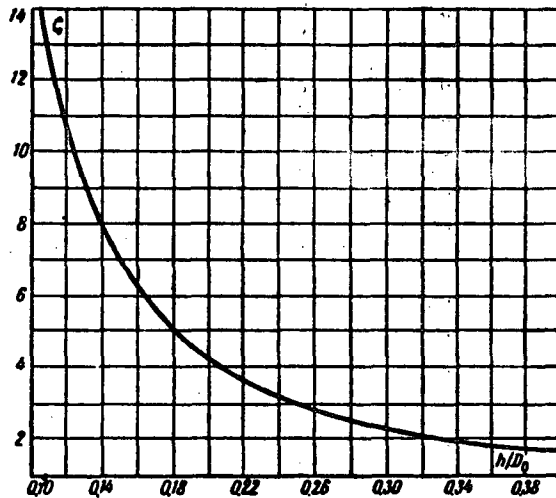
$$\zeta = \frac{\Delta H}{\gamma w_0^2} = 0.6 + \frac{0.15}{(h/D_0)^2}$$

is determined from the curve

$$\zeta = f\left(\frac{h}{D_0}\right).$$

 The formula is valid for $0.125 < \frac{h}{D_0} < 0.4$.

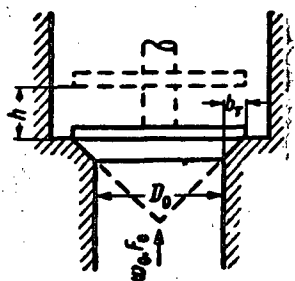
h/D_0	0.10	0.15	0.20	0.25	0.30	0.35	0.40
ζ	15.6	7.27	4.35	3.00	2.27	1.82	1.54



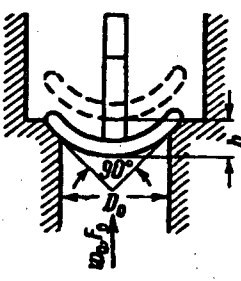
Conical valve on flat seat and ball valve on spherical seat

 Section IX
 Diagram 9-16

1. Conical valve



2. Ball valve



$$\zeta = \frac{\Delta H}{\gamma w_0^2} = 2.7 - \beta_1 + \beta_2,$$

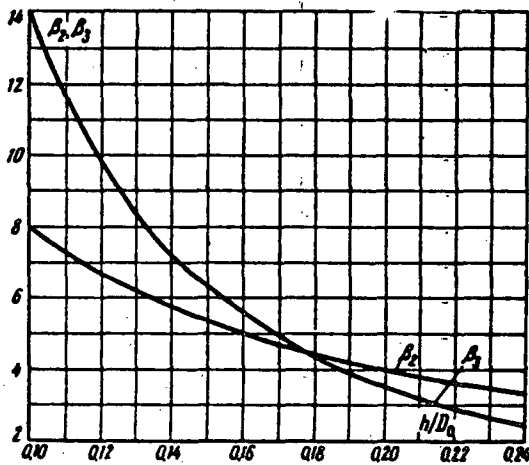
 where $\beta_1 = \frac{0.8}{h/D_0}$ is determined from curve $\beta_1 = f_1(h/D_0)$;

 $\beta_2 = \frac{0.14}{(h/D_0)^2}$ is determined from curve $\beta_2 = f_2(h/D_0)$;

The formula is valid for

$$0.1 < \frac{h}{D_0} < 0.25, \quad \frac{b_d}{D_0} = 0.1.$$

$\frac{h}{D_0}$	0.10	0.12	0.14	0.16	0.18	0.20	0.22	0.24	0.25
β_1	8.00	6.66	5.71	5.00	4.44	4.00	3.63	3.33	3.20
β_2	14.0	9.73	7.15	5.46	4.32	3.	2.90	2.43	2.24

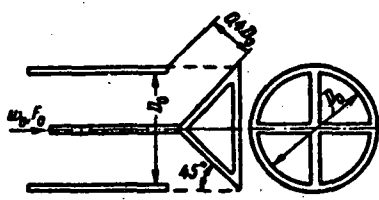


Ring-seal gate (free)

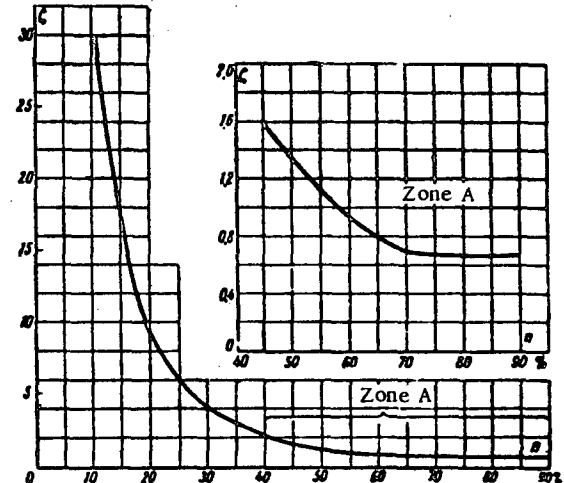
Section IX

Diagram 9-17

$n\%$	0	10	20	30	40	50	60	70	80	90	100
ζ	S	29.8	9.25	4.06	2.22	1.34	0.93	0.69	0.67	0.67	0.67



$$\zeta = \frac{\Delta H}{\frac{\gamma w_0^2}{2g}}$$
 is determined from curve $\zeta = f(n\%)$, where n is the degree of gate opening (%).

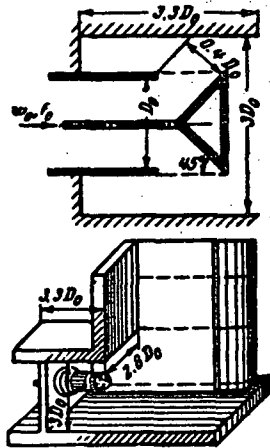


Ring-seal gate (in a chamber)

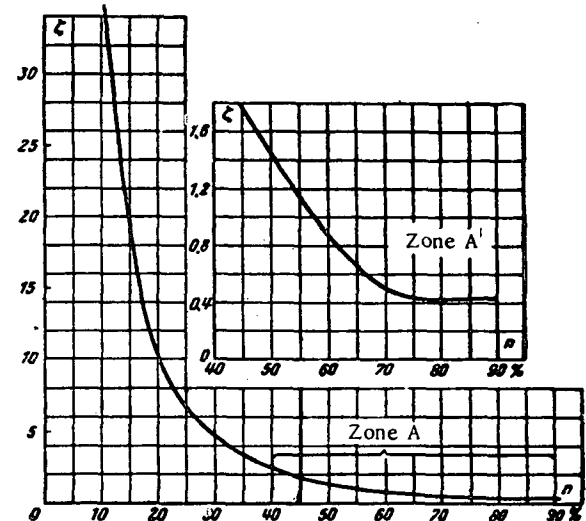
Section IX

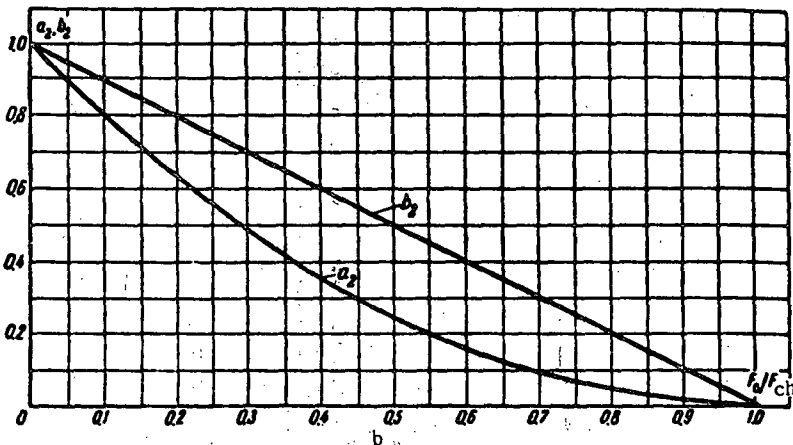
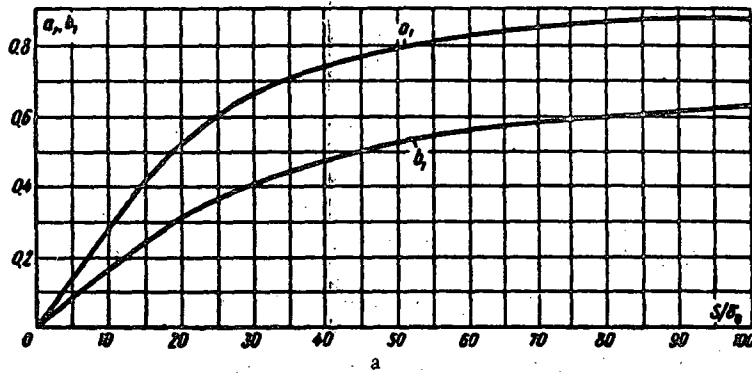
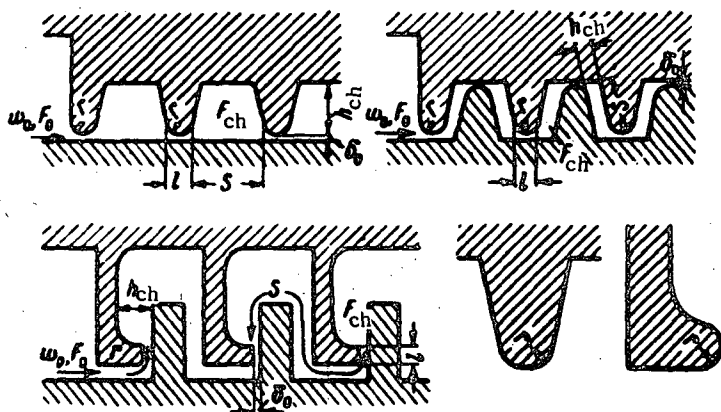
Diagram 9-18

$n\%$	0	10	20	30	40	50	60	70	80	90	100
ζ	S	36	10.6	4.85	2.45	1.45	0.89	0.50	0.43	0.43	0.43



$$\zeta = \frac{\Delta H}{\frac{\gamma w_0^2}{2g}}$$
 is determined from curve $\zeta = f(n\%)$, where n is the degree of gate opening (%).





\$F_0/F_{ch}\$	0.0	0.1	0.2	0.3	0.4	0.5	0.6	0.7	0.8	0.9	1.0
\$a_2\$	1.0	0.81	0.64	0.49	0.36	0.25	0.16	0.09	0.04	0.01	0
\$b_2\$	1.0	0.90	0.80	0.70	0.60	0.50	0.40	0.30	0.20	0.10	0

$$D_h = \frac{4F_0}{\Pi_0}; \quad \Pi_0 \text{ — perimeter}$$

$$1. \frac{h_{ch}}{s_0} > \frac{b_s}{s_0}:$$

$$\zeta = \frac{\Delta H}{\frac{1}{2} \frac{w_0^2}{g}} = 1 + \zeta' + z(a_1 + \zeta' b_1 + \zeta_{fr}).$$

$$2. \frac{h_{ch}}{s_0} < \frac{b_s}{s_0}:$$

$$\zeta = \frac{\Delta H}{\frac{1}{2} \frac{w_0^2}{g}} = 1 + \zeta' + z(a_2 + \zeta' b_2 + \zeta_{fr}).$$

where $a_1 = f_1 \left(\frac{s}{b_0} \right)$ and $b_1 = f_2 \left(\frac{s}{b_0} \right)$
are determined from graph a;

$$a_2 = \left(1 - \frac{F_0}{F_{ch}} \right)^2 \text{ and } b_2 = 1 - \frac{F_0}{F_{ch}}$$

are determined from graph b;

$$\zeta \text{ is determined as } \zeta = f \left(\frac{r}{D_h} \right)$$

from diagram 3-3;

$$\text{at } r/b_0 = 0, \zeta' = 0.5;$$

$$\zeta_{fr} = \lambda l/D_{hp};$$

λ is determined from diagrams 2-1 to 2-5;

z is the number of cells of the labyrinth;

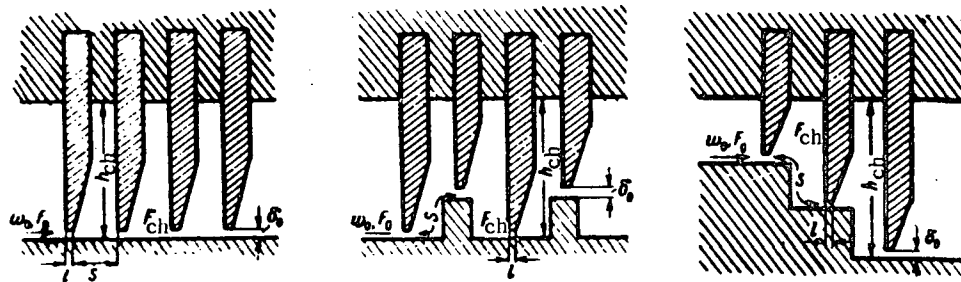
D_h is the hydraulic diameter of the gap;

F_0 is the area of the gap section;

F_{ch} is the area of the chamber cross section.

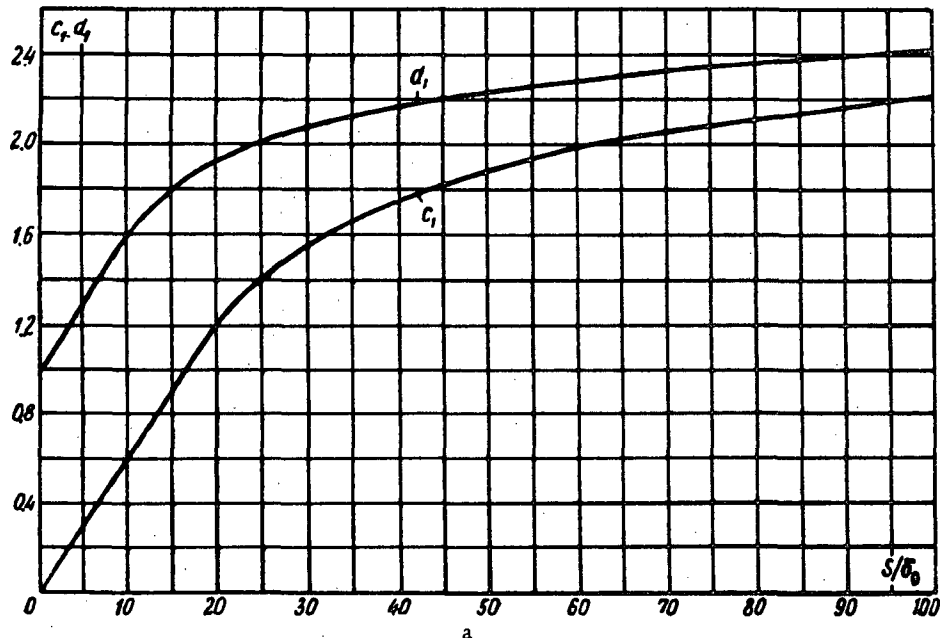
\$s/b_0\$	\$a_1\$	\$b_1\$
0	0	0
5	0.15	0.08
10	0.28	0.16
20	0.53	0.31
30	0.65	0.40
40	0.73	0.47
50	0.78	0.52
60	0.82	0.55
70	0.84	0.58
80	0.87	0.59
90	0.87	0.61
100	0.87	0.63

Comb-type labyrinth seal

 Section IX
 Diagram 9-20


$$1. \frac{h_{ch}}{\delta_0} > \frac{\delta_s}{\delta_0} : \\ \zeta = \frac{\Delta H}{\gamma w_0^2} = zc_1 + d_1$$

$$2. \frac{h_{ch}}{\delta_0} < \frac{\delta_s}{\delta_0} : \\ \zeta = \frac{\Delta H}{\gamma w_0^2} = zc_2 + d_2$$



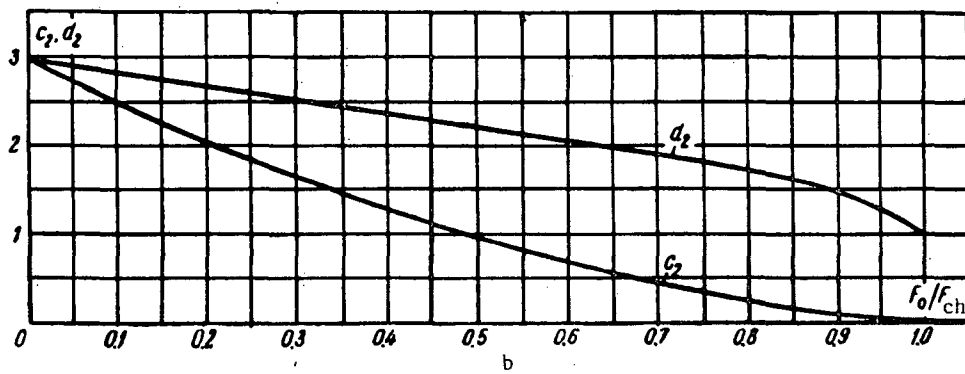
where $c_1 = f_1 \left(\frac{S}{\delta_0} \right)$ and $d_1 = f_2 \left(\frac{S}{\delta_0} \right)$
are determined from graph a;

$$c_2 = \left(1 + \frac{0.707}{\sqrt{1 - \frac{F_0}{F_{ch}}}} \right)^2 \left(1 - \frac{F_0}{F_{ch}} \right)^2$$

and

$$d_2 = \left(1 + 0.707 \sqrt{1 - \frac{F_0}{F_{ch}}} \right)^2$$

are determined from graph b;
 z is the number of cells of the labyrinth.



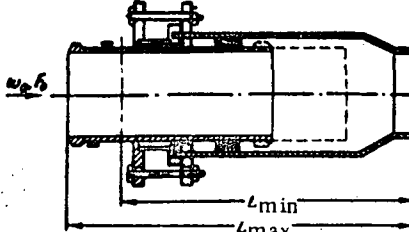
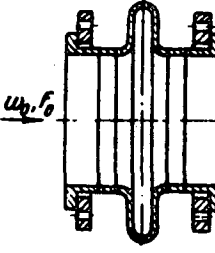
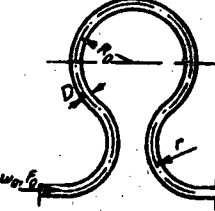
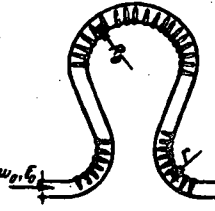
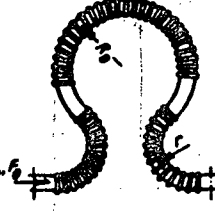
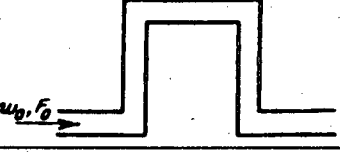
F ₀ /F _{ch}	0	0.1	0.2	0.3	0.4	0.5	0.6	0.7	0.8	0.9	1.0
c₁	2.92	2.50	2.05	1.67	1.32	1.00	0.72	0.47	0.27	0.11	0
d₁	2.92	2.81	2.68	2.54	2.39	2.25	2.09	1.92	1.73	1.50	1.0

S/\delta_0	c ₁	d ₁
0	0	1.00
5	0.32	1.31
10	0.63	1.62
20	1.24	1.96
30	1.60	2.10
40	1.78	2.19
50	1.92	2.26
60	2.02	2.32
70	2.10	2.36
80	2.16	2.40
90	2.20	2.42
100	2.26	2.46

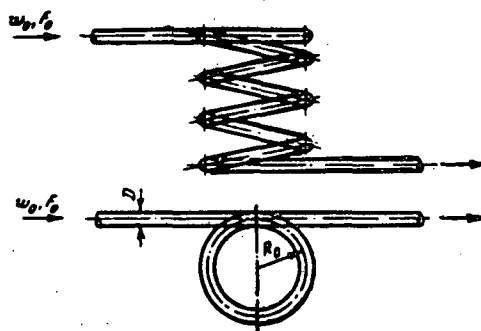
Various expansion joints

Section IX

Diagram 9-21

Type	View	Resistance coefficient $\zeta = \frac{\Delta H}{\frac{1}{2} w_0^2}$														
Stuffing box		$\zeta = 0.2$														
Bellows		<table border="1"> <thead> <tr> <th>D_0, mm</th><th>50</th><th>100</th><th>200</th><th>300</th><th>400</th><th>500</th></tr> </thead> <tbody> <tr> <td>ζ</td><td>1.7</td><td>1.6</td><td>1.6</td><td>1.8</td><td>2.1</td><td>2.3</td></tr> </tbody> </table>	D_0 , mm	50	100	200	300	400	500	ζ	1.7	1.6	1.6	1.8	2.1	2.3
D_0 , mm	50	100	200	300	400	500										
ζ	1.7	1.6	1.6	1.8	2.1	2.3										
Lyre-shaped, smooth $\frac{R_0}{d} = 6; \frac{r}{d} \approx 5$		<table border="1"> <thead> <tr> <th>D_0, min</th><th>50</th><th>100</th><th>200</th><th>300</th><th>400</th><th>500</th></tr> </thead> <tbody> <tr> <td>ζ</td><td>1.7</td><td>1.8</td><td>2.0</td><td>2.2</td><td>2.4</td><td>2.6</td></tr> </tbody> </table>	D_0 , min	50	100	200	300	400	500	ζ	1.7	1.8	2.0	2.2	2.4	2.6
D_0 , min	50	100	200	300	400	500										
ζ	1.7	1.8	2.0	2.2	2.4	2.6										
Lyre-shaped, with grooves $\frac{R_0}{d} \approx 6; \frac{r}{d} \approx 6$		<table border="1"> <thead> <tr> <th>D_0, mm</th><th>80</th><th>100</th><th>200</th><th>300</th><th>400</th><th>500</th></tr> </thead> <tbody> <tr> <td>ζ</td><td>2.0</td><td>2.2</td><td>2.5</td><td>2.8</td><td>3.1</td><td>3.5</td></tr> </tbody> </table>	D_0 , mm	80	100	200	300	400	500	ζ	2.0	2.2	2.5	2.8	3.1	3.5
D_0 , mm	80	100	200	300	400	500										
ζ	2.0	2.2	2.5	2.8	3.1	3.5										
Lyre-shaped, with corrugated tube $\frac{R_0}{d} \approx 5; \frac{r}{d} \approx 3.0$		<table border="1"> <thead> <tr> <th>D_0, mm</th><th>50</th><th>100</th><th>200</th><th>300</th><th>400</th><th>500</th></tr> </thead> <tbody> <tr> <td>ζ</td><td>3.0</td><td>3.3</td><td>3.7</td><td>4.2</td><td>4.6</td><td>5.0</td></tr> </tbody> </table>	D_0 , mm	50	100	200	300	400	500	ζ	3.0	3.3	3.7	4.2	4.6	5.0
D_0 , mm	50	100	200	300	400	500										
ζ	3.0	3.3	3.7	4.2	4.6	5.0										
Π-shaped		<table border="1"> <thead> <tr> <th>D_0, mm</th><th>50</th><th>100</th><th>200</th><th>300</th><th>400</th><th>500</th></tr> </thead> <tbody> <tr> <td>ζ</td><td>2.0</td><td>2.1</td><td>2.3</td><td>2.5</td><td>2.7</td><td>2.9</td></tr> </tbody> </table>	D_0 , mm	50	100	200	300	400	500	ζ	2.0	2.1	2.3	2.5	2.7	2.9
D_0 , mm	50	100	200	300	400	500										
ζ	2.0	2.1	2.3	2.5	2.7	2.9										

Coils

Section IX
Diagram 9-22

$$\zeta = \frac{\Delta H}{\frac{V^2}{2g}} \text{ is determined from diagram 6-3}$$

Complex passage from one volume to another through a 90° elbow

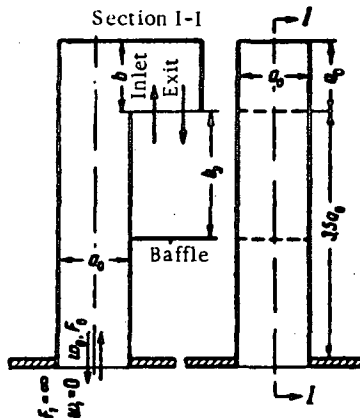
Section IX
Diagram 9-23

Elbow characteristic	View	Resistance coefficient $\zeta = \frac{\Delta H}{\frac{V^2}{2g}}$
With cut-off inlet (exit) stretch without vanes		$\zeta_{in} \approx 4.8$ $\zeta_{ex} \approx 3.7$
The same, but with vanes		$\zeta_{in} \approx 2.8$ $\zeta_{ex} \approx 2.3$
With inlet (exit) stretch of length $l_0 = a_0$, without vanes		$\zeta_{in} \approx 4.3$ $\zeta_{ex} \approx 3.7$
The same, but with vanes		$\zeta_{in} \approx 2.3$ $\zeta_{ex} \approx 1.7$

Complex passage from one volume to another through an
oblong 180° elbow

Section IX

Diagram 9-24



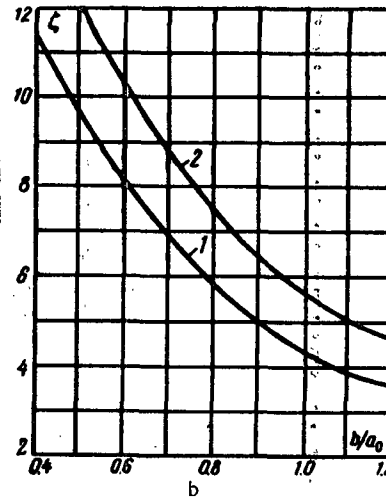
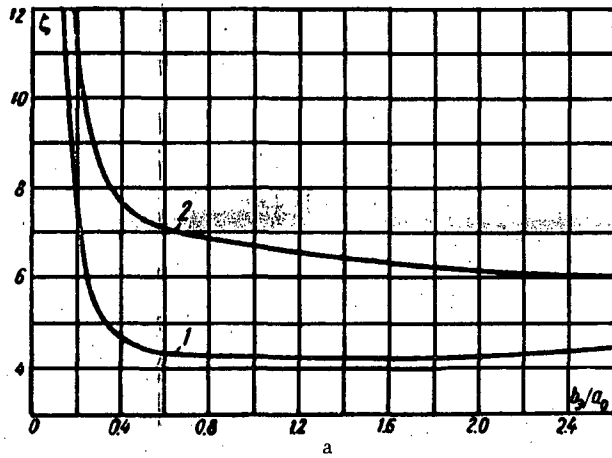
$$\zeta = \frac{\Delta H}{\frac{1}{2} u_0^2} \text{ is determined from the curves } \zeta = f\left(\frac{b}{a_0}\right)$$

1. With baffle, $\frac{b}{a_0} = 1.0$

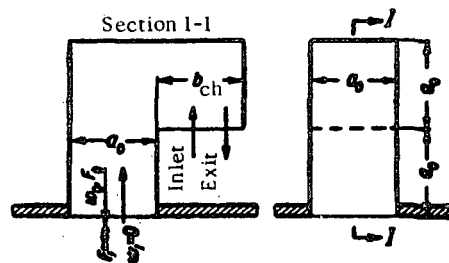
b/a_0	0.2	0.4	0.8	1.2	1.6	2.0	2.4	2.6
1. Inlet	7.3	4.6	4.3	4.3	4.3	4.3	4.4	4.4
2. Exit	13	7.6	6.8	6.6	6.3	6.1	6.0	5.9

2. Without baffle

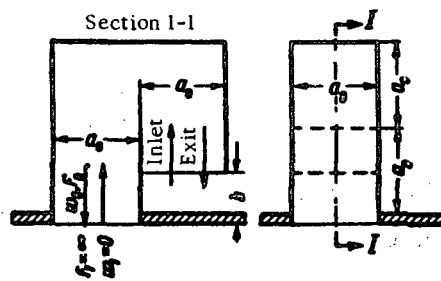
b/a_0	0.5	0.6	0.8	1.0	1.2	1.4
1. Inlet	9.5	8.0	5.8	4.4	3.6	3.2
2. Exit	12.0	10.1	7.4	5.7	4.6	4.1



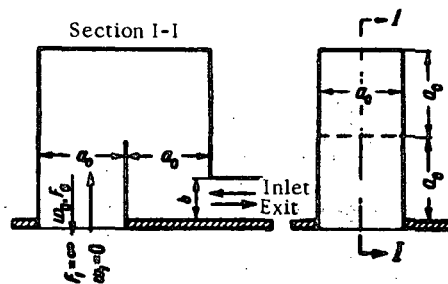
1. Short 180° elbow



2. Hood with three-sided inlet or exit



3. Hood with straight stretch at the inlet or exit



Complex passage from one volume to another through different labyrinth seals (continued)

Section IX

Diagram 9-25

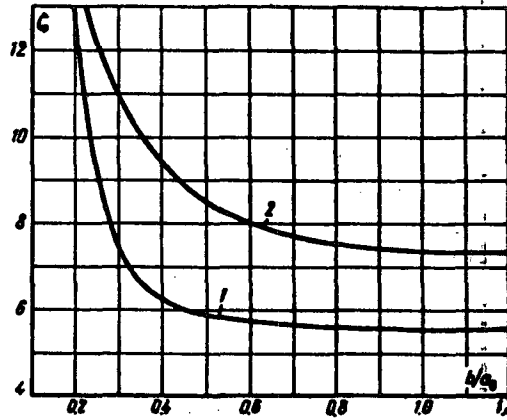
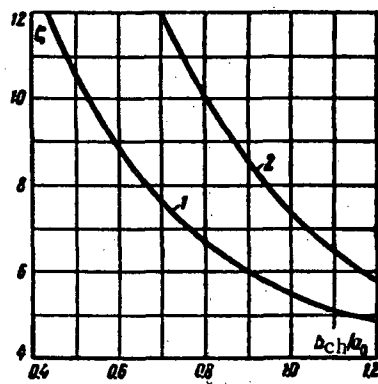
$$\xi = \frac{\Delta H}{\frac{\rho w_0^2}{2g}}$$
 is determined from the curves $\xi = f\left(\frac{b}{a_0}\right)$ or $\xi = \left(\frac{b_{ch}}{a_0}\right)$

1. Short 180° elbow

a_{ch}/a_0	0.5	0.6	0.8	1.0	1.2	1.4
1. Inlet						
ξ	11.0	9.0	6.7	5.5	4.9	4.5
2. Exit						
ξ	17.2	14.5	10.2	7.4	5.8	5.1

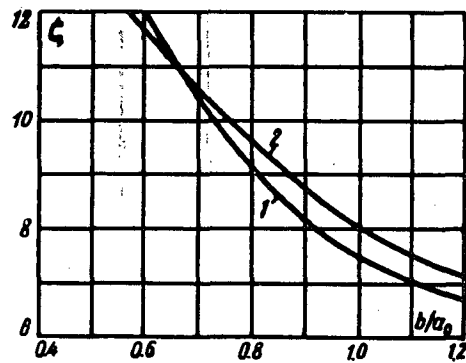
2. Hood with three-sided inlet or exit

b/a_0	0.18	0.2	0.4	0.6	0.8	1.0
1. Inlet						
ξ	13.3	12.4	6.2	5.7	5.6	5.5
2. Exit						
ξ	14.2	13.9	9.4	8.0	7.5	7.0



3. Hood with straight stretch at the inlet or exit

b/a_0	0.5	0.6	0.8	1.0	1.2	1.4
1. Inlet						
ξ	13.5	12.0	9.0	7.4	6.6	5.9
2. Exit						
ξ	13.0	11.7	9.5	8.0	7.1	6.3



Section Ten

FLOW PAST OBSTRUCTIONS IN A CONDUIT

(Resistance coefficients of stretches with projections, trusses, girders, and other obstructions)

10-1. LIST OF SYMBOLS

- F_0 = area of the conduit cross section before the obstruction, m^2 ;
 S_m = maximum cross section of a body, i.e., area of the projection of an obstruction in the pipe cross section, m^2 ;
 P_0 = perimeter of the section of the pipe or of the mine shaft (excavation), m;
 D_0 = diameter or side of the conduit cross section, m;
 d_m = characteristic dimension of the maximum cross section of the obstruction, m;
 $D_h = \frac{4F_0}{P_0}$ = hydraulic diameter of the conduit cross section, m;
 l = total length of the pipe stretch, m;
 l_1, l_2 = body length in the direction normal to the flow and the distance between adjacent obstructions arranged in a row, m;
 $\bar{l} = \frac{l_2}{d_m}$ = relative distance between adjacent obstructions arranged in a row;
 t = chord of the obstruction profile, m;
 $\bar{l} = \frac{t}{d_m}$ = relative length of obstruction;
 w_0 = mean stream velocity in the conduit before the obstruction, m/sec ;
 ΔH = pressure loss, kg/m^2 ;
 ζ = coefficient of local resistance of the obstruction in the conduit;
 c_x = drag coefficient of the obstruction;
 a_p = aerodynamic resistance coefficient of the mine shaft (or excavation), $\text{kg.sec}^2/\text{m}^4$;
 Re = Reynolds number of the conduit;
 Re' = Reynolds number of the obstruction.

10-2. EXPLANATIONS AND RECOMMENDATIONS

1. The resistance of conduit stretches containing obstructions is made up the resistance of the stretch proper and the resistance of the obstruction:

$$\zeta_{\text{sum}} = \frac{\Delta H}{\frac{\rho w_0^2}{2g}} = \zeta_{\text{st}} + \zeta, \quad (10-1)$$

where ζ_{st} is the resistance coefficient of the stretch; in the case of a straight stretch $\zeta_{\text{st}} = \zeta_{\text{fr}}$; ζ is the local resistance coefficient of the object placed in the conduit.

2. The coefficient of local resistance of a single object in a conduit is expressed as the drag coefficient of the object by the following formula, obtained by the author /10-5/:

$$\zeta = \frac{\Delta H}{\frac{\gamma w_0^2}{2g}} = c_x \frac{\frac{S_m}{F_0} k^3 \left(1 - \frac{2y}{D_0}\right)^{\frac{3}{m}}}{\left(1 - \frac{S_m}{F_0}\right)^3} = \frac{k_1 c_x \frac{S_m}{F_0} \left(1 - \frac{2y}{D_0}\right)^{\frac{3}{m}}}{\left(1 - \frac{S_m}{F_0}\right)^3}. \quad (10-2)$$

where

$$c_x = \frac{P_d}{\frac{\gamma w_0^2}{2g} S_m} \quad (10-3)$$

c_x is the drag coefficient of the object, depending on its shape, Reynolds number $Re' = \frac{w_0 d_m}{v}$, and other parameters, and is determined from the data of diagrams 10-1 to 10-13; P_d = drag force; S_m = mid-section of the object, m^2 ; d_m is the diameter or maximum width of its mid-section, m; y = distance of the center of gravity of an object from the channel axis, m; $k = \frac{w_{max}}{w_0}$ is the ratio of the maximum stream velocity in the free conduit to the mean velocity over its section; it is a function of the exponent m (cf. /10-1/) and is given in Table 10-1; m is a number depending on Reynolds number $Re = \frac{w_0 D_0}{v}$ of the conduit at steady velocity profile; it is given in Table 10-1; τ is a corrective coefficient, allowing for the influence of the shape and the mutual disposition of the separate objects; for smooth objects $\tau = 1.0$.

TABLE 10-1

Re	$4 \cdot 10^3$	$2.5 \cdot 10^4$	$2 \cdot 10^5$	$6 \cdot 10^5$	$3 \cdot 10^6$
m	5	6	7	8	9
k	1.32	1.26	1.23	1.20	1.17

At $Re > 6 \times 10^5$, m is practically equal to 9; in that case $k = 1.17$, and $k_1 = k^3 = 1.6$. This value of k_1 is true for objects of very small ratio of the mid-section to pipe section $\frac{S_m}{F_0}$ in the case of three-dimensional flow. The value of k_1 decreases with the increase of $\frac{S_m}{F_0}$ and tends toward unity. The values of k_1 given in the diagrams of this section have been approximated to allow for this fact.

3. The drag coefficient of oblong objects is determined by two factors: the frictional and the form resistances. This latter is a result of the stream separation from the object's surface and of the subsequent formation of eddies. The magnitude of these two resistance components and their ratio are a function of the body configuration and its position in the stream, the roughness of its surface, and Reynolds number. In the case of nonstreamlined bodies, the frictional resistance is very small compared with the

total drag. In the case of streamlined shapes, the frictional resistance and the form resistance are of comparable values.

4. The dependence of the drag coefficient of shapes such as a sphere, cylinder, etc. on the Reynolds number is very complex (Figure 10-1). The value of c_x is maximum at very small values of Re' ; decreasing with the increase of Re' , passes through a first minimum (at a value of $Re' \approx (2 \text{ to } 5) \times 10^3$), then increases somewhat and remains constant up to $Re' = (1 \text{ to } 2) \times 10^5$ (the critical Reynolds number). It then drops sharply to a second minimum ($Re' \approx 5 \times 10^5$), and increases negligibly to $Re' = 10^6$, where it becomes fairly constant.

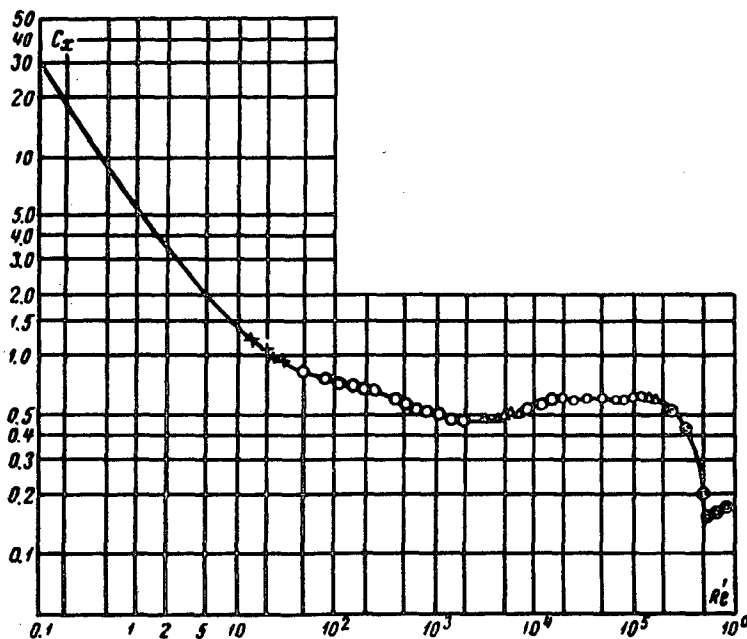


FIGURE 10-1. Drag coefficient of a sphere as a function of Reynolds number.

5. The flow pattern past spheres and cylinders is characterized by the absence of eddies at small values of Re' (Figure 10-2, a). The flow is purely laminar, and the resistance of the body is determined entirely by the viscosity forces. With the increase of the value of Re' the influence of the inertia forces begins to be felt, leading to the separation of the stream from the rear of the object (Figure 10-2, b).

The stream separation here is due to the same causes as in flow in a diffuser, i. e., to the increase of the pressure along the stream resulting from the decrease of velocity (§ 5-2). Therefore, at moderate values of Re' , when the boundary layer is still laminar and is characterized by a linear distribution of the velocities, giving a maximum thickness, the stream separation from the surface of the sphere or cylinder starts almost at its widest section (Figure 10-3, a).

With the further increase of Re' , the flow in the boundary layer passes from laminar to turbulent. This is accompanied by a decrease of the boundary layer thickness, and by an increased "fullness" of the velocity profile in the detached stream, which causes it to adhere again to the spherical surface. Since the inertia forces continue

to increase with the increase of Re' , the flow will separate once more after this adhesion; however, this will be a turbulent separation, taking place farther downstream beyond the widest section of the sphere. As a result, the eddy zone behind the sphere will be much narrower than with laminar separation (Figure 10-3, b).

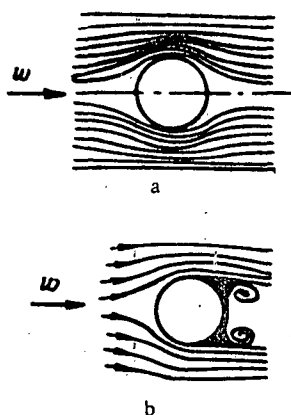


FIGURE 10-2. Pattern of flow past a sphere;

a—laminar flow without stream separation; b—flow with stream separation.

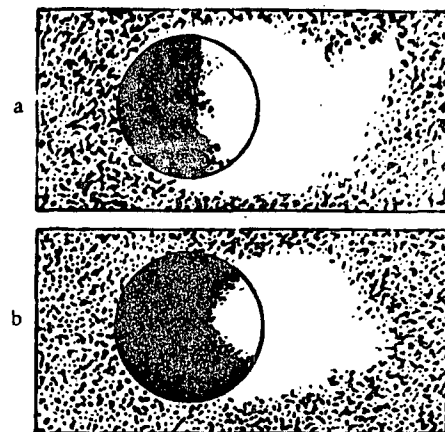


FIGURE 10-3. Pattern of flow past a sphere:

a—laminar boundary layer; b—turbulent boundary layer.

6. Transition of flow in the boundary layer from laminar to turbulent takes place at the critical value of Re' at which the value of c_x starts to drop sharply. The thickness of the zone of separation becomes a minimum at $Re' \approx 5 \times 10^5$, where c_x reaches the second minimum. The further small increase of c_x is probably explained by the state of the spherical surface, which starts to influence the resistance by the considerable decrease of boundary layer thickness at high values of Re' .

7. An artificial mixing of a stream impinging on a streamlined body, has the same effect as a natural mixing caused by the simple increase of Re' . The critical region in which a sharp drop of c_x is observed is shifted toward smaller values of Re' .

The value of c_x of nonstreamlined bodies does not materially vary with Re' and the degree of mixing of the stream. This may be seen from the instant the inertial forces exceed the viscous forces, since the separation point for nonstreamlined bodies is the same as for sharp corners.

8. The drag coefficient of a cylinder and other oblong bodies is a function of the relative length $t = \frac{t}{d_m}$ and increases with it.

9. When several objects are located in the same section of the pipe, the total coefficient of local resistance of these objects is calculated by the formula

$$\zeta = \frac{\Delta H}{\frac{\gamma w_0^2}{2g}} = k_1 \sum_{i=1}^n c_{xi} \frac{\frac{S_{mi}}{F_0} \left(1 - \frac{2y}{D_0}\right)^{\frac{3}{m}}}{\left(1 - \sum_{i=1}^n c_i \frac{S_{mi}}{F_0}\right)^2}, \quad (10-4)$$

where i is the ordinal number of the object of the given complex; n is total number of objects in the complex.

10. The total drag of two identical objects placed one behind the other in the stream direction is not equal to twice the drag of a single object; the drag coefficient of each of these objects and their total drag coefficient will be a function of the relative distance

$$\bar{l} = \frac{l_s}{d_m} \text{ between them.}$$

11. In the case of two cylinders placed close to each other in the stream flow, the rear cylinder will be completely immersed in the eddy zone created by the front one (Figure 10-4) and will not exert any drag. The rarefaction behind the first cylinder will be larger than the rarefaction behind the second and the resulting pressure gradient will cause the appearance of a force opposing the stream flow. This will cause the value of c_x for the rear cylinder to be negative, and the total drag coefficient of the two cylinders will be smaller than the drag coefficient of the first cylinder alone. The effect of "suction" of the rear cylinder toward the first one decreases with the increase of the distance between them; however, since the rear cylinder remains in the strongly mixed and slower "zone" of the first cylinder, its drag coefficient slowly approaches but remains lower than the value of c_x corresponding to an isolated cylinder, even with the increase of \bar{l} .

A lower value of c_x is obtained not only for cylinders, but also for any bodies located in the aerodynamic "shadow" of another body.

12. The mean value of the drag coefficient $c_{x,m}$ of a body placed in a longitudinal row of more than two bodies is smaller than the mean arithmetic value of $c_{x,m}$ of a couple of bodies, since the drag coefficient of each of the rear bodies is considerably smaller than the drag coefficient of the first body.

13. If several groups of bodies, arranged in longitudinal rows, are placed in a pipe, the coefficient of local resistance of a pipe stretch equal to one hydraulic diameter is calculated by the following formula /10-5/:

$$\lambda = \frac{\Delta H}{\frac{\rho w_0^2}{2g} \frac{L}{D_h}} = k_1 \sum_{i=1}^n c_{xi} \left(\frac{1}{\left(\frac{d_m}{D_h} \right)_i \bar{l}_i} \times \frac{\frac{S_m}{F_o} \left(1 - \frac{2y}{D_o} \right)^{\frac{3}{m}}}{\left(1 - \sum_{i=1}^n c_i \frac{S_m}{F_o} \right)} \right), \quad (10-5)$$

where i is the ordinal number of a body in a given complex or the ordinal number of a given longitudinal row of several bodies; n is the total number of longitudinal rows; c_{xi} is the drag coefficient of a single body belonging to the i -th row, determined as a function of the body profile shape, the Reynolds number Re' , and other parameters, by the data of diagrams 10-1 to 10-13.

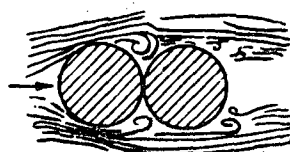


FIGURE 10-4. Flow past two cylinders placed close together.

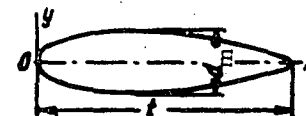


FIGURE 10-5. Profile of a streamlined body.

14. The coefficient of fluid resistance of all the bodies contained in the entire stretch considered will be equal to

$$\zeta = \frac{\Delta H}{\frac{\gamma w_0^2}{2g}} = \lambda \frac{L}{D_h} . \quad (10-6)$$

The friction coefficient of a straight pipe stretch of the same length is:

$$\zeta_{st} = \zeta_{fr} = \frac{\Delta H}{\frac{\gamma w_0^2}{2g}} = \lambda_{fr} \frac{L}{D_h} . \quad (10-7)$$

Hence

$$\zeta = \frac{\Delta H}{\frac{\gamma w_0^2}{2g}} = (\lambda + \lambda_{fr}) \frac{L}{D_h} , \quad (10-8)$$

where λ_{fr} is friction coefficient of unit pipe length, determined as λ from the data of diagrams 2-1 to 2-5.

15. An important factor influencing the drag coefficient of a body is the shape of its profile. The more streamlined the body, the smaller is the stream separation and formation of eddies and, therefore, the smaller is the drag coefficient. Streamlined bodies should thus be used wherever possible. The streamlined shape is characterized by a smoothly rounded nose and a tapering tail (Figure 10-5).

The sharper the contraction of the profile beyond the mid-section, the earlier will the separation occur upstream, and the more intense will be the formation of eddies behind the body. A correct selection of the tail profile can lead to a considerable shift of the beginning of separation toward the trailing edge of the body, or even to the avoidance of separation altogether.

16. The values of the dimensionless coordinates of several streamlined profiles are given in Table 10-2.

TABLE 10-2

	$\frac{x}{l_1}$	0	0.05	0.10	0.20	0.3	0.4	0.5	0.6	0.7	0.8	0.9	0.95	1.0
Profile No. 1	$\frac{2y}{d_m}$	0	0.528	0.720	0.917	0.987	1.00	0.960	0.860	0.738	0.568	0.340	0.195	0
Profile No. 2	$\frac{2y}{d_m}$	$r^* = 0.08^*$	0.490	0.750	0.960	1.00	0.980	0.930	0.840	0.720	0.560	0.370	—	$r^* = 0.10^*$
Profile No. 3	$\frac{2y}{d_m}$	0	0.530	0.720	0.940	1.00	0.995	0.940	0.860	0.910	0.520	0.300	—	0

* r^* is the radius of curvature of the profile nose and tail.

17. Elliptical cylinders and circular cylinders with tail fairings, likewise belong to the category of streamlined bodies. The drag coefficient of these bodies is higher than that of bodies shaped according to the data of Table 10-2. In view of their great simplicity, however, they are frequently used in practice.

18. The drag coefficient of systems of interconnected bodies, such as beams or trusses, is a function of their cross-section shape, the method of connecting the beams, the direction of impinging stream, and Reynolds number. The influence of the direction of the impinging stream for such a system is more complex than for a single body, since here the rear elements are oriented differently in relation to the aerodynamic shadow of the front elements (Figure 10-6).

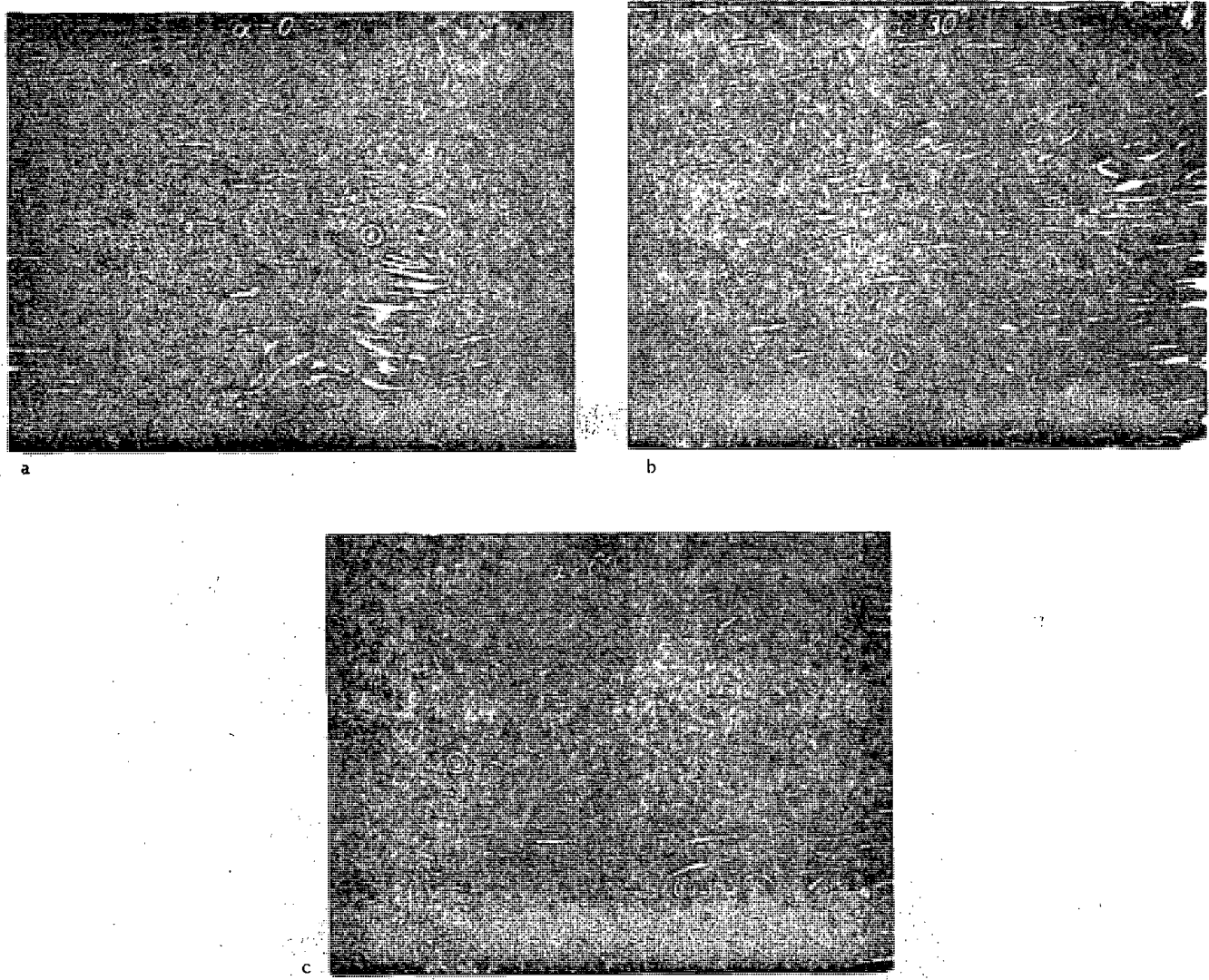


FIGURE 10-6. Pattern of stream flow past truss systems.

19. The coefficient of local resistance of a truss placed in a pipe is approximately determined by the formula:

$$\zeta = \frac{\Delta H}{\frac{Tw_0^2}{2g}} \cong 1.15 c_{ra}^* \frac{S_m/F_0}{\left(1 - \frac{S_m}{F_0}\right)^3}, \quad (10-9)$$

where in the given case

$\frac{S_m}{F_0} = \varphi' \frac{S}{F_0}$ = filling ratio of the pipe section by the truss elements;

$\varphi' = \frac{S_m}{S}$ = filling coefficient of the truss proper;

$c_{xa}^* = \text{drag coefficient of the truss at given Reynolds number } Re' = \frac{\omega d_m}{v}$ and given angle α of the impinging stream; it is determined by the formula (cf. Khanzhonkov's paper /10-6/):

$$c_{xa}^* = c_{xa} \frac{c_{x0}^*}{c_{x0}}, \quad (10-10)$$

where c_{x0} is the drag coefficient of the truss at $\alpha = 0$ and $Re' = Re'_1$; c_{x0}^* is the drag coefficient of the truss at $\alpha = 0$ and the given Re' ; c_{xa} is the drag coefficient of the truss at the given α and the value of Re' at which the relationship $c_{xa} = f(\alpha)$ was obtained.

20. The calculations of mine shafts and excavations are based on the dimensional coefficient of aerodynamic resistance, expressed by the following formula through the coefficient of local resistance λ :

$$\alpha_p = \frac{\gamma}{2g} \frac{\lambda}{4} [\text{kg} \cdot \text{sec}^2 / \text{m}^4]. \quad (10-11)$$

The resistance of the mine (excavation) is expressed by the following formula through the coefficient α_p :

$$\Delta H = \alpha_p \omega_0^2 \frac{4L}{D_h} = \alpha_p \left(\frac{Q}{F_0} \right)^2 \frac{\Pi_0}{F_0} L [\text{kg} / \text{m}^2]. \quad (10-12)$$

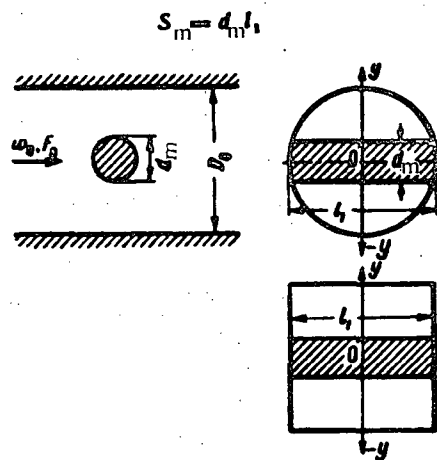
**10-3. LIST OF THE DIAGRAMS OF RESISTANCE COEFFICIENTS
OF SECTION X**

Diagram description	Source	Diagram number	Note
Single smooth cylinder placed in a pipe. Plane-parallel flow	/10-12/	10-1	c_x — according to the experimental data of the authors; calculating formula — according to the author's recommendations
Single stay rods and braces placed in a pipe. Plane-parallel flow	Kuznetsov /10-3/, Flaksbart /10-13/, Chesalov /10-8/, Yur'ev and Lesnikova /10-9/, Hütte /10-15/	10-2	
Single rolled sections placed in a pipe. Plane-parallel flow	/10-12/, Skochinskii, Ksenofontova, Kharev and Idel'chik /10-5	10-3	The same
Sphere placed in a pipe. Three-dimensional flow	/10-12/, Hütte /10-15/	10-4	" "
Smooth elliptical cylinder placed singly in a pipe. Three-dimensional flow	The same	10-5	" "
Single bodies of different shapes placed in a pipe. Three-dimensional flow	" "	10-6	" "
Single ellipsoid placed in a pipe. Three-dimensional flow	" "	10-7	" "
Circular cylinders placed in pairs in a pipe. Plane-parallel flow. $Re > 10^5$	Kuznetsov /10-4/	10-8	" "
Circular plates placed in pairs in a pipe. Three-dimensional flow.	/10-12/, Hütte /10-15/	10-9	" "
Rolled sections arranged in a row in a pipe. Plane-parallel flow	Skochinskii, Ksenofontova, Kharev and Idel'chik /10-5/	10-10	" "
Pipe reinforced by various stay rods and braces across the section	The same	10-11	" "
Triangular truss placed in a pipe. Plane-parallel flow	Khanzhonkov /10-6/	10-12	" "
Square truss placed in a pipe. Plane-parallel flow	The same	10-13	" "

10-4. DIAGRAMS OF THE RESISTANCE COEFFICIENTS

Single smooth cylinder placed in a pipe. Plane-parallel flow

Section X
Diagram 10-1



$$\zeta = \frac{\Delta H}{\frac{1}{2} w_0^2} \cong 1.15 c_x \frac{\frac{S_m}{F_0}}{\left(1 - \frac{S_m}{F_0}\right)} \left(1 - \frac{2y}{D_0}\right)^{\frac{1}{3}}$$

where c_x is taken from the curve $c_x = f(Re')$:

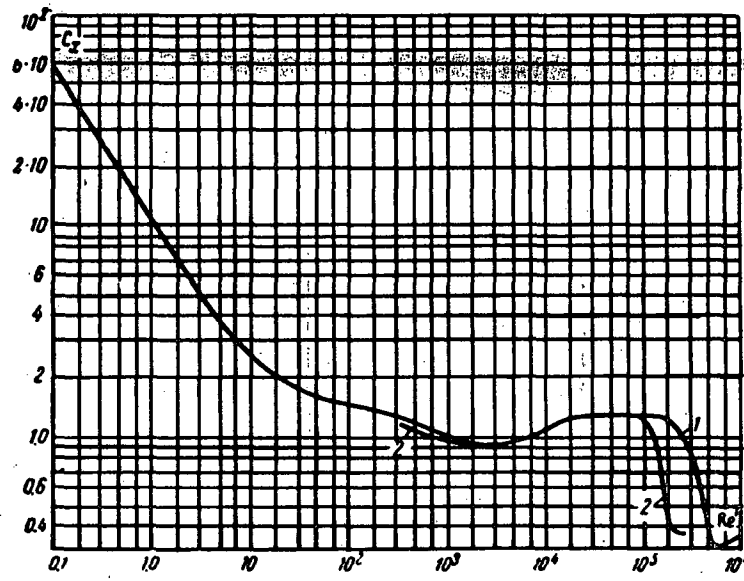
$$Re' = \frac{w_0 d_m}{v}$$

v is taken from § 1-3, b.

Re'	0.1	0.5	1.0	5	10	$5 \cdot 10^1$	10^2	$5 \cdot 10^2$	10^3	$5 \cdot 10^3$	10^4	$5 \cdot 10^4$	10^5	$2 \cdot 10^5$	$3 \cdot 10^5$	$4 \cdot 10^5$	$5 \cdot 10^5$	$6 \cdot 10^5$	$7 \cdot 10^5$	$8 \cdot 10^5$	10^6
-------	-----	-----	-----	---	----	----------------	--------	----------------	--------	----------------	--------	----------------	--------	----------------	----------------	----------------	----------------	----------------	----------------	----------------	--------

	1. Small turbulence																				
c_x	59.0	22.5	10.0	4.50	2.65	1.65	1.50	1.20	1.00	0.90	1.05	1.25	1.25	1.20	1.10	0.80	0.60	0.32	0.30	0.32	0.35

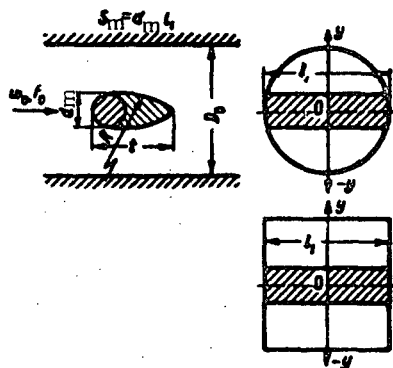
	2. Large turbulence																			
c_x	-	-	-	-	-	-	-	1.12	0.95	0.90	1.05	1.25	1.20	0.40	0.35	-	-	-	-	-



Single stay rods and braces placed in a pipe. Plane-parallel flow

Section X

Diagram 10-2



$$\zeta = \frac{\Delta H}{\frac{1}{2} \rho u_0^2} \approx 1.15 c_x \frac{\frac{S_m}{F_0}}{\left(1 - \frac{2y}{D_0}\right)^3} \left(1 - \frac{2y}{D_0}\right)^{1/3},$$

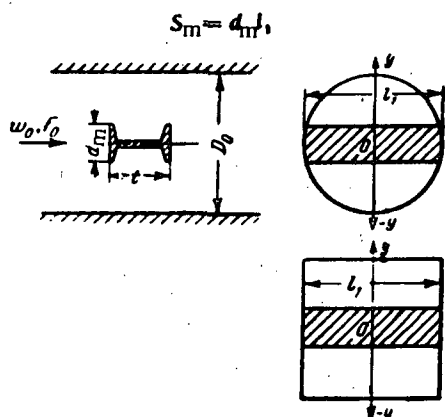
where c_x and τ are taken from the tables given here;
 τ is taken from § 1-3, b.

Type	Sectional view	Drag coefficient				
Circular cylinder with fairing at $Re' = \frac{\omega_0 d_m}{v} > 10^4$		t/d_m	2	3	3.5	4.0
		R/d_m	0	4.0	6.0	8.0
		c_x	0.20	0.10	0.07	0.06
Streamlined rod at $Re' = \frac{\omega_0 d_m}{v} > 10^4$		t/d_m	2	3	4	5
		c_x	0.09	0.06	0.06	0.08
		τ	1.0	0.10	0.10	0.19
Plate with rounded edges $r/d_m = 0.5$		$Re' = \frac{\omega_0 d_m}{v}$	$5 \cdot 10^5$	$2 \cdot 10^6$		
		c_x	0.78	0.66		
Wedge-shaped plate $d_1/t = 0.0417$; $\frac{d_2}{t} = 0.025$		$Re' = \frac{\omega_0 d}{v}$	$5 \cdot 10^5$	$2 \cdot 10^6$		
		c_x	0.53	0.46		
Square beam		α°	0	10	20	30
		c_x	2.00	1.43	1.35	1.50
		τ	≈ 1.5	1.52	1.54	

Single rolled sections placed in a pipe. Plane-parallel flow

Section X

Diagram 10-3



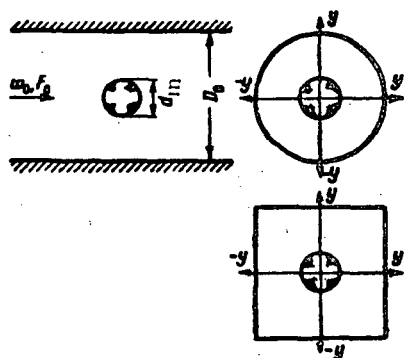
$$\xi = \frac{\Delta H}{\gamma w_0^2} \approx 1.15 c_x \frac{S_m}{F_e} \left(1 - \frac{2y}{D_0}\right)^{\frac{1}{3}}$$

where c_x and τ are taken from the table corresponding to the given profile for the indicated angle α° .

Rolled section	c_x	τ	Source
	2.76	1.5	10-21
	2.88	1.5	—
	2.68	1.5	—
	1.66	1.5	—
	1.76	1.5	—
	2.2	1.5	—

Rolled section	c_x	τ	Source
	1.20	1.5	10-51
	2.08	1.5	10-121
	0.80	1.5	10-51
	0.15	1.0	—
	0.50	1.0	—
	0.30	1.0	—
	2.40	1.5	—

$$S_m = \frac{\pi d_m^2}{4}$$



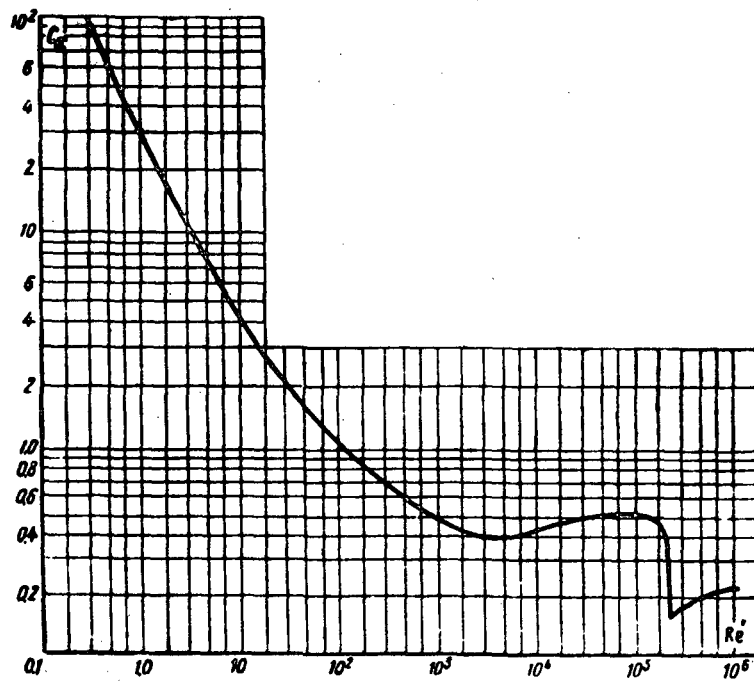
$$\zeta = \frac{\Delta H}{\frac{\gamma w_0^2}{2g}} \approx 1.30 c_x \frac{S_m}{F_0} \left(1 - \frac{2y}{D_0}\right)^{\frac{1}{3}}$$

where c_x is taken from the curve $c_x = f(\text{Re}')$:

$$\text{Re}' = \frac{w_0 d_m}{v}$$

v is taken from § 1-3, b.

Re'	0.5	1.0	5	10	5·10	10 ²	5·10 ²	10 ³	5·10 ³	10 ⁴
c_x	75.0	30.0	9.00	4.00	1.75	1.00	0.61	0.48	0.38	0.40
Re'	5·10 ⁴	10 ⁵	2·10 ⁵	3·10 ⁵	4·10 ⁵	6·10 ⁵	7·10 ⁵	8·10 ⁵	10 ⁶	
c_x	0.49	0.50	0.49	0.40	0.18	0.20	0.20	0.21	0.22	

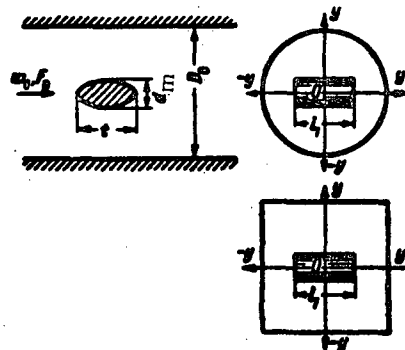


Smooth elliptical cylinder placed in a pipe.
Three-dimensional flow

Section X

Diagram 10-5

$$S_m = d_m l_s$$



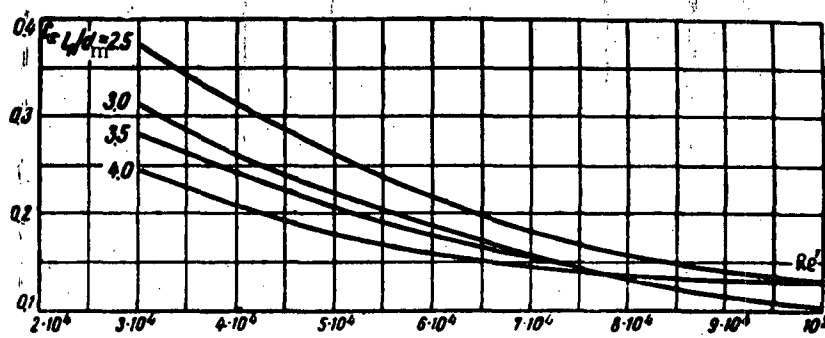
$$\xi = \frac{\Delta H}{\frac{w_0^2}{2g}} \approx 1.30 c_x \frac{\frac{S_m}{F_o}}{\left(1 - \frac{S_m}{F_o}\right)^3} \left(1 - \frac{2y}{D_o}\right)^{\frac{1}{3}}.$$

where c_x is taken from the curves $c_x = f(Re')$ corresponding to different l/d_m

$$Re' = \frac{w_0 d_m}{v};$$

\downarrow is taken from § 1-3, b.

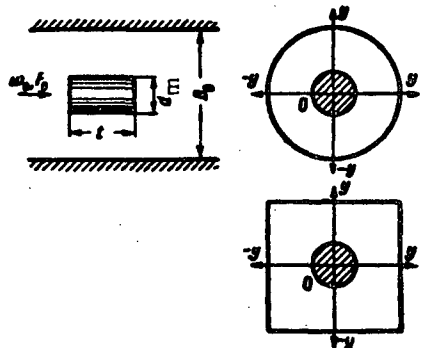
Re'	$3 \cdot 10^4$	$4 \cdot 10^4$	$5 \cdot 10^4$	$6 \cdot 10^4$	$7 \cdot 10^4$	$8 \cdot 10^4$	$9 \cdot 10^4$	10^5
c_x	0.38	0.31	0.26	0.22	0.18	0.16	0.14	0.13
	$l/d_m = 2.5$							
c_x	0.32	0.26	0.22	0.19	0.16	0.14	0.12	0.11
	$l/d_m = 3.0$							
c_x	0.28	0.24	0.21	0.18	0.16	0.14	0.12	0.11
	$l/d_m = 3.5$							
c_x	0.25	0.21	0.18	0.16	0.15	0.14	0.13	0.13
	$l/d_m = 4.0$							



Single bodies of different shapes placed in a pipe.
Three-dimensional flow

Section X

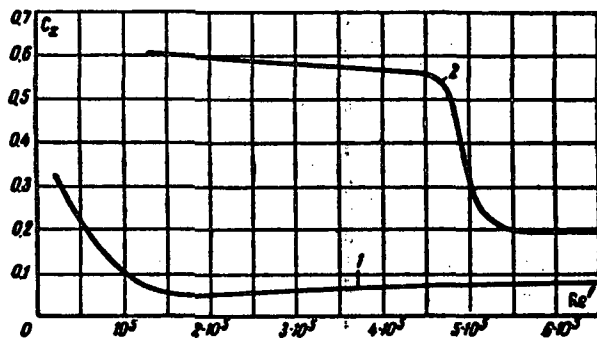
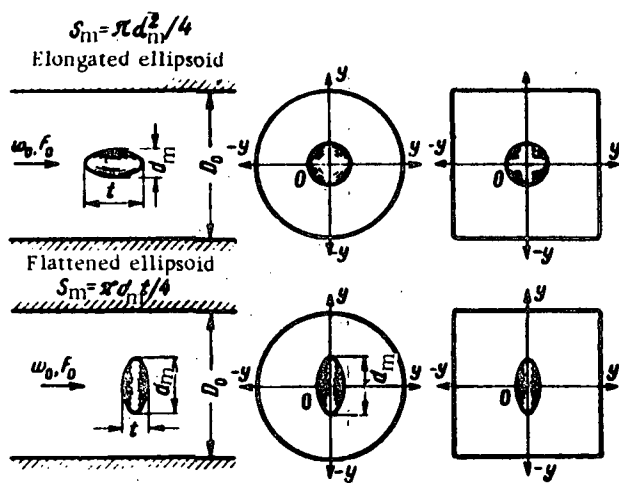
Diagram 10-6



$$\xi = \frac{\Delta H}{\frac{1}{2} \rho v_0^2} \approx 1.30 c_x \frac{\frac{S_m}{F_0}}{\left(1 - \frac{S_m}{F_0}\right)} \left(1 - \frac{2y}{D_0}\right)^{\frac{1}{3}},$$

where c_x and τ are taken from the tables given here;
 v is taken from § 1-3, b.

Type	View	Drag coefficient c_x																
Convex hemisphere		$c_x = 0.34; \tau \approx 1.0$																
Concave hemisphere		$c_x = 1.33; \tau \approx 2.5$																
Smooth cylinder, axis parallel to direction of flow		<table border="1" style="margin-left: auto; margin-right: auto;"> <tr> <td>t/d_m</td><td>1</td><td>2</td><td>3</td><td>4</td><td>5</td><td>6</td><td>7</td></tr> <tr> <td>c_x</td><td>0.91</td><td>0.85</td><td>0.85</td><td>0.87</td><td>0.90</td><td>0.95</td><td>0.99</td></tr> </table> $\tau \approx 1.5$	t/d_m	1	2	3	4	5	6	7	c_x	0.91	0.85	0.85	0.87	0.90	0.95	0.99
t/d_m	1	2	3	4	5	6	7											
c_x	0.91	0.85	0.85	0.87	0.90	0.95	0.99											
Smooth cylinder, axis perpendicular to direction of flow		<table border="1" style="margin-left: auto; margin-right: auto;"> <tr> <td>$\frac{d_m}{t_1}$</td><td>0</td><td>0.025</td><td>0.10</td><td>0.20</td><td>0.50</td><td>1.0</td></tr> <tr> <td>c_x</td><td>1.20</td><td>0.98</td><td>0.82</td><td>0.74</td><td>0.68</td><td>0.63</td></tr> </table> $t \approx 1.2$	$\frac{d_m}{t_1}$	0	0.025	0.10	0.20	0.50	1.0	c_x	1.20	0.98	0.82	0.74	0.68	0.63		
$\frac{d_m}{t_1}$	0	0.025	0.10	0.20	0.50	1.0												
c_x	1.20	0.98	0.82	0.74	0.68	0.63												
Cone		<table border="1" style="margin-left: auto; margin-right: auto;"> <tr> <td>α°</td><td>30</td><td>50</td><td>$\tau \approx 1.2$</td></tr> <tr> <td>c_x</td><td>0.35</td><td>0.51</td><td></td></tr> </table>	α°	30	50	$\tau \approx 1.2$	c_x	0.35	0.51									
α°	30	50	$\tau \approx 1.2$															
c_x	0.35	0.51																
Square beam		<table border="1" style="margin-left: auto; margin-right: auto;"> <tr> <td>α°</td><td>0</td><td>10</td><td>20</td><td>30</td><td>40</td><td>50</td></tr> <tr> <td>c_x</td><td>1.58</td><td>1.12</td><td>0.80</td><td>0.87</td><td>0.89</td><td>0.90</td></tr> </table> $\tau \approx 1.5$	α°	0	10	20	30	40	50	c_x	1.58	1.12	0.80	0.87	0.89	0.90		
α°	0	10	20	30	40	50												
c_x	1.58	1.12	0.80	0.87	0.89	0.90												



$$\zeta = \frac{\Delta H}{\frac{1}{2} w_0^2} \approx 1.30 c_x \frac{\frac{S_m}{F_c}}{\left(1 - \frac{S_m}{F_c}\right)^3} \left(1 - \frac{2y}{D_c}\right)^{\frac{1}{3}}$$

where c_x is taken from the curves $c_x = f(Re')$ for the different ellipsoids;

$$Re' = \frac{w_0 d_m}{v}$$

v is taken from § 1-3, b.

Re'	$2 \cdot 10^4$	$5 \cdot 10^4$	10^5	$2 \cdot 10^5$	$3 \cdot 10^5$	$4 \cdot 10^5$	$5 \cdot 10^5$	$6 \cdot 10^5$
-------	----------------	----------------	--------	----------------	----------------	----------------	----------------	----------------

1. Elongated ellipsoid $t/d_m = 5/9$

c_x	0.32	0.22	0.10	0.05	0.06	0.07	0.075	0.08
-------	------	------	------	------	------	------	-------	------

2. Flattened ellipsoid $t/d_m = 4/3$

c_x	-	-	0.62	0.59	0.58	0.57	0.31	0.20
-------	---	---	------	------	------	------	------	------

Diagram 10-6 (continued)

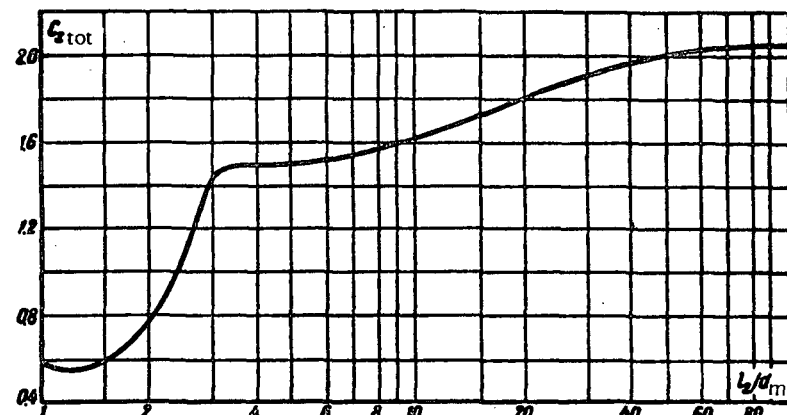
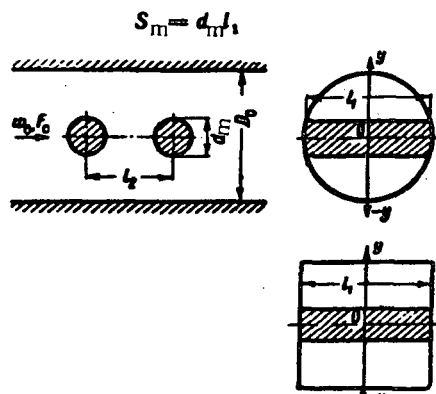
Type	View	Drag coefficient c_x																												
Rectangular plate	 $w_0 f_0$ $S_m = d_m l_s$	<table border="1"> <tr> <td>$\frac{d_m}{l_s}$</td> <td>0</td> <td>0.05</td> <td>0.10</td> <td>0.20</td> <td>0.25</td> <td>0.35</td> <td>0.50</td> <td>1.0</td> </tr> <tr> <td>c_x</td> <td>2.00</td> <td>1.40</td> <td>1.29</td> <td>1.21</td> <td>1.19</td> <td>1.17</td> <td>1.15</td> <td>1.10</td> </tr> </table> <p>$\tau \approx 1.5$</p>	$\frac{d_m}{l_s}$	0	0.05	0.10	0.20	0.25	0.35	0.50	1.0	c_x	2.00	1.40	1.29	1.21	1.19	1.17	1.15	1.10										
$\frac{d_m}{l_s}$	0	0.05	0.10	0.20	0.25	0.35	0.50	1.0																						
c_x	2.00	1.40	1.29	1.21	1.19	1.17	1.15	1.10																						
Washer	 $w_0 f_0$ $S_m = \frac{\pi}{4} (D^2 - d^2)$	<table border="1"> <tr> <td>$\frac{d}{D}$</td> <td>0</td> <td>0.1</td> <td>0.2</td> <td>0.3</td> <td>0.4</td> <td>0.5</td> </tr> <tr> <td>c_x</td> <td>1.10</td> <td>1.14</td> <td>1.15</td> <td>1.18</td> <td>1.20</td> <td>1.22</td> </tr> <tr> <td>$\frac{d}{D}$</td> <td>0.6</td> <td>0.7</td> <td>0.8</td> <td>0.9</td> <td>1.0</td> <td></td> </tr> <tr> <td>c_x</td> <td>1.25</td> <td>1.40</td> <td>1.78</td> <td>1.92</td> <td>2.00</td> <td></td> </tr> </table> <p>$\tau \approx 1.5$</p>	$\frac{d}{D}$	0	0.1	0.2	0.3	0.4	0.5	c_x	1.10	1.14	1.15	1.18	1.20	1.22	$\frac{d}{D}$	0.6	0.7	0.8	0.9	1.0		c_x	1.25	1.40	1.78	1.92	2.00	
$\frac{d}{D}$	0	0.1	0.2	0.3	0.4	0.5																								
c_x	1.10	1.14	1.15	1.18	1.20	1.22																								
$\frac{d}{D}$	0.6	0.7	0.8	0.9	1.0																									
c_x	1.25	1.40	1.78	1.92	2.00																									

Circular cylinders placed in pairs in a pipe. Plane parallel

$$\text{flow. } \text{Re} = \frac{w_0 d_m}{\nu} > 10^5$$

Section X

Diagram 10-8



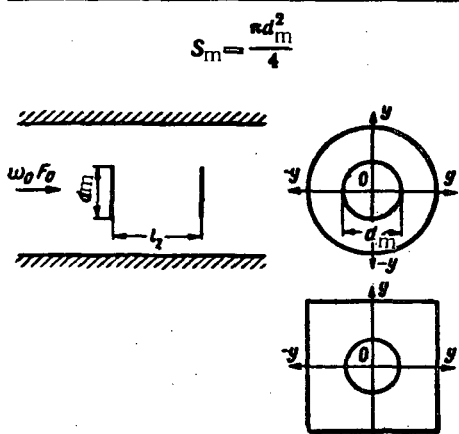
l_2/d_m	1.0	1.5	2.0	2.5	3.0	4.0	5.0	10	20	30	50	100
c_x, tot	0.60	0.60	0.76	1.10	1.44	1.50	1.52	1.62	1.82	1.92	2.0	2.06

$$\xi = \frac{\Delta H}{\frac{1}{2} w_0^2} \approx 1.15 c_x, \text{tot} \cdot \frac{\frac{S_m}{F_o}}{\left(1 - \frac{S_m}{F_o}\right)^3} \left(1 - \frac{2y}{D_o}\right)^{\frac{1}{3}},$$

where c_x, tot is taken from the curve $c_x, \text{tot} = f\left(\frac{l_2}{d_m}\right)$;
 y is taken from § 1-3, b.

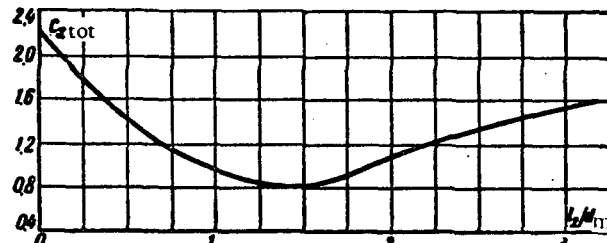
Circular plates placed in pairs in a pipe. Three-dimensional flow

Section X
Diagram 10-9



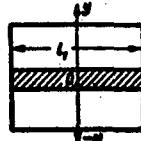
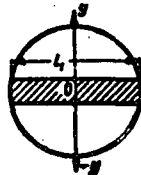
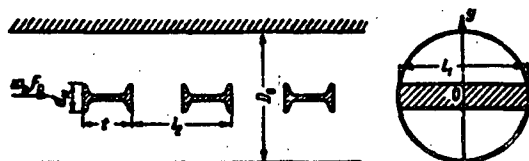
$$\xi = \frac{\Delta H}{\frac{1}{2} w_0^2} \approx 1.30 c_x, \text{tot} \cdot \frac{\frac{S_m}{F_o}}{\left(1 - 1.5 \frac{S_m}{F_o}\right)^3} \left(1 - \frac{2y}{D_o}\right)^{\frac{1}{3}},$$

where c_x, tot is taken from the curves $c_x, \text{tot} = f\left(\frac{l_2}{d_m}\right)$



l_2/d_m	0	0.25	0.5	0.75	1.0	1.25	1.5	1.75	2.0	2.5	3.0
c_x, tot	2.22	1.80	1.40	1.18	0.98	0.84	0.80	0.88	1.05	1.30	1.52

$$S_m = d_m l; D_h = \frac{4F_0}{\Pi_0}; \Pi_0 - \text{perimeter}$$



$$\zeta = \frac{\Delta H}{\gamma u_0^2} \approx 1.15 \frac{c_{x1}}{d_m} \frac{1}{l} \left(\frac{S_m}{1 - \epsilon \frac{S_m}{F_0}} \right)^{\frac{1}{3}} \left(1 - \frac{2y}{D_h} \right)^{\frac{1}{3}} \frac{l}{D_h} + \lambda \frac{l}{D_h}$$

where c_{x1} is taken from the curves $c_{x1} = f(l)$ for the different sections;
 ϵ is taken from the table for each section;
 λ is taken from diagrams 2-1 to 2-5;

$$l = \frac{l_0}{d_m}$$

$\bar{l} = \frac{l_0}{d_m}$	0	5	10	20	30	40	50	60	70	100
-----------------------------	---	---	----	----	----	----	----	----	----	-----

Section No. 1; $\epsilon \approx 1.5$

c_{x1}	0	0.24	0.44	0.75	0.95	1.00	1.14	1.18	1.18	1.18
----------	---	------	------	------	------	------	------	------	------	------

Section No. 2; $\epsilon \approx 1.5$

c_{x1}	0	0.17	0.28	0.45	0.60	0.71	0.80	0.85	0.88	0.88
----------	---	------	------	------	------	------	------	------	------	------

Section No. 3; $\epsilon = 1.0$

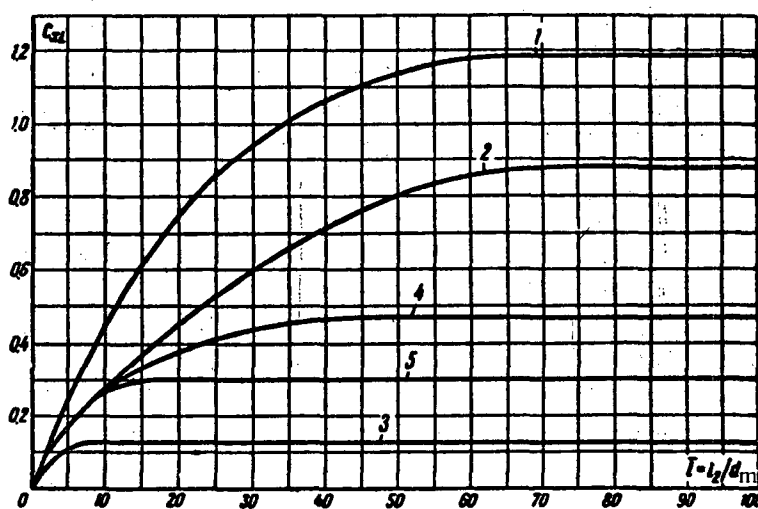
c_{x1}	0	0.11	0.12	0.12	0.12	0.12	0.12	0.12	0.12	0.12
----------	---	------	------	------	------	------	------	------	------	------

Section No. 4; $\epsilon = 1.0$

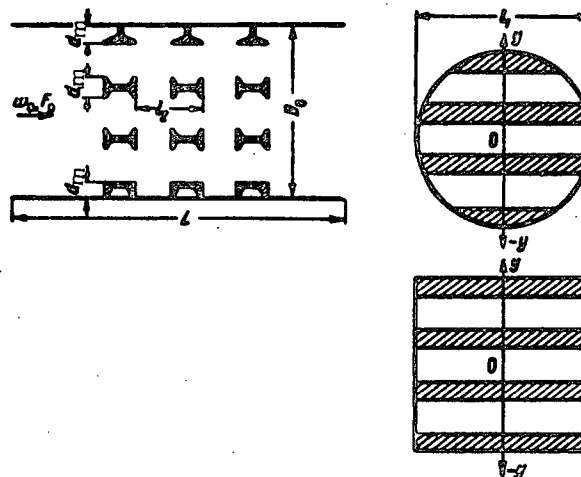
c_{x1}	0	0.17	0.27	0.37	0.43	0.46	0.47	0.47	0.47	0.47
----------	---	------	------	------	------	------	------	------	------	------

Section No. 5; $\epsilon = 1.0$

c_{x1}	0	0.17	0.26	0.30	0.30	0.30	0.30	0.30	0.30	0.30
----------	---	------	------	------	------	------	------	------	------	------



$$D_h = \frac{4F_0}{\Pi_0}; \Pi_0 - \text{pipe perimeter}$$



$$\zeta = \frac{\Delta H}{\frac{\gamma w_0^2}{2g}} \approx 1.15 \sum_{l=1}^n c_{xll} \frac{1}{\left(\frac{d_m}{D_h}\right)_l \bar{l}_l} \frac{\frac{S_{ml}}{F_0} \left(1 - \frac{2y}{D_h}\right)^{\frac{1}{3}}}{\left(1 - \sum_{l=1}^n c_l \frac{S_{ml}}{F_0}\right)^3 D_h} + \lambda \frac{L}{D_h},$$

where l = ordinal number of the reinforcement;

c_{xll} is taken as c_x for the given section, as a function of

$\bar{l} = l_2/d_m$ from diagrams 10-1 to 10-10;

λ is determined from diagrams 2-1 to 2-5;

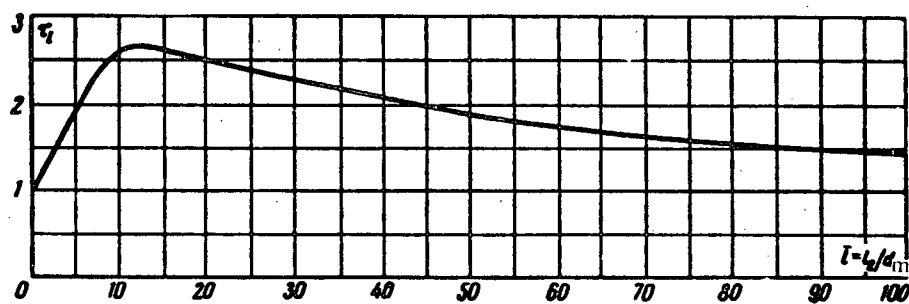
τ_l is determined as a function of the section shape;

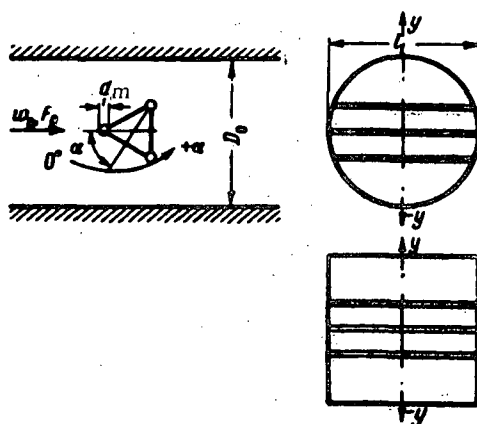
a) for ordinary rolled sections, plates with

frontal impingement of the stream, etc. by the curve $\tau_l = f(l)$

b) for cylinders and streamlined sections $\tau_l = 1.0$.

$\bar{l} = \frac{l_2}{d_m}$	0	2	4	6	8	10	15	20	30	40	50	60	80	100
τ_l	1.00	1.35	1.70	2.10	2.40	2.60	2.60	2.50	2.30	2.10	1.90	1.75	1.55	1.45





$$\zeta = \frac{\Delta H}{\frac{w_0^2}{2g}} \approx 115 c_{xa}^* \frac{S_m}{F_0} \frac{c_{xa}^*}{(1 - \frac{S_m}{F_0})},$$

$$\text{where } c_{xa}^* = c_{xa} \frac{c_{x0}^*}{c_{x0}},$$

c_{xa} is taken from the curves $c_{xa} = f(a)$ of graph a, obtained for $Re' = \frac{w_0 d_m}{v} = 1.18 \cdot 10^5$;

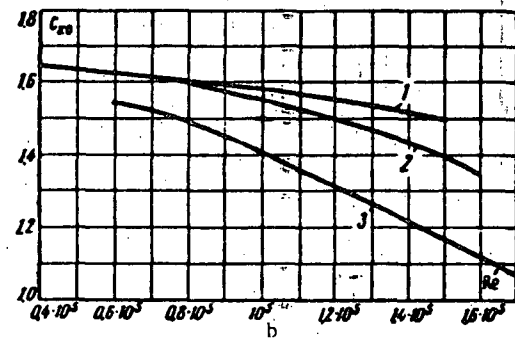
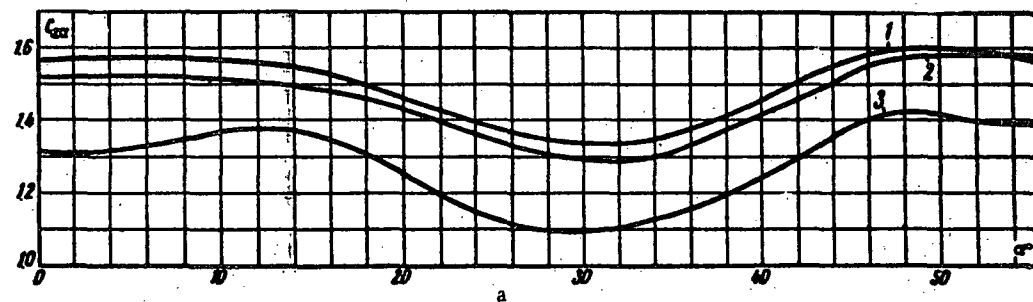
c_{x0}^* is taken from the curves $c_{x0}^* = f(Re')$ of graph b, obtained for $a = 0$;

c_{x0} is taken from graph a for $a = 0$;

$$\frac{S_m}{F_0} = \frac{bl}{F_0};$$

v is taken from § 1-3, b.

α°	0	10°	15°	20°	25°	30°	35°	40°	45°	50°	60°
Truss No. 1											
c_{xa}	1.32	1.37	1.37	1.25	1.13	1.00	1.15	1.25	1.39	1.42	1.40
Truss No. 2											
c_{xa}	1.52	1.52	1.49	1.43	1.35	1.30	1.32	1.42	1.53	1.58	1.58
Truss No. 3											
c_{xa}	1.57	1.57	1.54	1.47	1.39	1.35	1.37	1.46	1.57	1.60	1.55



No. 1

Welded truss without cross stays
 $\varphi = 0.183$

No. 2

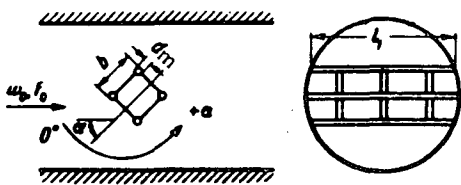
Welded lattice truss with cross stays
 $\varphi = 0.230$

No. 3

Lattice truss with cross stays and corner plates
 $\varphi = 0.241$

Re'	$0.5 \cdot 10^5$	$0.6 \cdot 10^5$	$0.8 \cdot 10^5$	$1.0 \cdot 10^5$	$1.2 \cdot 10^5$	$1.5 \cdot 10^5$	$1.6 \cdot 10^5$
Truss No. 1	1.65	1.63	1.61	1.58	1.55	1.50	-
Truss No. 2	1.65	1.63	1.60	1.55	1.50	1.40	1.35
Truss No. 3	-	1.55	1.50	1.41	1.32	1.17	1.12

Square truss placed in a pipe. Plane-parallel flow

 Section X
 Diagram 10-13


α°	0	5	10	15	20	30	35	40	45
Truss No. 1									
c_{xa}	1.35	1.42	1.55	1.78	1.79	1.78	1.67	1.54	1.50
Truss No. 2									
c_{xa}	1.50	1.60	1.78	1.93	1.95	1.95	1.93	1.83	1.81
Truss No. 3									
c_{xa}	1.49	1.56	1.73	1.89	1.93	1.93	1.91	1.80	1.77
Truss No. 4									
c_{xa}	1.59	1.68	1.88	2.03	2.05	2.03	1.99	1.90	1.88

$$\zeta = \frac{\Delta H}{\frac{w_0^2}{2g}} \approx 1.15 c_{xa}^* \frac{\frac{S_m}{F_0}}{\left(1 - \frac{S_m}{F_0}\right)^2}$$

$$\text{where } c_{xa}^* = c_{xa} - \frac{c_{x0}}{c_{x0}}$$

c_{xa} is taken from the curves $c_{xa} = f(\alpha)$ of graph a, obtained for

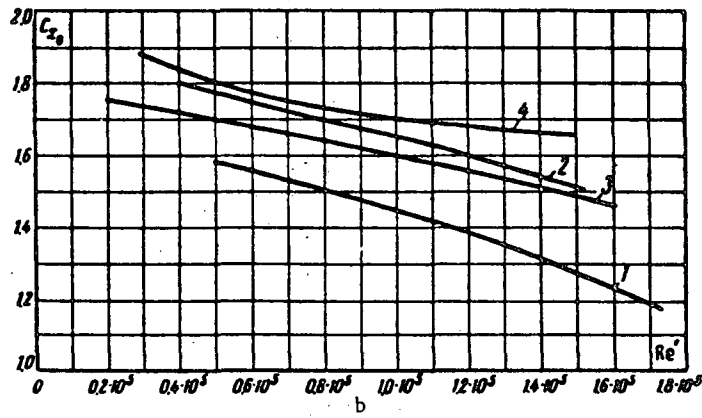
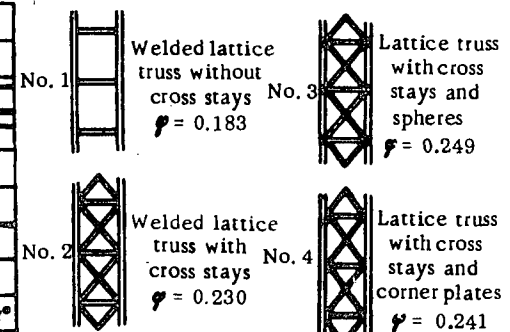
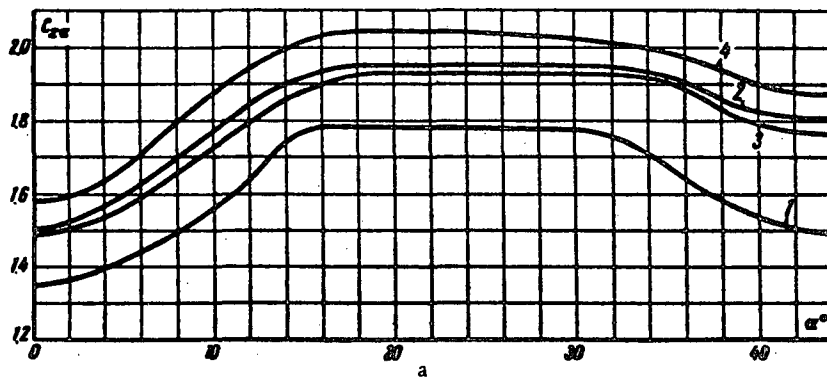
$$Re' = \frac{w_0 d_m}{\nu} = 1.18 \cdot 10^6$$

c_{x0}^* is taken from the curves $c_{x0}^* = f(Re')$ of graph b, obtained for $\alpha = 0$;

c_{x0} is taken from graph a for $\alpha = 0$;

$$\frac{S_m}{F_0} = \varphi \frac{b l_1}{F_0}$$

φ is taken from § 1-3, b.



Re'	$0.4 \cdot 10^5$	$0.6 \cdot 10^5$	$0.8 \cdot 10^5$	$1 \cdot 10^6$	$1.2 \cdot 10^6$	$1.4 \cdot 10^6$	$1.6 \cdot 10^6$
Truss No. 1	-	1.55	1.50	1.44	1.38	1.30	1.22
Truss No. 2	1.80	1.74	1.70	1.65	1.6	1.54	-
Truss No. 3	1.72	1.68	1.64	1.59	1.55	1.51	1.46
Truss No. 4	1.84	1.77	1.73	1.70	1.68	1.66	-

Section Eleven

STREAM DISCHARGE FROM PIPES AND CHANNELS (Resistance coefficients of exit stretches)

11-1. LIST OF SYMBOLS

- F_0, F_{ex} = area of narrowest and exit sections, respectively, m²;
 F_{or}, F_g = total flow area, and frontal area, respectively, of the grid, washer, screen, m²;
 f_0 = free area of one orifice of the grid, screen, m²;
 Π_0 = perimeter of the orifice section, m;
 $\bar{f} = \frac{F_{or}}{F_g}$ or $\bar{f} = \frac{F_{or}}{F_0}$ = area ratio;
 D_0, R_0 = diameter and radius of narrowest section of the exit or of the initial section of the free jet (nozzle), m;
 D_{or} = diameter of the orifices of the grid, washer, m;
 $D_h = \frac{4F_0}{\Pi_0}, d_h = \frac{4f_0}{\Pi_0}$ = hydraulic diameters of the conduit, grid, washer, or screen, m;
 a_0, b_0 = sides of narrowest rectangular section of the exit, m;
 b_1 = width of gaps between the louver slats, m;
 δ_0' = half-width of the initial section of a plane-parallel free jet, m;
 h = distance between the discharge orifice of the exit and the baffle, m;
 l = depth of the orifice or length of the exit stretch of a bend or elbow, m;
 l_d = diffuser length, m;
 S = free jet length, m;
 α = central angle of divergence of the diffuser or angle of the edges of the grid orifice, and also half-angle of divergence of the free jet;
 w_0, w_{wh} = mean velocity in narrowest and exit sections of the conduit, m/sec;
 w_{or} = mean velocity in the openings of the grid, m/sec;
 ΔH = total pressure losses or resistance in the exit stretch, kg/m²;
 ζ = resistance coefficient of the exit stretch;
 N = kinetic-energy coefficient.

11-2. EXPLANATIONS AND RECOMMENDATIONS

- When a stream flows out from a pipe, independent of the exit conditions, the kinetic energy of the discharged jet is always lost to the pipe; in general it follows that the exit losses will be:

$$\Delta H = \Delta H_{st} + \Delta H_{dyn}. \quad (11-1)$$

The resistance coefficient of the discharge in terms of the velocity in the narrow section

will be equal to:

$$\zeta = \frac{\Delta H}{\frac{\gamma w_0^2}{2g}} = \frac{\Delta H_{st}}{\frac{\gamma w_0^2}{2g}} + \frac{\Delta H_{dyn}}{\frac{\gamma w_0^2}{2g}} = \zeta_{st} + \zeta_{dyn}. \quad (11-2)$$

In general the velocity distribution at the exit is not uniform and, therefore, the dynamic pressure is determined on the basis of the specified distribution:

$$\Delta H_{dyn} = \frac{1}{Q} \int_{F_{ex}} \frac{\gamma w^3}{2g} dF \quad (11-3)$$

and

$$\zeta_{dyn} = \frac{\Delta H_{dyn}}{\frac{\gamma w_0^2}{2g}} = \frac{1}{F_0} \int_{F_{ex}} \left(\frac{w}{w_0} \right)^3 dF = \frac{1}{n^3} \frac{1}{F_{ex}} \int_{F_{ex}} \left(\frac{w}{w_{ex}} \right)^3 dF = \frac{1}{n^3} N, \quad (11-4)$$

where $n = \frac{F_{ex}}{F_0}$ is the expansion ratio of the exit stretch; and $N = \frac{1}{F_{ex}} \int_{F_{ex}} \left(\frac{w}{w_{ex}} \right)^3 dF$ is the kinetic-energy coefficient of the stream in the exit stretch.

2. In the case of free discharge into a large volume from a constant-section straight conduit, the total losses reduce to the loss of dynamic pressure at the exit; since $F_0 = F_{ex}$ ($n = 1$), the total resistance coefficient will be :

$$\zeta = \frac{\Delta H}{\frac{\gamma w_0^2}{2g}} = \frac{\Delta H_{dyn}}{\frac{\gamma w_0^2}{2g}} = N. \quad (11-5)$$

The coefficient N is a function of the velocity distribution at the exit and is larger than unity, except for a uniform distribution where it equals unity.

3. In the case of an exponential velocity distribution at the exit (cf. points 6 to 9 of § 4-2)

$$\frac{w}{w_{max}} = \left(1 - \frac{y}{R_0} \right)^{\frac{1}{m}}, \quad (11-6)$$

where w, w_{max} is the velocity at the given point and maximum velocity over the section, respectively, m/sec; R_0 is the radius of the section, m; y is the distance from the conduit axis, m; $m \geq 1$ is an exponent; the resistance coefficients of the discharge from conduits with circular and square sections are calculated by the following formula (cf. /11-9/):

$$\zeta = \frac{\Delta H}{\frac{\gamma w_0^2}{2g}} = \frac{(2m+1)^2 (m+1)^2}{4m^2 (2m+3)(m+3)}, \quad (11-7)$$

and the resistance coefficient of the discharge from a plane conduit by

$$\zeta = \frac{\Delta H}{\frac{\gamma w_0^2}{2g}} = \frac{(m+1)^3}{m^2(m+3)}. \quad (11-8)$$

In the case of a sinusoidal distribution of velocities at a discharge from a plane conduit (cf. (4-10))

$$\frac{w}{w_0} = 1 + \frac{\Delta w}{w_0} \sin 2k\pi \frac{2y}{b_0}, \quad (11-9)$$

where Δw is the deviation of the velocity from the mean at a given point over the section, m/sec; k is an integer; $\pi=3.14\dots$, the resistance coefficient of the discharge is calculated by the following formula /11-9/:

$$\zeta = \frac{\Delta H}{\frac{\gamma w_0^2}{2g}} = 1 + \frac{3}{2} \left(\frac{\Delta w}{w_0} \right)^2. \quad (11-10)$$

4. The pressure losses in a diffuser in the case of free discharge into a large volume are made up of the loss in the diffuser proper ζ_d and the loss of dynamic pressure at the exit ζ_{ex} :

$$\zeta = \frac{\Delta H}{\frac{\gamma w_0^2}{2g}} = \zeta_d + \zeta_{ex} = \zeta_d + \frac{N}{n^2}. \quad (11-11)$$

The velocity distribution at the discharge of a diffuser is assumed to be uniform ($N=1$); to compensate for this assumption, a corrective coefficient in the form $(1+\sigma')$ is introduced (cf. /11-8/, /11-11/):

$$\zeta = \frac{\Delta H}{\frac{\gamma w_0^2}{2g}} = (1+\sigma') \left(\zeta_d + \frac{1}{n^2} \right) = (1+\sigma') \zeta_{cal}. \quad (11-12)$$

where $\zeta_{cal} = \zeta_d + \frac{1}{n^2} = \zeta_{fr} + \zeta_{exp} + \frac{1}{n^2}$ is the calculated resistance coefficient of a diffuser with discharge into a large volume, and is determined from the corresponding graphs of diagrams 11-2 to 11-4; ζ_{fr} and ζ_{exp} are friction coefficient and resistance coefficient due to diffuser expansion, determined from the data of diagrams 5-2 to 5-4; σ' is the tentative corrective coefficient, allowing for the nonuniformity of velocity distribution at the diffuser exit.

The value of the correction for diffusers of near-optimum divergence angle lies within the limits 0 to 0.5, depending on the relative diffuser length $\frac{l_d}{D_h}$. The optimum divergence angle is the angle for which ζ_{cal} is minimum (cf. diagrams 11-2 to 11-4).

The optimum diffuser length l_d lies in the range 2.5 to 4.0 D_h for circular and rectangular diffusers with unobstructed exits, and in the range 5.0 to 6.0 a_0 for a plane diffuser.

5. If a stream encounters a baffle after its discharge from a pipe, the loss will depend on the relative distance between the baffle and the exit edge of the pipe. In some cases the installation of a baffle will lead to an increase of losses, and in other cases to a decrease. In particular, a baffle behind a cylindrical stretch or behind a straight diffuser of divergence angle $\alpha \leq 30^\circ$ will always cause an increase in losses. A baffle behind a curved diffuser or behind a straight diffuser of divergence angle larger than 30° can considerably decrease the total losses, provided the distance from the diffuser to the baffle is correctly chosen.

6. A baffle behind a diffuser creates a head forcing the stream to spread over the section. This leads to a decrease of the stream separation zone and, therefore, to a more efficient spreading of the stream. As a result, both the losses inside the diffuser and the losses of dynamic pressure at the exit are reduced. Simultaneously, the baffle forces the stream to be deflected at an angle of 90° before the exit. If the exit edge of the diffuser is not smoothly rounded, this deflection will be accompanied by a considerable contraction of the jet (Figure 11-1, a) and, therefore, by an increase of its kinetic energy; it follows that when a baffle is placed behind a diffuser of small area ratio (so that the mean stream velocity at the deflection is large) the gain obtained from the spreading and more complete expansion of the jet can be smaller than the additional losses caused by the jet contraction at the discharge. In the case of considerable area ratio (divergence angle), the losses due to the stream deflection are relatively small, and the influence of the baffle is greater.

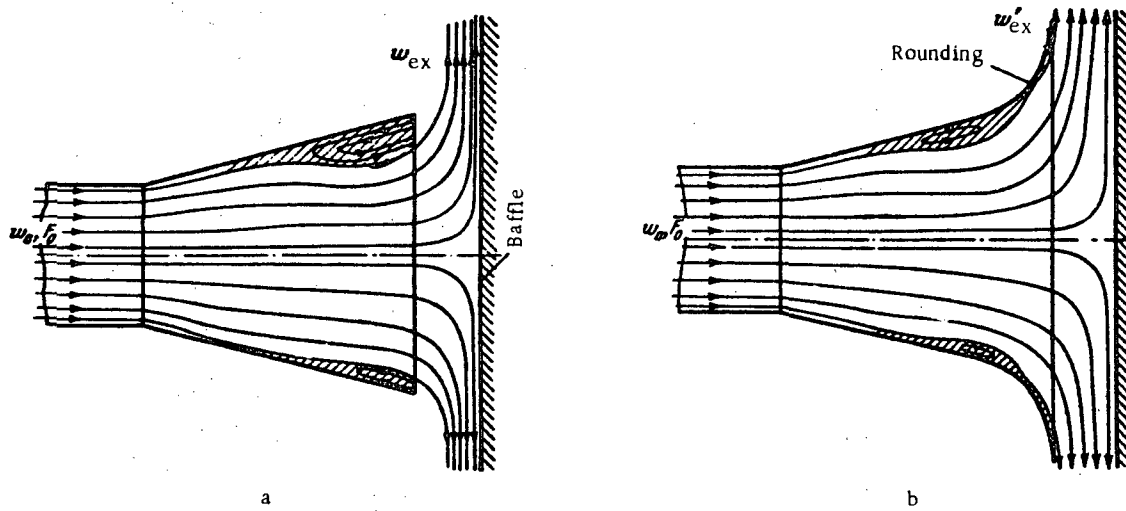


FIGURE 11-1. Flow pattern at a diffuser exit with baffle:

a—sharp discharge edge of the diffuser; b—rounded discharge edge of the diffuser.

7. The smooth rounding of the discharge edge of the diffuser or the straight stretch reduces the jet contraction (Figure 11-1, b) and leads to the formation of an annular diffuser, in which additional expansion takes place and kinetic energy is transformed into pressure energy. As a result, the installation of a baffle behind a diffuser with rounded edges is advantageous in all cases, independent of the area ratio.

8. The optimum distance $(\frac{h}{D_h})_{opt}$ between the baffle and the discharge orifice, at which the resistance coefficient of the stretch with discharge against a baffle is minimum, exists for rectilinear diffusers of wide divergence angle and for straight stretches with diffuser of rounded edges. When this distance is very large (of the order of $\frac{h}{D_h} > 0.6$), the baffle influence is not felt and the losses are equal to a discharge without baffle. When it is very small ($\frac{h}{D_h} < 0.15$), the flow velocity between the baffle and the discharge edge is increased and the losses increase sharply. Finally, when it is within the range $0.15 \leq (\frac{h}{D_h})_{opt} \leq 0.25$, the velocity of flow will substantially decrease and the eddy formation caused by the stream separation in the course of its deflection and expansion will also decrease; this is the optimum range of values of $\frac{h}{D_h}$.

9. The following parameters are recommended for diffusers with rounded edges and baffles: relative length $\frac{l}{D_h} = 2.5$; divergence angle $\alpha = 14$ to 16° ; relative radius of curvature of the discharge edge $\frac{r}{D_h} = 0.6$ to 0.7 ; relative baffle diameter $\frac{D_b}{D_h} = 3.0$; relative distance of the baffle from the diffuser $\frac{h}{D_h} = 0.24$ to 0.26 (cf. /11-8/).

The coefficient of total resistance of such a diffuser is equal to

$$\zeta = \frac{\Delta H}{\frac{T_{in}}{2g}} = 0.25 \text{ to } 0.35.$$

10. When an exit diffuser is installed behind a centrifugal fan, the recommendations stated under points 22 to 25 of § 5-2 should be taken into account. The installation of a diffuser behind an induced-draft fan is especially necessary, since it can reduce the exit losses by a factor of three to four (cf. Lokshin and Gazirbekova /11-13/).

The relative length of a pyramidal diffuser placed behind an induced-draft fan should not be larger than $\frac{l_d}{b_e} = 2.5$ to 3.0 at divergence angles $\alpha = 8$ to 12° , and that of a plane diffuser not larger than $\frac{l_d}{b_e} = 4$ to 5 at $\alpha = 15$ to 25° . The resistance coefficients of diffusers placed behind fans are determined from the data of diagrams 11-11 and 11-12.

11. In a free discharge of flow from a ring-type diffuser formed by a conical diffuser located behind an axial fan with a diverging back fairing, the resistance of the ring-shaped diffuser differs from the resistance of an equivalent conical diffuser to a much greater degree than in the case of a ring-shaped diffuser installed in a pipe network (cf. point 27 of § 5-2). Due to more uniform velocity distributions, the loss of kinetic energy at the discharge from an annular diffuser is much smaller than at the exit from an ordinary conical diffuser with equal discharge. The annular diffuser is also characterized by a more ordered stream flow along its entire length, contributing to the decrease of losses in the diffuser proper. The resistance coefficient of such a diffuser

placed behind an axial fan can be determined by the formula

$$\zeta = \frac{\Delta H}{\frac{1}{2} w_0^2} = k_1 \zeta' \quad (11-13)$$

where ζ' is the resistance coefficient of the same diffuser at uniform distribution of the velocities in its narrow section, determined from the data of Bushel /11-3/ (cf. Table 11-3 of diagram 11-8); k_1 is the corrective coefficient, determined by diagram 5-18.

12. The radial-annular or axial-radial-annular diffusers used in axial turbines (cf. points 28 and 29 of § 5-2), with induced draft and discharging the stream into a large volume, can also be considered as discharge stretches. The resistance coefficients of such diffusers are given in diagrams 11-9 and 11-10.

13. Another type of discharge is represented by exhaust vents having the same shapes and characteristics as supply vents. Their selection should be based on recommendations given in under points 14 and 15 of § 3-2.

14. Inlet nozzles (into a room) also belong to the category of discharge units. The main requirements of such nozzles are to ensure either a rapid dissipation of the kinetic energy or to give a concentrated jet. The nature of the losses in such nozzles is the same as in stream discharge from a pipe. These losses reduce to the loss of kinetic energy at the given degree of expansion or contraction of a jet.

The nozzles whose resistance coefficients are given in this handbook include not only the most effective types of nozzles, but also some less successful ones which, in view of their simplicity, are widely used. To this category belong such nozzles as ordinary bends and elbows.

15. In certain cases the distribution of the air is carried out through air ducts with perforated surfaces (Figure 11-2). Such a distribution ensures speedy dissipation of kinetic energy, which is desirable in many installations. At the same time, if the ratio of the total area of the orifices to the area of the duct cross-section is too large

$(\bar{f}_o = \frac{F_{or}}{F_o} > 0.5)$, the stream distribution along the duct will not be uniform, the nonuniformity increasing with the decrease of the relative length of the supply part of the duct.

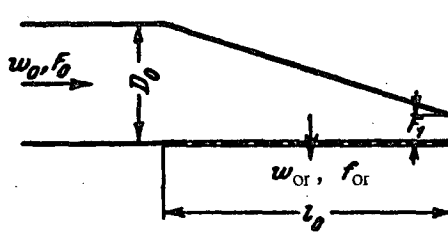


FIGURE 11-2. Air duct with perforated lateral outlet.

Tapered air ducts give a more uniform distribution of the stream along the perforated surface than straight ducts, if the ratio of the final area to the initial area lies in the range $0.15 \leq \frac{F_1}{F_0} \leq 1.0$.

16. The total resistance coefficient of an inlet nozzle with perforated surface within the limits $0.5 < \frac{F_1}{F_0} < 3.0$ and $0 < \frac{F_1}{F_0} < 1.0$ can be calculated by the following formula (cf. Grimitlin /11-4/):

$$\zeta = \frac{\Delta H}{\frac{\gamma w_0^2}{2g}} = \frac{1.8}{F_0^2} + \left(\frac{l_0}{D_h} \right)^{0.18} \quad (11-14)$$

For $\frac{F_1}{F_0} > 0$ this formula gives values approximately twenty per cent higher than the actual values.

More accurate results are obtained by another formula (cf. Grimitlin /11-5/):

$$\zeta = \frac{\Delta H}{\frac{\gamma w_0^2}{2g}} = 1.62 \bar{F}^{-2.2} \left(\frac{F_1}{F_0} \right)^{0.25\bar{F}} \left(1 \frac{l}{D_h} \right)^{-0.05} + 1. \quad (11-15)$$

The curves of diagram 11-18 have been plotted on the basis of the simplified formula (11-14).

17. Elbows and bends with large discharge volumes are frequently used as discharge nozzles. The resistance of such elbows and bends depends to a great extent on the length of the discharge stretch. At first, the losses increase with length, drop sharply, and finally become constant at some value of $\frac{l}{b_0}$. Such a variation of the resistance curve is explained by the shape and magnitude of the eddy zone formed along the inner wall of the elbow after the turn.

18. The eddy zone in an elbow starts from the turn, gradually expands, and attains its maximum width at a certain distance from this turn; it then contracts until finally the stream spreads over the entire section. Thus, when the discharge stretch of the elbow ends at the section where the eddy zone is widest and the cross section narrowest, the stream will be discharged into the larger volume at maximum velocity and with maximum energy loss. This corresponds to the maximum of ζ_m on the graphs of diagrams 11-20 to 11-23.

19. If the length of the stretch after the turn is reduced to zero, the eddy zone will be absent, the stream will be discharged into the larger volume with a lower velocity, and the resistance coefficient ζ will be smaller. The decrease of ζ will, however, be very small, since the stream presses by inertia toward the upper wall, and the velocity at the exit as a result is considerably higher than the mean velocity over the section.

20. If the discharge stretch is sufficiently long, the stream will spread over the entire section and the resistance coefficient ζ will be minimum. The subsequent increase $\frac{l}{b_0}$ will be accompanied by a certain increase of ζ due to the increase of the friction losses in the straight portion.

The resistance coefficient for elbows with free discharge of the stream and discharge section twice as large as the inlet section is lower by 40 to 50%.

21. Guide vanes can be used to decrease resistance of elbows discharging into a large volume. The relative reduction of resistance achieved here is even larger than

in elbows with lengthy discharge sections, since the absolute resistance value of discharge elbows alone is considerably larger than that of elbows with discharge stretches.

22. The resistance coefficient of a straight exit stretch with a grid or orifice at the exit ($F_s = \infty$, Figure 11-3) with $\text{Re} = \frac{\omega_0 d_h}{\nu} > 10^4$ is generally calculated by (cf. /11-10, 11-11/):

$$\zeta = \frac{\Delta H}{\frac{\rho w_0^2}{2g}} = \left[1 + \zeta' (1 - \bar{f}) + \tau \sqrt{1 - \bar{f}} + \lambda \frac{l}{d_h} \right] \frac{1}{\bar{f}}, \quad (11-16)$$

where ζ' is a coefficient which is determined as ζ from diagrams 3-3 to 3-6; τ is a coefficient allowing for the influence of the plate-wall thickness, the shape of the inlet edge of the orifice, and the conditions of flow through it; λ is the friction coefficient of unit length of the orifice plate wall, determined from diagrams 2-1 to 2-5; $\bar{f} = \frac{F_{\text{or}}}{F_g}$ is the cross-section coefficient of the plate.

23. The general case is reduced to several particular cases:

a) sharp-edged orifices ($\frac{l}{d_h} = 0$), for which $\zeta' = 0.5$, $\tau = 1.41$, $\lambda \frac{l}{d_h} = 0$, and expression (11-16) reduces to the following formula (cf. /11-7, 11-11/):

$$\zeta = \frac{\Delta H}{\frac{\rho w_0^2}{2g}} = (1 + 0.707 \sqrt{1 - \bar{f}})^2 \frac{1}{\bar{f}}; \quad (11-17)$$

b) thick-walled orifices, for which $\zeta' = 0.5$, and τ is determined from the curve $\tau = f(l/d_h)$ of diagram 11-28*.

c) orifice edges beveled toward the stream flow or rounded, for which one takes $\lambda \frac{l}{d_h} = 0$, $\tau \approx 2\sqrt{\zeta'}$ and obtains

$$\zeta = \frac{\Delta H}{\frac{\rho w_0^2}{2g}} = \left[1 + \sqrt{\zeta' (1 - \bar{f})} \right]^2 \frac{1}{\bar{f}}, \quad (11-18)$$

where the coefficient ζ' is determined in case of edges beveled toward the stream as ζ for a conical bell mouth with end wall, as a function of the convergence angle α° and of the relative length $\frac{l}{d_h}$, by graph a of diagram 11-29; and in the case of rounded edges as ζ for a circular bellmouth with end wall, as a function of $\frac{l}{d_h}$, by graph b of the same diagram.

24. The resistance coefficient of the exit through an orifice plate is calculated at

* Calculation by (11-14) and (11-18) can be made for $\text{Re} \approx 10^4$.

$\text{Re} < 10^5$ for sharp-edged orifices, by the following formula derived from expression (4-19):

$$\zeta = \frac{\Delta H}{\frac{\gamma w_0^2}{2g}} = \left\{ \left(\frac{1}{\varphi} - 1 \right) + \bar{\epsilon}_0^{\text{Re}} \left(1 + 0.707 \sqrt{1 - \bar{f}} \right)^2 \right\} \frac{1}{\bar{f}^2} = (\zeta_{\varphi} + \bar{\epsilon}_0^{\text{Re}} \zeta_0^2) \frac{1}{\bar{f}^2}. \quad (11-19)$$

Here $\zeta_{\varphi} = \frac{1}{\varphi}$ is determined from the curves $\zeta_{\varphi} = f_{\varphi}(\text{Re}, \bar{f})$ on graph a of diagram 4-10;

$\bar{\epsilon}_0^{\text{Re}} = \left(\frac{0.585}{\epsilon_0^{\text{Re}}} \right)^2$ is determined from the curves $\bar{\epsilon}_0^{\text{Re}} = f_{\bar{\epsilon}}(\text{Re})$ on the same graph; $\zeta_0 = 1 + 0.707 \sqrt{1 - \bar{f}}$ is determined from the curve $\zeta_0 = f(\bar{f})$ on graph b of the same diagram; φ is coefficient of the discharge velocity from a sharp-edged orifice, and depends on Re and \bar{f} ; ϵ_0^{Re} = coefficient of filling of a sharp-edged orifice at $\frac{F_{\text{or}}}{F_0} = 0$, and depends on Re.

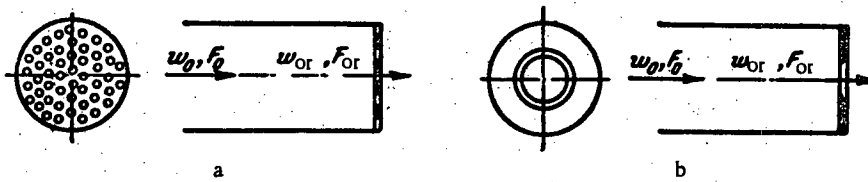


FIGURE 11-3. Stream discharge from a straight stretch through a grid or orifice:
a — grid; b — orifice; F_{or} — flow section.

The resistance coefficient is calculated at $\text{Re} < 10^5$ for thick-edged orifices by the following formula, also derived from (4-19):

$$\zeta = \frac{\Delta H}{\frac{\gamma w_0^2}{2g}} = \left\{ \zeta_{\varphi} + \bar{\epsilon}_0^{\text{Re}} \left[1 + 0.5(1 - \bar{f}) + \epsilon \sqrt{1 - \bar{f}} + 2 \frac{l}{d_h} \right] \right\} \frac{1}{\bar{f}^2}. \quad (11-20)$$

25. The resistance coefficient of louvers with fixed slats installed in the exit of a straight channel can be approximated by the following formulas:

a) $\frac{l}{b'_1} \geq \left(\frac{l}{b'_1} \right)_{\text{opt}}$

$$\zeta = \frac{\Delta H}{\frac{\gamma w_0^2}{2g}} = k \left[1 + 0.85 \left(1 - \bar{f} \frac{F_g}{F_0} \right) + \zeta_{\text{fr}} \right] \frac{1}{\bar{f}^2} \left(\frac{F_0}{F_g} \right)^2; \quad (11-21)$$

b) $\frac{l}{b'_1} < \left(\frac{l}{b'_1} \right)_{\text{opt}}$

$$\zeta = \frac{\Delta H}{\frac{\gamma w_0^2}{2g}} = k \left[1 + 0.85 \left(1 - \bar{f} \frac{F_g}{F_0} \right) + \zeta_{\text{fr}} \right] \frac{1}{\bar{f}^2} \left(\frac{F_0}{F_g} \right)^2 + \Delta \zeta. \quad (11-22)$$

where

$$\Delta \zeta \approx 0.5 \left[11 \left(1 - \bar{f} \right) - \frac{l}{b'_1} \right] \quad (11-23)$$

and

$$\zeta_{fr} = \lambda \frac{l}{b'_1};$$

$k = 1.0$ for a standard louver (vertically cut inlet edges); $k = 0.6$ for an improved louver (inlet edges cut horizontally); $\bar{f} = \frac{F_{or}}{F_g}$ is the cross-section coefficient of the louver; λ is the friction coefficient of unit relative length (depth) of the louver channels, determined from diagrams 2-1 to 2-5 as a function of $Re = \frac{w_{or} b'_1}{v}$.

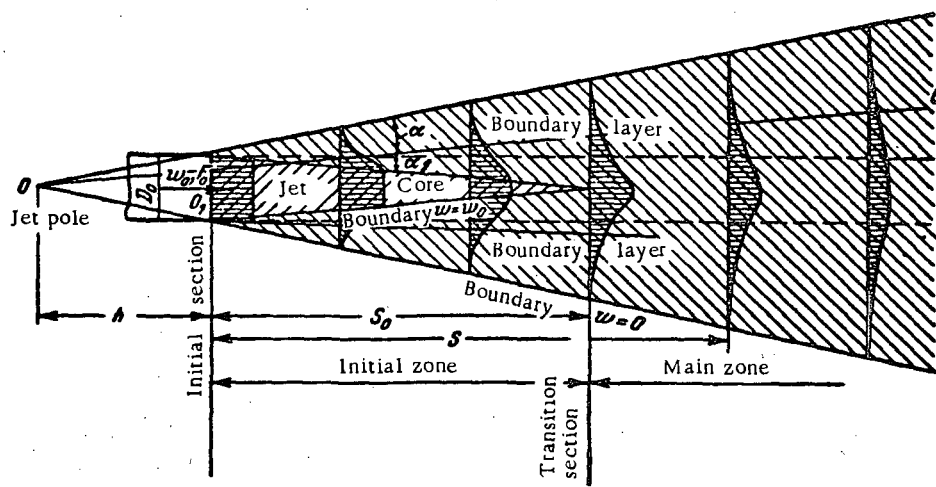


FIGURE 11-4. Pattern of a free jet.

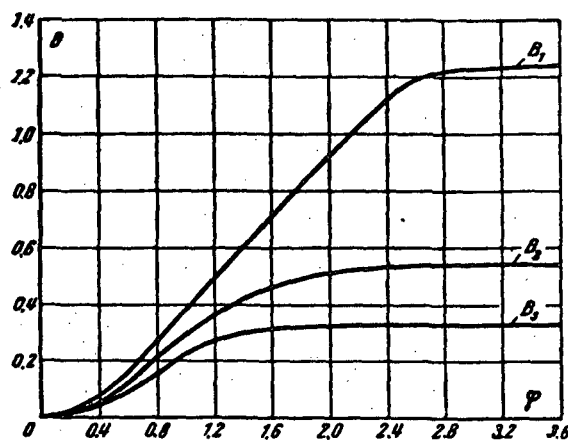


FIGURE 11-5. Auxiliary functions for calculating a circular free jet.

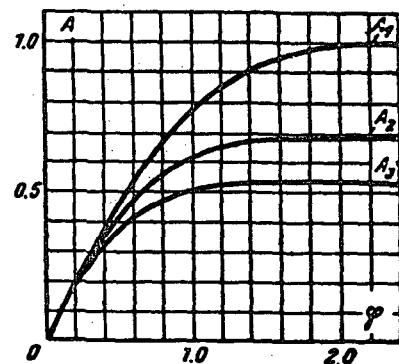


FIGURE 11-6. Auxiliary functions for calculating a plane-parallel free jet.

26. The energy of a free jet discharged from a system into an unlimited volume (Figure 11-4) is lost to the system. All the basic parameters of an incompressible free jet can be determined by the data of Abramovich /11-1/ given in Tables 11-1 and 11-2; these tables contain formulas for calculating the corresponding parameters of the free jet for both its initial and main zones. The initial zone is understood to mean the jet zone starting from the exit orifice of the channel and ending at the section where the velocity at the axis begins to differ from the initial velocity at the exit. The main zone is understood to mean the entire remaining part of the jet, characterized by a gradual decrease of the velocity at the axis. The section separating the two zones is called the transition region.

The coefficient of jet turbulence α' is equal to 0.08 for a circular jet and to 0.09 to 0.12 for a plane-parallel jet.

TABLE 11-1
Characteristics of a circular free jet at a distance S from its initial section

No.	Characteristics	Formulas for the initial jet zone	Formulas for the main jet zone
1	Dimensionless diameter of the outer boundary of the jet	$\frac{D_b}{D_0} = \frac{R_b}{R_0} = 3.4 \frac{a'S}{R_0} + 1$ $F = \frac{F_j}{F_0} = \left(3.4 \frac{a'S}{R_0} + 1 \right)^2$	$\frac{D_b}{D_0} = \frac{R_b}{R_0} = 3.4 \frac{a'S}{R_0} + 1$ $\frac{F_j}{F_0} = \left(3.4 \frac{a'S}{R_0} + 1 \right)^2$
2	Dimensionless area of the jet section		—
3	Dimensionless diameter of the constant-velocity core	$\frac{D_c}{D_0} = \frac{R_c}{R_0} = 1 - 1.5 \frac{a'S}{R_0}$	
4	Dimensionless diameter of the constant-mass core	$\frac{D_a}{D_0} = \frac{R_a}{R_0} = 1 + 0.32 \frac{a'S}{R_0}$	$\frac{D_a}{D_0} = \frac{R_a}{R_0} = \left(\frac{a'S}{R_0} + 0.29 \right) \varphi_a$
			In order to determine φ_a one calculates first
			$B_1 = \frac{0.52}{\frac{a'S}{R_0} + 0.29}$
			from the given value of $\frac{a'S}{R_0}$, the value of φ_a is then found from the curve $B_1 = f(\varphi)$ in Figure 11-5
5	Dimensionless distance of the end of the initial zone from the exit section of the discharge channel	$\frac{S_0}{R_0} = \frac{0.67}{a'}$	—
6	Tangent of the half-angle of jet divergence	$\operatorname{tg} \alpha = 3.4 a'$ (at $a' = 0.08 - \alpha = 15^\circ$)	$\operatorname{tg} \alpha = 3.4 a'$ (at $a' = 0.08 - \alpha = 15^\circ$)
7	Tangent of the half-angle of contraction of the constant-velocity core	$\operatorname{tg} \alpha_1 = 1.5 a'$ (at $a' = 0.08 - \alpha_1 = 7^\circ$)	—
8	Dimensionless velocity at the jet axis	$\frac{w_m}{w_0} = 1.0$	$\frac{w_m}{w_0} = \frac{0.96}{\frac{a'S}{R_0} + 0.29}$
9	Dimensionless arithmetic mean velocity of jet	$\frac{w_{av}}{w_m} = \frac{Q}{w_m F} = \frac{1 + 0.76 \frac{a'S}{R_0} + 1.32 \left(\frac{a'S}{R_0} \right)^2}{1 + 6.8 \frac{a'S}{R_0} + 11.56 \left(\frac{a'S}{R_0} \right)^2}$	$\frac{w_{av}}{w_m} = 0.2 = \text{const}$
10	Dimensionless mean-square jet velocity	$\frac{w'_{av}}{w_m} = \frac{\int_{m_1} w dm_1}{w_m m_1} = \frac{1}{1 + 0.76 \frac{a'S}{R_0} + 1.32 \left(\frac{a'S}{R_0} \right)^2}$ where $m_1 = \rho F w$	$\frac{w'_{av}}{w_m} = 0.48 = \text{const}$
11	Dimensionless fluid-discharge across the given section	$\bar{q} = \frac{Q}{Q_0} = 1 + 0.76 \frac{a'S}{R_0} + 1.32 \left(\frac{a'S}{R_0} \right)^2$	$\bar{q} = 2.22 \left(\frac{a'S}{R_0} + 0.29 \right)$
12	Dimensionless residue of kinetic energy of the jet in the given section	$\bar{e} = \frac{e}{m_{10} w_0^2} = \frac{e}{e_0} = \frac{1 - 1.03 \frac{a'S}{R_0} + 0.68 \left(\frac{a'S}{R_0} \right)^2}{2}$	$\bar{e} = \frac{0.59}{\frac{a'S}{R_0} + 0.29}$

Table 11-1(continued)

No.	Characteristics	Formulas for the initial jet zone	Formulas for the main jet zone
13	Dimensionless residue of kinetic energy of the constant-mass jet core in the given section	$\bar{e}_a = \frac{e_a}{e_0} = 1 - 1.14 \frac{a'S}{R_0} + 0.61 \left(\frac{aS}{R_0} \right)^2$	$\bar{e}_a = \frac{1.78 B_3}{\frac{a'S}{R_0} + 0.29}$ In order to determine B_3 one calculates first B_1 from the given value of $a'S/R_0$ (point 4 of the table). With B_1 known, one determines φ_a from Figure 11-5, and then the value of B_2 corresponding to this φ_a in the same figure
14	Resistance coefficient of the free jet	$\zeta = \frac{\Delta H}{\frac{1}{2} w_0^2} = 1 - \bar{e}$	$\zeta = 1 - \bar{e}$
15	Resistance coefficient of the constant-mass jet core	$\zeta_a = \frac{\Delta H}{\frac{1}{2} w_0^2} = 1 - \bar{e}_a$	$\zeta_a = 1 - \bar{e}_a$

TABLE 11-2
Characteristics of a plane-parallel free jet at a distance S from its initial section

No.	Characteristics	Formulas for the initial jet zone	Formulas for the main jet zone
1	Dimensionless half-width of the jet	$\frac{\delta'_b}{\delta'_0} = 2.4 \frac{a'S}{\delta'_0} + 1$	$\frac{\delta'_b}{\delta'_0} = 2.4 \frac{a'S}{\delta'_0} + 1$
2	Dimensionless area of the jet section	$\bar{F} = \frac{F_j}{F_0} = 2.4 \frac{a'S}{\delta'_0} + 1$	$\bar{F} = \frac{F_j}{F_0} = 2.4 \frac{a'S}{\delta'_0} + 1$
3	Dimensionless half-width of the constant-velocity core	$\frac{\delta'_c}{\delta'_0} = 1 - 0.96 \frac{a'S}{\delta'_0}$	$\frac{\delta'_c}{\delta'_0} = 1 - 0.96 \frac{a'S}{\delta'_0}$
4	Dimensionless half-width of the constant-mass core	$\frac{\delta'_a}{\delta'_0} = 1 + 0.275 \frac{a'S}{\delta'_0}$	$\frac{\delta'_a}{\delta'_0} = \left(\frac{a'S}{\delta'_0} + 0.41 \right) \varphi_a$ In order to determine φ_a one calculates first
5	Dimensionless distance of the end of the initial zone from the exit section of the discharge channel	$\frac{S_c}{\delta'_0} = \frac{1.03}{a'}$	$A_1 = \frac{0.833}{\sqrt{\frac{a'S}{\delta'_0} + 0.41}}$ from the given value of $\frac{a'S}{\delta'_0}$; the value of φ_a is then found from the curve $A_1 = f(\varphi)$ in Figure 11-6.

Table 11-2 (continued)

No.	Characteristics	Formulas for the initial jet zone	Formulas for the main jet zone
6	Tangent of the half-angle of jet divergence	$\tan \alpha = 2.4 \alpha'$ (at $\alpha' = 0.09$ to 0.12 $\alpha = 12$ to 16°)	$\tan \alpha = 2.4 \alpha'$ $\alpha' = 0.09 + 0.12 \alpha = 12$ to 16°
7	Tangent of the half-angle of contraction of the constant-velocity core	$\tan \alpha_1 = 0.98 \alpha'$ (at $\alpha' = 0.09$ to 0.12 $\alpha_1 = 5$ to 6.5°)	
8	Dimensionless velocity at the jet axis	$\frac{w_m}{w_0} = 1.0$	$\frac{w_m}{w_0} = \frac{1.2}{\sqrt{\frac{\alpha' S}{\delta'_0} + 0.41}}$
9	Dimensionless arithmetic-mean velocity of the jet	$\frac{w_{av}}{w_m} = \frac{Q}{w_m F} = \frac{1 + 0.43 \frac{\alpha' S}{\delta'_0}}{1 + 0.24 \frac{\alpha' S}{\delta'_0}}$	$\frac{w_{av}}{w_m} = 0.47 = \text{const}$
10	Dimensionless mean-square jet velocity	$\frac{w'_{av}}{w_m} = \frac{\int w dm_1}{w_m m_1} = \frac{1}{1 + 0.43 \frac{\alpha' S}{\delta'_0}}$	$\frac{w'_{av}}{w_m} = 0.7 = \text{const}$
11	Dimensionless fluid discharge across the given section	$\bar{q} = \frac{Q}{Q_0} = 1 + 0.43 \frac{\alpha' S}{\delta'_0}$	$\bar{q} = 1.2 \sqrt{\frac{\alpha' S}{\delta'_0} + 0.41}$ $\bar{e} = \frac{0.94}{\sqrt{\frac{\alpha' S}{\delta'_0} + 0.41}}$ $\bar{e}_a = \frac{1.73 A_2}{\sqrt{\frac{\alpha' S}{\delta'_0} + 0.41}}$
12	Dimensionless residue of kinetic energy of the jet in the given section	$\bar{e} = \frac{e}{m_1 w_0^2} = \frac{e}{e_0} = 1 - 0.21 \frac{\alpha' S}{\delta'_0}$	
13	Dimensionless residue of kinetic energy of the constant-mass jet core in the given section	$\bar{e}_a = \frac{e_a}{e_0} = 1 - 0.275 \frac{\alpha' S}{\delta'_0}$	In order to determine A_2 one calculates first A_1 from the given $\alpha' S / \delta'_0$. With known, one determines \bar{e}_a from Figure 11-6, and then the value of A_2 corresponding to this \bar{e}_a in the same figure.
14	Resistance coefficient of the free jet	$\zeta = \frac{\Delta H}{\frac{1}{2} w_0^2} = 1 - \bar{e}$	$\zeta = 1 - \bar{e}$
15	Resistance coefficient of the constant-mass jet core	$\zeta_a = \frac{\Delta H}{\frac{1}{2} w_0^2} = 1 - \bar{e}_a$	$\zeta_a = 1 - \bar{e}_a$

**11-3. LIST OF THE DIAGRAMS OF RESISTANCE COEFFICIENTS
OF SECTION XI**

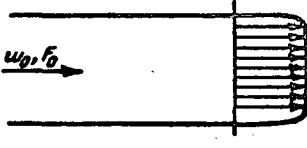
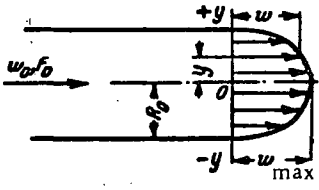
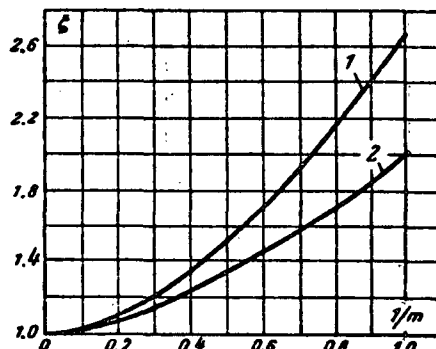
Diagram description	Source	No.of diagram	Note
Free discharge from a conduit at different velocity distributions	Idel'chik /11-9/	11-1	Calculating formulas
Free discharge from a circular rectilinear diffuser	Idel'chik /11-8/	11-2	Approximate calculations
Free discharge from a rectangular (square) diffuser	—	11-3	The same
Free discharge from rectilinear plane diffuser	—	11-4	" "
Discharge from a rectilinear diffuser against a baffle at $l_d/D_h = 1.0$	Khanzhonkov /11-18/ Nosova /11-14/	11-5	Experimental data
Discharge from a straight stretch with rounded edges against a baffle	Idel'chik /11-8/	11-6	The same
Discharge from a diffuser with rounded edges and optimum characteristics against a baffle	Idel'chik /11-8/	11-7	" "
Free discharge from an annular diffuser	Bushel' /11-3/	11-8	" "
Free discharge from an annular-radial diffuser; $\bar{d} = 0.688$	Dovzhik and Ginevskii /11-6/	11-9	" "
Free discharge from an axial-radial-annular diffuser; $\bar{D} = 2.06$, $\bar{d} = 0.688$, $a_2 = 8^\circ$, $c_{a0} = 0.5$	The same	11-10	" "
Free discharge from a plane asymmetric diffuser behind a centrifugal-induced-draft fan	Lokshin and Gazirbekova /11-13/	11-11	" "
Free discharge from a pyramidal diffuser behind a centrifugal induced-draft fan	The same	11-12	" "
Side discharge from the last orifice of a circular pipe	—	11-13	The author's experimental data
Straight rectangular exhaust vents; lateral openings with and without fixed louvers	Nosova and Tarasov /11-15/	11-14	Experimental data
Rectangular exhaust vents with elbows; lateral openings with and without fixed louvers	The same	11-15	The same
Straight circular exhaust vents.	Khanzhonkov /11-19/	11-16	" "
$Re > 10^4$	Baturin and Shepelev /11-2/	11-17	" "
Duct caps	Grimitlin /11-4, 11-5/	11-18	" "
Airduct with perforated lateral outlet	Baturin and Shepelev /11-2/	11-19	" "
Baturin-type outlet	Khanzhonkov and Taliev /11-21/	11-20	" "
Discharge from a 90° bend	According to the data of /11-16/	11-21	" "
Discharge from a square-section ($a_0/b_0 = 1.0$) sharp 90° elbow with contracted or expanded discharge section	The same	11-22	" "
Discharge from a rectangular-section ($a_0/b_0 = 0.25$) sharp 90° elbow with contracted or expanded discharge section	" "	11-23	" "
Discharge from a rectangular-section ($a_0/b_0 = 4.0$) sharp 90° elbow with contracted or expanded discharge section	" "	11-24	" "
Discharge from a smooth $\left(\frac{r}{b_0} = 0.2\right)$ 90° elbow with contracted or expanded discharge section	Yudin /11-22/	11-25	" "
Discharge from a smooth 90° elbow with discharge section contracted or expanded by a factor of two	The same	11-25	" "

Diagram description	Source	No. of diagram	Note
Discharge from a smooth 90° elbow with discharge section expanded by a factor of two ($b_1/b_0 = 2.0$) and with five thin guide vanes	Yudin /11-12/	11-26	Experimental data
Discharge from a straight conduit through a grid or orifice $0 \leq l/d_h \leq 0.15$	Idel'chik /11-10, 11-11, 11-12/ The same	11-27 11-28	Calculating formula; partially experimental data The same
Discharge from a straight conduit through a thick-walled orifice or grid	" "	11-29	Approximate calculating formulas
Discharge from a rectilinear conduit through an orifice or grid with orifice edges beveled or rounded toward the stream flow	—	11-30	According to the author's approximate formula, taking into account the experiments of Bevier /11-23/ and Cobb /11-24/ Tentatively
Discharge from a straight channel through a fixed louver	—	11-31	
Discharge stretches under different conditions	Abramovich /11-1/	11-32	"
Circular free jet	The same	11-33	"
Plane-parallel free jet			

11-4. DIAGRAMS OF RESISTANCE COEFFICIENTS

Free discharge from a conduit at different velocity distributions

 Section XI
 Diagram 11-1

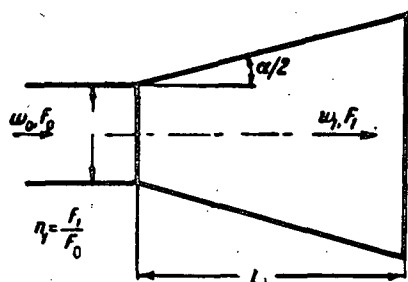
Type of velocity distribution	Scheme	Resistance coefficient $\xi = \frac{\Delta H}{\frac{V^2 g}{2}}$																								
Uniform velocity distributions		$\xi = 1.0$																								
Exponential distribution $w = w_{max} \left(1 - \frac{y}{R_o}\right)^{\frac{1}{m}}$ $m \geq 1.0$		<p>a. Circular or square pipe $\xi = \frac{(2m+1)^2(m+1)^2}{4m^2(2m+3)(m+3)}$ is determined from curve 1</p> <p>b. Plane pipe $\xi = \frac{(m+1)^2}{m^2(m+3)}$ is determined from curve 2</p> <table border="1" style="margin-left: auto; margin-right: auto;"> <tr> <td>m</td> <td>1.00</td> <td>1.35</td> <td>2.00</td> <td>3.00</td> <td>4.00</td> <td>7.00</td> <td>∞</td> </tr> <tr> <td>1. Circular pipe</td> <td>2.70</td> <td>2.00</td> <td>1.50</td> <td>1.25</td> <td>1.15</td> <td>1.06</td> <td>1.00</td> </tr> <tr> <td>2. Plane pipe</td> <td>2.00</td> <td>1.63</td> <td>1.35</td> <td>1.19</td> <td>1.12</td> <td>1.04</td> <td>1.00</td> </tr> </table> 	m	1.00	1.35	2.00	3.00	4.00	7.00	∞	1. Circular pipe	2.70	2.00	1.50	1.25	1.15	1.06	1.00	2. Plane pipe	2.00	1.63	1.35	1.19	1.12	1.04	1.00
m	1.00	1.35	2.00	3.00	4.00	7.00	∞																			
1. Circular pipe	2.70	2.00	1.50	1.25	1.15	1.06	1.00																			
2. Plane pipe	2.00	1.63	1.35	1.19	1.12	1.04	1.00																			

Free discharge from a conduit at different velocity distributions
(continued)

Section XI

Diagram 11-1

Type of velocity distribution	Scheme	Resistance coefficient $\xi = \frac{\Delta H}{\frac{1}{2} w_0^2}$																						
<p>Sinusoidal distribution of the velocities in a plane pipe:</p> $\frac{w}{w_0} = 1 + \frac{\Delta w}{w_0} \sin 2k\pi \frac{2y}{b_0}.$ <p>k = integer</p>		$\xi = 1 + \frac{3}{2} \left(\frac{\Delta w}{w_0} \right)^2$ <p>ξ determined from the curve $\xi = f \left(\frac{\Delta w}{w_0} \right)$ on the graph</p> <table border="1"> <tr> <td>$\frac{\Delta w}{w_0}$</td> <td>0.1</td> <td>0.2</td> <td>0.3</td> <td>0.4</td> <td>0.5</td> <td>0.6</td> <td>0.7</td> <td>0.8</td> <td>0.9</td> <td>1.0</td> </tr> <tr> <td>ξ</td> <td>1.00</td> <td>1.06</td> <td>1.13</td> <td>1.24</td> <td>1.38</td> <td>1.54</td> <td>1.74</td> <td>1.96</td> <td>2.20</td> <td>2.50</td> </tr> </table>	$\frac{\Delta w}{w_0}$	0.1	0.2	0.3	0.4	0.5	0.6	0.7	0.8	0.9	1.0	ξ	1.00	1.06	1.13	1.24	1.38	1.54	1.74	1.96	2.20	2.50
$\frac{\Delta w}{w_0}$	0.1	0.2	0.3	0.4	0.5	0.6	0.7	0.8	0.9	1.0														
ξ	1.00	1.06	1.13	1.24	1.38	1.54	1.74	1.96	2.20	2.50														
<p>Asymmetrical distribution in a plane pipe:</p> $\frac{w}{w_0} = 0.585 + 1.64 \sin \left(0.2 + 1.95 \frac{2y}{b_0} \right)$		$\xi = 3.67$																						
<p>Parabolic distribution:</p> $\frac{w}{w_0} = 1 - \left(\frac{y}{R_0} \right)^2$		<p>a. Circular (or square) pipe</p> $\xi = 2.0$ <p>b. Plane pipe</p> $\xi = 1.55$																						



$\frac{l_d}{D_0}$	Values of ϵ_{cal}									
	2	4	6	8	10	12	16	20	24	30
1.0	0.90	0.79	0.71	0.62	0.55	0.50	0.41	0.38	0.33	0.30
1.5	0.84	0.70	0.60	0.51	0.45	0.40	0.34	0.30	0.26	0.20
2.0	0.81	0.65	0.52	0.43	0.37	0.33	0.29	0.30	0.35	0.40
2.5	0.78	0.60	0.45	0.36	0.30	0.27	0.26	0.28	0.33	0.44
3.0	0.74	0.53	0.40	0.31	0.27	0.24	0.23	0.27	0.35	0.44
4.0	0.66	0.44	0.32	0.26	0.22	0.21	0.22	0.27	0.36	0.45
5.0	0.52	0.35	0.28	0.23	0.20	0.19	0.22	0.29	0.38	0.48
6.0	0.41	0.28	0.21	0.18	0.17	0.18	0.24	0.32	0.42	0.51
10.0	0.40	0.20	0.15	0.14	0.16	0.18	0.26	0.35	0.45	0.55

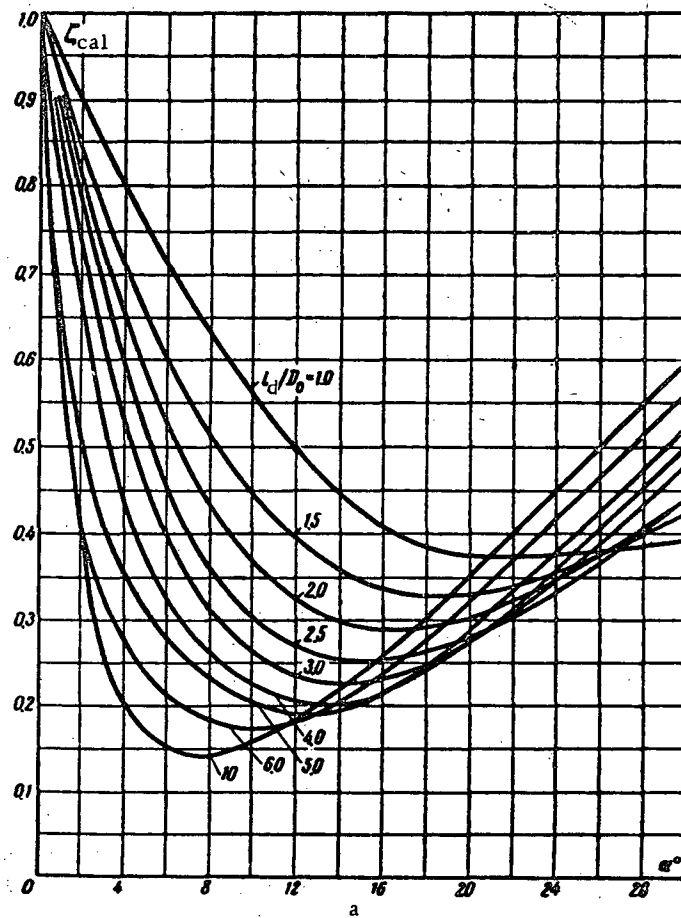
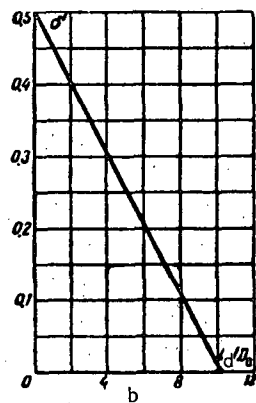
$$\zeta = \frac{\Delta H}{\frac{1}{2} w_0^2} = (1 + \alpha') \epsilon_{cal} \text{ (approximately),}$$

where ϵ_{cal} is determined from graph a;
 α' is determined tentatively from graph b.
When a screen is mounted in the exit

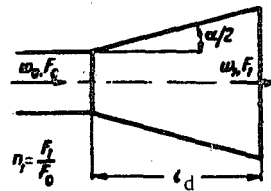
$$\zeta_{sum} = \frac{\Delta H}{\frac{1}{2} w_0^2} \approx \zeta + \frac{\zeta_s}{n^2},$$

where ζ is determined by the basic formulas;
 ζ_s is determined as ζ from the data of diagram
8-6

$\frac{l_d}{D_0}$	1.0	2.0	4.0	6.0	10.0
α'	0.45	0.40	0.30	0.20	0.0



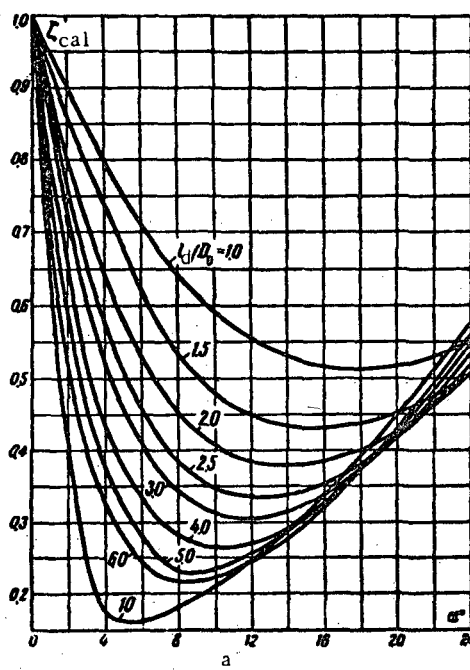
$$D_1 = \frac{4f_1}{\eta_0}; \quad \eta_0 = \text{perimeter}$$

Values of ζ_{cal} .

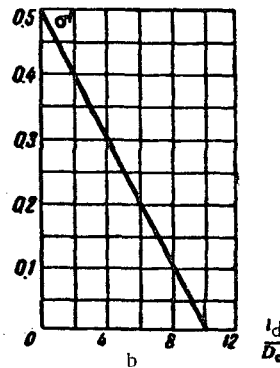
$\frac{l_d}{D_0}$	a'								
	0	2	4	6	10	12	16	20	24
1.0	1.0	0.89	0.79	0.64	0.59	0.56	0.52	0.52	0.55
1.5	1.0	0.84	0.74	0.53	0.47	0.45	0.43	0.45	0.50
2.0	1.0	0.80	0.63	0.45	0.40	0.39	0.38	0.43	0.50
2.5	1.0	0.76	0.57	0.39	0.35	0.34	0.35	0.42	0.52
3.0	1.0	0.71	0.52	0.34	0.31	0.31	0.34	0.42	0.53
4.0	1.0	0.65	0.43	0.28	0.26	0.27	0.33	0.42	0.53
5.0	1.0	0.59	0.37	0.23	0.23	0.26	0.33	0.43	0.55
6.0	1.0	0.54	0.32	0.22	0.22	0.25	0.32	0.43	0.56
10	1.0	0.41	0.17	0.18	0.20	0.25	0.34	0.45	0.57

$$\zeta = \frac{\Delta H}{\frac{\rho w_0^2}{2g}} = (1 + a') \zeta_{\text{cal}} \quad (\text{very approximately})$$

where ζ_{cal} is determined from graph a;
 a' is determined tentatively from graph b



$\frac{l_d}{D_0}$	1.0	2.0	4.0	6.0	10.0
a'	0.45	0.40	0.30	0.20	0.0

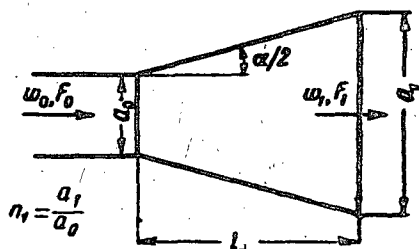


Free discharge from a rectilinear plane diffuser. $0.5 \leq \frac{a_0}{b_0} \leq 2.0$

Section XI

Diagram 11-4

b_0 = width, constant along the diffuser

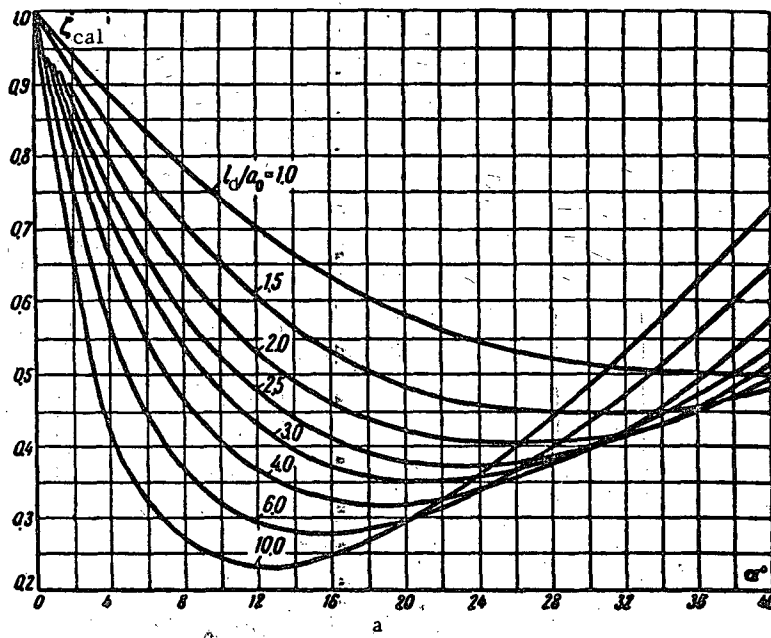


$$\zeta = \frac{\Delta H}{\frac{1}{2} w_0^2} = (1 + \alpha') \zeta_{cal} \text{ (approximately),}$$

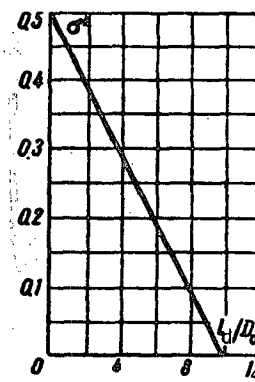
where ζ_{cal} is determined from graph a;
 α' is determined tentatively from graph b.

Values of ζ_{cal}

$\frac{l_d}{a_0}$	a_0													
	0	2	4	6	8	10	12	16	20	24	28	32	38	40
1.0	1.00	0.95	0.89	0.84	0.79	0.75	0.70	0.64	0.58	0.55	0.52	0.51	0.50	0.51
1.5	1.00	0.93	0.86	0.78	0.71	0.66	0.61	0.53	0.49	0.46	0.45	0.45	0.46	0.48
2.0	1.00	0.90	0.80	0.72	0.65	0.59	0.54	0.47	0.42	0.41	0.41	0.42	0.45	0.50
2.5	1.00	0.88	0.76	0.66	0.59	0.53	0.48	0.42	0.38	0.38	0.39	0.42	0.46	0.51
3.0	1.00	0.86	0.72	0.62	0.54	0.48	0.43	0.37	0.36	0.36	0.38	0.42	0.47	0.54
4.0	1.00	0.83	0.66	0.55	0.46	0.41	0.37	0.33	0.32	0.34	0.38	0.42	0.49	0.58
6.0	1.00	0.76	0.56	0.45	0.37	0.32	0.30	0.28	0.30	0.34	0.40	0.47	0.56	0.65
10.0	1.00	0.67	0.43	0.33	0.27	0.25	0.24	0.25	0.30	0.37	0.45	0.53	0.63	0.73



$\frac{l_d}{D_0}$	1.0	2.0	4.0	6.0	10.0
α'	0.45	0.40	0.30	0.20	0.0



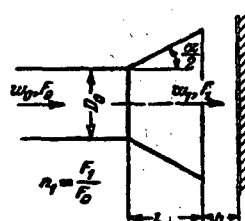
Section XI

 Discharge from a rectilinear diffuser against a baffle at $\frac{t_d}{D_h} = 1.0$

Diagram 11-5

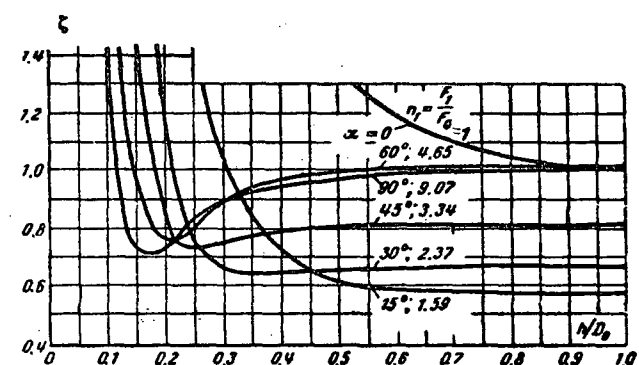
$$D_{II} = \frac{4F_0}{\Pi_0}; \Pi_0 - \text{perimeter};$$

$$\eta_1 = \frac{F_1}{F_0};$$



$\zeta = \frac{\Delta H}{\frac{\rho w_0^2}{2g}}$ is determined from the curves $\zeta = f\left(\frac{h}{D_0}\right)$.

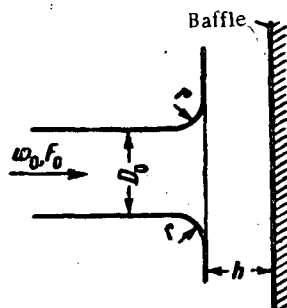
α°	n_1	Values of ζ									
		0.10	0.15	0.20	0.25	0.30	0.40	0.50	0.60	0.70	1.0
0	1.0	—	—	—	—	—	—	1.37	1.20	1.11	1.00
15	1.59	—	—	—	1.50	1.06	0.72	0.61	0.59	0.58	0.58
30	2.37	—	—	1.23	0.79	0.66	0.64	0.66	0.66	0.67	0.67
45	3.34	—	1.50	0.85	0.73	0.75	0.79	0.81	0.82	0.82	0.82
60	4.65	—	0.98	0.76	0.80	0.90	0.96	1.00	1.01	1.02	1.02
90	9.07	1.50	0.72	0.74	0.83	0.89	0.94	0.96	0.98	1.00	1.00



Discharge from a straight stretch with rounded edges against a baffle

Section XI

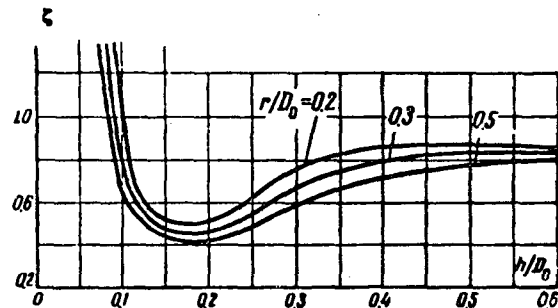
Diagram 11-6



h/D_0	0.05	0.07	0.10	0.15	0.20	0.25	0.30	0.35	0.40	0.50	0.60	1.0
$r/D_0 = 0.2$	2.30	0.90	0.52	0.51	0.62	0.75	0.82	0.85	0.86	0.85	0.85	—
$r/D_0 = 0.3$	1.60	0.75	0.47	0.48	0.55	0.66	0.73	0.78	0.81	0.82	0.82	—
$r/D_0 = 0.5$	2.50	1.30	0.63	0.44	0.41	0.49	0.58	0.65	0.71	0.76	0.87	0.78

$\zeta = \frac{\Delta H}{\frac{\rho w_0^2}{2g}}$ is determined from the curves $\zeta = f\left(\frac{h}{D_0}\right)$

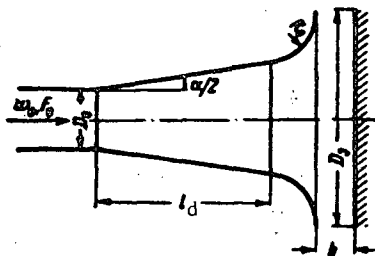
corresponding to different $\frac{r}{D_0}$:



Discharge from a diffuser with rounded edges and optimum characteristics against a baffle

Section XI

Diagram 11-7



$$\frac{l_d}{D_0} \approx 2.5; \alpha \approx 14^\circ.$$

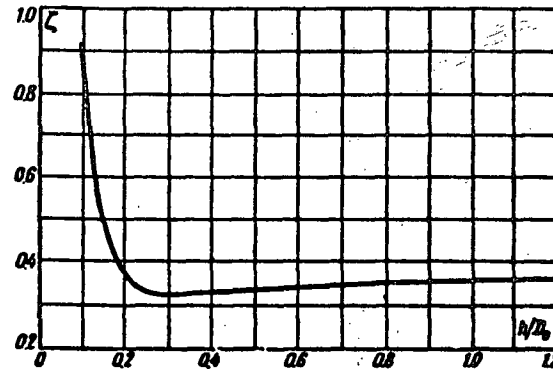
$$\frac{R_o}{D_0} \approx 0.7; \frac{D_2}{D_0} \approx 3.0$$

$$\zeta = \frac{\Delta H}{\frac{\rho w_0^2}{2g}}$$

is determined from the curve

$$\zeta = f\left(\frac{h}{D_0}\right).$$

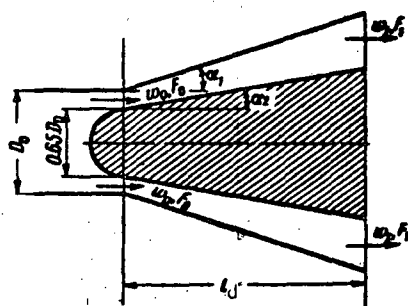
h/D_0	0.10	0.15	0.20	0.25	0.30	0.35	0.40	0.50	0.60	1.0
—	0.78	0.46	0.36	0.32	0.32	0.33	0.33	0.34	0.34	0.36



Free discharge from an annular diffuser

Section XI

Diagram 11-8

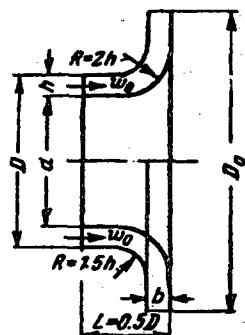


$$\zeta = \frac{\Delta H}{\frac{\rho w_0^2}{2g}} = k_1 \zeta'$$

where ζ' is taken from Table 11-3;
 k_1 is taken from diagram 5-18.

TABLE 11-3

l_d/D_0	0.75	1.0	1.5	1.8	2.0
a_1^0	12.5	12	6.7	8.7	6
a_2^0	0	9	3	6	3
ζ'	0.47	0.43	0.35	0.34	0.29



$$n = 2 \frac{b}{h} \bar{D} \frac{1}{1+\bar{d}}; \quad \bar{D} = \frac{D_d}{D_0}; \quad \bar{d} = \frac{d}{D_0};$$

$$\bar{c}_{a_0} = w_0 = \frac{Q}{\frac{\pi}{4} (D_0^2 - d^2) u};$$

Q = discharge, m^3/sec ;

u = peripheral velocity at maximum radius, m/sec .

$\zeta = \frac{\Delta H}{\frac{Tw_0^2}{2g}}$ is determined from the curves $\zeta = f(n, \bar{D})$.

Values of ζ

\bar{D}	n						
	1.1	1.8	2.2	2.6	3.0	3.4	3.8

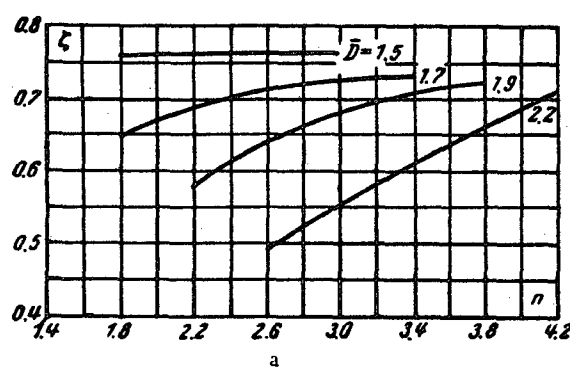
a. Diffuser behind an operating compressor

$$\bar{c}_{a_0} \approx 0.5$$

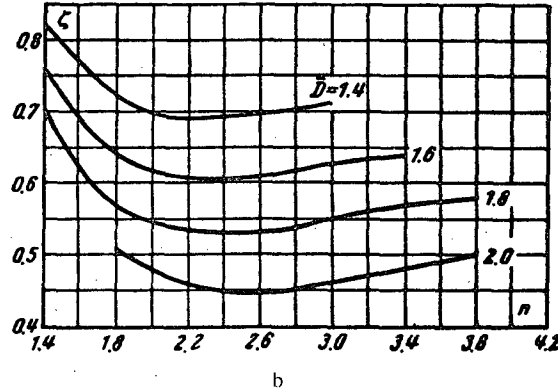
1.5	—	0.76	0.76	0.76	0.76	—	—	—
1.7	—	0.65	0.69	0.71	0.72	0.73	—	—
1.9	—	—	0.58	0.64	0.67	0.71	0.72	—
2.2	—	—	—	0.49	0.65	0.61	0.66	0.71

b. Diffuser behind nonoperative compressor

1.4	0.82	0.72	0.69	0.70	0.71	—	—	—
1.6	0.76	0.64	0.61	0.61	0.63	0.64	—	—
1.8	0.70	0.57	0.54	0.53	0.55	0.57	0.58	—
2.0	—	0.51	0.46	0.45	0.46	0.48	0.50	—



a

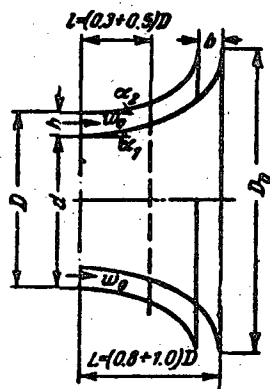


b

Free discharge from an axial-radial-annular diffuser
 $\bar{D} = 2.08$; $\bar{d} = 0.688$; $\alpha_2 = 8^\circ$; $c_{a_0} = 0.5$

Section XI

Diagram 11-10



$$n = 2 \frac{b}{h} \bar{D} \frac{1}{1 + \bar{d}}; \quad \bar{D} = \frac{D_d}{D_0}; \quad \bar{d} = \frac{a}{D_0};$$

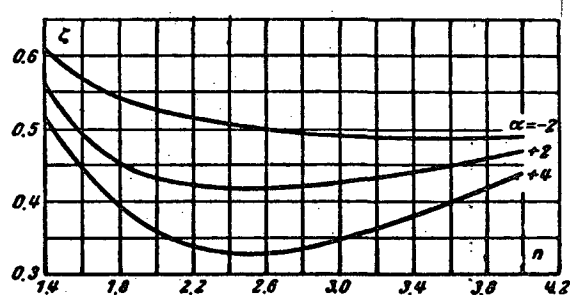
$$c_{a_0} = w_0 = \frac{Q}{\frac{\pi}{4} (D_0^2 - d^2) u};$$

Q = discharge, m^3/sec ;

u = peripheral velocity at maximum radius, m/sec .

$\zeta = \frac{\Delta H}{\frac{\gamma w_0^2}{2g}}$ is determined from the curves $\zeta = f(n, \alpha)$.

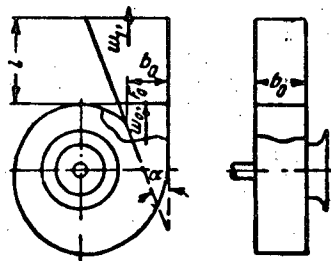
α°	Values of ζ							
	1.4	1.8	2.2	2.6	3.0	3.4	3.6	4.0
-2	0.61	0.54	0.52	0.50	0.49	0.49	0.49	0.49
+2	0.56	0.45	0.43	0.42	0.43	0.44	0.45	0.47
+4	0.52	0.39	0.34	0.33	0.35	0.38	0.40	0.46



Free discharge from a plane asymmetric diffuser behind a centrifugal induced-draft fan

Section XI

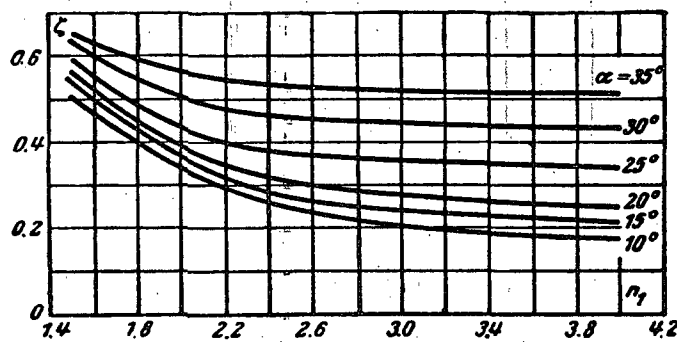
Diagram 11-11



$$n_1 = \frac{F_1}{F_0}$$

$$\zeta = \frac{\Delta H}{\frac{\gamma w_0^2}{2g}}$$

from the curves $\zeta = f(n_1)$ corresponding to different α°



n_1	1.5	2.0	2.5	3.0	3.5	4.0
-------	-----	-----	-----	-----	-----	-----

$\alpha = 10^\circ$

ζ	0.51	0.34	0.25	0.21	0.18	0.17
---------	------	------	------	------	------	------

$\alpha = 15^\circ$

ζ	0.54	0.36	0.27	0.24	0.22	0.20
---------	------	------	------	------	------	------

$\alpha = 20^\circ$

ζ	0.55	0.38	0.31	0.27	0.25	0.24
---------	------	------	------	------	------	------

$\alpha = 25^\circ$

ζ	0.59	0.43	0.37	0.35	0.33	0.33
---------	------	------	------	------	------	------

$\alpha = 30^\circ$

ζ	0.63	0.50	0.46	0.44	0.43	0.42
---------	------	------	------	------	------	------

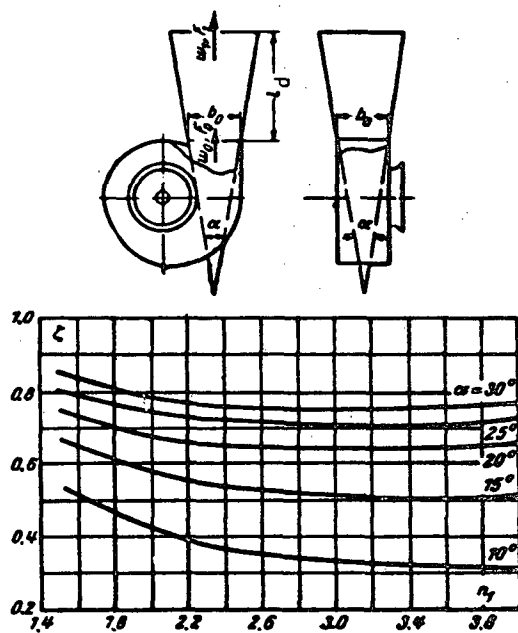
$\alpha = 35^\circ$

ζ	0.65	0.56	0.53	0.52	0.51	0.50
---------	------	------	------	------	------	------

Free discharge from a pyramidal diffuser behind a centrifugal induced-draft fan

Section XI

Diagram 11-12



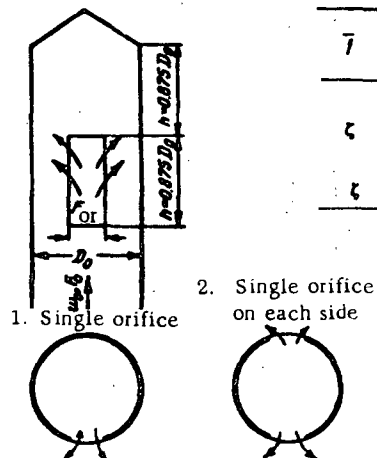
$$\zeta = \frac{\Delta H}{\frac{V^2}{2g}} \text{ is determined from the curves } \zeta = f(n_1) \text{ corresponding to different } \alpha^\circ$$

where $n_1 = \frac{F_1}{F_0}$

Side discharge from the last orifice of a circular pipe

Section XI

Diagram 11-13

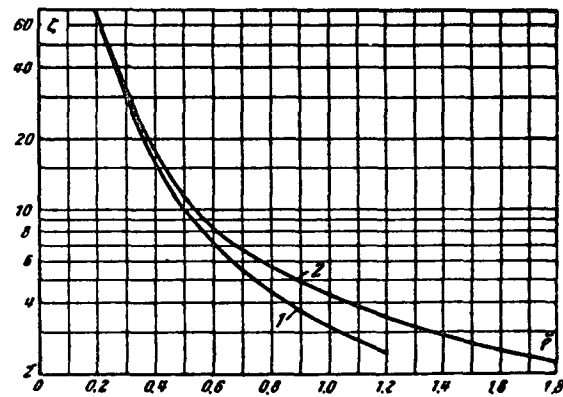


$$\zeta = \frac{\Delta H}{\frac{V^2}{2g}} \text{ is determined from the curves } \zeta = f(\bar{f}).$$

where $\bar{f} = \frac{F_{or}}{F_0}$.

\bar{f}	0.2	0.3	0.4	0.5	0.6	0.7	0.8	0.9	1.0	1.2	1.4	1.6	1.8
1. One orifice													
ζ	65.7	30.0	16.4	10.0	7.30	5.50	4.48	3.67	3.16	2.44	—	—	—
ζ	67.7	33.0	17.2	11.6	8.45	6.80	5.86	5.00	4.38	3.47	2.90	2.52	2.25

2. Two orifices

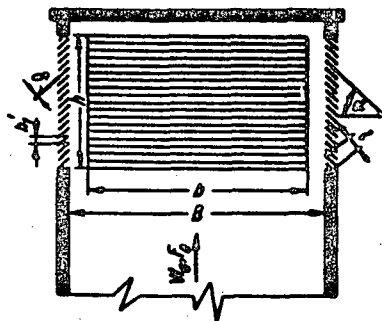


Straight rectangular exhaust vents; lateral openings with and without fixed louvers

Section XI

Diagram 11-14

$$\frac{h}{B} = 0.5; \quad f = \frac{nbh}{F_0}$$

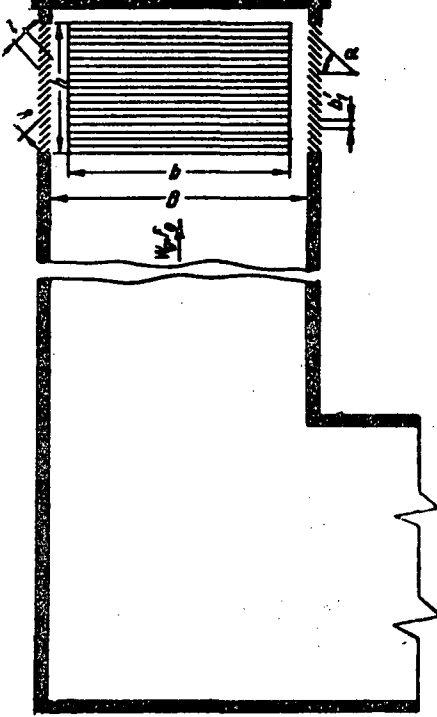
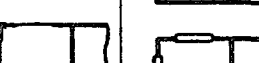
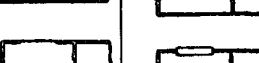
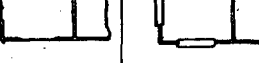
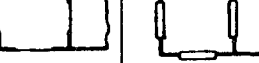
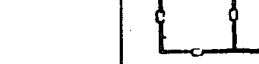
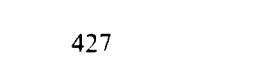
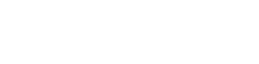
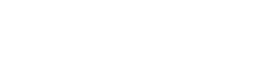


Number of openings n	Layout of the openings		$\frac{l}{l}$	$\frac{b}{B}$	Resistance coefficient		$C = \frac{\Delta H}{\frac{V^2}{2g}}$
	without louvers	with louvers			without louvers	with louvers	
One			0.36	1.5	15.5	22.0	—
Two			0.36	1.5	5.00	7.20	—
Three			0.36	1.5	3.50	5.00	—
Four			0.36	1.5	2.20	2.60	3.50
The same			0.24	1.0	5.30	7.00	10.0
			0.12	0.5	15.6	19.6	29.0

Rectangular exhaust with elbows; lateral openings with and without fixed louvers

Section XI

Diagram 11-15

Number of openings	Layout of the openings		$\frac{b}{h}$	Resistance coefficient $\zeta = \frac{\Delta H}{\frac{V^2}{2g}}$			
	without louvers	with louvers		$\alpha=30^\circ$: $\frac{b_1'}{h} = 0.029$; $\frac{l}{b_1'} = 1.8$;	$\alpha=45^\circ$: $\frac{b_1'}{h} = 0.024$; $\frac{l}{b_1'} = 1.4$; $\frac{s}{b_1'} = 0.058$; $\frac{s}{b_1'} = 0.07$		
One		 	0.36	1.5	14.0	18.6	—
"	 	 	0.36	1.5	17.6	26.0	—
Two	 	 	0.36	1.5	5.20	6.60	—
"	 	 	0.36	1.5	7.00	9.30	—
Three	 	 	0.36	1.5	4.00	4.60	—
"	 	 	0.36	1.5	7.00	9.00	—
Four	 	 	0.36	1.5	4.00	4.20	5.00
The same	 	 	0.24	1.0	6.60	8.00	10.7
			0.12	0.5	16.0	20.0	29.5

Straight circular exhaust vents. $Re = \frac{\omega_0 D_0}{\nu} > 10^4$

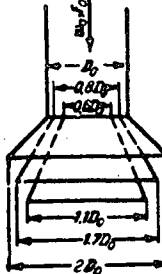
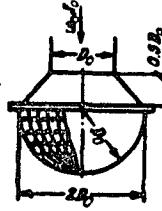
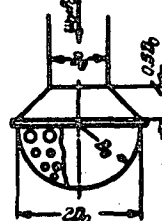
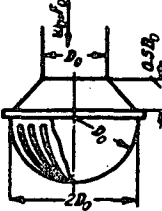
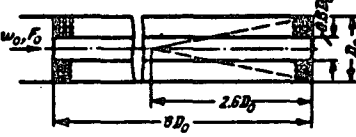
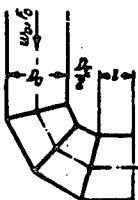
Section XI

Diagram 11-16

No.	Vent characteristic	Diagram	Resistance coefficient $\xi = \frac{AH}{\gamma v_0^2} \frac{2R}{D_0}$																																																																												
1	With plane baffle		Values of ξ																																																																												
2	With split canopy		<table border="1"> <thead> <tr> <th rowspan="2">N</th> <th colspan="10">h/D_0</th> </tr> <tr> <th>0.10</th> <th>0.20</th> <th>0.25</th> <th>0.30</th> <th>0.35</th> <th>0.40</th> <th>0.50</th> <th>0.60</th> <th>0.80</th> <th>1.0</th> </tr> </thead> <tbody> <tr> <td>1</td> <td>—</td> <td>—</td> <td>3.40</td> <td>2.60</td> <td>2.10</td> <td>1.70</td> <td>1.40</td> <td>1.20</td> <td>1.10</td> <td>1.00</td> </tr> <tr> <td>2</td> <td>—</td> <td>—</td> <td>—</td> <td>—</td> <td>—</td> <td>3.50</td> <td>2.00</td> <td>1.50</td> <td>1.20</td> <td>1.10</td> </tr> <tr> <td>3</td> <td>4.00</td> <td>2.30</td> <td>1.90</td> <td>1.60</td> <td>1.40</td> <td>1.30</td> <td>1.15</td> <td>1.10</td> <td>1.00</td> <td>1.00</td> </tr> <tr> <td>4</td> <td>—</td> <td>2.90</td> <td>2.30</td> <td>1.90</td> <td>1.70</td> <td>1.50</td> <td>1.30</td> <td>1.20</td> <td>1.10</td> <td>1.00</td> </tr> <tr> <td>5</td> <td>2.60</td> <td>1.20</td> <td>1.00</td> <td>0.80</td> <td>0.70</td> <td>0.65</td> <td>0.60</td> <td>0.60</td> <td>0.60</td> <td>0.60</td> </tr> </tbody> </table>	N	h/D_0										0.10	0.20	0.25	0.30	0.35	0.40	0.50	0.60	0.80	1.0	1	—	—	3.40	2.60	2.10	1.70	1.40	1.20	1.10	1.00	2	—	—	—	—	—	3.50	2.00	1.50	1.20	1.10	3	4.00	2.30	1.90	1.60	1.40	1.30	1.15	1.10	1.00	1.00	4	—	2.90	2.30	1.90	1.70	1.50	1.30	1.20	1.10	1.00	5	2.60	1.20	1.00	0.80	0.70	0.65	0.60	0.60	0.60	0.60
N	h/D_0																																																																														
	0.10	0.20	0.25	0.30	0.35	0.40	0.50	0.60	0.80	1.0																																																																					
1	—	—	3.40	2.60	2.10	1.70	1.40	1.20	1.10	1.00																																																																					
2	—	—	—	—	—	3.50	2.00	1.50	1.20	1.10																																																																					
3	4.00	2.30	1.90	1.60	1.40	1.30	1.15	1.10	1.00	1.00																																																																					
4	—	2.90	2.30	1.90	1.70	1.50	1.30	1.20	1.10	1.00																																																																					
5	2.60	1.20	1.00	0.80	0.70	0.65	0.60	0.60	0.60	0.60																																																																					
3	With hood																																																																														
4	With split hood																																																																														
5	With diffuser and hood																																																																														

Duct caps

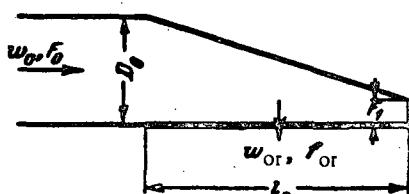
Section XI
Diagram 11-17

Type of cap	View	Resistance coefficient $\zeta = \frac{\Delta H}{T_0 \frac{V^2}{2g}}$						
With three diffusers		$\zeta = 1.0$						
Hemisphere with orifices $\frac{F_{or}}{F_0} = 0.56$		$\zeta = 1.0$						
Hemisphere with orifices $\frac{F_{or}}{F_0} = 3.9$		$\zeta = 1.0$						
Hemisphere with slots $\frac{F_{or}}{F_0} = 1.4$		$\zeta = 2.0$						
Cylinder with perforated surface $\frac{F_{or}}{F_0} = 4.7$		$\zeta = 0.90$						
Bend		<table border="1" data-bbox="1237 1614 1456 1730"> <tr> <td>$\frac{l}{D_0}$</td><td>0.4</td><td>0.8</td></tr> <tr> <td>ζ</td><td>1.52</td><td>1.41</td></tr> </table>	$\frac{l}{D_0}$	0.4	0.8	ζ	1.52	1.41
$\frac{l}{D_0}$	0.4	0.8						
ζ	1.52	1.41						

Air duct with perforated lateral outlet

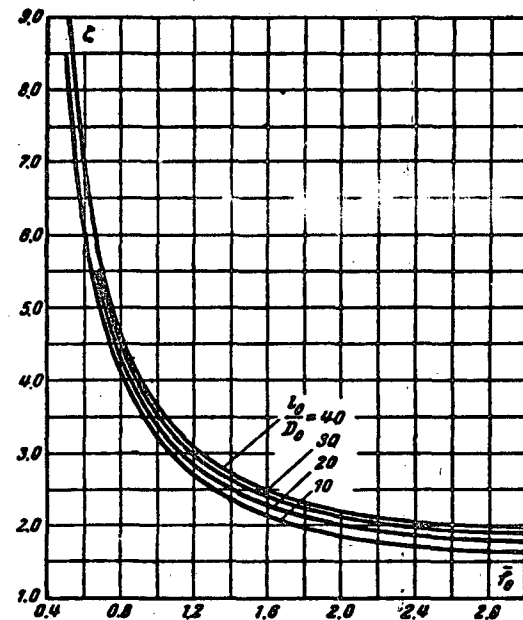
 Section XI
 Diagram 11-18

$$D_h = \frac{4F_0}{H_0}; H_0 - \text{perimeter}$$

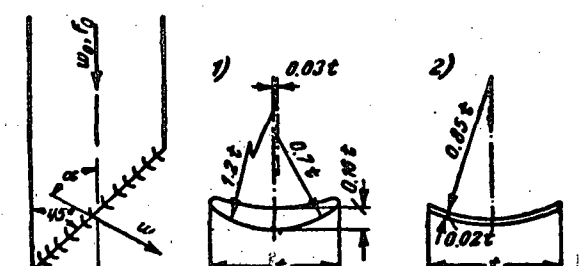


$0.5 < \bar{l}_0 < 3.0$ and $0 < \frac{F_1}{F_0} < 1.0$; $\zeta = \frac{\Delta H}{\frac{1}{2} w_0^2} \approx \frac{1.8}{f_0^2} + \left(\frac{l_0}{D_h} \right)^{0.15}$

l_0/D_h	\bar{l}_0							
	0.5	0.6	0.8	1.0	1.5	2.0	2.5	3.0
10	8.61	6.41	4.22	3.21	2.21	1.86	1.69	1.61
20	8.77	5.57	4.38	3.37	2.37	2.02	1.85	1.77
30	8.87	6.67	4.48	3.47	2.47	2.12	1.95	1.87
40	8.94	6.74	4.55	3.54	2.54	2.19	2.02	1.94



Baturin-type outlet

 Section XI
 Diagram 11-19


a_0	30	40	50	60	70	80	90	100	110
-------	----	----	----	----	----	----	----	-----	-----

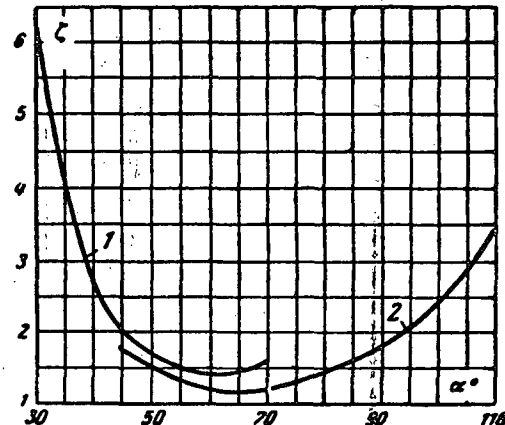
1. Airfoils

$$\zeta | 6.4 | 2.7 | 1.7 | 1.6 | - | - | - | - | -$$

2. Plane vanes

$$\zeta | - | - | 1.5 | 1.2 | 1.2 | 1.4 | 1.8 | 2.4 | 3.5$$

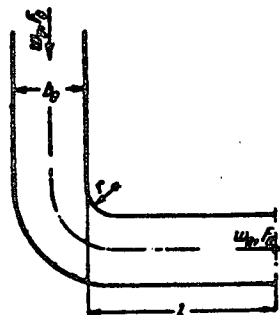
$$\zeta = \frac{\Delta H}{\frac{1}{2} w_0^2} \quad \text{is determined from the curves } \zeta = f(\alpha^\circ)$$



Discharge from a 90° bend

 Section XI
 Diagram 11-20

r/b_0	Values of ζ_m									
	l/b_0									
0	0.5	1.0	1.5	2.0	3.0	4.0	6.0	8.0	12.0	
0.0	2.95	3.13	3.23	3.00	2.72	2.40	2.24	2.10	2.05	2.00
0.2	2.15	2.15	2.08	1.84	1.70	1.60	1.56	1.52	1.49	1.48
0.5	1.80	1.54	1.43	1.36	1.32	1.26	1.22	1.19	1.19	1.19
1.0	1.46	1.19	1.11	1.09	1.09	1.09	1.09	1.09	1.09	1.09
2.0	1.19	1.10	1.06	1.04	1.04	1.04	1.04	1.04	1.04	1.04

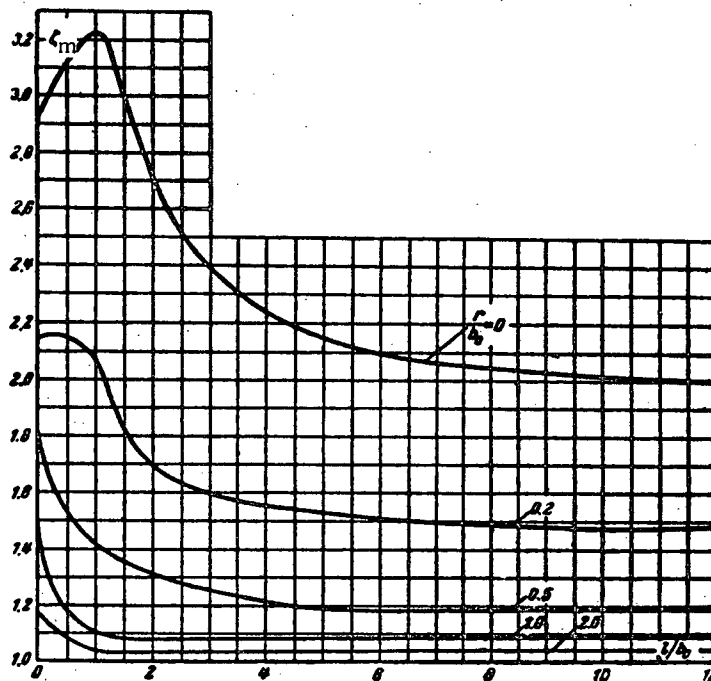


$$\zeta = \frac{\Delta H}{\frac{1}{2} w_0^2} = \zeta_m + \lambda \frac{l}{b_0},$$

where ζ_m is determined from the curve $\zeta_m =$

$= f \left(\frac{l}{b_0} \right)$ for different $\frac{r}{b_0}$; λ is determined

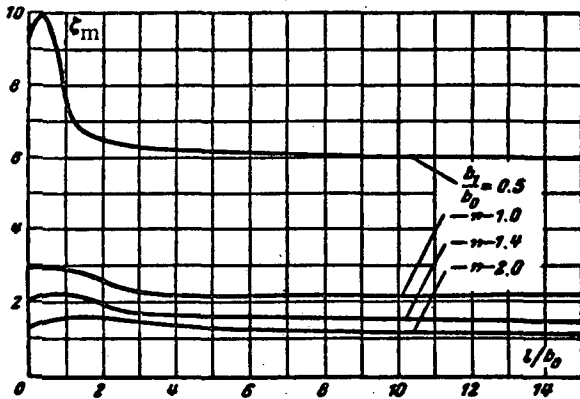
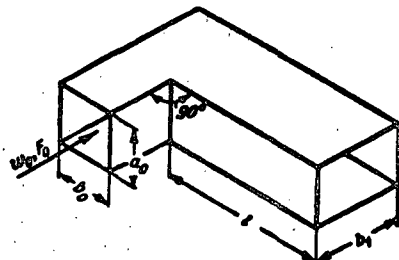
from diagrams 2-1 to 2-5.



Discharge from a square-section ($\frac{a_0}{b_0} = 1.0$) sharp 90° elbow
with contracted or expanded discharge section

Section XI

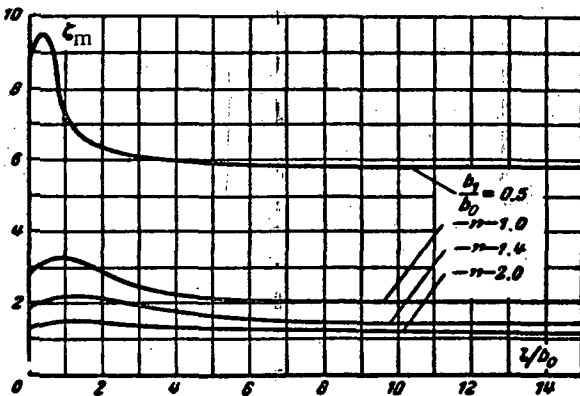
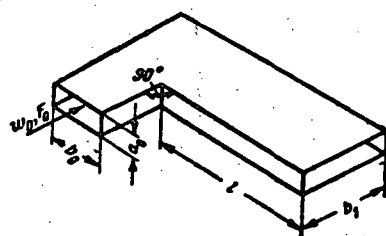
Diagram 11-21



Discharge from a rectangular-section ($\frac{a_0}{b_0} = 0.25$) sharp elbow
with contracted or expanded discharge section

Section XI

Diagram 11-22



$$\zeta = \frac{\Delta H}{\frac{1}{2} w_0^2} = \zeta_m + \lambda \frac{l}{b_1} \left(\frac{b_0}{b_1} \right)^n$$

where ζ_m is determined from the curves $\zeta_m = f\left(\frac{l}{b_1}\right)$ for different $\frac{b_1}{b_0}$; λ is determined from diagrams 2-1 to 2-5.

l/b_0	0	0.5	1.0	1.5	2.0	4.0	6.0	8.0	15.0
$b_1/b_0 = 0.5$									
ζ_m	9.0	10	7.6	6.7	6.5	6.2	6.2	6.1	5.9
$b_1/b_0 = 1.0$									
ζ_m	2.9	3.0	2.9	2.8	2.6	2.2	2.2	2.2	2.2
$b_1/b_0 = 1.4$									
ζ_m	2.0	2.2	2.2	2.1	1.9	1.7	1.6	1.5	1.5
$b_1/b_0 = 2.0$									
ζ_m	1.3	1.5	1.6	1.6	1.6	1.4	1.3	1.2	1.1

$$\zeta = \frac{\Delta H}{\frac{1}{2} w_0^2} = \zeta_m + \lambda \frac{l}{b_1} \left(\frac{b_0}{b_1} \right)^n$$

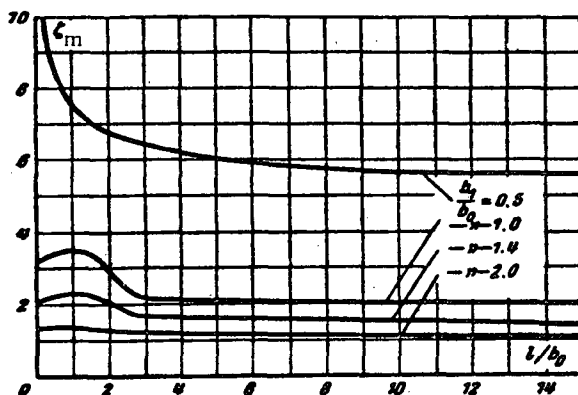
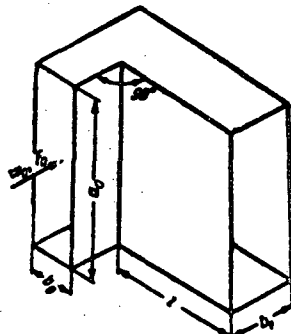
where ζ_m is determined from the curves $\zeta_m = f\left(\frac{l}{b_1}\right)$ for different $\frac{b_1}{b_0}$; λ is determined from diagrams 2-1 to 2-5.

l/b_0	0	0.5	1.0	1.5	2.0	4.0	6.0	8.0	15.0
$b_1/b_0 = 0.5$									
ζ_m	8.8	9.5	7.2	6.6	6.3	6.0	5.9	5.8	5.8
$b_1/b_0 = 1.0$									
ζ_m	2.7	3.2	3.3	3.1	2.9	2.3	2.1	2.0	2.0
$b_1/b_0 = 1.4$									
ζ_m	1.8	2.1	2.2	2.2	2.1	1.8	1.6	1.4	1.4
$b_1/b_0 = 2.0$									
ζ_m	1.3	1.5	1.6	1.5	1.4	1.3	1.2	1.1	

Discharge from a rectangular-section ($\frac{a_0}{b_0} = 4.0$) sharp 90° elbow
with contracted or expanded discharge section

Section XI

Diagram 11-23



$$\xi = \frac{\Delta H}{\gamma w_0^2} = \xi_m + \lambda \frac{l}{b_1} \left(\frac{b_0}{b_1} \right)^2.$$

where ξ_m is determined from the curves $\xi_m = f\left(\frac{l}{b_0}\right)$ for different $\frac{b_1}{b_0}$; λ is determined from diagrams 2-1 to 2-5.

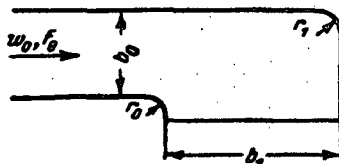
l/b_0	0	0.5	1.0	1.5	2.0	4.0	6.0	8.0	15.0
1) $\frac{b_1}{b_0} = 0.5$									
ξ_m	9.9	8.5	7.6	7.1	6.8	6.2	5.9	5.7	5.6
2) $\frac{b_1}{b_0} = 1.0$									
ξ_m	3.2	3.3	3.5	3.4	3.0	2.1	2.1	2.1	2.0
3) $\frac{b_1}{b_0} = 1.4$									
ξ_m	2.0	2.2	2.3	2.2	2.0	1.7	1.6	1.6	1.5
4) $\frac{b_1}{b_0} = 2.0$									
ξ_m	1.3	1.4	1.4	1.3	1.2	1.2	1.2	1.1	1.1

Discharge from a smooth ($\frac{r}{b_0} = 0.2$) 90° elbow with contracted or expanded discharge section

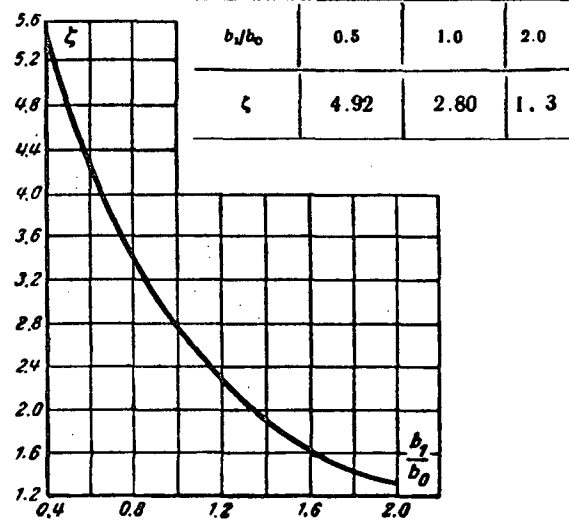
Section XI

Diagram 11-24

$$r_0 = r_1 = r$$



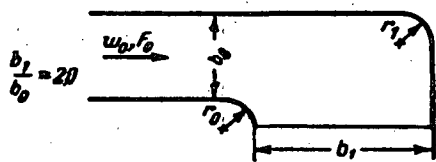
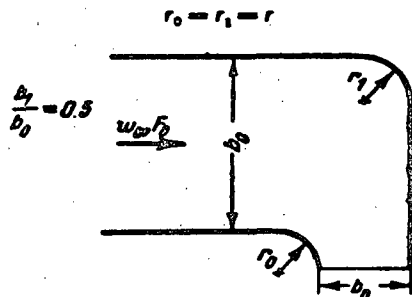
$$\xi = \frac{\Delta H}{\gamma w_0^2} \text{ is determined from the curve } \xi = f\left(\frac{b_1}{b_0}\right)$$



Discharge from a smooth 90° elbow with discharge section contracted or expanded by a factor of two

Section XI

Diagram 11-25

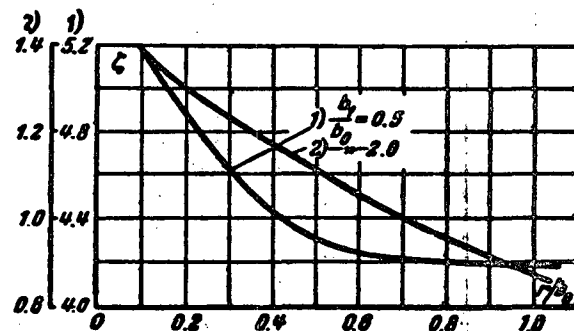


$$\zeta = \frac{\Delta H}{\frac{\gamma u_0^2}{2g}} \text{ is determined from the curves } \zeta = f\left(\frac{r}{b_0}\right).$$

r/b_0	0.1	0.2	0.3	0.4	0.5	0.6	0.8	1.0
---------	-----	-----	-----	-----	-----	-----	-----	-----

$$1) \frac{b_1}{b_0} = 0.5 \quad \zeta | 5.20 | 4.92 | 4.64 | 4.44 | 4.31 | 4.24 | 4.20 | 4.18$$

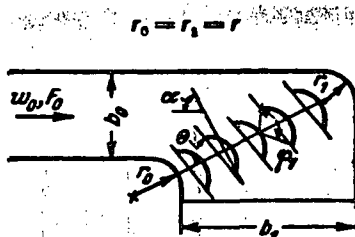
$$2) \frac{b_1}{b_0} = 2.0 \quad \zeta | 1.40 | 1.30 | 1.23 | 1.17 | 1.11 | 1.05 | 0.95 | 0.87$$



Discharge from a smooth 90° elbow with discharge section expanded by a factor of two ($\frac{b_1}{b_0} = 2.0$) and with five thin guide vanes

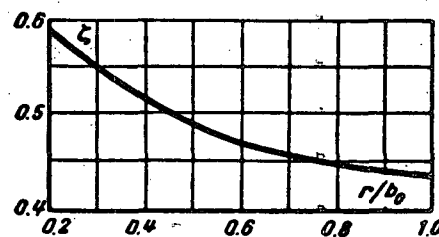
Section XI

Diagram 11-26



$$\zeta = \frac{\Delta H}{\frac{\gamma u_0^2}{2g}} \text{ is determined from the curve } \zeta = f\left(\frac{r}{b_0}\right).$$

r/b_0	0.2	0.5	1.0
θ°	70	72-74	72-74
φ_1°	154	99	90
ζ	0.59	0.49	0.44

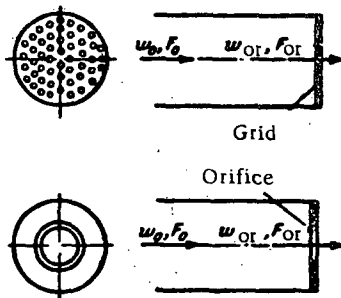


Discharge from a straight conduit through a grid or orifice
 $(0 \leq l/d_h \leq 0.15)$

Section XI

Diagram 11-27

$$d_h = \frac{4f_0}{P_{or}}; P_{or} - \text{perimeter};$$



f_0 = area of one orifice; P_{or} = total cross-section area of the grid openings

$$\text{a) } Re = \frac{w_{or} d_h}{v} > 10^5.$$

$$\zeta = \frac{\Delta H}{\frac{1}{2} w_0^2} = \left(1 + 0.707 \sqrt{1 - \bar{f}} \right)^2 \frac{1}{\bar{f}}$$

is determined from the curve $\zeta = f(\bar{f})$

b) $Re < 10^5$:

$$\zeta = \frac{\Delta H}{\frac{1}{2} w_0^2} = (\zeta_p + \epsilon_0^{Re} \bar{f}) \frac{1}{\bar{f}^2},$$

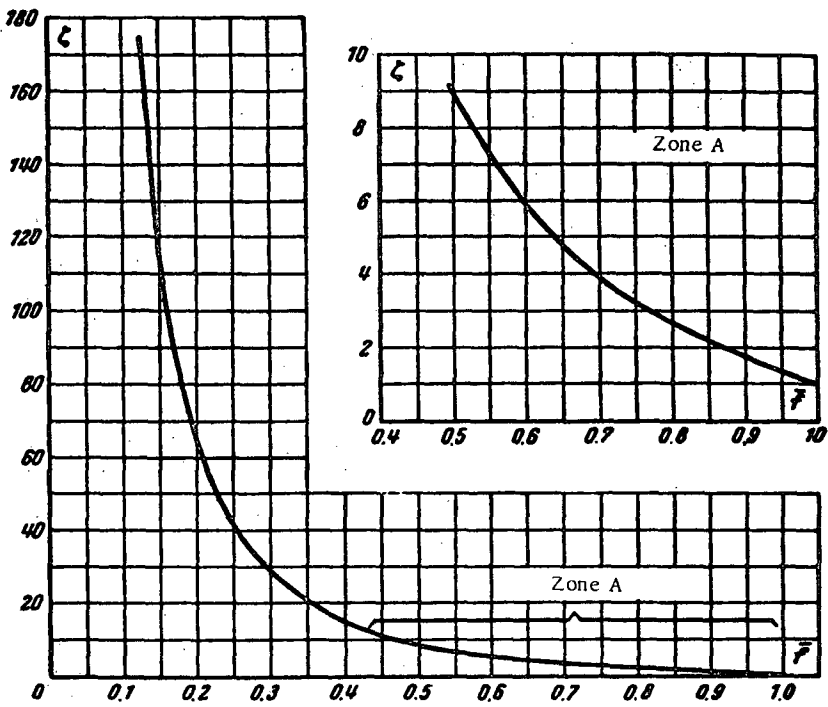
where ζ_p is determined from the curves $\zeta_p = f(Re, \bar{f})$ on graph a of diagram 4-10;

ϵ_0^{Re} is determined from the curve $\epsilon_0^{Re} = \bar{f}(Re)$ on the same graph a of diagram 4-10;

$\zeta_p = f(\bar{f})$ on graph b of diagram 4-10.

v is determined from § 1-3, b.

f	0.05	0.10	0.15	0.20	0.25	0.30	0.35	0.40	0.45	0.50	0.55	0.60	0.65	0.70	0.75	0.80	0.85	0.9	1.0
ζ	1140	280	122	67	41.6	30.0	20.2	15.0	11.5	9.00	7.40	6.20	4.80	3.90	3.30	2.70	2.22	1.80	1.0

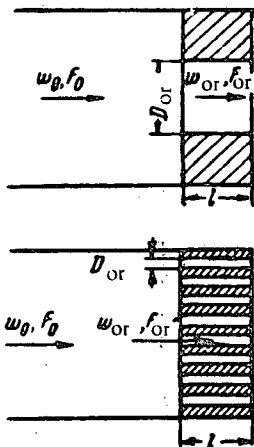


$$\bar{l} = \frac{F_{\text{or}}}{F_0}; d_h = \frac{4f_0}{H_{\text{or}}};$$

H_{or} = perimeter;

f_0 = area of one orifice;

F_{or} = total cross-section area of the grid openings.



$$\text{a) } Re = \frac{w_0 D_h}{v} > 10^4:$$

$$\zeta = \left\{ \left[1 + 0.5(1 - \bar{l}) + \varsigma \sqrt{1 - \bar{l}} \right] + \lambda \frac{l}{d_h} \right\} \frac{1}{\bar{l}^2} = \\ = \left(\zeta_0 + \lambda \frac{l}{d_h} \right) \frac{1}{\bar{l}^2}.$$

where ς is determined from the curve $\varsigma = f\left(\frac{l}{d_h}\right)$

$$\zeta_0 = 1 + 0.5(1 - \bar{l}) + \varsigma \sqrt{1 - \bar{l}},$$

λ is determined from diagrams 2-1 to 2-5;

b) $Re < 10^4$ (approximately):

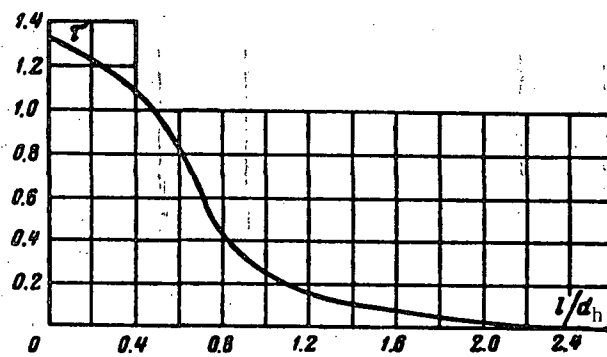
$$\zeta = (\zeta_p + \bar{\zeta}_0^{Re} \zeta_0) \frac{1}{\bar{l}^2},$$

where ζ_p and $\bar{\zeta}_0^{Re}$ are determined from diagram 4-10;

ζ_0 is determined as under a;

v is determined from § 1-3, b.

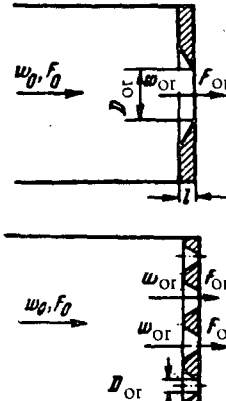
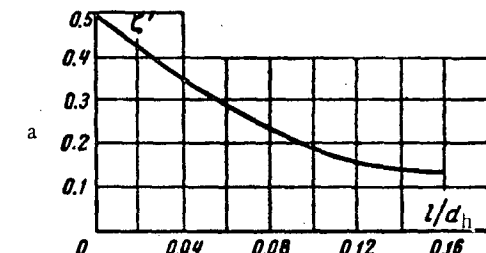
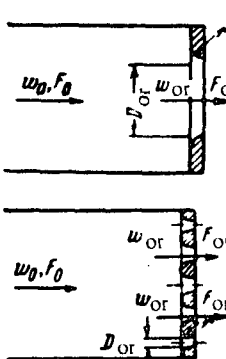
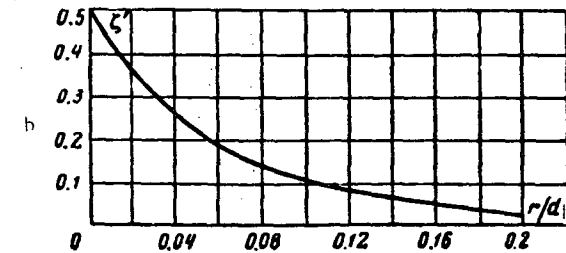
$\frac{l}{d_h}$	0	0.2	0.4	0.6	0.8	1.0	1.2	1.6	2.0	2.4
ς	1.35	1.22	1.10	0.84	0.42	0.24	0.16	0.07	0.02	0



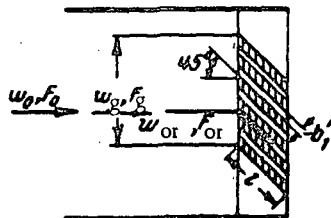
Discharge from a rectilinear conduit through an orifice or grid
with orifice edges beveled or rounded toward the stream flow

Section XI

Diagram 11-29

Shape of the orifice edges	Scheme	Resistance coefficient $\zeta = \frac{\Delta H}{\frac{1}{2} w_0^2}$																								
Beveled		$Re = \frac{w_{or} d_h}{v} > 10^3$ $\zeta = [1 + V \zeta' (1 - \bar{l})]^2 \frac{1}{\bar{l}^2}$ where ζ' is determined from the curve $\zeta' = f\left(\frac{l}{d_h}\right)$ <table border="1" data-bbox="922 675 1553 822"> <tr> <th>$\frac{l}{d_h}$</th><th>0.01</th><th>0.02</th><th>0.03</th><th>0.04</th><th>0.06</th><th>0.08</th><th>0.12</th><th>0.16</th> </tr> <tr> <th>ζ'</th><td>0.46</td><td>0.42</td><td>0.38</td><td>0.35</td><td>0.29</td><td>0.23</td><td>0.16</td><td>0.13</td> </tr> </table> 	$\frac{l}{d_h}$	0.01	0.02	0.03	0.04	0.06	0.08	0.12	0.16	ζ'	0.46	0.42	0.38	0.35	0.29	0.23	0.16	0.13						
$\frac{l}{d_h}$	0.01	0.02	0.03	0.04	0.06	0.08	0.12	0.16																		
ζ'	0.46	0.42	0.38	0.35	0.29	0.23	0.16	0.13																		
Rounded		$Re = \frac{w_{or} d_h}{v} > 10^3$ $\zeta = [1 + V \zeta' (1 - \bar{l})]^2 \frac{1}{\bar{l}^2}$ where ζ' is determined from the curve $\zeta' = f\left(\frac{r}{d_h}\right)$ <table border="1" data-bbox="922 1329 1553 1477"> <tr> <th>$\frac{r}{d_h}$</th><th>0</th><th>0.01</th><th>0.02</th><th>0.03</th><th>0.04</th><th>0.05</th><th>0.06</th><th>0.08</th><th>0.12</th><th>0.16</th><th>0.20</th> </tr> <tr> <th>ζ'</th><td>0.50</td><td>0.44</td><td>0.37</td><td>0.31</td><td>0.26</td><td>0.22</td><td>0.19</td><td>0.15</td><td>0.09</td><td>0.06</td><td>0.03</td> </tr> </table> 	$\frac{r}{d_h}$	0	0.01	0.02	0.03	0.04	0.05	0.06	0.08	0.12	0.16	0.20	ζ'	0.50	0.44	0.37	0.31	0.26	0.22	0.19	0.15	0.09	0.06	0.03
$\frac{r}{d_h}$	0	0.01	0.02	0.03	0.04	0.05	0.06	0.08	0.12	0.16	0.20															
ζ'	0.50	0.44	0.37	0.31	0.26	0.22	0.19	0.15	0.09	0.06	0.03															

No. 1. Inlet edges of the slats cut vertically



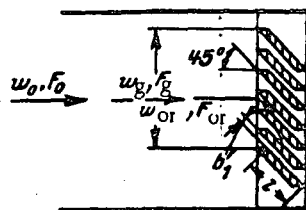
$$a) \frac{l}{b'_1} \geq \left(\frac{l}{b'_1} \right)_{\text{opt}} \quad \text{where } \left(\frac{l}{b'_1} \right)_{\text{opt}} \cong 11(1 - \bar{l})$$

$$\zeta = \frac{\Delta H}{\gamma w_0^2} = k \left[1 + 0.85 \left(1 - \bar{l} \frac{F_g}{F_{or}} \right) + \zeta_{fr} \right] \times \frac{1}{\bar{l}^2} \left(\frac{F_g}{F_{or}} \right)^2 = k' \zeta'$$

$$b) \frac{l}{b'_1} < \left(\frac{l}{b'_1} \right)_{\text{opt}}$$

$$\zeta = k' \zeta' + \Delta \zeta$$

2. Inlet edges of the slats cut horizontally

where $k = 1.0$ for No. 1; $k = 0.6$ for No. 2.

$$\Delta \zeta \cong 0.5 \left[11(1 - \bar{l}) - \frac{l}{b'_1} \right]; \quad \zeta_{fr} = \lambda \frac{l}{b'_1};$$

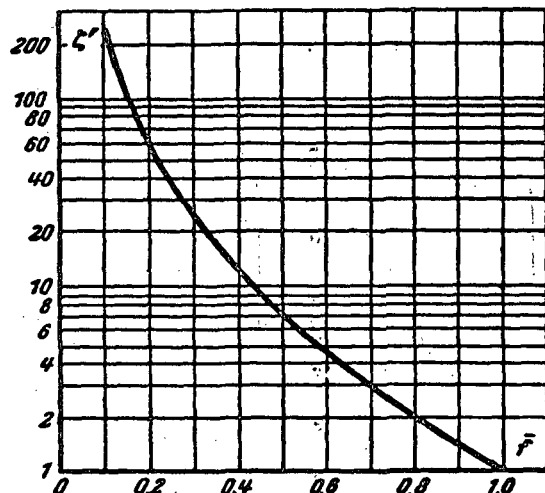
 λ is determined from diagrams 2-1 to 2-5;

$$\bar{l} = \frac{F_{or}}{F_g} \quad (F_g = \text{louver-grid front};$$

 F_{or} = free cross section of the louver.

$$\text{At } \frac{l}{b'_1} = \left(\frac{l}{b'_1} \right)_{\text{opt}}, \quad \frac{F_{or}}{F_g} = \frac{F_{or}}{F_0} \quad \text{and } \lambda = 0.064$$

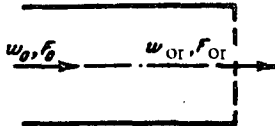
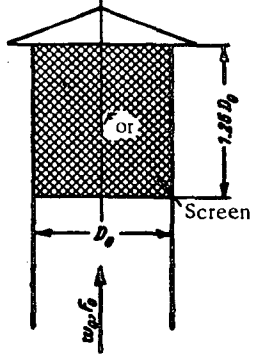
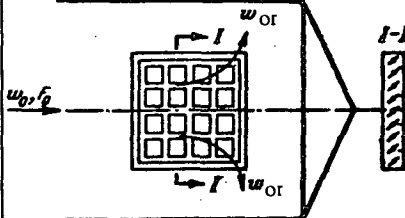
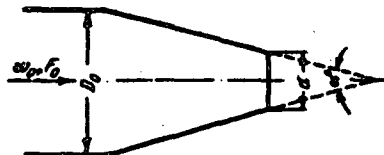
(at $Re = \frac{w_0 b'_1}{v} = 10^3$) the values of ζ' are determined from the curve $\zeta' = f(\bar{l})$

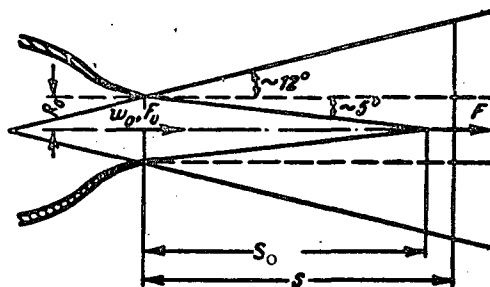
 v is taken from § 1-3.b.

\bar{l}	0.1	0.2	0.3	0.4	0.5	0.6	0.7	0.8	0.9	1.0
ζ'	247	55.0	23.8	12.3	7.00	4.60	3.00	2.06	1.43	1.00

Discharge stretches under different conditions

 Section XI
 Diagram 11-31

Conditions of discharge	View	Resistance coefficient $\xi = \frac{\Delta H}{\frac{V^2}{2g}}$
From a straight conduit with screen at the exit		$\xi = 1 + \xi_c$ where ξ_c is determined as ξ for a screen by diagram 8-6 (approximately)
From a gutter with screen $\bar{F} = \frac{F_{or}}{F_g} = 0.8$		$\xi = 1.1$ (approximately)
Through a stamped standard louver at $\bar{F} = \frac{F_{or}}{F_g} \approx 0.8$ with completely opened adjustable slats		$\xi \approx 3 - 3.5$ (approximately)
Through stamped or cast grids	cf. diagram 3-22 (p. 111)	ξ is determined from the curve $\xi = f(\bar{h})$ of diagram 11-27 (approximately)
Smoothly converging nozzle		$\xi = 1.05 \left(\frac{D_n}{d} \right)^4$

$\alpha' \approx 0.08$ 

$$\zeta = \frac{\Delta H}{\frac{1}{2} w_0^2} = 1 - \bar{e}$$

1. Initial zone ($S < 8$ to $10R_0$)

$$\bar{q} = 1 + 0.76 \frac{\alpha' S}{R_0} + 1.32 \left(\frac{\alpha' S}{R_0} \right)^2$$

$$\bar{e} = 1 - 1.03 \frac{\alpha' S}{R_0} + 0.68 \left(\frac{\alpha' S}{R_0} \right)^2$$

$$\bar{e}_a = 1 - 1.14 \frac{\alpha' S}{R_0} + 0.61 \left(\frac{\alpha' S}{R_0} \right)^2$$

2. Main zone ($S > 8$ to $10R_0$)

$$\bar{q} = 2.22 \left(\frac{\alpha' S}{R_0} + 0.29 \right)$$

$$\bar{e} = \frac{0.59}{\frac{\alpha' S}{R_0} + 0.29}$$

$$\bar{e}_a = \frac{1.78 B_2}{\frac{\alpha' S}{R_0} + 0.29}$$

(for B_2 cf. Table 11-1);

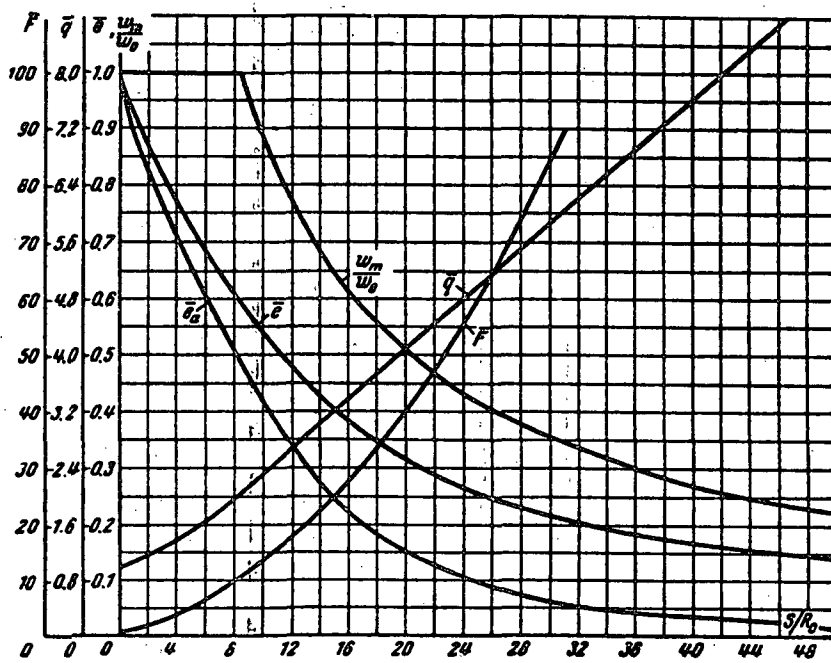
$$\frac{w_m}{w_0} = \frac{0.96}{\frac{\alpha' S}{R_0} + 0.29}$$

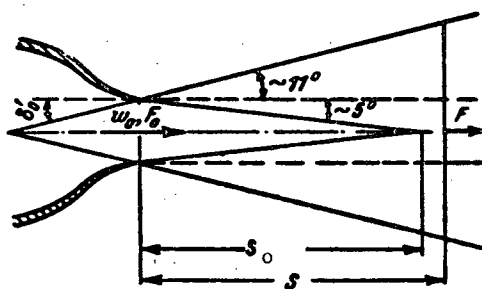
3. For the entire jet:

$$\bar{F} = \left(1 + 3.4 \frac{\alpha' S}{R_0} \right)^2$$

 \bar{q} = dimensionless discharge across the section of a jet; \bar{e} = dimensionless kinetic-energy residue in the section of a jet; \bar{e}_a = dimensionless kinetic-energy residue of the constant-mass jet core in the section; \bar{F} = dimensionless area of the jet section.The values of \bar{q} , \bar{e} , \bar{e}_a , $\frac{w_m}{w_0}$ and \bar{F} aredetermined from the graph as functions of $\frac{S}{R_0}$.

S/R_0	0	5	10	15	20	25	30	40	50
\bar{q}	1.00	1.52	2.38	3.24	4.12	5.00	5.86	7.62	9.37
\bar{e}	1.00	0.70	0.61	0.40	0.31	0.26	0.22	0.17	0.14
\bar{e}_a	1.00	0.64	0.48	0.24	0.16	0.10	0.07	0.04	0.01
$\frac{w_m}{w_0}$	1.00	1.00	1.00	0.64	0.51	0.42	0.36	0.27	0.22
\bar{F}	1.00	5.57	13.8	25.7	41.50	60.80	83.90	141.00	213.00



$\alpha \approx 0.09$ 

$$\zeta = \frac{\Delta H}{\gamma w_0^2} = 1 - \bar{e}$$

$$\frac{2g}{2g}$$

1. Initial zone ($S < 10$ to $12\delta_0'$):

$$\bar{q} = 1 + 0.43 \frac{\alpha' S}{\delta_0};$$

$$\bar{e} = 1 - 0.21 \frac{\alpha' S}{\delta_0};$$

$$\bar{e}_a = 1 - 0.275 \frac{\alpha' S}{\delta_0}.$$

2. Main zone ($S > 10$ to $12\delta_0'$):

$$\bar{q} = 1.2 \sqrt{\frac{\alpha' S}{\delta_0'} + 0.41};$$

$$\bar{e} = \frac{0.94}{\sqrt{\frac{\alpha' S}{\delta_0'} + 0.41}};$$

$$\bar{e}_a = \frac{1.73 A_3}{\sqrt{\frac{\alpha' S}{\delta_0'} + 0.41}}$$

(for A_3 cf. Table 11-2);

$$\frac{w_m}{w_0} = \frac{1.2}{\sqrt{\frac{\alpha' S}{\delta_0'} + 0.41}}.$$

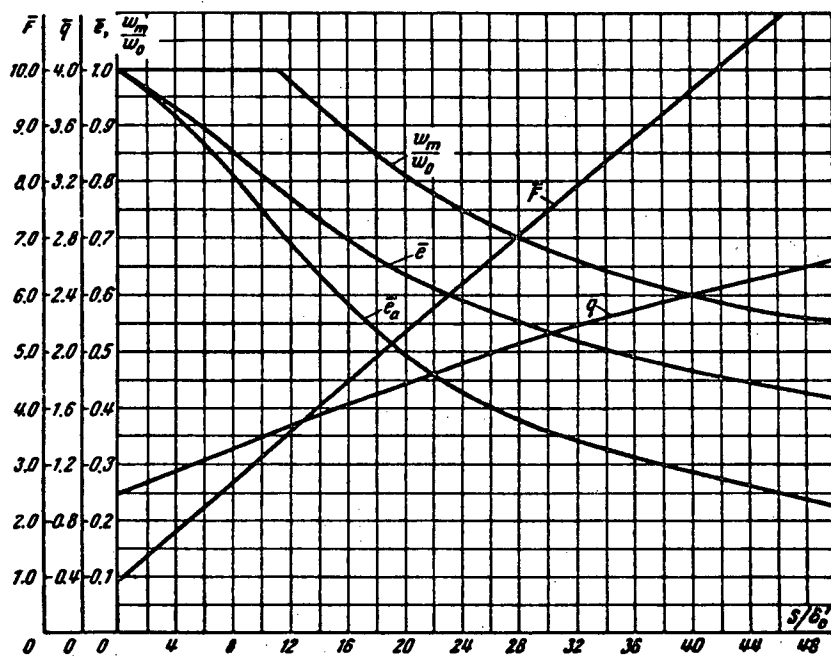
3. For the entire jet:

$$\bar{F} = 1 + 2.4 \frac{\alpha' S}{\delta_0'};$$

 \bar{q} = dimensionless discharge across the section of a jet; \bar{e} = dimensionless kinetic-energy residue in the section of a jet; \bar{e}_a = dimensionless kinetic-energy residue of the constant-mass jet core in the section; \bar{F} = dimensionless area of the jet section.

The values of \bar{q} , \bar{e} , \bar{e}_a , $\frac{w_m}{w_0}$ and \bar{F} are determined from the graph as functions of $\frac{S}{\delta_0'}$.

S/δ_0'	0	5	10	15	20	25	30	40	50
\bar{q}	1.00	1.19	1.39	1.60	1.79	1.96	2.11	2.40	2.66
\bar{e}	1.00	0.91	0.81	0.71	0.63	0.58	0.54	0.47	0.42
\bar{e}_a	1.00	0.88	0.75	0.60	0.49	0.42	0.36	0.29	0.23
$\frac{w_m}{w_0}$	1.00	1.00	1.00	0.90	0.81	0.74	0.68	0.60	0.56
\bar{F}	1.00	2.08	3.16	4.24	5.32	6.40	7.48	9.64	11.8



Section Twelve

STREAM FLOW THROUGH VARIOUS TYPES OF EQUIPMENT (Resistance coefficients)

12-1. LIST OF SYMBOLS

F_0 = area of the inlet section, or the narrowest section of a radiator, m^2 ;

F_1 = cross-section area of a filtering cloth, radiator, or total cross section of the dust-separator element, m^2 ;

F_{ch} = cross-section area of the working chamber of a unit, m^2 ;

$n = \frac{F_{ch}}{F_0}$ = area ratio;

D_0 = diameter of the inlet orifice, m;

w_0 = mean stream velocity at the inlet or in the narrowest section of a radiator, m/sec ;

w_1 = mean stream velocity before the filtering cloth (filtration rate), before the radiator, in the free section of the dust separator, m/sec ;

ΔH = pressure loss (resistance) of the apparatus, device, kg/m^2 ;

ξ = resistance coefficient;

M_0 = momentum coefficient for the inlet orifice;

N_0 = kinetic-energy coefficient for the inlet orifice.

12-2. EXPLANATIONS AND RECOMMENDATIONS

a. Gas or air scrubbers

1. Gas or air scrubbers can be divided into groups according to the principle used for separating suspended particles. The following types are treated here: inertial louver-type dust separators, ordinary and battery-type dust separators, porous and cloth filters, and electrostatic filters.

2. In inertial louver-type dust separators the entering gas stream is split by the louver slats into fine jets which turn sharply about these slats (Figure 12-1). As a result, centrifugal forces separate the dust particles from the stream. The impact of the dust particles on the slats and their reflection helps this separation.

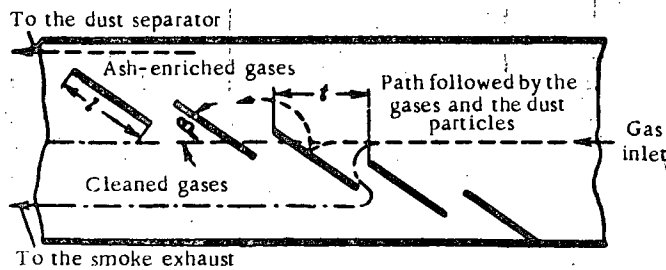


FIGURE 12-1. The working of a louver-type dust separator.

The degree to which the gas is cleaned is a function of: stream velocity upon reaching the louver slats, dust-particle size and specific gravity, viscosity and specific gravity of the gases, curvature of the trajectory of the jet passing through the louver, and dust separator design.

3. Cyclones are based on the utilization of inertia forces during the helical motion of the stream in the dust extractor, starting at the tangential inlet and ending at the dust discharge orifice in the body bottom (Figure 12-2). During the stream motion along the descending (outer) spiral, a part of the stream is directed with decreasing velocity toward the exhaust pipe, while the particles suspended in it are thrown toward the body wall and continue to move with the remaining part of the stream toward the dust discharge orifice.

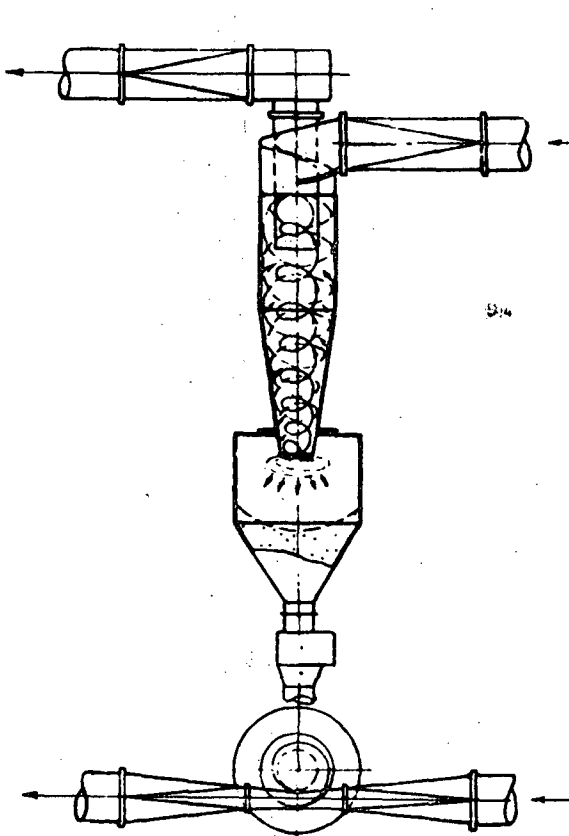


FIGURE 12-2. Pattern of stream motion in the body of a cyclone.

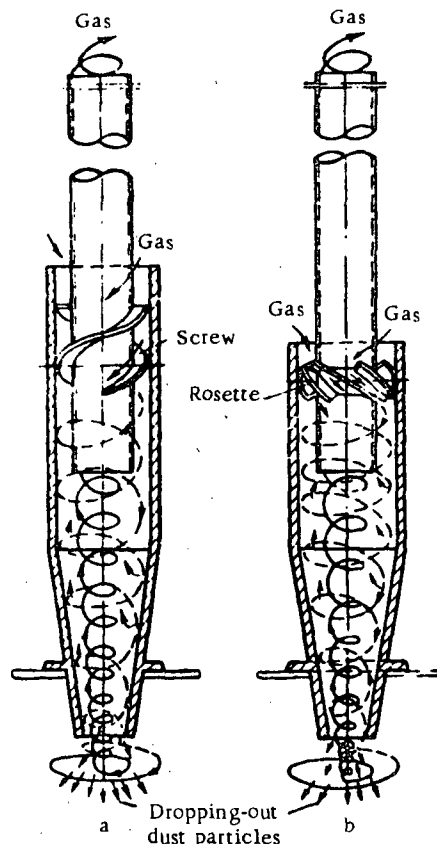


FIGURE 12-3. Extractor elements of a battery-type dust separator:
a—with screw blade; b—with rosette.

A certain part of the stream moving along the outer spiral passes through the dust discharge orifice into a bunker, carrying the suspended particles with it. In the bunker the stream gradually loses its velocity, and as a result the particles suspended in it settle out.

The clean stream re-enters the dust separator body through the same discharge orifice but along the ascending (inner) spiral. The stream flows along this spiral until it

enters the exhaust pipe, and then continues along the pipe. Here it is rejoined by the part of the stream which was separated from it during its descending motion.

4. The degree to which the stream is cleaned in cyclones is a function of the design and dimensions of the unit, stream velocity, physical properties and size of the dust particles, physical properties of the moving medium, dust concentration, etc. In general, cyclones operate efficiently when the dust particles are larger than 5 microns.

5. The capacity or output of a cyclone is in reverse ratio to its hydraulic resistance. Theoretically, the resistance coefficient of a cyclone can be assessed by the method of Klyachko /12-18/ or Minskii /12-25/.

The values of resistance coefficients of different types of cyclones, given in this handbook have been determined experimentally.

Since the performance of a given type of cyclone is best characterized by the stream velocity in its body, and it is more convenient in calculations to use the inlet velocity, two values of the resistance coefficient are given for each cyclone corresponding to the mean velocity at the inlet ($\zeta_0 = \frac{\Delta H}{\gamma w_0^2/2g}$) and to the mean velocity over the free cross section of the body ($\zeta_1 = \frac{\Delta H}{\gamma w_1^2/2g}$).

6. Since the output of a cyclone increases with an increase of its diameter, while the increase of diameter reduces the degree of cleaning, in the case of large streams it is more expedient to use a group of cyclones of smaller diameter, or a battery-type dust separator, instead of a single cyclone of large diameter. The difference between a battery-type dust separator and a group of cyclones lies in the considerably smaller dimensions of the separator elements of the former, and in the different design. The extractor elements of a battery-type separator have special guide wheels (a screw blade or a rosette with blades set at angles of 25 to 30° toward the separator axis (Figure 12-3) which ensure a rotary motion in the extractor elements.

7. Wet-scrubbing apparatus are used to increase the amount of removal of suspended particles. Here the gas stream is wetted by a liquid sprayed through nozzles, or by a water film on the scrubber surface.

The values of the resistance coefficients of different types of wet-scrubbing apparatus are given in diagrams 12-6 to 12-8.

8. A high-performance type of wet scrubber is the Venturi scrubber, consisting of two main parts: a tube sprayer (1), which represents a Venturi tube, and a drop catcher (2) (Figure 12-4). This unit is characterized by a high velocity at the throat (60 to 150 m/sec). The liquid, introduced in the tube sprayer in the form of jets or drops, is split as a result of the high stream velocity at the throat into fine particles with large total surface area (large number of particles per unit volume). In addition, the high velocity leads to an increase of the stream turbulence. These factors increase the probability of collision between the liquid and solid particles in the polluted gas. It follows that the cleaning process in this unit can be considered essentially a coagulation process. The coagulated particles are subsequently caught by the second part of the Venturi scrubber — the drop catcher.

9. The resistance coefficient of the tube sprayer is determined, on the basis of the data of Teverovskii, Zaitsev, and Murashkevich /12-9, 12-26, 12-34, 12-35/, by the following formula:

$$\zeta = \frac{\Delta H}{\gamma g w_g^2} = \zeta_g + \zeta_w \frac{w_1}{w_g} m, \quad (12-1)$$

where $\zeta_g = \frac{\Delta H}{\frac{1}{2} w_g^2}$ is the resistance coefficient of the tube sprayer without liquid wetting; it

can be determined approximately as the sum of the resistance coefficients of the straight stretch, the nozzle, and the diffuser, by the data given in Sections II, III, and V; ζ_w is the resistance coefficient of a tube sprayer, allowing for the influence of wetting by a liquid; values of this coefficient are given in diagram 12-6; w_g = mean velocity of the gas in the tube-sprayer throat, m/sec; γ_g , γ_l are the specific gravity of the gas at the tube throat, and of the wetting liquid, kg/m³; m is the specific discharge of the wetting liquid, l/m³ of the gas.

The hydraulic resistance of the drop catcher is determined from the data of this section as a function of its design.

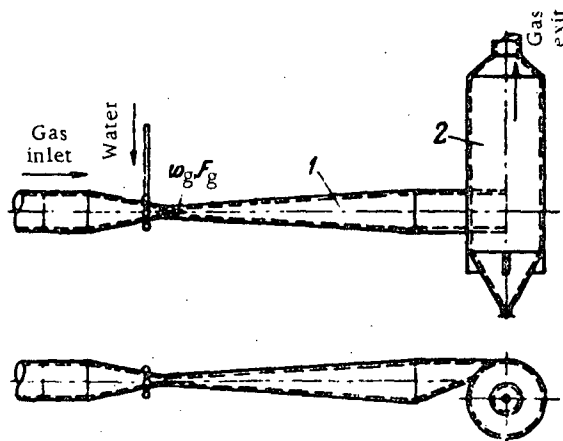


FIGURE 12-4. Venturi scrubber.

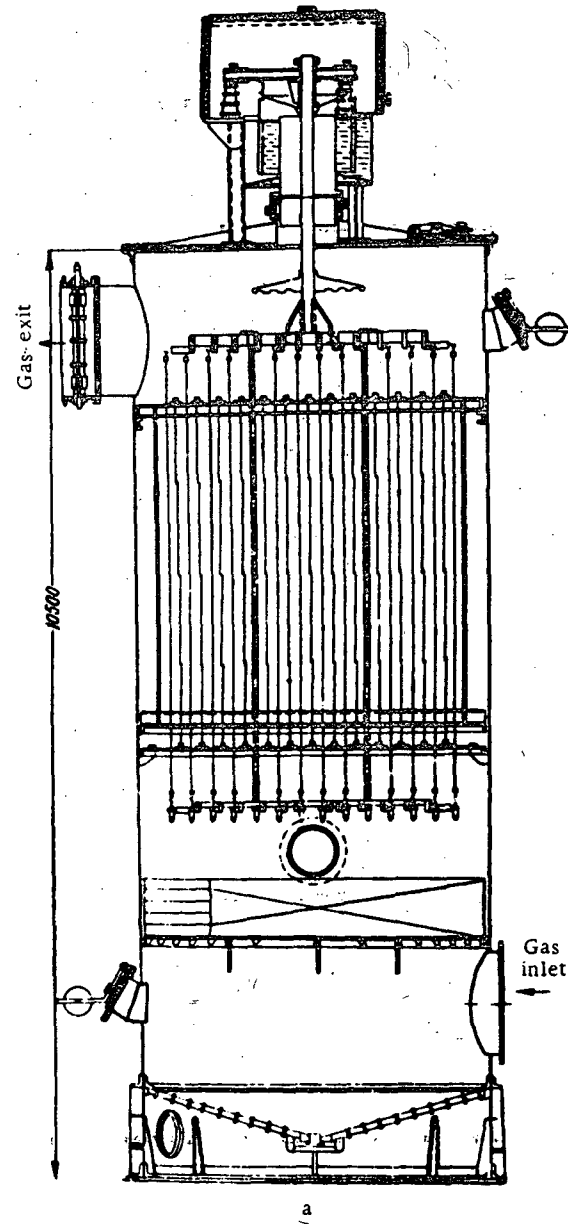
10. The dry cleaning of gas or air from fine dust is frequently achieved by means of cloth filters. The resistance of a filtering cloth increases with time during the passage of dirty gas through it. This increase in resistance is due to the settling of dust particles at the pore inlets; these coalesce and form a "secondary" porous partition which aids the dust separation. The resistance of the resulting filtering medium made of the cloth and dust increases with the increase of the dust-layer thickness.

11. The resistance of the contaminated filtering cloth can be considered (Zaitsev /12-8/) as made up of two parts: $\Delta H'$ = resistance caused by the unremovable dust, and $\Delta H''$ = resistance of the dust layer removed during the periodical cleanings of the cloth.

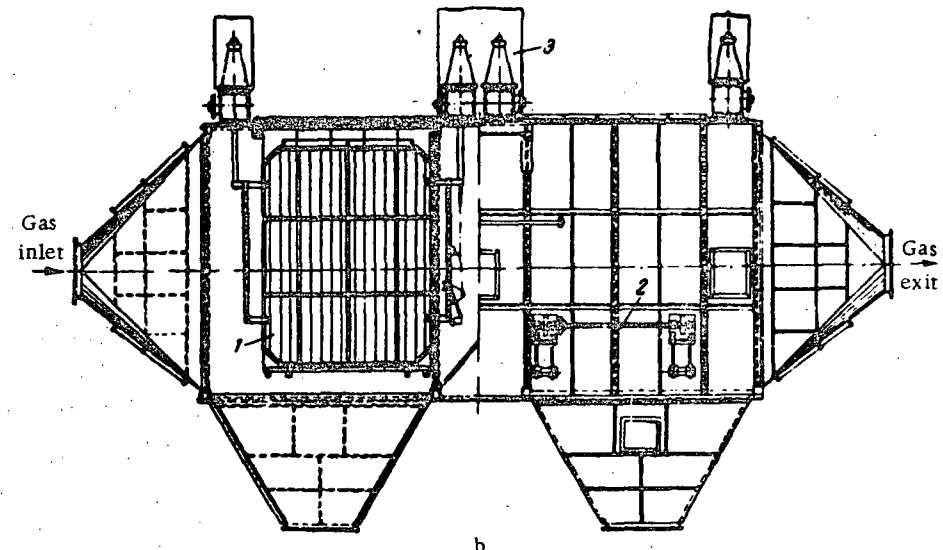
It is therefore recommended (Gordon and Aladzhalov /12-7/) that the total resistance of a contaminated filtering cloth be calculated by the following formula:

$$\Delta H = (A + Bp) \eta w_s, \text{ kg/m}^2, \quad (12-2)$$

where A is the experimental coefficient depending on the kind of dust, the cloth type, and the degree of contamination; B is the experimental coefficient depending on the dry weight



a



b

FIGURE 12-5. Electrostatic filters:

a —vertical; b—horizontal.

and permeability of the dust layer; η is the dynamic viscosity of the gas, $\text{kg}\cdot\text{sec}/\text{m}^2$; p is the degree of contamination of the gas, kg/m^2 ; w , is the filtration rate, $\text{m}^3/\text{m}^2\cdot\text{sec}$.

12. A different formula is sometimes used for the resistance of a contaminated cloth (Rekk /12-30/):

$$\Delta H = (A_0 + A'_0) Q^m. \quad (12-3)$$

where A_0 and A'_0 are proportionality coefficients depending on the kind of dust, the type of cloth, and the degree of contamination; $Q = \frac{Q_h}{F_1}$ is the specific loading of the cloth per hour, $\text{m}^3/\text{m}^2\cdot\text{hr}$; Q_h is the volume of gas filtered per hour, m^3/hr ; F_1 is the filtering-cloth area, m^2 .

The values of ΔH for different types of cloth are given in Tables 12-9 to 12-15.

13. The pressure losses in bag filters are mainly in the cloth sleeves, so that the resistance of such filters can be calculated on the basis of data for resistance of different types of cloth.

The characteristics and resistance of two specific types of bag filters (DIZ and MFU) are given in diagrams 12-13 and 12-14.

14. An efficient means of trapping the dust is also achieved by means of porous media, such as layers of loose or lump materials (sand, gravel, slag, Raschig rings, etc.), and also by sets of metallic gauze screens, specially prepared porous materials, filters from threadlike fibers and threads, paper filters, etc.

The fluid resistance of some of these filters can be determined from the data for checkerworks and screens (cf. Section VIII).

15. The pressure losses in industrial electrostatic filters of almost all types (Figure 12-5) are mainly made up of: 1) the loss at the inlet to the working chamber; 2) the loss at the exit from the working chamber; and 3) the loss at the passage through the interelectrode space. For a plate electrostatic filter, this is the passage between the settling plates, and in the case of a pipe electrostatic filter, this is along the settling pipes.

The total resistance coefficient of an electrostatic filter can be considered equal to:

$$\zeta = \frac{\Delta H}{\frac{\rho w_0^2}{2g}} = \zeta_{in} + \zeta_{dis} + \zeta_{ch} \quad (12-4)$$

where ζ_{in} is the resistance coefficient of the inlet stretch of the unit, calculated relative to the velocity w_0 at the inlet; ζ_{dis} is the resistance coefficient of the discharge stretch, calculated relative to this same velocity w_0 ; ζ_{ch} is the resistance coefficient of the working chamber of the unit with the settling elements, likewise calculated in relation to the velocity w_0 .

16. In almost all industrial apparatus the gas expands suddenly upon entering the working chamber* (Figure 12-5,a and b), and therefore the resistance coefficient of the inlet can be determined in the absence of gas-distributing devices by formula (4-3'):

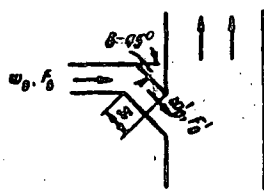
$$\zeta_{in} = \frac{\Delta H_{in}}{\frac{\rho w_0^2}{2g}} = N_0 \left(1 - \frac{2}{3n} \right) + \frac{1}{n^2} - \frac{4}{3n}. \quad (12-5)$$

* The case of a stream inlet through a diffuser (horizontal electrostatic filters) can also be considered as a case of inlet with sudden expansion, with the diffuser angle generally larger than 60 to 90°.

where $n = \frac{F_{ch}}{F_0}$ is the area ratio of the unit (ratio of the working-chamber area to the area of the inlet orifice); $N_0 = \frac{1}{F_0} \int \left(\frac{w}{w_0} \right)^3 dF$ is the kinetic-energy coefficient, characterizing the velocity distribution at the inlet. The values of this coefficient, and of the momentum coefficient $M_0 = \frac{1}{F_0} \int \left(\frac{w}{w_0} \right)^2 dF$ can be (very tentatively) determined from Tables 12-1 to 12-8, corresponding to different cases of stream inlet.

TABLE 12-1

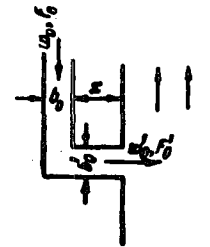
$$\text{Elbow, } \delta = 45^\circ; \frac{r}{b_0} = 0$$



$\frac{x}{b_0} \approx$	0-1.2	3.25	≥ 5.0
$M_0 \approx$	1.12	1.08	1.02
$N_0 \approx$	1.36	1.25	1.06

TABLE 12-2

$$\text{Elbow, } \delta = 90^\circ; \frac{r}{b_0} = 0; \frac{b'_0}{b_0} = 1.0$$



$\frac{x}{b_0} \approx$	1.2	3.0	6.0	10
$M_0 \approx$	1.80	1.50	1.10	1.02
$N_0 \approx$	3.50	2.80	1.30	1.06

TABLE 12-3

$$\text{Elbow, } \delta = 90^\circ; \frac{r}{b_0} = 0.1; \frac{b'_0}{b_0} = 1$$

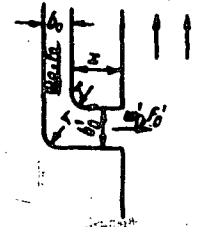


$\frac{x}{b_0} \approx$	0-0.5	1.5	3.0	6.0	8.0
$M_0 \approx$	1.40	1.25	1.12	1.06	1.02
$N_0 \approx$	2.30	1.75	1.36	1.18	1.06

TABLE 12-4

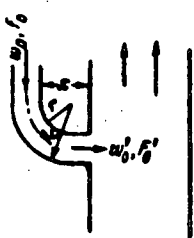
$$\text{Elbow, } \delta = 90^\circ \text{ with expansion}$$

$$\left(\frac{F'_0}{F_0} = 1.3 \right); \frac{r}{b_0} = 0.18$$



$\frac{x}{b_0} \approx$	0-0.5	1.5	3.0	6.0	10
$M_0 \approx$	1.70	1.40	1.25	1.10	1.02
$N_0 \approx$	3.20	2.30	1.75	1.30	1.06

TABLE 12-5

Bend, $\delta = 90^\circ$; $\frac{r}{b_0} = 0.5$ 

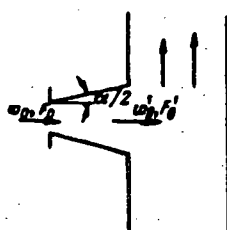
$\frac{s}{b_0}$	0-0.5	1.0	2.0	3.0	4.0
$M_0 \approx$	1.25	1.13	1.07	1.03	1.02
$N_0 \approx$	1.80	1.40	1.21	1.10	1.06

[TABLE 12-6]

$n = \frac{F'_0}{F_0}$	$\alpha = 6^\circ$				$\alpha = 10^\circ$			
	3.0	4.0	6.0	10	3.0	4.0	6.0	10
$M_0 \approx$	1.15	1.20	1.40	1.25	1.20	1.30	1.90	1.40
$N_0 \approx$	1.45	1.60	2.20	1.75	1.60	1.90	3.70	2.20
$\alpha = 15^\circ$				$\alpha = 30^\circ$				
$M_0 \approx$	1.50	1.85	2.30	1.80	2.00	2.50	3.10	2.55
$N_0 \approx$	2.50	3.50	4.80	3.40	4.00	5.30	7.20	5.70
$\alpha = 45^\circ$				$\alpha = 60^\circ$				
$M_0 \approx$	2.50	2.90	3.90	4.50	2.70	3.30	4.50	5.90
$N_0 \approx$	6.00	6.90	9.70	11.5	5.80	8.00	11.5	15.7
$\alpha = 90^\circ$				$\alpha = 180^\circ$				
$M_0 \approx$	2.80	3.75	5.20	7.00	4.00	5.10	7.30	9.00
$N_0 \approx$	6.90	9.00	13.5	19.0	10.0	13.0	20.0	25.0
$\alpha = 6^\circ$				$\alpha = 10^\circ$				
$n = \frac{F'_0}{F_0}$	3.0	4.0	6.0	10	3.0	4.0	6.0	10
$M_0 \approx$	1.10	1.15	1.35	1.15	1.12	1.20	1.60	1.30
$N_0 \approx$	1.30	1.45	2.05	1.45	1.36	1.60	2.80	1.90
$\alpha = 15^\circ$				$\alpha = 30^\circ$				
$M_0 \approx$	1.40	1.50	1.70	1.40	1.80	2.50	2.20	1.80
$N_0 \approx$	2.20	2.50	3.10	2.20	3.40	5.40	4.60	3.40
$\alpha = 45^\circ$				$\alpha = 60^\circ$				
$M_0 \approx$	2.00	2.60	2.30	2.00	2.10	2.90	3.70	3.50
$N_0 \approx$	4.00	5.80	4.90	4.00	4.30	7.00	9.00	8.50
$\alpha = 90^\circ$				$\alpha = 180^\circ$				
$M_0 \approx$	2.25	3.20	4.80	6.60	3.00	4.50	7.00	8.00
$N_0 \approx$	5.10	7.80	13.5	17.0	7.00	11.5	19.0	22.0

TABLE 12-7

Plane-diffuser



The resistance coefficient of the discharge can be determined on the basis of (3-3):

$$\zeta_{\text{dis}} = \frac{\Delta H_{\text{dis}}}{\frac{\rho v_0^2}{2g}} = \zeta' \left(1 - \frac{F_{\text{dis}}}{F_{\text{ch}}} \right) \left(\frac{F_e}{F_{\text{dis}}} \right)^2, \quad (12-6)$$

where ζ' is a coefficient which is determined as ζ for the inlet stretch from diagrams 3-1 to 3-3, 3-5, and 3-6; F_{dis} is the area of the narrowest section of the discharge stretch, m^2 .

The resistance coefficient of the chamber can be determined by the formula:

$$\zeta_{\text{ch}} = \frac{\Delta H_{\text{ch}}}{\frac{\rho v_0^2}{2g}} = \zeta'_{\text{in}} + \zeta'_{\text{dis}} + \zeta_{\text{fr}}, \quad (12-7)$$

where $\zeta'_{\text{in}} = 0.5 \left(1 - \frac{F_e}{F_{\text{ch}}} \right) \left(\frac{F_e}{F_e} \right)^2$ is the resistance coefficient of the discharge into the inter-electrode space; $\zeta'_{\text{dis}} = \left(1 - \frac{F_e}{F_{\text{ch}}} \right)^2 \left(\frac{F_e}{F_e} \right)^2$ is the resistance coefficient of the discharge from the interelectrode space; $\zeta_{\text{fr}} = \lambda \frac{l_e}{D_e} \left(\frac{F_e}{F_e} \right)^2$ is the friction coefficient of the interelectrode space; F_e is the total area of the gap between the settling plates, or total cross-section area of the settling pipes, m^2 ; l_e is the length of the settling plates or pipes, m ; $D_e = \frac{4F_e}{\Pi_e}$ is the hydraulic diameter of the gap between the settling plates, or diameter of settling pipe, m ; Π_e = perimeter of the gap between the settling plates or of the section of the settling pipe, m .

17. Many units including electrostatic filters use gas distributing grids for uniform distribution of a stream after its entrance into the working chamber. The entire stretch from the end section of the inlet branch pipe, including the grid, can be considered as a unit.

There are three ways of introducing a stream into the working chamber: 1) central impingement of a stream on the grid (Figure 12-6,a); 2) peripheral impingement of a stream on the grid (Figure 12-6,b); 3) side impingement of a stream on the grid (Figure 12-6,c).

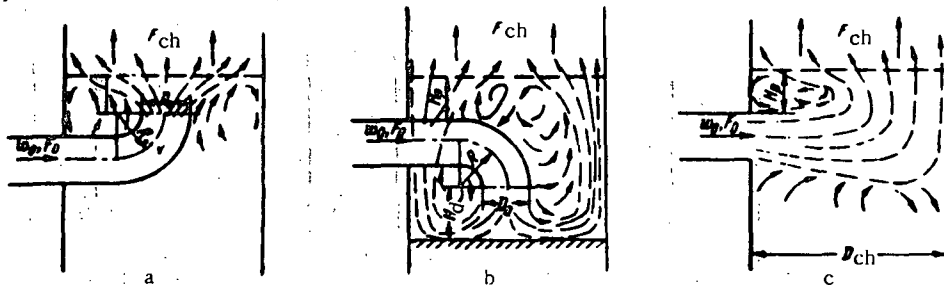


FIGURE 12-6. Different methods of stream introduction:

a — central impingement of the stream; b — peripheral impingement of the stream;
c — side impingement of the stream.

Either a single grid or a system of grids in series are used, depending on the area ratio $\frac{F_{ch}}{F_0}$ (cf. /12-15/ and /12-16/).

18. The resistance coefficient of the inlet stretch of the unit at central impingement of a stream on the grid*, is calculated by the following formula proposed by the author**:

$$\zeta_{in} = \zeta = \frac{\Delta H}{\frac{\rho w_0^2}{2g}} = \zeta'_{o.be} + N_o + 0.7\zeta_p \left(\frac{F_0}{F_{ch}} \right)^2 + \frac{0.013}{\left(\frac{H_g}{D_0} \right)^2} \sqrt{\zeta_p - \sqrt{\zeta_p}}, \quad (12-8)$$

where $\zeta'_{o.be} = 0.5\zeta_{o.be}$; $\zeta_{o.be}$ is the resistance coefficient of the bend through which the stream is discharged against the grid; it is determined as ζ from the corresponding diagrams of Section VI; ζ_p is the resistance coefficient of the grid, determined as ζ from diagrams 8-1 to 8-7; H_g is the distance from the exit opening of the intake bend to the grid, m; D_0 is the diameter of the discharge section of the intake bend, m.

The last term on the right-hand side of (12-8) is to be taken into account for $\frac{H_g}{D_0} < 1.2$ only.

The resistance coefficient of the inlet stretch of the unit at peripheral stream impingement on the grid is calculated by the following formula:

$$\zeta_{in} = \zeta = \frac{\Delta H}{\frac{\rho w_0^2}{2g}} = \zeta'_{o.be} + 0.9 \left[N_o + 0.7\zeta_p \left(\frac{F_0}{F_{ch}} \right)^2 \right] + \frac{0.05}{\left(\frac{H_d}{D_0} \right)^2}, \quad (12-9)$$

where $\frac{H_d}{D_0}$ is the relative distance from the exit of the intake bend to the apparatus bottom or to a baffle (if a baffle has been installed behind the bend).

The last term of the right-hand side of (12-9) is to be taken into account for $\frac{H_d}{D_0} < 1.2$ only.

The resistance coefficient of the inlet stretch of a unit at side impingement of the stream on a grid is calculated by the formula:

$$\zeta_{in} = \zeta = \frac{\Delta H}{\frac{\rho w_0^2}{2g}} = N_o + 0.7\zeta_p \left(\frac{F_0}{F_{ch}} \right)^2 + 0.1 + \left(2 - 20 \frac{H_p}{D_{ch}} \right), \quad (12-10)$$

where D_{ch} is the diameter or large side of the chamber section, m.

The last term on the right-hand side of (12-10) is to be taken into account for $\frac{H_p}{D_{ch}} < 0.1$ only.

In the case of a series of grids, the resistance coefficient of the inlet stretch is determined by the same formulas (12-8) to (12-10) but with ζ_p replaced by the sum of the

* The term "grid" is used here in a very general sense; it can mean not only a plane grid (perforated sheet), but also other types of uniformly distributed resistances (various checkerworks or layers of loose or lump material, Raschig rings, etc.)

** These formulas differ from the formulas in /12-15/, certain refinements having been introduced as a result of the author's subsequent experiments.

resistance coefficients of all the grids of the system:

$$\sum_{i=1}^{n_p} \zeta_i = \zeta_{1p} + \zeta_{2p} + \dots + \zeta_{np}, \quad (12-11)$$

where n = number of grids.

b. Heat exchangers

19. The total pressure losses in honeycomb radiators, used for cooling air, are made up of the loss at the inlet to the radiator tube, the frictional loss in the tubes, and the loss at sudden expansion at the discharge from the tubes into the common channel. The resistance coefficient of a honeycomb radiator is determined by the following formula (Mar'yamov, /12-23/):

$$\begin{aligned} \zeta &= \frac{\Delta H}{\frac{\tau_{in} w_1^2}{2g}} = \lambda \left(3 + \frac{l_o}{d_h} \right) \left(\frac{F_1}{F_0} \right)^2 + \left(\frac{F_1}{F_0} - 1 \right)^2 + \left(1.7 + \lambda \frac{l_o}{d_h} \right) \left(\frac{F_1}{F_0} \right)^2 \bar{T} = \\ &= \lambda \left(3 + \frac{l_o}{d_h} \right) \left(\frac{F_1}{F_0} \right)^2 + \zeta_{sh} + \Delta \zeta_r, \end{aligned} \quad (12-12)$$

where

$$\zeta_{sh} = \left(\frac{F_1}{F_0} - 1 \right)^2; \quad (12-13)$$

$$\Delta \zeta_r = \left(1.7 + \lambda \frac{l_o}{d_h} \right) \left(\frac{F_1}{F_0} \right)^2 \bar{T}; \quad (12-14)$$

$\bar{T} = \frac{T_{ex} - T_{in}}{T_{in}}$ is the ratio of the difference between the temperatures ($^{\circ}$ K) of the outflowing and incoming streams to the temperature of the incoming stream, in $^{\circ}$ K (absolute); w_1 is the velocity in the pipe before the radiator front, m/sec; F_0 is the total flow area of the radiator, m^2 ; F_1 is the cross-section area of the radiator front, m^2 ; l_o is the length of the radiator tube (radiator depth), m; $d_h = \frac{4l_o}{\Pi_o}$ is the hydraulic diameter of the radiator tube, m; Π_o is the perimeter of the radiator-tube section, m; λ is the friction coefficient of unit radiator depth.

The friction coefficient λ of honeycomb radiators with circular or hexagonal tubes is determined by the following formula (Mar'yamov /12-23/):

a) for $35 < Re^* = \frac{w_{0,in} \Delta}{v} < 275$

$$\lambda = 0.375 Re^{*-0.1} \bar{\Delta}^{0.4}; \quad (12-15)$$

b) for $275 < Re^* < 500$

$$\lambda = 0.214 \bar{\Delta}^{0.4}, \quad (12-16)$$

where $\bar{\Delta} = \frac{\Delta}{d_h}$ is the relative roughness of the radiator tubes.

20. The total pressure losses in ribbed-tube and tube-and-plate radiators are made up of friction loss and losses at contraction or expansion of the stream during its passage from one row of tubes to another.

The resistance coefficient of such radiators is determined by the following formula (Mar'yamov /12-24/):

$$\zeta = \frac{\Delta H}{\frac{\rho_0 w_0^2}{2g}} = \left(z\zeta_c + \lambda \frac{l_0}{d_h} \right) \left(\frac{F_1}{F_0} \right)^2 + \left(1.7 + \lambda \frac{l_0}{d_h} \right) \left(\frac{F_1}{F_0} \right)^2 \bar{T} = \left(z\zeta_c + \lambda \frac{l_0}{d_h} \right) \left(\frac{F_1}{F_0} \right)^2 + \Delta\zeta_r. \quad (12-17)$$

where

$$\zeta_c = 1.5 \left(1 - \frac{F_0'}{F_0} \right)^2 \quad (12-18)$$

is a coefficient allowing for the losses at contraction and expansion of the stream during its passage between the radiator tubes;

$$\Delta\zeta_r = \left(1.7 + \lambda \frac{l_0}{d_h} \right) \left(\frac{F_1}{F_0} \right)^2 \bar{T}; \quad (12-14)$$

F_0 is the area of the narrowest radiator section (between the tubes), m^2 ; F_0' is the area of the section between the plates in the zone between the rows, m^2 ;

$$d_h = \frac{2b_0 h_0}{b_0 + h_0};$$

b_0 is the mean gap between the fins or plates, m; h_0 is the gap between adjacent tubes of the radiator, m; z is the number of rows of tubes; λ is the friction coefficient of unit radiator depth; for the remaining symbols cf. point 19.

The friction coefficient λ for ribbed-tube radiators can be calculated approximately by the following formula (Mar'yamov):

$$\lambda = \frac{0.77}{\sqrt{Re}}, \quad (12-19)$$

which is correct for $3,000 < Re = \frac{\rho_0 w_0 d_h}{\mu} < 25,000$:

The friction coefficient λ for tube-and-plate radiators can be calculated by the following formulas (Mar'yamov /12-24/):

a) for $4 \cdot 10^4 < Re = \frac{\rho_0 w_0 d_h}{\mu} < 10^5$

$$\lambda = \frac{0.98}{\sqrt{Re}}; \quad (12-20)$$

b) for $Re > 10^5$

$$\lambda = \frac{0.21}{\sqrt{Re}} \quad (12-21)$$

21. The resistance of heaters is similar to the resistance of radiators. It is also made up of the loss at the inlet, the friction loss, and the shock loss at discharge from the narrow section between the tubes and plates of the heater. The main parameter used in the selection of a heater is the weight rate of flow in its cross section $\gamma_m w_0$, kg/m².sec, where γ_m kg/m³ = mean specific gravity of the heated air flowing through the heater.

This is the reason why the data on resistance of heaters given in the literature are presented in the form of a relation between ΔH (kg/m²) and $\gamma_m w_0$ (kg/m².sec). The same relationship is adopted in this handbook too.

With multipass heat exchangers, the transverse stream flowing over the tubes turns sharply through 180° on moving from one bundle into the next (Figure 12-7, a). The phenomenon is similar to the one taking place in a U-shaped elbow without bundles of tubes, i.e., an eddy zone is created at the inner wall after the second 90° turn, but is reduced somewhat due to the smoothing effect of the tube bundles.

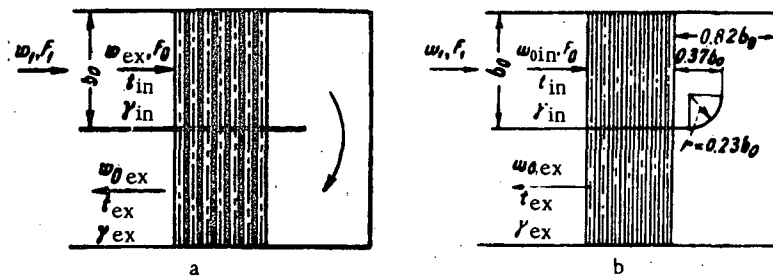


FIGURE 12-7. Two-pass cross-current heat exchanger:

a—straight partition in the intermediate channel; b—partition in the intermediate channel bent against the direction of stream flow.

The reduction or elimination of this eddy zone increases the efficiency of the heat exchange. To achieve this, guide vanes can be placed at the point of bending. Another method is (El'perin /12-44/) to place a partition, either straight or bent against the direction of stream flow at the point of bend (Figure 12-7).

c. Ventilating hoods, roof ventilators, and exhausts

23. Ventilating hoods are used when it is required to utilize the wind energy in order to achieve greater ventilation. When the wind blows on the hood, a negative pressure is created on part of its surface, and this contributes to the displacement of air from the room outside. The total pressure losses in the hood are made up of the loss in the duct proper and the loss of dynamic pressure at the exit.

The ventilating hoods of greatest interest are those of the "TsAGI", "Chanard-Etoile", and "Grigorovich" types. The resistance coefficients of these hoods are given in diagram 12-26.

24. Roof ventilators or exhausts are installed on the roof of industrial buildings for the natural elimination of polluted air. The most efficient types of such ventilators are the ventilator house, the LEN PSP ventilators, followed by the KTIS, double-level, Giprotis, and Ryukin-Ill'inskii ventilators (cf. Taliev /12-33/).

The rectangular ventilator with panels, the Baturin-Brandt LEN PSP, KTIS, PSK-2, and Giprotis ventilators and the ventilator house belong to the category of practically draftproof ventilators.

The values of the resistance coefficients of different types of ventilators are given in diagrams 12-27 and 12-28.

The resistance coefficient of rectangular ventilators with panels can be calculated by the following formula, which follows from the data of Taliev /12-33/ and Frukht /12-39/:

$$\xi = \frac{\Delta H}{\frac{w_0^2}{2g}} = a + \left(\frac{3}{\frac{l}{h}} \right)^3 + \frac{0.2}{\frac{l}{h}}$$

where w_0 is the mean velocity in the gaps of the ventilators, m/sec; a is an empirical coefficient, depending on the angle of opening of the ventilator flap α and determined from the following table:

TABLE 12-8

α°	35°	45°	55°
a	8.25	5.25	3.15

l is the distance from the panel to the outer edge of the flap, m; h = total height of all the gaps on one side of the flap, m.

**12-3. LIST OF THE DIAGRAMS OF RESISTANCE COEFFICIENTS
(OR RESISTANCE MAGNITUDES) OF SECTION XII**

Diagram description	Source	No. of diagram	Notes
Various dust separators	Geras'ev /12-6/, Zalgin and Shukher /12-12/, Kouzov /12-20/ Standards /12-42/ The same	12-1 12-2 12-3	Experimental data The same " "
NIIOGAZ cyclones	KTIS /12-3/, Kucheruk and Krasilov /12-21/, Shakhev /12-43/	12-4	" "
BTs battery-type dust separators	Zverev /12-13/, Kucheruk and Krasilov /12-21/, Shakhev /12-43/	12-5	" "
Inertial (louver-type) conical KTIS separator	Zaitsev and Murashkevich /12-9/, Teverovskii and Zaitsev /12-35/	12-6	" "
Inertial (louver-type) dust separators of different types	Zalgin and Shukher /12-12/ The same	12-7 12-8	" " " "
Venturi scrubber (tube sprayer)	Kucheruk /12-22/ The same	12-9 12-10	" " " "
Scrubber with wooden packing	" "	12-11	" "
VTI centrifugal scrubber	" "	12-12	" "
Twine wedge-shaped shaking two-stage MIOT-type filter	Rekk /12-30/ The same	Table No. 12-9 12-10	" " " " " "
Twine wedge-shaped shaking simple stage MIOT-type filter	" "	12-11	" "
Box-type filter from corrugated gauze with moist filter, of Rekk design	" "	12-12	" "
Porous box-type filter with moist packing	Rekk /12-30/ The same	Table No. 12-9 12-11	" " " "
Filtering cloth — "Mel'stroi" wool	Adamov	12-13 12-14 12-15	" " " " " "
Filtering cloth — serge wool mixture	Kucheruk /12-22/	Diagram No. 12-13	" "
Filtering cloth — unbleached coarse calico	Gordon and Aladzhalov /12-7/ —	12-14 12-15	" " According to the author's approximate calculations
Filtering cloth — wool flannelette	Idel'chik /12-15/, /12-6/	12-16	The same
Filtering cloth — cotton thread	Mar'yamov /12-23/	12-17	Experimental data
Filtering cloth — flax flimsy 2-ply thread	Mar'yamov /12-24/ The same	12-18 12-19	The same " "
Filtering cloths — calico, moleskin, and cottontread flannelette	Trichler and Egorov /12-36/, Polikarpov /12-29/ Trichler and Egorov /12-36/ The same	12-20 12-21 12-22	" " " " " "
DIZ cloth shaking filter with various types of cloth			
MFU suction-type hose filter with various types of cloth			
Industrial electrostatic filters			
Inlet stretches of unit with grid, packing, or other type of obstruction placed in the working chamber			
Honeycomb radiator with hexagonal or circular			
Ribbed-tube radiator			
Tube-and-Plate radiator			
Plate-type air heater			
Spiral-ribbed air heater			
Petaled fin heater			

(continued)

Diagram description	Source	No. of diagram	Notes
Plain pipe air heater	Taliev /12-32/	12-23	The same
Air heater made from heating elements	Ritshel' and Greber /12-31/	12-24	" "
Various heat exchangers	—	12-25	Approximate calculations
Various ventilating hoods	Khanzhonkov /12-40/, /12-41/	12-26	Experimental data
Eliminators	Taliev /12-33/	12-27	The same
Various types of roof ventilators	Frukht /12-39/	12-28	" "
Rectangular roof ventilators with panels	Uchastkin /12-38/	12-29	" "

12-4. DIAGRAMS OF THE RESISTANCE COEFFICIENTS

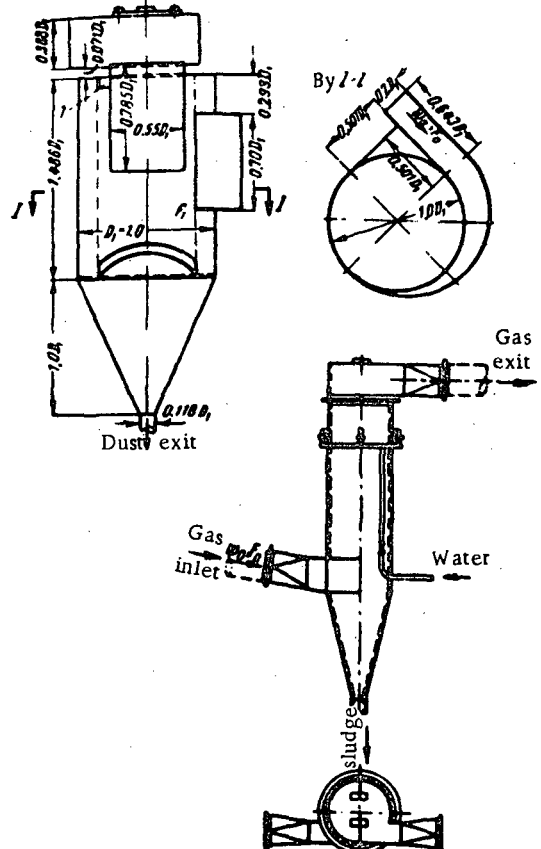
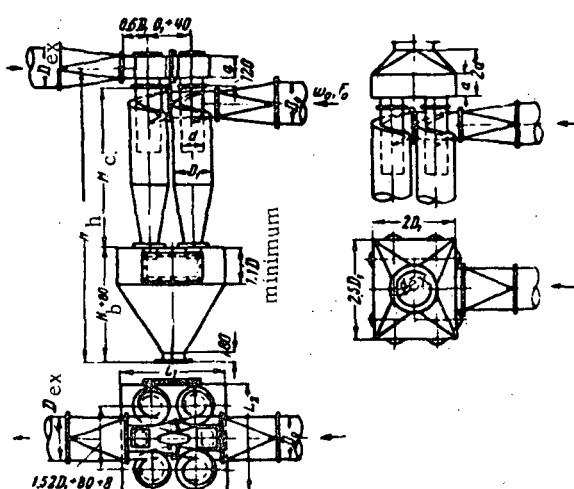
Various cyclones

 Section XII
 Diagram 12-1

Type	View	Resistance coefficient
Simple conical cyclone	<p>Front view (a) shows a cone with height $1.65D_0$, top diameter D_0, and bottom diameter $0.3D_0$. A gas inlet is at height $0.2D_0$ from the bottom, and a dust exit is at height $0.13D_0$ from the bottom. A gas exit is at the top. Cross-section (b) shows a circle with radius R_0 and velocity w_0.</p>	$\zeta_0 = \frac{\Delta H}{\frac{1}{2} w_0^2} = 7.0$ $\zeta_1 = \frac{\Delta H}{\frac{1}{2} w_1^2} = 1100$ $w_1 = \frac{Q}{F_1}$ $F_1 = \text{total cross-section area of cyclone body}$
Conical SIOT cyclone	<p>Front view (a) shows a cone with height $1.22D_0$, top diameter $1.9D_0$, and bottom diameter $0.4D_0$. A gas inlet is at height $0.71D_0$ from the bottom. A cross-section (b) shows concentric spirals with outer radius $2.2D_0$ and inner radius $1.55D_0$.</p>	$\zeta_0 = 4.2$ $\zeta_1 = 595$
Ordinary LIOT cyclone and shortened LIOT cyclone with untwisting spiral	<p>Front view (a) shows a cone with height $1.3D_0$, top diameter $1.9D_0$, and bottom diameter $0.4D_0$. A gas inlet is at height $0.87D_0$ from the bottom. A cross-section (b) shows concentric spirals with outer radius $1.17D_0$ and inner radius $0.67D_0$.</p>	$\zeta_0 = 2.5$ $\zeta_1 = 263$
The same without untwisting spiral	<p>Front view (a) shows a cone with height $1.13D_0$, top diameter $1.9D_0$, and bottom diameter $0.4D_0$. A gas inlet is at height $0.67D_0$ from the bottom. A cross-section (b) shows concentric spirals with outer radius $1.17D_0$ and inner radius $0.67D_0$.</p>	$\zeta_0 = 2.8$ $\zeta_1 = 293$

Various cyclones (continued)

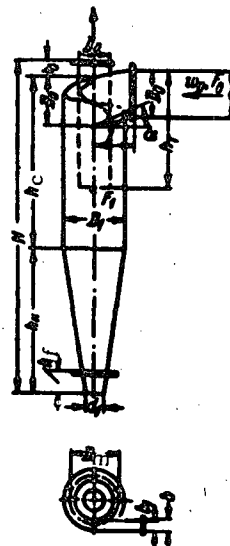
 Section XII
 Diagram 12-1

Type	View	Resistance coefficient
Cyclone with dust removal		$\zeta_0 = \frac{\Delta H}{\frac{1}{2} w_0^2} = 2.6;$ $\zeta_1 = \frac{\Delta H}{\frac{1}{2} w_1^2} = 133$
LIOT cyclone with water film and a specific liquid discharge of 0.13 to 0.30 liter/m³		$\zeta_0 = 3.0$
Grouped cyclones		$\zeta_0 \approx 1.1\zeta'_0$ where ζ'_0 = resistance coefficient of a single cyclone

NIIOGAZ cyclones

Section XII
Diagram 12-2

No.	Type							View	Resistance coefficient																
	NIIOGAZ-TsN-15																								
	<table border="1" style="width: 100%; border-collapse: collapse;"> <thead> <tr> <th>D_0</th><th>d_1</th><th>b</th><th>b_1</th><th>l</th><th>D_m</th><th>h_f</th><th>α</th></tr> </thead> <tbody> <tr> <td>$0.6D_1$</td><td>$0.3-0.4D_1$</td><td>$0.2D_1$</td><td>$0.26D_1$</td><td>$0.6D_1$</td><td>$0.8D_1$</td><td>$0.21-0.32D_1$</td><td>15°</td></tr> </tbody> </table>							D_0	d_1	b	b_1	l	D_m	h_f	α	$0.6D_1$	$0.3-0.4D_1$	$0.2D_1$	$0.26D_1$	$0.6D_1$	$0.8D_1$	$0.21-0.32D_1$	15°		
D_0	d_1	b	b_1	l	D_m	h_f	α																		
$0.6D_1$	$0.3-0.4D_1$	$0.2D_1$	$0.26D_1$	$0.6D_1$	$0.8D_1$	$0.21-0.32D_1$	15°																		
	<table border="1" style="width: 100%; border-collapse: collapse;"> <thead> <tr> <th>D_1</th><th>a</th><th>h_T</th><th>h_C</th><th>h_K</th><th>h_B</th><th>H</th></tr> </thead> <tbody> <tr> <td>40 to 800 mm</td><td>$0.66D_1$</td><td>$1.74D_1$</td><td>$2.26D_1$</td><td>$2D_1$</td><td>$0.3D_1$</td><td>$4.56D_1$</td></tr> </tbody> </table>							D_1	a	h_T	h_C	h_K	h_B	H	40 to 800 mm	$0.66D_1$	$1.74D_1$	$2.26D_1$	$2D_1$	$0.3D_1$	$4.56D_1$				
D_1	a	h_T	h_C	h_K	h_B	H																			
40 to 800 mm	$0.66D_1$	$1.74D_1$	$2.26D_1$	$2D_1$	$0.3D_1$	$4.56D_1$																			
	NIIOGAZ-TsN-15u																								
	<table border="1" style="width: 100%; border-collapse: collapse;"> <thead> <tr> <th>D_0</th><th>d_1</th><th>b</th><th>b_1</th><th>l</th><th>D_m</th><th>h_f</th><th>α</th></tr> </thead> <tbody> <tr> <td>$0.6D_1$</td><td>$0.3-0.4D_1$</td><td>$0.2D_1$</td><td>$0.26D_1$</td><td>$0.6D_1$</td><td>$0.8D_1$</td><td>$0.24-0.32D_1$</td><td>15°</td></tr> </tbody> </table>							D_0	d_1	b	b_1	l	D_m	h_f	α	$0.6D_1$	$0.3-0.4D_1$	$0.2D_1$	$0.26D_1$	$0.6D_1$	$0.8D_1$	$0.24-0.32D_1$	15°		
D_0	d_1	b	b_1	l	D_m	h_f	α																		
$0.6D_1$	$0.3-0.4D_1$	$0.2D_1$	$0.26D_1$	$0.6D_1$	$0.8D_1$	$0.24-0.32D_1$	15°																		
	<table border="1" style="width: 100%; border-collapse: collapse;"> <thead> <tr> <th>D_1</th><th>a</th><th>h_T</th><th>h_C</th><th>h_K</th><th>h_B</th><th>H</th></tr> </thead> <tbody> <tr> <td>200 to 800 mm</td><td>$0.66D_1$</td><td>$1.5D_1$</td><td>$1.51D_1$</td><td>$1.50D_1$</td><td>$0.3D_1$</td><td>$3.31D_1$</td></tr> </tbody> </table>							D_1	a	h_T	h_C	h_K	h_B	H	200 to 800 mm	$0.66D_1$	$1.5D_1$	$1.51D_1$	$1.50D_1$	$0.3D_1$	$3.31D_1$				
D_1	a	h_T	h_C	h_K	h_B	H																			
200 to 800 mm	$0.66D_1$	$1.5D_1$	$1.51D_1$	$1.50D_1$	$0.3D_1$	$3.31D_1$																			
	NIIOGAZ-TsN-24																								
	<table border="1" style="width: 100%; border-collapse: collapse;"> <thead> <tr> <th>D_0</th><th>d_1</th><th>b</th><th>b_1</th><th>l</th><th>D_m</th><th>h_f</th><th>α</th></tr> </thead> <tbody> <tr> <td>$0.6D_1$</td><td>$0.3-0.4D_1$</td><td>$0.2D_1$</td><td>$0.26D_1$</td><td>$0.6D_1$</td><td>$0.8D_1$</td><td>$0.24-0.32D_1$</td><td>24°</td></tr> </tbody> </table>							D_0	d_1	b	b_1	l	D_m	h_f	α	$0.6D_1$	$0.3-0.4D_1$	$0.2D_1$	$0.26D_1$	$0.6D_1$	$0.8D_1$	$0.24-0.32D_1$	24°		
D_0	d_1	b	b_1	l	D_m	h_f	α																		
$0.6D_1$	$0.3-0.4D_1$	$0.2D_1$	$0.26D_1$	$0.6D_1$	$0.8D_1$	$0.24-0.32D_1$	24°																		
	<table border="1" style="width: 100%; border-collapse: collapse;"> <thead> <tr> <th>D_1</th><th>a</th><th>h_T</th><th>h_C</th><th>h_K</th><th>h_B</th><th>H</th></tr> </thead> <tbody> <tr> <td>400 to 1000 mm</td><td>$1.11D_1$</td><td>$2.11D_1$</td><td>$2.11D_1$</td><td>$1.75D_1$</td><td>$0.4D_1$</td><td>$4.28D_1$</td></tr> </tbody> </table>							D_1	a	h_T	h_C	h_K	h_B	H	400 to 1000 mm	$1.11D_1$	$2.11D_1$	$2.11D_1$	$1.75D_1$	$0.4D_1$	$4.28D_1$				
D_1	a	h_T	h_C	h_K	h_B	H																			
400 to 1000 mm	$1.11D_1$	$2.11D_1$	$2.11D_1$	$1.75D_1$	$0.4D_1$	$4.28D_1$																			
	NIIOGAZ-TsN-11																								
	<table border="1" style="width: 100%; border-collapse: collapse;"> <thead> <tr> <th>D_0</th><th>d_1</th><th>b</th><th>b_1</th><th>l</th><th>D_m</th><th>h_f</th><th>α</th></tr> </thead> <tbody> <tr> <td>$0.6D_1$</td><td>$0.3-0.4D_1$</td><td>$0.2D_1$</td><td>$0.26D_1$</td><td>$0.6D_1$</td><td>$0.8D_1$</td><td>$0.24-0.32D_1$</td><td>11°</td></tr> </tbody> </table>							D_0	d_1	b	b_1	l	D_m	h_f	α	$0.6D_1$	$0.3-0.4D_1$	$0.2D_1$	$0.26D_1$	$0.6D_1$	$0.8D_1$	$0.24-0.32D_1$	11°		
D_0	d_1	b	b_1	l	D_m	h_f	α																		
$0.6D_1$	$0.3-0.4D_1$	$0.2D_1$	$0.26D_1$	$0.6D_1$	$0.8D_1$	$0.24-0.32D_1$	11°																		
	<table border="1" style="width: 100%; border-collapse: collapse;"> <thead> <tr> <th>D_1</th><th>a</th><th>h_T</th><th>h_C</th><th>h_K</th><th>h_B</th><th>H</th></tr> </thead> <tbody> <tr> <td>40 to 200 mm</td><td>$0.48D_1$</td><td>$1.56D_1$</td><td>$2.08D_1$</td><td>$2D_1$</td><td>$0.3D_1$</td><td>$4.38D_1$</td></tr> </tbody> </table>							D_1	a	h_T	h_C	h_K	h_B	H	40 to 200 mm	$0.48D_1$	$1.56D_1$	$2.08D_1$	$2D_1$	$0.3D_1$	$4.38D_1$				
D_1	a	h_T	h_C	h_K	h_B	H																			
40 to 200 mm	$0.48D_1$	$1.56D_1$	$2.08D_1$	$2D_1$	$0.3D_1$	$4.38D_1$																			



$$\zeta_0 = \frac{\Delta H}{\frac{1}{2} \rho g} = 2.98;$$

$$\zeta_1 = \frac{\Delta H}{\frac{1}{2} \rho g} = 105;$$

$\omega_i = \frac{Q}{F_i}$ (F_i = total cross-section area of the cyclone body)

$$\zeta_0' = 2.98;$$

$$\zeta_1' = 110$$

$$\zeta_0'' = 4.8;$$

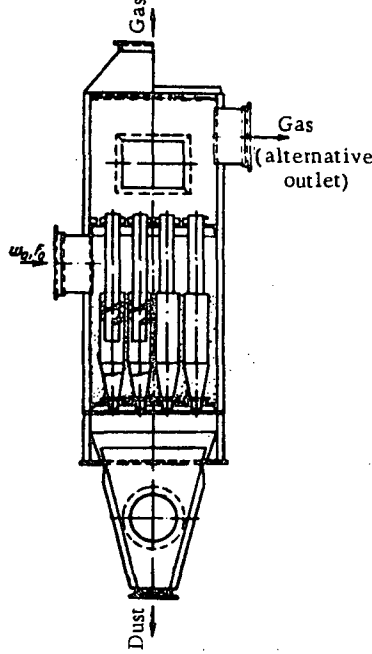
$$\zeta_1'' = 60$$

$$\zeta_0''' = 2.70;$$

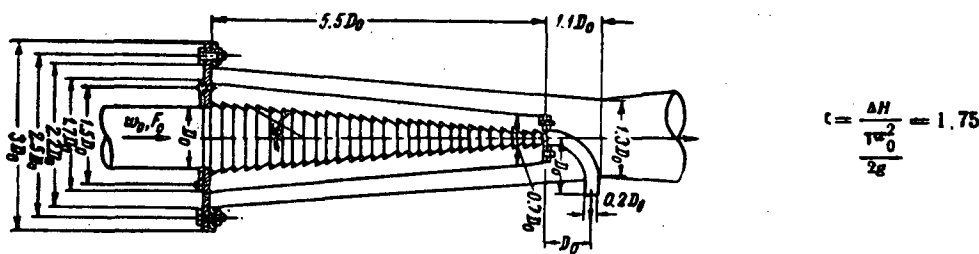
$$\zeta_1''' = 189$$

BTs battery-type dust separators

 Section XII
 Diagram 12-3

Type	View	Resistance coefficient $\zeta_1 = \frac{\Delta H}{\frac{V^2}{2g} F_1}$
with screw blade		$\zeta_1 = 85$
with rosette, $\alpha = 25^\circ$		$\zeta_1 = 90$
with rosette, $\alpha = 30^\circ$		$\zeta_1 = 65$ $\omega_1 = \frac{Q}{F_1}$ $(F_1 = \text{total cross-section area of the dust-separator body})$

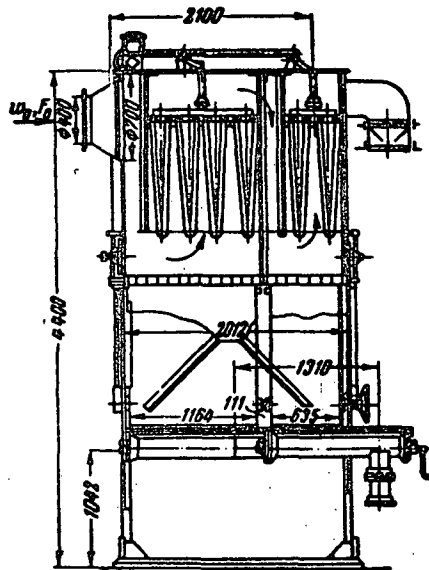
Inertial (louver-type) conical KTIS dust separator

 Section XII
 Diagram 12-4


Type	View	Resistance coefficient $\zeta = \frac{\Delta H}{\frac{P_0}{2g}}$
MIOT plane-grid wedge-shaped		$\zeta = 1.75$
VTL ash catcher		$\zeta = 3.2$

Twine wedge-shaped shaking two-stage MIOT-type filter

Section XII
Diagram 12-9



Resistance of the entire filter at $Q_T = 500 \text{ m}^3/\text{m}^2 \cdot \text{hr}$:

1) unsoiled filter layer $\Delta H = 6 \text{ kg/m}^2$;

2) after the feeding into the filter, of 400 g/m^2 dust; $\Delta H = 25 \text{ kg/m}^2$. The relationship $\Delta H = f(Q_T)$ for separate stages with clean layer is given in graph a. The relationship $\Delta H = f(p, \text{g/m}^2)$ for the first stage at $Q_T = 500 \text{ m}^3/\text{m}^2 \cdot \text{hr}$ is given in graph b.

The filtering layer of the first stage is binding twine (OST 6707/407, article 883).

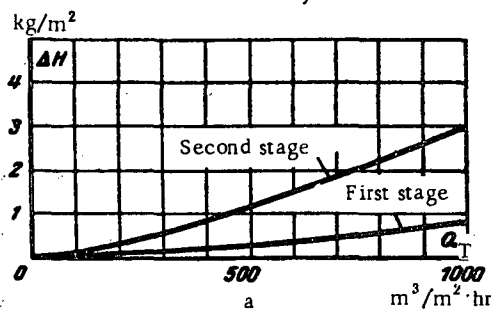
The filtering layer of the second stage is cable yarn No. 03 (GOST 905-41).

Asbestos dust

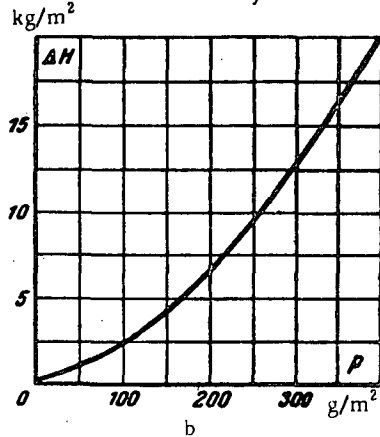
Particle size d , microns	2	2-10	10-25	25-100
Weight content, %	0.05	3.64	8.94	87.36

Cleaning efficiency at $Q_T = 500 \text{ m}^3/\text{m}^2 \cdot \text{hr}$, $k_{st} = 98\%$.

Clean twine layer

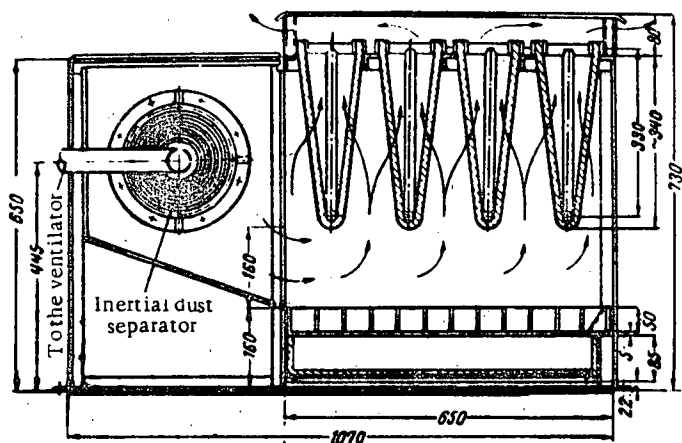


Soiled twine layer



Twine wedge-shaped shaking single-stage MIOT-type filter

Section XII
Diagram 12-10



Filtering layer — knitting twine wound in four rows;
material handled — asphalt road dust

Particle diameter <i>d</i> , microns	0-5	5-10	10-20	20-40	40
Weight content, %	9.00	49.6	21.9	18.4	1.06

Cleaning efficiency, $\alpha_{st} = 97\%$

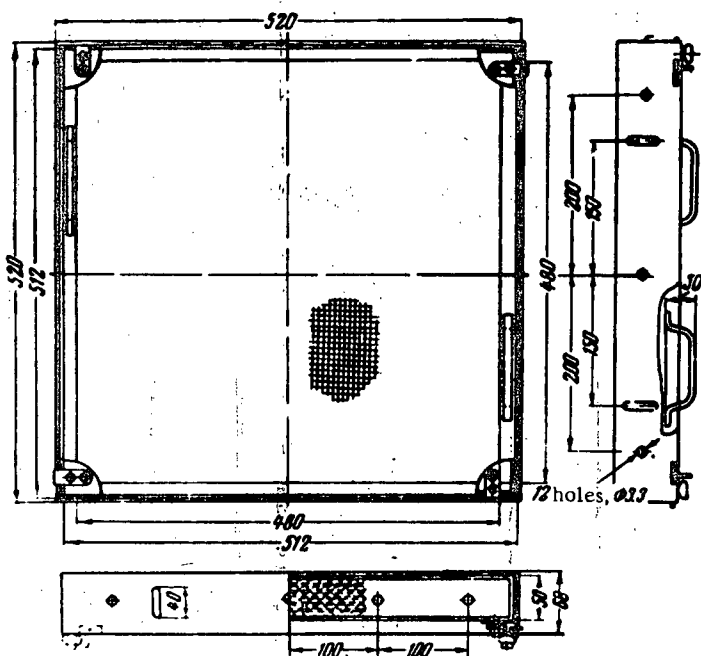
Resistance of the whole filter at $Q_T = 864 \text{ m}^3/\text{m}^2 \cdot \text{hr}$ and dust content $p = 1250 \text{ g/m}^2$:

- 1) before the shaking $\Delta H = 35 \text{ kg/m}^2$
- 2) after the shaking $\Delta H = 16 \text{ to } 19 \text{ kg/m}^2$

Box-type filter from corrugated gauze with moist filter, of Rekk design

Section XII

Diagram 12-11



Filler — corrugated gauze; pitch of the corrugation — 7 mm; height of the corrugation — 4 mm; wetted by almond oil.

Type of dust	Small model 1951		Small model 1952	
	α_{st} , %	p , g/m^2	α , %	p , g/m^2
Foundry . . .	88	350	39	400
Cement . . .	96	450	97	550
Cement . . .	86	280	87	400
Coal	94	240	92	500
Coal ashes . .	94	450	93	700

Filter resistance with clean air within the limits

$$1.1 < w < 2.4 \text{ m/sec}$$

- 1) small model 1951

$$\Delta H = 40 h w^{1.7} \text{ kg/m}^2$$

- 2) small model 1952

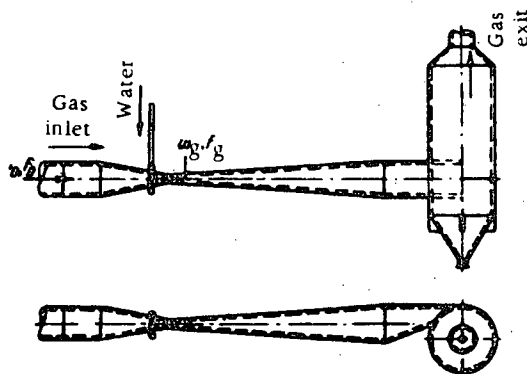
$$\Delta H = 1.6 h w^{1.7} \text{ kg/m}^2$$

where h = layer thickness, m.

The value of ΔH is doubled when the limiting dust content given in the table is reached.

Venturi scrubber (tube sprayer)

Section XII
Diagram 12-6



$$\Delta H = (\zeta_g + \zeta_w q) \frac{\tau_g w_g^2}{2g} \text{ kg/m}^2,$$

where $\zeta_g \approx 0.10-0.15$ depending on the manufacturing accuracy;

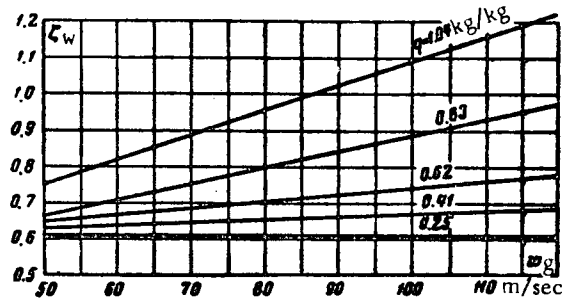
ζ_w is determined from the graph as a function of w_g and q :

$$q = m \frac{\tau_1}{\tau_g} \text{ kg/kg};$$

τ_g, τ_1 = specific gravity of the working gas in the throat and the sprayed liquid, respectively, kg/m^3 ;

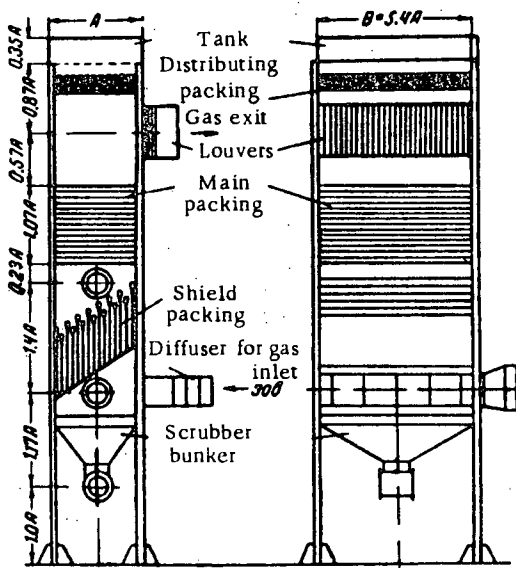
m = specific discharge of the sprayed liquid, $1/\text{m}^3$ of the gas

$q, \text{kg/kg}$	Values of ζ_w							
	$w_g, \text{m/sec}$							
	50	60	70	80	90	100	110	120
0.25	0.61	0.61	0.61	0.61	0.61	0.61	0.61	0.61
0.41	0.63	0.64	0.65	0.66	0.66	0.67	0.68	0.69
0.62	0.65	0.66	0.68	0.70	0.72	0.74	0.76	0.76
0.83	0.67	0.70	0.75	0.79	0.83	0.88	0.92	0.97
1.04	0.75	0.82	0.88	0.94	1.00	1.03	1.14	1.22



Scrubber with wooden packing

Section XII
Diagram 12-7

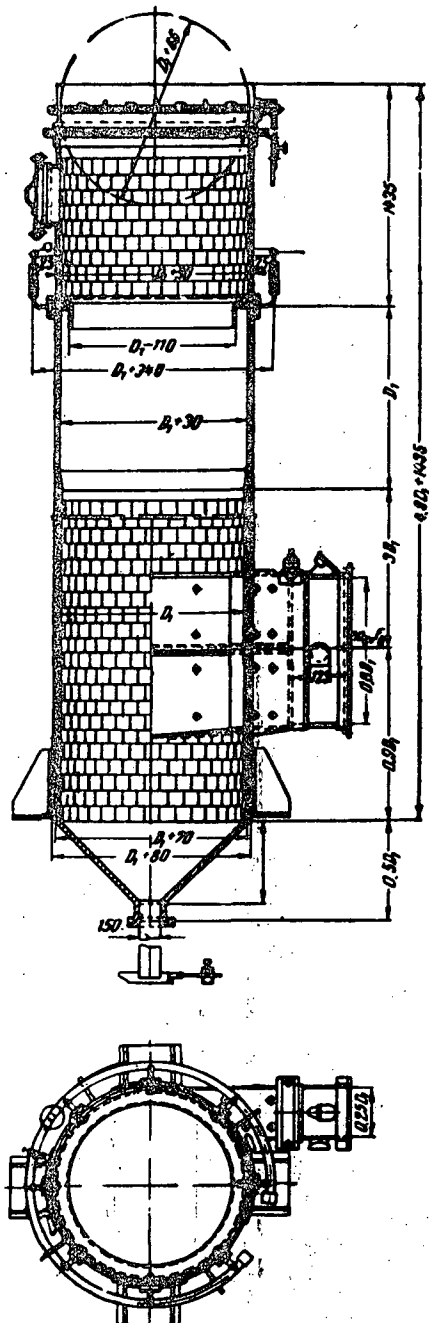


$$\text{Wetting intensity } A \approx 52 \frac{\text{m}^2}{\text{m}^2 \cdot \text{h}}$$

$$\zeta_1 = \frac{\Delta H}{\tau_1 w_1^2} = 960;$$

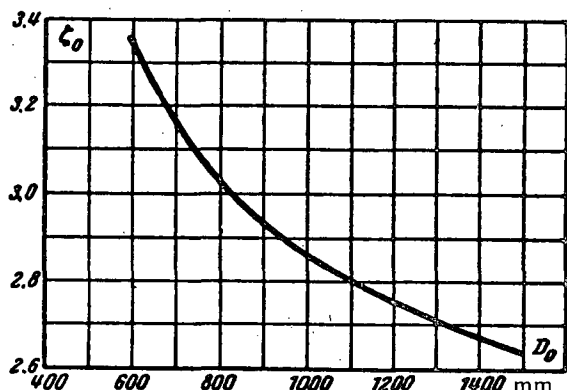
$$w_1 = \frac{Q}{F_1}$$

(F_1 = total cross-section area of the scrubber body)



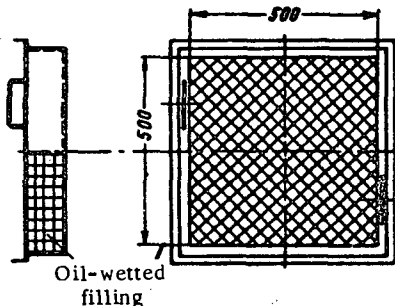
$$\zeta_0 = \frac{\Delta H}{\frac{\gamma w_0^2}{2g}} \text{ is determined from the curve } \zeta_0 = f(D_0)$$

D_0, mm	600	700	800	900	1 000	1 100	1 200	1 300	1 400	1 500
Discharge of water at spraying, kg/sec	0.22	0.28	0.33	0.39	0.45	0.50	0.56	0.61	0.70	0.78
ζ_0	3.38	3.17	3.04	2.94	2.87	2.81	2.76	2.72	2.68	2.65



Porous box-type filter with moist packing

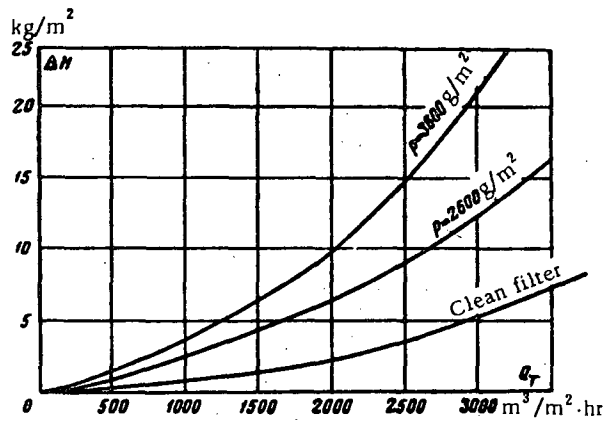
Section XII
Diagram 12-12



1. Filter dimensions 500x500x50mm (LIOT);

packing — 12.7x12.2x0.25 mm metal rings; wetted by turbine oil; dust — fine-ground coal, after passage through the LIOT dust separator

Particle size d , microns	>48	48-22.4	22.4-11.2	≤ 11.2
Weight content, %	1.0	17	60	22
Air load, Q_T , $m^3/m^2 \cdot hr$	Filter dust content p , g/m^2	Cleaning efficiency k_{st} , %	Resistance ΔH , kg/m^2	
4320	0	0	12.4	
4200	1200	76	18.5	
4120	1600	79	21.5	
4040	2000	80	24.4	



2. Filter dimensions 710x510x90 mm (LIOT);

packing — 13x15x8 mm china rings; wetted by Viscin oil; dust — a mixture of coal and cement

Particle size d , microns	11.2	11.2-5.6	5.6-0
Weight content, %	0	33.9	66.1

Air load Q_T , $m^3/m^2 \cdot hr$	Filter dust content p , g/m^2	Cleaning efficiency k_{st} , %	Resistance ΔH , kg/m^2
4000	0	0	25
4000	555	79	35
4000	1110	82	45
4000	1665	85	57

3. Filter dimensions 500x500x50 mm (MIOT);

packing: first half of the box — 9 rows of gauze (woven gauzes with cells 10x10 mm, 2 wicker gauzes with cells 10x10 mm, and 3 woven gauzes with cells 5x5 mm);

second half of the box — (6.8 to 7.7) × (2 to 5) × 0.1 mm copper-coated rings;

wetted by mineral oil;

dust — white Portland cement grade 300-400;

the large-size fractions (77.6 to 78.3 % of the weight)

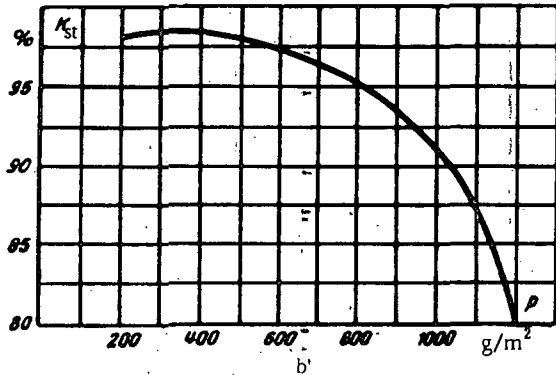
of the cement have been removed from the air by a LIOT dust separator;

mean dust concentration 500 mg/m³;

average cleaning efficiency at $Q_T = 2500-3600 m^3/m^2 \cdot hr$ and $p = 3000 g/m^2$; $k_{st} = 80\%$

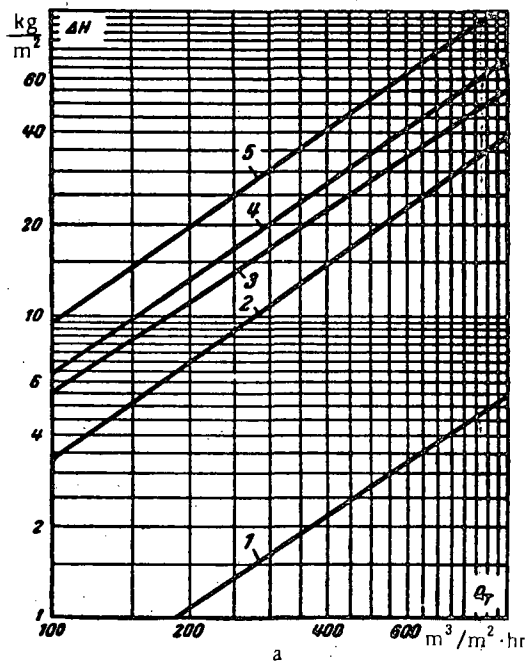
Air load Q_T , $m^3/m^2 \cdot hr$	Resistance ΔH , kg/m^2		
	Clean filter	Dust content $p = 2600, g/m^2$	Dust content $p = 3600, g/m^2$
1000	0.75	2.50	3.75
1500	1.50	4.25	5.25
2000	2.25	6.30	10.0
2500	3.75	9.00	14.7
3000	5.25	12.5	21.2
3500	7.50	16.5	—

Cloth characteristics	
Substance	Wool
Weave	Serge
Approximate cloth thickness, mm	3.75
Weight of 1 m ² cloth, g	463
Number of threads per 50 mm	warp woof
	59 44
Approximate thickness of the threads, mm	warp woof
	0.83 0.83
Twist of the threads per 2.5 cm	warp woof
	4.3 3.5
Presence of nap	Long nap on one side
Exponent <i>m</i>	1.012
Constant coefficient <i>A</i> ₀	5.03 · 10 ⁻³
Dust content <i>p</i> , g/m ²	Value of <i>A</i> ' ₀
0	0
305	241 · 10 ⁻⁴
589	466 · 10 ⁻⁴
894	605 · 10 ⁻⁴
1139	900 · 10 ⁻⁴
<i>p</i> , g/m ²	200 400 600 800 1000 1100 1200
<i>k</i> _{st} , %	98.6 98.6 97.5 95.0 92.0 86.5 80.0



$\Delta H = (A_0 + A'_0) Q_t$, [kg/m²] is determined from graph a, as a function of *Q*_t for different *p*;
*Q*_t = specific load per hour m³/m²·hr;
*k*_{st} = cleaning efficiency of the cloth (%), determined from graph b.
The values given for *A'*₀ and *k*_{st} have been determined for mineral dust (from a sand-blast machine) of particle size not larger than 90 microns.

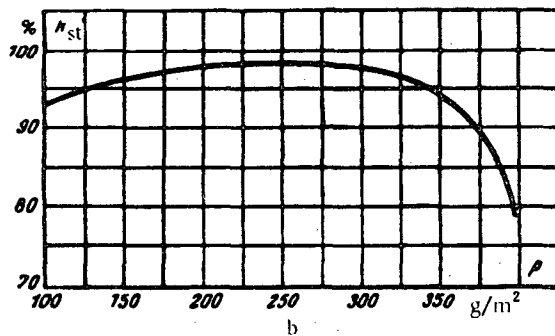
<i>Q</i> _t m ³ /m ² ·hr	100	200	300	400	500	600	800	1000
1. <i>p</i> = 0								
ΔH , kg/m ²	—	1.10	1.52	2.20	2.50	3.30	4.30	5.40
2. <i>p</i> = 305 g/m ²								
ΔH , kg/m ²	3.30	7.10	11.0	14.5	18.6	23.0	31.0	38.0
3. <i>p</i> = 589 g/m ²								
ΔH , kg/m ²	5.50	11.6	16.1	22.4	27.0	34.0	45.0	56.0
4. <i>p</i> = 894 g/m ²								
ΔH , kg/m ²	6.50	13.7	20.0	27.0	35.0	40.0	55.0	70.0
5. <i>p</i> = 1139 g/m ²								
ΔH , kg/m ²	9.50	20.0	30.0	40.5	51.0	62.0	83.0	103



Filtering cloth — serge wool mixture

 Section XII
 Table 12-10

Cloth characteristics							
Substance	warp	Cotton					
	woof	Wool					
Weave		Serge					
Approximate cloth thickness, mm		1.6					
Weight of 1 m ² cloth, g		300					
Number of threads per 50 mm	warp	118					
	woof	83					
Approximate thickness of the threads, mm	warp	0.40					
	woof	0.46					
Twist of the threads per 2.5 cm	warp	12.4					
	woof	7.3					
Presence of nap	Medium nap on one side						
Exponent m	1.11						
Constant coefficient A_0	$5.34 \cdot 10^{-3}$						
Dust content p , g/m ²	Value of A'_0						
0	0						
117	$232 \cdot 10^{-4}$						
308	$610 \cdot 10^{-4}$						
367	$726 \cdot 10^{-4}$						
p , g/m ²	100	150	200	250	300	350	370
k_{st} , %	93.5	96.0	98.0	98.0	97.5	94.0	90.0



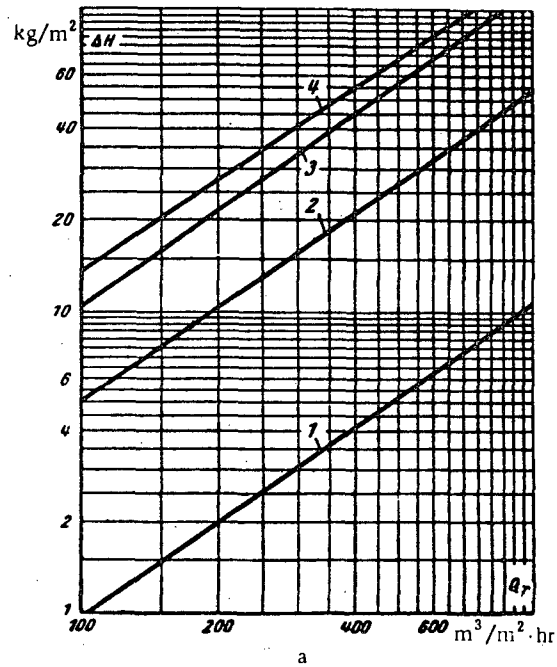
$\Delta H = (A + A'_0 Q_T^m)$, [kg/m²] is determined from graph a as a function of Q_T for different p ;

Q_T = specific load per hour m³/m².hr;

k_{st} = cleaning efficiency of the cloth (%), determined from graph b

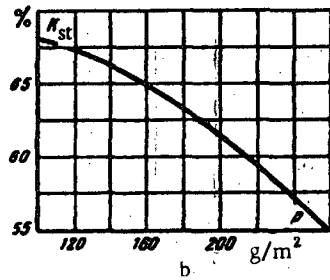
The values given for A'_0 and k_{st} have been determined for mineral dust (from a sand-blast machine) of particle size not larger than 90 microns.

Q_T m ³ /m ² . hr	100	200	300	400	500	600	800	1000
1. $p = 0$	2.00	3.16	4.00	5.50	6.80	8.60	11.4	
2. $p = 117$ g/m ²	5.00	10.0	15.6	21.0	27.0	32.0	44.0	55.0
3. $p = 308$ g/m ²	10.2	21.8	33.5	45.0	57.5	70.0	95.0	125
4. $p = 367$ g/m ²	13.8	27.6	40.0	54.0	68.0	82.0	120	148



Cloth characteristics

Substance	Cotton
Weave	Garnish
Approximate cloth thickness, mm	0.6
Weight of 1 m ² cloth, g	171
Number of threads per 50 mm	warp woof
Approximate thickness of the threads, mm	warp woof
Twist of the threads per 2.5 cm	warp woof
Presence of nap	Without nap
Exponent m	1.17
Constant coefficient A_0	$3.24 \cdot 10^{-3}$
Dust content p , g/m ²	Value of A'_0
0	0
201	$184 \cdot 10^{-4}$
277	$253 \cdot 10^{-4}$
361	$330 \cdot 10^{-4}$
p , g/m ²	100 150 200 250 300
k_{st} , %	67.7 65.6 61.2 56.0 51.0



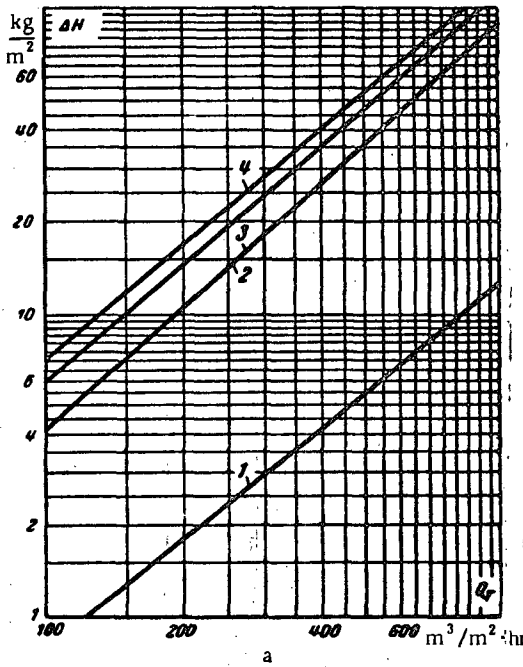
$\Delta H = (A_0 + A'_0) Q^m$ [kg/m²] is determined from graph a as a function of Q_T for different p :

Q_T = specific load per hour m³/m²·hr;

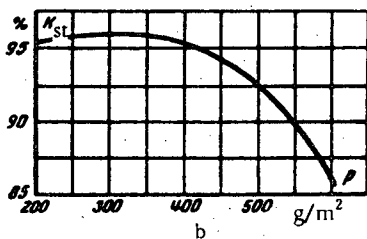
k_{st} = cleaning efficiency of the cloth (%), determined from graph b.

The values given for A'_0 and k_{st} have been determined for mineral dust (from a sand-blast machine) of particle size not larger than 90 microns.

Q_T m ³ /m ² ·hr	100	200	300	400	500	600	800	1000
1. $p = 0$								
ΔH , kg/m ²	—	1.78	3.00	4.20	5.50	6.50	9.20	11.8
2. $p = 201$ g/m ²								
ΔH , kg/m ²	4.20	10.8	17.8	26.2	35.0	45.0	65.0	80.0
3. $p = 277$ g/m ²								
ΔH , kg/m ²	6.00	14.6	25.4	36.0	46.0	60.0	94.0	120
4. $p = 361$ g/m ²								
ΔH , kg/m ²	7.10	17.0	29.6	41.0	52.0	73.0	108	140



Cloth characteristics	
Substance	Wool
Weave	Serge
Approximate cloth thickness, mm	1.56
Weight of 1 m ² cloth, g	355.6
Number of threads per 50 mm	warp woof
Approximate thickness of the threads, mm	warp woof
Twist of the threads per 2.5 cm	warp woof
Presence of nap	Medium nap on one side
Exponent <i>m</i>	1.1
Constant coefficient <i>A</i> ₀	$4.97 \cdot 10^{-3}$
Dust content <i>p</i> , g/m ²	Value of <i>A</i> ' ₀
0	0
145	$173 \cdot 10^{-4}$
313	$374 \cdot 10^{-4}$
468	$580 \cdot 10^{-4}$
603	$720 \cdot 10^{-4}$
<i>p</i> , g/m ²	200 300 400 500 600
<i>k</i> _{st} , %	95.2 96.0 95.5 92.0 86.0



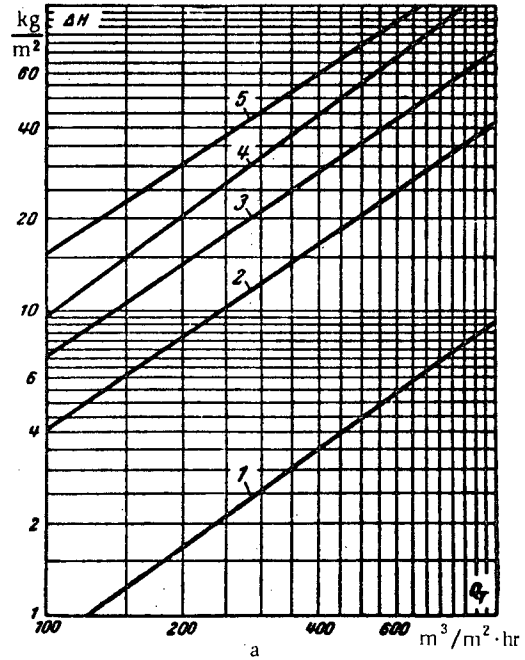
$\Delta H = (A_0 + A'_0 Q_T^m)$ [kg/m²] is determined from graph a as a function of *Q*_T for different *p*:

*Q*_T = specific load per hour m³/m²·hr;

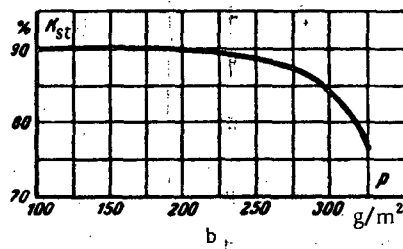
*k*_{st} = cleaning efficiency of the cloth (%), determined from graph b.

The values given for *A*₀ and *k*_{st} have been determined for mineral dust (from a sand-blast machine) of particle size not larger than 90 microns.

<i>Q</i> _T m ³ /m ² ·hr	100	200	300	400	500	600	800	1000
1. <i>p</i> = 0	—	1.70	2.60	3.50	4.50	5.50	7.50	9.50
2. <i>p</i> = 145 g/m ²	4.00	8.00	12.0	16.0	22.0	25.0	34.5	44.0
3. <i>p</i> = 313 g/m ²	7.00	14.5	22.0	30.0	36.0	44.0	60.0	76.0
4. <i>p</i> = 468 g/m ²	10.0	21.0	32.0	45.0	56.0	70.0	98.0	130
5. <i>p</i> = 603 g/m ²	15.0	30.0	45.0	60.0	75.0	90.0	120	160



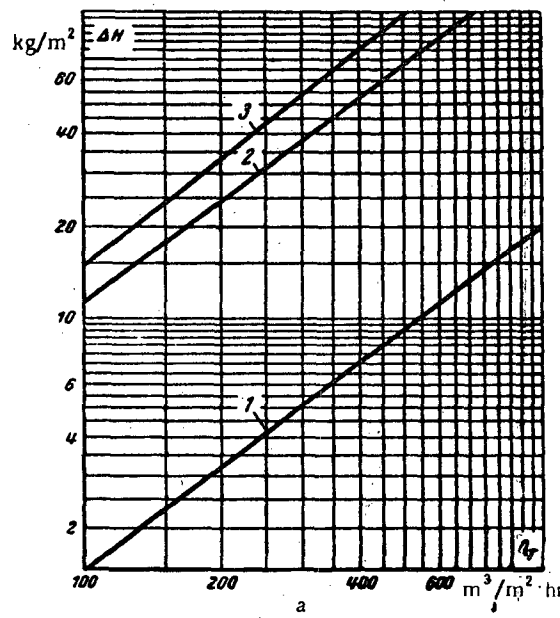
Cloth characteristics	
Substance	Cotton
Weave	Serge
Approximate cloth thickness, mm	1.07
Weight of 1 m ² cloth, g	362.5
Number of threads per 50 mm	warp woof
	105 180
Approximate thickness of the threads, mm	warp woof
	0.24 0.63
Twist of the threads per 2.5 cm	warp woof
	24.0 6.75
Presence of nap	Without nap
Exponent <i>m</i>	1.14
Constant coefficient <i>A₀</i>	7.56 · 10 ⁻³
Dust content <i>p</i> , g/m ²	Value of <i>A'_0</i>
0	0
183	448 · 10 ⁻⁴
330	810 · 10 ⁻⁴
<i>p</i> , g/m ²	100 200 250 300 325
<i>k_{st}</i> , %	90.0 90.0 89.0 85.0 77.0



$\Delta H = (A_0 + A'_0) Q_T^m$ [kg/m²] is determined from graph a as a function of Q_T for different *p*;
 Q_T = specific load per hour m³/m²·hr;
k_{st} = cleaning efficiency of the cloth (%), determined from graph b.

The values given for *A'_0* and *k_{st}* have been determined for mineral dust (from a sand-blast machine) of particle size not larger than 90 microns.

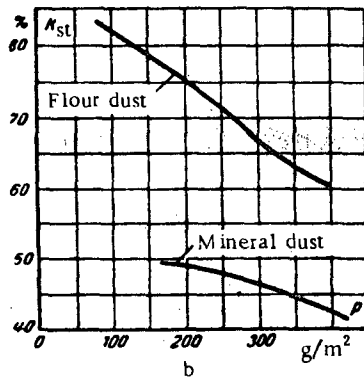
<i>Q</i> m ³ /m ² ·hr	100	200	300	400	500	600	800	1000
1. <i>p</i> = 0 ΔH , kg/m ²	14.5	31.5	50.0	70.5	91.0	110.0	162	200
2. <i>p</i> = 193 g/m ² ΔH , kg/m ²	11.0	23.5	37.5	52.5	67.0	81.0	120	150
3. <i>p</i> = 330 g/m ² ΔH , kg/m ²	15.0	39.5	53.0	75.0	95.0	115	170	210



Filtering cloth — flax flimsy 2-ply thread

 Section XII
 Table 12-14

Cloth characteristics		
Substance	Flax	
Weave	—	
Approximate cloth thickness, mm	1.0	
Weight of 1 m ² cloth, g	203	
Number of threads per 50 mm	warp woof	
Approximate thickness of the threads, mm	warp woof	
Twist of the threads per 2.5 cm	warp woof	
Presence of nap	Without nap	
Exponent m	1.46	
Constant coefficient A_0	$0.029 \cdot 10^{-3}$	
Dust content p , g/m ²	Value of A'_0	
Mineral dust	0 229 413	
Flour dust	123 253 362	
p , g/m ²	Flour dust	
	100 150 200 250 300 400	200 300 400
k_{st} , %	82.0 78.0 75.0 71.0 67.0 60.5	49.0 46.5 42.5



$\Delta H(A_0 + A'_0 Q_T^m)$ [kg/m²] is determined from graph a as a function of Q_T for different p :

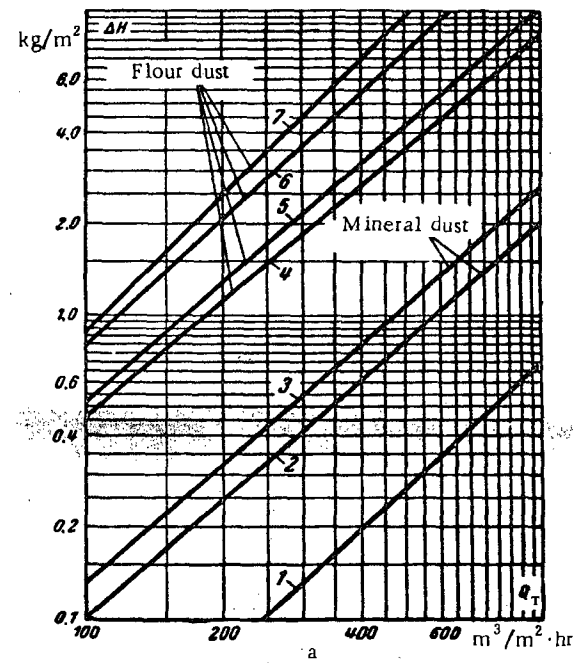
Q_T = specific load per hour m³/m²·hr;

k_{st} = cleaning efficiency of the

cloth (%), determined from graph b.

The particle size of the mineral dust is not larger than 90 microns.

Q_T , m ³ /m ² ·hr	100	200	300	400	500	600	800	1000
Mineral dust 1. $p = 0$								
ΔH , kg/m ²	—	—	0.120	0.20	0.25	0.35	0.51	0.70
ΔH , kg/m ²	0.10	0.25	0.42	0.60	0.81	1.05	1.50	2.02
2. $p = 229$ g/m ²								
ΔH , kg/m ²	0.12	0.37	0.56	0.80	1.05	1.40	2.00	2.55
Flour dust 4. $p = 97$ g/m ²								
ΔH , kg/m ²	0.45	1.10	1.76	2.60	3.50	4.45	6.20	8.20
3. $p = 413$ g/m ²								
ΔH , kg/m ²	0.12	0.37	0.56	0.80	1.05	1.40	2.00	2.55
5. $p = 123$ g/m ²								
ΔH , kg/m ²	0.50	1.25	2.10	3.10	4.10	5.20	7.50	10.0
6. $p = 253$ g/m ²								
ΔH , kg/m ²	0.80	2.00	3.50	5.10	7.20	9.20	13.2	19.6
7. $p = 362$ g/m ²								
ΔH , kg/m ²	0.90	2.50	4.50	7.00	9.60	10.4	19.4	28.0



Filtering cloths — calico, moleskin, and cottonthread
flannelette

Section XII

Table 12-15

Clean (unsoiled) filtering cloths

$$\Delta H \approx A Q_T^m \text{ kg/m}^2$$

Q_T = specific load per hour, $\text{m}^3/\text{m}^2 \cdot \text{hr}$

Cloth	Exponent m	Coefficient A ₀
Calico (without nap)	1.47	$0.06 \cdot 10^{-3}$
Moleskin (without nap)	1.20	$3.18 \cdot 10^{-3}$
Cottonthread flannelette (medium nap on the two sides)	1.18	$4.21 \cdot 10^{-3}$

Q_T , $\text{m}^3/\text{m}^2 \cdot \text{hr}$	600	800	1,000	2,000	3,000	4,000	5,000	6,000	7,000	8,000	9,000	10,000	20,000	30,000	40,000

1. Calico

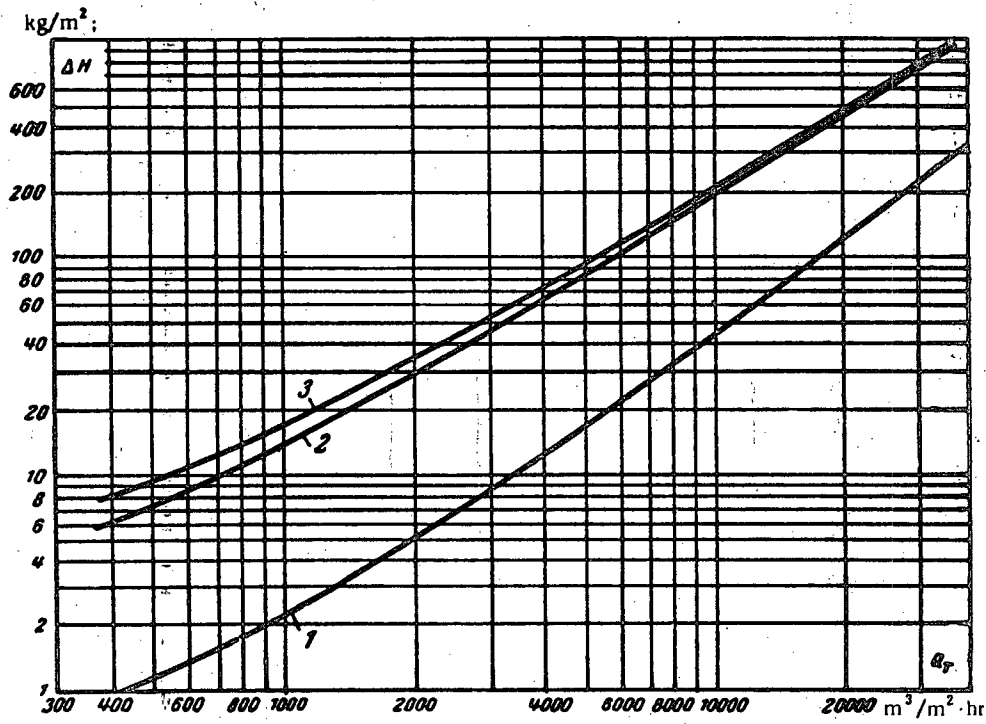
ΔH , kg/m^2	1.40	1.80	2.30	5.20	8.70	12.6	17.0	21.0	27.0	32.0	39.0	45.0	126	229	369

2. Moleskin

ΔH , kg/m^2	9.00	10.9	13.8	29.5	46.0	66.0	83.0	105	129	145	167	195	457	759	1,080

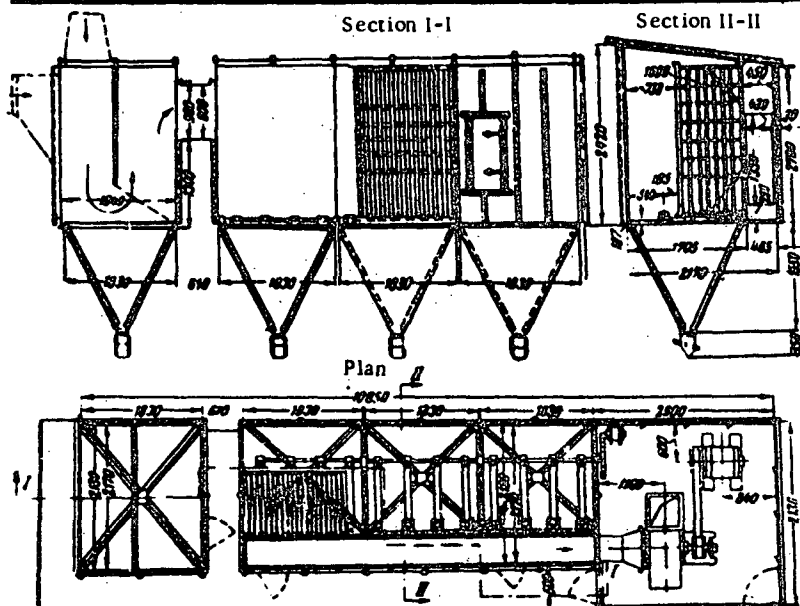
3. Cottonthread flannelette

ΔH , kg/m^2	10.9	13.9	17.0	35.0	53.0	73.0	93.0	115	138	160	182	209	470	767	1,110



DIZ cloth shaking filter with various types of cloth

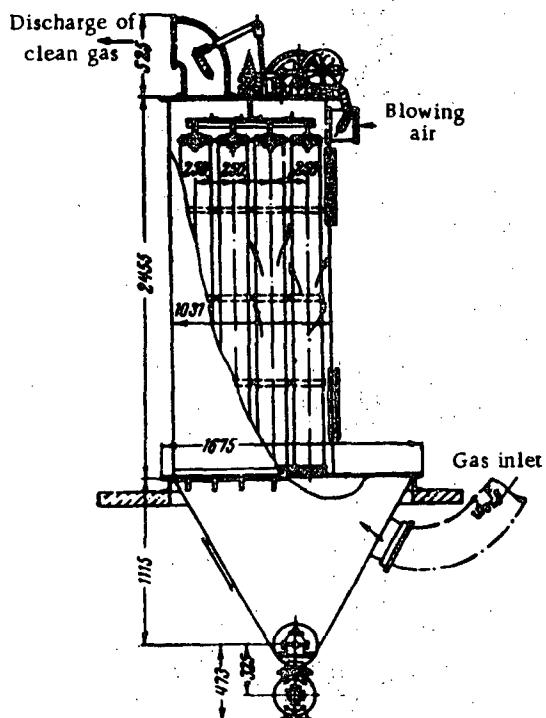
Section XII
Diagram 12-13



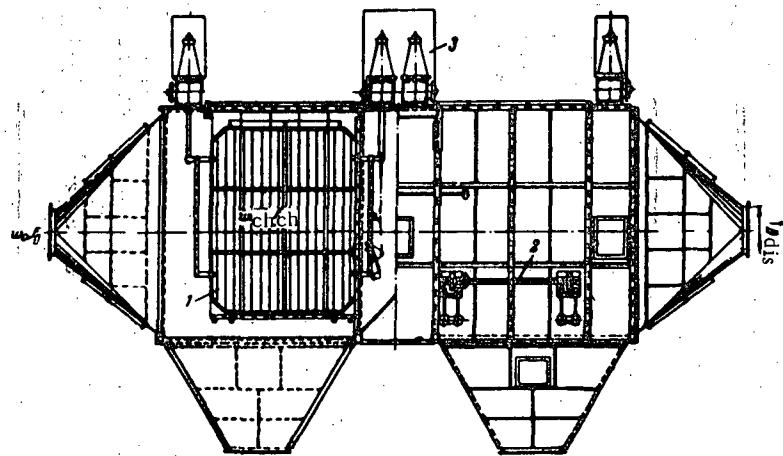
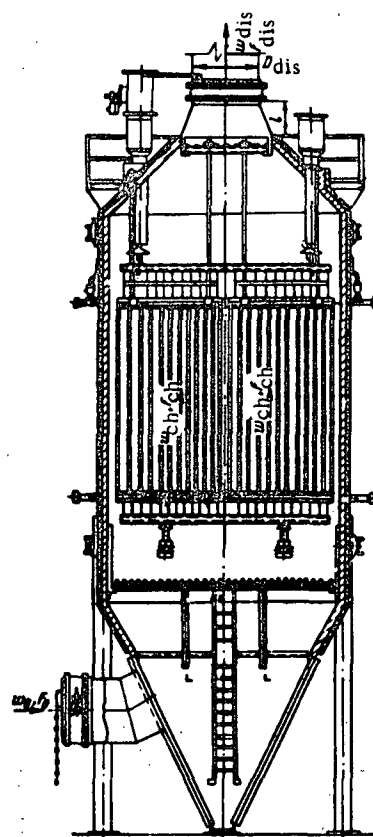
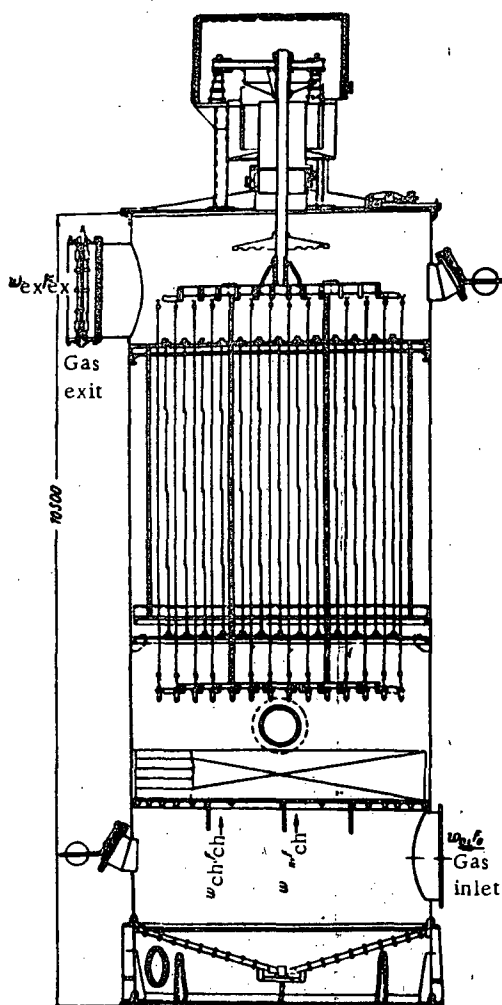
Cloth	Dust	Specific air load m ³ /m ² ·hr	Cleaning efficiency, %	Cloth resistance, kg/m ²
Tricot "melange"	Sand blast	34.7	99.19	60.5
Black mole- skin	From the shaking-out foundry screens of the "Kompress- or" plant	83.5	85.30	26.0
Moleskin (dense)	Sand blast	123.5 100.0	— 97.54	53.5 113.0

MFU suction-type hose filter with various types of cloth

Section XII
Diagram 12-14



Cloth	Dust	Specific gas (air) load, mg/m ² ·hr	Cleaning efficien- cy, %	Cloth re- sistance, dN kg/m ²
Velveteen	Flour dust	187.0	99.824	28.0
"	Sand blast	213.0	97.185	32.0
Chamois	The same	77.0	99.966	11.4
"	" "	141.0	99.886	26.2
"	" "	198.0	99.817	48.1
Linen for press filter	" "	75.9	99.907	18.1
The same	" "	13.5	99.707	37.3
" "	" "	194.0	99.929	94.7
Cloth No. 2	" "	77.1	99.020	9.80
" "	" "	142.3	99.733	53.5
" "	" "	181.0	98.968	156.2
" "	Flour dust	195.0	99.795	27.0
Velveteen	Sand blast	150.0	—	62.0
"	" "	150.0	—	40.0
"	" "	75.0	—	32.0
"	" "	75.0	—	14.0
"	Discharged from the bottom of flour mills	78.0	98.50	47.8
"	The same	87.0	99.00	53.3
"	" "	124.0	99.04	60.0
Cloth No. 2 for BET filters	Zinc and lead oxide	59.0	99.52	65.5
		59.0	99.12	61.0



$$\zeta = \frac{\Delta H}{\gamma w_0^2} = \zeta_{in} + \zeta_{ex} + \zeta_{ch}$$

where ζ_{in} is determined as ζ from diagram 12-16;

$$\zeta_{ex} = \zeta \left(1 - \frac{F_{ex}}{F_{ch}} \right);$$

ζ is determined as ζ from diagram 3-6 as a function of a and $\frac{l}{D_h}$.

$$\text{at } \frac{l}{D_h} = 0 \quad \zeta = 0.5;$$

$$\zeta_{ch} = \zeta_{in} + \zeta_{dis} + \zeta_{fr};$$

$$\zeta = 0.5 \left(1 - \frac{F_e}{F_{ch}} \right) \left(\frac{F_o}{F_e} \right)^2;$$

$$\zeta_{ex} = 0.5 \left(1 - \frac{F_e}{F_{ch}} \right)^2 \left(\frac{F_o}{F_e} \right)^2;$$

$$\zeta_{fr} = \lambda \frac{l_e}{D_e} \left(\frac{F_o}{F_e} \right)^2;$$

λ is determined from diagrams 2-2 to 2-5 as a function of Re and

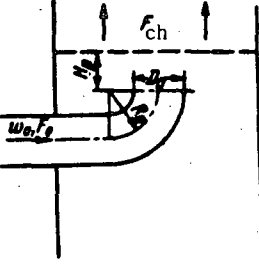
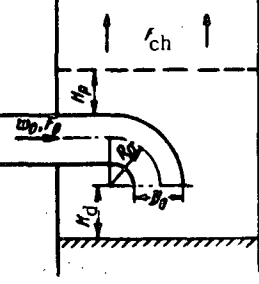
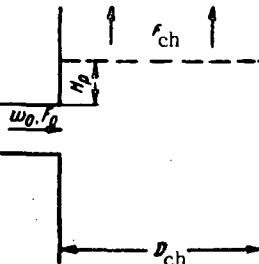
$$D_e = \frac{4F_e}{\Pi_e}$$

F_e and Π_e are, respectively, the cross-section area and the perimeter of the settling tubes or of the gap between the settling plates

Section XII

Inlet stretches of unit with grid, packing or other type of obstruction placed in the working chamber

Diagram 12-16

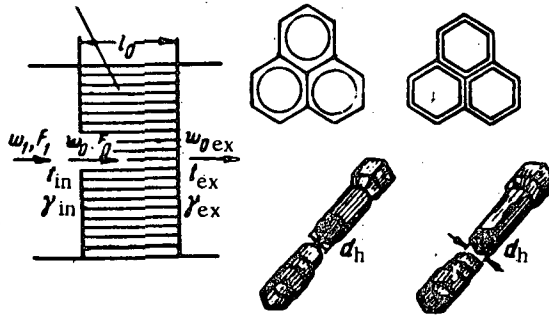
Stream-inlet conditions	Scheme	Resistance coefficient $\zeta = \frac{AH}{\frac{V^2}{2g}}$
Central impingement of the stream on the grid		$\zeta = \zeta'_{o.be} = N_o + 0.7\zeta_p \left(\frac{F_o}{F_{ch}} \right)^2 + \frac{0.013}{\left(\frac{H_p}{D_o} \right)^2} \sqrt{\zeta_p - \sqrt{\zeta_p}}$ <p>where $\zeta'_{o.be}$ is determined as $0.5 \zeta_o$ for the given bend from the diagrams of Section VI.</p> <p>N_o is determined from Tables 12-1 to 12-7;</p> <p>ζ_p is determined as ζ for a grid, packing, or other type of resistance, from diagrams 8-1 to 8-6 and 8-16 to 8-21;</p> <p>the term $\frac{0.013}{\left(\frac{H_p}{D_o} \right)^2} \sqrt{\zeta_p - \sqrt{\zeta_p}}$ is only taken into account if $0 < \frac{H_p}{D_o} < 1.2$.</p>
Peripheral impingement of the stream on the grid		$\zeta = \zeta'_{o.be} + 0.9 \left[N_o + 0.7\zeta_p \left(\frac{F_o}{F_{ch}} \right)^2 \right] + \frac{0.05}{\left(\frac{H_d}{D_o} \right)^2};$ <p>the term $\frac{0.05}{\left(\frac{H_d}{D_o} \right)^2}$ is only taken into account for $\frac{H_d}{D_o} < 1.2$</p>
Side impingement of the stream on the grid		$\zeta = N_o + 0.7\zeta_p \left(\frac{F_o}{F_{ch}} \right)^2 + 0.1 + \left(2 - 20 \frac{H_p}{D_{ch}} \right);$ <p>the term $\Delta\zeta = 2 - 20 \frac{H_p}{D_{ch}}$ is only taken into account for $\frac{H_p}{D_{ch}} < 0.1$.</p>

For a system of grids installed in series instead of a single grid, ζ_p is replaced by the sum

$$\sum_{i=1}^n \zeta_{ip} = \zeta_{1p} + \zeta_{2p} + \dots + \zeta_{np}$$

where n = number of grids arranged in series.

$$d_h = \frac{4f_0}{B_0}; B_0 - \text{perimeter}$$



f_0 = cross-section area of one tube;
 F_0 = total flow area of radiator

$$\zeta = \frac{\Delta H}{\gamma_{in} w_0^2} = \lambda \left(3 + \frac{l_0}{d_h} \right) \left(\frac{F_1}{F_0} \right)^2 + \zeta_{sh} + \Delta \zeta,$$

$$\text{where 1) at } 35 \leq Re^* = \frac{w_0 \sin \Delta}{v} \leq 275$$

$$\lambda = 0.375 Re^{*-0.1} \Delta^{0.4} \text{ is determined by graph a;}$$

$$2) \text{ at } 275 \leq Re^* \leq 500$$

$$\lambda = 0.214 \Delta^{0.4} \text{ is determined by graph a;}$$

$$\zeta_{sh} = \left(\frac{F_1}{F_0} - 1 \right)^2 \text{ is determined by graph b;}$$

$$\Delta \zeta_t = \left(1.7 + \lambda \frac{l_0}{d_h} \right) \left(\frac{F_1}{F_0} \right)^2 \bar{T};$$

$$\bar{T} = \frac{T_{ex} - T_{in}}{T_{in}}; \bar{\Delta} = \frac{\Delta}{d_h};$$

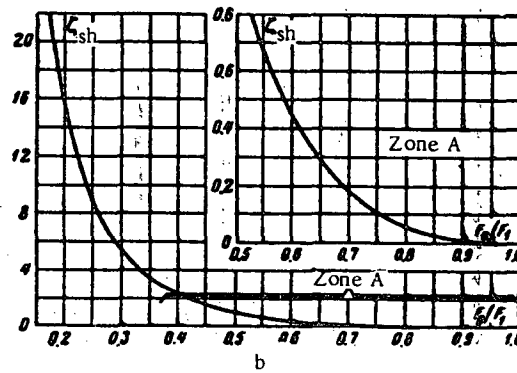
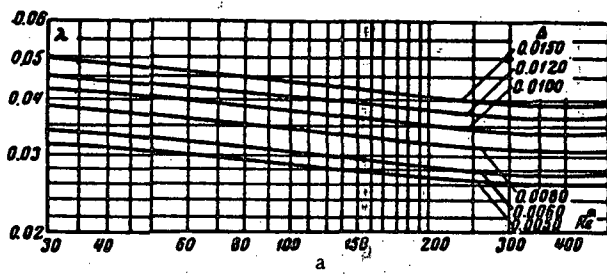
Δ is taken from Table 2-1;

v is determined by §1-3, b.

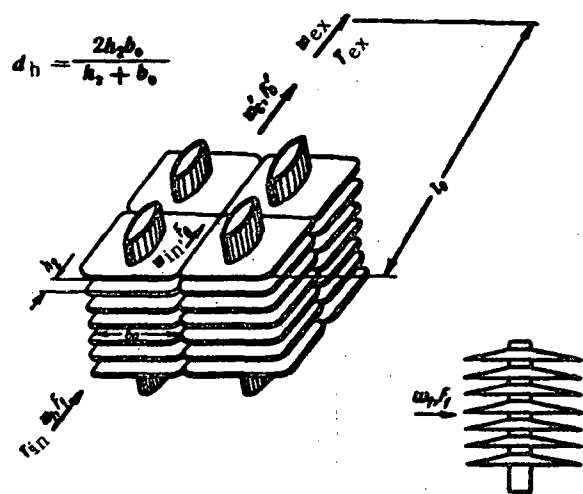
Values of λ

Re*	Δ					
	0.0050	0.0060	0.0080	0.0100	0.0120	0.0150
30	0.032	0.034	0.039	0.043	0.046	0.050
40	0.031	0.035	0.038	0.042	0.045	0.049
60	0.030	0.032	0.036	0.040	0.043	0.047
80	0.029	0.032	0.035	0.039	0.042	0.046
100	0.028	0.031	0.034	0.038	0.041	0.045
150	0.028	0.030	0.034	0.036	0.039	0.042
200	0.027	0.029	0.033	0.035	0.038	0.041
300	0.026	0.028	0.031	0.034	0.037	0.039
500	0.026	0.028	0.031	0.034	0.037	0.039

$\frac{F_1}{F_0}$	$\left(\frac{F_1}{F_0} \right)^2$	ζ_{sh}
0	∞	∞
0.1	100	81.0
0.2	25.0	16.0
0.3	11.1	5.43
0.4	6.25	2.25
0.5	4.00	1.00
0.6	2.76	0.45
0.7	2.04	0.18
0.8	1.56	0.06
0.9	1.23	0.01
1.0	1.00	0



Ribbed-tube radiator

 Section XII
 Diagram 12-18


$$\epsilon = \frac{\Delta H}{T_{in} w_1^2} = \left(\epsilon_{ct} + \lambda \frac{l_0}{d_h} \right) \left(\frac{F_1}{F_0} \right)^2 + \Delta \zeta_r$$

where $\lambda = \frac{0.77}{\sqrt{Re}}$ is determined from graph a as a function of Re

$$Re = \frac{w_0 \sin d_h}{v}, \text{ taken in the range } 3,000 \leq Re \leq 25,000;$$

$$\zeta_c = 1.5 \left(1 - \frac{F_0}{F'_0} \right)^2 \text{ is determined from graph b;}$$

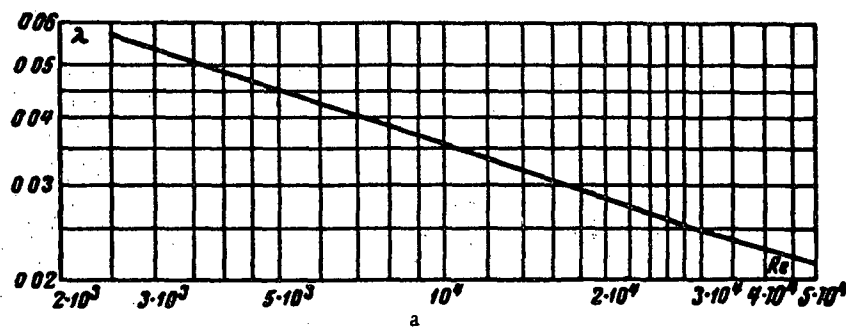
$$\Delta \zeta_r = \left(1.7 + \lambda \frac{l_0}{d_1} \right) \left(\frac{F_1}{F_0} \right)^2 \bar{T};$$

$$\bar{T} = \frac{T_{ex} - T_{in}}{T_{in}};$$

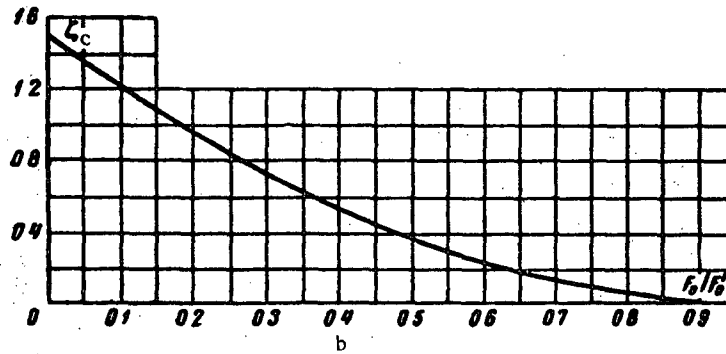
z = number of rows of tubes;

v = is taken from § 1-3, b.

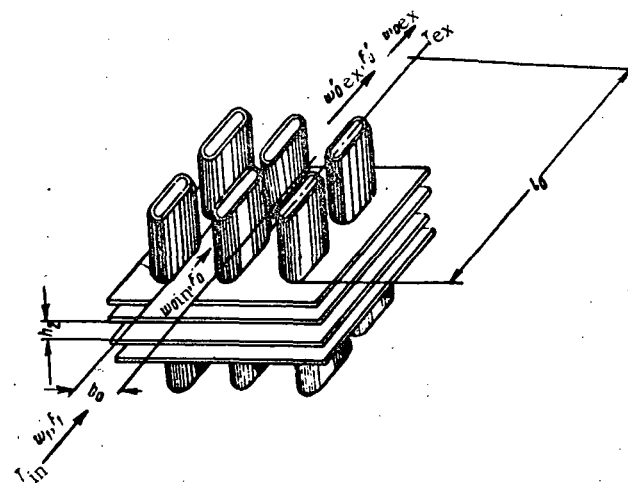
Re	$2.5 \cdot 10^3$	$3 \cdot 10^3$	$4 \cdot 10^3$	$5 \cdot 10^3$	$6 \cdot 10^3$	$8 \cdot 10^3$	10^4	$1.2 \cdot 10^4$	$1.6 \cdot 10^4$	$2.0 \cdot 10^4$	$2.5 \cdot 10^4$	$3.0 \cdot 10^4$
λ	0.057	0.540	0.049	0.045	0.043	0.039	0.036	0.034	0.030	0.029	0.027	0.025



$\frac{F_0}{F'_0}$	0	0.1	0.2	0.3	0.4	0.5	0.6	0.7	0.8	0.9	1.0
ϵ_c	1.50	1.22	0.96	0.74	0.54	0.38	0.24	0.14	0.06	0.02	0



$$d_h = \frac{2h_2 b_0}{h_2 + b_0}$$



$$\zeta = \frac{\Delta H}{\frac{\gamma_{in} w_1^2}{2g}} = \left(z\zeta_c + \lambda \frac{l_0}{d_h} \right) \left(\frac{F_1}{F_0} \right)^2 + \Delta \zeta_r$$

where 1) at $4000 < Re = \frac{w_0 in d_h}{v} < 10000$

$\lambda = \frac{0.98}{\sqrt[6]{Re}}$ is determined from the curve $\lambda = f(Re)$;

2) at $R > 10000$

$\lambda = \frac{0.21}{\sqrt[6]{Re}}$ is determined from the same curve $\lambda = f(Re)$;

ζ_c is determined from graph b of diagram 12-18;

$$\Delta \zeta_r = \left(1.7 + \lambda \frac{l_0}{d_h} \right) \left(\frac{F_1}{F_0} \right)^2 \bar{T};$$

$$\bar{T} = \frac{T_{ex} - T_{in}}{T_{in}}.$$

z = number of rows of tubes;

v is taken from § 1-3, b.

	$3 \cdot 10^3$	$4 \cdot 10^3$	$5 \cdot 10^3$	$6 \cdot 10^3$	$8 \cdot 10^3$	10^4	$1.4 \cdot 10^4$	$2.0 \cdot 10^4$	$2.5 \cdot 10^4$	$3.0 \cdot 10^4$
λ	0.068	0.062	0.057	0.054	0.050	0.046	0.043	0.040	0.039	0.038

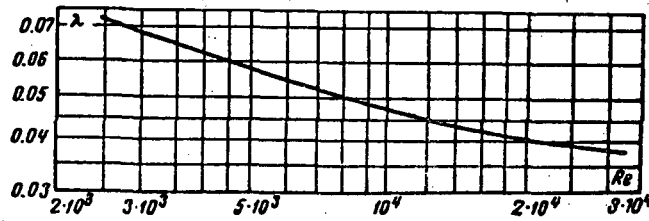
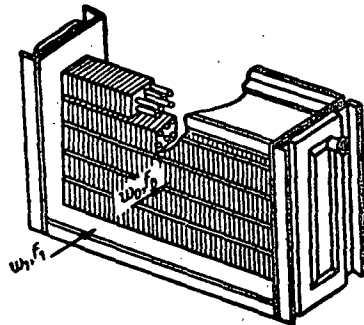


Plate-type air heater

Section XII
Diagram 12-20

$$w_0 = \frac{Q}{F_0}; F_0 - \text{flow area}$$



1. For model S

one-row

$$\Delta H = 0.138 (\gamma_m w_0)^{1.66} [\text{kg/m}^2] \text{ is determined from curve } S_1;$$

two-row

$$\Delta H = 0.276 (\gamma_m w_0)^{1.70} [\text{kg/m}^2] \text{ is determined from curve } S_2;$$

2. For model B

one-row

$$\Delta H = 0.150 (\gamma_m w_0)^{1.74} [\text{kg/m}^2] \text{ is determined from curve } B_1;$$

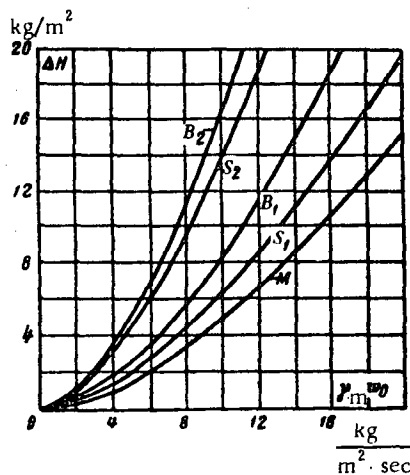
two-row

$$\Delta H = 0.326 (\gamma_m w_0)^{1.69} [\text{kg/m}^2] \text{ is determined from curve } B_2;$$

3. For model M

ΔH is determined from curve **M**;

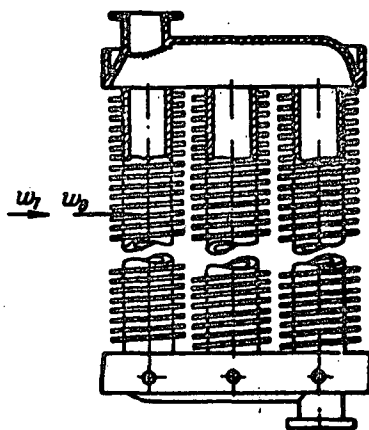
γ_m is specific gravity, kg/m^3 .



Values of ΔH , kg/m^2

$\gamma_m w_0$ $\text{kg/m}^2 \cdot \text{sec}$	0	2	4	6	8	10	12	14	16	18	20
M	0	0.30	0.90	1.90	3.10	4.60	6.40	8.50	10.5	13.0	15.2
S₁	0	0.40	1.40	2.70	4.40	6.30	8.50	11.0	13.8	16.3	19.9
S₂	0	0.90	2.90	5.80	9.50	13.8	18.8	24.6	31.0	39.6	45.9
B₁	0	0.50	1.70	3.40	5.60	8.30	11.3	14.8	18.9	23.0	27.5
B₂	0	1.00	3.40	6.70	10.9	15.9	21.7	28.0	35.3	42.9	54.6

$$w_0 = \frac{Q}{F_0}; F_0 - \text{flow area}$$



1. KB and T - twenty-tube

$\Delta H = 0.345 (\gamma_m w_0)^{1.84} [\text{kg/m}^2]$ is determined from curve No. 1;

2. Universal elements and KU heater

two-row

$\Delta H = 0.0824 (\gamma_m w_0)^{1.88} [\text{kg/m}^2]$ is determined from curve No. 2;

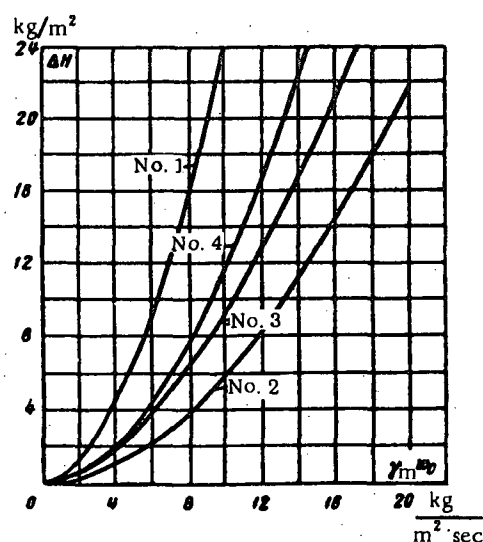
three-row

$\Delta H = 0.156 (\gamma_m w_0)^{1.77} [\text{kg/m}^2]$ is determined from curve No. 3;

four-row

$\Delta H = 0.130 (\gamma_m w_0)^{1.95} [\text{kg/m}^2]$ is determined from curve No. 4;

γ_m is the specific gravity, kg/m^3 .



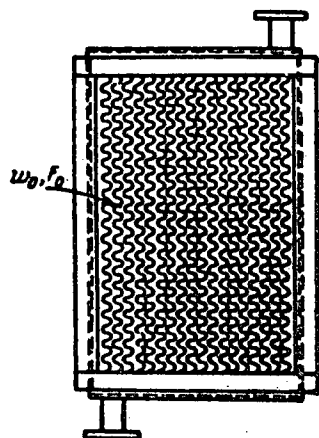
Values of ΔH , kg/m^2

$\gamma_m w_0$ $\text{kg/m}^2 \text{sec}$	0	2	4	6	8	10	12	14	16	18	20
No. 1	0	1.23	4.41	9.34	15.8	23.8	35.0	44.4	56.5	70.4	85.0
No. 2	0	0.30	1.09	2.31	3.94	5.97	8.38	11.6	14.3	17.7	21.7
No. 3	0	0.53	1.82	3.73	6.19	9.19	12.7	16.7	21.1	26.0	31.3
No. 4	0	0.50	1.94	4.48	7.50	11.6	16.6	22.3	29.0	36.5	45.1

Petaled fin heater

Section XII
Diagram 12-22

$$w_0 = \frac{Q}{F_0}; F_0 - \text{flow area}$$



1. One-channel

Three-row

$\Delta H = 0.118 (\gamma_m w_0)^{1.85} [\text{kg/m}^2]$ is determined from curve No. 1;

Six-row

$\Delta H = 0.315 (\gamma_m w_0)^{1.86} [\text{kg/m}^2]$ is determined from curve No. 2;

2. Two-channel

One-row

$\Delta H = 0.153 (\gamma_m w_0)^{1.78} [\text{kg/m}^2]$ is determined from curve No. 3;

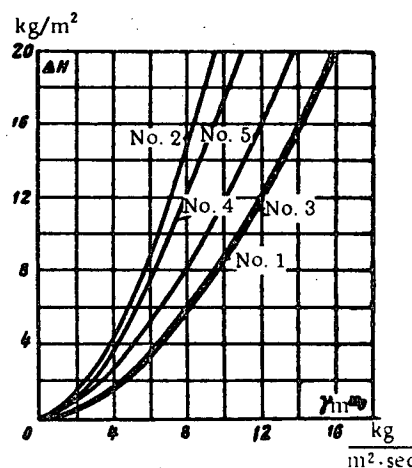
Two-row

$\Delta H = 0.336 (\gamma_m w_0)^{1.71} [\text{kg/m}^2]$ is determined from curve No. 4;

3. Three-channel one-row

$\Delta H = 0.227 (\gamma_m w_0)^{1.71} [\text{kg/m}^2]$ is determined from curve No. 5

γ_m is the specific gravity, kg/m^3 .



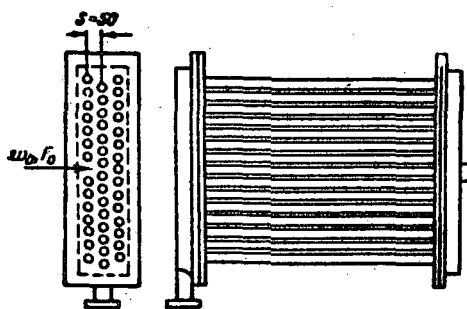
Values of ΔH , kg/m^2

$\gamma_m w_0$ $\text{kg/m}^2 \cdot \text{sec}$	0	2	4	6	8	10	12	14	16	18	20
No. 1	0	0.42	1.53	3.25	5.51	8.35	11.6	15.5	20.0	24.7	30.3
No. 2	0	1.13	4.04	8.52	14.4	21.8	30.5	40.6	52.0	64.4	78.0
No. 3	0	0.52	1.76	3.58	5.95	8.80	12.2	15.6	20.2	24.8	29.9
No. 4	0	1.10	3.60	7.20	11.8	17.2	23.3	30.0	38.5	47.3	56.1
No. 5	0	0.74	2.43	4.86	7.95	11.6	15.8	20.2	26.0	32.0	38.1

Plain pipe air heater

 Section XII
 Diagram 12-23

$$w_0 = \frac{Q}{F_0}; F_0 = \text{flow area}$$


 Two-row
 $\Delta H = 0.0625 (\gamma_m w_0)^{1.81}$

[kg/m²] is determined from curve No. 1;

Three-row

 $\Delta H = 0.0877 (\gamma_m w_0)^{1.81}$

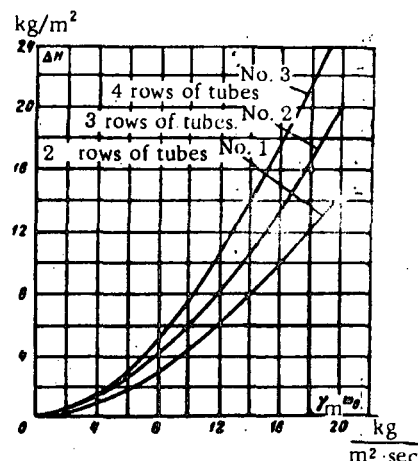
[kg/m²] is determined from curve No. 2

Four-row

 $\Delta H = 0.113 (\gamma_m w_0)^{1.81}$

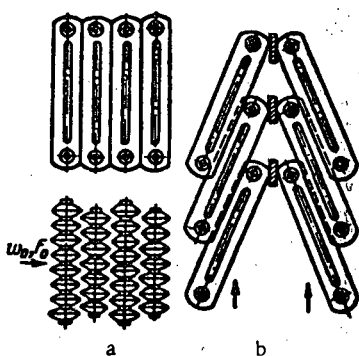
[kg/m²] is determined from curve No. 3.

γ_m = specific gravity, kg/m³.

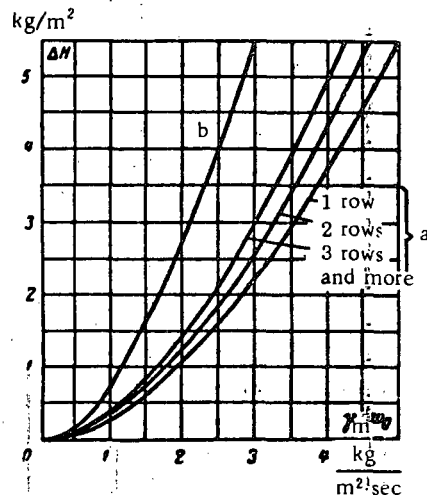

 Values ΔH , kg/m²

$\gamma_m w_0$, kg/m ² ·sec	0	1	2	4	6	8	10	12	14	16	18	20
2 rows No. 1	0	0.06	0.22	0.77	1.60	2.70	4.00	6.00	7.80	9.80	11.7	14.3
3 rows No. 2	0	0.08	0.31	1.10	2.20	3.80	5.70	7.90	10.4	13.2	16.3	20.1
4 rows No. 3	0	0.11	0.40	1.40	2.90	4.90	7.30	10.2	13.4	17.1	21.0	26.0

Air heater made from heating elements

 Section XII
 Diagram 12-24

 1. Radiator installed in a vertical position.
 ΔH is determined from curves a;

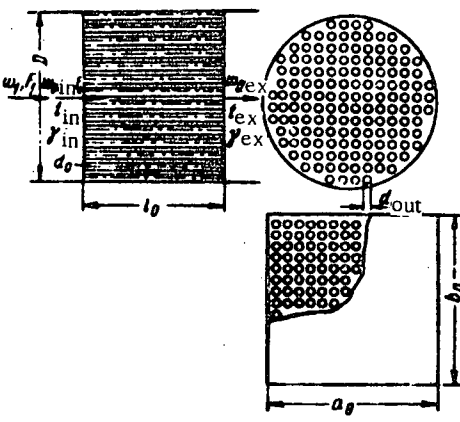
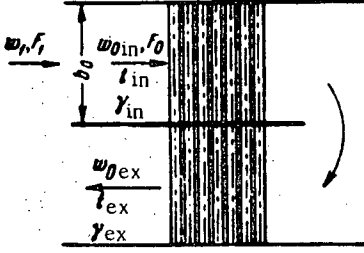
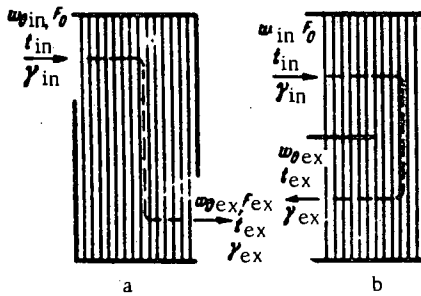
 2. Radiator installed in inclined position.
 ΔH is determined from curve b;
 γ_m = specific gravity, kg/m³.

 Values ΔH , kg/m²


$\gamma_m w_0$, kg/m ² ·sec	0	0.5	1.0	1.5	2.0	2.5	3.0	3.5	4.0	5.0	6.0
a) One row	0	0.01	0.03	0.06	0.11	0.16	0.22	0.29	0.37	0.55	0.76
a) Two rows	0	0.01	0.03	0.07	0.12	0.18	0.25	0.33	0.43	0.64	0.90
a) Three rows	0	0.01	0.04	0.08	0.14	0.21	0.29	0.39	0.49	0.73	0.99
b)	0	0.02	0.07	0.16	0.26	0.39	0.54	0.74	0.92	—	—

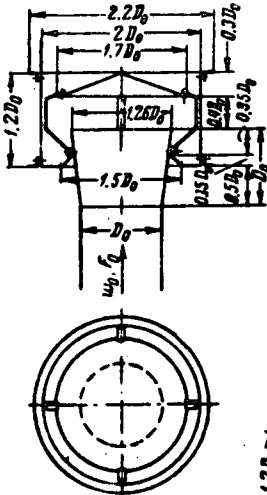
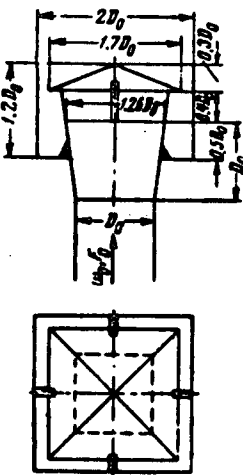
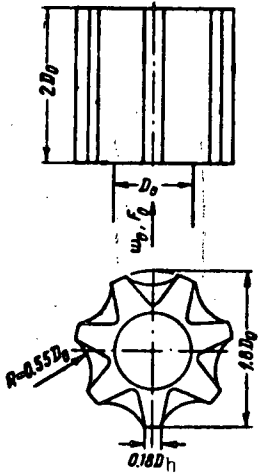
Various heat exchangers

 Section XII
 Diagram 12-25

Type	Schematic view	Resistance coefficient
Shell-tube exchanger with longitudinal stream flow around the tubes		$\zeta = 0.5 \left(1 - \frac{F_0}{F_1} \right) + \left(1 - \frac{F_0}{F_1} \right)^2 + \lambda \frac{l_0}{d_0} + \Delta \zeta,$ <p>where</p> $d_h = \frac{D_1^2 - z d_{\text{out}}^2}{z d_{\text{out}}},$ <p>for a shell of circular section, and</p> $d_h = \frac{4 \left(a_1 b_1 - z \frac{\pi}{4} d_{\text{out}}^2 \right)}{2 (a_1 + b_1) + z \pi d_{\text{out}}};$ <p>for a shell of rectangular section; λ is determined from diagrams 2-1 to 2-5.</p>
Shell-tube with stream flow through the tubes		$\zeta = 0.5 \left(1 - \frac{F_0}{F_1} \right) + \left(1 - \frac{F_0^2}{F_1} \right) + \lambda \frac{l_0}{d_0} + \Delta \zeta;$ <p>λ is determined from diagrams 2-1 to 2-5</p>
Two-stage heat exchanger with transverse flow around the tube bundle (180° turn)		$\zeta = \zeta_{180} + \zeta_{bd} + \Delta \zeta,$ <p>where ζ_{180} is determined as ζ for a U-shaped elbow at $\frac{l_0}{b_0} = 0$ from diagrams 6-21 to 6-24; ζ_{bd} is determined as ζ for the corresponding tube bundles from diagrams 8-11 and 8-12.</p>
With mixed flow around the tubes (alternating sections of transverse and longitudinal flows)		$\zeta = \zeta_{bd} + \Delta \zeta,$ <p>where in the case of design a ζ_{bd} is determined as ζ for the corresponding bundle from diagrams 8-11 and 8-12, taken only for half the rows of the tubes in each zone of transverse flow; in the case of design b as ζ_{bd} from the same diagrams, but for all the rows of tubes enclosed by the partition, and for half of the tubes protruding from it</p>
$\Delta \zeta_t = 2 \frac{t_{ex} - t_{in}}{273 + t_{in}} ; \quad t_{in} = \frac{t_{in} + t_{ex}}{2} ; \quad \gamma_m = \frac{\gamma_0}{1 + \frac{\gamma_0}{273}} ;$ $w_{0m} = w_{0in} \frac{273 + t_{in}}{273 + t_{in}}.$		

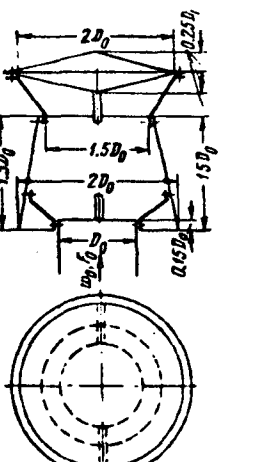
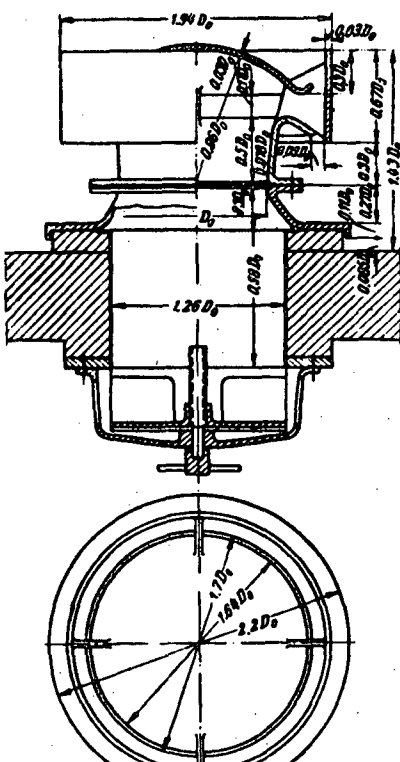
Various ventilating hoods

Section XII
Diagram 12-26

Type	Schematic view	Resistance coefficient $\zeta = \frac{\Delta H}{\frac{1}{2} \rho v_0^2}$
Circular TsAGI hood		$\zeta = 0.64$
Square TsAGI hood		$\zeta = 0.64$
Chanard-Etoile hood		$\zeta = 1.0$

Various ventilating hoods (continued)

Section XII
Diagram 12-26

Type	Schematic view	Resistance coefficient $\zeta = \frac{\Delta H}{\frac{V^2}{2g}} \cdot \frac{2g}{Re_0^2}$
Grigorovich hood		$\zeta = 1.04$
Standardized TsAGI hood without reducing piece for railroad cars		Without lid $\zeta = 1.4$ With lid $\zeta = 3.0$

Type	Schematic view	Resistance coefficient $\zeta = \frac{\Delta H}{V^2/2}$
Standardized TsAGI roof ventilator with reducing piece for railroad cars		With lid $\zeta = 2.6$
Chesnokov roof ventilator		Without lid $\zeta = 10.6$ With lid $\zeta = 11.6$

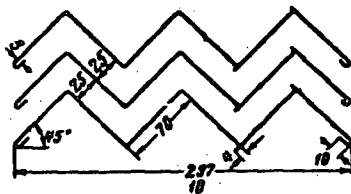
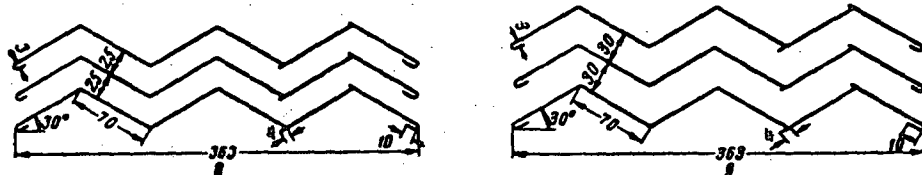
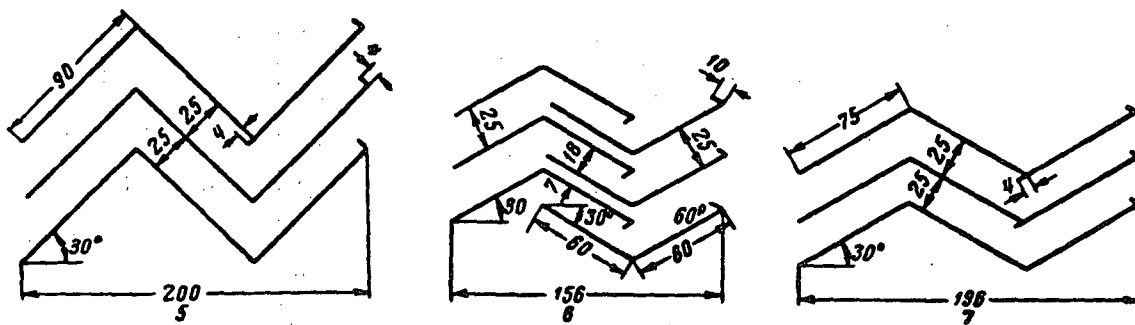
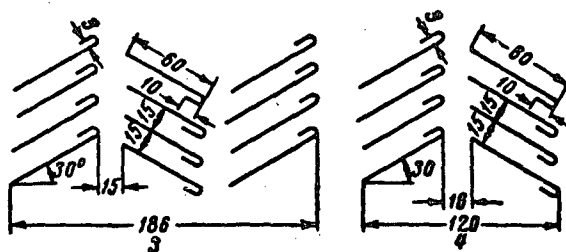
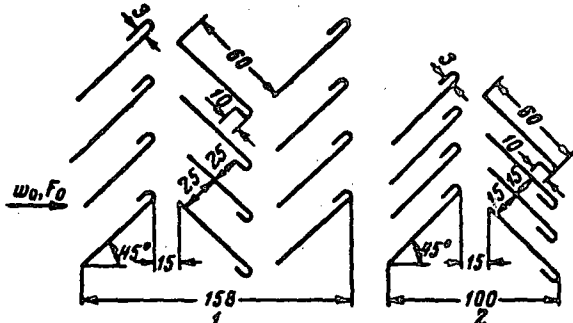
Eliminators

 Section XII
 Diagram 12-27

$\zeta = \frac{\Delta H}{\frac{V^2}{2g}}$ is taken from the table

$$w_0 = \frac{Q}{F_0}; F_0 = \text{flow area}$$

Eliminator type	Position	$\zeta = \frac{\Delta H}{\frac{V^2}{2g}}$
1	After the chamber	17.7
2	After the chamber	9.40
3	Before the chamber	7.30
4	After the chamber	8.40
5	Before the chamber	3.40
6	After the chamber	13.9
7	Before the chamber	8.90
8	After the chamber	10.7
9	" " "	8.00
10	" " "	5.50
		8.80
		9.60
		16.9



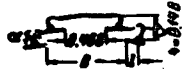
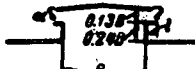
Various types of roof ventilators

 Section XII
 Diagram 12-28

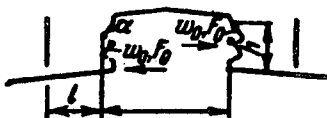
Type	Schematic view		I/A	$\frac{t = \Delta H}{T_{\text{out}} - T_0}$ 24
Baturin-Brandt ventilator with grid		45	1.3	6.5
The same with flaps		80	1.3	6.8
LD-4		0	1.46	8.3
LEN PSP ventilator with two flaps The same with three flaps		80 80	1.49 1.49	3.9 3.9
KTIS		40	1.12	4.3
MIOT-2 MIOT-2a		0 0	0.69 0.86	9.0 5.8
PSK-1		0	1.45	5.3
PSK-2 – summer conditions PSK-2 – winter conditions		—	1.0 1.0	5.1 5.6

Various types of roof ventilators (continued)

 Section XII
 Diagram 12-28

Type	Schematic view	a°	I/h	$\zeta = \frac{\Delta H}{\gamma w_0^2} \frac{2g}{2g}$
Two-circle		40	1.12	4.2
Giprotis		40	1.12	4.6
Ryukin-11'inskii		40	0.58	4.3
Ventilating house		40	1.12	3.3

Rectangular roof ventilators with panels

 Section XII
 Diagram 12-29


$$\zeta = \frac{\Delta H}{\gamma w_0^2} = a + \Delta \zeta,$$

$$\frac{2g}{2g}$$

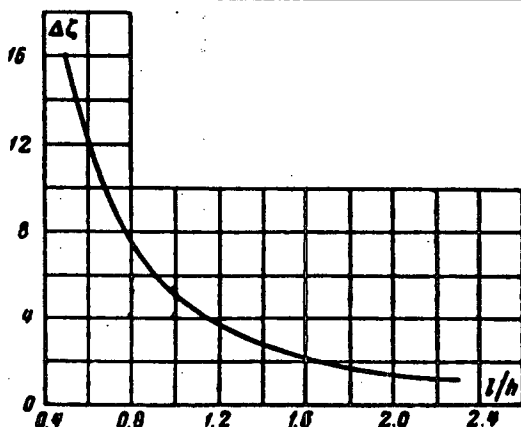
where a is taken from Table 12-8 as a function of a° ;

$\Delta \zeta = \left(\frac{3}{h}\right)^2 + \frac{0.2}{h}$ is taken from the curve $\Delta \zeta = f\left(\frac{l}{h}\right)$.

TABLE 12-8

a°	35	45	55
a	8.25	5.25	3.15

I/h	0.5	1.0	1.5	2.0	2.5	∞
$\Delta \zeta$	16	5.0	2.6	1.8	1.3	0.7



BIBLIOGRAPHY

Section One

- 1-1. Agroskin, I.I., G.T. Dmitriev, and F.I. Pikalov. Gidravlika (Hydraulics). — Gosenergoizdat. 1954.
- 1-2. Al'tshul', A.D. Istechenie iz otverstii zhidkostei s povyshennoi vyazkost'yu (Discharge of High-Viscosity Liquids through Orifices). — Neftyanoe khozyaistvo, No. 2. 1950.
- 1-3. Al'tshul', A.D. Raschetnye zavisimosti pri istechenii zhidkostei bol'shoi vyazkosti (Calculating Relationships for the Discharge of High-Viscosity Liquids). — Vestnik inzhenerov i tekhnikov, No. 4. 1951.
- 1-4. Al'tschul', A.D. Ob istechenii zhidkostei znachitel'noi vyazkosti pri peremennom uredzhenii teorii viskozimetra (On the Discharge of High-Viscosity Liquids at Variable Level, and Theories of the Viscosimeter). — Zhurnal tekhnicheskoi fiziki, Vol. XXVII, No. 4, AN SSSR. 1957.
- 1-5. Velikanov, M.A. Dinamika rul'sovykh potokov (Dynamics of Channel Flow). — Gostekhizdat. 1954.
- 1-6. Idel'chik, I.E. Gidravlicheskie soprotivleniya (fiziko-mekhanicheskie osnovy) (Fluid Resistances (Physical and Mechanical Fundamentals)). — Gosenergoizdat. 1954.
- 1-7. Makarov, A.N. and M.Ya. Sherman. Raschet drossel'nykh ustroistv (Calculation of Throttling Devices). — Metalurgizdat. 1953.
- 1-8. Malkov, M.P. and K.F. Pavlov. Spravochnik po glubokomu okhlazhdenu (Cooling Handbook). — Gostekhizdat. 1947.
- 1-9. Glinkov, M.A. (Editor). Metallurgicheskie pechi (Metallurgical Furnaces). — Metallurgizdat. 1951.
- 1-10. Mostkov, M.A. Gidravlicheskiy spravochnik (Handbook of Hydraulics). — Gosstroizdat. 1954.
- 1-11. Nevel'son, M.I. Tsentrrobezhnye ventilyatory (Centrifugal Fans). — Gosenergoizdat. 1954.
- 1-12. Normy aerodinamicheskogo rascheta kotel'nykh agregatov (Standards for the Aerodynamic Calculation of Boiler Units). — Mashgiz. 1949.
- 1-13. Normy rascheta tsirkulyatsii vody v parovykh kotlakh (Standards for Calculating the Water Circulation in Steam Boilers). — TsKTI, Mashgiz. 1950.
- 1-14. Normy teplovogo rascheta kotel'nogo agregata (Standards for the Thermal Calculation of a Boiler Unit). — VTI, Gosenergoizdat. 1954.
- 1-15. Polikovskii, V.I. Ventilyatory, vozdukhoduvki, kompressory (Fans, Blowers, Compressors). — Mashgiz. 1938.
- 1-16. Prandtl, L. Fundamentals of Hydro- and Aerodynamics. — McGraw Hill. 1934. [Russian translation], GIIL. 1953.
- 1-17. Rikhter, G. Gidravlika truboprovodov (Hydraulics of Pipe Lines). — ONTI. 1936.
- 1-18. Solodkin, E. and A.S. Ginevskii. Turbulentnoe techenie vyazkoi zhidkosti v nachal'nykh uchastkakh osesimmetrichnykh i ploskikh kanalov (Turbulent Flow of a Viscous Liquid in the Initial Stretches of Axisymmetric and Plane Channels). — Trudy TsAGI, No. 701, Oborongiz. 1957.
- 1-19. Spravochnik khimika (Handbook of Chemistry), Vol. I. — Goskhimizdat. 1951.
- 1-20. Spravochnik Hütte [Russian translation], Vol. I. — ONTI. 1936.
- 1-21. Vargaffik, N.B. (Editor). Spravochnik, teplotekhnicheskie svoistva veshchestv (Handbook of the Thermal Properties of Materials). — Gosenergoizdat. 1956.
- 1-22. Fabrikant, N.Ya. Aerodinamika (Aerodynamics). — Gostekhizdat. 1949.
- 1-23. Filippov, G.V. O vliyanii vkhodnogo uchastka na soprotivlenie truboprovodov (On the Influence of the Inlet Stretch on the Resistance of Pipelines). Doctorate's thesis. — Kuibyshevskii industrial'nyi institut. 1955.
- 1-24. Frenkel', V.Z. Gidravlika (Hydraulics). — Gosenergoizdat. 1956.
- 1-25. Shiller, D. Dvizhenie zhidkostei v trubakh (Flow of Liquids in Pipes). — Tekhizdat. 1936.
- 1-26. Yur'ev, B.N. Eksperimental'naya aerodinamika (Experimental Aerodynamics). — ONTI. 1936.

Section Two

- 2-1. Abramovich, G.N. *Prikladnaya gazovaya dinamika* (Applied Gas Dynamics). — Gostekhteorizdat. 1953.
- 2-2. Agroskin, I.I., G.T. Dmitriev, and F.I. Pikalov. *Gidravlika* (Hydraulics). — Gosenergoizdat. 1954.
- 2-3. Adamov, G.A. and I.E. Ideł'chik. *Eksperimental'noe issledovanie sопротивления фанерных труб круглого и квадратного сечения при полном развиившемся турбулентном течении* (Experimental Study of the Resistance of Plywood Pipes of Circular and Square Section at Fully Developed Turbulent Flow). — Trudy No. 670, MAP. 1948.
- 2-4. Adamov, G.A. and I.E. Ideł'chik. *Eksperimental'noe issledovanie турбулентного течения в начальных участках прямых труб круглого и квадратного сечения* (Experimental Study of the Turbulent Flow in Initial Stretches of Straight Pipes of Circular and Square Section). — Tekhnicheskie otchetы, No. 124, MAP. 1948.
- 2-5. Adamov, G.A. *Obshchee uravnenie dlya zakona sопротивления при турбулентном течении и новые формулы dlya koeffitsienta sопротивления шероховатых труб* (General Equation for the Law of Resistance at Turbulent Flow, and New Formulas for the Friction Coefficient of Rough Pipes). — Vestnik inzhenerov i tekhnikov, No. 1. 1952.
- 2-6. Adamov, G.A. *Priblizhennye raschetnye formuly dlya koeffitsientov gidrodinamicheskogo sопротивления* (Approximate Formulas for Calculating the Coefficients of Hydrodynamic Resistance). — Vestnik inzhenerov i tekhnikov, No. 2. 1953.
- 2-7. Adamov, G.A. *Priblizhennyi raschet gidravlicheskogo sопротивления и движениya gazov i zhidkosti v truboprovodakh* (Approximate Calculation of the Fluid Resistance and Motion of Fluids in Pipe Conduits). — In: Sbornik "Voprosy razrabotki i ekspluatatsii gazovykh mestorozhdenii", Gostopizdat. 1953.
- 2-8. Al'tshul', A.D. *O zakone turbulentnogo dvizheniya zhidkosti v gladkikh trubakh* (On the Law of Turbulent Flow of a Liquid in Smooth Pipes). — DAN SSSR, Vol. LXXV, No. 5. 1950.
- 2-9. Al'tshul', A.D. *O raspredelenii skorosti pri turbulentnom dvizhenii v trubakh* (Velocity Distribution at Turbulent Flow through Pipes). — Gidrotehnicheskoe stroitel'stvo, No. 1. 1951.
- 2-10. Al'tshul', A.D. *Zakon sопротивления truboprovodov* (Resistance Law of Pipelines). — DAN SSSR, Vol. XXVI, No. 6. 1951.
- 2-11. Al'tshul', A.D. *Obobshchennaya zavisimost' dlya gidravlicheskogo rascheta truboprovodov* (General Relationship for the Hydraulic Calculation of Pipelines). — Gidrotehnicheskoe stroitel'stvo, No. 6. 1952.
- 2-12. Al'tshul', A.D. *Soprotivlenie truboprovodov v kvadratichnoi oblasti* (Resistance of Pipes in Square Conduits). — Sanitarnaya tekhnika, Collection, No. 4. Gosstroizdat. 1953.
- 2-13. Al'tshul', A.D. *O raspredelenii skorosti pri turbulentnom techenii zhidkosti v tekhnicheskikh trubakh* (Velocity Distribution at Turbulent Flow of a Liquid in Commercial Pipes). — Teploenergetika, No. 2. 1956.
- 2-14. Al'tshul', A.D. *Osnovnye zakonomernosti turbulentnogo techeniya zhidkosti v tekhnicheskikh truboprovodakh* (Basic Laws of the Turbulent Flow of a Liquid in Commercial Pipes). — Sanitarnaya tekhnika, Collection, No. 6. Gosstroizdat. 1957.
- 2-15. Al'tshul', A.D. *K obosnovaniyu formuly Kol'bruka* (Substantiation of the Colebrook Formula). — Izvestiya AN SSSR, OTN, No. 6. 1958.
- 2-16. Ashe, B.M. and G.A. Maksimov. *Otoplenie i ventilyatsiya* (Heating and Ventilating), Vol. II. — Stroizdat. 1940.
- 2-17. Bakhmet'ev, B.A. *O ravnomernom dvizhenii zhidkosti v kanalakh i trubakh* (Uniform Flow in Pipes and Channels). 1931.
- 2-18. Gamburg, P.Yu. *Tablitsy i primery dlya rascheta truboprovodov otopleniya i goryachego vodosnabzheniya* (Tables and Examples for Calculating Heating and Hot-Water Piping). — Stroizdat. 1953.
- 2-19. Gandel'sman, A.F., A.A. Gukhman, N.V. Ilyukhin, and L.N. Naurits. *Issledovaniya koefitsienta sопротивления pri techenii s okolozvukovoi skorost'yu* (Studies of the Friction Coefficient at Near-Sonic Flow). Parts I and II. — ZhTF, Vol. XXIV, No. 12. 1954.
- 2-20. Ginevskii, A.S. and E.E. Solodkin. *Aerodinamicheskie kharakteristiki nachal'nogo uchastka truby kol'tsevogo sечения при turbulentnom techenii v pogranichnom sloe* (Aerodynamic Characteristics of the Initial Stretch of an Annular Pipe at Turbulent Flow in the Boundary Layer). — Promyshlennaya aerodinamika, col. No. 12, Oborongiz. 1959.
- 2-21. Zegzhda, A.P. *Gidravlicheskie poteri na trenie v kanalakh i truboprovodakh* (Frictional Hydraulic Losses in Pipes and Channels). — Gosenergoizdat. 1957.
- 2-22. Ideł'chik, I.E. *Opryedelenie koefitsienta treniya stal'nykh trub gazoprovoda Saratov-Moskva* (Determination of the Friction Coefficient of the Steel Pipes of the Saratov-Moscow Gas Main). — Tekhnicheskie otchetы, No. 50, BNT, NKAP. 1945.
- 2-23. Izbashev, S.V., B.T. El'tsev, and P.M. Sliskii. *Gidravlicheskie spravochnye dannye* (Hydraulic Reference Data). — MEI. 1954.
- 2-24. Ideł'chik, I.E. *Gidravlicheskie sопротивления (fiziko-mekhanicheskie osnovy)* (Fluid Resistance (Physical and Mechanical Fundamentals)). — Gosenergoizdat. 1954.

- 2-25. Izbaš, S.V. Osnovy gidravliki (Fundamentals of Hydraulics). — Stroiizdat. 1952.
- 2-26. Isaev, I.A. Novaya formula dlya opredeleniya koeffitsienta gidravlicheskogo soprotivleniya priamoi krugloj truby (New Formula for the Determination of the Coefficient of Fluid Resistance of a Straight Pipe of Circular Cross Section). — Neftyanoe khozyaistvo, No. 5. 1951.
- 2-27. Karman, von Th. Some Problems of the Theory of Turbulence [Russian translation in: Sbornik "Problemy turbulentnosti"], edited by M.A. Velikanov and N.G. Shveikovskii. — ONTI. 1936.
- 2-28. Kisim, M.I. Otoplenie i ventilyatsiya (Heating and Ventilating), Part II. — Stroiizdat. 1949.
- 2-29. Konakov, V.K. Novaya formula dlya koeffitsienta soprotivleniya gladkikh trub (New Formula for the Friction Coefficient of Smooth Pipes). — DAN SSSR, Vol. XXV, No. 5. 1950.
- 2-30. Lobanov, B.N. Novye formuly rascheta trub v perekhodnoi oblasti (New Formulas for Pipe Calculation in the Transitional Region). — In: Sbornik "Novoe v stroitel'noi tekhnike", Akademiya Arkhitektury USSR, Sanitarnaya tekhnika. 1954.
- 2-31. Lyatkher, V.M. Analiz i vybor raschetnykh formul dlya koeffitsienta treniya v trubakh (Analysis and Selection of Calculating Formulas for the Friction Coefficient in Pipes). — In: Sbornik Statei studencheskogo nauchnogo obshchestva, MEI. 1954.
- 2-32. Murin, G.A. Gidravlichesko soprotivlenie stal'nykh trub (Fluid Resistance of Steel Pipes). — Izvestiya VTI, No. 10. 1948.
- 2-33. Murin, G.A. Gidravlichesko soprotivlenie stal'nykh nefteprovodov (Hydraulic Resistance of Steel Pipelines). — Neftyanoe khozyaistvo, No. 4. 1951.
- 2-34. Nikuradze, I. Zakonomernosti turbulentnogo dvizheniya v gladkikh trubakh (Laws of Turbulent Flow in Smooth Pipes). [Russian translation in: Sbornik "Problemy turbulentnosti"], edited by M.A. Velikanov and N.G. Shveikovskii. — ONTI. 1936.
- 2-35. Ovsenyan, V.M. Vyrazhenie gidravlicheskih poter' cherez osredennuyu skorost' pri neustanovivshemsya dvizhenii zhidkosti v zhestkoi trube (Expressing Hydraulic Losses through the Mean Velocity at Unsteady Flow in a Rigid Pipe). — Erevan Polytechnic Institute, Sbornik nauchnykh trudov, No. 14, No. 2. 1952.
- 2-36. Pavlovskii, N.N. Gidravlicheskiy spravochnik (Handbook of Hydraulics). — ONTI. 1937.
- 2-37. Petukhov, B.S., A.S. Sukhomel, and V.S. Protopopov. Issledovanie soprotivleniya treniya i koeffitsienta vosstanovleniya temperatury stenki pri dvizhenii gaza v krugloy trube s vysokoi dozvukovo skorost'yu (Study of the Friction and Temperature Coefficients of Restoration of the Wall with Gas Flow in a Circular Pipe at High Subsonic Velocity). — Teploenergetika, No. 3. 1957.
- 2-38. Pozin, A.A. Printsipy rascheta i konstruirovaniya vsasyvayushchikh rukavov (Principles of the Calculation and Design of Suction Hoses), Doctorate's thesis. 1950.
- 2-39. Popov, V.N. Gidravlicheskiy raschet napornykh truboprovodov gidrostantsii (Hydraulic Calculation of Pressure Pipes of Hydroelectric Power Plants). — Gosenergoizdat. 1950.
- 2-40. Prandtl, L. Rezul'taty rabot poslednego vremeni po izucheniyu turbulentnosti (Results of Recent Studies of Turbulence). [Russian translation in: Sbornik "Problemy turbulentnosti"], edited by M.A. Velikanov and N.G. Shveikovskii. — ONTI. 1936.
- 2-41. Prandtl, L. Fundamentals of Hydro- and Aerodynamics. — McGraw Hill, 1953. [Russian translation], GIIL. 1953.
- 2-42. Rikhter, G. Gidravlika truboprovodov (Hydraulics of Pipelines). — ONTI. 1936.
- 2-43. Rysin, S.A. Ventilyatory obshchepromyshlennogo naznacheniya (General-Purpose Industrial Fans). — Stroiizdat. 1951.
- 2-44. Solodkin, E.E. and A.S. Ginevskii. Turbulentnyi pogranichnyi sloi i soprotivlenie treniya tsilindra s uchetom vliyaniya poperechnoi krivizny poverhnosti (Turbulent Boundary Layer and Friction Resistance of a Cylinder, Allowing for the Influence of the Transverse Surface Curvature). — Trudy MAP, No. 690. 1956.
- 2-45. Solodkin, E.E. and A.S. Ginevskii. Turbulentnoe techenie vyzakoi zhidkosti v nachal'nykh uchastkakh osesimmetrichnykh i ploskikh kanalov (Turbulent Flow of a Viscous Liquid in the Initial Stretches of Axisymmetric and Plane Channels). — Trudy TsAGI, No. 701, Oborongiz. 1957.
- 2-46. Tol'sman, V.F. and F.A. Shevelev. Gidravlichesko soprotivlenie rezinovykh rukavov (Fluid Resistance of Rubber Hose). — In: Sbornik VNII Vodgeo "Issledovanie po gidravlike truboprovodov". 1952.
- 2-47. Fedorov, N.F. Novye issledovaniya i gidravlicheskie raschety kanalizatsionnykh setei (New Studies and Hydraulic Calculations of Sewerage Systems). — Stroiizdat. 1956.
- 2-48. Filonenko, G.K. Formula dlya koeffitsienta hidravlicheskogo soprotivleniya gladkikh trub (Formula for the Coefficient of Fluid Resistance of Smooth Pipes). — Izvestiya VTI, No. 10 (162). 1948.
- 2-49. Filonenko, G.K. Gidravlichesko soprotivlenie truboprovodov (Hydraulic Resistance of Pipes). — Teploenergetika, No. 4. 1954.
- 2-50. Flyatau, R.S. Gidrotekhnicheskie raschety truboprovodov (Hydrotechnic Calculations of Pipes). — Gostoptekhizdat. 1949.

- 2-51. Frenkel', V. Z. Gidravlika (Hydraulics). — Gosenergoizdat. 1956.
- 2-52. Shevelev, F.A. Issledovanie osnovnykh gidravlicheskikh zakonomernostei turbulentnogo dvizheniya v trubakh (Study of the Main Hydraulic Laws of Turbulent Flow in Pipes). — Inzhenernaya gidravlika, VNII Vodgeo, Stroizdat. 1953.
- 2-53. Shevelev, F.A. Gidravlicheskoе sопротивление металлических труб больших диаметров (Hydraulic Resistance of Large-Diameter Steel Pipes). — Gidrotehnicheskoe stroitel'stvo, No.1. 1950.
- 2-54. Shevelev, F.A. Gidravlicheskiy raschet asbestosementnykh trub (Hydraulic Calculation of Asbestos-Cement Pipes). — VNII Vodgeo. 1954.
- 2-55. Shifrinson, B.L. Gidrodinamicheskii raschet teplovykh setei (Hydrodynamic Calculation of Heating Pipes). — Teplo i sila, No.1. 1935.
- 2-56. Yakimov, A.K. Novyi zakon turbulentnogo dvizheniya vyazkoi zhidkosti (A New Law of Turbulent Flow of a Viscous Liquid). — DAN SSSR, Novaya seriya, Vol.4. 1945.
- 2-57. Blasius. Das Ähnlichkeitsgesetz bei Reibungsvorgängen in Flüssigkeiten. — Mitt. Forschungsarbeiten VDI, Heft 131. 1913.
- 2-58. Colebrook, F. Turbulent Flow in Pipes with Particular Reference to the Transition Region between the Smooth and Rough Pipes. — J. Inst. Civil Engineers, No.4. 1938, 1939.
- 2-59. Hagen, G.—Poggendorffs Annalen, Bd.46. 1939.
- 2-60. Hering, F. Die Rohreibungszahl. — Brennst., Wärme, Kraft, Bd.4. 1952.
- 2-61. Kirschmer, O. Der gegenwärtige Stand unserer Erkenntnisse über die Rohreibung. — G.W.F. Ausgabe Wasser, H.16, 18. 1953.
- 2-62. Marechal, H. Pertes de charge continues en conduite forcée de section circulaire. — Annales des travaux publics de Belgique, No.6. 1955.
- 2-63. Moody, L.F. Friction Factor for Pipe Flow. — Trans. ASME, Vol.66. November 1944.
- 2-64. Morris, M. A New Concept of Flow in Rough Conduits. — Proc. Amer. Soc. Civil Engrs, No.390. 1954.
- 2-65. Müller, W. Druckverlust in Rohrleitungen. — Energietechnik, H.7. 1953.
- 2-66. Nikuradze, J. Strömungsgesetze in rauhen Rohren. — VDI, No.361. 1933.
- 2-67. Poiseuille. — Comptes rendus, Vol.11. 1840.
- 2-68. Richter, H. — Rohrhydraulik. 1954.

Section Three

- 3-1. Idef'chik, I.E. Gidravlicheskie sопротивления pri vkhode potoka v kanaly i protekanii cherez otverstiya (Fluid Resistance at the Inlet of a Stream in Channels and at the Flow through Orifices). — In: Sbornik "Promyshlennaya aerodinamika", No.2, BNT, NKAP. 1944.
- 3-2. Idef'chik, I.E. Opredelenie koeffisientov sопротивления pri istechenii cherez otverstiya (Determination of the Resistance Coefficients at Discharge through Orifices). — Gidrotehnicheskoe stroitel'stvo, No.5. 1953.
- 3-3. Idef'chik, I.E. Gidravlicheskie sопротивления (fiziko-mekhanicheskie osnovy) (Fluid Resistances (Physical and Mechanical Fundamentals)). — Gosenergoizdat. 1954.
- 3-4. Idef'chik, I.E. Uchet vliyaniya vyazkosti na gidravlicheskoе sопротивление diafragm i reshetok (Allowing for the Influence of Viscosity on the Fluid Resistance of Diaphragms and Grids). — Teploenergetika, No.9. 1960.
- 3-5. Karev, V.N. Poteri napora pri vnezapnom suzhenii truboprovoda i vliyanie mestnykh sопротивлений na narusheniya potoka (Head Losses at Sudden Contraction of a Pipe, and Influence of Local Resistances on the Stream Disturbance). — Neftyanoe khozyaistvo, No.8. 1953.
- 3-6. Nosova, M.M. Sопротивление vkhodnykh i vkhodnykh rastrubov s ekranami (Influence of Inlet and Exit Bells with Baffles). — In: Sbornik "Promyshlennaya aerodinamika", No.7. 1956.
- 3-7. Nosova, M.M. and N.F. Tarasov. Sопротивление pritochno-vtyazhnykh shakht (Resistance of Intake-Exhaust Vents). — In: Sbornik "Promyshlennaya aerodinamika", No.12, Oborongiz. 1959.
- 3-8. Khanzhonkov, V.I. Sопротивление setok (Resistance of Screens). — In sbornik: "Promyshlennaya aerodinamika", No.2, BNT, NKAP. 1944.
- 3-9. Khanzhonkov, V.I. Sопротивление pritochnykh i vtyazhnykh shakht (Resistance of Intake and Exhaust Vents). — In: Sbornik "Promyshlennaya aerodinamika", No.3, BNI, MAP. 1947.
- 3-10. Khanzhonkov, V.I. Aerodinamicheskie kharakteristiki kollektorov (Aerodynamic Characteristics of Headers). — In: Sbornik "Promyshlennaya aerodinamika", No.4. 1953.
- 3-11. Khanzhonkov, V.I. Umen'shenie aerodinamicheskogo sопротивления otverstii kol'tsevymi rebrami i ustupami (Reducing the Aerodynamic Resistance of Orifices by Means of Annular Ribs and Ledges). — In: Sbornik "Promyshlennaya aerodinamika", No.12. Oborongiz. 1959.

- 3-12. Chepaikin, G.A. Opredelenie poter' pri vkhode potoka v turbinnuyu kameru (Determination of the Losses at the Inlet of a Stream in a Turbine Scroll Case). — Izvestiya vysshikh uchebnykh zavedenii, Energetika, No.2. 1958.
- 3-13. Bevier, C.W. Resistance of Wooden Louvers to Fluid Flow. — Heating, Piping and Air-Conditioning. May 1955.
- 3-14. Cobb, P.R. Pressure Loss of Air Flowing through 45° Wooden Louvers. — Heating, Piping and Air-Conditioning. December 1953.
- 3-15. Weisbach, G.—Lehrbuch der Ingenieur- und Maschinenmechanik, II Aufl. 1850.

Section Four

- 4-1. Abramovich, G.N. Turbulentnye svobodnye strui zhidkostei i gazov (Turbulent Free Jets of Fluids). — Gosenergoizdat. 1948.
- 4-2. Alt'shul', A.D. Ispol'zovanie zadachi Zhukovskogo dlya opredeleniya mestnykh poter' v trubakh (Application of the Zhukovskii Problem to the Determination of Local Losses in Pipes). — Vestnik inzhenerov i tekhnikov, No.6. 1948.
- 4-3. Alt'shul', A.D. Istechenie iz otverstii zhidkosteis povyshennoi vyazkostyu (Discharge of High-Viscosity Liquids through Orifices). — Neftyanoe khozyaistvo, No.2. 1950.
- 4-4. Alt'shul', A.D. Raschetnye zavisimosti pri istechenii zhidkosteis bol'shoi vyazkosti (Calculating Relationships for the Discharge of High-Viscosity Liquids). — Vestnik inzhenerov i tekhnikov, No.4. 1951.
- 4-5. Alt'shul', A.D. Ob istechenii zhidkosteis znachitel'noi vyazkosti pri peremennom urovne i teorii viskozimetrii (On the Discharge of High-Viscosity Liquids at Variable Level, and Theories of the Viscosimeter). — Zhurnal tekhnicheskoi fiziki, Vol. XXVII, No.4, AN SSSR. 1957.
- 4-6. Brik, P.M. and D.A. Grossman. Rezul'taty issledovanii gidravlicheskikh soprotivlenii drossel'nykh shaib (Results of Studies of the Hydraulic Resistances of Throttling Plates). — Naladochnye i eksperimental'nye raboty ORGRES, No. IX, Gosenergoizdat. 1954.
- 4-7. Bromlei, M.F. Koefitsienty raskhoda otverstii, prikrytykh stvorkami (Discharge Coefficients of Orifices Covered by Flaps). — Sovremenkiye voprosy ventilyatsii, Stroizdat. 1941.
- 4-8. Egorov, S.A. Formula dlya poteri napora na vnezapnom rasshireniyu truby pri laminarnom techenii (Formula for Head Losses at Sudden Expansion of a Pipe with Laminar Flow). — Trudy MAI, No. II. 1946.
- 4-9. Zhukovskii, I.E. Vidooizmenenie metoda Kirchhoffa dlya opredeleniya dvizheniya zhidkosti v dvukh izmereniyakh pri postoyannoj skorosti, dannoj na neizvestnoj linii toka (Variation of the Kirchhoff Method for the Determination of a Liquid Flow in Two Dimensions at Constant Velocity, with an Unknown Streamline). — Collected Works, Vol.2, Gosizdat. 1949.
- 4-10. Ideł'chik, I.E. Gidravlicheskie soprotivleniya pri vkhode potoka v kanaly i protekanii cherez otverstiya (Fluid Resistance at the Inlet of a Stream in Channels and at the Flow through Orifices). — In: Sbornik "Promyshlennaya aerodinamika", No.2, BNT, NKAP. 1944.
- 4-11. Ideł'chik, I.E. Poteri na udar v potoke s neravnopravnym raspredeleniem skorostei (Shock Losses in a Stream with Nonuniform Velocity Distribution). — Trudy MAP, No. 662. 1948.
- 4-12. Ideł'chik, I.E. Opredelenie koefitsientov soprotivleniya pri istechenii cherez otverstiya (Determination of the Resistance Coefficients at Discharge through Orifices). — Gidrotekhnicheskoe stroitel'stvo, No. 5. 1953.
- 4-13. Ideł'chik, I.E. Gidravlicheskie soprotivleniya (fiziko-mekhanicheskie osnovy) (Fluid Resistances (Physical and Mechanical Fundamentals)). — Gosenergoizdat. 1954.
- 4-14. Ideł'chik, I.E. Uchet vliyaniya vyazkosti na gidravlicheske soprotivlenie diafragm i reshetok (Allowing for the Influence of Viscosity on the Fluid Resistance of Diaphragms and Grids). — Teploenergetika, No. 9. 1960.
- 4-15. Karev, V.N. Poteri napora pri vnezapnom rasshireniyu truboprovoda (Head Losses at Sudden Expansion of a Pipe). — Neftyanoe khozyaistvo, Nos 11 and 12. 1952.
- 4-16. Karev, V.N. Poteri napora pri vnezapnom suzhenii truboprovoda i vliyanie mestnykh soprotivlenii na narusheniya potoka (Head Losses at Sudden Contraction of a Pipe, and Influence of Local Resistances on the Stream Disturbances). — Neftyanoe khozyaistvo, No. 8. 1953.
- 4-17. Krylov, A.V. Nekotorye eksperimental'nye dannye ob istechenii zhidkosteis cherez ostrye diafragmy (Some Experimental Data on the Discharge of Liquids through Sharp Diaphragms). — Izvestiya AN SSSR, OTN, No.2. 1948.
- 4-18. Teplov, A.V. Znacheniya koefitsientov raskhoda, skorosti i poter' dlya vnutrennei tsilindricheskoi nasadki (Values of the Coefficients of Discharge, Velocity and Loss for an Internal Cylindrical Nozzle). — Gidrotekhnicheskoe stroitel'stvo, No. 10. 1953.
- 4-19. Frenkel', V.Z. Gidravlika (Hydraulics). — Gosenergoizdat. 1956.

- 4-20. Khanzhonkov, V.I. Aerodinamicheskie kharakteristiki kolletorov (Aerodynamic Characteristics of Headers). — In: Sbornik "Promyshlennaya aerodinamika", No. 4. 1953.
- 4-21. Cornell, W.G. Losses in Flow Normal to Plane Screens. — Trans. ASME, No. 4. 1958.
- 4-22. Iversen, H.W., Orifice Coefficients for Reynolds Numbers from 4 to 50,000. — Trans. ASME, Vol. 78, No. 2. 1956.
- 4-23. Johansen, F. Flow through Pipe Orifice of Flow Reynolds Numbers. — Proc. Royal Soc., A, Vol. 126, No. 801. 1930.
- 4-24. Kolodzie, P.A. and M. van Winkle. Discharge Coefficients through Perforated Plates. — A.J.Ch.E.Journal, No. 9. 1959.

Section Five

- 5-1. Abramovich, G.N. Aerodynamika mestnykh soprotivlenii (Aerodynamics of Local Resistances). — Promyshlennaya aerodinamika, Trudy No. 211. 1935.
- 5-2. Bam-Zelikovich, G.M. Raschet pogranichnogo sloya (Calculation of the Boundary Layer). — Izvestiya AN SSSR, OTN, No. 12. 1954.
- 5-3. Bam-Zelikovich, G.M. Vychislenie parametrov zhimaemogo gaza s neravnomernym profilem skorostei i temperatury, dvizhushchegosya v kanale proizvol'noi formy pri nalichii turbulentnogo peremeshivaniya (Calculating the Characteristics of Incompressible Bases with Turbulent Mixing, Flowing through a Channel of Arbitrary Shape at Nonuniform Velocity Distribution). — Institut imeni L.I. Baranova, Trudy No. 300. 1957.
- 5-4. Bushel', A.R. Snizhenie vnutrennikh poter' v shakhtnoi ustanovke s osevym ventilyatorom (Reduction of the Interior Losses in an Installation with Axial Fan). — Trudy, No. 673, BNT MAP. 1948.
- 5-5. Vederinkov, A.I. Eksperimental'nye issledovaniya dvizheniya vozdukh v ploskom rasshirayushchemsya kanale (Experimental Studies of the Motion of Air in a Plane Diverging Duct). — Trudy TsAGI, No. 21. 1926.
- 5-6. Gibson, A. Gidravlika i ee prilozheniya (Hydraulics and Its Applications). — ONTI. 1935.
- 5-7. Ginevskii, A.S. Energeticheskie kharakteristiki dozvukovykh diffuzornykh kanalov (Power Characteristics of Subsonic Diffuser Channels). — Izvestiya AN SSSR, OTN, No. 3. 1956.
- 5-8. Ginevskii, A.S. Raschet poter' v rasshirayushchikhsya i suzhayushchikhsya kanalakh (Calculation of the Losses in Converging and Diverging Channels). — Promyshlennaya aerodinamika, No. 7, BNI MAP. 1956.
- 5-9. Ginevskii, A.S. and E.E. Solodkin. Vliyanie poperechnoi krivizny poverkhnosti na kharakteristiki osesimmetricheskogo turbulentnogo pogranichnogo sloya (Influence of the Transverse Curvature of the Surface on the Characteristics of an Axisymmetrical Turbulent Boundary Layer). — Prikladnaya matematika i mehanika, Vol. XXII, No. 6. 1958.
- 5-10. Grishanin, K.V. Ustanovivsheesy turbulentnoe dvizhenie zhidkosti v konicheskem diffuzore s malym uglom raskrytiya (Steady Turbulent Flow of a Liquid in a Conical Diffuser of Low Divergence Angle). — Trudy Leningradskogo politekhnicheskogo instituta inzhenernogo transporta, No. 22. 1955.
- 5-11. Gurzienko, G.A. Ob ustanovivshemsya turbulentnom techenii v konicheskikh diffuzorakh s malymi ugлami rasshireniya (Steady Turbulent Flow in Conical Diffusers of Low Divergence Angles). — Trudy TsAGI, No. 462. 1939.
- 5-12. Dovzhik, S.A. and A.S. Ginevskii. Eksperimental'noe issledovanie napornykh patrubkov statsionarnykh osevykh mashin (Experimental Study of Pressure Connections of Stationary Axial Machines). — Tekhnicheskie otchety, No. 130, BNI MAP. 1955.
- 5-13. Evdomikov, I.F. Opyty po otsasyvaniyu pogranichnogo sloya v aerodinamicheskikh trubakh bol'sikh skorosteii (Experiments on the Suction of the Boundary Layer in High-Velocity Wind Tunnels). — Trudy TsAGI, No. 506. 1940.
- 5-14. Egorov, B.N. Opyty s diffuzorami aerodinamicheskikh trub (Experiments with Diffusers of Wind Tunnels). — TVF, No. 3. 1930.
- 5-15. Idel'chik, I.E. Aerodynamika vsasyvayushchikh patrubkov (Aerodynamics of Suction Connecting Pieces). — TVF, Nos 5-6. 1944.
- 5-16. Idel'chik, I.E. Aerodynamika potoka i poteri napora v diffuzorakh (Aerodynamics of the Stream, and Head Losses in Diffusers). — Promyshlennaya aerodinamika, Col. No. 3, BNT MAP. 1947.
- 5-17. Idel'chik, I.E. Vyravnivayushchee deistvie soprotivleniya, pomeshchennogo za diffuzorom (Equalizing Effect of a Resistance (Obstruction) Placed behind a Diffuser). — Trudy, No. 662, BNT MAP. 1948.
- 5-18. Idel'chik, I.E. Gidravlicheskie soprotivleniya (fiziko-mekhanicheskie osnovy) (Fluid Resistances (Physical and Mechanical Fundamentals)). — Gosenergoizdat. 1954.
- 5-19. Idel'chik, I.E. Issledovanie korotkikh diffuzorov s razdelitel'nymi stenkami (Study of Short Diffusers with Dividing Walls). — Teploenergetika, No. 8. 1958.
- 5-20. Levin, A.M. Polozenie tochki otryva v ploskikh diffuzorakh (Position of the Separation Point in Plane Diffusers). — DAN SSSR, Vol. XXXVII, No. 5. 1952.

- 5-21. Lifshits, A.G. O preobrazovanii skorosti gaza v davlenie v diffuzore (Transformation of Gas Velocity into Pressure in a Diffuser). — Trudy Ural'skogo politekhnicheskogo instituta imeni S. M. Kirova, No. 1. 1955.
- 5-22. Lokshin, I.L. and A.Kh. Gazirbekova. Rabota diffuzorov, ustanovlennykh za tsentrobezhnymi ventilyatorami (Operation of Diffusers Placed Behind Centrifugal Fans). — Promyshlennaya aerodinamika, col. No. 6, BNI MAP. 1955
- 5-23. Makarov, I.M. K raschetu koefitsienta poter' v diffuzornykh reshetkakh pri ploskom potoke (Calculation of the Coefficient of Loss in Diffuser Grids at Plane Stream). — Kotloturbostroenie, No. 1. 1950.
- 5-24. Ovchinnikov, O.N. Vliyanie vkhodnogo profilya skorosti na rabotu diffuzorov (Influence of the Inlet Velocity Distribution on the Operation of Diffusers). — Trudy Leningradskogo politekhnicheskogo instituta, No. 176. 1955.
- 5-25. Sanoyan, V.G. Dvizhenie zhidkosti v osesimmetrichnom kanale zadannogo profilya i raschet deistvitel'nykh davlenii (Motion of a Liquid in an Axisymmetrical Channel of Specified Shape, and Calculation of the Actual Pressures). — Trudy Leningradskogo politekhnicheskogo instituta, No. 176. 1955.
- 5-26. Solodkin, E.E. and A.S. Ginevskii. Turbulentnoe techenie vyazkoi zhidkosti v nachal'nykh uchastkakh osesimmetrichnykh i ploskikh kanalov (Turbulent Flow of a Viscous Liquid in the Initial Stretches of Axisymmetrical and Plane Channels). — Trudy TsAGI, No. 701, Oborongiz. 1957.
- 5-27. Solodkin, E.E. and A.S. Ginevskii. Stabilizirovannoje turbulentnoe techenie vyazkoi zhidkosti v ploskom diffuzornom kanale pri malykh uglokh raskrytiya (Steady Turbulent Flow of a Viscous Liquid in a Plane Diffuser Channel of Small Divergence Angle). — Trudy BNI MAP, No. 728. 1958.
- 5-28. Solodkin, E.E. and A.S. Ginevskii. Turbulentnoe techenie v nachal'nom uchastke ploskogo diffuzornogo kanala (Turbulent Flow in the Initial Stretch of a Plane Diffuser Channel). — Trudy BNI MAP, No. 728. 1958
- 5-29. Solodkin, E.E. and A.S. Ginevskii. K voprosu o vliyanii nachal'noi neravnomernosti na kharakteristiki diffuzornykh kanalov (The Influence of the Initial Nonuniformity on the Characteristic of Diffuser Channels). — Promyshlennaya aerodinamika, col. No. 12, BNI MAP. 1959.
- 5-30. Zsillard, C.S. Issledovanie diffuzorov aerodinamicheskikh trub bol'sikh skorostei (Study of Diffusers of High Velocity Wind Tunnels). — Tekhnicheskie zametki, TsAGI, No. 160. 1938.
- 5-31. Targ, S.M. Osnovnye zadachi teorii laminarnykh techenii (Basic Problems of Laminar Flow Theory). — Gostekh-teorizdat. 1951.
- 5-32. Fedyayevskii, K.K. Kriticheskii obzor rabot po zamedlennym i uskorenym turbulentnym pogranichnym sloyam (Critical Survey of the Papers on Decelerated and Accelerated Turbulent Boundary Layers). — Tekhnicheskie zametki, TsAGI, No. 158. 1937.
- 5-33. Ackeret, J. Grenzschichtberechnung. — ZVDL, Vol. 35. 1926.
- 5-34. Ackeret, J. Grenzschichten in geraden und gekrümmten Diffusoren. — Intern. Union für theor. und angew. Mechanik, Symposium, Freiburg (Br.) 1957. 1958.
- 5-35. Andres, K. Versuche über die Umsetzung von Wassergeschwindigkeit in Druck. — VDI Forschungsarbeiten, Heft 76, Berlin. 1909.
- 5-36. Bardil, Notter, Betz, and Evel. Wirkungsgrad von Diffusoren. — Jahrbuch der Deutschen Luftfahrtforschung.
- 5-37. Borry, H. Ducts for Heating and Ventilating. April 1953.
- 5-38. Dösch, F. Divergente und konvergente turbulente Strömungen mit kleinen Öffnungswinkeln. — VDI, Forschungsarbeiten, Heft 282. 1929.
- 5-39. Eiffel, G. Souffleries aerodynamiques. — Résumé de principaux travaux exécutés pendant la guerre au laboratoire aerodynamique. 1915-1918.
- 5-40. Fliegner, A. Versuche über das Ausströmen von Luft durch konisch-divergente Düsen. — 1. Zivilingenieur. 1875; 2. Schweiz. Bauztg. 31. 1898.
- 5-41. Frey, K. Verminderung der Strömungsverluste in Kanälen durch Leitflächen. — Forschung, No. 3. 1934.
- 5-42. Galle, K.R. and R.C. Binder. Two-Dimensional Flow through a Diffuser with an Exit Length. — J. Applied Mechanics, Vol. 20, No. 3. 1953.
- 5-43. Gibson, A. On the Flow of Water through Pipes and Passages Having Converging or Diverging Boundaries. — Proc. Royal Soc., Vol. 83, No. A-563. 1910.
- 5-44. Gibson, A. On the Resistance to Flow of Water through Pipes or Passages Having Diverging Boundaries. — Trans. Royal Soc., Vol. 48, Part 1, No. 5. 1911.
- 5-45. Hochschild, H. Versuche über Strömungsvorgänge in erweiterten und verengten Kanälen. — VDI, Forschungsarbeiten, Heft 114, Berlin. 1912.
- 5-46. Hofmann, A. Die Energieumsetzung in saugrohrähnlich erweiterten Düsen. — Mitteilungen, Heft 4. 1931.
- 5-47. Johnston, J.H. The Effect of Inlet Conditions on the Flow in Annular Diffusers. — C.P. No. 178, Memorandum No. M 167, No. 1. January 1953.

- 5-48. Johg, A.D. and G.L. Green. Tests of High-Speed Flow in Diffusers of Rectangular Cross Section. — Reports and Memoranda, No. 2201. July 1944.
- 5-49. Kmoníček, V.K. Unterschallströmungen in Kegeldiffusoren. — Acta Technica, No. 5. 1959.
- 5-50. Kröner, K. Versuche über Strömungen in stark erweiterten Kanälen. — VDI, Forschungsarbeiten, Heft 222, Berlin. 1920.
- 5-51. Little, B.H. and S.W. Wilbur. Performance and Boundary Layer Data from 12° and 23° Conical Diffusers of Area Ratio 2.0 at Mach Numbers up to Choking and Reynolds Numbers up to $7.5 \cdot 10^6$. — Report NACA, No. 1201. 1954.
- 5-52. Margoulis, W. Recherches experimentales et théorétiques effectuées de 1930-1933 sur la mécanique des fluides et la transmission de la chaleur dans les fluides en mouvement. — La technique aéronautique, No. 139. 1934.
- 5-53. Milliat, Z.P. Etude expérimentale de l'écoulement turbulent dans un conduit divergent par l'air. — La houille blanche, 11, No. B. 1956.
- 5-54. Naumann. Efficiency of Diffusers on High Subsonic Speeds. — Reports and Transaction, No. 11 A. June 1946.
- 5-55. Nikuradze, I. Untersuchungen über die Strömungen des Wassers in konvergenten und divergenten Kanälen. — VDI-Forschungsarbeiten, Heft 289. 1929.
- 5-56. Patterson, G. Modern Diffuser Design. — Aircraft Eng. 1938.
- 5-57. Peters, H. Energieumsetzung in Querschnittserweiterung bei verschiedenen Zulaufbedingungen. — Ingenieur-Archiv, No. 1. 1931.
- 5-58. Polzin, J. Strömungsuntersuchungen an einem ebenen Diffuser. — Ingenieur-Archiv, Heft. 5. 1940.
- 5-59. Prandtl, L. Neuere Ergebnisse der Turbulenzforschung. — VDI, Bd. 77, No. 5. 1933.
- 5-60. Robertson, J.M. and J.W. Holl. Effect of Adverse Pressure Gradients on Turbulent Boundary Layers in Axisymmetric Conduits. — J. Appl. Mech., VI, Vol. 24, No. 2. 1954.
- 5-61. Stratford, B.S. Turbulent Diffuser Flow. — ARC, C.P., No. 307. 1956.
- 5-62. Szablewski, W. Turbulente Strömungen in divergenten Kanälen. — Ingenieur-Archiv, Bd. XXII, Heft 4. 1954.
- 5-63. Turuwa, J. and K. Suzuki. Experiments on the Efficiency of Conical Diffusers (The Initial State of Separation of Flow). — Trans.Japan, Soc. Mech. Engrs., 23, No. 125. 1957.
- 5-64. Squire, H.B. Experiments on Conical Diffusers. — Reports and Memoranda, No. 2751. November 1950.
- 5-65. Winter, H. Strömungsverhältnisse in einem Diffusor mit vorgeschaltetem Krümmer. — Maschinenbau und Wärme-wirtschaft, Heft 2. 1953.

Section Six

- 6-1. Abramovich, G.N. Aerodinamika mestnykh soprotivlenii (Aerodynamics of Local Resistances). — Sbornik po promyshlennoi aerodinamike, Trudy, No. 211. 1935.
- 6-2. Aronov, I.Z. Teploobmen i gidravlicheskoе soprotivlenie v izognutyykh trubakh (Heat Exchange and Hydraulic Resistance in Bent Pipes). Doctorate's thesis. — Kievskii politekhnicheskii institut. 1950.
- 6-3. Baulin, K.K. and I.E. Ideł'chik. Eksperimental'noe issledovanie techeniya vozdukh v kolenakh (Experimental Study of Air Flow in Elbows). — Tekhnicheskie zametki, No. 23. 1934.
- 6-4. Grabovskii, A.M. Issledovanie vzaimnogo vliyaniya mestnykh soprotivlenii (Study of the Interaction of Local Resistances). — Nauchnye zapiski Odesskogo politekhnicheskogo instituta, No. 3. 1955.
- 6-5. Tu P'eng-Chi'iu. Issledovaniya vliyaniya stepeni sherokhovatosti vnutrennikh poverkhnostei ventilyatsionnykh otvodov na ikh koefitsienty mestnykh soprotivlenii (The Influence of Roughness of the Inner Surfaces of Ventilation Bends on Their Coefficients of Local Resistances). Author's summary of thesis for Cand. of Engineering Sciences. — Inzhenerno-sroitel'nyi institut, Leningrad. 1939.
- 6-6. Ideł'chik, I.E. Napravlyayushchie lopatki v kolenakh aerodinamicheskikh trub (Guide Vanes in Wind-Tunnel Elbows). — Tekhzametki, TsAGI, No. 133. 1936.
- 6-7. Ideł'chik, I.E. Gidravlicheskie soprotivleniya (fiziko-mekhanicheskie osnovy) (Fluid Resistances (Physical and Mechanical Fundamentals)). — Gosenergoizdat. 1954.
- 6-8. Ideł'chik, I.E. K voprosu o vliyanii chisla Re i sherokhovatosti na soprotivlenie izognutyykh kanalov (The Influence of the Reynolds Number and the Roughness on the Resistance of Bent Channels). — Promyshlennaya aerodinamika, col. No. 4, BNI MAP. 1953.
- 6-9. Kamershtein, A.G. and V.N. Karev. Issledovanie gidravlicheskogo soprotivleniya gnutykh, svarnykh, kruto-zagnutyykh i skladchatyykh kolen kompensatorov (Study of the Hydraulic Resistance of Bent, Welded, Steeply Bent, and Corrugated Elbows of Expansion Devices). — Vniistroineft' i MIIGS. 1956.

- 6-10. Klyachko, L.S. Utochnenie metoda teorecheskogo opredeleniya koeffitsientov sопrotivleniya otvodov razlichnogo profilya (Refining the Method of Theoretical Determination of the Resistance Coefficient of Bends of Different Profiles). — Trudy nauchnoi sessii LIOT, No. 1. 1955.
- 6-11. Nekrasov, B.B. Gidravlika (Hydraulics). — VVA, 1954.
- 6-12. Promyshlennaya aerodinamika (Industrial Aerodynamics). — Collection No. 6, BNI MAP. 1956.
- 6-13. Rikhter, G. Gidravlika truboprovodov (Hydraulics of Pipelines). — ONTI, 1936.
- 6-14. Richter, L.A. Tyagodut'evye ustroistva promyshlennykh parovykh kotlov i puti snizheniya raskhoda elektroenergii na sobstvennye nuzhdy (Fans and Blowers for Industrial Steam Boilers with Means of Reducing Their Electric-Energy Consumption). — Trudy nauchno-tekhnicheskoi sessii po ekspluatatsii promyshlennykh kotel'nykh ustanovok, Gosenergoizdat. 1953.
- 6-15. Richter, L.A. Issledovanie na modelyah elementov gazovozdukhoprovodov teplovykh elektrostantsii (Model Study of the Elements of Gas and Air Conduits for Thermal Power Plants). — Teploenergetika, No. 1. 1957.
- 6-16. Richter, L.A. Voprosy proektirovaniya gazovozdukhoprovodov teplovykh elektrostantsii (Problems of the Design of Gas and Air-Conduits for Thermal Power Plants). — Gosenergoizdat. 1959.
- 6-17. Tatarchuk, G.T. Soprotivlenie pryamougol'nykh otvodov (Resistance of Rectangular Bends). — Voprosy otopleniya i ventilyatsii, Trudy TsNIIIPS, Gosstroizdat. 1951.
- 6-18. Khanzhonkov, V.I. and V.I. Taliev. Umen'shenie soprotivleniya kvadratnykh otvodov napravlyayushchimi lopatkami (Reducing the Resistance of Square Bends by Means of Guide Vanes). — Tekhnicheskie otchety, No. 110, BNT MAP. 1947.
- 6-19. El'perin, I.T. Povorot gazov v trubnom puchke (Curve Flow of Gases through a Tube Bundle). — Izvestiya AN BSSR, No. 3. 1950.
- 6-20. Yudin, E.Ya. Kolena s tonkimi napravlyayushchimi lopatkami (Elbows with Thin Guide Vanes). — Promyshlennaya aerodinamika, col. No. 7, BNT MAP. 1956.
- 6-21. Flyatau, R.S. Gidravlicheskie raschety truboprovodov (Hydrotechnical Calculation of Pipes). — Gostoptekhizdat. 1949.
- 6-22. Adler, M. Strömung in gekrümmten Röhren. — Z. angew. Math. Mech., Bd. 14. 1934.
- 6-23. Bambach. Plötzliche Umlenkung (Stoss) von Wasser in geschlossenen unter Druck durchströmten Kanälen. — VDI, Heft 327. 1930.
- 6-24. Conn, H.G., H.G. Colborne, and W.G. Brown. Pressure Losses in 4-inch Diameter Galvanized Metal Duct and Fittings. — Heating, Piping and Air-Conditioning, No. 1. 1953.
- 6-25. De Graene, E.P. — Heating, Piping and Air-Conditioning, No. 10. 1955.
- 6-26. Franke, P.G. Perdite di carico nelle curve circolari. — L'energia Elettrica, No. 9. 1954.
- 6-27. Frey, K. Verminderung des Strömungsverlustes in Kanälen durch Leitflächen. — Forschung auf dem Gebiete des Ingenieurwesens, Bd. 5, No. 3. 1934.
- 6-28. Fritzsche und H. Richter. Beitrag zur Kenntnis des Strömungswiderstandes gekrümmter rauher Rohrleitungen. — Forschung auf dem Gebiete des Ingenieurwesens, Bd. 4, No. 6. 1933.
- 6-29. Haase, D. — Allgemeine Wärmetechnik, Nos 11-12. 1953.
- 6-30. Heating and Ventilating. January, February 1953.
- 6-31. Hilding, Beij K. Pressure Losses for Fluid Flow in 90° Pipe Bends. — J. Research of National Bureau of Standards, Vol. 21, No. 1. 1938.
- 6-32. Hofmann, A. Der Verlust in 90° Rohrkümmern mit gleichbleibendem Kreisquerschnitt. — Mitteilungen des Hydraulischen Instituts der Technischen Hochschule, München, Heft 3. 1929.
- 6-33. Garbrecht, G. Über die Linienführung von Gerinnen. — Wasserwirtschaft, No. 6. 1956.
- 6-34. Kirschbach. Der Energieverlust in Kniestücken. — Mitteilungen des Hydraulischen Instituts der Technischen Hochschule, München, Heft 3. 1929.
- 6-35. Krober, Schaufelgitter zur Umlenkung von Fluss-Strömungen mit geringem Energieverlust. — Ingenieur-Archiv, Heft V. 1932.
- 6-36. Nippert, H. Über den Strömungsverlust in gekrümmten Kanälen. — Forschungsarbeiten auf dem Gebiete des Ingenieurwesens, VDI, Heft 320. 1929.
- 6-37. Richter, H. Der Druckabfall in gekrümmten glatten Rohrleitung. — Forschungsarbeiten auf dem Gebiete des Ingenieurwesens, VDI, Heft 338. 1930.
- 6-38. Richter, H. Rohrhydraulik. 1954.
- 6-39. Schuhart. Der Verlust in Kniestücken bei glatter und rauher Wandung. — Mitteilungen des Hydraulischen Inst. der Technischen Hochschule, München, Heft 3. 1929.
- 6-40. Spalding. Versuche über den Strömungsverlust in gekrümmten Leitungen. — VDI, No. 6. 1933.

- 6-41. Vuskovic, G. Der Strömungswiderstand von Formstücken für Gasrohrleitungen (Fittings). — Mitteilungen des Hydraulischen Instituts der Technischen Hochschule, München, Heft 9. 1939.
- 6-42. Wasilewski, J. Verluste in glatten Rohrkrümmern mit kreisrundem Querschnitt bei weniger als 90° Ablenkung. — Mitteilungen des Hydraulischen Instituts der Technischen Hochschule, München, Heft 5. 1932.
- 6-43. Weisbach, J. Lehrbuch der Ingenieur und Maschinenmechanik, II. Aufl. 1850; Experimentalhydraulik. 1855.
- 6-44. White, C.M. Streamline Flow through Curved Pipes. — Proc. Roy. Soc. Lon. (A), Vol. 123. 1929.

Section Seven

- 7-1. Aver'yanov, A.G. Koeffitsienty mestnykh soprotivlenii v troinikakh vtyazhnykh vozdukhovodov (Coefficients of Local Resistance in Y-Branches of Exhaust Air Ducts). — Otoplenie i ventilyatsiya, No. 2. 1939.
- 7-2. Zusmanovich, V.M. Soprotivlenie troinikov stochnykh gazovodoprovodnykh trub (Resistance of Y-Branches of Sewer Pipes). — Voprosy otopleniya i ventilyatsii, Gosstroizdat.
- 7-3. Kamenev, P.N. Dinamika potokov promyshlennoi ventilyatsii (Flow Dynamics in Industrial Ventilation Systems). — Gosstroizdat. 1938.
- 7-4. Konokotin, V.V. Mestnye soprotivleniya bokovykh otverstii gladkikh vozdukhovodov pryamougol'nogo secheniya (Local Resistances of Lateral Orifices of Smooth Rectangular Air Conduits). — LISI. 1957.
- 7-5. Levin, S.R. Analiticheskoe opredelenie velichiny poter' napora v troinikakh vtyazhnykh ventilyatsionnykh setei (Analytic Determination of the Magnitude of Head Losses in Y-Branches of Ventilating Exhaust Systems). — Otoplenie i ventilyatsiya, No. 7. 1935.
- 7-6. Levin, S.R. Soprotivlenie troinikov vtyazhnykh vozdukhovodov (Resistance of Y-Branches of Exhaust Air Conduits), Novosibirsk. 1939; — Otoplenie i ventilyatsiya, Nos 10-11. 1940.
- 7-7. Levin, S.R. Delenie potokov v truboprovodakh (Stream Division in Pipes). — Trudy LTI im. S. M. Kirova, No. 2/3. 1948.
- 7-8. Levin, S.R. Smeshenie potokov v krestoobraznykh soedineniyakh truboprovodov (Stream Mixing in Cross-Shaped Pipe Joints). — Trudy LTI im. S. M. Kirova, No. 5. 1954.
- 7-9. Levin, S.R. Novyi metod teorecheskogo opredeleniya gidravlicheskih soprotivlenii pri smeshenii potokov v truboprovodakh (New Methods for the Theoretical Determination of Fluid Resistances at Stream Mixing in Pipes). — Trudy LTI im. S. M. Kirova, No. 6. 1955.
- 7-10. Levin, S.R. Soudarenie potokov neszhimaemoi zhidkosti v truboprovodakh (Collision of Incompressible-Liquid Streams in Pipes). — Trudy LTI im. S. M. Kirova, No. 8. 1958.
- 7-11. Maksimov, G.A. Raschet ventilyatsionnykh vozdukhovodov (Calculation of Ventilation Air Conduits). — Gosstroizdat. 1952; Ventilyatsiya i otoplenie, Part II, Gosstroizdat. 1955.
- 7-12. Pludemakher, A.S. and G.M. Itkin. Mestnye soprotivleniya troinikov vozdukhovodov pri nagnetanii (Local Resistances of Y-Branches of Forced Draft Air Conduits). — Otoplenie i ventilyatsiya, No. 9. 1934.
- 7-13. Pludemakher, A.S. Mestnye soprotivleniya v krestovinakh vodovodov pri rozlive (Local Resistances in Water Pipeline Crosses at Discharge). — Otoplenie i ventilyatsiya, No. 4. 1937.
- 7-14. Poletov, N.V. K gidravlicheskim raschetam soprotivlenii truboprovodov (Hydraulic Calculation of Pipe Resistances). — Vodosnabzhenie i sanitarnaya tekhnika, No. 4. 1957.
- 7-15. Pruzner, A.S. Soprotivlenie troinikov pri rabote na nagnetanii (Resistance of Forced Draft Y-Branches). — Sovremenye voprosy ventilyatsii, Stroizdat. 1941.
- 7-16. Taliev, V.N. and G.T. Tatarchuk. Soprotivlenie pryamougol'nykh troinikov (Resistance of Rectangular Y-Branches). — Voprosy otopleniya i ventilyatsii, Gosstroizdat. 1951.
- 7-17. Taliev, V.N. Raschet mestnykh soprotivlenii troinikov (Calculation of the Local Resistances of Y-Branches). — Gosstroizdat. 1952.
- 7-18. Taliev, V.N. Aerodinamika ventilyatsii (Aerodynamics of Ventilation). — Gosstroizdat. 1954.
- 7-19. Tatarchuk, G.T. Mestnye soprotivleniya chugunnykh krestovin (Local Resistances of Iron Crosses of Pipes). — Voprosy otopleniya i ventilyatsii, No. 3, Gosstroizdat. 1936.
- 7-20. Franke, P. Die zusätzlichen Verluste bei der Vereinigung von zwei Wasserströmen in einem gemeinsamen Steigschacht. — VDI-Zeitschrift, Bd. 97, No. 24. August 1955.
- 7-21. Gilman, S.F. Pressure Losses of Divided Flow Fittings. — Heating, Piping, and Air-Conditioning. April 1955.
- 7-22. Kinne, E. Der Verlust in 60° Rohrverzweigungen. — Mitteilungen des Hydraulischen Instituts der Technischen Hochschule, München, Heft 4. 1931.
- 7-23. Konzo, S., S.F. Gilman, J.W. Holl, and R.J. Martin. Investigation of the Pressure Losses of Takeoffs for Extended Plenum-Type Air-Conditioning Duct Systems. — University of Illinois Bulletin, Bulletin Series, No. 415. 1953.

- 7-24. Mc Nown, J.S. Mechanics of Manifold Flow. — Proc. Amer. Soc. Civil Engrs., No. 258. 1953.
- 7-25. Miller, L.G., C.H. Pesterfield, and R.J. Waalkes. Resistance of Rectangular Divided Flow Fittings. — Heating, Piping, and Air-Conditioning, No. 1. 1956.
- 7-26. Petermann, F. Der Verlust in schiefwinkligen Rohrverzweigungen. — Mitteilungen des Hydraulischen Instituts der Technischen Hochschule, München, Heft 3. 1929.
- 7-27. Vazsonyi, A. Pressure Loss in Elbows and Duct Branches. — Trans. ASME, Vol. 66. 1944.
- 7-28. Vogel, C. Untersuchungen über den Verlust in rechtwinkligen Rohrverzweigungen. — Mitteilungen des Hydraulischen Instituts der Technischen Hochschule, München, Heft 1. 1926; Heft 2. 1928.

Section Eight

- 8-1. Abramovich, G.N. Turbulentnye svobodnye strui zhidkostei i gazov (Turbulent Free Jets of Fluids). — Gosenergoizdat. 1948.
- 8-2. Abramovich, G.N. Prikladnaya gazovaya dinamika (Applied Gas Dynamics). — Gostekhteorizdat. 1953.
- 8-3. Antuf'ev, V.M. and L.S. Kazachenko. Teploperedacha i soprotivlenie konvektivnykh poverhnostei nagreva (Heat Transfer and Resistance of Convective Heating Surfaces). — Gosenergoizdat. 1938.
- 8-4. Antuf'ev, V.M. and G.S. Beletskii. Teploperedacha i aerodinamicheskoe soprotivlenie trubchatykh poverhnostei v poperechnom potoke (Heat Transfer and Aerodynamic Resistance of Tubular Surfaces in a Transverse Stream). — Mashgiz. 1948.
- 8-5. Bezrukin, I.P. Aerodinamicheskie svoistva zeren (Aerodynamic Properties of Grains). — In: Sbornik "Separirovaniye sypuchikh tel", Trudy Moskovskogo doma uchenykh. 1937.
- 8-6. Berezkin, A.R. Issledovanie poteri napora v reshetkakh vodozabornykh sooruzhenii (Study of Head Losses in the Water Intake Screens). — Trudy gidravlicheskoi laboratorii, VODGEO, No. 1, Gosstroizdat. 1941.
- 8-7. Bernshtein, R.S., V.V. Pomerantsev, and S.L. Shagalova. K voprosu o mekhanike soprotivleniya i teplopere-dachi v trubnykh puchkakh (Mechanics of Resistance and Heat Transfer in Tube Bundles). — "Voprosy aerodinamiki i teploperedachi v kotel'no-topochnykh protsessakh", Collection of papers edited by Knorre, Gosenergoizdat. 1958.
- 8-8. Bernshtein, R.S., V.V. Pomerantsev, and S.L. Shagalova. Obobshchennyi metod rascheta aerodinamicheskogo soprotivleniya zagruzheniykh sechenii (Generalized Method of Calculating the Aerodynamic Resistance of Loaded Sections) — "Voprosy aerodinamiki i teploperedachi v kotel'no-topochnykh protsessakh", Collection of papers edited by Knorre, Gosenergoizdat. 1958:
- 8-9. Denisenko, G.F. Fil'try iz poristogo metalla (Porous-Metal Filters). — Byulleten' "Kislorod", No. 6. 1952.
- 8-10. Dil'man, V.V., E.P. Darovskikh, M.E. Aerov, and L.S. Aksel'rod. O gidravlicheskem soprotivlenii reshetchatykh tarelok (On the Hydraulic Resistance of Grids and Perforated Plates). — Khimicheskaya promyshlennost', No. 3. 1956.
- 8-11. Dul'nev, V.B. Opredelenie poter' napora v reshetkakh (Determination of the Head Losses in Grids). — Gidro-tehnicheskoe stroitel'stvo, No. 9. 1956.
- 8-12. Zhavoronkov, N.M. Gidravlicheskie osnovy skrubbernogo protsessa i teploperedacha v skrubberakh (Hydraulic Foundations of the Scrubber Process, and Head Transfer in Scrubbers). — Sovetskaya nauka. 1944.
- 8-13. Zhavoronkov, N.M. Gidro-i aerodinamika nasadok skrubbernykh i rektifikatsionnykh koloni. Gidravlicheskie soprotivlenie sukhikh neuporyadochenykh nasadok (Hydro- and Aerodynamics of Packings for Scrubber and Rectification Columns. Fluid Resistance of Dry Random Arranged Packing Works). — Khimicheskaya promyshlennost', No. 9. 1948.
- 8-14. Zhavoronkov, N.M., M.E. Aerov, and N.I. Umnik. Gidro-i aerodinamika nasadok skrubbernykh i rektifikatsionnykh koloni. Gidravlicheskie soprotivlenie oroshaemykh neuporyadochenykh nasadok (Hydro- and Aerodynamics of Packing for Scrubber and Rectification Columns. Hydraulic Resistance of Wet, Random Arranged Packings). — Khimicheskaya promyshlennost', No. 10. 1948.
- 8-15. Zhavoronkov, N.M., M.E. Aerov, S.N. Babkov, and N.M. Umnik. Gidro-i aerodinamika nasadok skrubbernykh i rektifikatsionnykh koloni. Kriticheskie yavleniya v oroshaemykh neuporyadochenykh nasadkakh (Hydro- and Aerodynamics of Packings for Scrubber and Rectification Columns. Critical Phenomena in Wet, Random Arranged Packings). — Khimicheskaya promyshlennost', No. 3. 1949.
- 8-16. Zalogin, N.G. Ob aerodinamicheskem soprotivlenii shakhmatnogo puchka trub (Aerodynamic Resistance of a Checkerboard-Type Tube Bundle). — Izvestiya VTI, No. 5. 1951.
- 8-17. I del'chik, I.E. Gidravlicheskie soprotivlenie pri vkhode potoka v kanaly i protekanie cherez otverstiya (Hydraulic Resistance at Stream Entrance in Channels, and Flow through Orifices). — Promyshlennaya aerodinamika, col. No. 2, BNT NKAP. 1944.

- 8-18. Idel'chik, I.E. Vyravnivayushchee deistvie soprotivleniya, pomeshchennogo za diffuzorom (Equalizing Effect of a Resistance Placed Behind a Diffuser). — Trudy No. 662, BNT MAP. 1948.
- 8-19. Idel'chik, I.E. Opredelenie koeffitsientov soprotivleniya pri istechenii cherez otverstiya (Determination of the Resistance Coefficients at Discharge through Orifices). — Gidrotehnicheskoe stroitel'stvo, No. 5. 1953.
- 8-20. Idel'chik, I.E. Gidravlicheskie soprotivleniya (fiziko-mekhanicheskie osnovy) (Fluid Resistances (Physical and Mechanical Fundamentals)). — Gosenergoizdat. 1954.
- 8-21. Idel'chik, I.E. Prinuditel'naya razdacha potoka v gazoochistnykh, teploobmennykh i drugikh apparatakh (Forced Stream Distribution in Scrubbing. Heat-Exchange and Other Apparatus). — Collection of papers of NIIOGAZ, No. 1, Goskhimizdat. 1957.
- 8-22. Idel'chik, I.E. Uchet vliyaniya vyazkosti na gidravlichesko soprotivlenie diafragm i reshetok (Allowing for the Influence of Viscosity on the Hydraulic Resistance of Diaphragms and Grids). — Teploenergetika, No. 9. 1960.
- 8-23. Ishkin, N.P. and M.G. Kaganer. Gidravlichesko soprotivlenie poristykh sred (Hydraulic Resistance of Porous Media). — Kislorod, No. 3. 1952.
- 8-24. Kazakevich, F.P. Vliyanie ugla ataki gazovogo potoka na aerodynamicheskoe soprotivlenie puchkov trub (Influence of the Angle of Approach of a Gas Stream on the Aerodynamic Resistance of a Tube Bundle). — Izvestiya VTI, No. 8. 1952.
- 8-25. Kasalainen, N.N. Teploperedacha i soprotivlenie vozdukhopodogrevatelya s poperechno-omyvaemym puchkom trub (Heat Transfer and Resistance of an Air Heater with Transverse Flow Around the Tube Bundle). — Teploenergetika, No. 7. 1955.
- 8-26. Kafarov, V.V. Soprotivlenie v nasadochnykh kolonnakh pri zakhlebyvanii i pri optimal'nykh skorostyakh potoka (Resistance in Packed Columns at Clogging and at Optimum Stream Velocities). — Khimicheskaya promyshlennost', No. 6. 1948.
- 8-27. Komarovskii, A.A., M.S. Verteshev, and V.V. Strel'tsov. Gidravlichesko soprotivlenie sloya chasitst proizvol'noi formy (Hydraulic Resistance of a Layer of Particles of Arbitrary Shape). — Trudy Novocherkasskogo politehnicheskogo instituta imeni Ordzhonikidze, Vol. 41(55). 1956.
- 8-28. Konobeev, B.I., V.A. Malyusov, and N.M. Zhavoronkov. Gidravlichesko soprotivlenie i tolshchina plenki pri obrashchennom techenii zhidkosti pod deistviem gaza v vertikal'nykh trubakh (Hydraulic Resistance and Film Thickness at Reverse Liquid Flow Under the Action of a Gas in Vertical Pipes). — Khimicheskaya promyshlennost', No. 3. 1957.
- 8-29. Kolletov, L.D. Gidrodinamika porovykh sred (Hydrodynamics of Porous Media). — Khimicheskaya promyshlennost', No. 2. 1959.
- 8-30. Kuznetsov, N.V. and A.Z. Shcherbakov. Eksperimental'noe opredelenie teploperedachi i aerodynamicheskikh soprotivlenii chugunnogo rebristogo vozdukhopodogrevatelya (Experimental Determination of Heat Transfer and Aerodynamic Resistances of a Cast-Iron Ribbed Air Heater). — Izvestiya VTI, No. 2. 1951.
- 8-31. Kuznetsov, N.V., A.Z. Shcherbakov, and E.Ya. Titova. Novye raschetnye formuly dlya aerodynamicheskogo soprotivleniya poperechno obtekaemykh puchkov trub (New Calculating Formulas for the Aerodynamic Resistance of Transverse Flow Around Tube Bundles). — Teploenergetika, No. 9. 1954.
- 8-32. Kuznetsov, N.V. and S.I. Turilin. Vliyanie temperaturnykh uslovii na teplootdachu i soprotivlenie trubchatykh poverkhnostei v poperechnom potoke (Influence of the Temperature Conditions on Heat Transfer and Resistance of Tubular Surfaces in a Transverse Stream). — Izvestiya VTI, No. 11. 1952.
- 8-33. Kuzovnikova, E.A. Gidravlichesko soprotivlenie puchkov trub s peremennym shagom po vysote (Hydraulic Resistance of Tube Bundles Varying over Height Pitch). — Sbornik nauchnykh trudov AN BSSR, 44 (VI). 1954.
- 8-34. Lev, E.S. Fil'tratsiya gaza cherez sloi sypuchego tela (sostoyanie voprosa) (Gas Filtration through a Layer of Loose Material (State of the Problem)). — "Voprosy aerodinamiki i teploperedachi v kotel'no-topochnykh protsessakh", Collection of articles edited by Knorre, Gosenergoizdat. 1958.
- 8-35. Leibenzon, L.S. Dvizhenie prirodnnykh zhidkosteii i gazov v poristoi srede (Flow of Natural Fluids in a Porous Medium). — Gostekhizdat. 1947.
- 8-36. Linchevskii, V.P. (Editor). Metallurgicheskie pechi (Metallurgical Furnaces). — Metallurgizdat. 1948.
- 8-37. Lyapin, M.F. Teploperedacha i aerodynamicheskoe soprotivlenie gladkotrubnykh puchkov pri bol'shikh chislakh Re gazovogo potoka (Heat Transfer and Aerodynamic Resistance of Bundles of Smooth Pipes at High Reynolds Numbers of the Gas Stream). — Teploenergetika, No. 9. 1956.
- 8-38. Minskii, E.M. O turbulentnoi fil'tratsii v poristykh sredakh (Turbulent Filtration in Porous Media). — DAN SSSR, Vol. 78, No. 3. 1951.
- 8-39. Mints, D.M. and S.A. Shubert. Gidravlika zernistykh materialov (Hydraulics of Granular Materials). — Izdatel'stvo Ministerstva komunal'nogo khozyaistva RSFSR. 1955.
- 8-40. Mikheev, M.A. Osnovy teploperedachi (Fundamentals of Heat Transfer). — Gosenergoizdat. 1949.
- 8-41. Mochan, I.S. Mestnye soprotivleniya pri dvizhenii odnofaznogo i dvukhfaznogo potokov (Local Resistances at the Flow of Single- and Two-Phase Streams). — BTI TsKTI. 1959.

- 8-42. Mollokandov, F.N. Gidravlicheskoе sопротивление слоя сферических частиц при изотермическом и неизотермическом воздушном потоке (Fluid Resistance of a Layer of Spherical Particles at Isothermal and Nonisothermal Air Streams). — ZhTF, Vol. XVIII, No. 8. 1948.
- 8-43. Panchenko, A.V. Ventilyatsionnye уstanовки mel'niits i elevatorov (Ventilating Installations of Grinding Mills and Elevators). — Zagotizdat. 1954.
- 8-44. Planovskii, A.N. and V.V. Kafarov. Optimal'nye skorosti potokov v nasadochnykh kolonnakh (Optimum Stream Velocities in Packed Columns). — Khimicheskaya promyshlennost', No. 4. 1946.
- 8-45. Ramzin, L.K. Gazovoe sопротивление сypuchikh materialov (Gas Resistance of Loose Materials). — Izvestiya VTI, No. 7(20). 1926.
- 8-46. Salikov, A.P., Ya.L. Polynovskii, and K.I. Belyakov. Issledovanie teploperedachi i sопротивleniya v prodol'nykh puchkakh gladkikh trub (Study of Heat Transfer, and Resistance in Longitudinal Bundles of Smooth Tubes). — Teploenergetika, No. 8. 1954.
- 8-47. Teben'kov, B.P. Rekuperatory dlya promyshlennykh pechei (Heat Recuperators for Industrial Furnaces). — Metalurgizdat. 1955.
- 8-48. Timofeev, V.N. and E.S. Karasina. Teploobmen v puchkakh trub chugunnogo rebristogo ekonomizera (Heat Exchange in Bundles of Tubes of a Cast-Iron Ribbed Waste-Gas Heater). — Izvestiya VTI, No. 5. 1952.
- 8-49. Tulin, S.N. Teploperedacha i sопротивление v puchkakh trubok s provolochnym orebreniem (Heat Transfer and Resistance in Bundles of Tubes with Wire Ribbing). — Teploenergetika, No. 3. 1958.
- 8-50. Usyukin, I.P. and L.S. Aksel'rod. Osnovy gidravlicheskogo rascheta setchatykh rektifikatsionnykh koloni (Fundamentals of the Hydraulic Calculation of Screen-Packing Rectification Columns). — Kislorod, No. 1. 1949.
- 8-51. Uchastkin, P.V. Issledovanie effektivnosti i гидродинамического sопротивления eliminatorov (Study of the Efficiency and Hydrodynamic Resistance of Roof Ventilators). — Otoplenie i ventilyatsiya, No. 6. 1940.
- 8-52. Federov, I.M. Koeffitsienty ispareniya, teplootdachi i sопротивleniya pri sushke zernistykh materialov s produvkoi vozdukh cherez sloi (Coefficients of Evaporation, Heat Transfer, and Resistance when Granular Materials Are Dried by Blowing Air through a Layer). — In: Sbornik "Sovremennye problemy sushil'noi tekhniki", Gosenergoizdat. 1941.
- 8-53. Fuks, S.N. Soprotivlenie trubnogo puchka pri kondensatsii v nem para (Resistance of a Bundle of Tubes at Condensation Stream in It). — Teploenergetika, No. 4. 1954.
- 8-54. Khanzhonkov, V.I. Soprotivlenie setok (Resistance of Screens). — Promyshlennaya aerodinamika, col. No. 2, BNT NKAP. 1944.
- 8-55. Chavtoraev, A.I. O poteryakh napora v reshetke (Head Losses in a Grid). — Gidrotekhnicheskoe stroitel'stvo, No. 5. 1958.
- 8-56. Chudnovskii, A.F. Teploobmen v dispersnykh sredakh (Heat Exchange in Dispersed Media). — Gostekhtheoretizdat. 1954.
- 8-57. Shepelev, I.A. Osnovy rascheta vozдушных zaves, pritochnykh strui i poristykh fil'trov (Fundamentals of the Calculation of Air Locks, Influx Streams, and Porous Filters). — Stroizdat. 1950.
- 8-58. Shcherbakov, A.E. and N.I. Zhirnov. Teploperedacha i aerodinamicheskoe sопротивление chugunnogo rebristo-zubchatogo vozdukhopodgrevatelya (Heat Transfer and Aerodynamic Resistance of a Cast-Iron Radiator-Type Air Heater). — Teploenergetika, No. 8. 1954.
- 8-59. Cornell, W.G. Losses in Flow Normal to Plane Screens. — Trans. ASME, No. 4. 1958.
- 8-60. Flachsbart, O. Widerstand von Seidengazefiltern, Runddraht und Blechstreifensieben mit quadratischen Maschen. Ergebnis der aerodynamischen Versuchsanstalt zu Göttingen, IV Lieferung. 1932.
- 8-61. Kirschmer, O. Untersuchungen über den Gefallsverlust an Rechen. — Mitteilungen des Hydraulischen Instituts der Technischen Hochschule, München, Heft 1. 1926.
- 8-62. Spandler, I. Untersuchungen über den Verlust an Rechen bei schräger Zuströmung. — Mitteilungen des Hydraulischen Instituts der Technischen Hochschule, München, Heft 2. 1928.
- 8-63. Wallis, R.P. and C.M. White. Resistance to Flow through Wests of Tubes. — Engineering, Vol. 146, Nos. 3802, 3804, 3806. 1938.

Section Nine

- 9-1. Abramovich, G.N. Turbulentnye svobodnye strui zhidkostei i gazov (Turbulent Free Jets of Fluids). — Gosenergoizdat. 1948.
- 9-2. Aronov, I.Z. Teploobmen i гидравлическое sопротивление v izognutyykh trubakh (Heat Exchange and Fluid Resistance in Bent Pipes), Doctorate's thesis, Kiev Polytechnic Institute. 1950.

- 9-3. Aronovich, V.A. Vybor razmera reguliruyushchikh klapanov (Selecting the Size of Control Valves). — Khimicheskaya promyshlennost', No. 4. 1950.
- 9-4. Aronovich, V.V. and M.S. Slobodkin. Armatura reguliruyushchaya i zapornaya (Control and Shutoff Valves). — Mashgiz. 1953.
- 9-5. Baulin, K.K. Ispytanie labirintnykh uplotnenii (Testing Labyrinth Seals). — In: Sbornik 'Statei po kompressornym mashinam', VIGM, No. 10. 1940.
- 9-6. Gurevich, D.F. Osnovy rascheta truboprovodnoi armatury (Fundamentals of Calculation of Pipe Fittings). — Mashgiz. 1956.
- 9-7. Dub, B.I. Armatura vysokogo davleniya dlya truboprovodov (High-Pressure Pipe Fittings). — Gosenergoizdat. 1954.
- 9-8. Idel'chik, I.E. Gidravlicheske soprotivlenie pri vkhode potoka v kanaly i protekanie cherez osterstiya (Hydraulic Resistance at Stream Entrance in Channels, and Flow through Orifices). — Promyshlennaya aerodinamika, col. No. 2, BNT NKAP. 1944.
- 9-9. Idel'chik, I.E. K raschetu soprotivleniya labirintnykh uplotnenii (Calculating the Resistance of Pipe Seals). — Kotloturbostroenie, No. 3. 1953.
- 9-10. Idel'chik, I.E. Gidravlicheskie soprotivleniya (fiziko-mekhanicheskie osnovy) (Fluid Resistances (Physical and Mechanical Fundamentals)). — Gosenergoizdat. 1954.
- 9-11. Kuznetsov, L.A. and B.V. Rudomin. Konstruirovaniye i raschet truboprovodov teplosilovykh ustankov (Design and Calculation of Pipes of Thermal-Power Installations). — Mashgiz. 1949.
- 9-12. Murin, G.A. Gidravlicheske soprotivlenie pramotochnykh ventilei (Hydraulic Resistance of Direct-Flow Valves). — Otoplenie i ventilyatsiya, No. 5. 1941.
- 9-13. Osipovskii, N.F. Ekspluatatsiya barabannyykh kotlov vysokogo davleniya (Operation of High-Pressure Drum Boilers). — Gosenergoizdat. 1953.
- 9-14. Rolle, N.L. Koefitsienty soprotivleniya i raskhoda kol'tsevogo zatvora (Resistance and Discharge Coefficients of a Ring-Seal Gate Valve). — Gidrotekhnicheskoe stroitel'stvo, No. 4. 1953.
- 9-15. Chebysheva, K.V. K voprosu o raschete labirintnogo uplotneniya (Calculating a Labyrinth Seal). — Tekhnicheskie zametki, TsAGI, No. 142. 1937.
- 9-16. Frenkel', V.Z. Gidravlika (Hydraulics). — Gosenergoizdat. 1956.
- 9-17. Erlikh, A.M. Paroprovody, ikh armatura i prochie detali (Steam Conduits, Their Fittings and other Parts). — ONTI. 1937.
- 9-18. Bach, C. Versuche über Ventilbelastung und Ventilwiderstand. 1884.
- 9-19. Hottinger, M. Bericht über die an Rohrverschraubungen, Rohrschweissen, und Ventilen durchgeföhrten Untersuchungen. — Gesundheitsingenieur, No. 45. 1928.
- 9-20. Guilleaume, M. Die Wärmeausnutzung neuerer Dampfkraftwerke und ihre Ueberwachung. — VDI-Zeitschrift, No. 17. 1915, u. "Feuerungstechnik". 1913/1914.
- 9-21. Pfleiderer, G. and A. Closterhalfen. Versuche über den Strömungswiderstand von Heissdampfventilen verschiedener Bauart. — "Die Wärme", No. 43. 1930, und "Archiv für Wärmewirtschaft", No. 1. 1931.
- 9-22. Weisbach, J. Lehrbuch der technischen Mechanik. 1875.

Section Ten

- 10-1. Idel'chik, I.E. Poteri na udar v potoke s neravnomernym raspredeleniem skorosti (Shock Losses in a Stream with Nonuniform Velocity Distribution). — Trudy MAP, No. 662. 1948.
- 10-2. Krasnoperov, E.V. Eksperimental'naya aerodinamika (Experimental Aerodynamics). — ONTI. 1935.
- 10-3. Kuznetsov, B.Ya. Lobovoe soprotivlenie trosov, provolok, tenderov i aviationskikh lenth (Drag of Ropes, Wires, Ties, and Stays). — Trudy TsAGI, No. 97. 1931.
- 10-4. Kuznetsov, B.Ya. Aerodinamicheskie issledovaniya tsilindrov (Aerodynamic Studies of Cylinders). — Trudy TsAGI, No. 98. 1931.
- 10-5. Skochinskii, A.A., A.I. Ksenofontova, A.A. Kharev, and I.E. Idel'chik. Aerodinamicheskoe soprotivlenie shakhtnykh stvolov i sposoby ego snizheniya (Fluid Resistance of Mineshafts and Methods of Reducing It). — Ugletekhizdat. 1953.
- 10-6. Khanzhonkov, V.I. Aerodinamicheskoe soprotivlenie trubchatykh ferm (Aerodynamic Resistance of Tubular Girders). — Tekhnicheskie otchety, No. 131, BNI MAP. 1955.
- 10-7. Kharev, A.A. Mestnye soprotivleniya shakhtnykh ventilyatsionnykh setei (Local Resistances of Mine-Ventilating Systems). — Ugletekhizdat. 1954.

- 10-8. Chesalov, A.V. Koeffitsienty vrednykh sопrotivlenii samoletov (Coefficients of Aircraft Resistance). — Trudy TsAGI, No.42. 1929.
- 10-9. Yur'ev, B.N. and M.P. Lesnikova. Aerodinamicheskie issledovaniya (Aerodynamic Studies). — Trudy TsAGI, No.33. 1928.
- 10-10. Yur'ev, B.N. Ekspérimental'naya aerodinamika (Experimental Aerodynamics). — ONTI, 1932.
- 10-11. Eiffel. Resistance de l'air et l'aviation, Paris. 1910.
- 10-12. Ergebnisse der aerodynamischen Versuchsanstalt zu Göttingen, Lieferung II. 1923; Lieferung III. 1927.
- 10-13. Frachsbart, O. Neue Untersuchunge über den Luftwiderstand von Kugeln.— Phys. Z. 1927.
- 10-14. Jacobs. Sphere Drag Tests in the Variable Density Wind Tunnel. — Nat. Advisory Commission for Aeronautics. 1929.
- 10-15. Hütte, Handbuch [Russian translation].—ONTI. 1936.

Section Eleven

- 11-1. Abramovich, G.N. Turbulentnye svobodnye strui zhidkoste i gazov (Turbulent Free Jets of Fluids). — Gosenergoizdat. 1948.
- 11-2. Baturin, V.V. and I.A. Shepelev. Aerodinamicheskie kharakteristiki pritochnykh nasadkov (Aerodynamic Characteristics of Intake Nozzles). — Sovremennye voprosy ventilyatsii, Stroizdat. 1941.
- 11-3. Bushel', A.R. Sniženie vnútrennikh poter' v shakhtnoi ustanovke s osevym ventilyatorom (Reduction of the Interior Losses in an Installation with Axial Fan). — Trudy, No.673, BNT MAP. 1948.
- 11-4. Grimitlin, M.I. Gidravlicheskiy raschet pritochnykh perforirovannykh truboprovodov na zadannyyu stepen' ravnomennosti razdachi (Hydraulic Calculation of Intake Perforated Pipes for a Specified Degree of Uniformity of Stream Distribution). — Promyshlennaya energetika, Trudy LIOT. 1958.
- 11-5. Grimitlin, M.I. Vremennye rukovodyashchie ukazaniya po gidravlicheskому raschetu, primeneniyu i izgotovleniyu pritochnykh perforirovannykh vozdukhovodov (Provisional Instructions for Hydraulic Calculation, Application, and Manufacture of Perforated Intake Air Conducts). — Nauchno-tehnicheskaya informatsiya po voprosam okhrany truda, LIOT, No.19. 1959.
- 11-6. Dovzhik, S.A. and A.S. Ginevskii. Ekspertimental'noe issledovanie napornykh patrubkov statsionarnykh osevykh mashin (Experimental Study of Pressure Connections of Stationary Axial Machines). — Tekhnicheskie otchety, No.130, BNI MAP. 1955.
- 11-7. Ideł'chik, I.E. Gidravlicheskie sопrotivleniya pri vkhode potoka v kanaly i protekanii cherez otverstiya (Fluid Resistance at the Inlet of a Stream in Channels and at the Flow through Orifices). — In: Sbornik "Promyshlennaya aerodinamika", No.2, BNT, NKAP. 1944.
- 11-8. Ideł'chik, I.E. Aerodinamika potoka i poteri napora v diffuzorakh (Aerodynamics of the Stream, and Head Losses in Diffusers). — Promyshlennaya aerodinamika, col. No.3, BNT MAP. 1947.
- 11-9. Ideł'chik, I.E. Poteri na udar v potoke s neravnomernym raspredeleniem skorosti (Shock Losses in a Stream with Nonuniform Velocity Distribution). — Trudy MAP, No.662. 1948.
- 11-10. Ideł'chik, I.E. Opredelenie koeffitsientov sопrotivleniya pri istechenii cherez otverstiya (Determination of the Resistance Coefficients at Discharge through Orifices). — Gidrotehnicheskoe stroitel'stvo, No.5. 1953.
- 11-11. Ideł'chik, I.E. Gidravlicheskie sопrotivleniya (fiziko-mekhanicheskie osnovy) (Fluid Resistances (Physical and Mechanical Fundamentals)). — Gosenergoizdat. 1954.
- 11-12. Ideł'chik, I.E. Uchet vliyanija vyazkosti na hidravlicheskoе sопrotivlenie diafragm i reshetok (Allowing for the Influence of Viscosity on the Hydraulic Resistance of Diaphragms and Grids). — Teploenergetika, No.9. 1960.
- 11-13. Lokshin, I.L. and A.Kh. G a z i t b e k o v a. Rabota diffuzorov, ustanovленных за центробежными вентиляторами (Operation of Diffusers Placed Behind Centrifugal Fans). — Promyshlennaya aerodinamika, col. No.6, BNI MAP. 1955.
- 11-14. Nosova, M.M. Sопrotivlenie vkhodnykh i vkhodnykh rastrubov s ekranom (Influence of Inlet and Exit Bells with Baffles). — In: Sbornik "Promyshlennaya aerodinamika", No.7. 1956.
- 11-15. Nosova, M.M. and N.F. Tarasov. Soprotivlenie pritochno-vtyazhnykh shakht (Resistance of Intake-Exhaust Vents). — In: Sbornik "Promyshlennaya aerodinamika", No.12, Oborongiz. 1959.
- 11-16. Promyshlennaya aerodinamika (Industrial Aerodynamics), Collection No.6, BNI MAP. 1956.
- 11-17. Khanzhonkov, V.N. Soprotivlenie setok (Resistance of Screens). — Promyshlennaya aerodinamika, col. No.2, BNT NKAP. 1944.
- 11-18. Khanzhonkov, V.N. Uluchshenie effektivnosti diffuzorov s bol'shimi uglami raskrytiya pri pomoshchi ploskikh ekranov (Improving the Efficiency of Diffusers with Large Divergence Angles by Means of Plane Baffles). — Promyshlennaya aerodinamika, col. No.3, BNT MAP. 1947.

- 11-19. Khanzhonkov, V.I. Soprotivlenie pritochnykh i vtyazhnykh shakht (Resistance of Intake and Exhaust Vents). — In: Sbornik "Promyshlennaya aerodinamika", No. 3, BNI, MAP. 1947.
- 11-20. Khanzhonkov, V.I. Umen'shenie aerodinamicheskogo soprotivleniya oterstii kol'tseyimi rebrami i ustupami (Reducing the Aerodynamic Resistance of Orifices by Means of Annular Ribs and Ledges). — In: Sbornik "Promyshlennaya aerodinamika", No. 12, Oborongiz. 1959.
- 11-21. Khanzhonkov, V.I. and V.I. Taliev. Umen'shenie soprotivleniya kvadratnykh otvodov napravlyayushchimi lopatkami (Reducing the Resistance of Square Bends by Means of Guide Vanes). — Tekhnicheskie otchety, No. 110, BNT MAP. 1947.
- 11-22. Yudin, E.Ya. Kolena s tonkimi napravlyayushchimi lopatkami (Elbows with Thin Guide Vanes). — Promyshlennaya aerodinamika, col. No. 7, BNT MAP. 1956.
- 11-23. Bevier, C.W. Resistance of Wooden Louvers to Fluid Flows. — Heating, Piping, and Air-Conditioning. May 1955.
- 11-24. Cobb, P.R. Pressure Loss of Air Flowing through 45° Wooden Louvers. — Heating, Piping, and Air-Conditioning. December 1953.
- 11-25. Hofmann, A. Die Energieumsetzung in saugrohrähnlichen erweiterten Düsen. — Mitteilungen, Heft 4. 1931.

Section Twelve

- 12-1. Abramovich, G.N. Turbulentnye svobodnye strui zhidkosti i gazov (Turbulent Free Jets of Fluids). — Gosenergoizdat. 1948.
- 12-2. Atlas "Inertionnye pyleuloviteli" (Inertial Dust Separators). — Series OV-122, Lenpromstroiproekt. 1947.
- 12-3. Atlas KTIS, Series V-327. 1943.
- 12-4. Batareinye tsiklony, rukovodyashchie ukazaniya po proektirovaniyu, izgotovleniyu, montazhu i ekspluatatsii (Battery-Powered Dust Separators, Instructions Relative to Their Design, Manufacture, Installation, and Running). — Goskhimizdat. 1956.
- 12-5. Gazoochistnoe oborudovanie (Gas-Scrubbing Equipment). — Catalog of the Fazoochistka Trust, Goskhimizdat. 1958.
- 12-6. Geras'ev, A.M. Pyleuloviteli SIOT (SIOT-Dust Separators). — Profizdat. 1954.
- 12-7. Gordon, G.M. and I.A. Aladzhalov. Gazoochistka rukavnymi fil'trami v tsvetnoi metallurgii (Gas Cleaning by Bag-Type Filters in Nonferrous Metallurgy). — Metallurgizdat. 1956.
- 12-8. Zaitsev, M.M. Raschet rukavnogo fil'tra (Calculation of a Bag-Type Filter). — Trudy NIItsegment, No. 3. 1950.
- 12-9. Zaitsev, M.M. and F.I. Murashkevich. Vremennye rukovodyashchie ukazaniya po raschetu truby-raspilyatelya dlya optychno-promyshlennyykh ustanovok (Provisional Instructions for Calculation of Tube-Sprayers for Pilot Plants). — Report of NIIOGAZ. 1954.
- 12-10. Zaitsev, M.M. Normali giprogazoochistki na batareinye tsiklony i tsiklony NIIGAZ (Standards for Gas Cleaning by Battery-Powered Dust Separators and NIIGAZ Dust Separators). — Trudy konferentsii po voprosam zoloulavlivaniiya, shlakoulavlivaniiya, shlakozoloispol'zovaniya, Gosenergoizdat. 1955.
- 12-11. Zaitsev, M.M. Ochistka gazov v tsiklonakh i gruppovykh tsiklonakh (Gas Cleaning in Dust Separators and Group Dust Separators). — Sbornik materialov po pyleulavlivaniiyu v tsvetnoi metallurgii, Metallurgizdat. 1957.
- 12-12. Zalogin, N.G. and S.M. Shukher. Ochistka dymovykh gazov (Cleaning of Exhaust and Waste Gases). — Gosenergoizdat. 1954.
- 12-13. Zverev, N.I. Malogabaritnyi zhalyuziiniy zoloulovitel' (Small-Size Louver-Type Dust Collector). — Izvestiya VTI, No. 3. 1946.
- 12-14. Zverev, N.I. Proektnaya normal' zhalyuziinogo zoloulovitelya VTI (Design Standard for the VTI Louver-Type Collector). 1948.
- 12-15. Idechik, I.E. Prinuditel'naya razdacha potoka s pomoshch'yu reshetok v gazoochistnykh, teploobmennyykh i drugikh apparatov (Forced Stream Distribution by Means of Grids in Gas Cleaning, Heat Exchange and other Instruments). — Trudy NIIOGAZ, col. No. 1, Goskhimizdat. 1957.
- 12-16. Idechik, I.E. Vyravnivayushche deistvie sistemy posledovatel'no ustanovlennykh reshetok (The Equalizing Effect of a System of Grids Arranged in a Series). — Teploenergetika, No. 5. 1956.
- 12-17. Kirichev, V.F. and A.A. Tsar'kov. Sravnitel'nye ispytaniya razlichnykh tsiklonov na stende (Comparative Tests of Different Dust Separators on a Test Bend). — Teploenergetika, No. 10. 1957.
- 12-18. Klyachko, L.S. Metod teorecheskogo opredeleniya propusknoi sposobnosti apparatov s vrashchayushchimsya osesimmetrichnym techeniem zhidkosti (Theoretical Determination of the Discharge Capacity of Apparatus with Rotating Axisymmetrical Flow of the Liquid). — Teoriya i praktika obesplyivayushchey ventilyatsii, LIOT (Leningrad), Profizdat. 1952.

- 12-19. Kouzov, P.A. Ochistka vozdukha ot pyli (Dust Removal from Air). — LIOT. 1938.
 12-20. Kouzov, P.A. Tsiklony LIOT s vodyanoj plenkoj (LIOT Dust Separation with the Aid of Water Film). — Vsesoyuznyj nauchno-issledovatel'skij institut okhrany truda v Leningrade. 1953.
 12-21. Kucheruk, V.V. and G.I. Krasilov. Novye sposoby ochistki vozdukha ot pyli (New Methods for Removing Dust from the Air). — Mashgiz. 1950.
 12-22. Kucheruk, V.V. Ochistka ot pyli ventilyatsionnykh i promyshlennykh vybrosov (Dust Removal from Ventilating and Industrial Exhaust Air). — Stroizdat. 1955.
 12-23. Mar'yamov, N.B. Eksperimental'noe issledovanie i raschet aviatsionnykh radiatorov (Experimental Study and Calculation of Aviation Radiators). — Trudy TsAGI, No. 367. 1938.
 12-24. Mar'yamov, N.B. Raschet trubchato-plastinchatykh i trubchato-rebristykh radiatorov (Calculation of Tube- and Plate and Fin- and-Tube Radiators). — Trudy LII, No. 18. 1946.
 12-25. Minskii, E.M. and M.P. Korchazhkin. K raschetu propusknoi sposobnosti tsiklonnykh separatorov (Calculation of the Discharge Capacity of Dust Separators). — Gazovaya promyshlennost', No. 11. 1956.
 12-26. Murashkevich, F.I. Effektivnost' pyleulavlivaniya turbulentnym promyvatel'm (Efficiency of Dust Collection by a Turbulent Washer). — Inzhenerno-fizicheskii zhurnal, AN BSSR, Vol. II, No. 11. 1959.
 12-27. Normy aerodinamicheskogo rašcheta kotel'nykh agregatov (Standards of the Aerodynamic Calculation of Boiler Units). — Mashgiz. 1948.
 12-28. Ochistka vozdukha ot pyli, inertionnye pyleotdeliteli IP-20, rabochie chertezhi (Cleaning the Air of Dust, Inertial IP-20 Dust Separators, Working Drawings). — TsBSP, Stroizdat. 1948.
 12-29. Polikarpov, V.F. Ispytanie plastinchatykh kaloriferov (Testing Baffle Feed Air Heaters). — TsNILOV, Promstroiproekt. 1936.
 12-30. Rekk, E.E. Sravnitel'naya otsenka tkanej, primenayushchikhsya dlya ochistki vozdukha ot pyli v ventilyatsionnykh fil'trakh (Comparative Evaluation of the Fabrics Used for Cleaning the Air from Dust in Ventilation Filters). — Otoplenie i ventilyatsiya, No. 1. 1933; No. 4. 1934.
 12-31. Ritshel', G. and G. Greber. Rukovodstvo po otopleniyu i ventilyatsii (Manual of Heating and Ventilating). Vols I and II. — Gosstroizdat. 1932.
 12-32. Taliev, V.N. Raschet gladkotrubchatykh kaloriferov (Calculating Smooth-Tube Air Heaters). — Otoplenie i ventilyatsiya, No. 6. 1940.
 12-33. Taliev, V.N. Aerodinamicheskie-kharakteristiki novykh konstruktii aeratsionnykh fonarei (Aerodynamic Characteristics of New Designs for Roof Ventilators). — Gosstroizdat. 1955.
 12-34. Teverovskii, E.N. Opty ekspluatatsii i promyshlennykh ispytanii razlichnykh zoloulovitelei i rekomendatsii po ikh vyboru (Experience Accumulated in Operating and in Testing Various Ash and Slag Collectors, and Recommendations for Their Selection). — Trudy konferentsii po voprosam zoloulavlivaniya, shlakoulavlivaniya i shlakozoloispol'zovaniya. Gosenergoizdat. 1955.
 12-35. Teverovskii, E.N. and M.M. Zaitsev. Pyleulavlivayushchii, absorbtionnyi i teploobmennyi apparat "TP" s vysokoskorostnym potokom gaza (Collecting, Absorbing, and Heat Exchanging Apparatus Type "TP" with High-Speed Gas Stream). — Trudy NIIOGAZ, No. 1, Goskhimizdat. 1957.
 12-36. Trichler, A.L. and L.D. Egorov. Metallicheskie kalorifery diya nagreva vozdukha (Steel Air Heaters). — Stroizdat. 1940.
 12-37. Uzhov, V.N. Sanitarnaya okhrana atmosfernogo vozdukha (Air-Pollution Control). — Medgiz. 1955.
 12-38. Uchastkin, P.V. Issledovanie effektivnosti i gidravlicheskogo soprotivleniya eliminatorov (Study of the Efficiency and the Fluid Resistance of Roof Ventilators). — Otoplenie i ventilyatsiya, No. 6. 1940.
 12-39. Frukt, I.A. Gidravlicheskoе soprotivlenie fonarei, snabzhennykh vetrootboinymi shchitkami (Fluid Resistance of Roof Ventilators Equipped with Wind Shields). — Stroitel'naya promyshlennost', No. 1. 1958.
 12-40. Khanzhonkov, V.I. Ventilyatsionnye deflektory (Ventilation Hoods). — Stroizdat. 1947.
 12-41. Khanzhonkov, V.I. Aerodinamicheskie kharakteristiki unifitsirovannogo deflektora TsAGI dlya wagonov (Aerodynamic Characteristics of the Unified TsAGI Ventilation for Railroad Cars). — Promyshlennaya aerodinamika, col. No. 10, Oborongiz. 1958.
 12-42. Tsiklony NIIOGAZ, rukovodystvie ukazaniya po proektirovaniyu, izgotovleniyu, montazhu i ekspluatatsii (NIIOGAZ Dust Separators, Instructions for Their Design, Manufacture, Mounting, and Operation). — Goskhimizdat. 1956.
 12-43. Shakhov, T.F. Siaavnitel'noe izuchenie razlichnykh konstruktii reshetok zhalyuziinykh (inertionnykh) pyleulovitelei (Comparative Study of Different Designs of Louvers for Louver-Type (Inertial) Dust Collectors). — NIIOGAZ report. 1949.
 12-44. El'perin, I.T. Povorot gazov v trubnom puchke (Gas Flow through the Bends of Tube Bundles). — Izvestiya AN BSSR, No. 3. 1950.

SUBJECT INDEX

- Bar grating with an angle of approach
 $\alpha_0 = 0^\circ$, 330
- — — — and $d_0 > 0.5$, 331
- Bell, cf. Bellmouth, conical, 86, 87, 95, 96, 98
- Bellmouth, conical, converging orifice, cf. Inlets, various, into a conduit with a screen at the inlet, 109
- Bellmouth, conical, with end wall, 96
- , — without end wall, 95
- , converging, cf. Inlet with smooth contraction, 96
- , set in a large wall, 146
- , smooth, made by an arc of a circle, with flat end wall and with screen, cf. Bellmouth, smooth, 94
- , — — —, without screen and without end wall, 82
- , — — —, —, with end wall, 93
- Bend, 90° corrugated at $\frac{R_0}{D_0} = 2.5$, 227
- , discharge from, 431
- , standard threaded cast-iron, 30° , 211
- , standard threaded cast-iron, 45° , 211
- , standard threaded cast-iron, 90° , 211
- , — — —, at $\frac{R_0}{D_0} = 1.36-1.67$, 211
- , twin bent, by-pass, 213
- , twin bent, S-shaped, gooseneck shape, 213
- , U-shaped, twin bent, bends at different θ and $\frac{R_0}{D_0} \geq 0.5$, 213
- Bends, sharp at $0.5 < \frac{R_0}{D_h} < 1.5$ and $0 < \theta < 180^\circ$, 206, 207
- , smooth at $\frac{R_0}{D_h} > 1.5$ and $0 < \theta < 180^\circ$, 208, 209
- , standard threaded cast-iron, 211, 212
- , turn, bent at different θ° and $\frac{R_0}{D_h} \geq 0.5$, 212, 213
- , — — —, S-shaped with turn in two planes, 213
- , very smooth ($\frac{R_0}{D_h} \gg 1.5$) in conduits (coils at arbitrary angle of bend θ°). $50 < Re = w_0 D_h / V < 2 \cdot 10^4$, 211
- Bundle of ribbed tubes (air heater) with circular or square ribs, 335
- Bundles of tubes of different cross-section shapes:
- 1) checkerboard bundle of ribbed tubes;
 - 2) parallel bundle of oval tubes;
 - 3) checkerboard bundle of oval tubes;
 - 4) checkerboard bundle of drop-shaped tubes;
 - 5) checkerboard bundle of "Elesko" type tubes;
 - 6) tubes with wire ribbing, 336, 337
- Checkerwork, regenerator (furnaces).
- 1) simple Siemens checkerwork;
 - 2) Siemens checkerwork;
 - 3) checkerwork of "Stal'proekt" design;
 - 4) fence-type checkerwork of V. E. Grune-Grzhimailo system, 349
- Circular free jet, 440
- Cloth, DIZ, shaking filter of various types of cloth, 475
- , filtering, coarse calico, unbleached, 470
- , —, cotton thread, 472
- , —, flax, flimsy, 2-ply thread, 473
- , —, serge-wool mixture, 469
- , —, wool "Mel'stroi", 468
- , various types, MFU suction-type hose filter, 475
- Cloths, filtering, calico, moleskin, and cotton-thread flannelette, 474
- Conduit, friction coefficient at laminar flow $Re < 2000$, 66
- with nonuniform wall roughness (commercial pipes), friction coefficient $Re > 2000$, 70, 71
- with rough walls, friction coefficient, flow conditions according to square law of resistance, 72

- Conduit with smooth walls, friction coefficient $Re > 2000$, 67
 - with uniform wall roughness, friction coefficient $Re > 2000$, 68, 69
- Conical converging bellmouth, cf.
 Inlet with smooth contraction, 96
- Contraction, smooth, cf. Bellmouth:
 (a) rectilinear; (b) converging, 96
 - sudden, at the inlet, cf. Inlet with sudden contraction, $Re < 10^4$, 99
 - - - inlet section in the end wall, $Re = \frac{W_0 D_h}{V} < 10^4$
 cf. Inlet with sudden contraction, 98
 - - - moved forward relative to the end wall $(\frac{b}{D_h} > 0.5)$, $Re > 10^4$ - cf. Inlet with sudden contraction, 98
- Converging bellmouth orifice along the arc of a circle, cf. Inlets, various to a conduit with a screen at the inlet, 109
 - T of type $F_s + F_b > F_c$; $F_s = F_{cs}$; of improved shape, $\alpha = 90^\circ$, 274
 - - - standard threaded from malleable-iron, $\alpha = 90^\circ$, 275
 - Y-branch of type $F_s + F_b = F_c$; $\alpha = 15^\circ$, 267
 - - -; $\alpha = 30^\circ$, 268
 - - -; $\alpha = 45^\circ$, 269
 - - -; $\alpha = 60^\circ$, 270
 - - -; 271
 - - - circular, with smooth side bend $(\frac{R_o}{D_b} = 2.0)$, $\alpha = 12-15^\circ$; branch, 276
 - - -; - - -; - , straight passage, 277
 - - - rectangular, smooth $(\frac{r}{b_b} = 1.0)$, $\alpha = 90^\circ$, branch, 278
 - - -; - , - , main passage, 279
 - - - $F_s + F_b > F_c$; $F_{st} = F_c$, $\alpha = 30^\circ$, branch, 260
 - - -; - ; $\alpha = 45^\circ$, branch, 262
 - - -; - ; $\alpha = 60^\circ$, branch, 264
 - - -; - ; $\alpha = 45^\circ$, main passage, 263
- - -; - ; $\alpha = 60^\circ$; main passage, 265
 - - -; - ; of improved shape, $\alpha = 45^\circ$, 272
 - - -; - ; - ; $\alpha = 60^\circ$, 273
 - Y-branches of type $F_s + F_b > F_c$
 $F_{st} = F_c$, asymmetrical with smooth bends $(\frac{R_o}{D_c} = 2.0)$, $\alpha = 90^\circ$: a) side branch edge D_c slightly rounded $(\frac{r}{D_c} = 0.1)$; b) smooth side branch $(\frac{R_o}{D_c} = 2.0)$, 288
- Corrugated elbows from galvanized sheet for $\frac{R_o}{D_o} = 0.7$: a) elbow $\delta' = 45^\circ$; b) elbow 2 $\delta' = 2 \times 45^\circ$; c) elbow $\delta' = 90^\circ$; d) gooseneck 2 $= 2 \times 45^\circ$; e) gooseneck 2 $\delta' + 2 \times 90^\circ$, 239
- Cross of type $F_{1b} = F_{2b}$; $F_s = F_c$; $\alpha = 90^\circ$: 1) Junction of streams (converging cross); 2) Diversion of a stream (diverging cross), 299, 300
- Curve, 90° , with concentric guide vanes, 240
- Cyclones, NILOGAZ, 1) TsN-15; 2) TsN-15u; 3) TsN-24; 4) TsN-11, 460
 - various, a) simple conical; b) conical SIOT; c) ordinary LIOT and shortened LIOT with untwisting spiral; d) same without untwisting spiral; e) with dust removal; f) LIOT; with water film and a specific liquid discharge; g) grouped cyclones, 458, 459
- Cylinder, elliptical smooth, placed in a pipe, three-dimensional flow, 392
 - single, smooth, placed in a pipe, plane-parallel-flow, 388
- Cylinders, placed in pairs in a pipe, plane parallel flow, 395
- Diaphragm with edges bevelled or rounded at the passage of a stream from one conduit to another, 138
 - (orifice), sharp edged $(\frac{l}{D_h} = 0 \div 0.015)$ in a straight conduit, 139

- Diffuser, annular, free discharge
 from, 422
 -, -, with converging fairing, 187
 -, -, with diverging fairing, 187
 -, axial-radial-annular, free
 discharge, 424
 -, --- in a line, 188
 -, conical, in a line, 167, 168
 -, curved ($\frac{dp}{dx} = \text{const}$), of
 circular or pyramidal sections
 in a line, 175
 -, curved plane in a line, 175
 -, (discharge from) with rounded
 edges and optimum character-
 istics against a baffle, 422
 -, multistage, of optimum
 divergence angle behind a
 centrifugal fan in a duct
 (forced draft), 186
 -, plane asymmetrical at $\alpha = 0$
 behind a centrifugal fan in a
 duct (forced draft), 183
 -, -, asymmetrical behind a
 centrifugal induced-draft fan,
 free discharge, 424
 -, -, in a line, 171, 172
 -, plane, symmetrical behind
 a centrifugal fan in a duct
 (forced draft), 183
 -, pyramidal, behind a centri-
 fugal fan in a duct (forced
 draft), 185
 -, -, behind centrifugal induced-
 draft fan, free discharge, 425
 -, radial-annular, in a line, 188
 -, pyramidal, in a line, 169, 170
 -, rectilinear, discharge against
 a baffle at $\frac{ld}{D_h} = 1.0$, 421
 -, short, with dividing walls, 182
 -, -, with guiding devices or
 with resistance at the exit,
 182
 -, stepped circular; optimum
 divergence angle α^* opt, 176, 177
 -, -, plane; optimum divergence
 angle, 180, 181
 -, -, pyramidal; optimum divergence
 angle, α^* opt, 178, 179
 -, transitional (from circle to rect-
 angle or from rectangle to circle)
 in a line, 174
 -, with baffles, 182
 Diffusers, annular, with deflecting
 baffles in a duct, 187
 - of arbitrary shape, at $\alpha = 8-12^\circ$
 located at discharges of
 branches or other fitting at
 similar velocity profiles, 174
 - - - located at the discharge of
 long stretches with nonuniform
 but symmetric velocity profile,
 166
 - with resistance at the exit
 (screen, perforated plate), 182
 Discharge from a straight conduit
 through grid or orifice
 ($0 < l/d_h < 0.15$), 435
 - from a straight conduit through
 fixed louvre. 1) Inlet edges
 of the slots cut vertically;
 2) Inlet edges of the slots cut
 horizontally, 438
 - - - thick-edged orifice or
 grid, 436
 - - - stretch with rounded edges
 against a baffle, 421
 -, side, from the last orifice of a
 circular pipe, 425
 - stretches under different conditions:
 1) From a straight conduit with
 screen at the exit;
 2) from a gutter with screen;
 3) through a stamped standard
 louvre with completely open
 adjustable slots; 4) through
 cramped or cast grids; 5) Smoothly
 converging nozzle, 439
 Diverging T of type $F_s + F_b > F_c$:
 $F_s = F_c$, $\alpha = 90^\circ$, standard
 threaded from malleable iron,
 285
 - Y of type, $\alpha = 90^\circ$, branch, 280
 - - - $F_s + F_b = F_c$, $\alpha = 0-90^\circ$,
 281
 - - - -, - rectangular smooth
 ($\frac{r}{b_s} = 0.1$), $\alpha = 90^\circ$, branch,
 286
 - - - - ($\frac{r}{b_b} = 1.0$), $\alpha = 90^\circ$,
 main passage, 287
 - - - - and $F_s + F_b = F_c$:
 $\alpha = 0-90^\circ$, straight passage,
 282
 - - - - $F_{st} = F_c$, of improved
 shape, 283, 284
 Double flaps, top and bottom
 hinged, 149
 - Y- of type $F_s + F_b = F_c$:
 $F_s = F_c$; $\alpha = 15^\circ$, 291, 292
 - - - - ; $\alpha = 30^\circ$, 293, 294
 - - - - ; $\alpha = 45^\circ$, 295, 296

- Double flaps, top and bottom
 hinged; $\alpha = 60^\circ$, 297, 298
 Dust separator, inertial (louvre-type) conical [KTIS, 461
 - separators, battery-powered
 BTs: 1) with "screw" blade;
 2) with "rosette", $\alpha = 25^\circ$;
 3) with "rosette", $\alpha = 30^\circ$, 461
 Dynamic viscosity, 4, 6-9, 11, 12

 Elbow, composite, made from two
 90° elbows lying in different
 planes, 229
 - π -shaped (180°) with contracted exit section, 231
 - -- with enlarged exit section

$$\left(\frac{F_1}{F_0} = \frac{b_1}{b_0} = 1.4 \right) 232$$

 - --- $\left(\frac{F_1}{F_0} = \frac{b_1}{b_0} = 2.0 \right) 233$
 - -- with equal inlet and exit
 areas $\left(\frac{F_1}{F_0} = \frac{b_1}{b_0} = 1.0 \right) 230$

 Elbow, sharp, rectangular section
 with contracted or expanded
 discharge section, 432
 - , - , - with contracted or expanded discharge section, 433
 - , - , square section with contracted or expanded discharge section, 432
 - , smooth with contracted or expanded discharge section, 433
 - , U-shaped (180°) with contracted exit section $\left(\frac{F_1}{F_0} = \frac{b_1}{b_0} = 0.5 \right) 234$
 - -- with equal inlet and exit
 areas $\left(\frac{F_1}{F_0} = \frac{b_1}{b_0} = 1.0 \right) 235$
 - -- with widened exit section

$$\left(\frac{F_1}{F_0} = \frac{b_1}{b_0} = 1.4 \right) 236$$

 - --- $\left(\frac{F_1}{F_0} = \frac{b_1}{b_0} = 2.0 \right) 237$
 - with rounded corners and converging or diverging exit section

$$\left(\frac{F_1}{F_0} \geq 1.0 \right), 217, 218$$

 - -- at $0.05 < r/D_h < 0.5$ and
 $0^\circ < \delta < 180^\circ$, 219, 220
 - Z-shaped made from two 30° elbows, 227
 - -- $\text{Re } \frac{w_0 D_h}{v} > 10^4$, 228
 - 45°; three 22.5° elements, 223
 - 60°; - 30° elements, 223
 - 90°, five 22.5° elements, 224
 - 90°, made from five elements, 225

- --- at different $\frac{r}{b_0}$ with profiled guide vanes, 241
 - --- with thin guide vanes ($\Phi_1 = 90^\circ$), 242
 - --- with rounded inner corner and sharp outer corner, 221

 Elbow 90° rectangular section with thin guide vanes. ($\Phi_1 = 95^\circ$) under different conditions:
 1) sharp inner corner, normal number of vanes; 2) same as 1), but $\alpha = 50^\circ$; 3) same as 1), but most advantageous (reduced number of vanes); 4) same as 1), but inner corner cut off; 5) elbow with expansion, normal number of vanes; 6) same as 5), but reduced (minimum) number of vanes, 243
 - -- with cut-off corners, 222
 - -- smooth $\left(\frac{r}{b_0} = 0.2 \right)$ rectangular at $\frac{F_1}{F_0} = 0.5$ with thin guide vanes ($\Phi_1 = 103^\circ$), 244
 - --- $\frac{F_1}{F_0} = 1.0$ with thin guide vanes ($\Phi_1 = 107^\circ$), 244
 - --- at $\frac{F_1}{F_0} = 2.0$ with thin guide vanes, 245
 - -- with discharge section expanded by a factor of two

$$\left(\frac{b_1}{b_0} = 2.0 \right)$$
 and with five thin guide vanes, 434
 - -- with discharge section contracted or expanded by a factor of two, 434
 - -- three 45° elements, 226
 - --- at $\frac{R_0}{D_0} \approx \text{welded (with welding joints) at } Re = \frac{\rho D_0}{v} > 10^5$, 226

 Elbows made from separate elements at different δ° , 223
 - , square $\left(\frac{r}{D_h} = 0 \right)$ at $0^\circ < \delta < 180^\circ$, 215

 Elbows, square $\left(\frac{r}{D_h} = 0 \right)$ rectangular section with converging or diverging exit section, 214
 - 90° circular with profiled guide vanes: a) smooth turn with

- normal number of vanes;
 b) the same with reduced number of vanes; c) cut-off corners and normal number of vanes; d) the same with reduced number of vanes; e) cut-off corners with reduced number of vanes, 246
- Electrostatic filters, industrial, 476
- Eliminators, 489
- Ellipsoid, placed in a pipe, three-dimensional flow, 394
- Entrance, straight into a conduit mounted flush in the wall at an arbitrary angle, 93
- , - of constant cross section with various mountings, 92, 100
 - , - made by the arc of a circle without screen and without end wall, cf. Bellmouth, smooth, 93
 - , - to a conduit through a perforated plate with rounded orifice edges, 108
 - through a fixed louver:
 - a) inlet edges of the fins cut vertically; b) inlet edges of the fins cut horizontally, 110
 - to a straight channel through a fixed louver, 110
 - conduit through a perforated plate with orifice edges beveled or rounded, 108
 - with thick-edged orifices $(\frac{l}{d_h} > 0.015)$, 107
 - with sharp-edged orifices $(\frac{l}{d_h} = 0 \div 0.015)$
- Entrances to a conduit with a screen at the inlet, 109
- Exhaust flap, single, top hinged, 147
- Exhaust vents, bent rectangular, lateral opening with and without louvers, 427
- -, straight circular: 1) with plane baffle; 2) with split canopy; 3) with hood; 4) with split hood; 5) with diffuser and hood, 428
 - -, rectangular; lateral openings with and without fixed louvers, 426
- Expansion joints, various: 1. Stuffing box; 2. Bellows; 3. Lyre-shaped smooth; 4. Lyre-shaped with grooves; 5. Lyre-shaped with
- corrugated tube; 6. Π-shaped, 374
- , sudden, after a long straight stretch, diffuser, etc., with exponential velocity distribution. Circular or rectangular cross section, 129
 - , - long plane and straight stretches, plane diffusers, etc., with exponential velocity distribution, 130
 - , - stretches with parabolic velocity distribution, 133
 - , - behind plane diffusers with $\alpha > 10^\circ$, elbow, etc., with asymmetric velocity distribution, 133
 - , - of a plane channel behind orifice plates, baffles in elbows, etc., with sinusoidal velocity distribution, 131
 - , - with uniform distribution of the velocities, 128
- Filter, box-type from corrugated gauze with moist filter of Rekk design, 466
- , -- porous with moist packing, 467
 - , twine, wedge-shaped shaping single stage of MIDT-type, 466
- Filters, cloth, 468-475
- Fixed louvers at the inlet to a straight channel: a) inlet edges of the fins cut vertically; b) inlet edges of the fins cut horizontally - cf. Entrance to a straight channel through a fixed louver, 110
- at side orifice in an intake shaft of rectangular section - cf. Straight intake shafts of rectangular section with fixed louvers, 104
 - in a straight intake shaft - cf. Straight intake shafts with fixed louvers, 103
- Flap, 366
- , exhaust, single, top hinged, 147
 - , intake, single, top hinged, 147
 - , single, center hinged, 148
 - , double, both top hinged, 148
- Free discharge from an annular radial diffuser, 423
- from a circular rectilinear

- diffuser, 418
- - from a conduit at different velocity distributions: 1) uniform; 2) exponential; 3) sinusoidal; 4) axisymmetrical; 5) parabolic, 416, 417
 - - from a plane diffuser, 420
 - - from a rectangular diffuser, 419
- Friction coefficient with nonuniform wall roughness (commercial pipes), 70, 71
- - of conduit with rough walls at square resistance law, 72
 - - - with uniform wall roughness, 68, 69
 - - of a pipe at laminar flow, $Re < 2000$, cf. Conduit at laminar flow, 66
 - - - from rubberized material, cf. Pipe from rubberized material, 78
 - - - with smooth walls, cf. Conduit with smooth walls, 59
 - - of a plywood pipe, cf. Pipe, plywood, 79
 - - of a steel or cast-iron water pipe - cf. Pipe, water, 74
 - - of a welded pipe - cf. Pipe welded with joints, 73
- Gate valve: a) cylindrical pipe; b) rectangular pipe, 359
- - , with symmetric contraction, 360
- Globe and gate valves: a. Globe valve "Rey" type; b. Forged globe valve; c. Wedge-type gate valve; d. Steam-gate valve with lever gate; e. Gate valve with mushroom head and sliding tube, 365
- valve, direct-flow, 364
 - - , standard with dividing walls: a) dividing walls at an angle of 45°; b) vertical dividing walls, 363
 - - , Y-pattern ("Kosva"): 1) with 30% contraction of the seat; 2) with full seat section, 363
- Grid, flat (perforated plate), with sharp-edged orifice ($\frac{l}{D_t} = 0 \div 0.015$) at the inlet of a conduit - cf. Entrance to a straight conduit
- through a perforated plate with sharp-edged orifices, 106
- or orifice, thick-walled through with discharge from a straight conduit, 436
 - - - with rounded or beveled edges through which discharge passes from a rectilinear conduit toward the stream flow, 437
 - , plane (perforated sheet or strip), with sharp-edged orifices ($\frac{l}{D_t} = 0 \div 0.015$). Large Reynolds numbers ($Re = \frac{w_0 d_h}{V} > 10^5$) 321
 - - - , with sharp-edged orifices ($\frac{l}{D_h} = 0 \div 0.015$). Small Reynolds numbers ($Re = \frac{w_0 d_h}{V} < 10^5$), 322
 - , thick (perforated plate or laths), 324, 325
 - with orifice edges beveled facing the flow or made from angle iron, 323
 - with orifices with beveled edges - cf. Entrance to a straight conduit through a perforated plate with orifice edges beveled or rounded, 108
 - with rounded orifice edges, 326
 - - - at the inlet of a conduit - cf. Entrance to a straight channel through a fixed louver, 110
 - , with orifice edges cut or rounded and screens at high stream velocities (large Mach numbers), 329
 - , with sharp inlet in the orifice of a wall of arbitrary thickness at high stream velocities (large Mach numbers), 328
- Header, with transition stretches, 302
- Heat exchangers, various:
1. Shell-tube, with longitudinal stream flow around the tubes; 2. Shell-tube, with stream flow through the tubes; 3. Two-stage flow exchanger with transverse flow

- around the tube bundle (180° turn); 4. With mixed flow around the tubes (alternating sections of transverse and longitudinal flows), 485
- Heater, air, made from heating elements,** 484
 —, —, plain pipe, 484
 —, —, plate-type, 481
 —, —, spiral-ribbed, 482
 —, fin, petaled, 483
- Indraft shaft, straight circular,** with diffuser and hood, 105
 —, —, with flat screen, 105
 —, —, with hood and section, 105
 —, —, with hood at sharp inlet edge, 105
 —, —, with section, 105
 —, —, square with hood at thickened inlet edge, 105
 —, shafts, straight circular section, 105
 —, air duct with perforated lateral outlet, 430
 —, conical, with end wall — cf. Bellmouth, conical, 96
 —, side, to a circular straight pipe through the first orifice, 102
 —, straight, in a conduit clamped between three walls, 101
 —, —, — mounted between two walls, 101
- Inlet, straight, in a conduit mounted on a wall,** 101
 —, —, — with reinforced inlet edge, 109
 —, —, — with sharp inlet edge through a screen, 109
 —, —, with end wall on one side of the conduit, 100
 —, —, — on two adjacent sides of the conduit, 100
 —, —, — three sides of conduit, 100
 —, —, — two opposite sides of the conduit, 100
 —, — with orifices on the one side of the conduit, 102
 —, —, — on the two sides of the conduit, 102
 —, stretches of unit with grid packing or other type of obstruction placed in the working chamber; 1. Cen-
- tral impingement of the stream on the grid. 2. Peripheral impingement of the stream on the grid. 3. Side impingement of the stream on the grid, 477
- with smooth contraction:
 a) rectilinear converging bell-mouth; b) converging bell-mouth — Bellmouth, 96
- with sudden contraction (or sudden contraction only); inlet cross section in the end wall
 $Re = \frac{w_e D_h}{V} < 10^4$, 99
- (—); — section in the end wall ($\frac{b}{D_h} = 0$); $Re > 10^4$; a) rounded inlet edge; b) inlet edge cut, beveled; c) blunt inlet edge, 98
- ; — moved forward relative to the end wall ($\frac{b}{D_h} = 0$); a) rounded inlet edge; b) sharp or thick inlet edge; c) beveled inlet edge, 98
- Inlets, various, with screen,** 97
- Kinematic viscosity,** 4, 6, 7, 8, 10-12
- Labyrinth seal, comb-type,** 373
 — with increased gap, 372
- Labyrinths; various:** a) short 180° elbow complex; b) hood with three-sided inlet (exit); c) hood with straight stretch at the inlet or exit, 377, 378
- Louver, dust separators,** 461, 462
 — fixed at inlet to a straight channel: a) inlet edges of the fins cut vertically; b) inlet edges of the fins cut horizontally — cf. Entrance to a straight channel through a fixed louver, 110
 — at side orifice in an intake shaft; cf. Straight intake shafts . . . side orifice with fixed louvers, 103, 104
 — stamped with adjustable slots in a large wall; $F \approx 0.8$ complete opening of the louver, 149

- Orifice plate — cf. Entrance to a straight conduit through a perforated plate with sharp-edged orifices, 106
- , sharp-edged ($\frac{l}{d_h} = 0+0.015$),
at the passage of a stream from one size conduit to another,
 $Re = \frac{w_0 D_h}{\nu} > 10^5$, 136
 - , — — — , in a large wall, 143
 - , — — — , in a straight conduit, 139
 - , thick-walled ($\frac{l}{D_h} > 0.015$)
at the passage of the stream from one size conduit unto another, 137
 - , — — — , in a large wall, 114
 - , — — — , in a straight conduit, 140
 - with edges beveled facing the stream flow ($\alpha = 40-60^\circ$) in a straight pipe, 141
 - , — or rounded at the passage of a stream from one conduit to another — cf. Diaphragm, 138
 - , — cut along the stream in a large wall, 144
 - with rounded edges in a large wall, 144
 - — — in a straight pipe, 142
- Orifices with various edges in a large wall, 144

- Packing, bonded porous medium (not granulated), 345
- , ceramic, Raschig rings, ($\frac{d_{out}}{d_{in}} = 1.2$)
dry or wetted: 1) rings in vertical columns; 2) rings in staggered, 346
 - of wooden laths; dry or wetted:
1) chords placed in parallel;
2) chords placed crosswise, 347, 348
 - , loose layer of spherical (granular) bodies or porous cemented layer from granular material (constant diameter), 343, 344
 - , material deposited at random (loose layers from bodies of irregular shape) at given d_h dry and wetted, 339-342.
- Parallel bundle of circular tubes, 332, 333
- Passage complex from one volume to another through a 90° elbow:

- 1) with cut-off inlet (exit) stretch without vanes; 3) the same, but with vanes; 3) with inlet (exit) stretch of length $l_0 = d_0$ without vanes; 4) the same, but with vanes, 375
 - — — — through an oblong elbow: 1) with baffle;
2) without, 376
 - — — — through different labyrinth seals, 377
 - through a side opening of a header pipe of constant section, 303, 304
- Perforated plate at high Mach numbers, 145
- Pipe from tarpaulin-type, rubberized material, friction coefficient, 78
- plywood (birch with longitudinal grain), friction coefficient at turbulent flow, 79
 - reinforced by various stay rods and braces across the section, 397
 - , water, of steel or cast iron, allowing for the increase of resistance with use, friction coefficient, 74
 - welded with joints, friction coefficient, 73
- Plane-parallel free jet, 441
- Plates, circular, placed in pairs in a pipe, three-dimensional flow, 395
- Radiator, honeycomb with hexagonal or circular tubes, 478
- , ribbed-tube, 479
 - , tube- and plate, 480
- Recuperators (air heaters): 1) ribbed cast-iron air heaters; 2) ribbed-toothed air heaters, 338
- Reinforced rubber hose, friction coefficient, 75
- steel rubber hose, friction coefficient, 77
- Ring-seal gate (free), 371
- — — (in a chamber), 371
- Rolled section, arranged in a row in a pipe, plane-parallel flow, 396
- Roof ventilation openings, rectangular with panels, 491
- — — , various types: 1) Baturin-Brandt with grid; 2) same with

- flaps; 3) LD-4; 5) LEN PSP with 2 flaps, same with 3 flaps; 6) KTIS; 7) MIOT 2, MIOT 2a; 8) PSK-1; 9) PSK-2 summer conditions, PSK-2 winter conditions; 10) two-circle; 11) Giprotis; 12) Ryukin-ll'yanskii; 13) Ventilating house, 490, 491
 Roughness, 61, 62, 65
- Screens: a) circular metal wire; b) silk threads, 327
 Scrubber with wooden packing, 463
 Shapes, different, placed in a pipe. Three-dimensional flow:
 1) convex hemisphere; 2) concave hemisphere; 3) smooth cylinder, axis parallel to direction of flow; 4) smooth cylinder, axis perpendicular to direction of flow; 5) cone; 6) square beam, 393
 Single rolled sections placed in a pipe, plane-parallel flow, 390
 Specific gravity, 3, 4
 Sphere placed in a pipe, three-dimensional flow, 391
 Stay rods and braces, single, placed in a pipe, plane-parallel flow:
 1) circular cylinder with fairing; 2) streamlined rod; 3) plate with rounded edges; 4) wedge-shaped plate; 5) square beam, 389
 Steel-reinforced hose, friction coefficient, 75
 Stopcock: a) rectangular pipe; b) cylindrical pipe, 362
 Straight intake shafts of rectangular section; side orifice with fixed louvers and without them, 103
 Stream deformation in a straight conduit with the entry of a free jet into it (ejection), 134
 Symmetric tee, $\alpha = 90^\circ$, 289
- Tee of type $F_b + F_{st} > F_c$; $F_s = F_c$
 $\alpha = 90^\circ$, 266
 Thickened grid (perforated plate or laths), 324
 Throat of a wind-tunnel, 150
 Transition, cf. Diffuser, transitional, 174
 Truss, square, placed in a pipe, plane-parallel flow, 399
 —, triangular, placed in a pipe, plane-parallel flow, 398
 Type of cap: 1) with three diffusers;
 2) hemisphere with orifices
 $\frac{F_{or}}{F_0} = 0.56$; 3) hemisphere with orifices $\frac{F_{or}}{F_0} = 3.9$;
 4) hemisphere with slots $\frac{F_{or}}{F_0} = 1.4$; 5) cylinder with perforated surface $\frac{F_{or}}{F_0} = 4.7$, 429
- Valve, ball, on spherical seat, 370
 —, butterfly: 1) cylindrical pipe; 2) rectangular pipe, 361
 —, check, 368
 —, conical on conical seat, 370
 —, — on flat seat, 370
 —, control, double seat, 367
 —, disk, with bottom guide, 369
 —, disk, without bottom guide, 368
 Valve, suction with screen, 368
 Ventilating hoods, various: 1) circular TsAGI; 2) square TsAGI; 3) Chanard-Etoile; 4) Grigovich; 5) standardized TsAGI without reducing piece for railroad cars; 6) standardized TsAGI roof ventilator with reducing piece for railroad cars; 7) Chesnokov roof ventilator, 486-488
 Venturi scrubber (tube-sprayer), 463
 VT1 centrifugal scrubber, 464
 Y of type $F_c = 2F_s$, 301